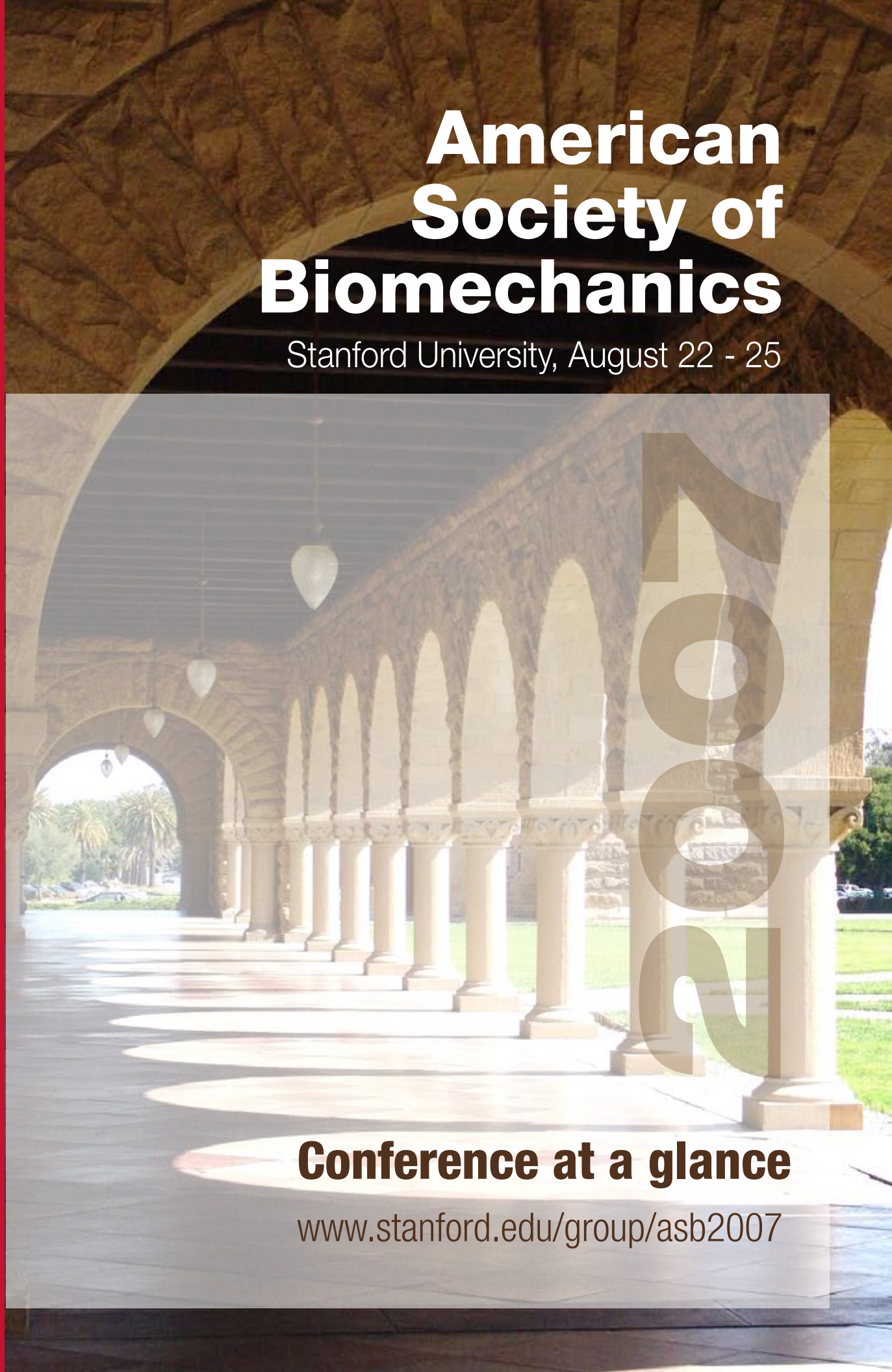

American Society of Biomechanics

Stanford University, August 22 - 25

2007

Conference at a glance

www.stanford.edu/group/asb2007

ASB
founded 1977
AMERICAN SOCIETY OF BIOMECHANICS


AMTI


BERTEC
www.bertec.com


Innovative
Sports Training
...The Total Solution in Motion Capture


Innovision Systems
INCORPORATED


KISTLER
measure. analyze. innovate.


mic
Motion Imaging and Analysis


MotionAnalysis


NORAXON®
EMG & Sensor Systems


novel


O
Z
ENGINEERING, INC.
N


VICON

Dear Friends and Fellow Biomechanists:

Welcome to Stanford University! We are excited to host you and hope that you all have a stimulating conference experience.

Biomechanics research began on the Stanford farm when Leland Stanford took a position on a hotly debated question: whether during a horse's trot, all four hooves were ever off the ground at the same time. Stanford sided with this assertion, and wanted to prove it scientifically. He hired Eadweard Muybridge to settle the issue. Muybridge developed a scheme for instantaneous motion picture capture. Muybridge's technology involved novel methods for photographic processing and a camera trigger developed by Stanford's engineer, John Isaacs. In 1877, Muybridge settled Stanford's question with a single photographic negative showing Stanford's race-horse, Occident, airborne during trot.

This conference marks the 30th anniversary of ASB. The Society was founded in October 1977 by a group of 52 scientists and clinicians (listed later in this program). The mission of ASB — to foster the exchange of ideas among biomechanists working in different disciplines and fields of application, including biological sciences, exercise and sports science, health sciences, ergonomics and human factors, and engineering, and to facilitate the development of biomechanics as a basic and applied science — is still vital today.

Over 450 abstracts were submitted for presentation at the conference. This is the largest number of abstracts ever submitted to an ASB conference. Two or three reviewers read and scored each abstract, and the top-rated abstracts were selected for presentation at the meeting.

Many people have helped prepare for this conference. A special thanks goes to the program committee and the local organizers listed in this program. We also want to thank the Stanford students, fellows, and staff who put in many hours to make the meeting special. You will see these local volunteers wearing their "Cardinal" shirts. Please ask them for help, directions and advice. Kam Morrella and Carolyn Mazenko put forth a huge effort to organize the conference; please thank them when you see them.

We hope you enjoy the conference. Engage in the science… ask 100 questions… go to every poster… meet a new mentor… find an old friend. Maybe even take a walk to Stanford's barn to see the place where Muybridge "stopped time."

Sincerely,

Scott Delp	**Chris Jacobs**	**Francisco Valero-Cuevas**
Conference Co-Chair	*Conference Co-Chair*	*Program Chair*

SOCIAL PROGRAM

Opening Reception, Wednesday, August 22, Clark Center, 5:00-7:30pm

Night on the Town, Thursday, August 23, Downtown Palo Alto, 7:00pm-midnight

Conference Dinner, Friday, August 24, Frost Amphitheater, Stanford Campus, 6:00-9:00pm

CONFERENCE REGISTRATION

Wednesday, August 22, Clark Center noon-7:00pm

Wednesday, August 22, Governor's Corner dorms 2:00-7:00pm

Thursday, August 23, Memorial Auditorium Lobby 8:00am-2:30pm

Friday, August 24, 2007 Memorial Auditorium Lobby 8:00am-2:30pm

Saturday, August 25 Memorial Auditorium Lobby 8:00am-noon

COMMITTEE MEETINGS

ASB Executive Committee, Wednesday August 22, 3:00-5:00pm Clark Center Room S363

ASB Past President's Breakfast, Friday, August 24, 7:15-8:15am, Green Room, Memorial Auditorium

ASB Executive Committee, Saturday August 25, 4:00-6:00pm Green Room, Memorial Auditorium

INDUSTRIAL EXHIBITS

Thursday, August 23, Memorial Auditorium Lobby 8:00am – 6:00pm

Friday, August 24, Memorial Auditorium Lobby 8:00am – 6:00pm

INDUSTRIAL SPONSORS and EXHIBITORS

Motion Analysis Corporation (Gold Sponsor)

Innovision Systems, Inc.

Innovative Sports Training, Inc.

Kistler Instrument Corporation

Novel Inc.

AMTI

Bertec Corporation

Vicon

Ozen Engineering

Motion Imaging Corporation

Noraxon USA, Inc.

Program Committee

Francisco Valero-Cuevas (Program Chair)

Art Kuo, Christine Raasch, Darryl Thelen, Jack Dennerlein, James Ashton-Miller, Larry Bonassar, Lena Ting, Max Donelan, Richard Hughes, Rick Lieber, Silvia Blemker, Wendy Murray, Yasin Dhaher, Mont Hubbard, Kai An, Eric Perreault, Glen Niebur, Joseph Crisco

Local Organizing Committee

Christopher Jacobs (Co-chair), Scott Delp (Co-chair)

Dennis Carter, Thomas Andriacchi, Thor Besier, Ellen Kuhl, Marc Levenston, Charles A.Taylor

ASB Executive Committee

President: Kenton Kaufman

Past-President: Ted Gross

President-Elect: Rodger Kram

Secretary/Treasurer: Don Anderson

Secretary/Treasurer-Elect: Paul DeVita

Program Chair: Francisco Valero-Cuevas

Program Chair-Elect: Richard Hughes

Meeting Chair: Scott Delp

Membership Chair: Max Kurz

Education Committee Chair: Steve McCaw

Communications Committee Chair: Andy Karduna

Newsletter Editor: Michelle Sabick

Student Representative: Katie Bieryla

ASB FOUNDING MEMBERS AND PAST PRESIDENTS

FOUNDING MEMBERS

Thomas Andriacchi
Thomas Armstrong
Michael Askew
Eugene Bahniuk
Barry Bates
Richard Brand
Albert Burstein
David Butler
Dennis Carter
Don Chaffin
Krishnan Chandran
Jerome Danoff
Dwight Davy
Robert Deusinger
Roger Enoka
F. Gaynor Evans
Carl Gans
Edward Grood
James Hay
H.K. Huang
Maury Hull
Ronald Huston
Martha Jack
J. Lawrence Katz
Jonathan Kofman
William Krause
Shrawan Kumar
Jean Landa Pytel
R. Bruce Martin
Bruce Mason
Doris Miller
Manssour Moeinzadeh
Richard Nelson
Sally Phillips
Gerald Pijanowski
Carol Putnam
George Rab
Herbert Reynolds
Verne Roberts
Subrata Saha
Albert Schultz
Robert Shapiro
Gary Soderberg
Robert Soutas-Little
Christopher Vaughan
Stephen Wainwright
James Walton
Frederick Werner
William Whiting
Keith Williams
Timothy Wright
Charles Wunder

PAST PRESIDENTS

F. Gaynor Evans (1977)
Albert Burnstein (1978)
James Hay (1980)
Stephen Wainwright (1981)
Albert Schultz (1982)
Doris Miller (1983)
Richard Brand (1984)
Savio Woo (1985)
Peter Cavanagh (1986)
Don Chaffin (1987)
Malcolm Pope (1988)
Roger Enoka (1989)
George Rab (1990)
Thomas Andriacchi (1991)
Ronald Zernicke (1992)
Thomas Brown (1993)
Philip Martin (1994)
Kai An (1995)
Robert Gregor (1996)
Mark Grabiner (1997)
Bruce Martin (1998)
Melissa Gross (1999)
James Ashton Miller (2000)
Andrew Biewener (2001)
Joan Bechtold (2002)
Walter Herzog (2003)
Trey Crisco (2004)
Ted Gross (2005)
Kenton Kaufman (2006 –)

SCIENTIFIC SESSIONS

Thursday, August 23, 2007

Podium 1: Motor Control I
Chair: Eric Perreault
Memorial Auditorium 9:45 - 11:00 AM
Thursday, August 23, 2007

Podium 2: Methods I
Chair: Steve Piazza
Annenberg Auditorium 9:45 - 11:00 AM
Thursday, August 23, 2007

Podium 3: Bone I
Chair: Glen Niebur
Cubberley Auditorium 9:45 - 11:00 AM
Thursday, August 23, 2007

Podium 4: Aging I
Chair: James Ashton-Miller
Memorial Auditorium 11:15 AM - 12:30 PM
Thursday, August 23, 2007

Podium 5: Computational Biomechanics I
Chair: Richard Hughes
Annenberg Auditorium11:15 AM - 12:30 PM
Thursday, August 23, 2007

Podium 6: Ergonomics and Occ. Biomech. I
Chair: Devin Jindrich
Cubberley Auditorium11:15 AM - 12:30 PM
Thursday, August 23, 2007

Podium 7: Walking
Chair: Clay Anderson
Memorial Auditorium 1:45 - 3:00 PM
Thursday, August 23, 2007

Podium 8: Injury
Chair: Jack Dennerlein
Annenberg Auditorium 1:45 - 3:00 PM
Thursday, August 23, 2007

Podium 9: Sports I
Chair: Mont Hubbard
Cubberley Auditorium 1:45 - 3:00 PM
Thursday, August 23, 2007

Podium 10: Running
Chair: Rick Neptune
Memorial Auditorium 3:15 - 4:30 PM
Thursday, August 23, 2007

Podium 11: Upper Extremity
Chair: Wendy Murray
Annenberg Auditorium 3:15 - 4:30 PM
Thursday, August 23, 2007

Podium 12: Tendon and Ligament
Chair: Zachary Domire
Cubberley Auditorium 3:15 - 4:30 PM
Thursday, August 23, 2007

Friday, August 24, 2007

Podium 13: Locomotion Energetics
Chair: Young-Hui Chang
Memorial Auditorium 9:45 - 11:00 AM
Friday, August 24, 2007

Podium 14: Hand
Chair: Zong-Ming Li
Annenberg Auditorium 9:45 - 11:00 AM
Friday, August 24, 2007

Podium 15: Knee
Chair: Heidi-Lynn Ploeg
Cubberley Auditorium 9:45 - 11:00 AM
Friday, August 24, 2007

Podium 16: Comparative Biomechanics
Chair: Andrew Biewener
Memorial Auditorium 11:15 AM - 12:30 PM
Friday, August 24, 2007

Podium 17: Muscle Mechanics
Chair: Silvia Blemker
Annenberg Auditorium11:15 AM - 12:30 PM
Friday, August 24, 2007

Podium 18: Rehabilitation I
Chair: Yasin Dhaher
Cubberley Auditorium11:15 AM - 12:30 PM
Friday, August 24, 2007

Podium 19: Neurorehabilitation
Chair: David Reinkensmeyer
Memorial Auditorium 1:45 - 3:00 PM
Friday, August 24, 2007

Podium 20: Motor units
Chair: Rick Lieber
Annenberg Auditorium 1:45 - 3:00 PM
Friday, August 24, 2007

Podium 21: Ergonomics and Occ. Biomech. II
Chair: Joseph Crisco
Cubberley Auditorium 1:45 - 3:00 PM
Friday, August 24, 2007

Podium 22: Neuromechanics
Chair: Jonathan Dingwell
Memorial Auditorium 3:15 - 4:30 PM
Friday, August 24, 2007

Podium 23: Muscle
Chair: Kevin Keenan
Annenberg Auditorium 3:15 - 4:30 PM
Friday, August 24, 2007

Podium 24: Rehabilitation II
Chair: Matt Tresch
Cubberley Auditorium 3:15 - 4:30 PM
Friday, August 24, 2007

Saturday, August 25, 2007

Podium 25: Aging II
Chair: Darryl Thelen
Memorial Auditorium 9:45 - 11:00 AM
Saturday, August 25, 2007

Podium 26: Computational Biomechanics II
Chair: Veronica Santos
Annenberg Auditorium 9:45 - 11:00 AM
Saturday, August 25, 2007

Podium 27: Sports II
Chair: Alison Sheets
Cubberley Auditorium 9:45 - 11:00 AM
Saturday, August 25, 2007

Podium 28: Motor Control II
Chair: Boris Prilutsky
Memorial Auditorium 11:15 AM - 12:30 PM
Saturday, August 25, 2007

Podium 29: Methods II
Chair: Li-Shan Chou
Annenberg Auditorium11:15 AM - 12:30 PM
Saturday, August 25, 2007

Podium 30: Bone II
Chair: Katherine Boyer
Cubberley Auditorium11:15 AM - 12:30 PM
Saturday, August 25, 2007

Thursday, August 23, 2007

Poster 1: Skeletal Tissue
Memorial Auditorium 4:30 - 6:15 PM
Thursday, August 23, 2007

Poster 2: Aging
Memorial Auditorium 4:30 - 6:15 PM
Thursday, August 23, 2007

Poster 3: Motor Control
Memorial Auditorium 4:30 - 6:15 PM
Thursday, August 23, 2007

Poster 4: Injury
Memorial Auditorium 4:30 - 6:15 PM
Thursday, August 23, 2007

Friday, August 24, 2007

Poster 5: Rehabilitation
Memorial Auditorium 4:30 - 6:15 PM
Friday, August 24, 2007

Poster 6: Computational Biomechanics
Memorial Auditorium 4:30 - 6:15 PM
Friday, August 24, 2007

Poster 7: Muscle
Memorial Auditorium 4:30 - 6:15 PM
Friday, August 24, 2007

Poster 8: Sports
Memorial Auditorium 4:30 - 6:15 PM
Friday, August 24, 2007

Poster 9: Locomotion
Memorial Auditorium 4:30 - 6:15 PM
Friday, August 24, 2007

Poster 10: Manipulation
Memorial Auditorium 4:30 - 6:15 PM
Friday, August 24, 2007

PLENARY SESSIONS AND TUTORIALS

Wednesday August 22, 2007 1:00 – 3:00 PM

Tutorial 1: Biomechanical Modeling and Simulation

Clark Center Auditorium

Faculty: Scott Delp, Stanford University

Computational models provide a framework for exploring the biomechanics and neural control of movement. In recent years, simulations of human and animal movement have become widely used to explore a range of basic scientific questions, study the mechanisms of various diseases, and assist in the design of medical devices. This tutorial will provide an introduction to musculoskeletal modeling and the application of simulations in the study of movement. Specifically, the tutorial will:

- motivate the use of simulations in studies of human and animal movement,
- review the components of a simulation, including models of muscle-tendon mechanics, musculoskeletal geometry, skeletal dynamics, and neural control,
- provide examples of simulations that have provided insight into important scientific questions and clinical problems,
- discuss some of the limitations of current simulations and suggest future research directions.

Wednesday August 22, 2007 3:00 – 5:00 PM

Tutorial 2: Molecular Biology in Biomechanics

Clark Center Auditorium

Faculty: Rick Lieber, University of California at San Diego

The scientific community has experienced a virtual explosion in applications of molecular biological methods to the fields of medicine, biotechnology, computing and engineering. All of the highest scientific impact papers from 1994-to date used molecular biology to understand transduction of information by cells. These papers could justifiably be considered within the purview of biomechanics. In this tutorial, the basic tenets of molecular biology will be presented including basic cell structure and the flow of information from DNA to RNA to proteins. The most common methods used to study cells and tissues will be reviewed including gene cloning, sequencing, blotting methods and the use of reverse transcription (RT) and the polymerase chain reaction (PCR). Finally, application of these methods will be illustrated using examples of vascular, muscle and ligament cell response to mechanical signals provided by applications of exercise, strain fields and temperature. The main point of this presentation is to demonstrate that molecular biological methods provide powerful tools for studying tissue response, but the careful mechanical characterization of cells, receptors and even isolated proteins remain within the area of expertise we know as biomechanics. This is a field on which we all should have great impact.

Thursday August 23, 2007 8:30 – 9:30 AM

Plenary Session: Singing, breathing and wing waving

Biomechanics of vocal behavior in birds

Memorial Auditorium

Franz Goller: University of Utah

In birds as in humans, sound production involves coordinated activity of two main motor systems, vocal muscles and respiratory muscles. The vocal organ of songbirds, the syrinx, contains two independent sound generators, each controlled by six muscles. Although the major functional roles of these syringeal muscles are documented, the biomechanics of the vocal organ are not well understood. As an example, I will discuss the evidence for direct muscular control of sound frequency and gating of airflow. Singing also involves drastic changes to breathing patterns, including rapid switching between expiration and inspiration. I will discuss the avian respiratory system and its contributions to song production, including fine control of the driving pressure for phonation. In addition, some visual displays affect respiratory mechanics and their simultaneous performance with song must require complex coordination of these multi-modal displays.

Friday August 24, 2007 8:30 – 9:30 AM

Plenary Session: Single Molecule Measurements of Motor Proteins, In vitro and In vivo

Memorial Auditorium

Paul Selvin: University of Illinois

The standard diffraction limit of light is about 250 nm, meaning that you cannot "resolve" objects closer than this distance. Despite this, we have come up with a method to measure 1.5 nm in 1-500 msec, using a technique we call Fluorescence Imaging with One Nanometer Accuracy (FIONA). We have chosen to study molecular motors, which are involved in moving things around within the cell, both in purified systems, and inside living cells. There has been a question as to whether molecular motors move things in an "inchworm" fashion, or in a "hand-over-hand" fashion (i.e. by "walking".) We have definitively determined that myosin, and kinesin, two important motors, walk in a "hand-over-hand" manner in purified systems. In living cells (that is, in Drosophila, or fruit fly cells), we have seen cargos being moved by individual "conventional" kinesin and dynein. We find that both kinesin and dynein move cargo 8 nm per ATP. Amazingly, these two molecular motors do not engage in a tug-of-war, but appear to be cooperative, taking terms hauling the cargo.

Saturday August 25, 2007 8:30 – 9:30 AM
Plenary Session: Borelli Award Lecture
Lessons in skeletal muscle design and plasticity
Memorial Auditorium
Richard Lieber: University of California at San Diego

Skeletal muscles represent a classic biological example of a structure-function relationship. As such, muscle mechanical and muscle physiological studies over the past 100 years have exploited tools that permit comparison between structure and function. In this lecture, I will review some of our findings based on "fancy" as well as "simple" tools. The key concept to be conveyed is that science progresses by asking great questions and using whatever tool is appropriate to answer that question. If the tool does not exist, make it! If it does, use it! I would argue that the converse approach (having a tool and looking for a question) is not as fruitful. Biomechanists are uniquely positioned in the scientific community to have high impact by asking the right questions and applying the right tools.

Saturday August 25, 2007 1:45 – 1:50 PM
Plenary Session:
Announcement of Awards:
Microstrain Award
Journal of Biomechanics Award
Clinical Biomechanics Award
Memorial Auditorium

Saturday August 25, 2007 1:50 – 2:05 PM
Plenary Session: Pre-Doctoral Young Scientist Award
Biofidelity requirements for the focus headform for the prediction of eye injuries
Memorial Auditorium
Eric Kennedy: Virginia Tech-Wake Forest University

In recent military action the rate of eye injuries has dramatically increased compared to historical trends. In order to assess the capability of protective equipment in preventing these injuries, a new advanced headform has been developed that can predict eye injury from impact events. Biofidelic response requirements for the synthetic eye and orbit were defined based on experimental impact tests on post-mortem human eyes, for both force-deflection response as well as eye injury criteria. The Facial and Ocular CountermeasUre Safety (FOCUS) headform will be used to reduce both eye and facial injuries for military troops, as well as sports participants and victims of motor vehicle accidents.

Saturday August 25, 2007 2:05– 2:20 PM
Plenary Session: Post-Doctoral Young Scientist Award
The effect of collagen fibres on permeability of articular cartilage
Memorial Auditorium
Salvatore Federico: University of Calgary

The macroscopic, physico-mechanical properties of soft tissue depend on the tissue microstructure. For articular cartilage, several microstructural models have been proposed to account for the effect of collagen fibres on the elastic properties. In contrast, collagen fibres have been neglected in any considerations regarding permeability, as permeability has been considered to be dependent exclusively on the proteoglycan part of the extra-cellular matrix. However, early experimental results (Maroudas and Bullough, 1968, *Nature* 219) suggest that the depth-dependence of the permeability cannot be explained in terms of proteoglycans alone, and that collagen fibres may significantly affect cartilage permeability.

In this work, we show that the collagen fibril network introduces local anisotropies in articular cartilage. In particular, permeability is shown to be lower orthogonal compared to longitudinal to the fibre. At the global level, the anisotropy of permeability depends on the directional distribution of the fibres.

We used this result to explain why cartilage axial permeability is lower in the superficial zone compared to the middle and deep zones, where the fibres are orthogonal to the cartilage axial direction (i.e., parallel to the articular surface) These results are in good agreement with the experimental findings of Maroudas and Bullough (1968) which could not be explained with previous theoretical models. All results specifically found here for articular cartilage can be used for any fibre reinforced soft tissue.

Saturday August 25, 2007 2:20 – 3:20 PM
Plenary Session: James Hay Lecture Memorial Auditorium
Paradigm Shifts for Impact Forces and Foot Control
Benno M. Nigg: University of Calgary

The conventional paradigms used for running shoes (cushioning and foot control) are currently challenged since impact force peaks during heel-toe running are not different for soft or hard materials, subjects that are or are not exposed to impact activities have the same frequency of short or long term injuries, bone showed bio-positive effects as a result to impact loading, and foot pronation can not be used as a predictor for injuries. Thus new paradigms are proposed, the paradigm for muscle tuning (impact forces produce soft tissue vibrations, which are damp-ened through muscle activity) and the paradigm for instability (unstable shoes are effective in training the small muscles and improving general stability).

SCIENTIFIC SESSIONS: Podium

Author lists are in alphabetical order

Thursday, August 23, 2007 9:45 - 11:00 AM

Podium 1: Motor Control I
Memorial Auditorium

Chair: Eric Perreault

9:45 **Goal equivalent control of variability in human walking**
Joseph Cusumano, Jonathan Dingwell, Michelle Garel
Corresponding Author: Jonathan Dingwell
University of Texas

10:00 **Low dimensional motor control and muscle synergies**
Max Berniker, Emilio Bizzi, Matthew Tresch
Corresponding Author: Max Berniker
Northwestern University

10:15 **The transition between muscle coordination patterns is context dependent**
Sherry L. Backus, Kevin Keenan, Robert V. McNamara III, Flor Alicia Medina, Stanley Song, Carolyn Price , Francisco Valero-Cuevas Madhu sudhan Venkadesan,
Corresponding Author: Flor Medina
Cornell University & The University of Southern California

10:30 **Can electromyography asymmetries during gait be explained by limb dominance?**
Matthew Seeley, Robert Shapiro, Brian Umberger
Corresponding Author: Matthew Seeley
Brigham Young University

10:45 **Swing phase interruption in a slip: active or passive response?**
Rakie Cham
Corresponding Author: Rakie Cham
University of Pittsburgh

Thursday, August 23, 2007 9:45 - 11:00 AM

Podium 2: Methods I
Annenberg Auditorium

Chair: Steve Piazza

9:45 **Posturographic analysis is possible without ground reaction forces measurement through markerless motion capture**
Thomas Andriacchi, Stefano Corazza
Corresponding Author: Stefano Corazza
Stanford University

10:00 **Procrustes analysis applied to relative motion plots of locomotor patterns in sprint**
Leslie Decker, Francoise Natta, Sabine Renous
Corresponding Author: Leslie Decker
University of Nebraska-Omaha

10:15 **Estimation of hip-muscle geometry using automated, non-rigid atlas-based registration of MR images**
Ilse Jonkers, Dirk Loeckx, Lennart Scheys, Arthur Spaepen, Paul Suetens and Anja Van Campenhout,
Corresponding Author: Lennart Scheys
K.U. Leuven

10:30 **Characterizing hamstrings muscle dynamics during knee flexion-extension using real-time MRI**
Silvia Blemker, Andy Derbyshire, Nicholas Evoy, Niccolo Fiorentino, Michael Guttman, Jonathan Lin, Dimitru Mazilu, Elliot McVeigh
Corresponding Author: Niccolo Fiorentino
University of Virginia

10:45 **A new method for quantifying foot bone-to-bone positions**
Michael J. Fassbind, David R. Haynor, Yangqiu "Patrick" Hu, William R. Ledoux, Eric S. Rohr, Bruce J. Sangeorzan
Corresponding Author: William Ledoux
VA Puget Sound

Thursday, August 23, 2007 9:45 - 11:00 AM

Podium 3: Bone I
Cubberley Auditorium

Chair: Glen Niebur

9:45 **The enhanced daily load stimulus (EDLS): Accounting for saturation, recovery and standing**
Peter Cavanagh, Kerim Genc, Brad Humphreys, Gail Perusek
Corresponding Author: Kerim Genc
Case Western Reserve University

10:00 **A computational approach to bone remodeling postoperative to facet fusion**
Dennis Abernathie, Ferris Pfeiffer, Douglas Smith
Corresponding Author: Ferris Pfeiffer
University of Missouri

10:15 **Episodic subluxation increases third body ingress and embedment in the THA bearing surface**
Anneliese D Heiner, Hannah J Lundberg, Thomas E Baer, Douglas R Pedersen, John J Callaghan, Thomas D Brown
Corresponding Author: Anneliese Heiner
University of Iowa

10:30 **A new method for studying the anabolic effects of vibrational loading of bone: constrained tibial vibration in mice**
Philip Bayly, Blaine Christiansen, Matthew Silva
Corresponding Author: Blaine Christiansen
Washington University in St. Louis

10:45 **Measurements of in vivo patellofemoral joint kinematics with real-time MRI**
Gary Beaupre, Thor Besier, Christine Draper, Garry Gold, Juan Santos, and Scott Delp
Corresponding Author: Christine Draper
Stanford University

Thursday, August 23, 2007 11:15 AM - 12:30 PM

Podium 4: Aging I
Memorial Auditorium

Chair: James Ashton-Miller

11:15 ***Journal of Biomechanics Award Finalist Effects of lateral stabilization and arm swing on metabolic cost of walking in young and elderly adults**
Claire Farley, Leslie Fehlman, Justus Ortega
Corresponding Author: Justus Ortega
University of Colorado

11:30 **Human cervical spine mechanics across the maturation spectrum**
Randal Ching, David Linders, David Nuckley
Corresponding Author: David Nuckley
University of Washington

11:45 **Load-modifying footwear intervention lowers knee adduction moment, reduces pain, and improves function in subjects with medial compartment knee osteoarthritis**
Thomas Andriacchi, Jennifer Erhart, Nicholas Giori
Corresponding Author: Jennifer Erhart
Stanford University

12 noon **Eccentric but not concentric muscle work is retained with age in level walking**
Paul DeVita, Patrick Rider, Allison Gruber, Ken Steinweg, Mandana Fisher, Allison Mazzenga, Stanislaw Solnik and Tibor Hortobagyi
Corresponding Author: Paul DeVita
East Carolina University

12:15 **Effect of age on shear modulus of skeletal muscle**
Kai-Nan An, Zachary Domire, Matthew McCullough
Corresponding Author: Zachary Domire
Mayo Clinic College of Medicine

Thursday, August 23, 2007 11:15 AM - 12:30 PM

Podium 5: Computational Biomechanics I
Annenberg Auditorium

Chair: Richard Hughes

11:15 **Experimental evaluation of model-based lower extremity induced accelerations**
Yasin Dhaher, Betsy Hunter, Darryl Thelen
Corresponding Author: Betsy Hunter
Northwestern University

11:30 **3D Finite element simulation of bone remodeling under the tibial component of an Oxford knee replacement**
Harinderjit Gill, Hans Gray, Amy Zavatsky
Corresponding Author: Amy Zavatsky
University of Oxford

11:45 **Predicting outcomes of treatment for stiff-knee gait using supervised learning**
Scott Delp, Melanie Fox, Jeffrey Reinbolt, Michael Schwartz
Corresponding Author: Jeffrey Reinbolt
Stanford University

12 noon **Influence of quadriceps muscle force distributions on cartilage stresses at the patellofemoral joint during running**
Gary Beaupre, Thor Besier, Scott Delp, Garry Gold
Corresponding Author: Thor Besier
Stanford University

12:15 **Stresses on movable core and loads on facets are higher by implanting a cervical artificial disc prosthesis as compared to bone grafting fusion technique - a finite element model study**
Howard An, Gunnar Andersson, Mozammil Hussain, Raghu Natarajan
Corresponding Author: Mozammil Hussain
Rush University Medical Center

Thursday, August 23, 2007 11:15 AM - 12:30 PM

Podium 6: Ergonomics and Occupational Biomechanics I
Cubberley Auditorium

Chair: Devin Jindrich

11:15 **Movement height affects kinematic variability during fatigue**
Jonathan Dingwell, Deanna Gates
Corresponding Author: Deanna Gates
University of Texas at Austin

11:30 **Postural control strategies during prolonged standing: is there a relationship with low back discomfort?**
Jack Callaghan, Diane Gregory, Erika Nelson-Wong, David Winter
Corresponding Author: Erika Nelson-Wong
University of Waterloo

11:45 **The effect of friction and arm posture on max pull / push force**
Thomas Armstrong, Kathryn Dannecker, Na Jin Seo
Corresponding Author: Na Jin Seo
University of Michigan

12 noon **Algorithm for identification of running, walking, and standing activity in foot force data**
Peter Cavanagh, Kerim Genc, Brad Humphreys, Gail Perusek
Corresponding Author: Brad Humphreys
ZIN Technologies

12:15 **Birth of the super pen: an innovative approach to studying handwriting kinetics**
Alexander Hooke, Jae Kun Shim
Corresponding Author: Alexander Hooke
University of Maryland

Thursday, August 23, 2007 1:45 - 3:00 PM

Podium 7: Walking
Memorial Auditorium
Chair: Clay Anderson

1:45 ***Clinical Biomechanics Award Finalist**
The anterior-posterior thickness variation of femoral cartilage in the tibiofemoral joint is influenced by the knee flexion angles during walking
Thomas Andriacchi, Seungbum Koo, Jonathan Rylander
Corresponding Author: Seungbum Koo
Stanford University

2:00 **Walking in simulated hyper-gravity**
Stephen Cain, Daniel Ferris
Corresponding Author: Stephen Cain
University of Michigan

2:15 **Obstacle crossing behavior is affected by Parkinson's disease**
Thomas Buckley, Chris Hass, Chris Pitsikoulis
Corresponding Author: Chris Hass
University of Florida

2:30 **Effect of felt and recognized emotions on gait kinematics**
Elizabeth Crane, Barbara Fredrickson, Melissa Gross
Corresponding Author: Melissa Gross
University of Michigan

2:45 **Detecting asymmetries in braced and unbraced limbs**
Elizabeth T. Hsiao-Wecksler, John D. Polk, Karl Rosengren, K. Alex Shorter
Corresponding Author: Elizabeth T. Hsiao-Wecksler
University of Illinois

Thursday, August 23, 2007 1:45 - 3:00 PM

Podium 8: Injury
Annenberg Auditorium
Chair: Jack Dennerlein

1:45 **Anterior cruciate rupture due to excessive internal torque of the human tibia**
Roger Haut, Eric Meyer
Corresponding Author: Roger Haut
Michigan State University

2:00 **Biomechanics of impact loading of goat skull (capra hircus) using CT image based finite element modeling**
Andrew Biewener, Ashkan Vaziri, Edwin Yoo
Corresponding Author: Edwin Yoo
Harvard University

2:15 **A three-dimensional nonlinear kinematic finite element model of the human cervical spine under dynamic inertial loading**
Ronald Anderson, Gerald Harris, Richard Hart, Brad Probst, Bradley Probst
Corresponding Author: Bradley Probst
Tulane University

2:45 **Female necks are not uniformly scaled versions of male necks**
Jonathan Danaraj, Gunter Siegmund, Anita Vasavada
Corresponding Author: Anita Vasavada
Washington State University

Thursday, August 23, 2007 1:45 - 3:00 PM

Podium 9: Sports I
Cubberley Auditorium
Chair: Mont Hubbard

1:45 **The effect of compression pants on postural steadiness before and after tiring exercise**
Gary Heise, Katharine Mack, Minoru Shinohara
Corresponding Author: Gary Heise
University of Northern Colorado

2:00 **Changes in spring-mass characteristics during 400m sprint**
Kouki Gomi, Hiroaki Hobara, Kazuyuki Kanosue, Tetsuro Muraoka
Corresponding Author: Hiroaki Hobara
Waseda University

2:15 **Trunk muscle activation and low-back loading during the performance of standard and suspended push-up exercises**
Tyson A.C. Beach, Jack P. Callaghan, Samuel J. Howarth
Corresponding Author: Tyson A.C. Beach
University of Waterloo

2:30 **Interactive effects of running speed and weight support on metabolic cost and ground reaction forces**
Alena Grabowski, Rodger Kram
Corresponding Author: Alena Grabowski
University of Colorado, Boulder

2:45 **Determination of heading frequency in youth soccer**
Cynthia Bir, Erin Hanlon
Corresponding Author: Cynthia Bir
Wayne State University

Thursday, August 23, 2007 3:15 - 4:30 PM

Podium 10: Running
Memorial Auditorium

Chair: Rick Neptune

3:15 **Integrating the mechanical and metabolic energetics of the swing phase of walking and running**
Richard Marsh, Jonas Rubenson
Corresponding Author: Jonas Rubenson
Northeastern University

3:30 **Walking, skipping, and running produced from a single bipedal model**
Arthur Kuo, Shawn O'Connor
Corresponding Author: Shawn O'Connor
University of Michigan

3:45 **Running stability is enhanced by a proximo-distal gradient in joint mechanics**
Biewener Andrew, Monica Daley
Corresponding Author: Biewener Andrew
Harvard University

4:00 **Changing the demand on specific muscle groups affects the walk-run transition speed**
Jamie Bartlett, Rodger Kram
Corresponding Author: Jamie Bartlett
University of Colorado

4:15 **Criteria for dynamic similarity in bouncing gaits**
Sharon Bullimore, Jeremy Burn, Max Donelan
Corresponding Author: Sharon Bullimore
University of Calgary

Thursday, August 23, 2007 3:15 - 4:30 PM

Podium 11: Upper Extremity
Annenberg Auditorium

Chair: Wendy Murray

3:15 **Upper limb moment-generating capacity in middle aged adults**
Garry Gold, Katherine Holzbaur, Wendy Murray
Corresponding Author: Katherine Holzbaur
Stanford University/VA Palo Alto HCS

3:30 **Effect wrist and forearm muscle architecture on wrist radial-ulnar deviation and forearm pronation supination moment**
Roger Gonzalez, John Ramsay
Corresponding Author: Roger Gonzalez
LeTourneau University

3:45 **Glenohumeral joint reaction forces following latissimus tendon transfer**
Marcus Pandy, Kevin Shelburne, Michael Torry, Takashi Yanagawa
Corresponding Author: Takashi Yanagawa
Steadman Hawkins Research Foundation

4:00 **A three-dimensional model of the supraspinatus muscle**
Silvia Blemker, Scott Delp, Joshua Webb
Corresponding Author: Joshua Webb
Stanford University

4:15 **Moment arm measurement to validate a closed-loop feedback-controlled elbow joint simulator**
Laurel Kuxhaus, Pat Schimoler, Angela M. Flamm, Jeffrey S Vipperman, Mark E. Baratz, and Mark Carl Miller
Corresponding Author: Laurel Kuxhaus
University of Pittsburgh, Allegheny General Hospital

Thursday, August 23, 2007 3:15 - 4:30 PM

Podium 12: Tendon and Ligament
Cubberley Auditorium

Chair: Zachary Domire

3:15 **A technique for determination of transverse material properties of human flexor digitorum tendons**
Thomas D. Brown, Cheolwoong Ko, M. James Rudert
Corresponding Author: Thomas D. Brown
University of Iowa

3:30 **Relationship between knee flexion moment and early cartilage changes in the ACL reconstructed knee**
Sean Scanlan, Katerina Blazek, Joshua Schmidt, Seungbum Koo, Ajit Chaudhari, Jason Dragoo, and Tom Andriacchi
Corresponding Author: Sean Scanlan
Stanford University

3:45 **The influence of patellar ligament insertion angle on quadriceps usage during walking in ACL reconstructed subjects**
Thomas Andriacchi, Ajit Chaudhari, Chris Dyrby, Choongsoo Shin
Corresponding Author: Choongsoo Shin
Stanford University

4:00 **An algorithm for automated tracking of tendon excursion from ultrasound images**
Sabrina Lee, Gregory Lewis, Stephen Piazza
Corresponding Author: Stephen Piazza
The Pennsylvania State University

4:15 **Cruciate ligament force during the wall squat and one-leg squat**
Rafael F. Escamilla, Naiquan Zheng, Alan Hreljac, Rodney Imamura, Toran D. MacLeod, William B. Edwards, Glenn S. Fleisig, Kevin E. Wilk
Corresponding Author: Rafael Escamilla
California State University, Sacramento

Friday, August 24, 2007 **9:45 - 11:00 AM**

Podium 13: Locomotion Energetics
Memorial Auditorium

Chair: Young-Hui Chang

9:45 **Comparison of two methods of determining relative effort during sit-to-stand**
Dennis Anderson, Kathleen Bieryla, Michael Madigan
Corresponding Author: Kathleen Bieryla
Virginia Tech

10:00 **Independent effects of body weight and mass on the metabolic cost of running**
Alena Grabowski, Rodger Kram, Lennart Teunissen
Corresponding Author: Alena Grabowski
University of Colorado, Boulder

10:15 **Disintegrating the metabolic cost of human running: weight support, forward propulsion, and leg swing**
Rodger Kram, Erin Warddrip
Corresponding Author: Rodger Kram
University of Colorado - Boulder

10:30 **Mechanics and energetics of level walking with powered ankle exoskeletons**
Daniel Ferris, Gregory Sawicki
Corresponding Author: Gregory Sawicki
University of Michigan-Ann Arbor

10:45 **Center of mass velocity redirection predicts COM work in walking**
Peter Gabriel Adamczyk, Arthur D. Kuo
Corresponding Author: Peter Gabriel Adamczyk
University of Michigan

Friday, August 24, 2007 **9:45 - 11:00 AM**

Podium 14: Hand
Annenberg Auditorium

Chair: Zong-Ming Li

9:45 **Comparison of finger force enslaving and sharing between mvf and oscillatory finger force production tasks**
Qi Li, Marcio A. Oliveira, Jae Kun Shim
Corresponding Author: Qi Li
University of Maryland

10:00 **A data-driven Markov Chain Monte Carlo Metropolis-Hastings algorithm for a model of the human thumb**
Carlos Bustamante, Veronica Santos, Francisco Valero-Cuevas
Corresponding Author: Veronica Santos
Cornell University & The University of Southern California

10:15 **Modeling of the muscle/tendon excursions in an index finger using the commercial software AnyBody**
Kai-Nan An, Robert G Cutlip, Ren G Dong, John Z Wu
Corresponding Author: John Z Wu
National Institute for Occupational Safety and Health

10:30 **Variation in force and moment stabilizing synergies with different finger combinations: an uncontrolled manifold analysis**
Sohit Karol, Jae Kun Shim
Corresponding Author: Sohit Karol
University of Maryland, College Park

10:45 **Blind inference of tendon networks through minimal testing**
Hod Lipson, Anupam Saxena, Francisco Valero-Cuevas
Corresponding Author: Anupam Saxena
Cornell University & The University of Southern California

Friday, August 24, 2007 **9:45 - 11:00 AM**

Podium 15: Knee
Cubberley Auditorium

Chair: Heidi-Lynn Ploeg

9:45 **The effect of collagen fibres on permeability of articular cartilage**
Salvatore Federico, Walter Herzog
Corresponding Author: Salvatore Federico
The University of Calgary

10:00 **Changes in patellofemoral contact pressure due to imbalance of the knee extensors**
Doug Bourne, Walter Herzog, Azim Jihna, Andrew Sawatsky
Corresponding Author: Andrew Sawatsky
University of Calgary

10:15 **Regional variations in the depth-dependent strain distribution in the tibial plateau**
Thomas Andriacchi, Scott Bevill, Paul Briant, Gabriel Sanchez
Corresponding Author: Gabriel Sanchez
Stanford University

10:30 **Decreased knee flexion during landing increases frontal plane loading of the knee**
Christine Pollard, Christopher Powers, Susan Sigward
Corresponding Author: Christine Pollard
University of Southern California

10:45 **3d joint contact forces at the hip, knee, and ankle during running at different stride lengths**
Timothy Derrick, W. Brent Edwards, Joshua Thomas
Corresponding Author: W. Brent Edwards
Iowa State University

Friday, August 24, 2007 11:15 AM - 12:30 PM

Podium 16: Comparative Biomechanics
Memorial Auditorium

Chair: Andrew Biewener

11:15 **A biomechanical study of vertebral allometry in primates**
Andrew L. Schifle, Leah C. Anderson, David A. Loomis, Charles Kunos, Bruce Latimer, Christopher J. Hernandez
Corresponding Author: Andrew Schifle
Case Western Reserve University

11:30 **Effective fields in control muscles: efficacy of control depends on biomechanical context in an insect**
Robert Full, Chris Mullens, Andrew Spence, Simon Sponberg
Corresponding Author: Simon Sponberg
University of California, Berkeley

11:45 **A hexapedal jointed-leg model for insect locomotion in the horizontal plane**
Philip Holmes, Raghavendra Kukillaya
Corresponding Author: Raghavendra Kukillaya
Princeton University

12 noon **Minimal muscle atrophy during hibernation in captive brown bears**
John Hershey, David Lin, O. Lynne Nelson, Charles Robbins
Corresponding Author: David Lin
Washington State University

12:15 **Functional heterogeneity within and between hind limb muscles during running in guinea fowl**
Andrew Biewener, Timothy Higham
Corresponding Author: Timothy Higham
Harvard University

Friday, August 24, 2007 11:15 AM - 12:30 PM

Podium 17: Muscle Mechanics
Annenberg Auditorium

Chair: Silvia Blemker **Microstrain Award Winner*

11:15 **In vivo sarcomere length measurement by minimally invasive microendoscopy**
Robert P. J. Barretto, Scott L. Delp, Michael E. Llewellyn, Mark J. Schnitzer
Corresponding Author: Michael E. Llewellyn
Stanford University

11:30 **Force transmission from soleus muscle in the cat; is m. Soleus an independent actuator?**
Huub Maas, Thomas G. Sandercock
Corresponding Author: Huub Maas
Northwestern University

11:45 **Functional implications of optimal muscle fiber lengths of the ankle plantarflexors**
Edith Arnold, Scott Delp, Richard Lieber, Samuel Ward
Corresponding Author: Edith Arnold
Stanford University

12 noon ***Journal of Biomechanics Award Finalist**
Active and passive force enhancement in rabbit psoas myofibrils
Walter Herzog, Venus Joumaa, Tim Leonard
Corresponding Author: Venus Joumaa
University of Calgary

12:15 **Strains in the biceps brachii during dynamic el bow flexion show concentric, eccentric and isometric behavior simultaneously**
Brian Knarr, John Novotny, Hehe Zhou
Corresponding Author: John Novotny
University of Delaware

Friday, August 24, 2007 **11:15 AM - 12:30 PM**

Podium 18: Rehabilitation I
Cubberley Auditorium

Chair: Yasin Dhaher

11:15 **Upper extremity kinematics of crutch-assisted gait in children with myelomeningocele**
Gerald Harris, Brooke Slavens, Peter Sturm
Corresponding Author: Brooke Slavens
Marquette University

11:30 **Correlation between knee adduction moment and the ratio of medial-to-lateral compartment compression in subjects with knee osteoarthritis undergoing high-tibial osteotomy.**
Timothy Bhatnagar, Trevor Birmingham, Thomas Jenkyn
Corresponding Author: Thomas Jenkyn
University of Western Ontario

11:45 **Mechanical vibrations reduce the intervertebral disc swelling and muscle atrophy from bed rest**
Nilsson Holguin, Jesse Muir, Harlan J. Evans, Yi-Xian Qin, Clinton Rubin, Mark Wagshul, and Stefan Judex
Corresponding Author: Nilsson Holguin
Stony Brook University

12 noon **Asymmetric stability margin of postural response to perturbation in unilateral transtibial amputees**
Lena Ting, Yi-Ying Tsai
Corresponding Author: Lena Ting
Emory University and Georgia Institute of Technology

12:15 **Effect of visual uncertainty on adaptation to ankle perturbations**
Timothy N. Judkins, Lewis A. Wheaton, J.C. Mizelle, Hermano I. Krebs, Richard F. Macko, and Larry W. Forrester
Corresponding Author: Timothy Judkins
University of Maryland School of Medicine

Friday, August 24, 2007 **1:45 - 3:00 PM**

Podium 19: Neurorehabilitation
Memorial Auditorium

Chair: David Reinkensmeyer

1:45 **Spinal cord injured subjects use ankle-foot load feedback to modulate hip torque during locomotion**
Keith Gordon, Brian Schmit, Ming Wu
Corresponding Author: Keith Gordon
Rehabilitation Institute of Chicago

2:00 **Motor adaptation during dorsiflexion-assisted walking with a powered orthosis**
Daniel Ferris, Pei-Chun Kao
Corresponding Author: Pei-Chun Kao
University of Michigan

2:15 **Metabolic costs and walking symmetry of trans-tibial amputees are influenced by prosthetic mass distribution**
Philip Martin, Jeremy Smith
Corresponding Author: Jeremy Smith
Ball State University

2:30 **Regulating shoulder net joint moments during wheelchair propulsion**
Jill McNitt-Gray, Shashank Raina, Philip Requejo
Corresponding Author: Shashank Raina
University of Southern California

2:45 **Gait adaptability in people with unilateral trans-tibial amputations in response to variable walking speed and body weight support**
Jason Johanning, Iraklis Pipinos, Nicholas Stergiou, A. Joseph Threlkeld, Clinton Wutzke
Corresponding Author: A. Joseph Threlkeld
Creighton University

Friday, August 24, 2007 **1:45 - 3:00 PM**

Podium 20: Motor units
Annenberg Auditorium

Chair: Rick Lieber

1:45 **Detecting the transient recruitment of motor units in the surface electromyogram during a sustained contraction**
Roger Enoka, Jane Litsey, Zachary Riley, Mary Terry, Alberto-Mendez Villaneuva
Corresponding Author: Zachary Riley
University of Colorado, Boulder

2:00 **Improving models of motor unit function is best done by refining their neural mechanisms**
Kevin Keenan, Francisco Valero-Cuevas
Corresponding Author: Kevin Keenan
Cornell University & The University of Southern California

2:15 **DTI-based fiber tracking reveals a multifaceted alteration of pennation angle in tibialis anterior muscle upon muscle lengthening**
Bruce Damon, Zhaohua Ding, Anneriet Heemskerk, Tuhin Sinha
Corresponding Author: Anneriet Heemskerk
Vanderbilt University

2:30 **Maximising the resolution of EMG characteristics from dynamic contractions by combining a muscle model and wavelet analysis**
Steph Forrester, Matt Pain
Corresponding Author: Matt Pain
Loughborough University

2:45 **The effect of temperature on residual force enhancement in single skeletal muscle fibers**
Walter Herzog, Eun-Jeong Lee
Corresponding Author: Eun-Jeong Lee
University of Calgary

Friday, August 24, 2007 1:45 - 3:00 PM

Podium 21: Ergonomics and Occupational Biomechanics II
Cubberley Auditorium

Chair: Joseph Crisco

1:45 **Modeling of the dynamic muscle force in an index finger during tapping**
Kai-Nan An, Robert G Cutlip, Ren G Dong, Kristine Krajnak, John Z Wu
Corresponding Author: John Z Wu
National Institute for Occupational Safety and Health

2:00 **Hammering and dart throwing are kinematically different**
Joseph Crisco, Patrick Curran, Douglas Moore, Michael Rainbow
Corresponding Author: Joseph Crisco
Brown University

2:15 **Sagittal lumbar intervertebral angles in seated postures using fluoroscopy**
Jack Callaghan, Nadine Dunk, Tom Jenkyn, Angela Kedgley
Corresponding Author: Nadine Dunk
University of Waterloo

2:30 **Predicting slow changes in muscle fatigue from kinematics**
David Chelidze, Jonathan Dingwell, David Segala, Miao Song
Corresponding Author: Jonathan Dingwell
University of Texas

2:45 **Modeling 3D knee torque surfaces for males and females**
Laura Frey Law, Andrea Laake
Corresponding Author: Andrea Laake
University of Iowa

Friday, August 24, 2007 3:15 - 4:30 PM

Podium 22: Neuromechanics
Memorial Auditorium

Chair: Jonathan Dingwell

3:15 ***Clinical Biomechanics Award Finalist**
Evidence of gender specific motor templates to resist a valgus perturbation at the knee
Martha Cammarata, Tobey DeMott, Yasin Dhaher
Corresponding Author: Martha Cammarata
Northwestern University

3:30 **Visual perturbation of walking balance**
Arthur Kuo, Shawn O'Connor
Corresponding Author: Shawn O'Connor
University of Michigan

3:45 **Effect of neuromuscular resistance training on multi-finger synergy**
Jeffrey Hsu, Sohit Karol, Jae Kun Shim
Corresponding Author: Jeffrey Hsu
University of Maryland

4:00 **Effects of repetitive drop jumps on lower extremity landing mechanics**
Eric Dugan, Holmes Finch, Jeremy Smith, Joshua Weinhandl
Corresponding Author: Joshua Weinhandl
Ball State University

4:15 **Torque coupling post stroke: implication for gait**
Yasin Dhaher, Theresa Hayes
Corresponding Author: Theresa Hayes
Northwestern University

Friday, August 24, 2007 3:15 - 4:30 PM

Podium 23: Muscle
Annenberg Auditorium

Chair: Kevin Keenan

3:15 **Is a passive element responsible for the enhancement of isometric muscle force following active stretch?**
Sharon Bullimore, Walter Herzog
Corresponding Author: Sharon Bullimore
University of Calgary

3:30 **Crouched gait postures reduce the capacity of uni-articular muscles to extend the hip and knee joints**
Scott Delp, Jennifer Hicks, Michael Schwartz
Corresponding Author: Jennifer Hicks
Stanford University

3:45 **Growth-dependent enhancement of mouse neonatal muscle morphology and contractile function**
David Gokhin, Richard Lieber
Corresponding Author: Richard Lieber
University of California, San Diego

4:00 **Increased stress production and response to injury in desmin knockout muscles rescued by plasmid transfection**
Shannon Bremner, Richard Lieber, Michelle Palmisano
Corresponding Author: Richard Lieber
University of California, San Diego

4:15 **EMG characteristics of dynamic knee extensions determined by combined muscle modelling and wavelet analysis**
Steph Forrester, Matt Pain
Corresponding Author: Matt Pain
Loughborough University

Friday, August 24, 2007 3:15 - 4:30 PM

Podium 24: Rehabilitation II
Cubberley Auditorium

Chair: Matt Tresch

3:15 **Effects of UHMWPE surface roughness and lubrication on the frictional properties of total knee replacements**
Ryan Landon, Ryan Lucking, Stephen Piazza
Corresponding Author: Stephen Piazza
The Pennsylvania State University

3:30 **Point markers versus cluster triads: multi-segment foot model performance is insensitive to the architecture of the reflective markers used in optical motion analysis**
Kiersten Anas, Colin Dombroski, Thomas Jenkyn, Shawn Robbins
Corresponding Author: Thomas Jenkyn
University of Western Ontario

3:45 **Effect of the knee joint contact path on the quadriceps extension moment during gait**
Hannah Lundberg, Valentina Ngai, Andrea Swanson, Markus Wimmer
Corresponding Author: Hannah Lundberg
Rush University Medical Center

4:00 **Variability in secondary motions of the knee following total joint replacement**
Valentina Ngai, Markus Wimmer
Corresponding Author: Valentina Ngai
Rush University Medical Center

4:15 **Gait stability following total hip replacement**
Li-Shan Chou, Dennis Collis, Brian Jewett, Virginia Klausmeier, Vipul Lugade
Corresponding Author: Li-Shan Chou
University of Oregon

Saturday, August 25, 2007 9:45 - 11:00 AM

Podium 25: Aging II
Memorial Auditorium

Chair: Darryl Thelen

9:45 **Biomechanical modeling to identify risk factors in knee OA: model dependence upon source MRI field strength**
Donald Anderson, Thomas Brown, Neil Segal, James Torner
Corresponding Author: Donald Anderson
The University of Iowa

10:00 **Hip joint moments and bone mineral density in healthy older women**
Thomas Andriacchi, Gary Beaupre, Katherine Boyer
Corresponding Author: Katherine Boyer
Stanford University

10:15 **Lateral falls after a slip are affected by medial/lateral slipping foot displacement**
Stephanie Donovan, Mark Grabiner, Karen Troy
Corresponding Author: Mark Grabiner
University of Illinois at Chicago

10:30 **Rapid shoulder flexion after a slip may assist fall avoidance**
Stephanie Donovan, Mark Grabiner, Karen Troy
Corresponding Author: Mark Grabiner
University of Illinois at Chicago

10:45 **Young adults adapt to prevent falls from unpredictable balance disturbances**
Michael Pavol, Lisa Welsh
Corresponding Author: Michael Pavol
Oregon State University

Saturday, August 25, 2007 9:45 - 11:00 AM

Podium 26: Computational Biomechanics II
Annenberg Auditorium

Chair: Veronica Santos

9:45 **Long-duration muscle-actuated simulations of walking at multiple speeds**
Frank (Clay) Anderson, Scott Delp, Eran Guendelman, Jill Higginson, Chand John
Corresponding Author: Chand John
Stanford University

10:00 **OPENSIM: an open-source platform for simulating and analyzing musculoskeletal dynamics**
Frank (Clay) Anderson, Eran Guendelman, Peter Loan, Ayman Habib, Chand John, Allison Arnold, Darryl Thelen, and Scott Delp
Corresponding Author: Frank (Clay) Anderson
Stanford University

10:15 **Biomechanical neck model based on the visible human female**
Richard Lasher, Linda Rico, Anita Vasavada, Liying Zheng
Corresponding Author: Liying Zheng
Washington State University

10:30 **Can a passive dynamic walking robot exhibit a deterministic nonlinear gait?**
Chris Arellano, Timothy Judkins, Max Kurz, Melissa Scott-Pandorf
Corresponding Author: Timothy Judkins
University of Maryland School of Medicine

10:45 **Simulation insights into experimental techniques for estimating walking stability**
Kevin Granata, Anthony Marsh, James Norris
Corresponding Author: James Norris
WFU - VT

Saturday, August 25, 2007 9:45 - 11:00 AM

Podium 27: Sports II
Cubberley Auditorium

Chair: Alison Sheets

9:45 **Design of safe ski jump landing surfaces**
Mont Hubbard
Corresponding Author: Mont Hubbard
University of California, Davis

10:00 **Reduced shoe-surface friction can increase the risk of non-contact ACL injury during cutting movements**
Ariel Dowling, Stefano Corazza, Lars Mundermann, Todd Alamin, Thomas Andriacchi, and Ajit Chaudhari
Corresponding Author: Ariel Dowling
Stanford University

10:15 **Regulation of reaction forces during the impact phase of landings**
Henryk Flashner, Jill McNitt-Gray, Joseph Munaretto
Corresponding Author: Joseph Munaretto
University of Southern California

10:30 **The influence of maturation and lower extremity kinetics on swing limb foot velocity in young females during a soccer kick**
Mark Lyle, Christine Pollard, Christopher Powers, Susan Sigward
Corresponding Author: Mark Lyle
University of Southern California, Los Angeles, CA

10:45 **Roles of leading and trailing arms in baseball bat swing**
Richard Hinrichs, Young-Kwan Kim
Corresponding Author: Young-Kwan Kim
Arizona State University

Saturday, August 25, 2007 11:15 AM - 12:30 PM

Podium 28: Motor Control II
Memorial Auditorium

Chair: Boris Prilutsky

11:15 **Enhanced inter-joint reflex coupling may contribute to impaired coordination in hemiparetic stroke**
Yasin Dhaher, James Finley, Eric Perreault
Corresponding Author: James Finley
Northwestern University

11:30 **Quantifying stretch reflex contributions to multijoint coordination following stroke**
Eric Perreault, Vengateswaran Ravichandran, Randy Trumbower
Corresponding Author: Randy Trumbower
Rehabilitation Institute of Chicago & Northwestern University

11:45 **Movement stability is affected by muscle fatigue**
Jonathan Dingwell, Deanna Gates
Corresponding Author: Deanna Gates
University of Texas at Austin

12 noon **Stability criteria reduce neuromuscular redundancy in postural control**
Nathan E. Bunderson, Thomas J. Burkholder, Lena H. Ting
Corresponding Author: Nathan E. Bunderson
Georgia Institute of Technology

12:15 **Cortical networks for controlling instabilities in dexterous manipulation**
Chad Lau, Kristine Mosier, Francisco J. Valero-Cuevas, Madhusudhan Venkadesan, Yang Wang
Corresponding Author: Madhusudhan Venkadesan
Cornell University, The University of Southern California & Indiana University

Saturday, August 25, 2007 11:15 AM - 12:30 PM

Podium 29: Methods II
Annenberg Auditorium
Chair: Li-Shan Chou

11:15 **Tracking the position of insole pressure sensors during walking and running**
Elizabeth Chumanov, Christian Remy, Darryl Thelen
Corresponding Author: Elizabeth Chumanov
University of Wisconsin - Madison

11:30 **Automatic generation of a subject specific model for accurate markerless motion capture and biomechanical applications**
Thomas Andriacchi, Stefano Corazza, Emiliano Gambaretto, Lars Mündermann
Corresponding Author: Stefano Corazza
Stanford University

11:45 **In vivo knee loading measured by an instrumented total knee replacement during activities of daily living**
Thomas Andriacchi, Cliff Colwell, Darryl D'Lima, Chris Dyrby, Anne Muendermann
Corresponding Author: Chris Dyrby
Stanford University

12 noon **Temporomandibular joint kinematics in osteoarthritic patients pre- and post-surgery: The combination of electromagnetic motion data with patient-specific CT images**
Kai-Nan An, Evre Baltali, Eugene Keller, Matthew Koff, Kristin Zhao
Corresponding Author: Kristin Zhao
Mayo Clinic

12:15 **A novel method for patient specific finite element mesh development of the spine**
Nicole Grosland, Nicole Kallemeyn, Kiran Shivanna
Corresponding Author: Nicole Grosland
The University of Iowa

Saturday, August 25, 2007 11:15 AM - 12:30 PM

Podium 30: Bone II
Cubberley Auditorium
Chair: Katherine Boyer

11:15 **Subject specific geometry reconstruction of knee bones**
Anthony G Au, Darren Palathinkal, Adrian B Liggins, V James Raso, Jason Carey, Robert G Lambert, Alidad Amirfazli
Corresponding Author: Alidad Amirfazli
University of Alberta

11:30 **Compressive properties of trabecular bone in the distal femur**
Travis Burgers, Jim Mason, Glen Niebur, Heidi Ploeg
Corresponding Author: Travis Burgers
University of Wisconsin-Madison

11:45 **Displaced soft tissue volume as a metric of comminuted fracture severity**
Donald Anderson, Thomas Brown, J Lawrence Marsh, Thaddeus Thomas
Corresponding Author: Thaddeus Thomas
University of Iowa

12 noon **Determining site-specific bone loss in mice**
Brandon Ausk, Ted Gross, Philippe Huber, Sundar Srinivasan
Corresponding Author: Brandon Ausk
University of Washington

12:15 **A biomechanical comparison of an all-locked vs. Hybrid screw configuration of proximal tibial plates**
Kristine Csavina, Chris Estes, David Jacofsky, Wade Shrader
Corresponding Author: Kristine Csavina
SHRI-CORE Orthopedic Research Labs

SCIENTIFIC SESSIONS: Poster

Author lists are in alphabetical order

Thursday, August 23, 2007 4:30 - 6:15 PM

Poster Session 1: Skeletal Tissue
Memorial Auditorium

P1-1 **Transverse damage and failure behavior of trabecular bone**
Jaqueline Keilty, Glen Niebur, Constance Slaboch
Corresponding Author: Glen Niebur
University of Notre Dame

P1-2 **A calibration method for stereo fluoroscopic imaging systems**
J. Erik Giphart, Bart Kaptein, Kevin Shelburne, Michael Torry
Corresponding Author: J. Erik Giphart
Steadman-Hawkins Research Foundation, Vail, CO

P1-3 **A finite element analysis of femoral stresses in a simulated falling on the hip condition**
Kevin E. Bennet, Mark E. Bolander, Dan M. Dragomir-Daescu, Sean McEligot, Miranda N. Shaw, Michael J. Burke, and Geraldine K. Bernard
Corresponding Author: Dan M. Dragomir-Daescu
Mayo Clinic Division of Engineering

P1-4 **The effect of loading rate on porcine lumbar spinal segments: an in-vitro biomechanical study**
Kornelia Kulig, Gadi Pelled, John Popovich, Wafa Tawackoli, Judson Welcher, D. Gazit
Corresponding Author: John Popovich
University of Southern California

P1-5 **Stresses in the L2 vertebra under different loading conditions**
Ibrahim Erdem, Eeric Truumees, Marjolein C.H. van der Meulen
Corresponding Author: Marjolein C.H. van der Meulen
Cornell University

P1-6 **Refinements in modeling the mechanical properties of laryngeal soft tissue**
Eric Hunter, Ingo Titze
Corresponding Author: Eric Hunter
National Center for Voice and Speech; Denver Center for the Performing Arts

P1-7 **Non-rigid registration of deformable shape models produces a superior normative femur model**
Weidong Luo, Frances Sheehan, Steven Stanhope
Corresponding Author: Weidong Luo
Catholic University of America

P1-8 **Difference in biomechanical properties between a cervical pedicle screw construct and lateral mass cervical fixation**
Brad Dunlap, Eldin Karaikovic, Hyung-Soon Park, Li-Qun Zhang
Corresponding Author: Li-Qun Zhang
Rehabilitation Institute of Chicago

P1-9 **Effect of facet arthroplasty on the biomechanics of the lumbar spine — a finite element study**
Jorge Ochoa, David Rosler, Sasidhar Vadapalli
Corresponding Author: Sasidhar Vadapalli
Archus Orthopedics Inc.,

P1-10 **Bone surface tracking for standing knee MRI: a validation study**
Peter Barrance, Joaquin Barrios, Irene Davis, Brian Noehren, Michael Pohl
Corresponding Author: Peter Barrance
Kessler Medical Rehabilitation Research and Education Center

P1-11 **Carpal cartilage thickness mapping using micro-CT**
Jane Casey, Joseph Crisco, Douglas Moore
Corresponding Author: Douglas Moore
Department of Orthopaedics, Brown Medical School/RI Hospital

P1-12 **Effects of labrum thickness and modulus on glenohumeral capsule and labrum strains**
Richard Debski, Nick Drury, Ben Ellis, Jeff Weiss
Corresponding Author: Jeff Weiss
University of Utah

P1-13 **Effects of area selection choice on quantifying proximal tibia bone density**
David Hudson, Todd Royer
Corresponding Author: Todd Royer
University of Delaware

P1-14 **Biomechanics of the prodisc artificial disc using finite element analysis**
Yabo Guan, Dennis J. Maiman, Frank A. Pintar, Narayan Yoganandan, Jiangyue Zhang
Corresponding Author: Yabo Guan
Medical College of Wisconsin

P1-15 **Strand-based simulation of tendinous systems**
Dinesh K. Pai, Shinjiro Sueda
Corresponding Author: Shinjiro Sueda
University of British Columbia

P1-16 **Accuracy of radiographic intervertebral kinematics as a determinant of lumbar fusion**
Amir Fayyazi, Bruce Fredrickson, Nathaniel Ordway, Soo-An Park, Mike Sun, Hansen Yuan
Corresponding Author: Soo-An Park
SUNY-Upstate Medical University

P1-17 **A novel approach to design knee implants for wear and stress shielding performance**
Alidad Amirfazli, Anthony Au, Il Yong Kim, Ryan Willing
Corresponding Author: Il Yong Kim
Queen's University

P1-18 **3.5 mm lag screws as compared with 6.5 mm lag screws for fixation of the distal femur: implications for reconstruction of complex joint injuries**
Anjali Gupta, John McCamley, M. Wade Shrader, Kristine Csavina, David J. Jacofsky, Paul Tornetta III
Corresponding Author: Kristine Csavina
SHRI-CORE Orthopedic Research Labs, Sun City West, AZ

P1-19 **An in vivo 3d articular model of the radioscapho-capitate (RSC) ligament during wrist flexion/extension and ulnar/radial deviation**
Edward Akelman, Joseph Crisco, Douglas Moore, Michael Rainbow, Scott Wolfe
Corresponding Author: Joseph Crisco
Department of Orthopaedics, Brown Medical School/Rhode Island Hospital

P1-20 **North American perception of the prestige of biomechanics serials**
John Chow, Duane Knudson
Corresponding Author: Duane Knudson
California State University, Chico

P1-21 **Fatigue induced damage in cemented total hip arthroplasty can be investigated by acoustic emission**
Jihui Li, Gang Qi
Corresponding Author: Jihui Li
Columbia University

P1-22 **Finite element parameters affecting micromotion and strain energy density predictions in tibial model as determined by factorial analysis**
Michael Dunbar, Adam Henderson, Heidi Ploeg, Jill Schmidt
Corresponding Author: Jill Schmidt
University of Wisconsin-Madison

P1-23 **The influence of using one or two lag screws on the mechanical environment of a femoral neck fracture.**
Chris Brown, Philip Procter, David Simpson, Alan Yettram
Corresponding Author: David Simpson
University of Oxford

P1-24 **The effect of using modular necks with an uncemented hip stem on primary stability**
Harinderjit Gill, Paige Little, David Simpson
Corresponding Author: David Simpson
University of Oxford

P1-25 **Polyethylene stresses in unicompartmental knee replacements during a step-up activity.**
Harinderjit Gill, David Simpson
Corresponding Author: David Simpson
University of Oxford

P1-26 **Dynamic loading and biological growth**
Samer Adeeb, Marcelo Epstein, Walter Herzog
Corresponding Author: Samer Adeeb
University of Calgary

P1-27 **The effect of bone microstructure on microcracks propagation trajectory**
Ahmad Reza Arshi, Mohamad Reza Eslami, Hamid Reza Katoozian, E. Mallakin, Manssour Moeinzadeh, Ahmad Raeisi Najafi
Corresponding Author: Manssour Moeinzadeh
University of Illinois at Urbana- Champaign

P1-28 **Biomechanical effects of minimally invasive treatment for cervical spondylotic myelopathy**
Gunnar B.J. Andersson, Lacey E. Bresnahan, Richard G. Fessler, Mozammil Hussain, Raghu N. Natarajan
Corresponding Author: Lacey E. Bresnahan
The University of Chicago

P1-29 **Calibration of the ZETOS bone loading system**
Sylvana Garcia, Heidi Ploeg, Everett Smith
Corresponding Author: Sylvana Garcia
University of Wisconsin - Madison

P1-30 **Anisotropic stress analysis of the second metatarsal**
Timothy Derrick, W. Brent Edwards, Stacey Meardon, Erin Ward
Corresponding Author: W. Brent Edwards
Iowa State University

P1-31 **In vitro validation of a dynamic finite element tkr model**
Randy Ellis, Joel Lanovaz
Corresponding Author: Joel Lanovaz
University of Saskatchewan

P1-32 **Joint loads and bone strains associated with a resurfaced femoral head**
Donald L. Bartel, Christopher T. Cheng, Jason P. Long
Corresponding Author: Jason P. Long
Cornell University

P1-33 **The evaluation of tribological properties of biomaterials used for knee replacements**
Radek Sedlacek, Jana Vondrova
Corresponding Author: Radek Sedlacek
Czech Technical University in Prague, Faculty of Mechanical Engineering

P1-34 **Marrow space used for high resolution image segmentation of cancellous and cortical bone**
Robert Burden, Michael Voor, Seid Waddell, Qian Xu
Corresponding Author: Qian Xu
University of Louisville

P1-35 **A finite element investigation into the biomechanical effects of minimally invasive treatment for cervical spondylotic myelopathy**
Gunnar B.J. Andersson, Lacey E. Bresnahan, Richard G. Fessler, Mozammil Hussain, Raghu N. Natarajan
Corresponding Author: Lacey E. Bresnahan
The University of Chicago

P1-36 **Effects of ACL interference screws on articular cartilage thickness measurements with 1.5T and 3T MRI**
Megan Bowers, Braden Fleming, Evan Leventhal, Nhon Trinh, Glenn Tung, JJ Crisco, BB Kimia
Corresponding Author: Braden Fleming
Brown Medical School/Rhode Island Hospital

P1-37 **Can height loss across a functional spinal unit modified by static rest breaks mitigate cumulative compression induced injury?**
Jack P. Callaghan, Robert J Parkinson
Corresponding Author: Robert J Parkinson
University of Waterloo

P1-38 **Ankle angle and localized muscle fatigue effects on tibial response during heel impacts**
David Andrews, Adriana Holmes
Corresponding Author: Adriana Holmes
University of Windsor

P1-39 **Biomechanics of adjacent segments with number of inter-body bone grafts and spinal instrumentations for a multi-level fusion construct using a finite element model**
Howard An, Gunnar Andersson, Mozammil Hussain, Ahmad Nassr, Raghu Natarajan
Corresponding Author: Mozammil Hussain
Rush University Medical Center

P1-40 **Relationship between failure progression in a lumbar disc and manual lifting - a poroelastic finite element model study**
Howard An, Gunnar Andersson, Steve Lavender, Raghu Natarajan
Corresponding Author: Raghu Natarajan
Rush University of Medical Center

P1-41 **Finite element simulation of nanoindentation tests for cortical bone using a damaged plastic model**
Satya Paruchuru, Xuanliang Dong, Xiaodu Wang
Corresponding Author: Xuanliang Dong
University of Texas at San Antonio

P1-42 **Mechanical testing of tendon in transverse compression**
C. Paul Buckley, S.T. Samuel Salisbury, Amy B. Zavatsky
Corresponding Author: Amy B. Zavatsky
University of Oxford

Thursday, August 23, 2007 4:30 - 6:15 PM

Poster Session 2: Aging
Memorial Auditorium

P2-1 **Effects of age and loss of balance direction on the kinematics of the threshold of balance recovery**
Cecile Smeesters, Alessandro Telonio
Corresponding Author: Cecile Smeesters
Universite de Sherbrooke

P2-2 **Stair descent knee power changes following minimally invasive computer navigated total knee arthroplasty**
Kristine Csavina, David Jacofsky, John McCamley, M. Wade Shrader
Corresponding Author: John McCamley
SHRI-CORE Orthopedic Research Labs, Sun City West, AZ

P2-3 **Dynamic postural stability during sit-to-walk transitions in the healthy young and healthy elderly**
Thomas Buckley, Chris Hass, Chris Pitsikoulis
Corresponding Author: Thomas Buckley
Georgia Southern University

P2-4 **Effect of Parkinson's disease on step response to a backwards pull**
Stephen D. Jernigan, Carl Luchies, Kelly Lyons, Molly McVey, Rajesh Pahwa, Antonis Stylianou
Corresponding Author: Carl Luchies
The University of Kansas

P2-5 **Passive and active contributions to joint kinetics in elderly gait**
Bryan Heiderscheit, Amy Silder, Darryl Thelen, Ben Whittington
Corresponding Author: Amy Silder
University of Wisconsin - Madison

P2-6 **Altered response to a backwards pull in Parkinson's disease.**
Carl Luchies, Kelly Lyons, Molly McVey, Rajesh Pahwa, Antonis Stylianou
Corresponding Author: Carl Luchies
University of Kansas

P2-7 **Age and fatigue effects on lower extremity joint torque development**
Gregory King, Carl Luchies, Molly McVey, Antonis Stylianou
Corresponding Author: Gregory King
University of Missouri - Kansas City

P2-8 **Separating the influence of age and speed on gait variability**
Jonathan Dingwell, Hyun Gu Kang
Corresponding Author: Jonathan Dingwell
University of Texas at Austin

P2-9 **Pad causes alterations in the variability of gait patterns**
Jason Johanning, Naomi Kochi, Sara Myers, Iraklis Pipinos, Nick Stergiou
Corresponding Author: Sara Myers
University of Nebraska at Omaha

P2-10 **Center of mass and ankle inclination angles during walking: an alternative detection of gait instability**
Chu-Jui Chen, Li-Shan Chou
Corresponding Author: Li-Shan Chou
University of Oregon

P2-11 **Cruciate ligament removal contributes to abnormal knee motion during posterior stabilized total knee arthroplasty**
Melinda Cromie, Scott Delp, Nicholas Giori, Robert Siston
Corresponding Author: Melinda Cromie
Stanford University

Thursday, August 23, 2007
4:30 - 6:15 PM
Poster Session 3: Motor Control
Memorial Auditorium

P3-1 **Muscle synergies for human postural control are robustly used across multiple postural configurations**
Lena Ting, Gelsy Torres-Oviedo
Corresponding Author: Lena Ting
Emory University and Georgia Institute of Technology

P3-2 **Solutions of a redundant motor task with sub-task conflict**
Jaebum Park, Jae Kun Shim
Corresponding Author: Jaebum Park
University of Maryland

P3-3 **Bidirectional neural coupling between upper and lower limbs**
Daniel Ferris, Helen Huang
Corresponding Author: Helen Huang
University of Michigan

P3-4 **Changes in the postural control system following localized muscle fatigue: a time-delayed stability analysis**
Bradley Davidson, Michael Madigan, Maury Nussbaum
Corresponding Author: Bradley Davidson
Virginia Tech

P3-5 **Electromyographic correlates of internal models of target reaching tasks in randomized force fields**
Wen Liu, Mukul Mukherjee
Corresponding Author: Mukul Mukherjee
University of Kansas Medical Center

P3-6 **Processing effects on joint moments during impact landings**
Jeffery Podraza, Scott White
Corresponding Author: Scott White
University at Buffalo

P3-7 **Presentation of target torque level and error information enhance maximal voluntary elbow flexion torque**
Makoto Fukuda, Tetsuo Fukunaga, Yasuo Kawakami, Yohei Takai
Corresponding Author: Makoto Fukuda
Waseda University

P3-8 **A non-linear analysis of kinematic variability during cyclic reach-and-point movements.**
Robert Gregory, David Heller
Corresponding Author: Robert Gregory
United States Military Academy

P3-9 **Modelling static force generation of rat hindlimb muscles by direct stimulation**
Dinesh Pai, Matthew Tresch, Sang Hoon Yeo
Corresponding Author: Matthew Tresch
Northwestern University

P3-10 **Critical time-to-contact after postural perturbations**
Graham Caldwell, Catherine Gariepy, Christopher Hasson, William McDermott, Richard Van Emmerik
Corresponding Author: Christopher Hasson
University of Massachusetts

P3-11 **Adaptations to task mechanics alter stretch reflex gain but not intermuscular coordination**
Kuifu Chen, Gwyn Lewis, Eric Perreault
Corresponding Author: Eric Perreault
Northwestern University

P3-12 **Effect of surface compliance on stepping responses to trunk perturbations**
James Ashton-Miller, Manuel Hernandez
Corresponding Author: Manuel Hernandez
University of Michigan

P3-13 **The optimal release angles of elite discus throwers**
Steve Leigh, Hui Liu, Bing Yu
Corresponding Author: Steve Leigh
The University of North Carolina at Chapel Hill

P3-14 **Switching control to actuate elbow motion**
Mark E. Baratz, Daniel Budny, Angela Flamm, Laurel Kuxhaus, Mark Carl Miller, Pat Schimoler, Jeffrey Vipperman
Corresponding Author: Pat Schimoler
University of Pittsburgh

P3-15 **Stabilization of locomotion by a musculoskeletal model of cat hindlimbs with hill-type actuators**
Alexander Klishko, Boris Prilutsky
Corresponding Author: Boris Prilutsky
Georgia Institute of Technology

P3-16 **Rambling-trembling decomposition in two dimensions**
Marcos Duarte, Mark Latash, Thomas Robert, Vladimir Zatsiorsky
Corresponding Author: Thomas Robert
The Pennsylvania State University

P3-17 **Angular momentum control of forward dynamic walking**
Mark Able, Bradford Bennett, Alexandre Ledoux, Shawn Russell, Pradip Sheth
Corresponding Author: Bradford Bennett
University of Virginia

P3-18 **Examination of cutting knee mechanics using principal components analysis**
Michael Bottum, Kristian O'Connor
Corresponding Author: Kristian O'Connor
University of Wisconsin - Milwaukee

P3-19 **Joint moments are coordinated to stabilize vertical endpoint forces during human locomotion**
Young-Hui Chang, Jasper Yen
Corresponding Author: Jasper Yen
Georgia Institute of Technology

P3-20 **Selecting among neuromechnical control architectures using kinematic phase and perturbation experiments**
Robert Full, Daniel Koditschek, Shai Revzen
Corresponding Author: Shai Revzen
University of California, Berkeley

P3-21 **Mechanics of bipedal running turns**
Devin Jindrich
Corresponding Author: Devin Jindrich
Arizona State University

P3-22 **Test-retest reliability of sitting posture in typically developing infants.**
Joan Deffeyes, Stacey DeJong, Regina Harbourne, Anastasia Kyvelidou, Wayne Stuberg, Nicholas Stergiou, Junfeng Sun
Corresponding Author: Anastasia Kyvelidou
University of Nebraska at Omaha

P3-23 **Neuromechnical modeling of functional muscle synergies for postural control in the cat**
J. Lucas McKay, Lena H. Ting, Gelsy Torres-Oviedo
Corresponding Author: Lena H. Ting
Georgia Institute of Technology and Emory University

P3-24 **Muscle function is biased towards positive over negative work in level human gait**
Paul DeVita, Allison Gruber, Tibor Hortobagyi, Lars Janshen, Brian Moscicki, Patrick Rider, Stanislaw Solnik, Paul Zalewski
Corresponding Author: Paul DeVita
East Carolina University

P3-25 **Upper and lower limb disturbance rejection of self-triggered and computer-cued load perturbations**
Kari Danek, Daniel Ferris, Brent Gillespie, Jessy Grizzle
Corresponding Author: Kari Danek
University of Michigan

P3-26 **Biomechanical constraints on equilibrium point control of multi-joint arm postures**
James Gordon, Ning Lan, Dan Song
Corresponding Author: Ning Lan
University of Southern California

P3-27 **Lower limb force production and bilateral force asymmetries are based on sense of effort**
Daniel Ferris, Ann Simon
Corresponding Author: Ann Simon
University of Michigan

P3-28 **Revisiting the EMG-torque relationship of the trunk musculature: effects of antagonistic co-contraction**
Stephen Brown, Stuart McGill
Corresponding Author: Stephen Brown
University of Waterloo

P3-29 **Muscular contributions to vertebral joint rotational stiffness during the standard pushup**
Tyson Beach, Jack Callaghan, Samuel Howarth
Corresponding Author: Samuel Howarth
University of Waterloo

P3-30 **Muscle activation patterns change the inherent stiffness of the human trunk**
Stephen Brown, Stuart McGill
Corresponding Author: Stephen Brown
University of Waterloo

P3-31 **Joint kinetic contributions to acute performance enhancement & degradation**
Loren Chiu, George Salem
Corresponding Author: Loren Chiu
University of Southern California

P3-32 **Gender differences in spinal posture and user positioning on a prototype seat pan**
Jack Callaghan, Diana De Carvalho, Nadine Dunk
Corresponding Author: Diana De Carvalho
University of Waterloo

P3-33 **Effects of gender on lower extremity muscle activation in children performing a single-leg unanticipated landing task**
David Clark, Kristof Kipp, Kristin Kipp, Seth Kuhlman, Ronald Pfeiffer, Michelle Sabick, Kevin Shea
Corresponding Author: Ronald Pfeiffer
Boise State University

P3-34 **Effects of breathing on muscle strength of large muscle groups**
Adam Borg, Devn Brown, Elizabeth Ikeda, Sheng Li, Jessica Malouf
Corresponding Author: Sheng Li
University of Montana

P3-35 **Obstacle avoidance with varying ability to spatailly orient attention following mild traumatic brain injury**
Robert Catena, Li-Shan Chou, Charlene Halterman, Paul van Donkelaar
Corresponding Author: Li-Shan Chou
University of Oregon

Thursday, August 23, 2007 4:30 - 6:15 PM

Poster Session 4: Injury
Memorial Auditorium

P4-1 **Lower extremity kinematic consequences during vertical to horizontal momentum redirection**
Henryk Flashner, Laura Held, Jill McNitt-Gray
Corresponding Author: Laura Held
University of Southern California

P4-2 **Factors affecting lumbar kinetics during dependent transfers on an aircraft.**
Brian Higginson, Welsh Lisa, Michael Pavol
Corresponding Author: Michael Pavol
Oregon State University

P4-3 **Muscle forces at the knee during walking and running in patients with patellofemoral pain**
Gary Beaupre, Thor Besier, Garry Gold, Michael Fredericson, Scott Delp
Corresponding Author: Thor Besier
Stanford University

P4-4 **The effect of hand position on subscapularis force during the belly-press test**
Marcus Pandy, Kevin Shelburne, Michael Torry, Takashi Yanagawa
Corresponding Author: Takashi Yanagawa
Steadman Hawkins Research Foundation

P4-5 **Effect of orientation on failure criteria for lumbar spine segments**
David Burnett, Naira Campbell-Kyureghyan, Sai Vikas Yalla
Corresponding Author: Naira Campbell-Kyureghyan
University of Louisville

P4-6 **Deformation at branch points in human cerebral arteries**
Louis Cheng, Geoffrey Manley, Kenneth Monson, Joshua Smith
Corresponding Author: Joshua Smith
University of California, San Francisco

P4-7 **The influence of stride length on impact shock and metabolic cost during walking in obese women**
Joseph Hamill, Elizabeth Russell
Corresponding Author: Elizabeth Russell
University of Massachusetts

P4-8 **Spinal mechanics during drop landing: effects of gender and landing technique**
John W. Chow, Soo-An Park, Mark D. Tillman
Corresponding Author: Soo-An Park
SUNY-Upstate Medical University

P4-9 **A stochastic biomechanical model for the risk and risk factors for non-contact ACL injury**
Bing Yu, Chengfeng Lin, Chuanshu Ji, Paul S. Weinhold, Michael T. Gross, Darin A. Padua, and William E. Garrett
Corresponding Author: Bing Yu
The University of North Carolina at Chapel Hill

P4-10 **Meniscal injury in conjunction with acute and chronic ACL tears increase peak cartilage stresses**
Thomas Andriacchi, Nathan Netravali
Corresponding Author: Nathan Netravali
Stanford University

P4-11 **Prospective study of kinetic factors associated with tibial stress fractures in runners**
Irene Davis, Joseph Hamill, Michael Pohl
Corresponding Author: Michael Pohl
University of Delaware

P4-12 **Validation of tri-axial accelerometer for the calculation of elevation angles**
Tal Amasay, Andrew Karduna, Laurel Kincl, Keely Zodrow
Corresponding Author: Tal Amasay
University of Oregon

P4-13 **Acute torsional failure: do physiological loading rates effect the spine's limit?**
Jack Callaghan, Janessa Drake
Corresponding Author: Janessa Drake
University of Waterloo

P4-14 **Sagittal ACL graft orientation influences passive and dynamic anterior tibial translation**
Katerina Blazek, Ajit Chaudhari, Jason Dragoo, Sean Scanlan, Joshua Schmidt, and Tom Andriacchi
Corresponding Author: Sean Scanlan
Stanford University

P4-15 **Correlation of dynamic cartilage contact stress aberration with severity of joint instability**
Thomas Brown, Todd McKinley, Douglas Pedersen, M. James Rudert, Yuki Tochigi
Corresponding Author: Yuki Tochigi
University of Iowa

P4-16 **Frontal plane knee joint stiffness: gender and hormonal effects**
Martha Cammarata, Tobey DeMott, Yasin Dhaher, Jennifer Moore
Corresponding Author: Yasin Dhaher
Northwestern University

P4-17 **Electromyographic and kinematic evaluation of provocative tests for slap lesions**
Seth M. Kuhlman, Michelle B. Sabick, Ronald P. Pfeiffer, Kurt Nilsson, Kevin G. Shea, Mike Curtin, and David Clark
Corresponding Author: Seth Kuhlman
Boise State University

P4-18 **Model for occupants ejected from vehicles with roll and yaw**
Chad Hovey, Matthew Kaplan, Robert Piziali
Corresponding Author: Chad Hovey
Piziali and Associates, Inc.

P4-19 **Evaluation of injury criteria for predicting commotio cordis**
Cynthia Bir, Nathan Dau, Mark Link, Christopher Madias
Corresponding Author: Nathan Dau
Wayne State University

P4-20 **Prospective study of the biomechanical factors associated with patellofemoral pain**
Irene Davis, Brian Noehren
Corresponding Author: Brian Noehren
University of Delaware

P4-21 **Glucosamine and chondroitin sulfate affect the response of exercised articular cartilage to blunt impact loading**
Nurit Golenberg, Roger Haut, Eugene Kepich, Feng Wei
Corresponding Author: Roger Haut
Michigan State University

P4-22 **Biofidelity requirements for an advanced headform for the prediction of eye injuries**
Fred Brozoski, Paul Depinet, Stefan Duma, Eric Kennedy
Corresponding Author: Eric Kennedy
Virginia Tech - Wake Forest University Center for Injury Biomechanics

P4-23 **The effect of cardiovascular fatigue on trunk muscle activation and spine postures during firefighting tasks**
Jack Callaghan, Diane Gregory, Samuel Howarth, Sonia Narula
Corresponding Author: Diane Gregory
University of Waterloo

P4-24 **Effect of linear wheelchair velocity on a new manual wheelchair user joint injury index**
Mohammadreza Mallakzadeh, Farrokh Sassani, Bonita J Sawatzky
Corresponding Author: Mohammadreza Mallakzadeh
The University of British Columbia

P4-25 **Whiplash causes increased laxity of cervical capsular ligament**
Erik J. Carlson, Marcus Coe, Shigeki Ito, Paul Ivancic, Anthony B. Ndu, Manohar M. Panjabi, Wolfgang Rubin, Yasuhiro Tominaga
Corresponding Author: Paul Ivancic
Yale University School of Medicine

Friday, August 24, 2007 4:30 - 6:15 PM

Poster Session 5: Rehabilitation
Memorial Auditorium

P5-1 **Gait adaptations and recovery rates following minimally invasive total hip replacement**
Richard Berger, Kharma Foucher, Robert Trombley, Markus Wimmer
Corresponding Author: Markus Wimmer
Rush University Medical Center

P5-2 **Functional gait outcomes after intertrochanteric hip fracture**
Ellen Boeke, Kristine Csavina, M. Wade Shrader, Kimberly Yarnall
Corresponding Author: Kimberly Yarnall
SHRI-CORE Orthopedic Research Labs, Sun City West, AZ

P5-3 **Post-TKA effects of prehabilitation on standing knee kinetics**
Peter M. Quesada, James E. Doane, Ann M. Swank, Claudia A. Angeli, John Nyland, and Robert V. Topp
Corresponding Author: Peter Quesada
University of Louisville

P5-4 **Surgical recession of the gastrocnemius for isolated contracture: a case study**
Michael Castro, Nicole Chimera, Kurt Manal
Corresponding Author: Kurt Manal
Center for Biomedical Engineering Research, University of Delaware

P5-5 **Assessment of function of an orthotic brace control mechanism**
Steven Anderson, Jessica Hagan, William Hnat, John Lilly, Kenneth A. Mook, Peter Quesada
Corresponding Author: Peter Quesada
University of Louisville

P5-6 **Effects of wheelchair propulsion training on pushrim kinetics**
Michael Boninger, Rachel Cowan, Alicia Koontz, Ian Rice
Corresponding Author: Alicia Koontz
Human Engineering Research Laboratories

P5-7 **Disease severity influences trunk sway and knee loading during walking in patients with medial compartment knee OA**
Thomas P. Andriacchi, Jessica L. Asay, Annegret Muendermann
Corresponding Author: Annegret Muendermann
Stanford University

P5-8 **Reflex and nonreflex characterization of spasticity in children with cerebral palsy: dependence of catch angle on velocity**
Jia-Jin Chen, Deborah Gaebler, Hyung-Soon Park, Yi-Ning Wu, Li-Qun Zhang
Corresponding Author: Li-Qun Zhang
Northwestern University

P5-9 **Can intervertebral kinematics predict clinical outcome of lumbar discectomy?**
Jerry Calabrese, Amir Fayyazi, Nathaniel Ordway, Soo-An Park, Hansen Yuan
Corresponding Author: Soo-An Park
SUNY-Upstate Medical University

P5-10 **Lower limb synergy patterns of stroke subjects while walking in a lokomat robotic orthosis**
Joseph Hidler, Nathan Neckel, Diane Nichols
Corresponding Author: Nathan Neckel
Catholic University of America

P5-11 **Integer programming models for optimizing shoulder rehabilitation**
James Carpenter, Christopher Gatti, Richard Hughes, Jason Scibek, Oleg Svintsitski
Corresponding Author: Richard Hughes
University of Michigan

P5-12 **Control system development for automatic standing balance using functional neuromuscular stimulation (FNS) following spinal cord injury (SCI)**
Musa Audu, Robert Kirsch, Raviraj Nataraj, Ronald Triolo
Corresponding Author: Raviraj Nataraj
Case Western Reserve University

P5-13 **Effect of the lateral wedged insoles on the joint load of knee and ankle in patients with medial knee osteoarthritis**
Yuji Kuroyanagi, Hideo Matsumoto, Takeo Nagura, Toshiro Otani, Yasumori Suda, and Y. Toyama
Corresponding Author: Yuji Kuroyanagi
Department of Orthopedic Surgery, Keio University

P5-14 **3-d joint motion of ACL deficient and reconstructed knees during daily activities**
Bo Gao, Peter Indelicato, Michael Moser, Nigel Zheng
Corresponding Author: Nigel Zheng
University of Florida

P5-15 **Is gait after unilateral total knee arthroplasty similar to healthy adults?**
Clare Milner
Corresponding Author: Clare Milner
University of Tennessee

Friday, August 24, 2007 4:30 - 6:15 PM

Poster Session 6: Computational Biomechanics
Memorial Auditorium

P6-1 **Analytical expression of musculotendon model including viscoelastic properties of tendon**
Miloslav Vilimek
Corresponding Author: Miloslav Vilimek
Czech Technical University in Prague

P6-2 **Influence of loading on knee extensor mechanics in total knee replacement: a computer simulation study**
Michael Hast, Ryan Landon, Stephen Piazza
Corresponding Author: Stephen Piazza
The Pennsylvania State University

P6-3 **Musculo-skeletal modeling software (MSMS) for biomechanics and virtual rehabilitation**
Rahman Davoodi, Mehdi Khachani, Gerald E. Loeb
Corresponding Author: Mehdi Khachani
Alfred Mann Institute and Department of Biomedical Engineering - University of Southern California

P6-4 **Criteria for wrapping surface parameters for spinal nuscles**
Richard Lasher, Travis Meyer, Anita Vasavada
Corresponding Author: Anita Vasavada
Washington State University

P6-5 **Robust contact spring placement using trimmed nurbs surfaces for simulation of articular contact**
Ryan Landon, Stephen Piazza
Corresponding Author: Stephen Piazza
The Pennsylvania State University

P6-6 **Validation of orthopaedic related image segmentation techniques**
Nicole DeVries, Esther Gassman, Nicole Grosland, Nicole Kallemeyn, Vincent A. Magnotta, Kiran Shivanna
Corresponding Author: Nicole Grosland
University of Iowa

P6-7 **Three-dimensional hyperelastic model of the human knee: a parametric sensitivity study**
Yasin Dhaher, Qunli Sun
Corresponding Author: Yasin Dhaher
Northwestern University and Rehabilitation Institute of Chicago

P6-8 **Virtue of boundary element method in calculation of pressure distribution on boundary based segmented medical images**
Nasser Fatouraee, Ali Pashaee
Corresponding Author: Nasser Fatouraee
Amirkabir University of Technology

P6-9 **A musculoskeletal model of the rat hindlimb**
V Reggie Edgerton, Devin Jindrich, William Johnson, Roland Roy
Corresponding Author: William Johnson
UCLA

P6-10 **A genetic algorithm approach to singularity avoidance in the analysis of weight lifting performance**
Ahmed Reza Arshi, Amir Homayoun Javadi, Manssour Moeinzadeh, Elham Shirzad
Corresponding Author: Manssour Moeinzadeh
University of Illinois at Urbana-Champaign

P6-11 **Magnetic resonance image segmentation for biomechanical modeling of the orbit**
Joseph L. Demer, Joel M. Miller, Dinesh K. Pai, Qi Wei
Corresponding Author: Qi Wei
Rutgers University

P6-12 **Shoulder mechanics: analytical modeling and validation**
Noshir Langrana, Sue Ann Sisto, Sarah Sullivan
Corresponding Author: Sarah Sullivan
Rutgers University

P6-13 **Forward dynamics simulations of human gait using neuromusculoskeletal tracking**
Hyung Joo Kim, Marcus Pandy, Ajay Seth
Corresponding Author: Ajay Seth
Stanford University

P6-14 **Muscle activation, joint position and muscle mass distribution: considerations for musculoskeletal modeling**
Timothy Clark, David Hawkins
Corresponding Author: David Hawkins
University of California - Davis

P6-15 **A rigid body model of a lacrosse shot underestimates measured ball velocities**
Joseph Crisco, Michael Rainbow, Eileen Wang
Corresponding Author: Joseph Crisco
Bioengineering Laboratory, Department of Orthopaedics, Brown Medical School/Rhode Island Hospital

P6-16 **Simulation study of walking patterns with knee osteoarthritis using opensim**
Jill Higginson, Ming Xiao
Corresponding Author: Ming Xiao
University of Delaware

P6-17 **A proposed new obstacle-set algorithm for modeling the wrapping path of deltoid**
Brian Garner, Bo Xu
Corresponding Author: Brian Garner
Baylor University

P6-18 **Using distributions of forward dynamic simulations to investigate model inaccuracies**
Matt Camilleri
Corresponding Author: Matt Camilleri
Sacramento City College

P6-19 **A novel elastic foundation contact detection algorithm for use in a six degree of freedom knee model**
Roger Gonzalez, Nathan Green
Corresponding Author: Roger Gonzalez
LeTourneau University

P6-20 **A neuro-musculoskeletal motor control model with somatosensory and vestibular feedback**
Kamran Iqbal, Anindo Roy
Corresponding Author: Kamran Iqbal
University of Arkansas at Little Rock

P6-21 **Patient specific finite element modeling of lumbar vertebrae**
Dennis Abernathie, Dirk Alander, Ferris Pfeiffer, Douglas Smith, Carol Ward
Corresponding Author: Ferris Pfeiffer
University of Missouri

P6-22 **Expressing joint axis orientation**
Kevin A Ball, Thomas M Greiner
Corresponding Author: Kevin A Ball
University of Hartford

P6-23 **A model of maximum voluntary joint torque variation with joint angle and angular velocity**
Dennis Anderson, Michael Madigan, Maury Nussbaum
Corresponding Author: Dennis Anderson
Virginia Tech

P6-24 **Exclusion of the subtalar joint affects significantly the calculated ankle muscle forces during gait.**
Ilse Jonkers, Gerlinde Lenaerts, Friso Hagman, Louis Peeraer, Jos Vander Sloten, and Georges Van der Perre
Corresponding Author: Ilse Jonkers
Katholieke Universiteit Leuven

P6-25 **Reliability of lower extremity anthropometric measures and their effect on wobbling mass tissue predictions**
David Andrews, Timothy Burkhart, Katherine Teigrob
Corresponding Author: Timothy Burkhart
University Of Windsor

P6-26 **Bayesian techniques improve human motion estimation**
Friedl De Groote, Tinne De Laet, Joris De Schutter, Ilse Jonkers
Corresponding Author: Friedl De Groote
Katholieke Universiteit Leuven

P6-27 **Response-surface mapping to generate distributions of forward dynamic simulations**
Matt Camilleri
Corresponding Author: Matt Camilleri
Sacramento City College

P6-28 **Muscle contributions to body segment mechanical power during able-bodied toe walking**
Judith Burnfield, Sara Mulroy, Richard Neptune, Kotaro Sasaki
Corresponding Author: Richard Neptune
Department of Mechanical Engineering, The University of Texas at Austin, Austin, TX

P6-29 **Automated hexahedral meshing of anatomical structures using deformable registration**
Ritesh Bafna, Nicole Grosland, Vincent Magnotta
Corresponding Author: Nicole Grosland
The University of Iowa

P6-30 **A new trunk volume representation for geometric body segment models**
Genevieve Dumas, Jason Wicke
Corresponding Author: Jason Wicke
Texas A&M University - Commerce

P6-31 **A check of mesh quality**
Nicole Grosland, Curtis Lisle, Vincent Magnotta, Steve Pieper, Kiran Shivanna
Corresponding Author: Nicole Grosland
The University of Iowa

P6-32 **Patient-specific orthopaedic surgical planning: image datasets to fe models**
Nicole M Grosland, Vincent A Magnotta, Kiran H Shivanna, Srinivas C Tadepalli
Corresponding Author: Srinivas C Tadepalli
The University of Iowa

P6-33 **Determining vertical ground reaction forces without a force platform using a mass-spring-damper model**
Graham Caldwell, Timothy Derrick, Ross Miller
Corresponding Author: Ross Miller
University of Massachusetts Amherst

Friday, August 24, 2007 4:30 - 6:15 PM

Poster Session 7: Muscle
Memorial Auditorium

P7-1 **A comparison of force-velocity properties of single muscle fibers obtained under dynamic and steady-state conditions**
Sampath Gollapudi, David Lin
Corresponding Author: David Lin
Washington State University

P7-2 **Muscle architecture of extensor carpi radialis longus and brevis: a comprehensive volumetric modeling approach**
Anne Agur, Eugene Fiume, Victor Ng-Thow-Hing, Kajeandra Ravichandiran, Karan Singh
Corresponding Author: Anne Agur
University of Toronto

P7-3 **Emg-based estimates of pennation angle for the primary ankle dorsi and plantarflexors during isometric contractions**
Thomas Buchanan, Kurt Manal, Dustyn Roberts
Corresponding Author: Kurt Manal
Center for Biomedical Engineering Research, University of Delaware

P7-4 **In vivo examinations of medial gastrocnemius: change of force-generating capacity in stroke survivors**
Fan Gao, Li-Qun Zhang
Corresponding Author: Li-Qun Zhang
Rehabilitation Institute of Chicago & Northwestern University

P7-5 **Trade-offs in performance associated with muscle fiber type composition**
Brian Umberger
Corresponding Author: Brian Umberger
University of Massachusetts Amherst

P7-6 **Architecture of the first dorsal interosseous muscle**
John Challis, Daniel Gales, Benjamin Infantolino
Corresponding Author: Benjamin Infantolino
Pennsylvania State University

P7-7 **Determination of the psoas major muscle thickness by B-mode ultrasonography**
Tetsuo Fukunaga, Yoichi Katsumata, Yasuo Kawakami, Yohei Takai
Corresponding Author: Yoichi Katsumata
Waseda University

P7-8 **An unconstrained workloop approach to study stability in frog muscle in vitro**
Stephen DeWeerth, Kartik Sundar, Lena Ting
Corresponding Author: Kartik Sundar
Georgia Institute of Technology

P7-9 **Temperature-dependent mechanical properties of human type-i muscle fibers**
Sampath Gollapudi, David Lin
Corresponding Author: Sampath Gollapudi
Washington State University

P7-10 **Estimation of myotendinous junction displacement using a cross correlation algorithm for ultra-sound images**
Daniel Alves, Liliam Oliveira, Carolina Peixinho, Taian Vieira
Corresponding Author: Liliam Oliveira
Federal University of Rio de Janeiro

P7-11 **Influence of isometric muscle fatigue on the human force-length relationship**
Eric Berton, Stuart Binder-Macleod, Thomas Buchanan, Ramu Perumal, Guillaume Rao
Corresponding Author: Guillaume Rao
Department of Mechanical Engineering, University of Delaware

P7-12 **Human lower extremity design: architecture of hip, knee, and ankle muscles**
Jacqueline Braun, Carolyn Eng, Trevor Kingsbury, Richard Lieber, Kristin Lieber, Laura Smallwood, Samuel Ward, Taylor Winters
Corresponding Author: Samuel Ward
University of California San Diego

P7-13 **Scaling of joint mechanics and muscle architecture in the human knee**
Samuel R. Ward, Trevor Kingsbury, Taylor Winters, Kristin M. Lieber, Jacqueline Braun, Carolyn M. Eng, and Richard L. Lieber
Corresponding Author: Samuel Ward
University of California San Diego

P7-14 **The relationship between muscle force and intramuscular pressure during dynamic muscle contractions**
Jennifer Davis, Kenton Kaufman, Richard Lieber, Samuel Ward
Corresponding Author: Samuel Ward
University of California San Diego

P7-15 **Cyclic compressive loading facilitates functional and histological recovery following strain induced damage in skeletal muscle**
Sudha Agarwal, Thomas Best, Timothy Butterfield, Yi Zhao
Corresponding Author: Timothy Butterfield
The Ohio State University

P7-16 **Continuum-based model of skeletal muscle**
Tammy Haut Donahue, Kenton Kaufman, Duane Morrow, Gregory Odegard
Corresponding Author: Gregory Odegard
Michigan Technological University

P7-17 **Human lower extremity design: architecture of human hamstring and quadriceps muscles**
Jacqueline Braun, Carolyn Eng, Trevor Kingsbury, Kristin Lieber, Taylor Winters
Corresponding Author: Kristin Lieber
University of California

P7-18 **The effect of muscle fatigue on correlations in timing errors**
Jonathan Dingwell, Deanna Gates
Corresponding Author: Deanna Gates
University of Texas at Austin

P7-19 **Evaluation of three methods for determining EMG-muscle force parameter estimates for the shoulder muscles**
Christopher J. Gatti, Lisa Case Doro, Joseph E. Langenderfer, Amy G. Mell,
Joseph D. Maratt, James E. Carpenter, Richard E. Hughes
Corresponding Author: Richard Hughes
University of Michigan

P7-20 **Effect of glutathione depletion and age on skeletal muscle performance during a chronic stretch-shortening contraction exposure**
Brent Baker, Robert Cutlip, Melinda Hollander, Michael Kashon
Corresponding Author: Robert Cutlip
National Institute for Occupational Safety and Health

P7-21 **Reliability of hand-free ultrasound measurement for vastus medialis obliquus**
Gabriel Ng, Yiu Ming Wong
Corresponding Author: Yiu Ming Wong
Hong Kong Polytechnic University

P7-22 **Residual force depression is not abolished following a quick shortening step**
Walter Herzog, Timothy Leonard
Corresponding Author: Walter Herzog
University of Calgary

Friday, August 24, 2007 4:30 - 6:15 PM

Poster Session 8: Sports
Memorial Auditorium

P8-1 **Stroke resumption following flip turns in swimming**
Richard Hinrichs, Bethany Larsen
Corresponding Author: Richard Hinrichs
Arizona State University

P8-2 **Cruciate ligament force between the forward lunge long and short with and without a stride**
Rafael F. Escamilla, Naiquan Zheng, Alan Hreljac, Rodney Imamura, Toran D. MacLeod, William B. Edwards, Glenn S. Fleisig, Kevin E. Wilk
Corresponding Author: Rafael Escamilla
California State University, Sacramento

P8-3 **Changes in leg stiffness and sprint characteristics during the acceleration phase of running in top sprinters**
Kai Kobayashi, Shigeo Iso, Kazuyuki Kanosue, Hiroyasu Tsuchie, Tetsuo Fukunaga, Yasuo Kawakami
Corresponding Author: Kai Kobayashi
Waseda University

P8-4 **Contributions of passive-tension vs. inertial effects on gravity correction for strength training**
Colleen Delmonaco, Laura Frey Law, Andrea Laake
Corresponding Author: Laura Frey Law
University of Iowa

P8-5 **Ground reaction forces between running shoes, racing flats and distance spikes in runners**
Iain Hunter, Suzanna Logan
Corresponding Author: Iain Hunter
Brigham Young University

P8-6 **The effect of stroke length on active drag in swimming**
Richard Hinrichs, Bryan Morrison
Corresponding Author: Bryan Morrison
Valparaiso University & Arizona State University

P8-7 **Influence of cycling intensity on running kinematics and electromiography in well trained triathletes**
Javier Mon, Ramón Maañón, Oscar Viana, Jose A. Sánchez, Rafael Martín, Miguel Fernández del Olmo
Corresponding Author: Miguel Fernández del Olmo
Faculty of Sciences of Sport and Physical Education (INEF Galicia)

P8-8 **Multi-segment foot kinematics in high- and low-arched females recreational athletes during walking and running**
Benjamin Long, Clare Milner, Douglas Powell, Songning Zhang
Corresponding Author: Douglas Powell
The University of Texas of the Permian Basin

P8-9 **Lumbar motion during pitching in professional baseball players**
Ajit Chaudhari, Christopher McKenzie
Corresponding Author: Ajit Chaudhari
The Ohio State University

P8-10 **Dynamic and static changes in foot shape**
Sharna Clark-Donovan, Gordon Valiant
Corresponding Author: Sharna Clark-Donovan
Nike Sport Research Lab

P8-11 **Comparison of split double twists and split triple twists in pairs figure skating**
Deborah L. King, Sarah L. Smith, Michele R. Brown, Jean L. McCrory, Barry A. Muncasy, Gary L. Scheirman
Corresponding Author: Deborah King
Ithaca College

P8-12 **Stepping aerobics: how do the stepping direction and height affect joint kinetics?**
Man-Ying Wang, Hsin-Chang Wu
Corresponding Author: Man-Ying Wang
University of Southern California

P8-13 **Push up bars and hand position affect upper extremity muscle activity during the push up exercise**
Aaron Decker, Siufong Lam, Steven McCaw, Amanda Somers, Mitch Waller
Corresponding Author: Steven McCaw
Illinois State University

P8-14 **A mechanical cause of body rotation about the vertical axis in baseball batting**
Toshimasa Yanai
Corresponding Author: Toshimasa Yanai
Chukyo University

Friday, August 24, 2007 4:30 - 6:15 PM

Poster Session 9: Locomotion
Memorial Auditorium

P9-1 **Effects of physical assistance on narrow beam walking**
Antoinette Domingo, Daniel Ferris
Corresponding Author: Antoinette Domingo
University of Michigan

P9-2 **Walking with increased push-off decreases hip flexion moment**
Daniel Ferris, Cara Lewis
Corresponding Author: Cara Lewis
University of Michigan

P9-3 **Comparison of the plantarflexion moment arms of lateral gastrocnemius between sprinters and non-sprinters**
Sabrina Lee, Stephen Piazza
Corresponding Author: Stephen Piazza
The Pennsylvania State University

P9-4 **Kinematic correlates of the free moment and combined loads during running**
Timothy Derrick, PhD, William Edwards, Stacey Meardon
Corresponding Author: Stacey Meardon
Iowa State University

P9-5 **Mechanics and energetics of incline walking with powered ankle exoskeletons**
Daniel Ferris, Gregory Sawicki
Corresponding Author: Gregory Sawicki
University of Michigan-Ann Arbor

P9-6 **In vivo measurement of the inversion-eversion moment arms of gastrocnemius and tibialis anterior**
Sabrina Lee, Stephen Piazza
Corresponding Author: Stephen Piazza
The Pennsylvania State University

P9-7 **Functional gait outcomes in stair climbing after intertrochanteric hip fracture**
Ellen Boeke, Kristine Csavina, M. Wade Shrader, Kimberly Yarnall
Corresponding Author: Kimberly Yarnall
SHRI-CORE Orthopedic Research Labs, Sun City West, AZ

P9-8 **Estimating lean angle through application of the gravity line projection algorithm**
Elizabeth Hsiao-Wecksler, Pilwon Hur, Seiji Naito
Corresponding Author: Elizabeth Hsiao-Wecksler
University of Illinois at Urbana Champaign

P9-9 **An innovative diagnostic tool for reducing traumatic knee injuries**
Brian Armstrong, Michael Bottum, Mustafa Farrah, Kristian O'Connor, Stephen Watts
Corresponding Author: Kristian O'Connor
University of Wisconsin - Milwaukee

P9-10 **A functional method for locating the subtalar joint axis: in vivo assessment of accuracy**
Gregory S. Lewis, Andrea R. Seisler, Tamara L. Cohen, Kevin A. Kirby, Frances T. Sheehan, Stephen J. Piazza
Corresponding Author: Gregory Lewis
The Pennsylvania State University

P9-11 **Measurement of ground reaction force in single limb support through markerless motion capture**
Thomas Andriacchi, Stefano Corazza
Corresponding Author: Stefano Corazza
Stanford University

P9-12 **Finite helical axes of ACL-deficient and ACL-reconstructed knees during walking**
Bo Gao, Nigel Zheng
Corresponding Author: Nigel Zheng
University of Florida

P9-13 **A hybrid methodology using ultrasonography and motion analysis for estimation of achilles tendon moment arms in vivo**
Thomas Buchanan, Nicole Chimera, Justin Cowder, Kurt Manal
Corresponding Author: Kurt Manal
Center for Biomedical Engineering Research, University of Delaware

P9-14 **Effects of an elastic knee orthosis on unilateral hopping**
Michael S. Cherry, Daniel P. Ferris, Sridhar Kota
Corresponding Author: Michael S. Cherry
The University of Michigan

P9-15 **Independent effects of weight and mass on muscle activity during walking**
Rodger Kram, Craig McGowan, Richard Neptune
Corresponding Author: Craig McGowan
University of Colorado at Boulder

P9-16 **Traditional vs. continuous data collection for gait evaluation**
James Doane, Peter Quesada, Ann Swank, Robert Topp
Corresponding Author: Peter Quesada
University of Louisville

P9-17 **Does weight influence locomotive stability?**
Christopher J. Arellano, Max J. Kurz, Charles S. Layne, Daniel P. O'Connor, Melissa Scott-Pandorf
Corresponding Author: Christopher J. Arellano
University of Houston

P9-18 **Exploring the impulse response of the postural control system**
Brett Duiser, Elizabeth Hsiao-Wecksler, Pilwon Hur
Corresponding Author: Elizabeth Hsiao-Wecksler
University of Illinois at Urbana-Champaign

P9-19 **Power required to maintain balance on a moving platform**
Jerome Allen, Thomas Edwards, Venkata Gade, Nitin Moholkar, David Tung
Corresponding Author: Venkata Gade
Kessler Medical Rehabilitation Research and Education Center

P9-20 **Evaluation of the assessment of symmetry during gait**
John Challis, Daniel Gales
Corresponding Author: Daniel Gales
Pennsylvania State University

P9-21 **Estimation of knee joint compression forces in subjects with medial compartment knee osteoarthritis**
Jill Higginson, Joseph Zeni, Jr
Corresponding Author: Joseph Zeni, Jr
University of Delaware

P9-22 **Static postural stability of individuals with mental retardation before and after weight and balance training**
Courtney Haynes, Thurmon Lockhart
Corresponding Author: Courtney Haynes
Virginia Tech

P9-23 **Height estimation of an obstacle is scaleable to toe elevation at obstacle crossing**
Chris Rhea, Shirley Rietdyk
Corresponding Author: Chris Rhea
Purdue University

P9-24 **Sensitivity of functional hip joint center location to body mass index, movement pattern and marker cluster**
Annegret Mündermann, Stefano Corazza, Priyanshu Gupta, Valentina Camomilla, Chris O. Dyrby, Thomas P. Andriacchi
Corresponding Author: Annegret Muendermann
Stanford University

P9-25 **Variability of joint coupling within the lower extremity in runners with patellofemoral pain during a prolonged run**
Irene Davis, Tracy Dierks, Joseph Hamill, John Scholz
Corresponding Author: Tracy Dierks
Indiana University

P9-26 **Feedforward postural control in standing: role of lateral muscles and body orientation**
Alexander Aruin, Marcio Santos
Corresponding Author: Marcio Santos
University of Illinois at Chicago

P9-27 **Comparison of kinematic methods for determining footstrike and toe-off during overground running**
Irene Davis, Rebecca Fellin
Corresponding Author: Rebecca Fellin
University of Delaware

P9-28 **Energetics and biomechanics of walker assisted gait**
Rodger Kram, Jonathon Priebe
Corresponding Author: Jonathon Priebe
University of Colorado

P9-29 **A gait modification to reduce the external adduction moment at the knee: a case study**
Joaquin Barrios, Irene Davis
Corresponding Author: Joaquin Barrios
University of Delaware

P9-30 **Sensitivity of lyapunov exponent estimation for human gait**
Joseph Hamill, Trampas TenBroek, Richard Van Emmerik
Corresponding Author: Trampas TenBroek
University of Massachusetts

P9-31 **Older adults exhibit reduced lateral acceleration of the center of mass at fast walking speeds**
Bryan Heiderscheit, Antonio Hernandez, Amy Silder, Darryl Thelen
Corresponding Author: Antonio Hernandez
University of Wisconsin - Madison

P9-32 **Postural control of self-initiated weight shifts in children and adults**
James Abbas, Andrea Downing, K Narayanan
Corresponding Author: Andrea Downing
Center for Adaptive Neural Systems, Arizona State University

P9-33 **The effects of stepping off vs. hopping off a box on calculated drop heights in two-legged landings**
Mostafa Afifi, Richard Hinrichs
Corresponding Author: Mostafa Afifi
Arizona State University

P9-34 **Reducing errors in inverse dynamics-based joint torques through optimized body segment parameters and segment motion profiles**
Elizabeth T. Hsiao-Wecksler, Raziel Riemer
Corresponding Author: Raziel Riemer
Ben-Gurion University

P9-35 **Effects of attention on dynamic stability of walking**
Jonathan Dingwell, Mark Grabiner, Roland Robb, Karen Troy
Corresponding Author: Jonathan Dingwell
University of Texas

P9-36 **A mechanism to reduce the knee adduction moment during walking**
Thomas Andriacchi, Jennifer Erhart, Anne Mündermann, Lars Mündermann
Corresponding Author: Jennifer Erhart
Stanford University

P9-37 **An elusive talus: re-thinking the ankle complex**
Kevin A Ball, Thomas M Greiner
Corresponding Author: Kevin A Ball
University of Hartford

P9-38 **Approximate entropy is robust to non-stationarity in analysis of infant sitting postural sway**
Joan Deffeyes, Stacey DeJong, Regina Harbourne, Anastasia Kyvelidou, Nicholas Stergiou, Wayne Stuberg
Corresponding Author: Joan Deffeyes
Biomechanics Laboratory, University of Nebraska at Omaha

P9-39 **Accuracies of skin marker based knee motion analysis using different techniques**
Bryan Conrad, Bo Gao, Nigel Zheng
Corresponding Author: Nigel Zheng
University of Florida

P9-40 **Lower limb local or global asymmetry in gait of people without impairments**
Heydar Sadeghi
Corresponding Author: Heydar Sadeghi
Tarbiat Moallem University

P9-41 **Contact stress elevation with lateral talar shift**
Daniel Fuchs, Tina Maxian, Robert Spilker, Richard Uhl, Jeremy Winston
Corresponding Author: Tina Maxian
Eastern Maine Medical Center

P9-42 **Importance of preswing rectus femoris activity**
Allison Arnold, Scott Delp, Melanie Fox, Sylvia Ounpuu, Jeffrey Reinbolt
Corresponding Author: Melanie Fox
Stanford University

P9-43 **The effect of manipulating subject mass on lower extremity torque patterns during locomotion**
Ronita Cromwell, John De Witt, R Donald Hagan
Corresponding Author: John De Witt
Bergaila Engineering Services

P9-44 **Gait adaptations and high implant twisting moments during stair climbing in subjects with total hip replacements**
Kharma Foucher, Debra Hurwitz, Markus Wimmer
Corresponding Author: Kharma Foucher
Rush University Medical Center

P9-45 **Origins of the long-range correlations in stride times**
Jonathan Dingwell, Deanna Gates, Jimmy Su
Corresponding Author: Deanna Gates
University of Texas at Austin

P9-46 **The short-term effect of whole body vibration training on collegiate sprint athletes**
Mike Bishop, Iain Hunter, Brad Roberts, Robert Thiebaud
Corresponding Author: Iain Hunter
Brigham Young University

P9-47 **How precise is the hip joint centre position found using functional methods?**
Richard Good, Julie Stebbins, Tim N. Theologis, Amy B. Zavatsky
Corresponding Author: Amy B. Zavatsky
University of Oxford

P9-48 **Comparison of two alternate methods for tracking toe trajectory**
Jacob Bloomberg, Rachel Brady, Al Feiveson, Chris Miller, Ajitkumar Mulavara, Brian Peters, Liz Warren
Corresponding Author: Chris Miller
Wyle Laboratories; Houston, TX

Friday, August 24, 2007 4:30 - 6:15 PM

Poster Session 10: Manipulation
Memorial Auditorium

P10-1 **The effect of handle friction and torque on axial push force**
Thomas Armstrong, Yoko Konishi, Na Jin Seo
Corresponding Author: Na Jin Seo
University of Michigan

P10-2 **Principal component analysis reveals control strategies in static grasp at multiple time scales**
Daniel Brown, Francisco Valero-Cuevas
Corresponding Author: Francisco Valero-Cuevas
Cornell University

P10-3 **Asymmetry of wheelchair pushrim biomechanics over varying surfaces**
Kai-Nan An, Kenton Kaufman, Melissa Morrow
Corresponding Author: Kenton Kaufman
Mayo Clinic

P10-4 **Reference hand configurations during grip force adjustments**
Sun W Kim, Mark L. Latash, Vladimir M. Zatsiorsky
Corresponding Author: Mark L. Latash
Penn State University

P10-5 **Coactivation of hand muscles and movement fluctuations in old adults**
Roger Enoka, Adam Marmon, Minoru Shinohara
Corresponding Author: Minoru Shinohara
Georgia Institute of Technology

P10-6 **Analysis of strains in extensor mechanism of index finger**
Hua Chen, Derek Kamper, Sang Wook Lee, Joseph Towles
Corresponding Author: Sang Wook Lee
Rehabilitation Institute of Chicago

P10-7 **Quantitative analysis of finger movements during reaching and grasping tasks**
Thomas Armstrong, Jaewon Choi
Corresponding Author: Jaewon Choi
University of Michigan

P10-8 **Effective moment arm estimation of index finger muscles**
Hua Chen, Derek Kamper, Sang Wook Lee, Joseph Towles
Corresponding Author: Sang Wook Lee
Rehabilitation Institute of Chicago

P10-9 **Simultaneous performance of two tasks by the fingers of the human hand**
Mark Latash, John Scholz, Vladimir Zatsiorsky, Wei Zhang
Corresponding Author: Wei Zhang
The Penn State University

P10-10 **Prehension synergies: effects of finger manipulation**
Mark Budgeon, Mark Latash, Vladimir Zatsiorsky
Corresponding Author: Mark Budgeon
Pennsylvania State University

P10-11 **Upper extremity kinematic model for walker assisted gait**
Jeffrey Ackman, Kevin Cao, Gerald F. Harris, Jeffrey Schwab, Kelly Strifling, Mei Wang
Corresponding Author: Kelly Strifling
Marquette University

P10-12 **Effect of elevation angle on movement velocity in a non-visually-guided reaching task**
David Harmer, David Suprak
Corresponding Author: David Harmer
University of Colorado, Colorado Springs

P10-13 **Prehension of the objects with complex friction patterns**
Mark Latash, Xun Niu, Vladimir Zatsiorsky
Corresponding Author: Xun Niu

NOTES

NOTES

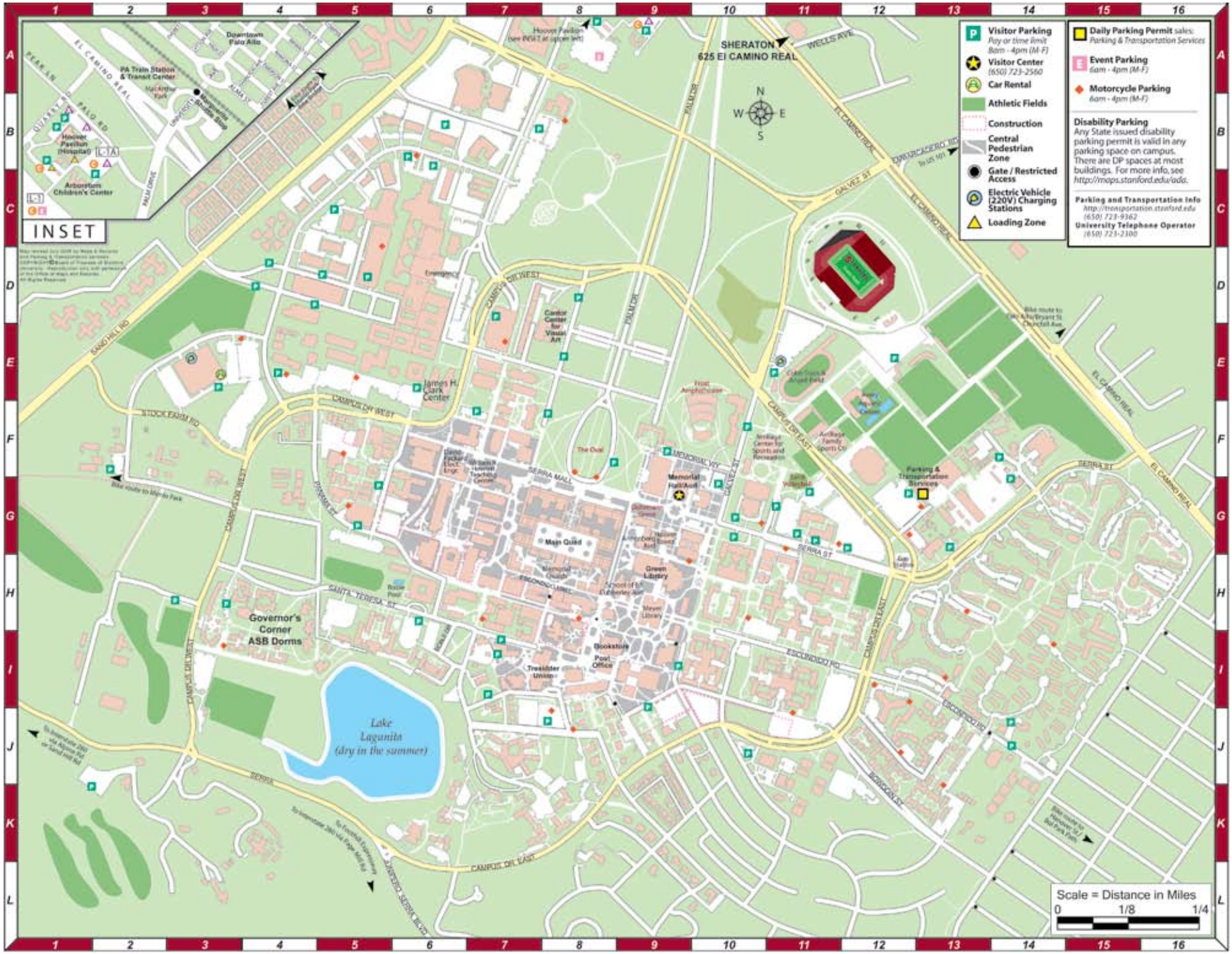
INSET
Downtown Palo Alto
PA Train Station & Transit Center
Hoover Pavilion (Hospital)
Arboretum Children's Center
SHERATON
625 El CAMINO REAL
Visitor Parking
Pay or time limit
8am - 4pm (M-F)
Visitor Center
(650) 723-2560
Car Rental
Athletic Fields
Construction
Central Pedestrian Zone
Gate / Restricted Access
Electric Vehicle (220V) Charging Stations
Loading Zone
Daily Parking Permit sales:
Parking & Transportation Services
Event Parking
6am - 4pm (M-F)
Motorcycle Parking
6am - 4pm (M-F)
Disability Parking
Any State issued disability parking permit is valid in any parking space on campus. There are DP spaces at most buildings. For more info, see http://maps.stanford.edu/ada.
Parking and Transportation Info
http://transportation.stanford.edu
(650) 723-9362
University Telephone Operator
(650) 723-2300
Governor's Corner
ASB Dorms
Lake Lagunita
(dry in the summer)
Main Quad
The Oval
Memorial Hall/Auditorium
Green Library
Bookstore
Post Office
Tresidder Union
James H. Clark Center
Cantor Center for Visual Art
Parking & Transportation Services
Scale = Distance in Miles
0 1/8 1/4

	Wed, Aug 22, 2007	Thurs, Aug 23, 2007	Fri, Aug 24, 2007	Sat, Aug 25, 2007
7:30 AM	**Breakfast**	**Breakfast**	**Breakfast**	**Breakfast**
8:15 AM		**Welcome**	**Memorial**	**Announcements**
8:30 AM				
8:45 AM	**OpenSim workshop (8am-5pm)** **Clark Center Room S360**	**Keynote Address** **Memorial Auditorium** **Franz Goller**	**Keynote Address** **Memorial Auditorium** **Paul Selvin**	**Borelli Lecture** **Memorial Auditorium** **Richard Lieber**
9:00 AM				
9:15 AM				
9:30 AM		**Break**	**Break**	**Break**
9:45 AM				
10:00 AM		**Podium 1** **Motor Control I** Memorial Auditorium **Podium 2** **Methods I** Annenberg Auditorium **Podium 3** **Bone I** Cubberley Auditorium	**Podium 13** **Locomotion Energetics** Memorial Auditorium **Podium 14** **Hand** Annenberg Auditorium **Podium 15** **Knee** Cubberley Auditorium	**Podium 25** **Aging II** Memorial Auditorium **Podium 26** **Computational Biomech. II** Annenberg Auditorium **Podium 27** **Sports II** Cubberley Auditorium
10:15 AM				
10:30 AM				
10:45 AM		**Break**	**Break**	**Break**
11:00 AM				
11:15 AM		**Podium 4** **Aging I** Memorial Auditorium **Podium 5** **Computational Biomech. I** Annenberg Auditorium **Podium 6** **Erg. & Occ. Biomech. I** Cubberley Auditorium	**Podium 16** **Comparative Biomechanics** Memorial Auditorium **Podium 17** **Muscle Mechanics** Annenberg Auditorium **Podium 18** **Rehabilitation** Cubberley Auditorium	**Podium 28** **Motor Control II** Memorial Auditorium **Podium 29** **Methods II** Annenberg Auditorium **Podium 30** **Bone II** Cubberley Auditorium
11:30 AM				
11:45 AM				
12 NOON				
12:15 PM				
12:30 PM		**Lunch Boxes / Exhibits**	**Lunch Boxes / Exhibits**	**Lunch Boxes**
12:45 PM				
1:00 PM		**Dohrmann Grove**	**Student Luncheon with ASB Founding Members** **Dohrmann Grove**	**Women in Science Luncheon** **Tresidder Union**
1:15 PM	**Tutorial I** **Biomechanical Modeling and Simulation** **Scott Delp** **Clark Center**	**Tours I** **Durand Building** **Biomotion Lab** **Arrillaga Center Human Performan Lab**		
1:30 PM				
1:45 PM				**Awards Session - Memorial Auditorium** ASB Pre-Doctoral Young Scientist Award ASB Post-Doctoral Young Scientist Award
2:00 PM		**Podium 7** **Walking** Memorial Auditorium **Podium 8** **Injury** Annenberg Auditorium **Podium 9** **Sports I** Cubberley Auditorium	**Podium 19** **Neuro-rehabilitation** Memorial Auditorium **Podium 20** **Motor Injury** Annenberg Auditorium **Podium 21** **Erg. & Occ. Biomech. II** Cubberley Auditorium	**James Hay Lecture** Dr. Benno Nigg
2:15 PM				
2:30 PM				
2:45 PM				
3:00 PM		**Break**	**Break**	
3:15 PM	**Tutorial 2** **Molecular Biology in Biomechanics** **Richard Lieber** **Clark Center**	**Tours 2** **Clark Center** **Neuromuscular Biomechanics** **3D Radiology Lab**		
3:30 PM				**ASB Business Meeting** **Memorial Auditorium**
3:45 PM		**Podium 10** **Running** Memorial Auditorium **Podium 11** **Upper Extremity** Annenberg Auditorium **Podium 12** **Tendon & Ligament** Cubberley Auditorium	**Podium 22** **Mechanics** Memorial Auditorium **Podium 23** **Muscle** Annenberg Auditorium **Podium 24** **Rehabilitation I** Cubberley Auditorium	
4:00 PM				**Closing Ceremonies**
4:15 PM				
4:30 PM				
4:45 PM				
5:00 PM				
5:15 PM	**ASB Executive Board Meeting** **Clark Center**	**Poster Session / Exhibits**	**Poster Session / Exhibits**	**ASB Executive Board Meeting**
5:30 PM				
5:45 PM				
6:00 PM	**Reception** **(Clark Center)**			
6:15 PM		**Night on the town**	**Conference Dinner** **(Frost Amphitheater)**	
6:30 PM				
6:45 PM				
7:00 PM				

WHIPLASH CAUSES INCREASED LAXITY OF CERVICAL CAPSULAR LIGAMENT

Paul C. Ivancic, Shigeki Ito, Yasuhiro Tominaga, Wolfgang Rubin,
Marcus P. Coe, Anthony B. Ndu, Erik J. Carlson, Manohar M. Panjabi

Biomechanics Research Laboratory, Yale University School of Medicine, New Haven, CT, USA
E-mail: paul.ivancic@yale.edu

INTRODUCTION

Whiplash neck injuries, caused by relative acceleration between the head and thorax during motor vehicle collisions, produce acute and chronic neck pain, headache, dizziness, and parasthesias in the upper extremities. Clinical studies have targeted the cervical facet joints and capsular ligaments (CLs), as sources of chronic pain in whiplash patients (Barnsley et al., 1995; Lord et al., 1996). The purpose of this study was to determine whether whiplash caused increased CL laxity by applying quasi-static loading to whiplash-exposed and control bone-CL-bone preparations.

METHODS

Facet-CL-facet specimens were prepared from 12 osteoligamentous whole cervical spines (6 whiplash-exposed and 6 control) (Tominaga et al., 2006). The whiplash-exposed spines had been previously rear impacted using the incremental trauma protocol at a maximum peak T1 horizontal acceleration of 8 g (Ivancic et al., 2005). All spines had no history of any disease that could have affected the osteoligamentous structures. The spines were divided into two equal groups with each group consisting of three whiplash-exposed and three control spines. Facet-CL-facet specimens were prepared using C2/3, C4/5, and C6/7 spinal levels in the first group and C3/4, C5/6, and C7/T1 spinal levels in the second group. Left and right facet-CL-facet specimens from each spinal level were prepared separately and then mounted for mechanical testing (**Figure 1**). In total, 66 facet-CL-facet specimens were prepared.

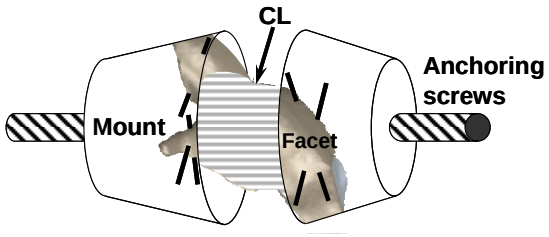

Figure 1. Facet-CL-facet preparation.

Each specimen was mounted in a custom designed, displacement-controlled mechanical testing apparatus (Panjabi et al., 1996). To standardize the neutral CL position, the facets were preloaded to 1 N of compression immediately prior to testing and this was defined as zero CL elongation. The facet-CL-facet specimen was elongated at 1 mm/s in increments of 0.05 mm until a tensile force of 5 N was achieved and subsequently was returned to neutral position. Force and elongation data were recorded at each motion step following a 0.5 second rest period. Four pre-conditioning cycles were performed and data from the load phase of the fifth cycle were used for subsequent analyses.

CL elongation was computed at tensile forces of 0, 0.25, 0.5, 0.75, 1, 2.5, and 5 N. Data from left and right CLs and all spinal levels were combined within each group. Students unpaired t-tests ($P<0.05$) were performed to determine significant differences in CL elongation between the whiplash-exposed and control groups.

RESULTS

The force-elongation curve is shown for each whiplash-exposed CL (**Figure 2A**), control CL (**Figure 2B**), along with the average curves (**Figure 2C**).

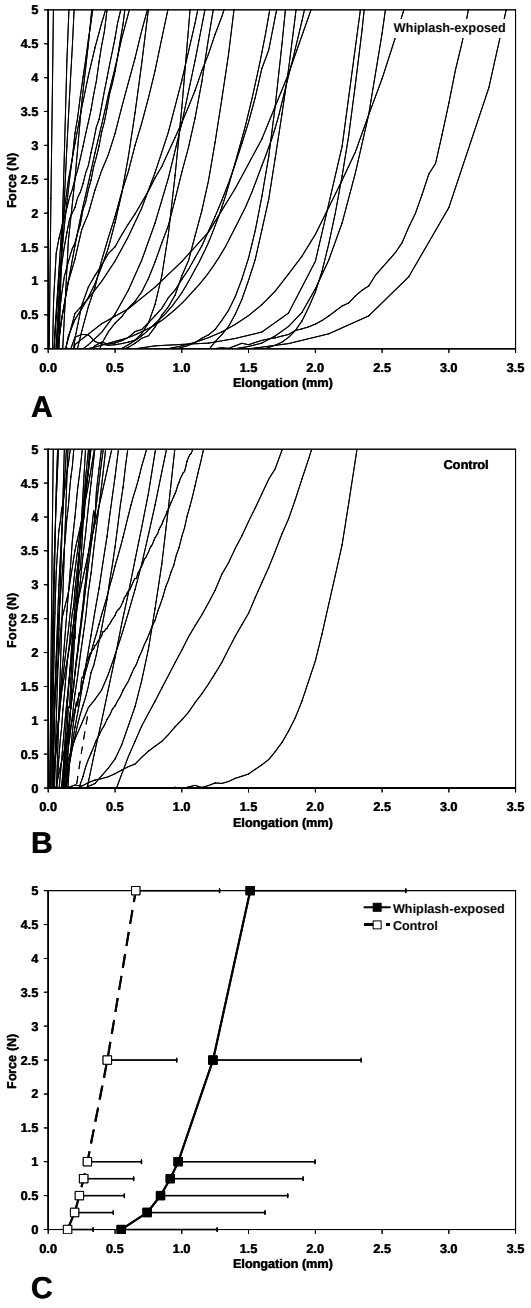

Figure 2. CL force-elongation curves: A) whiplash-exposed, B) control, C) averages.

The average elongation of the whiplash-exposed CLs was significantly greater than that of the control CLs at each tensile force. The difference between the average elongation of the whiplash-exposed and control CLs progressively increased from 0.4 mm (P=0.021) at 0 N to 0.9 mm (P=0.007) at 5 N.

DISCUSSION AND CONCLUSIONS

Whiplash injuries and the causes of the resulting chronic symptoms are not fully understood. The present study documented statistical increases in CL laxity due to whiplash. The average force-elongation curves were nonlinear, with greater flexibility at low forces and increasing stiffness at higher forces. Greater flexibility was generally observed in the whiplash-exposed CLs, as compared to the control CLs, particularly at low forces. Increased CL laxity due to whiplash may lead to chronic pain and clinical instability.

REFERENCES

Barnsley, L.et al. (1995). *Spine,* **20**, 20-25; discussion 26.

Ivancic, P.C.et al. (2005). *Eur Spine J,* **14**, 346-355.

Lord, S.M.et al. (1996). *Spine,* **21**, 1737-1744; discussion 1744-1735.

Panjabi, M.M.et al. (1996). *J Orthop Res,* **14**, 216-222.

Tominaga, Y.et al. (2006). *BMC Musculoskelet Disord,* **7**, 103.

ACKNOWLEDGEMENTS

This research was supported by NIH Grant 1 RO1 AR45452 1A2.

OBSTACLE AVOIDANCE WITH VARYING ABILITY TO SPATAIALLY ORIENT ATTENTION FOLLOWING MILD TRAUMATIC BRAIN INJURY

Robert D. Catena, Charlene I. Halterman, Paul van Donkelaar, and Li-Shan Chou

Department of Human Physiology, University of Oregon, Eugene, OR, USA
E-mail: chou@uoregon.edu, Web: http://biomechanics.uoregon.edu/MAL/

INTRODUCTION

Safety during motor tasks is imperative to decreasing the likelihood of permanent brain damage following mild traumatic brain injury (mTBI). Crossing over an obstacle is a real-world task that has revealed conservative adaptations by mild (Catena et al 2007) and severe TBI populations (McFadyen et al 2003). Reduced performance during this task could result in trips, and subsequent brain injuries. The spatial orientation component of attention allows for the disengagement, shift and reengagement of attention to quickly and accurately process information and formulate a response. Deficits in the spatial orientation of attention have been shown following mTBI (Halterman et al. 2006). Recently, obstacle avoidance during reaching has been proposed as a parietal lobe process (Schindler et al. 2004), similar to where spatial orientation of attention is said to occur. The purpose of this study was to examine how the spatial orientation of attention is correlated to obstacle crossing performance, specifically following mTBI and during recovery from such an injury.

METHODS

Seventeen grade II mTBI subjects were tested within 48 hours post-injury. Testing was repeated at 6, 14 and 28 days post-injury. Seventeen gender, age, stature and athletic participation matched controls were tested at four equivalent intervals. Markers located between the 2nd and 3rd metatarsals of each foot just proximal to the metatarsophalangeal joints were tracked with an 8-camera motion analysis system. Obstacle clearance heights (toe marker to obstacle) were measured for each foot during walking. Two walking tasks were conducted: single task obstacle-crossing at 10% of body height (OB), and with a concurrent attention dividing cognitive task (DOB). After each testing session, the spatial orienting of attention was measured with an Attentional Network Test (ANT). Linear regressions were performed between the spatial orientation of attention effect size and each obstacle crossing parameter during each day and within each group. Two-way ANOVAs were performed between group and day for each task.

RESULTS AND DISCUSSION

Individuals following mTBI demonstrated deficits in spatial orientation only at the first testing session. No significant group differences were detected for obstacle clearances.

Without a secondary cognitive task, only lead clearance over an obstacle seems to have a significant relationship with an ability to spatially orient attention following an mTBI. Specifically, obstacle clearance height (OC) was directly related to an ability to effectively spatially orient attention following an mTBI, but not in healthy individuals (Table 1). The relation between spatial orientation of attention and obstacle

crossing clearance exhibited signs of decreasing as healing progressed.

While performing a secondary cognitive task, both lead foot and trailing foot clearance over an obstacle seems to have a significant relationship with an ability to spatially orient attention following an mTBI. We found that obstacle clearance heights of both feet are directly related to an ability to effectively spatially orient attention following an mTBI, but not in healthy individuals (Table 1). The relation between spatial orientation of attention and obstacle clearance also tended to decrease as healing progressed.

The results from this study indicate that as one is able to spatially orient attention better, the lead foot is lifted higher to avoid obstacle contact. This could prove important for mTBI subjects that have been shown to suffer from deficits in the spatial orientation of attention immediately following an injury. When attention is divided, there is a significant relationship between obstacle clearance of each foot and increased spatial orientation. As one is able to spatially orient attention better, both feet are lifted higher over the obstacle. This would seem to indicate that mTBIs use a more conservative strategy for crossing with both feet when attention is divided but spatial orientation of attention is still intact. One caveat to these results is that the spatial effect was usually only able to predict around 27% of the variance in each of the mentioned variables. This leaves other factors to play an important role in obstacle clearance parameters, including natural human variation.

SUMMARY/CONCLUSIONS

Measuring a concussed individual's ability to avoid obstacles is of particular relevance, but may not always be feasible in clinical examinations. This study may support the use of either one of these tests to predict performance in the other following mild traumatic brain injury.

REFERENCES

Catena, R.D. et al. (2007) *Gait & Posture* **25**, 406-411.

Halterman**,** C.I. et al. (2006) *Brain* **129**, 747-753.

McFadyen, B.J. et al. (2003) *J Head Trauma Rehabil* **18**, 512-525.

Schindler, I. et al. (2004) *Nature Neurosci* **7**, 779-784.

ACKNOWLEDGEMENTS

This study was supported by the Center for Disease Control and Prevention (R49/CCR023203).

Table 1: R^2 values reported indicate the linear relationship between spatial orientation of attention and the given obstacle variable for the given task, group and day. *P*-values are shown in parentheses.

Task	Foot Clearance	Group	Time (days)			
			<2	5-7	13-15	27-29
OB	Lead	mTBI	**.294 (.037)**	**.282 (.028)**	.176 (.093)	.182 (.100)
		Cont.	.041 (.455)	.055 (.382)	.073 (.293)	.017 (.618)
DOB	Lead	mTBI	**.477 (.004)**	.099 (.218)	.094 (.232)	.185 (.096)
		Cont.	.045 (.411)	.005 (.801)	.131 (.153)	.029 (.514)
	Trailing	mTBI	**.265 (.050)**	.174 (.095)	.048 (.396)	.050 (.486)
		Cont.	.080 (.273)	.055 (.382)	.044 (.418)	.054 (.370)

3D FINITE ELEMENT SIMULATION OF BONE REMODELLING UNDER THE TIBIAL COMPONENT OF AN OXFORD KNEE REPLACEMENT

Hans A Gray[1] Amy B Zavatsky[1], and Harinderjit S Gill[2]

[1] Dept of Engineering Science, University of Oxford, UK
[2] Nuffield Department of Orthopaedic Surgery (NDOS), University of Oxford, UK
E-mail: amy.zavatsky@eng.ox.ac.uk

INTRODUCTION

Two distinct types of radiolucency can be observed at the bone-implant or bone-cement interface. The first type is usually thicker than 2mm, has no definite boundary, and is usually an indication that the implant is loose [1]. The second type has a distinct boundary and is usually less than 2mm thick. This type is commonly seen under the Oxford Unicompartmental Knee Replacement (OUKR) (Biomet, Swindon, UK) tibial component and is not an indication that the implant is loose [2]. Confusion about the two types of radiolucency has led to unnecessary revisions of OUKRs [3].

Histological studies of retrieved implants have shown that soft tissues such as fibrocartilage and fibrous tissue are formed at the bone-implant interface. There is evidence that radiolucency is a result of this tissue, but the reasons for this tissue formation are not entirely understood. Similar tissue formation takes place in the callus during fracture healing.

The aim of the current study was to investigate whether tissue remodeling rules proposed for fracture healing can explain formation of radiolucencies under OUKRs.

METHODS

A 3D finite element (FE) model of the medial half of the proximal 75mm of a tibia implanted with a cemented OUKR was created and run over 365 iterations linked with a simple remodelling rule. The model consisted of 110,555 ten-node tetrahedral elements and was based on a previously experimentally validated FE model of a complete human cadaveric tibia with an OUKR tibial component [4]. The model was initially run under a load of 1157N perpendicular to the implant, the peak load seen by the medial plateau of the tibia of an 82kg (mass of cadaveric tibia donor) person during normal gait [5]. The model was also run under 578N (half load) and 2314N (double load).

After each iteration, new material properties were calculated for elements in a 2mm thick remodelling area which was adjoining the bone cement. An element's new material property was a function of the stress-strain condition [6] at its centre of gravity, its current material property, and a rate of change. The rate of change was set so that an iteration represented roughly a day of in vivo remodelling. It was assumed that these elements represented granulation tissue before the first iteration with Young's modulus and Poisson's ratio assumed to be 0.2MPa and 0.47 respectively.

The material properties of the elements which represented bone were changed based on a set of established remodelling rules [7]. The initial properties of these elements were calculated from radiographic density (RD) values from CT scans [8].

The variation of material properties of each element was plotted against the iteration number in order to visualise the evolution of material properties with time (iterations).

Next "synthetic AP radiographs" were generated by reverse calculating RDs from material properties for the model after 365 iterations. Comparisons were made between these plots and patient AP radiographs.

RESULTS AND DISCUSSION

The material properties of the remodelling zone stabilised after about 365 iterations, which is consistent with stabilisation of radiolucent lines which occurs about a year after surgery [3].

Application of smaller loads resulted in more of the elements in the 2mm remodelling zone turning to bone than did the application of larger loads, suggesting that radiolucency is related to patient weight or activity level (Figure 1). An investigation is now being carried out using patient follow-up radiographs to find out if this in fact is the case.

In the trabecular bone adjacent to the 2mm remodeling zone an increase in RD was observed. A similar observation was made on some of the radiographs where a sclerotic line was observed just below the radiolucent line (Figure 1).

Although based on a simple remodelling rule, the model was able to simulate the formation of soft tissue in a realistic manner, providing synthetic radiographs which compared well with patient radiographs.

REFERENCES

1. Ritter M.A., et al. (1999). *J Bone Joint Surg Br*, **81**, 982-986.
2. Tibrewal S.B., et al. (1984). *J Bone Joint Surg Br*, **66**, 523-528.
3. Goodfellow J, et al. (2006). *Unicompartmental Arthroplasty with the Oxford Knee*, Oxford University Press.
4. Gray, H.A., et al. (2006). *Proc Brit Orthop Res Soc*, 35-36 (OP11).
5. D'Lima, D.D., et al. (2006). *J Arthroplasty*, **21**, 255-262.
6. Claes L.E., Heigele, C. A. (1999). *J Biomech*, **32**, 255-266.
7. Beaupre G.S., et al. (1990). *J Orthop Res*, **8**, 651-661.
8. Rho, J.Y. et al. (1995). *Med Eng Phys*, **17**, 347-355.

ACKNOWLEDGEMENTS

Hans Gray was funded by a Felix Scholarship at the University of Oxford.

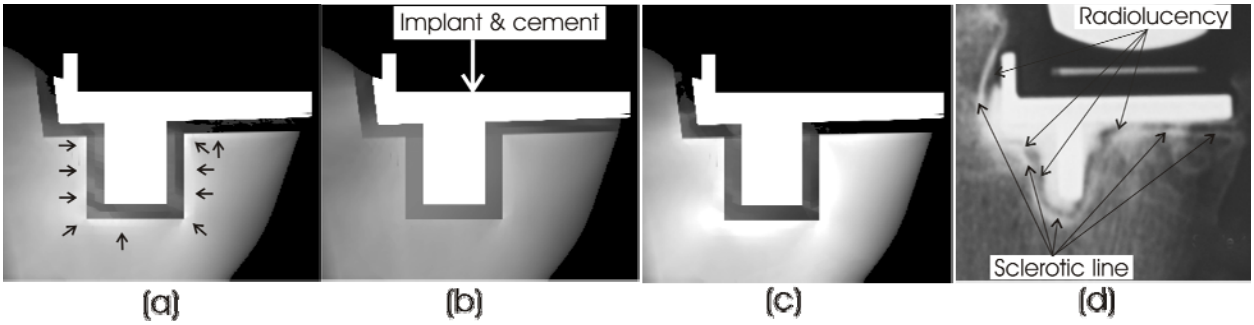

Figure 1: "Synthetic radiographs" (a, b, and c) and patient radiograph (d). (a) 1157N load (b) half load and (c) double load applied on implant. Radiolucency (the dark area under the implant) in increasing order – (b) < (a) < (c). Arrows in (a) point to stiffened bone.

JOINT LOADS AND BONE STRAINS ASSOCIATED WITH A RESURFACED FEMORAL HEAD

Jason P. Long[1], Christopher T. Cheng[1], and Donald L. Bartel[1,2]

[1] Cornell University, Ithaca, NY; [2] Hospital for Special Surgery, New York, NY
E-mail: jpl38@cornell.edu

INTRODUCTION

In the short-term, the primary mode of failure for hip resurfacing systems is femoral neck fracture near the implant rim (Shimmin, 2005), which may be associated with damage accumulation in this region. Bone damage caused by localized yielding and low-cycle fatigue is associated with high strains (Haddock, 2004; Morgan, 2001). Additionally, likely due to patient selection, motion analysis during normal walking has shown that hip resurfacing patients produce significantly larger adduction/abduction and flexion/extension hip moments than traditional hip replacement patients (Mont, 2007). These larger moments may result in larger joint loads that would increase the likelihood of high strains forming within the femoral neck.

The purposes of this study were: 1) to calculate joint loads associated with hip resurfacing patients and compare these loads to those in patients with traditional hip replacements, 2) to analyze the effect of hip resurfacing on bone strains near the implant rim using the calculated joint loads and nonlinear finite element analysis.

METHODS

The hip loads were calculated using a quasi-static, reduction model (Paul, 1967). Mean and standard deviations for the peak hip abduction and extension moments associated with hip resurfacing and traditional hip replacement patients (Mont, 2007) were used to determine the distribution of hip joint loads (head, abductor, and extensor loads) for each patient group. Since ground reaction forces associated with these moments were not provided, a distribution of the head load direction was based on data from telemetrically implanted patients (Bergmann, 1993 & 2001). Additionally, force equilibrium was constrained by requiring the vertical component of the resultant forces across the hip to equal 1.1BW (Crowninshield, 1979). This approach gave a distribution of joint loads, and ten consecutive draws from these distributions were analyzed for each patient group.

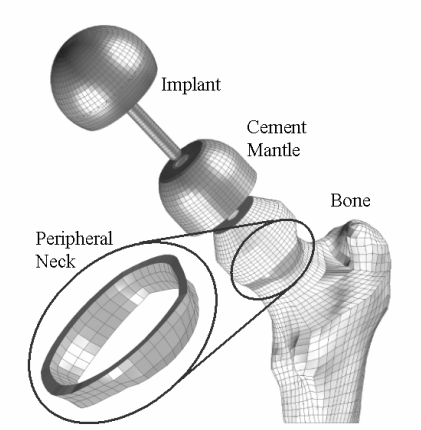

Figure 1: An exploded view of the finite element model of the implanted bone showing the peripheral neck near the implant rim.

Finite element (FE) models of a bone were created from computed tomography (CT) scans for the intact (pre-op) and implanted (immediate post-op) cases. The bone-implant system consisted of the surgically-altered bone, a cement mantle, and an

implant (Fig. 1). Bone material properties were assigned element by element using empirical relationships between CT number, apparent density, and elastic modulus (Morgan, 2003). Head and abductor loads were applied to the FE models based upon the ten draws for the hip resurfacing patient group. To analyze the potential for neck fracture, max. and min. principal strains were analyzed in the peripheral bone near the implant rim (Fig. 1).

RESULTS

The head load magnitudes for the hip resurfacing patient group were 3.12$\pm$0.32BW compared to 2.66$\pm$0.39BW for the traditional hip replacement group ($P < 0.05$). For the hip resurfacing group, the head load components were -0.88$\pm$0.26BW medial, 0.33$\pm$0.03BW posterior, and -2.96$\pm$0.31BW superior; the abductor load components were 0.71$\pm$0.09BW medial, -0.16$\pm$0.02BW posterior, and 1.52$\pm$0.20BW superior.

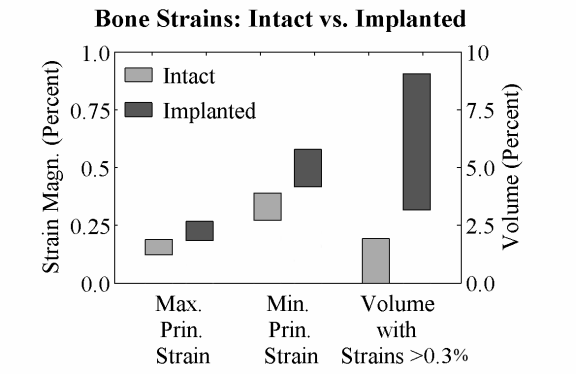

Figure 2: The range of peak principal strains in the peripheral neck and the percent volume of this region with large compressive strains were substantially higher for the implanted compared to the intact bone.

Comparing the intact to the implanted bone, the peak max. and min. principal strains in the peripheral neck increased in magnitude for each load trial, and for all load trials the range of strain magnitudes was substantially higher for the implanted bone compared to the intact bone (Fig. 2). Additionally, the percent volume of the peripheral neck that had min. principal strain magnitudes greater than 0.30% (Burr, 1996) was substantially higher for the implanted compared to the intact bone (Fig. 2).

DISCUSSION

Hip joint loads were found to be significantly higher in the hip resurfacing group compared to the traditional hip replacement group. Additionally, the strains in the peripheral neck, associated with these larger joint loads, were substantially higher in magnitude for the implanted bone compared to the intact bone. This increase in bone strain indicates a possibility of damage accumulation in the femoral neck due to localized yielding and low-cycle fatigue (Haddock, 2004; Morgan, 2001), which may be associated with short-term neck fracture after hip resurfacing.

REFERENCES

Bergmann G et al. (1993). *J Biomech*, **26**, 969-990

Bergmann G et al. (2001). *J Biomech*, **34**, 859-871

Burr DB et al. (1996). *Bone*, **18**, 405-410

Crowninshield RD et al. (1978). *Clin Orthop Relat Res*, **132**, 140-144

Haddock SM et al. (2004). *J Biomech*, **37**, 181-187

Mont MA et al. (2007). *J Arthroplasty*, **22**, 100-108.

Morgan EF, Keaveny TM (2001). *J Biomech*, **34**, 569-577

Morgan EF et al. (2003). *J Biomech*, **36**, 897-904

Paul JP (1967). *Proc Inst Mech Eng*, **181**, 8-15

Shimmin AJ et al. (2005). *Orthop Clin N Am*, **36**, 187-193

REVISITING THE EMG-TORQUE RELATIONSHIP OF THE TRUNK MUSCULATURE: EFFECTS OF ANTAGONISTIC CO-CONTRACTION

Stephen H.M. Brown and Stuart McGill

Department of Kinesiology, University of Waterloo, Waterloo, ON, Canada
E-mail: shmbrown@uwaterloo.ca

INTRODUCTION

The use of electromyographic signals in the modeling of muscle forces and joint loads requires an understanding of the relationship between the acquired electrical signals and their generated joint torques. This relationship has been studied for the trunk extensor musculature and predominantly been shown to be non-linear (Stokes et al., 1987; Potvin et al., 1996), with a reducing increase in torque output for a given increase in electrical activity. This relationship has been studied very limitedly in the abdominal musculature (rectus abdominis only), with similar results (Stokes et al., 1989). However, in neither case has the effect of torque produced by muscles acting antagonist to the dominant moment been thoroughly considered. Thus, the purpose of this study was to reveal the sensitivity of the EMG-torque relationship of the trunk musculature to the consideration of antagonist muscle torque.

METHODS

Eight healthy male individuals sat with knees supported and a harness secured across the upper torso and attached to a wall. Participants were instructed to slowly generate either isometric extensor or flexor trunk torques from rest to maximum and back to rest. This was done both with an upright neutral torso, and with the torso flexed to 50% of maximum about the hips. EMG was recorded from 6 bilateral abdominal muscles and 8 bilateral extensor muscles. EMG was rectified, LP filtered (2.5 Hz) and, using an anatomically detailed biomechanical model, an estimation was made of the torques generated by both the extensor and abdominal musculature. The agonist muscle torques (abdominal muscles in the flexor condition and back muscles in the extensor condition) were then either linearly or non-linearly normalized to maximum and compared (RMS difference) to: 1) externally calculated torque alone; 2) externally calculated torque combined with antagonist muscle torque.

RESULTS AND DISCUSSION

A great deal of co-activation between the abdominal and extensor muscle groups occurred in each condition. Thus, the degree and form of non-linearity in the EMG to torque relationship depended heavily on whether or not antagonist muscle activity was considered. When antagonist activity was not considered the relationship was slightly non-linear, similar to previous work (Stokes et al., 1987; Potvin et al., 1996). The relationship was consistently more non-linear when torques were generated in the 50% flexed posture, and consistently more non-linear in the abdominal as compared to the extensor muscle groups. However, when the additional muscle torque generated by the antagonist muscle groups was accounted for, the relationship became much more linear, displaying only very slight non-linearities.

Most striking, these slight non-linearities were opposite to those previously found experimentally, with rising increases in torque outputs for a given increase in electrical activity. It is interesting to note that this opposite non-linear form has been theorized using motor unit driven models of EMG (Milner-Brown & Stein, 1975; Fuglevand et al., 1994). Figure 1 displays the EMG-FlexorMoment (50% hip flexion) relationship in both cases: where antagonist muscle activity has not (A) and has (B) been accounted for.

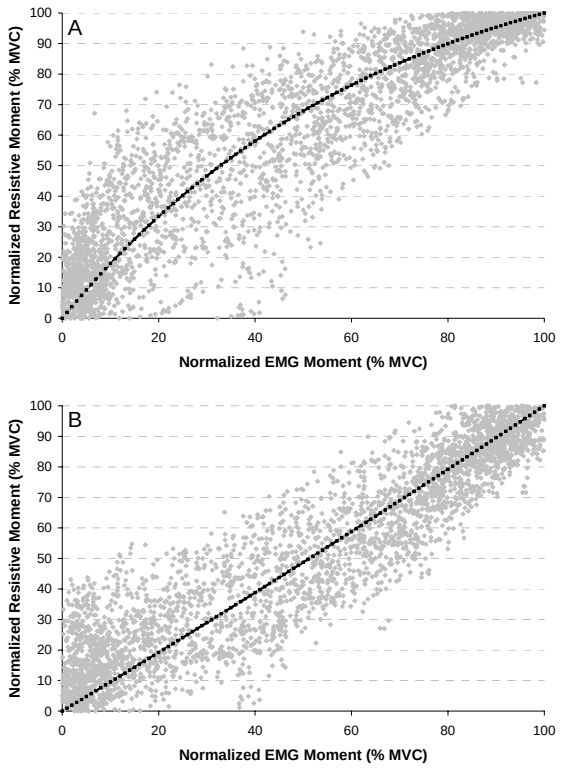

Figure 1: Scatterplots (all participants and trials) for the Flexor Moment 50% flexed condition displaying the Agonist EMG Moment normalized to 100% of maximum versus the Resistive Moment normalized to 100% of maximum. A: Resistive Moment is the externally calculated moment alone; B: Resistive Moment is the combined externally applied moment and antagonist muscle moment.

Finally, the non-linear differences between abdominal and extensor muscle groups were reduced when antagonist activity was accounted for.

SUMMARY/CONCLUSIONS

Proper modeling of the EMG-torque relationship of the trunk musculature requires consideration of the activity of both agonist and antagonist muscles, at least for the type of isometric exertions studied here. This study suggests that the relationship is primarily linear, and that non-linear impressions are most likely due to disproportionate antagonist activity as torso muscles increase force. It also appears that very little difference exists between the EMG-torque relationship between the trunk extensor and abdominal musculature; therefore they can be treated in a similar manner during the EMG processing stage.

REFERENCES

Fuglevand, A.J. et al. (1993). *J. Neurophysiology*, **70**, 2470-2488.

Milner-Brown, H.S., Stein, R.B. (1975). *J. Physiology*, **246**, 549-569.

Potvin., J.R. et al. (1996). *Eur. J. Appl. Physiol.*, **74**, 119-132.

Stokes, I.A. et al. (1987). *Spine*, **12**, 770-776.

Stokes, I.A. et al. (1989). *Spine*, **14**, 857-861.

LOWER LIMB FORCE PRODUCTION AND BILATERAL FORCE ASYMMETRIES ARE BASED ON SENSE OF EFFORT

Ann M. Simon[1] and Daniel P. Ferris[1]

[1]Human Neuromechanics Laboratory, University of Michigan, Ann Arbor, MI, USA
E-mail: asimon@umich.edu

INTRODUCTION

Humans control force production in their limbs by using an internal model of musculoskeletal mechanics to calculate appropriate neural signals (Wolpert & Ghahramani 2000). Subjects produce less force during an isometric force matching task when one limb is fatigued (Carson et al. 2002), presumably because they have not updated their internal model. Carson et al. (2002) also found that upper limb force production after fatigue scales with maximum voluntary strength. This suggests that individuals use a sense of effort (Gandevia & McCloskey 1977), rather than proprioceptive feedback, to gauge upper limb force production.

We have adopted the isometric force matching task used by Carson et al. (2002) to study normal force asymmetry in the lower limbs of humans. The goal of this study was to determine if force asymmetry during bilateral force production results from a neural mechanism related to sense of effort. We hypothesized that subjects attempting to produce equal forces in their lower limbs would generate equal percentages of their bilateral maximum voluntary strength rather than equal absolute limb forces. If true, this could provide critical insight into the neural origins of lower limb force asymmetry during movement.

METHODS

Ten healthy subjects performed isometric lower limb extensions on a leg press exercise machine (Figure 1). We recorded individual limb forces from a dual force platform and muscle activity from electromyography electrodes. We assessed subjects' isometric strength with three trials each of bilateral, left limb, and right limb maximum voluntary contractions (MVC) in a randomized order with three minutes rest between trials. Lower limb MVC values were determined as the peak force measured within the three trials of each condition. We identified the stronger limb as the limb that produced the higher peak force during the bilateral MVC condition.

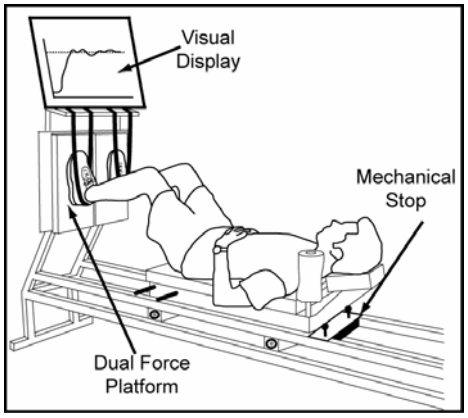

Figure 1. Leg press exercise machine.

After a ten minute rest period, we assessed subjects' ability to match forces in their lower limbs with nine force matching trials. Subjects were asked to exert a force using the stronger limb equal to 20, 40, or 60% of the peak force recorded from the weaker limb during the bilateral MVC condition. Subjects received visual feedback of the target force level and the stronger limb force. When subjects reached the target force level in the stronger limb, they began applying force with the weaker limb. Subjects verbally signaled to the experimenter once they believed they had matched forces in both lower limbs. No

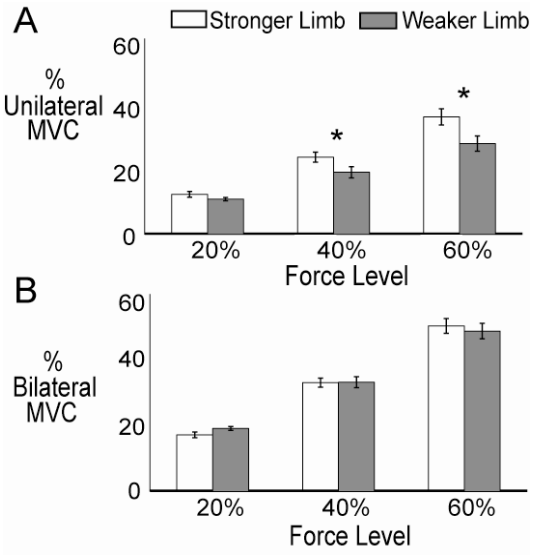

Figure 2. Average forces for all subjects during three different levels of force matching. Force levels were 20%, 40%, and 60% of the maximum force recorded at the weaker limb during the bilateral MVC condition. A) Forces normalized to unilateral MVC for each limb show significant differences for 40% and 60% force levels. B) Forces normalized to bilateral MVC shows no differences between limbs. Error bars are standard error of the mean.

feedback was given about weaker limb force. Subjects performed three trials at each of the three force levels in a randomized order. Subjects were unaware of the study's purpose and which limb produced more force during the bilateral MVC condition.

For all force matching trials, we calculated the average force applied by each limb for three seconds after subjects indicated they believed the forces were equal. We normalized foot forces to a) each limb's unilateral MVC and b) to each limb's bilateral MVC. We used a repeated measures ANOVA and Tukey-Kramer Honestly Significant Difference (HSD) post-hoc tests to determine if there were differences between limbs and force levels.

RESULTS AND DISCUSSION

MVC trials showed significant differences in peak force between limbs and conditions (ANOVA, $p < 0.001$). Subjects produced average peak forces of 1143 N ± 130 N (mean ± s.e.m.) and 904 N ± 111 N for their stronger and weaker limbs during bilateral MVC trials, respectively (interlimb difference $p < 0.05$). Subjects produced average peak forces of 1625 N ± 180 N and 1582 N ± 157 N for their stronger and weaker limbs during unilateral MVC trials, respectively (interlimb difference $p > 0.05$). All subjects demonstrated a decrease in the peak force generated during the bilateral MVC trials when compared to the unilateral MVC trials for each limb ($p < 0.05$).

During the force matching trials, subjects consistently produced less force in their weaker limb during both the 40% and 60% force matching levels as a percentage of their unilateral MVC force ($p < 0.05$) (Figure 2A). However, normalizing force magnitudes by bilateral MVC forces revealed no significant differences between limbs at all three force matching levels (ANOVA, $p=0.8506$) (Figure 2B).

CONCLUSIONS

These results indicate that normal limb force asymmetry during bilateral activation has a neural origin. Regardless of whether humans produce maximal or submaximal forces, limb force asymmetry results from an uneven neural drive to the lower limbs. Our findings have implications for bilateral asymmetries during movement in healthy and neurologically impaired populations such as individuals with post-stroke hemiparesis.

REFERENCES

Carson, R.G. et al. (2002). *J Physiol*, **539**(Pt 3), 913-25.

Gandevia, S.C., McCloskey, D.I. (1977). *Brain* **157**(1), 32-42.

Wolpert, D.M., Ghahramani Z. (2000). *Nat Neurosci,* **3**(Suppl), 1212-1217.

ACKNOWLEDGEMENTS

Supported by NIH R01NS045486 and NSF GRFP.

BAYESIAN TECHNIQUES IMPROVE HUMAN MOTION ESTIMATION

Friedl De Groote Tinne De Laet Ilse Jonkers, and Joris De Schutter

Katholieke Universiteit Leuven, Leuven, Belgium
E-mail: friedl.degroote@mech.kuleuven.be

INTRODUCTION

During motion analysis the motion of the human body is derived from the position of surface mounted markers. Important sources of measurement errors are soft tissue artifacts (STA) and noise. Data processing is based on a generic, kinematic model with degrees of freedom q. The traditional approach, inverse kinematics (IK), estimates q by a nonlinear least squares fit between the measured marker positions and the model. By estimating q at each time step separately, the a priori knowledge that human motion is smooth can not be included. Furthermore, numerical differentiation of q leads to large errors on q' and q'' and will therefore influence the joint reaction torques T.

Cerveri et al. (2005) describe the use of a Kalman filter to estimate q. This method allows us to use the knowledge about the smoothness of the motion and to estimate q, q' and q'' simultaneously along with a covariance which reflects the reliability of the estimate. In this abstract, we show that Kalman smoothing yields significantly better results than Kalman filtering. A comparison of our results and those obtained with IK implemented in SIMM is presented for both q and T. The proposed method is applied to a simulated as well as to an experimental gait motion.

METHODS

Bayesian filtering and smoothing techniques are based on a process and a measurement model. The nth order process model, used for prediction, describes the joint motion assuming $q^{(n)}$ to be constant. The measurement model, used for correction, describes the relation between the states (q … $q^{(n)}$) and the measurements (the marker positions) and is based on the musculoskeletal model provided in SIMM (Delp, 1990). Modeling and measurement errors are accounted for by considering well chosen uncertainty in both models.

The developed framework is first validated in simulation and is thereafter applied to and evaluated on experimentally obtained gait data. In simulation, STA are modeled by a systematic error on the simulated marker positions proportional to q with an order of magnitude of 10mm over the motion range (S1). Noise is simulated by corrupting the simulated marker positions with Gaussian noise with mean 0 and standard deviation 1mm (S2). In simulation the true states are known, allowing a comparison between the estimation errors ε_{est} on the IK estimates and on the Bayesian estimates:

$$\varepsilon_{est} = 100 \frac{\sqrt{\frac{1}{N}\sum_{t=1}^{N}(q^*(t) - q(t))^2}}{\max(q) - \min(q)},$$

with q^* the estimate of q, t time and N the number of time samples. In the experimental case, the estimations are based on a subset of the measured markers, whereas the other markers are used as validation markers. The positions of these validation markers are calculated from q^*. The discrepancy between the calculated and measured positions of the validation markers is a measure for the quality of q^*.

RESULTS AND DISCUSSION

For the simulated case, table 1 shows ε_{est} obtained by IK and three different Bayesian techniques for 6 out of the 21 estimated degrees of freedom. More importantly, in view of application to inverse dynamic calculations, figure 1 shows that for both S1 and S2, 3rd order Kalman smoothing yields a much better estimate of the minimum and maximum joint torques than IK (relative percentage error reduced by factor 2 (S1), 12 (S2)). In the experimental case, one marker on the thigh is used for estimation while two markers on the same cluster are used for validation. Figure 2 shows that for all three markers the RMS distance between their calculated and measured position is smaller for 3rd order Kalman smoothing than for IK.

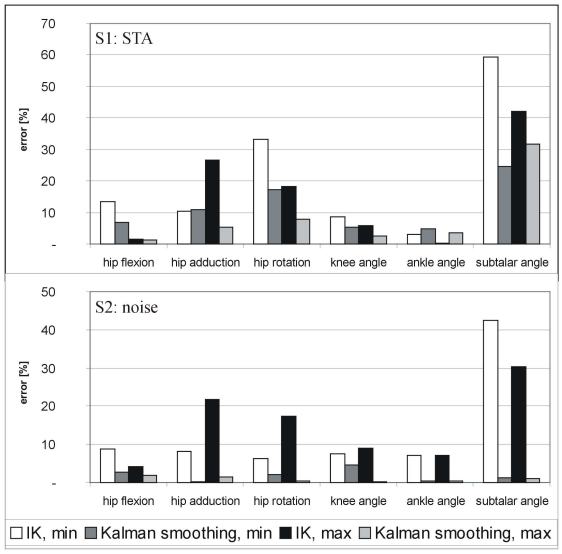

Figure 1: Percentage relative error on the minimum and maximum joint torques for the right leg (S1: top, S2: bottom).

CONCLUSIONS

Our results show that the use of 3rd order Kalman smoothing substantially improves the estimate of joint kinematics and kinetics as compared to the currently used techniques: inverse kinematics implemented in SIMM and 2nd order Kalman filtering proposed by Cerveri et al. (2005). Furthermore we can show that the local marker estimation technique of Cerveri et al. (2005) is only applicable to a limited number of markers.

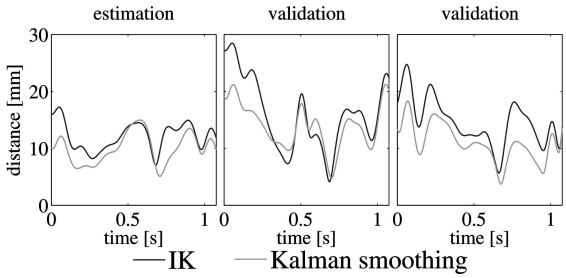

Figure 2: RMS distance between calculated and measured position of thigh markers.

REFERENCES

Cerveri, P. et al. (2005). *J. Biomech.*, **38**, 2228-2236

ACKNOWLEDGEMENTS

Friedl De Groote and Tinne De Laet are Research Assistants of the Research Foundation – Flanders (FWO-Vlaanderen). Ilse Jonkers is a Postdoctoral Fellow of the Research Foundation – Flanders.

Table 1: Pecentage error on the estimates of the generalized coordinates of the right leg obtained by four different methods for a simulated gait motion corrupted by noise (S1) or STA (S2).

estimation error	hip flexion		hip adduction		hip rotation		knee angle		ankle angle		subtalar angle	
	noise	STA	noise	STA	noise	STA	noise	STA	noise	STA	noise	STA
inverse kinematics	1,04	2,90	6,37	8,93	12,2	13,0	0,33	1,25	1,87	4,82	2,34	10,2
Kalman filter (n = 2)	0,44	2,63	0,76	6,12	1,76	13,4	0,22	1,24	1,28	4,81	1,55	10,1
Kalman smoothing (n = 2)	0,24	2,62	0,39	6,13	0,93	13,4	0,13	1,26	0,62	4,79	0,77	10,1
Kalman smoothing (n = 3)	0,23	2,62	0,36	6,13	0,88	13,4	0,11	1,25	0,56	4,80	0,69	10,1

IN VITRO VALIDATION OF A DYNAMIC FINITE ELEMENT TKR MODEL

Joel L. Lanovaz [1] and Randy E. Ellis [2]

[1] University of Saskatchewan, Saskatoon, SK, Canada
[2] Queen's University, Kingston, ON, Canada
E-mail: joel.lanovaz@usask.ca

INTRODUCTION

The objective of this study was to develop and validate a 3D dynamic finite element (FE) model of a total knee replacement (TKR) that could be used to simulate implant mechanics under functional loading conditions.

To date, dynamic FE TKR models have mainly been used to simulate implant testing environments (Godest *et al*, 2002). The ability to simulate the loading conditions and movement constraints experienced by a TKR in vivo would greatly enhance understanding of knee implant mechanics. Recently, dynamic FE models that simulate the implanted environment have begun to appear (Halloran *et al*, 2005; Barink *et al*, 2005). The model presented here is unique by virtue of 1) representing the full degrees of freedom (DOF) of all components (femur, tibia and patella) simultaneously under the control of a quadriceps load and 2) validation by direct comparison with in vitro kinematic and force data. The model is capable of reproducing experimental data as well as predicting responses to perturbations.

METHODS

A knee specimen was prepared by resecting all tissue surrounding the joint, leaving the joint capsule and quadriceps muscle. A posterior-cruciate-retaining TKR (PFC Sigma, Size 4, DePuy, Warsaw, IN), including patellar resurfacing, was implanted by an experienced orthopaedic surgeon using standard procedures. The specimen was mounted in a modified Oxford rig (Zavatsky, 1997) and a 6 DOF force transducer (MC3A-250, AMTI, Watertown, MA) was placed at the distal tibia in line with the bone. Kinematic tracking arrays (Optotrak 3020, NDI, Waterloo, ON) were fixed to the femur, tibia and patella and a probe was used to register the implant components and bones to corresponding computer models.

Kinematic and force data were collected as the knee joint was extended via a cable fixed to a clamp on the quadriceps muscle. The cable was wound by a motor attached to the proximal femur (cable velocity 16 mm/s). Trials were performed at Q-angles of 10° and 15°. Afterwards, the specimen was dissected and insertion locations of the major ligaments were recorded with the probe.

The Oxford rig was simulated with the non-linear dynamic explicit FE code LS-DYNA (LSTC, Livermore, CA) using built-in penalty-based mechanical joints to simulate the various connections in the rig. Rigid masses were used to connect the various joints together and to model the inertial properties of the rig. Hexahedral FE meshes with element edge lengths of 1.0 mm were constructed for the TKR components based on CAD representations of the implants. The femoral component was modelled as rigid, while the UHMWPE tibial insert and patellar button were represented using a non-linear elastic-plastic material model. The bones were considered rigid and the tibial insert was fixed to the tibia. A coefficient of friction of 0.09 was used.

Six ligament bundles were modelled (LCL, superficial MCL, deep MCL, PMC, anterior PCL and posterior PCL) along with the patellar ligament and the quadriceps muscle. For each bundle, nine non-linear cable elements were used. Stiffness and reference strain values were obtained from the literature and insertion locations relative to the femoral and tibial components were generated from the experimental data. Registration data from the experimental trials were used to set initial poses. Simulations were performed for both Q-angles.

RESULTS AND DISCUSSION

The 3D joint kinematics for the tibiofemoral joint (TFJ) and patellofemoral joint (PFJ), along with ankle joint reaction forces and moments, were extracted from the simulations and compared to data from the experimental trials. Trends for individual trials were evaluated along with the changes due to the Q-angle increase.

The simulated TFJ kinematics produced trends of motion that were consistent with the experimental data. The simulations had a TFJ varus angle offset along with an internal rotation relative to the experimental data, possibly due to a lack of posterior-lateral soft tissues in the model. The simulated PFJ kinematics produced correct trends but were offset from the experimental data with an increased medial tilt and medial spin. The reaction force and moment data were reproduced accurately by the simulation with only minor offsets.

The increase in Q-angle produced a valgus and lateral shift in the experimental TFJ kinematics which were not reproduced well in the simulation. However, the increased medial tilt and lateral spin observed for the PFJ were accurately simulated. The Q-angle change produced a lateral force shift and varus moment shift that were both captured by the simulations (Figure 1).

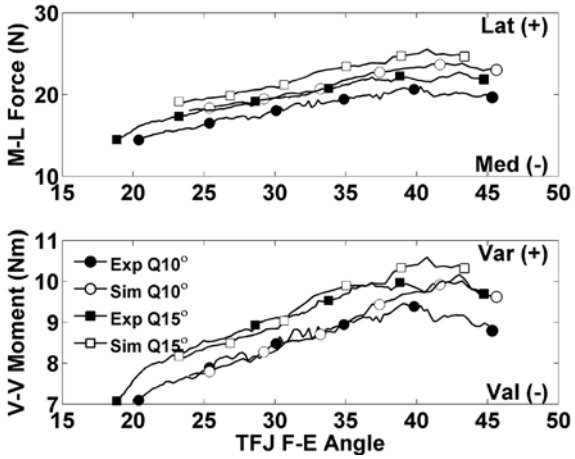

Figure 1: Comparison of experimental (Exp) and simulated (Sim) medial-lateral (M-L) forces and varus-valgus (V-V) moments for both Q-angles (Q10° & Q15°) as a function of TFJ flexion (F-E) angle.

SUMMARY/CONCLUSIONS

A unique 3D dynamic TKR model has been presented that simulates full TFJ and PFJ function during a weight bearing extension motion controlled by quadriceps loading. The model was validated by direct comparison to an in vitro experiment and was able to reproduce measured kinematic and reaction force data. Changes in PFJ kinematics and reaction force data due to an increase in Q-angle were accurately predicted by the model.

REFERENCES

Godest, A.C. et al. (2002) *J. Biomech.*, **35**:267–275.
Halloran, J.P. et al. (2005) *J. Biomech.*, **38**:323-331.
Barink, A. et al. (2005) *Proc. I. Mech. E. Part H*, **219**:415-424
Zavatsky, A.B. (1997) *J. Biomech.*, **30**:277-280

The Effect of Manipulating Subject Mass on Lower Extremity Torque Patterns During Locomotion

John K. DeWitt[1], Ronita L. Cromwell[2] and R. Donald Hagan[3]

[1]Bergaila Engineering Services, Houston, TX, USA; [2]The University of Texas Medical Branch, Galveston, TX, USA; [3]NASA Johnson Space Center, Houston, TX, USA
email: john.k.dewitt@nasa.gov

INTRODUCTION

During locomotion, humans adapt their motor patterns to maintain coordination despite changing conditions (Reisman et al., 2005). Bernstein (1967) proposed that in addition to the present state of a given joint, other factors, including limb inertia and velocity, must be taken into account to allow proper motion to occur.

During locomotion with added mass counterbalanced using vertical suspension to maintain body weight, vertical ground reaction forces (GRF) increase during walking but decrease during running, suggesting that adaptation may be velocity-specific (De Witt et al., 2006). It is not known, however, how lower extremity joint torques adapt to changes in inertial forces.

The purpose of this investigation was to examine the effects of increasing body mass while maintaining body weight upon lower-limb joint torque during walking and running. We hypothesized that adaptations in joint torque patterns would occur with the addition of body mass.

METHODS

Vertical GRF was measured while ten subjects (5M/5F) walked (1.34 $m \cdot s^{-1}$) and ran (3.13 $m \cdot s^{-1}$) on a Kistler Gaitway treadmill (Amherst, NY). Sagittal plane kinematics were obtained using an optical motion capture system (Smart Elite System, BTS Bioengineering Spa, Milanese, IT).

Subjects completed trials with 5 added mass (AM) conditions (0%, 10%, 20%, 30% and 40% of body mass) applied in random order. The added mass was achieved by having subjects wear a weighted vest (X-Vest, Perform Better, Cranston, RI). Body weight was maintained using a pneumatic unweighting system (H/P/Cosmos Airwalk, Nussdorf-Traunstein, Germany).

Ten consecutive strides were analyzed after each subject achieved steady-state within each trial. Left hip and knee joint torques were computed using inverse dynamics. Positive torques represent hip and knee extension. Positive and negative angular impulse (AI) for each joint was found during the stance and swing phase of each stride, respectively. Trial means for each variable were computed for each condition.

Analysis of variance with repeated measures was used to determine the affect of AM conditions on angular impulse. Separate analyses were conducted for walking and running. Tukey-Kramer post-hoc tests were used to determine differences when a significant AM effect ($p<0.05$) was found.

RESULTS AND DISCUSSION

For all conditions, knee flexor torque dominated during the early stance phase of walking (see Figure 1), which is contrary to the presence of extensor torque reported in literature (De Vita et al., 1996). This may be a specific characteristic of treadmill

locomotion that is not apparent during overground gait.

During the stance phase, hip extensor AI increased with AM during walking, but was not affected during running. Hip flexor AI increased with AM during running, but was unaffected during walking. Knee extensor AI was not affected by AM, but knee flexor AI increased with AM during running.

During the swing phase, AM did not affect hip AI during walking, but both flexor and extensor AI decreased with increasing AM during running. Knee extensor AI decreased with increasing AM during both walking and running. Knee flexor AI during swing was unaffected by AM in either gait mode.

SUMMARY/CONCLUSIONS

Our findings suggest that when mass is increased while maintaining body weight, adaptations in joint torques occur that are specific to each locomotion style (walking or running). Hip and knee AI were affected by AM, but the effects were different between walking and running, and were inconsistent. It appears that the control system adapts differently to walking with AM than running.

REFERENCES

Bernstein, NA. (1967). *The Coordination and Regulation of Movements*, 15-59.

Reisman, D. et al. (2005). *J Neurophysiol*, ***94***, *2403-2415*.

De Witt, J. et al. (2006). *ASB Annual Meeting, www.asbweb.org/conferences/ 2006/pdfs/160.pdf*.

De Vita, P et al. (1996). *J Biomech*, **26**, 583-588.

AKNOWLEDGEMENTS

We would like to thank the Exercise Countermeasures Program at NASA – Johnson Space Center for funding this study.

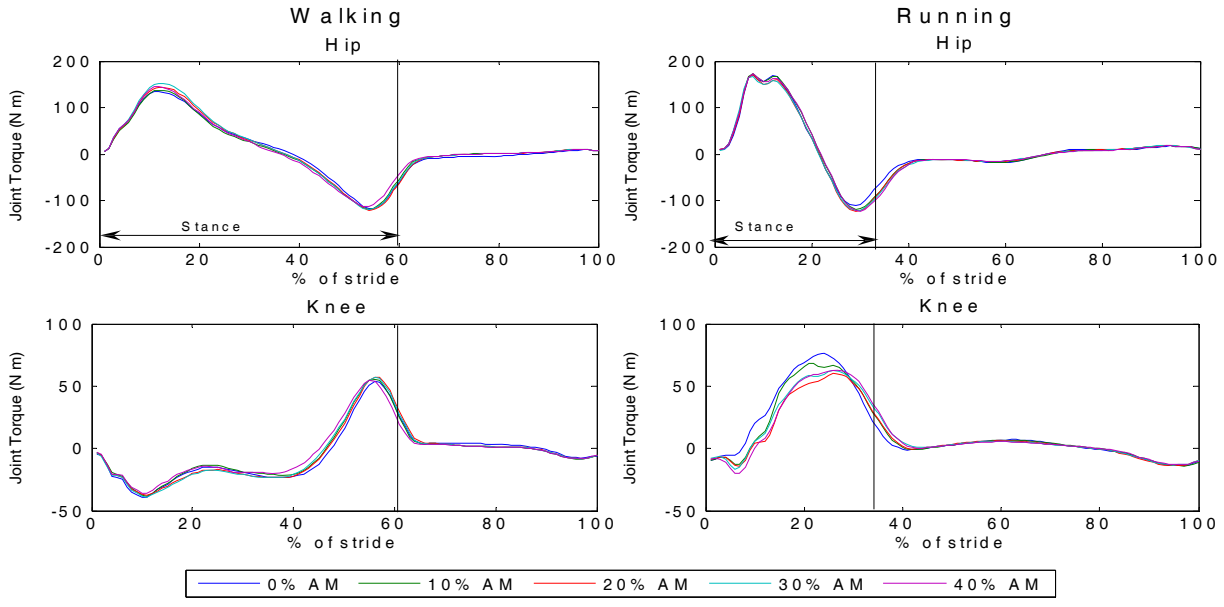

Figure 1. Hip and knee joint torque trajectories during walking and running. Extensor torques are positive and flexor torques are negative.

TEMPOROMANDIBULAR JOINT KINEMATICS IN OSTEOARTHRITIC PATIENTS PRE- AND POST-SURGERY: THE COMBINATION OF ELECTROMAGNETIC MOTION DATA WITH PATIENT-SPECIFIC CT IMAGES

Kristin D. Zhao [1], Matthew F. Koff [1], Evre Baltali [1,2] , Eugene E. Keller[2], and Kai-Nan An[1]
[1] Orthopedic Biomechanics Laboratory, Mayo Clinic, Rochester, MN, USA
[2] Department of Surgery, Mayo Clinic, Rochester, MN, USA

E-mail: zhao.kristin@mayo.edu

INTRODUCTION

The temporomandibular joint (TMJ) of the jaw is a unique and complex structure composed of a concave articular surface (fossa) on the temporal bone, a convex articular surface (condylar head) on the mandible and a bi-concave fibrocartilagious articular disc inter-positioned between the two bony structures. Motion of the articulating disc is constrained by surrounding ligaments. Interruption of normal articular disc motion causes temporomandibular joint disorders (TMDs). TMDs are characterized by altered disc displacement and osteoarthritis of the joint.

Surgical intervention provides relief of pain and improvement in quality of life for patients, especially in end-stage advanced TMJ osteoarthritis (OA), when bone-on-bone contact and/or fibroosseous ankylosis cause unbearable conditions for patients. Therefore, understanding joint mechanics and kinematics of the TMJ is essential for determining proper treatment of the TMJ during OA.

Previous studies have typically assessed TMJ function and surgical outcomes subjectively by patient response questionnaires and objectively by measuring the borderline movement of the incisors (Mercuri, 2004;Wolford et al., 2003; Nitzan et al., 2001). However, more recently, investigators (Gallo, 2005) have suggested the combination of medical imaging and kinematic data acquisition methods represent and quantify the motion of the condyles and incisors with greater accuracy.

The purpose of this study was to quantify movement of the mandibular condyles and the incisors in TMJ OA patients before and after TMJ metal fossa-eminence hemi-joint replacement surgery. These motions were quantified using an electromagnetic motion tracking system combined with patient-specific CT images.

METHODS

Fourteen patients with TMJ OA were enrolled in the study according to IRB guidelines prior to receiving a hemi-joint implant. Subjects were fit with custom plastic dental stents. Six 0.8 mm diameter metal beads were embedded in the stents on the vestibular surface of all four first molars and both upper and lower central incisors. The stents were form fitted and no adhesive materials were required to fix them to the teeth.

The subjects wore the dental stents on their upper and lower teeth during both the CT imaging and the kinematic recording sessions. CT scans were obtained on a 64-slice MDCT system (Sensation 64, Siemens, Forchheim, Germany). Locations of the metal beads and the volumetric centroids of the condyles were obtained in the CT coordinate system using Analyze image analysis software (Robb et al., 1989).

Pre-and post-operatively, an electromagnetic tracking device (Polhemus, Inc.) and accompanying software (The Motion Monitor, Innovative Sports Training, Inc., Chicago, IL) were used to record the three-dimensional kinematics of the mandible relative to the temporal bone in the in-vivo coordinate system. A calibrated Plexiglas digitizing probe was used to locate the metal bead locations within the in-vivo coordinate system. Four trials of maximal opening-closing movements were performed starting and ending in the maximum intercuspal position.

The transformation between the two coordinate systems (in-vivo and CT) was determined using the 3D positions of the metal beads (Fig. 1). The CT image data (including the condyle centers and incisor locations) were then transformed to the in-vivo coordinate system for analysis and animation.

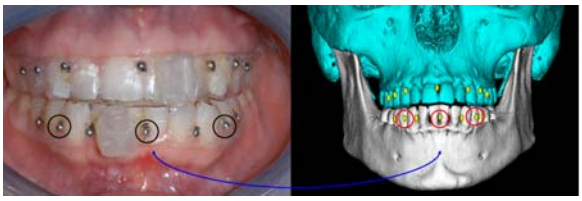

Figure 1: Kinematic data and CT images were aligned using markers on the upper and lower custom dental stents.

Three opening portions of the mandibular movements were selected from the trial with the greatest mouth opening. Condylar and incisor linear distances (LD, 3D distance), and curvilinear distance (CP, length along 3D path) were calculated for incisor and condylar points defined from the CT images during jaw opening and closing. Rotation of the mandible was evaluated using helical axis parameters.

RESULTS AND DISCUSSION

The mean calculated LD and CP traveled by the incisors increased significantly from 30.36 mm ± 6.87 mm and 31.53 mm ± 7.03 mm pre-operatively, to 35.52 mm ± 5.28 mm and 36.58 mm ± 5.52 mm post-operatively ($p<0.05$), respectively. The mandibular rotation significantly increased from $19.30^{o}\pm4.92^{o}$ pre surgically to $24.81^{o}\pm3.86^{o}$ degrees post surgically. Condylar LD and CP values did not change significantly from pre- to post-implant surgery.

SUMMARY/CONCLUSIONS

This kinematic method documented preservation of operated and unoperated condyle motion, improved incisal opening and increased mandibular body rotation and allowed for objective measures of surgical outcome. More advanced analysis methods including helical axis locations and orientations, and inter-boney (joint space) distances will highlight the benefits and applicability of TMJ kinematic analysis in a clinical setting.

REFERENCES

Gallo, L.M. (2005) *Cells Tissues Organs*; **180**, 54-68.

Mercuri, L.G. et al. (2004). *J Oral Maxillofac Surg*; **62**, 1088-96.

Nitzan, D.W. et al. (2001). *J. Oral Maxillofac Surg*; **59**, 1154-59.

Robb, R.A. et al. (1989) *Comput Med Imaging Graph*; **13**, 433-54.

Wolford, L.M. et al. (2003). *J Oral Maxillofac Surg*; **61**, 685-90.

ACKNOWLEDGEMENTS

This project was supported by The Mayo Clinic Department of Surgery, Rochester, MN and the National Institutes of Health (NIAMS: F32 AR053430-01).

RELIABILITY OF LOWER EXTREMITY ANTHROPOMETRIC MEASUREMENTS AND THEIR EFFECT ON WOBBLING MASS TISSUE PREDICTION

Timothy A. Burkhart, Katherine Teigrob, and David M. Andrews

University of Windsor, Windsor, ON, Canada
E-mail: burkha3@webmail1.uwindsor.ca

INTRODUCTION

Many biomechanical models of the lower extremities do not take into consideration soft tissue motion effects relative to bone. The motion of segmental soft tissues or wobbling masses (WM) has been shown to significantly influence the magnitude of impact kinetics (Gruber et al., 1998). Since there is a lack of information regarding WM tissues for living people that can be put into such models, Holmes et al. (2005) developed and validated regression equations to predict the WM of the lower extremity (thigh, leg, and leg and foot segments) of young healthy adults. These equations require inputs such as segment length, circumference, breadth and skin-fold thickness, and subject data such as height, weight and sex. However, the reliability of these measurements and the effect on predicted WM estimates from the equations has yet to be determined. Therefore, the purposes of this study were to measure the inter- and intra-measurer reliability of the anthropometric dimensions necessary as inputs into the prediction equations (Holmes et al., 2005), and to quantify the effects on the predicted WM magnitudes.

METHODS

Fifty participants (25 males and 25 females with a mean (S.D.) age of 22.5 (2.79) years, height 1.72 (0.09) m and mass of 72.3 (13.3) kg), were recruited from the University of Windsor population. Two measurers were each responsible for collecting two sets of unilateral measurements from the right upper and lower limb (the upper limb data were recorded for a subsequent study). 9 upper limb and 10 lower limb anatomical landmarks were marked with 0.64 cm diameter stickers that were used to quickly identify the start and end points of the segment dimensions. Following landmark identification, segment measurements were taken using standard measuring equipment (soft measuring tape, anthropometer, and callipers). 6 lengths, 6 circumferences, 8 breadths, and 4 skin-fold thicknesses for the upper and lower limbs were acquired. Measurements were made in different planes (e.g. frontal, sagittal) and at different points on each segment (e.g. proximal, midway, distal), where possible. Landmark stickers were removed and a new set attached before the second set of measurements took place. Once the second set of measurements were collected by the first measurer, the second measurer followed with the identical protocol. Mean differences in measurements between and within measurers were statistically evaluated using ANOVA, and correlational analyses (Intra-class correlation coefficients or ICCs) were conducted using a 2-way random effects model for absolute agreement (Weir, 2005) to quantify reliability. The four sets of measurements were input into the prediction equations of Holmes et al. (2005) to produce WM tissue estimates for both attempts by each measurer. Differences in tissue estimates were quantified in terms of percent error and RMSerror.

RESULTS AND DISCUSSION

Significant differences were found between measurers and between sexes ($p<0.05$) in half of the measurement sites. However, the mean measurement differences were relatively small in general (e.g. 90% of between-measurer differences were < 1 cm).

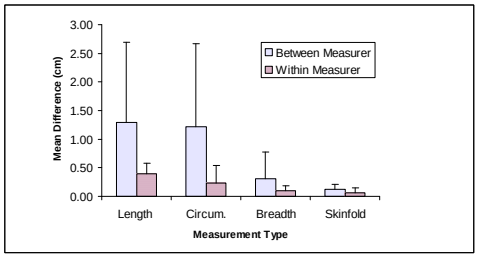

Figure 1: Mean (S.D.) measurement type differences by segment.

Differences between attempts were found not to be statistically significant for almost all the measurements. Mean measurement type differences were also small ranging from only 0.13 to1.29 cm for skinfold and lengths, respectively (Figure 1). Circumference differences were higher on average because of the compressibility of the soft tissues. These types of measurements were less affected where they occurred around bony processes with little underlying soft tissue. Discrepancies in landmark positions between measurers led to higher length differences overall.

The average measurement type ICCs were 0.79, 0.86, 0.85 and 0.86 for lengths, circumferences, breadth and skinfolds, respectively, which indicates good to excellent reliability. Measurement site ICCs also showed good to excellent reliability (mean ICC = 0.84). The higher reliability within-measurer vs. between-measurer was expected as small differences in marker placement between measurers were noted. Difference in placement of a single marker could contribute to errors in multiple measures (e.g. the location of the mid-calf marker has an effect on one circumference, one length, and two breadth measurements).

WM magnitude predictions were moderately affected by the measurement differences with maximum errors of 13.3% and 4.7% for between- and within-measurers, respectively (Table 1).

Table 1: Mean RMSerror and % error in WM predictions.

Segment	Mean (S.D.)	RMSe	% Error	
			Btwn	Within
Thigh	8443.82 (1369.13)	218.92	13.3	0.9
Leg	2817.24 (393.71)	147.43	9.2	4.7
Leg and Foot	3469.97 (509.71)	172.35	10.7	3.6

SUMMARY/CONCLUSIONS

Overall, the measurement differences between- and within-measurers were found to be small, with within-measurer estimates more consistent than between. Almost all measurements had high to excellent reliability. The WM predictions from the equations were moderately affected by the measurement differences, but within-measurer effects were considerably lower in general. This highlights the importance of measurer training and limiting the number of measurers in large scale studies when the WM prediction equations will be used.

REFERENCES

Gruber, K. et al. *J. Biomech.*; **31**: 439-444, 1998

Holmes, J. D. et al. *J. Appl. Biomech.*; **21**: 371-382, 2005.

Weir, J., P. *J. Streng. Cond. Res.*; **19**: 231-240

ACKNOWLEDGEMENT

This study was funded by NSERC.

FUNCTIONAL IMPLICATIONS OF OPTIMAL MUSCLE FIBER LENGTHS OF THE ANKLE PLANTARFLEXORS

Edith M. Arnold[1], Samuel R. Ward[3, 4], Richard L. Lieber[4, 5] and Scott L. Delp[1,2]

Departments of [1]Mechanical Engineering and [2]Bioengineering, Stanford University, Departments of [3]Radiology, [4]Orthopaedic Surgery and [5]Bioengineering, University of California and Department of Veterans Affairs Medical Centers, San Diego, CA
E-mail: emarnold@stanford.edu Web: http://www.stanford.edu/group/nmbl

INTRODUCTION

Computer models of the lower limb that characterize the geometry and force-generating properties of muscles are widely used. Models of the lower limb have been created primarily from descriptions of muscle architecture published by Wickiewicz et al. (1983) and Friederich and Brand (1990). These reports of muscle architecture were based on a small number of subjects, three and two, respectively, and the models that incorporate these data have several limitations. One important limitation is that lower-limb models predict that the ankle plantarflexors generate force over a more narrow range of ankle angles than human subjects do (Delp et al., 1990). Two possible reasons for this discrepancy are; the assumption that all fibers within a muscle are the same length is incorrect or the fiber lengths reported in previous studies are incorrect.

Ward et al. recently measured lower extremity muscle architecture in 20 subjects (submitted to ASB 2007). The purpose of our study was to evaluate the functional consequences of the new architecture data—specifically, to model how differences in the optimal fiber lengths of the ankle plantarflexors affect their force-generating capacities over a range of ankle angles.

METHODS

We developed two models of the ankle plantarflexors. The first was based on data reported by Wickiewicz et al. (1983) and the second was based on the data reported by Ward et al. (2007). The two models had identical bone geometry, muscle paths, and joint kinematics. As a result, differences in the relationship between muscle fiber length and ankle angle arose solely from differences in muscle architecture.

Wickiewicz et al. (1983) reported the cross-sectional area of gastrocnemius as a single muscle instead of separating the two heads. For the model based on these data, we divided cross-sectional area between the two compartments according to proportions used by Delp et al. (1990).

For the model based on the optimal fiber lengths reported by Ward et al., we estimated tendon slack lengths (L^T_s) by making adjustments until we obtained the L^T_s value that produced a fiber length that matched the experimentally derived fiber lengths at the same joint angles measured in the specimens. This process resulted in tendons that produced too much passive force during dorsiflexion. We lengthened the tendons slightly, 9.0, 6.1, and 6.6% for soleus, and medial and lateral gastrocnemius respectively, so that passive forces were more consistent with experimental results (Siegler 1988).

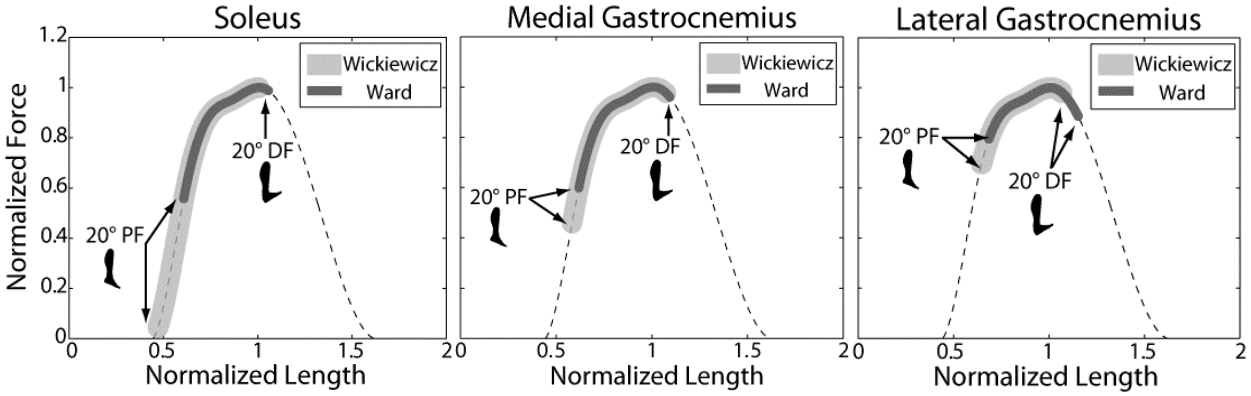

Figure 1: Normalized force-length curves for soleus, and medial and lateral gastrocnemius. The models of soleus and medial gastrocnemius with properties based on the architecture data of Ward et al. (2007) operate on a more narrow region of the force-length curve and maintain greater force-generating capacity over a 20° plantarflexion to 20° dorsiflexion range of motion than models of these muscles based on architecture data from Wickiewicz et al. (1983).

RESULTS AND DISCUSSION

Average optimal fiber length of soleus was significantly longer in the data from Ward et al. (2007) compared to the data reported by Wickiewicz et al. (1983; Table 1). This produced a substantial change in the force-generating characteristics of the soleus. Soleus was able to exert a greater fraction of its maximum force over the 20° plantarflexion to 20° dorsiflexion range of motion with the longer fiber length (Figure 1). Additionally, the slightly longer fibers of the medial gastrocnemius reported by Ward et al. increased the muscle's force-generating capacity over the range of motion. Lateral gastrocnemius had similar fiber lengths in the two data sets; thus, the range of operating lengths was similar in the two models.

These changes represent a significant improvement for musculoskeletal modeling because the plantarflexors are predicted to exert force over a broader, more experimentally-consistent range of ankle angles than previous models. This result is particularly important for creating simulations of actions such as walking and jumping in which the plantarflexors generate large moments about the ankle. Previous simulations based on shorter fiber lengths result in over-activation of these muscles to compensate for the fact that they were predicted to exert low forces when the ankle joint was plantarflexed.

Table 1: Mean optimal fiber lengths ± SD (cm) for the major plantarflexors in the two data sets.

	Wickiewicz	**Ward**
Soleus	2.39±0.09*	4.40±0.99 §
Medial Gas	4.34±0.43**	5.10±0.98 §
Lateral Gas	6.22±1.19**	5.88±0.95 §

* n = 2; ** n = 3; § n = 20

REFERENCES

Delp, et al., (1990) *IEEE Trans. Biomed. Eng.*, **37**, 557-567.

Freiderich and Brand (1990), *J. Biomech.*, **23**, 91-95.

Siegler et al. (1988) *J. Biomech. Eng.,* **110**, 264-373

Wickiewicz et al. (1983), *Clin. Orthop. Rel. Res.*, **179**, 275-283.

ACKNOWLEDGEMENTS

The Stanford Bio-X Program, NIH grants 1042779-2-PAGKZ, HD048501 and HD050837.

STEPPING AEROBICS: HOW DO THE STEPPING DIRECTION AND HEIGHT AFFECT JOINT KINETICS?

Man-Ying Wang [1], and Hsin-Chang Wu [2]

[1] University of Southern California, Los Angeles, CA, USA
[2] National Cheng Kung University, Tainan, Taiwan
E-mail: mwang@usc.edu

INTRODUCTION

Stepping aerobics are getting popular because of its similarity to daily living activities, accessibility to general population, safety to practice, and adjustable intensity with various forms (i.e., varying stepping speed, height, and direction) (Wang et al, 2003). Unfortunately, musculoskeletal loadings associated with this popular exercise program are rarely quantified. Thus, prescribing stepping aerobics as a potential intervention program for improving physical function has become difficult. The purpose of this study is using biomechanical methods to systemically quantify the influence of stepping regimen including 2 different directions (forward and lateral stepping) and 3 different step heights (6, 8, and 10 inches) on joint kinetics in healthy adults.

METHODS

Fifteen male and fifteen female healthy adults, aged from 19 to 29 years, participated in this study. Eighteen reflective markers were attached to anatomical landmarks of bilateral lower-extremities and pelvis. Subjects were then required to perform stepping aerobics on 3 different step heights (6, 8, and 10 inches) while recorded by a six-camera motion analysis system (120 Hz, Vicon 460, Oxford Metrics, Oxford, UK) and a force platform (Kistler, Model #9284, Winterthur, Switzerland).. They were also asked to perform the stepping aerobics in 2 movement directions, forward (FS) and lateral stepping (LS). The speed of the stepping aerobics was controlled at 120 steps/min by a metronome. The stepping activities were performed in a random manner and 3 successful trials of each activity were collected. The primary outcomes were the average peak joint moments and powers generated during the landing phase of each stepping activity at the ankle, knee, and hip. Data in sagittal and coronal planes were analyzed. Repeated-measure ANOVAs and Bonferroni post-hoc analyses were used to examine the differences in joint kinetics produced among the movement directions and different heights.

RESULTS

There were no statistically significant interactions between the movement direction and stair height in each variable accessed (joint moments and powers). Statistically significant main effects were identified between the directions of movements for the joint moments and powers at the hip, knee, and ankle joint ($p < .05$) (Fig. 1); except for the hip flexor moment ($p = .47$) and ankle dorsiflexor moment ($p = .06$). Joint powers and coronal-plane joint moments produced during LS were significantly greater than those generated during FS at the hip, knee, and ankle ($p < .001$). However, moments in the sagittal plane did not show a consistent trend between FS and LS among the 3 joints. There were also statistically significant main effect differences among

the 3 stair heights. Joint moments and powers were the greatest while performing the stepping aerobics on the 10-inch step and the lowest while performing the activities on the 6-inch step ($p < .05$).

CONCLUSIONS

A dose-response relation between the lower-extremity joint kinetics and step height was identified in this study. Stepping aerobics performed on the 10-inch step produced greater lower-extremity musculoskeletal loadings than those performed on the 6-inch step. The kinetic responses were also direction- and joint-specific.

REFERENCES

Wang, M-Y. et al. (2003). *Clin. Biomech.,* **18**, 214-221.

ACKNOWLEDGEMENTS

This study is supported by National Science Council, Taiwan NSC 92-2320-B-006-075

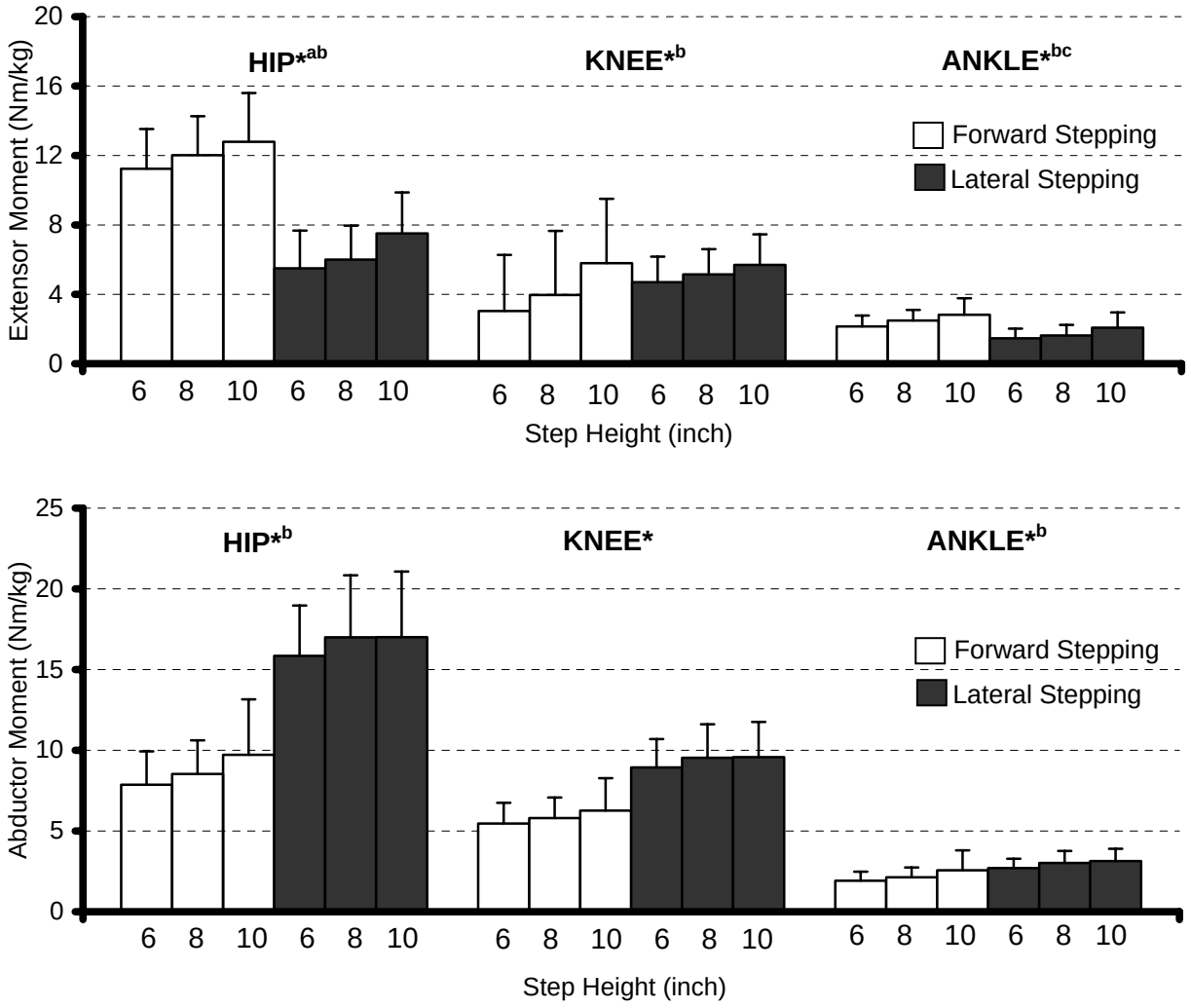

Figure 1: *Significant differences between FS and LS. [a]Significant differences between 6- and 8-inch step heights. [b]Significant differences between 6- and 10-inch step heights. [c]Significant differences between 8- and 10-inch step heights.

IMPORTANCE OF PRESWING RECTUS FEMORIS ACTIVITY IN STIFF-KNEE GAIT

Melanie D. Fox[1], Jeffrey A. Reinbolt[2], Allison S. Arnold[1], Silvia Õunpuu[3] and Scott L. Delp[1,2]
Departments of Mechanical Engineering[1] and Bioengineering[2], Stanford University
Center for Motion Analysis, Connecticut Children's Medical Center[3]
Email: melanief@stanford.edu Web: http://www.stanford.edu/group/nmbl/

INTRODUCTION

Stiff-knee gait, a common pathological walking pattern of persons with cerebral palsy, is characterized by reduced and delayed peak knee flexion during the swing phase of gait. This abnormality may lead to tripping or energy-inefficient compensatory movements due to inadequate toe clearance (Sutherland and Davids, 1993). The reduction in knee flexion has commonly been attributed to over-activity of the rectus femoris during swing phase (Perry, 1987). However, abnormal muscle activity during the stance phase, such as excessive force in vasti or rectus femoris, may decrease knee flexion velocity at toe off and limit knee flexion in swing (Goldberg et al., 2006).

Rectus femoris transfer surgery, which is intended to decrease the muscle's knee extension moment while preserving its hip flexion moment, is a common treatment for stiff-knee gait. It is generally indicated when a patient exhibits abnormal rectus femoris excitation during swing phase. However, if stance phase factors also inhibit knee flexion, excessive excitation of rectus femoris during preswing may also be an important indication for rectus femoris transfer surgery. The purpose of this study was to evaluate the relative importance of preswing rectus femoris activity to peak knee flexion in patients with stiff knee gait.

METHODS

We assessed the effects of rectus femoris activity during stance and swing by creating dynamic gait simulations of ten patients with cerebral palsy. These subjects, with an average age of 10.6 years, were each categorized as exhibiting stiff-knee gait in at least one limb by Goldberg et al. (2006). The gait analysis data were collected at Connecticut Children's Medical Center in Hartford, CT, as a routine part of treatment planning. No subject exhibited excessive knee extension moments or diminished hip flexion moments during swing (Goldberg et al., 2006). Most subjects displayed excessive knee extension moments during double support. A musculoskeletal model with 21 degrees-of-freedom and 92 muscle actuators was scaled to represent the size of each subject. Using computed muscle control (Thelen et al., 2003) we determined a set of muscle excitation patterns for each subject that produced kinematics similar to the subject's measured motions when used to drive a forward dynamic simulation. The computed excitation patterns were generally consistent with each subject's measured EMG data. Forward dynamic simulations were performed for the period of preswing through peak knee flexion.

To investigate the relative contribution of rectus femoris activity during preswing and swing on knee flexion, two more simulations were created for each patient; one in which rectus femoris excitation was eliminated during preswing only, and a second in which rectus femoris excitation was eliminated during swing only (Fig. 1). Preswing was defined to be a time period before toe-off equal in length to early swing. Early swing was defined to be the period of gait from toe-off to peak knee flexion. The difference in amount of peak knee flexion

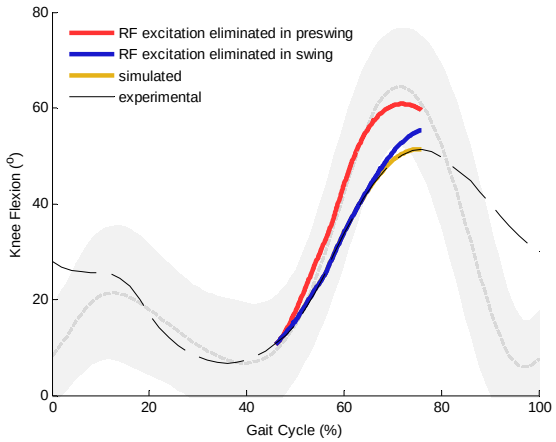

Figure 1: Simulated knee flexion angles when rectus femoris excitation was eliminated during different phases. Shaded region represents normal knee flexion ± 2 SD.

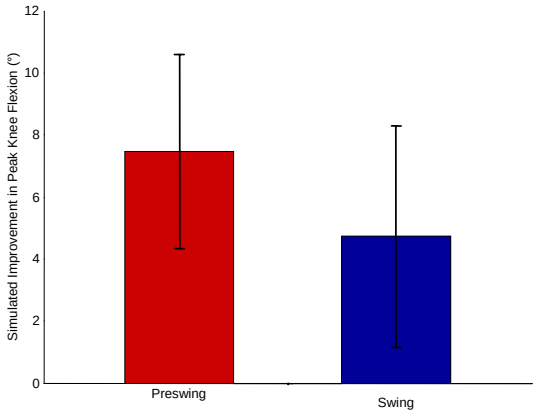

Figure 2: Average simulated improvement in peak knee flexion among all 10 subjects when rectus femoris excitation was eliminated in preswing or swing. Error bars signify ± 1 SD.

improvement between the two cases was compared for each patient.

RESULTS AND DISCUSSION

Simulated improvement in peak knee flexion when rectus femoris excitations were eliminated during preswing was greater than that when rectus femoris excitations were eliminated during early swing in eight out of ten subjects. Using a paired t-test ($p<0.05$), the amount of peak knee flexion improvement attained by eliminating rectus femoris excitations during preswing was significantly greater than the amount of peak knee flexion improvement attained by eliminating rectus femoris excitations during swing (Fig. 2). This result suggests that rectus femoris activity during preswing may have greater influence on peak knee flexion than rectus femoris activity during early swing in some patients with stiff-knee gait. In evaluating the causes of stiff-knee gait, one should examine rectus femoris EMG in preswing as well as early swing (before peak flexion is attained) for abnormal activity.

Dynamic simulations allow one to evaluate the changes in body motions caused by alterations in the timing of muscle activity. This provides a valuable tool for assessing and investigating the mechanisms leading to improvements in some patients following treatment for stiff knee gait. Our future work will focus on simulating the postoperative gait of subjects with good and poor surgical outcomes to determine why some subjects have a dramatic improvement with treatment while others improve very little or get worse.

REFERENCES

Goldberg, S. et al. (2006). *J Biomech*, **39**, 689-698.

Perry, J. (1987). *Dev Med Child Neurol*, **29**, 153-158.

Sutherland, D.H., Davids, J.R. (1993). *Clin Orthop Relat Res*, **288**, 139-147.

Thelen, D.G. et al. (2003). *J Biomech*, **36**, 321-328.

ACKNOWLEDGEMENTS

The authors thank the staff of the Center for Motion Analysis at the Connecticut Children's Medical Center. This research was funded by the NSF, NIH R01 HD046814, and NIH Roadmap for Medical Research U54 GM072970.

Tracking the Position of Insole Pressure Sensors during Walking and Running

Elizabeth S. Chumanov, Christian D. Remy, Darryl G. Thelen

University of Wisconsin-Madison, Madison, WI, USA
E-mail: easchmerr@wisc.edu, Web: www.engr.wisc.edu/groups/nmbl/

INTRODUCTION

Pressure sensitive insoles have emerged as a powerful tool for assessing the pressure distribution on the sole of a foot. The pressures measured by the insole sensors can also be combined to determine a partial set of net ground reactions (COP-center of pressure, vGRF - vertical ground reaction force) (Barnett, *et.al*, 2000, Chesnin, *et.al*, 2000). Such information could conceivably be used within a least-squares inverse dynamics approach (Kuo, 1998) to estimate joint kinetics, thereby providing an alternative to fixed forceplates. However, using insoles for inverse dynamics analysis would require the global position of the insole sensors be tracked with high fidelity. This is a challenging requirement to achieve since the flexible insoles are embedded in a shoe which can undergo large motion and deformations. The objective of this study was to develop and evaluate the use of an array of motion capture markers affixed to a shoe to track insole sensor positions during walking and running. The accuracy of the approach was assessed by comparing the estimated position of the COP and the net vGRF with values measured using a fixed forceplate.

Figure 1. Ten markers (15 mm) affixed around the periphery of a running shoe were used to track insole sensor positions.

METHODS

Five healthy young adults (25 ±2 yrs, 68.9 ± 6.8 kg, 172.5 ±5.5 cm) were tested. Each subject walked at three speeds (slow, preferred, fast) and ran at two speeds (preferred, fast) over a fixed forceplate (AMTI). Three repeated trials at each speed were performed. Each subject also performed a standing static calibration trial, in which he/she stood on a fixed forceplate while voluntarily shifting the center of pressure in the anterior-posterior and medio-lateral directions.

A motion capture system (Motion Analysis) was used to measure the kinematics of ten markers affixed to the periphery of a pair of running shoes (Figure 1). Pressure sensitive insoles (99 capacitive sensors per insole, Novel Inc.) were fitted into the shoes to measure the pressure on the bottom of the feet for all trials. Pressure data was acquired at 100Hz synchronously with the kinematic (200Hz) and forceplate data (2000Hz). At each frame, we used a natural cubic spline through the positions of the 10 motion capture markers to infer the positions of 100 virtual markers around the periphery of the shoe.

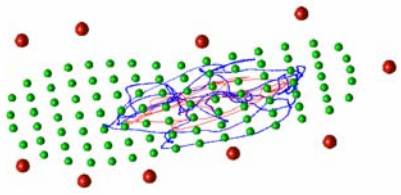

Figure 2. A standing calibration trial was used to establish the location of the sensors (small dots) that optimized agreement between the insole and forceplate measured COP trajectories.

A two stage transformation was used to map the insole sensor locations into the lab reference frame. The first transformation determined the global position of the insole sensors in the calibration trial. Numerical optimization was used to determine a linear transformation from the ground to the insole reference frame that minimized the differences between the insole COP trajectory and the forceplate COP trajectory (Figure 2).

The second stage used piecewise affine transformations to describe the position of the moving insole sensors with respect to the calibration trial. At each frame of a motion trial, a separate affine transformation was used for each sensor. This transformation was obtained from the measured relative motion of the virtual markers with respect to the calibration trial. It was quantified by placing an orthonormal basis in the nearest virtual marker to the sensor, and defining the principal axes of the transformation using the neighboring markers.

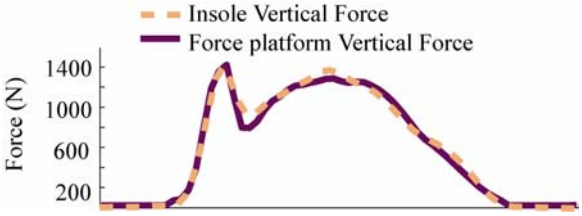

Figure 3. Agreement between net vertical force recorded by the insole and forceplate.

RESULTS

The proposed affine transformation approach generated estimates of the vGRF and COP that were remarkably similar to that measured by the forceplate (Figure 3). Root mean square (RMS) differences in the vGRF were <1% of peak vertical force for walking and <2% of peak vertical force for running. RMS differences in the COP were <5 mm during walking and <9 mm during running (Table 1). The largest errors in the COP trajectory occurred at heel strike.

Table 1: Mean (SD) RMS differences between the forceplate and insole in the vGRF and global position of the COP.

Speed	**vGRF (N)**	**COP (mm)**
Slow Walk	5.3 (4.0)	3.5 (0.5)
Preferred Walk	6.7 (4.4)	4.6 (0.7)
Fast Walk	6.7 (4.7)	4.5 (0.9)
Preferred Run	23.3 (11.2)	8.4 (1.5)
Fast Run	26.8 (12.9)	7.5 (1.9)

DISCUSSION

We have demonstrated a novel approach to tracking the global position of the pressure on the bottom of the feet during human walking and running. There are two important uses of this information in biomechanics. One application is the refinement of foot-floor contact models used to simulate human locomotion. Most current models use an array of discrete visco-elastic units on the sole of the foot (Gilchrist and Winter, 1996). Accurate pressure distribution could be used to both estimate contact model parameters and validate model predictions. A second application is in least squares inverse dynamics (LSID), which uses the kinematics of a whole body model to calculate the missing ground reaction components (Kuo, 1998). Such an approach would be a powerful alternative to the use of fixed forceplates for calculating internal joint torques during human locomotion.

REFERENCES

Barnett, S, et.al. (2000). *Clin Biomech* **15**, 781-785.

Chesnin, KJ, et.al. (2000). *Gait Posture* **12**, 128-133.

Kuo, AD. (1998). *J Biomech Eng* **120**, 148-159.

Gilchrist, LA and DA Winter. (1996). *J Biomech* **29**, 795-798

ACKNOWLEDGEMENTS

Aircast Foundation, NFL Charities, Simbios, NSF Graduate Fellowship (EC), an ASB Grant-in-aid, and a SDE-GWIS Ruth Dickie Research Scholarship.

BIOFIDELITY REQUIREMENTS FOR AN ADVANCED HEADFORM FOR THE PREDICTION OF EYE INJURIES

Eric Kennedy[1], Paul Depinet[2], Fred Brozoski[3], and Stefan Duma[1]

[1] Virginia Tech – Wake Forest University Center for Injury Biomechanics, Blacksburg, VA
[2] Denton ATD, Milan, OH
[3] United States Army Aeromedical Research Laboratory, Ft. Rucker, AL
E-mail: eric_kennedy@vt.edu, Web: www.cib.vt.edu

INTRODUCTION

The rate of eye injuries has dramatically increased in warfare from approximately 2% during World War I and World War II, to nearly 13% during Operation Desert Storm (Heier 1993, Wong 2000) (Figure 1). In order to assess the capability of protective equipment in reducing eye and facial injuries, a new advanced headform is being developed that can predict fracture of facial bones, as well as eye injury from impact loading. Because of its emphasis on eye and orbital injuries, the name of this new advanced headform will be the FOCUS Headform, which stands for Facial and Ocular CountermeasUre Safety Headform (Figure 2).

METHODS

In order to develop the FOCUS headform for eye injury response, the response of the human eye to impact was characterized. A two-part study was utilized to develop biofidelity requirements and develop eye injury risk functions.

First, the force-deflection response of the human eye was determined by dynamic impact testing of eyes in-situ. Human eyes were impacted by a spring powered impactor to determine the amount of force required to displace the eye a given distance into the orbit. The FOCUS synthetic eye was subjected to the same test to assess its biofidelic response to impact.

Second, injury risk functions for five frequently occurring eye injuries were developed based on data from blunt projectile impacts. In addition to existing data reported in the literature, 126 projectile tests were conducted to determine injury response. Logistic regression was used to determine the eye injury risk based upon the normalized energy (J/m^2) of the projectile.

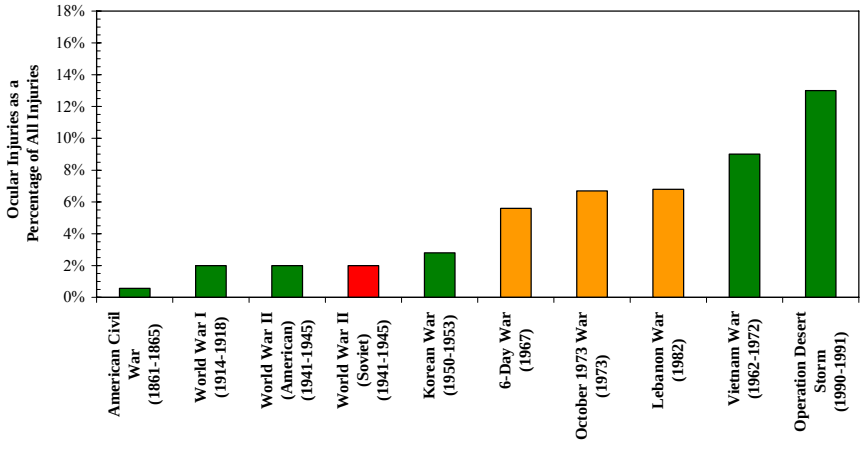

Figure 1: Ocular injuries shown as a percentage of total war casualties from 1861 to present (Heier 1993, Wong 2000). The incidence of ocular injuries has risen from approximately 2% during World War II to over 10% in modern conflicts.

Figure 2: The FOCUS headform is designed to predict eye and facial injuries.

RESULTS AND DISCUSSION

Force-deflection results for individual tests were determined from test data, and from the complete dataset the overall force-deflection corridor is generated (Figure 3). This corridor defines the biofidelity requirements for the FOCUS headform, so that the force-deflection response of the synthetic eye in the headform matches that of the human eye *in-situ*.

Eye injury risk functions were developed based on an extensive database of all eye injury impact tests reported in the literature and from experimental tests (Figure 4). Using over data from 251 eye impact tests, normalized energy (energy per projected area) value was found to be a significant predictor for corneal abrasion, hyphema, lens dislocation, retinal damage, and globe rupture ($p \leq 0.001$ in all cases). These injury risk functions will serve as the basis for the development of new injury risk criteria that use the load measured by the FOCUS eye load cells to predict injury risk.

SUMMARY/CONCLUSIONS

The relative severity of both eye and facial injuries is much greater for the military than in the civilian population; however, these injuries in both the civilian and military sectors can be severely debilitating and pose an enormous health cost. Due to a lack of instrumentation, the prediction of eye and facial injuries using anthropomorphic test devices is not currently possible. The current study presents biofidelity design requirements for a new headform to determine the risk of eye and facial injuries from impacts. This technology will be useful not only for the military to evaluate protective equipment prior to deployment, but also will be useful in the civilian population for evaluation of various facial impact scenarios, such as sports injuries and automotive accidents.

REFERENCES

Heier JS et al. (1993) Archives of Ophthalmology 111: 795-798.

Wong TY et al. (2000) American Journal of Ophthalmology 129(5): 645-650.

ACKNOWLEDGEMENTS

The authors would like to acknowledge the United States Army Medical Research and Materiel Command for their support of this research and development program

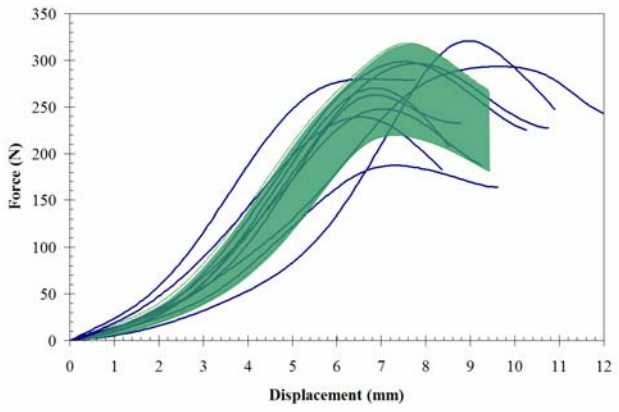

Figure 3: Force-deflection curve of *in-situ* human eye from blunt impact at 10 m/s. The individual lines represent each test. The shaded region represents the corridor for typical force-deflection response.

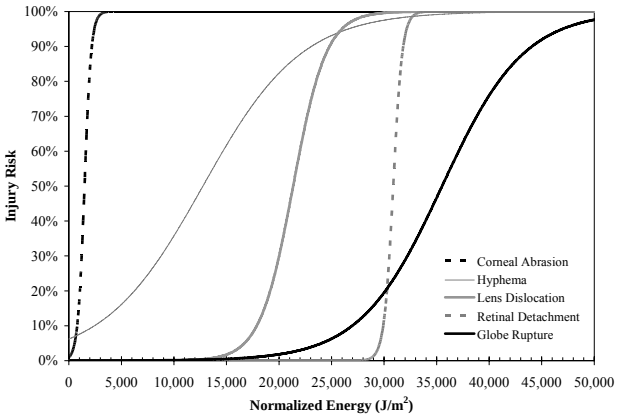

Figure 4: Parametric eye injury risk functions for predicting corneal abrasion, hyphema, lens dislocation, retinal detachment, and globe rupture from impact. These are the basis for eye injury risk functions for the FOCUS.

ROTATIONAL LAXITY OF ACL DEFICIENT AND RECONSTRUCTED KNEES

Naiquan (Nigel) Zheng, Bo Gao, Michael Moser, Peter Indelicato

University of Florida, Gainesville, FL, USA
E-mail: nigelz@ufl.edu, Web: www.ortho.ufl.edu/BMAL

INTRODUCTION

Anterior cruciate ligament (ACL) injury has been associated with progressive development of knee osteoarthritis (Daniel et al, 1994). The ACL plays a role in controlling axial rotation in the knee in addition to its primary function of limiting anterior translation of the tibia relative to the femur (Andersen et al, 1997; Wilson et al 2000). A recent study showed that rotational changes at the knee will cause cartilage thinning (Andriacchi et al, 2006). It is still under debate whether or not the reconstruction of the anterior cruciate ligament (ACL-R) restores normal tibial rotation. The purpose of this study is to investigate the knee rotational laxity of healthy subjects and those following ACL injury and reconstruction.

METHODS

Both left and right knees from 6 subjects with unilateral ACL-R knee (4 male and 2 female), 7 subjects with unilateral ACL-deficient (ACL-D) knee (6 male and 1 female) and 19 healthy subjects (8 male and 11 female) were tested using an IRB approved protocol. ACL-R and ACL-D subjects at the time of test were 3 months to 2 years after surgery and after injury respectively. Using an 11-camera motion analysis system (MAC, Santa Rosa, Ca) and a JR3 universal load cell, the internal and external rotation of the knee and applied internal and external torque were recorded (Fig. 1) (Zheng et al, 2006). Motion data were collected at 60 Hz and the torque data were collected at 1200 Hz. Data from three trials were collected from both legs during internal and external rotation. The rotational laxity of the knees was measured at 2 and 7 Nm torque. Total ranges of motion (ROM) of the internal and external rotation at both 2 and 7 Nm were measured (Fig. 1). Rotational stiffness between 2 and 7 Nm was calculated for both the internal and external rotation. The internal and external rotational stiffness from 2 to 7 Nm and the ROMs from internal 2 and 7 Nm to external 2 and 7 Nm were analyzed. A repeated measure ANOVA (SPSS, Chicago, IL) was used to test the differences between involved and uninvolved knees of ACL-R and ACL-D subjects, and between knees of ACL-R and healthy subjects.

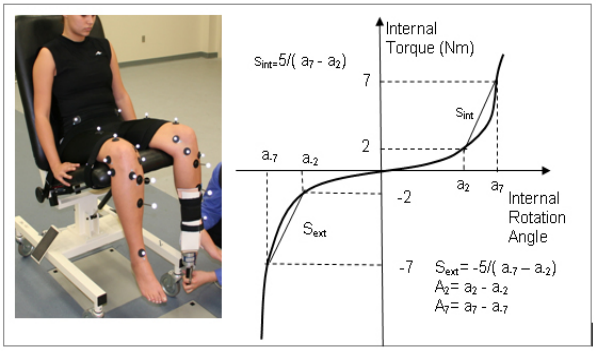

Figure 1: Test Set Up and Variable Definitions

RESULTS AND DISCUSSION

Figure 2 shows the internal and external rotation stiffness. The internal rotation stiffness (S_{int}) of the right knee was significantly higher than that of the left knee ($p=0.014$). There were significant differences of rotational stiffness (S_{int} and S_{ext}) and ROM (A2 and A7) between males and females (Table 1).

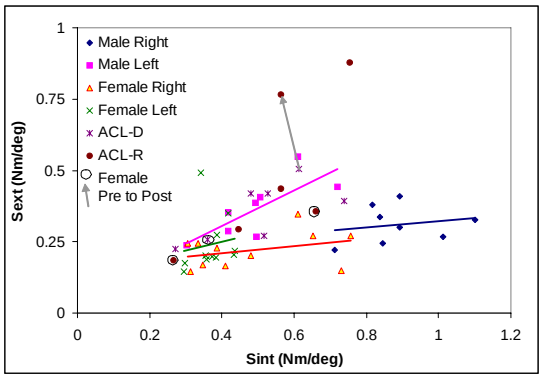

Figure 2 Internal *vs* External Rotation Stiffness.

One subject was tested pre- and post-surgery. The external rotation stiffness of the involved knee was increased 52% post-surgery while the internal rotation stiffness was slightly decreased (8%). In the ACL-R group, the external rotation stiffness of the involved knee was significantly higher than the healthy group (p=0.016). ROMs (A2 and A7) in the ACL-R group were significantly smaller than those in the healthy group. With the knee flexed at 90 degrees, the contribution of reconstructed ACL to rotational stiffness may result from higher tension of the graft.

No significant differences were found between the ACL-D and healthy groups. Significant differences of rotation stiffness and ROM between left and right knees and between male and female were found in the healthy group. Due to the small sample size, no conclusions can be reached regarding the effect of the ACL-R on rotational laxity of the knee. However, there was evidence that the ACL-R group was different than the healthy group. Because there were significant differences between males and females and between left and right knees, a larger sample size will be needed in order to study the influences of the ACL-R on rotational laxity of the knee.

SUMMARY/CONCLUSIONS

Subjects in the ACL-R group had different characteristics from the healthy group. Some ACL-R subjects had significant higher external rotation stiffness while the internal rotation stiffness was not different. Gender differences exist in the healthy group. Subjects in the ACL-D group did not show significant differences in the rotational stiffness and ROM.

REFERENCES

Andersen HN et al (1997) *Knee Surg Sports Traumatol Arthrosc* **5**,145-9

Andriacchi TP *et al* (2006) *Clin Orthop Relat Res* **442**, 39-44

Daniel DM et al (1994) *Am J Sports Med* **22**, 632-44

Wilson DR et al (2000) *J Biomech* **33**, 465-73

Zheng N et al (2006) *Proceedings of ASB'06*, 56

ACKNOWLEDGEMENTS

The authors would like to students for their assistance in data collection and reduction.

Table 1: Ranges of motion and rotational stiffnesses (mean± SD).

	A2 (deg)**		A7 (deg)**		S_{INT}(Nm/ deg)*		S_{EXT}(Nm/ deg)**	
	F	M	F	M	F	M	F	M
Left	30±7.8	17±6.5	67±12	42 ± 12	0.37±0.05	0.50±0.13	0.24±0.1	0.37±0.10
Right	29±9.6	17±5.8	65±15	42 ± 9	0.48±0.17†	0.57±0.08†	0.22±0.06	0.31±0.06
ACL-D	30	19±11	64	45±21	0.36	0.52±0.15	0.25	0.37±0.13
ACL-R	22±15	9.8±3.8‡	55±32	29±10‡	0.46±0.27	0.57±0.12	0.27±0.12	0.56±0.27‡

† Significant differences between right and left (p=0.014), * and ** significant differences between male and female (*p<0.05, **p<0.01), ‡ significant differences between ACL-R and Healthy group (p<0.05).

CONTACT STRESS ELEVATION WITH LATERAL TALAR SHIFT

Tina Maxian [1], Jeremy Winston [2], Richard Uhl [3], Robert Spilker [2], and Daniel Fuchs [4]

[1] Eastern Maine Medical Center, Bangor, ME, USA
[2] Rensselaer Polytechnic Institute, Troy, NY, USA
[3] Albany Medical Center, Albany, NY, USA
[4] Harvard University, Boston, MA, USA
E-mail: tmaxian@emh.org

INTRODUCTION

One of the most widely cited papers in the orthopaedic literature, used to argue for fixation of lateral malleolus fractures to avoid articular cartilage contact stress elevations that contribute to degenerative joint disease, is that by Ramsey and Hamilton (1976), despite more recent studies that have been unable to reproduce their results (Vrahas *et al.*, 1994). Using a cadaveric model, they investigated contact stress between the tibia and talus, with the talus located, then with varying amounts of lateral talar shift. With increasing lateral shift, they found that the contact area medialized on the talus, and decreased in size. Since they used carbon black to indicate contact, they were unable to document the magnitude of increase, and inferred that contact stress increased because the contact area decreased, since the applied load remained the same. Using a contact finite element (FE) formulation, we set out to model the same system, and to document the contact stress increases that occur.

METHODS

We used the frozen male dataset from the NIH Visible Human® Project for our patient-specific model. First, we extracted the geometry of bone and articular cartilage from the distal tibia and talus from the CT scans and anatomic photographs, respectively, by segmentation using the Marching Squares algorithm in VTK (Kitware, Inc., Clifton Park, NY). We then interpolated these ordered sets of points by non-uniform rational B-spline (NURBS) curves, which were lofted, capped, and converted to Parasolid models in Rhino (Robert McNeel and Associates, Seattle, WA). We meshed the models using Patran (MSC Software, Santa Ana, CA) (Figure 1).

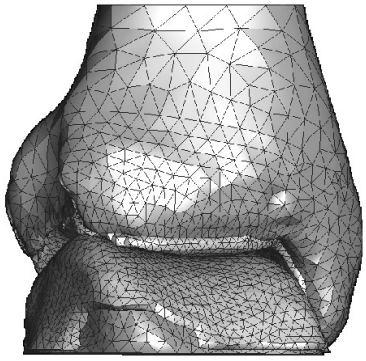

Figure 1. FE mesh of distal tibia and talus.

Previous FE work has shown that if one is interested in contact stress analysis, homogenous bone and cartilage material properties produce acceptable results (Donahue *et al*., 2002); consequently the bone was modeled using a homogeneous linearly elastic modulus of 20 GPa, and the cartilage modeled with an elastic modulus of 15 MPa.

After convergence testing, the analyses were performed using ABAQUS (ABAQUS Inc., Pawtucket, RI) with contact assumed to be nonlinear, finite sliding, frictionless contact between one deformable body and

another deformable body. The boundary conditions for the applied loads and displacements were applied through a rigid surface attached to the bottom of the talus. We brought the tibia and talus into contact using a resultant load of 687 N (70 kg), representing a vertically directed load. We then repeated the test with the talus shifted laterally 5 mm, and determined the contact areas, as well as the peak and overall contact stress distributions.

RESULTS AND DISCUSSION

For the joint in neutral position, the FE model required a vertical load of 687 N (70 kg), with small loads (20 N (2.9 %) and 10 N (1.5%)) in the other two directions to keep the talus from undergoing a rigid body motion. (Percentages are of the resultant load magnitude). For the laterally displaced talus, much larger nonaxial loads were required to prevent rigid body motion, 180 N (26 %) and 21 N (2.0 %). (The axial load was decreased to 663 N to keep the resultant load magnitude at 687 N). The contact area on the talus decreased in size and medialized with lateral talar shift, and the peak contact stresses increased from 5.9 MPa to 9.1 MPa (Figure 2).

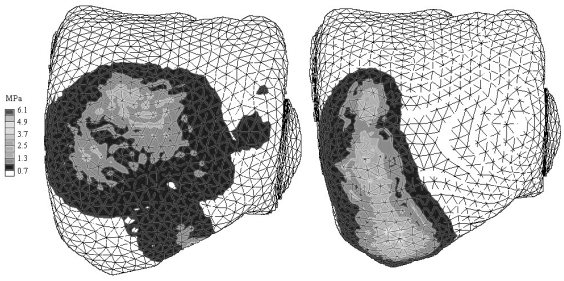

Figure 2. Stress distribution on the talar contact surface showing in a located talus (left) and a laterally shifted talus (right).

The model was able to reproduce the trend found by Ramsey and Hamilton, namely, that the talar contact area decreases, and shifts medially with lateral talar displacement. However, we may have demonstrated why others have been unable to verify the findings of Ramsey and Hamilton (1976) despite being widely cited in the clinical orthopaedic literature. The only way we were able to achieve stable contact between the isolated talus and the tibia when the talus was shifted laterally, was by strongly constraining the model, which forced the talus into the tibia in one position, and consequently generated a small area of contact with high contact stresses. In the work by Vrahas, *et al*. (1994), they simulated a fibular malunion in a cadaveric model in which they allowed the talus to shift position, and encountered no increase in contact stress with lateral talar displacement. Most likely by allowing the talus to move, it can "settle" into a position that distributes the contact stresses more equally, something that could not happen in Ramsey and Hamilton's experimental set-up.

SUMMARY/CONCLUSIONS

With most malreduced ankle fractures not having a purely fixed deformity as in this model, the degenerative changes that occur clinically after a poorly reduced ankle fracture may not necessarily be due solely to elevations in normal contact stress, and instead, may be due to shear forces or instabilities that are not measured by this experimental system.

REFERENCES

Donahue *et al*., (2002). *J Biomech Eng*, **124**, 273 - 280.

Ramsey PL and Hamilton W (1976). *JBJS*, **58A**, 356 - 357.

Vrahas et al, (1994) *J Orthop Trauma*, **8**, 159 – 166.

EFFECT OF AGE ON SHEAR MODULUS OF SKELTAL MUSCLE

Zachary J. Domire[1], Matthew B. McCullough[1] and Kai-Nan An[1]

[1] Mayo Clinic College of Medicine, Rochester, MN, USA
E-mail: Domire.Zachary@mayo.edu

INTRODUCTION

With an increasing percentage of the population reaching old age, researching negative health consequences associated with aging has become increasingly important. Aging has many detrimental consequences in skeletal muscle. Because of resulting functional limitations, the bulk of research attention focuses on the progressive loss of muscle strength accompanying aging. However, changes in passive structures within muscle may also have negative health effects.

It is known that during aging advanced glycation endproducts result in cross-linking of collagen fibers in tissues throughout the body (Avery and Bailey, 2005). These cross-links result in increased tissue stiffness. Negative effects of this stiffening have been seen in numerous tissues, including cardiac muscle (Asif et al, 2000), bone (Vashishth et al, 2001), and articular cartilage (Verzijl et al, 2000). Cross-links have also been shown to accumulate in the skeletal muscle of aged rats (Gosselin et al, 1998). Potential negative effects of this stiffening in muscle include decreased ability to remodel and increased risk for injury.

Magnetic Resonance Elastography (MRE) is a novel imaging technique that allows measurement of tissue shear modulus in vivo (Muthupillai et al, 1995). In this technique a small amplitude shear wave is induced in a tissue. At the same time a motion-sensitizing gradient synchronized to the shear wave is applied. From this process a phase shift can be measured using phase-contrast MRI. The displacement at each voxel can be directly calculated from this phase shift and the shear wave can be imaged as it moves through the tissue.

The purpose of the following study is to examine muscle stiffness changes associated with aging using MRE.

METHODS

20 female subjects were included in the study with an age range of 50-70 years. Scans were performed with the ankle in 20 degrees of plantarflexion. Vibration was applied by a small bar tapper to the distal end of the tibialis anterior muscle belly. The tapper was oriented parallel to the long axis of the leg and secured tightly in place with a Velcro band.

Strain modulus was calculated at each voxel by determining the phase gradient for a small window around each point. The magnitude of the shear modulus within the muscle was calculated as the mean value for each voxel within a central region of the muscle. The standard deviation of the moduli within this region was used as a measure of tissue homogeneity.

RESULTS AND DISCUSSION

There was not a significant relationship between age and shear modulus (Figure 1). However, several older subjects (over 65) had a much higher modulus than average. On the other hand, there was a significant relationship ($p<.05$) between age and the

standard deviation of the modulus (Figure 2). The R squared value for a linear fit to the data was 0.53.

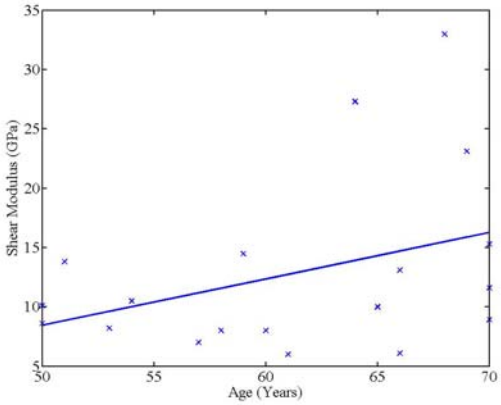

Figure 1: Shear Modulus vs. Age

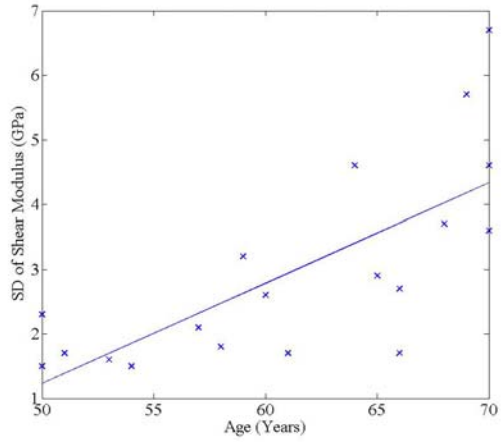

Figure 2: Standard Deviation of Shear Modulus vs. Age

The lack of a significant relationship between age and shear modulus is likely explained by the relatively narrow age range studied as well as the fact the other factors, such as physical activity, are likely to contribute to crosslinking (Gosselin et al, 1998). Given this however, the relationship between age and the standard deviation of the shear modulus is relatively strong. A less homogeneous muscle may be a result of age related crosslinking.

Identifying individuals with high concentrations of collagen crosslinking is important considering the negative health consequences and that potential treatments exist. Exercise has been shown to significantly reduce collagen crosslinking in muscle (Gosselin et al, 1998). Though, the effects may be site specific (Thomas et al, 2001). A novel pharmaceutical crosslink breaker (Alt-711) is currently being tested and shows promise in treating stiffening of the cardiovascular system (Asif et al 2000) and may be useful elsewhere.

SUMMARY/CONCLUSIONS

Though there was not a significant relationship between age and shear modulus, all subjects with high values were amongst the oldest tested. The standard deviation of the modulus did increase with age indicating a less homogeneous tissue. More research is needed to determine if the changes seen here are reflective of increased tissue cross-linking. MRE shows promise as a tool to study development of cross-links or to evaluate treatments.

REFERENCES

Asif, M. et al. (2000). *Proc Natl Acad Sci USA*, 97, 2809-13.

Avery, N.C., Bailey, A.J. (2005). *Scand J Med Sci Sports*, 15, 231-40.

Gosselin, L.E. et al. (1998). *J Appl Physiol*, 85, 1011-6.

Muthupillai, R. et al. (1995). *Science*, 269, 1854-7.

Thomas, D.P. et al. (2001). *Eur J Appl Physiol*, 85, 164-9.

Vashishth, D. et al. (2001). *Bone*, 28, 195-201.

Verzijl, N. et al. (2000). *Biochem J*, 350, 381-7.

ACKNOWLEDGEMENTS

This study was supported by a grant from the NIBIB R01 EB 00812

Biomechanical Constraints on Equilibrium Point Control of Multi-Joint Arm Postures

Dan Song, Ning Lan and James Gordon

University of Southern California, Los Angeles, CA 90089
Web: www. http://pt.usc.edu/labs/cel/

INTRODUCTION

Modeling and simulation appear to reveal a plausible role of fusimotor command in controlling equilibrium point (EP) of the limb (Lan et al. 2005). In this study, we use a comprehensive sensorimotor model of the virtual arm (VA) (Song et al. 2006) to evaluate the impact of biomechanical properties on the EP control. The results help to understand the constraining effect of neuro-musculoskeletal properties of the peripheral plant on EP control in particular, and on motor control in general.

METHODS

A systems model of virtual arm in cascade with spinal reflex circuits was used in this simulation studies (Figure 1). The equilibrium points of the planar shoulder and elbow joints were steered by the gamma static fusimotor commands to the spindles of a pair of mono-articular antagonistic muscles acting at each joint. The virtual muscle (VM) implemented here captured the most realistic properties of mammalian muscle (Cheng et al. 2000). The musculoskeletal structure also incorporated realistic features of muscle moment arms at shoulder and elbow joints (Song et al. 2006). Spinal circuitry at the output of motoneuron pools included Ia stretch reflex, reciprocal inhibition, as well as Renshaw cell recurrent inhibition. Neural transmission delays and synaptic delays were considered in the spinal feedback loops. Reflex gains were selected

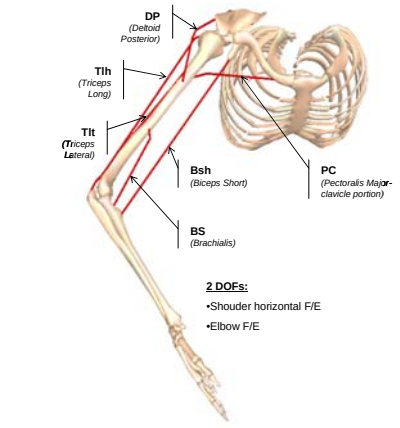

(a)

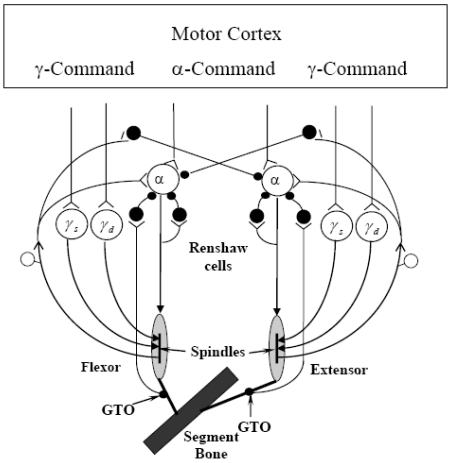

(b)

Figure 1, (a) six-muscle, virtual arm model, and (b) spinal reflex circuits that are implemented in the systems model for simulation.

so that the closed-loop response was stable.

RESULTS AND DISCUSSION

Simulation indicated that the choice of architectural parameters of the virtual muscles had a limiting effect on the range

of equilibrium angles that can be modulated by the full range of gamma fusimotor control, i.e. from 0 ~ 1. This was mainly due to the fact that a low level of muscle activation was used for postural control under normal conditions. This tended to have a length-tension property combined with a moment arm profile together that produced little or no active force near the bounds of joint motion. Thus, passive forces overtook the active forces, and limited the effective EP range that can be achieved.

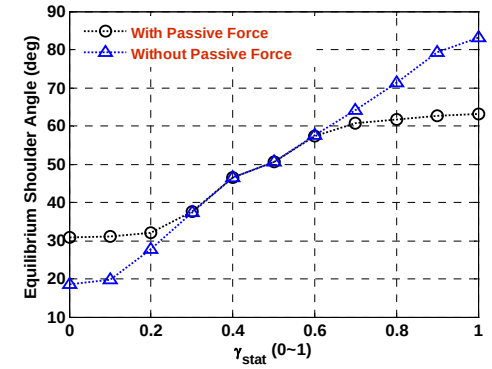

(a)

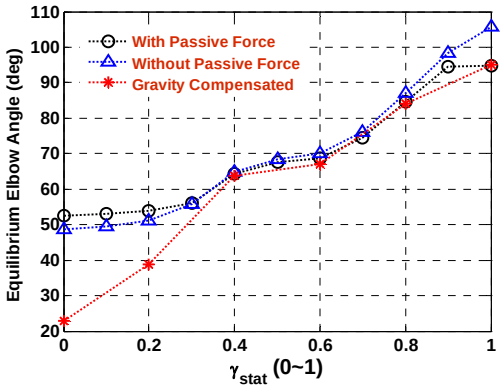

(b)

Figure 2, (a) the θ_{eq}–γ_s relation at shoulder joint when the elbow joint is fixed; (b) the θ_{eq}–γ_s relation at the elbow joint when the shoulder joint is fixed.

As shown in Figure 2, the range of equilibrium angle achieved with full range of γ command was limited by the presence of gravity influence and passive muscle force (Figure 2, with open circles). With gravity influence compensated at elbow and passive muscle force removed from all muscles, the range of equilibrium angle achieved was expanded significantly at both shoulder and elbow joints (Figure 2, with open triangles and stars). We believe that with proper tuning of muscle architectural parameters, particularly length-tension property, the range of equilibrium angle can be further expanded. However, these factors are realistic, and will present an inevitable constraint to the neural control of the brain.

CONCLUSION

This study illustrates the utility of realistic models to understand the limits of spinal sensorimotor control. Results suggest that, in order to overcome these biomechanical nonlinear constraints, an adaptive scheme for reflex gain control by supraspinal centers may be necessary in order to achieve a full range of EP control.

REFERENCES

Cheng EJ, Brown IE, and Loeb GE. *Journal Of Neuroscience Methods* 101: 117-130, 2000.
Lan N, Li Y, Sun Y and Yang FS, *IEEE Tran. NSRE*, 13(1):60-71, 2005.
Song D, Mileusnic M, Lan N, and Gordon J. In: *16th Annual Neural Control of Movement Meeting*. Key biscayn Florida, USA: 2006.

ACKNOWLEDGEMENTS

This work is supported by a grant from NSF, IOB #0352117.

Upper and Lower Limb Disturbance Rejection of Self-Triggered and Computer-Cued Load Perturbations

Kari A. Danek, Daniel P. Ferris, J.W. Grizzle, and R. Brent Gillespie

University of Michigan, Ann Arbor, MI, USA
E-mail: danekk@umich.edu

INTRODUCTION

People are capable of producing changes in grip and postural support forces in one hand to anticipate load perturbations that are self-generated by the other hand (Dufosse et al., 1985; Blakemore et al., 1998; Diedrichsen et al., 2003). We investigated whether humans could produce similar anticipatory actions in the lower limbs in response to perturbations triggered by a hand. In addition to testing upper/lower limb task coordination, we replicated bimanual results from the literature to gauge the upper limb effect with our protocol. For both the upper and lower limbs, we compared disturbance rejection when the perturbations were self-triggered, randomly automated, or predictably automated with visual and auditory stimuli.

METHODS

Healthy subjects (n = 12) were presented with a simple motor task: to minimize the motion of their hand or feet when exposed to a large and sudden change in load. We used a custom apparatus capable of presenting programmable loads to a subject through a motorized platform. For each trial, subjects were asked to oppose a load and attempt to maintain a stationary position while the load was rapidly removed according to the time-function: $W \cdot e^{-20t}(1+10t)$, where W was 14 N at the hand or 20 Nm about the ankles.

The experiment included three conditions for unloading: a) after an unpredictable delay (*Uncued*), b) upon a computer-initiated trigger accompanied by predictable audio-visual cues (*Computer-Cued*), and c) upon a subject-initiated trigger through a handheld pushbutton (*Self-Triggered*). In addition to regular trials, we included *catch trials* where the load was surreptitiously held upon triggering. Subjects completed one series of testing using a hand to oppose the load and a second series of testing using both feet to oppose the load.

Acceleration following unloading was used as a measure of performance, where small acceleration magnitude indicated better compensation for the load release. We used peak acceleration in the first 200 ms following triggering as a performance metric. We used ANOVAs to test for significant differences between conditions.

RESULTS

In both hand and feet disturbance rejection tests, subjects were able to compensate for the unloading better when it was self-triggered than when it was triggered by computer. The general response showed similar characteristics for both sets of tests (hand and feet). When computer-triggered, subjects were able to compensate better when a timing cue was presented. The mean acceleration waveforms were smallest for Self-Triggered, intermediate for Computer-Cued, and largest for Uncued (Figure 1).

Post hoc analyses of variance with multiple comparison procedures indicate significant differences in the peak acceleration. When compared to the Uncued condition in the upper limb tests, the Computer-Cued and Self-Triggered conditions produced smaller peak accelerations by 6.7% and 24.2%,

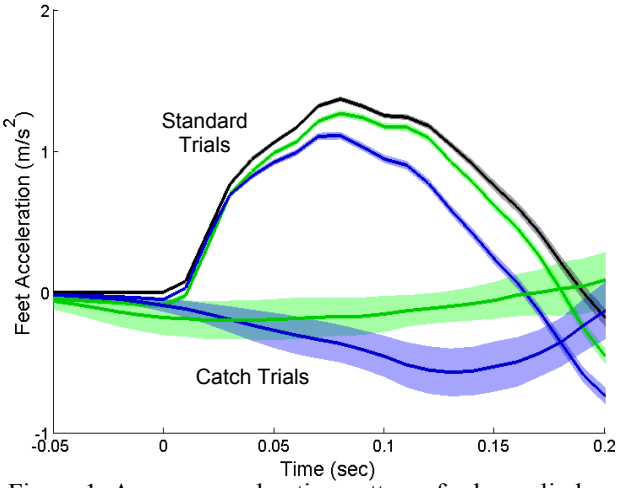

Figure 1: Average acceleration patterns for lower limb tests of all subjects showed larger magnitudes for Uncued (grey) and Computer-Cued (green) standard trials than for Self-Triggered (blue). Self-Triggered catch trials (blue) generally had larger magnitudes than Computer-Cued catch trials (green). The shaded regions indicate 95% confidence intervals. These results were consistent with those from the upper limb analysis.

respectively ($p < 0.001$). Likewise, for the lower limb tests, Computer-Cued was 5.3% smaller ($p = 0.0031$) and Self-Triggered was 16.3% smaller ($p < 0.001$) than the Uncued. The peak accelerations for both Self-Triggered conditions were also significantly smaller than their respective Computer-Cued conditions ($p < 0.001$).

Subjects exhibited more active compensation for the expected but missing load release during the catch trials for the Self-Triggered condition than for the catch trials for the Computer-Cued condition. Although acceleration for some trials remained flat, indicating no active compensation, the acceleration profile for many catch trials resembled the inversion of that produced in standard trials. Mean acceleration waveforms depicted in Figure 1 were intermediate between flat and large inversion profiles.

Peak acceleration magnitudes in the Self-Triggered catch conditions were larger than peak accelerations in the Computer-Cued catch conditions for both hand and feet ($p < 0.001$).

DISCUSSION

Our results indicate that subjects develop anticipatory adjustments in the lower limbs based on upper limb dynamics. The effects observed were similar in character and magnitude as those demonstrated from bimanual unloading tasks performed on the same apparatus. Given that lower limb neuromuscular commands incorporate predictions of interaction forces from the upper limbs, we suggest that upper limb guided lower limb motion may be a productive means of neurological rehabilitation (Danek et al., 2005), similar to what has been suggested for bimanual guidance (Lum et al., 2002). In contrast, interaction forces from external agents (i.e. robots or therapists) can not be anticipated or incorporated into lower limb neuromuscular control during therapy in the same manner demonstrated here by upper limb interaction forces.

REFERENCES

Blakemore SJ, et al. (1998) Predicting the consequences of our own actions: The role of Sensorimotor context estimation. *J Neurosci* **18**:7511-7518.

Danek KA, et al. (2005) A dual input device for self-assisted control of a virtual pendulum. In: *ICORR*. Chicago, IL.

Diedrichsen J, et al. (2003) Anticipatory adjustments in the unloading task: Is an efference copy necessary for learning? *Exp Brain Res* **148**:272-276.

Dufosse M, et al. (1985) Postural forearm changes induced by predictable in time or voluntary triggered unloading in man. *Exp Brain Res* **60**:330-334.

Lum PS, et al. (2002) Robot-assisted movement training compared with conventional therapy techniques for the rehabilitation of upper-limb motor function after stroke. *Arch Phys Med Rehabil* **83**:952-959.

AKNOWLEDGEMENTS

The work was supported in part by NSF grants ECS-0600869 and IIS-0093290

LOWER LIMB LOCAL OR GLOBAL ASYMMETRY IN GAIT OF PEOPLE WITHOUT IMPAIRMENTS

Heydar Sadeghi[1]

[1]Department of Kinesiology, Tarbiat Moallem University, Ministry of Sciences, Research and Technology, Tehran, IRAN

sadeghih@yahoo.com

INTRODUCTION

Because pathological conditions can affect gait [1-4], understanding the fundamental tasks of the lower limbs in able-bodied subjects can guide clinicians in refining their clinical evaluation or rehabilitation treatment. This gait study was undertaken to determine whether the main actions taken by the ankle, knee and hip extensors/flexors and overall lower limb muscle activity during able-bodied gait appear to be symmetrical or not.

METHODS

Sixty gait trials were obtained from 20 healthy male subjects having an average age of 25.3 ±4.1 years, height of 1.77±0.06 m and average mass was 80.6 ±13.8 kg. The model and the procedure have been explained in detail elsewhere [5]. Bilateral gait data were collected with an eight video-based camera system (90 Hz) synchronized to two AMTI force plates (360 Hz). Direct Linear Transformation software from the Motion Analysis Expert Vision system was used to reconstruct the image markers into three-dimensional coordinates. A fourth order zero-phase lag Butterworth low-pass filter was applied to reduce the noise in the video data. The cut-off frequency was 6 Hz for the body segments and 30 Hz for the force data. For averaging purposes, moments were normalized with respect to body mass. Joint moments were expressed according to the convention proposed by the International Society of Biomechanics and included in Winter [6], where the extensor and plantarflexor moments are considered positive. Kinematic and force plate data were used in an inverse dynamic approach to calculate the net sagittal muscle moments at the hip, knee and ankle of the lower limbs during the stance phase. Student's t-test for paired data with a $p<0.05$ threshold was performed on the right and left limb peak muscle moments as a primary evaluation of limb symmetry. PCA was applied to identify the main structure of the data throughout the variation in the data. To determine what each PC measures, the muscle moment having the highest correlation within each PC (called the factor loading) was used. In this instance, a factor loading higher than 0.70 was used for further biomechanical interpretation [7]. We proposed that the role of the muscles could be identified using PCA. We presumed that gait symmetry between two corresponding lower limb joints could be quantified by means of the PC curves derived from each joint or from each of the lower limbs described the same portion of the stance phase.

RESULTS AND DISCUSSION

The objective of this bilateral gait study was to determine whether the role of the sagittal plane joint moments taken appears to be symmetrical or not.

The average sagittal muscle moment curves and their standard deviation developed at the right and left ankles, knees and hips during the stance phase are presented in Table 1 and Fig 1. Muscle moment curves reported in this study were in close agreement in shape and magnitude with previously published findings [1,8,9].

Table 1: Peak muscle moments and standard deviation (SD) values calculated at the ankles, knees and hips for 20 healthy young male subjects (* $p < 0.05$)

Joint	Peak	Right		Left	
		Mean	SD	Mean	SD
Ankle	A1	-0.15	0.09	-0.12	0.02
	A2	1.53	0.30	1.46	0.10
Knee	K1	0.27	0.17	0.28	0.10
	K2	-0.40*	0.25	-0.26*	0.15
	K3	0.26	0.24	0.36	0.22
	K4	-0.31*	0.14	-0.20*	0.13
Hip	H1	-0.83	0.34	0.83	0.35
	H2	0.77*	0.32	0.40*	0.24

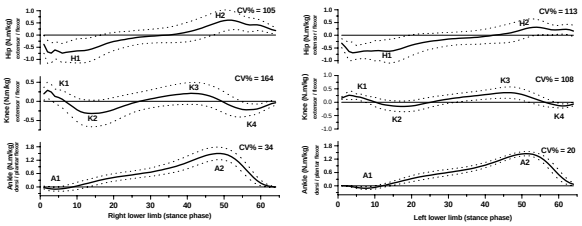

Figure 1: Average sagittal muscle moment curves and standard deviation (1SD) developed at the ankle, knee and hip joints during the stance phase of 20 able-bodied young male subjects

The two first representative curves (PC1 and PC2) accounted for the largest and an almost equal proportion of the observed variables' variance for the right (93%) and left (93%) limbs in the sagittal plane. In both PC1 and PC2, the significant loading factor values were similarly distributed over 20 to 40% and 5 to 20% of the gait cycles. These results might explain in part the idea of gait symmetry (global – Fig 3), while discrepancies were noted for group of muscles acting at each two corresponding joints (local – Fig 2). It seems that compensatory mechanisms might be the best explanation to describe global gait symmetry while different actions are taken by the joints.

Table 2: The variance extracted by each PC from the right and left lower limb muscle moment data

Joint	% Right lower limb			% Left lower limb		
	PC1	PC2	TEV	PC1	PC2	TEV
Ankle	51	21	72	40	20	60
Knee	80	11	91	73	12	85
Hip	73	15	88	82	6	88
Lower limb	64	29	93	63	30	93

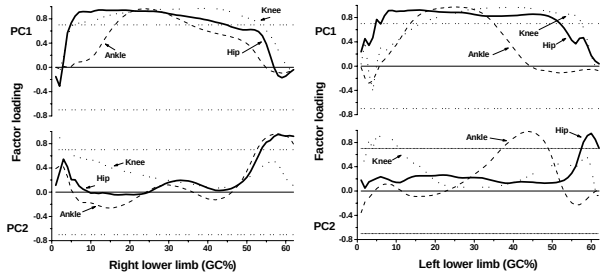

Figure 2: The first two PCs extracted from muscle moment curves calculated at the right and left ankles, knees and hips

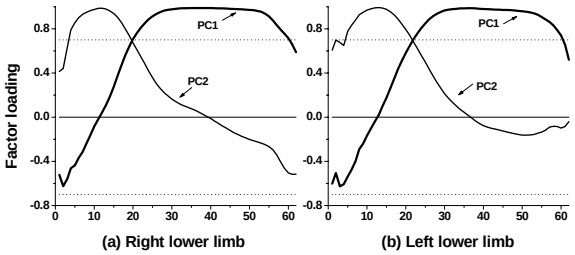

Figure 3: The first two PCs for the muscle moments developed at the lower limb during the stance phase of 20 healthy young male subjects

CONCLUSIONS

Local asymmetry in the gait of people without impairment is suggested, based on different functional tasks between the right and left hips, knees and ankles to control balance, between limb coordination and propulsion functions. The lower limbs, on the other hand, appeared to behave symmetrically when the total behavior of the limbs is considered. Compensation is recognized as an explanation for the existence of local asymmetry.

REFERENCES

1. **Crowinshield, R.D. et al. (1978).** *Clin Orthop,* **132:140-44.**
2. Winter, D.A., Sienko, S.E. (1989). *J Biomech,* **21:361-67.**
3. Gitter, A.. et al. (1997). *Am J Phys Med & Rehabil,* **76(2):114-120.**
4. Sadeghi, H. et al. (2001). *Am J Phys Med Rehabil,* **80: 25-32.**
5. Sadeghi, H. et al. (2000). *Phys Ther,* **80(12): 1188-196.**
6. Winter, D.A. (1990). John Wiley and Sons Publisher.
7. Sadeghi, H. et al. (2001). *J Aging Phys Activity,* **9: 172-83.**
8. Apkarian, J. et al. (1989). *J Biomech,* **22:143-55.**
9. Eng, J.J., Winter, D.A. (1995). *J Biomech,* **28(6):753-58.**

EXCLUSION OF THE SUBTALAR JOINT AFFECTS SIGNIFICANTLY THE CALCULATED ANKLE MUSCLE FORCES DURING GAIT.

Ilse Jonkers[1] Gerlinde Lenaerts[1] Friso Hagman[2] Louis Peeraer[1]
Jos Vander Sloten[1] and Georges Van der Perre[1]

[1] Katholieke Universiteit Leuven, Belgium
[2]Vrije Universiteit Brussel, Belgium
E-mail: Ilse.jonkers@faber.kuleuven.be

INTRODUCTION

In routine clinical gait assessment, the foot segment is often defined as a line segment between a marker on the forefoot and a marker on the heel. Such a 2 D model allows the calculation of dorsi- and plantarflexion movement at the ankle but does not account for movements in the subtalar joint, i.e. inversion and eversion. Consensus exists that for the description of the gait pattern in terms of kinematics and kinetics, a 2D ankle model suffices, especially if no gross foot deformities are present.

Based on the measured kinematics and kinetics, the muscle force contribution underlying the observed gait pattern can be calculated using dynamic simulations of gait, using either an inverse or forward approach. The current work focuses on the question whether exclusion of a subtalar joint significantly alters the muscle force production in the muscles crossing the ankle joint, calculated using an inverse dynamics analysis.

METHODS

Gait kinematics were measured at 250 Hz in 10 adult control subjects, walking at their self-selected walking speed (1.2 ±0.1 m/s) using Vicon system (Oxford Metrics). A modified Cleveland marker placement protocol was used. At the foot, the marker placement protocol was extended to four markers attached to the calcaneus and three markers attached to the forefoot. Ground reaction forces were measured simultaneously using an AMTI force plate.

Kinematics are calculated through an inverse kinematics procedure (SIMM, Motion Analysis Corp) based on a scaled musculoskeletal model, matching the subject's weight and height. Two distinct models were used: The first one (16 DOF) represented the foot as a line segment between the marker on the forefoot and heel. The second model (18 DOF) incorporated the subtalar joint as defined by Inman. In this model, ankle and subtalar kinematics were calculated using the postition of the four markers on the calcaneus and three markers on the forefoot.
For both models, joint moments were calculated for the generalized coordinates in each of the models using SIMM dynamics pipeline.

In a second analysis, muscle force distribution was calculated during stance phase of gait (Matlab). An optimization problem was solved to calculate the muscle moments and hence muscle forces that constitute the external joint moments while minimizing the overall muscle activity. Input were the moment arms and maximal force generating capacity of 43 muscles, given the kinematics of the generalized coordinates during stance. Additional constraints were imposed to the solver to

constrain the rate of muscle activation raise and decay within physiological limits and limit the level of maximal activation.

This analysis was repeated for the kinematics and kinetics calculated using the model with a 2D ankle, as well as the model incorporating the subtalar joint axis. To account for the anatomical variation of the subjects in the study population, the muscle force was expressed as a fraction of body weight (Force/BW). Muscle force production profiles were compared with reference data on muscle activation. The differences in the forces of the muscles crossing the ankle joint were compared statistically using a Wilcoxon Signed Rank test.

RESULTS

We found no significant differences in maximal dorsiflexion angle and maximal plantarflexor moment in stance, using both models. The 2D ankle model significantly overestimates maximal plantarflexor power generation (2D:1.53 - 3D:1.39; $p<0.05$), but underestimates maximal plantarflexor power absorption (2D:-0.34 - 3D:-0.55; $p<0.01$).

Figure1 presents the average difference in maximal muscle force production of 12 muscles crossing the ankle, using both models.

The 2D ankle model significantly under-estimates the muscle force production in M. peroneus longus, brevis and tertius, M. tibialis posterior and M. soleus. M. peroneus longus shows the largest difference in maximal force production up to 0.4 BW. M. tibialis posterior and M. Peroneus Brevis differ up to 0.1 BW. Although similar in magnitude, the overestimation of muscle force production for M. tibialis anterior using a 2D model, is not significant. The differences in maximal muscle forces for M. gastrocnemius medialis and lateralis are smaller than 0.1 BW and not statistically significant.

DISCUSSION AND CONLUSION

Estimation of individual muscle force production during gait is crucial in several applications, especially in evaluating the effectiveness of therapeutic interventions. We show that the calculated maximal force production in muscles that provide medio-lateral control of the foot position is significantly under- or overestimated when a 2D ankle model is used. Measurement and modelling of subtalar joint kinematics are crucial for reliable muscle force estimates during gait.

ACKNOWLEDGEMENTS

Ilse Jonkers is a Postdoctoral Fellow of the Research Foundation – Flanders

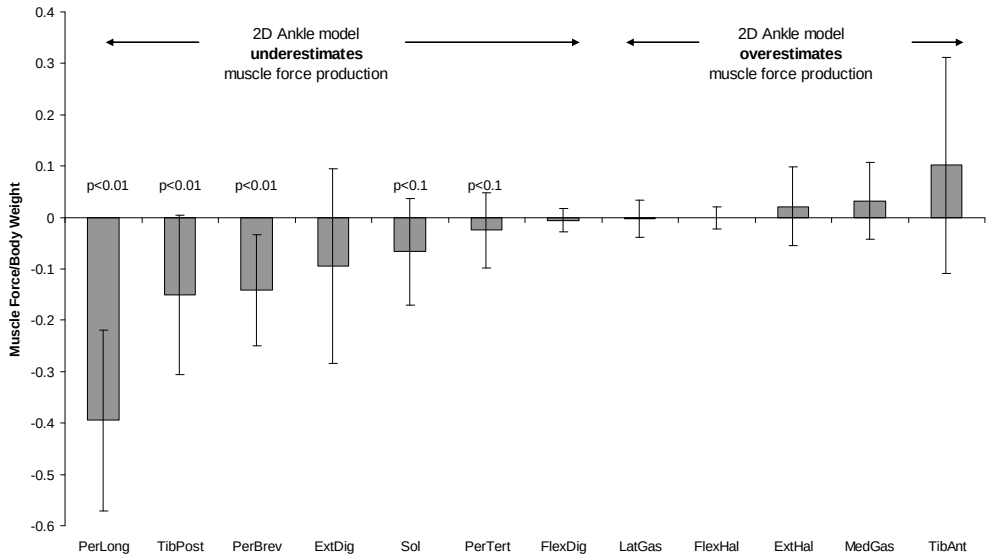

DETERMINING VERTICAL GROUND REACTION FORCES WITHOUT A FORCE PLATFORM USING A MASS-SPRING-DAMPER MODEL

Ross H. Miller[1,2], Graham E. Caldwell[1], and Timothy R. Derrick[2]
[1]Department of Kinesiology, University of Massachusetts Amherst, Amherst, MA, USA
[2]Department of Health and Human Performance, Iowa State University, Ames, IA, USA
Email: rhmiller@kin.umass.edu Web: http://www.umass.edu/sphhs/kinesiology

INTRODUCTION

The mechanics and stiffness characteristics of the body during running are often described by mass-spring (MS) models (Farley & Gonzalez, 1996) or mass-spring-damper (MSD) models (Derrick *et al*., 2000; Nigg & Liu, 1999). Using models to generate ground reaction forces (GRF) could be beneficial when no force measurement is possible. While MS models can replicate the active mid-stance vertical GRF peak (Morin *et al*., 2005), MSD models can also produce the passive impact peak present in heel-toe running (Derrick *et al*., 2000). The feasibility of using an MSD model to predict GRF in the absence of a force platform depends on how well MSD parameters can be predicted from simple measurements that can be made outside the laboratory. Our purpose was to investigate the ability of an MSD model to produce model GRF (*MGRF*) that replicate experimental GRF (*EGRF*) without using a force platform. MSD parameters were predicted by correlating kinematic and anthropometric measurements with optimized parameters.

METHODS

EGRF were collected for ten healthy young subjects running over a force platform at their preferred pace for seven trials each. Joint kinematics were computed from reflective markers on the dominant leg. Each subject's kinematics and *EGRF* were averaged across trials. *MGRF* were generated with a MATLAB-based MSD model (Derrick *et al*., 2000; Fig. 1). The lower mass M_2 represents the effective mass of the body accelerated at impact. The upper mass M_1 is the remainder of the body's mass.

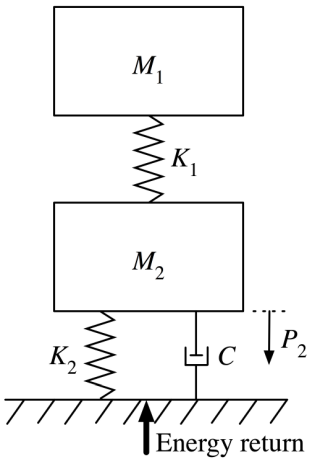

Figure 1. The MSD model used to generate GRF.

For each subject, stiffness parameters (K_1 and K_2) and the initial lower mass height (P_2) were optimized using a genetic algorithm to minimize the mean square error and timing errors between *MGRF* and *EGRF*. Optimal MSD parameters were then correlated by multiple linear regression with eight anthropometric and kinematic measures: sex, height, weight, leg length, thigh length, running speed, knee flexion angle at heel-strike, and knee flexion range of motion (ROM) during stance. GRF generated by parameters predicted by regression (*RGRF*) were compared to *EGRF* and *MGRF*.

RESULTS & DISCUSSION

The damping coefficient *C*, energy return, effective mass, and error between *MGRF*

and *EGRF* were comparable to previous MSD models (Derrick *et al*., 2000). Linear regression predicted strong correlations for K_1, K_2, and P_2 (R^2 = 0.99, 0.95, and 0.99, respectively) between optimal MSD parameters and the anthropometric and kinematic measures. Table 1 shows the average parameters from optimization and regression. Height, weight, and knee flexion ROM were the most sensitive regression parameters. Leg length was a sensitive parameter for P_2. *MGRF* and *RGRF* profiles were nearly identical for all subjects. Figure 2 shows *EGRF*, *MGRF*, and *RGRF* profiles for a representative subject.

Table 1. Optimal and regressed MSD parameters.

	K_1 (N/m)	K_2 (N/m)	P_2 (mm)
Optimization	14557	104565	8.45
Regression	14556	104612	8.46

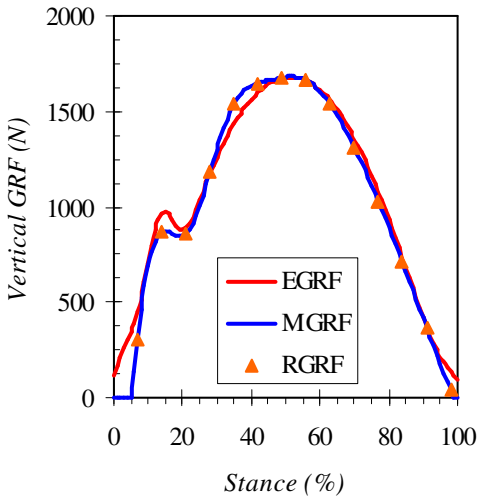

Figure 2. *EGRF*, *MGRF*, and *RGRF* curves.

Results indicate that the MSD model with parameters predicted by regression can accurately represent experimental GRF without kinetic measures. Previous research that modeled GRF without kinetic data depended on stance time, which is difficult to measure without a force platform or motion capture system (Morin *et al*., 2005). The MSD model with parameters estimated by regression can generate relatively accurate GRF using lower extremity anthropometrics and sagittal knee kinematics, quantities easily measured by anthropometry and electrogoniometry.

The MSD model had difficulty matching the GRF profile near heel-strike and toe-off (Fig. 2) and typically provided a better fit between *EGRF* and *MGRF* for the mid-stance peak (average error of 3%) compared to the impact peak (average error of 10%). Model performance can be improved by using a cost function that emphasizes peak magnitudes, or by including wobbling masses (Nigg & Liu, 1999).

SUMMARY & CONCLUSIONS

Vertical GRF during running were determined using a mass-spring-damper (MSD) model. By optimizing the MSD parameters, the model could generate GRF that closely matched experimental data. Model parameters were strongly correlated with data that are easy to measure without force platforms or motion capture systems. Therefore model parameters could be estimated from regression and used to determine vertical GRF outside a laboratory setting. The next step, predicting the anterior-posterior GRF by a Fourier series model, has shown promising early results.

REFERENCES

Derrick *et al*. (2000). *Journal of Applied Biomechanics*, *16(1)*, 36-51.

Farley & Gonzalez (1996). *Journal of Biomechanics*, *29(2)*, 181-186.

Morin *et al*. (2005). *Journal of Applied Biomechanics*, *21(2)*, 167-180.

Nigg & Liu (1999). *Journal of Biomechanics*, *32(8)*, 849-856.

ACKNOWLEDGEMENTS

Thanks to Jason Gillette and Brent Edwards for help with data collection and coding.

EFFECT OF MUSCLE WEAKNESS ON HIP CONTACT FORCES DURING GAIT IN PATIENTS WITH PRIMARY OSTEOARTHROSIS

Gerlinde Lenaerts[1], Ilse Jonkers[1], Michiel Mulier[2], Arthur Spaepen[1] and George Van der Perre[1]

[1] Katholieke Universiteit Leuven, Leuven, Belgium
[2] Universitaire Ziekenhuizen Leuven, Pellenberg, Belgium
E-mail: gerlinde.lenaerts@faber.kuleuven.be

INTRODUCTION

Hip abductor weakness is a typical limitation in patients with osteoarthrosis (Jandric, 1997, Sims et al., 2002) but is also reported in healthy elderly people (Johnson et al., 2004). The activity of the muscles that span the hip joint affects the hip contact forces. Muscular forces and hence joint loading can be calculated with musculoskeletal models and inverse dynamic analyses (Heller et al., 2001; Pedersen et al., 1997; Stansfield and Nicol, 2002). The aim of the present study is to explore the relation between hip muscle weakness, evaluated through dynamometry, and the calculated hip contact forces during gait. We hypothesize that more pronounced muscle weakness results in less physiologic loading of the hip joint.

METHODS

Ten patients (mean age 62.6 ± 9.6 yr) with primary osteoarthritis of the hip were included in the study. Clinical gait analysis was performed prior to total hip replacement surgery. Kinematic and kinetic data were collected during gait using an integrated 3D movement analysis system (Vicon, Oxford Metrics). All patients performed a maximal voluntary contraction (MVC), during which the peak force generated during hip flexion, hip extension and hip abduction was measured with a hand-held dynamometer (MicroFET, Biometrics, NL) in a standardized upright position. For each patient, a musculoskeletal model was created by scaling a standardized model (Simm, Motion Analysis corp.) based on the marker positions during a static pose. Maximal force generating capacity of the muscles was not scaled to represent muscle weakness. These models were used to calculate (1) joint moments (2) individual muscle force generating capacity and (3) muscle moment arms over the gait cycle. Muscle activation patterns balancing the external joint moments were computed using a static optimization algorithm, minimizing the sum of the muscle activation (Matlab, MathWorks Inc.). The 3D hip contact forces were computed taking into account the muscle forces resulting from the muscle activation patterns, as well as external forces (the ground reaction forces – inertial forces and gravity). The maximal hip contact forces and the associated inclination angles are reported.

RESULTS

In the studied population, a high correlation (0.72) was found between the peak MVC values for hip abduction en and hip extension. Decreased MVC values are indicative for more pronounced muscle weakness. There was no clear relation between peak MVC values and walking velocity.
The total peak contact forces are within the range reported in literature (Heller et al., 2001; Stansfield et al., 2002). Weakness of the hip extensor muscles is associated with a decrease of the vertical contact force component and an increase of the posterior-

anterior contact force component at the moment of peak loading. Weakness of the hip abductor muscles increases the anterior-posterior and medio-lateral force component, but does not affect the vertical component. These tendencies are confirmed in the changes in inclination angles of the total contact force vector (fig. 1). There was no clear relation between the peak MVC values of the hip flexors and the 3D hip contact forces.

DISCUSSION

We demonstrated a relation between weakness of hip extensors and abductors and hip contact forces, dictated by alterations in the gait pattern. The components of the hip contact forces and hence the inclination angles of the total contact force are affected: The angles in the sagittal and especially transverse plane increase, resulting in a less physiologic loading condition of the hip joint. Further research will aim to extend the study population, in order to establish stronger relations between muscular force and hip contact forces during gait.

SUMMARY/CONCLUSIONS

Hip extensor and abductor weakness in patients with osteoarthrosis, tend to increase the anterior-posterior and medio-lateral contact force component, resulting in a reduced vertical loading condition of the hip joint.

REFERENCES

Heller, M.O. et al. (1997). *J Biomech*, **30**, 959-965.

Jandric, S. (1997). *Med Preg*, **50**, 301-304.

Johnson, M.E. et al. (2004). *Arch.Phys.Med.Rehabil.*, **85**, 593-597.

Sims, K.J. et al. (2002). *Ann.Rheum.Dis*. **61**, 687-692.

Stansfield, B.W., Nicol A.C. (2002). *Clin Biomech*, **17**, 130-139.

ACKNOWLEDGEMENTS

The support of the KU Leuven research council trough grant OT/03/31 is gratefully acknowledged.

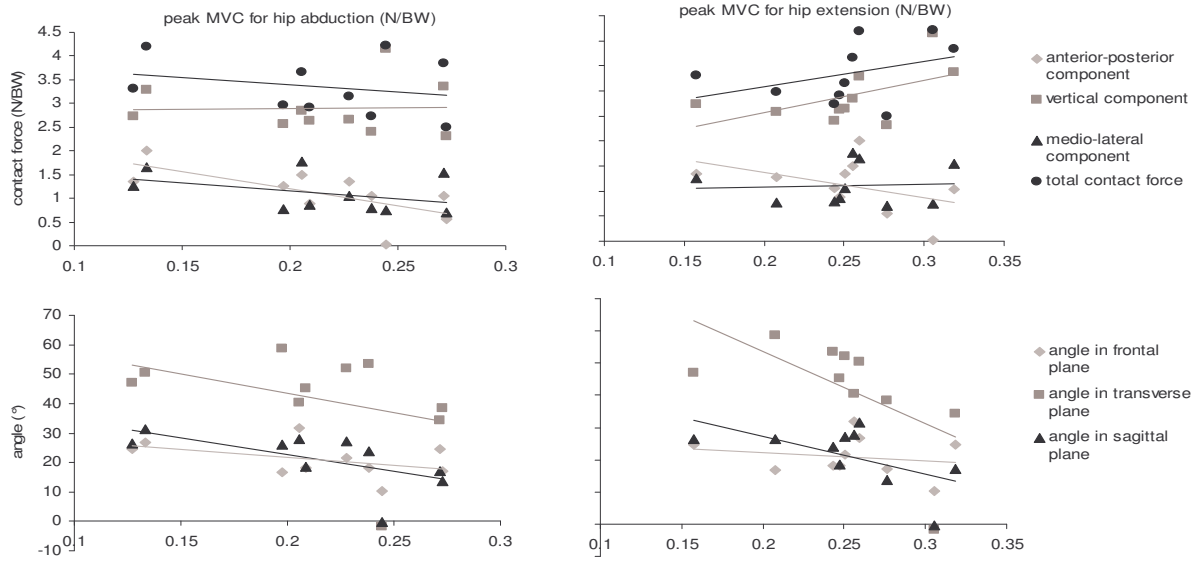

Figure 1: Peak hip contact forces and associated inclination angles during gait, as a function of peak MVC of hip abduction (left pane) and hip extension (right pane).

NEW TRENDS IN ORTHOPEDIC IMPLANTS

Aliotti, A[1,2] , Turri, S[3], Stindel, E[1,4], Hamitouche, C[1,2] and Roux, C[1,2]
[1] INSERM U650, Brest, F-29200 France ;
[2] ENST Bretagne, GET-ENST, Brest, F-29200 France ;
[3] LIME, UBO, Brest, France;
[4] CHU Brest, Service d'Orthopédie-Traumatologie, Brest, F-29200 France ;
email: antoine.aliotti@enst-bretagne.fr, web: http://latim.univ-brest.fr

INTRODUCTION

Since the beginning of this new century, the micro electromechanical technology is more present in the day - life. This evolution is mainly met in medical surgeries like cardiac or abdominal. They solve some medical deficiencies, and most of them are powered by chemical batteries like Lithium Ion batteries [1], which have to be recharged or replaced during a revision surgery.

Figure 1 : Theken eDisc

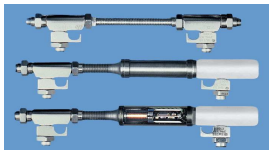

Figure 2 : Spinal Device

The main goal of the orthopaedic surgery is to contribute to the restoration of articular deficiency with total or unit compartmental orthopaedic implant. However, the morphological patient dataset is not the same during and after the surgery. As the patient is under the influence of general anaesthesia, the surgery procedure increases the risk of loosening of prosthesis due to the non-optimal position of the implant. The traditional solution is to carry out a new revision surgery in order to replace bad prosthesis. Others personal characteristics are likely to disturb the prosthesis's life like patient's age, walk, day life, the tibial plateau erosion, etc. These constraints modify the conditions of the patients and also increase the difficulty of the surgeon's work. The implants present challenges to their designers and manufacturer in term of high level of safety and reliability. Such orthopaedic implant has to be active and not passive to give some information about risks.

The aim of our study is to stand a brief comparative review of various developments of new trends in orthopedic implants, developed by laboratories or companies. The main goal is to know what happened inside implant about in-vivo load measurements, temperature distribution or information during the performed surgeries. Most of them use telemetry technology to transmit their datasets in order to process the computation, and, the provided energy is transmitted by induction coils between the implant and extern devices. However, none of them is self alimented by micro mechanism or batteries.

METHODS AND SOLUTIONS

SPINAL JOINT

The instrumented spinal devices are present in two versions. The first, defined by [2], presents an artificial spinal disc, which incorporates a microelectronic device (Figure 1). The information gathered from the eDisc empowers surgeons to better manage their patient's post-operative course. The second device [3] presents an internal spinal fixation, using semiconductor strain gauges in order to control and measure three force components, three moments and the implant temperature.

HIP JOINT

For this joint, the principal idea is still to develop a device around the temperature measure and the force measurements between the cup and the femoral head [4 - 5] (Figure 3).

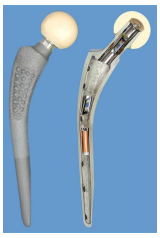

Figure 3: Hip implant

KNEE JOINT

The knee is the joint, where the trend is more present than the other joints. In addition, the Total

Knee Arthroplasty (TKA) needs to improve the ligament balancing to intraoperatively procedure. The first used approach consists in a distraction device or a model, which helps the surgeons to release the ligament [6]. The second solution is a device with two piezoelectric blades [7], one for each condyle, to improve the ligament balancing (Figure 4).

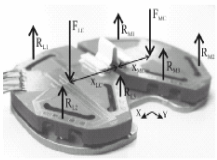

Figure 4: Device sensitive plate

Also, joint implant is evaluated. In addition, several studies incorporated sensors to measure joint forces and environmental conditions [8]. In vivo measurements are taken during walking or stair climbing (Figure 5)

Figure 5 : Instrumented Tibial tray

CONCLUSIONS

All devices proposed here allow to the improvement of the implant technology. Their main goal is to define the force distribution in the implant and also improving their future designs. However, they are limited by their power autonomy, because they need to be supplied by external energy from large equipment (such induction process). To optimally this trends and give total free, it could be interesting to study the self powered and other localized failuress.

REFERENCES

1.Venkateswara et al., *IPEJ* **4**, 201 – 212, 2004
2.Theken Discl.. *MdNews* , 1 - 4**,**, 2004.
3.Greichen et al. *Med. Eng. Phys*. **18**, 167-174, 1996.
4.Greichen et al. *J Biomech **32,** 1113 – 1117*,1999
5.Davy et al., *J Bone Joint Surgery* **70**, 45 – 50, 1988
6.Marmignon, *Phd thesis*, 115 p, 2004
7.Crottet, *IEEE TBE* **52**, 109 – 1611, 2005
8.Morris, *J Bone Joint Surgery* **83**, 62 – 66, 2001

A NOVEL METHOD FOR PATIENT SPECIFIC FINITE ELEMENT MESH DEVELOPMENT OF THE SPINE

Nicole A. Kallemeyn, Kiran H. Shivanna, Nicole M. Grosland

The University of Iowa, Iowa City, IA, USA
E-mail: nicole-grosland@uiowa.edu, Web: www.ccad.uiowa.edu/mimx

INTRODUCTION

Finite element analysis is an invaluable tool in the field of musculoskeletal biomechanics because it allows for a detailed investigation of normal and pathological conditions of a variety of anatomical structures. Once validated, a finite element (FE) model can be used to explore conditions that might not otherwise be feasible in an experimental setting.

Due to the complexity of the bony structures of the human body, it is difficult and time consuming to create a FE mesh of high quality. In the case of orthopaedic biomechanics, it is common to create a single model based on an 'average' geometry. However, a potential limitation of this method is that the results for one subject may not necessarily apply to the general population.

The spine is a very complex component of the skeletal system. A number of spine FE models exist in the literature (Fagan 2002); however, most use simplified or idealized geometry. Those which incorporate a more realistic geometry often are comprised of tetrahedral elements or a mixture of hexahedral and tetrahedral elements. Hexahedral elements are generally accepted as being preferable for 3D nonlinear strain calculations (Bowden 2006).

We propose an automated hexahedral meshing technique for the spine. The method addresses many of the previously reported difficulties with regard to spine FE modeling. A bounding box technique is used, with a special emphasis on the attachment of the posterior region to the vertebral body. The method has been applied to both the cervical and lumbar levels, and helps pave the way for patient-specific spine FE modeling.

METHODS

CT scans were acquired of a cadaveric specimen. The C5 vertebra was segmented and an STL was created (Figure 1A). The solid meshing process consists of two stages; meshing the vertebral body, and meshing the posterior elements directly from the vertebral body mesh.

Using ParaView (www.paraview.org), the vertebral STL surface definition was initially clipped so that the posterior region was removed. The resulting vertebral body was meshed using the technique shown in Figure 1B. The mesh was initiated by manually tracing the bounds of the superior and inferior vertebral endplate periphery, in addition to the nucleus. A butterfly bounding box (BB) pattern was then automatically generated and applied to subdivide the vertebral body as illustrated.

The posterior region was meshed by creating a system of bounding boxes which surround the posterior surface (Figure 1C). At the junction between the vertebral body and the posterior region (pedicle), the BB's were defined directly from the nodes of the predefined vertebral body mesh, which later

provided a mutual platform for the body and posterior meshes to be merged (Figure 2A).

After the BB's were created, mesh seeds were automatically assigned to each box based on a specified average element length. The seeding for the boxes at the pedicle was governed by the mesh seeding on the corresponding vertebral body mesh. Finally, the posterior element mesh was created and automatically attached to the vertebral body mesh at the pedicle.

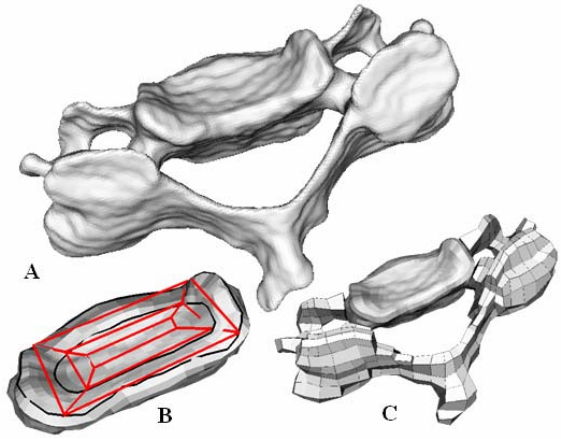

Figure 1: A) C5 STL surface. B) Vertebral body mesh. C) BB's for C5.

RESULTS AND DISCUSSION

The final C5 mesh is shown in Figure 2B, with a 50N compressive load applied to the superior body surface. The meshing technique was also applied to the lumbar spine (L5, Figure 2C). Once the bounding boxes have been created, the entire meshing process takes only a few minutes. After the BB's have been created for one spinal level, only slight modifications are needed for meshing adjacent levels.

SUMMARY/CONCLUSIONS

This method brings a novel approach to subject-specific spine modeling through the merging of the vertebral body and posterior region meshes using the BB methods described above. The automated techniques dramatically decrease the amount of time required to mesh the spine as compared to previous methods, while maintaining the geometrical complexities inherent to the spine. Further work will include the automated creation of the intervertebral disc between spinal levels, and model validation through biomechanical testing.

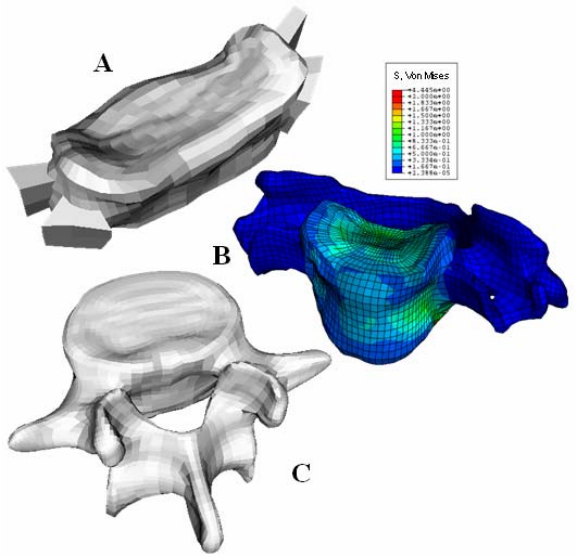

Figure 2: A) Posterior BB attachment to vertebral body mesh (other BB's removed). B) C5 mesh with 50 N compressive load applied to the body. C) L5 final mesh.

REFERENCES

Bowden, A. (2006). *Spine Technology Handbook*. Ed. by S.M. Kurtz and A.A. Edidin. Elsevier Academic Press.

Fagan, MJ, et al. (2002). *Proc Instn Mech Engrs Part H*, **216,** 281-298.

ACKNOWLEDGEMENTS

The authors gratefully acknowledge the financial support provided by The University of Iowa Biological Sciences Funding Program (BSFP).

GLUCOSAMINE AND CHONDROITIN SULFATE AFFECT THE RESPONSE OF EXERCISED ARTICULAR CARTILAGE TO BLUNT IMPACT LOADING

Feng Wei, Nurit Golenberg, Eugene Kepich, and Roger Haut

Michigan State University, East Lansing, MI, USA
E-mail: haut@msu.edu, Web: www.obl.msu.edu

INTRODUCTION

Cyclic compression of articular cartilage has been shown to modulate metabolism and turnover of proteoglycan (PG) and collagen in a complex and multifactorial manner. More recent studies in our lab showed that physiologically moderate in vitro exercise plays a positive role in articular cartilage response to injurious compression (Wei et al. 2006). However, in vitro studies by Thibault et al. (2002) have shown an increase of cell death and matrix damage due to the cyclic loading of cartilage explants. Furthermore, strenuous exercise of cartilage has shown a significant modulus decrease of 13-14% and a reduction of PG content (Helminen et al. 1992).

Osteoarthritis (OA) is a manifestation of an imbalanced synthesis of articular cartilage matrix and the associated growth factors. The use of potentially chondro-protective agents such as glucosamine (glcN) and chondroitin sulfate (CS) has been explored to treat OA. The mixture of glcN and CS has been observed to function as biological response modifiers (BRMs), which may boost natural protective responses of tissue under adverse environmental conditions (Lippiello 2003). Since both glcN and CS have minimal effects on normal cartilage in vivo, we hypothesized that stressed cells under exercise in the presence of high doses of glcN and CS might be more responsive and enhance the protective metabolic response of chondrocytes to injurious blunt impact loading.

METHODS

A biopsy punch was used to make 54 6mm diameter chondral explants from the lower metacarpal surface of bovine forelegs. All specimens were randomly assigned to three groups: 7, 14 and 21 days of exercise with (n=6) and without (n=6) glcN and corresponding controls (n=6). All explants were placed in DMEM: F12 medium inside of a humidity-controlled incubator. Six explants in each of the 3 groups were treated with 500 μg/ml glcN and 250 μg/ml CS in the medium. Prior to and after exercise loading, each explant was subjected to an indentation stress relaxation test. The relaxation data were analyzed using a fibril-reinforced biphasic model (Soulhat et al. 1999) to determine values of matrix modulus, fiber modulus and hydraulic permeability. Intermittently applied uniaxial exercise loading was introduced by using a sinusoidal 0.5MPa-0.2Hz waveform for 10 cycles once per hour. After exercise, all explants were exposed to an unconfined compression of 25MPa in 1 sec to peak between two highly polished stainless steel plates. For matrix damage analysis, the surfaces of all impacted explants were wiped with India ink and photographed to determine the total length of surface fissures. Two-way repeated measures ANOVA and Student-T tests were performed to determine differences from control and within exercise groups. Statistical significance was indicated for $p < 0.05$.

RESULTS AND DISCUSSION

Previous studies in our lab showed that up to 21 days of exercise all cells remained alive before injurious compression. The matrix modulus of explants exercised with glcN and CS stayed in a high level in all 3 groups, while after 21 days exercise without glcN and CS decreased the matrix modulus by about 50% (Figure 1). Both exercise with and without glcN and CS decreased the fiber modulus about 60%. There was no significant difference between exercise with and without glcN and CS (Figure 2). Up to 14 days exercise without glcN and CS significantly decreased the explant permeability, while after 21 days the permeability increased dramatically. However, with glcN and CS in the media exercise decreased the permeability significantly in all 3 groups (Figure 3). Exercise without glcN and CS significantly decreased the explant surface fissure length after 7 days, while after 21 days the fissure length increased to about 130% of control. However, when exercised with glcN and CS a significant decrease of fissure length from control was observed in all three groups (Figure 4).

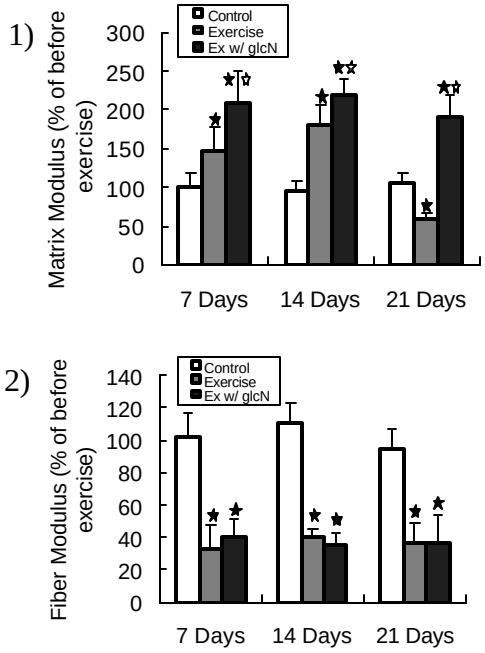

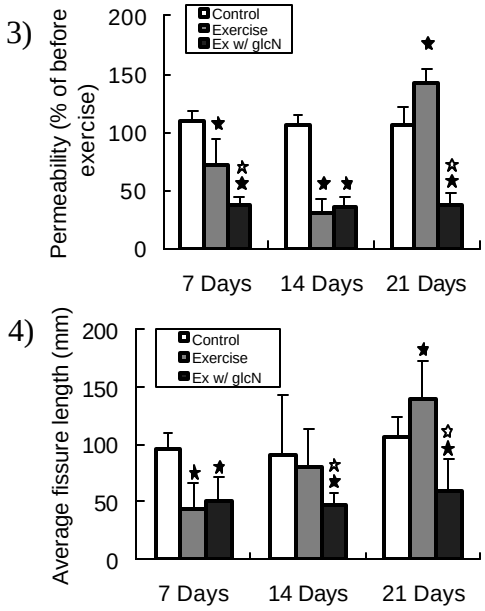

Figure 1-4. Statistically significant differences were observed: ★ from control, and ☆ from exercise.

SUMMARY/CONCLUSIONS

The mechanical response of cartilage to glcN and CS under simulated conditions of in vivo exercise was significantly greater than that seen without supplementation. By enhancing the protective response of cartilage to impact loading, glcN and CS may help to reduce the susceptibility of cartilage to mechanical injury in the normal population during sports, recreation and exercise.

REFERENCES

Helminen, H.J. et al. (1992). *Articular Cartilage and Osteoarthritis*. Raven Press.

Lippiello, L. (2003). *OA & Cart*, **11**, 335-42.

Soulhat, J. et al. (1999). *J. Biomech Eng*, **121**, 340-7.

Thibault, M. et al. (2002). *J. Orthop Res*, **20**, 1265-73.

Wei, F. et al. (2006). *Trans of the 53rd Annual Meeting of the Orthop Res Soc*.

ACKNOWLEDGEMENTS

This research was supported by a grant from the CDC (R49/CE000623). The nutraceutical was supplied by Nutramax Laboratories Inc.

ANISOTROPIC STRESS ANALYSIS OF THE SECOND METATARSAL DURING THE STANCE PHASE OF GAIT

W. Brent Edwards [1], Stacey A. Meardon [1] Erin D. Ward [2], and Timothy R. Derrick [1]

[1] Iowa State University, Ames, IA, USA
[2] Central Iowa Foot Clinic, Perry, IA, USA
E-mail: edwards9@iastate.edu Web: www.hhp.hs.iastate.edu

INTRODUCTION

The second metatarsal (2nd Met) is a common site for stress fracture among athletes and military recruits. Although the exact cause of stress fractures remains unclear, it is believed to result from repetitive, cyclical loading. Understanding the loading environment at the 2nd Met may help to elucidate the etiology and aid in the prevention of stress fractures at this site.

In locomotion, peak longitudinal bone strain at the 2nd Met occurs during late stance, and tends to coincide with peak Achilles tendon force (Donahue et al., 2000). During this phase, the stresses acting along the principal material axes (Figure 1) of the 2nd Met are important, because models of stress fracture damage, repair and adaptation are based on stresses occurring in these directions (Taylor et al., 2004).

The purpose of this study was to: (a) quantify the stresses acting along the principal material axes of the 2nd Met during the stance phase of gait, (b) and determine the relationship between longitudinal stress and Achilles tendon force.

METHODS

Four fresh cadaver foot specimens were utilized for this study. A stacked rosette strain gage was mounted to the dorsal surface of the 2nd Met, and an intra-medullary rod was used to connect the tibia to a dynamic gait simulator.

The dynamic gait simulator is capable of simulating the stance phase of walking in approximately 1.0 sec and can replicate human ground reaction forces. Eight extrinsic muscles crossing the ankle joint are connected to load cells in series with motors to simulate muscle activity.

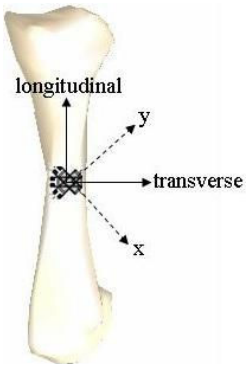

Figure 1: Principal material axes (trans-long) and rosette axes (x-y).

Each cadaver foot was outfitted with a sandal, and walked multiple trials across a force platform. Ground reaction force, bone strain, and muscle force data were collected concurrently at 1200 Hz. The data were exported to Matlab 7.0.4., and smoothed using a low-pass Butterworth filter with a cutoff frequency of 30 Hz. An anisotropic stress analysis of the strain rosette information during the stance phase of gait was then performed in accordance with Carter (1978). The principal strains and axes of orientation were calculated and rotated into the principal material directions. The stresses in the principal material directions were then calculated using material constants provided by Reilly and Burstein (1975).

The mean and standard deviation for peak longitudinal stress (σ_{long}), transverse stress (σ_{tran}), and shear stress (τ) were calculated

for each specimen. To determine the relationship between σ_{long} and Achilles tendon force (F_{at}) during stance, a cross-correlation at zero-lag was used. The mean correlation for all trials was calculated by converting the correlations to z-scores, calculating the average, and converting back to the correlation scale.

RESULTS AND DISCUSSION

A substantial amount of compressive σ_{long} was observed during the later portions of stance, while the σ_{tran} and τ appeared to be negligible in comparison (Figure 2). The mean peak σ_{long} for each specimen ranged between 11.18 MPa and 30.54 MPa (Table 1), and tended to occur near 70% of stance.

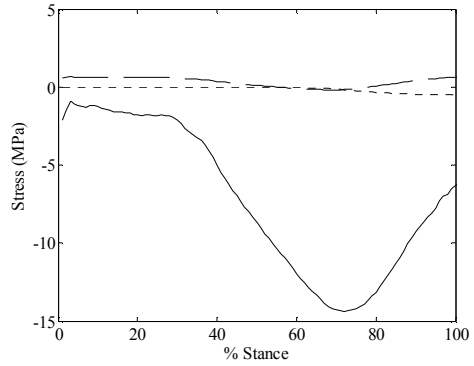

Figure 2: Principal material stresses for one representative trial. Solid line = σ_{long}; Dashed line = σ_{tran}; Dotted line = τ.

A strong cross-correlation was observed between σ_{long} and F_{at} (Figure 3). The correlation ranged from -0.85 to -0.99, with a mean of -0.97. The large correlation suggested that the σ_{long} was highly dependent on the plantarflexor moment that occurred during late stance.

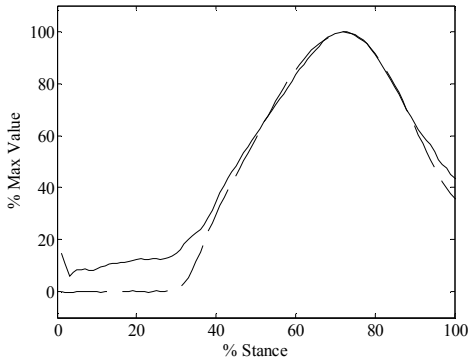

Figure 3: Relationship between σ_{long} and F_{at} for one representative trial. Solid line = $|\sigma_{long}|$; Dashed line = F_{at}.

SUMMARY/CONCLUSIONS

According to our model, the primary mode of loading on the dorsal 2nd Met during walking is compressive σ_{long} with little σ_{tran}. The small τ also suggested negligible torsional loading, although this may be due to the restricted tibial rotation in our model. The compressive σ_{long} is most likely due to bending caused by late stance plantarflexion. Stress fracture intervention should look to decrease this large bending stress, possibly with the use of orthotics.

REFERENCES

Donahue, S. W. et al. (2000). *Bone*, **27**(6), 827-833.

Taylor, D. et al. (2004). *J. Orthop. Res.*, **22**, 487-494.

Carter, D. R. (1978). *J. Biomech.*, **11**, 199-202.

Reilly, D. T. & Burstein, A. H. (1975). *J. Biomech.,* **8***,* 393-405.

Table 1: Mean (1SD) peak stresses in principal material directions for the four specimens.

	Foot 1	**Foot 2**	**Foot 3**	**Foot 4**
σ_{long} (MPa)	30.54 (6.53)	18.17 (2.07)	11.34 (1.31)	11.18 (3.23)
σ_{trans} (MPa)	0.47 (0.13)	0.77 (0.10)	0.53 (0.04)	0.40 (0.08)
τ (MPa)	0.39 (0.17)	0.53 (0.22)	0.10 (0.04)	0.22 (0.07)

MUSCLE FUNCTION IS BIASED TOWARDS POSITIVE OVER NEGATIVE WORK IN LEVEL HUMAN GAIT

Paul DeVita[1], Lars Janshen[2], Allison Gruber[1], Patrick Rider[1],
Stanislaw Solnik[1], Paul Zalewski[1], Brian Moscicki[1], and Tibor Hortobagyi[1]

[1]East Carolina University, Greenville, NC, USA [2] Humboldt University, Berlin, Germany
E-mail: devitap@ecu.edu

INTRODUCTION

Level gait at constant average velocity includes the generation and dissipation of equal amounts of mechanical energy (i.e. positive and negative work) through the stride cycle (4). Surprisingly, Elftman (4) and Dutto et al (1) showed net positive joint work in level human running and in level horse trotting. Positive and negative joint work were derived from joint powers and were attributed to shortening (concentric) or lengthening (eccentric) muscle contractions. To our knowledge no subsequent studies of the potential imbalance in joint and therefore muscle work over the stride cycle have been reported.

Theoretically positive mechanical work can be produced in mammals only by converting chemical energy into mechanical energy within muscle sarcomeres (i.e. the power stroke of the cross bridges, 3). In contrast, negative work can be produced by muscles but also other body tissues through compression and tension (5). This suggests that to maintain constant mechanical energy over a stride muscle positive work would have to overcome energy losses from these other tissues. Based on Elftman's and Dutto's empirical data and on these theoretical concepts, we hypothesize that muscles produce a net positive work during level gait despite the maintenance of a constant level of mechanical energy (total mechanical work = 0). The purpose of the study was to determine total negative, positive and net lower extremity joint work during level human walking and running.

METHODS

Ground forces and 3D kinematics were obtained from 21 adults while walking (1.5 m/s) and 16 other adults while running (3.5 m/s). Inverse dynamics were used to derive 3D joint powers throughout the stride. Positive, negative, and total work at each lower limb joint were derived from these data and assumed to be due to muscle forces (6). We verified that mechanical energy did not change over the stride by comparing the height and velocity of a marker on the L5/S1 joint at the start and end of the stride cycle. T-tests ($p<0.05$) compared negative and positive work at each joint and total negative and positive work summed across the joints.

RESULTS AND DISCUSSION

The pattern of results was identical in walking and running tests. Total positive joint work was 16% and 8% larger then total negative joint work in these gaits (both $p<0.05$) producing 9 J and 10 J of net positive work in the two gaits (fig 1). 20 of the 21 subjects in walking and all 16 subjects in running had net positive joint work. Based on the L5/S1 marker kinematics, total body energy changed less than 1% over the stride in walking and running. These results indicated the observed positive bias in joint work was a consistent finding and was not due to a

change in body vertical position or running velocity (i.e. an increase in body mechanical energy).

Hip and ankle joint work were positively biased in both gaits however the hip bias was much larger. Positive vs. negative hip work was 2.6 and 3.3 fold larger in walking and running whereas positive vs. negative ankle work was only 0.2 fold larger in both gaits (fig 1.). Knee joint work was largely negatively biased in both gaits. Negative vs. positive knee work was ~2.5 fold larger in walking and running. These data indicated the hip muscles were primary energy generators and functioned more concentrically than eccentrically, knee muscles were primary energy dissipaters and emphasized eccentric function and ankle muscles had, to a large extent a balance of generating-dissipating or concentric-eccentric functions.

SUMMARY/CONCLUSIONS

Level human gait at a constant average velocity does not balance muscle work through concentric and eccentric contractions but emphasizes the, "over-production," of energy through shortening contractions to maintain a constant level of total mechanical energy. The net positive muscle work along with the nearly constant vertical position and horizontal velocity over the stride indicated that some of the positive work produced by muscles was not used to maintain upright posture (i.e. potential energy) and gait velocity (i.e. kinetic energy) but was wasted through various energy sinks. These sinks might be spinal discs, joint cartilage, and the shoe and floor however these and other possible energy sinks need further investigation.

REFERENCES

1) Dutto et al. (2000), *J. Exp. Biol.* **209**, 3990-3999.
2) Elftman. (1940), *Am. J. Physiol.* **129**, 672-684.
3) Huxley. (1969), *Science* **164**, 1356-1365.
4) Minetti et al. (1993). *J Physiol* **472**, 725-735
5) Williams et al. (1983) *J. Biomech.* **16**, 115-128.
6) Winter (1983). *J. Biomech.* **16**, 91-97.

ACKNOWLEDGEMENTS

NIA AG16192

A)

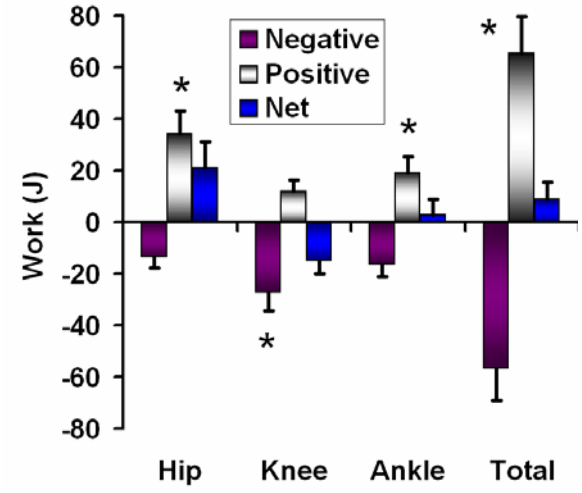

B)

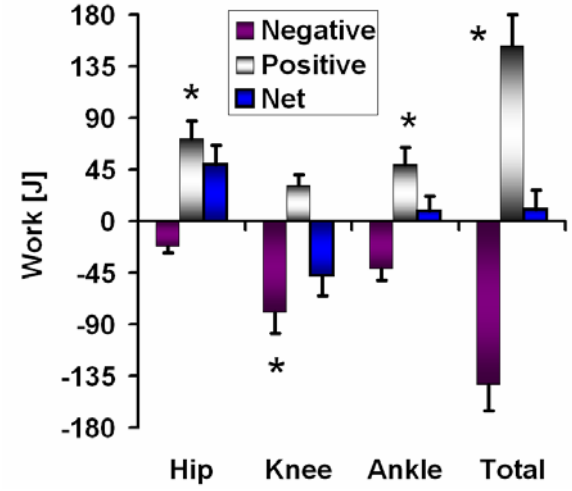

Figure 1, Negative, positive, and net work at each joint and their sums (Total) in A) walking and B) running. ***** positive or negative work significantly larger than the other ($p<0.05$).

A MODEL OF MAXIMUM VOLUNTARY JOINT TORQUE VARIATION WITH JOINT ANGLE AND ANGULAR VELOCITY

Dennis E. Anderson, Michael L. Madigan and Maury A. Nussbaum

Virginia Polytechnic Institute and State University, Blacksburg, VA, USA
E-mail: dennisa@vt.edu, Web: www.biomechanics.esm.vt.edu

INTRODUCTION

Maximum voluntary joint torque varies substantially with joint angle and angular velocity. In some studies of human movement, joint torques determined by inverse dynamics analysis are compared to strength, defined as a single value of maximum joint torque (e.g. Hughes, 1996). However, because of the variation in available joint torque with angle and angular velocity, representing strength as a single value could lead to erroneous conclusions about the effort exerted during a dynamic activity. Thus, a method for determining available joint torque given joint angle and angular velocity may be of importance.

A model was developed to represent the maximum voluntary joint torque as a function of joint angle and angular velocity. There are a few examples of torque-angle-angular velocity models in the literature, such as those of Chow (1999) and King (2002). However, these have only been used in limited cases. The goal of this work was to develop a relatively simple model of maximum joint torque that is applicable to a variety of joints and populations.

METHODS

Maximum voluntary joint torque data was collected from 34 healthy adults ages 18-73, half male and half female, using an isokinetic dynamometer. Informed consent was obtained prior to participation. Data was collected for six different exertion directions: hip extension (HE), hip flexion (HF), knee extension (KE), knee flexion (KF), ankle plantar flexion (PF), and ankle dorsiflexion (DF). For each exertion direction, tests were made in eccentric isokinetic, isometric, concentric isokinetic and high speed concentric modes. Passive torques, or torques while the subjects were relaxed, were recorded throughout the range of motion (ROM).

The model for joint torque included both passive and active torques. Passive torques, caused by the stretching of tissues, were modeled with an exponential equation:

$$T_{PASSIVE} = B_1 e^{k_1 \theta} + B_2 e^{k_2 \theta}$$

Active joint torques, caused by the activation of muscles crossing the joint, were modeled based in part on muscle force-length and force-velocity relationships. For isometric and concentric cases:

$$T_{ACTIVE}(\theta, \dot{\theta}) = T_{ISO}(\theta) \cdot R(\dot{\theta})$$

Here, the isometric torque is given by:

$$T_{ISO}(\theta) = C_1 \cos\left(C_2 (\theta - C_3)\right)$$

and the torque-velocity relation, based on the hyperbolic Hill (1938) force-velocity model, is:

$$R(\dot{\theta}) = \frac{2C_4C_5 + \dot{\theta}(C_5 - 3C_4)}{2C_4C_5 + \dot{\theta}(2C_5 - 4C_4)}$$

For eccentric motion, the active torque is multiplied by an additional velocity dependent term, giving:

$$T_{ECC}(\theta, \dot{\theta}) = T_{ACTIVE}(\theta, -\dot{\theta}) \cdot (1 - C_6 \dot{\theta})$$

The torque-angle-angular velocity model is the sum of the active and passive torque equations. The model includes a total of 10 parameters: four for passive joint torque, and six for active joint torque.

Model parameters were determined using optimization techniques. Passive torque parameters and gravity corrections were based on the passive torque data. The active torque parameters were calculated with a simulated annealing optimization algorithm.

RESULTS AND DISCUSSION

The model fit the individual data well in most cases. Mean R^2 across all exertion directions was 0.89, (range 0.46 to 0.99).

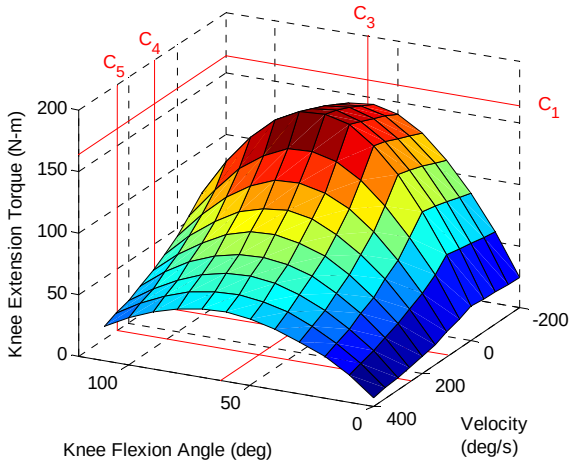

Figure 1: Example surface for KE torque, showing a distinct peak in the ROM. Red lines indicate values of C_1, C_3, C_4 and C_5.

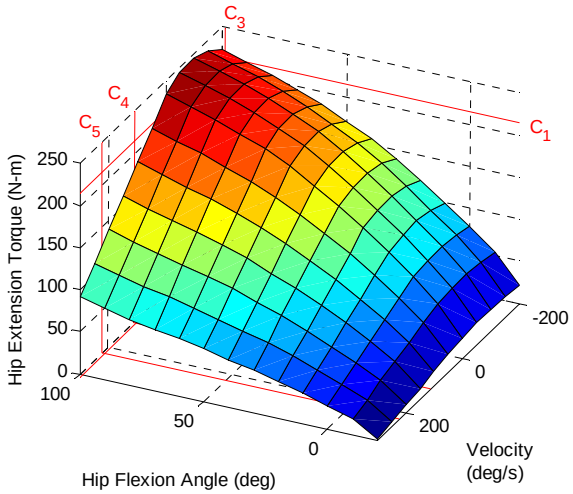

Figure 2: Example surface for HE torque, showing torque increase with hip flexion throughout the ROM. Red lines indicate values of C_1, C_3, C_4 and C_5.

The shapes of the torque-angle-angular velocity surfaces were similar between subjects, but differed between exertion directions. One major difference was whether maximum torque occurred centrally in the ROM or near one end. KE models generally fell into the first case. An example KE surface is shown in Figure 1. HE and PF models generally fell into the second case. An example HE surface is shown in Figure 2. HF, KF and DF generally fell somewhere in between the two cases.

Several of the model parameters have a simple physical interpretation. Specifically, C_1 is the maximum active joint torque and C_3 the corresponding joint angle. C_4 and C_5 are angular velocities at which torque is 75% and 50% of the isometric torque, respectively. In Figures 1 and 2, these four parameters are indicated by red lines.

SUMMARY/CONCLUSIONS

The relatively simple model presented can estimate maximum voluntary joint torques given joint angle and angular velocity. When compared to actual joint torques, these indicate the relative effort required to perform muscle-driven dynamic activities.

REFERENCES

Chow, J.W., et al. (1999). *J. Applied Biomechanics*, **15**, 200-209.

Hill, A.V. (1938). *Proc. Royal Society London B*, **126**, 132-195.

Hughes, M.A., et al. (1996). *J. Biomechanics*, **29**, 1509-1513.

King, M.A., Yeadon, M.R. (2002). *J. Applied Biomechanics*, **18**, 207-217.

ACKNOWLEDGEMENTS

This work was supported in part by a grant R03 OH007821 from the CDC.

CALIBRATION OF THE ZETOS BONE LOADING SYSTEM

Sylvana García[1], Heidi-Lynn Ploeg[1] and Everett L. Smith[2]

[1]Department of Mechanical Engineering, University of Wisconsin ï Madison, USA;
[2]Department of Population Health Sciences, University of Wisconsin ï Madison, USA
e-mail: garcia1@wisc.edu

INTRODUCTION

An ex vivo bone culture and loading system, ZETOS, has been developed to evaluate morphological and physiological cellular responses of trabecular bone cylinders (10 mm diameter, 5 mm height). A cylindrical piezoelectric actuator (PZA) expands while compressing the specimen. Strain gauges and a load cell measure PZA expansion and applied load, respectively. These, however, are not representative of the specimenôs compressive deformation due to the compliance of the system. Therefore force, expansion and specimen deformation are related by means of a calibration table (Jones et al, 2003; Smith et al, 2001).

Calibration was performed at manufacture, but the compliance of the system may change with time, thus the requirement of recalibration. The purpose of this investigation was to develop and validate a recalibration protocol for the ZETOS bone loading system.

METHODS

Ten aluminum reference bodies (RBs) with a known stiffness were designed and manufactured (Figure 1). The RB stiffness ranged from 40 MPa to 2000 MPa which is a reprehensive range of trabecular bone. The main feature of the RB design was a diaphragm which would deflect under a compressive axial load applied to a central piston. In order to comply with geometric and mechanical limitations, two groups of RB geometries were required, differing in lateral wall thickness and fillet radii. A range of diaphragm thicknesses was determined for each geometry to span the desired range of stiffness.

Calibration of the PZA expansion under no load was performed using a fiberoptic distance sensor. All RBs were tested, ten times each, in ZETOS to record force and PZA expansion.

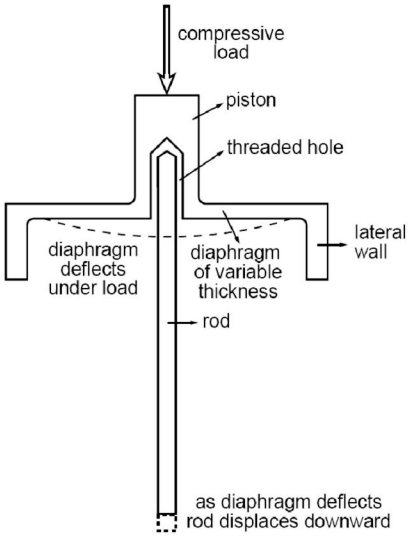

Figure 1: Schematic of a section view of a RB and stainless steel rod.

Finite element analysis (FEA) was used to model compression of the RBs in ZETOS. The model included all interface surfaces: a steel base (ZETOS loading platform), the RB, a sapphire cylinder (10 mm diameter, 10 mm height, used to avoid RB indenting) and the convex, sapphire crystal on the

loading end of the PZA. A displacement of 60 μm was assigned to the top of the PZA crystal. The reaction force was divided by deformation to find RB stiffness, which was found at the top of the surface and at the threaded cavity.

The reference body (RB) stiffness determined with FEA was validated with physical testing in an Instron device. Six RBs were compressed using a setup replicating the FE model. Compressive deformation of the RBs was derived from measurements with a 10x microscope. Percent differences of the FEA-determined stiffness were calculated with respect to stiffness found with Instron testing.

ZETOS force and expansion, and compression derived from FEA were related by generating a calibration table through spline interpolation. All the RBs were tested in random order in ZETOS, ten times each. For further verification, three metal specimens of unknown stiffness were also tested in ZETOS and compared to FEA. Comparisons of these tests with respect to FEA were made with percent differences.

RESULTS

Two sites were analyzed in the FEA: at the top of the RB piston and at the threaded cavity. The first was the stiffness of interest, used for calibration; the second analysis site was for comparison with experimental testing aimed to validate the model.

FEA results had a mean percent difference (absolute value) with respect to Instron testing of 5.08%, ranging from -3.21 to 10.6%. This comparison used the stiffness calculated at the threaded cavity in the FEA to mimic the displacement measurements taken during physical testing. Results from Instron testing served as FEA validation.

A calibration table was generated, based on the displacement results found at the top of the piston from the FEA. Verification of the RB stiffness determined using the ZETOS loading system after calibration found a mean percent difference (absolute value) of 1.10%, ranging from -2.07 to 0.877%. Finally, the verification of the calibration procedure using metal springs found a mean percent difference in stiffness compared with their FE models of 2.25%, ranging from -3.31 to 2.78%.

DISCUSSION AND CONCLUSIONS

The calibration procedure of the ZETOS loading system is important to assure accuracy of stiffness measurements of trabecular bone. FEA was an essential tool in this study, both for design of the RBs and for calculation of their stiffness. The combination of experimental testing and FEA enabled a more precise determination of RB stiffness for the generation of the calibration table. The test results were used to validate the FEA; and subsequently, the FEA provided results that could not otherwise be measured to generate the calibration table. The successful calibration of the ZETOS loading system assures continuing accuracy of stiffness measurements of trabecular bone.

REFERENCES

Jones, D.B. et al. (2003). *European Cells and Materials*, **5**, 48-60.
Smith, E.L. et al. (2001). *J. Bone and Mineral Research*, **16**(Suppl 1), S481.

ACKNOWLEDGEMENTS

The authors thank the Univ. of Wisconsin graduate school and AO, research fund 02-S52. Also, Professors Greg Nellis and Wendy Crone, Univ. of Wisconsin.

NEUROMECHANICAL MODELING OF FUNCTIONAL MUSCLE SYNERGIES FOR POSTURAL CONTROL IN THE CAT

J. Lucas McKay[1], Gelsy Torres-Oviedo[1,2], and Lena H. Ting[1,2]

[1] Georgia Institute of Technology, Atlanta, GA, USA
[2] Emory University, Atlanta, GA, USA
E-mail: jlmckay@neuro.gatech.edu

INTRODUCTION

In a recent study, we demonstrated that EMG and kinetic data from the automatic postural response in cats could be decomposed into five "functional" muscle synergies, each specifying a pattern of hindlimb muscle activation and a correlated "synergy force vector" at the ground (Torres-Oviedo et al., 2006). The analysis showed that these functional muscle synergies could explain both muscle activation patterns and endpoint forces in a range of postural configurations that alter the biomechanical conditions of the task. However, this generalization was apparent only when we expressed the kinetic data in a coordinate system that rotated with the sagittal hindlimb axis. This suggests that muscle synergies provide the nervous system with a simple mechanism to generate forces consistent in the reference frame of the limb.

Here, we used a static 3D musculoskeletal model of the cat hindlimb (McKay et al. 2006) to test the hypothesis that muscle synergies could produce endpoint force vectors across a range of postural configurations corroborating our experimental observations. We then examined the neuromechanical implications of the functional muscle synergy architecture by examining changes in the feasible force set (FFS; Valero-Cuevas 2006) after a synergy organization was imposed.

METHODS

First, we tested whether muscle synergies could produce endpoint forces that were consistent with respect to the sagittal hindlimb axis in a range of postural configurations. For each of three animals, we generated five simulated muscle synergies that could reproduce the experimentally derived synergy force vectors in the nominal postural configuration. We then examined the endpoint forces generated by these muscle synergies in the three other postural configurations using kinematic data from each cat (Torres-Oviedo et al., 2006).

We investigated whether the simulated muscle synergies limited or spanned the force-production capabilities of the hindlimb. We calculated FFSs for all conditions as in (McKay et al. 2006); first assuming individuated control of muscles and later assuming individuated control of only the simulated synergies.

RESULTS AND DISCUSSION

Consistent with our hypothesis, simulated synergies produced force vectors that rotated monotonically with the limb axis in the sagittal plane as postural configuration varied (Figure 1, colored lines). Synergy force vector orientation was highly correlated to limb axis angle in the sagittal plane ($r^2 = 0.94 \pm 0.08$, $\mu \pm \sigma$), and less so in the dorsal plane (0.75 ± 0.3), confirming the quasi-planar variation we observed

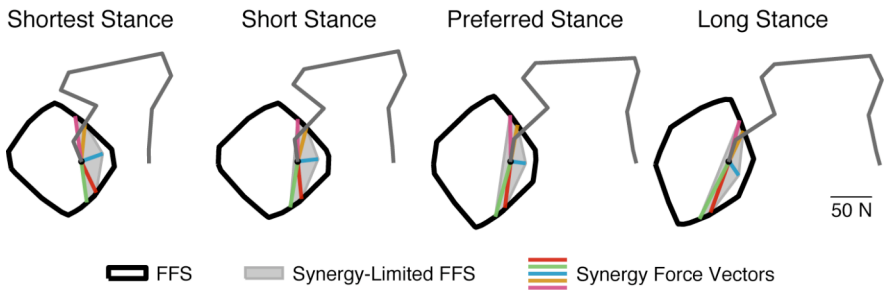

Figure 1: Rotation of synergy force vectors and feasible force sets with hindlimb axis when the animal stands using various postural configurations.

experimentally. This result suggests that postural forces can be coordinated by the nervous system throughout the workspace with a relatively simple polar transformation from intrinsic to extrinsic coordinates. This is consistent with the encoding of limb orientation in sensory signals traveling from the spinal cord to higher brain centers (Bosco et al. 1996).

When compared with the nominal FFS (Figure 1, thick black lines), the synergy-limited FFS (Figure 1, gray shaded areas) varied much more acutely with postural configuration, particularly in the sagittal plane ($r^2 = 0.92 \pm 0.05$ vs. 0.77 ± 0.2). The synergy-limited FFS was also considerably more elongated at all postures. We have previously demonstrated that the nominal FFS is a weak determinant of postural force, due to its generally isotropic shape (McKay et al, 2006) – taken together, these results suggest that the synergy-limited FFS may be a much stronger determinant of force magnitude in the hindlimb, particularly as postural configuration changes.

Our results illustrate that the muscle synergies recruited for postural control do not span the force-producing capabilities of the limb, so that only a limited range of forces are available for the postural task. Similar reductions in FFS volume occur in conditions of neural deficit (cf. Valero-Cuevas 2006). Based on these results, we predict that tasks like locomotion will recruit additional synergies to reach the remainder of the FFS (e.g., d'Avella and Bizzi 2005).

Muscle synergies appear to limit the biomechanical outputs of the limb based on a parsimonious control strategy rather than musculoskeletal constraints. Our results suggest that it may be valuable to consider the changes to the FFS associated with muscle synergies when predicting muscle coordination and biomechanics for some natural behaviors, as opposed to "maximal" tasks where coordination is determined uniquely by biomechanical limitations (e.g., Valero-Cuevas 2006).

REFERENCES

Bosco, G., et al. (1996). *J. Neurophys*, **76**, 715-726.
d'Avella, A., Bizzi, E. (2005). *PNAS*, **102**, 3076-3081.
McKay, J.L., et al. (2006). *J. Biomech*, doi:10.1016/j.jbiomech.2006.10.013.
Torres-Oviedo, G., et al. (2006). *J. Neurophys*, **96**, 1530-1546.
Valero-Cuevas. F. (2006). *Progress in Motor Control V*, in press.

ACKNOWLEDGEMENTS

Experimental data courtesy of Jane Macpherson. Support provided by NIH HD46922

A FINITE ELEMENT INVESTIGATION INTO THE BIOMECHANICAL EFFECTS OF MINIMIALLY INVASIVE TREATMENT FOR CERVICAL SPONDYLOTIC MYELOPATHY

Lacey E. Bresnahan [1], Mozammil Hussain [2], Richard G. Fessler [1], Raghu N. Natarajan [2], and Gunnar B.J. Andersson [2]

[1] The University of Chicago, Chicago, IL, USA
[2] Rush University Medical Center, Chicago, IL, USA

INTRODUCTION

Cervical spondylotic myelopathy is one of the most common diseases of the vertebral column frequently caused by degenerative processes (1). The degenerative changes that occur in the cervical spine result in compression of the spinal cord and nerve roots leading to radicular pain and numbness. Posterior surgical approaches for the management of cervical spondylosis are well established and among the oldest spinal procedures known. Recent advancements in minimally invasive surgical techniques have produced the same surgical result while minimizing bone and ligament resection as well as preserving the surrounding tissue (1). These surgical advancements have shown clinical improvements such as a decrease in post operative pain and improved clinical outcomes (2) however, the biomechanical impact of cervical microendoscopic decompression for stenosis (MEDS) is unknown. In this study we will quantify the change in intersegmental motion of the cervical spine in response to a decompressive laminotomy at C4-6 using the standard open procedure and the new MEDS technique.

METHODS

A three dimensional finite element model of an intact C3-T1 cervical spine motion segment was developed from the CT scan of a 38 year-old female normal subject. The model was previously validated with the *in vivo* study under diurnal compressive load of 40 – 350N (3). A compressive pre-load of 150N was simulated using the follower load technique. Two additional C3-T1 models with a C4-C6 laminectomy were developed one with traditional open posterior approach and the other a cervical MEDS approach. The open procedure was modeled by removal of the spinous process, a bilateral laminectomy and removal of the ligamentum flavum and interspinous ligaments. The cervical MEDS was modeled by unilateral removal of the right lamina and the ligamentum flavum. Moment loads were created by applying appropriate equal and opposite loads on the superior surface of C3 keeping the inferior surface of T1 fixed. A 1.5 Nm flexion, extension, axial rotation and lateral bending moment were applied to the model. The values selected represent the mean motion generated in the three principle planes computed from the *in vivo* studies. Rotation of the vertebral body was studied for the three FE models using the commercially available software ADINA.

RESULTS AND DISCUSSION

Rotation of the vertebral bodies in the sagittal, axial and coronal planes was compared between a cervical MEDS and open laminectomy at C4-6 to an intact control using finite element analysis. The open procedure resulted in an overall increase in motion at all segment levels for each of the three loading conditions (Figure 1), with the largest overall increases in axial

rotation and lateral bending. Increased motion in the axial plane ranged from 100% at C7-T1 to 141% at C6-7. The range of increase in motion during lateral bending was from 26% at C3-4 to 108% at C4-5.

MEDS resulted in minimal increased motion at all segment levels for each of the three loading conditions. The most significant changes were seen in axial rotation and flexion-extension with no significant change in lateral bending. Motion for the MEDS in the axial plane increased in the range of 0% at C7-T1 to 20% at C6-7. Flexion-extension increased from less than 1% at C3-4 to 29% at C6-7.

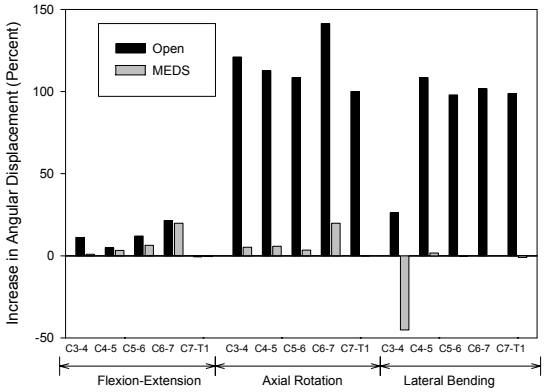

Figure 1. Change in percent segmental rotation for open and MEDS normalized to control under flexion, extension, lateral bending and axial rotation.

Axial rotation resulted in the most significant increases in motion for both the open and MEDS with a maximum of 1% and 20% at C6-7 respectively. Lateral bending resulted in the second largest overall increase in motion with the maximum occurring at C4-5 with a 108% and 2% increase for open and MEDS. The total motion (C3 with respect to T1) of the open was increased relative to the MEDS in flexion-extension (10% and 5%), axial rotation (115% and 6%) and lateral bending (101% and -1%). A comparison of the segments directly adjacent to the operative site resulted in a consistent maximum increase in motion at the caudal end (C6-7) for both open and MEDS (Table 1).

SUMMARY/CONCLUSIONS

The limitations of the finite element analysis are known. However, our application of the finite element method for comparison of segmental motion as a result of two different surgical treatments for cervical spondylotic myelopathy provide biomechanical data to verify results seen clinically (1). The data show that the posterior elements of the cervical spine provide resistance to segmental rotation in the three anatomic planes. Surgical manipulation of these elements can lead to substantially increased motion as can be seen by the results of the open data. Minimization of bone and ligament removal associated with MEDS results in greater preservation of the normal motion of the cervical spine after surgery.

REFERENCES

1. Santiago P, Fessler RG (2007) *Neurosurgery,* **60 (Suppl 1),** S160-5.
2. Fessler RG, Khoo LT (2002) *Neurosurgery,* **51 (Suppl 5)**, S37-45.
3. Natarajan RN et al. (2000) *Spine,* **25(8)**, 955-61.

Table 1: Percent increase in segmental rotation of levels adjacent to operative site (C4-6).

	Flexion-Extension		Axial Rotation		Lateral Bending	
Level	**Open**	**MEDS**	**Open**	**MEDS**	**Open**	**MEDS**
C3-4	11	1	121	5.	26	-45
C6-7	21	20	141	20	102	0

CROUCHED GAIT POSTURES REDUCE THE CAPACITY OF UNI-ARTICULAR MUSCLES TO EXTEND THE HIP AND KNEE JOINTS

Jennifer L. Hicks[1], Michael H. Schwartz[2,3], and Scott L. Delp[1]
[1]Departments of Bioengineering and Mechanical Engineering, Stanford University
[2]Center for Gait and Motion Analysis, Gillette Children's Specialty Healthcare
[3]Departments of Orthopaedic Surgery and Biomedical Engineering, University of Minnesota
Email: jenhicks@stanford.edu Web: http://www.stanford.edu/group/nmbl/

INTRODUCTION

Many children with cerebral palsy (CP) walk with a crouched posture during the stance phase of the gait cycle, exhibiting excess knee flexion, hip flexion, and internal hip rotation. This pathological gait pattern increases the energy cost of walking and can lead to chronic knee pain and joint degeneration if left uncorrected. Further, without intervention, crouch gait typically worsens over time (Bell et al., 2002).

Understanding the impact of a crouched gait posture on muscle function may shed light on the progression of the pathology and improve the efficacy of corrective and preventative treatments. The goal of this study was to determine the effect of crouch gait on the capacity of the major limb extensor muscles to accelerate the hip and knee joint during the single limb support phase of the gait cycle.

METHODS

We assessed the effect of crouched gait postures on the capacity of muscles to extend the joints using a modeling technique known as an induced acceleration analysis (e.g. Zajac and Gordon, 1989). In this analysis, a model of the musculoskeletal system is positioned with joint angles corresponding to a given gait cycle. The model's equations of motion are then used to calculate the capacity of the muscles to accelerate each of the joints.

We used a 3D, 15-segment, 23 degree-of-freedom model of the musculoskeletal system (Delp et al., 1990). This model was positioned using four distinct gait patterns: normal, mild crouch, moderate crouch and severe crouch (Figure 1). The normal gait pattern was based on the averaged gait kinematics of 83 able-bodied children. The crouch gait patterns were based on averaged gait kinematics from subjects with CP, classified based on their knee flexion angle at initial contact. Mild crouch subjects had between 20º and 30º of knee flexion at initial contact (N=103), moderate crouch between 30º and 40º (N=171), and severe crouch over 40º (N=197). All gait data was collected using a 3D motion capture system at Gillette Children's Specialty Healthcare.

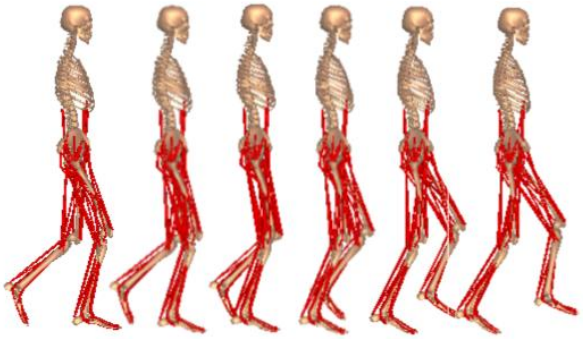

Figure 1: The musculoskeletal model in postures corresponding to the single limb support phase of moderate crouch gait.

For all four gait patterns, the capacity of the major limb extensors to accelerate the hip and knee joints toward extension was calculated for every 2% of single limb support (14-50% of the gait cycle). First, the contribution of each muscle to the ground reaction force was determined using an approach developed by Anderson and Pandy (2001): five contact points were distributed over the sole of the foot, a unit muscle force was applied to the model, and the resulting ground reaction force was determined by solving for the minimum force that would constrain the acceleration of each contact point to be zero. Second, a unit muscle force plus its contribution to the ground reaction force were applied to the model. The resulting accelerations of the hip and knee were then calculated using the model's equations of motion. This quantity represents the capacity of a muscle to accelerate the joint at that pose of the gait cycle, per unit muscle force.

RESULTS AND DISCUSSION

Major limb extensors were defined as the muscles that had an average extension capacity of at least $5^o/s^2/N$ and are active during normal single limb support (Perry, 1992). Of these muscles, the gluteus maximus was found to have the greatest potential to extend both the hip and knee joints (Figure 2). The bi-articular hamstrings was found to have an extension capacity at both the hip and knee. Vasti, soleus, and the posterior gluteus maximus also had significant hip and knee extension potentials.

When walking with a crouched gait posture, the extension capacities of almost all muscles were markedly reduced (Figure 2). The more severe the crouch gait pattern, the larger the impact on muscle extension capacity. For moderate crouch, the capacities of the limb extensors to accelerate the knee joint were reduced by 25-70%. At the hip joint, the capacities of the gluteal muscles, vasti and soleus were reduced by 15-50% for moderate crouch. The lone exception was the bi-articular hamstrings: the capacity of hamstrings to extend the hip *increased* slightly with crouch gait.

Two major factors must be considered when interpreting the results of this analysis. First, the actual angular acceleration of a joint induced by a muscle depends on the muscle's activation level as well as its force-generating capacity, which depends in turn on the muscle's physiological cross-sectional area and the muscle's length and velocity during the movement. Second, the results of this analysis depend on the musculoskeletal geometry and inertial properties of the model, which are variable, especially in children with CP.

The results of this analysis provide several valuable insights into muscle function during crouch gait. First, as crouch gait worsens, muscle extension capacities are further reduced in a negative cycle. This is consistent with the clinically observed worsening of crouch gait over time. Conversely, small improvements in hip or knee flexion may help reverse the process, especially if intervention occurs early in the progression of crouch gait. The only muscle whose extension capacity was not reduced by a crouched posture, at least at the hip joint, was the hamstrings. Over-activity of hamstrings is common in patients with crouch, which may be related to this maintenance of extension capacity in a crouched posture.

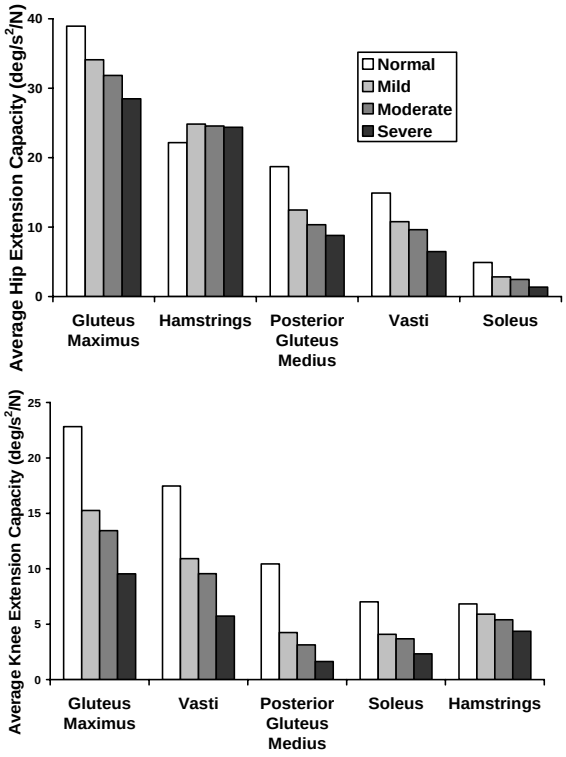

Figure 2: Effect of crouch gait on the average capacity of the major limb extensors to accelerate the hip (top) and knee (bottom) towards extension during single limb support.

REFERENCES

Anderson, F.C., Pandy, M.G. (2001) *J Biomech Eng*, **123**, 381-390.

Bell, K.J. et al. (2002) *J Pediatr Orthop*. **22**, 677-682.

Delp, S.L. et al. (1990) *IEEE Trans Biomed Eng*, **37**, 757-767

Perry J. (1992), *Gait Analysis: Normal and Pathological Gait*. SLACK Inc.

Zajac, F.E., Gordon, M.E. (1989) *Exerc Sport Sci Rev*, **17**, 187-230.

.

ACKNOWLEDGEMENTS

The authors thank Clay Anderson, Allison Arnold, and the staff of the Gillette Gait Lab. Supported by the NSF and NIH Roadmap for Medical Research, Grant U54 GM072970 and through NIH Grants HD33929 and HD04681

EFFECT OF ELEVATION ANGLE ON MOVEMENT VELOCITY IN A NON-VISUALLY-GUIDED REACHING TASK

David J. Harmer and David N. Suprak

Department of Health Sciences, University of Colorado, Colorado Springs, CO, USA
email: dsuprak@uccs.edu

INTRODUCTION

Joint position sense (JPS) is important in the maintenance of optimal movement coordination and injury prevention of limb segments in functional activities. It is well established that the accuracy of visually guided reaching movements declines as movement speed increases. However, very few studies have examined the influence of movement speed on accuracy of 3D reaching movements to memorized targets without visual feedback (Messier et al. 2003). Previous data from our laboratory indicate that joint position sense acuity improves as the presented position is moved toward an elevation of 90° (Suprak et al., 2006). Therefore, the purpose of this study was to examine the effects of elevation angle on movement velocity. We hypothesized that velocity would increase as the elevation angle increased from 30° to 110°.

METHODS

A total of 22 subjects (12 males, 10 females), with a mean age of 23.3 yrs. (± 4.8 yrs.) participated in the study. Following a standardized warm-up procedure, subjects were fitted with a head-mounted display and asked to remove shirts (females wore sports bras) to minimize visual and tactile cues (Figure 1). Kinematic data were collected via the Polhemus Fastrak magnetic tracking system, with one receiver on the thorax and one on the humerus. Testing involved the presentation of five target positions, consisting of various elevation angles in the scapular plane (35° plane). These positions were presented via custom-made Labview software through the head-mounted display. Once the target position was achieved, the display turned black and remained so for the remainder of the trial. Subjects held the position for five seconds, and returned to the side. Subjects then attempted to replicate the target position in three dimensions, in the absence of visual cues. Target positions were presented in a randomized order. Vector position data collected during the repositioning phase was processed via a forth order Butterworth filter. Peak angular velocity was calculated from the filtered position data using the central difference method.

Figure 1: Experimental Set-up.

RESULTS AND DISCUSSION

A one-way repeated measures ANOVA revealed a significant main effect of elevation angle on peak velocity (Figure 2). Analysed data also showed a significant cubic polynomial contrast. However, previous data using the same protocol to assess position sense acuity indicated that repositioning accuracy improved as the elevation angle of the presented position approached 90° (Figure 3). Cordo et al. (1994) studied the role of velocity on the proprioceptive coordination of movement

sequences using passive rotation of the elbow at fixed speeds. There results suggested that the nervous system uses velocity information to coordinate movement sequences. Our results indicate that movement velocity increases in a cubic pattern with increase elevation angle at the shoulder. This finding, along with previous data, may indicate that in an unconstrained active repositioning movement, the accuracy of movement without vision is not exclusively affected by velocity.

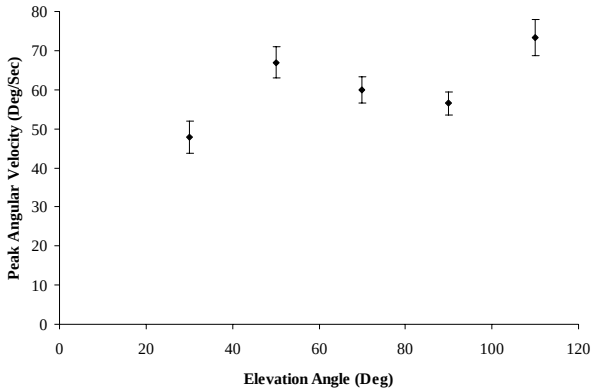

Figure 2: Angular velocity with Elevation Angle (Mean ± SEM).

CONCLUSIONS

The results of this study indicate that angular velocity increases with an increase in elevation angle of the shoulder. Taken together with previous accuracy data (Suprak et al., 2006), these findings may indicate that in an unconstrained reaching task to remembered targets, movement velocity does not play a dominant role in determining movement accuracy. More investigation is necessary to elucidate the role of velocity in the processing of proprioceptive information by the central nervous system.

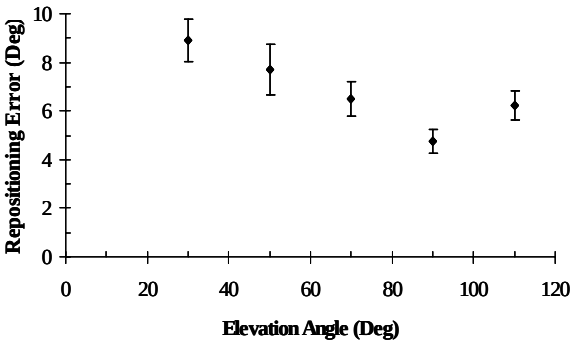

Figure 3. Repositioning Error Across Elevation Angle (Mean ± SEM).

REFERENCES

Cordo, P. et al. (1994). *Journal of Neurophysiology*. **71**: 1848-1861.

Messier, J. et al. (2003). *Exp Brain Res.* **150**:399–416.

Suprak, D. et al. (2006). *J Orthop Res*. **24**: 559-5.68

MOTOR ADAPTATION DURING DORSIFLEXION-ASSISTED WALKING WITH A POWERED ORTHOSIS

Pei-Chun Kao[1] and Daniel P. Ferris[1]

[1]Human Neuromechanics Laboratory, University of Michigan, Ann Arbor, MI, USA
E-mail: kaop@umich.edu

INTRODUCTION

The ankle dorsiflexors have two main mechanical functions during gait. One function is eccentric control at heel strike and a second function is concentric control during swing. Correspondingly, in healthy persons, the ankle dorsiflexors show two bursts of electromyographic (EMG) activity during walking. A large burst is seen around heel strike to prevent the forefoot from colliding with the floor at a high velocity (i.e. foot slap). A second burst is seen after toe off to prevent the toes from hitting the floor on swing through (i.e. drop foot).

Post-stroke patients often have very weak dorsiflexor recruitment at the stance to swing transition. Rigid AFOs are frequently prescribed to improve walking ability and to prevent stumbling. However, rigid AFOs impede push-off plantar flexion and do not allow the user to make step-to-step changes in motion dynamics for terrain. The purpose of this study was to determine how people adapt their walking patterns to a powered orthosis with dorsiflexion assist. The advantage of a powered orthosis is that it would not impede plantar flexion at the end of stance.

Our preliminary results using a powered orthosis under proportional myoelectric control of the tibialis anterior (TA) revealed different motor adaptation responses for the two mechanical functions of the dorsiflexors (Kao and Ferris 2006). Although TA EMG amplitude decreased for the first burst by about 22% as subjects adapted, TA EMG amplitude did not change for the second burst. In order to clarify the different responses, we tested a second group of subjects that received the active dorsiflexion assist **ONLY** during the swing phase. We hypothesized that subjects would demonstrate similar adaptation as before for the second TA burst (i.e. no change in dorsiflexor EMG amplitude).

METHODS

Ten healthy subjects were fitted with custom-made polypropylene orthosis (Fig. 1). An artificial pneumatic muscle attached on the foot and shank portions powered the orthosis to provide dorsiflexor torque. A real-time computer controller modulated force in the artificial muscle proportional to tibialis anterior EMG amplitude via a pressure regulator. Foot-switches were used for gating control signals.

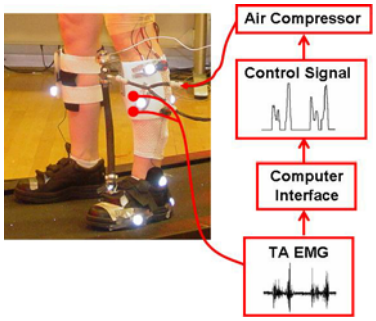

Figure 1: The powered orthosis uses TA EMG to control air pressure in an artificial dorsiflexor muscle.

We collected lower body kinematics, EMG, and artificial muscle force while subjects walked on a treadmill for two training sessions. Subjects walked with

the orthosis first without power for 10 minutes (baseline), with power for 30 minutes (active), and without power again for 15 minutes (post-passive). We repeated the same protocol 3 days later. During active orthosis walking, subjects in the first group (n=5) received powered assistance **BOTH** at heel strike and during swing. Subjects in the second group (n=4) received assistance **ONLY** during the stance-to-swing transition (50-90% of step cycle). We calculated root-mean-square EMG for each burst of TA EMG individually and normalized data to the last minute of baseline. We also correlated every minute's ankle angle profile to the baseline trial. We used the method described by Noble and Prentice (2006) to define steady state dynamics

RESULTS AND DISCUSSION

At the end of Day 2, the orthosis provided peak dorsiflexor torques ~0.22 Nm/kg at heel contact for Group One subjects and ~0.10 Nm/kg during swing for both Group One and Two subjects. The assist provided was ~150% of the normal peak dorsiflexor moments (~0.1 Nm/kg at heel contact and ~0.06 Nm/kg during swing (Mills, 2001)).

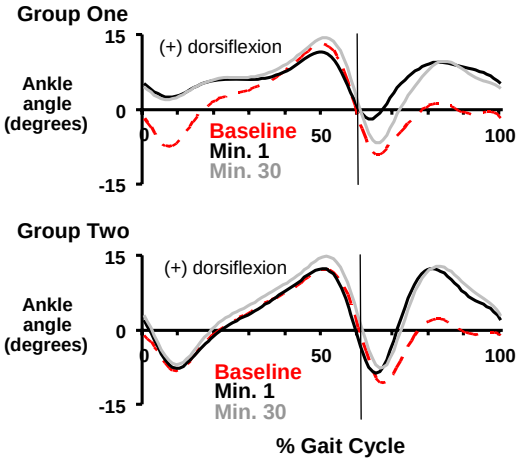

Figure 2: Ankle kinematics on Day 2.

Subjects walked with increased ankle dorsiflexion (Fig. 2) and had tibialis anterior muscle activation patterns similar to passive orthosis trials (Fig. 3). In comparison with the baseline condition, amplitude of the second TA EMG burst did not change during the active condition for Group Two subjects (baseline 1.17 ±0.10 (m±s.d.); active 1.6±0.10; $F_{1,40}$=0.0534, p=0.82). Both Group One and Two subjects reached steady state more rapidly on the second day.

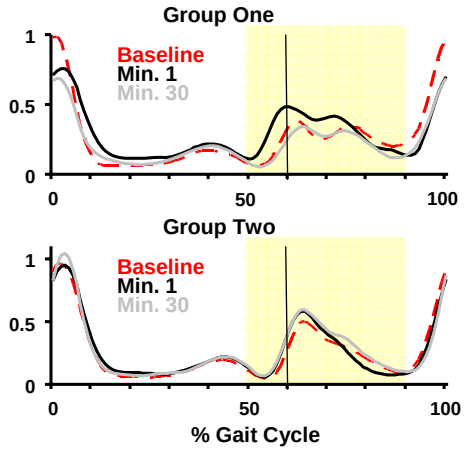

Figure 3: TA EMG on Day 2.

SUMMARY/CONCLUSIONS

When wearing a powered orthosis providing dorsiflexor assist, healthy subjects walked with increased dorsiflexion without altering TA EMG amplitude during the stance to swing transition. In contrast, subjects decreased TA EMG amplitude during the swing to stance transition when dorsiflexor assist was provided at that time. These findings indicate that the nervous system modulates the two TA EMG bursts differently in regards to motor adaptation. In addition, active dorsiflexion assist controlled by EMG has potential for assisting people with drop-foot gait.

REFERENCES

Kao, P.C., and Ferris, D.P. (2006). Proc 5th World Cong Biomech.

Noble, J.W., Prentice, S.D. (2006). Exp Brain Res, 169(4):482-95.

ACKNOWLEDGEMENTS

This project was supported by NIH R01NS045486.

FAMILIARIZATION WITH CARRYING NOVEL BACKPACK LOADS AFFECTS THE BIOMECHANICS AND OXYGEN CONSUMPTION OF TREADMILL WALKING

Jeffrey M. Schiffman, Carolyn K. Bensel, Louis Piscitelle, Leif Hasselquist,
Karen N. Gregorczyk, and John P. Obusek

Natick Soldier Research, Development and Engineering Center, Natick, MA USA
E-mail: Jeffrey.Schiffman@natick.army.mil

INTRODUCTION

Treadmills provide a convenient means for collecting biomechanical and physiological data to assess the effects of walking with backpack loads (Quesada et al., 2000). Researchers have reported on the time it takes for individuals unencumbered by external loads to habituate to treadmill walking in terms of achieving stable biomechanical (Van de Putte et al., 2006) and oxygen consumption measures (Keefer et al., 2005). However, little research exists on how long it takes individuals to become familiar with carrying novel backpack loads while walking on a treadmill. The purpose of this study was to investigate the effects on walking biomechanics and oxygen consumption of repeated exposure to carrying loads.

METHODS

Fourteen U.S. Army enlisted men (mean age = 21.3 yrs, SD = 4.9; mean height = 1.79 m, SD = 3.9; mean body mass = 82.3 kg, SD = 11.7) participated in the study. Informed consent was obtained and the study was conducted in accordance with DOD regulations.

Volunteers attended four study sessions. The first two sessions were within one week. They were followed, after a 1-week interval, by the last two, which were also within one week. Seven volunteers performed treadmill walking at the first two sessions and agility maneuvers at the last two; the remaining seven volunteers engaged in treadmill walking and agility activities in the opposite order.

Six backpack conditions were tested, all with different moments of inertia (MOI). Steel weights totaling 26 kg were placed in a pack in various locations to produce MOIs that ranged from 0.5 to 2.5 $kg \cdot m^2$ about the three principal axes (Ixx, Iyy, Izz). An external-frame backpack was used for all conditions. All conditions had the same total mass (35 kg) and the same mass center location (about 0.3 m away from the frame, 0.3 m away from the bottom, and centered on the midline of the load carrier's back).

The treadmill activity consisted of 10-min trials of walking on a level treadmill (AMTI, Watertown, MA) set at 4.8 km/h. During the fifth minute, 20 s of kinematic data were collected (Qualisys, Gothenburg, Sweden). After six minutes, $\dot{V}O_2$ (ml/min) data were collected (K4b^2, COSMED, Rome, Italy). There were three walking trials at a session, each with a different backpack condition. The agility maneuvers were timed, maximal effort tasks: running a 32-m zigzag course; climbing over a 1.4-m sheer wall; and moving from a standing to a prone position and returning to the standing position. There were three trials on each agility task at a session, with a different backpack condition being carried on each trial. The order in which the participants were exposed to the load conditions was based on a Latin square.

$\dot{V}O_2$ data were averaged over the 90-s collection period. Rate of oxygen consumption was expressed relative to the individual's body mass (ml/kg/min). Five strides of kinematic data were analyzed using Visual3D (C-motion Inc., Rockport, MD) and were averaged across sides (left and right) and strides. ANOVAs were performed on the dependent measures with alpha set at .05. A hierarchical design was used with one between- (Order: Treadmill Week 1-2) and two within-subjects factors (Day: 1-2; Trial: 1-3). Two of the volunteers tested only two conditions at one session. Their data were excluded from the analyses, resulting in n = 5 for the Treadmill Week 1 group and n = 7 for the Treadmill Week 2 group.

RESULTS AND DISCUSSION

Mean $\dot{V}O_2$ analysis yielded a significant Order x Day interaction (p = .008). Follow-up comparisons revealed that Treadmill Week 1 group mean $\dot{V}O_2$ was significantly lower on Day 2 (15.30 ml/kg/min) than on Day 1 (17.02 ml/kg/min), improving 11%. No significant Day effect was obtained for the Treadmill Week 2 group; the mean $\dot{V}O_2$ for this group was approximately 15.55 ml/kg/min each day.

A significant main effect of Order was found for a number of the kinematic measures. Compared with those who did the treadmill walking activity the first week, the volunteers who were tested on the treadmill the second week revealed increased cycle time (p=.005), stance time (p=.014), step time (p=.005), swing time (p =.005) and stride length (p =.005). The second order interaction (Order x Day x Trial) was significant for one kinematic variable, maximum ankle ROM (p=.048). Those who walked on the treadmill the 2nd week, as compared to walking on the treadmill first, took longer strides and had greater ankle joint movement.

Research conducted without external loads on the body indicates that 5 min of treadmill walking is sufficient to achieve stable $\dot{V}O_2$ levels between trials on a single day and across days (Keefer et al., 2005). Based on the oxygen consumption data from the present study, it appears that treadmill walking with a backpack load requires more extensive practice and that, with practice, the energy cost of the activity may decrease. Further, study findings suggest that carrying a load while performing physical activities other than treadmill walking may subsequently affect walking biomechanics when carrying the load on a treadmill.

CONCLUSIONS

In studies of the effects of novel backpack loads on oxygen consumption and biomechanics during walking, volunteers must be provided a period of familiarization with carrying the load. At least two days of carrying the load intermittently for a few hours each day seem to be necessary. To achieve efficient energy usage during treadmill walking with a load, it appears that practice in that specific activity is required. Future research should address the changes over time that occur in walking patterns and oxygen consumption during familiarization with carrying novel backpack loads while walking on a treadmill.

REFERENCES

Keefer, D.J. et al. (2005). *Gait and Posture*, **21**, 80-84.

Quesada, P.M. et al. (2000). *Ergonomics*, **43**, 293-309.

Van de Putte, M. et al. (2006). *Biomedical Materials and Engineering*, **16**, 43-52.

3-D JOINT MOTION OF ACL DEFICIENT AND RECONSTRUCTED KNEES DURING DAILY ACTIVITIES

Naiquan (Nigel) Zheng, Bo Gao, and Michael Moser, Peter Indelicato

University of Florida, Gainesville, FL, USA
E-mail: nigelz@ufl.edu, Web: www.ortho.ufl.edu/BMAL

INTRODUCTION

Anterior cruciate ligament (ACL) injury has been associated with progressive development of knee osteoarthritis (OA) (Daniel et al, 1994). ACL reconstruction is often performed to restore the joint stability. Current literature does not lend support to the efficacy of ACL reconstruction in retarding progression of OA after knee injury. Altered knee kinematics and loading pattern are believed to be responsible for premature OA. Knee kinematic changes were observed after ACL injury using dynamic MRI (Barrance et al, 2006). A recent study reported that rotational changes at the knee would cause cartilage thinning (Andriacchi et al, 2006). Some differences during level walking between ACL injured knees and healthy knees have been reported (Zheng et al, 2007). The purpose of this study is to study 3-D joint motion of ALC-deficient (ACL-D), ACL-reconstructed (ACL-R) and ACL-intact (ACL-I) knees during level walking, ascending and descending stairs.

METHODS

Twenty nine subjects were recruited in this study, including 15 healthy subjects, 6 subjects with unilateral ACL-R knee and 8 with unilateral ACL-D knees. ACL-R and ACL-D subjects at the time of test were 3 months to 2 years after injury or surgery. Both left and right knees were tested using an IRB approved protocol. An 11-camera motion analysis system (MAC, Santa Rosa, CA) was used to collect motion data using 89 reflective markers (Fig. 1) (Zheng et al, 2007). Three translations and rotations at the knee were determined using a modified point cluster technique with accuracy of 1.8^{o} for rotation and 3.5 mm for translation (Gao and Zheng, 2007). Peak and valley values during the stance phase and swing phase were determined for each variable. Each test was repeated three times. Differences of three translations and three rotations between two knees were analyzed and compared between ACL-R and healthy group. Multivariate analysis of variance (MANOVA) was used to compare the differences (SPSS, Chicago, IL).

Figure 1: A subject in test

RESULTS AND DISCUSSION

Figure 2 shows the three rotations and three translations at the knee during level walking, ascending and descending stairs. There were significant differences of the knee flexion between the ACL-R and ACL-I and between the ACL-D and ACL-I. Subjects in the ACL-D and ACL-R groups had more knee flexion at the mid stance during level walking (Table 1). Subjects in the ACL-R group had greater peak knee flexion during the swing phase in all three daily activities. Tibiae in the ACL-R and ACL-D groups had significant less external rotation during the swing phase and at heel strike of three daily activities. Significant differences for the maximum valgus at the stance phase, the maximum varus and valgus at both the

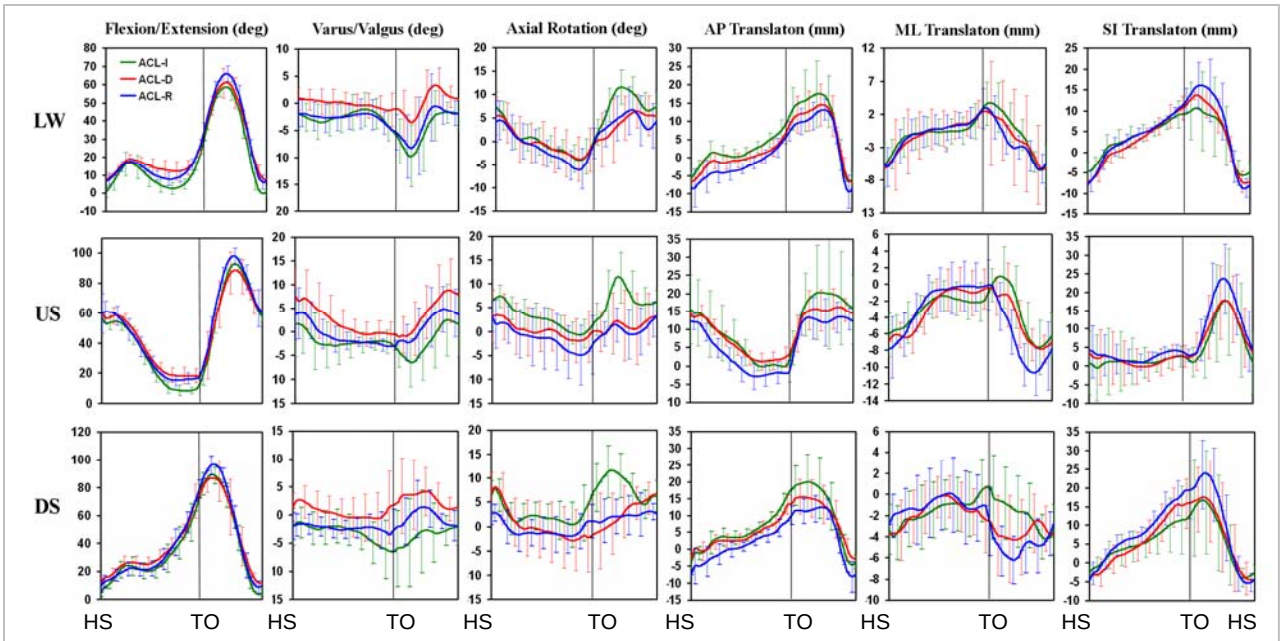

Figure 2: 3-D knee motion during walking on a level (LW), upstairs (US) and downstairs (DS). Data were normalized from heel strike (HS) to HS. Three translations were determined from a reference point located in the femur condyle relative to the tibia (anterior, medial and superior translations were positive). Rotations were calculated as the femur relative to the tibia (flexion, varus and internal rotation positive).

stance and swing phases were also found for three daily activities.

Findings from this study allow us to identify the individuals who have abnormal joint motion. Future studies will be focused on how changes in knee joint kinematics in ACL-D and ACL-R groups lead to cartilage degenerative changes of the articular cartilage and how to apply appropriate interventions and treatment to prevent degenerative changes of the knee joint.

SUMMARY/CONCLUSIONS

Three dimensional knee joint motions in ACL-D, ACL-R and healthy groups were studied and significant differences of joint motion were found. Their long-term influences on the joint degenerative change need to be monitored and studied.

REFERENCES

Andriacchi TP *et al* (2006) *Clin Orthop Relat Res* **442**, 39-44

Barrance PJ et al (2006), *J Orthop Res* **24**, 132-40

Daniel DM et al (1994) *Am J Sports Med* **22**, 632-44

Gao and Zheng (2007) *ISB XXI Congress*.

Zheng N et al (2007) *ORS paper 164*

Table 1 Rotations (deg) with significant differences among groups during level walking (mean± SD).

Group	ACL-I	ACL-R	ACL-D	p
Flexion at stance phase	2.4 ± 3.3	7.6 ± 4.4	12.4 ± 1.8	**, p<0.01
Flexion at heel strike	0.1 ± 3.7	5.4 ± 4.0	6.9 ± 4.7	**, p<0.01
External Rotation at swing phase	12.7 ± 3.7	8.5± 5.1	7.8 ± 4.3	*, p<0.05
Valgus at stance phase	6.3 ± 2.8	5.5 ± 2.9	2.0 ± 2.6	*, p<0.05

ACCURACIES OF SKIN MARKER BASED KNEE MOTION ANALYSIS USING DIFFERENT TECHNIQUES

B Gao, BP Conrad, N Zheng
University of Florida, Gainesville, Florida USA,
Email: nigelz@ufl.edu

INTRODUCTION

Accurate determination of bone motion is important in understanding the normal function as well as clinical problems of musculoskeletal system. Skin marker based optical stereophotogrammetry provides a non-invasive and radiation-free approach for in vivo skeletal kinematics measurement, but the accuracy is limited mainly by soft tissue artifact (STA) errors (Leardini et al. 2005). In the present study, accuracies of three STA reduction techniques were evaluated. The techniques included point cluster technique (PCT) (Andriacchi et al, 1998), a modified least square method (MLS) (Spoor et al, 1980), and a marker triad technique (MTT) newly proposed (Gao et al, 2007). Outcome of each technique was evaluated using human cadaver knees by comparing with movement derived from intracortical pin markers.

METHODS

Six fresh human cadaver knees were tested in this study. Specimens included bilateral lower extremities with intact pelvis to keep all lower extremity muscles intact. The specimens had not been frozen before the test so the soft tissue flexibility was well maintained. Intracortical pins were fixed into the femur and the tibia to assess the skeletal motion. Seven retro-reflective markers (10 mm in diameter) and 4 marker triads were attached to the thigh and also to shank. Four markers were fixed to the end of each bone pin (Fig.1). An 11-camera motion analysis system (MAC, Santa Rosa, CA) was utilized to collect the motion data. The pelvis of the specimen was held by a frame and an upright pose of the leg was captured as a neutral position where the local coordinates of each marker were calibrated. Then dynamic trials were recorded while the leg was manipulated to stimulate the range of motion of level walking. Three trials were collected for each knee with each trial containing 3 to 5 motion cycles.

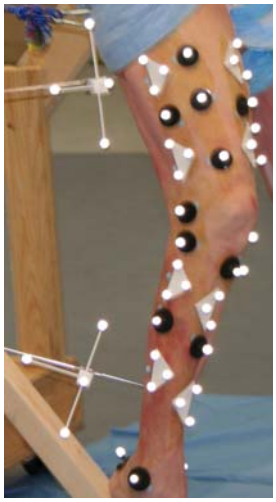

Figure 1: Marker placement on a specimen leg.

Based on marker positions, three different techniques were employed to derive the skeletal movement. All markers were used in MLS method. To make marker distribution even in PCT method, triads were treated as single markers by referring their center positions. Only the four triads on each segment were used in MTT method. In this method, each triad's rotation was determined by the three vertex markers and the results of the four triads on one segment were averaged to derive the rotation of the underlying bone. Translations of the bone could be consequently determined.

Using each method, the 3-D motions derived from skin markers (SM) were compared with those derived from bone pin (BP) markers in three ways:

1) *(*Femur_{SM} + Tibia_{BP}*) VS (*Joint_{BP}*)*
2) *(*Femur_{BP} + Tibia_{SM}*) VS (*Joint_{BP}*)*
3) *(*Joint_{SM}*) VS (*Joint_{BP}*)*

The first and second comparisons evaluated the accuracies of femoral and tibial motion calculation, and the third one evaluated the accuracies of the joint kinematics determination.

RESULTS AND DISCUSSION

Table1 lists the average errors of PCT, MLS, and MTT methods in 3-D knee kinematics determination. Parameters include flexion/extension (FE), axial rotation (AR), varus/valgus (VV), anterior/posterior (AP), medial/lateral (ML), and superior/inferior translations (SI). Joint motion was expressed as femur relative to tibia and translations were described in terms of the tibia origin located at the middle of tibial plateau.

For all the three methods, the average errors of femoral motion determination (0.60° to 2.14° for rotations and 1.85 mm to 3.53 mm for translations) were overall larger than those of tibial motion determination (0.31° to 1.84° for rotations and 0.86 mm to 2.96 mm for translations). This is consistent with the fact that thigh has greater soft tissue movement than shank. The errors of knee joint kinematics were generally larger than errors of either segment.

Among the three techniques, MLS achieved the best accuracy in knee joint kinematic analysis, with less than 3.5mm /2° errors for translational/rotational measurements. PCT method which used non-rigid optimization did not show higher accuracy than MLS, especially in translations. This finding is in agreement with other studies (Cereatti et al, 2006, Taylor et al, 2005). MTT method was less accurate than MLS but comparable with PCT, with errors less than 4mm/2.6° for translational/rotational measurements. This performance shows the potential of MTT technique given its simpler marker set.

Among the six kinematic parameters, AP translation had slightly larger errors than the other two translations. Axial rotation appeared largest errors among all the three rotations. The non-uniform error distribution is consistent for all the techniques and could be associated with the anatomical structure of lower extremity.

REFERENCES

Leardini A. et al. (2005). *Gait and Posture*, **21**, 212–225.

Andriacchi TP. et al.(1998). *J Biomech Eng*, **120**, 743–9.

Spoor CW. et al. (1980). *J Biomech*, **13**, 391-393.

Gao B. et al. (2007). *ISB XXIth Congress*.

Cereatti A. et al. (2006). *J NeuroEng and Rehab*, **3**:7.

Taylor WR, et al. (2005). *J Ortho Res*, **23**, 726-734.

Table 1: Average errors of knee kinematics using different techniques (mean± SD).

Technique	Segment	FE (°)	AR (°)	VV (°)	AP (mm)	ML (mm)	SI (mm)
PCT	**Femur**	1.55±1.26	2.14±1.14	1.00±0.57	3.09±1.99	3.35±2.14	3.53±1.83
	Tibia	0.76±0.38	1.43±0.55	0.36±0.09	2.96±2.17	1.62±0.71	1.29±0.59
	Knee	**1.24±0.73**	**1.99±0.83**	**1.01±0.53**	**5.14±4.45**	**3.90±3.11**	**3.96±1.55**
MLS	**Femur**	0.84±0.64	1.51±0.75	0.85±0.56	1.85±0.67	1.93±0.95	2.46±1.41
	Tibia	0.70±0.32	1.10±0.30	0.31±0.12	2.47±1.65	0.86±0.32	0.86±0.16
	Knee	**0.74±0.35**	**1.81±0.49**	**0.77±0.53**	**3.30±2.34**	**1.96±0.45**	**2.74±1.31**
MTT	**Femur**	0.60±0.13	1.77±0.82	1.27±0.73	2.72±1.31	2.33±0.83	2.89±2.26
	Tibia	0.87±0.41	1.84±0.61	0.61±0.21	2.43±1.49	1.59±0.70	1.03±0.28
	Knee	**1.13±0.33**	**2.54±1.19**	**1.56±0.66**	**3.77±1.78**	**2.89±0.68**	**3.02±1.84**

BIOMECHANICAL NECK MODEL BASED ON THE VISIBLE HUMAN FEMALE

Liying Zheng, Linda Rico, Richard Lasher and Anita Vasavada

Washington State University, Pullman, WA, USA
E-mail: liying_zheng@wsu.edu

INTRODUCTION

Studies have shown that females are more likely to experience neck injuries than males. A female neck model is requisite for analysis of gender difference in neck injuries, especially the effect of size, geometry and biomechanical properties. Male neck models have been developed (Vasavada *et al.*, 1998; Chancey *et al.*, 2003), but to our knowledge a female model does not exist. The goal of this study is to develop a musculoskeletal model of the female neck and head system based upon female anatomy from the National Library of Medicine's Visible Human Female (VHF), and compare the female to male neck models.

METHODS

The VHF subject was 1.65m tall (65th percentile height female) and 59 years old. Although her exact weight is not available, Bajka *et al.* (2004) estimated her weight from her liver volume, to be about 124-131kg. Her external neck and head size were estimated to be over or around 90th percentile female (Gordon *et al.*, 1989). However most of her vertebrae are in the 40th -60th stature percentile female range for vertebral height and depth (Katz *et al.*, 1975).

Head and neck skeletal anatomy: Computed tomographic (CT) images of VHF skull, vertebrae (C1-T6), ribcage, clavicle, scapula and hyoid bone were traced using image analysis software (3D-doctor, Able Software, Lexington, MA). The biomechanical model (Figure 1a) was built in SIMM (Software for Interactive Musculoskeletal Modeling, Santa Rosa, CA).

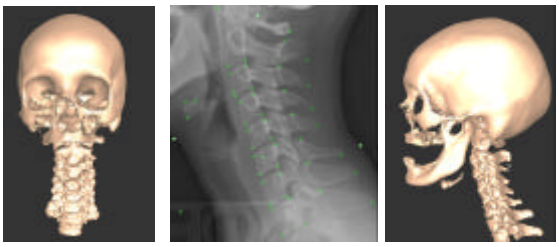

(a) **(b)** **(c)**

Figure 1: (a) Frontal view of VHF; (b) Lateral x-ray of a 65th percentile height female subject in neutral posture; (c) Aligned neck model

Joint kinematics: The visible female was scanned in the supine posture, resulting in a neck posture, which was different from the upright neutral posture. We used a lateral x-ray of a height-matched female subject (1.65m, 48.6kg, similar vertebrae size) in the upright neutral posture (standing) to align the VHF bones to upright neutral (Figure 1b, 1c). This ensured a neutral posture, which fell within the range reported in the literature (Harrison *et al.*, 2004).

The rotation centers of skull and vertebrae were estimated from subjects in which gender was not specified (Amevo *et al.*, 1991) and scaled by the vertebral size of VHF.

Muscle anatomy and force-generating parameters: The muscle volumes were obtained from the reconstruction of 3D muscle surfaces by tracing the color cryosection photographs of VHF. Physiological cross-sectional (PCSA) was obtained by dividing muscle volume by muscle fiber length, which was estimated by calculating the length of a cubic B-spline curve that used least squares approximation

fitting to the muscle centroids at each slice. Other parameters were scaled from the male neck model.

The origin and insertion of each neck muscle were attached to the same bony landmarks as those of male model and connected by a straight line (Figure 2).

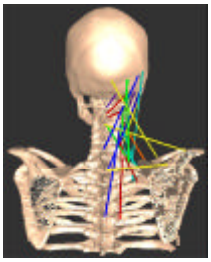

Figure 2: biomechanical female neck model

RESULTS AND DISCUSSION

The VHF model predicted that the extension moment at the neutral position was 28 Nm, which was larger than experimental data from females (Vasavada *et al*., 2001). The VHF data were compared to two male models representing a 50th percentile male, where the only difference between those two was that one ("M_1") used PCSA measured from older male and female cadavers (Kamibayashi *et al.* 1998) and the other one ("M_2") used PCSA estimated from *in vivo* MRI of young 50th percentile males (Chancey *et al*., 2003). The ratio of female model maximum extension moment to "M_1" and to "M_2" were within the range from the literature (Suryanarayana et al., 2004; Vasavada *et al*., 2001) (Table 1).

The maximum moment analysis was broken down to two parts: the effect from the peak muscle forces and from the muscle moment arms (Table 1). The peak muscle force is proportional to PCSA. The average PCSA of VHF is close to PCSA obtained from cadaver data and is smaller than that from *in vivo* MRI data. However, even if female PCSA is slightly larger than male, the smaller moment arms result in lower total moment. The smaller moment arms of the female model mainly result from her smaller skeletal structure compared to 50th percentile male. However the slightly different neutral postures and use of straight-line muscle paths could also affect the differences in moment arm.

Table 1: The comparisons of maximum extension moment in neutral position among female model (F), *in vitro*-PCSA male model (M_1) and *in vivo*-PCSA male models (M_2)

	Ratio$_1$ (F/M$_1$)	Ratio$_2$ (F/M$_2$)
PCSA	1.05	0.74
Moment arm	0.77	0.77
Max. Moment	0.84	0.59

It was obvious that we could not scale a male neck model to a female one by a simple ratio, since there were many gender differences in size, geometry and biomechanical properties.

SUMMARY/CONCLUSIONS

The results predict lower neck strength in females, even when muscle size is comparable to males, as in this very large female (VHF). The skeletal structure appears to play a very important role in our current straight-line neck model. Gender-specific neck models are necessary for further research.

REFERENCES

Amevo B., et al. (1991) *Clin Biomech.* **6**(2): 111-117.

Bajka, M., et al. (2004) *Clin Anat.* **17**:252-260.

Chancey, V. C. et al. (2003) *Stapp Car Crash J.* **47**:135-153.

Gordon, C. C. et al. (1989). *1988 anthropometric survey of U.S. army personnel: methods and summary statistics.*

Harrison D. D. et al. (2004) *Spine*. **29**(22):2485-2492.

Katz, P. R., et al. (1975) *Am J Phys Anthropol.* **43**(3): 319-26.

Kamibayashi L. K. et al. (1998) *Spine.* **23**(12): 1314-1323.

Suryanarayana, L. et al. (2004) *Clin Biomech.* **20**: 138-144.

Vasavada, A. N., et al. (1998) *Spine.* **23**(4): 412-422.

Vasavada, A. N., et al. (2001) *Spine.* **26**(17): 1904-1909.

ACKNOWLEDGEMENTS

WSU Bioengineering Research Center, Whitaker Foundation and Centers for Disease Control (R49 CE000660-01)

COMPARISON OF TWO METHODS OF DETERMINING RELATIVE EFFORT DURING SIT-TO-STAND

Kathleen A. Bieryla, Dennis A. Anderson, and Michael L. Madigan

Virginia Tech, Blacksburg, VA, USA
E-mail: kbieryla@vt.edu, Web: www.biomechanics.esm.vt.edu/msbiolab/

INTRODUCTION

Older adults have a reduced ability to perform activities of daily living (ADLs), and one possible reason is older adults perform ADLs at a higher level of relative effort compared to young adults. Relative effort has been quantified by expressing joint torques during an activity as a percentage of the maximum voluntary torque (Hortobagyi 2003).

Anderson et al. (2007) developed a model to predict maximum voluntary joint torque as a function of joint angle and angular velocity using a regimen of isokinetic and isometric measurements. This model could be used to estimate maximum voluntary torque when assessing relative effort.

The main purpose of this study was to compare two methods of determining relative effort during sit-to-stand (STS). It was hypothesized that relative effort values that account for variations in maximum voluntary joint torque with joint angle and angular velocity will be higher than relative effort values that do not account for these variations.

METHODS

Thirty participants (mean 43.5 ± 21.6 years) performed six STS trials at three self-selected speeds (slow, normal, fast). Participants rose from an armless, backless chair that was positioned on a forceplate with feet spaced shoulder width apart and each resting on a forceplate.

Sagittal plane joint torques in the right lower extremity were estimated using a 2-D rigid-link model. Body segment data was sampled at 100 Hz (Vicon, CA) and force plate data were sampled at 1000 Hz. Isometric and isokinetic maximum voluntary contractions (MVC) for knee extension were collected using a Biodex System 3 dynamometer and used for model parameters to predict the participant-specific theoretical maximum voluntary joint torque (Anderson 2007).

Two methods were used to calculate relative effort (Figure 1). Method 1 (M1) first determined the peak joint torque during STS, then normalized this torque by dividing it by the maximum isometric torque recorded from the Biodex. Method 2 (M2) first normalized joint torques throughout STS by dividing each instantaneous value by the theoretical maximum voluntary joint torque at the specific joint angle-angular velocity combination, then determined peak relative effort.

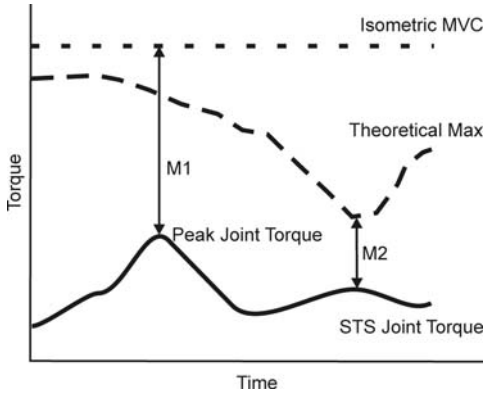

Figure 1: Sample STS data to illustrate the two methods of calculating relative effort.

A two-way ANOVA was conducted on relative knee extension effort with method (M1 or M2) and speed (slow, normal, or fast) as independent variables.

RESULTS AND DISCUSSION

Relative knee extension effort showed main effects of speed ($p<0.001$), method ($p<0.001$), and a speed x method interaction ($p<0.001$) (Figure 2). Pair-wise comparisons between speeds revealed the relative effort at a fast speed (82.5 ± 31.8%) was higher than at a normal speed (66.8 ± 23.0%), and both were higher than at a slow speed (45.5 ± 13.4%). Pair-wise comparisons between methods revealed the relative effort calculated using M2 (78.4 ± 32.1%) was higher than M1 (51.7 ± 15.0%). Pair-wise comparisons to evaluate the speed x method interaction revealed relative effort calculated using M2 increased at a higher rate as speed increased compared to relative effort calculated using M1.

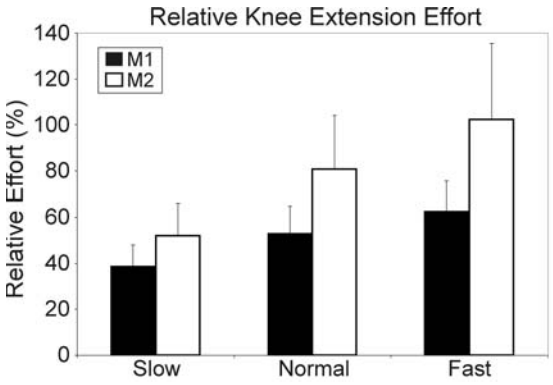

Figure 2: Mean relative knee extension effort during STS for all three speeds and both methods. Error bars represent standard deviation.

In general, accounting for variations in maximum voluntary joint torque with joint angle and angular velocity led to higher levels of relative effort compared to methods which do not account for these variations.

At higher velocities, the difference in calculating relative effort with respect to isometric MVC or incorporating joint angle and angular velocity becomes more evident. The difference between M2-M1 was significantly higher in the fast STS trials than in the slow trials. These results support the importance of including angular velocity in a model when calculating relative efforts during tasks with higher velocities.

SUMMARY/CONCLUSIONS

In conclusion, incorporating variations in joint torque production with joint angle and angular velocity was shown to have an effect on calculated relative effort, especially for tasks with higher velocities.

REFERENCES

Anderson, D.E., et al. (2007). *J Biomech*, in press.

Hortobagyi T., et al. (2003). *J Gerontol A Biol Sci Med Sci*, **58**, M453-460

ACKNOWLEDGEMENTS

This work was supported in part by grant R03 OH007821 from Centers for Disease Control and Prevention.

MOVEMENT HEIGHT AFFECTS KINEMATIC VARIABILITY DURING FATIGUE

Deanna H. Gates [1] and Jonathan B. Dingwell [2]

[1] Department of Biomedical Engineering, University of Texas, Austin, TX, USA
[2] Nonlinear Dynamics Laboratory, Dept. of Kinesiology, University of Texas, Austin, TX, USA
E-mail: jdingwell@mail.utexas.edu Web: http://www.edb.utexas.edu/faculty/dingwell/

INTRODUCTION

Muscle fatigue may be an important intermediary to the development of repetitive stress injuries (RSIs). Changes in kinematics (Cote, 2005) or muscular coordination (Corcos, 2002) can occur with fatigue. These changes may reflect the person's inability to maintain a proper posture which in turn could lead to the development of a RSI. Most research has focused on fatiguing *specific* muscle groups, so little is known about the effect of *global* muscle fatigue on coordination and variability.

This study examined the mean and variability of the kinematic range of motion (ROM) and EMG median frequencies (MdPF) during a high and low height repetitive task similar to a sawing motion. We hypothesized that the mean values of ROM and MdPF would change significantly over the course of each trial, reflecting a shift away from the initially more optimal movement patterns. We also hypothesized that the cycle-to-cycle variability of ROM and MdPF would increase significantly over the course of each trial, possibly reflecting an increasing attempt to maintain performance.

METHODS

10 healthy right-handed (28 ± 2 years) subjects sat in an adjustable chair with seat belts to help them maintain a constant posture (Fig.1). They then pushed a weight back and forth along a low friction horizontal track in time with a metronome until volitional exhaustion. The weight was set to 15% of the subject's maximum pushing/pulling force. The height of the track was set to either sternum level (Low) or shoulder level (High). Each subject performed both tasks in random order on 2 different days. The 3-D movements of markers on the arm and trunk were recorded continuously at 60 Hz using VICON (Oxford Metrics, Oxford, UK). EMG were collected at 1080 Hz from 9 arm and trunk muscles.

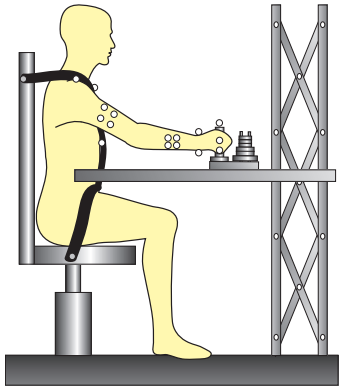

Figure 1. The experimental set-up.

Three rotational angles of the shoulder, elbow, and wrist were calculated using Euler angles. Dependent measures were calculated by splitting each time series into 10 bins. Mean values of MdPF and ROM were calculated for each bin and variability was measured as the standard deviation of each measure across that bin. A series of 3-factor (Subject x Condition x Bin) ANOVAs were used to identify differences over time (bins) and between conditions for each measure.

RESULTS AND DISCUSSION

The high height significantly reduced the time to failure ($p = 0.007$; Low: 24.1 ± 10.3

minutes; High: 12.1 ± 3.9 minutes). MdPFs decreased over time, indicating that both tasks significantly fatigued the arm and trunk muscles tested ($p < 0.001$ for 8 of 9 muscles). MdPF variability decreased in the triceps and anterior and posterior deltoid ($p < 0.011$) and increased in the Low condition for the triceps and middle deltoid ($p < 0.031$) (Fig. 1).

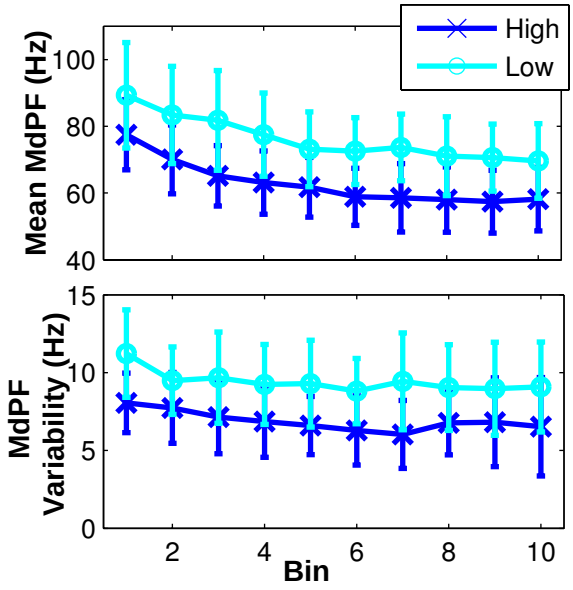

Figure 1. MdPF mean and variability of the anterior deltoid decreased significantly. Error bars are 1 standard deviation.

The ROM of the 3 shoulder angles and the wrist flexion angle were significantly lower in the High condition ($p < 0.001$; Fig 2). This was likely due to the constraining nature of the High task. Only the humeral plane angle ROM significantly decreased in across the task. Thus, subjects were largely able to maintain their ROM despite muscle fatigue. Variability was significantly reduced in the High condition for humeral rotation and elevation angles and all 3 wrist angles ($p < 0.033$). There was a significant subject x condition interaction for all comparisons, indicating that each subject responded differently to the change in height.

SUMMARY/CONCLUSIONS

The increase in height had a much stronger effect on mean ROM and ROM variability than did muscle fatigue. Large between subject variations reflect the numerous functional solutions that exist, even a highly controlled task. This large between subject variability agrees with previous work on EMG intensity patterns during a fatiguing cycling task (von Tscharner, 2002). Our results suggest that it may difficult to generalize results from *localized* muscle fatigue studies to *globally* fatiguing tasks.

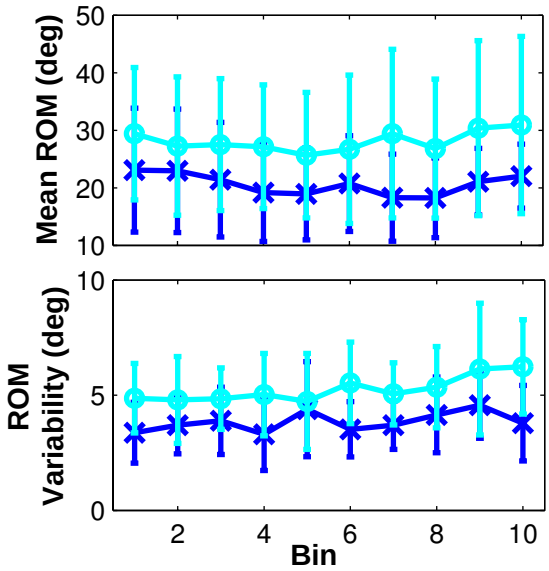

Figure 2. Humeral rotation ROM mean and variability were significantly lower for the high condition. There was no effect for bin. Error bars are 1 standard deviation.

REFERENCES

Corcos, D. et al. (2002) *Exp Brain Res* **142**: 1-12.

Cote, J. et al. (2005) *Clin Biomech* **20**: 581-590.

von Tscharner, V. (2002) *J Elec Kinesiol* **12**: 479-492.

ACKNOWLEDGEMENTS

Supported by NIH Grant #EB003425

APPROXIMATE ENTROPY IS ROBUST TO NON-STATIONARITY IN ANALYSIS OF INFANT SITTING POSTURAL SWAY

Joan E. Deffeyes[1], Regina T. Harbourne [2], Stacey L. DeJong [2], Wayne A. Stuberg [2], Anastasia Kyvelidou[1], Nicholas Stergiou[1]

[1] Biomechanics Laboratory, University of Nebraska at Omaha, Omaha, NE, USA
[2] Munroe-Meyer Institute, University of Nebraska Medical Center, Omaha, NE, USA
E-mail: jdeffeyes@mail.unomaha.edu Web: http://biomech.unomaha.edu/

INTRODUCTION

Upright sitting is one of the first developmental milestones an infant achieves in normal development. This seemingly static posture involves considerable subtle movement as the weight shifts, requiring specific behavioral control strategies to keep the body upright. Center-Of-Pressure (COP) data obtained from a force platform is used to gain insight into these control strategies (Harbourne & Stergiou, 2003). However, suitable mathematical techniques must be employed to quantify the postural control information from the COP data. Techniques such as path length or range of movement can be used to describe how much the center of pressure moves around (quantity of movement), but these techniques don't give any information about how well coordinated the movement is (quality of movement). Approximate entropy (ApEn) is a measure of the randomness in a time series, and can be used to assess quality of movement. However, stationarity is often a concern in the analysis of time series data, and was an explicit assumption in the derivation of the commonly used ApEn algorithm (Pincus, 1991). Differencing is a commonly employed method for removing nonstationarity from time series data (Chatfield, 2003). Thus, we have explored the use of differencing on the approximate entropy analysis of infant sitting COP data.

METHODS

Infants were recruited when they were just developing the ability to sit upright (started at age 145.1 days old, *sd*=15.9 days, n=11). Infants were screened for normal development by a physical therapist prior to admission into the study, being excluded if they failed to score above 0.5 standard deviations below the mean on the Peabody Developmental Motor Scales (Folio & Fewell, 2000). Infants came to the laboratory twice per month for a period of four months, until they were beginning to crawl, and would thus no longer sit still for data acquisition.

For data acquisition, infants sat on an AMTI force plate (Watertown, MA), interfaced to a computer system running Vicon data acquisition software (Lake Forest, CA). COP data was analyzed using custom MatLab software (MathWorks, Nantick, MA), and ApEn was calculated using code developed by Kaplan and Staffin (1996), implementing the methodology of Pincus (1991) and Kaplan et al (1996). Stage of sitting was assessed by a physical therapist on a scale of 1 to 3 (1=prop sitting, 3=extended time in upright sittting) based on the length of time the infant was able to maintain upright sitting without a fall. ApEn was calculated for the COP data from the anterior-posterior axis for each of 244 trials, both with and without differencing. Differencing is calculating the difference between each data point and the data point preceding it in the time series, reducing the length of the time series by one. The ApEn

results were then correlated with 1) age of the infant at data acquisition, and 2) stage of sitting.

RESULTS AND DISCUSSION

Differencing the data appears to remove most, if not all, of the nonstationarity in the data (Figure 1).

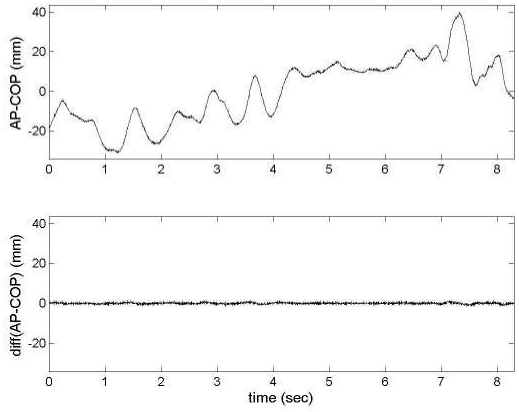

Figure 1: Representative COP time series data in anterior-posterior axis (top) and that same data after differencing (bottom). Differenced data appears more stationary than raw data.

Correlation coefficients of ApEn with developmental variables were larger in magnitude when no differencing was used, and largest when lag 4 was used in the ApEn calculation (Table 1). This is likely due to the presence of 60 Hz noise in the 240 Hz data.

SUMMARY/CONCLUSIONS

Approximate entropy originally was derived as being applicable only to stationary processes (Pincus, 1991). However, one can examine the necessity of this requirement by differencing the data to remove nonstationarity (Chatfield, 2003). Our results indicate, that for postural sway data, differencing is not beneficial. Approximate entropy appears to be robust to nonstationarity of the data.

REFERENCES

Chatfield, C. (2003). *The Analysis of Time Series Data: An Introduction, 6th ed.* Chapman & Hall/CRC: Boca Raton.

Harbourne, R.T., Stergiou, N. (2003) *Dev Psychobiol.* **42,** 368-77.

Folio M.R., Fewell R.R.(2000). *Peabody Developmental Motor Scales, 2nd Edition.* Pro-ed, Inc., Austin, TX.

Kaplan, D. et al. (1991). *Biophys.J.* 59, 945-949.

Pincus SM. (1991) *Proc Natl Acad Sci USA*, **88**, 2297-2301.

Rapp, P.E. (1994). *Integr Physiol Behav Sci.* **29,** 311-327.

Kaplan, D., Staffin, P. (1996). http://www.macalester.edu/~kaplan/hrv/doc/

ACKNOWLEDGEMENTS

This work was supported by NIH (K25HD047194) and NIDRR (H133G040118).

Table 1. Correlation coefficients of ApEn with age and with stage of sitting.

Differencing used	none	none	1	4
Lag used in ApEn	4	1	1	1
r (ApEn w/ age)	-0.315	-0.166	-0.124	-0.031
r (ApEn w/ sit stage)	-0.437	-0.251	-0.198	-0.173

Prospective Study of the Biomechanical Factors Associated with Patellofemoral Pain Syndrome

Brian Noehren[1] and Irene Davis [1,2]

[1] University of Delaware, Newark, DE, USA
[2] Drayer Physical Therapy institute, Hummelstown, PA, USA E-mail: bwn51@yahoo.com

INTRODUCTION

Patellofemoral pain syndrome (PFPS) is the leading cause of knee pain in runners. Despite the high incidence of PFPS, the etiology of this injury is not well-understood. Most of the focus on PFPS has been on factors directly associated with patellofemoral joint. However, abnormal mechanics of joints proximal and distal to the knee may also contribute to this injury.

At the hip, increased adduction, as well as internal rotation may alter the patellofemoral contact area, thereby adversely affecting patellar stress. In support of this, cadaveric studies revealed that increased hip adduction (Huberti et al. 1984) and internal rotation (Lee et al, 2003) both resulted in increased stress on the lateral patellar facet. With the repetitive loading of running, this can lead to PFPS. Increased hip motions may place greater demands on the hip musculature leading to greater joint moments in these individuals as well.

At the rearfoot, abnormal eversion has been suggested to contribute to PFPS. Tiberio (1987) hypothesized that if eversion is prolonged into the second half of stance, tibial internal rotation would also be extended. However, relative tibial external rotation is necessary for knee extension to occur. As the tibia is coupled tightly with the talus, it cannot externally rotate at this time. Thus, the femur must increase its internal rotation to obtain the necessary knee external rotation needed for knee extension to occur. This internal rotation of the femur and associated external rotation of the knee increases the Q-angle and can lead to abnormal patellofemoral joint loading (Huberti et al.1984).

To date, there are no prospective studies of mechanics proximal and distal to the knee in runners who develop PFPS. Therefore, the purpose of this study was to compare running mechanics in a group of female runners who later went on to develop PFPS to a group of healthy controls. It was hypothesized that runners who go on to develop PFPS would exhibit greater hip adduction, hip internal rotation, less knee internal rotation and greater time to peak rearfoot eversion. Additionally, we hypothesized that the PFPS group would exhibit greater hip abduction and hip external rotation moments.

METHODS

These data are part of a larger, ongoing study of injuries in female runners. Thus, females between the ages of 18-45, running a minimum of 20 mpw and free from current injury were recruited for the study.

Upon entry into the study all subjects underwent an instrumented gait analysis. Retroreflective markers were placed on the lower extremities. Subjects then ran along a 25m runway at 3.7m/s striking a forceplate (Bertec OH, USA) at its center. Kinematic data were captured using a 6-camera motion capture system at 120Hz (Vicon, Oxford metrics, UK). Kinetic data were captured at 1080 Hz using a force platform. Five running trials were collected. Joint angles and moments during the stance phase were

calculated using visual3D software (Visual 3D, C motion, MD, USA).

To date, 13 female runners have gone on to develop PFP on 15 knees. All injuries were confirmed by a medical professional. They were compared to a control group of 15 age and mileage matched uninjured runners Variables of interest were compared between groups using an independent t-test.

RESULTS AND DISCUSSION

Discrete variables of interest and joint angular curves are presented in Table 1 and Figures 1-2 respectively.

Table 1 Variables of Interest

	PFP	CON	P
Peak Hip Add (Deg)	12.1	8.1	0.007
Peak Hip Abd Mom (Nm)	-1.3	-1.3	0.896
Peak Hip Int Rot (Deg)	4.5	3.0	0.47
Peak Hip Ext Rot Mom (NM)	-0.04	-0.02	0.07
Peak Knee Int Rot (Deg)	0.01	1.9	0.39
Time to Peak Ev (% stance)	51.3	51.4	0.94

As hypothesized, hip adduction was significantly greater in the PFPS group (Fig 1). The greater hip adduction seen may increase the loading on the lateral patella (Huberti et al. 1984). With greater hip adduction we were surprised hip abduction moment was not greater as well. However, it is possible that differences in neuro-muscular factors, such as timing of activation are more important. The PFPS group was in greater hip internal rotation throughout stance, although this was not significantly different. However there was a trend towards greater hip external rotation moment in the PFPS group.

At the knee, the PFPS group exhibited greater external rotation (Fig 2). However this was not significantly different between groups. There was no difference in the time to peak rearfoot eversion between groups (Fig 2). While contrary to Tiberios theory, these results are similar to the retrospective findings of Duffey et al. (2000).

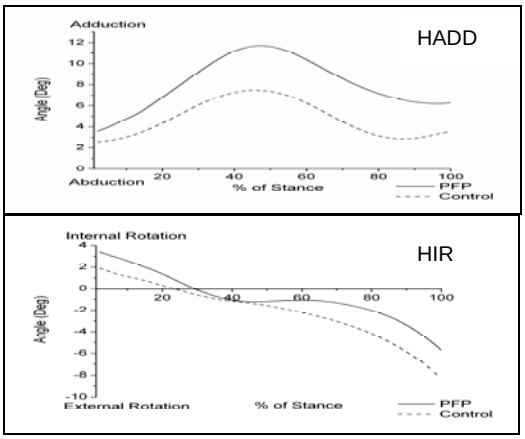

Figure 1 Hip Add (top) and B: Hip Int rot (bottom)

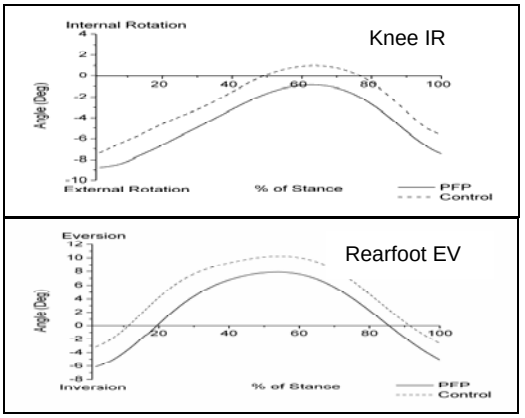

Figure 2 Knee IR (top) and RF EV (bottom)

SUMMARY/CONCLUSIONS

Based on these preliminary results, proximal factors may have a greater impact in the development of PFPS than distal ones. Also frontal and transverse plane mechanics of the knee may be controlled by the hip. This suggests that interventions should focus on proximal factors.

REFERENCES

Dierks et.al (2005) ASB Mta, Clevland, OH
Duffey et.al (2000). *MSSE* , **27**, 951-60
Lee et al. (2002) *JOSPT*, **33**, 686-693
Huberti et al. (1984) *JBJS* **66** 715-724
Tiberio (1987) *JOSPT,**17,*** 160-169

ACKNOWLEDGEMENT

Supported by Dept of Defense grant DAMD17-00-1-0

A TECHNIQUE FOR DETERMINATION OF TRANSVERSE MATERIAL PROPERIES OF HUMAN FLEXOR DIGITORUM TENDONS

Cheolwoong Ko[1], M. James Rudert[1], and Thomas D. Brown[1]

[1] Department of Orthopaedics and Rehabilitation, University of Iowa, Iowa City, IA, USA
E-mail: tom-brown@uiowa.edu Web: http://poppy.obrl.uiowa.edu/Home%20Page/index.html

INTRODUCTION

Carpal tunnel syndrome (CTS) is among the most important of the family of musculo-skeletal disorders. Mechanical insult to the median nerve, due to contact with the flexor digitorum tendons, is considered a proximate cause. However, there is little biomechanical information available for transverse compressive properties of the flexor tendons to explain the objective characterization of this local biomechanical insult. To obtain apparent tendon transverse compressive properties, biaxial tests were undertaken using human cadaver tendons. The apparent tendon anisotropic material behavior was characterized using finite element (FE) analysis.

METHODS

Tendon behavior in compression is presumably influenced by longitudinal tension, owing to the composite-like tissue architecture of collagen fibers embedded in extra-fibrillar matrix. To measure transverse compressive stiffness of the flexor tendons as a function of independently prescribed levels of longitudinal tension, an MTS-mounted biaxial testing device was developed (Figure 1). The tendon specimen is oriented horizontally, with a pneumatic actuator used to apply longitudinal loads. After tensioning to a physiologically representative level (16.9 N, 33.8 N, and 50.7 N), the MTS actuator-mounted upper platen applied transverse displacement at a rate of 0.25mm/sec, while the transverse

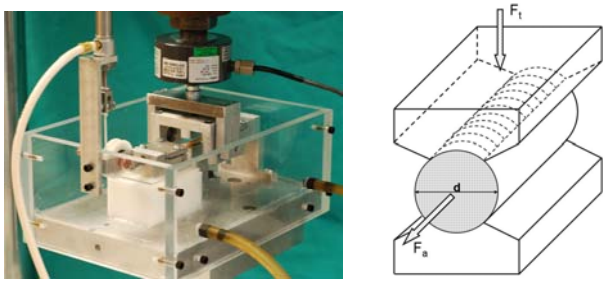

Figure 1: Test Apparatus and Parameter Definitions

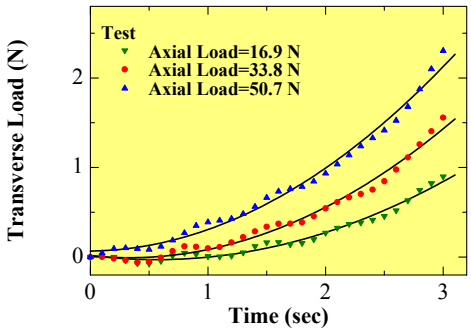

Figure 2: Transverse Load History (normal digital flexor tendon, from a 55-year old fresh-frozen cadaver specimen)

load was continuously measured by an in-line load cell during 3.0 sec (Figure 2).

A three-dimensional finite element (FE) model of the experimental set-up was created (Figure 3). The tendon FE model was positioned between the two rigid platen surfaces, with the lower surface model being completely fixed. ABAQUS Standard (v6.5) was used as a solver. To quantitatively identify flexor tendon material properties, two types of tendon material characteriza-

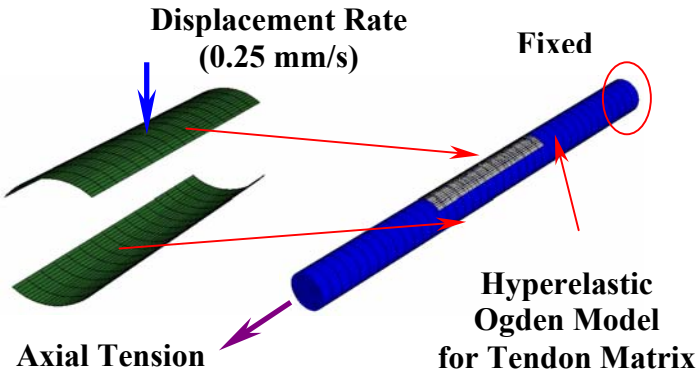

Figure 3: 3-D FE Modeling and Boundary Conditions of Test Set-up

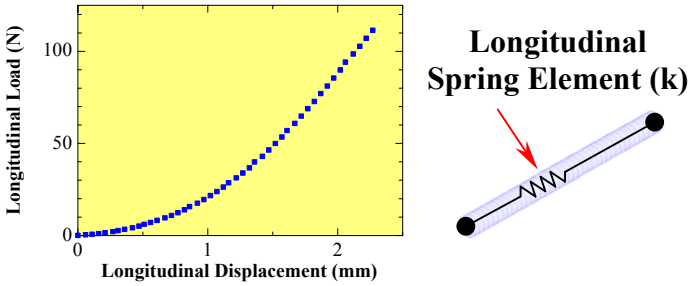

Figure 4: Tendon Longitudinal Test and Spring Element Application

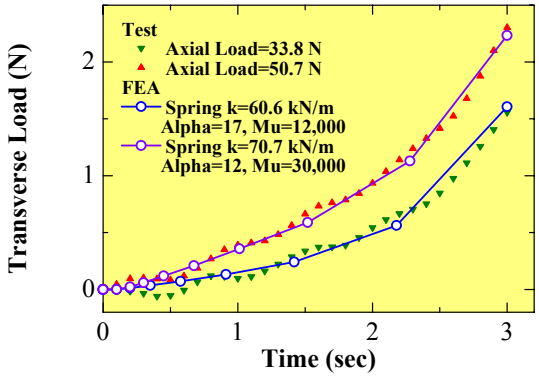

Figure 5: Comparison of FEA and Test Results

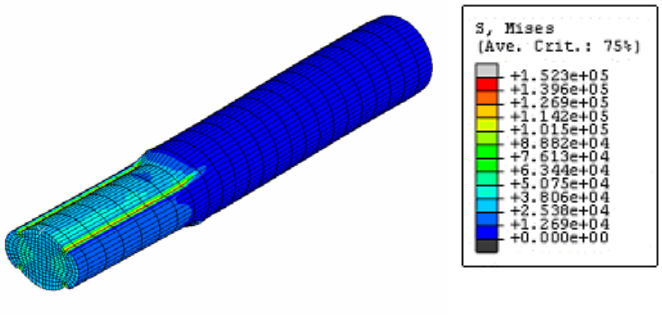

Figure 6: Example of 3-D FE Simulation

tions were introduced. Isotropic Ogden hyperelasticity was applied for the tendon matrix. With an incompressible Ogden model condition, only two material parameters α, μ are considered, with strain energy U being expressed as a function of stretch ratios $\lambda_1, \lambda_2, \lambda_3$ (Equation 1). Also, to describe tendon anisotropy, a spring element was superimposed between the end nodes of the tendon FE model, within the tendon isotropic matrix (Figure 4). The spring stiffness data (k) were estimated from tendon longitudinal displacement-load data.

$$U = \frac{2\mu}{\alpha}(\lambda_1^{\alpha} + \lambda_2^{\alpha} + \lambda_3^{\alpha} - 3) \qquad (1)$$

RESULTS AND DISCUSSION

Iterative parameter searching with α, μ was used to obtain transverse load history matching with experimental data (Figure 5). The determined Ogden model parameters were α=17, μ=12,000 in case of axial tension 33.8 N, and α=12, μ=30,000 in case of axial tension 50.7 N, respectively. An example of mid-cross section deformation and stress contours is illustrated in Figure 6. It was found that the present FE analysis method is effective to determine the apparent transverse compressive material properties of the flexor digitorum tendons, which then can be used for patho-physiological study of the role of median nerve entrapment and compression by tendons, in CTS.

ACKNOWLEDGEMENT

The authors greatly appreciate technical assistance provided by Dr. Y. Tochigi.

AMPUTEE GAIT TRAINING USING VIRTUAL REALITY AND REAL-TIME FEEDBACK

Wilken, J.M. and Marin, L.C.
Military Performance Lab, Center for the Intrepid, Fort Sam Houston, TX
E-mail: Jason.Wilken@amedd.army.mil

INTRODUCTION

Gait training is a key component of the rehabilitation process following trans-femoral amputation. Training frequently focuses on minimizing abnormal trunk and pelvic motion and decreasing loading asymmetries, as these factors are believed to contribute to disabling long-term morbidity such as low back pain and contralateral limb osteoarthritis, respectively (Cappozzo et al. 1982; Kulkarni et al. 1998). However, clinical gait training for pelvic motion is limited by issues such as poor reliability of observational gait assessment, the complex tri-planar motion of the pelvis and a limited ability to provide feedback in a manner that will optimize motor learning.

Although optoelectronic motion capture technologies allow the ability to accurately and reliably assess pelvic kinematics, the ability to synthesize this information and present it in an easily accessible format for use by the patient and therapist is limited. Furthermore, there is frequently a considerable delay in feedback and a limited ability to provide information regarding the results of training interventions.

Recently, studies have shown that real-time feedback during treadmill-based training can produce rapid effects in amputees, resulting in improved gait symmetry (Dingwell et al. 1996) and decreased metabolic cost (Davis et al. 2004). These studies demonstrate the potential of real-time feedback as a tool for amputee gait training.

The rapid results achieved by these training protocols are likely due, in part, to the fact that the subject's attention was focused on a display screen providing real-time feedback rather than their physical self. An emphasis on an external point of feedback, also known as external focus, has been found to result in improved motor learning relative to more conventional internal focus based programs (McNevin et al. 2000).

In an effort to maximize efficiency and effectiveness of gait training for trans-femoral amputees, a protocol has been designed which combines the real-time feedback capacity of a virtual reality based training environment with the accuracy of optoelectronic motion capture.

EQUIPMENT

The training protocol will be conducted within a one-of-a-kind dome-shaped Computer Assisted Rehabilitation Environment (Motek B.V.). Eight DLP projectors display a custom immersive virtual environment on the inner surface of the 21ft diameter dome, yielding a 300° horizontal field of view and -40° to +80° vertical field of view. Subjects interact with the virtual environment while standing or walking on a 4m diameter Stewart platform (Rexroth Hydraudyne B.V.) in the center of the dome. In addition to being capable of motion with six degrees-of-freedom, the Stewart platform features an integrated 3m x 2m instrumented treadmill (Bonte). Data

collected using the included 24-camera optoelectronic motion capture system (Vicon, Inc.) allows kinematic assessment and can also be used to provide feedback, control treadmill speed, guide navigation through the virtual world and influence the motion of the platform.

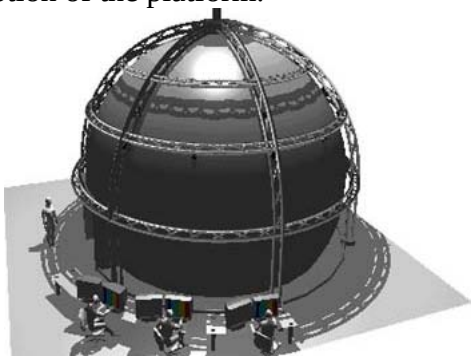

METHODS

Eighteen subjects with unilateral trans-femoral amputation will participate in 12 physical therapist-directed training sessions over a period of three weeks. As subjects walk through a speed-appropriate virtual environment they will be provided visual feedback including 1) an animation of the subject (avatar), presenting real-time full-body gait kinematics as determined using the optoelectronic motion capture system 2) a Lissajous plot presenting vertical and medial-lateral translation of the pelvis relative to normal and 3) a correlation score indicating the extent to which the subject's pelvic kinematics are similar to normal pelvic kinematics.

Additional graphical feedback will be displayed out of view of the subject. The physical therapist guiding the training session will monitor graphs of the frontal, transverse and sagittal plane pelvic kinematics relative to normative data. This enables the therapist to rapidly assess the subject's performance and provide verbal feedback in near real-time.

To evaluate the effectiveness of this new gait training protocol, subjects' gait performance will be assessed during both training and over-ground ambulation. Over-ground ambulation will be assessed four times in a separate, traditional gait lab to describe changes without intervention, changes due to intervention and the persistence of intervention-related changes (an A-B-A design). Gait training is expected to produce pelvic angular excursions, pelvic kinematic patterns and peak vertical loads that are more similar to non-pathologic subjects.

DISCUSSION

The described study will be the first known attempt to use external focus and real-time feedback for the systematic modification of pelvic kinematics. The reliability and accuracy provided by the motion capture system, combined with easy to interpret real-time feedback is expected to improve both the rate and quality of learning.

REFERENCES

Cappozzo, A., et al. (1982). *Prosthet Orthot Int* 6, 131-8.

Davis, B., et al. (2004). *J Prosthet Orthot* 16, 49-54.

Dingwell, J.B., et al. (1996). *Prosthet Orthot Int* 20, 101-10.

Kulkarni, J., et al. (1998). *Clin Rehabil* 12, 348-53.

McNevin, N.H., et al. (2000). *Phys Ther* 80, 373-85.

ACKNOWLEDGEMENTS

Project funded by the Military Amputee Research Program.

EVALUATION OF INJURY CRITERIA FOR PREDICTING COMMOTIO CORDIS

Nathan Dau[1], Mark S. Link MD[2], Christopher Madias MD[2], and Cynthia Bir PhD[1]

[1]Wayne State University, Detroit, MI, USA
[2]Tufts-New England Medical Center, Boston, MA, USA
E-mail: nate.dau@wayne.edu Web: www.bioengineeringcenter.org/home/labs/sports/

INTRODUCTION

Commotio Cordis (CC) is defined as sudden cardiac death (SCD) due to blunt thoracic impact without any observable thoracic or cardiac damage. It is the second leading cause of death in youth sports, taking the lives of 85% of those afflicted (Link, 2005).

Research has provided substantial insight into the pathophysiologic mechanism of CC. It can result from a chest wall impact that occurs in a 10-30 ms vulnerable window during cardiac repolarization, corresponding to the upstroke of the T wave on the ECG. Rapid rise of left ventricular (LV) pressure following impacts directly over the heart results in SCD due to induction of ventricular fibrillation (VF) mediated through resultant myocardial stretch and activation of stretch-sensitive ion channels. Survival is most dependent on institution of early resuscitation including cardiac defibrillation. However, even early resuscitation cannot revive all those affected (Maron, 2005).

The need to identify the most appropriate injury criterion for CC is the next critical step. Currently the only reliable method to test the efficacy of chest protectors in preventing CC is in an animal model. This method requires a large number of animals in order to achieve statistical significance. The goal of the current study is to investigate two possible injury criteria: force and LV pressure. The hope is one of these criteria will be an effective injury criterion for predicting induction of VF from blunt, thoracic impacts.

METHODS

Twelve anesthetized swine ranging from 21 to 45 kgs were impacted using a free flight projectile according to the protocol established by Link et al. (2001). The impacts were timed to occur during the vulnerable period of the cardiac cycle (10-30 ms before the T-wave peak) and aimed directly over the LV. A lacrosse ball attached to an aluminum shaft instrumented with an Endevco 7270 20K accelerometer (Figure 1) was used as the impact projectile. This system provided accurate impact locations, consistent velocities, and a site for mounting the accelerometer.

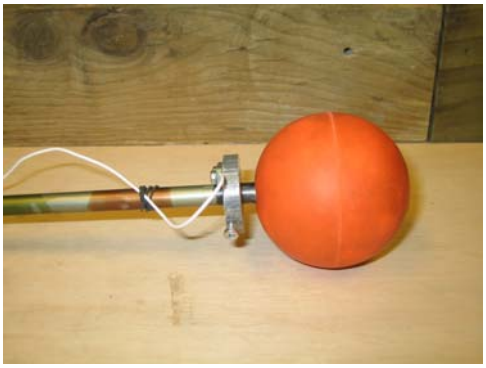

Figure 1: Impact Projectile

Intracardiac pressures were recorded with a Millar Mikrotip catheter placed into the LV via the femoral artery, and the data was collected at 1 KHz using

AD Instruments PCLab Chart software. Accelerometer data was collected at 10 KHz using a TDAS data acquisition system (DTS, Inc) and was filtered using a CFC1000 filter within Diadem (National Instruments).

Specimens were impacted at velocities from 13.4 to 26.8 m/s. The acceleration and pressure data were recorded for each impact along with the incidence of VF. A biphasic defibrillator was used to restore sinus rhythm if VF was induced. Testing continued once normal cardiac physiology was restored.

The Animal Research Committee of the Tufts-New England Medical Center reviewed and approved the protocol.

RESULTS AND DISCUSSIONS

Logistic regression analysis was performed independently for both LV pressure and peak force with incidence of VF as the dependant variable (SPSS v15.0). Both peak LVP and peak force predicted the incidence of VF. However, peak force was a more accurate predictor compared to LVP (Table 1). Figure 2 represents the injury risk curve for the predictive levels of CC in terms of level of force.

This study represents the first prospective investigation into the validation of impact force as an injury criterion to predict the incidence of CC. Previous research has indicated that other criteria, such as the viscous criterion and peak chest compression, might also have significant predictive abilities (Bir, 1999). Future research could compare these variables to peak force to determine the most appropriate criterion.

Table 1: Statistical Results of Logistic Regression Analysis

	$\propto$	B	X^2	p	R^2
LVP	-2.25	.003	9.5	.002	.096
Force	-3.43	.001	22.3	< .001	.270

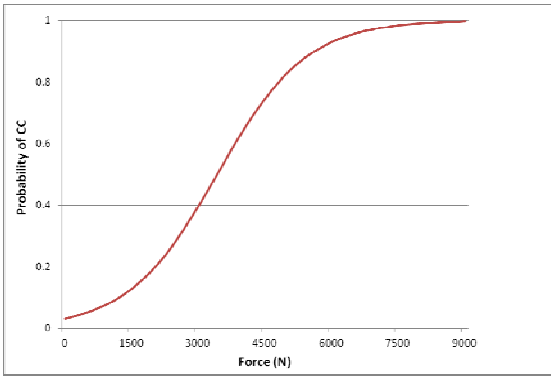

Figure 2: Logistic regression graph for peak impact force

CONCLUSIONS

This study shows that peak impact force has the ability to predict the occurrence of CC more reliably than peak LV pressure. Further research is required to identify the most appropriate predictors of CC for blunt thoracic impacts. These data will be critical in the future design of a reliable mechanical model of CC.

REFERENCES

Link, M. S., Maron, B. J. (2005). *Ital Heart J.* **6**(4): 281-3.

Maron, B. J., et al. (2005). *Heart Rhythm* **2**(9): 991-3.

Link, M. S., et al. (2001). *J. of Am Coll of Cardiology* **37**(2): 649-54.

Bir, C. A., Viano, D. C. (1999). *J. of Trauma.* **47**(3): 468-473.

ACKNOWLEDGEMENTS

Supported by grants from the Acompora Foundation

THE RELATIONSHIP BETWEEN MUSCLE FORCE AND INTRAMUSCULAR PRESSURE DURING DYNAMIC MUSCLE CONTRACTIONS

Samuel R. Ward[1], Jennifer Davis[2], Kenton R. Kaufman[3], Richard L. Lieber[4]

[1]Departments of Radiology, [4]Orthopaedic Surgery and Bioengineering, University of California and Veterans Administration Medical Center, San Diego, CA, USA
[2] Department of Physiology, University of Michigan, Ann Arbor, Michigan USA
[3] Department of Orthopaedics, Mayo Clinic, Rochester, Minnesota USA
E-mail: rlieber@ucsd.edu, Web: http://muscle.ucsd.edu/

INTRODUCTION

The fact that skeletal muscles generate significant intramuscular pressure (IMP) during active contraction was established by A.V. Hill (Hill, 1938). While there is evidence in the literature that IMP is a good predictor of relative isometric joint torque in humans (Hargens, 1989) and relative passive and active isometric stress in animal models (Davis *et al.*, 2003), the extent to which such a relationship is maintained during dynamic muscle movement is not known.

For IMP to serve a useful role in understanding *in vivo* human muscle function, it must provide unique information that reflects muscle force under all conditions, not just the precisely controlled conditions that may be created in a laboratory setting. Therefore, the purpose of this study was to determine the extent to which IMP is a valid surrogate for muscle force during dynamic contractions.

METHODS

The experimental model used was the tibialis anterior (TA) muscle of the New Zealand White rabbit (mass = 2.5 kg ± 0.5; n=4). Rabbits were maintained on gas anesthesia (2% isoflurane) during instrumentation (Fig. 1) and the following testing procedures.

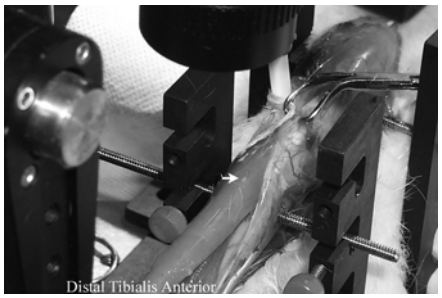

Figure 1. A photograph of the experimental setup shows the TA muscle was isolated from its fascial and bony boundaries and the leg was rigidly fixed to a frame. After attaching the distal TA tendon to a dual-mode servomotor, a pressure transducer (Fig. 1, white arrow) was inserted into the muscle.

The experimental test consisted of an isometric contraction, followed by a 10% shortening contraction at 1 L_f/s, followed by an isometric contraction at the new muscle length. Second, a an isometric contraction, followed by a 10% lengthening contraction at 1 L_f/s, followed by an isometric contraction at the new muscle length. The order of these contraction paradigms was randomized.

Length, tension, pressure, and temperature were recorded for each contraction. A high speed video system (400Hz) was used to measure transducer position relative to the muscle surface. Following testing, the relationship between muscle force and muscle pressure was analyzed using linear regression.

RESULTS AND DISCUSSION

Transducer position measurements demonstrated that significant tip movements occurred when muscle length was changed (Fig. 2), and this movement was related to the usefulness of the IMP signal. In general, transducer movement followed muscle length change (Fig. 2).

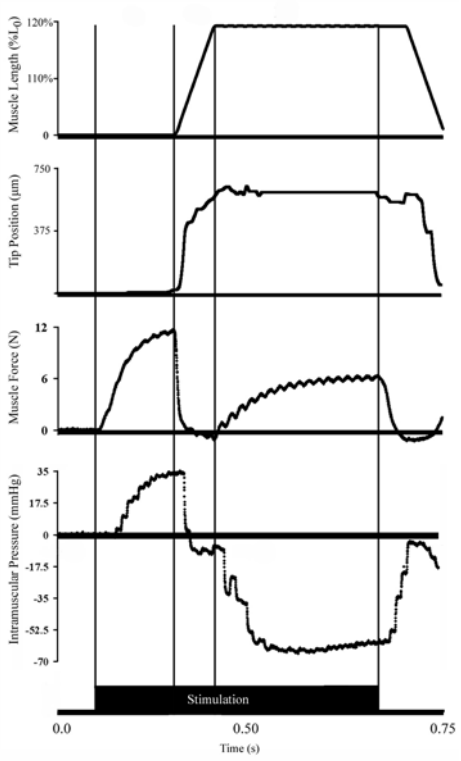

Figure 2. Schematic of synchronized length, transducer position, force, and pressure measurements during a combined isometric – lengthening- isometric contraction.

Quantitative analysis of the predictability of muscle force based on IMP demonstrated that, when the muscle was not moving, IMP explained 89% ± 0.5% of the variance in muscle force (i.e., r^2=0.89). However, when attempting to predict muscle force from IMP either during movement or during the isometric period after movement, the relationship between IMP and stress was no longer valid (Fig. 3).

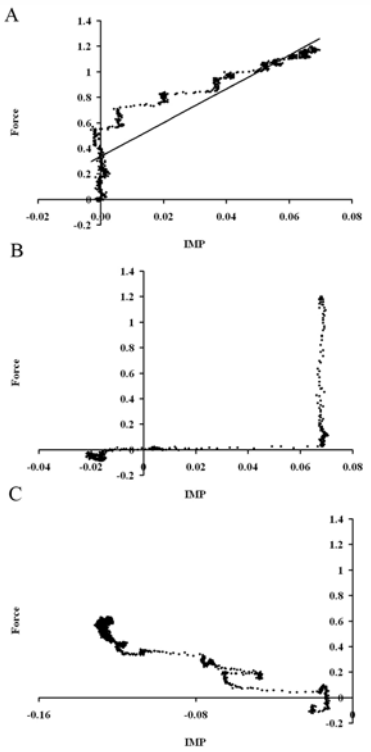

Figure 3. Scatter plots of IMP versus muscle force during (A) an initial isometric contraction (r^2 = 0.89) followed by (B) shortening and (C) isometric contraction.

These findings suggest that when transducer movement is well controlled, there is a strong correlation between IMP and muscle force. This highlights the need to control transducer movement if muscle force is to be inferred from IMP measurements such as might be desired during clinical gait testing.

REFERENCES

Hargens AR, Akeson WH, Mubarak SJ, *et al. J Orthop Res.* **89**, 902-909.
Hill AV. (1938) *Proc R Soc Lond B Biol Sci* **126,** 136-195.
Davis J, Kaufman KR, Lieber RL. (2003). *J Biomech.* **36**, 505-512.

ACKNOWLEDGEMENTS

This work was supported by NIH grant HD031476.

UPPER EXTREMITY KINEMATICS OF CRUTCH-ASSISTED GAIT IN CHILDREN WITH MYELOMENINGOCELE

Brooke Slavens [1,2], Peter Sturm [1-3], and Gerald Harris [1-3]

[1] Orthopaedic and Rehabilitation Engineering Center, Milwaukee, WI
[2] Marquette University, Milwaukee, WI
[3] Shriners Hospitals for Children, Chicago, IL
E-mail: brooke.slavens@mu.edu

INTRODUCTION

Currently, there are limited biomechanical models for quantitative evaluation of upper extremity (UE) dynamics in children with myelomeningocele (MM). While the lower extremities have been studied extensively in MM during crutch-assisted gait (Vankoski, et al., 1997; Galli, et al., 2002; Gutierrez, et al., 2003), UE dynamics have received very limited attention (Requejo, et al., 2005). In order to study UD dynamics, a three-dimensional (3D) biomechanical model of the UEs was developed for dynamic analysis of reciprocal and swing-through Lofstrand crutch-assisted gait in children with MM.

A pediatric model that describes joint motions of the upper body during crutch-assisted gait may be a valuable tool for clinicians. The study findings may also prove useful for improving crutch prescription and in planning ambulatory rehabilitation of children with MM.

METHODS

The UE motion model includes seven rigid body segments: 1) trunk, 2) right upper arm, 3) right forearm, 4) right hand, 5) left upper arm, 6) left forearm, and 7) left hand. Three degree-of-freedom shoulder (glenohumeral) joints and two degree-of-freedom elbow and wrist joints connect the segments. The upper extremity model incorporates ISB recommendations for modeling (Wu, et al., 2005). Eighteen markers are placed on bony landmarks of the upper body in order to determine the kinematics of the trunk, shoulders, elbows and wrists during crutch-assisted gait. To calculate the kinematics of the crutches, four markers are placed strategically. Rotations are described using Euler angles (Z-X-Y order). The trunk and crutch segments are described with reference to the lab (global) coordinate system.

Nine subjects (mean ± S.D. age: 11 ± 4 years) volunteered and gave written consent to participate in the research study. All subjects had an L3 or L4 level myelodysplasia and were ambulatory using Lofstrand crutches in both reciprocal and swing-through gait patterns. Subjects who had undergone orthopaedic surgery in the past year were excluded from the study. The subjects walked at a self-selected pace using Lofstrand crutches until five successful trials were completed with each gait pattern. A 14-camera Vicon MX system captured the marker motions.

RESULTS AND DISCUSSION

The mean cadence, walking speed, stride length, and stance duration during reciprocal gait and swing-through gait were calculated. All temporal-spatial parameters were greater during swing-through gait compared to reciprocal gait, except stance duration (Table 1). Stride length and stance duration were found to be statistically different between gait patterns ($p<0.05$).

Table 1: Mean temporal-spatial parameters. *Gait patterns are significantly different ($p<0.05$)

	Cadence (steps/min)	Walking Speed (m/s)	Stride Length* (m)	Stance Duration* (s)
Reciprocal	69.55	0.46	0.77	0.62
Swing-through	77.36	0.68	1.00	0.54

The mean flexion/extension joint motion, for right and left sides, during reciprocal gait and swing-through gait were also determined (Figure 1). Although reciprocal and swing-through gait have distinguishable characteristics, the flexion/extension motions were similar throughout the gait cycles. Joint ranges of motion were greatest during swing-through gait. Significant differences were found in trunk and elbow ranges of motion between swing-through and reciprocal gait ($p<0.05$). Right and left elbow and wrist ranges of motion were significantly different during reciprocal gait.

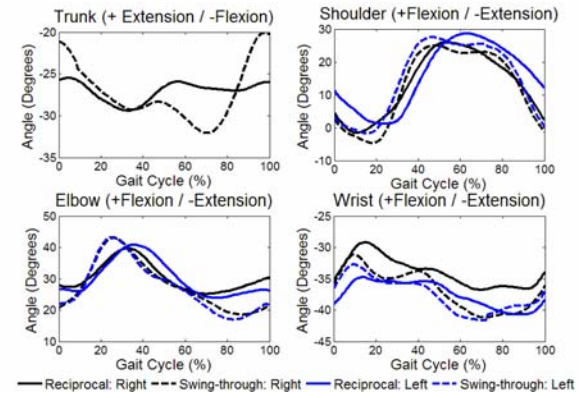

Figure 1. Joint kinematics during reciprocal and swing-through gait.

The model is effective in detecting significant differences in upper extremity joint motion. The model is considered to be suitable for further application to quantify upper extremity dynamics in pediatric subjects with MM. The information gained may be useful for developing injury prevention strategies, rehabilitation protocols, and/or improving the design of Lofstrand crutches.

SUMMARY/CONCLUSIONS

The current study aids physicians in treatment planning of children with MM, which may ultimately improve quality of life. Further subject testing is currently underway, as well as, a kinetic analysis of the UE joints. Future work includes identifying correlations among dynamics and standardized outcomes assessment tools.

REFERENCES

Vankoski, S. et al. (1997) *Dev Med Child Neurol*, **39**, 614-619.

Galli, M. et al. (2002) *Funct Neurol*, **17**, 203-210.

Gutierrez, E.M. et al. (2003) *Gait Posture*, **18**, 170-177.

Requejo, P.S. et al. (2005) *Med Eng Phys*, **27**, 19-29.

Wu, G. et al. (2005). *J. Biomechanics*, **38**, 981-992.

ACKNOWLEDGEMENTS

This project was supported by Shriners Hospitals for Children and OREC. The authors would like to thank Ms. Sahar Hassani, Ms. Kathy Reiners, Ms. Vicky Young and Mr. Adam Graf for their helpful suggestions, assistance and contributions to this project.

SCALING OF JOINT MECHANICS AND MUSCLE ARCHITECTURE IN THE HUMAN KNEE

Samuel R. Ward[1], Trevor Kingsbury[1], Taylor Winters[1], Kristin M. Lieber[2], Jacqeline Braun[3], Carolyn M. Eng[1], and Richard L. Lieber[1]

[1]Departments of Bioengineering, Orthopaedic Surgery, and Radiology, University of California and Veterans Administration, San Diego, La Jolla, CA, USA
[2]University of Southern California, Los Angeles, CA, USA
[3]Baylor University, Waco, TX, USA
E-mail: srward@ucsd.edu, Web: http://muscle.ucsd.edu

INTRODUCTION

Skeletal muscle performance depends on a variety of intrinsic and extrinsic factors. One important intrinsic factor is the degree of actin and myosin overlap. This length-dependent behavior was quantified in isolated frog muscle fibers Gordon *et al.* (1966) and Edman (1966).

In situ, the relationship between sarcomere length (L_s) and joint angle dictates the length-dependent behavior of muscle. In this situation, L_s changes are the result of an initial L_s-joint angle configuration, modified as length changes are imposed by joint motion. Although it has been suggested that L_s-joint angle relationships are stereotypic in humans, this has only been experimentally demonstrated in the wrist (Lieber, *et al.*, 1997). Mechanically, if this is assumption is true, length changes imposed upon a muscle and muscle fiber length (L_f) must scale linearly.

Recently, indirect measurements of excursion and L_f measured by ultrasound suggested that this assumption was not true in the human lower extremity (Maganaris *et al.*, 2006). Here we directly measure muscle excursion and L_f in identical specimens to define the scaling relationship (if any) between lower extremity muscle architecture and joint kinematics.

METHODS

Ten cadaveric lower quarters were harvested and used for the following procedures. First, muscle architecture measurements were made on the four vasti and four hamstring muscles according to methods previously described (Lieber *et al.* 1997). Most importantly, L_s was measured in each fiber bundle using laser diffraction and was used to normalize muscle fiber length (L_{fn}) to 2.7 μm. (Eq. 1):

$$L_{fn} = L_f \times \frac{2.7\,\mu m}{L_s} \qquad \text{(Equation 1)}$$

Physiological cross-sectional area (PCSA), a measure of a muscle's capacity for force generation (Powell *et al.* 1984), was calculated according to (Eq. 2), where M is mass, θ is pennation angle and ρ is muscle density (1.055 g/cm^3).

$$PCSA = \frac{M \times \cos\theta}{\rho \times Lf} \qquad \text{(Equation 2)}$$

After architectural measurements, each knee was instrumented in a custom jig and the tendon excursion-joint angle relationship of each muscle was measured (Fig. 1).

Following these measurements, data were log transformed and linear regression was used to define the mathematical relationship between tendon excursion, mass, fiber length, and PCSA in the exponential form originally described by Alexander *et al.* (1979).

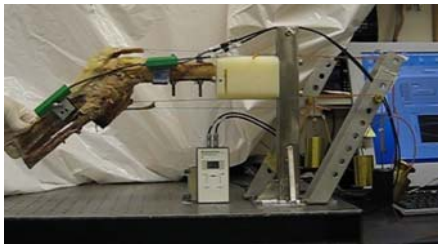

Figure 1. Experimental apparatus to measure simultaneously all tendon excursions and joint angles.

RESULTS AND DISCUSSION

Excursion and muscle mass were not related for any muscle studied (Table 1). This suggests that muscle mass and volume are relatively constant relative to the amount of excursion imposed on these muscles.

Surprisingly, excursion was negatively related to muscle fiber length in the quadriceps muscles (r^2 0.26-0.59) and not related to fiber length in the hamstring muscles (Table 1, Fig. 2). This suggests that *larger* changes in muscle length are associated with *shorter* muscle fibers in the quadriceps and are unrelated to fiber length in the hamstrings.

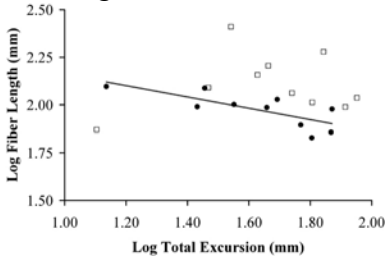

Figure 1. Total excursion versus L_f in the vastus lateralis (filled circles) and semitendinosus (open squares).

Muscle excursion was significantly positively related to PCSA in the vastus lateralis muscle, but not related to PCSA in any other muscle (Table 1, Fig. 3). This suggests that larger changes in muscle length are associated with greater force producing capacity in the key antigravity muscle.

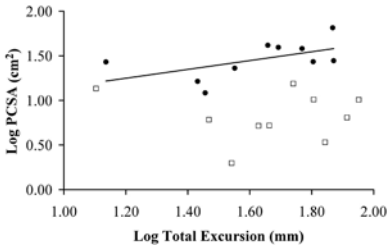

Figure 3: Total excursion versus PCSA (B) in the vastus lateralis (filled circles) and semitendinosus (open squares).

SUMMARY/CONCLUSIONS

Joint mechanics and muscle architecture do scale in some human lower extremity muscles. However, the scaling rules are; 1) not intuitive, 2) appear to vary by muscle and muscle group, and 3) may have profound functional implications.

REFERENCES

Alexander, R.M., *et al.*(1979). *J. Zool. Lond.* **189**, 305-314.

Edman, K.A.P.(1966). *J Physiol (Lond)*, **183**, 407-417.

Gordon, A.M., Huxley, A.F., Julian, F.J.(1966). *J Physiol (Lond)*, **184**, 170-192.

Lieber, R.L. Ljung B.-O., Friden, J.(1997). *J Exp Biol*, **200**, 19-25.

Lieber *et al.*(1992). *J Hand Surg,* **17**:787-798.

Powell P.L.(1984) *J Appl Physiol*, **57:**1715-1721

Maganaris, C.N., Baltzopoulos V., Tsaopoulos D.(2006). *J Biomech,* **39**, 1663-1668.

Table 1. Relationships between muscle excursion and muscle architectural features in the form $y = Excursion^X + C$

Muscle	Excursion versus Mass			Excursion versus Fiber Length			Excursion versus PCSA		
	Exponent	Constant	r^2	Exponent	Constant	r^2	Exponent	Constant	r^2
rectus femoris	0.11 ± 0.27	1.85 ± 0.45	0.02	**-0.15 ± 0.60***	2.15 ± 0.10	0.43	0.26 ± 0.29	0.65 ± 0.47	0.09
vastus lateralis	0.18 ± 0.28	2.20 ± 0.45	0.05	**-0.30 ± 0.09***	2.46 ± 0.14	0.59	**0.50 ± 0.27#**	0.65 ± 0.44	0.30
vastus intermedius	0.03 ± 0.23	2.29 ± 0.37	< 0.01	**-0.16 ± 0.10#**	2.23 ± 0.16	0.26	0.19 ± 0.28	1.02 ± 0.46	0.05
vastus medialis	< 0.01 ± 0.24	2.33 ± 0.39	< 0.01	**-0.30 ± 0.15#**	2.48 ± 0.25	0.33	0.25 ± 0.32	0.82 ± 0.53	0.07
biceps femoris (LH)	0.15 ± 0.29	1.76 + 0.40	0.03	0.05 ± 0.07	1.94 ± 0.10	0.07	0.10 ± 0.29	0.79 ± 0.40	0.02
biceps femoris (SH)	0.17 ± 0.18	1.53 ± 0.26	0.09	0.04 ± 0.13	1.95 ± 0.18	0.01	0.14 ± 0.19	0.54 ± 0.27	0.06
semitendinosus	0.02 ± 0.23	1.95 ± 0.38	< 0.01	0.11 ± 0.22	1.93 ± 0.36	0.03	-0.08 ± 0.39	0.95 ± 0.65	< 0.01
semimembranosus	-0.16 ± 0.18	2.30 ± 0.27	0.09	-0.31 ± 0.27	2.22 ± 0.41	0.14	0.18 ± 0.27	1.01 ± 0.41	0.05

***(P < 0.05); # (P < 0.1)**

MODEL FOR OCCUPANTS EJECTED FROM VEHICLES WITH ROLL AND YAW

Chad B. Hovey, Matthew L. Kaplan, and Robert L. Piziali

Piziali & Associates Inc., San Carlos, CA, USA
E-mail: hoveyc@piziali.com, Web: www.piziali.com

INTRODUCTION

In the fields of accident reconstruction and injury biomechanics, it is often of interest to know details of an occupant's ejection from a vehicle during a rollover. Determining the trajectory of an occupant, both in the air and on the ground, assists in the understanding of injury mechanisms.

The ejection event consists of three general phases: (1) occupant in the vehicle, (2) occupant in the air, and (3) occupant on the ground. During phase (1), the occupant is moving in a vehicle that is rolling over. The vehicle has translational and angular velocity, and may be yawing. In phase (2), the occupant has been ejected from the vehicle. The occupant is thrown from the vehicle with a trajectory that is dependent on the dynamics of both the vehicle and the occupant at time of ejection. Gravity causes the occupant to fall, and the occupant impacts the ground. In phase (3), the occupant may bounce and slide, the degree of which depends on the impact dynamics, to the point-of-rest (POR).

METHODS

We model the vehicle as a cylinder moving in the ground plane. There are two translational degrees of freedom: longitudinal—in the direction of the vehicle's heading at roll inception, and lateral—perpendicular to the vehicle's initial heading. There are two rotational degrees of freedom: roll and yaw. The dynamics of the vehicle are governed by a drag factor, which allows the translational time history to be determined. The roll and yaw rates are obtained from the time values at discrete roll and yaw positions. We interpolate functions of all vehicle degrees of freedom to describe the vehicle's motion during the rollover event.

We model the occupant as a point mass ejected from the vehicle at any time except for when the occupant's ejection portal is blocked by the ground. For each admissible ejection time, we construct an occupant trajectory based on the dynamics of the vehicle moving in the inertial frame, and the occupant moving within the vehicle. Each trajectory gives rise to a landing point, where the occupant impacts the ground. The occupant may then have continued motion, consisting of bouncing and sliding on the ground, from impact to rest. Each trajectory produces candidate occupant PORs. Candidate PORs that match the actual occupant's POR are considered possible occupant ejection solutions.

RESULTS AND DISCUSSION

We calculate the occupant landing position and occupant rest position for each admissible ejection time, as a function of roll position, as shown in Figures 1 and 2. We superimpose the actual occupant POR, indicated with the red dashed line, in both the longitudinal and lateral directions. Possible ejection solutions exist where candidate PORs intercept actual PORs.

In this case study, we have a four roll event and a leading-side occupant ejection. We find seven ejection candidates from the longitudinal solutions. We rule out two of

these candidates since their lateral solutions do not satisfy the actual occupants POR, leaving five possible occupant ejection solutions.

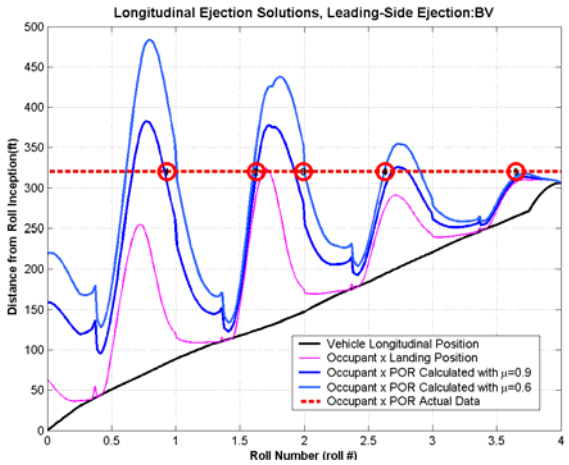

Figure 1: Longitudinal direction solutions.

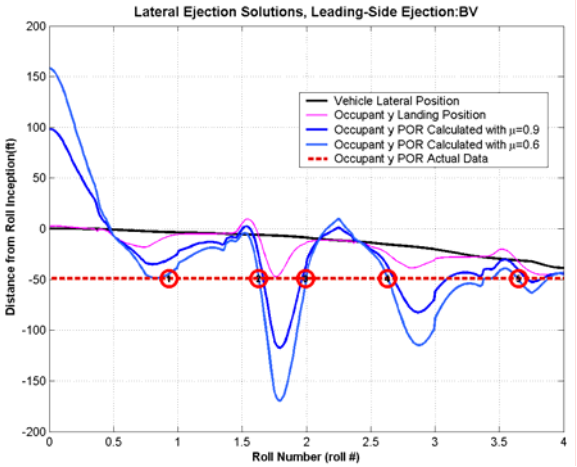

Figure 2: Lateral direction solutions.

Table 1 shows numeric values for vehicle and occupant positions and speeds for each of the ejection solutions. The occupant launch speed, launch angle, and maximum height indicate if the occupant is thrown up in the air, through a high arc; or, if the occupant is thrown horizontally or downward from the vehicle. The occupant's vertical landing speed is used to quantify the severity of occupant's impact with the ground. The slide distance is used to determine if the occupant slid for a significant distance after ground impact, or if the occupant came to rest at or near the point of impact. The occupant's injuries can be correlated with the vertical impact speed and slide distance help to identify likely ejection points from the possible ejection solutions.

Table 1: Vehicle and occupant positions and speeds for each ejection solution.

Ejection Solutions Results, Leading Side Occupant:BV

Solution (#)	$\Theta^{vehicle}_{launch}$ (roll #)	$\Theta^{vehicle}_{launch}$ (deg)	$s^{vehicle}_{launch}$ (ft)	$(v.s)^{vehicle}_{launch}$ (mph)	$\rho^{ejectee}_{launch}$ (deg)	$\|v\|^{ejectee}_{launch}$ (mph)	$(v.z)^{ejectee}_{land}$ (mph)	$z^{ejectee}_{max}$ (ft)	$\Delta s^{ejectee}_{air}$ (ft)	$\Delta s^{ejectee}_{slide}$ (ft)
1	0.93	334.8	83.5	58.2	-3.48	76.4	-15.2	7	53.9	223
2	1.63	586	124	52.7	29	53.5	-28.3	26.8	170	53.8
3	1.99	717	147	49.3	-9.94	64.8	-17.5	6.09	27.1	145
4	2.63	947	195	41.4	21.5	40.8	-18.8	11.9	85.8	40.4
5	3.65	1314	268	25.1	23.5	26.8	-16.1	8.66	44	14

SUMMARY/CONCLUSIONS

We created a model of occupant ejection that incorporates vehicle roll and yaw. Candidate solutions, calculated from the model, and actual occupant PORs, obtained from physical evidence, give rise to possible solutions. Possible solutions, correlated with occupant injury, indicate likely points of occupant ejection. Knowing when and how an occupant is ejected is useful for explaining an occupant's injury mechanism.

REFERENCES

Parenteau, C., *et al.* (2001). *SAE 2001-01-0176.*

Searle, J.A. (1993). *SAE 930659.*

Searle, J.A., Searle, A. (1983). *SAE 831622.*

Wood, D.P. (1991). *SAE 910814.*

ACKNOWLEDGEMENTS

We thank Piziali & Associates Inc. for funding this work.

AN ELUSIVE TALUS: RE-THINKING THE ANKLE COMPLEX

Kevin A. Ball[1] and Thomas M. Greiner[2]

[1] University of Hartford, West Hartford, CT, USA
[2] University of Wisconsin – La Crosse, La Crosse, WI, USA
E-mail:keball@hartford.edu

INTRODUCTION

The classic investigations of Inman and colleagues focused attention upon the subtalar joint and its interplay within the ankle complex (Inman, 1976). In 1988, Siegler and colleagues reported on the joints' interactions. Today, despite decades of technical advances, identification of the individual functional contributions within this joint complex remains a challenge. Motion of the talus is not easily measured *in vivo*, thus motion of the rearfoot (calcaneus) is typically measured with respect to the leg (tibia). Sets of "tri-planar" motion patterns are produced where the talocrural joint is often considered to produce the sagittal effects, while the subtalar is assumed to be jointly responsible for transverse and coronal plane motions. Yet, Inman's mitered hinge model does not suggest bi-planar subtalar motion. Instead, the model describes movement about a single, obliquely oriented, axis. Is Inman's mitered hinge model of the subtalar joint appropriate? Should the ankle complex be reported as tri-planar? Surprisingly, we found both perspectives have merit, but perhaps for the wrong reasons.

METHODS

Joint integrity was maintained in the preparation of 18 cadaveric specimens (leg, ankle and foot). Ligaments and joint capsules were left intact, while all other soft tissues were removed. A rigid cluster of 4 markers attached to a threaded rod was inserted into each tibia, talus and calcaneus. An OptoTRAK 3D active marker camera system (Northern Digital, Waterloo, ON) recorded marker motion (30Hz). Each leg was tested in upright stance. The internal bones of the foot and ankle moved freely as three driving actions were used to manually manipulate the leg: Plantar/Dorsiflexion (PD), Inversion/Eversion (IE), and Medial/Lateral rotation (ML). All 3D movement data were processed using rigid-segment pose algorithms. The results were reprocessed using the Functional Alignment algorithm (Ball *et al.*, 2004) to identify mean best-fit axes of rotation for each bone-to-bone combination with respect to each applied driving action. Analyses focused on reporting joint axis orientation of three joint combinations: (1) Talus to Calcaneus – to evaluate subtalar joint motion; (2) Tibia to Talus – used as a surrogate of talocrural motion; and (3) Tibia to Calcaneus – used to replicate marker cluster placement as is typically employed for the evaluation of this joint complex in living subjects.

RESULTS AND DISCUSSION

Table 1 presents results for the PD driving action. Table 2 compares the oblique joint axes for the Tibia to Calcaneus "joint" with respect to the Subtalar (Talocalcaneal) joint. For the

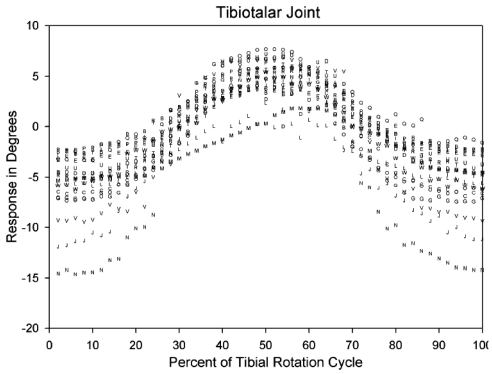

Figure 1. The ML driving action produced transverse plane rotation in the Tibiotalar joint.

ML driving action, figure 1 shows that transverse plane rotation occurred within the Talocrural (Tibiotalar) joint itself.

The results in Table 1 demonstrate that measurement of the rearfoot (calcaneus) yields appropriate estimates of ankle function. In comparison with the Subtalar joint however, the easier to measure Tibia to Calcaneus "joint" was significantly different in joint orientation ($p<0.05$). Considerable transverse plane rotation occurred within the tibiotalar joint; ROM was 14.2º (5.1). This supports a previous hypothesis of Nester et al. (2003).

SUMMARY AND CONCLUSION

When examining "triplanar ankle" data, *in vitro* findings suggest that it is inappropriate to infer that transverse and frontal plane motion patterns are the result of subtalar joint function alone. The subtalar joint does respond as a mitered hinge, yet its orientation is also modifiable. The ankle complex does provide tri-planar action, yet much transverse plane motion is allowed within the talocrural joint itself.

REFERENCES

Ball, K.A., *et al.* (2004) *Proceedings of the ISB 3D*, 77-80.

Inman, V.T. (1976) *The Joints of the Ankle*. Williams & Wilkins.

Nester, C.J. *et al.* (2003). *Foot Ankle Int,* 164-168.

Siegler S. *et al.* (1988) *J Biomech Eng.* 110, 364-373.

Table 1. PD driving action: Statistical comparisons showed no significant differences between the Talocrural joint and the Tibia to Calcaneus "joint" ($p>0.05$).

Joint (n=18)	Joint Axis Orientation		Range of Motion (º)
	Lateral decline (º)	Posterolateral (º)	
Talocrural	4.9 (4.9)	12.5 (4.9)	66.9 (13.3)
Tibia to Calcaneus "joint"	7.1 (4.9)	13.7 (4.0)	70.7 (13.7)

Table 2. Statistical comparisons showed significant differences ($p<0.05$) for the orientations of the axes of the Subtalar (Talocalcaneal) joint and the Tibia to Calcaneus "joint" for both driving actions.

Driving Action	Joint (n=18)	Joint Axis Orientation		Range of Motion (º)
		Elevation (º)	Medial deviation (º)	
IE	Subtalar	38.4 (4.8)	16.3 (7.6)	19.0 (5.2)
	Tibia - Calcaneus	30.0 (7.3)	7.8 (13.6)	22.4 (7.4)
ML	Subtalar	50.2 (6.6)	13.9 (13.4)	12.7 (4.4)
	Tibia - Calcaneus	72.9 (6.6)	-8.8 (7.1)	21.3 (4.7)

EXPRESSING JOINT AXIS ORIENTATION

Kevin A. Ball[1] and Thomas M. Greiner[2]

[1] University of Hartford, West Hartford, CT, USA
[2] University of Wisconsin – La Crosse, La Crosse, WI, USA
E-mail: keball@hartford.edu

INTRODUCTION

As the techniques for measuring human movement improve, researchers will experience an increasing need to express the finer details of human joint performance. While standardization protocols have been developed over the past decade to bring order to the expression of joint rotations (Wu et al. 2005), little attention has been paid to the process of numerically expressing the orientation of individual joint axes of rotation. This may seem somewhat surprising since the "oblique" orientation of human joints is well known (Inman, 1976).

Early efforts measured joint axis of rotation through manual inspection. Each oblique axis is described as a linear projection onto the cardinal planes. Mathematically, each projection can equate to the concept of "rise over run", thus the tangent function is used to compute each angle of orientation. In theory, three cardinal planes exist, thus three planar angles of orientation can be described, but in practice only the angular orientations of two selected cardinal planes are typically reported.

Given the recent popularity of the Cardan angle sequence, current researchers are just as likely to borrow from these calculations. It should be noted, however, that such Cardan angle variants do not correspond directly with values calculated using the cardinal plane method. The Cardan system involves order-dependent body-fixed rotations, while the cardinal plane system is simply plane dependent.

In 1994 Woltring introduced a novel "attitude vector" concept for the purpose of expressing time-series joint rotations. The attitude vector system shares characteristics with the axis/angle expression of joint rotations (i.e. helical axis) yet it also possesses the 3-element convenience of the Cardan angle system. The attitude vector system has no plane dependence, and no order dependence, thus it avoids the possible confusion that surrounds such specifications. The attitude vector approach can be adapted to express joint axis orientation. Here, the three-element attitude vector conveniently reduces to just two nonzero elements, and a zero element that indicates the referent axis. Thus, a measure of (0°,10°,10°) suggests the concept of rotating away from the X-axis, 10° in elevation, and 10° in deviation.

In this presentation we demonstrate the importance of choosing an appropriate method for expressing joint axis orientation. We highlight some unexpected effects associated with increasingly oblique orientations.

METHODS

The experimental procedure starts with a rotation matrix that incorporates a description of the axis of rotation. The rotation matrix is modified in several steps to describe a change in the elevation and deviation of the axis. With each modification the appropriate direction cosines are selected from the rotation matrix and converted into a suitable expression of joint axis orientation using: a cardinal plane system, and Y-Z Cardan angle sequence, a Z-Y Cardan angle sequence, and an attitude vector system. The resulting expressions of the axis orientations represent four different ways of describing the same underlying phenomenon. These expressions are plotted graphically so that patterns and implications can be explored.

RESULTS AND DISCUSSION

Figure 1 shows the differences that exist between the four methods of expressing joint axis of orientation. Note that all four systems agree when just one angle is changed. As axis orientation steps away from the origin, the attitude vector system demonstrates equal step changes. The other three systems change at increasingly different rates and directions. As obliquity increases the two Cardan angle systems produce the most disparate expressions of the same physical phenomena. A tendency to exaggerate the obliquity is the most visible response of the cardinal plane system – at its extreme the two angles converge at 90°.

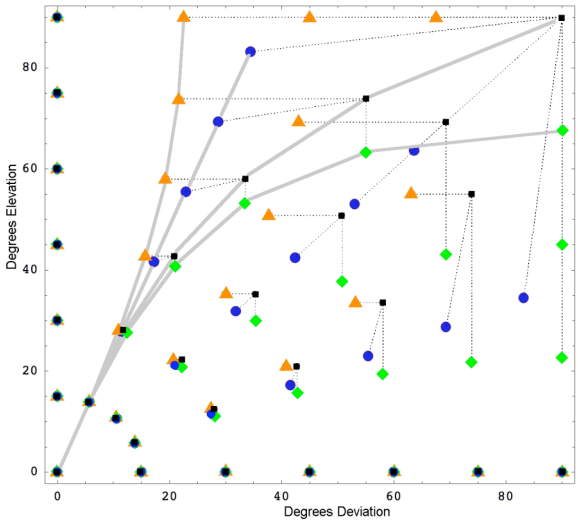

Figure 1. Comparison of joint axis orientations. Blue circles represent attitude vectors results. Black squares represent cardinal plane results. Green diamonds represent Y-Z Cardan sequence results. Orange triangles are results of the Z-Y Cardan sequence. Expressions based upon the same joint axis are joined by a dotted line. The solid gray lines follow one example of changes within each system during equal step progression away from the origin.

SUMMARY AND CONCLUSION

There are a few joints in the lower limb, and many more in the upper limb, that demonstrate widely oblique joint axes. In these cases, selection of the system used to describe joint axis orientation becomes critical. Biomechanists may want to consider the use of a system that can provide methodological transferability among subjects and across all joints in the body.

REFERENCES

Inman, V.T. (1976) *Joints of the Ankle.* Williams & Wilkins.

Woltring, H.J. (1994) *J. Biomech.* **27,** 1399-1414.

Wu,G., et al (2005) *J. Biomech.* **38,** 981-992.

THE EFFECT OF COLLAGEN FIBRES ON PERMEABILITY OF ARTICULAR CARTILAGE

Salvatore Federico and Walter Herzog
Human Performance Laboratory, Faculty of Kinesiology, The University of Calgary
2500 University Drive NW, Calgary, Alberta, T2N1N4, Canada
Email: salvatore@kin.ucalgary.ca, walter@kin.ucalgary.ca

INTRODUCTION

The proteoglycan meshwork is deemed to be the main source of resistance to fluid flow in articular cartilage. Maroudas (1968) showed that the decrease in proteoglycan volumetric fraction from the tidemark (bone-cartilage interface) to the articular surface corresponds to an increase in permeability from tidemark to surface, which is consistent with the well accepted "proteoglycan paradigm". However, Maroudas and Bullough (1968) also found that, in the upper layers of the superficial zone, permeability decreased instead of the expected increase. They ascribed this to the fact that, in the superficial zone, the collagen fibres are parallel to the surface, and have a higher volumetric fraction.

Nevertheless, there are no microstructural models of cartilage permeability in which the effect of the arrangement of the collagen fibres or the inhomogeneity caused by the depth-dependent proteoglycan content, were considered. Based on the perfect analogy between the laws of fluid filtration in porous media (Darcy's law) and the electric induction in dielectric media, we recently proposed a model for the permeability of fibre-reinforced porous materials (Federico and Herzog, 2007), exploiting results for dielectrics reported by Landau and Lifshitz (1960). Here, we use this model to verify whether the collagen fibres cause the anisotropy, and affect the inhomogeneity of articular cartilage permeability.

METHODS

Articular cartilage is considered as a composite comprised of a porous matrix (the proteoglycans), with volumetric fraction ϕ_0 and isotropic intrinsic permeability k_0, a phase of impermeable fibres ($k_1 = 0$), with fraction $\phi_1 = \phi$, and the fluid phase with fraction $\phi_f = 1 - (\phi_0 + \phi)$. A "unit cell" describing the *local* properties of this composite material is comprised of a segment of a fibre, together with its cylindrical neighbourhood, filled with the mixture of matrix and fluid. The volume Ω of the embedding cylinder is such that the ratio between the volume Ω_1 occupied by the fibre and Ω equals the fibre volumetric fraction, ϕ (Fig. 1).

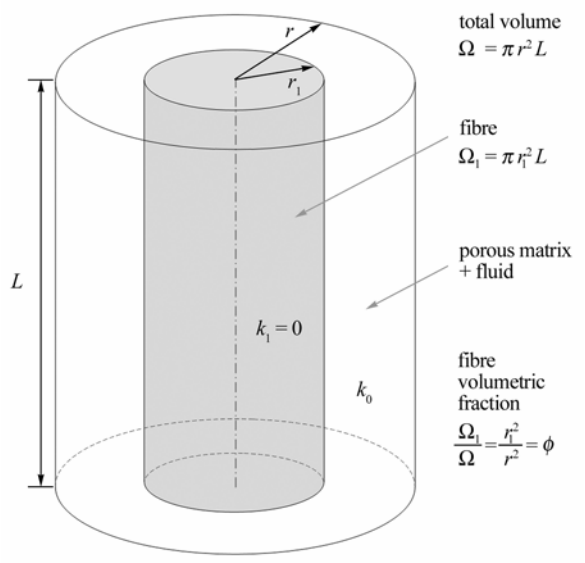

Figure 1: Unit cell, with an impermeable fibre embedded in the porous matrix

According to our model (Federico and Herzog, 2007), the *local* permeability tensor is given by

$$\boldsymbol{k} = \begin{bmatrix} (1-\phi) & 0 & 0 \\ 0 & (1-\phi)^2 & 0 \\ 0 & 0 & (1-\phi)^2 \end{bmatrix} k_0 . \quad (1)$$

The overall permeability, $\boldsymbol{K}$, at a given normalised depth ξ (such that $\xi = 0$ at the tidemark and $\xi = 1$ at the surface) is then obtained through the directional averaging integral

$$\boldsymbol{K}(\xi) = \int_{\mathbb{S}^2} \psi(\boldsymbol{w};\xi)\ \boldsymbol{k}(\boldsymbol{w};\xi)\ dS(\boldsymbol{w}) , \quad (2)$$

where $\mathbb{S}^2 = \{\boldsymbol{w} \in \mathbb{R}^3 : \| \boldsymbol{w} \| = 1\}$ is the set of all directions in space, $\boldsymbol{k}(\boldsymbol{w},\xi)$ is the permeability of the unit cell oriented in the direction $\boldsymbol{w}$, which depends on ξ through the proteoglycan permeability k_0, and $\psi(\boldsymbol{w},\xi)$ is the probability to find, at depth ξ, a unit cell oriented in the direction $\boldsymbol{w}$.

RESULTS AND DISCUSSION

In order to compare our theoretical predictions to the experimental results obtained by Maroudas and Bullough (1968), we assumed a linear increase of the proteoglycan permeability and the collagen volumetric fraction from the tidemark to the articular surface. The probability distribution, ψ, describing the arrangement of the collagen fibres, was constructed from the X-ray diffraction measurements of Mollenhauer et al. (2003) which showed that the fibres were oriented parallel to the surface in the surface zone, randomly oriented in the middle zone, and perpendicular to the tidemark in the deep zone. Our model was able to catch the decrease in permeability in the superficial zone that is associated with the parallel-to-the-surface fibre orientation, and gave good agreement with the experiments by Maroudas and Bullough (1968) (Fig. 2). We demonstrated that the structural arrangement of the collagen fibres plays a crucial role in the depth-dependent permeability of articular cartilage, and causes anisotropy. Unfortunately, there are no experimental data to compare the predicted anisotropy in cartilage permeability, although such experiments seem possible and should be performed in the near future.

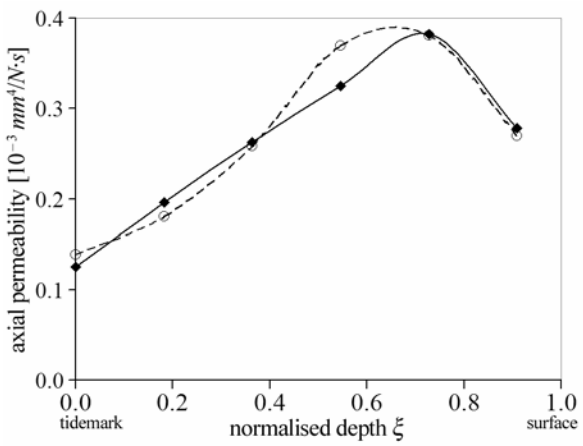

Figure 2: Axial permeability measured by Maroudas and Bullough (1968) (dashed line with open circles) and model predictions (solid line with solid diamonds)

REFERENCES

Federico, S., Herzog, W., 2007. *J. Mech. Phys. Solids*, submitted.

Landau., L.D., Lifshitz., E.M., 1960. *Electrodynamics of Continuous Media*, Pergamon Press.

Maroudas, A., 1968. *Biophys. J.*, **8**, 575-595.

Maroudas, A., Bullough, P., 1968. *Nature*, **219**, 1260-1261.

Mollenahuer, J., et al., 2003. *Conn. Tiss. Res.*, **44**, 201-207.

ACKNOWLEDGEMENTS

The Canada Research Chair Programme, the Canadian Institute of Health Research (CIHR), the Alberta Heritage Foundation for Medical Research (AHFMR, Canada)

FORCE TRANSMISSION FROM SOLEUS MUSCLE IN THE CAT. IS M. SOLEUS AN INDEPENDENT ACTUATOR?

Huub Maas and Thomas G. Sandercock

Northwestern University, Chicago, IL, USA
E-mail: h-maas@northwestern.edu, Web: heckmanlab.physiology.northwestern.edu

INTRODUCTION

It has been shown that muscle fiber force can be transmitted via connective tissues surrounding the muscle and that this is affected by changes in muscle relative position (e.g. Huijing and Baan, 2003; Maas et al., 2004). However, the extent of such myofascial force transmission for normal muscle function *in vivo* is still unclear. Myofascial pathways may also serve to transmit force in conditions of muscle or connective tissue injury. Therefore, the purpose of the present study was to assess the mechanical interactions between the one-joint soleus muscle (SO) and its two-joint synergists in physiological muscle-tendon unit (MTU) lengths and relative positions as well as following tenotomy.

METHODS

Deeply anesthetized cats (n = 7, 2.8-4.6 Kg) were mounted in a rigid frame with the left foot secured to a 6 degree-of-freedom load cell (JR3) coupled to a robotic arm (Staubli). The load cell was used to calculate ankle moments exerted in the sagital plane. The robotic arm was used to impose isolated rotations of the knee joint. The SO nerve bundle was isolated, but all nerves to its synergists and antagonists were cut. Ankle moment at the ankle upon tetanic activation of SO was measured for various knee angles (70-140°), changing the length of the two-joint gastrocnemius (GAS) and plantaris (PL) muscles and hence their passive force and relative position to the SO. Ankle angle and, thus, SO MTU length, was kept constant (~90°).

In addition, ankle moment was assessed after cutting the distal SO tendon (tenotomy), which prevented any myotendinous force transmission to its insertion (the calcaneus). Connective tissues at the muscle belly level were minimally disrupted. Subsequently, the distal tendon of SO was attached to a force transducer. The muscle was lengthened distally from the length it obtained after tenotomy to its physiological length. Both ankle joint moment and tendon force were measured.

RESULTS AND DISCUSSION

SO ankle moment was not significantly affected by changes in knee angle (Fig. 1), despite the fact that this involved substantial changes in length and relative position of GAS and PL muscles. Also half-relaxation time and the maximal rate of relaxation of SO muscle contraction, which varied strongly with ankle angle, were insensitive to changes in knee angle. These results suggest that changing the length of the passive two-joint synergists and, consequently, the position relative to the one-joint SO, does not affect force transmission from SO muscle fibers.

Following tenotomy, SO ankle moment decreased substantially (by ~60%) but did not reach zero (Fig. 2). SO muscle shortened to a much greater extent during contraction than in the intact case, which resulted in a

major position shift relative to its synergists (16.3 mm, SD 0.3). These results indicate force transmission from SO muscle fibers to the achilles tendon and calcaneus, likely through intermuscular connective tissues linking the muscle belly to GAS and PL. The shortening of the SO fibers along the ascending limb of the length-tension curve probably explains the decreased moment.

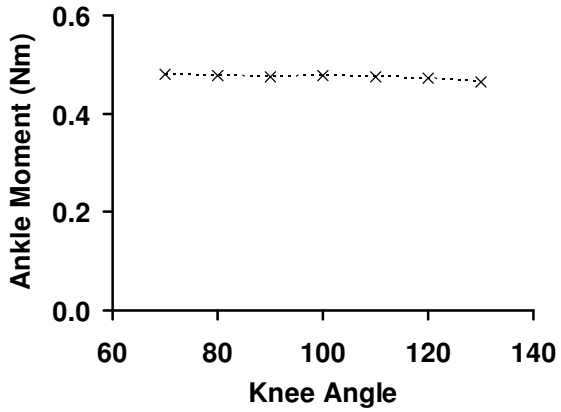

Figure 1: SO Ankle moment plotted as a function of knee angle for one cat.

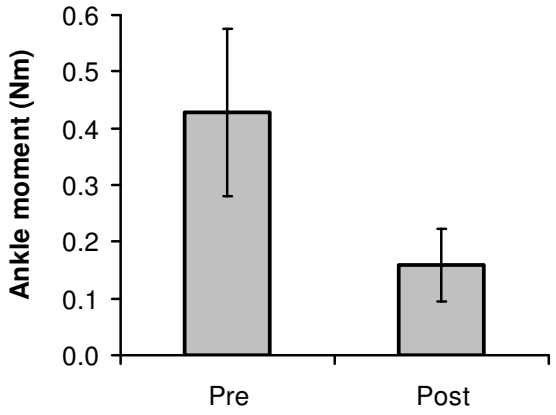

Figure 2: Ankle moment exerted upon activation of SO muscle before and after tenotomy of the distal tendon (n = 3).

Measuring SO ankle joint moment and tendon force at several MTU lengths of SO muscle yielded a clearly linear relationship (Fig. 3). This indicates a partitioning of muscle fiber force between two pathways: (1) via the distal tendon of SO and (2) via the connective tissues linking SO muscle to its synergists. At the physiological length, SO activation did not yield an ankle moment.

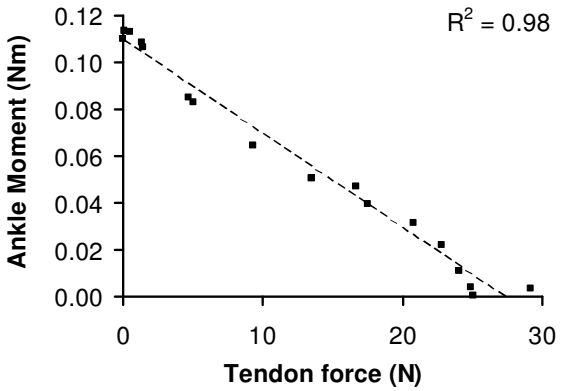

Figure 3: Relationship between force exerted at the SO tendon and ankle moment generated by SO muscle fibers (n = 1).

SUMMARY/CONCLUSIONS

In physiological conditions of the ankle plantar flexors, SO force appears to be predominantly transmitted to bone via its tendons. This suggests that in the intact cat SO muscle acts as an independent actuator.

However, strong mechanical connections between SO and synergistic muscles exist. Such intermuscular connective tissues may bear muscle forces after traumatic events in muscle or tendon.

REFERENCES

Huijing, P.A. and Baan, G.C. (2003). *J Appl Physiol*, **94**, 1092-107.

Maas, H., Baan, G. C. and Huijing, P.A. (2004). *J Biomech*, **37**, 99-110.

ACKNOWLEDGEMENTS

This work was supported by National Institute of Arthritis and Musculoskeletal and Skin Diseases Grant AR-041531

TEST-RETEST RELIABILITY OF SITTING POSTURE IN TYPICALLY DEVELOPING INFANTS.

Anastasia Kyvelidou[1], Wayne Stuberg[2], Regina Harbourne[2], Stacey DeJong[2], Joan Deffeyes[1], Junfeng Sun[3] and Nicholas Stergiou[1]

[1]University of Nebraska at Omaha, Omaha, NE, USA
[2]Munroe-Meyer Institute, University of Nebraska Medical Center, Omaha, NE, USA
[3]Preventive and Societal Medicine, University of Nebraska Medical Center, Omaha, NE, USA
Email: akyvelidou@mail.unomaha.edu, Web: http://biomech.unomaha.edu

INTRODUCTION

The study of the center of pressure (COP) in standing has led to specific therapy programs to improve standing postural control. Clinical rehabilitation programs use force plate technology and the COP for both assessment and treatment of balance disorders. Research has revealed the benefits of these programs. However, the use of this technology has been limited to adults and older children who can achieve the standing position (Cherng *et al.* 1999). Researchers have not yet shown its usefulness for the infant population or for postural control in the sitting position. Furthermore, COP data have recently been analyzed with nonlinear measures which have provided additional insights into behavioral strategies during posture (Newell *et al.* 1993) However, the reliability of this methodology for evaluating COP time series during sitting posture in infants has not been investigated. Therefore, the purpose of our study was to determine the reliability of linear and nonlinear tools, including intra-session and inter-session reliability, for the sitting posture in typically developing infants.

METHODS

Ten typically developing (TD) infants participated in the study. All TD infants scored above –0.5 SD on the Peabody Developmental Scales. Infants were recruited when they were just developing the ability to sit upright. Each came to the lab twice per month for four months. The first three acceptable trials at each session were used to determine intra-session reliability. The TD infants returned for a repeat testing within one week of each month's testing for the inter-session reliability portion of the study. Each trial consisted of recording COP data at 240 Hz for 8.3 sec of unsupported sitting on an AMTI force plate (Advanced Mechanical Technology Inc. Newton, Massachusetts, Model OR6-7-1000). The COP data were analyzed using two common linear and two nonlinear parameters. Linear tools consisted of Root Mean Square (RMS) and Range for both the anteriorposterior and the mediolateral direction. Nonlinear parameters consisted of the Approximate Entropy (ApEn) and the Lyapunov Exponent (LyE) for both directions. Intra-session and inter-session reliability was quantified by the Intraclass Correlation Coefficient (ICC). Specifically, a one way ANOVA model with a random subject effect was used to estimate the intra-session reliability based on data from the first visit for each child. A two way ANOVA model with a random subject effect and a random session effect was used to estimate the inter-session reliability based on the average measurement during each session. Based on Rosner (2000), an ICC of less than 0.4 indicates poor reproducibility while an ICC between 0.4 and 0.75 indicates fair to good reproducibility. Lastly, an ICC over 0.75 indicates excellent reproducibility.

RESULTS

Inter-session ICC's for all parameters were between 0.37 to 0.56. ApEn presented similar ICC's with range and RMS in both directions, which is a fair to good reproducibility. However, LyE presented poor reproducibility (Table 1).

Nonlinear Variables	***ICC's***	***Linear Variables***	***ICC's***
ApEn x	0.50	Range x	0.52
ApEn y	0.56	Range y	0.40
LyE x	0.37	RMS x	0.51
LyE y	0.40	RMS y	0.37

Table 1. Inter-session correlation coefficients.

Intra-session ICC's for all parameters were between 0.26 to 0.66 (Table 2). ApEn presented the higher ICC's falling in the fair to good category. Both linear parameters presented fair to good reproducibility, however lower than ApEn. Lastly, LyE presented poor reproducibility.

Nonlinear Variables	***ICC's***	***Linear Variables***	***ICC's***
ApEn x	0.58	Range x	0.50
ApEn y	0.66	Range y	0.43
LyE x	0.26	RMS x	0.47
LyE y	0.37	RMS y	0.49

Table 2. Intra-session correlation coefficients.

CONCLUSIONS

Linear parameters showed fair to good reproducibility in both inter- and intra-session analysis. ApEn presented the highest ICC values in both inter- and intra-session analysis, while LyE showed poor reproducibility. Reproducibility of linear parameters during infant sitting task showed similar results to standing in adults (Brouwer *et al.* 1998). In addition, the ICCs of linear parameters during infant sitting were similar to those of children without disabilities during standing balance tasks (Liao *et al.* 2001). However, regarding nonlinear parameters, no comparison can be made, since the reliability of nonlinear analysis of COP time series has not yet been explored. We need to state here, that these are preliminary data of an ongoing project. The limited number of subjects may have influenced the results. However, even with this limitation taken into account, ApEn, which is a measure that can quantify the regularity of posture over time, was able to show higher reproducibility within and between session of infant sitting posture in comparison to other linear and nonlinear parameters.

REFERENCES

Brouwer B. *et al.* (1998). Scandinavian Journal of Rehabilitation Medicine, **30**:131-137.

Cherng R.J. et al. (1999). American Journal of Physical Medicine and Rehabilitation, **78**:336-343.

Liao H. et al. (2001). Developmental Medicine and Child Neurology **43**: 180-186.

Newell K.M. et al. (1993). Gait & Posture, **1**:225-230.

Rosner B. (2000). *Fundamentals of Biostatistics.*5th Edition.

ACKNOWLEDGMENTS

This work was supported by NIH (K25HD047194) and NIDRR (H133G040118), and the Nebraska Research Initiative.

EFFECT OF THE LATERAL WEDGED INSOLES ON THE JOINT LOAD OF KNEE AND ANKLE IN PATIENTS WITH MEDIAL KNEE OSTEOARTHRITIS

Kuroyanagi Y, Nagura T, Matsumoto H, Otani T, Suda Y, and Toyama Y
Department of Orthopedic Surgery, Keio University, Tokyo, Japan
E-mail: yuji-kuro@nifty.com

INTRODUCTION

Knee osteoarthritis (OA), which occurs symptomatically in approximately 11% of 65 years of age and older, account for more mobility disability in the elderly than other disease. Although surgical treatment such as high tibial osteotomy and total knee replacement have been providing successful results for knee osteoarthritis, there is a need to improve conservative treatment as cost-effective and non-invasive care for the patients.

A lateral wedged insole is widely used as conservative treatment for patients with medial knee OA. Several studies have reported clinical and biomechanical effect of the insole. Toda [1] reported that the lateral wedged insoles with elastic strapping of the subtalar and ankle joint changed femorotobial angles (FTA) and talar tilt angles in medial knee OA patients. They showed that the strapping insole had clinically better effects than conventionally used lateral wedged insole. Our previous study revealed that the knee joint load in medial compartment was reduced with use of ankle strapping insoles in patients with moderate knee OA [2]. However, it was not clear whether the insole have any adverse effects on the ankle.

The purpose of this study was to quantify the changes in knee and ankle joint loads during gait with use of two types of lateral wedged insole in medial knee OA patients. We hypothesized that the strapping insole changes the dynamic loads in the knee as well as the load in the ankle joint.

METHODS

Twenty-eight OA knees in 17 patients (16 women, 1 man) were involved in this study. The patients were 67 to 81 (mean 73) years old and had radiographic OA of at least grade 2 severity according to the Kellegren-Lawrence scale. Before the examination, Institutional Review Board for this study and informed consent were obtained for all subjects. The patients were tested at gait laboratory, using a four camera system (Pro-reflex, Qualysis) and a force plate (AM6110, Bertec) with a sample frequency of 120Hz and with 6 retro- reflective markers on the limb [3]. Knee mechanics was calculated using an inverse dynamics approach. The patients performed level walking at their comfortable walking speed. They were tested barefoot (without insoles), wearing lateral wedged insoles (conventional insole) and wearing lateral wedged insoles with strapping (strapping insole) on both sides. The order of testing of each condition was randomized. A silicon rubber of 10mm lateral wedge was used for two types of insoles. The peak knee adduction moment in stance phase and walking speed were evaluated by Wilcoxon signed-ranks test. Statistical significance level was set at $p<0.05$.

RESULTS AND DISCUSSION

Peak knee varus moment (knee adduction moment) during walking without insole, with the conventional insole and with the strapping insole were 4.5±2.0, 4.3±1.9, 4.1±1.7 (%BW*Ht) respectively and they were statistically different (Figure 1). The reductions in the peak knee adduction moment were larger with the strapping insole compared to the conventional insole. The strapping insole reduced the peak knee varus moment by 7.9% compared to bare foot, and the conventional insole reduced the moment by 4.4% compared to bare foot. On the other hand, peak ankle varus moment during walking without insole,

with the conventional insole and with the strapping insole were 1.8±1.1, 1.8±1.2, 1.8±1.0 (%BW*Ht), respectively. There were no statistically differences among the three conditions (Figure 2).

There were no statistically differences in walking velocity and cadence among the three conditions (Table 1).

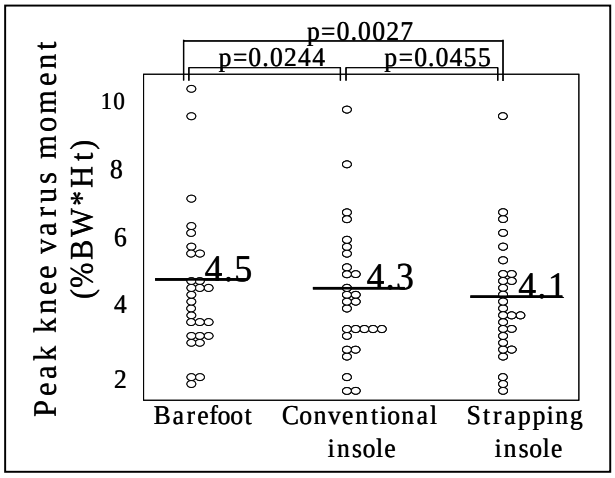

Figure 1 Peak knee varus moment during gait.

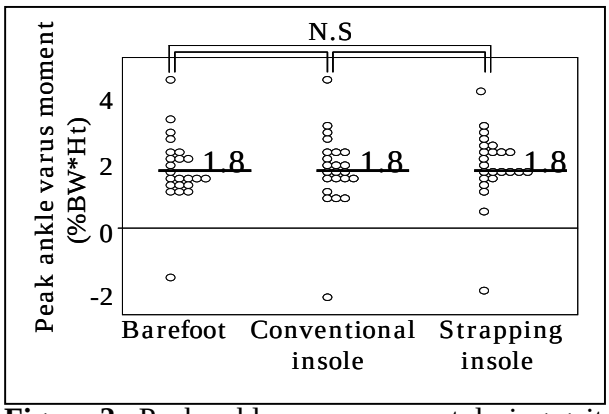

Figure 2 Peak ankle varus moment during gait.

Table 1 Walking speed and cadence with each condition (mean±SD).

	Barefoot	Conventional insole	Strapping insole
velocity (m/s)	0.68±0.21	0.71±0.22	0.69±0.22
cadence (stride/min)	104±13	107±12	108±15

The results supported our hypothesis that both insoles changed the dynamic loads at the knee, but did not change the loads at the ankle.

Valgus in talocalcaneal angle would be induced by both lateral wedged insoles. The varus deformity of the knee should not be changed by conventional lateral wedged insole, because valgus inclination of the calcaneus occurs in the subtalar joint, and it should cancel the effect of the lateral wedge. Since the elastic strap would fix the subtalar and ankle joint, the strapping insole should cause valgus inclination of the talus and tibia, and result in correction of varus alignment of the limb in patients with knee OA. As the varus deformity was corrected by strapping insoles and mechanical axis shifts laterally, they may effect to reduce the load in medial compartment of the knee.

Toda el at reported that the FTA was corrected when wearing strapping insole in patients with knee OA [2]. However, the influences on the ankle joints during gait wearing strapping insoles were not examined. Although our analysis was limited on the coronal plane moment, there was no change in the dynamic load in the ankle with use of the strapping insole. Therefore, it is recommended to use this type of insole as an effective and primary treatment for medial knee OA.

SUMMARY/CONCLUSION

Strapping insoles had greater effect to reduce the joint load at the knee and had little influence to the load at the ankle joint. The strapping insole can be used as an effective conservative treatment for the medial knee OA patients.

REFERENCES

[1]Toda, Y. et al. (2001).
J Rheumatol, **28**: 2705-10.
[2] Kuroyanagi et al. (2007).
Osteoarthritis Catilage, (in press)
[3] Nagura, T. et al. (2002).
J Orthop Res, **20**: 881-881.

A MECHANISM TO REDUCE THE KNEE ADDUCTION MOMENT DURING WALKING

Jennifer Erhart [1,2], Anne Mündermann [1,2], Lars Mündermann[1], and Thomas P. Andriacchi [1,2,3]

[1] Department of Mechanical Engineering, Stanford University, Stanford, CA, USA
[2] Bone and Joint Center, Palo Alto VA, Palo Alto, CA, USA
[3] Department of Orthopedic Surgery, Stanford University, Stanford, CA, USA
E-mail: jerhart@stanford.edu Web: www.stanford.edu/group/biomotion

INTRODUCTION

A high maximum adduction moment at the knee during walking has been associated with an increased rate of progression (Miyazaki et al. 2002) and worse treatment outcome (Andriacchi 1994) of medial compartment osteoarthritis (OA) of the knee. Laterally-wedged inserts and shoes have been shown to reduce the knee adduction moment in healthy and osteoarthritic populations (Krenshaw et al. 2000, Kerrigan et al. 2002, Fisher et al. 2007). However, the mechanism of the effectiveness of such interventions is not well understood, since it is possible that the change in adduction moment could be affected by a change in foot contact patterns or alternatively, medio-lateral trunk sway has been shown to effectively reduce the knee adduction moment during walking (Mündermann et al. 2006). Thus it remains unclear whether the reduced adduction moment produced by a lateral wedge is influenced more by foot alignment changes or upper body movements.

The overall goal of this study was to gain a better understanding of the mechanism of reduction in the knee adduction moment. The following alternative hypotheses were proposed: (1) the change in knee adduction moment will be correlated with a change in pressure distribution of the foot, and (2) the change in knee adduction moment will be correlated with a change in hip adduction moment.

METHODS

Fifteen physically active subjects (6 male, 9 female; age: 31.9 ± 5.9 yrs; height: 1.74 ± 0.10 m; mass: 70.7 ± 15.9 kg) without pain or previous injury in their lower extremity participated in this study after giving written consent in accordance with the Institutional Review Board. Subjects performed 3 walking trials at a self-selected normal speed in each of 3 shoes with identical uppers: 0° lateral wedge (control); 4° lateral wedge; and 8° lateral wedge. Kinematic and kinetic data were collected using an 8-camera optoelectronic motion capture system (Qualisys) and reflective markers. External inter-segmental forces and moments were calculated for the lower limb using previously described methods (Andriacchi et al. 2004). Pressure distribution data were collected synchronously using a pressure mat placed on the force plate level with the walkway. The pressure region was divided into four zones, medial and lateral heel and forefoot, respectively. The first peak knee adduction moment and peak hip adduction moment were calculated for each trial. The ratio between the medial and lateral maximum pressure values was calculated for the heel region. Average values for each shoe and subject were calculated. Differences in heel pressure ratio, peak knee adduction moment, and peak hip adduction moment for the 4^o and 8^o laterally-wedged shoes versus the 0^o control shoe were detected using repeated measures analysis of variance (ANOVA) (α=0.05). Upon

significant result of the ANOVA, Bonferroni adjusted t-tests were used for post hoc analyses. Linear regression analyses were used to determine correlations between changes in knee adduction moment with the 4^o and 8^o laterally-wedged shoes versus control and (1) heel pressure ratio and (2) hip adduction moment.

RESULTS AND DISCUSSION

The results of this study did not support the first hypothesis, since no correlation was found between knee adduction moment and heel pressure ratio. However, the second hypothesis was supported by the finding that the changes in knee adduction moment with the 4^o and 8^o laterally-wedged shoes versus control were significantly correlated with changes in hip adduction moment (Figure 1) ($R^2 = 0.57$; $p<0.01$ and $R^2=0.45$; $p<0.01$, respectively).

Interestingly, the heel pressure ratio was significantly increased with the 4^o and 8^o laterally-wedged shoes versus control ($p<0.01$), with average increases of 16.8% and 26.3%, respectively. However the magnitude of the pressure change did not predict the magnitude of the knee adduction moment change.

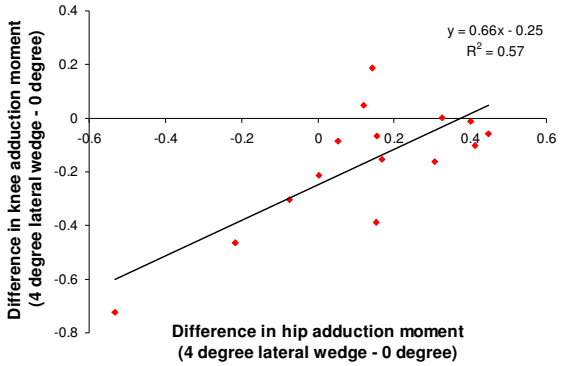

Figure 1: Difference in knee adduction moment vs. hip adduction moment with the 4^o lateral wedge vs. control. Similar results were seen with the 8^o lateral wedge.

SUMMARY/CONCLUSIONS

These results suggest that although the foot placement is changed with a load-altering intervention, the reduction in knee adduction moment may actually be caused by a change in upper body motion, as evidenced by a change in hip adduction moment. Thus, the mechanism of reduction in the knee adduction moment by laterally-wedged footwear interventions may be greatly influenced by upper body movement induced by a change of placement of the foot.

As expected, the laterally-wedged interventions successfully reduced the knee adduction moment during walking. However, the primary mechanism of the change appears to be related to dynamically changing upper body movement as reflected by changes in the hip adduction moment, rather than changing the static alignment of the limb caused by the lateral wedge. Thus the intervention appears to create a stimulus that produces overall changes in the pattern of locomotion. These results suggest that interventions directed towards stimulating changes in patterns of locomotion can be more effective than static interventions such as a lateral wedge.

REFERENCES

Andriacchi TP et al. (1994) *Orthop Clin North Am* **14**, 289-295.

Andriacchi TP et al. In *Basic Orthopaedic Biomechanics*, 3rd ed., 91-121, 2004.

Crenshaw SJ et al. (2000) *Clin Orthop* **375**, 185-192.

Fisher DS et al. (2007) *J Orthop Res* **25(4)**, 540-546.

Kerrigan DC et al. (2002) *Arch Phys Med Rehabil* **83**, 889-893.

Miyazaki T et al. (2002) *Ann Rheum Dis* **61**, 617-622.

Mündermann L et al. (2006) *Trans Orthop Res Soc* **52**, 170.

ACKNOWLEDGEMENTS

RSscan (pressure mat); VA A02-2577R.

PROCRUSTES ANALYSIS APPLIED TO RELATIVE MOTION PLOTS OF LOCOMOTOR PATTERNS IN SPRINT

Leslie Decker [1,2], Sabine Renous [1], and Françoise Natta [3]

[1] FRE CNRS 26 96, Muséum National d'Histoire Naturelle, Paris, France.
[2] HPER Biomechanics Laboratory, University of Nebraska-Omaha, Omaha, USA.
[3] LMAP, Institut National du Sport et de l'Éducation Physique, Paris, France.
E-mail: ldecker@mail.unomaha.edu, Web: biomech.unomaha.edu

INTRODUCTION

A crucial aspect of motion analysis is the ability to quantify and identify movement strategies for a specific task. This is particularly important in human motion, because more than one movement strategy can be used to accomplish the same objective. While the importance of alternate movement techniques has been acknowledged in certain fields (e.g., motor control, ergonomics), quantitative methods for identifying movement strategies have not been developed. Thus, we sought to quantify a methodology that can clearly show us how two performers could use different combinations of segmental movements while producing identical gait features (speed, frequency and amplitude). To accomplish this task, we proposed to use geometric morphometry algorithms (e.g. Procrustes method; Bookstein, 1991) which allow to describe curve shape and shape changes in a mathematical and statistical framework, regardless of time and size factors. We applied the Procrustes method to the shape of gait patterns by using relative motion plots (i.e. fifth metatarsal head trajectory relative to hip trajectory). We utilized the 100-meter event and we compared the motor behaviors adopted by runners with different levels of expertise in order to identify the characteristics of motor performance in high level sprinting. We hypothesized that the difference between novices versus experts would not rely exclusively on the optimization of physical ability. In other words, there will be no continuity, but different levels of organization between these two populations.

METHODS

Fifty-five male sprinters with 12 highly advanced (international level), 19 advanced (national level), 13 intermediate (regional level) and 10 novice athletes participated in the study. They all performed two 80-meter sprints at maximal effort. The three-dimensional kinematics of the lower extremity were collected at 200 Hz along the track between 42- and 54-m marks of a 100-m race using a Vicon™ 612 motion capture system including six high speed cameras (Oxford Metrics, Ltd., Oxford, UK). The 3D coordinate data were smoothed using a zero-lag, fourth-order Butterworth filter. After superimposition of the hip marker positions, the resultant relative trajectory of the fifth metatarsal head was smoothed using a Fast Fourier Transform in order to both reduce errors and eliminate the data disjunction to form a completed cyclogram. Seven gait events were determined by our customized mathematical algorithms. We selected 112 cyclograms from the running sequences and they were superimposed using the Procrustes method (Bookstein, 1991) (Figure 1).

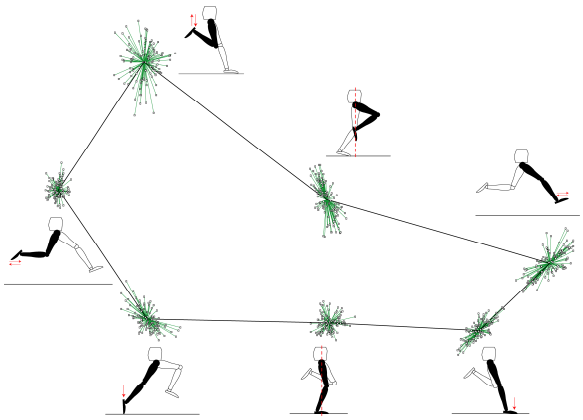

Figure 1. Procrustes superimposition of 112 ankle cyclograms in the sagittal view.

The shape of each cyclogram was defined as "Procrustes residuals", i.e. landmarks deviating from the "consensus" (mean shape) (Rohlf & Slice, 1990). A principal components analysis (PCA) in conjunction with a Hierarchical Ascendant Classification (HAC) was performed on all the Procrustes residuals. A multivariate regression was used in which the dependent variables were the principal component (PC) scores, and the independent variable corresponded to the different sprint expertise-levels. The graphic representations of the cyclograms along the PC are useful to identify atypical patterns. Multivariate regression provides the linear combination (called "vector V") of the most significant PCs to express the changes in conformation associated with expertise (Kraznowski, 1988). A one-way ANOVA with Bonferroni adjustment was performed in order to ensure the statistical validity of the expertise groups.

RESULTS AND DISCUSSION

The analyses (PCA and HAC) revealed the main shape changes of the cyclogram relative to expertise (PC1: novices vs. experts) and the sport speciality (PC2: sprinters vs. athletes non sprinters but "trained" in sports requiring qualities for sprint performance e.g. soccer, rugby). Multivariate regression calculated with the first two PCs was significant: $R^2 = 0.77$; $F = 20.26$; $p < 10^{-6}$. The equation of the V shape vector ($V=0.99\times PC1-0.010\times PC2$) showed that PC1 makes an overwhelming (even almost exclusive) contribution. Although the vector V guarantees the existence of a "continuum" or "gradient" towards expertise ($F= 72.10$, $P<0.001$), it creates a "hurdle to cross" in the progression from the national level to the international level (HSD: $p<0.001$). Moreover, the cyclograms of the sprinters and "trained" athletes are scarcely different regarding the vector V (HSD: $p=0.096$), thus suggesting two distinct "pathways" towards expertise: the first relates to the learning process as an effect of practice and experience; the second is related to the "transfer of the learning" process (e.g., speed skills in soccer transferred in high-speed races).

SUMMARY/CONCLUSIONS

In conclusion, by evaluating the size, shape, and orientation of these relative motion plots, it is possible to examine variation in gait patterns within and among groups. Recourses from morphometry applied in the area of movement analysis provided useful gait indicators to select and correct performances in Track and Field running.

REFERENCES

Bookstein F.L. (1991). *Morphometric tools for landmark data: geometry and biology*. Cambridge University Press.

Kraznowski W.J. (1988). *Principles of multivariate analysis*. Clarendon Press.

Rohlf F.J. & Slice D.E. (1990). *Syst. Zool.*, **39**: 40-59.

ACKNOWLEDGEMENTS

This study was supported by the CNRS (FRE 2696), the Muséum National d'Histoire Naturelle, the Ministère de la Jeunesse, des Sports & de la Vie Associative, and the Fédération Française d'Athlétisme.

BIOMECHANICS OF IMPACT LOADING OF GOAT SKULL (*CAPRA HIRCUS*) USING CT IMAGE BASED FINITE ELEMENT MODELING

Edwin Yoo[1], Ashkan Vaziri[2], and Andrew A. Biewener[1]

[1]Organismic and Evolutionary Biology, Harvard University, Cambridge, MA, USA
[2] School of Engineering and Applied Sciences, Harvard University, Cambridge, MA, USA
E-mail: edwinyoo@oeb.harvard.edu

INTRODUCTION

Intrasexual male combat is a critical determinant of social status and reproductive success within the order bovidae. Horn on horn collisions between male goats (*Capra hircus*) at speeds up to 2.5 m/s can pose a serious risk of brain and spinal cord injuries. Kitchener (1988) modeled these horn collisions in Big Horn rams (*Ovis candaensis*) as concentrated quasi-static forces using curved beam theory and reported peak stress at the base of the horns, ignoring the role of inertia and wave propagation on different components.

Dynamic loading however might suggest otherwise. Jaslow and Biewener (1995) studied *in vitro* strain patterns of a goat skull during drop tests that supported Kitchener's findings. However, their study measured strain at a limited number of sites around the horn base and the skull.

Figure 1: Male goat (*Capra hircus*) skull showing skull. (Keratin sheath removed from left horn).

Horns are composed of an inner bone core covered by an external keratin sheath (Figure 1). Keratin is not as stiff or strong as bone but has differing material properties, most notably, a ten-fold increase in work of fracture compared to bone (Bertram and Gosline 1987). We present a finite element analysis of the dynamic response of this composite structure to impact loading.

METHODS

The 3D finite element model (Figure 2) was constructed using ABAQUS/Explicit (Abaqus, Inc., Providence, RI) based on 2.5mm thick computed tomography (CT) scan images using a method developed by Dumont, Piccirillo, and Grosse (2005). The bone core and keratin sheath were assigned appropriate Young's modulus, density, and yield stress values. The surface interactions between the two parts were modeled as frictionless and infinite friction. The model was composed of 20,500 3D stress hex-

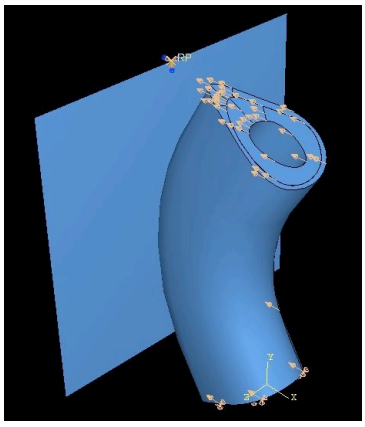

Figure 2: Simplified 3D Model

dominated elements using mid-axis symmetry. The horns were set to impact a rigid wall given an initial horizontal velocity.

RESULTS AND DISCUSSION

Our initial findings disagree with predictions based on Kitchener's (1987) analysis utilizing quasi-static beam theory. Our model shows that maximum stress occurs near the site of the point of impact, a few millimeters below the surface (Figure 3) and not at the base of the horn. In addition, we found that the stress magnitude at the base of support was greater on the cranial (front) surface and than the caudal (rear) surface of the horn bone core (Figure 4).

Finally, there is a 5-fold increase in stress in the keratin sheath impact site compared to the bone horn core. This is a phenomenon that has not been addressed in previous studies. We believe that the role of keratin under dynamic loading needs further attention.

It should be noted that several assumptions were made in the development of this model. We modeled bone as isotropic material although cortical bone is known to be orthotropic. We did not attempt to model adhesion between the keratin and bone, as

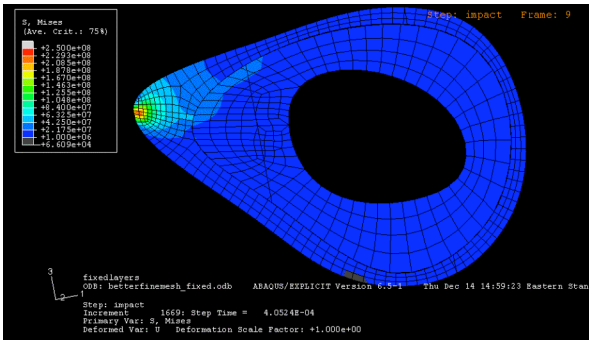

Figure 3: Cross section of horn at the point of contact showing von Mises stress 400 μs after initial contact with the wall.

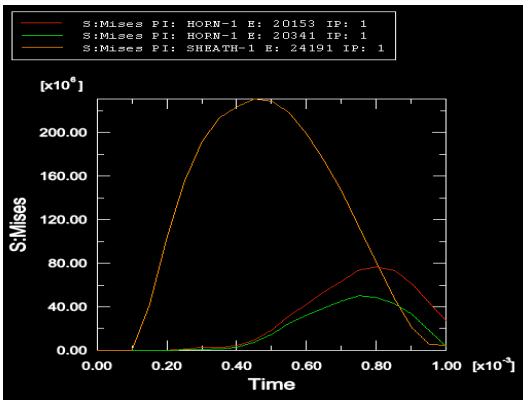

Figure 4: Time varying von Mises stress patterns during impact. Keratin element (orange), cranial bone (red) and caudal bone (green) at the base.

we are unaware of any studies investigating this. In the future, we plan to incorporate materials testing of horn samples to further refine our model.

SUMMARY

We found that maximum stress in the FEM developed here occurs in the keratin sheath at the site of impact. In the base of the bone horncore, the maximum von Mises stresses on the cranial surface exceed the maximum von Mises stresses on the caudal surface.

REFERENCES

Bertram., J.E. and Gosline, J.M. (1987). *J. Exp. Biol.*, **130**, 121-136.

Dumont, E.R., Piccirillo, J., and Grosse, I.R. (2005). *Anat. Rec.,* **283A**, 319-330.

Jaslow CR, and Biewener AA. (1995). *J. Zool,* **235**, 193-210.

Kitchener, A. (1988). *J. Zool*, **214**, 1-20.

Richmond, B.G. et al. (2005). *Anat. Rec.,* **283A**, 259-274.

ACKNOWLEDGEMENTS

Thanks to Shelten Yuen, Harvard U. and Betsy Dumont, UMASS Amherst, for assistance in development of FEM model.

ANTERIOR CRUCIATE RUPTURE DUE TO EXCESSIVE INTERNAL TORQUE OF THE HUMAN TIBIA

Eric G Meyer and Roger C Haut
Michigan State University, East Lansing, MI, USA
E-mail: haut@msu.edu, Web: www.obl.msu.edu

INTRODUCTION

The knee is one of the most frequently injured joints in the human body. Epidemiological studies have shown there are over 80,000 anterior cruciate ligament (ACL) tears in the USA each year, with a total cost of one billion dollars (Griffen, 2000). Many clinical studies have proposed the loading mechanisms that cause injury to the ACL. In one study of 361 ACL patients, 78% were from athletic activities, primarily football and basketball, and approximately 82% of the patients could describe the injury mechanism as internal tibial rotation (Arnold, 1979). Skiing in particular, has one of the highest rates of ACL injuries, accounting for 25-30% of knee injuries (Speer, 1995). These injuries are mainly associated with internal twisting or combined loading during a hard landing (Ettlinger, 1995). In fact, biomechanical studies have shown that internal tibial torque is an important loading mechanism of the ACL (Markolf, 1995), especially when the knee is between full extension and 30º of flexion. The hypothesis of the current study was that the primary injury in an isolated human cadaver knee joint under excessive internal torsion would be isolated ACL rupture. Unlike previous experimental knee torsion studies, the proposed experiments would allow normal unconstrained joint motion of the knee in all the degrees of freedom with the exception of flexion and the applied internal rotation of the tibia.

METHODS

Torsion experiments were conducted on seven cadaver tibiofemoral joints (55.8 ± 5.7 yrs) that were sectioned 15cm proximal and distal to the center of the knee. The femur and tibia shafts were cleaned with 70% alcohol and potted in cylindrical aluminum sleeves with room temperature curing epoxy. The tibia was attached to a rotary hydraulic actuator through a biaxial (torsion-axial) load cell. The femur was placed in a fixture that allowed the joint flexion angle to be set at 30º while the varus/valgus angle was left unconstrained and recorded with a rotary encoder. This fixture was attached to an X/Y translational table that had linear encoders attached to record anterior and posterior as well as medial and lateral motions of the femur relative to the tibia. The X/Y table was in turn attached to a rotation-locked, linear hydraulic actuator and a compressive preload of approximately 1000 N was applied. Repeated, increasing levels of internal torque where applied to each specimen until catastrophic injury of the joint. Additionally a CT scan of each specimen was acquired and the bone mineral density (BMD), in Hounsfield units (Hu), was measured from trabecular bone regions on the medial and lateral tibial plateaus using coronal slices. Statistical t-tests were used to test for significant differences, where $p < 0.05$.

RESULTS AND DISCUSSION

Four of seven knee joints suffered ligamentous damage including a complete or partial ACL rupture at 45.7 ± 14.9 Nm. The remaining three joints suffered avulsion fractures at the ACL insertion into the tibia at a lower peak torque of 26.3 ± 13.9 Nm ($p=0.07$). The BMD was significantly higher in specimens with ligamentous rupture versus avulsion fracture ($p=0.001$). BMD values were 163.5 ± 58.7 Hu versus 61.3 ± 17.9 Hu, respectively. The failure torque and

BMD also showed a slight correlation using linear regression (Figure 1). Torque values from all the tests were used in a logistic regression analysis to predict the 50% likelihood of joint failure (Figure 2). The compressive load, rotation and displacement values were similar between injury types (p values between 0.18-0.37) so the average for all specimens is reported. The average external rotation at joint failure was 66.6 ± 17.3° and the average valgus rotation was 20.3 ± 5.7°. There was 10 ± 4.1 mm of posterior motion of the femur relative to the tibia. The linear actuator moved 7.4 ± 4.9 mm proximally in order to compensate for small drops in the compressive preload.

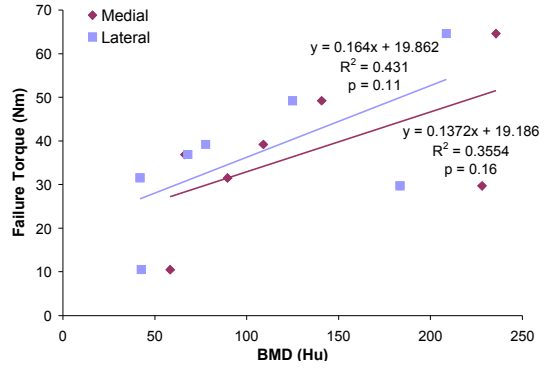

Figure 1.Linear regression.

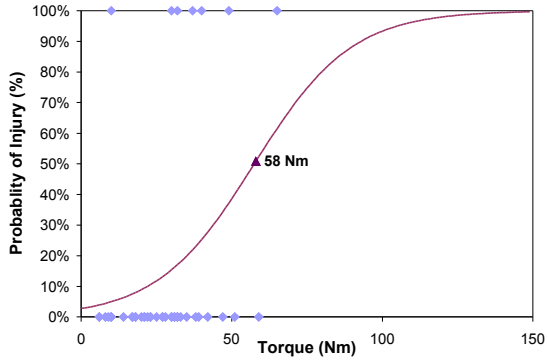

Figure 2. Logistic regression.

SUMMARY/CONCLUSIONS

The current study showed that ACL injuries occurred at torques of approximately 37 Nm applied to the tibia. Our laboratory has previously documented ACL rupture with approximately 5 kN of tibio-femoral compressive loading. Others have also noticed a similar "anterior neutral shift" of the tibia with respect to the femur during weight bearing (Flemming, 2001) that could predispose the ACL towards rupture. A combined loading scenario with higher joint compressive loads than applied in the current study may in fact reduce the peak torque required to cause ACL injury. However, muscle contraction also plays an important role in sports related injuries and male subjects have been shown to voluntarily produce internal tibial torques as high as 99 Nm without injury (Shoemaker, 1988). The tibia is able to withstand approximately 115 Nm before failure while the average torque for ankle injury is approximately 70 Nm (Hirsch and Lewis, 1965). Thus, the knee joint is the weak link in the lower leg for torsion related injuries and this may account for the relatively high rates of ACL injuries in athletes.

REFERENCES

Arnold JA, et al. (1979) *Am J Sports Med.* **7 (6)** 305-313.

Ettlinger CF, et al. (1995) *Am J Sports Med.* **23 (5)**, 531-537.

Flemming BC, et al. (2001) *J Biomech*. **34**, 163-170.

Griffen LY, et al. (2000) *J Am Acad Orthop Surg* **8 (3)**, 141-150.

Markolf KL, et al. (1995) *J Orthop Res*. **13**, 930-935.

Meyer EG and Haut RC. (2005) *J Biomech* **38**, 2311-2316.

Shoemaker SC, et al. (1988) *Clin Orthop Relat Res*. **228**, 164-170.

Speer KP, et al. (1995) *Am J Sports Med*. **24 (5)**, 676-683.

ACKNOWLEDGEMENTS

This study was supported by a grant from the CDC (R49/CE000623).

EFFECTS OF ATTENTION ON DYNAMIC STABILITY OF WALKING

Roland T. Robb [1], Mark D. Grabiner [2], Karen L. Troy [2], and Jonathan B. Dingwell [1]

[1] Nonlinear Biodynamics Lab, Department of Kinesiology, University of Texas, Austin, TX
[2] Department of Movement Sciences, University of Illinois at Chicago, Chicago, IL, USA
E-mail: jdingwell@mail.utexas.edu, Web: www.edb.utexas.edu/faculty/dingwell/

INTRODUCTION

Performing attention-distracting tasks while walking may increase fall risk. Increased step kinematic variability has also been associated with fall risk, suggesting that attention-distracting tasks should increase step variability. However, young healthy subjects exhibited *decreased* step width variability while performing an attention- distracting task and walking (Grabiner, 2005).

The relationship between step width variability and fall risk has not been unambiguously characterized. Measures of kinematic variability are not well correlated with measures of dynamic stability that directly quantify the sensitivity of walking kinematics to small perturbations (Dingwell, 2006). This study determined if performing a concurrent attention-demanding task would affect the dynamic stability of walking.

METHODS

Data analyzed in this study were collected previously (Grabiner, 2005). 15 healthy volunteers (8 M / 7 F, age: 24.5±3.4 yrs) participated. Subjects walked on a motorized treadmill at their self-selected constant speed for 10 minutes while performing an attention-distracting Stroop test (ST) (Stroop, 1935; Grabiner, 2005) and also during undisturbed walking (CO). 3-D motions of a marker attached at the 1st thoracic vertebra were recorded continuously at 60 Hz (Motion Analysis, Santa Rosa, CA, USA). Marker velocities in each direction (V_{AP}, V_{ML}, and V_{VT}) were calculated over 3 equal intervals of 200 sec each and analyzed.

Mean variability (MeanSD) was calculated for each time series as the average standard deviation across all strides (Dingwell, 2006).

Local stability was estimated by calculating the mean local divergence between nearest neighbor trajectories using previously established methods (Dingwell, 2006; Kang, 2006). Time constants, τ_S and τ_L, from double-exponential fits to these curves defined, respectively, the short-term and long-term exponential rates of divergence in response to small naturally-occurring perturbations to the walking kinematics (Kang, 2006).

Orbital stability was quantified by calculating magnitudes of maximum Floquet Multipliers (MaxFM) for the system (Dingwell, 2007) for Poincaré sections defined at 0%, 25%, 50%, 75%, and 100% of the gait cycle. MaxFM quantify how much small initial perturbations from the mean trajectory grow or decay from one cycle to the next.

For each dependent measure, differences between CO and ST walking were evaluated using a 2-factor repeated measures ANOVA. For the local dynamic stability variables (τ_S and τ_L), the data were log transformed first to satisfy linearity and normality constraints.

RESULTS AND DISCUSSION

MeanSD's for upper body movements were significantly smaller during ST walking for all three movement directions (Fig. 1A). Long-term time constants (τ_L; Fig. 1B) were larger (more stable) during ST walking trials

for AP movements, but tended to be slightly smaller (more unstable) for ML movements. Similar (but not statistically significant) trends were observed for short-term time constants (τ_S; not shown).

Max FM values were , on average, slightly larger (more unstable) during the ST trials for AP and VT movements, but tended to be slightly smaller (more stable) for ML movements (Fig. 1C). Most of these differences were not statistically significant.

The Stroop test led to decreased trunk movement variability, consistent with decreased step width variability (Grabiner, 2005). Trunk movements in the AP directions were also locally more stable. However, the Stroop test also led to slightly greater local *in*stability for ML movements and greater orbital *in*stability for VT movements. Thus, the decreased variability associated with the Stroop task did *not* translate to reduced dynamic instability.

These young healthy subjects likely altered their gait patterns to adapt to the imposed task (Grabiner, 2005). It is likely we might observe more pronounced effects in more impaired (e.g., elderly) populations and/or by imposing more complex cognitive tasks.

REFERENCES

Dingwell, J.B. Marin, L.T. (2006). *J. Biomech.*, **39**(3), 444-52.

Dingwell, J.B. et al. (2007). *J. Biomech.*, doi: 10.1016/j.jbiomech.2006.08.006.

Grabiner, M.D. Troy, K.L. (2005). *J. Neuroengin. Rehabil.*, **2**(1), 25.

Kang, H.G. Dingwell, J.B. (2006). *Exp. Brain Res.*, **172**(1), 35-48.

Stroop, J.R., (1935). *Exp. Psychol.*, **18**, 643-661.

ACKNOWLEDGEMENTS

Partially funded by NIA R01AG10557 to MDG, Whitaker Grant #RG-02-0354 to JBD and UT Preemptive Fellowship to RTR.

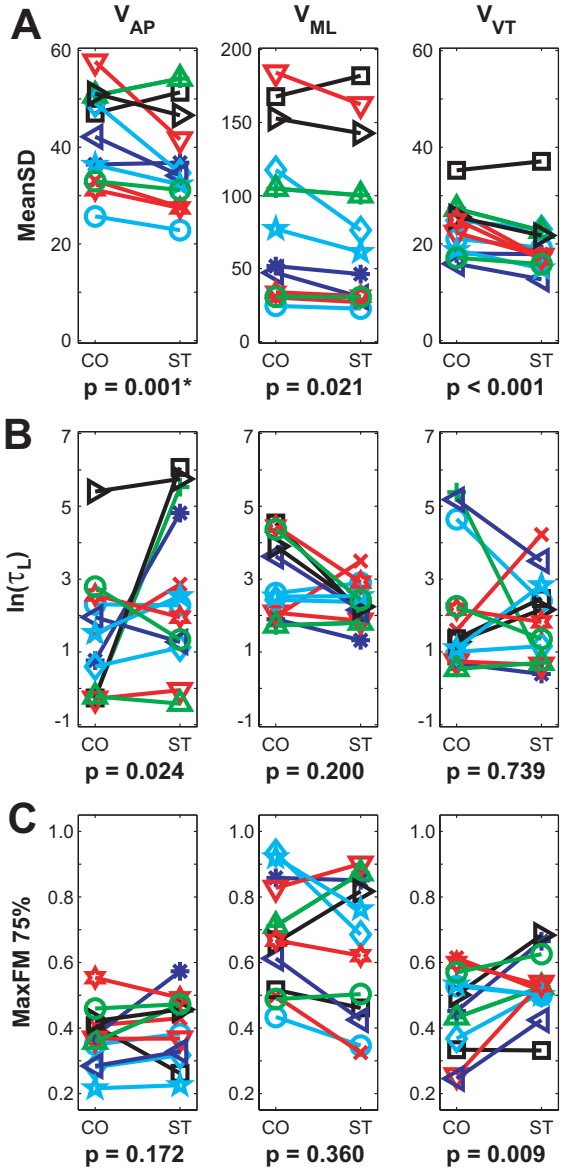

Figure 1: Variability and dynamic stability results. **A:** Kinematic variability (MeanSD), **B:** Long-term local divergence time constants (ln(τ_L)), and **C:** Maximum Floquet Multipliers (MaxFM) for the Poincaré section at 75% of the gait cycle. Asterisk indicates significant Subject × Condition interaction. Subplots in **B** are plotted on a log scale, consistent with statistical analyses.

PATIENT SPECIFIC FINITE ELEMENT MODELING OF LUMBAR VERTEBRAE

Ferris M. Pfeiffer [1,2], Dr. Carol V. Ward [1], Dr. Dennis L. Abernathie [2,3],
Dr. Douglas E. Smith [1], and Dr. Dirk H. Alander[4]

[1] University of Missouri, Columbia, MO, USA
[2] Brenoak Labs LLC, Columbia, MO, USA
[3] Columbia Orthopaedic Group, Columbia, MO, USA
[4] Saint Louis University, St. Louis, MO, USA
E-mail: f.pfeiffer@brenoaklabs.com

INTRODUCTION

The ability to identify the extent of variation in anatomical, and commensurate mechanical, variation among patients stands to make a significant contribution to evaluating individual patient outcomes.

There are often geometric asymmetries in lumbar vertebrae, and there certainly are differences in geometry between the vertebrae of different patients. It is reasonable to expect that these differences will lead to differences in stress within spinal tissues and deflection of spinal components resulting from the same loading condition.

It is the purpose of this work to investigate whether it is feasible to develop Finite Element (FE) models that take into account the geometric differences between the lumbar vertebrae of patients. It is also the purpose of this work to determine whether or not such patient specific differences affect the results of the FE analysis in such a significant way that they should be considered in future patient modeling analysis. Because the spine is a complex system consisting of many tissues, developing an accurate patient-specific FE model is complex. Thus, our initial goal is to evaluate the nature and extent of differences in mechanical response within individual lumbar vertebrae. In this paper, the FE simulated responses of 7 vertebrae are compared under similar loading conditions to biomechanical testing of 7 cadaver specimens.

METHODS

The cadaver specimen tested was a 72 year old African American woman with no known history of back problems or spinal abnormalities. The spinal components of interest are extracted from the cadaver these include T11 to L5 and consist of seven vertebrae.

A CT scan of the specimen was performed using a slice interval of 1mm to ensure maximum resolution of the reconstructed vertebral geometry. A dual energy X-ray absortiometry (DEXA) scan is performed on the specimen to provide a measure of the bone quality. According to DEXA scan results, the specimen is osteopenic which means the bone density is weaker than normal healthy bone.

Each vertebra is loaded to failure using an Instron (Instron, Norwood, MA) model 1122 load frame. The vertebral body is held securely in a vise. The endplates are oriented perpendicular to the direction of the applied load, and the vertebrae are mounted upside down from anatomical position.

Axial force is then applied to the spinous process from the inferior to superior direction. The load is applied at a rate of

1mm/min. The load and deflection of the specimen are recorded, and the load is increased until ultimate failure of the specimen. The location of failure is recorded for later comparison to FEA simulations.

The commercial software package Amira (Mercury Computers, Berlin) is used to reconstruct the 3D geometric data of the cadaver specimens. Each vertebra is segmented into two materials, cortical bone and cancellous bone, each of which is assigned different material properties.

Table 1. Material properties used in cadaver finite element modeling

Material	Young's Modulus MPa	Poisson ratio
Healthy Cortical bone	12000	0.3
Healthy Cancellous bone	100	0.2
Cadaver Cortical bone	900	0.3
Cadaver Cancellous bone	75	0.2

Each vertebra is meshed using between 160000 and 230000 quadratic tetrahedral elements. The material properties used for the finite element simulations of the cadaver specimens are shown in table 1.

Table 1 presents two values for cortical bone and cancellous bone. The first values denoted in table 1 as healthy bone are reported values of healthy bone taken from literature (Goel, Kim, Lim et al. 1986). The second values are calculated from the bone density information acquired from the DEXA scan.

RESULTS AND DISCUSSION

Figure 1 shows the measured stiffness from the cadaver specimens and the predicted stiffness from the finite element simulations for each vertebral level. In figure 1 we see that the stiffness trends between the measured stiffness and the stiffness predicted by the finite element analysis are similar. That is when the measured stiffness is low so is the predicted stiffness.

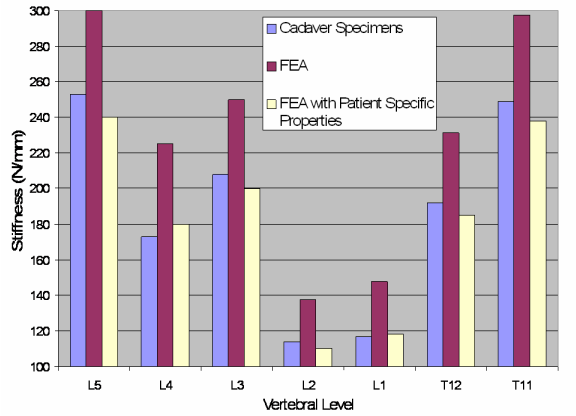

Figure 1. Measured and predicted stiffness for various vertebral levels.

We can also see from figure 1 that the predicted stiffness is higher than the measured stiffness for each vertebral level when normal bone properties are used in the analysis. When patient specific materials are taken into consideration, the stiffness values for the finite element models are reduced slightly and appear to more accurately represent the measured stiffness.

SUMMARY/CONCLUSIONS

The results of this work indicate the response to loading varies between vertebral level. This variation is expected to be due to geometric variation. The results of the patient specific finite element models presented in this work show good correlation to the results of the biomechanical testing for the cadaver specimens tested.

REFERENCES

Goel, V. K., Y. E. Kim, et al. (1986). "An Analytical Investigation of the Mechanics of Spinal Instrumentation." Spine **13**: 1003-1011.

INDEPENDENT EFFECTS OF BODY WEIGHT AND MASS ON THE METABOLIC COST OF RUNNING

Alena M. Grabowski [1], Lennart P.J. Teunissen [2], and Rodger Kram [1]

[1] University of Colorado, Boulder, Colorado, USA
[2] Vrije Universiteit, Amsterdam, The Netherlands.
E-mail: alena.grabowski@colorado.edu
Web: www.colorado.edu/intphys/research/locomotion.html

INTRODUCTION

The metabolic cost of running is substantial, despite savings from elastic energy storage and return. Previous studies suggest that the major determinants of the metabolic cost of running are generating vertical force to support body weight (Kram and Taylor, 1990) and horizontal forces to brake and propel body mass (Chang and Kram, 1999). However, the independent metabolic costs of supporting body weight and braking/propelling body mass have not been previously measured in running.

We hypothesized that supporting body weight would proportionally decrease metabolic power demand (as per Farley and McMahon, 1992), adding mass and weight would proportionally increase metabolic power demand, and adding mass alone would not substantially affect metabolic power demand.

METHODS

10 recreational human runners (6 M, 4 F, mass: 63.3 ± 9.8 kg, mean ± s.d.) volunteered. Subjects performed a standing trial and 10 running trials at 3 m/s on a force-measuring treadmill. Trials were 7 minutes long with 5 minutes rest between trials. Subjects ran normally (100% M & 100% BW; M = mass, BW = body weight), at 3 levels of weight support (100% M & 75, 50, 25% BW), with added mass and weight (110, 120, 130% M & BW), and with added mass alone (110, 120, 130% M at 100% BW).

We measured rates of oxygen consumption and carbon dioxide production during minutes 4-6 of each trial and calculated net (gross – standing) metabolic power (Brockway, 1987). We measured ground reaction forces (GRFs) at 1000 Hz during 10 strides.

We reduced body weight using a harness system (Fig. 1), increased mass and weight using lead worn about the waist, and increased mass alone using a combination of reduced weight and added load as described by Grabowski et al. (2005).

We used repeated measures ANOVA with Tukey HSD follow-up tests when warranted ($P < 0.05$).

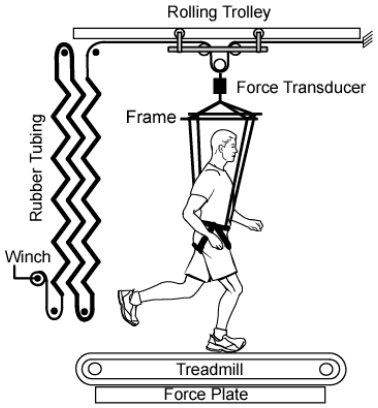

Figure 1. Weight support system

RESULTS AND DISCUSSION

Net metabolic power decreased in less than direct proportion to weight support. When subjects ran at 75% of normal body weight,

net metabolic power decreased by 19 ± 1.7% (mean ± s.e.m.). At 50 and 25% of normal body weight, net metabolic power decreased by 38 ± 2.1% and 55 ± 2.7%, respectively (Fig. 2). By extrapolating the line shown in Fig. 2 ($y = 0.73x + 26.18$; $R^2 = 0.999$) to zero weight, the intercept indicates a 74% reduction in metabolic power suggesting that weight support comprises 74% of the net cost of normal running. This estimate supports the idea that muscular force generation acting in opposition to gravity is the primary determinant of the metabolic cost of running (Kram and Taylor, 1990; Taylor, 1994).

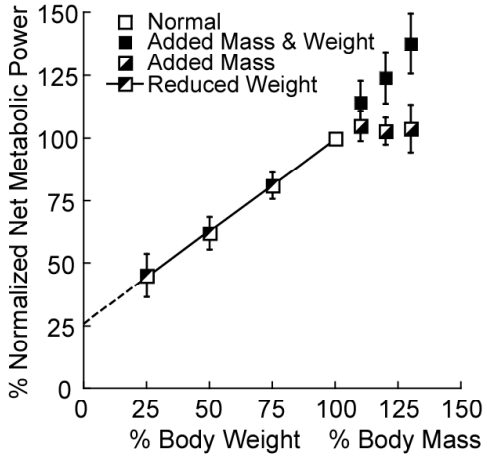

Figure 2. Means (n=10) +/- s.e.m.

Further, our metabolic data closely parallel our force data for running with weight support (Fig. 3). Net metabolic rate shows a substantial linear decrease that is similar to vertical and horizontal impulses.

Net metabolic power increased in slightly more than direct proportion to added load (added mass and weight). When subjects ran at 110% of normal body mass and weight, net metabolic power increased by 14 ± 2.7% of normal running. At 120 and 130% of normal body mass and weight, net metabolic power increased by 24 ± 3.2 and 38 ± 3.8%, respectively (Fig. 2).

Net metabolic power was not substantially different from normal running with added mass alone (Fig. 2). Runners loaded with mass alone did not generate greater vertical or horizontal impulses than normal running. Thus, adding mass alone was not an effective method for determining the cost attributable to braking/propelling body mass.

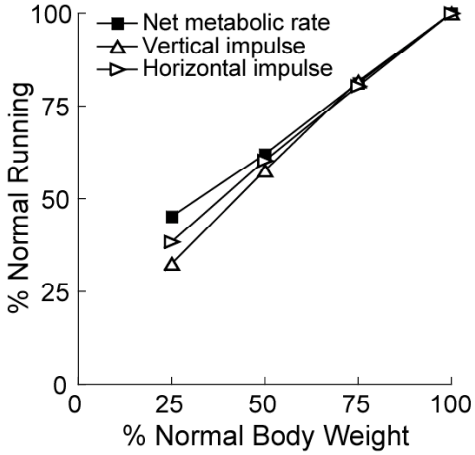

Figure 3. Means (n=10)

SUMMARY/CONCLUSIONS

Our results show that generating force to support body weight is the primary determinant of the metabolic cost of running. We deduce that the net metabolic cost to support body weight is about 74% of the total net cost of running.

REFERENCES

Brockway, J. M. (1987). *Human Nutrition. Clin Nutrition,* **41**, 463-471.

Chang, Y.-H. and Kram, R. (1999). *J Appl Physiol,* **86**, 1657-1662.

Farley, C.F. and McMahon, T.A. (1992). *J Appl Physiol,* **73**, 2709-2712.

Grabowski, A., Farley, C.F., and Kram, R. (2005). *J Appl Physiol*, **98**, 579-58.

Kram, R. and Taylor, C.R. (1990). *Nature* **346**, 265-267.

Taylor, C.R. (1994). *Adv vet sci comp med* **38A**, 181-21

THE EFFECT OF HANDLE FRICTION AND TORQUE ON AXIAL PUSH FORCE

Na Jin Seo, Thomas J. Armstrong, and Yoko Konishi

Department of Industrial and Operations Engineering, University of Michigan, Ann Arbor, MI
E-mail: najins@umich. edu

INTRODUCTION

Insufficient hand-handle friction can limit coupling between the hand and handle, thus reducing maximum axial push force on a handle that a person can exert or increasing required grip force to complete a given axial push task. Previous studies investigated push force without friction constraints only, e.g., pushing against a wall (Chaffin et al., 1983; Daams, 1993; Peebles and Norris, 2003).

It has been demonstrated that when the hand applies torque about the long axis of a cylindrical object in a power grip, inward torque (in the direction fingertips point) resulted in increased normal force on the fingertips and thus greater maximum torque, compared to outward torque (in the direction the thumb points) (Seo and Armstrong, 2006). Based on this finding, it can be expected that increased grip force from inward torque would result in increased axial push force on a cylindrical handle.

This study tested 2 hypotheses: 1) Maximum axial push force is related to handle friction. 2) Subjects voluntarily apply inward torque to increase grip force and axial push force.

METHODS

Twelve healthy right-handed university students (6 males, 6 females, age=21-35 yrs) grasped a horizontal cylindrical handle with their right hand and performed isometric maximum axial push force exertions along the long axis of a cylindrical handle for 5 sec, in a standing posture. The handle was adjusted to each subject's elbow height. Subjects were allowed to freely choose a posture, e.g., lean forward.

Dependent variables were maximum axial push force, torque and grip force. Independent variables were handle friction (low friction aluminum vs. high friction rubber) and push method (straight vs. preferred). For the straight method, subjects were instructed to exert only axial push force with no torque about the long axis of the handle. For the preferred method, no specific instruction was given but to exert the maximum axial push force. Each condition was presented twice to subjects in a random order. A two-minute break was given between successive trials.

Grip force was measured by a split cylinder (Edgren et al., 2004) which was covered with a smooth 3.5 mm-thick rubber sheet, or smooth 0.2 mm-thick aluminum sheet. With the sheet of rubber or aluminum, the tested handle diameters were 57.8 and 51.2 mm for the rubber and aluminum, respectively. Via universal joints, the handle was connected to a load cell that measured axial push force and torque. Data were averaged over 2 sec during maximum exertions.

RESULTS AND DISCUSSION

Hypothesis 1: The data support the first hypothesis. Maximum axial push force was 10% greater for the high friction rubber handle than for low friction aluminum handle (see Table 1, $p<0.01$), although grip force was not different between the two handle materials (see Table 1, $p>0.05$). Maximum axial push force measured in this

Table 1: Max axial push force, grip force and inward torque for the two methods, handle materials and gender (mean ± SD)

Method	Push (N)	Grip (N)	Torque (Nm)
Male (n=6), aluminum handle			
Prefer	123 ±11	143 ±78	1.9 ±1.8
Straight	119 ±12	109 ±51	0.7 ±0.5
Male (n=6), rubber handle			
Prefer	137 ±26	121 ±51	1.1 ±2.1
Straight	130 ±18	115 ±50	0.3 ±0.6
Female (n=6), aluminum handle			
Prefer	62 ±21	56 ±24	0.5 ±0.5
Straight	59 ±23	51 ±19	0.2 ±0.2
Female (n=6), rubber handle			
Prefer	64 ±26	45 ±19	0.6 ±1.1
Straight	61 ±29	39 ±35	0.1 ±0.1

study is about the half of push strength in the absence of friction constraints (Chaffin et al., 1983; Daams, 1993; Peebles and Norris, 2003). It suggests that the weakest link in the chain was the friction between the hand and handle in this study.

Axial push force may also have been limited by wrist strength. The reaction force from push generates a moment about the wrist joint in the ulnar direction, requiring radial deviators' activities for stabilizing the wrist. The voluntary wrist abduction strength reported by Delp et al. (1996) is only 7% greater than the maximum axial push force measured in this study, suggesting that wrist strength may have been the limiting factor; however, when the wrist becomes deviated in the ulnar direction more with pushing, the passive force of the wrist will increase and the wrist may not limit axial push. Also, a fixed handle (with no universal joints) may increase axial push force, as subjects can apply downward force to the handle: The reaction force from downward push can counterbalance the moment about the wrist joint produced by the reaction force from an axial push exertion.

Hypothesis 2: The data support the hypothesis that subjects voluntarily apply inward torque during maximum axial push force exertions (see Table 1, $p<0.01$). This voluntary inward torque appears to increase grip force and thus axial push force 7%, compared to the straight method (see Table 1, $p<0.01$). Within the preferred method, high axial push force was associated with high grip force and high inward torque ($p<0.01$), as predicted based on our previous study (Seo and Armstrong, 2006).

CONCLUSIONS

- Higher axial push force can be produced with higher handle friction by a worker of a given strength.
- Design of work objects or consumer products should assume that workers or users use inward torque to increase grip force and thus axial push force.

REFERENCES

Chaffin, D.B. et al. (1983). *Human Factors*, **25**, 541-550.

Daams, B. J. (1993). *Ergonomics*, **36**, 397-406.

Delp, S.L. et al. (1996). *Journal of Biomechanics*, **29** (10) 1371-1375.

Edgren, C. S. et al. (2004). *Human Factors*, **46** (2) 2 44-251.

Peebles, L., Norris, B. (2003). *Applied Ergonomics*, **34**, 73-88.

Seo, N., Armstrong, T. J. (2006). *ASB 30th meeting, Blacksburg, VA.*

ACKNOWLEDGEMENTS

This project was funded in part by joint funds from the UAW-GM National Joint Committee on Health and Safety and in part by NIOSH pilot grant.

RESIDUAL FORCE DEPRESSION IS NOT ABOLISHED FOLLOWING A QUICK SHORTENING STEP

Walter Herzog and Tim R. Leonard

University of Calgary, Calgary, Alberta, Canada
E-mail: walter@kin.ucalgary.ca

INTRODUCTION

When a muscle is actively shortened and then held at a constant length until all transient force recovery has disappeared, the force following shortening is smaller than the corresponding steady-state force obtained for a purely isometric contraction at the corresponding length. This phenomenon has first been described systematically by Abbott and Aubert (1952) and is referred to as (residual) force depression.

Recently, the idea that force depression is caused by an inhibition of cross-bridge attachment in the actin-myosin zone that is newly formed during shortening has received strong support (Herzog, 2004). The "cross-bridge inhibition theory" predicts that when stress on actin is released, force depression should be abolished. This observation has been made when force-depressed muscles were deactivated just long enough for force to drop to zero.

Stress in force-depressed muscles can also be released by shortening the muscle at great speed. The purpose of this study was to shorten a force-depressed muscle quickly so that force dropped to zero. We hypothesized, in accordance with the cross-bridge inhibition theory, that force depression would be abolished following the quick shortening step.

METHODS

All testing was performed with cat soleus muscles (n=8) as described in detail previously (Herzog and Leonard, 1997).

Each set of tests consisted of ten contractions. The first two and last two contractions were isometric reference contractions performed at optimal length (hereafter referred to as 0mm length) and 9mm shorter than optimal length (-9mm). The reference contractions were complemented by six test contractions. The first consisted of a 1s isometric contraction at a length 9mm greater than optimal, followed by shortening at 4.5mm/s, followed by an isometric contraction at 0mm. The second test contraction was identical except that shortening occurred from +9mm to -9mm. The third was identical to the second, except that the speed of shortening was 200mm/s. The remaining three test contractions consisted of slow shortening (4.5mm/s), followed by quick shortening (200mm/s) with a delay between the slow and quick shortening of 0, 1 and 2s.

Mann-Whitney statistics were used to identify differences between the forces obtained for the reference and shortening contractions. Kruskal-Wallis statistics were used to identify differences in force depression between the slow, fast and the slow-followed-by-fast shortening tests. The level of significance was 0.05 for all tests.

RESULTS AND DISCUSSION

Slow shortening of soleus produced statistically significant force depression for both magnitudes of shortening (Figure 1) with mean values of 5.3% (± 1.9%) for the 9mm shortening and 5.8% (± 1.3%) for the 18mm shortening distance.

Active shortening at the quick speed (200mm/s) resulted in a drop of the active force to zero (Figure 2) and there was no force depression. When force depression was induced by shortening at the slow speed and then followed by the quick shortening step, active forces dropped to zero. However, there remained a significant force depression of 3.2% (± 0.5%), 3.7% (± 0.5%); and 4.2% (± 1.5%) when the quick and slow shortening were delayed by 0, 1, and 2s, respectively.

If the cross-bridge inhibition theory was correct, force depression should have been abolished after the quick shortening step. However, that was not observed in this study. Rather, quick shortening steps following slow shortening known to induce force depression were associated with a small but consistent and statistically significant force depression (Figure 2), while the quick shortening steps alone were not. This result indicates that loss of force depression during deactivation is not caused by stress release on actin, but by changes associated with deactivating the muscle.

SUMMARY/CONCLUSIONS

We conclude from these results that a small amount of force depression persists following stress release caused by quick shortening, and therefore that the cross-bridge inhibition theory cannot be the sole cause of force depression. We suggest that force depression might be associated with an inhibition of cross-bridge attachment that is controlled in the cross-bridge itself.

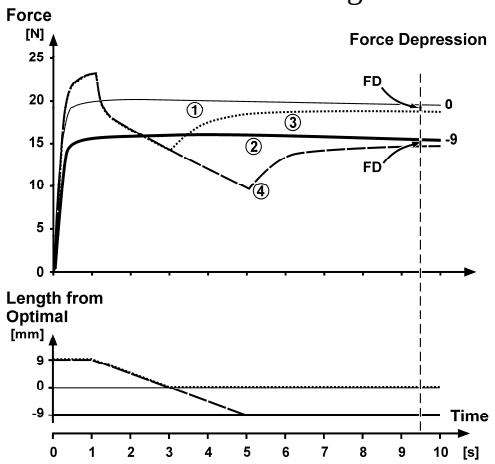

Figure 1: Force depression following slow shortening of soleus for 9 and 18mm.

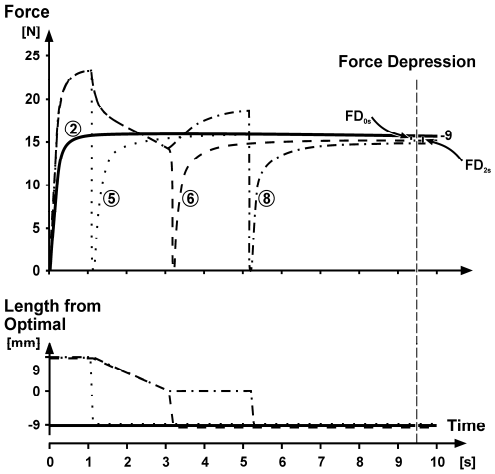

Figure 2: Force depression persists when slow shortening is followed by a quick shortening step

REFERENCES

Abbott, B. C. & Aubert, X. M. (1952). *J. Physiol (Lond)*, **117**, 77-86; Herzog, W. (2004). *Hum Mvmnt Sci*, **23**, 591-604; Herzog, W. & Leonard, T. R. (1997). *J. Biomech*, **30(9)**, 865-872; Maréchal, G. & Plaghki, L. (1979). *J. Gen Physiol*, **73**, 453-467.

ACKNOWLEDGEMENTS

CRC, NSERC and CIHR of Canada

The Influence of Maturation and Lower Extremity Kinetics on Swing Limb Foot Velocity in Young Females During a Soccer Kick

Mark A. Lyle, Susan M. Sigward, Christine D. Pollard and Christopher M. Powers
Musculoskeletal Biomechanics Research Laboratory
Division of Biokinesiology and Physical Therapy
University of Southern California, Los Angeles, CA, USA
E-mail: mlyle@usc.edu, Web: www.usc.edu/go/mbrl

INTRODUCTION

Kicking is the most fundamental activity in the sport of soccer. Information concerning kicking biomechanics is necessary to develop strategies that optimize performance. Previous studies evaluating soccer kicking have been limited in that they have focused solely on swing limb kinematics and kinetics. (Kellis et al. 2006; Nunome et al. 2006; Apriantono et al. 2006). Evaluation of the swing limb provides only partial insight into this activity as stance limb mechanics can have an influence on swing limb dynamics. Furthermore, evaluation of younger soccer players at different stages of maturation may provide insight into the developmental aspects of kicking.

The purposes of this study were to 1) compare the swing and stance limb kinetics of pre-pubertal and post-pubertal female soccer players during kicking, and 2) identify predictors of peak swing limb foot velocity. Peak foot velocity of the swing leg was chosen as the dependent variable of interest as this parameter has been shown to be related to ball velocity following foot contact. (Kellis et al. 2006; Nunome et al. 2006; Apriantono et al. 2006)

METHODS

Twenty healthy female soccer players participated in this study. The Pubertal Maturation Observational Scale (Davies et al. 2000) and a self-report of Tanner stages (Schlossberger et al. 1992) were used to classify subjects as pre-pubertal (n=10) or post-pubertal (n=10).

Bilateral three-dimensional kinematics (eight camera Vicon motion analysis system, 250 Hz) and ground reaction forces (AMTI force platform, 1500 Hz) were collected while each subject kicked a soccer ball into a net. Each subject was allowed a two step approach and kicked with their preferred foot. Four kicking trials were obtained. Net joint moments at the knee and hip (normalized by body mass) were calculated using inverse dynamics equations.

Variables of interest during the kicking cycle included peak foot velocity of the swing limb, peak hip extensor, peak knee flexor and peak knee extensor moments of the stance limb, as well as peak hip flexor, peak hip adductor and peak knee extensor moments of the swing limb. The start of the kicking cycle was defined by initial contact of the stance limb on the force plate while the end of the kicking cycle was determined when maximum vertical displacement of the swing limb foot was achieved following ball contact (i.e. follow-through).

Independent samples t-tests were used to evaluate group differences for each of the kinetic and kinematic variables noted above. Stepwise regression analysis using a forward stepping approach was used to determine which of the kinetic variables were

predictive of peak swing limb foot velocity (both groups combined). For all analyses, the P-value was set at 0.05.

RESULTS AND DISCUSSION

Peak foot velocity was 16% greater in the post-pubertal group when compared to the pre-pubertal group (p=006; Table 1). Additionally, the post-pubertal group demonstrated significantly greater peak knee extensor moments of the stance limb as well as significantly greater swing limb kinetic variables (peak hip flexor, hip adductor, and knee extensor moments; Table 1).

Stepwise regression revealed that the peak swing hip flexor moment was the best predictor of peak foot velocity of the swing limb ($R=0.82$, $P<0.001$). No other kinetic variables entered the regression equation.

Both swing and stance limb kinetics likely contributed to the observed differences in peak foot velocity between pre-pubertal and post-pubertal soccer players. The fact that all swing limb variables were greater in the post-pubertal group suggests that increases in swing limb foot velocity are primarily achieved through forward acceleration of the swing limb. The stance limb knee extensors appear to assist in swing limb acceleration and may contribute to the transfer of energy from the stance to swing limb.

Peak hip flexor moment explained 67% of the variance in peak foot velocity during kicking. This finding suggests that dynamic hip flexor strengthening may improve kicking performance in young female soccer players. However, a training study would be needed to confirm this hypothesis.

SUMMARY/CONCLUSIONS

Post-pubertal female soccer players demonstrate greater swing limb foot velocities during kicking compared to pre-pubertal athletes. More mature athletes achieve greater foot velocities through a combination of higher swing and stance limb moments. The ability to generate a large hip flexor moment appears to be an important factor with respect to improving kicking performance.

REFERENCES

Davies PL et al. (2000). *Occup Ther Pediatr* **20**, 19-24.

Apriantono, T. et al. (2006). *J Sports Sciences*, **24**(19), 951-960.

Kellis, E. et al. (2006). *Scand J Med Sci Sports*, **16**, 334-344.

Nunome, H. et al. (2006). *J Sports Sciences*, **24**(5), 529-541.

Schlossberger, NM. Et al (1992). *J Adolesc Health*, 13, 109-113.

ACKNOWLEDGEMENTS

This study was funded by the National Institutes of Health (R01 AR053073-02)

Table 1: Group comparisons of kinetic variables (mean ± SD)

	Pre-Pubertal	Post-Pubertal	P value
Peak Foot Velocity (swing limb)	11.6 ± 0.8	13.4 ± 1.4	0.006
Peak Knee Extensor Moment (stance limb)	1.6 ± 0.3	2.0 ± 0.3	0.014
Peak Knee Flexor Moment (stance limb)	1.0 ± 0.2	1.0 ± 0.3	0.9
Peak Hip Extensor Moment (stance limb)	3.7 ± 0.7	4.3 ± 0.9	0.1
Peak Hip Flexor Moment (swing limb)	1.5 ± 0.2	1.9 ± 0.3	0.001
Peak Hip Adductor Moment (swing limb)	0.9 ± 0.4	1.1 ± 0.4	0.04
Peak Knee Extensor Moment (swing limb)	0.5 ± 0.1	0.6 ± 0.2	0.04

INTERACTIVE EFFECTS OF RUNNING SPEED AND WEIGHT SUPPORT ON METABOLIC COST AND GROUND REACTION FORCES

Alena M. Grabowski and Rodger Kram
University of Colorado, Boulder, CO, USA
E-mail: alena.grabowski@colorado.edu
Web: www.colorado.edu/intphys/research/locomotion.html

INTRODUCTION

Training at fast running speeds can enhance cardiovascular function due to increased metabolic demands and may also enhance neuromuscular function, thereby improving running performance (Daniels, 2005). Yet, running fast likely increases the risk of over-use injury due to greater peak ground reaction forces (GRFs) (Hreljac, 2000). Weight support decreases peak GRFs (Chang et. al, 2000), but also demands less metabolic power (Farley and McMahon, 1992) than normal weight running.

Our goal was to determine running speed and weight combinations that demand the same metabolic power, but differ in peak vertical impact and active GRFs. We predicted that running at fast speeds with weight support would decrease peak vertical GRFs, yet demand the same metabolic power compared to running at slower speeds with normal weight.

METHODS

We used a novel device called the G-trainer, created by Alter-G, Inc., to acutely reduce body weight (Fig. 1). The G-trainer is an enclosed treadmill body-weight-support system that uses a small increase in air pressure around the user's lower body to create a lifting force approximately at the person's center of mass. The controlled air pressure (less than 10.3 kPa or 1.5 psi) can support up to 100% of body weight. The G-trainer is comfortable, easily adjustable, and allows runners to retain normal mechanics, unlike water running.

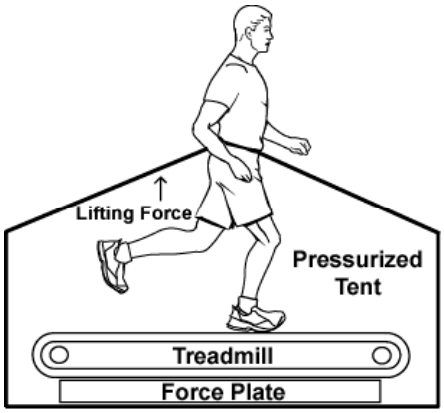

Figure 1. G-trainer (Alter-G, Inc.)

10 healthy recreational runners volunteered [7 M, 3 F, 64.4 ± 7.4kg (mean ± s.d.)]. Subjects completed 12 trials during 2 experimental sessions on a force-measuring treadmill. Trials were 7 minutes with at least 3 minutes rest given between. Subjects began each day with a standing trial at 100% body weight (BW). We randomly assigned the order of the other trials. Subjects ran 3.0 m/s at 1.0, 0.75, 0.50, and 0.25 BW, 4.0 m/s at 1.0, 0.75, 0.50, and 0.25 BW, and 5.0 m/s at 0.50, and 0.25 BW.

We measured rates of oxygen consumption and carbon dioxide production during minutes 4-6 of each trial and calculated net (gross-standing) metabolic power (Brockway, 1987). We measured GRFs at 1000 Hz during 10 strides.

We used repeated measures ANOVAs with Tukey HSD follow-up tests when warranted

($P < 0.05$). We used linear least-squares regression equations to compare body weight and net metabolic power and to compare body weight and peak GRFs.

RESULTS AND DISCUSSION

We found multiple running speed and weight combinations that demanded the same net metabolic power, but resulted in different peak vertical impact and active GRFs. Running at faster speeds with weight support decreased peak vertical GRFs in most cases, yet maintained the same metabolic power demand as running at slower speeds with normal weight.

For example, running 3 m/s at 1.0 BW, 4 m/s at 0.83 BW, and 5 m/s at 0.43 BW all demand the same net metabolic power of 9.95 W/kg (Fig. 2).

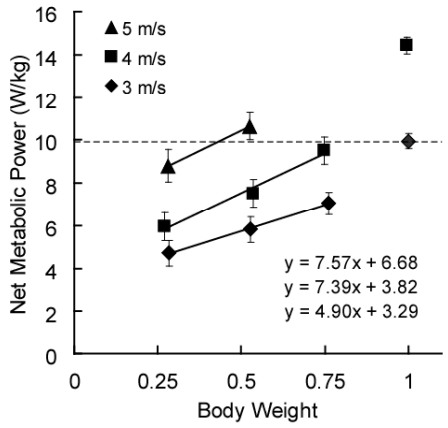

Figure 2. Metabolic demand during normal and weight supported running. (n=10) means ± s.e.m.

Peak impact and active GRFs running 3 m/s at 1.0 BW were 941 N and 1480 N, respectively (Fig. 3). Running 4 m/s at 0.83 BW, peak impact GRF increased to 1170 N and peak active GRF decreased to 1398 N. Running 5 m/s at 0.43 BW both peak impact and active GRFs decreased to 910 N and 955 N, respectively. Therefore, a person who normally runs 3 m/s could run 5 m/s in the G-trainer at 0.43 BW and reduce their impact GRF by ~3% and active GRF by ~35%.

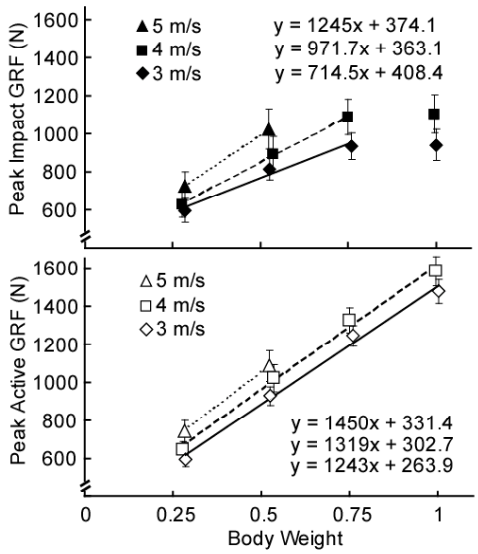

Figure 3. Peak vertical GRFs during normal and weight supported running (impact n=6, active n=10) means ± s.e.m.

SUMMARY/CONCLUSIONS

The G-trainer is a unique lower-body positive pressure system that can assist runners in training and rehabilitation. By running at faster speeds with weight support, runners can achieve the same aerobic intensity while decreasing peak vertical GRFs.

REFERENCES

Brockway, J. M. (1987). *Human Nutrition. Clin Nutrition,* **41**, 463-471.

Chang, Y.-H., Huang, H.W., Hamerski, C.M., and Kram, R. (2000). *J Exp Biol,* **203**, 229-238.

Daniels, J.D. (2005) *Daniels' Running Formula*. Human Kinetics Publishers, Inc.

Farley, C.F. and McMahon, T.A. (1992). *J Appl Physiol,* **73**, 2709-12.

Hreljac, A., Marshall, R.N., and Hume, P.A. (2000). *Med Sci Sport Exer,* **32**, 1635-41.

ACKNOWLEDGEMENTS

Supported by Alter-G.com.

ELECTROMYOGRAPHIC AND KINEMATIC EVALUATION OF PROVOCATIVE TESTS FOR SLAP LESIONS

Seth M. Kuhlman, Michelle B. Sabick, Ronald P. Pfeiffer, Kurt Nilsson, Kevin G. Shea, Mike Curtin, and David Clark

Center for Orthopaedic & Biomechanics Research, Boise State University, Boise, Idaho, USA
E-mail: sethkuhlman@boisestate.edu, Web: http://coen.boisestate.edu/cobr/

INTRODUCTION

Clinicians have a choice between several modalities when diagnosing Superior Labrum Anterior to Posterior (SLAP) lesions: arthroscopy, MRI, and clinical tests. However, surgical and imaging techniques have the disadvantage of being costly. Therefore, effective clinical tests that can diagnose SLAP lesions without the expense associated with surgery or MRI are needed.

Consequently, at least 17 different provocative tests have been used to detect SLAP lesions. A subset of 10 of these tests consists of active provocative tests which cause symptoms by simulating one of the two proposed SLAP injury mechanisms. The first mechanism involves actively straining the Long Head of the Biceps Brachii (LHBB) muscle. The second involves passively straining the LHBB through an external load applied by the physician administering the test.

The purpose of this study was to biomechanically assess the effectiveness of the clinical tests by quantifying the amount of LHBB muscle activation, muscle selectivity, and the relative motion between the glenoid and head of the humerus (HH) in 10 clinical tests developed specifically for detecting SLAP lesion pathology.

METHODS

Performance of each provocative test was evaluated using electromyography (EMG) (Noraxon Telemyo 900, 1250 Hz) and an electromagnetic motion capture system (Polhemus Fastrak, 30Hz). Male subjects (n=11), without history of shoulder pathology were recruited to participate. Surface electrodes were placed over the muscle belly of the LHBB, short head of biceps brachii, anterior deltoid, pectoralis major, latissimus dorsi, and infraspinatus muscles (Figure 1). An intramuscular electrode was placed in the supraspinatus due to its deep location.

To collect kinematic data, seven of the subjects were instrumented with three electromagnetic sensors placed on the humerus, scapula, and thorax segments. Kinematic data collection was performed according to the recommended ISB shoulder procedures (Wu et al., 2005).

Figure 1: Subject instrumented with EMG electrodes and electromagnetic sensors

Subjects performed a 3-second maximum voluntary isometric contraction (MVIC) for each muscle monitored. The peak activation

level in any of the processed MVIC trials was considered 100% effort and used to normalize the provocative test data.

A physician performed 3 repetitions each of the following 10 provocative tests on the right arm of each subject in random order:

- Active Compression
- Anterior Slide
- Biceps Load
- Biceps Load II
- Compression Rotation
- Crank
- Pronated Load
- Resisted Supination External Rotation
- Speed's
- Supination Sign

One way repeated measures ANOVA and a paired t-test post-hoc analysis (α=0.05) was used to compare peak normalized LHBB activation, selectivity, and translation of the HH relative to the scapula across the tests. Selectivity was defined as the proportion of EMG signal received from all muscles monitored that is attributable to the LHBB.

RESULTS

There were significant differences in LHBB activation (p=0.000), muscle selectivity (p=0.005), and superior/inferior translation (p=0.023) between the 10 tests (Table 1). LHBB activation resulted in three distinct groups with no statistical difference within the groups. The top group included the Biceps Load, Biceps Load II, Speed's, and Active Compression (palm up) tests. Muscle selectivity resulted in four statistically distinct groups with the top group being comprised of the Biceps Load, Biceps Load II, Speed's, and the Resisted Supination External Rotation tests. The only test that showed any significant difference in superior/inferior translation was the Supination Sign test.

DISCUSSION

The Biceps Load, Biceps Load II, and Speed's tests best reproduced the first mechanism of injury, traction on the LHBB origin. These tests not only had the highest LHBB muscle activations, but best isolated the LHBB, which should help avoid confounding pain in the other rotator cuff structures. Before a final conclusion can be made about the overall effectiveness of these 10 tests, the methodology pertaining to the kinematics must be improved. The large values of HH superior translation obtained appear infeasible. Once this adjustment is made, the next phase of this study is to evaluate the top tests on patients with suspected SLAP lesions and verify the results with arthroscopy.

REFERENCES

Wu, G., et al. (2005). *J. Biomech*, **38**(5), 981-992.

Table 1: Results from the 10 active provocative tests, muscle activation, muscle selectivity, and superior/inferior translation (mean ± standard deviation).

Test	Muscle Activation (% MVIC)	Muscle Selectivity	Superior/Inferior Translation (mm)
Active Compression (Palm Down)	34.8 ± 35.8	0.10 ± 0.08	-4.3 ± 8.4
Active Compression (Palm Up)	63.5 ± 50.8	0.12 ± 0.08	-9.0 ± 13.9
Anterior Slide	15.5 ± 11.3	0.07 ± 0.07	9.4 ± 17.8
Biceps Load	66.7 ± 32.4	0.19 ± 0.12	-9.7 ± 10.9
Biceps Load II	73.8 ± 35.7	0.20 ± 0.04	-9.1 ± 14.5
Compression Rotation	12.1 ± 8.9	0.09 ± 0.08	-5.6 ± 5.5
Crank	18.8 ± 19.8	0.12 ± 0.06	11.4 ± 21.1
Pronated Load	36.2 ± 16.0	0.13 ± 0.10	-18.3 ± 36.3
Resisted Supination External Rotation	42.6 ± 31.1	0.17 ± 0.04	-26.5 ± 10.2
Speed's	76.2 ± 67.4	0.15 ± 0.03	-4.3 ± 9.3
Supination Sign	42.8 ± 23.7	0.13 ± 0.04	19.3 ± 11.5

THE EFFECT OF FRICTION AND ARM POSTURE ON MAX PULL / PUSH FORCE

Na Jin Seo, Thomas J. Armstrong, and Kathryn L. Dannecker

University of Michigan, Ann Arbor, MI
E-mail: najins@umich. edu

INTRODUCTION

An individual's limited pull/push capability can pose safety risks in situations such as climbing a ladder or propelling a wheel chair. An understanding of pull/push force in relation to hand-handle friction and arm posture is important to design grip objects that prevent slippage or overexertion.

Previous studies used handles that produced mechanical interference to prevent the hands from slipping (e.g., pushing against a wall, Davis and Stubbs, 1977; Mital et al., 1995). In many cases, however, it is necessary to rely on friction for coupling between the hand and handle.

This study tests the hypotheses that 1) maximum pull/push force is limited by hand-handle friction and 2) maximum pull force varies with different arm postures.

METHODS

Eight healthy right-handed subjects (4 male, 4 female, average age = 26.4 yrs, SD = 5.3 yrs) grasped a cylindrical handle with the right hand and performed maximum pull/push exertions. They were seated on a chair that supported the back and feet to minimize the effect of balance and slip on pull/push force. The handle height was adjusted to each subject's elbow height.

Independent variables were handle material (aluminum, rubber), gloves (bare hand, cotton glove – GoldKnit™ Mediumweight 70-227, PVC dot glove – Performers Extra™ Knit Series D2-09), handle orientation (long axis of the handle parallel to the pull/push direction and the floor, vs. perpendicular to the pull/push direction and the floor), and elbow angle (flexed at 90˚ vs. extended). The dependent variable was maximum pull/push force, measured using a load cell. The cylindrical handle diameter was 40 mm. Each condition was repeated twice and randomized.

RESULTS AND DISCUSSION

Pull/push forces for different friction conditions and elbow postures are shown in Fig 1 and 2. When the handle was oriented parallel to the exertion direction, pull/push forces decreased 10% ($p<0.01$), compared to the handle perpendicular to the exertion direction. Pull/push force further decreased 17% for the low friction aluminum handle, compared to the high friction rubber handle. These results support the first hypothesis that axial pull/push force is limited by hand-handle friction.

Use of the PVC dot glove and cotton glove resulted in 18% and 42% reduced pull force compared to the bare hand, respectively ($p<0.01$, Fig 1). It is probably due to decreased friction with gloves, especially for the cotton glove.

Similar with Davis and Stubbs (1977), pull force was 29% greater for the extended elbow than for the flexed elbow ($p<0.01$). The shoulder strength to move the upper arm backwards may have limited pull force when the elbow was 90º flexed. For the

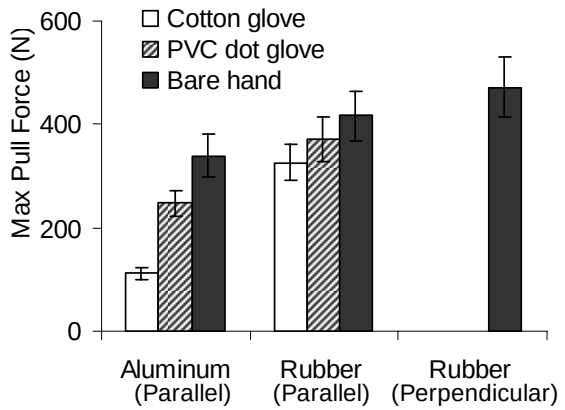

Figure 1. Mean ± SE pull force for different gloves (cotton glove, PVC dot glove, bare hand), handle materials and orientations. Low friction aluminum and high friction rubber handles were tested for a handle parallel to the pull/push direction. A handle perpendicular to the pull/push direction was also tested. (n=8, extended elbow only)

extended elbow, torso extension strength may have limited pull force. Pull force was greater than push force ($p<0.01$, Fig 1), probably because push force was primarily exerted by the upper arm whereas subjects could engage the torso for pull exertion in the apparatus provided in this study.

SUMMARY/CONCLUSIONS

Pull/push capabilities can increase 22% by orienting the long axis of a handle perpendicular (as opposed to parallel) to the pull/push direction so that pull/push force is not limited by hand-handle friction. When the handle should be oriented parallel to the pull/push direction, a high friction handle is preferred over a low friction handle, to improve hand-handle friction and thus the pull/push capability, as exampled by wheelchair rim design (Richter et al., 2006).

Gloves are often used in industry. Low friction gloves such as cotton gloves can reduce friction and the pull/push capability 42% (compared to the bare hand), and may

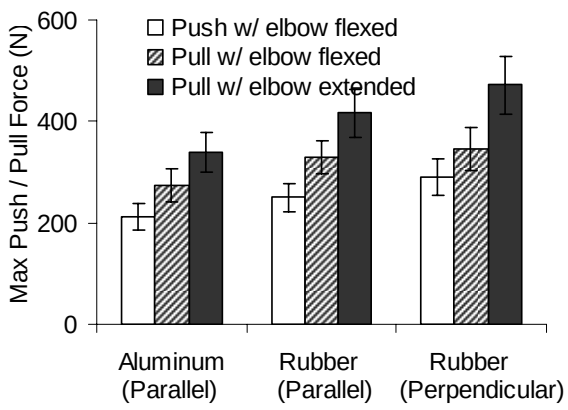

Figure 2. Mean ± SE push/pull force for different elbow postures, handle materials and orientations. (n=8, bare hand only)

result in hand slippage. In addition, use of gloves can decrease tactile sensitivity (Kinoshita, 1999). Reduced sensitivity or low hand-handle friction can result in high grip force exertions which, if repeated, can cause local fatigue and musculoskeletal disorders (Armstrong et al., 1993).

Pull force can be limited by shoulder extension strength. This limitation can be relieved by elbow extension.

REFERENCES

Armstrong, T.J. et al. (1993). *Scand J Work Environ Health*, **19** (2) 73-84.

Davis, P.R., Stubbs, D.A. (1977). *Applied Ergonomics*, **8** (4) 219-228.

Kinoshita (1999). *Ergonomics*, **42** (10) 1372-1385.

Mital, A. et al. (1995). *Clinical Biomechanics*, **10** (2) 110-112.

Richter, W.M. et al. (2006). *Arch Phys Med Rehabil*, **87** (12) 1643-1647.

ACKNOWLEDGEMENTS

This project was funded in part by joint funds from the UAW-GM National Joint Committee on Health and Safety and in part by NIOSH pilot grant.

CAN ELECTROMYOGRAPHIC ASYMMETRIES DURING GAIT BE EXPLAINED BY LIMB DOMINANCE?

Matthew K. Seeley [1], Brian R. Umberger [2], and Robert Shapiro [3]

[1] Brigham Young University, Provo, UT, USA
[2] University of Massachusetts, Amherst, MA, USA
[3] University of Kentucky, Lexington, KY, USA
E-mail: matt_seeley@byu.edu

INTRODUCTION

Subtle asymmetries exist in kinematic, kinetic, and electromyography (EMG) data describing able-bodied gait, yet the causes of these asymmetries remain unclear (Sadeghi *et al*., 2000). Some scientists have suggested that these bilateral asymmetries may reflect differences in functional roles of the lower limbs, with the non-dominant (ND) limb contributing more to support, while the dominant (D) limb contributes more to propulsion (Sadeghi *et al.,* 2000). However, bilateral symmetry has been demonstrated for impulses due to vertical (i.e., support) and propulsive ground reaction forces during normal gait (Seeley *et al.,* submitted) indicating that, at a global level, each lower limb contributes equally to support and propulsion. Symmetrical impulses, however, do not necessarily imply "local" bilateral symmetry for measures such as EMG or joint kinetics. Sadeghi et al. (2003) proposed that such local asymmetries may represent compensatory strategies that help ensure global symmetry of lower-limb function.

The purpose of this study was to determine if local asymmetries in EMG are related to hypothesized functional differences (support and propulsion) of the lower limbs during normal gait, and to see if these differences depend on walking speed. Bilateral EMG was monitored for specific muscles throughout intervals of the gait cycle during which these muscles have been shown to contribute to support or propulsion (Anderson & Pandy, 2003; Neptune *et al.,* 2004). Two general hypotheses were expected to be supported if EMG asymmetries are related to functional asymmetry. First, support-related muscles would be more active for the ND limb and propulsion-related muscles would be more active for the D limb. Second, with increases in walking speed, D-limb muscle activity related to propulsion would increase disproportionately compared to ND-limb counterparts. This limb × speed interaction was not predicted for support-related muscles, as gravity is independent of speed.

METHODS

Bilateral surface EMG data were collected (1200 Hz) from the gluteus maximus (GMX), gluteus medius (GMD), vastus lateralis (VLA), semitendinosis (SMT), and soleus (SOL) during walking for 20 subjects (age = 25 ± 3 yr; ht = 1.7 ± 0.1 m; mass = 70 ± 14 kg) at three speeds: preferred (1.61 ± 0.01 m/s), -20% (1.37 ± 0.01 m/s), and +20% (2.02 ± 0.04 m/s). EMG data were normalized to maximal voluntary isometric contraction amplitude and time normalized to a full gait cycle. Mean muscle amplitudes during intervals of the gait cycle for which those muscles have been shown to contribute to support or propulsion were averaged across five trials for each subject, limb, and speed. Mean amplitudes associated with support were GMX, GMD, VLA, and SOL during the first 30% of the

gait cycle. Mean amplitudes associated with propulsion were SMT during the first 30% of the gait cycle, and SOL between 30 and 50% of the gait cycle. A repeated measures ANOVA ($\alpha = 0.05$) was performed to detect effects of limb and walking speed on dependent variables. Bonferroni-Holm *post hoc* analyses were conducted to detect bilateral differences at each walking speed.

RESULTS AND DISCUSSION

No significant limb × speed interactions were indicated, so data pooled from each speed were compared bilaterally for each dependant variable. GMD activity related to support was 25% less for the ND limb. SOL amplitudes related to support and propulsion were 55% and 31% less for the ND limb, respectively (Table 1).

The data offered little support for the first hypothesis and no evidence for the second hypothesis. Support-related muscles (GMX, GMD, VLA, and SOL during the first 30% of the gait cycle) were expected to be greater for the ND limb. However, only GMD and SOL were bilaterally different, and these differences were opposite to the predictions. Propulsion-related muscles (SMT between 0 and 30%, and SOL between 30 and 50%) amplitudes offered limited support for the first hypothesis. SMT activity was not bilaterally different, yet, as was predicted, mean propulsion-related SOL amplitude was greater for the D limb. Present data failed to support the second hypothesis, as no limb × speed interactions were indicated. During gait, propulsion requirements increase disproportionately in comparison to support requirements as walking speed increases. This is because gravity remains constant. Consequently, propulsive D-limb SMT and SOL activity were expected to increase disproportionately in comparison to ND-limb counterparts as walking speed increased, yet this was not observed.

Table 1: Mean EMG amplitudes (%MVIC) during specific intervals of the gait cycle (see text for details). *Asterisks indicate statistical significance.

	Mean Amplitude	
Support	**ND**	**D**
GMX	8.6 ± 0.9	11.8 ± 1.9
GMD* (p = 0.02)	8.1 ± 0.5	10.1 ± 0.7
VLA	8.8 ± 1.1	7.7 ± 0.7
SOL* (*p* = 0.02)	10.8 ± 0.9	16.7 ± 1.9
Propulsion		
SMT	4.9 ± 0.4	5.5 ± 0.6
SOL* (p = 0.03)	31.8 ± 2.8	41.6 ± 4.4

SUMMARY/CONCLUSIONS

Present results indicate that bilateral EMG asymmetries are not likely related to lower-limb task differences, as conceptualized within the functional asymmetry framework (Sadeghi *et al.,* 2000). Only one of the six bilateral comparisons supported the first hypothesis that was based on functional asymmetry. Additionally, the walking speed manipulation failed to support the idea that EMG asymmetries are related to lower-limb functional differences. Other plausible causes of local EMG asymmetries during normal gait including lower-limb morphological asymmetry or environmental issues should now be explored. Elucidation of this issue may advance our understanding regarding the role of the neuromuscular system during cyclic activities such as gait.

REFERENCES

Anderson F. & Pandy M. (2004). *Gait Post,* **17,** 159-169.

Neptune R. et al. (2004). *Gait Post,* **19,** 194-205.

Sadeghi, H. et al. (2000). *Gait Post,* **12**, 34-45.

Sadeghi, H. (2003). *Gait Post,* **17**, 197-204.

Seeley, M. et al. (submitted). *Gait Post.*

THE ANTERIOR-POSTERIOR THICKNESS VARIATION OF FEMORAL CARTILAGE IN THE TIBIOFEMORAL JOINT IS INFLUENCED BY THE KNEE FLEXION ANGLES DURING WALKING

Seungbum Koo [1], Jonathan Rylander [1] and Thomas Andriacchi [1,2]

[1] Stanford University, Stanford, CA, USA
[2] VA Palo Alto Health Care System, Palo Alto, CA, USA
E-mail: skoo@stanford.edu, Web: Biomotion.stanford.edu

INTRODUCTION

Knee articular cartilage sustains high loading during common activities such as walking. Cartilage morphology has been reported to be regulated by mechanical loading conditions (Kiviranta, 1988, Smith, 2004), suggesting that the joint loading conditions during normal activities can affect knee articular cartilage morphology. While it has been suggested that loading during activities such as walking influence the medial-lateral variations in cartilage thickness (Andriacchi, 2004, Koo, 2007), the factors that affect anterior-posterior (AP) variations in cartilage thickness are still not well understood. However, the mechanics of walking offer the opportunity to test the relationship between gait mechanics and AP variations in cartilage thickness since the femoral contact regions during the stance phase of walking can largely be predicted by the knee flexion angle. The purpose of this study was to test if the AP spatial cartilage thickness distributions in the medial and lateral condyles of the distal femur were influenced by the knee flexion angle during walking.

METHODS

Gait data and knee MR images were obtained for seventeen healthy subjects (age 33.2±9.8 years, 10 males, 7 females, BMI 23.0±2.4 kg/m^2, no previous knee injures) after IRB approval and informed consent were obtained. In this study, only the data from the left knee of the subjects were processed. The knee flexion angle at heel strike and the average knee flexion angle during the stance phase of normal walking were measured using the previously describe six marker link system. Three-dimensional models of the distal femoral cartilage were created from the knee MR images using custom software (Koo, 2005) (Figure 1 left).

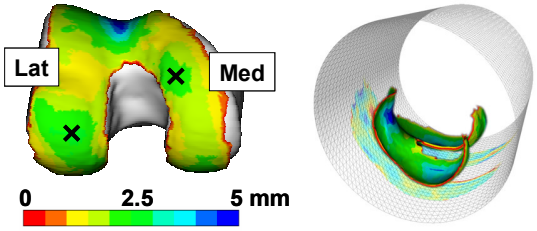

Figure 1: The locations of the centroids of the thickest cartilage in the medial and lateral condyles (left); Creating a two-dimensional cartilage thickness map by projecting a three-dimensional map onto a cylindrical surface (right).

To identify the locations (centroids) of the thickest cartilage on the condyles of the distal femur (Figure 1 left), two dimensional thickness maps were generated by projecting the three-dimensional models onto a cylindrical surface (Figure 1 right). These centroids, determined through the use of a Gaussian optimization algorithm over the regions of interest, were used to determine a sagittal plane angle relative to the femoral axis to locate the AP position of the centroid of thickest cartilage (Figure 2). The associations between the angular AP location of the centroids in the medial and lateral condyles and the knee flexion angles

(at heel strike and average over stance phase) during walking were tested.

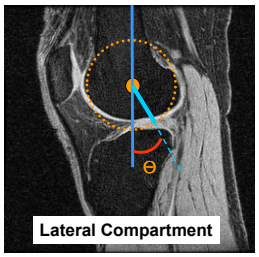

Figure 2: The angle between the femoral axis and the location of the centroid of the thickest cartilage

RESULTS

The angular AP location of the medial femoral cartilage centroid was correlated with the knee flexion angle at heel strike (R^2=0.41, P<0.01) (Figure 3) and the average knee flexion angle during the stance phase of walking (R^2=0.34, p=0.01). No correlation was found on the lateral side. The subjects with more hyper-extended knee positions at heel strike had the thickest cartilage in the more anterior part of the medial femoral cartilage.

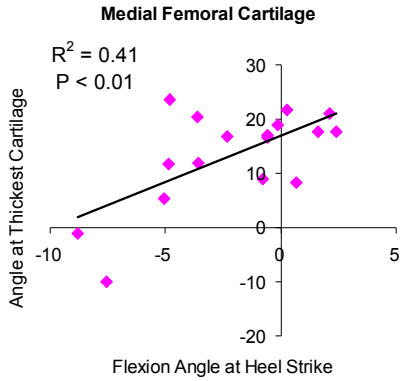

Figure 3: The angle of the thickest cartilage in the medial femoral cartilage and the knee flexion angle at heel strike

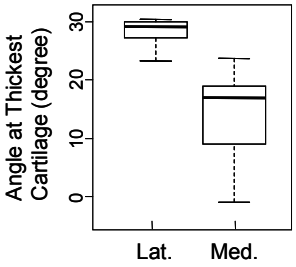

Figure 4: Distribution of the angle of the thickest cartilage in the medial and lateral femoral cartilage

The centroids of the thickest cartilage in the lateral femoral condyles had smaller variations (Standard deviation 5.3° vs. 8.9°) and were located in more posterior regions (median location 29.1° vs. 16.9°) than the medial femoral cartilage (Figure 4).

DISCUSSION

The results showed that the angular AP position of the thickest femoral cartilage morphology in the tibiofemoral joint was influenced by the knee flexion angle during walking only in the medial compartment. The tibiofemoral contact surfaces in the medial compartment are more conforming (convex-concave), so the contact location is sensitive to small differences in knee joint kinematics. On the other hands, the contact regions in the lateral compartment may not vary as much as in the medial compartment with the differences in the knee joint kinematics because of the shape of contact surfaces (Andriacchi, 2005), which may have resulted in a small variation of the centroids in the lateral compartment. This result supports the functional adaptation of the knee articular cartilage morphology to the mechanical loading conditions in the knee (Koo, 2007).

REFERENCES

Andriacchi, T.P. et al. (2004). *Ann Biomed Eng*, **32**:447-457.

Andriacchi, T.P., Briant, P.L., Bevill, S.L., Koo, S. (2005). *Clin Orthop Relat Res*, **442**, 39-44.

Kiviranta, I. et al. (1988). *J Orthop Res*, **6**, 188-195.

Koo, S., Gold, G.E., Andriacchi, T.P. (2005). *Osteoarthritis Cartilage*, **13**, 782-789.

Koo, S., Andriacchi, T.P. (2007). *J Biomech*, **In press**.

Li, G. et al. (2005). *Clin Biomech*, **20**, 736-744.

Smith, R.L., Carter, D.R., Schurman, D.J. (2004). *Clin Orthop Relat Res*, **427 Suppl**, 89-95.

ACKNOWLEDGEMENTS

NIH grant # 1R01AR049790

HUMAN LOWER EXTREMITY DESIGN: ARCHITECTURE OF HIP, KNEE, AND ANKLE MUSCLES

Samuel R. Ward[1], Carolyn M. Eng[2,3], Laura H. Smallwood[2,3], Richard L. Lieber[2,3]

[1]Departments of Radiology, [2]Orthopaedic Surgery and [3]Bioengineering, University of California and Veterans Administration Medical Center, San Diego, CA, USA
E-mail: srward@ucsd.edu, Web: http://muscle.ucsd.edu/

INTRODUCTION

Models of the musculoskeletal system depend on accurate muscle architecture inputs. To date, models of the human lower extremity are based on the muscle architecture of either two (Friederich and Brand, 1990) or three (Wickiewicz *et al.*, 1983) cadaveric specimens of unknown age, gender, and size. As models become more sophisticated, accurate depiction of inter- and intra-muscular architectural features is becoming more important (Blemker and Delp 2006). The purpose of this project was to generate a high resolution human lower extremity muscle architecture database and compare these data to the most widely used data set currently in use.

METHODS

Twenty formaldehyde-fixed cadaveric lower extremities were used for this project (age: 82.5 ± 9.4 yrs.; gender: 9 female – 11 male; height 168.4 ± 9.3 cm; weight 82.7 ± 15.3 kg). The use of human tissue was approved by the Anatomical Services Committee of the University of California, San Diego.

Muscle architectural measurements were made on twenty-seven (n=20/muscle) lower extremity muscles (540 total samples) according to methods previously described (Lieber *et al.* 1990). Briefly, mass and muscle length were measured for each muscle. Fiber bundles from three to five predetermined regions of each muscle were microdissected and sarcomere length was measured in each fiber bundle using laser diffraction (Lieber *et al.* 1984) to calculate normalized fiber length (L_f) and physiological cross-sectional area (PCSA) as previously illustrated (Lieber *et al.* 1990).

To report the large number of muscles studied, descriptive data for each joint are reported in the form of L_f versus PCSA scatter plots. Comparisons between these data and those of Wickiewicz *et al.* (1983) are reported as relative differences between functional groups. Results are shown as mean ± SE.

RESULTS AND DISCUSSION

At the hip, the gluteus maximus and medius were predicted to produce the largest forces based on PCSA, while sartorius and gracilis would operate over the widest range of lengths based on their long L_f (Fig. 1). Comparisons of these data with those of Wickiewicz *et al.* (1983), reveal larger PCSAs (10.3 ± 2.8%) and shorter fiber lengths (11.0 ± 4.7%) than previously expected.

At the knee, quadriceps had larger PCSAs than hamstrings ($P < 0.05$), but these functional groups had similar L_f values, contrary to previous reports. Comparisons of these data with those of Wickiewicz *et al.* (1983), revealed larger PCSAs (12.4 ± 3.8%) and longer L_f values (21.5 ± 3.3%) than previously reported (Fig. 2).

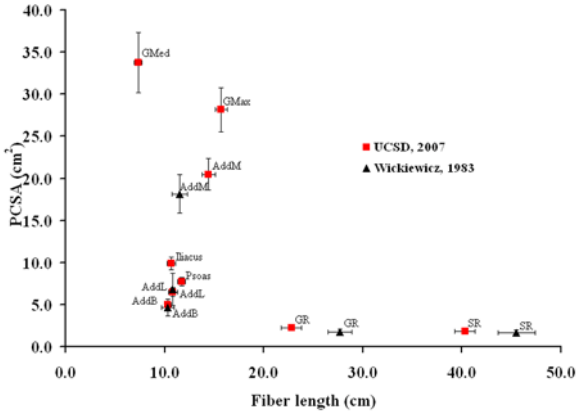

Figure 1. Scatter plot (L_f v. PCSA) of hip muscles (■) and comparison to Wickiewicz 1983 (▲).

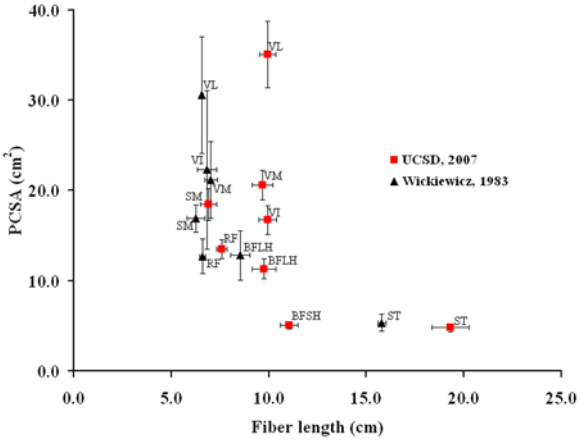

Figure 1. Scatter plot (L_f v. PCSA) of knee muscles (■) and comparison to Wickiewicz 1983 (▲).

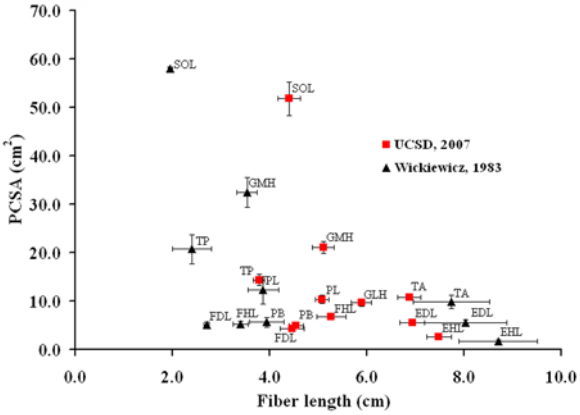

Figure 1. Scatter plot (L_f v. PCSA) of ankle muscles (■) and comparison to Wickiewicz 1983 (▲).

At the ankle, the plantarflexors clearly favored force production over operating range, while the dorsiflexors demonstrated the opposite pattern. Comparisons of these data with those of Wickiewicz *et al.* (1983), demonstrate that the plantarflexors had smaller PCSAs (29.7 ± 8.1%) and longer L_f values (35.3 ± 5.5%), while the dorsiflexors had larger PCSAs (14.2 ± 8.1%) and shorter L_f values (14.9 ± 1.2%). Interestingly, since cadaveric ankles are fixed in plantarflexion, the L_f data suggest previous fiber length data may not have been normalized.

SUMMARY/CONCLUSIONS

Functionally, these data highlight the important force producing roles of gluteus maximus and medius at the hip, vastus lateralis at the knee, and soleus and the medial head of gastrocnemius at the ankle.

Conceptually, these data suggest that the force producing capacities and operating ranges of human lower extremity muscles have previously been underestimated. At the level of individual muscles, these discrepancies are in the 10%-50% range which will; 1) have a substantial impact on the way these muscles are individually modeled and 2) have a substantial impact on the way muscle groups will interact during function.

REFERENCES

Blemker and Delp (2006). *J Biomech* **39**:1383-1391.
Friederich and Brand (1990). *J Biomech* **23**:91-95.
Lieber *et al.* (1984). *Biophys. J.* **45**, 1007-1016.
Lieber *et al.* (1990). *J. Hand Surg.* **15A**, 244-250.
Wickiewicz *et al.* (1983). *Clin Orthop* **179**:275-283.

ACKNOWLEDGEMENTS

This work was supported by the Department of Veterans Affairs and NIH grants HD048501 and HD050837.

REDUCING ERRORS IN INVERSE DYNAMICS-BASED JOINT TORQUES THROUGH OPTIMIZED BODY SEGMENT PARAMETERS AND SEGMENT MOTION PROFILES

Raziel Riemer [1] and Elizabeth T. Hsiao-Wecksler [2]

[1] Ben-Gurion University, Beer-Sheva, Israel
[2] University of Illinois at Urbana-Champaign, Urbana, IL, USA
E-mail: rriemer@bgu.ac.il

INTRODUCTION

Errors in inverse dynamics calculations range from 4 to 140% of the estimated joint torque (Riemer et al. 2005). The accuracy of these calculations depends on errors in estimation of the body segment parameters (BSP; i.e., mass, moment of inertia, and center of mass location). It also depends on errors in the motion profiles of the body segments. These motion errors arise from two main sources: noise in the motion capture system and skin movement artifacts of skin-mounted markers.

One approach for reducing the error in inverse dynamics calculations exploits the "overdetermined" nature of this method. This refers to the fact that, in the ideal case (one in which no error is present), the measured ground reaction forces (GRF) should match the GRF calculated using a top-down approach. This phenomenon was used by Vaughan et al. (1982), to determine an optimal set of subject-specific body segment parameters. Kuo (1998) and Cahouet et al. (2002) proposed static optimization methods to reduce the effect of noise in measured data (i.e., ground reaction measurements and segment motion). The performance of these methods, however, significantly deteriorates when additional sources of error exist.

The current study presents a method to increase the accuracy of joint torque calculations through the optimization of both BSP and motion data. The goal of the optimization is to produce improved estimates for subject-specific BSP and angular motion profiles of each segment. These values are then used in inverse dynamics calculations of joint torques.

METHODS

Our approach used a three-step iterative optimization procedure. Prior to performing this procedure, a set of three "calibration" movements were collected. In step one, initial guesses for BSP and segment motions were used by the optimization to compute first approximations for each movement. In step two, BSP estimates were further refined (through optimization) by using a combined motion profile derived from the optimized motions found in step one. In step three, this optimal set of BSP were used to calculate joint torques and further refined segment motions for each calibration movement. In general, however, this optimal set of BSP could be applied to calculating optimized joint torques and segment motions for any movement that the subject performs. The optimization was based on solving constrained (on motion and BSP) nonlinear optimization problems. The objective function minimized the difference between the GRF measured from an external device (e.g., force plate) and the GRF calculated via a top-down inverse dynamics approach.

We assessed the efficacy of this approach using a simulated experiment with known true values of BSP, angular profiles, GRF, and joint torques. A human model was

developed under the assumption of a rigid body model and was represented by a three-link system (HAT, thigh, and shank). Ground reaction forces and moments were calculated with respect to the ankle joint. The simulated experiment used motion capture data from a test subject (1.8m, 80kg) performing three movements to create true BSP and motions. The movements were: squat, sway, and a "long movement" (flexion and hyperextension of the hips followed by flexion and extension of the knees). To imitate real-world data, we introduced various noise conditions to these true movements (Lu and O'Connor 1999) and BSP. Ten noise conditions were applied to each of the movements and BSP for a total of 30 movements. These were used as the initial guess for the optimization.

RESULTS AND DISCUSSION

To assess the performance of the proposed approach compared to traditional (top-down or bottom-up) approaches, we computed the average root mean square error (RMSE) relative to the true joint torques for each movement (Table 1). Comparison of results from our approach (after step three) versus the bottom-up approach (smallest RMSE for traditional approaches) showed: (1) for the long movement, average RMSE was reduced by ~ 35% in the knee and 61% in the hip; (2) for the squat movement, RMSE was reduced by 10% in the knee and 60% in the hip; and (3) for sway, ~ 43% at the knee, 80% at the hip. Further, compared to the initial guess for BSP, the final optimized set of BSP (after step two) reduced the average RMSE, due to BSP alone for all joints, by 77%.

CONCLUSIONS

The proposed approach yielded smaller errors in calculations of joint torques compared to traditional non-optimized inverse dynamics methods. The average reduction in RMSE due to our method was 48%, while prior methods found an overall reduction of 30% (Kuo 1998). This error reduction in our approach was found for all joints; whereas the reduction in previous work was due to improvement only in hip errors, while ankle and knee errors became larger. In sum, the presented method deals with the main sources of errors in inverse dynamics, and resulted in a significant improvement in the accuracy of calculated joint torques. Future research should expand the capability of the method, such as developing the method for 3D, adding degrees of freedom, and dealing with additional sources of errors.

Table 1: Comparison of the average joint torque RMSE for the three movements using the optimization approach (step-three) and traditional top-down or bottom-up inverse dynamics approaches

		Long mvmt (Nm)	Squat (Nm)	Sway (Nm)
After optimization step three	Ankle	0.02	0.00	0.02
	Knee	3.36	4.37	2.89
	Hip	3.53	3.92	1.77
Top-down	Ankle	22.41	15.30	40.84
	Knee	16.48	11.86	29.19
	Hip	16.11	11.92	16.37
Bottom-up	Ankle	0.00	0.00	0.00
	Knee	5.20	4.84	5.07
	Hip	9.16	9.79	8.62

REFERENCES

Cahouët, V. et al. (2002) *J Biomech,* 35: 1507-1513.

Kuo, A.D. (1998) *J Biomech En.*, 120: 148-159,

Lu, T.W. and J.J.O'Connor (1999) *J Biomech **32**(2): 129-34.*

Riemer, R. et al. (2005) *ISB XXth Congress*.

Vaughan, C.L. et al. (1982) *J Biomech Eng* 104(1): 38-44.

ACKNOWLEDGEMENTS

We thank Professor Placid Ferreira for assistance with optimization and Farooq Khan for help with experiments. Partial funding was provided by the CRB at UIUC.

MECHANICS OF BIPEDAL RUNNING TURNS

Devin L. Jindrich

Arizona State University, Tempe, AZ, USA
E-mail: devin.jindrich@asu.edu, Web: www.limblab.org

INTRODUCTION

Maneuvering is an essential aspect of locomotion. Efforts to design rehabilitation strategies or neural prostheses to assist locomotion following neuromotor injury must ultimately confront the need for maneuverability. Moreover, maneuvering is a controlled perturbation that may reveal control strategies used for stable locomotion under many conditions. However, relatively little is known about the mechanical requirements for maneuvers and the control strategies used for their execution.

To begin to understand the mechanical requirements for maneuvers, I developed a simple algebraic model for legged maneuvers based on the hypothesis that body rotation should match movement deflection (the change in velocity direction) over the course of a turn. The model leads to two predictions: (1) humans will over-rotate if they only generate the lateral forces necessary to turn during running; and (2) ostriches, with more horizontal body orientation and higher inertias relative to their mass, can effectively turn using only the lateral forces necessary for deflection. I used experimental data on humans and ostriches to test these predictions.

METHODS

The model assumes that a biped of mass M and moment of inertia about the vertical axis I, traveling at velocity V, seeks to deflect the direction of movement by θ_d during a step. At the beginning of the step, the foot is placed at an anterior extreme position $P_{AEP,imd}$ with respect to the center of mass (COM) parallel to the initial movement direction (*imd*), and generates a sinusoidal lateral force $F_p(t)$ for the duration of stance. If the foot does not remain directly lateral to the COM, generating the lateral impulse necessary to change the movement direction will result in a torque that rotates the body by θ_p. The proportion that θ_p matches θ_d can be estimated by a "leg effectiveness number", an indication of the degree to which generating the forces necessary for deflection maintains body orientation aligned with movement deflection. The leg effectiveness, ε, is determined by a simple algebraic equation based on behavioral and morphological parameters,

$$\varepsilon = \frac{\theta_p}{\theta_d} = \frac{MV\tau}{2I}\left(P_{AEP,imd} - \frac{4V\tau}{\pi^2}\right), \quad (1)$$

where τ is the stance period. Values of ε close to 1 represent conditions where little modulation of *imd* forces is required for body rotation to match movement deflection at the end of the turn. In the case where *imd* forces are required, their magnitude can be predicted using the equation

$$F_{imd,\max} = \frac{\pi I(1-\varepsilon)\theta_d}{\tau^2 P_p}, \quad (2)$$

where P_p is the foot placement relative to the COM, perpendicular to the *imd*.

Humans (74 kg) and ostriches (22 kg) ran at 3 m s^{-1} and executed sidestep (left turns with the right leg) or crossover (left turns with the left leg) cutting turns on a force platform. Forces in the *imd* were calculated for each turn using eq. (2), and compared to *imd* forces used by humans and ostriches (Jindrich et al., 2006; Jindrich et al., 2007).

RESULTS AND DISCUSSION

Whereas humans generated almost exclusively deceleratory (braking) forces in the *imd* during crossover and sidestep cuts (Fig. 1), ostriches generated braking forces in only 60% of turning trials (Fig. 2). This difference can be explained by differences in leg effectiveness. Humans had leg effectiveness numbers of 2.0-4.2 depending on turn magnitude, indicating that over-rotation must be overcome by braking forces. In contrast, ostriches showed values for ε of 0.9 - 1.2 for crossovers and sidesteps. Ostrich ε values were close to 1, indicating that mis-rotation is less likely to occur. On average, ostriches can effectively turn using primarily the forces necessary for deflection.

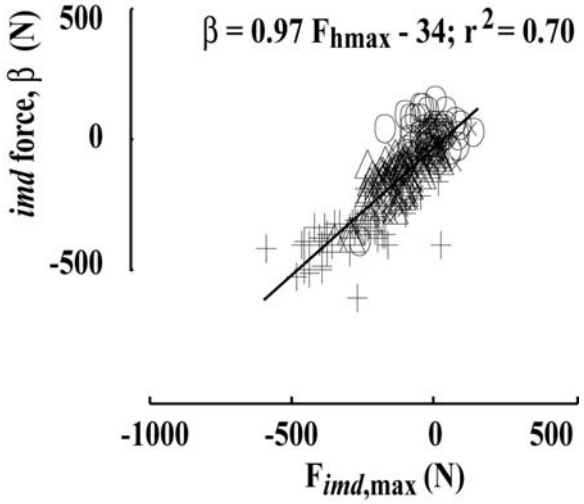

Figure 1. Comparison of forces predicted using eq. (2) to forces in the *imd* for humans. Sidesteps of 28°±1° (triangles) and 42°±5° (plus signs), crossovers of -24°±4° (crosses) and straight-running trials (circles) are shown. Black line is a linear fit.

Despite differences in body shape, body mass, and turn type, the simple algebraic turning model was able to explain over 70% of the variance in *imd* forces for both humans and ostriches (Figs. 1 and 2).

Although ostriches generated small *imd* forces on average, the range of forces observed shows that for individual trials, forces in the *imd* were used to modulate body rotation.

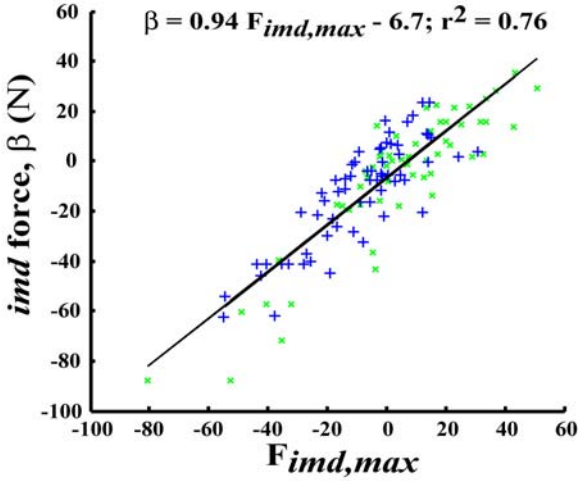

Figure 2. Comparison of forces predicted using eq. (2) to forces in the *imd* for ostriches. Sidesteps of 18°±0.6° (blue plus signs) and crossovers of 14°±0.6° (green crosses) are shown. Black line is a linear fit.

SUMMARY/CONCLUSIONS

Differences in body shape influence the forces necessary to control maneuvers in a predictable way that can be captured by a simple algebraic model.

REFERENCES

Jindrich, D. L., Besier, T. F. and Lloyd, D. G. (2006). A hypothesis for the function of braking forces during running turns. *J Biomech*, 1611-1620.

Jindrich, D. L., Smith, N. C., Jespers, K. and Wilson, A. M. (2007). Mechanics of cutting maneuvers by ostriches (*Struthio camelus*). *J Exp Biol* 210, 1378-90.

ACKNOWLEDGEMENTS

This work was conducted in collaboration with Thor Besier, David Lloyd, Nicola Smith, Karin Jespers, and Alan Wilson.

A NEURO-MUSCULOSKELETAL MOTOR CONTROL MODEL WITH SOMATOSENSORY AND VESTIBULAR FEEDBACK

Kamran Iqbal [1] and Anindo Roy [2]

[1] University of Arkansas at Little Rock, Little Rock, AR, USA
[2] Massachusetts Institute of Technology, Cambridge, MA, USA
E-mail: kxiqbal@ualr.edu, Web: www.ualr.edu/kxiqbal

INTRODUCTION

The use of dynamic systems theory to provide insight into neurophysiology has a long history (Barin, 1989; He et al., 1991; Kuo, 1995; van der Helm and Rozendaal, 2000; Iqbal and Roy, 2004). The motivation for this work is to develop a simple yet physiologically accurate model of human biomechanics and use it to study fundamental aspects of the central nervous system (CNS) control of posture and movement. Specifically, we are interested to explore answers to the following questions: a) how can a simple CNS control models be integrated into the mathematical description of the body derived from anatomy and physiology, and b) how does proprioception involving position, velocity, and force feedback support stability and facilitate control of posture and movement. To answer these questions, we consider a simplified characterization of the postural control system that broadly speaking has two components: one, representing the musculoskeletal dynamics in the sagittal plane, the other representing the sensors (muscled spindle, GTO, and the vestibular system), and the CNS. The model includes important physiological parameters such as muscle (active and passive) stiffness properties, length and velocity feedback from the muscle spindle, force feedback from GTO, vestibular feedback from the Otolith system, and transmission latencies in the neural pathways. Finally, a neural PID controller is assumed to represent the CNS analogue in the model theoretic framework.

METHODS

The human body is modeled as a multi-segment structure comprising of skeletal, muscular, and sensory subsystems. The musculoskeletal system model consists of four planar rigid-body segments that approximate sagittal plane biomechanics. The segments represent a bilateral symmetrical arrangement of the feet, legs, thighs, and head-arm-trunk (HAT) with stationary foot segment. The model parameters, i.e., the segment length, mass, centre of gravity and moment of inertia, are based on gross anatomical properties of the human body (Stroeve, 1999). The length of the stationary foot segment defines the base of support (BOS) in the anterior-posterior direction. The leg, thigh, and HAT each have a single-rotational degree of freedom.

The CNS commands and active force generation in the muscle are represented by a second order muscle model (Winter and Stark, 1985) that consists of: a) the excitation dynamics from the motor control signal to the neural signal, b) the activation dynamics from the neural signal to the active state, and c) the contraction dynamics that characterizes the force velocity relation in combination with the fiber and series elastic (SE) force-length relation. The active and passive muscle stiffness and viscosity are modeled as intrinsic muscle impedance. The dynamics of muscle spindle and GTO are characterized by constant gains. The corresponding block diagram for posture and movement control is shown in Fig. 1.

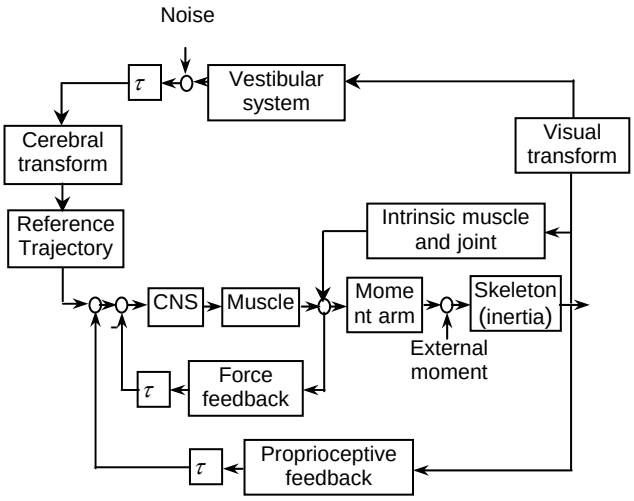

Figure 1: Conceptual block diagram of the human musculoskeletal control system with inherent muscle stiffness and viscosity, and physiological latencies in position, velocity, force, and vestibular feedback.

RESULTS AND DISCUSSION

For illustration purposes, an initial posture of $\varphi_i^0 = 0.15 \times [\pi/6 \;\; -\pi/3 \;\; \pi/12]'$ rad and a terminal posture of $\varphi_t = [\pi/8 \;\; -\pi/4 \;\; \pi/16]'$ rad are assumed; such a trajectory may, for example, represent stand-to-sit movement. The resulting limb trajectories are plotted in Fig. 2. It can be seen that the kinematics are dynamically stable and attain the desired steady-state posture. Further, the movement has negligible overshoot (~ 0.1%), and a low settling time (≤ 1 sec).

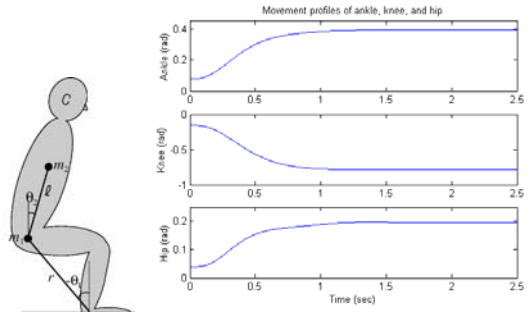

Figure 2: Physiological significance (left) and limb trajectories (right) for sit-to-stand transfer.

SUMMARY/CONCLUSIONS

Mechanisms of posture and movement control in the human body are investigated via a four-segment planar neuro-musculoskeletal model The model includes position, velocity, force, and vestibular feedback, the intrinsic stiffness properties of the muscle, and the physiological latencies of the motor servo system. The CNS control of the postural stabilization process is represented by three autonomous PID controllers, one each for the ankle, knee, and hip joints (Roy and Iqbal, 2006). Our simulation results confirm that the anatomical arrangement, active muscle stiffness, force and vestibular feedback, and physiological latencies of the body segments play a major role in shaping motor control processes in the human body.

REFERENCES

Barin, K. (1989). *Biol. Cybern.*, **61**, 37-50.

He, J., et al. (1991). *IEEE Trans. Autom. Cont.*, **36**, 322-332.

Kuo, A.D. (1995). *IEEE Trans. Biomed. Eng.*, **42**, 87-101.

Stroeve, S. (1999). *Biol. Cybern.*, **81**, 475-495.

Winters, J.M., Stark, L. (1985). *IEEE Trans. Biomed. Eng.*, **32**, 826-839.

van der Helm, F., Rozendaal, L. (2000). in *Biomechanics and Neural Control of Movement and Posture*, Springer-Verlag, Chapter 11, 164-174.

Iqbal, K., Roy, A. (2004). *ASME J. Biomechanical Eng.*, **126**, pp. 838-843.

Roy, A., and Iqbal, K. (2006). *ASME J. Biomechanical Eng.*, in review process.

3D JOINT CONTACT FORCES AT THE HIP, KNEE, AND ANKLE DURING RUNNING AT DIFFERENT STRIDE LENGTHS

W. Brent Edwards [1], Joshua M. Thomas[2], and Timothy R. Derrick [1]

[1] Iowa State University, Ames, IA, USA
[2] Trinity International University, Deerfield, IL, USA
E-mail: edwards9@iastate.edu Web: www.hhp.hs.iastate.edu

INTRODUCTION

Repetitive mechanical loading has been associated with lower limb joint pain (Radin et al., 1991). The joint contact forces that arise from mechanical loading are due to a combination of reaction forces and muscle forces. During running, ground reaction forces can be reduced by shortening stride length (Mercer et al., 2005). It is unclear if shortening stride length has similar effects on joint contact forces.

The purpose of this study was to determine if reducing stride length decreased joint contact forces and joint contact loading rates during running.

METHODS

Five experienced male runners participated in this study (age: 21.6 ± 3.3 yrs, height: 176.5 ± 2.9 cm, mass: 68.5 ± 4.6 kg). Kinematic and kinetic data were collected while subjects ran at their preferred stride length (PSL) and -10% their preferred stride length (-10%PSL). Subjects performed ten trials at each condition. Stride length was adjusted by having the subjects strike targets placed on the floor. A trial was considered successful if the subject consistently hit the targets and was within ± 5% their preferred running velocity. The average preferred running velocity was 4.2 ± 0.3 m/s.

Three dimensional kinematics of the thigh, leg, and foot were calculated using a flex/ext, abd/add, introt/extrot sequence. Inverse dynamics was used to obtain three dimensional joint reaction forces and joint moments at the hip, knee, and ankle. Muscle forces for 45 lower extremity muscles were then calculated using computer optimization.

The kinematic data were imported into a scaled SIMM 4.0 model to obtain maximal dynamic muscle forces, muscle moment arms, and muscle orientations at each 1% of stance. This information was then exported into Matlab 7.0.4 to calculate muscle forces using the *fmincon* optimization routine. The cost function to be minimized was the sum of cubed muscle stresses. The optimization was constrained so that the resulting hip, knee, and ankle moments equaled experimental data. Six moments were used in the optimization including: Hip flex/ext, abd/add, introt/extort; Knee flex/ext; Ankle flex/ext, inver/ever. The lower and upper bound muscle forces were originally set to zero and the maximal dynamic muscle forces respectively. These bounds were then adjusted in subsequent frames to prevent non-physiological changes in muscle force (Pierrynowski & Morrison, 1985).

Joint contact forces were calculated in the distal segment reference frame as the sum of reaction force and muscle forces crossing the joint. Peak instantaneous forces and loading rates were then calculated for the hip, knee and ankle joint in the axial and shear directions (anterior-posterior, or AP; medial-lateral, or ML). Peak forces and loading rates were averaged across trials for

each subject and effect sizes between conditions were calculated. We used Cohen's (1992) suggestion that effect sizes of .20 are small, .50 are medium, and .80 are large. Only variables with medium effect sizes, or better, are reported below.

RESULTS AND DISCUSSION

Axial joint contact forces were similar to those previously reported for running (Glitsch & Baumann, 1997). While axial forces were always compressive, the direction of AP and ML shear forces were dependent upon the joint and percentage of stance (Figure 1). Peak axial loading rates always occurred during the impact phase of stance between 0 and 30%. The occurrence of peak shear loading rate varied.

Medium effects were observed for ML hip force (-0.64), ML ankle force (-0.56), and ML ankle loading rate (-0.61). Large effects were observed for axial hip loading rate (-1.07), ML hip loading rate (-1.33), and axial knee loading rate (-0.82). For each variable the effect size was negative indicating a lower value during -10%PSL.

SUMMARY/CONCLUSIONS

These findings suggest that decreasing stride length may be an effective way to minimize repetitive mechanical loading that occurs during running. Future research will look to increase sample size to see if these trends are statistically significant.

REFERENCES

Radin, E. et al. (1991). *J. Orthop. Res.*, **9**, 398-405.

Mercer, J. et al. (2005). *J. Sport. Sci. Med.*. **4**, 144-152.

Pierrynowski, M., Morrison, J. (1985). *Math. Biosci.*, **75**(1), 43-101.

Cohen, J. (1992). *Psychol. Bull.,* **112***,* 155-159.

Glitsch, U., Baumann, W. (1997). *J. Biomech.,* **30,** 1123-1131.

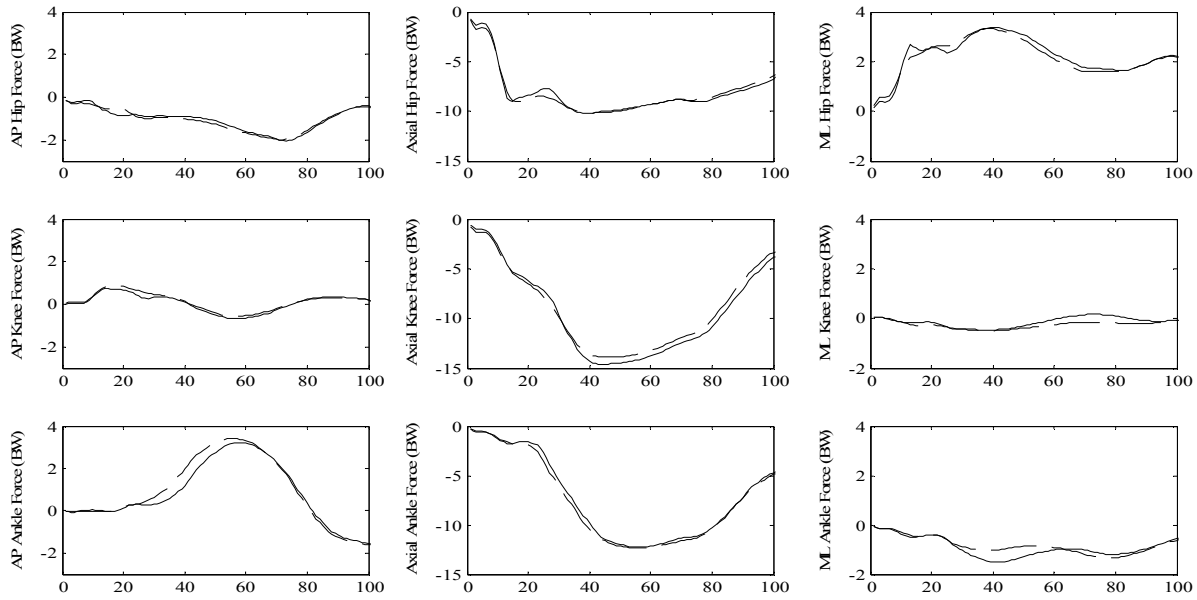

Figure 1: Ensemble average axial and shear joint contact forces at the hip, knee, and ankle for one subject. Solid line = PSL; Dashed line = -10%PSL; +AP = anterior shear; +Axial = tension; +ML = lateral shear.

Control System Development for Automatic Standing Balance using Functional Neuromuscular Stimulation (FNS) Following Spinal Cord Injury (SCI)

Raviraj Nataraj[1,3], Musa L. Audu[1,2,3], Robert F. Kirsch[1,2,3], and Ronald J. Triolo[1,2,3]

[1] Case Western Reserve University, Cleveland, OH, USA
[2] Louis Stokes Cleveland Veterans Affairs Medical Center, Cleveland, OH, USA
[3] Cleveland Functional Electrical Stimulation Center, Cleveland, OH, USA
E-mail: rxn25@case.edu, Web: http://fescenter.case.edu/

INTRODUCTION

Complete thoracic-level spinal cord injury (SCI) causes motor function loss at and below the chest/abdomen. This may result in the inability to stand or step independently. The CWRU/VAMC system (Davis et al., 2001) for standing uses open-loop stimulation via implantable stimulator to artificially activate extensor musculature to restore basic standing function. However, a user still requires an assistive device (e.g., walker) whereby he/she exerts significant upper-body effort to make postural corrections and maintain balance against potentially de-stabilizing perturbations. This can precipitate considerable fatigue and hinder manual functionality.

The goal of this project is to develop a sensor-feedback control system that will automatically detect postural disturbances and modulate muscle stimulation levels to assist in balance maintenance. For purposes of cosmesis and subsequent clinical acceptance, we look to develop a feedback system that requires a minimal number of sensors yet sufficiently describes changes in posture.

These sensor feedbacks will be used to drive an artificial neural network (ANN) actuator that is trained to output changes in muscle stimulation consistent with making postural corrections. The ANN is capable of mapping a non-linear input-output relationship that considers muscle actuation across multiple joints in a three-dimensional space.

METHODS

To minimize live patient testing during controller development, we prototype various control schemes initially in simulation. For this purpose, our lab has developed a three-dimensional model of human bipedal stance (Zhao et al., 1998). The model includes twelve degrees of freedom (DOFs) across the lower extremities (ankles, knees, hips), 3 DOFs for the trunk, passive joint properties, and Hill-type musculature targeted by 16 channels of stimulation.

The actuator ANN used for steady-state PD (proportional-derivative) control is trained on statically optimized joint angle and muscle excitation data across a comprehensive three-dimensional posture space. For each test posture configuration, the optimization routine is required to determine the muscle excitations necessary to produce joint moments corresponding to that posture. The joint moments required for a particular posture are proportional to the joint angle errors relative to the erect position. This is consistent with the notion that a simple static stiffness may sufficiently describe basic standing perturbation responses (Matjacic, 2001).

Assuming an effective closed-chain for bipedal standing, we hypothesize that

minimal instrumentation can sufficiently estimate lower extremity joint angles for feedback control. The aforementioned posture space is used to non-linearly map pelvic position inputs to estimated lower extremity joint angle outputs. These estimates are subsequently used for feedback. Finally, another ANN actuator is trained to respond to trunk accelerations induced during a perturbation to act as a predictive controller necessary to compensate for the non-linear delay in muscle force production. This ANN is trained to produce muscle excitations that are consistent with maintaining an inverted pendulum model of stance.

RESULTS AND DISCUSSION

A globally convergent solution is not feasibly determined from the aforementioned ANNs. Therefore during forward simulations, a point-force controller is included at each shoulder position. This controller is representative of the upper-body effort the user may exert upon an assistive device for stabilization. Automatic controller performance is thereby evaluated by a reduction in the shoulder point-force output. During a successful crouch-to-erect restoration, the joint-angle estimates used for steady-state PD control feedback are sufficiently well correlated (table 1) to the actual joint angles. For simulations whereby a 100-Newton, 300 msec, forward perturbation is applied from erect stance at the thorax center of mass, the results are shown in figure 1.

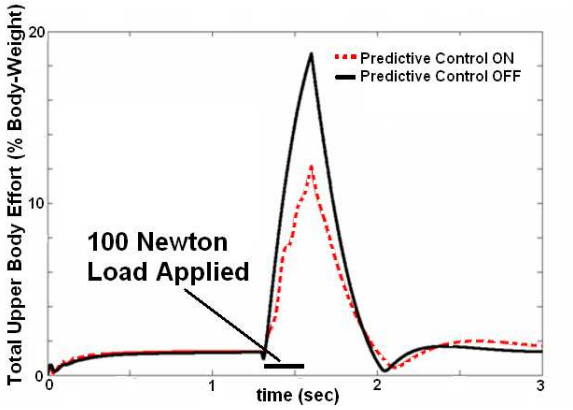

Figure 1: Total upper-body (all shoulder forces) load necessary for stabilization with and without the predictive controller module against 100-Newton perturbation at thorax.

Overall, the steady-state controller with joint angle feedbacks was successful in providing assistance (reduction in upper body effort) for erect postural restoration from several different initial positions. The inclusion of the predictive controller provides the necessary fast-acting response for reducing upper body effort used for re-stabilization given a perturbation from erect stance.

REFERENCES

Davis et al., (2001).
Journal Rehab Res Dev, **38 (6)**, 609-617
Zhao et al., (1998).
Proc IEEE EMBS, **20 (5)**, 2605-2608
Matjacic, Zalatko (2001).
Neuromodulation, **4 (1)**, 37-46.

ACKNOWLEDGEMENTS

This work is funded by NIH: R01NS040547-03 Research Project Grant

Table 1: Correlation between actual joint angle and joint angle estimate used for feedback during three-second forward simulation for crouch-to-erect restoration.

Joint Angles:	**Hip**	**Knee**	**Ankle**
Left:	0.996	0.889	0.782
Right:	0.998	0.896	0.774

EFFECTIVE FIELDS IN CONTROL MUSCLES: EFFICACY OF CONTROL DEPENDS ON BIOMECHANICAL CONTEXT IN AN INSECT

Simon N. Sponberg[1], Andrew J. Spence[2], Chris H. Mullens[1] and Robert J. Full[1]

[1]University of California at Berkeley, Berkeley, CA, USA
[2]Royal Veternary College, University of London, North Mymms, Hatfield, UK
E-mail: sponberg@berkeley.edu, Web: http://polypedal.berkeley.edu

INTRODUCTION

Recent research (e.g. Koditschek et al. 2005) suggests an axis of neuromechanical control for locomotion in animals. On one side the slowest movements are dominated by long-latency, slow, precise responses from neural feedback. On the other side, the fastest behaviors with high-bandwidth constraints demand passive dynamic stability arising from mechanical feedback or preflexes. The majority of behaviors must integrate these two mechanisms, requiring an understanding of how reflex modulation of neuromuscular commands are decoded through the musculo-skeletal system.

To probe this relationship of reflexes and mechanics we must quantify the effect of modifying motor activation patterns on the center of mass (COM) dynamics of the body. We define this set of responses to a muscle's activation as its *effective field*, a motor version of a sensory neuron's receptive field. If we alter the pattern of muscle activation in a manner identical to its range of possible reflex response then the effective field is a quantification of a muscle's potential to control the body during a behavior.

Using this approach we can explicitly describe an individual muslce's *in vivo* function. Reflex modulation is often assumed to function similarly in different behavioral contexts. We can now directly address this hypothesis by compared a muscle's effective field under different behavioral circumstances.

METHODS

As a first step, we focus specifically on a putative control muscle in a cockroach because it has a known, simple pattern of reflex modulation. We target muscle 137, a femoral extensor, which plays a role in the control of body orientation during obstacle negotiation and perturbation recovery. Previous studies (Sponberg, *et al.* 2004) have shown that the critical parameter of the motor code that is modulated in the femoral extensors like muscle 137 is the number of fast motor neuron action potentials received per step.

To repeatedly and precisely represent these changes in the motor code, we stimulated muscle 137 in a phase locked manner. We record EMGs in real-time and convert these signals into logic pulses that can be used to trigger a stimulator with variable delay. Tuning stimulus voltage and timing enables phase locked spike addition through a second pair of electrodes (Figure 1).

To record the kinematic and kinetic responses of the cockroach's COM we mount a 3-axis MEMS accelerometry backpack on its back. High-speed videography of a 3D cross on top of the accelerometer provides g correction and gives pitch, roll, and yaw of the body.

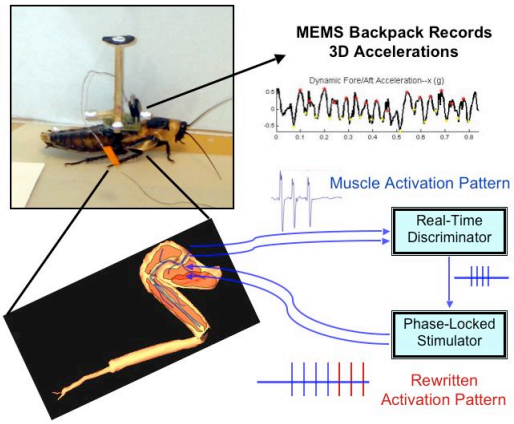

Figure 1: A cockroach mounted 3-D accelerometer backpack and neural recording/stimulus diagram for simultaneous real-time modulation of muscle activation patterns and recording of body dynamics.

RESULTS AND DISCUSSION

Activation of muscle 137 leads primarily to roll responses with vertical and lateral accelerations ($p<0.0001$). Comparison of muscle effective fields shows that muscle 137 can provide finely graded control responses during station-keeping ($p=0.007$), with each additional spike addition resulting in approximately a 1 degree roll response.

Interestingly, similar rewriting of the motor code in running cockroaches produces significantly different effects (Figure 2). Precise reflex control of the peak roll response is lost at high speeds ($p=0.35$). Further, the response is not a simple summation of running kinematics with stationary effects of spike additions. Whereas modifying muscle activation by even a single spike during station-keeping significantly altered the maximum roll, equivalent stimulation during rapid running did not produce similar increases.

Our results demonstrate that changes in motor activation from neural feedback produce behaviorally dependent changes in the animal's dynamic state. This suggests that the motor coding depends on the mechanical state of the organism.

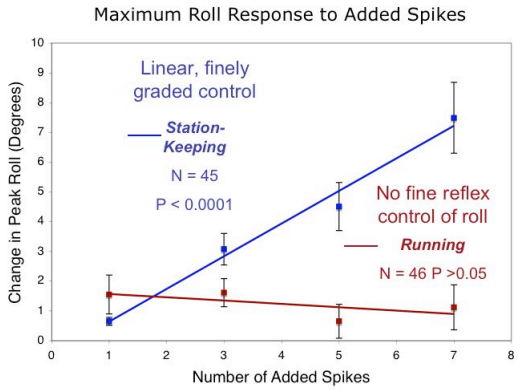

Figure 2: The control effects of adding spikes to muscle 137 differ between the two behaviors, station-keeping and running.

More generally, constructing effective fields enables us to quantify control and can be directly translated to dynamical systems models. In biology, this holds important implications for interpreting neural signals in the motor code and understanding what constitutes a "control muscle." In engineering, using the same actuators with different control strategies could provide valuable insight into the biologically inspired design of legged robots.

SUMMARY/CONCLUSIONS

We have developed a method for real-time phase locked stimulation of muscles while recording the biomechanical responses to stimulation. We quantify these relationships and have shown that interpreting the control potential reflex modulation of muscle activation depends on the state of the system. Neuromechanical integration is therefore required to understand reflex control of locomotion.

Koditschek, *et al.* (2004). *Arthropod Structure and Development*. **33**(3): 251-272.
Sponberg, S. *et al.* (2004). *Integrative and Comparative Biology.* 44 (6): 644.

INCREASED STRESS PRODUCTION AND RESPONSE TO INJURY IN DESMIN KNOCKOUT MUSCLES RESCUED BY PLASMID TRANSFECTION

Michelle P. Palmisano[1], Shannon N. Bremner[1], and Richard L. Lieber[1]

[1]Departments of Orthopaedic Surgery and Bioengineering
University of California-San Diego and Veterans Affairs Medical Center, La Jolla, CA, USA
E-mail: rlieber@ucsd.edu, Web: muscle.ucsd.edu

INTRODUCTION

The muscle intermediate filament protein desmin provides structural support and integrates muscle force throughout the cell (Lazarides, 1980). In the absence of desmin, muscles have disorganized myofibrils (Shah *et al.* 2002) and are injured less compared to their wild-type counterparts during eccentric contraction-induced injury (Sam *et al.* 2000). These changes could result directly from lack of desmin or could be due to secondary changes that result from development in the absence of desmin. To determine whether desmin plays a direct role in stress generation and response to injury, desmin knockout muscles were transfected with a GFP-desmin DNA plasmid and their mechanical function was probed using a high stress eccentric contraction model.

METHODS

All procedures were performed on mice in accordance with the NIH Guide for the Use and Care of Laboratory Animals. For transfection, GFP-desmin plasmids were injected into the tibialis anterior (TA) muscles of desmin-null mice and DNA incorporation facilitated by electroporation (Ichor Med. Systems. Inc., San Diego, CA). Seven days later, the fifth toe extensor digitorum longus (EDL), which was also transfected, was excised and mounted in a chamber bathed in Ringer's solution from one of five groups (n=7-12/group): (1) wild-type (WT), (2) desmin knockout (KO), (3) KO transfected with a plasmid encoding GFP-desmin, (4) KO transfected with GFP plasmid alone, and (5) KO transfected with PBS (EP only). For mechanical testing, muscle sarcomere length was set to 2.91 μm by laser diffraction and maximum isometric tension was measured twice at 3 min intervals.

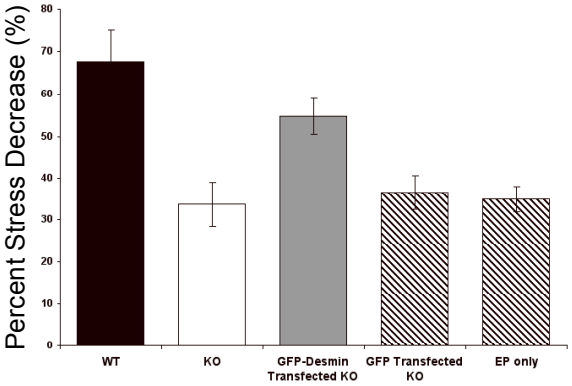

Figure 1: Percent stress decrease of five experimental groups. KOs (open bar) have about the same stress decrease of either KO transfected with GFP or PBS controls (hatched bars). KOs transfected with GFP-desmin (grey bar) were injured almost to the level of WT muscles (black bar).

Muscles were then eccentrically-activated by stimulating isometrically for 200 ms, stretching the muscles by 15% of the fiber length (L_f) and holding this length for an additional 500 ms. This procedure was repeated for 10 eccentric contractions every 3 min as previously described (Sam *et al.* 2000) to produce muscle injury. Maximum isometric tension was measured twice after the exercise bout. Percent stress decrease (change in post-eccentric maximum isometric stress relative to pre-eccentric maximum isometric stress) was compared across groups by one-way ANOVA as the

index of muscle injury. Paired comparisons were made between groups with post hoc Tukey tests. All results are presented as mean±standard error. Significance level (α) was set to 0.05. To quantify GFP-desmin expression, western blots were obtained using monoclonal antibodies against desmin (DER11, Novacastra Laboratories) for endogenous GFP-desmin using an exogenous desmin standard for calibration. All bands were quantified using enhanced chemiluminescence (ECL; Amersham Pharmacia Biotech).

RESULTS AND DISCUSSION

Injury due to eccentric contraction is represented by percent decrease in maximum isometric stress. As previously demonstrated (Sam *et al.* 2000) WT muscles had the largest drop in stress (Fig. 1, black bar), decreasing by 67.5%±7.7, which was significantly greater than KO controls which decreased by only 33.7%±5.2 (Fig. 1, open bar; $p<0.05$). KO muscles transfected with GFP or PBS were not significantly different from KO controls (Fig. 1, hatched bars 36.5%±4.1 and 34.9%±2.9, $p>0.05$, respectively). In contrast to all other KO muscle groups, KO muscles that were successfully transfected with GFP-desmin showed a significantly greater stress decrease of 54.8%±4.3 (Fig. 1, grey bar) compared to other KO muscle groups ($p<0.05$). A nonlinear relationship between desmin expression levels and injury level was observed with higher desmin levels corresponding to greater amounts of injury (Fig. 2). This may imply some type of biomechanical cooperativity across the fiber.

SUMMARY/CONCLUSIONS

Here we provide direct evidence that the desmin protein increases the efficiency of stress production by the muscle and increases injury resulting from eccentric contraction. Thus, GFP-desmin not only correctly localizes at the Z-disk, but also incorporates and plays a functional role in skeletal muscle after expression.

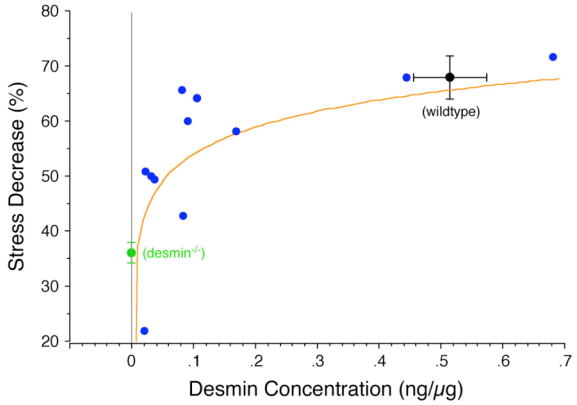

Figure 2: Percent stress decrease as a function of desmin concentration. Wildtype muscles have the greatest stress injury (black bars) while desmin null muscles have the least (green bars). Individual transfected muscles are shown as blue circles and have intermediate injury levels.

To date there are over 20 known different mutations in the desmin gene that result in an accumulation of desmin into clumps scattered throughout the cytoplasm (Goldfarb *et al.* 2004). This study has important implications in the pursuit of gene therapy models for rehabilitation and in understanding the apparently biomechanical etiology of desmin related muscle diseases.

REFERENCES

1. Lazarides (1980) . *Nature* **283**:249-256.
2. Shah *et al.* (2002). *J. Exp. Biol.* **205**:321-325.
3. Sam *et al.* (2000). *Am. J. Physiol.* **279**:C1116-C1122
4. Goldfarb *et al.* (2004. *Brain* **127**:723-734.

ACKNOWLEDGEMENTS

We acknowledge NIH grant AR40050 and the Department of Veterans Affairs.

THE EFFECTS OF TASK ROTATION AND ORDER ON DELTOID MUSCLE FATIGUE

Sachin Raina [1] and Clark Dickerson [1]

[1] University of Waterloo, Waterloo, ON, CAN
E-mail: smraina@uwaterloo.ca

INTRODUCTION

Job rotation is an industrial practice that is often applied with the intention of reducing muscle fatigue, exposure, or workload. It is believed that this reduction can help lower the risk of developing or exacerbating work-related musculoskeletal disorders (WMSDs). Recent survey results indicated that 42.7% of 178 manufacturers evaluated in the Midwest United States used job rotation as part of their administrative work design (Jorgensen, 2005).
Despite its popularity, the specific effects of job rotation on the musculoskeletal system are not well known (Jorgensen, 2005; Kuijer, 2005). While it is intuitive that rotating between jobs that involve different regions of the body over a period of time may pose less risk of developing a WMSD than performing one job over this same period of time, the same cannot be said for jobs that involve similar muscles. In the shoulder, for instance, many muscles are frequently active, albeit differentially, in movements that are apparently unique (Sigholm, 1984). The effect job rotation would have in this scenario is not obvious.

This study aimed to determine: 1) the impact of rotating between two tasks involving the same principal muscles; and 2) the importance of the order of task rotation, both with respect to muscle fatigue.

METHODS

Ten healthy subjects (5 male, 5 female, mean age = 25.7) took part in this study. Two repetitive, unloaded arm movements were used: forward shoulder flexion (A) and shoulder abduction in the frontal plane (B). Subjects completed four task combinations, generating four conditions: AA: four continuous minutes of task A; AB: two minutes of task A, then two minutes of task B, and their counterparts, BA and BB. Maximum voluntary force (MVF) for shoulder elevation was measured at the hand immediately before and after each trial. Electromyographic (EMG) signals from the anterior, middle, and posterior deltoids were measured during the trials, as were ratings of perceived exertions (RPE). Raw EMG was full-wave rectified and low pass filtered with a cut off frequency of 3Hz. EMG amplitude (AMP) was normalized to 100% maximum voluntary contraction (MVC). Because EMG AMP varies during a movement with joint angle (Potvin, 1997), peak AMP values were used for comparisons. Integrated EMG (iEMG) values were calculated using a trapezoidal method on the linear enveloped data. Mean power frequencies (MPF) were also used to assess muscle fatigue. One way ANOVAs were used to compare AMP, iEMG, MPF, and RPE between conditions for each muscle part. Changes in MVF post-exercise were also evaluated.

RESULTS AND DISCUSSION

Overall Indicators of fatigue: While each condition caused an MVF decrease (mean = 16.8 ± 9%, $p<0.05$) after exercise, there were no differences between the magnitude of the decrease across conditions. Further,

though minor RPE variations existed, end-state RPE was consistent across conditions.

EMG Indicators of fatigue: There were no differences in EMG amplitude between conditions for anterior deltoid. Movement B resulted in greater levels of EMG AMP than movement A in the middle (Figure 1) and posterior deltoids ($p<0.05$). Differences in end-state MPF were seen between AA and BB in these same deltoid parts. iEMG for BB was higher than all other conditions for middle and posterior deltoid ($p<0.0005$).

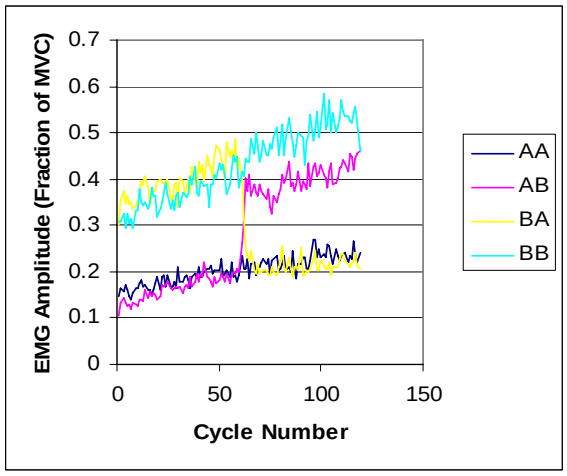

Figure 1: Linear enveloped EMG amplitude of middle deltoid during 4 different trials; AA, AB, BA, BB. Peak EMG and iEMG were greatest during trial BB

In the middle deltoid, task A was found to be less demanding than task B. The iEMG results (Table 1) showed significant differences between task conditions. Results indicate that combining less and more stressful tasks resulted in significantly less muscular demand than performing only the more stressful task. A combination of the two tasks did not require more muscular demand than performing just the less stressful task. These results also suggest that varying the order of task rotation (AB vs. BA) has no impact.

Table 1: iEMG values for all muscles across all conditions. Bolded values are significantly greater than other conditions for a given muscle.

	Condition			
Muscle	**AA**	**AB**	**BA**	**BB**
ANT	47.91	51.86	47.94	52.92
MID	28.89	32.84	43.13	**53.30**
POST	5.869	17.99	15.53	**24.63**

SUMMARY/CONCLUSIONS

Two findings relating to job rotation and the risk of injury emerged from this study:
1. When performing two tasks with different muscular demands, fatigue may be reduced by rotating between the tasks rather than only performing the higher demand task.
2. Rotation order (AB vs. BA) had no apparent impact on localized muscle fatigue.

REFERENCES

Jorgensen, M., et al. (2005).
Ergonomics, **48**, 1721-1733.
Kuijer, P.P., et al (2005).
Am J Ind Med, **47**, 394-402.
Potvin, J.R., (1997).
J Appl Physiol, **82**, 144-151.
Sigholm, G. et al. (1984).
J Orthop Res, **1,** 379-86.

ACKNOWLEDGEMENTS

Partial funding for this study was provided by the Workplace Safety and Insurance Board of Ontario and the Centre for Research Expertise for the Prevention of Musculoskeletal Disorders.

Selecting Among Neuromechnical Control Architectures using Kinematic Phase and Perturbation Experiments

Shai Revzen[1], Daniel E Koditschek [2], and Robert J Full [1]

[1] University of California, Berkeley, CA, USA
[2] University of Pennsylvania, Philadelphia, PA, USA
shrevz @ berkeley.edu, http://polypedal.berkeley.edu

INTRODUCTION

We use an experimental paradigm grounded in dynamical systems (DS) theory to select which among several competing neuro-mechanical control architectures (NCA) could be in use in a given rhythmic motor behavior by using kinematic data alone.

Our method allows us to extrapolate animal motions based on a few consecutive video frames, and compare the predicted motion to perturbation experiment outcomes.

We apply the method to the study of control of running in the cockroach *Blaberus discoidalis,* and discuss its broader utility in a variety of biomechanical problems, e.g. in potential clinical application of motor learning tasks such as [Sternad-04].

NEURAL CONTROL FRAMEWORK

We describe neuromechanical control as occurring in the framework outlined by the block diagrams in Figure 1. The figure presents several alternative NCA that may be used to stabilize a running gait against environmental perturbations. These differ in how far up the neural control hierarchy they employ feedback, if at all. In each NCA the "Brain" specifies parameters to a pattern generator (CPG) emitting a pattern modulated by proprioceptive Tracking that applies sensory feedback to the signal before using it to drive the muscles. Mechanics generate their own feedback dynamics with the body, and motions produce sensory

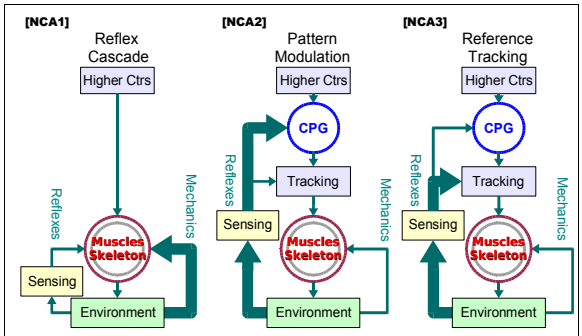

Figure 1: Neuro-mechanical Control Architecture block diagrams

changes that are processed through reflex pathways. [NCA1] motions cause interactions triggering subsequent motions reflexively; [NCA2] feedback strongly modulates the pattern generator; [NCA3] proprioceptive feedback makes the body track a reference signal from an immutable pattern generator.

THEORETICAL FRAMEWORK

Dynamical systems that function as nonlinear oscillators are a natural choice of model for equations governing rhythmic behaviors such as rapid locomotion. One of the fundamental tools of the mathematical theory of such oscillators is the idea of "phase" [Guckenheimer-83].

We suggest that phase, in its strict mathematical sense, can be estimated effectively from "kinematic phase" - the phase of the kinematic state of the animal along its characteristic rhythmic cycle of poses (Figure 2 below [A,B]). Kinematic phase provides a means for predicting

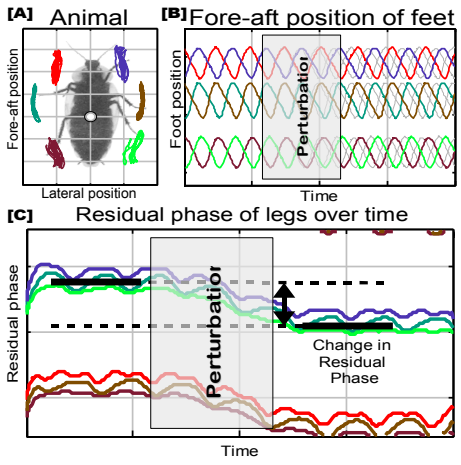

Figure 2: [A] Cockroach tarsi (foot) tracks in body frame. [B] Fore-aft positions of feet (color) and extrapolated model (gray). [C] Residual kinematic phase of the tarsi (feet).

animal motions by extrapolating the trend of the phase variable and converting it back to a pose (Figure 2,[B] gray).

While continuous phase resetting is likely in NCA1 reflex cascade controllers like WalkNet [Cruse-98], NCA2 feed-forward control as suggested in [Jindrich-02] maintains phase or resets it in discrete jumps. Figure 2 [C] illustrates a phase change observation using our technique. Long term frequency changes provide evidence that feedback has modified the functioning of the pattern generators, possible only in NCA3 (see Figure 1).

METHODS

Adult *B. discoidalis* cockroaches were induced to run and filmed with a high speed video camera, tracking body and tarsus motions in the horizontal plane. We collected 42 runs of animals running over a 3mm obstacle, 75 runs of a lateral impulse perturbation of 50 cm/sec and 20 unperturbed runs for validation.

The tarsus motions in the fore-aft direction were used to generate a kinematic phase estimate, and the pre-perturbation trend fitted with a robust least squares regression line. The post perturbation residuals were used to select among the NCA alternatives.

RESULTS

In 40 out of 42 obstacle trials significant phase changes were observed, but average frequency change was 0 and independent of phase change. All lateral impulse trials showed significant frequency changes at with a delayed onset that depended strongly on the phase at perturbation time.

SUMMARY/CONCLUSIONS

The lateral perturbation results reconfirm the result of [Jindrich-02] that initial lateral perturbation recovery is mechanically mediated and neural feedback is evident only after times on the order of a step. The structure of the obstacle perturbation outcomes suggest a novel control model that we will briefly present.

Kinematic phase has been shown to be a useful tool for generating experimentally tractable quantitative predictions and elucidating some of the interconnections in the feedback pathways governing running in *B. discoidalis* cockroaches.

REFERENCES

Cruse H., Kindermann T., Schumm M., Dean J., Schmitz J. (1998). *Neural Networks*, v. 11, **7-8**, 1435-1447

Guckenheimer J., Holmes P. (1983). *Nonlinear Oscillations, Dynamical Systems, and Bifurcations of Vector Fields*. Springer-Verlag

Jindrich D. L., Full R. J. (2002) *J. Exp. Biol.,* v. 205, **18**, 2803-2823.

Sternad D., Dijkstra T. M. H. (2004) *J. Clin. Neurophysiol.*, **21,** 215–227.

THE EFFECT OF BONE MICROSTRUCTURE ON MICROCRACKS PROPAGATION TRAJECTORY

A. Raeisi Najafi[1], A.R. Arshi[1], M.R. Eslami[1], H.R. Katoozian [1], M.H. Moeinzadeh[2],E. Mallakin[1]

[1] Amirkabir University of Technology, Tehran, Iran
[2] University of Illinois at Urbana-Champaign, USA
E-mail: manssour@uiuc.edu

INTRODUCTION

Haversian cortical bone is a biological fiber – ceramic matrix composite material (Yang et al. 2006) with varying microstructural arrangements at different scales that provides sites for microcracking. In this composite material, osteons are considered as fibers and interstitial tissue as a matrix (Raeisi Najafi et al. 2007a). The interface between the osteons and interstitial tissue is also presented by cement line.

Fracture phenomena in the Haversian cortical bone are primarily affected by the morphology and heterogeneity of the microstructure (Huang et al. 2006; Raeisi Najafi et al. 2007b). Any variations in these parameters caused by the aging process, on the other hand, make the problem rather more complicated. As an example, the aging process increases the differences in the mechanical properties of osteons and interstitial tissue. This has a profound effect upon the fracture behavior of bone. It was thus necessary to enhance the understanding of the mechanisms governing fracture in haversian cortical bone.

To this effect, the focus of this paper is to evaluate the microstructural effect of osteonal cortical bone upon the fracture phenomenon. The approach is to provide a suitable fracture model of the microstructure using finite element method (FEM) and then to evaluate the modeling outcomes by studying the SEM micrographs of a fracture test.

METHODS

Finite element model
In this study, the osteons are considered as fibers since they are approximately circular in shape and orientated parallel to the longitudinal axis of the bone. Furthermore, the interstitial tissue which fills the space between the osteons is considered as a matrix. The cement line or the interface between the osteon and the interstitial tissues is also included in the model.

Mechanical properties of bone constituents could be severely affected by factors such as bone type, anatomical location, age, gender and others. To this effect, values of 15-25 GPa for osteonal effective elastic modulus (E_o) and 20-27 GPa for interstitial tissue elastic modulus (E_i) are thus adopted for the evaluation of the effect of mechanical properties upon microcrack behavior. Here, Poisson's ratio for the osteon and the interstitial bone is assumed to be 0.3.

The mechanical characteristics of the cement line tissue have also been the subject of different studies. A series of reports consider this tissue softer than its surrounding tissues (Hogan, 1992). Other researchers such as Curry (1984) suggest a more mineralized structure and thus a higher modulus of elasticity (Hogan, 1992). In this paper, following the suggestion made by Advani et al (1987), the simulation is repeated twice for values of 10 and 30 GPa with the assumed Poisson's ratio of 0.4 (Hogan, 1992).

The computer program Casca Version 1.4 is used to produce a two-dimensional mesh. Fracture analysis is performed using Franc2D which is a Finite Element Modeling tool. The model is then used to analyze fracture propagation.

Experimental test
Compact bone samples are removed from bovine femur within 24 hours of slaughter. Distal and proximal ends are removed and the remaining section is divided into six approximately 5 cm long portions. The portions are cleaned from any soft tissues, preparing the way to obtain 23 standard (ASTM-E399) CT samples. Samples are mounted on a dynamic testing machine (Zwik/Roell 321 htm 123) using specially prepared fixtures. Slow fracture condition occurs during tension loading at a crosshead rate of 0.005 mm/sec. Fractured samples are gold coated at the pressure of 0.001 mbar and the SEM produces photographs of the fracture surfaces.

RESULTS AND DISCUSSION

Finite element model
In the first case, the edge microcrack is situated in a vertical direction to the loading (Figure 1). It is shown that within the adopted range of elastic moduli for different tissues, the microcrack trajectories are deviated from the osteon.

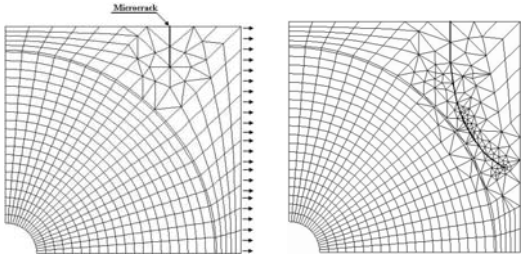

Figure 1: Microcrack propagation trajectory under tension.

Fracture test
A fracture surface is shown in Figure 2. The precrack orientation is perpendicular to longitudinal bone axis. The microcrack deviation from the osteon or its halt, once approaching the cement line boundary is evident in this picture.

Microcrack propagation trajectory is influenced by the Haversian cortical bone microstructure. The Scanning Electron Microscope photographs of fracture surfaces and the results of finite element modeling seem to be supporting one another. Results indicate that some of the microcracks are deviated as they approach the osteons. This deviation is dependant upon such parameters as osteon density. When the distance between osteons is small and the osteon density is higher, then microcrack propagation can not follow a trajectory between the osteons and stops at the cement line boundary. It could therefore be concluded that osteons act as a barrier against microcrack propagation.

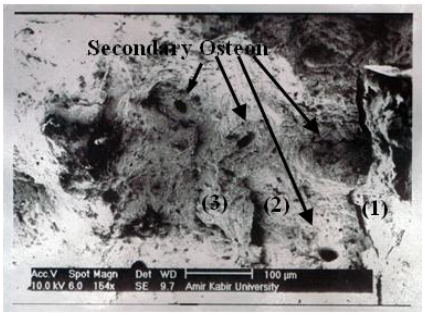

Figure 3: SEM fracture surface picture of a bovine femur sample.

REFERENCES

Hogan, H.A. (1992), *Journal of Biomechanics*, **25**(5), 549-556.
Huang, J.et al. (2006). *Materials and Design*, **27**, 461–469.
Raeisi Najafi, A. et al. (2007a). *Medical Engineering and Physics*, **29**, 708-717.
Raeisi Najafi, A. et al. (2007b). *Journal of Biomechanics*, in press.
Yang, Q.D. et al. (2006). *Biomaterials*, **27**, 2095–2113.

UPPER EXTREMITY KINEMATIC MODEL FOR WALKER ASSISTED GAIT

Kelly M.B. Strifling [1], Mei Wang [2], Kevin Cao [1], Jeffrey Ackman [3], Jeffrey Schwab [2], and Gerald F. Harris [1,2]

[1] Orthopaedic and Rehabilitation Engineering Center (OREC), Marquette University, Milwaukee, WI, USA
[2] Department of Orthopaedic Surgery, Medical College of Wisconsin, Milwaukee, WI, USA
[3] Motion Analysis Laboratory, Shriners Hospital for Children, Chicago, IL, USA
E-mail: kelly.strifling@mu.edu

INTRODUCTION

Recent literature has begun to explore the value of upper extremity (UE) modeling. Existing UE models vary according to task being performed (Newsam 1999, Petuskey 2007). The International Society of Biomechanics (ISB) has played a leading role in standardizing UE motion through joint recommendations (Wu, 2005). However, UE joint motion is very complex, so there is considerable difficulty in developing a standard model for all applications. The focus of this study is to design and evaluate an upper extremity model to be used with children with cerebral palsy using walkers. Our group previously developed and validated an UE model to be used with normal adults (Bachschmidt, 2001). The adult model aided in the development of the current pediatric model.

METHODS

The design of the pediatric model separates the UEs into seven segments: the torso, humeri, forearms, and hands. During data collection, all segments were represented by a minimum of three markers, with the torso having six, for a total of eighteen anatomical markers. When recorded in space the markers described the positions of the seven defining segments and create coordinate systems for each segment. Each adjacent segments' coordinate systems are related to one another through joints. The torso and humerus are connected by a three degree of freedom shoulder (glenohumeral) joint, with motion described as ab/adduction, flexion/extension, and internal/external rotation. The humerus is connected to the forearm by a two degree of freedom elbow joint, with motion of flexion/extension and pronation/supination. The forearm joins the hand through a two degree of freedom wrist joint, with motion in ulnar/radial deviation, and flexion/extension. The torso orientation is described with respect to the lab coordinate system. All segments are defined by local coordinate systems (Fig. 1).

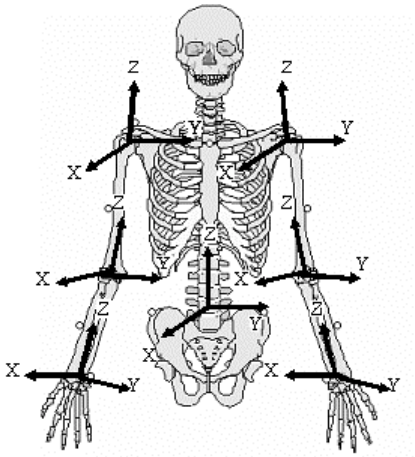

Figure 1: Segmental Axes

The local coordinate systems are related to one another by a series of Euler angle rotations, sequenced flexion/extension – ab/adduction – internal/external rotation. Equations 1-4 give the individual rotation matrices and equation 2 is the rotation matrix. A Vicon 524 motion analysis

system comprised of 15 cameras, and 120 Hz capturing rate, recorded the data.

$$(1)\quad [R_Y(\alpha)] = \begin{bmatrix} \cos\alpha & 0 & \sin\alpha \\ 0 & 1 & 0 \\ -\sin\alpha & 0 & \cos\alpha \end{bmatrix}$$

$$(2)\quad [R_X(\beta)] = \begin{bmatrix} 1 & 0 & 0 \\ 0 & \cos\beta & -\sin\beta \\ 0 & \sin\beta & \cos\beta \end{bmatrix}$$

$$(3)\quad [R_Z(\gamma)] = \begin{bmatrix} \cos\gamma & -\sin\gamma & 0 \\ \sin\gamma & \cos\gamma & 0 \\ 0 & 0 & 1 \end{bmatrix}$$

$$(4)\quad [R] = [R_Z(\gamma)]^T [R_X(\beta)]^T [R_Y(\alpha)]^T$$

Previously our group completed a static linear, dynamic linear, and dynamic angular validation of segmental models of the UE (Hingtgen, 2006). The resulting pediatric UE model was then evaluated by comparing it to our adult model (Bachschmidt, 2001). The same subject data was processed with each model and analyzed. Following evaluation, the current model was applied to three subjects with spastic diplegic cerebral palsy using posterior walkers. Assessment included a biomechanical evaluation of the shoulder joint in the coronal, sagittal, and transverse planes.

RESULTS AND DISCUSSION

The validation testing indicated a static linear accuracy (RMS error) of 31% (x-axis), 20% (y-axis), and 73% (z-axis). Dynamic linear and angular results showed 36% and 160% accuracy, respectively (Hingtgen, 2006). Model comparisons illustrated a maximum absolute error difference of ≤ 0.62 degrees in all planes of the shoulder, elbow, and wrist joints. Clinical results of the model application in three subjects are displayed in Figure 2. The average motions of the shoulders are plotted.

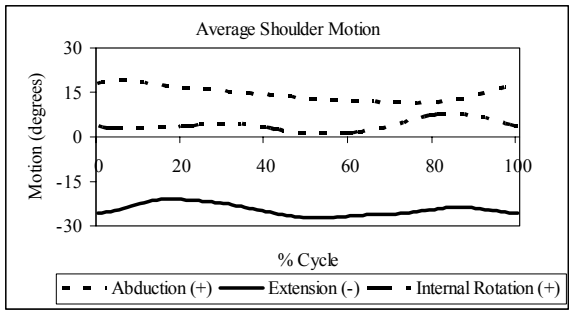

Fig. 2: Average Shoulder Motion

Results indicate that the shoulder is abducted, extended and internally rotated. The average joint motion is 14.3 degrees of abduction, 24.5 degrees of extension, and 3.7 degrees of internal rotation. The positioning of the joint is affected by the location of the posterior walker behind the subjects. This may also be due to the amount of spasticity in the UEs or lower extremities, and hand dominance. The UE kinematic model has been successfully evaluated and applied to these subjects with cerebral palsy. Additional testing is currently underway with a larger population. These results may enable clinicians to quantitatively evaluate joint movement and more effectively prescribe appropriate walker geometry.

REFERENCES

Bachschmidt, R.A. (2001). IEEE TRE, **9**(1), 96-105.

Hingtgen, B. et al. (2006). *J. Biomechanics*, **39**, 681-688.

Kreulen, M. et al. (2007). *Gait and Posture*, **25**, 485-492.

Newsam, C. et al. (1999). *Gait and Posture*, 10, 223-232.

Petuskey, K. et al. (2007). *Gait and Posture*, **25**, 573-579.

Wu, G. et al. (2005). J. Biomechanics, **38**, 981-992.

ACKNOWLEDGEMENTS

This project is supported by NIDRR grant H133G010069.

THE EFFECTS OF STEPPING OFF VS. HOPPING OFF A BOX ON CALCULATED DROP HEIGHTS IN TWO-LEGGED LANDINGS

Mostafa Afifi and Richard Hinrichs
Arizona State University, Tempe, AZ, USA
e-mail: mostafa.afifi@asu.edu

INTRODUCTION

When studying the mechanics of landing, the common practice is to have study participants step off or hop off a box onto the ground below. The box is intended to control for the height of the jump (Swartz et al., 2005). Thus, the step off or hop off studies assume that dropping in this case will be similar to landing from an actual countermovement jump from the ground. Recently we have reported the difference in mechanics of landing from a counter-movement jump and stepping off a box (Afifi and Hinrichs, 2006). Although both landings are different, stepping of a box may still be used when investigating other tasks such as falling if the drop height is consistent. However, in our study we noticed that calculated drop heights were approximately 10 cm less than the actual box height putting in question the validity of many studies that assumed drop heights were the same as box heights.

The purpose of the study was to investigate the difference in calculated drop heights from stepping off and hoping off boxes of different heights.

METHODS

Twenty active college students (10 males, 10 females) volunteered to participate in the study. Participants were excluded if they had any orthopedic condition that would prevent them from jumping.

Subjects were asked to do a series of stepping off and hopping off drops to a force platform (1200 Hz, AMTI). The box heights were adjusted to range from 20 to 45 cm with 5 cm increments in a balanced order such that each subject performed step off (SO) and hop off (HO) drops three times at six different heights. Participants were given instructions and shown an example of how to perform each type of drop. Landing impulse was used to calculate an equivalent dropping height (the fall height from rest of the body center of mass prior to touchdown). All trials were videotaped for qualitative analysis purposes.

A series of single sample t-tests were used to examine if calculated drop heights were significantly different from actual box heights. A mixed design three-way ANOVA with repeated measures (drop type × box height × gender) with gender as the between subjects condition was used to analyze the difference in calculated center of mass (CM) drop heights.

RESULTS AND DISCUSSION

Both types of drops showed significantly lower calculated drop heights than the actual box height (Figure 1). The magnitude of height difference gradually increased as the box height increased (Table 1). Regardless of the landing type, participants lowered their CM prior to takeoff. This is in agreement with our earlier study (Afifi and Hinrichs, 2006) for the SO condition. This may not have been expected for the HO condition; however, pilot testing had shown that HO differs with subject standing position in relation to the box edge. In this study, participants stood with their toes past

the edge of the box. A lower calculated drop height for the HO condition was confirmed by qualitatively observing limb positions at takeoff.

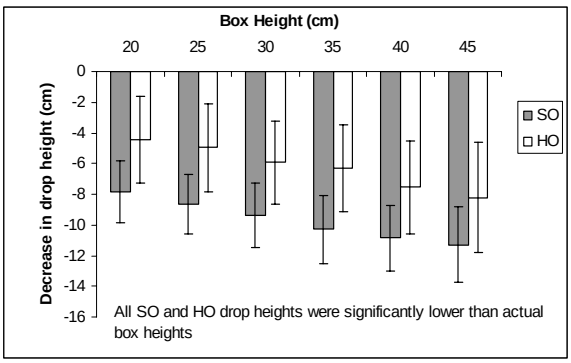

Figure 1. Mean CM height lost for each condition

The greater the difference between calculated drop height and actual box height as box height increased suggests that that subjects may have been subconsciously attempting to lower their centers of mass prior to takeoff, thus, reducing the risk of injury upon landing.

Table 1. The difference in height lost for each pair of box heights

BoxHt	20 cm	25 cm	30 cm	35 cm	40 cm	45 cm
20 cm		.79	1.51*	2.44*	2.99*	3.43*
25 cm	.55		.72	1.65*	2.20*	2.63*
30 cm	1.50*	.95*		.93	1.48*	1.92*
35 cm	1.91*	1.37*	.42		.55	.98*
40 cm	3.12*	2.57*	1.62*	1.20*		.43
45 cm	3.80*	3.25*	2.30*	1.88*	.68	

SO condition shown above the diagonal
HP condition shown below the diagonal
* Significant difference between pair of box heights, $p<.05$

A significant main effect for drop type was seen as SO heights were significantly lower than HO heights, $F(1,18) = 36.01$, $p<.001$,with no gender by drop type interaction, $F(1,18) = 3.7$, $p=.07$, no drop type by drop height interaction, $F(5, 90) = 1.33$, $p= .259$, and no gender by drop type by drop height interaction, $F(5, 90) = 2.13$, $p= .069$.

Participants in the SO condition decreased drop height more than the HO condition for all heights as one foot left the box first and they had control over when to leave the box with the other leg. This was not the case in the HO case where both feet left at once and there was no room for adjustment.

The decrease in drop height from actual box height ranged from 7.86 to 11.28 cm for SO and from 4.41 to 8.22 cm for HO. If precise control over the drop height is not needed then countermovement jumps should be studied as they relate to what happens in real-life jumping. However, when precise control of the drop height is needed then other methods to control height should be assessed. When studying falls, height may be controlled by having participants hold on to a bar and dropping. This methods has been used by some researchers, however, accuracy in controlling drop height remains to be tested.

SUMMARY/CONCLUSIONS

The difference in drop height when stepping off and hopping off a box were investigated. Both stepping off and hopping off lead to a decrease in drop height compared to the actual box height. The loss of height shows that the assumption that stepping or hopping off a box controls drop height is incorrect suggesting it would be best to study jump landing from actual jumps and fall landing from hanging on a bar and dropping. If SO or HO landings are to be used then the actual box height should be adjusted for each subject and each trial separately to ensure a relatively constant drop height and verified by impulse upon landing.

REFERENCES

Afifi, M. and Hinrichs, R.N. (2006). *Proceedings of ASB '06.*

Swartz, E.E. et al. (2005). *Journal of Athletic Training, 40,* 9-14.

ROLES OF LEADING AND TRAILING ARMS IN BASEBALL BAT SWING

Young-Kwan Kim and Richard N. Hinrichs

Arizona State University, Tempe, AZ, USA
E-mail: Young-Kwan.Kim@asu.edu

INTRODUCTION

Baseball is a popular team sport in North America, Latin America, and East Asia. Throwing and hitting are two important skills. Hitting a ball is perhaps the most difficult fundamental motor skill because it requires both temporal and spatial accuracy.

Bat swing is considered an open kinetic chain motion because there are sequential segmental rotations (proximal-to-distal order) to get the highest linear speed at the tip of the bat (Welch et al., 1995). Even though there have been arguments of "hips driving arm swing" and "arms driving hip rotation" among coaches and players (Lau, 1986), kinematics and inter-segmental coordination of leading arm and trailing arm were not reported. Also the arms motion itself is considered as a closed kinetic chain motion until the hands possibly separate following impact. Anecdotally players believe the trailing arm (dominant arm) is the "power" and the leading arm (non-dominant arm) is the "guide" in the bat swing.

The main objective of this study was to investigate 3D angular kinematics of the upper body in order to see the sequence of segmental angular velocity. In addition, the kinematics and intra-limb coordination of an overloaded bat swing were analyzed to justify the roles of each arm.

METHODS

Nine college students (7 males and 2 females) who had played baseball or softball in high school and/or community college participated in this study. They were informed of the purpose of this study and signed informed consent prior to data collection. Ten high speed (200 Hz) cameras (Eagles system, Motion Analysis) were used to collect position data of markers on the body. Twenty-five markers were defined on the subject's upper body, bat, and a tee to provide 3D position data and to build angular kinematics.

Subjects were asked to perform five bat swings with a standard bat (909 g) as fast as possible at an imaginary target on a tee (no ball contact). Following a 5-min break, they performed the same task with an overloaded bat (a standard bat + 568-g donut mass). Neither model nor feedback was given to the subjects. Collected data were smoothed by a second order zero-lag Butterworth filter (cutoff frequency of 10 Hz) and used for segmental angular velocity.

The local reference frame and direction cosine relative to the global reference frame were calculated. Then component angular velocities and resultant angular velocities with respect to the global reference frame were calculated. The resultant angular velocity profiles were used to provide the variables of intra- and inter-limb coordination.

RESULTS AND DISCUSSION

Segmental angular velocity profiles for a typical subject (Figure 1) and means of time-to-peak velocity difference and peak angular velocity differences between

adjacent segments for 9 subjects (Figure 2) showed that there was no significant temporal delay within leading arm segments and core sections, but there was significant temporal delay between lower and upper arms of the trailing arm (p<.05).

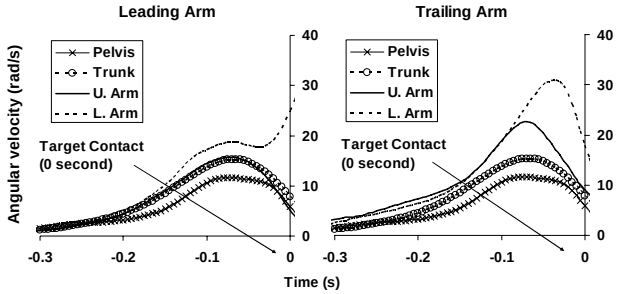

Figure 1: Resultant segmental angular velocity profile for leading and trailing arm separately. U. Arm=upper Arm, L. Arm=lower Arm.

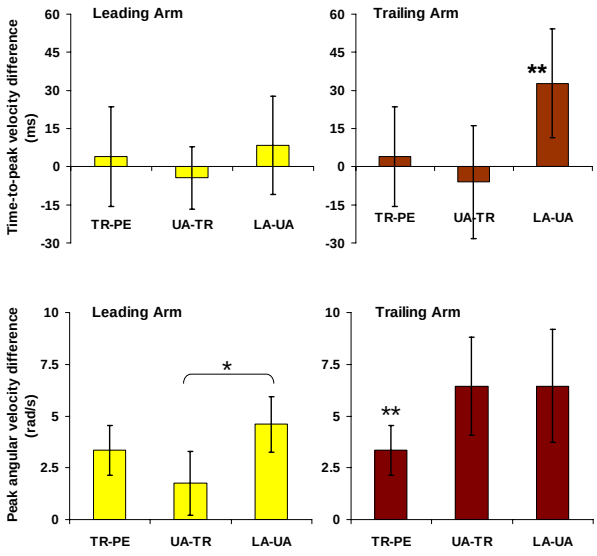

Figure 2: Time-to-peak velocity differences and peak angular velocity differences between adjacent segments for leading and trailing arms, respectively. TR–PE = trunk – pelvis, UA–TR= upper arm – trunk, LA–UA = lower arm – upper arm. * means significantly different between two conditions (p<.05) and ** significantly different than the other two conditions (p<.05).

Positive angular velocity contribution to bat speed mainly came out from the trailing arm motion (see Figures 1 and 2). A paired sample t-test (p<.001) indicated that the bat speeds at the target were significantly different between standard bat (25.3 ± 3.65 $m \cdot s^{-1}$) and overloaded bat (21.8 ± 4.40 $m \cdot s^{-1}$).

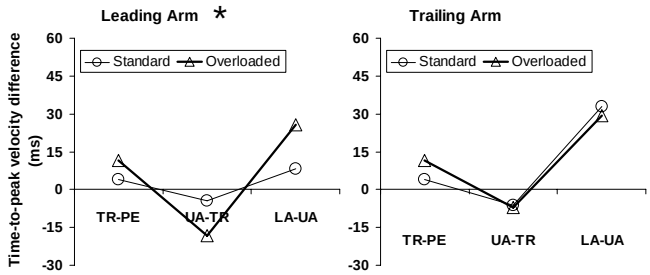

Figure 3: Change in time-to-peak velocity differences between adjacent segments due to overloaded bat swing. * Significant interaction in the leading arm (p<.05).

Only the two-way repeated measures ANOVA on time-to-peak velocity differences in the leading arm showed a significant interaction of bat weights and adjacent segments (p<.05) (see Figure 3). The overloaded bat induced a negative temporal delay of upper arm and trunk significantly and that was compensated by a longer positive temporal delay of lower arm and upper arm in the leading arm.

SUMMARY/CONCLUSIONS

Neither opinion of "hips driving arm swing" and "arms driving hip rotation" was fully supported by angular kinematics. The core section and lead arm segments rotated simultaneously as a unit in the bat swing. Significant temporal delay of upper and lower arms was found in the trailing arm. The significant peak angular velocity differences in the trailing arm supported the role of the trailing arm generating power during bat swing. Intra-limb coordination of the leading arm was significantly affected by the overloaded bat, while the trailing arm was invariant.

REFERENCES

Welch et al. (1995). *J Ortho Sports Phy Ther*, **22,** 193-201.

Lau (1986). *The art of hitting .300* (2nd Ed.).

THE ENHANCED DAILY LOAD STIMULUS (eDLS): ACCOUNTING FOR SATURATION, RECOVERY AND STANDING

Kerim O. Genc [1, 2], Brad T. Humphreys[3], Gail P. Perusek [4] and Peter R. Cavanagh [1, 2]

[1] Case Western Reserve University, Cleveland, OH, USA
[2] Cleveland Clinic, Cleveland, OH, USA
[3]ZIN Technologies, Cleveland, OH, USA
[4]NASA Glenn Research Center, Cleveland, OH, USA
E-mail: genck@ccf.org, Web: http://www.lerner.ccf.org/bme/cavanagh/lab/

INTRODUCTION

The Daily Load Stimulus (DLS), first proposed by Carter *et al.* (1987), is a method of quantifying daily stress histories of bone in terms of daily cyclic stress magnitudes and the number of daily loading cycles.

$$DLS = \left[\sum_{j=1}^{k} n_j \left(Gz_j \right)^m \right]^{1/2m} \quad (1)$$

Gz = Peak magnitude of vertical component of ground reaction force (GRF)
j = Number of loading conditions
m = Weighing factor {eg. 4}
k = Number of different loading conditions

Recent studies, however, indicate that the osteogenic potential of bone can also be influenced by temporal factors such as saturation (Turner and Robling, 2004), recovery (Robling *et al*., 2001, Gross and Srinivasan, 2006), and standing (Fritton *et al*., 2000). Based on animal data from Umemura et al. (1997), Turner and Robling (2004) demonstrated that bone tissue sensitivity to cyclical mechanical loading can be described by 1/(N+1) where N is the number of cyclic loads after saturation. Robling et al. (2001) were able to show that increasing the time of recovery between bouts of cyclical mechanical loading can enhance bone formation. The recovery of osteogenic potential can then be described by: Recovery (%) = $100(1-e^{-t/\tau})$, where t is time in hours between bouts and τ is a time constant (2hrs). Standing can also play a role in the maintenance of bone due to the micro strains imparted through postural stabilization (Fritton et al, 2000).

Currently, the DLS model does not account for saturation, recovery or standing. Therefore, the purpose of this study is to propose an updated method of determining the DLS that accounts for variables such as saturation and recovery of osteogenic potential with cyclical loading and standing.

METHODS

Ground reaction force (GRF) data was obtained from a previous experiment (Cavanagh *et* al. 2004) in which subjects wore Pedar force measuring insoles (NOVEL Gmbh. Munich, Germany) for entire typical work days. Data were collected using a wearable, portable computer and downloaded for data analysis completed using custom Matlab software (Mathworks Inc. Natick MA).

A peak detection algorithm was used to detect all fluctuations in the GRF data above 5% of body weight (BW). The GRF data was then categorized into sitting, standing, walking, running or other. This was done by an algorithm that took advantage of the repetitive and predictable nature of walking

and running profiles by examining their power spectral density. After 5 min. of continuous running or 10 min. of continuous walking, saturation was assumed to be achieved and each successive peak load (Gz) was multiplied by 1/(1+N). Each successive bout of walking or running that occurred after saturation was then multiplied by the recovery equation ($1-e^{-t/\tau}$) (Figure 1).

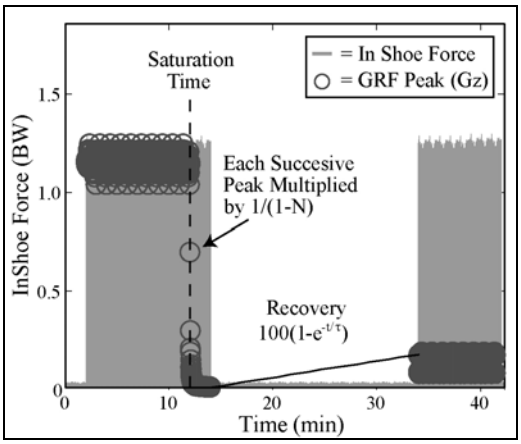

Figure 1: Exemplar walking GRF data with peaks detected and adjusted to account for saturation and recovery.

Eq. (1) can also be simplified as follows:

$$DLS = [DAL]^{1/2m} \qquad (2)$$

where DAL equals Daily Accumulated Load. To account for standing, the DAL from one minute of standing is defined to be equivalent to one quarter of the DAL from one minute of slow walking at 1.0m/s.

The peak magnitudes (Gz) are finally divided into bins (n) and input into Eq. (1) to calculate eDLS (Figure 2).

SUMMARY

This new method of calculating eDLS is currently being validated in an ongoing bedrest study in which the "dose" of exercise prescribed as a countermeasure

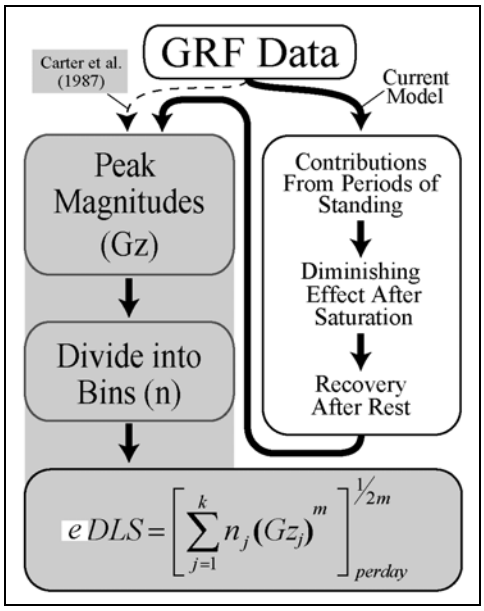

Figure 2: Flow chart of the proposed method of calculating eDLS versus the original method used by Carter et al. (1987).

to bone loss is based on the calculation of the DLS. This new method may also prove useful for exercise prescription for crewmembers on long-term missions to the moon or Mars.

REFERENCES

Cavanagh P.R. et al. (2004) *50th Annual Orthopaedic Research Society Meeting.*

Fritton. S.P. et al. (2000) *J Biomechanics* **33**, 317-325.

Gross T.S. and Srinivasan. S. (2006) *Br J Sports Med*, **40** 2-3.

Robling. A.G. et al. (2001) *J Exp Biol* **(204)**, 3389-3399.

Turner. C.H and Robling. A.G. (2003) *Exerc Sport Sci Rev*, **31(1)**, 45-50.

Umemura. Y. et al. (1997). *J Bone Miner Res*, **12(8)**, 1480-1485.

ACKNOWLEDGEMENTS

This research was supported by the National Space Biomedical Research Institute Grant BL0042 through NASA NCC 9-58.

CRUCIATE LIGAMENT REMOVAL CONTRIBUTES TO ABNORMAL KNEE MOTION DURING POSTERIOR STABILIZED TOTAL KNEE ARTHROPLASTY

Melinda J. Cromie[1,4], Robert A. Siston[1,2,4,5], Nicholas J. Giori[3,4], Scott L. Delp[1,2,3,4]
Departments of Mechanical Engineering[1], Bioengineering[2], and Orthopaedic Surgery[3]
Stanford University, Stanford California
Veterans Affairs Palo Alto Health Care System, Palo Alto California[4]
Department of Mechanical Engineering, The Ohio State University, Columbus Ohio[5]
Email: melindaj@stanford.edu Web: http://nmbl.stanford.edu

INTRODUCTION

Total Knee Arthroplasty (TKA) is performed to relieve the pain of osteoarthritis. When posterior stabilized knee prostheses are implanted, the cruciate ligaments are removed and mechanical interaction between the femoral and tibial components is intended to stabilize the anterior-posterior motion of the knee. However, these implants result in abnormal anterior translation of the femur relative to the tibia (Siston, 2006). This motion can lead to accelerated wear of the prosthesis and alter the moment arms of the muscles. The causes of this abnormal motion are unknown. We measured passive kinematics of the knee during surgery to answer two specific questions: Does posterior cruciate ligament removal introduce abnormal anterior translation of the femur? Does prosthesis implantation change the kinematics from the cruciate deficient case?

METHODS

We measured passive knee kinematics in 10 male subjects undergoing primary total knee arthroplasty for the treatment of osteoarthritis. Prostheses used were NexGen Legacy Posterior Stabilized Knees from Zimmer Inc. Institutional Review Boards approved the protocol and subjects gave informed consent.

We used a surgical navigation system to record the passive kinematics of the knee during surgery (Siston, 2006). Sterilized infrared-reflective trackers were affixed directly to the femur and tibia, and a stylus was used to digitize anatomic landmarks to establish the anatomic reference frames. The origin of the femur frame was the anterolateral edge of the posterior cruciate ligament attachment, and the origin of the tibia frame was the center of the anterior cruciate ligament attachment.

We measured the anterior-posterior translation of the knee throughout the range of flexion. We defined anterior position of the femur relative to the tibia by projecting the origin of the femur frame onto the anterior axis of the tibia frame. By this definition, anterior position is zero when the origin of the femur frame is directly above the origin of the tibia frame. The surgeon moved the knee through its range of motion three times. We calculated the flexion angle and anterior position of the femur relative to the tibia throughout the range of motion. We fit a fifth order polynomial to the resulting curves of anterior femur position vs. flexion angle (Fig. 1). We then measured the anterior translation, the forward distance traveled by the femur on the tibia (Fig 1, arrow). The anterior translation was recorded at four surgical stages: (1) Intact, before removing the ligaments, (2) No ACL, after removing the anterior cruciate

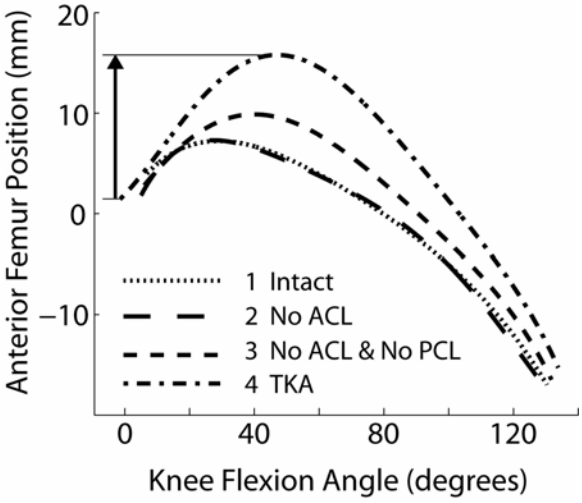

Figure 1: Anterior femur position throughout the range of knee flexion for one subject at the four surgical stages (see methods). Arrow indicates anterior femur translation.

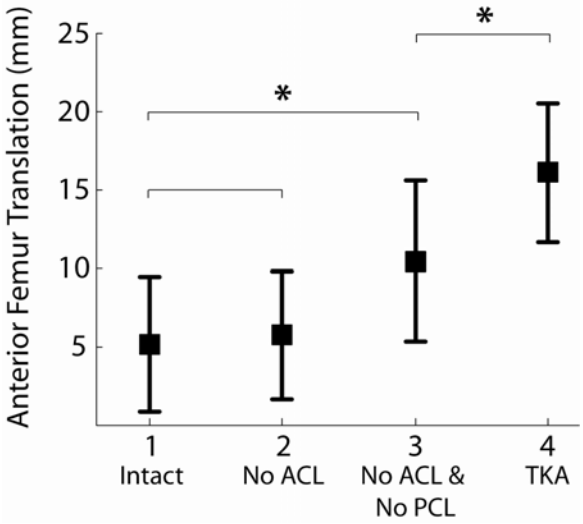

Figure 2: Anterior femur translation at the four surgical stages (mean ± SD). *α=0.05

ligament, (3) No ACL & No PCL, after removing the posterior cruciate ligament, and (4) TKA, after implanting the prosthesis. Surgical stages were compared with paired student's *t*-tests (stage 1 vs. 2, 1 vs. 3, 3 vs. 4) with Bonferroni correction for multiple comparisons.

RESULTS AND DISCUSSION

Removing the anterior cruciate ligament did not change the anterior motion of the femur (compare surgical stages 1 and 2 in Fig. 2). Removing the posterior cruciate ligament doubled the distance of anterior translation relative to the intact stage (compare surgical stages 1 and 3 in Fig. 2). Implanting the prosthesis increased the anterior translation of the femur relative to the cruciate deficient stage (compare surgical stages 3 and 4 in Fig. 2). Anterior translation after prosthesis implantation was three times that of the intact knee.

The increased anterior femur translation in early flexion following posterior stabilized total knee arthroplasty observed here in passive motion also occurs in voluntary movement, during the stance phase of gait (Dennis, 2003) and in the swing and stance phases of stair climbing (Andriacchi, 2003).

The abnormal anterior translation observed following posterior stabilized total knee arthroplasty was caused largely by removing the posterior cruciate ligament. Normal motion was not restored by the posterior stabilized prosthesis.

REFERENCES

Andriacchi et al. (2003) *Clin Orthop Relat Res*, **410**, 44–53

Dennis et al. (2003) *Clin Orthop Relat Res*, **416**, 37-57

Siston et al. (2006) *J Orthop Res*, **24**, 1607-1614

ACKNOWLEDGEMENTS

National Defense Science and Engineering Graduate Fellowship

PREHENSION SYNERGIRES: EFFECTS OF FINGER MANIPULATION

[1]Mark K. Budgeon, [1]Mark L. Latash and [1]Vladimir M. Zatsiorsky
[1]Department of Kinesiology, The Pennsylvania State University, University Park
Email: mkb167@psu.edu

INTRODUCTION

The purpose of this study was to investigate how equilibrium of a hand-held object is maintained when the index (I) or little (L) finger was removed or added during different external torques: counter-clockwise, clockwise and zero torque (CCW, CW, ZERO). We were interested in how the finger-tip forces were organized to maintain equilibrium, whether these forces followed the principle of superposition (Zatsiorsky et al., 2004), and if they were controlled in a feed-forward manner. Subjects had to exert a pronation effort (PRO) to resist a CCW torque and a supination effort (SUP) to resist a CW torque. The study was inspired by the literature data on the effects of finger removal/addition in multi-finger tapping (Latash et al., 1998) and pressing tasks (Li et al., 2003). The data were interpreted at the virtual finger (VF) level for the thumb and fingers.

METHODS

Seven male subjects with (mean +/- STD) age = 27.6 ± 4.3, height = 177.7 ± 3.8 cm, weight = 82.6 ± 12.8 kg, hand width = 9.4 ± 0.4 cm and hand length, measured from middle fingertip to distal crease while the hand was extended, = 19.1 ± 1.2 cm participated in the study. Each subject was identified as right-handed by their reported daily activity of the use of their hands. No history of neuropathies or traumas to the upper extremities was reported by the subject. All subjects gave informed consent in accordance with the Office of Research Protections of The Pennsylvania State University.

A handle with five sensors (four for the fingers, one for the thumb) arranged such that the vertical location of the thumb was between the M and R fingers, described in more detail in Aoki et al. (2003), was used to collect data. A beam was attached to the bottom of the handle and a load of 0.55 kg was suspended from the beam at three locations to create three torques: CCW, CW and ZERO.

The data were recorded at 200Hz and low pass filtered at 10Hz. Steady state values were calculated as the average for one second at the beginning and end of the trials.

Table 1: Changes in normal and tangential force when the I or L finger is manipulated during CW, ZERO or SUP efforts. The torque agonists are in bold text, "=" indicates no significant change, "+" indicates a significant increase in force, "-" indicates a significant decrease in force. Significance was tested at $p < 0.05$.

Manipulated finger	Finger addition, 3-to-4 tasks			Finger removal, 4-to-3 tasks		
	CW/PRO	ZERO	CCW/SUP	CW/PRO	ZERO	CCW/SUP
I, normal	**=1.56**	+2.55	+2.77	**+3.60**	=0.97	-1.60
L, normal	+3.02	+2.24	**=0.16**	=0.12	=0.88	**+2.31**
I, tangential	**+2.88**	+1.70	+0.70	**–3.15**	–1.67	–0.64
L, tangential	=0.29	–0.30	**–0.87**	+0.88	+0.96	**+1.54**

A one-way repeated measures ANOVA was performed on the factor PERTURBATION (before, after); one ANOVA per moment condition and finger manipulation, for a total of 24.

RESULTS AND DISCUSSION

The normal forces significantly changed depending on the role of the finger, i.e. whether it was an agonist (helped in the exerted effort, like the I finger during PRO effort) or antagonist, see the first two rows of Table 1. The increases in normal force were not mechanically necessary because the force prior to the increase was sufficient to prevent slipping. The tangential forces significantly changed depending on the finger manipulated (I or L), see the last two rows of Table 1.

The thumb and VF normal forces highly correlated with each other, as we expected, but the normal forces did not correlate with the normal moment. The thumb and VF tangential forces correlated with each other as well as with the tangential and normal moment. The correlations were grouped into two subsets (see Figure 1), like the findings of Zatsiorsky et al. (2004), which support the principle of superposition – two

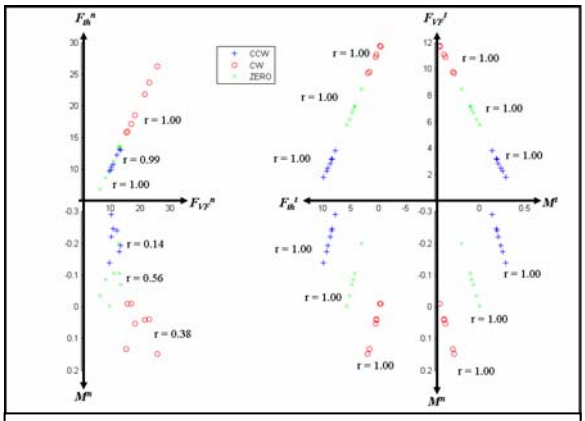

Figure 1: Correlations between the final steady state values for normal and tangential forces and moments.

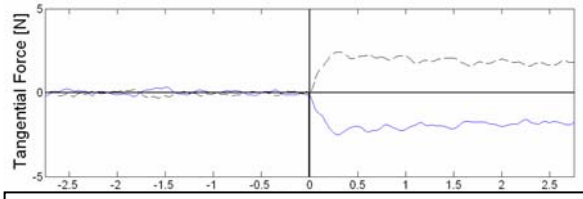

Figure 2: Thumb vs. VF (dotted and solid lines) tangential forces during an I addition, PRO effort trial.

commands were sent to the hand: "grasp the object stronger/weaker" and "prevent tilting."

The normal and tangential force of the VF and thumb changed synchronously, see Figure 2. This was supported by high Pearson correlation coefficients (~0.99) between the thumb and VF forces. Also, standard deviations of the performance variables — total tangential and total normal force and total moment — were low (the highest value for force was 0.41 N and for moment was 0.24 Ncm). These immediate compensations indicate that the CNS plans adjustments of the forces before the manipulation.

SUMMARY

Changes in normal digit force depend on the role of the manipulated finger while changes in tangential force depend on the finger manipulated. The changes were made according to the principle of superposition and in a feed-forward manner.

REFERENCES

Latash, et al.(1998). *Exp Brain Res* , **122**, 131-138.

Li, et al. (2003). *Exp Brain Res* **150**, 230-236.

Aoki, et al. (2006). *Exp Brain Res* **172**, 425-438.

Zatsiorsky et al. (2004). *Exerc Sport Sci Rev* **32**(3): 75-80.

EFFECTS OF LATERAL STABILIZATION AND ARM SWING ON METABOLIC COST OF WALKING IN YOUNG AND ELDERLY ADULTS

Justus D. Ortega, Leslie A. Fehlman, and Claire T. Farley

University of Colorado, Boulder, CO, USA
E-mail: jdo1@humboldt.edu

INTRODUCTION

Elderly adults consume more metabolic energy for walking than young adults across a range of speeds (Martin et al., 1992). It is possible that the elevated energy consumption by elderly adults is related to decreased stability during walking. In young adults, it is known that the metabolic cost of lateral stabilization accounts for as much as 6% of the cost of walking (Donelan et al., 2004). Elderly adults appear to be less stable during walking than young adults (Winter et al. 1990) and, thus, may have a greater metabolic cost of lateral stabilization. Moreover, because instability during walking may be partially counteracted by arm swing (Shibukawa et al., 2001), we examined its role in determining the metabolic cost of walking.

This study tests two hypotheses: 1) elderly adults consume more metabolic energy during walking than young adults because they have a greater metabolic cost of lateral stabilization, and 2) arm swing reduces the metabolic cost of stabilization during walking in young and elderly adults.

METHODS

Twelve healthy elderly adults (74.5 ± 2.9 years; mean ± s.d.) and twelve healthy young adults (22.7 ± 3.7 years) performed seven minute trials of treadmill walking at 1.3 m s^{-1}. We examined the effect of external stabilization on metabolic cost and kinematics during walking with and without arm swing.

We provided external lateral stabilization by applying bilateral forces (10% body weight) to the walking subject using a device similar to that in Donelan et al. (2004). This device consisted of two elastic cords attached to the left and right sides of the waist via a padded belt that allowed normal arm swing. Each cord included a 14 m long nylon string in series with 0.5 m of hollow latex rubber tubing. Given this long length, small deviations from the intended cord orientation created negligible vertical or horizontal (fore-aft) forces applied to the subject. The entire system produced an effective spring constant of approximately 1900 N m^{-1} and minimal damping (26 Ns m^{-1}).

Metabolic power consumption was determined for the last two minutes of each trial using indirect calorimetry and standard equations (Brockway 1987). We calculated net metabolic power (W/kg) by subtracting standing metabolic power from gross metabolic power and dividing by body mass. We also measured step frequency and step width using high-speed video (200 Hz).

RESULTS AND DISCUSSION

External stabilization reduced metabolic power consumption to a similar extent in young and elderly subjects (6-7%; $p < 0.0001$; Fig. 1) when they walked without arm swing. Moreover, for both groups walking without arm swing, external stabilization reduced step width by 63-67% ($p < 0.0001$) and its variability by 64-71% ($p < 0.0001$). Finally, when subjects walked

with normal arm swing, external stabilization affected metabolic power consumption and step width less than when they walked without arm swing (Fig. 1).

These results show that young and elderly adults have a similar metabolic cost of lateral stabilization during walking. External stabilization allowed subjects to reduce step width and step width variability because walking required less active control of stability. These changes probably reduced the individual limb work performed by the subjects and thereby reduced metabolic cost (Donelan et al., 2001).

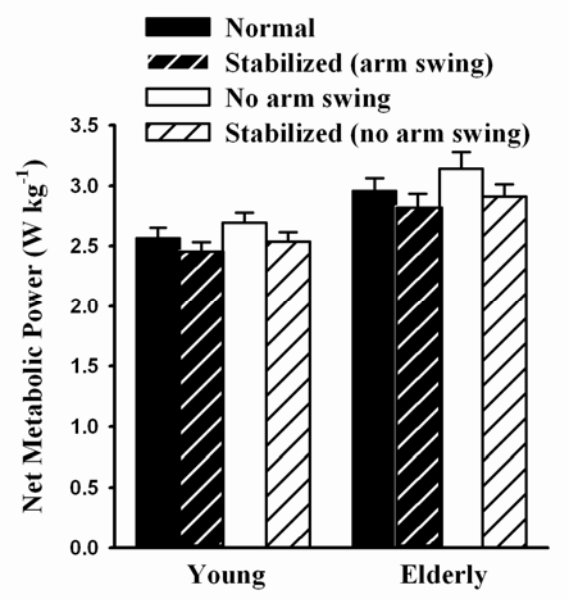

Figure 1: Net metabolic power for young and elderly subjects. External stabilization reduced metabolic power more when subjects walked with no arm swing than with arm swing. Also, eliminating arm swing increased metabolic power to a greater extent without external stabilization than with it.

Eliminating arm swing increased metabolic power consumption to a similar extent in young and elderly subjects when they walked without external stabilization (5-6%; $p < 0.014$; Fig. 1). In contrast, when either group walked with external stabilization, eliminating arm swing did not significantly affect metabolic power ($p = 0.160$).

These findings show that external stabilization compensates for arm swing elimination. This observation suggests that arm swing reduces the metabolic cost of walking in young and elderly adults by contributing to stabilization.

SUMMARY/CONCLUSIONS

Elderly adults have a similar metabolic cost of lateral stabilization as young adults. Thus, the high metabolic cost of walking in elderly adults is likely due to other factors, such as greater muscle force generation for supporting body weight. Moreover, arm swing reduces the metabolic cost of walking in young and elderly adults likely by contributing to stability.

REFERENCES

Brockway, J. M. (1987). *Hum. Nutr. Clin. Nutr.* **41**(6): 463-471.

Donelan, J. M., R. Kram, et al. (2001) *Proc. R. Soc. Lond. [Biol]*. **268**(1480): 1985-1992.

Donelan, J. M., D. W. Shipman, et al. (2004). *J. Biomech.* **37**(6): 827-835.

Martin, P. E., D. E. Rothstein, et al. (1992). *J. App. Physiol.* **73**(1): 200-206.

Shibukawa, M., K. Sugitani, et al. (2001). *Proceedings of EMBS'01,* 1139-1144.

Winter, D. A., A. E. Patla, et al. (1990). *Phys. Ther.* **70**(6): 340-347.

ACKNOWLEDGEMENTS

We thank Dr. Max Donelan and Dr. Rodger Kram for their technical assistance with the external stabilizing device. Funding provided by NIA T32 AG00279.

POSTURAL CONTROL STRATEGIES DURING PROLONGED STANDING: IS THERE A RELATIONSHIP WITH LOW BACK DISCOMFORT?

Erika Nelson-Wong, Diane E. Gregory, David A. Winter, Jack P. Callaghan

University of Waterloo, Waterloo, ON, Canada
E-mail: enelsonw@ahsmail.uwaterloo.ca

INTRODUCTION

Static postures such as prolonged standing have been associated with development of low back discomfort in the workplace (MacFarlane et al. 1997). Factors such as the number of shifts in the antero-posterior centre of pressure (CoP), and gluteus medius (GM) muscle activity, have shown promise in predicting development of low back discomfort in individuals during prolonged standing (Gregory & Callaghan 2007).

Differences in postural responses to a balance challenge have also been observed in people with and without low back pain. People with low back pain were found to have a decreased use of hip strategy for balance recovery in response to an anterior-posterior balance challenge (Mok et al. 2004). Winter has proposed a load-unload mechanism at the hip abductors as a 'hip strategy' for control of medio-lateral CoP (CoP_{M-L}) in normal individuals during unperturbed, quiet standing (Winter DA 1996). Use of this 'hip strategy' mechanism for CoP_{M-L} control has not been investigated during occupational standing or in those with low back discomfort exacerbated by prolonged standing.

The purpose of this work was to investigate differences in motor control strategies between groups with and without low back discomfort during prolonged standing while performing simulated occupational tasks. A second purpose was to determine whether identification of individuals who would develop low back discomfort during prolonged standing could be accomplished based upon their muscle coordination patterns.

It was expected that use of a load-unload 'hip strategy' would be seen in all participants for CoP_{M-L} control during prolonged standing. A second hypothesis was that there would be differences in trunk and hip muscle coordination patterns between groups. It was expected that these differences would be sufficient to enable separation of subjects into discomfort and non-discomfort groups prior to viewing their discomfort ratings.

METHODS

Fifteen participants stood for two hours in a constrained area while performing four different occupational tasks. Participants were required to have no history of low back pain during the previous 12 months. Participants rated their level of low back discomfort on a visual analog scale (VAS) every fifteen minutes. Ten channels of continuous electromyography (EMG) were collected from bilateral trunk and GM muscles. Force plate measurements were used to determine CoP_{M-L}.

Cross-correlation analyses were used to quantify the common signal and phase relationship between EMG signals to provide muscle coordination information. Cross-correlations between muscle activation and CoP_{M-L} migration were also used as a measure of CoP_{M-L} control.

RESULTS AND DISCUSSION

Eight of the fifteen participants reported low back discomfort with prolonged standing during the study protocol. Participants were clearly separated (one-tailed t-test p = 0.00001) based upon their VAS scores; low back discomfort (41.4 ± 5.16) and non-low back discomfort (7.0 ± 2.39).

All participants demonstrated the load-unload mechanism at the hip for CoP_{M-L} control as shown by strong cross correlations of GM activation and CoP_{M-L} movement to the ipsilateral side. There was also some evidence of a similar mechanism at the trunk, shown by correlations of left and right lumbar erector spinae (LLES, RLES) muscle activation with contralateral CoP_{M-L} movement (Figure 1).

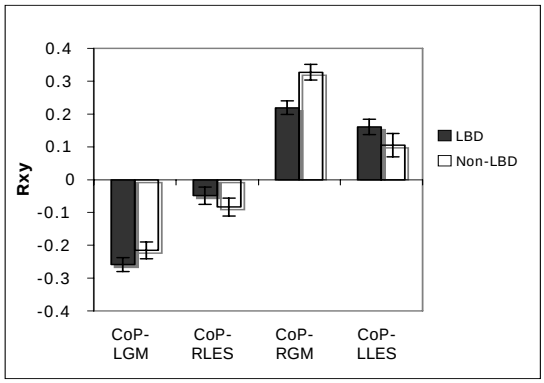

Figure 1: Both groups demonstrated load-unload mechanism for CoP_{M-L} control (CoP + Right)

Participants with low back discomfort had stronger co-activation of bilateral GM muscles than the non-low back discomfort group (one-tailed t-test, p = 0.047). Both groups had similar co-activation of LLES and RLES muscles (Figure 2).

Separation of participants into groups prior to viewing VAS scores was successfully done in 12 of the 15 cases based on the single factor of presence of co-contraction of left and right GM muscles. All of the participants in the low back discomfort group (n=8) were correctly predicted based on this factor.

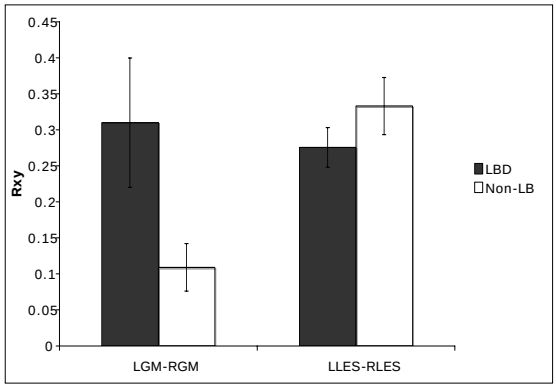

Figure 2: Co-activation of bilateral GM muscles was greater in the LBD group (p=0.047).

SUMMARY/CONCLUSIONS

The findings suggest an apparent increase in co-activation at the hip in individuals with increased low back discomfort when exposed to a prolonged standing task. This factor appears to be a useful predictive variable in identifying which individuals will develop low back discomfort with standing.

REFERENCES

MacFarlane, et al. (1997). *Spine*, **22**:1143-1149.
Gregory, D.E. & Callaghan, J.P. (2007). *Human Mov Sci*, Accepted-In-Revision.
Mok, N., et al. (2004). *Spine*, **29**(6):E107-E112.
Winter, D.A., et al. (1996). *J Neurophys*, **75**(6):2334-2343.

ACKNOWLEDGMENTS

Support for Dr. Nelson-Wong provided by the Foundation for Physical Therapy, APTA - USA

POSTURAL CONTROL OF SELF-INITIATED WEIGHT SHIFTS IN CHILDREN AND ADULTS

Andrea L. Downing, K. Narayanan, and James J. Abbas

Center for Adaptive Neural Systems, Harrington Dept. of Bioengineering, and IGERT: Neural & Musculoskeletal Adaptations in Form & Function at Arizona State University, Tempe, AZ, USA
E-mail: andrea.downing@asu.edu, Web: http://www.biodesign.asu.edu/centers/ans/

INTRODUCTION

The development of postural control has been evaluated using quantitative measures, such as quiet standing and perturbations (Forssberg and Nashner 1982). This work focuses on self-initiated weight shifts, which have been used for balance training in individuals with neurologic injuries (Ledebt et al 2005, Haart et al 2005), and may be a better indicator of postural performance during activities of daily living.

METHODS

Subjects: Healthy subjects were recruited into 3 groups: adults (AD, n=14, 8 males, age range 18-30, mean age 23.2), young children (YC, n=5, 2 males, age range 8-10, mean 9.2), and old children (OC, n=5, 4 males, age range 12-14, mean 13.1). Informed consent was given by the adults and the parents of the children.

Protocol and Data Collection: Subjects participated in a series of self-initiated weight shifts. For testing, subjects stood on a force plate (Bertec, Columbus OH) with their feet side-by-side, a hips width apart. Center of pressure (COP) was calculated and displayed as biofeedback (a cursor) on a computer monitor at eye-level, ~2.5 feet in front of the subject.

For each of 3 trials, subjects were presented with 10 targets (5 outer, 5 center). Outer targets were located E, NE, N, NW and W of the center target. Subjects were instructed to move the cursor to the target center as quickly as possible by shifting their weight. After the subject maintained the cursor in the target for 2 seconds (or the 10-second time limit was reached) the next target appeared. All outer targets were followed by the presentation of the center target. The distance from the center to the outer targets and the target size were scaled (40% and 10%, respectively) by each subject's theoretical limit of stability, which was calculated as an 8° anterior rotation of the navel about the ankle (Hamman et al 1992). Data were collected at 500 Hz and stored on a personal computer for post-processing. Subjects practiced moving the cursor before data collection began.

Data Analysis: COP data were low-pass filtered at 20 Hz with a dual-pass 4th order Butterworth filter. Data were divided into 2 zones, zone 1 (Z_1) - target presentation to entry point for the target, and zone 2 (Z_2) - entry point to completion of the target. The following measures were calculated: *error* (*Er*)-mean distance from the target center (Z_2); *unsteadiness* (*UnST*)-standard deviation of the distance from the target center (Z_2); *path lengths* PL_1 (Z_1) and PL_2 (Z_2); *mean velocity* V_1 (Z_1) and V_2 (Z_2); *reentry count* (*RC*)-number of times subject reentered the target; and *total time per target* (T_T). All measures, except *RC* and T_T, were normalized by ankle to navel height. An ANOVA with a Dunnett T3 post-hoc analysis (accounting for unequal variances) was used to compare the groups.

RESULTS

Significant differences ($p<0.05$) were found for all measures. The post-hoc analysis indicated that YC had significant increases in all measures compared to AD, while OC had significant increases in PL_2, V_2, and RC compared to AD (Table 1). Decreasing PL and V measures with age are demonstrated in Figure 1.

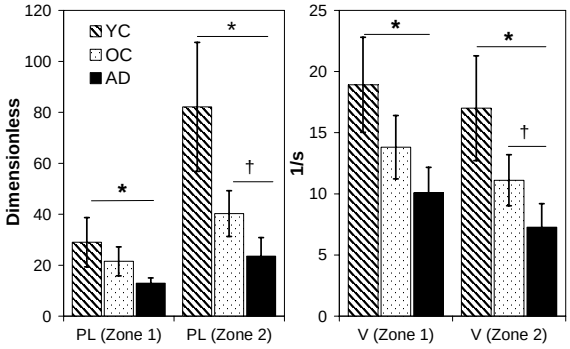

Figure 1: *PL* and *V* decrease with age. Error bars are ± 1 SD. Differences ($p<0.05$) between AD and YC and AD and OC are indicated with * and †, respectively.

DISCUSSION & CONCLUSIONS

During self-initiated weight shifts, YC demonstrated increased movement velocities and *Er*. This is similar to increased COP velocity during quiet standing. It has been suggested that children utilize larger, faster corrections (a ballistic postural control strategy) that results in less accurate movement (Riach & Starkes 1994). Increased V_2 was also seen in OC. Differences between the OC and AD were unexpected since other studies have shown adult-like postural responses in 7-10 year olds (Shumway-Cook & Woollacott 1985). However, this may be due to the difficulty of the task utilized in this study. Furthermore, it has been suggested that subtle changes in neuromuscular control continue throughout childhood (Sparto et al 2006).

Future studies will expand the number of healthy children and include children with disabilities, as well as compare this postural task to results of quiet standing trials. This functional postural task may increase the understanding of the development of postural control in healthy children as well as the impact of disability on the posture control system.

REFERENCES

Forssberg H. and Nashner L.M. (1982). *J. Neuroscience*, **2**, 545-52.

Haart M. et al. (2005). *Arch Phys Med Rehabil*, **86**, 755-62.

Hamman, R.G. et al. (1992). *Arch Phys Med Rehabil*, **73**, 738-44.

Ledebt, A. et al. (2005). *Motor Control*, **9**, 459-68.

Riach, C.L., Starkes, J.L. (1994). *Gait & Posture*, **2**, 167-72.

Shumway-Cook, A., Woollacott, M.H. (1985). *J. of Motor Behavior*, **17**, 131-47.

Sparto P.J. et al (2006). *Exp Brain Res*, **168**, 505-16.

ACKNOWLEDGEMENTS

Funding was provided by NSF-IGERT (NSF-DGE-9987619) and NINDS: NRSA (1 F31 NS053010) (A. Downing).

Table 1: Summary of Postural Control Measures (mean ± 1 SD). Differences ($p<0.05$) between AD and YC and AD and OC are indicated with * and †, respectively.

Group	*Er*	*UnST*	PL_1	PL_2	V_1	V_2	*RC*	T_T
YC	1.20±0.15*****	0.84±0.16*****	29.02±9.64*****	82.13±25.29*****	18.92±3.89*****	17.00±4.29*****	10.00±4.29*****	6.35±0.61*****
OC	1.02±0.15	0.63±0.16	21.53±5.70	40.25±8.95†	13.82±2.59	11.11±2.09†	4.41±1.14†	5.21±0.44
AD	0.90±0.11	0.52±0.11	12.97±2.01	23.54±7.31	10.10±2.06	7.28±1.92	2.28±0.89	4.52±0.32

THE EFFECTS OF CONSERVATIVE TREATMENT ON BIOMECHANICAL PARAMETERS IN PERIPHERAL ARTERIAL DISEASE PATIENTS

Matija Radovic [1], Jason Johanning[2], Iraklis Pipinos[2], Sara Myers[1], Jessie M. Huisinga[1], Nicholas Stergiou[1,2] and Shing-jye Chen[1]

[1] University of Nebraska at Omaha, NE, USA
[2] University of Nebraska Medical Center, Omaha, NE, USA
E-mail:mradovic@mail.unomaha.edu, Web: biomech.unomaha.edu

INTRODUCTION

Peripheral arterial disease (PAD) consists of atherosclerotic blockages in the arteries supplying the lower extremities and affects more than 12 million people in USA. The most common clinical sign of PAD is intermittent claudication (IC), a condition where muscle ischemia is induced during walking and subsequently relieved by rest. Recently PAD and intermittent claudication were recognized as one of the leading gait disabilities in the elderly population (Newman, 1999). The therapeutic goal for PAD patient is to regain lost physical function and normal gait through different treatment approaches. One of the most widely used therapeutic protocols is conservative treatment. Conservative treatment includes atherosclerosis risk factor control (smoking cassation, weight loss, hypertension, dislipidemia and diabetes control) and unsupervised exercise. A previous study from our laboratory has shown that PAD patients have impaired gait characteristics as compared to healthy controls (Scott, 2005). However the efficacy of conservative treatment with respect of changing gait characteristics towards normative values is currently unknown. Our specific aim was to investigate if conservative treatment can affect the biomechanical gait characteristics in PAD patients. Here we present preliminary data from this work, which is part of a large on going clinical trial on database of PAD in our research facilities.

METHODS

Four male PAD patients (three unilateral PAD and one bilateral) with lower extremity claudication (age=60 ± 7.8 yrs; mass=90.03 ± 14.1 kg) and 5 healthy controls (CON; age=54.7 ± 7.4 yrs; mass=87.0 ± 16.03 kg) walked through a 10 meter walkway at their self selected pace while kinetics were collected. Both groups performed five trials with each leg during a pain free condition (PF), or with no claudication symptoms. The subjects were required to rest between trials to ensure pain free data collection. This procedure was repeated for the post treatment collection for the PAD group following approximately three months of conservative treatment. The subjects were screened by two certified vascular surgeons and no other pathologies in the lower limbs of all subjects were detected. The kinetics data were acquired with a Kistler force plate (600Hz). Discrete points of ground reaction forces (GRF) data (local minimums and maximums) were calculated using custom laboratory software (Matlab; Math works Inc., MA). Independent t-tests were used to assess differences between CON and pre and post treatment conditions in the PAD patients. Paired t-tests were used to assess differences between pre and post treatment in the PAD patients. The level of significance was set at P=0.05.

RESULTS AND DISCUSSION

Significant differences were found for several parameters in all GRF directions between the CON group and pre treatment. These differences were located at: (a) the second peak of the vertical GRF; (p=0.013), (b) the minimum of the vertical GRF; (p=0.001), (c) the difference between the first peak and the minimum of the vertical GRF; (p=0.002), (d) the difference between the second peak and the minimum of the vertical GRF; (p=0.003), and (e) the anterior/posterior propulsion impulse: (p=0.009). After conservative treatment was completed, significant differences were found for: (a) the first peak of the vertical GRF; (p=0.0020), (b) the minimum of the vertical GRF; (p=0.001), (c) the difference between the first maximum and minimum of vertical GRF, (p=0.000), (d) the difference between the second maximum and the minimum of vertical GRF; (p=0.001), (e) the loading rate; (p=0.004), (f) the braking peak of anterior/posterior GRF; (p=0.009), (g) the anterior/posterior propulsion impulse; (p=0.001) and (h) the difference between maximum and minimum of anterior/posterior GRF; (p=0.002).

In general, the reduced vertical curve fluctuation in the PAD patients prior to and following treatment indicates that the PAD group has difficultness in going over the straight leg at single support and they increase stability by maintaining double leg support. PAD also had reduced braking and propulsion forces, indicating slower walking speed and less ability to push off during walking. When comparing gait parameters before and after treatment, the PAD group had significantly decreased values following conservative treatment for (a) the first peak of the vertical GRF; (p=0.012), (b) the second peak of the vertical GRF; (p=0.018), (c) the difference between the first peak and the second peak of vertical GRF, (p=0.019) and (d) the minimum of vertical GRF; (p=0.025), (e) the braking peak of the anterior/posterior GRF (p=0.01), (f) the difference between maximum and minimum of the anterior/posterior GRF (p=0.044) and (g) the anterior/posterior propulsion impulse (p=0.001). These findings collectively show that altered gait parameters still exist and some actually worsen following conservative therapy. Reduced forward push and lower braking forces indicate PAD is still unable to properly propel themselves forward during walking.

Decreased loading peaks for the vertical GRF and increased minimums at the vertical GRF show that PAD patients are still trying to create a more stable gait pattern following conservative therapy.

SUMMARY/CONCLUSIONS

These preliminary results suggest that unsupervised conservative rehabilitation treatment fails to restore normal gait parameters in PAD patients. This study suggests that although clinically useful, unsupervised conservative treatment fails to restore gait parameters in PAD patients. Other types of treatment, including supervised conservative therapy should be analyzed to assess gait improvements after intervention. These findings need to be further substantiated with more subjects and the incorporation of kinematics and joint moment data.

REFERENCES

1. Newman et al. (1999). JAGS 39, 142-148.

2. Scott, M. et al. (2005). *Proceedings of ISB'05*. Cleveland, OH. 2001

ACKNOWLEDGEMENTS

Supported by the American Geriatric Society's Hartford Foundation Dennis W. Jahnigen Award and the Nebraska Research Initiative.

HUMAN CERVICAL SPINE MECHANICS ACROSS THE MATURATION SPECTRUM

David J Nuckley, David R Linders, and Randal P Ching

University of Washington, Seattle, WA, USA
E-mail: dnuckley@u.washington.edu

INTRODUCTION

Pediatric cervical spine injury diagnosis, treatment, and prevention require an integrated knowledge of spinal development anatomically and biomechanically. Anthropometric patterns of cervical spine maturation have been well documented in the literature [Fesmire, 1989]. Despite the fact that head and neck injuries are the leading cause of death for children in the U.S., there exists a dearth of data describing the biomechanical response of the human cervical spine throughout development [FARS, 2003].

A number of studies have examined spinal maturation biomechanics in post-mortem animal models, discovering spinal level, loading rate, and sex specificity with unique ontogenetic growth curves describing the material and structural properties of the maturing spine [Nuckley, 2006; Pintar 2000]. Ouyang et al.[2005] examined ten human head and neck complexes from 2-to-12 years of age and reported sagittal bending curves and tensile failure loads. This study did not evaluate the spectrum of maturation mechanics, but provided excellent data describing spinal mechanics in the young.

Therefore, this research effort aimed to define relationships between spinal maturation and the functional (prior to injury) and failure mechanics of the human cervical spine in multi-axis loading.

METHODS

A correlation study design was used to determine the relationships linking spinal tissue maturation and biomechanics. Eleven human cadaver cervical spines from across the developmental spectrum (2-to-28 years) were dissected into segments (C1-C2, C3-C5, and C6-C7), wired and embedded in PMMA for biomechanical testing (Figure 1). Utilizing a servohydraulic MTS and custom Spine Motion Simulator, non-destructive (functional) and failure experiments were performed. Non-destructive flexibility tests were performed in tension, compression, flexion, and extension. After measuring their intact biomechanical responses, each specimen was failed to measure the tissue tolerance in tension (C1-C2), compression (C3-C5), and extension (C6-C7).

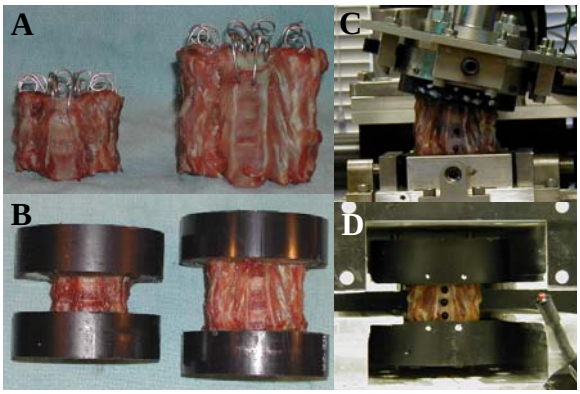

Figure 1. Sample Preparation and Testing. Each specimen (5 and 18 years shown) is dissected, wired (A), embedded in PMMA (B), then exercised in bending (C), tension (D), and compression prior to failure.

RESULTS AND DISCUSSION

The non-destructive spinal mechanics exhibited maturation dependent increased stiffness ($p<0.014$) and decreased range of motion. Nonlinear flexibility curves described the functional properties of the cervical spine throughout maturation and

elucidated age, spinal level, and mode of loading specificity (Figures 2 & 3).

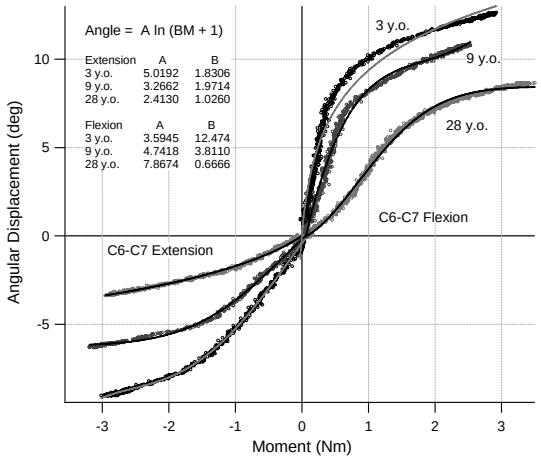

Figure 2. Sagittal Bending Flexibility as a Function of Age. Moment controlled inputs to C6-C7 segments elucidated these response curves as a function of maturation.

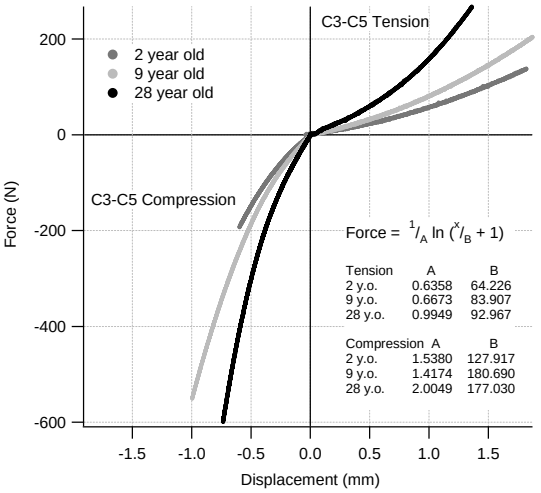

Figure 3. Compression / Tension Flexibility as a Function of Age. Response of the C3-C5 spinal segment to displacement controlled axial loading.

Together these functional data describe the biomechanics of the maturing cervical spine in multiple axes of loading. The failure mechanics (load/moment) were also found to significantly increase with advancing age (Figure 4). Classical injury patterns were observed in all of the specimens tested.

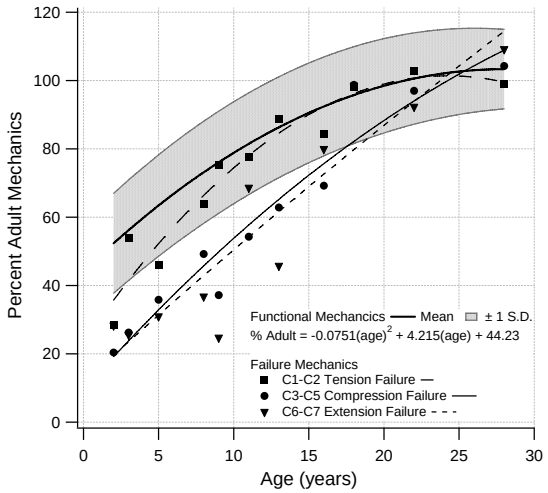

Figure 4. Scaling of Spinal Mechanics. The functional mechanics from all tests are grouped, displaying the maturation function of spinal stiffness. Failure data are overlaid defining the tolerance in multiple axes.

SUMMARY/CONCLUSIONS

The age dependent biomechanics of the human cervical spine are reported for functional and failure experiments. The adult data collected herein are consistent with the literature validating our maturation scaling curves. These data support previous animal studies and together facilitate the generation of injury prevention or treatment schema to mitigate child spine injuries.

REFERENCES

NCSA: FARS (2003).

Fesmire, F.M., Luten, R.C. (1989). *J. Emerg Med*, **7**, 133-42.

Nuckley, D.J., Ching, R.P. (2006). *J Biomech*, **39**, 3045-54.

Ouyang, J. et al. (2005). *Spine*, **30**, E716-23.

Pintar, F. et al. (2000). Stapp Car Crash J. **44**, 1-7.

ACKNOWLEDGEMENTS

Financial support by the National Highway Traffic Safety Administration and the CDC and made possible by the tissue donations of grieving parents whose gift to child injury prevention and science we honor.

LONG-DURATION MUSCLE-ACTUATED SIMULATIONS OF WALKING AT MULTIPLE SPEEDS

Chand T. John [1], Frank C. Anderson [1], Eran Guendelman [1], Jill S. Higginson [2], Scott L. Delp [1]
[1] Stanford University, Stanford, CA, USA
[2] University of Delaware, Newark, DE, USA
E-mail: ctj@stanford.edu Web: http://nmbl.stanford.edu

INTRODUCTION

Forward dynamic simulation is a powerful tool for investigating muscle function during normal and pathological walking. However, most existing 3D muscle-actuated simulations are of short duration (e.g., half a gait cycle) due to either high computational cost or dynamic inconsistencies between experimental kinematic and kinetic data. Recent advances in controller design along with methods for reducing dynamic inconsistencies have enabled more rapid simulation of long-duration movements. The purpose of this study is to evaluate the efficacy of these new methods by generating muscle-actuated simulations of full gait cycles for multiple subjects walking over a range of speeds, and to make our simulations available to others for examination and analysis.

METHODS

Data were collected on 2 healthy adult male subjects walking at 3 speeds (50%, 100%, and almost 200% of self-selected speed) on a Bertec split-belt instrumented treadmill. A 6-camera Motion Analysis system was used to record the positions of reflective markers placed according to a modified Cleveland Clinic marker set. These movements were simulated using OpenSim (Delp et al., in press). A 3D, 10-segment, 21-degree-of-freedom musculoskeletal model (Thelen and Anderson, 2006) with 92 muscles and 41 markers was scaled to match the anthropometry of each subject. For each motion, an inverse kinematics problem was solved to compute the joint angles that minimized the difference between model and experimental marker positions.

A residual reduction algorithm (RRA) was used to reduce dynamic inconsistency between the model kinematics and ground reaction forces in each motion. Unlike previous approaches, which may apply large "residual" forces and moments from the ground to the pelvis or dramatically change torso angles to enforce dynamic consistency (Thelen and Anderson, 2006), RRA makes small changes to the torso mass center location and overall model mass and kinematics (e.g., joint angles) that result in smaller residuals. Computed muscle control (CMC) (Thelen and Anderson, 2006) was then used to estimate the muscle excitations needed to track the altered joint angles over a full gait cycle. Some muscle excitations were constrained based on EMG data (Perry, 1992) to guide CMC in generating realistic excitations.

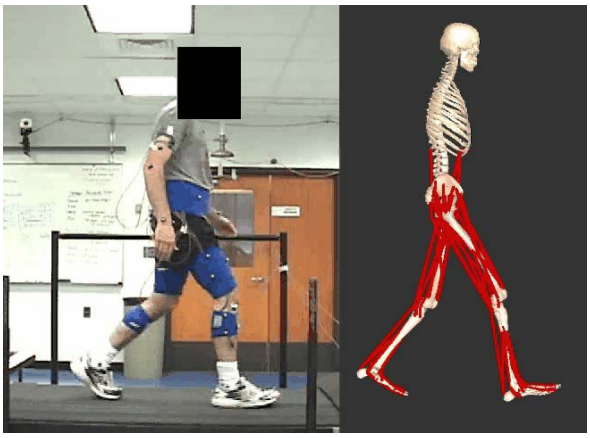

Figure 1: A 3D muscle-actuated simulation generated from motion capture data.

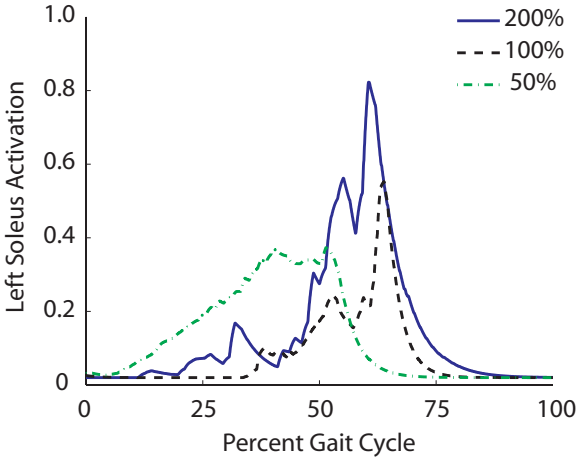

Figure 2: Left soleus activation for three walking speeds over one gait cycle.

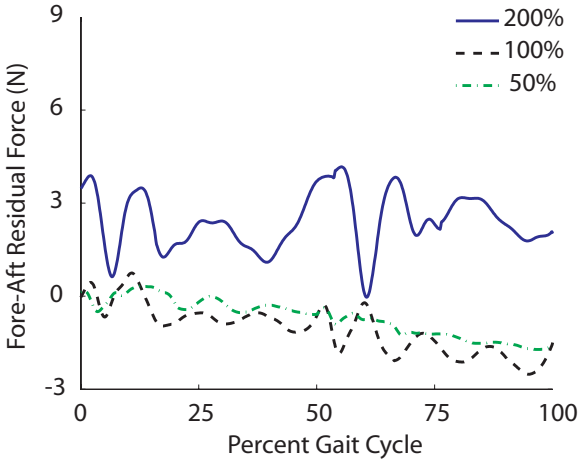

Figure 3: Fore-aft residual force for three walking speeds over one gait cycle.

RESULTS AND DISCUSSION

Each simulation was generated in less than 2 hours on a PC with a 2.8 GHz processor. Tracking accuracy was generally within 1 degree for all joint angles. However, for the fast trials, some tracking errors were as high as 6.2 degrees and the largest RMS error was 2.9 degrees. Muscle excitations were generally consistent with EMG data (Perry, 1992) and modulated with speed. Peak activations for soleus increased consistently with walking speed (Fig. 2). Hip, knee, and ankle joint moments were generally consistent with literature data as well (Inman et al., 1981). The residual forces were reduced significantly by RRA (Fig. 3). The residual moments, which also increased with speed, were more difficult to reduce. For all trials except the fast trials, the residual moments computed by RRA were generally less than 25 Nm. For one subject's near-200% trial, however, the peak absolute value of the sagittal plane residual moment's magnitude was only reduced from 210 Nm to 170 Nm.

CMC has dramatically reduced the computer time needed to generate 3D simulations with complex models, but its application to movements like walking where stability must be preserved, has been limited to movements about 0.5 seconds in duration. RRA allows much longer movements to be simulated, allowing CMC to be used to simulate more activities (e.g., full gait cycles, walk to run transitions). However, RRA does not completely eliminate the residuals, especially in faster movements. Future work will focus on quantifying how large residuals can be before they affect interpretation of muscle function. Our simulations and OpenSim will be made freely available on the web for testing and use by others.

REFERENCES

Delp et al. (in press) *IEEE Trans Biomed Eng*.

Inman et al. (1981) *Human walking*. Williams and Wilkins, Baltimore.

Perry (1992) *Gait analysis: Normal and pathological function*. Slack Inc., Thorofare, NJ.

Thelen and Anderson (2006) *J Biomech* **39**: 1107-1115.

ACKNOWLEDGEMENTS

We thank Ayman Habib, Peter Loan, Paul Mitiguy, May Liu, Allison Arnold, and Darryl Thelen. Supported by NIH Roadmap for Medical Research, U54 GM072970, NIH 18082170-30501-B, GM63495, HD33929, and HD046814.

Dynamic Loading and Biological Growth

Marcelo Epstein, Samer Adeeb and Walter Herzog

University of Calgary, Calgary, AB, Canada
E-mail: mepstein@ucalgary.ca

INTRODUCTION

Biological materials are complex structures that can undergo processes of growth (or resorption) in response to mechanical stimuli. Roughly speaking, these processes are of two kinds: (i) bulk growth, whereby the material particles retain their identity and experience a possible rearrangement (remodeling) with or without increase of mass; and (ii) surface growth, which may affect the very topology of the body (for example, by closing voids). Bulk growth, which is the subject of this paper, can be accompanied by mass diffusion (mass flux), but this effect is disregarded in the present work. One of the first complete models of biological growth was proposed by Hegedus and Cowin (1976). Although not explicitly stated, one of the limitations of this pioneering model is that the new mass finds a way to accommodate itself within the available space without altering the underlying tissue. In some models (e.g., Mullender et al. (1994)), the process of remodeling is accompanied by a change of material properties. A different point of view was advocated by Rodriguez et al. (1994), who introduced a model akin to that of nonlinear plasticity theory based on a multiplicative decomposition of the deformation gradient. A full thermodynamic treatment along those lines was proposed by Epstein and Maugin (2000). From this point of view, one can distinguish between "compliant" processes that can evolve naturally without the need for the intervention of active controlling mechanisms (entropy sinks) and those that cannot. In particular, we investigate the influence of a periodical loading and conclude that, within very general parameters, growth is stimulated in a compliant manner. The model is then incorporated into a finite element package and some examples are presented.

MODEL FORMULATION

As time (t) goes on, a stress-free archetype, representing the basic material constitution, is linearly mapped into each body point (**X**) by means of an *implant* **P(X**, t**)**. The deformation gradient **F** has its usual meaning of mapping the chosen arbitrary fixed reference configuration to the current deformed configuration. The Piola stress **T** is then considered a function of the linear mapping between the stress-free state and the current deformed configuration. This mapping is the composition of **FP**. In addition to the constitutive equations of the archetype, an *evolution law* for the implant **P** is sought that would satisfy thermodynamic requirements. In the absence of mass diffusion and of external entropy sinks, the Clausius-Duhem inequality in its local Lagrangian form is expressed as:

$$\rho_R \dot{\psi}_\rho + \rho_R \theta \dot{s}_\rho - T_i^I v^i{}_{,I} + \frac{1}{\theta} Q^I \theta_{,I} \leq 0$$

where: ρ_R denotes the density of the material in the reference configuration; ψ_ρ is the Helmholtz free-energy per unit mass; θ denotes the absolute temperature; s_ρ is the entropy per unit mass; T_i^I denotes the (mixed) components of the Piola stress **T**; v^i is the velocity field; and Q^I are the components of the heat-flux vector in the reference configuration. A comma preceding

an index indicates partial differentiation with respect to the corresponding coordinate in the underlying (Cartesian) system of coordinates and a dot indicates time derivatives. Following the standard procedure, the residual inequality for the implant evolution is obtained as:

$$\dot{P}^I_\alpha P^{-\alpha}_J m_I^J \leq 0$$

where **m** is the Mandel stress defined as:

$$m_I^J = F^i_I T_i^J$$

A possible law for evolution of the implant **P** can thus be assumed as:

$$\dot{\mathbf{P}} = -kJ_P \, \mathbf{P} \, \mathbf{P}^T \, \boldsymbol{m} \, \mathbf{P}^{-T}$$

where k is a positive material constant and J_P is the determinant of the implant **P**.

EXAMPLE AND FINITE ELEMENT ANALYSIS INCORPORATION

An example is presented to show the behaviour of the evolution law under sinusoidal load and to validate a user subroutine finite element code that was written to incorporate this material model in ABAQUS. A ball of material is assumed to be subjected to a sinusoidal applied load $a(t)=a_0\sin(\omega t)$. The deformation gradient **F** and the implant **P** are equal to $h(t)\mathbf{I}$ and $q(t)\mathbf{I}$, respectively. The constitutive law for Piola stress in the reference configuration is taken as $\mathbf{T} = \mu J_P^{-1} (\mathbf{FPP}^{\mathrm{T}}–\mathbf{F}^{-\mathrm{T}})$ from which the following relation: $h^2 a = \mu/q^3 (h q^2-1/q)$ can be written. The evolution law suggested in the previous section can be used to write the following equation: $\dot{q} = -kq^4h^3a$. The two equations were solved for μ and k =1 using the Mathematica Package. The average value of q obtained is shown to be decreasing with time (Figure 1). This indicates that the model predicts that the material grows under the effect of the sinusoidal load as compared to a static load of the same magnitude. The same problem was solved using ABAQUS by incorporating a user subroutine, UMAT, for the calculation of the Cauchy stress as a function of the deformation gradient and the implant. The nine components of the implant were calculated at the end of each time increment using an Euler time integration scheme and were stored as solution dependent variables to be used in the next increment. The finite element analysis and the Mathematica package produced the exact results.

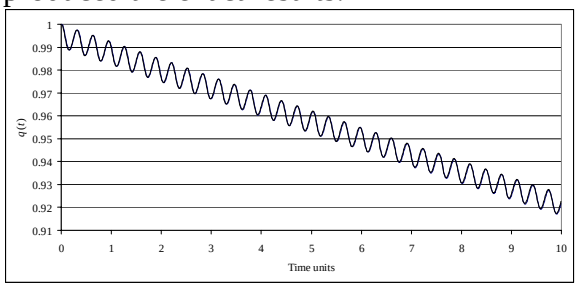

Figure 1. Evolution of the implant $q(t)$.

On the basis of this Benchmark test, more realistic examples will be presented.

SUMMARY

A model for the growth of biological material is formulated and shown to predict the growth of biological material under harmonic loading. The model was incorporated into a finite element package and can be easily calibrated against experimental data to mathematically model growth and resorption in biological tissues.

REFERENCES

Hegedus, D. H. and Cowin, S. C. (1976). *J Elasticity*, **6**, 337-352.

Mullender, M. G. et al. (1994). *J Biomechanics*, **27**, 1389-1394.

Rodriguez, E.K.et al. (1994). *J Biomechanics*, **27**, 455-467.

Epstein, M., Maugin, M.A. (2000). *International Journal of Plasticity*, **16**, 951-978.

ACKNOWLEDGEMENTS

This work has been supported by NSERC

INTEGRATING THE MECHANICAL AND METABOLIC ENERGETICS OF THE SWING PHASE OF WALKING AND RUNNING

Jonas Rubenson[1], Richard L. Marsh[1]
[1]Department of Biology, Northeastern University, web: www.biology.neu.edu

INTRODUCTION

One of the biggest challenges facing biomechanists and physiologists remains explaining the underlying determinants of the metabolic cost of locomotion. Traditional approaches have been hampered by their inability to partition metabolic energy between individual muscles.

Here we use estimates of muscle-specific metabolic rates from bloodflow measurements (Marsh et al., 2004; Rubenson et al., 2006) to explore the determinants of metabolic energy expenditure in an avian model system (domestic guinea fowl). Specifically, we examine whether the metabolic cost of swinging the leg is determined by mechanical energetics.

Given that a considerable component of the overall energy expenditure occurs during the swing phase (Marsh et al., 2004, Doke et al., 2005), knowledge of its determinants will prove important for our understanding of the energetics of normal and dysfunctional gait.

METHODS

Muscle-specific metabolic rates were estimated from previous studies in our laboratory combining whole body oxygen consumption and muscle bloodflow measurements from guinea fowl (*Numida meleagris*) moving on a motorized treadmill (Marsh et al., 2004; Rubenson et al., 2006).

Intramuscular EMG was used to partition the muscles recruited during the swing- and stance-phase.

Using similar size guinea fowl (n = 4; 1.47 ± 0.12 kg; ± S.D.), joint mechanical work was measured using 2-D inverse dynamic modeling as the animals walked and ran on the same treadmill at equivalent speeds. The major joints of the hind limb were identified with reflective markers and videod at 500 Hz (NAC). Center of mass and inertial properties of limb segments from sacrificed animals were determined using a suspension and pendulum method, respectively.

RESULTS AND DISCUSSION

Typical joint angle, moment and power curves for guinea fowl running at 2.5 m s^{-1} are depicted in Fig. 1. Interestingly, both the hip and knee exhibit similar kinematic and kinetic patterns to that of human running (Winter, 1983), whereas the ankle exhibits proportionately greater loading and power generation. The majority of positive work is generated at the hip and ankle and the majority of negative work is generated at the knee.

Metabolic and positive mechanical power of swinging the limb increases with speed, although not proportionately (Table 1). Consequently, the positive mechanical efficiency of swinging the limb during walking remains low (~ 5%), whereas efficiencies during running are greater (~ 12-17%). Interestingly, when the

mechanical efficiency is calculated for ankle flexion, in which all of the mechanical and metabolic work is attributed to a single muscle (*tibialis cranialis*), similar values are obtained as that for the entire limb.

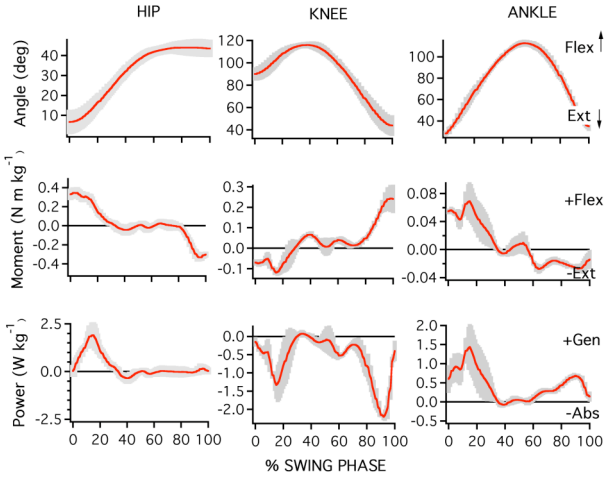

Figure 1: Anglel, moment and power curves for the swing phase (mean ± S.D.) in guinea fowl running at 2.5 m s^{-1}.

SUMMARY/CONCLUSIONS

Given that the maximum positive efficiency of skeletal muscle is ~ 25%, our results indicate that, for running speeds, muscular work may determine a major portion of the metabolic cost of swinging the limb. The situation is, however, complicated due to possible transfer of energy via bi-articular muscles, co-contraction and passive joint moments, which are not accounted for in the present study. These factors are currently being explored and may help to explain the discrepancy between efficiencies during walking and running.

REFERENCES

Marsh RL, et al. (2004). *Science*, **303**, 80-83.

Doke J, et al. (2005). *J Exp Biol* **208**, 439-445.

Rubenson J. et al. (2006) *J Exp Biol* **209**, 2395-2408.

Winter DA. (1983) *J Biomech* **16**, 91-97.

ACKNOWLEDGEMENTS

Supported by NIH grant AR47337 to RLM.

Table 1: Metabolic power, positive mechanical power, and positive mechanical efficiency of swinging the limb.

	Walking Speed (m s^{-1})	**Running Speed (m s^{-1})**	
	0.5	**1.5**	**2.5**
Metabolic Power (W kg^{-1})	1.78	4.34	6.32
+'ve Mechanical Power (W kg^{-1})	0.06 ± 0.02	0.43 ± 0.11	0.88 ± 0.13
+'ve Mechanical Efficiency	5.0 ± 1.0	12.2 ± 3.5	17.0 ± 3.4

A NOVEL ELASTIC FOUNDATION CONTACT DETECTION ALGORITHM FOR USE IN A SIX DEGREE OF FREEDOM KNEE MODEL

G. Nathan Green and Roger V. Gonzalez

LeTourneau University, Longview, TX, USA
E-mail: RogerGonzalez@letu.edu

INTRODUCTION

To estimate intersegmental contact forces between complex geometric surfaces, elastic foundation contact models must treat contacting surfaces as though they are "beds of springs" that, when in contact, apply viscoelastic forces on each other. Such models have been used by Neptune et al. (2000); Fregly et al. (2003); and Bei and Fregly (2004); to represent ground contact events, artificial knee replacements, and biological knees without the meniscus. One of the algorithms (Neptune et al., 2000), has been made commercially available as a part of Software for Interactive Musculoskeletal Modeling (SIMM), while the other (Fregly et al., 2003) is not commercially available. The former algorithm is used solely for ground contact events. As such, it is not suitable to model complex surface geometries. We propose a novel contact detection algorithm that utilizes the strengths of the elastic foundation models of Fregly et al., within a SIMM™ environment.

This new algorithm is currently being verified with a six degree of freedom SIMM knee model. Contact forces at the tibiofemoral joint are calculated with the algorithm and verified with experimental data of contact pressure and ligament strain in cadaver specimens. Once verified, we believe the model will be a stand alone method for descriptive and predictive analysis of intersegmental contact forces for complex geometric bone surfaces.

METHODS

To incorporate our elastic foundation contact algorithm into SIMM, existing spring based algorithms were altered to progress beyond the planar contact detection in SIMM. Currently, SIMM allows the user to have one *spring floor* (2D) per body segment to simulate contact detection. For our purposes, these spring floors have been replaced with *spring contact surfaces* (3D). Each surface is a polyhedron that is allowed to rest on a bed of *spring points* (e.g. surface – femur, spring points – tibial plateau).

During a simulation, spring points pass through their corresponding spring surface with spring forces calculated based on the equation by Neptune, 2000:

$$F_{contact}(i) = \max \begin{bmatrix} 0 \\ area(i) \cdot (c_1 \cdot dz(i)^{c_2} \\ + c_3 \cdot dz(i)^{c_4} \cdot d\dot{z}(i)^{c_5}) \end{bmatrix}$$

Where constants $c_1 - c_5$ are material specific constants and area(i) is the representative area of the i^{th} spring point. The values $dz(i)$ and $d\dot{z}(i)$ are the displacement and velocity normal to the plane of contact. The plane of contact is defined by the triangles of the polyhedron that defines the contact surface. Each spring point is compared spatially to each triangle of the contact surface to determine if the point is directly below the triangle. Forces are then calculated and applied in the standard SIMM environment.

The method presented is a general contact detection algorithm in that it can be used for any number and any type of geometric surfaces in a SIMM model. Currently, it is being applied to four contact regions: the

medial and lateral cartilage and meniscus of our knee model. Verification of our model is in progress by means of cadaver knee specimen experiments using Tekscan™ pressure sensors for intersegmental forces (Bowen, et al. 2007).

RESULTS

Contact for complex geometries has been visualized using MATLAB™ (Green, et al. 2007). The contact points match visual expectations well (Figs. 1 and 2). This was the first indication that the algorithm was accurate. Simulations calculating contact forces have since been performed.

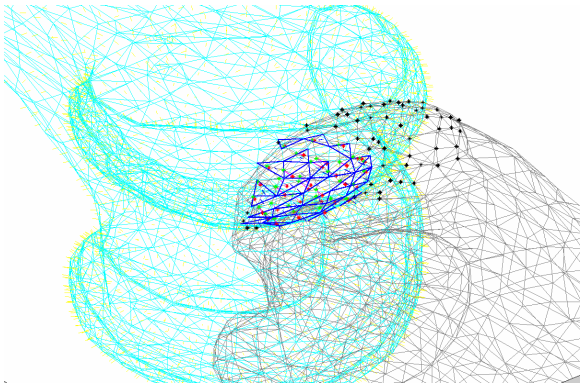

Figure 1: Cyan – Femur, Gray – Tibia, Dark Blue – penetrated regions of the femur, Green – penetrated spring points on tibia, Red – points of contact on femur, Black non-penetrated spring points.

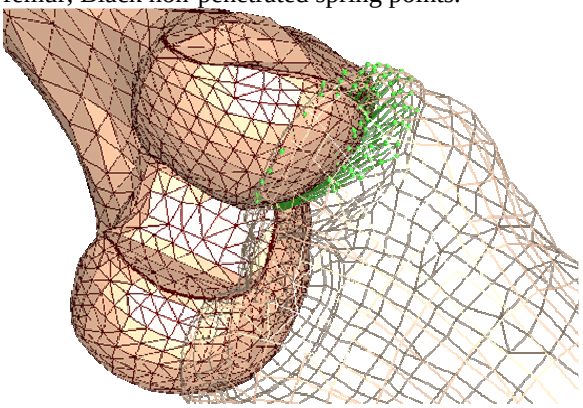

Figure 2: The same knee in SIMM, corresponding to the penetrations as shown in figure 1.

Preliminary results have shown that the new algorithm yields identical results to the method of Neptune et al. in cases for which their approach is still valid. Currently, we have only validated this model on a planar surface, requiring further assessment to be performed soon.

Toward this more comprehensive assessment, experimental data of subjects performing cutting and jumping maneuvers have been performed measuring joint kinematics and muscle activity. Muscle activity is used to estimate muscle forces as per Manal et al (2002). These muscle forces, along with the knee flexion extension angle, are used to drive an experiment utilizing a cadaver specimen test fixture previously mentioned. The same data is used as the input to a constrained, forward dynamic simulation of our SIMM knee model based upon the geometry of the cadaver knee. Comparison of the experiments and simulations will verify both the model and the algorithm.

CONCLUSION

This paper seeks to present a novel contact detection algorithm that has produced results consistent with literature. Further research is needed to extend verification to experimental data so that the algorithm, and SIMM models that employ it, can be used for predictive purposes.

REFERENCES

Bei, Y. and Fregly, B. J. (2004). *Medical Engineering & Physics*, **26**, 777-789.

Bowen, J. and Gonzalez, R.V. (2007). *24th Houston Soc Eng Med Bio*, p. 71.

Fregly, B. J., et al. (2003). *J. Biomechanics*, **36**, p. 1659-68.

Manal, K., et. al. (2002) *Coms Bio Med* **32**: 25-36.

Green, G.N. and Gonzalez, R.V. (2007). *24th Houston Soc Eng Med Bio*, p. 72..

Neptune, R. R., et al. (2000) *Comp Meth Biomech Biomed Eng*, **3**, 321–34.

ACKNOWLEDGMENTS

This work was funded in part by:
NSF-BES Grant (RUI-0201889) and NIH (R15-AR051316)

MECHANICAL TESTING OF TENDON IN TRANSVERSE COMPRESSION

STS Salisbury, CP Buckley, and AB Zavatsky

Department of Engineering Science, University of Oxford, Oxford, UK
E-mail: amy.zavatsky@eng.ox.ac.uk, Web: www.eng.ox.ac.uk

INTRODUCTION

Tendons primarily experience tensile loading along their fibre-aligned direction. They may at the same time also undergo compression and shear. Some of these complex loadings occur normally, as when a tendon wraps around a bone and is subjected to longitudinal tension and transverse compression. Other complex loadings are abnormal and may lead to rupture, as occurs at the rotator cuff (Józsa and Kannus, 1997).

Most mechanical testing of tendon has been performed in tension along the fibre-aligned direction. Testing in the transverse direction is far less common and has only been performed in tension (Bonifasi-Lista et al., 2005; Lynch et al., 2003; Quapp and Weiss, 1998). There appear to be no data in the literature on the transverse compressive properties of tendon. Such information is very important for the creation of finite element models of tendon.

The aim of this study was to measure the mechanical properties of tendon in compression transverse to the fibre-aligned axis.

METHODS

Ten digital extensor tendons from the bovine foot were dissected immediately after slaughter and frozen at -18°C. Samples were defrosted the day before testing and soaked in 10% sucrose solution overnight. Prior to testing, samples were rinsed with phosphate buffered saline (PBS).

Mechanical tests were done on ten specimens using a specially designed rig which also allowed measurement of tendon cross-sectional area (Salisbury et al., 2006a, 2006b). The tendon sample hung under its own weight and was compressed at mid-substance between two glass backing plates, one a window (40mm×50mm) in a paddle used to compress the tendon (Y-displacement). Paddle movement was measured with an LVDT (RDP Electronics DCT-500A, UK). A digital video camera (Basler A631f, Germany) recorded the change in transverse width of the specimen through the glass window (X-displacement) every 5s. All tests were carried out at room temperature.

Each sample was first preconditioned by applying a 20.8 N compressive load ten times for 10s at a time with 10s recovery between each successive load. Then sample cross-sectional area was measured at five sections along the tendon at the same level as the glass window, after which the tendon was placed in a 10% sucrose solution bath for 1 hr while still mounted in the test rig.

Subsequently, for three of the tendon samples, six load profiles were applied, each lasting 13 min, with 1 hr recovery time in the sucrose solution between each. The load magnitudes were 2.8 N, 20.8 N, 39.7 N, 2.8 N, 20.8 N, and 39.7 N. Each load was applied for 120s followed by 660s of recovery. Prior to the application of each load profile, a 0.9 N compressive load was applied for 5s and then removed. The peak value of displacement during this time was taken as the zero point. From this data, repeatability was

calculated using the method advocated by Hayward (1977).

For the remaining seven tendon samples, ten load profiles were applied. The procedure was the same as for the previous three tendons; however, the load magnitudes were 0.9 N, 2.3 N, 3.8 N, 5.7 N, 8.5 N, 12.3 N, 17.0 N, 22.7 N, 30.2 N, and 39.7 N.

RESULTS AND DISCUSSION

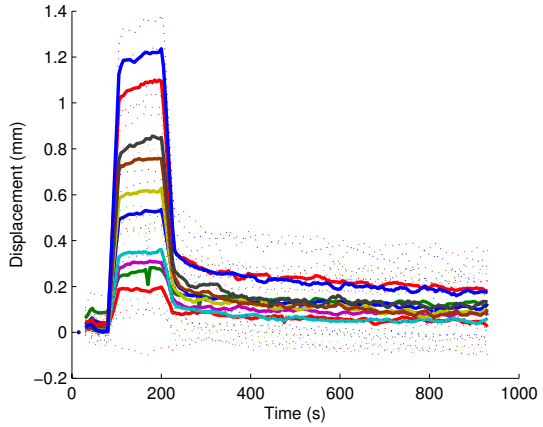

Figure 1: Mean *X*-displacement ± one standard deviation vs. time curves for seven tendon samples under ten load magnitudes.

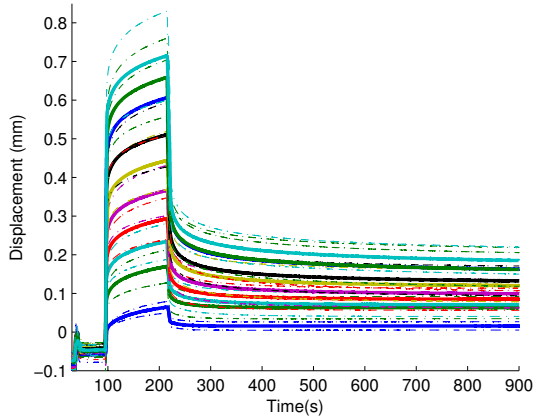

Figure 2: Mean *Y*-displacement ± one standard deviation vs. time curves for seven tendon samples under ten load magnitudes.

Loading responses are shown in Figures 1 and 2. For a given load, variability was found in mechanical response between tendon samples. This is due to variation both in tendon shapes and in mechanical properties. Tendons did not recover fully upon removal of load – the amount of plastic deformation increased in both the *X*- and *Y*- directions as greater loads were applied. The mean cross-sectional area of the samples was 39.1 mm^2. Repeatability of displacements in the *X*-direction was ±0.04 mm 10s after load application, ±0.05 mm 100s after load application, and ±0.02 mm in recovery.

SUMMARY/CONCLUSIONS

A new method for studying transverse compressive creep of tendons has been presented. With the load, displacement, and sample shape data collected, enough information is available to perform finite element simulations of the test, and hence obtain constitutive model parameters by inverse analysis.

REFERENCES

Bonifasi-Lista, C. et al. (2005) *J Orthop Res* **23**, 67-76.

Hayward, A.T.J. (1977) *Repeatability and Accuracy*. Mechanical Engng Publications.

Józsa, L.G. and Kannus, P. (1997) *Human tendons*. Human Kinetics.

Lynch, H.A. et al. (2003). *J Biomech Eng* **125**, 726-731.

Quapp, K.M. and Weiss, J.A. (1998) *J Biomech Eng* **120**, 757-763.

Salisbury, S.T.S. et al. (2006a) *Proc Brit Orthop Res Soc*, 35-36.

Salisbury, S.T.S. et al. (2006b) *J Biomech* **39(S1)**, S498.

ACKNOWLEDGEMENTS

This work was supported in part by the Leverhulme Trust (UK).

CHANGES IN SPRING-MASS CHARACTERISTICS DURING 400M SPRINT

Hiroaki Hobara [1], Kouki Gomi [2], Tetsuro Muraoka [3], and Kazuyuki Kanosue [1-3]

[1] Graduate School of Human Sciences, Waseda University
[2] Faculty of Sport Sciences, Waseda University
[2] Consolidated Research Institute for Advanced Science and Medical Care, Waseda University, Saitama, JAPAN
E-mail: h_hobara@moegi.waseda.jp, Web: www.f.waseda.jp/kanosue/

INTRODUCTION

For the biomechanical analysis of running, the whole body is often modeled with a spring-mass model composed of a body mass and a linear leg spring (Butler et al., 2003). Vertical stiffness (K_{vert}), which is defined as the ratio of the vertical leg spring compression at a given force during ground contact, is known to strongly influence the running performance (Butler et al., 2003).

How the K_{vert} during running changes with fatigue is still a matter of debate. Morin et al. (2006) clearly showed that the K_{vert} decreased with repetitive 100-m sprint running. However, Dutto and Smith (2002) failed to see a consistent change in K_{vert} during treadmill running to exhaustion.

The purpose of the present study was to investigate whether the fatigue induces the change in K_{vert} during 400 m sprinting, because it requires runners to run till the full exhaustion at the goal (Nummela et al. 1992).

METHODS

Eight male athletes participated in the study. Before the start of experiment, the subjects warmed up for 20 min. Then, each subject was instructed to run for 400 m with a maximal effort on an outdoor field track.

According to the previous study (Morin et al., 2005), the K_{vert} was calculated as the ratio of the estimated peak force (F_{max}) and the estimated vertical center of mass displacement ($\triangle y_c$):

$$K_{vert} = F_{max} \cdot \triangle y_c^{-1}$$

$$\text{with } F_{max} = mg\pi/2\,(t_f / t_c + 1)$$

where m is the total body mass, t_f the flight time and t_c the ground contact time

$$\text{and } \triangle y_c = F_{max}\, t_c^2 / m\pi^2 + g t_c^2 / 8$$

The t_f and t_c were determined by the output waveform of the accelerometer, which was attached to the subject's right heel with sampling frequency at 1 kHz. Obtained signals were averaged over each interval of 50 m during the entire running period.

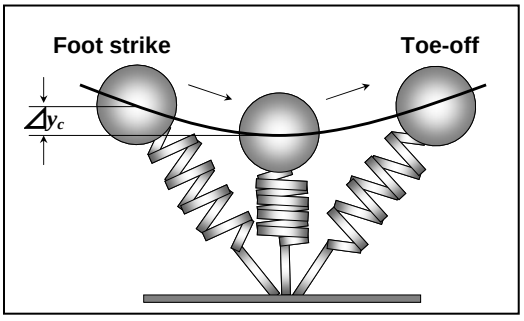

Figure 1: Spring-mass model in running. The leg spring is compressed during the first half of the stance phase and rebounds during the second half. $\triangle y_c$ represents the vertical displacement of the center of mass.

The effect of fatigue on the K_{vert} was analyzed with the one-way repeated measures ANOVA. Dunnet's post-hoc multiple comparison test were performed if a significant main effect was observed.

RESULTS AND DISCUSSION

The subjects ran 400 m in 52.67 ± 0.92 s. Running speed peaked at 50-100 m period, and it consistently decreased from the middle to the later part of the entire running period (Fig. 2). This result is in line with the earlier findings that the running performance began to decrease during the first quarter of the 400 m sprint, due to the fatigue (Nummela et al. 1992).

Figure 2 also shows the consistent decrease in K_{vert} over an entire 400 m sprinting. The K_{vert} peaked at 50-100 m period, and it gradually decreased until the last interval. Because the K_{vert} during sprinting depends on the knee joint stiffness (Kuitunen et al., 2002), observed changes in K_{vert} would be due to the decrease in knee stiffness.

SUMMARY/CONCLUSIONS

During 400 m sprinting, vertical stiffness peaked at 50-100 m interval and then gradually decreased towards the end of the race, which is in parallel with the change in running speed.

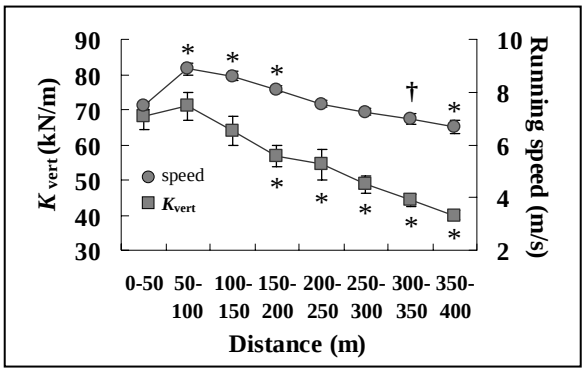

Figure 2: Changes in K_{vert} through an entire running period. A dagger (†) and an asterisk (*) indicate significant differences between two conditions; $p < 0.05$ and 0.01, respectively.

REFERENCES

Butler, R.J. et al. (2003). *Clinical Biomechanics,* **18**, 511-517.

Dutto. J., Smith. G.A. (2002). *Medicine & Science in Sports & Exercise,* **34**, 1324-1331.

Kuitunen S. et al. (2002). *Medicine & Science in Sports & Exercise,* **34**, 166-173.

Morin J.B. et al. (2005). *J. Appl Biomech,* **21**, 167-180.

Morin J.B. et al. (2006). *Int J. Sports Medicine,* **27**, 158-165.

Nummela. A. et al. (1992). *J. Sports Science,***10**, 217-228.

ESTIMATION OF HIP-MUSCLE GEOMETRY USING AUTOMATED, NON-RIGID ATLAS-BASED REGISTRATION OF MR IMAGES

Lennart Scheys [1], Ilse Jonkers [1], Dirk Loeckx [1], Anja Van Campenhout [2], Arthur Spaepen [1] and Paul Suetens [1]
[1] Katholieke Universiteit Leuven, Belgium
[2] Universitaire Ziekenhuizen Leuven, Pellenberg, Belgium
E-mail: lennart.scheys@uz.kuleuven.ac.be, Web: http://mic.uzleuven.be

INTRODUCTION

The analysis of parameters related to the muscle-tendinous structures (such as muscle tendon length, moment arm) during gait is highly relevant in patients presenting motor coordination dysfunction as well as skeletal deformity. Such analysis requires the use of musculoskeletal (MS) models. In general, these models are created by rescaling and deforming generic models based on data of healthy adult men. However fast, this procedure leads to models suffering from low accuracy and little patient-specific detail. Especially when analyzing gait in a paediatric and/or pathologic population, accommodation of the models for inter-individual variability in musculoskeletal geometry is needed. Modelling based on Magnetic Resonance Imaging (MRI) has great potential to generate individualized MS models. However, at present, the level of user interaction required for parameter extraction based on manual segmentation limits the applicability of this approach in a broader context.

This work presents the potential of a method to automatically identify muscle geometry (attachments and muscle path) by atlas-based non-rigid image registration in patients with increased femoral anteversion (FA).

METHODS AND PATIENTS

A pediatric atlas (age 9y, FA 31˚) was build by manual delineation of muscle geometry in a full-leg MRI volume, using a custom build software tool [ref]. Based on this atlas, muscle paths were automatically identified in MR images from 3 cerebral palsy (CP) subjects (average age 10.3y, average FA 38˚) using non-rigid image registration: in a first step the geometrical relation between both image volumes was determined by matching the image volumes using intensity-based, non-rigid image registration. The non-rigid deformation of the atlas image was modelled by a B-spline deformation mesh. The cost function uses mutual information as a similarity measure while a volume penalty term discourages improbable or impossible deformations. In a second step, the patient's muscle paths were retrieved by applying the resulting 3D deformation field to the original musculoskeletal geometry from the atlas. For each subject, a reference model was build using manual delineation. Hip joint centres were calculated by fitting a sphere to the segmented femoral head, using the iterative closest point algorithm.

Absolute differences in musculotendon (MTL) and moment arm lengths (MAL) for 21 major hip muscles are calculated between (1) the automatically and (2) the manually defined MS model using SIMM (Musculographics, Inc.). This was done for the scanned supine position. For MTL, differences are normalized to the MTL of the manually defined MS model. For MAL, absolute differences are reported for each plane of movement (adduction, rotation and flexion).

RESULTS

Table 1 presents the differences in MTL and MAL for the 21 muscles in the model. The average differences in normalized MTL remain below 10% in each of the subjects, with a maximum over 20% for the M. adductor longus and brevis. Larger MTL-errors are present in muscles with two or more lines of action (e.g. adductor magnus and glutei). The average error in these muscles measured 10.8, 11.1 and 10.8 compared to 6.7, 5.5 and 7.0 for each subject respectively. Average errors in MAL range between 3.51 mm in hip rotation, 4.62 mm in hip adduction and 6.68 mm in flexion, with maximum errors just over 20 mm reported in M. Gracilis for flexion and M. Adductor brevis for adduction.

DISCUSSION

Comparison of muscle tendon lengths and muscle moment arm lengths between the automatically and manually defined MS models shows that non-rigid, atlas-based registration of the MR images results in a valid estimate of the muscle paths, even in the presence of a large variation in femoral geometry. The proposed method therefore yields a good initial guess for user evaluation of the automatically proposed muscle line of action combined with the MR images. Consequently, the amount of user interaction as well as the total modelling time required for the creation of subject-specific musculoskeletal models can be reduced substantially. Careful selection of the appropriate atlas image will be essential to further improve the performance of the presented methodology and test the generalization of its performance in other pathological conditions.

SUMMARY/CONCLUSIONS

Automatic identification of muscle geometry using atlas-based, non-rigid registration of MR images enhances the feasibility to build detailed, subject-specific musculoskeletal models for biomechanical analysis of gait deviations in subjects suffering aberrant musculoskeletal geometry**.**

ACKNOWLEDGEMENTS

We acknowledge the support from the research council Flanders (Grant.0570.05)

Table 1: calculated absolute differences between manual and automatic delineation for all muscles from subject A (age 8, FA 42°,, ♂), B (age 11, FA 27°, ♂) and C (age 12, FA 46°, ♀).

	Hip Adduction MAL (mm)			**Hip Rotation MAL (mm)**			**Hip Flexion MAL (mm)**			**Normalized MTL**		
Subject =>	A	B	C	A	B	C	A	B	C	A	B	C
Glut max (n=3)	6.9	5.4	4.6	7.4	4.1	3.4	2.4	8.4	3.2	10.1	11.7	12.5
Glut med (n=3)	1.5	1.8	3.6	3.5	6.3	3.4	6.4	3.2	5.1	12.1	12.3	22.5
Glut min (n=3)	2.4	2.7	3.8	7.1	7.9	3.4	1.5	0.7	8.4	8.3	13.5	4.9
Add mag (n=3)	14.3	0.6	3.2	1.6	2.7	4.1	14.4	14.5	10.7	12.5	6.8	3.0
Tensor FL	3.5	2.5	5.8	5.5	4.6	8.3	1.7	8.5	0.7	3.4	6.8	2.6
Add long	11.7	0.2	6.4	3.6	3.6	9.2	3.8	11.6	3.9	7.3	26.7	24.8
Add brev	21.1	7.9	5.6	7.4	4.0	0.4	8.4	17.5	2.6	24.8	11.0	10.1
Gracilis	11.3	2.7	13.9	1.6	1.3	1.2	18.3	27.1	8.6	3.2	0.3	8.2
Semimem	2.4	0.4	1.3	0.4	0.5	0.7	4.5	10.5	0.4	2.1	0.2	0.2
Semiten	1.8	3.1	3.3	1.5	9.4	2.6	5.0	8.4	3.8	4.8	2.0	0.2
Bi Fem LH	0.8	3.8	2.9	0.5	0.2	0.8	1.5	8.4	6.6	3.8	0.2	6.7
Sartorius	2.8	3.2	2.4	3.2	3.3	4.8	4.9	7.1	3.0	4.2	2.3	4.7
Rect fem	3.1	3.5	2.2	1.5	0.2	1.5	3.4	1.2	0.5	6.6	0.2	5.7
Average	**4.62 ± 4.4**			**3.51 ± 2.69**			**6.68 ± 5.73**			**7.78 ± 7.07**		

Polyethylene stresses in Unicompartmental knee replacements during a step-up activity.

D.J Simpson[1] and H.S Gill[1]

[1]Nuffield Department of Orthopaedic Surgery, University of Oxford, UK.
email: david.simpson@ndos.ox.ac.uk

INTRODUCTION

The use of a thin bearing in Unicompartmental knee replacements is advantageous because more bone is preserved. However, very thin bearings can be associated with bulk failure and increased wear.

Osteolysis, resulting from a foreign body response to particulate debris, is a significant failure mechanism with knee arthroplasty [1]. The primary cause of osteolysis around knee replacements is from wear debris produced at the articulating surfaces. Wear rate of polyethylene can increase exponentially with increasing contact pressure [2] therefore contact stress analysis of knee arthroplasty designs can be used to predict performance.

Finite Element (FE) analysis is usually carried out at discrete points of an activity. The aim of this study was to compare the peak contact stress in a fully congruent mobile polyethylene (PE) bearing and a fixed flat PE bearing throughout the entire step-up activity, using a validated FE model.

METHODS

A validated FE model of a cadaver tibia implanted with a cemented tibial tray was used in this study [3].

Two implanted tibia models were used with a common spherical femoral component. A mobile, fully congruent, Oxford Unicompartmental bearing, (Biomet, Swindon, UK), and a generic flat bearing were inserted into the FE models. In both cases the minimum thickness was 3.5mm.

The tibial tray and femoral component were modelled as cobalt chromium, linear elastic and isotropic. The cement layer was modelled as linear isotropic. A nonlinear material model was used for the PE bearing [4].

Kinematic data from fluoroscopy measurements during a step-up activity was used to determine the relative tibial-femoral positioning for each model; this was a function of knee flexion angle.

The load data was adapted from in-vivo measured loads using an instrumented implant during a step-up activity [5]. Separate loads were applied to the medial and lateral compartment and these were scaled to a subject of mass 74kg (mass of tibia donor).

A Coulomb friction contact model was used to simulate the PE / metal bearing surfaces; for the fixed bearing the PE was fully bonded to the tibia. A coefficient of friction was taken from literature [6].

The peak stresses in the fixed flat bearing were assessed as a function of bearing thickness. The thickness of the flat fixed bearing was varied from 2.5mm to 6.5mm.

RESULTS AND DISCUSSION

Fully congruent articulating surfaces between the femoral component and the PE bearing significantly reduce the peak contact stress and peak von Mises stress in the bearing over the entire step-up activity (Figures 1 and 2).

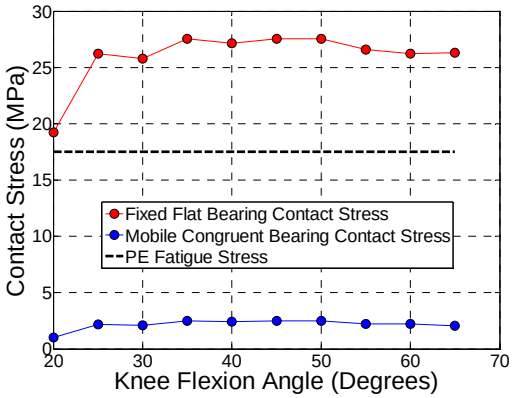

Figure 1 – Peak contact stress on the bearing surface over entire step-up activity.

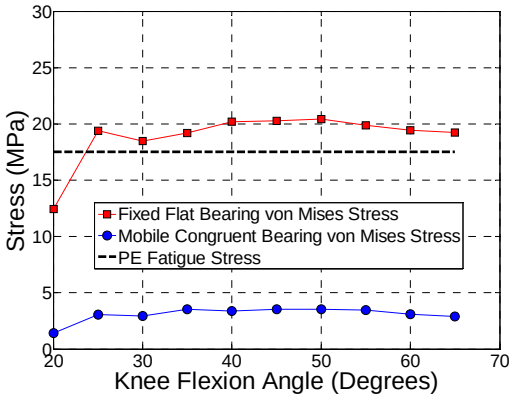

Figure 2 - Peak von Mises stress in the bearing over entire step-up activity.

A bearing thickness greater than 4mm ameliorates the stresses in the flat fixed bearing to below the fatigue limit. A minimum thickness of 6.5mm is required to achieve the lowest von Mises stress in the fixed flat bearing (Figure 3).

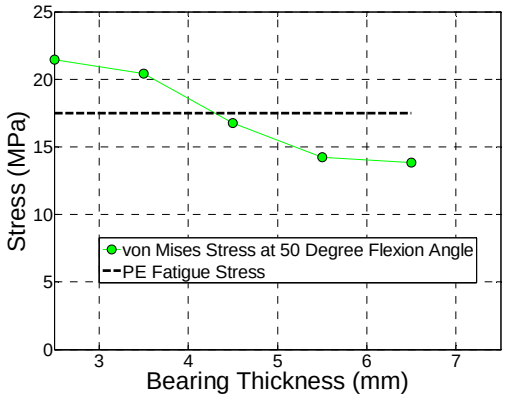

Figure 3 – Peak von Mises stress in the flat fixed bearing for 50^{o} flexion angle.

This study has compared the stresses on a fixed flat and mobile congruent bearing for a Unicompartmental knee arthroplasty over an entire step-up activity. The danger with thin fixed bearings is the stresses are close to the fatigue limit. The results of the model raise concerns about using relatively thin, fixed PE bearings and demonstrate that congruent designs can be markedly thinner without approaching the material limit.

Mobile congruent bearings have a greater potential for being bone conserving. A minimum potential saving of 3mm is possible with a mobile congruent bearing.

REFERENCES

1. Naudie DD, et al. *Instr Course Lect*, ***53***, 251-259, 2004.
2. Bartel DL, et al. *JBJS*, ***68***(7), 1041-1051, 1986.
3. Gray HA, et al. *Proceed. 5th World Congress of Biomechanics, Munich, Germany: J Biomech, 2006.*
4. Kurtz SM, et al. *J Orthop Res, **14**, 755-761, 1996.*
5. D'Lima DD, et al. J Arthroplasty, **21**, 255-262, 2006.
6. Shen C, et al. Wear, **30**, 349-364, 1974.

THE EFFECT OF USING MODULAR NECKS WITH AN UNCEMENTED HIP STEM ON PRIMARY STABILITY

D.J Simpson[1], J.P Little[2] and H.S Gill[1]

[1]Nuffield Department of Orthopaedic Surgery, University of Oxford, UK
[2]Queensland University of Technology, Australia
email: david.simpson@ndos.ox.ac.uk

INTRODUCTION

Total Hip arthroplasty (THA) carried out using modular implants affords the surgeon greater intro-operative flexibility [1] and permits more controlled stem positioning.

Long term survivorship of a hip stem can be predicted in terms of primary and secondary stability; a lack of primary stability is associated with early loosening [2].

The aim of this study was to compare a modular neck design to a proven uncemented stem design using finite element analysis and to look at the primary and secondary stability of each.

METHODS

An uncemented modular-neck THA (Profemur-Z, Wright Medical, USA) and a Zweymuller type device (Hipstar, Stryker, Europe) were separately modelled implanted in the same femoral geometry, an intact femur using the Muscle Standardised Femur (MuscleSF) [3]. Effects of a short extended (41mm), long extended (50mm), long retroverted and a long anteverted modular neck were examined. The interface surfaces between the implant and bone were represented with contact models. Bonded (no sliding or separation), and rough (separation permitted but no sliding) contact were used to investigate the secondary stability of the stems, and a Coulomb frictional contact model (μ ranged from 0.1 to 0.5) was used to investigate the primary stability of the stems. A physiological loading condition simulating an instant at 10% gait of the gait cycle was applied to all models and solved using ANSYS. Boundary conditions at the distal femur simulated the physiological constraint from the tibial condyles and the patella. Linear elastic, isotropic material properties were assigned to the model materials.

Principal stresses on the outer, medial surface of the cortical bone were compared between the Intact, Profemur-Z and Hipstar.

RESULTS AND DISCUSSION

A contact gap of between 0 and 8μm was observed on the medial contact interface for each configuration (Figure 1). The contact gap between implant and bone changed significantly with the coefficient of friction (Figure 2). The surface roughness of an implant can promote boney in-growth, but may also result in a larger separation between the bone and implant. Surface roughness of the stem was more dominant than neck length when considering the interface surface gap. Furthermore, the longer neck design was more comparable to the intact femur (Figure 3). The modular-neck device did not differ significantly from the non-modular stem in terms of primary stability.

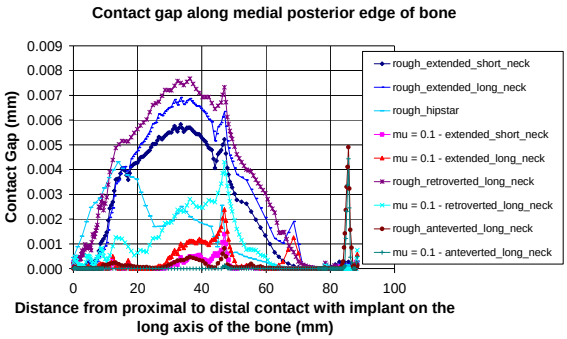

Figure 1: Contact gap on medial contact interface.

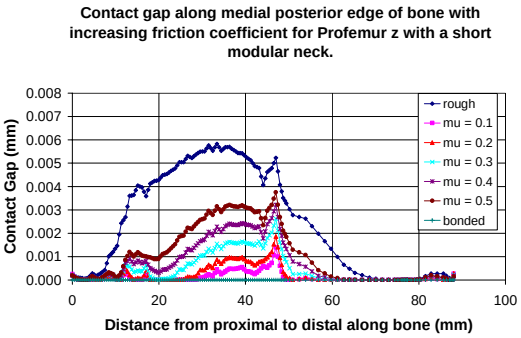

Figure 2: Contact gap as a function of Friction coefficient

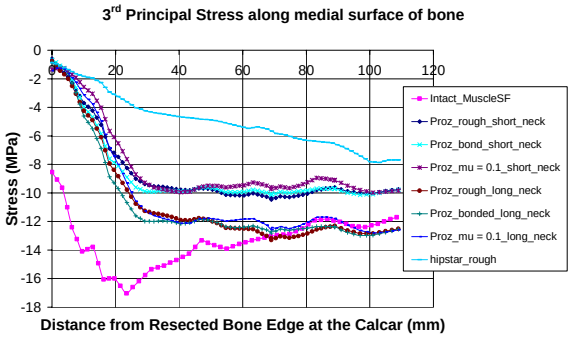

Figure 3: Variation of principal stress on the medial cortical bone surface.

REFERENCES

1. McCarthy, et al. *Clin. Orthopaedics.* **344**, 162-171, 1997.
2. Viceconti, et al. *J Biomech* **39**, 1169-1179, 2006.
3. Viceconti, et al. *J Biomech* **36**, 145-146, 2003.

A COMPUTATIONAL APPROACH TO BONE REMODELING POSTOPERATIVE TO FACET FUSION

Ferris M. Pfeiffer [1,2], Dr. Dennis L. Abernathie [2,3], and Dr. Douglas E. Smith [1]

[1] University of Missouri, Columbia, MO, USA
[2] Brenoak Labs LLC, Columbia, MO, USA
[3] Columbia Orthopaedic Group, Columbia, MO, USA
E-mail: f.pfeiffer@brenoaklabs.com

INTRODUCTION

The mechanical and biologic factors that drive bone fusion can be better understood. This is evident in the fact that of the approximately 200,000 spine fusion procedures performed each year failure to achieve a bony union can occur in as many as 40% of the cases (Boden 2002). Advances in computational methods and mathematical modeling of bone fusion make it advantageous to use numerical methods such as the finite element method, to better understand bone remodeling mechanics.

It has been observed for some time that bone adapts due to mechanical stimulus. Wolff described bone as a self optimizing material. Mullender et. al. (Mullender and Huiskes 1995) described the process of maintenance and adaptation in the hip as a local, cell-based control process.

Jovanovic and Jovanovic (Jovanovic and Jovanovic 2004) used a similar method to model the 2D structure of a cross section through the body of a vertebra. These studies demonstrate the usefulness of applying methods of bone remodeling to answer biologic questions, and they give a sound justification for the methods proposed here.

METHODS

In this work, a bone remodeling algorithm is adapted from the methods introduced by Mullender et al. (Mullender and Huiskes 1995). A general outline of the remodeling algorithm is shown in figure 1.

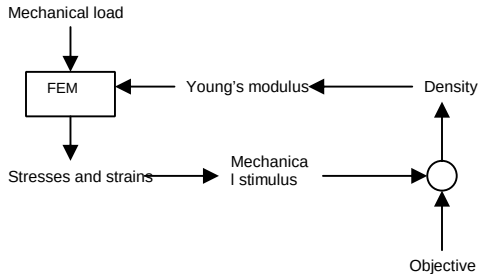

Figure 1. Proposed remodeling algorithm

A user material is developed for integration into Abaqus finite element software. Each Gauss point is assigned a material property based upon the strain energy density calculated from the previous analysis step. Using a gauss point approach eliminates discontinuous solutions. A 4^{th} order Runge-Kutta solution approach is used to calculate the density change for each analysis step.

A vascular model is developed from literature and clinical observation. This model is incorporated into the remodeling approach, and is shown to improve the accuracy of the solution when compared to data from a study of posterolateral fusion in sheep.

Geometric data is taken from computed tomography (CT) scans of sheep specimens and is digitally instrumented in a manner consistent with actual surgical alteration used in an animal study. Figure 2a shows the digital model, and figure 2b gives a

surface representation of the actual specimen.

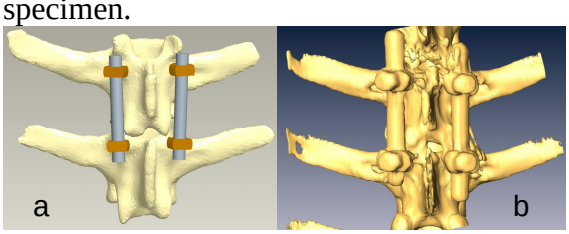

Figure 2. Instrumented a) CAD model and b) isosurface of specimen 1.

Loading is determined from static analysis of an adult sheep. This load is applied to the superior surface of the superior vertebra while the inferior surface of the inferior vertebra is fixed. The remodeling algorithm presented previously is applied and the simulation is run until steady state is reached.

RESULTS AND DISCUSSION

The predicted results agree well with actual results. Accuracy is improved when the vascular model is included as is seen in figure 3. Figure 4 shows the final configuration of bone with an increased mass at the facet joint and a reduction of the lateral mass consistent with clinical practice and study data.

SUMMARY/CONCLUSIONS

Once adequate validation is achieved, the method is applied to human CT scans to evaluate the response to loading subsequent to facet fusion surgery. This method allows for simulation of bone remodeling response to an altered stress state. A better understanding of the response to surgical alteration can benefit surgeon and patient. This can also lead to improved designs of fixation instrumentation that improves the environment for bone growth and leads to increased rates of fusion.

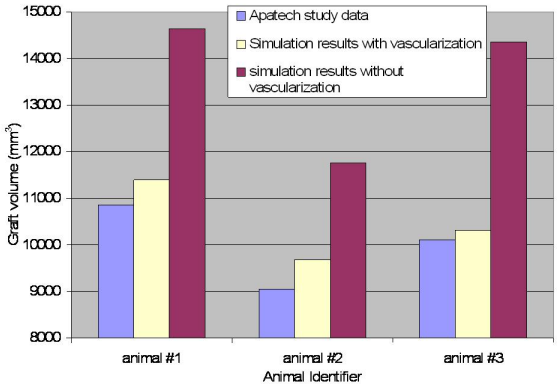

Figure 3. Volume of graft from physical study and simulations.

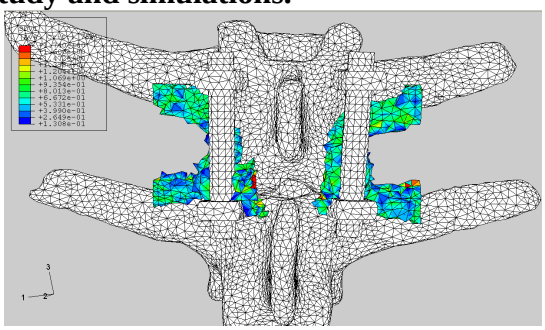

Figure 4. Approximate geometry for remodeled bone graft predicted by simulation including vascular effects for animal #1.

ACKNOWLEGEMENTS

The authors would like to thank Apatech Ltd for the use of fusion study material.

REFERENCES

Boden, S. D. (2002). "Overview of the Biology of Lumbar Spine Fusion and Principles for Selecting a Bone Graft Substitute." Spine **27**: S26-31.

Jovanovic, J. D. and M. L. Jovanovic (2004). "Biomechanical Model of Vertebra Based on Bone Remodeling." Facta Universitatis **11**: 35-9.

Mullender, M. G. and R. Huiskes (1995). "Proposal for the Regulatory Mechanism of Wolff's Law." J of Orthop Research **13**: 503-12.

ALOGRITHM FOR IDENTIFICATION OF RUNNING, WALKING, AND STANDING ACTIVITY IN FOOT FORCE DATA

Brad T. Humphreys[1], Kerim O. Genc [2, 3], Gail P. Perusek[4] and Peter R. Cavanagh [2, 3]

[1]ZIN Technologies, Cleveland, OH, USA
[2]Case Western Reserve University, Cleveland, OH, USA
[3]Cleveland Clinic, Cleveland, OH, USA
[4]NASA Glenn Research Center, Cleveland, OH, USA
E-mail: humphreysb@zin-tech.com, Web: www.zin-tech.com

INTRODUCTION

In-shoe total foot force data collected with a portable device, can provide valuable insight into a subject's free daily activity both in and outside of the laboratory (Hurkmans et al, 2006). However, as the length of data collection increases, the feasibility of manually classifying ground reaction forces (GRFs) into different activities decreases.

The accuracy of a magnitude-based activity identification algorithm can be compromised by the pseudo-random activity of subjects. For example, transferring weight between feet during rocking could incorrectly indicate walking.

A spectral-based method can be inherently problematic due to the relatively small differences and/or overlap in the fundamental frequencies of walking and running. (Figure 1, Table 1).

The following must be considered in the development of an algorithm that utilizes both frequency and magnitude criterions: 1) Running can have harmonics with significant magnitude content outside of the running and walking band (Figure 1). 2) A large transient movement, like a sudden jumping motion, can have broad frequency content that "spreads" frequency content into the running/walking band. 3) The base frequency peak of running and walking can vary with locomotion speed.

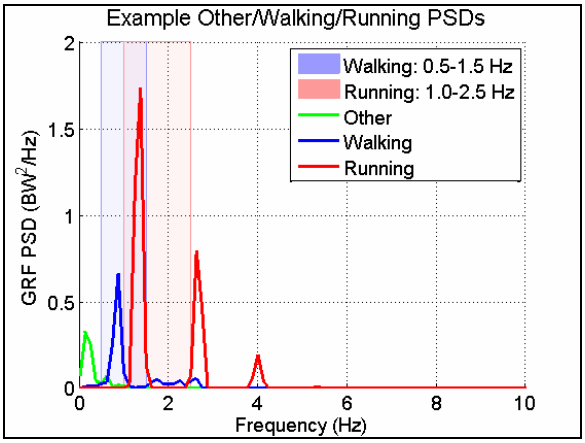

Figure 1: Typical power spectral density (PSD) of standing, walking, and running.

Therefore, an adaptive comb filter algorithm that utilizes both frequency and magnitude criteria for the identification of activity type from total foot force data has been developed. This algorithm can be utilized in either real-time applications or in post-processing.

METHODS

The GRF data used for the development of the algorithm was collected at 128Hz during a previous experiment (Cavanagh *et* al. 2004) in which subjects wore Pedar force measuring insoles (NOVEL Gmbh. Munich, Germany) for entire typical work days. Data were collected using a wearable, portable computer, normalized to body weight (BW)

and downloaded for data analysis completed using custom Matlab software (Mathworks Inc. Natick MA).

The GRF data was analyzed in 8 sec. increments, shifting every 0.1 sec. The PSD of the GRF data was calculated using a Discrete Fast Fourier Transform (DFFT) to find the peak frequency. If the peak frequency was within the defined band for running or walking, the data was further investigated. Using the peak frequency as the first harmonic (or fundamental) and a user selected filter bandwidth, 5 harmonic bands were calculated (Figure 2).

The magnitudes of the GRF in these bands were calculated using Parsevals theorem:

$$M_{RMS} = \sum_{1}^{k} \sqrt{\int_{f_{peak}(k)-w}^{f_{peak}(k)+w} PSD(GRF)} \quad [1]$$

k = number of harmonics
w = comb filter half band width
f_{peak} = peak base frequency (fundamental)

SUMMARY

The authors have performed parameter sensitivity analyses on factors such as sample rate, number of points in the DFFT, and varying activity types to demonstrate the robustness of the algorithm. While it is currently used in numerical post processing, the spectral analytical basis of the algorithm lends itself to straightforward deployment in a real-time digital signal processing (DSP) chip.

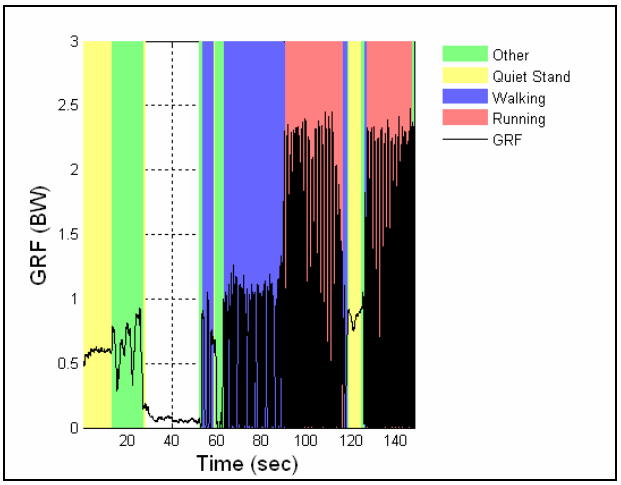

Figure 2: Typical GRF data separated into standing, walking, running and other activities by the algorithm.

The algorithm has been successfully utilized to expeditiously identify activity type in long duration data sets (Figure 2). While there are numerous practical applications for the algorithm, it was specifically developed to identify activity type for calculation of an enhanced Daily Load Stimulus (eDLS), a method of quantifying daily stress histories on the feet which are relevant to bone homeostasis.

REFERENCES

Cavanagh P.R. et al. (2004). *50th Annual Orthopaedic Research Society Meeting.*
Hurkmans H.L.P. et al. (2006). *J Biomechanics,* **39,** 110-118.

ACKNOWLEDGEMENTS

This research was supported by NASA contract #NAS-99155.

Table 1: Peak frequency and magnitude in PSD of running and walking from collected data.

Activity	Peak Frequency (Hz)	Magnitude at Peak Frequency (BW)
Walking:	0.5 – 1.5	0.6 – 1.6
Running:	1.0 – 3.0	1.4 – 2.6

THE INFLUENCE OF USING ONE OR TWO LAG SCREWS ON THE MECHANICAL ENVIRONMENT OF A FEMORAL NECK FRACTURE.

D.J Simpson[1], C.J Brown[2] A.L Yettram[2] and P Procter[3]

[1]Nuffield Department of Orthopaedic Surgery, University of Oxford, UK.
[2]School of Engineering & Design, Brunel University, UK.
[3]Stryker Trauma, Switzerland.
email: David.simpson@ndos.ox.ac.uk

INTRODUCTION

Fracture healing requires two major pre-requisites; sufficient blood supply and mechanical stability [1-2]. Optimum mechanical conditions for fracture healing remain unknown, but micro-movements of the fracture fragments are significant to a developing healing callus [2-3]. This study uses Finite Element analysis to evaluate an idealized neck fracture callus, for single, and two lag screw intramedullary nails, with two load conditions.

METHODS

A validated Finite Element model of a fractured femur, stabilized with an intramedullary nail was used to investigate the effects of loading and the mechanical environment on an idealized fracture callus, as the callus stiffness increased.

Load sharing between the device and bone was assessed for different fixation techniques, nail material properties, and callus size and stiffness. Titanium and Stainless steel constructs were investigated with a callus thickness of 0.5mm and 1.5mm. Strain energy and strain energy density were examined in the fracture callus on a comparative basis to evaluate the use of four different lag screw configurations. The four configurations are:

- Single lag screw of 12mm in diameter (12).
- Two lag screws of 7mm and 9mm diameter with the 7mm lag screw placed more proximally to the 9mm lag screw (7-9).
- Two lag screws of 7mm and 9mm diameter with the 9mm lag screw placed proximally to the 7mm lag screw (9-7).
- Two lag screws of 8mm diameter each (8-8).

Femur geometry was based on computerized tomography data. Bending and torsion loads were applied to the femur [4]. These load conditions use a joint reaction force and an abductor load.

A Coulomb frictional contact model was used to model the interface surfaces between the implant and bone. Sliding friction was permitted at the lag screw interface with the implant. Material properties were assigned in regions as linear elastic and isotropic.

RESULTS AND DISCUSSION

Strain energy varies significantly in the early developing callus (Figure 1). For a two-screw construct, the load sharing in each component changes as the callus stiffens. Two-screw configurations demonstrate smaller strain energy in the fracture callus at the early stages of healing, and more into the healed (stiff) fracture callus (Figure 2). The use of two screws may therefore be beneficial to a healing facture callus, by reducing the load carried into the callus at the early stages and countering stress shielding in the repaired bone.

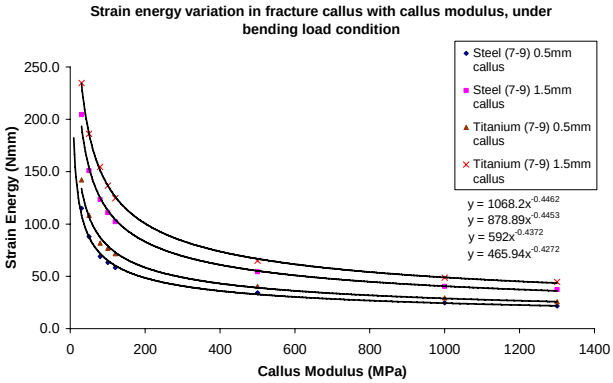

Figure 1 – Strain energy in the fracture callus as the callus stiffens for a bend load case.

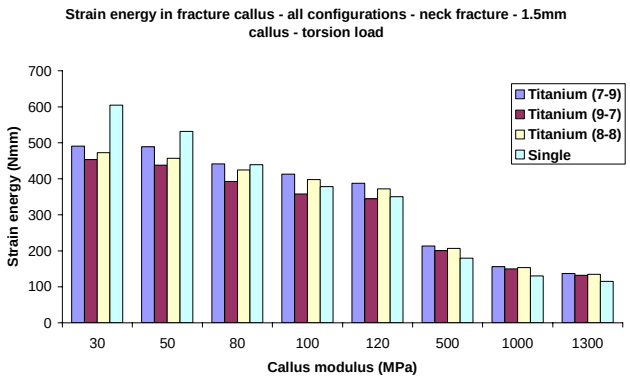

Figure 2 – Strain energy in the fracture callus for all configurations under a torsion load case.

The strain energy in the callus decreases as the fracture callus stiffens and the trend is an inverse power relationship.

Titanium lag screws share the load more evenly between them, particularly at low callus moduli, and the use of titanium significantly reduces the peak stress in the lag screw insertion hole.

Two lag screws are a more stable configuration with respect to a stiffening callus.

REFERENCES

1. Goodship AE, et al. *J.Bone & Jt Surg*, **67-B**:650-655, 1985.
2. Claes LE, et al. *J Orthop. Res*, **38**, 1099-1105, 2002.
3. Claes LE, et al. *Clin. Biomechanics*, **10**, 227-234, 199
4. Simpson DJ, et al. PhD Thesis, Brunel University, 2005.

ASYMMETRIC STABLITY MARGIN OF POSTURAL RESPONSES TO PERTURBATION IN UNILATERAL TRANSTIBIAL AMPUTEES

Yi-Ying Tsai[1] and Lena H. Ting[1,2]

[1] Georgia Institute of Technology, Atlanta, GA, USA
[2] Emory University, Atlanta, GA, USA
E-mail: lting@emory.edu, Web: http://www.neuro.gatech.edu/groups/ting/

INTRODUCTION

Falling is an important clinical problem in amputee population. Among community living people with lower extremity amputation (average age 62 ± 15.7 years), 52% have fallen in the past 12 months (Miller 2001). In unilateral transtibial amputees, increased postural sway in quiet standing and asymmetric EMG reactions in anticipatory postural adjustments to rapid arm raises have been previously identified (Fernie and Holliday 1978, Aruin et al. 1997, Isakov et al. 1992, Hermodsson et al. 1994, Buckley et al. 2002, Aruin et al. 1997).

However, there have been no prior studies of examining dynamic postural responses to perturbations in the amputee population. Reactions to support-surface perturbation have been a useful tool in advancing our understanding of basic postural control mechanisms, as well as for quantifying postural control deficits in various clinical populations such as Parkinson's disease (Horak et al. 2005).

The goal of this study is to quantify directional deficits in postural control in individuals with unilateral transtibial amputation. We used the concept of *stability margin*, which is the difference of peak center of pressure (COP) and center of mass (COM) displacement, to characterize directional stability in response to multiple directions of support-surface perturbations in the horizontal plane.

METHODS

Four subjects with unilateral, traumatic, transtibial amputation and four able-bodied subjects as a control group we recruited. Subjects were instructed to stand quietly with their arms crossed on the perturbation platform and were presented with a randomized set of support surface perturbation in the horizontal plane. We collected five replicates of each of the 8 perturbation direction (0º, 45º, 90º, 135º, 180º, 225º, 270º, 315º). Kinematic, kinetic and EMG data were recorded.

CoP and CoM trajectories were calculated from kinematic and kinetic data. For each subject we found the average peak CoP and CoM for each perturbation direction. Stability margin for each subject was computed as the difference of the peak COP and COM in each direction. Data from right-side amputees group was reflected, so that the left side could be considered the amputated side for group analyses.

RESULTS AND DISCUSSION

We found no significant difference between the peak COP or COM in the amputee vs. the control group in all directions ($p > 0.19$).

However, an asymmetric stability margin was found in amputee group. The stability margin of the control group is symmetric and round shape (Figure 1A); however, stability margin of amputee group is asymmetrical (Figure 1B).

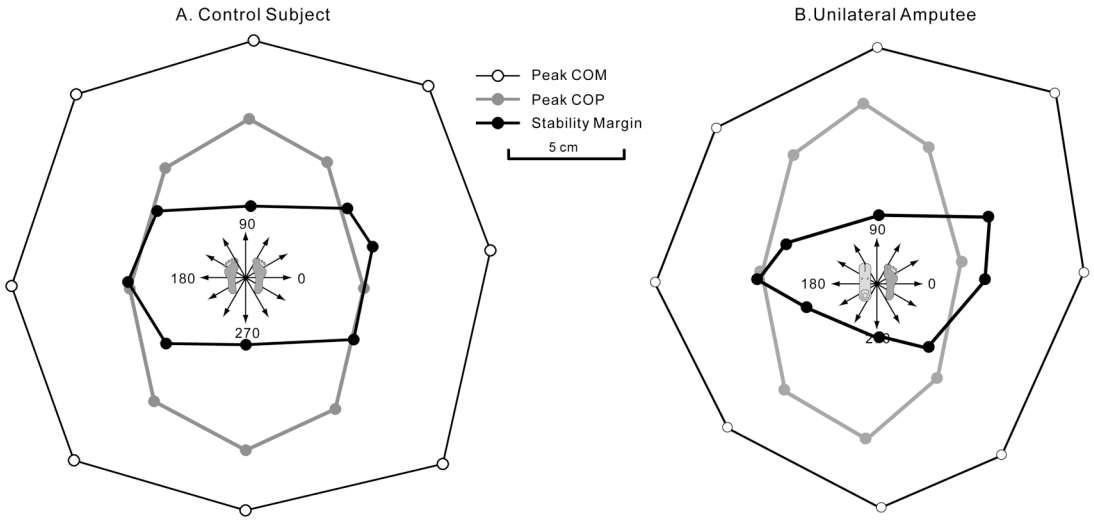

Figure 1: Peak CoP, Peak CoM, and stability margin of an individual in the A) control group and B) unilateral transtibial amputee group

Surprisingly, the stability margin in anterioposterior and mediolateral directions in amputee group was not significantly different from controls. However, stability margin was significantly reduced in the diagonal directions when the amputated side was loaded (Figure 2, 45° and 315° perturbations, $p < 0.05$).

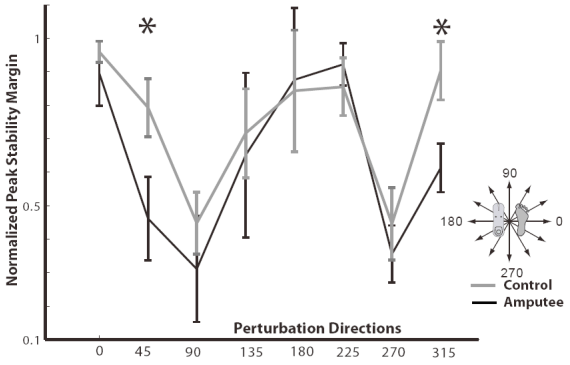

Figure 2: Stability margin as a function of perturbation direction for control group (gray lines) and amputee group (black lines). Stability margin in significantly les in the diagonal perturbation direction where the amputated side is loaded (45º, 315º, *p<0.05)

CONCLUSIONS

Our results show that the stability margin in amputees is reduced in diagonal directions where the amputated side in loaded and the intact side is unloaded. This reveals directions of postural instability which may be important in the fitting and training patients with prostheses. Surprisingly, we also showed that stability margin was not significantly reduced in the anterior-posterior or medial lateral directions.

REFERENCES

Aruin A.S., et al. (1997) Clin Biomech, 12(1) : 52-59.

Buckley J.G. et al. (2002) Am J Phys Med, **81(1)**: 13-20.

Fernie G.R., Holliday P.J. (1978) J Bone Joint Surg Am, **60(7)**: 895-898.

Hermodsson Y, et al. (1994) Prosthet Orthot Int, **18(3)**:150-158.

Horak F.B. et al.(2005) Exp Neurol, **193(2)**: 504-21.

Isakov E. et al.(1992) Arch Phys Med Rehabil, 73**(2)**: 174-178

Miller W.C. et al. (2001) Arch Phys Med Rehabil, **82(9**): 1238-44.

ACKNOWLEDGEMENTS

The authors thank whole the Neuromechanics Lab. Supported by NIH NS 053822

Using Distributions of Forward Dynamic Simulations to Investigate Model Inaccuracies

Matt J. Camilleri

Sacramento City College, Sacramento, CA, USA
E-mail: camillm@scc.losrios.edu

INTRODUCTION

Muscle forces and work are estimated using forward dynamic simulations because forces cannot be measured readily. Input muscle excitations are transformed into forces that act on the body segments to produce a simulated motion. Solutions may be generated by optimizing (minimizing) the error between experimental and simulated data, or by generating a distribution of simulation results (Camilleri, 2006).

However, large tracking errors exist in the total intersegmental moments in both the distribution and optimization solutions (Figure 1). The tracking errors are a result of high frequencies in the total simulated intersegmental moments that are not evident in the experimental data. This indicates an inaccuracy in the neuro-musculo-skeletal model. Identifying the source of this inaccuracy and correcting it would provide more confidence in the neuro-musculo-skeletal model and the attendant forward simulation results.

The muscle velocities affect the intersegmental moments and demonstrate little variability across simulations. Thus, it is reasonable to assume that particular muscle velocities are associated with the high frequencies. The objective of this work was to determine any such associations.

METHODS

To achieve these objectives, pedaling was used as a demonstration task. Fifteen subjects pedaled at 90 rpm and 250 W. Inverse dynamics were used to compute the intersegmental moments. A forward dynamic model of recumbent pedaling was implemented to simulate the input muscle excitations and output intersegmental moments. Specifically, the descent-ascent distributor was used to simulate an experimental distribution (Camilleri, 2006).

Muscles that demonstrated high frequencies in their contribution to the total intersegmental moments, over the same region that the total intersegmental moment demonstrated high frequencies ("error region", Figure 1), indicated that these muscles contributed to the high frequencies. The muscle velocities were extracted from each simulation, for each of these muscles, over the corresponding error region, and averaged. The averaged velocities were normalized to both the optimal fiber length (i.e., rest length) and the unloaded maximum shortening velocity.

Frequency histograms of the averaged and normalized velocities were plotted with the frequency histograms of the normalized velocities over the crank cycle. Histograms of the averaged velocities, producing a mean value consistent across muscles, indicated that the mean value was associated with the high frequencies in the intersegmental moments.

RESULTS AND DISCUSSION

Muscles that demonstrated high frequencies in their contribution to the total intersegmental moment were the psoas (PSO) and gluteus maximus (GMAX) for

the hip (Figure 1), soleus and gastrocnemius for the ankle, and vastii for the knee. The high frequencies were associated with muscle velocities near zero (Figure 2).

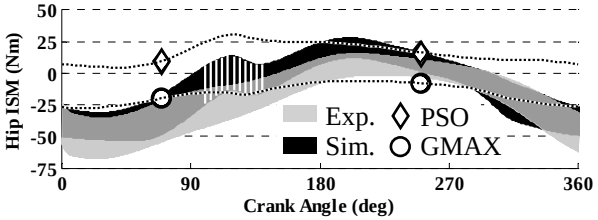

Figure 1. Intersegmental (ISM) hip moments (Exp. is total experimental and Sim. is total simulated, ± 1 st. dev.). Hatched region is the error region.

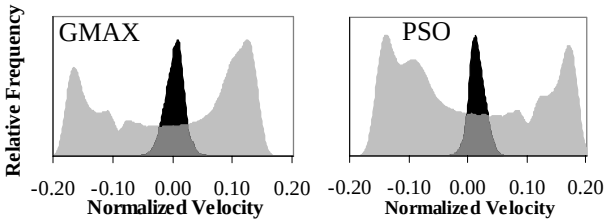

Figure 2. Relative frequencies of the normalized velocities. Black distributions are the frequencies for the error region, and gray distributions are the frequencies over the crank cycle.

This association is readily explained when the sensitivity of muscle force to velocity in the muscle model is considered. As is common, a Hill-type force-velocity relationship was used in the forward model. This relationship demonstrates the greatest sensitivity of muscle force to velocity (Δforce/Δvelocity) at zero velocity (Figure 3). This sensitivity causes rapidly changing muscle forces and thus high frequencies.

The finding of higher frequencies in the simulated versus experimental intersegmental moments is consistent with experimental results and the implemented muscle model. In-vivo experiments demonstrate that for a particular shortening velocity and length, the force is depressed with preceding shortening ('force depression'), and that the depression is magnified when the amplitude of the preceding shortening is increased (Herzog, 2004). The opposite effects are demonstrated for lengthening muscle ('force enhancement'). If history effects had been included in the forward dynamic model, then the high frequencies in the simulated intersegmental moments may have been diminished. This is because during both muscle shortening and lengthening, the force depression and enhancement, respectively, should cause the sensitivity of force to velocity, near zero velocity, to decrease with respect to the conventional model (Figure 3).

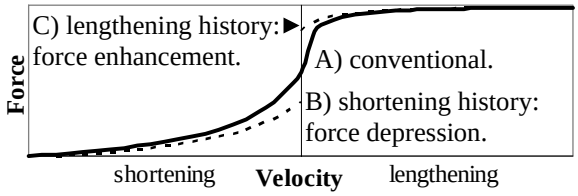

Figure 3. The force velocity relationship from a conventional Hill-type equation (A) and the hypothetical effects of history on the relationship (B and C, dashed). In both B and C, sensitivity of force to velocity, at zero velocity, is less than that of A.

SUMMARY

High frequencies in the simulated intersegmental moments: 1) were associated with muscle velocities near zero, 2) resulted in part from the simulated high sensitivity of muscle force to velocity at zero velocity, and 3) may be reduced if the history of the muscle velocity is included within the muscle model. These findings support the use of distributions of simulation results to diagnose simulation errors and address inaccuracies in the underlying models, to increase confidence in conclusions drawn from simulation analyses.

REFERENCES

Camilleri, M.J. (2006). *Ph.D. Dissertation*, **Chapters 2 and 3**.

Herzog, W. (2004). *Hum Mov Sci*, **23**, 591-604.

VARIATION IN FORCE AND MOMENT STABILIZING SYNERGIES WITH DIFFERENT FINGER COMBINATIONS: AN UNCONTROLLED MANIFOLD ANALYSIS

Sohit Karol[1] and Jae Kun Shim[1]
1. Department of Kinesiology, University of Maryland, College Park, USA
Email: skarol@umd.edu web: http://www.hhp.umd.edu/KNES/faculty/jkshim/

INTRODUCTION

One of the challenges of motor control is to demystify the mechanism by which the Central Nervous System (CNS) controls the apparently redundant systems for the effective movement of human body. The human hand is an excellent example of both kinetic as well as kinematic redundancy. However, it has been suggested that the CNS might actually use this apparent redundancy to incorporate better control strategies. This hypothesis has been called the principle of abundance. We presented an isometric force production task to the subjects and used the framework of Uncontrolled Manifold Hypothesis (UCM) for our analysis [2]. The current study addresses the question that which performance variable, total force or total moment is stabilized by different combinations of multi-finger synergies and how the stability and the constant errors in force production change with the number of fingers involved in the task.

METHODS

Nine right handed subjects (4 males and 5 females) participated in the experiment (age: 27 ± 4.3 years; weight: 64.2 ± 7 kg; height 1.69 ± 0.09m). The experimental setup can briefly be described as follows: the wrists and the forearms of the subject were rested in a wrist-forearm brace and held by Velcro straps. The subject sat in a chair and watched the computer screen to perform a task. The two-directional force sensors (tension and compression) were attached to an aluminum frame and the C – shaped thimbles were attached to the bottom of the sensors. The subject inserted the distal phalange of each finger in the thimbles. Signals from the sensors were conditioned, amplified, digitized at 1,000 Hz and low pass filtered at 20Hz. A custom software program made in LabVIEW and a desktop computer were used for data acquisition and data was processed using MATLAB.

Maximum Voluntary Force (MVF) was measured for all the fifteen finger combinations. This single digit task MVF data was used to estimate the enslaving matrix **E** as described previously [3]. A target force line representing 0% of MVF (in multi finger tasks) for the first three seconds and 20% of MVF for the next seconds for a particular subject was displayed on the computer screen. The summed force output of the task fingers was also shown with a different color. Subjects were asked to focus on the task fingers only, and no visual feedback about the non task finger forces was provided to them. Trials in which the non task finger was lifted from the force sensors were rejected and performed again. Subjects were asked to follow the target force lines.

Finger forces were converted into force modes (central commands) and the UCM was computed for both force and moments separately (see [3] for details). The total amount of variance (V_{TOT}) in the mode

space, computed for each time sample (0.01s) across trials of each series performed by each subject (between 7s and 12s) was divided into two components, V_{ORT} (variability orthogonal to UCM) and V_{UCM} (variability within UCM). A normalized index ΔV of multi-digit synergies was computed [3].

Constant Errors were measured using the formula: CE= $(\Sigma(xi - T)/n)/MVC$, where 'x_i' is average force produced in a ramp trial between 5-8s, 'T' is target force and 'n' is number of trials. The errors were normalized by the MVC for each subject.

RESULTS AND DICSUSSION

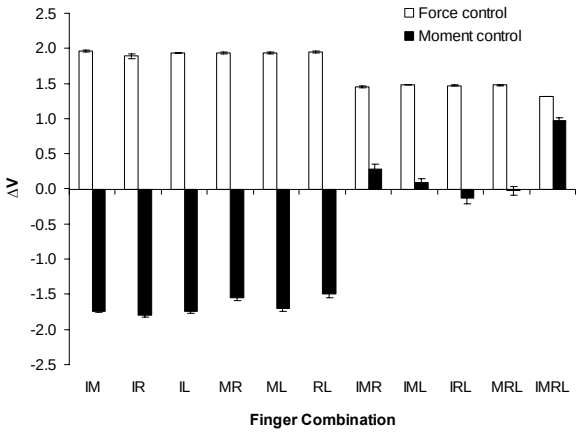

Fig. 1 The index of covariation of finger modes (ΔV) was computed with respect to the (A) force control hypothesis (white bars) and (B) moment control hypothesis (black bars) and averaged for the time interval 7s to 12 s for the constant force production task. Mean values and standard error bars are shown for both the hypothesis.

For the force control hypothesis, the index ΔV was 1.9 ± 0.045 (mean ± SD) for two finger combinations and

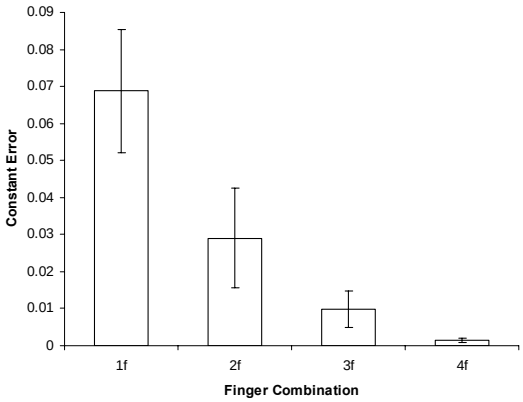

Fig. 2 Constant errors normalized by the MVC values of the four, three, two and one finger combination respectively. Mean values and standard error bars are shown.

decreased to 1.4 ± 0.025 for the four finger task (ANOVA: $p<.05$.ΔV was negative for all the two finger tasks for the moment control hypothesis, thus suggesting that the moments are not stabilized by these combinations of fingers (ANOVA: $p<.05$). The constant errors decreased from *0.07 ± 0.0019 to 0.002 ± 0.0006* from single finger combinations to four finger combinations (ANOVA: $p<.05$).These results suggest that the choice of stabilized task variable is task dependent. Also, the constant errors decreased by adding the number of fingers, suggesting that the principle of abundance might be used by the CNS in an isometric pressing task.

REFERENCES

1. Shim J.K., Olafsdottir H., Zatsiorsky V.M. and Latash M.L. (2005). *Exp Brain Res* **164(2)**: 260-270.

2. Scholz J.P., Schöner G. (1999). *Exp Brain Res* **126**:289-306.

3. Kang N., Shinohara M, Zatsiorsky VM, Latash ML. (2004). *Exp Brain Res* **157(3)**: 336-350.

SPINAL CORD INJURY DURING CERVICAL BILATERAL FACET DISLOCATION

Paul C. Ivancic, Adam M. Pearson, Yasuhiro Tominaga,
Andrew K. Simpson, James J. Yue, and Manohar M. Panjabi

Biomechanics Research Laboratory, Yale University School of Medicine, New Haven, CT, USA
E-mail: paul.ivancic@yale.edu

INTRODUCTION

Bilateral facet dislocation (BFD) of the cervical spine results in complete cord lesions and quadriplegia in 50 to 84% of cases. The majority of those not rendered quadriplegic sustain incomplete cord lesions and significant neurological morbidity. Clinically, it is not known whether dynamic spinal canal narrowing during BFD exceeded that observed on post-trauma radiographs or MRIs. Thus, the severity of the spinal cord injury may be underestimated. The goals of this study were to: (1) quantify the cervical spinal canal narrowing during simulated BFD of a functional spinal unit model with muscle force replication, (2) determine if the peak canal narrowing during dislocation exceeded that observed post-trauma, and (3) extrapolate the present results to quantify the dynamic cord compression in individuals with normal canal diameters and in those with cervical canal stenosis.

METHODS

Ten functional spinal units were dissected of all non-osteoligamentous soft tissues (C3/4, C5/6, or C7/T1) and mounted in resin at the upper and lower vertebrae. Motion tracking flags, each with three non-collinear markers, were rigidly fixed to both mounts. The lower mount was rigidly fixed to a 55° extension wedge on a sled apparatus (**Figure 1**). A 3.3 kg mass with sagittal, horizontal, and frontal plane moments of inertia of 0.019, 0.014, 0.015 kg m^2, respectively, was rigidly attached to the upper mount. The functional spinal unit and mass were stabilized using simulated compressive muscle forces, applied via bilateral cables originating from the upper mount at the four locations indicated in **Figure 1**. This model, developed through extensive preliminary trials, consistently produced dynamic BFD. Horizontal acceleration of increasing severity was applied to the lower mount with frontal impact using the sled apparatus until BFD was achieved. High-speed cameras recorded spinal motions at 500 f/s.

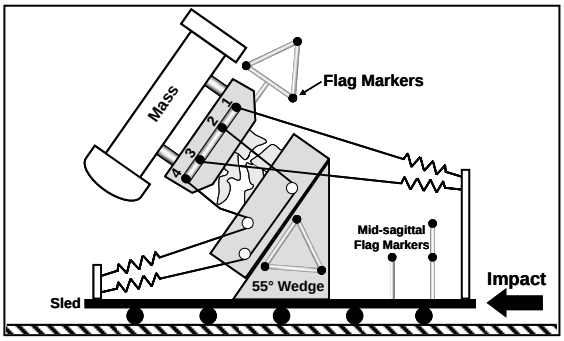

Figure 1. Functional spinal unit model with mass, ready for BFD.

To compute canal pinch diameter (CPD) narrowing, the CPD was measured in neutral posture, during dynamic impact, and post-impact (**Figure 2**) (Ivancic et al., 2006).

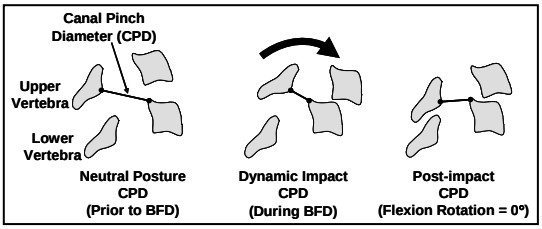

Figure 2. Schematics demonstrating the CPD under various experimental conditions.

The CPD was defined as the distance between the two CPD points: the inferior corner of the spinolaminar line of the upper vertebra and the posterosuperior corner of the lower vertebral body. The dynamic impact CPD was defined as the minimum CPD observed during dynamic BFD, while: *dynamic impact CPD narrowing = neutral posture CPD − dynamic impact CPD.*

The post-impact CPD was determined following dynamic BFD at the time of flexion rotation = 0°, while: *post-impact CPD narrowing = neutral posture CPD − post-impact CPD*.

Student's paired t-test was performed using data from all spinal levels combined to determine a significant difference ($P<0.05$) between the average dynamic impact and post-impact CPD narrowing.

RESULTS

The post-impact CPD narrowing combined across spinal levels was significantly less ($P<0.05$) than the dynamic impact CPD narrowing (0.8 mm vs. 6.2 mm). The earliest occurrence time of the peak CPD narrowing was 71.0 ms at C7/T1. The post-impact CPD narrowing occurred between 265.0 ms at C3/4 and 318.0 ms at C5/6. The peak CPD narrowing velocity did not exceed 0.25 m/s and occurred as early as 59.7 ms.

DISCUSSION AND CONCLUSIONS

Our results demonstrated that the average peak dynamic impact CPD narrowing significantly exceeded the post-impact CPD narrowing. These data indicate that the spinal canal narrowing observed on post-trauma radiographs or MRIs of BFD patients is likely substantially less than the dynamic narrowing that occurred during the dislocation event.

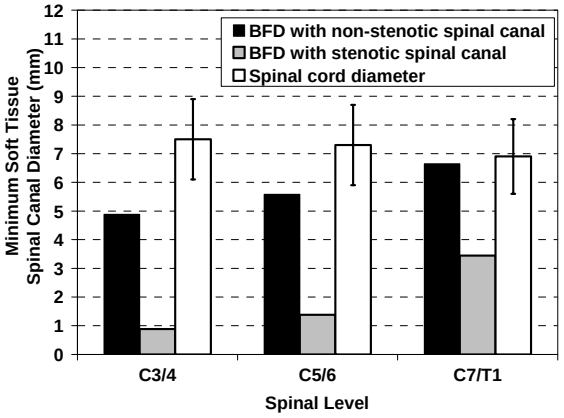

Figure 3. Minimum soft tissue canal diameter during BFD in those with non-stenotic and stenotic canals.

The present CPD narrowing data may be extrapolated to quantify cord compression during BFD, using averages of the previously reported anterior-posterior soft tissue canal and spinal cord diameters (**Figure 3**). The minimum canal diameter was obtained for C3/4, C5/6, and C7/T1 by subtracting the peak CPD narrowing of the present study from the corresponding previously reported average soft tissue canal diameter data. For comparison, the average spinal cord diameter data are also shown in **Figure 3**. These results demonstrate spinal cord compression of 88% at C3/4, 81% at C5/6, and 50% at C7/T1 in those with stenotic spinal canals. In those with normal canal diameters, spinal cord compression of 35% at C3/4, 24% at C5/6, and 4% at C7/T1 was observed. These results are consistent with the wide range of neurological injury severity observed clinically due to BFD.

REFERENCES

Ivancic, P.C.et al. (2006). *Traffic Inj Prev,* **7**, 81-87.

ACKNOWLEDGEMENTS

This research was supported by a grant from the Cervical Spine Research Society.

ISB SHOULDER POSITION METHOD AND "GLOBE" METHOD ARE IDENTICAL

George T. Rab, M.D.

University of California Davis, Sacramento, CA, 95817, USA
e-mail: george.rab@ucdmc.ucdavis.edu

INTRODUCTION

The ISB standard for measuring shoulder position and motion is based on work of An, et al.[1], who used a Z-Y'-Z'' rotation sequence to study humero-scapular motion. However, actually rotating an arm through this sequence is counterintuitive and confusing to clinicians, which has led to the development of "globe" methods[2,3] based on a simpler concept of plane of elevation, angle of elevation, and comparison of the flexed forearm with a global line of latitude to determine humeral rotation. The "globe" method has been described as "unambiguous" and "sequence-independent."

METHODS

An articulated model was placed in numerous shoulder positions, analyzed by both methods using the technique and descriptions found in references[1,2,3]. Numerical results were compared.

RESULTS

When critically analyzing the two methods, it is obvious that the first 2 elements (plane of elevation, angle of elevation) are the same for both, although the ISB method requires sequential rotations, whereas the "globe" method requires only measurement of projected angles. However, the first two sequential rotations in the ISB method leave the 90 degree flexed forearm *horizontal*, since the plane of elevation is reached by rotation the laterally-directed humerus axis until it points to that plane[1] (see figs. 1 and 2 below).

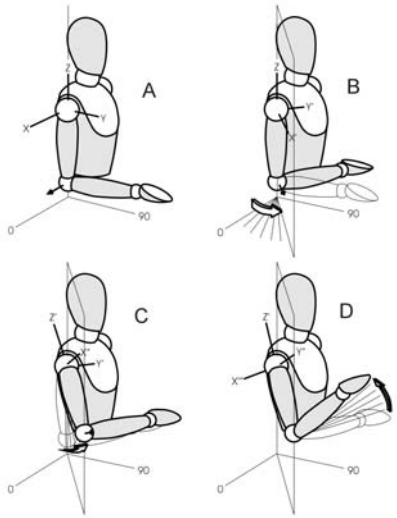

Fig. 1. ISB method sequential rotations

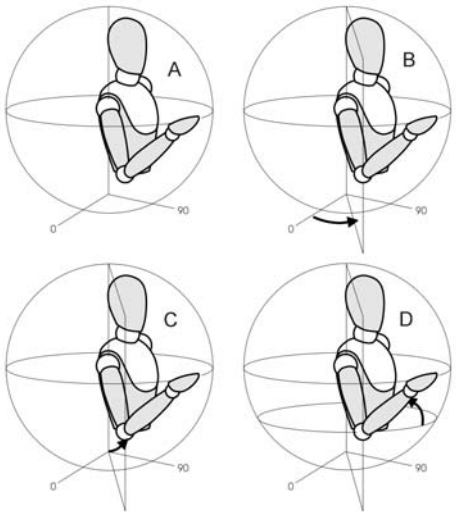

Fig. 2. "Globe" method measurements

Elevation then raises this axis, leaving the forearm still in the transverse plane, since it is 90 degrees apart from the lateral humerus axis. The third rotation then deconstructs to a rotation about the humerus from the latitude of the elbow, which is exactly the "globe" definition of humeral position[2,3].

CONCLUSION

The ISB and "globe" methods produce an identical numerical set. The ISB method appeals to engineers and investigators with mathematical understanding. The "globe" method appeals to clinicians, therapists, etc. who appreciate it's similarity to practical clinical measurement techniques and who are confused by sequential rotations that bear no relationship to their personal understanding of natural motion. Both methods are mathematically and numerically equivalent and interchangeable.

REFERENCES

1. An K-N, Browne AO, Korinek S, Tanaka S, Morrey BF. Three-dimensional kinematics of gleno-humeral elevation. *J Orthop Res* 9:143-149, 1991.

2. Doorenbusch CAM, Harlaar J, Veeger HEJ. The globe system: an unambiguous description of shoulder positions in daily life movements. *J Rehab Res Dev* 40:147-156, 2003.

3. Pearl ML, Harris SL, Lippett SB, Sidles JA, Harryman DT II, Matsen FA. A system for describing positions of the humerus relative to the thorax and its use in the presentation of several functionally important arm positions. *J Shoulder Elbow Surg* 1:113-118, 1992.

OBSTACLE CROSSING BEHAVIOR IS AFFECTED BY PARKINSON'S DISEASE

Chris Hass [1] Thomas Buckley [2], and Chris Pitsikoulis [3]

[1] University of Florida, Gainesville, FL, USA
[2] Georgia Southern University, Statesboro, GA, USA
[3] Teachers College Columbia University, New York, NY, USA
E-mail: cjhass@hhp.ufl.edu

INTRODUCTION

Postural instability and falls among individuals with idiopathic Parkinson's disease (PD) are common. It is estimated that over two-thirds of community dwelling individuals with PD have fallen at least once in the last year compared to an estimated one third of the healthy population over the age of 65 (Ashburn 2001).

Imbalance and tripping over obstacles during gait were reported as one of the most common causes of falls in older adults (American Geriatrics Society, 2001). Thus, it is not surprising that numerous studies have been devoted to uncovering age-related differences in locomotion during obstacle crossing. Joint kinematics and kinetics of either the trailing (i.e., limb crossing the obstacle last) or leading (i.e., limb crossing the obstacle first) limb as well as balance maintenance during obstacle crossing have been investigated. However, no studies, to our knowledge, have examined whether PD itself modifies gait behavior during obstacle-crossing. This is surprising considering the increased likelihood of falling in this population. Thus, the purpose of this investigation was to examine whether gait behavior while walking over an obstacle is affected by PD.

METHODS

Ten individuals with idiopathic PD (age: 62±9 yrs; height: 172±11 cm; mass: 88±20 kg; Hoehn and Yahr disability 2.4±0.6) and ten age- and gender-matched healthy control subjects (age: 62±9 yrs; height: 170±8 cm; mass: 77±14 kg) were evaluated. Individuals with PD were tested in the "ON medication" state within 1-1.5hours of taking their antiparkinson's medication.

Subjects walked barefoot along a 9m walkway at a normal comfortable pace. They were instructed to step over an obstacle placed in the middle of the path of progression and to continue walking. The obstacle was constructed of a wooden dowel (91 cm long and 1.27cm in diameter) supported by two stands which were set so that the dowel height was at 10% of the subject's height. The obstacle was placed between two adjacent force plates (AMTI, Watertown, MA) positioned end to end along the path of motion. Ground reaction forces were collected (1560Hz) from the two force plates embedded level with the walkway surface and halfway down the walkway length. Subjects performed 2 practice trials followed by 5 experimental trials of obstacle crossing.

Kinematic data were collected using an 8-camera optical capture system (Vicon Peak Motion Systems, Oxford UK) that was sampled at 120 Hz. Thirty-nine reflective markers were attached to the subjects in accordance with the Plug-in-gait marker system. Markers were also placed on the ends of the dowel.

For each experimental trial 3 consecutive steps were examined: 1 "approach", 1

"crossing", and 1 "recovery." The steps were defined at heel strike based on previous research (Ramachandran, 2006). Average values for the 5 trials for each person were recorded for each of the dependent variables. The following gait parameters were evaluated: step length, step velocity, and step width during each step. Obstacle clearance characteristics that were measured included: vertical clearance over the obstacle for the toe and heel of the lead and trail limbs; horizontal clearance between the obstacle and the toe and heel of the lead limb; and single limb support time while crossing. Center of mass displacements were also evaluated in the anteroposterior, vertical, and medial-lateral directions.

Our primary hypothesis was that differences would be observed in the dependent variables between the 2 participant groups Three separate (gait parameters, obstacle clearance, center of mass motion) multivariate analysis of variance (MANOVA) were used to test for overall group differences while controlling for type I error. Separate analyses of variance (ANOVAs) were then performed for follow-up testing when appropriate.

RESULTS AND DISCUSSION

None of the subjects came in contact with the obstacle, tripped, nor fell while crossing the obstacle.

The MANOVA detected significant differences between groups for the gait parameters ($F= 9.5$, $p= 0.001$). The individuals with PD walked more slowly and took shorter steps fore each step analyzed. The stepping velocity and step length was on average 33% slower and 22% shorter for the individuals with PD compared to the controls. Step width was not different between groups.

The MANOVA also detected significant differences between experimental groups in the obstacle clearance parameters ($F=3.3$, $p= 0.034$). Follow up univariate testing revealed that only time spent in single limb support and horizontal distance between the heel of the trail limb and the obstacle were different. The individuals with PD spent more time in single limb support (17% longer) during obstacle crossing and placed the limb closer to the obstacle when crossing.

COM displacements in the anterior direction where significantly reduced in the individuals with PD when crossing over the obstacle.

Combined these finding of significantly reduced gait speed and step length, closer placement of the limb to the obstacle, and reduced COM motion in the anterior direction indicate that a conservative strategy is adopted by the individuals with PD. However, the larger amount of time spent in single limb support as the lead limb crosses the obstacle increases the chances for balance loss in these individuals.

SUMMARY/CONCLUSIONS

Individuals with PD possess altered gait behavior during obstacle crossing compared to age matched controls. It is likely these differences are a result of a conservative approach to reduce the likelihood of tripping but this behavior may inadvertently increase the balance demands of the task.

REFERENCES

American Geriatrics Society. (2001). *J. Am. Geriatr. Soc.* **49**, 664-672.
Ashburn A, et al. (2001) *Age & Ageing* **30**, 47-523.
Ramachandran et al. (2006) *Gait Posture*. **Epub** October

BIOMECHANICAL MODELING TO IDENTIFY RISK FACTORS IN KNEE OA: MODEL DE ENDENCE U ON SOURCE MRI FIELD STRENGTH

Donald D. Anderson, Neil A. Segal, James C. Torner, and Thomas D. Brown
– for the Multicenter Osteoarthritis Study Group –

The University of Iowa, Iowa City, IA, USA
E-mail: don-anderson@uiowa.edu, Web: poppy.obrl.uiowa.edu

INTRODUCTION

The Multicenter Osteoarthritis (MOST) study is an investigation of the incidence and progression of knee osteoarthritis (OA) in a cohort of 3026 men and women, 50–79 years old. It aims to determine the effects of physical activity, weight, diet and other factors on knee pain and OA. In addition to routine physical check-ups, 1.0T (T=Tesla; magnetic field strength) MRI scans were obtained of subjects' knees at baseline and at regular intervals over a 30-month period, providing a unique opportunity to identify mechanical risk factors for knee OA.

Discrete element analysis (DEA – Li et al. 1997) is a means of estimating articular joint contact stress, using surfaces derived from CT or MRI. DEA treats apposed bones at an articular joint as rigid bodies, while the cartilage is modeled as a continuous system of springs. Bone displacements or loads are input to the model. Using DEA, contact stress solutions can be obtained orders of magnitude more quickly than for finite element analysis (FEA), making it especially well suited for studying a large cohort.

In addition to 2522 MOST subjects who underwent 1.0T MRI scans, 350 also had knees scanned at 1.5T. In general, MRI image quality is directly related to field strength. Given the desire to study as large a cohort as possible, using 1.0T scans for study would be preferable. The current study investigates the influence of source MRI field strength upon DEA estimates of joint contact stress in a series of MOST subjects.

METHODS

Standardized MRI scans (both 1.0T and 1.5T field strength) were obtained for seven subjects' knees at study commencement. The MRI images were segmented using OsiriX software (homepage.mac.com/rossetantoine/osirix), yielding a 3D cloud of points defining the subchondral bone surfaces of both the femur and the tibia.

Smoothed surfaces were then fit to the points using Geomagic Studio software (Geomagic; Research Triangle Park, NC). The smoothed surfaces were imported into MATLAB (The Mathworks, Inc.; Natick, MA), where DEA solutions were computed (Figure 1). The cartilage was assumed to be 6 mm thick, with an elastic modulus of 12 MPa, and a Poisson's ratio of 0.45. A 1000 N axial load and moments as necessary to resist tibial rotation (determined iteratively) were applied to the tibia, with the femur fixed against both translations and rotations.

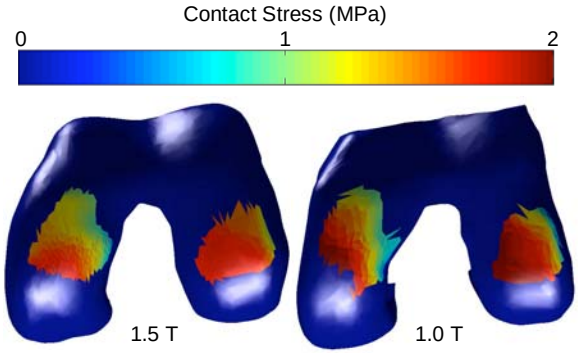

Figure 1: DEA-computed contact stress distributions for the left knee of a subject, derived from 1.5T scan (left) and 1.0T scan (right). Computed peak stress values were 2.17 MPa, and 2.02 MPa, and contact areas were 666.4 and 686.7 mm^2, respectively.

RESULTS AND DISCUSSION

DEA solutions took less than a minute to solve for each case. Estimates of peak contact stress (MPa), as well as the contact stress distributions, were highly consistent, independent of MRI field strength (Figure 1 and Table 2).

T e : Comparison of DEA results obtained working from 1.0T and 1.5T MRI scans.

Peak Contact Stress (MPa)				
Case	1.5 T	1.0 T	Diff	%Diff
1	1.51	1.36	0.15	10%
2	1.70	1.79	-0.09	-5%
3	2.16	1.98	0.17	8%
4	2.30	2.43	-0.14	-6%
5	2.49	2.47	0.01	1%
6	3.17	3.47	-0.30	-10%
7	3.63	3.39	0.25	7%
Mean	2.4	2.4	0.0	0.0
StDev	0.8	0.8	0.2	0.1

SUMMARY CONCLUSIONS

This study incorporates biomechanical modeling of knee joint stress (using discrete element analysis), working only from baseline MRI images. It bridges the gap between associative and physical models of knee OA, enabling an epidemiological model to test whether risk factors identified at baseline may act through increased articular surface loading.

The close agreement between contact stress estimates derived from source MRI data of 1.0T and 1.5T field strength indicates that the 1.0T scans are equally acceptable for estimating contact stress. As a result, a much larger cohort of patients may be included in these epidemiologic investigations.

The versatility of this method for estimating knee joint contact stresses makes its application to subject-specific modeling highly attractive. This type of study has not previously been possible with more complex conventional (i.e., FEA) techniques. By identifying thresholds of contact stress that predict development of painful knee OA, this type of study has the potential to improve patient care, and to guide the utilization of expensive interventions as they become available.

REFERENCES

Kawai T and Takeuchi N. *ASCE Int. Conf. Comput. Civ. Engng*, New York, 1981.

Li G, Sakamoto M, Chao EY. *J Biomech* :635-8, 1997.

ACKNOWLEDGEMENTS

This work was funded by grants from

NIH: University of Iowa (AR48939 & AG18832); Boston University (AG18820); University of Alabama at Birmingham (AG18947); University of California - San Francisco (AG19069)

Association of Academic Physiatrists (5K12HD001097-08).

AGE AND FATIGUE EFFECTS ON LOWER EXTREMITY JOINT TORQUE DEVELOPMENT

Gregory W. King[1,2,3], Carl W. Luchies[2,3] Antonis P. Stylianou [2,3], and Molly A. McVey [2,3]

[1] University of Missouri – Kansas City, Kansas City, MO, USA
[2] University of Kansas, Lawrence, KS, USA
[3]University of Kansas Medical Center, Kansas City, KS, USA
E-mail: kinggr@umkc.edu

INTRODUCTION

Muscle strength decreases with age [Ditor & Hicks 2000], a phenomenon that is prominent in the lower extremities [Whipple et al. 1987]. This affects joint torque development, which likely plays a role in balance recovery [Robinovitch et al. 2002; Mackey & Robinovitch 2006]. Therefore age-related reductions in torque development may increase fall risk among older adults. Localized muscle fatigue induced by exercise or other activities of daily living may compound this risk by further reducing strength output. Therefore the purpose of this study was to investigate the combined effects of age and fatigue on joint torque development characteristics. We hypothesized that a) older adults, compared to young, would have reduced torque development performance; and b) localized muscle fatigue would have a more debilitating impact on older adults, compared to young.

METHODS

Participants. Thirteen young (YA: mean age 26 ± 2.5 years) and twelve older (OA: mean age 71 ± 2.8 years) male adults participated in this study after providing written informed consent as approved by the institution's human subjects committee.

Tasks. Each participant performed isometric contractions of ankle plantarflexors or knee extensors to produce joint torque equal to 40% of his maximum voluntary contraction torque on a Cybex 6000 dynamometer (CSMI, Norwood, MA). One task was performed before and after a fatiguing exercise. Fatigue was induced by performing isokinetic contractions on the dynamometer using the ankle plantarflexors and knee extensors at rates of 30 and 60 degrees per second, respectively. Ankle and knee testing sessions were done separately within a single laboratory visit.

Measurements. During each 15-second trial, torque data was sampled at a rate of 2 kHz using a personal computer running LabVIEW (National Instruments, Austin, TX) through a 16-bit A/D data acquisition card (National Instruments).

Analysis. Data was processed using MATLAB (Mathworks, Natick, MA). Torque development was quantified using onset time (t_{onset}): the time from stimulus to torque development; settling time (t_{settle}): the first time at which torque remained within 5% of the target level for 1 second; and rate of torque development (S): the slope of a line fit between t_{onset} and the time at which torque reached 70.7% of the target value. Statistical analyses were done with SPSS 14.0 (SPSS Inc., Chicago, IL). Independent samples t-tests were used to detect age effects among pre-fatigue trials. Paired samples t-tests were used to assess fatigue effects within each age group. Age-related differences in fatigue effect were detected by calculating the difference (Δ) in each

variable between pre- and post-fatigue, and performing independent samples t-tests on Δ with age as the independent variable.

RESULTS AND DISCUSSION

Results are summarized in **Table 1**. OA, compared to YA, exhibited longer settling times (ankle) and slower torque development (ankle and knee). Post-fatigue trials, compared to pre-fatigue, were characterized by slower rates of torque development in YA only (ankle and knee). In the ankle joint, this resulted in a significant age-related difference in fatigue effect: rate of torque development decreased with fatigue in YA, but not in OA. These results suggest that aging reduces the ability to quickly generate a submaximal torque about the knee and ankle joints. The age effects observed have implications for balance recovery if age-related declines progressed to a level at which joint torque was not produced quickly enough to restore balance, increasing fall risk. These results also suggest fatigue-related performance declines in YA, but no fatigue-related performance changes in OA. This result does not support our hypothesis. This may be partially explained by preferential atrophy of type II fibers and motor unit remodeling [Merletti et al. 2002], whose combined effects may result in increased fatigue resistance among OA.

SUMMARY/CONCLUSIONS

Joint torque development performance appears to decline with age; however, localized muscle fatigue does not further diminish performance in OA. This suggests that muscle fatigue does not compound the existing fall risk among OA; however, aging alone may present a significant fall risk if torque development performance falls below the level needed for balance recovery.

REFERENCES

Ditor, D. S., Hicks, A. L. (2000). *Can J Physiol Pharmacol*, **78**, 781-790.

Whipple, R. H. et al. (1987). *J Am Geriatr Soc*, **35**, 13-20.

Robinovitch, S. N. et al. (2002). *J Neurophysiol*, **88**, 613-620.

Mackey, D. C., Robinovitch, S. N. (2006). *Gait Posture*, **23**, 59-68.

Merletti, R. et al. (2002). *Muscle Nerve*, **25**, 65-76.

ACKNOWLEDGEMENTS

Support is acknowledged from Department of Defense (DAAD 19-02-0222), Landon Center on Aging; and assistance from Rebecca Maletsky and Laura Zahner.

Table 1: Means ± SD of primary outcome variables. Superscripts denote significant age^{A} and fatigue^{F} effects ($p<0.05$).

	Ankle				Knee			
	Pre-Fatigue		Post-Fatigue		Pre-Fatigue		Post-Fatigue	
	YA	OA	YA	OA	YA	OA	YA	OA
t_{onset} (ms)	332±162	580±369	288±206	571±399	280±127	328±171	258±62	305±173
t_{settle} (ms)	2196±1106	4614±2899^{A}	3089±2532	6088±3584	2022±1357	3577±2408	1885±866	3561±2408
S (Nm/s)	96.3±51.5	52.0±28.3^{A}	44.9±21.9^{F}	40.8±47.7	119.9±67.0	51.4±23.7^{A}	70.4±45.1^{F}	39.5±28.0

FUNCTIONAL MEASURES AFTER DEPROGRAMMING OF MASTICATORY MUSCLES IN ADOLESCENTS WITH MAXILLOFACIAL SKELETAL DEFORMITIES: A PRELIMINARY STUDY

Linping ZHAO[1] Patricia V. M. ALVES[3, 4] Pravin K. PATEL[1, 2, 3]

[1] Shriners Hospital for Children, Chicago, IL 60707
[2] Northwestern University Medical School, Chicago, IL 60611
[3] University of Illinois at Chicago, Craniofacial Center, Chicago, IL 60612
[4] Orthodontics at Federal University of Rio de Janeiro. Brazil.
Email: lzhao@shrinenet.org

INTRODUCTION

Adolescents with severe maxillofacial skeletal deformities and consequent malocclusion can develop temporomandibular joint (TMJ) signs and symptoms such as pain, clicking and poping. It is common that these patients present dental compensation and adjust their mandible to a more comfortable position trying to improve their masticatory function. This leads to the habitual occlusion, in which the masticatory neuromuscular system has been adapted to this new relationship of the jaws. Consequently the centric relation at the TMJ is altered and can cause TMJ problems.

The habitual neuromuscular adaptation can be "deprogrammed", in other words allowing the masticatory muscles to relax. When this procedure is completed usually the centric relation at TMJ can be reached. It is conceivable that the functional measures such as maximal voluntary bite force and occlusal contact area would be altered as a consequence of the 'deprogramming'. The hypothesis to be tested in this preliminary study is that both the maximal voluntary bite force and occlusal contact area decrease after the masticatory muscle deprogramming in patients with severe maxillofacial skeletal deformity.

METHODOLOGY

In this preliminary study, seventeen (n=17) subjects have been recruited. The recruited population included adolescents between the ages of 14 and 20 who presented with maxillofacial skeletal deformity of developmental origin and were considered candidates for orthodontic and orthognathic surgery treatment. Both subject recruitment and data acquisition followed a protocol with an Institutional Review Board (IRB) approval.

Subjects were asked to bite on the T-Scan II sensors (Tekscan Inc., Boston, MA) before and after a 'deprogramming' procedure. The 'deprogramming' procedure involved the placement of cotton rolls between the teeth for at least 5 minutes. The subject had approximately 1 mm of separation between upper and lower first molars and thus relaxed the jaw elevation muscles. The bite force (F) vs. time (t) movie was recorded. The maximum voluntary bite force and occlusal contact area were then extracted and calculated using I-scan software (Tekscan Inc., Boston, MA). A comparison was made between these functional measurements before and after the 'deprogramming' procedure.

RESULTS AND DISCUSSION

In a total of seventeen (n = 17) subjects, maximal voluntary bite force increased in four (4) subjects (24 %), and decreased in thirteen (13) subjects (76%), as shown in Figure 1. Similarly, occlusal contact area (OCA) increased in two (2) subjects, representing 12 % of the sample, no change in one (1) case, or 6%, and decreased in fourteen (14) subjects, or 82%, as shown in Figure 2.

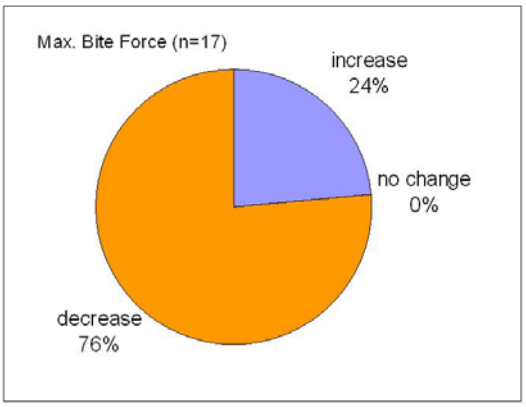

Figure 1. The change of the maximal voluntary bite force after 'cotton roll deprogramming' in seventeen (n=17) adolescents with maxillofacial deformity.

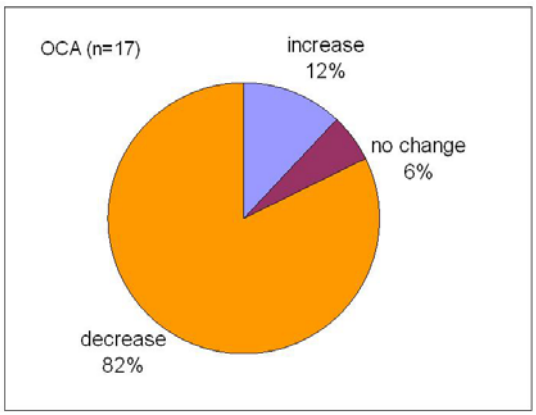

Figure 2. The change of the occlusal contact area (OCA) after 'cotton roll deprogramming' in seventeen (n=17) adolescents with maxillofacial deformity.

Most of subjects in this study had various degrees of decreases in maximal voluntary bite force (76%) and occlusal contact area (82%) after the 'cotton roll deprogramming" procedure. This suggests that the neuromuscular adaptation to the habitual bite in these patients is considerable. It also suggests that the 'cotton roll deprogramming' procedure allows the masticatory muscles relax and the TMJ returns to central relation. However, further investigation with larger sample size is needed.

The increasing maxillary bite force and occlusal contact area occurred in subjects with either facial asymmetry or severe open bite. This suggests that subjects with either facial asymmetry or severe open bite need additional functional measures to monitor the effect of the deprogramming procedure.

SUMMARY

The 'cotton roll deprogramming' procedure led to a reduction in both maximal bite force and occusal contact area in most adolescents who have severe maxillofacial deformity and undergo orthodontic and orthognathic surgery treatment.

ACKNOWLEDGEMENT

This study is supported by Shriners Hospitals for Children (SHC Grant # 8510).

REFERENCES

Bachus KN, DeMarco AL, Judd KT, Horwitz DS, Brodke DS. Med Eng Phys.2006; 28: 483-488.

Kerstein RB, Lowe M, Harty M, Radke J. Cranio. 2006 Jan; 24(1): 15-24.

Orent T. In the face of pain. Vol. 14, No. 6. DDS updates: a Doctor's Resource Book 2002.

INFLUENCE OF ISOMETRIC MUSCLE FATIGUE ON THE HUMAN FORCE-LENGTH RELATIONSHIP

Guillaume Rao [1], Ramu Perumal [2], Stuart A. Binder-Macleod [2],
Eric Berton [3], and Thomas S. Buchanan [1]

[1] Department of Mechanical Engineering, University of Delaware, Newark, DE, USA
[2] Department of Physical Therapy, University of Delaware, Newark, DE, USA
[3] Movement and Perception Laboratory, University of the Mediterranean, Marseille, France
E-mail: grao@udel.edu

INTRODUCTION

An important feature of the active force production in muscles is its dependence on muscle length. The physiological causes of the force-length property are well understood and rely on the overlap between the actin and myosin filaments. Another factor that influences the force produced is the presence of muscle fatigue. Previous animal studies investigated the influence of fatigue on the muscle torque-angle or force-length curves (Katz 1939; Wood et al. 1993; Butterfield and Herzog, 2005). These studies reported that with fatigue the peak torque shifted towards longer muscles lengths and that there was a change in the shape of the relationship.

The aim of the present study was to assess the influence of isometric muscle fatigue on the force-length relationship using a force dynamometer and electrical stimulation of the human quadriceps femoris muscle group.

METHODS

Three subjects were seated on a KinCom with their hips flexed at ~70°. Knee extension force was recorded through a force transducer pad placed against the anterior distal part of the tibia. Subjects performed a maximum voluntary isometric contraction (MVIC) with the knee joint flexed to 90° using a burst superimposition technique (Snyder-Mackler et al., 1994). Electrical stimulation of the quadriceps muscle group was achieved using a Grass S8800 stimulator with a SIU8T stimulation isolation unit. Electrical stimulation was used to assess the torque-angle relationship, and to fatigue the muscle. Throughout this study, the pulse duration was fixed at 600µs and the duration of the stimulation trains was 500 ms. The stimulation amplitude was adjusted so that a 100Hz train would result in a force output corresponding to 40% MVIC. Once the amplitude was set, it was held constant for the remainder of the experiment. In the Non-Fatigue condition (NF), force was produced using three 30Hz-trains with 5 s between each train. Forces were recorded at knee flexion angles of 15, 30, 40, 50, 55, 60, 65, 70, 75, 80, and 90° in a random order (with 0° for full extension). The knee angle that produced the peak force was then determined. Fatigue was then produced at each angle tested using 30Hz stimulation trains with1.5s between each train. For the fatigue portion of the protocol, we slightly modified the angles at which the muscles were tested; we tested the knee flexion angles with values of ±15º of the peak angle in steps of 5º and the remaining knee flexion angles in steps of 10-15º to cover the range of angles from 15 to 90º of knee flexion. The angles were tested in a random order and then repeated in the reverse order. The 30-Hz trains were repeated until at least three successive trains

produced no further decreases in force. Force data were sampled at 200Hz. Force values were computed by averaging the force peaks obtained from last three trains tested at each angle for each condition. Only the data collected during the second fatigue testing was used for the analysis of the fatigue condition. The knee torque-angle relationship was transformed into a force-length relationship using averaged moment-arms and muscle length data of the four quadriceps muscles (data obtained from SIMM software).

RESULTS AND DISCUSSION

Preliminary results revealed a mean decrease in peak force of 54% (± 8.5%) following the fatiguing stimulation. Moreover, the presence of muscle fatigue also modified the torque-angle and force-length relationships. Indeed, the angle (length) at which the maximal torque (force) is produced was shifted toward lower angles/lengths in presence of fatigue (see Fig. 1). While the relative shift in optimal muscle length was small (1.3% ± 0.2), the corresponding peak angle was shifted by (7° ± 2).

Surprisingly, the direction of the shift of the optimal length with fatigue towards shorter lengths was opposite to that of previously observed in human muscles following eccentric fatigue (Jones et al., 1997) and in other animal studies (Katz 1939; Wood et al. 1993; Butterfield and Herzog, 2005).

SUMMARY/CONCLUSIONS

This study was designed to identify the influence of isometric muscle fatigue on the force-length relationship of the human quadriceps femoris muscle group. The length/angle of maximal force/torque production was shifted to lower lengths/angles in presence of fatigue.

Our findings may need to be taken into account when estimating forces from fatigued muscle, as most of biomechanical models use the force-length relationship as a fundamental property.

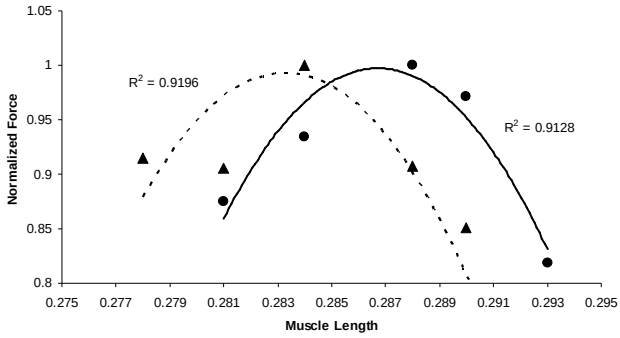

Figure 1: Representative normalized force-length relationships for the non-fatigue (solid line and circles) and the fatigue (dashed line and triangles) conditions. Forces that were >80% of the normalized force were fit with a second order polynomial.

REFERENCE

Butterfield, T.A., Herzog, W. (2005). *J. Biomech*, **38**, 1932-7.

Jones, C. et al. (1997). *Eur. J. Appl. Physiol*, **76**, 21-31.

Katz, B. (1939). *J. Physiol*, **96**, 45-64.

Snyder-Mackler, L. et al. (1994). *J. Bone Joint Surg. Am*, **76**, 555-560.

Woods, S.A. et al. (1993). *Am. J. Physiol*, **265**, C792-800.

ACKNOWLEDGEMENTS

This work was supported by the NIH grant R01-HD38582 as well as a special funding of the University of the Mediterranean.

FRONTAL PLANE KNEE JOINT STIFFNESS: GENDER AND HORMONAL EFFECTS

Martha Cammarata [1,2], Tobey DeMott[2], Jennifer Moore[2], Yasin Dhaher[1,2]
[1] Department of Biomedical Engineering, Northwestern University, Chicago, IL, USA
[2] Sensory Motor Performance Program, Rehabilitation Institute of Chicago, Chicago, IL, USA
E-mail: y-dhaher@northwestern.edu

INTRODUCTION

Emerging findings have associated the incidences of ACL injury in female athletes to abnormal abduction loading at the knee (Hewett et al. 2005). Passive frontal plane knee joint stiffness is one component that would act to resist these abduction torques. It has been shown that passive knee stiffness in this plane is gender specific with males exhibiting a greater joint stiffness (Bryant and Cooke 1988). This gender specificity may partly be attributed to anthropometric differences (weight, height, and joint structure) and hormonal environment. In females, anterior knee laxity was found to vary throughout the menstrual cycle as hormone levels changed (Zazulak et al. 2006). It has also been demonstrated that female athletes using hormonal contraceptives (HC) have significantly decreased anterior-posterior joint laxity than non-users (Martineau et al. 2004), a result which was attributed to the stabilization of hormones in HC users over time. While significant, this study failed to control for the potential effect of hormonal variations between subjects by not testing all subjects at the same time point in the menstrual cycle.

Given that many female athletes use HC, it is important to understand how hormonal modulation affects joint stability. The purpose of this study was to examine the effect of gender and HC use in females on frontal plane knee joint stiffness. Also, we sought to quantify the statistical association between joint varus/valgus stiffness and anthropometric measures within females.

METHODS

Ten male and 31 female subjects with no history of musculoskeletal disorders were tested. Female subjects were placed into three groups based on HC usage: non-users (F1, N = 11), monophasic HC users (F2, N = 11), and triphasic HC users (F3, N=9). All female subjects were tested within 3 days of the start of menses, when hormone levels are the lowest/most stable.

Subjects were seated in an experimental chair with the right knee fully extended. The right ankle was placed in a cast and then secured to a servomotor actuator, via a rigid cantilever beam. Brackets were securely fastened around the knee to prevent medial/lateral translation of the knee during the mechanical perturbation. With subjects under a volitionally relaxed state, torque-angle relationships were obtained for each subject by stretching the joint ±7° at a constant velocity (3°/s) in the frontal plane, while a 6 degree of freedom load cell recorded force and torque signals. Stiffness was estimated from the slope of the loading portion of the torque-angle relationship (Dhaher et. al. 2005) and was determined at 30%, 50%, 70%, and 90% of each subject's maximum varus and valgus torque. Independent sample 2-tailed *t* tests were used to compare the stiffness estimates between the four subgroups. Linear correlation analysis was performed to quantify the association between female stiffness estimates and height, weight, body mass index (BMI), quadriceps (Q) angle, and knee diameter.

RESULTS AND DISCUSSION

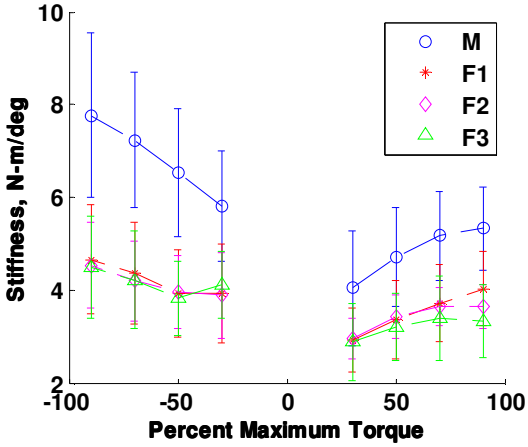

Figure 1. Frontal plane knee joint stiffness increased with increasing load

Frontal plane knee joint stiffness was found to increase with increasing load at the joint (Figure 1). Between genders, males exhibited significantly ($p<0.05$) greater stiffness than females at all loading conditions, consistent with previous reports (Bryant and Cooke 1988). Within the female population, there were no statistically significant differences in stiffness between the three subgroups at any load. However, there was a trend ($p = 0.08$) toward a significant difference in varus stiffness at 90% maximum torque between group F1 (non-users) and group F3 (triphasic users).

For the female population, adduction stiffness was not significantly correlated to any of the anthropometric parameters. The abduction stiffness was significantly correlated to height ($R = 0.63$, $p<0.05$ at 90% max torque) and weight ($R = 0.38$, $p<0.05$), but not to BMI or knee diameter. Our statistical analysis revealed that abduction stiffness was also negatively correlated to Q angle ($R = -0.43$, $p<0.05$).

SUMMARY/CONCLUSIONS

We found a significant correlation between female stiffness and height and weight, which suggests that stature has an effect on stiffness; however, due to the low R value, its predictive worth is questionable.

At the phase of the menstrual cycle considered, our results indicate that HC usage has no effect on frontal plane knee joint stiffness. This finding is contrary to earlier results from Martineau et al. suggesting a decrease in A-P laxity as a function of HC usage (2004). However, natural hormonal variations between subjects at different time points in the menstrual cycle could have skewed their results. It remains to be seen how joint stiffness is affected by HC usage throughout the menstrual cycle and future studies should investigate this question.

The trend toward greater varus stiffness in group F1 over F3 at higher load levels may be an artifact of our experimental set-up. Future investigations with a larger sample size would be able to determine if this is a true effect.

We found a significant negative correlation between female joint stiffness and Q angle. As a posture of dynamic knee valgus could increase the risk of ACL injury in females (Hewett et al. 2005), women with larger Q angles coupled with reduced knee abduction stiffness may need to engage the neuromuscular system to a higher degree to maintain joint stability during sports.

REFERENCES

Bryant JT, Cooke DT. (1988), *J. Orthop Res* **6**(6):863-70.

Dhaher, YY et al. (2005), *J. of Neurophysiology,* **93**(5):2698-709.

Hewett, TE et al. (2005). *Am J. Sports Med,* **33**(4):492-501.

Martineau, PA et al. (2004). *Clin J Sport Med,* **14**(5):281-6.

Zazulak, BT et al. (2006). *Sports Med*, **36**(10):847-62

ACKNOWLEDGEMENTS

This work was supported by the National Institute of Health (1-R01-AR049837-01

FINITE ELEMENT PARAMETERS AFFECTING MICROMOTION AND STRAIN ENERGY DENSITY PREDICTIONS IN TIBIAL MODEL AS DETERMINED BY FACTORIAL ANALYSIS

Jill Schmidt[1], Adam Henderson[2], Michael Dunbar[3], Heidi-Lynn Ploeg[1]

[1] University of Wisconsin-Madison, Madison, WI, USA
[2] Dalhousie University, Halifax, NS, Canada
[3] QEII Health Science Center, Halifax, NS, Canada
E-mail: jschmidt1@wisc.edu, Web: www.engr.wisc.edu/groups/BM/

INTRODUCTION

The population group receiving total knee replacements is being extended to both older and younger patients, which has lead to an increase in the number of surgeries performed each year. Between 1991 and 2000 the number of surgeries doubled (Dixon et al. 2006), which will lead to an increase in revision total knee arthroplasties (rTKAs) even as the failure rate decreases. Generally, tibial implants with stem extensions are used to increased implant stability and transfer loads away from the weak proximal tibial bone. Yet, surgeons performing rTKAs are faced with many decisions including the mode of fixation, stem diameter, length, and geometry. In order to maximize the survival rates of the implant, the effects of these stem configurations on implant stability and bone loading need to be quantified. Therefore the goal of this study was to quantify the effects stem length, load distribution, and friction coefficient have on the micromotion and proximal bone strain energy density (SED) in a finite element (FE) model of a tibial bone with a revision tibial implant.

METHODS

A FE model of the tibial bone and rTKA component (Zimmer, Warsaw, IN) was created using a previously defined computed tomography (CT) to FE protocol (Schmidt et al. 2006). Two 2^3 unreplicated factorial analyses were performed on three factors: stem length, bone-stem friction coefficient, and medial to lateral compartment load distribution. The low and high levels of the friction coefficient represent smooth and rough surface finishes, respectively. A 60:40 load distribution represents normal knee joint loading, whereas, 100:0 represents a varus deformity. The high and low states of each factor are shown in Table 1. The first analysis considered maximum bone-stem micromotion, while the second analysis evaluated average SED in the proximal 20 mm of the tibial bone. All statistics were performed using MiniTab.

Table 1: Factors and Levels

Factor	Level	
	–	+
A. Stem Length	145 mm	200 mm
B. Friction Coefficient	0.1	0.4
C. Load Distribution	60:40	100:0

RESULTS AND DISCUSSION

As seen in the normal probability plot, friction coefficient and load distribution significantly affected proximal SED since they did not lie near the line (Figure 1). Similarly, Figure 2 shows all three main factors (stem length, friction coefficient and load distribution) had a significant effect on maximum micromotion. In general, maximum micromotion increased with either increased stem length or normal knee joint loading, while average proximal SED increased with varus load distribution.

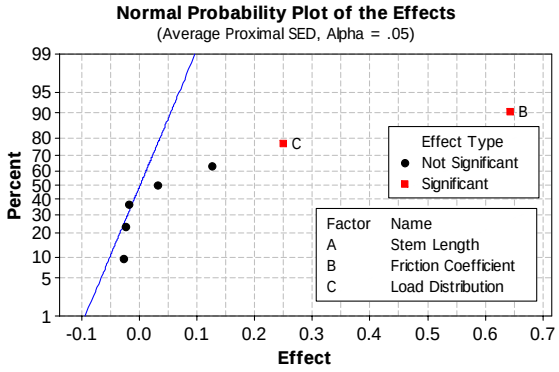

Figure 1: Normal probability plot of effect from proximal SED data.

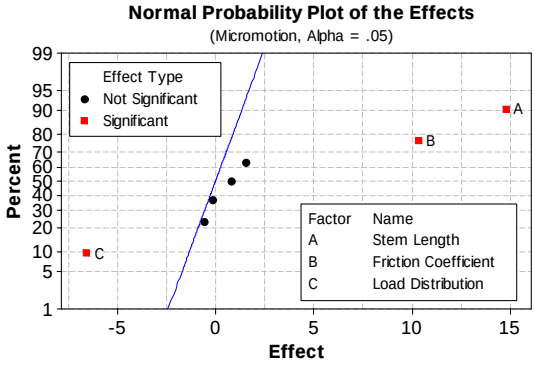

Figure 2: Normal probability plot of effect from micromotion data.

Figure 3 shows no interaction between factors when considering micromotion. Two distinct trends can be seen in the results for proximal bone SED. The first trend is, with a stem-bone friction coefficient of 0.1, a change in stem length had no effect on proximal SED. Second, there is an interaction between load distribution and stem length.

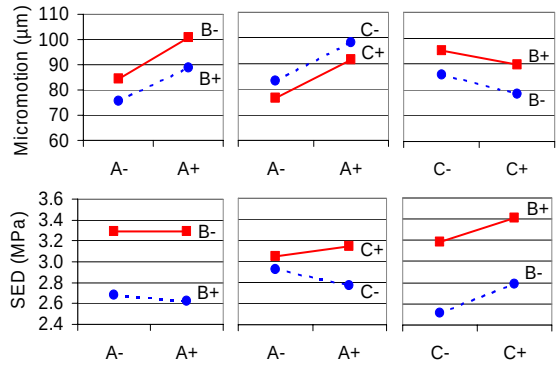

Figure 3: Factor interaction plots of stem length (A), friction coefficient (B) and load distribution (C).

SUMMARY/CONCLUSIONS

This study provided initial steps in developing an accurate FE model of the tibial component to better understand the parameters that affect implant stability and bone loading after an rTKA. In addition, it has shown factorial analysis combined with FEA can be a valuable tool to perform parametric studies. The statistical analysis provided information about which boundary conditions have the most significant effect on the results of the model. This study showed friction coefficient has a significant effect on both micromotion and SED results; and therefore, efforts need to be directed towards in-vitro testing to quantify this parameter more accurately. Load distribution also affected both results, thus offering encouragement to investigate the effect of this parameter in other regions of the model, such as stress at the stem tip. Finally, the information obtained from the interaction plots led to the conclusion that proximal tibial bone loading was not affected by stem length when a smooth stem was used. In contrast bone loading decreased when a long stem with high surface roughness was used, when compared to a short stem.

REFERENCES

Dixon, T. et al. (2006). *Public Health*, **120**, 83-90.

Schmidt, J. et al. (2006). *Proceedings of World Congress of Biomechanics.*

ACKNOWLEDGEMENTS

Funding was provided by Zimmer Inc., Warsaw, IN and the National Science Foundation (NSF) Graduate Research Fellowship.

LUMBAR MOTION DURING PITCHING IN PROFESSIONAL BASEBALL PLAYERS

Christopher McKenzie and Ajit Chaudhari

The Ohio State University, Columbus, OH, USA
E-mail: Christopher.Mckenzie@osumc.edu Web: sportsmedicine.osu.edu

INTRODUCTION

The stress placed upon a pitchers throwing arm has been the subject of many previous research studies [Aguinaldo 2007, Escamilla 2007, Feltner 1986]. Some of these studies have focused solely on the throwing arm, while others have suggested an influence by the lower body on the loads in the throwing arm [Matsuo 2001]. However, the effect in which core stability has on controlling the lumbar spine's range of motion during a pitch has not been examined. Core stability is needed to optimize the transfer of forces generated from the lower extremities to the upper extremity during a pitch [Putnam 1993]. Core stability also may be necessary to minimize the distal joint loads experienced during the throwing motion [Kibler 2006].

Lumbar rotation utilized during the throwing motion may affect joint stresses experienced at the throwing arm. To date, little is known about how the lumbar spine moves during the baseball pitch. Lumbar movement first needs to be quantified before attempting to identify what effect it may have on the throwing shoulder. The purpose of this study was to identify the movement of the lumbar spine during baseball pitching among professional baseball pitchers.

METHODS

Eighteen healthy professional baseball pitchers volunteered to participate in this study. Subject's ages ranged from 21 to 25 years. Signed informed consents were collected before the testing.

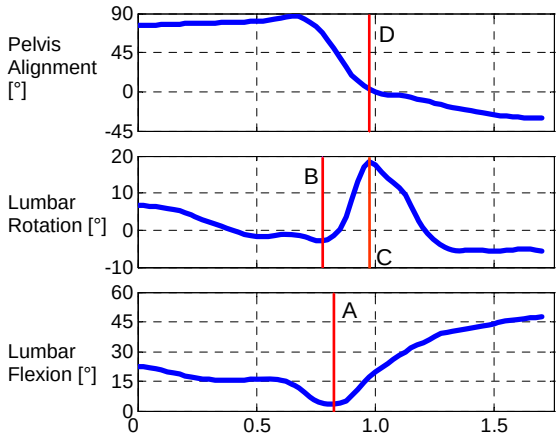

Figure 1. Typical curves for pelvis alignment towards home plate (top), lumbar rotation (middle), and lumbar flexion (bottom) during a pitch from the stretch.

A magnetic motion analysis system (Polhemus FasTrak) was utilized to collect lumbar data during the pitching motion. Sensors were attached at the sacrum and the spinous process of the first lumbar spine on each subject. After a normal warm-up routine, each subject threw six fastballs, three from the wind-up and three from the stretch position. Only the stretch pitches were analyzed in this study. Pitches were performed off a standard mound to a catcher located 18.4 meters away from the pitching rubber.

Lumbar rotation and flexion were calculated based on the relative orientations of the lumbar sensor with respect to the sacrum sensor. The angular motion of the pelvis in the horizontal plane was also calculated. The minimum flexion (Fig. 1A) and total range of motion for lumbar rotation (Fig. 1B-C) were identified during the cocking

and acceleration phases of the throwing motion [DiGiovine 1992]. This motion began upon the initiation of forward progression of the pelvis, and ended at the instant when the pelvis faced home plate (Fig. 1D). Average values were calculated for each pitcher.

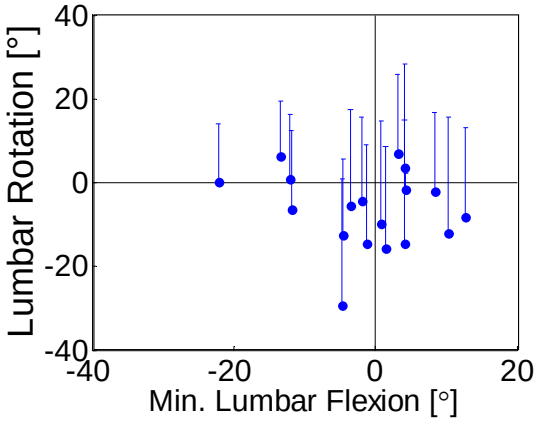

Figure 2. Lumbar rotation and minimum lumbar flexion during pitches from the stretch. Points show minimum lumbar rotation, and bars show range to peak lumbar rotation.

RESULTS AND DISCUSSION

The minimum lumbar flexion point ranged from -22° to 13° (Fig. 2, x-axis). The minimum lumbar rotation point ranged from -29° to 7° (Fig. 2, points on y-axis). Pitchers rotated through a net range of motion of 4° to 30° (Fig. 2, bars on y-axis).

Lower values of lumbar flexion and lumbar rotation are indicative of a more open position during the pitch. In a more open position, lower body motion precedes upper body motion. As they reach the limits of their flexibility, the anterior shoulder and medial elbow are subject to increased stretch, which could lead to higher peak loads on the joint structures.

Variations in the total range of lumbar rotation were identified among the subject population. It remains unknown what the optimal lumbar rotation range of motion is for the baseball pitcher, but a smaller range of motion may enhance the transfer of forces generated by the lower body to the throwing arm and reduce joint stresses in the shoulder and elbow.

This ongoing study will assess the relationship between the observed motions in these pitchers and the injuries they experience during the 2007 baseball season.

SUMMARY/CONCLUSIONS

This study represents the first work examining lumbar motion in baseball pitchers to the authors' knowledge. The considerable variability observed in minimum lumbar flexion, minimum lumbar rotation, and lumbar range of motion across the observed population may indicate different injury risk through the baseball season. Future studies will attempt to identify this relationship.

REFERENCES

Aguinaldo AL, et al. *J.Appl.Biomech.* **23**, 42-51, 2007.

DiGiovine NM, et al. *J Shoulder Elbow Surg* **1**, 15-25, 1992.

Escamilla RF, et al. *Am.J.Sports Med.* **35**, 23-33, 2007.

Feltner ME, et al. *Int J Sport Biomech* **2**, 235-259, 1986.

Kibler WB, et al. *Sports Med.* **36**, 189-198, 2006.

Matsuo T, et al. *J Appl Biomech* **17**, 1-13, 2001.

Putnam CA. *J.Biomech.* **26**(Suppl. 1), 125-135, 1993.

ACKNOWLEDGEMENTS

The authors would like to thank the Pittsburgh Pirates and Boston Red Sox baseball organizations for their participation.

MAXIMISING THE RESOLUTION OF EMG CHARACTERISTICS FROM DYNAMIC CONTRACTIONS BY COMBINING A MUSCLE MODEL AND WAVELET ANALYSIS

S.E. Forrester and M.T.G. Pain

Loughborough University, Loughborough, UK
Email: S.Forrester@lboro.ac.uk, Web: www.lboro.ac.uk

INTRODUCTION

When utilising surface electromyography (EMG) the amplitude and / or frequency content of the processed EMG signals can be used to investigate neural aspects of muscle function (De Luca, 1997). However, signal interpretation is complicated by the influence of a number of factors in addition to neural strategy and remains the subject of ongoing debate (Farina *et al.*, 2004). This is particularly true for dynamic contractions (Beck *et al.*, 2006), where the signals are non-stationary and require processing with a combined time–frequency approach.

The purpose of this study was to develop methods to improve the measurement and understanding of EMG signal characteristics from dynamic contractions. Based on a continuous wavelet transform (CWT) time–frequency analysis, the methods comprised of: (i) a muscle model to estimate the fibre kinematics beneath the recording electrodes; and (ii) selection of wavelet parameters to give the required resolution properties of the instantaneous amplitude (IAMP) and mean frequency (IMNF) estimates. Given the added dimension in resolution provided by the CWT, neglecting the muscle model would hamper the interpretation of time dependent EMG as the length, velocity and position of the fibres would be unknown.

METHODS

Eight strength trained male volunteers (age 27.5 ± 5.0 yrs, body mass 81 ± 11 kg, height 1.77 ± 0.05 m) gave informed consent prior to performing maximal effort knee extensions. Eccentric–concentric contractions at velocities ranging from ±50 to ±300° s^{-1} (Yeadon *et al.*, 2006) were conducted on a Cybex NORM dynamometer (CSMI, USA).

EMG signals from the rectus femoris (RF), vastus medialis (VM), and vastus lateralis (VL) were recorded using active bipolar electrodes (Biovision, Germany). Synchronous dynamometer and EMG signals were recorded at 2 kHz. The dynamometer data were used in a Hill-type muscle models, scaled to each subject, to give the force, length and velocity characteristics of the VM, VL and RF.

EMG signals were processed using a CWT analysis to provide estimates of the IAMP and IMNF. This employed a complex Morlet wavelet function (Wavelet Toolbox in Matlab):

$$\Psi(t) = \frac{1}{\sqrt{\pi f_B}} \times \exp(2i\pi f_C t) \times \exp\left(\frac{-t^2}{f_B}\right) \quad \text{eqn. 1}$$

where the wavelet shape is described by the bandwidth parameter, f_B and the central frequency parameter, f_C. The value of $f_C\sqrt{f_B}$, the wavelet shape factor, sets the resolution properties of the IAMP and IMNF estimates.

The influence of the wavelet shape factor on resolution was examined based on specifying time, angle and frequency resolutions for the knee extension task.

RESULTS AND DISCUSSION

The muscle model illustrated that the fibre kinematics could deviate markedly from those of the joint. Across eccentric and low concentric velocities the fibre velocity was up to 50% lower than that of the muscle-tendon complex for extended knee angles and up to 50% higher at flexed knee angles. Across concentric velocities the fibre length showed marked non-linearity with the length up to 12 mm shorter across mid-range joint angles. These differences were greater for the RF than the vastii.

For investigating time-based events a single velocity independent value of the wavelet shape factor gave the optimal time and frequency resolutions of the IAMP and IMNF estimates. Resolutions of better than 100 ms and 10 Hz were achievable across all trials using a wavelet shape factor of 4 (Figure 1). For investigating angle-based events wavelet shape factor selection was velocity dependent; at low velocities a high value provided the optimal angle and frequency resolutions, and vice versa at high velocities. Setting resolution limits of 10° and 10 Hz, and the requirement to minimise their sum, the optimal wavelet shape factor was 6 in the low velocity trial, and 3 in the high velocity trial (Figure 1). Individual values for f_B and f_C, were found by minimising the entropy of the resulting wavelet coefficients; giving f_C, of 1.5 and f_B, obtained from the optimised shape factor values given above.

Thus, through careful selection of the wavelet shape factor, the IAMP and IMNF can be estimated with resolutions specific to the investigation, and thereafter directly related to the instantaneous muscle fibre kinematics predicted by the muscle model.

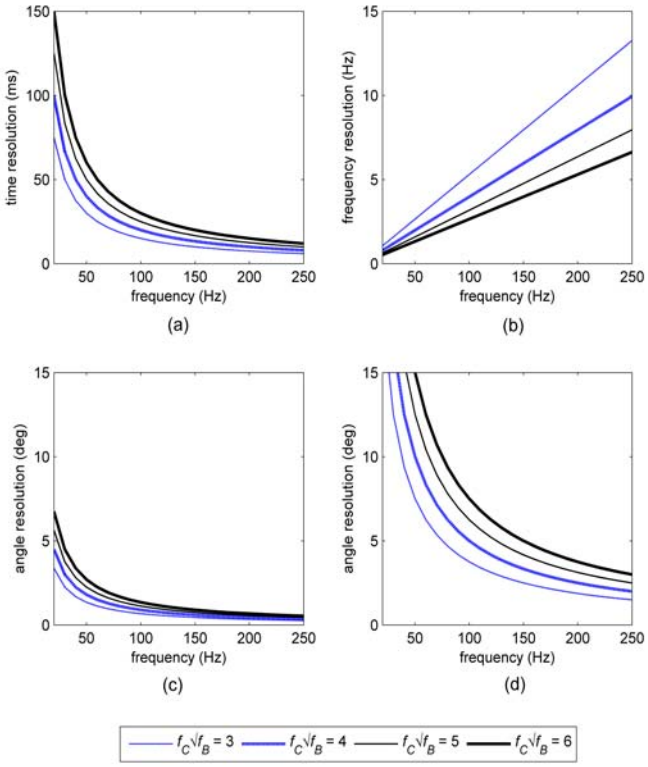

Figure 1 – Time, frequency and angle resolutions as a function of frequency. (a) time; (b) frequency (c) angle, (velocity = ±45° s^{-1}); (d) angle, (velocity = ±250° s^{-1}).

CONCLUSIONS

Combining the muscle model and CWT results allowed for a substantial improvement in measuring and interpreting time dependent EMG data since the length, velocity and position of the muscle fibres are known at the same time as specific frequency and amplitude events.

REFERENCES

Beck *et al.* (2006). *J Electromyography Kinesiol.*, **16**, 531–539.

De Luca, C.J. (1997). *J. Appl. Biomech.*, **13**, 135–163.

Farina *et al.* (2004). *J. Appl. Physiology*, **96**, 1486–1495.

Yeadon *et al.* (2006). *J. Biomech.*, **39**, 476–482.

SIMULTANEOUS PERFORMANCE OF TWO TASKS BY THE FINGERS OF THE HUMAN HAND

Wei Zhang [1] John P. Scholz [2] Vladimir M. Zatsiorsky [1], and Mark L. Latash [1]

[1] Pennsylvania State University, University Park, PA, USA
[2] University of Delaware, Newark, DE, USA
E-mail: wuz107@psu.edu
Web: www.kinesiology.psu.edu/research/laboratories/mcl/index.html

INTRODUCTION

Several studies used the framework of the uncontrolled manifold (UCM) hypothesis (Scholz and Schöner 1999) to quantify the multi-finger synergies stabilizing the total force (F_{TOT}) and total moment of force (M_{TOT}) in multi-finger tasks. The method of the UCM hypothesis allows to separate variance of the commands to fingers into two components, within a sub-space (UCM_F or UCM_M) that corresponds to multiple solutions of finger coordination that all achieve the same desired value of a performance variable such as F_{TOT} and M_{TOT} and within another sub-space that corresponds to finger force combinations that change the value of that variable. Most studies compared the amounts of variance in those two sub-spaces to find out whether a synergy existed stabilizing the performance variable (reviewed in Latash et al. 2002).

In this study, we explored the patterns of variance within the UCM computed for F_{TOT} (corresponding to the explicit task, UCM_F) when implicit requirements for M_{TOT} changed. We expected the subjects to be able to stabilize both F_{TOT} and M_{TOT} (Latash et al. 2001; Scholz et al. 2002). However, since four fingers form a redundant set with respect to tasks with two constraints, we expected the subjects to use flexible combinations of commands to fingers to satisfy the task requirements.

METHODS

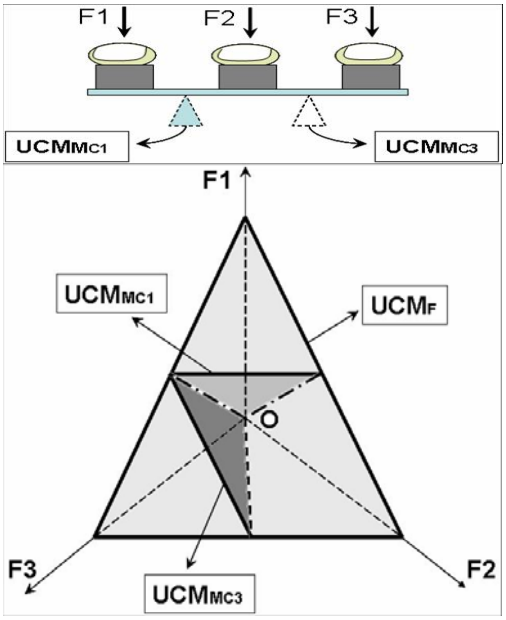

Figure 1: A simplified illustration of the task conditions (C1, C3) and UCM for F_{TOT} (UCM_F) and M_{TOT} stabilization (UCM_M). Note that a 3-finger case is illustrated!

Ten (5M, 5F) healthy, young, right-handed subjects participated in this study. Subjects sat comfortably facing a test table and placed the fingertips of the right hand on the four force sensors. The forearm/hand position was fixed. Subjects were instructed to produce a series of accurate steady-state values of the total force at 5%, 7.5% and 10% of the four-finger maximal force, following a template displayed on the computer screen. The force sensors could rest on the table (***Stable***) or on a narrow support (***Unstable***) placed between the index and middle fingers (**Pivot_IM**), middle and

ring fingers (***Pivot_MR***), or ring and little fingers (***Pivot_RL***).

The UCM hypothesis was used to compute an index (ΔV) reflecting the multi-finger F_{TOT} and M_{TOT} stabilizing synergies at each time sample over sets of trials for each condition and each subject separately. The upper panel of Figure 1 illustrates task conditions but for only three finger instead of four, such that we can illustrate the UCM (UCM_F and UCM_M) in the 3-dimensional space of finger forces (the lower panel). Principal component analysis (PCA) was performed within the UCM computed for F_{TOT}. All analyses were run within the space of hypothetical commands to fingers (modes).

RESULTS AND DISCUSSION

Indices ΔV indicated synergies stabilizing F_{TOT} in all the conditions and M_{TOT} only in the ***Unstable*** conditions. PCA of the projections of the finger modes onto the UCM for F_{TOT} stabilization showed two PCs ("default PCs") accounting for over 90% of variance in all conditions. In the ***Pivot_MR*** conditions, significant loadings in these PCs corresponded to negative co-variation of modes between fingers within the IM and RL pairs. In the other two ***Unstable*** conditions, these two PCs were seen less frequently, and only in about 50% of their occurrence they contributed to stabilization of the M_{TOT}. In the ***Stable*** condition, these PCs were all but absent. In addition, eight 2-finger, eight 3-finger, and four 1-finger PCs were observed. Most of the 2-finger PCs (87%) benefited M_{TOT} stabilization in the ***Unstable*** conditions. All the 3-finger PCs could be viewed as derived from the default PCs by adding a third finger that helped M_{TOT} stabilization.

SUMMARY/CONCLUSIONS

The results show that the redundancy of the four fingers allows subjects to achieve F_{TOT} stabilization together with stabilization of M_{TOT} with flexible means. Adding a secondary constraint did not interfere with the force stabilizing synergy. The flexible solutions used by the subjects in ***Unstable*** conditions emphasize the main advantage of using multi-finger synergies and comply with the principle of superposition (Arimoto et al.; Zatsiorsky et al.).

REFERENCES

Arimoto S. et al. (2001). *Robotica*, **19**, 21-28

Latash, M.L. et al. (2001). *Exp Brain Res*, **141**, 153-165.

Latash, M.L. et al. (2002). *Exerc. Sport Sci. Rev.*, **30**, 26-31

Scholz J.P., Schöner G (1999). *Exp Brain Res*, **126**, 289-306.

Scholz J.P. et al. (2002). Biol Cybern, **86**, 29-39

Zatsiorsky V.M. et al. (2004). *Robotica*, **22**, 231-234

Zhang, W. et al. (2006). *Exp Brain Res*, **175**, 68-82.

Zhang, W. et al. (2007). *Exp Brain Res*, **177**, 243-254.

ACKNOWLEDGEMENTS

This research was supported in part by NIH grants AG-018751, NS-035032, and AR-048563

HOW PRECISE IS THE HIP JOINT CENTRE POSITION FOUND USING FUNCTIONAL METHODS?

AB Zavatsky [1], R Good [1], J Stebbins [2], and TN Theologis [2]

[1] Department of Engineering Science, University of Oxford, Oxford, UK
[2] Oxford Gait Laboratory, Nuffield Orthopaedic Centre NHS Trust, Oxford, UK
E-mail: amy.zavatsky@eng.ox.ac.uk, Web: www.eng.ox.ac.uk & www.noc.nhs.uk

INTRODUCTION

The location of the hip joint centre (HJC) plays an essential role in the calculation of hip kinematics and kinetics in motion analysis studies. Mislocation of the HJC can lead to errors in hip joint moments and in hip flexion-to-extension timing (Stagni et al., 2000).

The most common way of estimating the position of the HJC is to use regression equations derived from anthropometric data (for example, Davis et al., 1991, Harrington et al., 2007). The accuracy of such equations depends on the size and variability of the data set and on the independent parameters chosen for the regression.

So-called functional methods for finding the HJC (Cappozzo, 1984) should be superior to regression equations since they are subject-specific. Functional methods involve a movement of the thigh relative to the pelvis and calculation of HJC position from the positions of skin-mounted markers.
For functional methods to be useful, they must be not only accurate, but precise. In theory, they should give the same HJC position regardless of the leg movement undertaken or the calculation method used.

The aim of this study was to assess the precision of the HJC position found using functional methods.

METHODS

One healthy adult male subject (age 23, height 183 cm, weight 67 kg) performed six repeats each of four functional motions (right leg only): hip flexion-extension-abduction, hip circumduction, forward walking, and sideways walking. Four retro-reflective markers (14 mm dia) were placed on the pelvis (ASIS and PSIS, left and right), and five similar markers were placed on the thigh (two on the anterior side, two on the lateral side, and one on the lateral femoral epicondyle). Motion data were collected at 100 Hz using a twelve-camera Vicon 612 (Vicon, Oxford, UK). Marker trajectory data was neither filtered nor smoothed. Data are reported in *mm*.

For each trial, the HJC position in a pelvis-based coordinate system (Wu, 2002) was calculated from the marker trajectories using several mathematical methods: Reuleaux method (Halvorsen et al., 1999), sphere-fitting methods (1-Piazza et al., 2001; 2-Halvorsen, 2003) and symmetrical estimation (SCoRE, Ehrig et al. 2006). A first estimate of the HJC position was calculated using the single-variable regression equations in Harrington et al. (2007). All calculations were implemented in Matlab (The Math Works, MA, USA).

Tests on a mechanical ball-and-socket joint gave a joint centre position accurate to just over 1 mm and repeatable to within 0.3 mm for the sphere-fit and SCoRE methods. The

Reuleaux method was accurate to 1.6 mm and repeatable to 0.6 mm.

RESULTS AND DISCUSSION

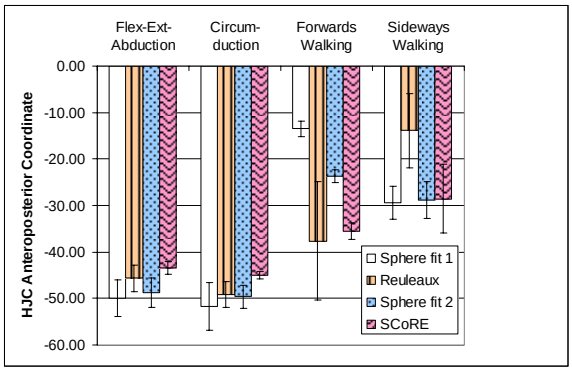

Figure 1: Anteroposterior (*x*) coordinate.

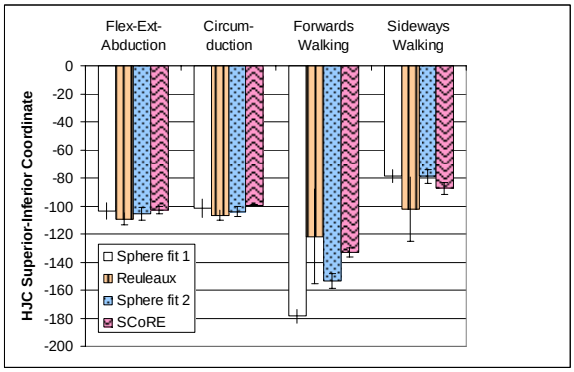

Figure 2: Superior-inferior (*y*) coordinate.

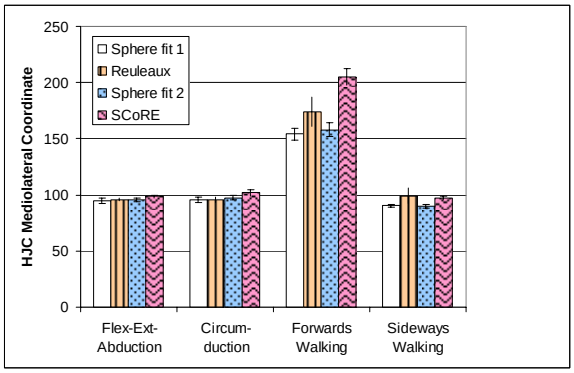

Figure 3: Mediolateral (*z*) coordinate.

Regression equations gave the HJC antero-posterior, superior-inferior, and mediolateral position coordinates (*x*, *y*, *z*) as (-50, -88, 92). Functional HJC position varied both with motion type and calculation method (Figs. 1-3). HJC position calculated from all motion trials and all calculation methods (*n*=94) was (-37±13, -110±27, 115±35).

The standard deviations (stdevs) of the calculations were used to indicate the precision, or repeatability, of functional HJC position. Overall, the SCoRE method gave the smallest stdevs in *x* and *y* (8 and 17), whilst the Sphere fit 1 method was most consistent in *z* (27). Flex-ext-abduction and circumduction had the smallest stdevs in *x*, *y*, and *z* (range 2-5). Sideways walking was similarly consistent in *z* (6). See Figs. 1-3.

SUMMARY/CONCLUSIONS

This study quantifies the precision of functional HJC methods. It does not give the accuracy of the methods (how close the calculations are to the true HJC) or indicate any bias in the HJC coordinate directions.

REFERENCES

Cappozzo, A. (1984) *Human Mov Sci* **3**: 27-50.

Davis, R.B. et al. (1991) *Human Mov Sci* **10**: 575-587.

Ehrig, R.M. et al. (2006) *J Biomech* **39** : 2798-2809.

Halvorsen, K. et al. (1999) *J Biomech* **32**: 1221-1227.

Halvorsen, K. (2003). *J Biomech* **36**, 999-1008.

Harrington, M.E. et al. (2007) *J Biomech* **40**: 595-602.

Piazza, S.J. et al. (2001) *J Biomech* **34**: 967-973.

Stagni, R. et al. (2000) *J Biomech* **33**: 1479-1487.

Wu, G. (2002) *J Biomech* **35**: 543-548.

ACKNOWLEDGEMENTS

This study was supported in part by the Leverhulme Trust (UK).

EMG CHARACTERISTICS OF DYNAMIC KNEE EXTENSIONS DETERMINED BY COMBINED MUSCLE MODELLING AND WAVELET ANALYSIS

M.T.G. Pain and S.E. Forrester

Loughborough University, Loughborough, UK
Email: M.T.G.Pain@lboro.ac.uk, Web: www.lboro.ac.uk

INTRODUCTION

Maximum effort movements are common in sport and surface EMG can be used to investigate their neural characteristics. The amplitude of the EMG signal is generally taken to represent the level of muscle activation (De Luca, 1997). However, EMG signals recorded under dynamic conditions are difficult to interpret due to their non-stationarity and the influence of several factors in addition to neural strategy (Farina *et al.*, 2004). Numerous studies have reported EMG amplitude to vary with movement velocity in a multitude of ways.

The objective of this study was to quantify the effects of fibre length and contraction velocity on the surface EMG characteristics of maximum effort knee extensions, through combining time–frequency processing of the EMG signals with a muscle model of the contractions. Given the added dimension in resolution obtained from the time–frequency analysis, neglecting the muscle model would hamper the interpretation of time dependent EMG data as the length, velocity and position of the muscle fibres at any given time would be unknown.

METHODS

Eight strength trained male volunteers who gave informed consent participated in the study (age 27.5 ± 5.0 yrs, body mass 81 ± 11 kg, height 1.77 ± 0.05 m). Maximal effort knee extensions were conducted on a Cybex NORM dynamometer (CSMI, USA). The protocol comprised of isometric contractions at five crank angles spanning 15 to 75° (0° = full extension), followed by eccentric–concentric contractions at preset crank velocities ranging from ±50 to ±300° s^{-1}, as described by Yeadon *et al.* (2006).

EMG signals from the rectus femoris (RF), vastus medialis (VM), and vastus lateralis (VL) were recorded using an active bipolar electrode system (Biovision, Germany). Synchronous dynamometer and EMG signals were recorded at 2 kHz. The dynamometer data were used in a Hill-type muscle model to give the force, length and velocity characteristics of the VM, VL and RF. The EMG signals were processed using the continuous wavelet transform (CWT) time–frequency method to give the instantaneous amplitude and mean frequency. This employed a complex Morlet wavelet (Wavelet Toolbox in Matlab) with wavelet shape parameters specifically selected to give the required resolution in frequency, time and angle. The amplitudes were normalised (AMPN) based on their values at the isometric location of peak force. The effects of contraction velocity and fibre length were assessed using two-way repeated measures ANOVAS (SPSS, v13.0) with a significance level set at $p = 0.05$.

RESULTS AND DISCUSSION

For a fixed joint angle the fibre length varied considerably with contraction velocity, especially for the RF (Figure 1). Fibre length

and contraction velocity simultaneously affected the AMPN, supporting the inclusion of both parameters and the contour maps used to present the results (Figure 1). These length and velocity effects were muscle specific, and differed for the RF compared to the vastii. For eccentric contractions the AMPN of the vastii decreased significantly ($p \leq 0.05$), by 15 – 20%, with increasing lengthening velocity from -25 to -100 mm s^{-1}. For concentric contractions the AMPN of the vastii decreased significantly, by 15 – 25%, with fibre shortening from 100 to 70 mm. Across all contraction velocities and knee extensors the mean frequency (MNF) increased significantly, by 5 – 15%, across the fibre shortening length range. The MNF was not affected by either eccentric or concentric

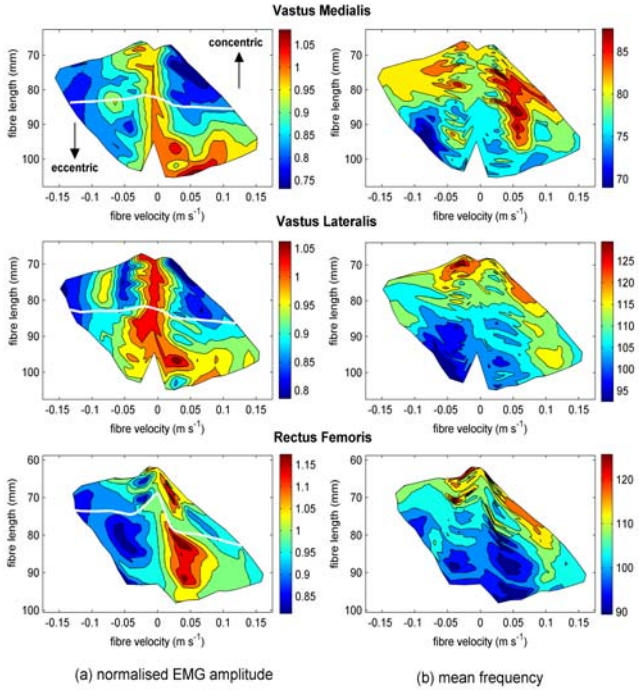

Figure 1. AMPN – length – velocity and MNF – length – velocity results for the VM, VL and RF. The white lines represent a fixed joint angle of 50°.

Simultaneous decreases in AMPN with increases in MNF in regions of the contour graphs suggest that the increase in MNF is more likely to be associated with changing fibre length rather than neural strategy. The two areas of reduced AMPN have previously been observed in studies of maximal knee extensions (*e.g.* Westing *et al.*, 1991 and Aagaard *et al.*, 2000) and linked to neural protection mechanisms. The AMPN results for the RF differed to those for the vastii. The muscle model may help to identify possible reasons for these differences. Notably that the fibre kinematics for this muscle showed the greatest differences to those of the joint.

CONCLUSIONS

Both fibre length and contraction velocity affected the EMG characteristics of maximal knee extensions, and in a muscle specific manner. Hence, including both these parameters has allowed for a more complete understanding of the results compared to previous studies that investigated contraction velocity alone. In particular, the AMPN contour graphs illustrated that the effect of shortening velocity is dependent on the region of the graph under investigation. Inconsistencies across previous studies may have resulted from the different angle ranges employed, leading to differing operating regions on the contour graphs.

REFERENCES

Aagaard *et al.* (2000). *J. Appl. Physiology*, **89**, 2249–2257.

De Luca, C.J. (1997). *J. Appl. Biomech.*, **13**, 135–163.

Farina *et al.* (2004). *J. Appl. Physiology*, **96**, 1486–1495.

Westing *et al.* (1991) *Euro. J. Appl. Physiology*, **62**: 104–108.

Yeadon *et al.* (2006). *J. Biomech.*, **39**, 476–482.

FATIGUE INDUCED DAMAGE IN CEMENTED TOTAL HIP ARTHROPLASTY CAN BE INVESTIGATED BY ACOUSTIC EMISSION

Jihui Li[1] and Gang Qi[2]

[1] Columbia University, New York, New York, USA
[2] University of Memphis, Memphis, TN, USA

INTRODUCTION

Cemented total hip arthroplasty (THA) has been reported with a failure rate from 3% to 16% after 10 years of surgery [1]. Numerous clinical and biomechanical studies have been done to identify its failure mechanism [2]. It is well accepted that fatigue induced damage accumulating in the cement mantle and along the cement-bone or cement-stem interfaces is a primary mechanism. However, little is known about the cement damage progression and related causes, due to the lack of continuous information on damage location and severity.

Recent research indicated that Acoustic Emission (AE) is a noninvasive evaluation tool that can monitor the location, growth trend and severity of fatigue damage in real time [3]. In this work, we further used AE technique to test a series of cemented THA models to explore their fatigue process. We hypothesized that: 1) AE signals could be used to study damage sites and severity; 2) cement defects, when occur in THA, would be a major cause of fatigue damage; 3) fatigue damage would be directional dependent, meaning that the damage level is different along the femoral axis.

METHODS

Eighteen cemented THA models were prepared using Spectron hip stems (Smith Nephew Inc., Memphis, TN), 2nd generation composite femora (Pacific Research Lab., Vashon, WA) and Versabond cement (Smith Nephew, Inc., Memphis, TN). Radiographs were taken to examine cement defects. The THA models were hinge-hinge constrained onto a servohydraulic testing machine (Fig.1) and subjected to a sinusoidal compressive load of 267/2670 N at 2 Hz for over 24 hours. Eight piezoelectric sensors (Physical Acoustics Corp., Princeton Junction, NJ) were glued onto the THA surface to monitor AE microcrack activities.

Fig. 1: Setup of the fatigue test.

The locations of fatigue induced AE microcracks were computed using a customized program 3DMem [3]. Based on the number of microcracks in the fatigue process, THA models were divided into two groups: Group 1 (G1) models would have significant AE microcracks (>10,000), while Group 2 (G2) models would have few microcracks. In G1 models, possible damage causes were identified according to the microcrack locations. For those without obvious causes, microcrack locations were presented in terms of proximal third, middle third, and distal third along the femoral axis. All models were transversely sectioned after fatigue tests, in 20 mm intervals from the collar to the distal tip. Cracks on section

surfaces were examined with a scanning electronic microscope (SEM). Crack location and severity were compared with AE microcrack locations and numbers.

RESULTS AND DISCUSSION

G1 had 12 THA models since a good amount of AE microcracks were detected. In these models 8 had obvious cement defects that attracted the majority of the AE microcracks (Fig.2). No obvious cause could be identified in the other 4 models, but more microcracks could be sorted into distal and proximal areas (Fig.3). In G2 models (totally 6), the number of microcracks was limited and their distribution was random. Two models had cement defects, but they did not induce any detectable microcracks.

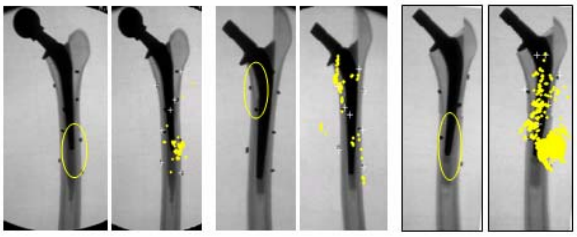

Fig. 2 Three THA models had cement defects (marked by yellow ovals) that attracted significant AE microcracks (dots).

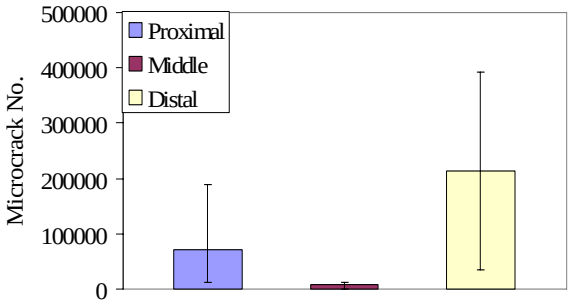

Fig. 3 AE microcrack distribution along the femoral axis in the four G1 models that had no observable defects.

SEM observations were consistent with AE results. Notable damage/cracks were found in G1 models, close to computed microcrack locations (Fig.4). No obvious cracks were observed in G2 models. This shows that the number of AE microcracks can be used as an indicator to evaluate the damage severity.

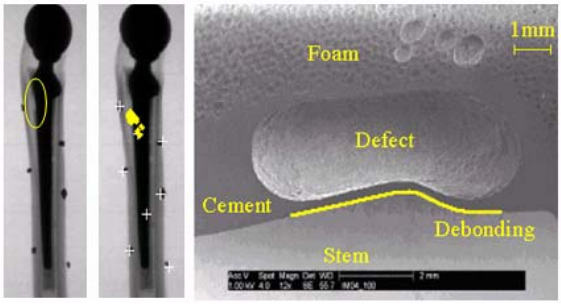

Fig. 4 A THA model that had cement defect (left) attracted AE microcracks (middle). SEM found a debonding along the stem-cement interface next to the defect (right).

SUMMARY/CONCLUSIONS

This study proved that AE is an efficient tool to investigate the fatigue induced damage occurred in cemented THA. Locations of computed AE microcracks were consistent with those of observed cracks with limited errors. The number of AE microcracks could be used as a parameter to evaluate the damage severity. Cement defects, although rarely seen in clinical environments, was found to be a significant damage initiator in this study. For the damaged models without obvious causes, more AE microcracks were found in the proximal and distal areas.

REFERENCES

[1] Verdonschot N. et al. (1997) Clin Orthop Relat Res., 336:297-307. [2] Halley D. et al. (2003) J Arthroplasty, 18(7 Suppl 1):79-85. [3] Qi G. and Li J., (2004) J Biomed Relat Res., 71(3):391-402

ACKNOWLEDGEMENTS

The project was supported by the Whitaker Foundation, RG-01-048.

NORTH AMERICAN PERCEPTION OF THE PRESTIGE OF BIOMECHANICS SERIALS

Duane V. Knudson [1] and John W. Chow [2]

[1] California State University, Chico, CA, USA
[2] Methodist Rehabilitation Center, Jackson, MS, USA
E-mail: dknudson@csuchico.edu, Web: www.csuchico.edu/kine/biomech/biomechanics.html

INTRODUCTION

Since 1975, the Institute of Scientific Information (ISI) has published Journal Citation Reports (JCR) annually and reported impact factors (IF's) of scientific journals (http://portal.isiknowledge.com/). The IF is essentially the mean number of citations an average article in a journal had in a year in the over 12,000 journals indexed relative to the number of papers published in that journal in the last two years.

Biomechanics is a discipline with many applications and sub-areas so scholars often publish their work in journals in different subject categories used in JCR. It is not known whether the quality/prestige of journals in the discipline of biomechanics matches the IF reported in JCR. Therefore, the purpose of this study was to document the perceived quality/prestige of English language peer-reviewed serials publishing biomechanical papers by the North American biomechanics community and evaluate the association between these ratings and the IF. A secondary purpose was to explore the potential differences in perceived quality/prestige of journals publishing biomechanical papers across different interest areas within biomechanics.

METHODS

An electronic mail survey including a list of 62 English language journals and regularly published proceedings that represented the variety of fields and publications focusing on biomechanics or using biomechanical research (Table 1) was sent to 610 members the American Society of Biomechanics (ASB) in the early 2007. They were asked to rate the journals based on their assessment of the mean quality or impact of papers from these journals in the field of biomechanics on a 5-point scale:

4 Likely High Quality/Impact
3
2 Likely Moderate Quality/Impact
1
0 Likely Low Quality/Impact or Unknown

A total of 78 members (13%) responded to the survey. A correlation coefficient between mean prestige ratings (PR's) and IF's reported for 2005 was determined ($p = 0.05$) and serials without IF in 2005 were excluded from the correlation analysis.

RESULTS AND DISCUSSION

Although the response rate was low, the respondents were representative of the ASB with a similar distribution of interest areas (biol sci-10%, eng/appl physics-39%, ergo/hum factors-6%, exerc/sport sci-23%, & health sci-22%) to the ASB membership (7, 50, 10, 20, 13%, respectively).

There was a significant but weak correlation between PR and the IF for 2005 ($r_{45} = 0.35$, $p < 0.05$). The weak correlation ($r^2 = 12\%$) suggests that the IF along is inappropriate for evaluating journal prestige within the field of biomechanics.

There was high variability of journal ratings across respondents probably because of the differences in research interests among respondents (Table 2). However, several journals were consistently highly rated across interest areas. Several respondents recommended additional journals that are considered relevant to their fields (e.g., IEEE Trans Biomed Eng, J Gerontol, Proc ISB, Spine, etc.) for future studies.

SUMMARY/CONCLUSIONS

It was concluded that IF's should be used with caution in evaluating the quality/prestige of journals publishing biomechanics research. Furthermore, investigators should consider interest area specific ratings within biomechanics when selecting journals for publishing their research.

Table 1: Prestige ratings (PR's) of biomechanics serials (mean ± SD).

Serial	PR's	Serial	PR's	Serial	PR's
J Biomech	3.8 ± 0.5	Muscle Nerve	1.9 ± 1.5	Clin J Sports Med	1.1 ± 1.2
Clin Biomech	3.0 ± 1.0	Eur J Appl Physiol	1.9 ± 1.3	J Sport Rehabil	1.1 ± 1.2
J Bone Joint Surg	2.9 ± 1.3	Ergonomics	1.8 ± 1.3	J Mech Med Biol	1.1 ± 1.3
J Orthop Res	2.9 ± 1.3	Hum Mov Sci	1.8 ± 1.3	J Sports Sci	1.1 ± 1.2
Nature	2.8 ± 1.5	Am J Phys Med Rehabil	1.7 ± 1.2	Eur J Sports Sci	1.0 ± 1.2
Science	2.8 ± 1.6	Phys Ther	1.7 ± 1.3	Res Q Exerc Sport	1.0 ± 1.1
Gait Posture	2.7 ± 1.2	Comput Methods Biomech Biomed Engin	1.7 ± 1.4	Proc Int Soc Biom Sports	1.0 ± 1.2
J Biomech Eng	2.7 ± 1.3	Motor Control	1.7 ± 1.4	Scand J Sci Med Sport	1.0 ± 1.2
J Appl Biomech	2.5 ± 1.2	J Orthop Sports Phys Ther	1.6 ± 1.3	J Strength Cond Res	0.9 ± 1.0
J Appl Physiol	2.4 ± 1.5	Hum Factors	1.5 ± 1.3	J Athl Train	0.9 ± 1.1
Med Sci Sports Exerc	2.4 ± 1.5	J Hum Mov Stud	1.5 ± 1.3	J Sports Med Phys Fitness	0.9 ± 1.0
Am J Sports Med	2.3 ± 1.3	J Mot Behav	1.5 ± 1.3	Percept Mot Skills	0.9 ± 1.1
J Biomed Eng	2.3 ± 1.4	Acta Physiol Scand	1.4 ± 1.3	Pediatr Exerc Sci	0.8 ± 1.1
J Electromyogr Kinesiol	2.2 ± 1.3	Med Biol Eng Comput	1.4 ± 1.3	Sports Eng	0.8 ± 1.1
Exp Brain Res	2.2 ± 1.6	Appl Ergonomics	1.3 ± 1.2	Int J Sport Health Sci	0.8 ± 1.2
J Physiol	2.2 ± 1.7	Br J Sports Med	1.3 ± 1.3	Isokinet Exerc Sci	0.7 ± 1.0
Arch Phys Med Rehabil	2.1 ± 1.2	Sports Biomech	1.3 ± 1.3	Proc: Sport-specific	0.7 ± 1.0
Am J Physiol	2.1 ± 1.5	Int J Sports Med	1.3 ± 1.3	Proc Int Sports Eng Assn	0.7 ± 1.0
J Neurophysiol	2.1 ± 1.7	J Biomech Sci Eng	1.3 ± 1.4	Jap J Biomech Sport Exerc	0.6 ± 1.0
Exerc Sport Sci Rev	2.0 ± 1.6	J Sci Med Sports	1.2 ± 1.3	Res Sports Med	0.6 ± 1.0
J Exp Biol	1.9 ± 1.5	Sports Med	1.2 ± 1.3		

Table 2: Top 10 original research journals by respondent ASB interest area

Biol Sci (n = 8)		Eng & Appl Physics (n = 30)		Ergonomics & Hum Factors (n = 5)		Exerc & Sports Sci (n = 18)		Health Sci (n = 17)	
J Biomech	3.6	J Biomech	3.7	J Biomech	4.0	J Biomech	3.9	J Biomech	3.8
J Appl Physiol	3.5	J Biom Eng	3.2	Clin Biomech	3.8	Med Sci Sp Ex	3.6	Gait Posture	3.4
J Neurophysiol	3.3	J Orthop Res	3.0	J Orthop Res	3.4	J Appl Biom	3.3	J Orthop Res	3.2
J Physiol	3.1	Clin Biom	2.8	Ergonomics	3.0	Clin Biom	3.2	J B Joint Surg	3.1
Exp Brain Res	3.1	J B Joint Surg	2.8	J Biom Eng	3.0	Am J Sp Med	2.8	Clin Biomech	2.9
J Exp Biol	2.9	Gait Posture	2.5	Hum Factors	2.8	Gait Posture	2.8	Exp Brain Res	2.9
Am J Physiol	2.9	J Appl Biom	2.3	J EMG Kines	2.8	J EMG Kines	2.8	J Physiol	2.9
J B Joint Surg	2.8	J Biomed Eng	2.2	J Appl Physiol	2.6	J B Joint Surg	2.7	J EMG Kines	2.6
Clin Biomech	2.5	J Appl Physiol	2.1	J Biomed Eng	2.4	Exp Brain Res	2.6	J Neurophysiol	2.6
J Biom Eng	2.5	Comp M Biom Biomed Eng	1.8	J Appl Physiol	2.6	J Appl Physiol	2.5	J Biomed Eng	2.6

CORRELATION OF DYNAMIC CARTILAGE CONTACT STRESS ABERRATION WITH SEVERITY OF JOINT INSTABILITY

Yuki Tochigi, M. James Rudert, Todd O. McKinley,
Douglas R. Pedersen, and Thomas D. Brown

University of Iowa, Iowa City, IA
E-mail: yuki-tochigi@uiowa.edu Web: http://poppy.obrl.uiowa.edu/

INTRODUCTION

Joint instability has been implicated closely in development of osteoarthritis. Abnormality in joint kinematics is thought to involve injurious-level cartilage contact stress aberrations, although the patho-mechanical details are still unclear. In this study, a human ankle cadaver model was utilized to create various levels of instability, and associated changes in dynamic articular contact mechanics were quantified. The purpose was to identify the correlation of dynamic contact stress aberrations with severity of joint instability.

METHODS

To model joint instability, potentially unstable cadaver ankles were created by impairing passive restraints. To reduce articular surface restraint, a step-off incongruity was created on the distal tibial surface. A full-width coronal osteotomy was made at the anterior one-third of the distal tibia (Fig. 1A), and the osteotomized fragment was rigidly secured in a proximally-displaced position (Fig. 1B). Ligamentous restraint was reduced by transecting the anterior talo-fibular ligament. With these alterations, a posteriorly directed force to the tibia was expected to subluxate the talus anteriorly under the tibia (Fig. 1C).

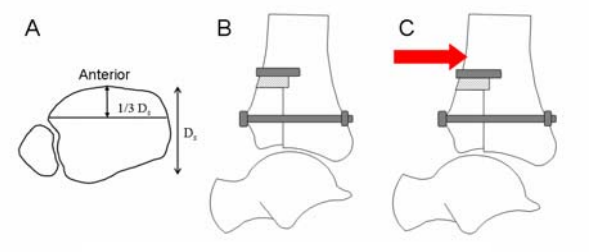

Figure 1: Modeling concept

Six cadaver specimens were subjected to a loading experiment, in which a custom fixture mounted in an MTS machine applied simulated stance-phase ankle motion at a rate of 0.5 Hz, under a compressive load held at 300N. The A/P tibial loading protocol consisted of a constant anteriorly directed "baseline" force (30N, for initial stabilization) and a superimposed posteriorly directed force pulse (for subluxating the ankle transiently, in some cases). The force pulse was applied at 45 to 70 % of cycle time, and the peak magnitude ranged from 0 to 120 N in 20 N increments.

Each specimen was first tested intact. After a baseline test (with no force pulse), tests were repeated while varying pulse magnitude randomly. After tibial osteotomy, tests were repeated with the tibial surface reduced anatomically and with 1mm and 2mm step-off conditions, both before and after ligament transection. A/P tibial displacement during testing was measured; the data were utilized to quantify abnormality of joint kinematics.

Ankle contact stresses were measured by a thin and flexible TekScan® sensor inserted into the joint. The sensor measured instantaneous contact stresses at 1472 sites (32 by 46 array), at a sampling rate of 132 Hz. Data from the 40 to 90 % cycle-time were analyzed. To evaluate changes in dynamic contact stress mechanics, the rates of change of contact stress were computed using a Lagrange four-point central differencing formula (positive/negative values indicate instantaneously increasing/decreasing cartilage contact stress, respectively).

RESULTS

In every specimen, visually distinct instability events occurred when a step-off incongruity was introduced, with pulse load magnitudes beyond a threshold specific to each specimen/condition (range, 20 to 100 N). Peak tibial displacement data (Fig. 2) revealed that instability occurred primarily due to step-off incongruity, and more severe instability occurred with the higher step-off. Instability was enhanced by ligament transection, although ligament transection alone did not lead to detectable change. (One-way ANOVA, significance-level p = 0.05.)

The effect of instability on dynamic cartilage contact mechanics was characterized by elevated rates of contact stress change, as evidenced by the expanded width of the 95% distribution range of the rate data (absolute difference between positive and negative 95th percentile values). Gathering the data across test series in each specimen (which yielded a wide spectrum of instability situations), this measure was found to be correlated linearly with the severity of instability (R^2 ranged from 0.79 to 0.97, averaging 0.92) (Fig. 3).

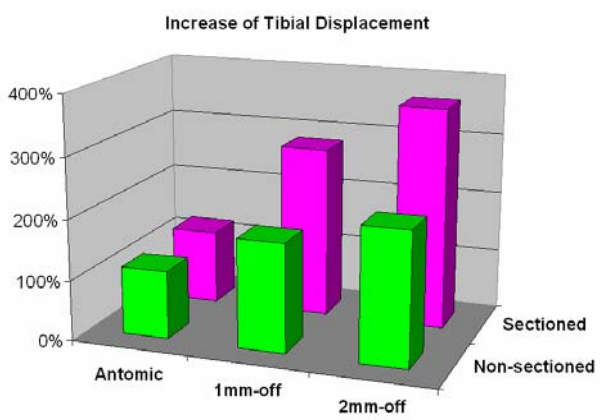

Figure 2: Relative increase of peak tibial displacement in 120N-pulse tests. (n = 6, 100% = data in the intact condition)

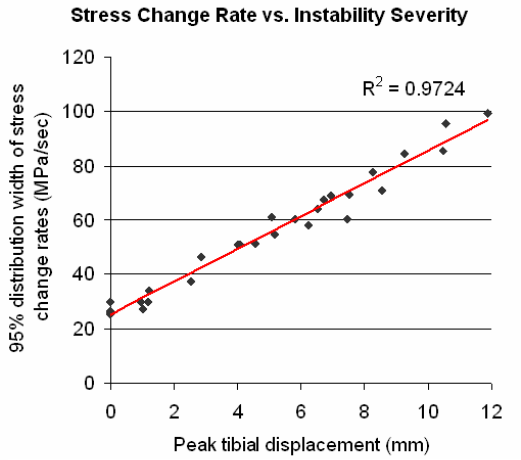

Figure 3: Correlation of contact stress change rate with instability severity, in an example specimen.

CONCLUSIONS

In this study, abnormal tibial surface geometry caused unstable ankle motion during dynamic loading, and its severity was dependent on the level of abnormality. It is suggested that altered joint geometry after mal-reduced distal tibial intraarticular fracture can cause joint instability, supporting the clinical belief that anatomical fracture reduction is essential for minimizing biomechanical residuals after intraarticular fractures. Parametric analysis with a contact FE model would allow identifying an acceptable form/range of geometric abnormality, and patient-specific modeling would also be helpful for planning effective reduction/reconstruction surgeries.

The rates of contact stress change were correlated linearly with the severity of joint instability. In experimental settings, evaluation of dynamic cartilage contact stress aberrations appears to be reasonable means to explore the small, fast abnormal joint motions that involve contact stress aberrations potentially injurious to cartilage. For example, application of this paradigm to a human cadaver knee experiment would allow study of potential pathomechanisms of osteoarthritis secondary to ACL injury.

ACKNOWLEDGEMENTS

CDC Grant R49 CCR721745
NIH Grant 5 P50 AR048939

Spinal Cord Injured Subjects use Ankle-Foot Load Feedback to Modulate Hip Torque during Locomotion

Keith Gordon[1], Ming Wu[1, 2], Brian Schmit[1, 2, 3]

[1] Rehabilitation Institute of Chicago, Chicago, IL, USA
[2] Northwestern University, Chicago, IL, USA
[3] Marquette University, Milwaukee, WI, USA
E-mail: keith-gordon@northwestern.edu

INTRODUCTION

The purpose of this research was to examine the effect of ankle-foot load on hip joint torque production during locomotion in people with spinal cord injury (SCI). In adult SCI subjects, the amplitude of limb load has an effect on the muscle activity during stepping (Harkema et al. 1997). Similarly, temporal modulations of limb loading have been shown to modulate the timing of stance / swing transitions in an infant population (Pang and Yang 2000). Although these effects have been identified, there is a tight coupling between gait kinematics and the timing of limb loading during walking. This interaction has made it difficult to investigate the afferent source and specific effects of limb load feedback on locomotor activity independent of kinematics. The likely sources of limb load feedback for locomotion are the muscle afferents of the ankle plantarflexors and the cutaneous afferents of the foot sole based on studies in animals (Conway et al. 1987). As a result, we tested the following hypotheses using a novel method to manipulate the timing of limb loading within the gait cycle of adult SCI subjects: 1) subjects increase both hip flexor and extensor torque when ankle-foot load feedback is presented during the stance phase and 2) temporal variations in the timing of ankle-foot loading result in subsequent temporal modulations in hip torque profile.

METHODS

Nine incomplete SCI subjects (ASIA C - D) stepped with assistance from a Lokomat during treadmill and airstepping conditions. During airstepping, subjects wore a powered ankle-foot orthosis on one limb. The orthosis allowed sagittal plane rotation about the ankle. A pneumatic cylinder, attached to the orthosis was used to apply an ankle-foot load to the subjects. When pressurized the cylinder created a dorsiflexor torque (~0.5 Nm/kg) about ankle. The timing of the applied load within the gait cycle was

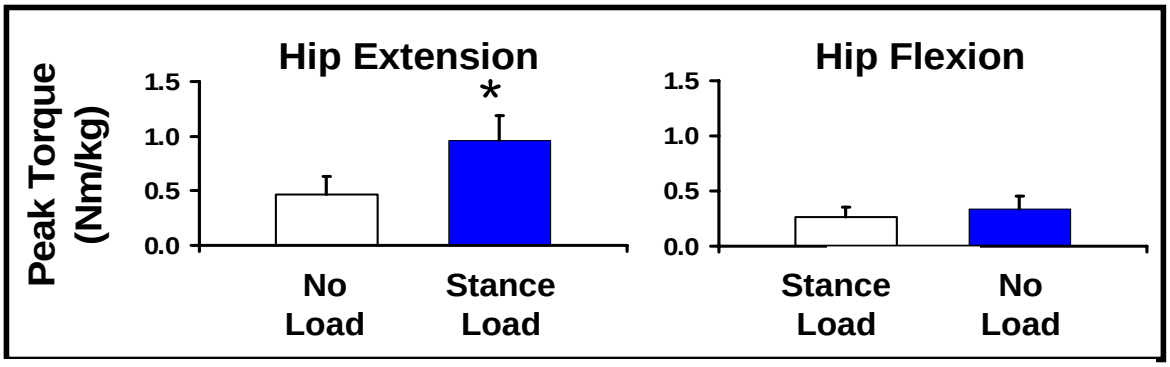

Figure 1: Mean + S.E. peak hip torques from all subjects during the NO LOAD and STANCE conditions.

triggered by hip position. We recorded EMG, joint kinematics and joint torques from both lower limbs. Subjects stepped during a TREADMILL (standard treadmill walking, no ankle-foot orthosis) and five airstepping conditions. The airstepping conditions consisted of NO LOAD (ankle-foot orthosis allowed unrestricted ankle sagittal rotation), STANCE (dorsiflexion torque applied during normal stance time), EARLY (dorsiflexion torque applied 200 msec earlier in the gait cycle than STANCE), LATE (dorsiflexion torque applied 200 msec later in the gait cycle than STANCE) and SWING (dorsiflexion torque applied during normal swing time).

RESULTS AND DISCUSSION

Peak hip extension torque increased significantly from 0.47 Nm/kg to 0.96 Nm/kg (104% increase) and peak hip flexion torque increased 25% from 0.09 Nm/kg to 0.12 Nm/kg between NO LOAD and STANCE (Figure 1). During STANCE, subjects also increased positive hip extensor work by 215% (7.4 to 23.2 J) and positive hip flexor work by 22% (5.1 to 6.2 J) compared to NO LOAD. In addition, negative hip extensor work increased by 10% (3.7 to 4.1) while negative hip flexor work decreased by 29% (3.0 to 2.1 J). Similar changes were also observed during the EARLY and LATE conditions compared to NO LOAD (Figure 2). During SWING, subjects increased peak hip flexion by 80% compared to NO LOAD.

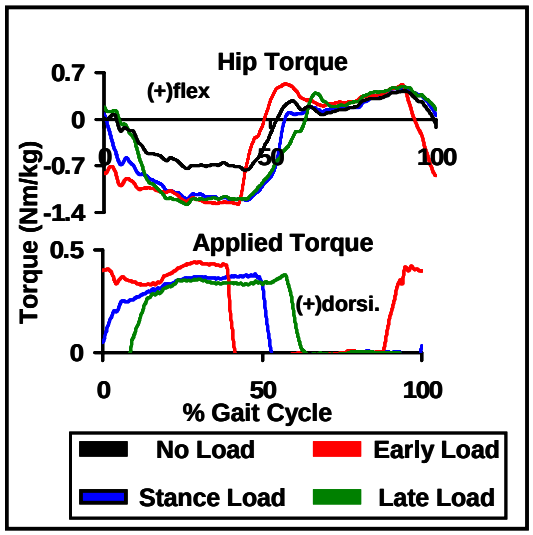

Figure 2: Mean hip torque and applied limb load from a single subject.

The timing of hip torque profiles was modulated by varying the timing of applied ankle loading (Figure 2). When the onset of the applied load was shifted, a corresponding shift in the onset time of hip extension was observed. The onset of hip flexion occurred earlier when ankle load was removed earlier in the gait cycle during the EARLY condition. However, when load release was delayed during the LATE condition the onset of hip flexion did not make a corresponding shift.

SUMMARY/CONCLUSIONS

These findings are consistent with previous research and support our hypotheses that humans with incomplete SCI use ankle-foot load feedback to modulate the amplitude and timing of hip joint kinetics. Subjects increased hip torque when provided with cyclical ankle loading. When the timing of limb load was shifted within the gait cycle subjects made a corresponding shift in hip joint torque profile.

REFERENCES

Conway BA et al. (1987) *Exp. Brain Res.* 68: 643-56.

Harkema, S.J., et al. (1997) *J. Neurophysiology*, **77**: 797-811.

Pang, M.Y.C., Yang, J.F. (2000) *J. Physiology*, **528.2**, 389-404.

ACKNOWLEDGEMENTS

This research was supported by the Coolidge Fellowship, NIDRR Switzer Fellowship and the Searle Research Fund. Jennifer Kahn, DPT contributed to this work.

Altered Response to a Backwards Pull in Parkinson's Disease

Antonis P. Stylianou [1,2], Molly A. McVey [2], Carl W. Luchies [1,2], Kelly E. Lyons [1], Rajesh Pahwa[1]

[1] University of Kansas Medical Center, Kansas City, KS, USA
[2] University of Kansas, Lawrence, KS, USA
E-mail: luchies@ku.edu, Web: www2.kumc.edu/coa

INTRODUCTION

Postural instability is one of the primary symptoms of Parkinson's disease (PD). In the early stages of the disease, postural instability is usually evident in the response used to recover from a postural perturbation (pushed or tripped) but as the disease progresses it may deteriorate to the point that support is needed to stand or sit. Postural instability often leads to falls, fear of falling, reduced mobility and quality of life (Adkin et al. 2003; Bloem et al. 2001). The mechanics of postural instability are not known but one hypothesis is that PD impairs the ability to make fast and accurate postural responses to a perturbation because of slower reaction and movements. This study attempts to answer the question of whether PD patients, compared to aged matched healthy controls, require more time to initiate and to execute responses to a postural perturbation.

METHODS

Subjects: Five healthy elderly adults (EA: mean age = 74.8, SD = 4.1) and five Parkinson's disease patients (PD: mean age = 68.2, SD = 6.5) with idiopathic PD and moderate impairment of postural control (H&Y = 2) participated in this study after signing an informed consent as approved by the KUMC Human Subjects Committee.

Task: Data were collected to quantify the response used to recover from a normalized backwards displacement at the waist. The destabilizing pull was produced using an electronically released weight and cable system which allowed the subject to sway freely prior to the onset of pull. The weight drop was 20% of the subject's body weight and the pull distance was 8.7% of the waist height, which corresponds to 5.0° equivalent disturbance angle (Luchies et al. 1994). The waist pull was applied to a waist harness, which incorporates padded adjustable blocks to secure contact with the anterior-superior iliac spines to transmit the disturbing force to the body. The subject stood upright, looking straight ahead, arms folded across the chest and feet placed in a shoulder width stance position with a force plate under each foot.

Data: Kinematic marker data were collected at a sampling rate of 120 Hz while force plate data (AMTI, Watertown, MA, USA) and surface EMG data (Noraxon, Scottsdale, AZ) from the tibialis anterior and gastrocnemius (medial head) were sampled at 1080 Hz using a Vicon 512 system (Vicon Peak, Lake Forest, CA).

Analysis: The disturbance onset time, EMG onset time, step foot liftoff time and step foot landing time were determined. The reaction time (RT): time between the disturbance onset and EMG onset time; the liftoff time (LT): time between disturbance onset time and step foot liftoff time; the weight shift time (WST): time between EMG onset and step foot liftoff time; and the step duration time (SDT): time between

step foot liftoff time and step foot landing time were extracted. The step length (STL) was defined as the distance traveled by the heel marker between step foot liftoff and step foot landing. The center of pressure trajectories (COP) prior to the disturbance and up to step foot liftoff were also calculated from the force plate data.

T-tests were used to look for group differences ($p<.05$) in the temporal outcomes.

RESULTS AND DISCUSSION

Table 1 demonstrates temporal parameter results. Significant group differences were found in the LT, WST, and STL. Group differences were observed in the COP trajectories: for all EA subjects the COP trajectory moved anterior after disturbance onset; in four of the five PD subjects the COP trajectory moved posterior.

Table 1. Temporal and Step Length Results for EA and PD groups (mean (SD))

	EA	PD	t-test
RT	138.0 (43.3)	138.1 (30.0)	.994
LT	373.6 (42.4)	557.2 (83.0)	.002*
WST	235.6 (67.7)	419.0 (65.4)	.002*
SDT	153.9 (41.4)	118.4 (48.6)	.249
STL	209.8 (70.0)	105.6 (64.5)	.04*

Our results indicate that in response to a posterior waist pull, moderate severity PD patients, compared to healthy controls, have similar EMG latencies, require more time for step foot liftoff, have similar step duration times, but utilize a significantly shorter first step which is often inadequate to arrest a fall. The increased WST along with the differences in the COP trajectories indicate a different recovery strategy in PD.

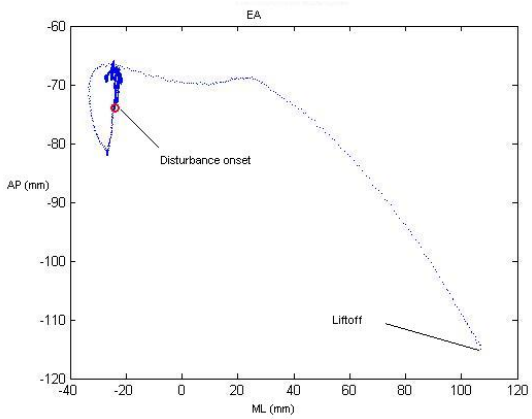

Figure 1. COP trajectory from EA subject.

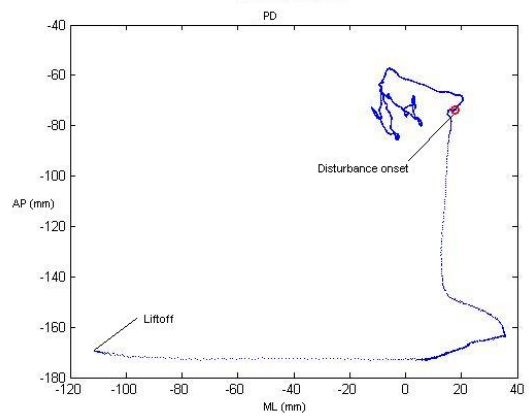

Figure 2. COP trajectory from PD subject.

SUMMARY/CONCLUSIONS

The group differences observed point to a different motor plan in PD. A stepping response is initiated immediately after the perturbation in PD patients whereas in healthy controls an attempt at regaining balance is made before the step is initiated.

REFERENCES

Adkin, A.L. et al. (2003). *Movement Disorders*, **18**, 496-502.

Bloem, B.R. et al. (2001). *Advances in Neurology*, **87**, 209-223.

Luchies, C.W. et al. (1994). *J Am Geriatr Soc*, **42**, 506-512.

OLDER ADULTS EXHIBT REDUCED LATERAL ACCELERATION OF THE CENTER OF MASS AT FAST WALKING SPEEDS

Antonio Hernández, Amy Silder, Bryan Heiderscheit and Darryl Thelen
University of Wisconsin-Madison, Madison, WI, USA
E-mail: ahernandez2@wisc.edu, Web: www.engr.wisc.edu/groups/nmbl/

INTRODUCTION

Aging induces a shift in power production, with elderly adults exhibiting reduced ankle plantar flexor power during push-off (Winter et al., 1990) and increased hip extensor power during mid-stance (DeVita and Hortobagyi, 2000). This shift persists even when statistically controlling for differences in gait speed (McGibbon et al., 2004). However, it is not currently understood how this change in joint kinetics affects the three dimensional motion of the center of mass (COM) during specific phases of the gait cycle. Simulations of healthy young gait suggest that the ankle musculature induces forward and vertical acceleration of the COM during double limb support (DLS) (Neptune et al., 2001). Based on these observations, we hypothesized that aging would induce a decrease in the forward and vertical accelerations of the COM during DLS, and an increase in the forward acceleration during single limb support (SLS). We also investigated lateral accelerations to determine how age-related changes in kinetics may influence frontal plane movement.

METHODS

20 healthy elderly (age, 72±5 y; height 1.69±0.09 m; mass, 69±11 kg) and 21 healthy young (age, 26±3 y; height 1.73±0.11 m; mass, 69±12 kg) adults participated in this study. Each subject performed five walking trials at 80, 100, and 120% of preferred speed along a 10m walkway. The order of speeds was randomized. Preferred speed was established prior to testing by averaging each subject's normal gait speed in the laboratory. Ground reaction forces (GRFs) were recorded (2000Hz) for two successive foot strikes using three fixed force plates. COM accelerations were calculated by dividing the forward, vertical and lateral components of the GRFs by subject mass. In the vertical direction, the acceleration due to gravity was subtracted.

For each subject, the accelerations of the COM were averaged across trials by speed. These accelerations were then averaged for each subject during DLS, and during early, mid and terminal SLS. Because DLS consists of pre-swing in the trailing limb and loading of the leading limb, we divided the DLS phase in two halves, corresponding with the dominant event in each. T-tests were performed between the mean values of young and elderly at each phase and significance reported if $p \leq 0.05$.

RESULTS AND DISCUSSION

Average gait speed and step length were not significantly different between young and elderly subjects at the slow, preferred or fast walking speeds. However, as hypothesized, the elderly adults walked with different COM acceleration patterns throughout the gait cycle (Fig. 1), with these differences becoming more pronounced with increasing gait speed. In particular, the forward accelerations in the elderly subjects were significantly smaller during pre-swing and significantly higher during late midstance at

the fast walking speed (Fig. 2). The vertical accelerations were significantly smaller during pre-swing. The absolute magnitude of the lateral accelerations were significantly lower both during pre-swing and early mid stance.

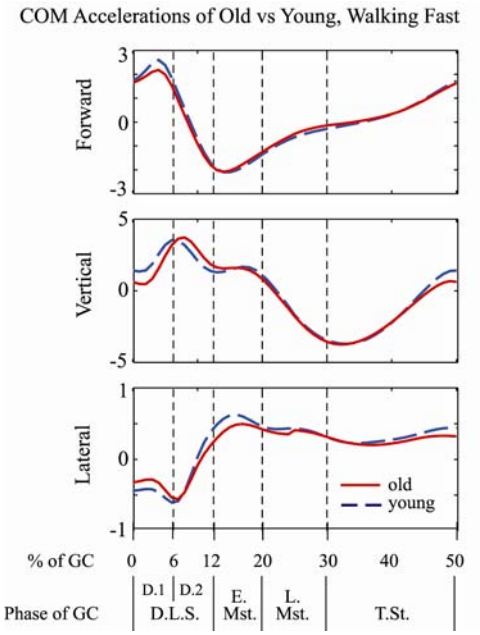

Figure 1. Center of mass accelerations for young and older adults walking at fast speeds. Shown is ½ of the gait cycle (GC), starting at heel strike, with corresponding phases labeled. D.L.S.=double limb support (D.1=pre-swing of trailing limb, D.2=loading of leading limb), E.Mst.=early midstance, L.Mst. = late midstance, T.St.=terminal stance.

This study shows that age-related changes in joint kinetics affect the motion of the center-of-mass during human walking. The differences seen in the sagittal plane are consistent with what would be predicted from prior forward dynamics studies (Neptune, 2001). Reduced ankle plantarflexor power in the old adults lowers the forward and vertical acceleration of the COM during DLS. This reduction seems to be compensated for by an increase in forward acceleration during midstance, perhaps via increased hip-extensor action.

Interestingly, age-related changes in coordination also seem to reduce the medio-lateral accelerations of the center of mass. It is known that lateral balance is challenging to older adults, as indicated by the difficulties they have with frontal plane balance tasks (Mille et al., 2004) Thus, it is feasible that age-related changes in the coordination of walking may, in part, be adapted to accommodate lateral balance concerns at fast walking speeds.

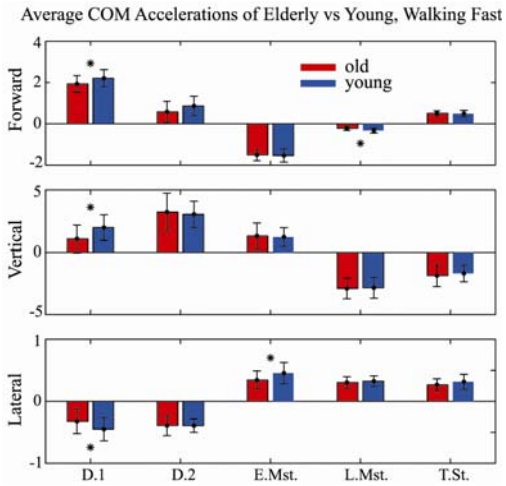

Figure 2. Average COM accelerations±s.d. during phases of the gait cycle (∗ $p \leq 0.05$). Abbreviations given in Fig. 1.

REFERENCES

Winter, D.A. et al. (1990). *Physical Therapy* **70**, 340-347.

DeVita, P. and Hortobagyi, T. (2000). *J Appl Physiol* **88**, 1804-1811.

McGibbon, C.A., Krebs, D.E. (2004). *J Appl Physiol* 96: 149-160.

Neptune R.R., et al. (2001). *J Biomechanics* **34**, 1387-1398.

Mille M.L. et al., (2005). *Clinical Biomechanics*, **20**, 607-616.

ACKNOWLEDGEMENTS

Jane Mahoney, MD; Funding provided by NIH AG20013, AG24276 and NSF graduate fellowship (AS).

A Proposed New Obstacle-Set Algorithm for Modeling Deltoid

Brian A. Garner and Bo Xu

Baylor University, Waco, TX, USA
E-mail: brian_garner@baylor.edu, Web: www.ecs.baylor.edu/engineering/faculty/garner

INTRODUCTION

Proper representation of muscle paths in musculoskeletal models is important for accurately modeling the magnitude and line-of-action of muscle forces. Muscle force magnitude depends on muscle path because of the force-length-velocity properties of the muscle sarcomeres.

Fairly complex muscle path algorithms have been developed which account for muscle tissue mechanics, connectivity between the muscle fibers, and surface contact with underlying anatomical structures (Blemker 2005). Although realistic, these methods are computationally demanding and may be impractical for widespread use in prolonged simulations.

Other algorithms, such as the obstacle-set method (Garner 2000), are simpler, solve quickly, and compute realistic muscle moment arms. However, modeling some broad muscles crossing joints with wide ranges of motion can be difficult.

The obstacle-set method models muscle paths as frictionless elastic bands wrapping around simple geometric shapes. Broad muscles are modeled with multiple bands – each band having its own obstacle set, and each band's path computed independently (ignoring connectivity between muscle fibers).

For muscles such as the deltoid crossing the shoulder, a sphere obstacle is a natural choice to model underlying structures. However, as the shoulder moves over its wide range of motion, the independent bands of the deltoid have a tendency to slip around to unrealistic positions behind the sphere. To address this slipping, Garner (2000) implemented a stub obstacle (sphere-capped cylinder) which uses the cylinder to catch the band from the sphere. However, it proved difficult to design appropriate stub obstacles which produce realistic paths for each band at all joint positions.

The aim of this study was to develop a new obstacle-set algorithm that accounts for connectivity between muscle fibers while quickly computing the paths of broad muscles wrapping around sphere obstacles.

METHODS

The new algorithm was developed using a hypothetical model of deltoid. The anterior, middle, and posterior heads of deltoid were modeled using three muscle bands. For each band, origin sites on a fixed clavicle/scapula bone, and insertion sites on a moving humerus, were defined. A sphere obstacle was defined to represent the shape of the humeral head and other underlying tissues.

The algorithm computes the minimum-distance path of each muscle band around the sphere and within a "path plane" of specified orientation. The absolute-shortest path happens to lie in the plane containing both attachment sites and the sphere center. However, this plane is fixed for each band without regard to the other bands. To permit a link between the respective bands, the new algorithm allows each path plane to stray from the sphere center, and instead form an

angle with a known reference plane. That is, it computes a minimum-distance path within the plane containing both attachment sites and forming a given angle relative to a specified reference plane.

For one of the bands (dubbed the "primary band") the reference plane is selected as an arbitrary plane of known orientation. For the remaining bands the reference plane is selected as the path plane of an adjacent muscle band. For example, for the hypothetical deltoid the anterior head was chosen as the primary band, and horizontal was chosen as its reference plane. The path planes of the anterior and middle heads were then chosen to be the reference planes for the middle and posterior heads, respectively (**Figure 1**).

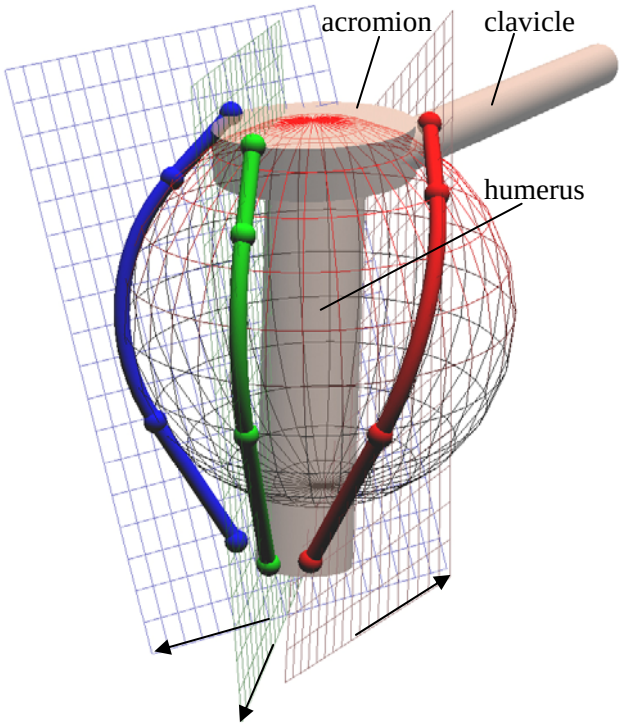

Figure 1: Hypothetical deltoid muscle wrapping around a sphere obstacle. The anterior (red), medial (green), and posterior (blue) heads of deltoid lie within respective planes that are constrained to form fixed angles relative to each other.

Fixed angles between the path and reference planes of the non-primary bands were chosen offline to reflect the breadth of the deltoid muscle between bands. The angle between path and reference planes of the primary (anterior) band was computed so as to produce the minimum sum of path lengths over all the bands. That is, for a given position of the shoulder joint, 1) the primary plane angle was varied, 2) the corresponding orientations of the three path planes were determined, 3) the minimum-distance path of each band within its respective plane was computed, and 4) steps 1 through 3 were repeated to find the primary plane angle which minimized the sum of path lengths.

RESULTS AND DISCUSSION

The algorithm converged to realistic configurations of the hypothetical deltoid, even at joint positions where solutions of isolated bands would slip around the sphere. Computational times for the three bands were less than a millisecond on a standard PC. Solutions were computed effectively over a wide range of shoulder joint motion.

Advantages of this algorithm include its simplicity, realism, computational efficiency, and simultaneous solution of all bands to account for the connectivity between muscle fibers. The algorithm requires definition of a sphere obstacle common to all bands, and fixed angles to define muscle breadth between adjacent bands. The algorithm is flexible so that an arbitrarily large number of muscle bands could be used to model broad muscles.

REFERENCES

Garner, B.A., Pandy, M.G. (2000). *Computer Methods in Biomechanics and Biomedical Engineering.* **3**(1), 1-30.

Blemker, S.S., Delp, S.L. (2005) *Annals of Biomedical Engineering*, **33**, 661-673.

SENSITIVITY OF LYAPUNOV EXPONENT ESTIMATION FOR HUMAN GAIT

T.M. TenBroek, R.E.A. Van Emmerik, J. Hamill

Biomechanics & Motor Control Laboratories, University of Massachusetts,
Amherst, MA, USA; email: ttenbroe@kin.umass.edu

INTRODUCTION

Dynamic stability is a major objective of human locomotion. Lyapunov Exponents (LE) can quantify dynamic stability by measuring the exponential rates of average divergence or convergence of nearby trajectories on an attractor as a system evolves in time. LE have been reported for a variety of signals including trunk and joint position, trunk acceleration, as well as joint angles for human locomotion. Each of these signals can result in different LE within the same system (Dingwell et al., 2006), which makes comparing dynamic stability across studies using LE challenging.

LE analysis assumes data stationarity (Kantz, 1997) indicating that: a) the system is sufficiently sampled to capture its dynamics; and b) system parameters remain constant across the trial. Stationarity in treadmill walking data is improved by computing the first difference time series (Dingwell et al., 2006). Since detecting and removing non-stationarity from data can be difficult, differences in calculated LE between seemingly non-stationary data and corrected data is of interest.

Properly capturing the dynamics of a system also requires a sufficient sampling frequency. Calculated LE over a range of capture frequencies should be consistent if a system's full dynamics are represented.

Therefore, the purpose of this study was to investigate LE sensitivities to differences in: signal type (acceleration/displacement), capture frequency, and stationarity of the signal.

METHODS

Five college aged males walked on a treadmill at their preferred speed for 15 minutes, while acceleration and displacement of the trunk in the AP direction were recorded at 240 Hz. Preferred speed was chosen using Dingwell et al.'s (2006) method. A uni-axial accelerometer (T45-10, Coulbourn Instruments, Allentown, PA) and a retro-reflective marker (Qualisys AB, Partille, Sweden) were attached to each subject's sternum using elastic tape.

To calculate LE, an appropriate state space was reconstructed from time series data and time delayed copies using the embedding theorem (Takens, 1980). An embedding dimension of 5 was used on all trials, as per a nearest neighbors analysis (Kennel, 1992; Dingwell et al., 2006). Rosenstein et al. (1993a) and Wolf et al. (1985) suggest a minimum of 10^d data points for Lyapunov estimation, where d is the dimension of the attractor. Therefore, the theoretical minimum number of data points required was 100,000. For this reason, a 100,000-point section was used from the middle of each 15-minute trial. In addition, for each data set, time delay was determined using the average displacement method (Rosenstein et al., 1993b); computed values ranged from 4 to 25 samples.

To establish LE sensitivity to signal type, raw displacement data were compared to

raw acceleration data. All LE were calculated using Rosenstein et al.'s algorithm (1993a), which requires calculating the slope of a portion of the divergence-time curve (Figure 1).

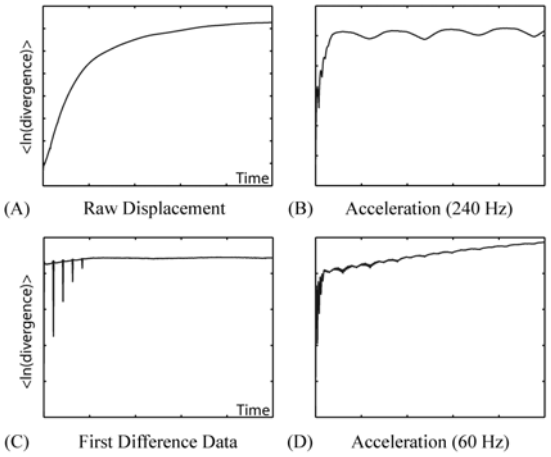

Figure 1: Representative plots of natural log of divergence versus time. Slope of linear portion of line represents Lyapunov exponent.

To improve displacement data stationarity, the first difference time series was computed for each displacement trial. LE for raw position data were compared to first difference data.

Finally, to determine LE sensitivity to collection frequency, raw acceleration data collected at 240 Hz were compared to acceleration data of 60 Hz. To obtain 60 Hz acceleration data with as many points as possible, every fourth point from the original 216,000-point trials was used. This resulted in about half as many points as the other conditions.

RESULTS AND DISCUSSION

LE computed using raw displacement signals were similar to those computed using raw acceleration signals of the same frequency (Table 1 & Figure 1-plots A & B). LE decreased substantially from raw displacement data to first difference data (Table 1 & Figure 1-plots A & C). Reducing the acceleration collection frequency from 240 Hz to 60 Hz also resulted in lower LE (Table 1 & Figure 1-plots B & D). The same dynamics may not be captured in an acceleration signal at 60 Hz that are captured at 240 Hz.

Table 1: Estimated Lyapunov exponent for each subject and condition.

	Acceleration		Displacement	
Sub#	240 Hz	60 Hz	Raw	F. Diff
1			7.2	0.2
2	7.0	1.2	7.8	0.2
3	3.8	1.4		
4	3.0	0.9		
6	3.3	0.9	6.8	0.18
7	5.7	1.2	6.8	0.15

Choosing the portion of the curve to fit a least square line to, in order to calculate slope, can lead to repeatability errors (Figure 1). Locating the linear portion of the divergence curve proved difficult in many cases.

CONCLUSIONS

LE estimation is sensitive to potential implementation differences. Data stationarity corrections and sampling frequency changes lead to significant changes in LE. Investigators comparing results from different studies must be extremely cautious given the substantial effects of some parameters on LE.

REFERENCES

Dingwell, J.B., et al. (2006). *Journal of Biomechanics* **39**, 444-452.

Kantz, H., Schreiber, T. (1997). *Nonlinear Time Series Analysis.* Cambridge University Press.

Kennel, M.B., et al. (1992). *Phys. Rev. A* **45**, 3403-3411.

Rosenstein M.T., et al. (1993). *Physica D: Nonlinear Phenomena* **65**, 117-134. (a)

Rosenstein, M.T., et al. (1993). *Physica D* **73**, 82-98. (b)

Takens F, *Dynamical Systems and Turbulence, Warwick 1980*, Springer-Verlag, Berlin.

Wolf JB, et al. (1985). *Physica D: Nonlinear Phenomena* **16**, 285-317.

ACKNOLEDGEMENT

Funded by NSF grant BCS 0341767

A GAIT MODIFICATION TO REDUCE THE EXTERNAL ADDUCTION MOMENT AT THE KNEE: A CASE STUDY

Joaquin A. Barrios [1] and Irene S. Davis [1,2]

[1] University of Delaware, Newark, DE, USA
[2] Drayer Physical Therapy Institute, Hummelstown, PA, USA
E-mail: joaquin@udel.edu

INTRODUCTION

Knee osteoarthritis (OA) is the most common form of arthritis, and affects approximately one-third of the elderly population. The medial tibiofemoral compartment is most commonly involved. This is due, in part, to the ground reaction force vector passing medial to the knee joint center during gait. This distance increases with genu varus malalignment, resulting in an increased external adduction moment at the knee (KEAM). A high KEAM has been previously associated with medial tibiofemoral OA disease progression and severity (Mundermann, et al., 2004, Miyazaki, et al., 2002). Reduction of the KEAM has been reported after high tibial osteotomy, and to a lesser extent with the use of conservative measures such as wedged orthoses (Prodromos, et al., 1985, Kerrigan, et al., 2002). In an asymptomatic, varus-aligned population without diagnosed knee OA, reducing the KEAM may serve to delay or prevent the onset of the disease.

Recently, walking with an increased medial-lateral trunk sway has been proposed to reduce the KEAM (DeMarre, et al., 2006). However, this could lead to adverse effects at the lumbar spine. Our research group has been studying the use of real-time feedback to improve abnormal lower extremity dynamic alignment in runners with patellofemoral pain. We believe these techniques may be beneficial in individuals with knee OA as well. Therefore, the purpose of this proof of concept study was to assess the effect of verbal and visual feedback on the KEAM in an asymptomatic individual with genu varus malalignment. We hypothesized that the subject would be able to reduce the KEAM in a single session using mirror and verbal feedback.

METHODS

The subject for this case study was an asymptomatic 29 year-old male (BMI: 28.3) with severe genu varus malalignment. The frontal plane mechanical axis of his shank was measured at 13° from the vertical (Hinman, et al., 2006). Retro-reflective markers were placed on the lower extremity. Three-dimensional motion analysis was performed as the subject walked at a self-selected speed along a 25m walkway. Kinematic data were captured using an 8-camera VICON motion analysis system (120 Hz). Kinetic data were captured using a Bertec force platform (1080 Hz).

The subject first walked with his normal gait pattern. He was then given verbal instructions to internally rotate his hips, and to bring his knees closer to midline as he walked. A mirror was positioned directly anterior to the subject's line of progression to provide a visual component to the feedback. The subject was provided approximately ten minutes to practice his new gait pattern. Gait analysis was again performed on the modified gait pattern. Five trials were averaged for each condition, and compared to a normative group mean.

RESULTS AND DISCUSSION

The subject was able to modify his gait without any musculoskeletal complaints. Subjectively, he felt the modified gait

visually approximated a normal gait pattern. The subject increased his peak hip internal rotation by 8°, providing evidence of an appropriate response to the feedback (Table 1). A reduction in both the knee varus angle and KEAM are seen throughout most of stance (Figure 1). The first peak of the KEAM was reduced by 28%, and brought within 1 SD of the normative group mean. Further, this order of magnitude of change surpasses the 6-13% reduction seen with wedged orthoses (Crenshaw, et al., 2000, Kerrigan, et al., 2002).

This case study has demonstrated the feasibility of using visual and verbal feedback in an individual with genu varus malalignment to reduce the KEAM. Currently, our lab is investigating the use of real-time angular feedback to improve dynamic valgus malalignment during running in subjects with patellofemoral pain. Based on the preliminary results of this case study, we believe these techniques could be applied to individuals with genu varus malalignment and a high KEAM.

SUMMARY/CONCLUSIONS

The results of this case study suggest that individuals appear to be able to reduce the KEAM with a single session of feedback. We hope to develop an intervention for individuals with identifiable genu varus malalignment to reduce the risk of development of knee OA.

REFERENCES

Mundermann, et al (2004), *Arth Rheum*, 50, 1172-78.
Miyazaki, et al (2002). *Ann Rheum Dis*, 61, 617-622.
Prodromos, et al (1985). *JBJS(A)*, 67, 1188-94.
Kerrigan, et al (2002). *AMPR*, 83, 889-893.
DeMarre, et al (2006). *Proceedings from ASB'06*
Hinman, et al (2006). *Arth Care & Res*, 55, 306-313.
Crenshaw, et al (2000). *Clin Orthop*, 375, 185-192.

Table 1: Comparison between mean (SD) baseline and modified discrete variables with normative values for peak hip internal rotation angle, knee adduction angle, and peak knee external adduction moment

	Peak Hip Internal Rotation Angle (deg)	Peak Knee Adduction Angle (deg)	First Peak Knee External Adduction Moment (Nm/kgm)
Subject Baseline	4.6 (0.4)	10.6 (0.3)	0.47 (.02)
Subject Modified	13.3 (2.8)	6.5 (0.6)	0.34 (.02)
Normative Mean	3.0 (7.7)	1.7 (4.8)	0.33 (.10)

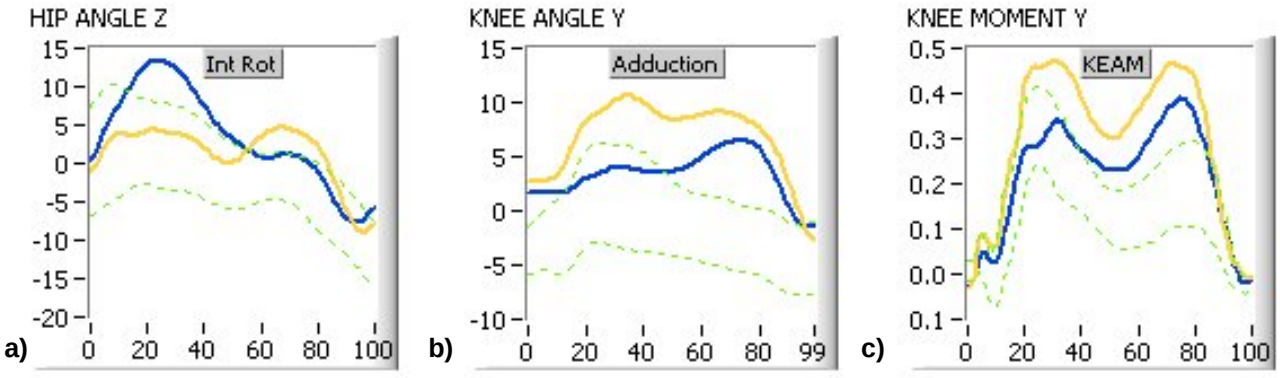

Figure 1: Comparison of a) hip rotation, b) knee adduction angle and c) knee external adduction moment during normal (light line) and realigned (dark line) gait. Mean normative walking data (± 1 SD) presented in dashed lines. Angles reported in degrees, moments in Nm / kg*m.

RELIABILITY OF HAND-FREE ULTRASOUND MEASUREMENT FOR VASTUS MEDIALIS OBLIQUUS

Y.M. Wong, G.Y.F. Ng
Dept. of Rehabilitation Sciences
The Hong Kong Polytechnic University
e-mail: rswongym@polyu.edu.hk

INTRODUCTION

Atrophy of the vastus medialis obliquus (VMO) muscle is relatively common among patients with patellofemoral pain syndrome. In order to monitor the effectiveness of rehabilitation program for strengthening the muscle, clinicians may measure the distal circumference of the thigh with tape. However, the distal thigh contains VMO as well as other muscles, the circumference measurement may not precisely address the change for the VMO muscle.

B-mode ultrasound can visually quantify muscular cross-sectional area, and is usually controlled by the operator manually holding the ultrasound probe. However, little has been done to reveal the reliability of such measurement for the VMO. Electromagnetic tracking (e.g. pciBird, Ascension, USA) and 3D digitizing (e.g. Microscribe, Immersion, USA) instruments have been used to ensure accurate positioning of the ultrasound probe at the same muscle for periodical scanning. Despite the costs of these positioning devices, the accuracy of the electromagnetic tracker is susceptible to adjacent metal (e.g. hospital bed) and a lack of mobility of the 3D digitizer is not very compatible to clinical settings.

The present study aimed (1) to design a hand-free ultrasound system with economic and portable manner; (2) to examine the reliability of the system for measuring the VMO cross-sectional area by comparing it with a gold standard and between-day measurements.

METHODS

Design: A custom-made mechanical stand adjustable in height and tilt angle was used to statically hold an ultrasound probe (Voyager, Ardent Sound, USA) (fig 1).

Figure 1: Ultrasound probe holder

A laser pointer projected a cross mark at the suprapatellar level and a sliding ruler was used to measure the distance between the sole of feet and the suprapatellar border (fig 2). The distance and laser-cross acted as landmarks for the repeatable positioning of the ultrasound probe while a subject supine lying with knee extended and feet secured.

Figure 2: Cross-section locator

An ultrasound gel pad (Aquaflex, Parker Lab, USA) was molded to match the shape of the ultrasound probe and the VMO underneath. The pad weighed about 15g, thus it would not deform the VMO significantly (fig 3).

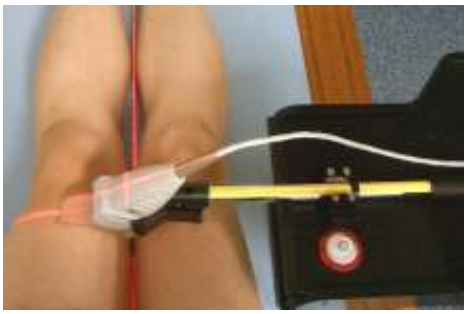

Figure 3: B-mode ultrasound

Testing procedures: Twelve VMO muscles (6 healthy volunteers, 4 males & 2 females) at suprapatellar level were imaged using the B-mode ultrasound and MRI (Magneton Avanto, Siemens AG, Germany) within 3 hours. Both set of the images were saved in DICOM format for offline comparison of the cross-sectional area of VMO (fig 4).

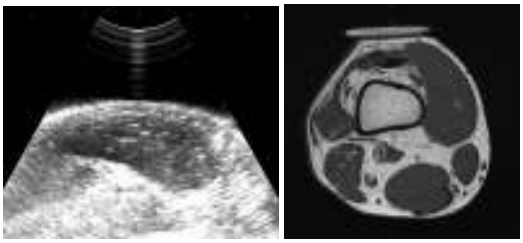

Figure 4: VMO in ultrasound and corresponding MRI image

The twelve VMO muscles were ultrasonically scanned at one week later. Intraclass correlation coefficient (p=0.05) was calculated for the consistency of the two sets of the VMO cross-sectional area.

RESULTS

The mean difference was 5.7% (SD=3%) between the VMO measurement based on the ultrasound and MRI images (12 knees). The ultrasound method slightly underestimated the muscle size compared with the MRI.

The ICC result for the 7-day interval for the VMO ultrasound measurement (12 knees was 0.96 (95% CI=0.89-0.99).

DISCUSSION

Results of this study reveal that the hand-free ultrasound measurement to be comparable with MRI measurements and the system has satisfactory between-day repeatability for the VMO muscle. The application should not be limited to the VMO; it is potentially applicable to other skeletal muscles for diagnostic or biofeedback training purpose.

Simulation Study of Walking Patterns with Knee Osteoarthritis using OpenSim

Ming Xiao and Jill Higginson

University of Delaware, Newark, DE, USA
E-mail: mx@udel.edu

INTRODUCTION

Although knee joint load and torque are the primary biomechanical factors assessed in knee osteoarthritis (OA) studies, patients with OA frequently report muscle weakness and fatigue. Previous studies have shown the effect of muscle dysfunction (e.g. quadriceps) on the development and even pathogenesis of OA. However, the relationship between muscle function and OA is still not clear (Hurley, 2003).

Forward simulation is a powerful tool to understand muscle function, but currently no such tools are used for OA. In the current study, we generated dynamic simulations of patients with knee OA using OpenSim (Thelen and Anderson, 2006; Delp et al, in press). The aims of this study were to evaluate the feasibility of applying OpenSim for pathological gait and compare muscle function between limbs for individuals with bilateral knee OA.

METHODS

Three-dimensional kinematic and kinetic data were collected from 12 patients with knee OA on a split-belt treadmill. Experimental data were then processed in Evart. Recorded raw EMG data were rectified, low-pass filtered and normalized to peak magnitude. Subjects signed an informed consent approved by the human subjects review board.

One subject was selected for this case study. The subject was diagnosed with grade I on the right knee and grade IV on the left knee, which resulted in an asymmetric walking pattern.

A 3D musculoskeletal model was generated by OpenSim. It has 10 segments, 23 degrees-of-freedom and is articulated by 54 Hill-type musculotendon actuators. The model was first scaled to subject dimensions. Inverse dynamics and residual reduction algorithms were then used to find the joint angles that best reproduce the experimental kinematics. Computed muscle control (CMC) was applied to compute the set of muscle excitations that drives the model to track the desired kinematics (Thelen and Anderson, 2006). A fast target optimization was used to minimize the sum of squared actuator forces. Finally, the computed excitations were used to drive a forward dynamics simulation. The output of OpenSim included muscle excitation, muscle force, and joint kinematics.

We generated three simulations for the subject at self-selected speed. Each simulation duration was more than a full gait cycle.

RESULTS AND DISCUSSION

Each simulation was completed within 30 minutes on a personal computer with a 3.0GHz Pentium 4 processor. Simulation joint angles were within ± 2º of the experimental data (Figure 1). Ground reaction forces were within ±1 standard deviation of experimental data.

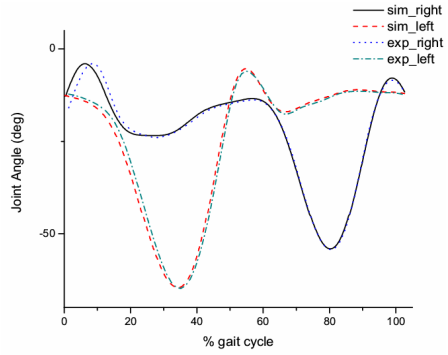

Figure 1: The simulated result of knee angles were very close to experimental data for both legs for a representative trial.

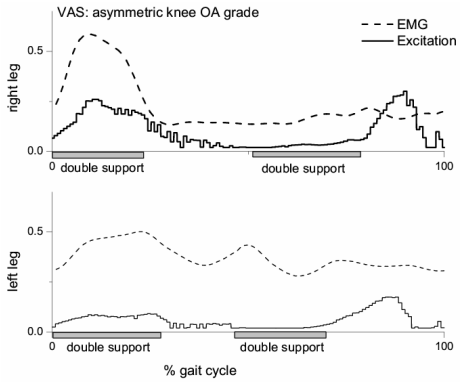

Figure 2: Excitation pattern compares with recorded EMG signals for VAS.

Vastus is one of the knee extension muscles and demonstrates changes in activity with OA. Our EMG data suggested that right VAS was active at early stance (0 - 20% gait cycle) and slightly active at terminal swing phase (80 - 100% gait cycle) (Figure 2, upper half, thick dashed line). Using OpenSim, we found similar excitation patterns which parallel stance phase EMG timing and magnitude (thick solid line). We believe that VAS was active at early stance to provide support for COM and active at swing phase to extend the leg in preparation for heel strike. On the left leg, the peak value of excitation was much smaller than the right side, especially in stance phase (Figure 2, lower half, thin solid line). Considering the left leg has more severe OA than the right leg, we believe that the patient was using less VAS so that the load on left knee would be reduced which is consistent with quadriceps weakness implicated in previous studies.

We noticed that the simulated excitation patterns were not perfectly matched with recorded EMG signals. However, they were more consistent with literature (Thelen and Anderson 2006, den Otter et al. 2004). One explanation for the difference may be the choice of cost function in CMC which may not be perfect for OA subjects, who potentially minimize joint load on the knee while walking. Future work will explore the effect of altering the cost function on predicted excitation patterns.

SUMMARY/CONCLUSIONS

With OpenSim, we are able to generate accurate OA simulations in a few minutes. We believe that these tools will be of great use in prediction of muscle excitation patterns, muscle function analysis and clinical treatment.

REFERENCES

Hurley M.V., (2003) *Arth & Rheu.*, 49(3): 444-452.

Thelen D.G., Anderson F.C. (2006) *J of Biomech.*, 39(6):1107-15.

Delp S. L. et al., (in press) *IEEE Trans Biomed Engr.*

den Otter A.R. et al. (2004) *Gait Posture*, 19:270-278.

ACKNOWLEDGEMENTS

We would like to acknowledge Joe Zeni for access to OA data, the Simbios team especially Chand John, Eran Guendelmann, Clay Anderson and Scott Delp for assistance with OpenSim, and our funding sources (NIH 18082170-30501-B, NIH P20-RR16458).

AN IN VIVO 3D ARTICULAR MODEL OF THE RADIOSCAPHOCAPITATE (RSC) LIGAMENT DURING WRIST FLEXION/EXTENSION AND ULNAR/RADIAL DEVIATION

Michael Rainbow[1], Joseph Crisco[1], Douglas Moore[1], Edward Akelman[1], and Scott Wolfe[2]
[1]Department of Orthopaedics, Brown Medical School/Rhode Island Hospital, Providence, RI
[2]Hospital for Special Surgery, New York, NY
E-mail: joseph_crisco@brown.edu

INTRODUCTION

The stability and function of the wrist are dependent on the ligaments that traverse the carpus. The ligaments stabilize the wrist by tightly approximating the congruent surfaces of neighboring bones, while at the same time allowing limited relative motion.

The radioscaphocapitate ligament (RSC) is an important extrinsic ligament of the wrist. It originates from the palmar surface of the radial styloid, and the majority of its fibers traverse obliquely to insert on the waist of the capitate (Berger, 1990). The RSC passes beneath the waist of the scaphoid, forming a supporting sling as the scaphoid flexes and extends during wrist motion.

There is limited data on the mechanical properties of the RSC, and the data that has been reported differs substantially from the properties of other ligaments. For example, the failure strain of the RSC has been reported to be 20 to 50% (Mayfield, 1979), which is much higher than that of other skeletal ligaments (the major knee ligaments fail at 12%-15% strain). We question whether the ligaments of the wrist are fundamentally different than those of the knee, or whether these findings were secondary to differences in testing methodologies.

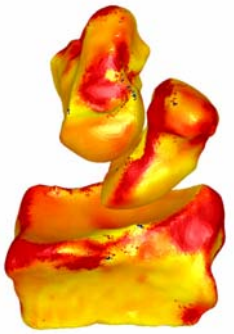

Figure 1: The radius scaphoid and lunate's color maps correspond to distance from the surrounding soft tissue. This Micro-CT model combined with dissection and anatomy texts provides a map of the insertion regions

This study was performed to estimate the elongation of the RSC at various wrist positions. To do so we analyzed an extensive database of 3-D *in vivo* carpal kinematic data using a computer algorithm designed to compute ligament fiber path lengths, with the constraint that the ligaments wrap over the bone surfaces. In particular, we tested the hypothesis that RSC elongation would change as a function of wrist position.

METHODS

Following IRB approval and informed consent, a comprehensive digital database of bone surfaces and carpal kinematics was generated from serial CT scans of 27 healthy subjects (mean age 24.6; range 21-34).

Anatomy texts, wrist dissections, and micro-CT (Fig. 1) were used to define the insertion sites of the RSC on the radial styloid and capitate of the average-sized subject from our database. A central fiber was placed at the centroid of the insertion sites and 12 other fibers were distributed around the periphery. The path of each fiber was computed as the shortest straight-line distance between its insertion sites, constrained to wrap around the bone surfaces, avoiding penetration. These paths were computed based upon distance-field maps and the tessellated scaphoid surface. The assembled wrist model was animated using the 3-D kinematic data from 80 different positions of wrist flexion/extension and 41 different positions of wrist ulnar/radial deviation. The 3-D kinematic

data for each subject was scaled to remove the effect of carpus size.

At each wrist position, fiber elongation was defined as the percent change in length relative to the neutral wrist position. Linear regression was used to determine if elongation of the central fiber differed with wrist position ($P < 0.05$).

RESULTS AND DISCUSSION

The central fiber of the RSC significantly ($P<0.01$) lengthened as the wrist moved from full flexion to full extension, and as the wrist moved from radial deviation to ulnar deviation (Fig. 2a). The elongation of the central fiber ranged from -15% to 25%, relative to its length at the neutral wrist position. The maximum elongation was observed in ulnar deviation and the maximum shortening was observed in radial deviation. There was a positive linear relationship between the elongations of the each of the 12 peripheral fibers and the central fiber. This relationship varied only slightly with insertion location and extent of wrapping (Fig 2b).

SUMMARY/CONCLUSIONS

Elongations of the RSC during wrist flexion/extension and radial/ulnar deviation were computed using kinematic data and bone surface models of the capitate, scaphoid and radius from an extensive *in vivo* digital kinematic database. The range of elongation was approximately 40%. While our findings are generally consistent with previous *in vitro* studies of RSC failure strains, they are still much greater than values typically reported for other ligaments (i.e. those around the knee). It is important to emphasize that our ligament elongations were derived computationally and that our results do not necessarily reflect actual ligament strain values. This is because we do not know precisely how the RSC fibers traverse the scaphoid, and because we arbitrarily selected our "zero" elongation at the neutral wrist positions. Therefore, negative elongations reflect decreased length relative to the length at the neutral wrist position, not necessarily a state of negative strain or "slack". The large range of elongations, however, does suggest either highly elastic structure or slack or both. *In vitro* biomechanical testing data will be required to resolve this issue.

REFERENCES

1. Beger and Landsmeer, *J Hand Surg [Am]* **15**: 847-854, 1990. 2. Mayfield et al. *Ortho. Trans*. 143-144, 1979. *IEEE Trans Biomed Eng* 79-799, 2004.

ACKNOWLEDGEMENTS

Funded by NIH HD052127.

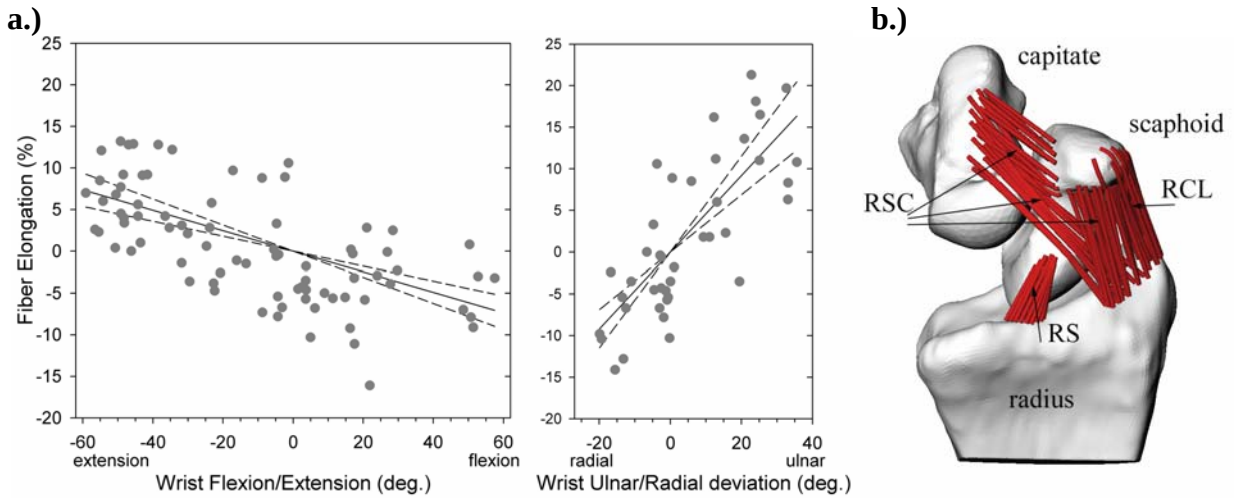

Figure 2. a.) Elongation of the central fiber of the RSC, relative to neutral wrist position, and constrained to wrap over the scaphoid bone surface. Each datum corresponds to a single wrist position. **b.)** Multiple fiber models of various ligaments. Radioscaphocapitate (RSC), radio collateral (RCL), radio scaphoid (RS). Note that the RSC forms a supporting sling around the waist of the scaphoid.

3.5 mm Lag Screws as Compared With 6.5 mm Lag Screws for Fixation of the Distal Femur: Implications for Reconstruction of Complex Joint Injuries

Anjali Gupta[2], John McCamley[2], M. Wade Shrader[1,2], Kristine Csavina[2], David J. Jacofsky[1,2], Paul Tornetta III [3]

[1] The CORE Institute, Sun City West, AZ, USA
[2] SHRI-CORE Orthopedic Research Labs, Sun City West, AZ, USA
[3] Boston University Medical Center, Boston, MA
E-mail: wade.shrader@thecoreinstitute.com, Web: www.thecoreinstitute.com

INTRODUCTION

Distal femur fractures result from high energy impacts such as vehicular trauma in the younger population, but are also common in osteoporotic patients. Approximately 85% of the distal femoral fractures occur in the over 50's age group (Forster, 2006). These fractures generally include an intra-articular line, which make it necessary to achieve anatomical reduction permitting a faster healing process and enabling early range of motion.

The fixation of complex distal femur fractures has evolved over the past 5 years to be dominated by locked plating as opposed to DCS or blade plate fixation. These plates fill a greater area of the lateral portion of the lateral condyle, leaving less room for lag screws outside of the implants. Many surgeons have moved away from 6.5mm screws in favor of smaller lag screws that can be placed around the plate. The purpose of this study was to evaluate the stiffness and strength of 3.5mm vs. 6.5 mm screws for the fixation of a unicondylar fracture of the distal femur in osteopenic human bone (mimicking the intercondylar component of more complex injuries).

METHODS

Seven unembalmed, matched pairs of human femurs (average age 82±7 yrs.) underwent biomechanical testing. Fresh specimens were stored, frozen vacuum sealed and wrapped in saline then thawed to room temperature prior to testing. The pairs were tested with (DEXA) scanning to confirm correlation within matched pairs. Lateral condyle fractures were created at a 25° angle from the intercondylar notch. One of each pair was fixed with three 3.5mm lag screws placed in the periphery of the joint and the other with two 6.5mm lag screws (Smith & Nephew, Memphis, TN) anteriorly and posteriorly, simulating fixation that would be placed around a plate (Figure 1). After pilot testing, axial loading tests were conducted using a uniaxial servo-hydraulic load frame (Dynamic Testing Systems, Phoenix, Arizona) with a digitally-monitored analog controller (Lynx, Michigan) and a closed-loop, vector drive hydraulic pump (LeBlond & Associates, Phoenix, Arizona). Specimens were potted in a vertical position .

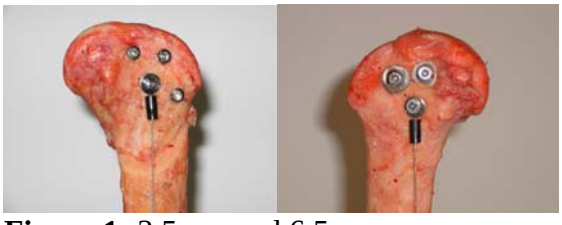

Figure 1: 3.5mm and 6.5mm screws

A lateral tibial plateau component of a total knee prosthesis was used for loading purposes. An axial preload of 50N was applied to the femur to stabilize the construct. After preloading for ten seconds

a ramped load increasing at 25N/s was applied to the lateral condyle until clinical failure of the bone, defined as a displacement greater than 3mm. Data were recorded at 500 Hz.

RESULTS AND DISCUSSION

The load at failure (3mm of displacement) was 919 ± 368 N for the 3.5mm and 1041 ± 33N for the 6.5mm screws (p=0.5, 95% CI difference -544 - +300). See Figure 2 for incremental load-displacement curves. The stiffness of the constructs (slope of the curve between 0.2 and 1.2 mm displacement) was 289 ± 150 N/mm for the 3.5 screws and 371 ± 170 N/mm for the 6.5 screws (p=0.29). The low number of pairs likely contributed to the variability in the study.

The smaller diameter screws are preferred for ease of placement in distal femur fractures especially when plating is required for further reduction of a fracture. Additional studies are recommended to include additional pairs and fatigue testing to further compare the screw sizes.

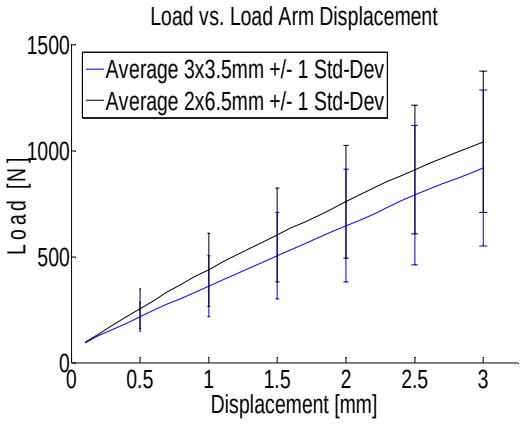

Figure 2: Load vs. displacement for 3x3.5mm and 2x6.5mm screws showing ± one standard deviation

SUMMARY/CONCLUSIONS

There was no difference seen in the ability of the 3.5mm screws to resist vertical displacement in a model of a shearing lateral condyle fracture. This study, done in osteoporotic fresh human cadaveric distal femur pairs supports the use of smaller lag screws that are more easily placed around the current distal femoral plates with a larger footprint than traditional DCS or blade plates, which had room for 6.5mm lag screws.

REFERENCES

Forster, M.C. et al. (2006). *Injury*, **37(2),** 97-108.

JOINT MOMENTS ARE COORDINATED TO STABILIZE VERTICAL ENDPOINT FORCES DURING HUMAN LOCOMOTION

Jasper Yen[1] and Young-Hui Chang[2]

[1] Dept. of Biomedical Engineering, Georgia Tech and Emory University, Atlanta, GA, USA
[2] School of Applied Physiology, Georgia Tech, Atlanta, GA, USA
E-mail: jaspery@gatech.edu Web: www.ap.gatech.edu/chang/cnlyhchang.html

INTRODUCTION

Because joints of the human leg are redundant for endpoint force production, there are infinite joint moment trajectory solutions for any given endpoint force trajectory. Therefore, there should exist a "buffer", or an uncontrolled manifold (UCM), where joint torques may vary without affecting the endpoint force. We hypothesized that locomotor systems do not choose specific joint moment trajectories during the locomotor cycle but instead allow solutions to vary within the UCM.

Previous studies have suggested similar hypotheses for upper extremity tasks.[1] The stability of a task level variable was assessed through across-trial variability. For each time point, the variance of local degrees of freedom was measured and split into two components: that which lay in the UCM (redundant variance) and that which lay outside the UCM (task error variance). If redundant variance was greater than task error variance, then the task level variable was deemed to be stabilized.

The purpose of the present study was to determine if joint moments are coordinated to vary within the UCM to stabilize endpoint force during human locomotion. We used human hopping because of its simple and reliable mass-spring-like dynamics, and it is a minimal locomotor behavior that can be studied under highly controlled conditions.[2]

METHODS

Sagittal plane kinematics and ground reaction forces were collected at 120 and 1080 Hz respectively from seven healthy, right-leg dominate subjects that gave informed consent to participate in this study. Subjects hopped in place on their right leg at frequencies of 2.2, 2.8, and 3.2 Hz. Three trials of each condition were collected in a random order for 30 seconds each. 30 hops were taken from each trial and pooled from each frequency condition for analysis.

We used a three link biomechanical model relating ankle, knee, and hip moments to endpoint force. The null space of the model represents the UCM. We normalized time and calculated the variance of joint moments for every one percent of stance phase. For each time point, we calculated the Redundant Fraction (RF) of total variance that lay in the UCM. An $RF > 0.5$ indicated that the joint moments were being coordinated to stabilize endpoint force.

RESULTS AND DISCUSSION

Variations of joint moments and GRF were evident from hop to hop. No clear correlation between joint moment variability and endpoint force variability, however, was evident without employing the UCM analysis. In accordance with the UCM hypothesis, coordination of joint moments acted to stabilize the vertical component of endpoint force (Fv).

Fv was stabilized at the beginning, middle, and end of stance phase (Figure 1). While redundant variance increased as the mean Fv value increased through the middle of stance, the task error variance decreased at mid-stance. This suggested that joint moments were coordinated synergistically to reduce Fv variability.

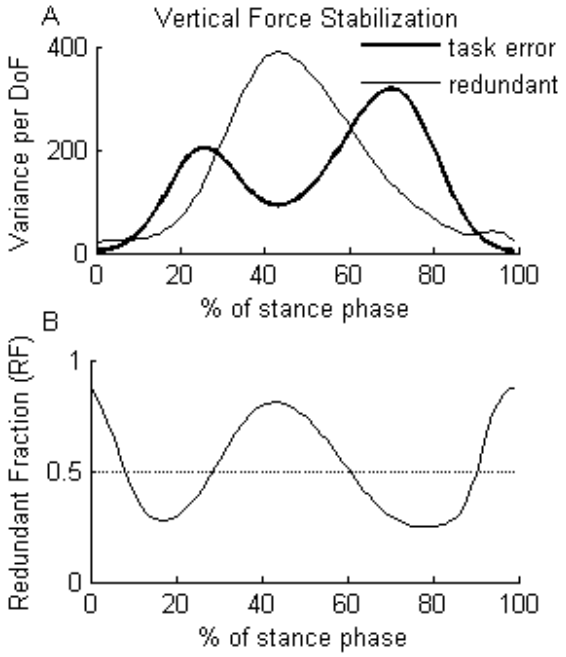

Figure 1: Total joint moment variance of a representative subject hopping at 2.2 Hz. The total variance was split into two components: task error and redundant (A), and RF was calculated as redundant / (redundant + task error) (B).

To test whether our results could be explained by interjoint coordination, any such coordination was artificially removed by randomly shuffling the joint moments at each time point. Hops were reconstructed by matching joint moments from random hops and re-running the UCM analysis. With no coordinating strategy, the RF during mid-stance was decreased to approximately 0.5, which corresponds to a random distribution of variance within and outside of the null space (UCM).

We did not observe significantly different control strategies for different hopping frequencies. The strategy employed between subjects was consistent. In contrast to Fv, the horizontal component of endpoint force (Fh) was consistently destabilized (RF < 0.5) throughout stance.

SUMMARY/CONCLUSIONS

Humans appear to coordinate joint moments to stabilize vertical endpoint force during hopping. Control of endpoint force generated by the leg may be especially important during mid-stance to ensure proper vertical acceleration of the CoM. Proper acceleration in this experimental scenario is linked to meeting the prescribed hopping frequency. The destabilization of Fh likely corresponded to subjects attempting to hop in place without looking down at their feet as instructed.

Redundant variance had the same unimodal trajectory as the average Fv trajectory. Task error variance had the same bimodal trajectory as the average time derivative of Fv. These results are in agreement with previous UCM analysis on finger force production tasks[3].

REFERENCES

[1]Latash M.L. et al. (2002). *Exerc Sport Sci Review*, **30**, 26-31.
[2]McMahon, T.A., Cheng, G.C. (1990). *J. Biomech.* **23 Suppl 1**, 65-78.
[3]Latash M.L. et al. (2002). *Exp Brain Research*, **146**, 219-32.

ACKNOWLEDGEMENTS

We would like to thank Arick Auyang for sharing his data with us and for advice from Dr. Lena Ting. This work was supported by an NSF IGERT fellowship to J.Y.

HIP JOINT MOMENTS DURING WALKING AND BONE MINERAL DENSITY IN HEALTHY OLDER WOMEN

Katherine A. Boyer, Thomas P. Andriacchi, and Gary S. Beaupre

VA Bone and Joint Rehabilitation R & D Center, Palo Alto, CA USA
Stanford University, Stanford, CA, USA
E-mail: kboyer@stanford.edu

INTRODUCTION

The relationship between proximal femoral bone density and the stress stimulus provided by normal walking is of interest because of the relationship between bone mineral density (BMD) and fracture risk in falls. While, body strength, exercise and ambulation have been suggested (Snow-Harter et al., 1992; Yanagimoto et al., 2000) as important factors in the maintenance of bone mass at the hip, it remains unclear if there are specific characteristics of walking that influence BMD to a greater extent than static characteristics such as body weight. During walking the joint moments are major factors influencing the hip joint load as they are balanced by muscle forces. Thus it is useful to consider how the variations in the dynamic moments influence the variation in BMD. The purpose of this study was to test the hypothesis that the dynamic moments during walking are a stronger predictor of BMD than the static effect of purely body weight using previously developed theoretical relationships between applied stress and bone density.

METHODS

Kinematic, kinetic, and bone density data were collected for 22 healthy, older women (age: 63.4 +/- 1.6 yrs; height: 1.64 +/- 0.01. m; mass: 64.3 +/- 2.5 kg). All subjects provided informed consent according to the Stanford institutional review board. Subjects walked along an 11m long walkway with an embedded force platform (4060H, Bertec Corp.) at a self-selected normal walking speed. Motion data were collected with an optoelectronic system (ProReflex 240, Qualisys Inc.). Both force and motion data were captured synchronously at 120Hz. Only subjects who did not participate in high-impact type sports were included, thus measures of the net joint moments and forces during the gait test were expected to be representative of habitual hip joint loading patterns.
An inverse dynamics approach was used to calculate external moments at the hip. The RMS joint moment was calculated from the directional components. BMD (g/cm^2) of the proximal femur was quantified using dual-energy X-ray absorptimetry (Hologic QDR-1000W).

A relationship between effective stress and apparent density has previously been shown (Carter et al., 1987):

$$\sigma \propto \rho^2 .$$

Introducing a simplified measure of stress, we obtain:

$$\frac{F}{A_{neck}} \propto \rho^2 .$$

Using scaling principles this relationship can be extended to a theoretical relationship between surrogate measures of the hip joint force and the BMD, where the measured BMD is related to the apparent density as (Carter et al., 1992):

$$\rho \propto \frac{BMD}{\sqrt{A_{neck}}} \propto \frac{BMD}{h}$$

Therefore, the relationship between the joint force and the BMD is:

$$\frac{BMD}{h} \propto \sigma^{1/2} \propto \left(\frac{F_{hip}}{A_{neck}}\right)^{1/2}$$

$$BMD \propto F_{hip}^{1/2}.$$

In walking

$$M \propto BW * h \text{ and } F_{hip} \propto M/h.$$

Therefore,

$$\rho \propto \left[\left(\frac{M}{h}\right)/h^2\right]^{1/2}$$

$$BMD \propto \left(\frac{M_{external}}{h}\right)^{1/2},$$

where F_{hip} = force in hip joint
A_{neck} = cross sectional area of hip
M = joint moment
h = height
σ = effective stress
ρ = bone apparent density.

RESULTS AND DISCUSSION

There was a significant relationship between the dynamic $M_{external}/h$ and BMD (Figure 1). After performing a log-log transformation, the slope of the regression of BMD vs. $(M/h)^{1/2}$ was found to be 0.33 (95% CI: 0.07- 0.58; $p < 0.05$). While significant, the relationship was not as strong when mass was used in place of the moment. The slope is 0.28 (95% CI:0.00- 0.56; $p = 0.05$; $r^2 = 0.17$) for $F_{hip} \propto BW$.

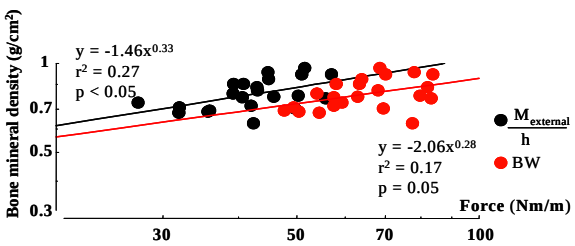

Figure 1: A log-log plot of BMD vs the resultant joint moment divide by height and BMD vs. body weight.

SUMMARY/CONCLUSIONS

This study demonstrated that the relation between BMD, joint moment and body size explained more variance than a relationship between BW and BMD. The fact that joint moments are most closely related to muscle forces and therefore the dynamic joint forces in walking suggests that the dynamics of walking play an important role in the maintenance of bone density at the hip and the resultant joint moment can be a useful predictor of BMD. In addition, these results indicate that interventions that modify the joint moments may have an impact on BMD.

ACKNOWLEDMENTS

Supported by the Department of Veterans Affairs, Rehabilitation R&D Service, merit review grant A4067R. Thanks to Barbara Elspas, Joe Guerricabeitia, Jenny B. Kiratli, and Sparkle Williams for data collection and Dennis Carter for thoughtful discussion.

REFERENCES

Carter, D. R., Bouxsein, M. L., Marcus, R., (1992). *J Bone Miner.Res* 7**,** 137-145.

Carter, D. R., Fyhrie, D. P., Whalen, R. T., (1987). *J Biomech* 20**,** 785-794.

Snow-Harter, C., Whalen, R., Myburgh, K., Arnaud, S., Marcus, R., (1992). *J Bone Miner.Res* 7**,** 1291-1296.

Yanagimoto, Y., Oshida, Y., Sato, Y., (2000). *Scandinavian Journal of Medicine and Science in Sports* 10**,** 103-108.

ACTIVE AND PASSIVE FORCE ENHANCEMENT IN RABBIT PSOAS MYOFIBRILS

Venus Joumaa [1] Tim R Leonard [1], and Walter Herzog [1]

[1] Human Performance Laboratory, University of Calgary, AB, Canada
E-mail: vjoumaa@kin.ucalgary.ca

INTRODUCTION

It has been accepted that the steady state force produced by a muscle following active stretch is greater than the corresponding purely isometric force (Abbott and Aubert, 1952; Herzog and Leonard, 2002). This phenomenon, called residual force enhancement, has been described in a variety of muscle preparations, ranging from human muscles (Lee and Herzog, 2002), isolated muscles (Abbott and Aubert, 1952; Herzog and Leonard, 2002) and single fibers (Rassier et al., 2003). The mechanisms of residual force enhancement are not known. It has been proposed that it has a passive component, related to titin filaments, and an active component, related to cross-bridge formation and actin-myosin interaction (Herzog and Leonard 2002).

The aim of this study was to investigate 1) residual force enhancement at the myofibril level and 2) the amount of contribution of the passive and active components to the residual force enhancement in single myofibrils. Residual force enhancement is accompanied by an increase in passive force after deactivation. This so-called passive force enhancement reflects the contribution of the passive component to the total residual force enhancement (Herzog and Leonard, 2005). The contribution of the active component can be approximated by subtracting the passive force enhancement from the total residual force enhancement. This calculation is possible in myofibrils where all sarcomeres are arranged in series, and therefore mechanical properties can be directly related to the intra-sarcomeric passive (titin) and active (cross-bridges) components.

METHODS

Myofibrils isolated from the rabbit psoas muscle were fixed to a glass needle at one end and to a nanolever at the other end, allowing for length change and force measurement respectively. The striation pattern of the myofibrils was projected onto a linear photodiode array for sarcomere length computation.

Myofibrils (n=6) were fixed at a sarcomere length (SL) of 2.4µm then stretched passively, in a relaxing solution, to a SL of 3.4µm; the stretch was held for 1min (Fig.1). After a period of ten-minute rest, the myofibril was chemically activated, by replacing the relaxing solution by an activating solution with a high calcium concentration, then stretched to a SL of 3.4µm. The stretch was held for 1min; deactivation occurred 30s after the stretch (Fig. 1).

Residual force enhancement was defined as the difference between the steady state force obtained after stretch (Fs, Fig. 1) and the force obtained before stretch (Fi, Fig. 1) corrected for the final sarcomere length according to the force length relationship (Fc, Table 1).

Passive force enhancement was measured as the difference between the steady state force reached after passive stretch (Fp, Fig. 1) and

the force after active stretch and deactivation (Fa, Fig. 1). Forces were normalized to the myofibril cross-sectional area.

RESULTS AND DISCUSSION

All six myofibrils showed residual force enhancement and passive force enhancement, as shown for a typical myofibril in figure 1. This result is in accordance with previous results obtained in whole muscles and single fibres (Herzog et al., 2002; Rassier et al., 2003).

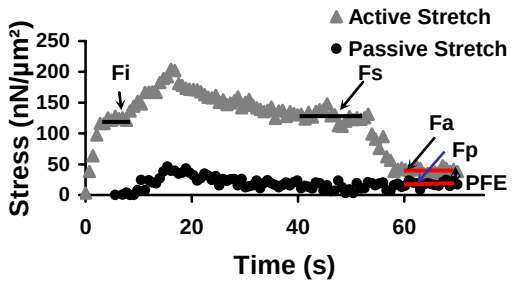

Figure 1: Typical myofibril response when stretched passively (●) and actively (▲). Passive force enhancement (PFE) is Fa-Fp. Residual force enhancement is Fs-Fc, where Fc is Fi minus the decrease in force when going from a SL of 2.4µm to a SL of 3.4µm, according to the force length relationship.

The average residual force enhancement and passive force enhancement were respectively 140 ± 24 nN/µm^2 and 39 ± 8 nN/µm^2 (Table 1). Accordingly, the contribution of the passive component to the residual force enhancement cannot exceed 28 ± 5% of the residual force enhancement. The contribution of the active component to the residual force enhancement would then be more than 70%.

Knowing that titin is the main structure responsible for passive force in single myofibrils, we propose that titin is responsible for about 28% of the residual force enhancement for the conditions tested here. Titin's stiffness might be calcium-dependent and therefore increasing upon muscle activation (Labeit et al., 2003).

The active component of the residual force enhancement is directly related to the cross-bridges. It might be caused by an increase in the number of attached cross-bridges induced by a decrease in the rate of detachment (Herzog and Leonard, 2002).

	Fi	Fs	Fc	FE	PFE
Mean	177	199	57	140	39
SD	24	30	8	24	8

Table 1: Forces (Mean ± SD) produced by 6 myofibrils normalized to the cross-sectional area (nN/µm^2).

CONCLUSION

The active component, represented by the cross-bridges, is the major contributor to residual force enhancement in myofibrils stretched from 2.4 to 3.4µm average sarcomere length. It accounts for more than 70% of the force enhancement while the passive contribution is about 28%.

REFERENCES

Abbott, B.C., Aubert, X.M. (1952). *J. Physiol* **117**, 77-86.

Herzog, W. and Leonard, T.R. (2002). *J Exp Biol* **205,** 1275-1283

Herzog, W. and Leonard, T.R. (2005). *J Biomech* **38,** 409-415

Lee, H.D. and Herzog, W. (2002). *J. Physiol* **545**, 321-330.

Rassier, D.E., et al. (2003). *J. Biomech* **36**, 1309-1316.

Labeit, D. et al. (2003). *Proc Natl Acad Sci U S A* **100,** 13716-13721.

ACKNOWLEDGEMENTS

NSERC, CIHR, CFI.

A DATA-DRIVEN MARKOV CHAIN MONTE CARLO METROPOLIS-HASTINGS ALGORITHM FOR A MODEL OF THE HUMAN THUMB

Veronica J. Santos, Carlos D. Bustamante, and Francisco J. Valero-Cuevas

Cornell University, Ithaca, NY, USA
E-mail: fv24@cornell.edu, Web: www.mae.cornell.edu/nmbl/

INTRODUCTION

Monte Carlo techniques are gaining acceptance in complex biomechanical modeling to explore the effects of anatomical variability and measurement uncertainty on model predictions in an open-loop manner (e.g., Langenderfer *et al.*, 2006; Santos and Valero-Cuevas, 2006). However, creating realistic models will require advanced stochastic methods to perform closed-loop, data-driven searches when model parameter spaces are large. We present what, to our knowledge, is the first use of Markov chain Monte Carlo (MCMC) techniques in biomechanics with synthetic data from a model of the human thumb as a proof-of-concept of the MCMC Metropolis-Hastings algorithm to explore a complex 36-dimensional (36D) model parameter space.

METHODS

Previously, we described an MCMC Metropolis-Hastings algorithm (Santos and Valero-Cuevas, 2004) that uses the single-site updating technique to explore a 36D model parameter space in a manner similar to a biased random walk: thumb bone dimensions (8), kinematic axes of rotation (16) (Giurintano *et al.*, 1995), and frame transformations at the proximal base (6) and distal tip (6) of the thumb. Here, we apply the algorithm to a model with 36 arbitrarily defined model parameters. To validate the algorithm, we used a truth model to simulate experimental data (thumbnail location, orientation, and linear and angular velocities) for nine active motions (e.g., flexion/extension). We also added zero-mean, uncorrelated multivariate Gaussian "measurement noise" to our deterministic truth model outputs. Ten independent Markov chains driven by these noisy data searched the 36D model parameter space for the subspace that best fit the data (i.e., the posterior distribution) until the Gelman-Rubin convergence diagnostic fell below a threshold of 1.2. We used posterior-predictive sampling to compare the MCMC results to the truth model and cross-validated the results using a separate set of simulated experimental data that were not used to drive the MCMC simulations.

RESULTS AND DISCUSSION

We ran each Markov chain for 105,000 iterations on 2.4GHz dual Intel® Xeon® machines, which took 255.5 hours (49 hrs. for MCMC simulations in C and 206.5 hrs. for post-analysis in MATLAB®). Six chains converged to the true posterior distribution while the remaining four chains located other local minima in the 36D landscape (Figure 1).

The errors in the posterior predictive samples for the six chains were minimal (Figure 2). Despite the fact that we provided noisy simulated data to our Metropolis-Hastings algorithm, the algorithm estimated and accounted for the noise to find the true values and successfully locate the true posterior distribution. The errors in the posterior predictions for the cross-validation data set were also minimal, demonstrating

that the algorithm did not simply over fit the data given, but actually found the true parameters in the 36D space.

CONCLUSIONS

We have successfully demonstrated the unprecedented use of our Metropolis-Hastings sampling algorithm to a large 36D biomechanical model parameter space with practical application to experimental data. MCMC techniques in biomechanics may provide clinical benefits such as the ability to determine sensitivity of model predictions and functional clinical outcomes to changes in model parameters, and to categorize clinically-relevant subpopulations. Convergence of a majority of chains to the true values demonstrates that the method is able to accommodate the expected redundancies of large parameter spaces.

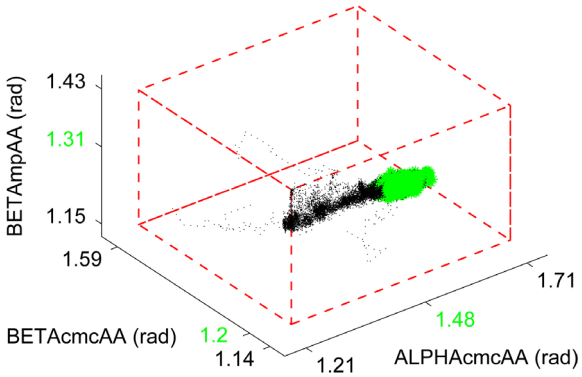

Figure 1: Convergence (green points) of the six Markov chains for three representative parameters. The chains located the true posterior distribution in the cuboid defined by the bounds on the prior distributions (red dashed lines). A Monte Carlo integrator must randomly sample from the entire volume. The MCMC simulations, in contrast, are more computationally efficient because they behave like biased random walks that converge to the model parameter subspace that best fits the data (true values in green). While only 3D results are shown here, convergence occurred in 36D.

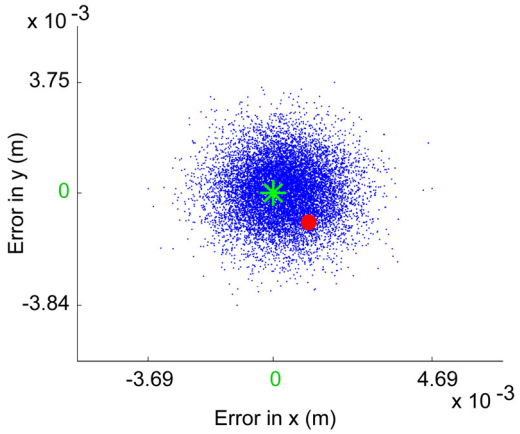

Figure 2: The posterior predictive sample errors (blue points) are shown for two experimental outputs (x and y coordinates for thumbnail location) for a single representative data point. The green asterisk indicates the true error value of zero. The red circle is the offset of the noisy simulated data point actually used to drive the MCMC simulations. Note that the algorithm estimated the variance in the noisy simulated data and recovered the true parameter values (blue cloud of points is centered around the true error value of zero).

REFERENCES

Giurintano, D.J., Hollister, A.M.., Buford, W.L., Thompson, D.E., and Myers, L.M. (1995). *Med. Eng. Phys.,* **17**, 297-303.

Langenderfer, J.E., Carpenter, J.E., Johnson, M.E., An, K.N., and Hughes, R.E. (2006). *Ann. Biomed. Eng.*, **34**, 465-476.

Santos, V.J. and Valero-Cuevas, F.J. (2004). *Proc. of IEEE EMBS '04,* 4626-4629.

Santos, V.J. and Valero-Cuevas, F.J. (2006). *IEEE Trans. Biomed. Eng.,* **53**, 155-163.

ACKNOWLEDGEMENTS

NSF Graduate Research Fellowship (to V.J. Santos), Grant Nos. AR050520 and AR052345 from the NIH, and NSF CAREER Award BES-0237258 (to F.J. Valero-Cuevas).

A NOVEL APPORACH TO DESIGN KNEE IMPANTS FOR WEAR AND STRESS SHIELDING PERFORMANCE

Ryan Willing [1] Anthony G Au [2] Il Yong Kim [1] and A. Amirfazli [2]

[1] Queen's University, Kingston, ON, Canada; iykim@me.queensu.ca
[2] University of Alberta, Edmonton, AB, Canada; a.amirfazli@ualberta.ca

INTRODUCTION

Total knee replacement (TKR) has long been the standard operation to relieve pain and restore range of motion to knee joints damaged by osteoarthritis. TKR frequency has been steadily increasing, and has been forecasted to increase to over 3.5 million primary and 270 thousand revision surgeries per year by 2030 [Kurtz et al., 2006]. The need for revision surgery can be the product of a number of factors, which include wear of the implant components, especially the ultra high molecular weight polyethylene (UHMWPE) bearing, and bone weakening caused by stress shielding, a bone remodeling process caused by stiff implant components "shielding" neighboring bone from load. While patient specific characteristics greatly influence success or failure of TKR, implant design is primarily related to these failure modes.

Wear of the UHMWPE insert in TKR is an issue because wear particles released into the body can cause an adverse tissue reaction, called osteolysis, which leads to density loss in neighboring bones. Previous work has shown that optimizing implant design for reduced wear results in lower conformity between the femoral component and UHMWPE insert [Willing and Kim, 2006].

Such reduced conformity can be detrimental to the bone as recent results have shown that, in addition to stiff implant materials, loading conditions as a result of altered condylar geometry can themselves cause stress shielding [Au et al., 2007]. Stress shielding will lead to bone resorption adjacent to the implant, potentially compounding the effects of osteolysis, and ultimately leaving inadequate bone stock for TKR support.

Whereas it is clear that some design characteristics play significant roles in determining the wear and stress shielding performance of an implant individually, it is unknown whether or not any of these characteristics are shared and, more importantly, would be considered competing factors. For example, a design factor that is beneficial for wear would be detrimental for stress shielding performance. In this research we have used a novel approach which combines the finite element (FE) methods for load and stress calculations with design optimization techniques to answer the above question.

METHODS

A parametric FE model of a TKR has been developed, where design variables such as frontal and sagittal femoral condyle radii can be modified to simulate different implant designs *in-silico*. Wear simulation is performed within the commercial FE package ANSYS (Swanson Inc., Houston, PA). A wear model based on Archard's law estimates wear at the contact surface of the UHMWPE during simulations of ISO-14243-1, a set of load and displacement waveforms for force controlled wear

simulators. This study has focused on the femoral component and the UHMWPE insert.

Following the wear simulation, the contact pressure contours are mapped onto an identical FE UHMWPE insert assembled to a titanium tray and tibia. The validated tibia FE model features 25 different material properties to represent heterogeneous bone. Quasi-static loading is applied to the TKR model to determine the stress shielding effects within the bone. A parameter study is performed after the computational framework has been completed. Parameters governing the shape of the implant components are modified in order to observe the impact on the wear rates and patterns at the contact surface, as well as the stress levels within the tibia. Design optimization follows, where TKR designs are optimized to reduce UHMWPE wear. Pre- and post-optimization stress levels within the tibia are then compared to wear results to determine if stress shielding is elevated with reduced wear levels.

RESULTS

Preliminary results include the development of the FE models and optimization for wear. It was found that the radius of curvature of the femoral condyles in the sagittal plane, as well as the conformity with the UHMWPE insert in this plane, carried the highest impact on expected wear rates. The radius of curvature is minimized, and the conformity in this plane is minimized as well, which results in smaller contact patches with higher contact stresses. Wear rates, however, decrease as the contact patch between the two components decreases (Fig 1). Preliminary results using the tibia FE model show that bone stresses decrease when load is concentrated on a smaller area. Thus, it is anticipated that reducing wear rates would potentially increase stress shielding.

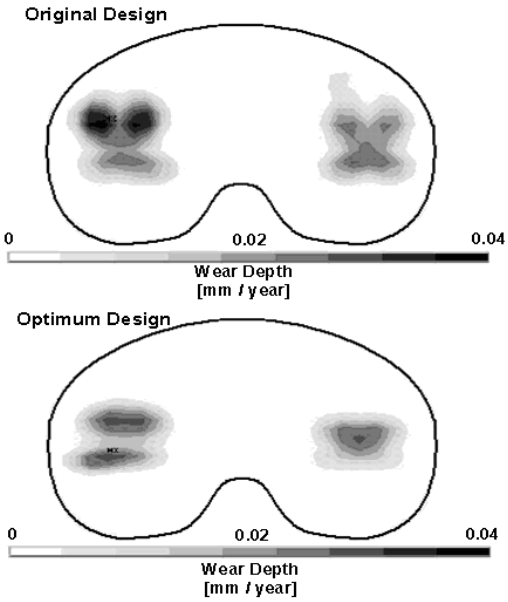

Figure 1: Initial wear pattern (above) compared to optimized wear pattern (below) shows reduction in patch size and depth

CONCLUSIONS

For the first time, the relationship between TKR design considering wear and stress shielding simultaneously is being studied. The study investigates whether there is a coupled relationship between wear and stress shielding, and discusses its consequences to improve TKR implant design. A wear-optimized design has been completed; its impact on stress shielding in the bone will be analyzed shortly.

REFERENCES

Kurtz, S. et al. (2006). Proceedings of AAO, Chicago, USA, March 2006.
Willing, R. and Kim, I.Y. (2006). *Proceedings of the CSME Forum*, Kananaskis, CAN, May 2006.
Au, A.G. et al. (2007). *J Biomech*, **40**, 1410–1416.

Effects of breathing on muscle strength of large muscle groups

Sheng Li, Elizabeth Ikeda, Adam Borg, Devn Brown, Jessica Malouf, Kathy Showers

University of Montana, Missoula, MT, USA
E-mail: sheng.li@umontana.edu

INTRODUCTION

The Valsalva maneuver (VM) refers to a forced expiration against a closed glottis. This technique is usually recommended for athletes during maximal voluntary contraction (MVC), because the VM could potentially maximize force output. However, the VM has associated potential negative effects on the cardiovascular system compared to normal breathing, such as increased blood pressure. Recently, Li and Laskin (2006) reported that peak force of the finger flexors increased significantly from forced inspiration to forced expiration. Interestingly, the peak forces were not significantly different from that produced during the VM. Since the VM is generally used in large muscles, the purpose of this study was to generalize these results to large muscles by examining the ventilation effects on muscle strength of big muscles, including knee muscles, shoulder muscles, and elbow muscles.

METHODS

Muscle strength of the knee joint was tested in one group (N=10), while muscle strength of shoulder and elbow joints was tested in another group (N=10). In the knee group, subjects were seated in a KimCom dynamometer chair with a face mask connected to a pneumotachometer to monitor ventilation. The trunk was restrained with the both arms crossed in front of the chest. The hip and knee joints were approximately 90º of flexion. After a 10-minute warm-up, subjects were instructed to produce 3~5 second maximal isometric knee flexion and extension force, respectively, under the following breathing conditions: 1) Normal breathing; 2) Valsalva maneuver (VM); 3) Synchronized forceful inhalation (i.e., MVC is synchronized with inhalation, IN), and 4) Synchronized forceful exhalation (OUT).

Similarly, the hip, knee, and ankle joints of both sides rested at about 90º of flexion in the shoulder elbow group. The elbow joint was tested at 90º of flexion for both elbow flexion and extension MVC when the shoulder joint was kept at approximately the neutral position; the forearm was fully supinated, and the mechanical stop was secured to the distal quarter of the test forearm for both elbow flexion and extension. The shoulder joint was tested at 45º of abduction when the mechanical stop was secured to the middle upper arm, and the elbow was maintained at about 90º of flexion. Note that the trunk was not restrained during experiments. Specific instructions were given to assure there was no tilting or leaning of the trunk during the experiments. The same procedures and breathing conditions were used for both elbow and shoulder joints. Within each group, breathing conditions and muscle contractions were randomized. Two trials were tested for each condition.

The peak force of each trial was calculated. To compare the effect of breathing, the peak forces during IN, OUT, and VM, were normalized to that measured during normal breathing. A two-way ANOVA was used. Factors were BREATH (3 levels, IN, OUT, VM) and MUSCLE (2 levels, FLEX/EXT).

RESULTS AND DISCUSSION

The effect of voluntary breathing on muscle strength was consistently observed in all tested muscle groups. In agreement of previous reports, the effects were respiratory phase-dependent and muscle-specific (Fig 1). Shoulder addition MVC was significantly decreased during forceful inhalation (IN) ($F[2,18]=7.74$, $p=0.004$); elbow extension MVC was significantly decreased during IN ($F[2,18]=3.90$, $p=0.039$); knee extension MVC was enhanced during OUT ($F[1,9]=9.35$, $p=0.014$).

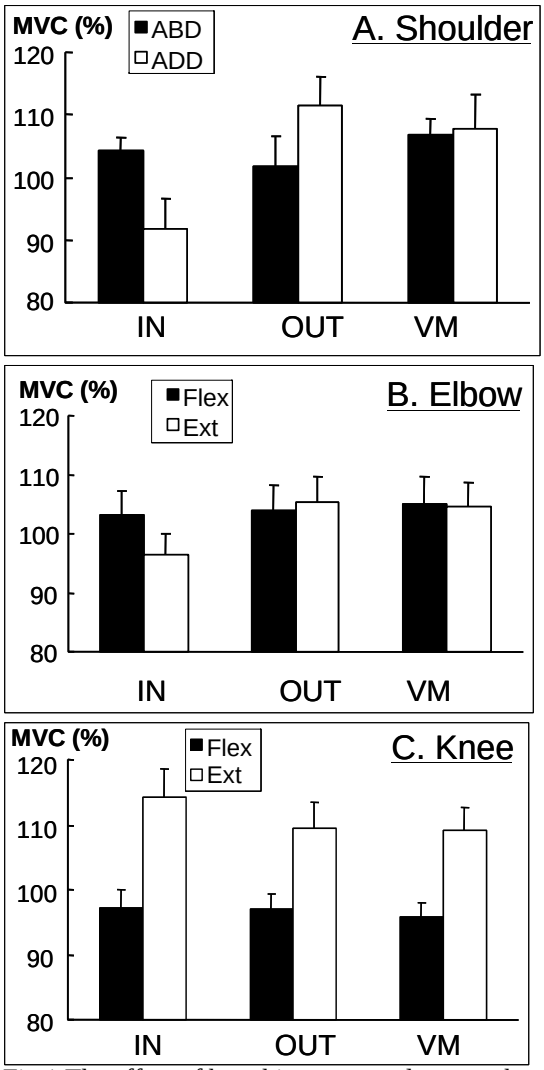

Fig 1 The effect of breathing on muscle strength. Muscle strength was normalized to the peak force during normal breathing.

Interestingly, MVC during the Valsalva maneuver was not significantly different from MVC measured during OUT.

In addition, synchronized forceful exhalation (OUT) imposed positive effects on muscle strength during shoulder adduction (Fig 1A), elbow extension (Fig 1B), and knee extension (Fig 1C). When taking into count the finding of increased finger flexion MVC during OUT (Li and Laskin 2006), a combination of shoulder adduction, elbow extension, fingers into a fist, and knee extension during forceful exhalation creates an image of a forward punching, e.g., during boxing.

SUMMARY AND CONCLUSION

1) We generalize our previous results to large muscle groups that synchronized breathing influences MVC production during ballistic isometric muscle contractions.
2) The VM is not superior to synchronized breathing during ballistic MVC production. Given the negatives associated with the VM, synchronized forceful ventilation (assumed to impose minimal risks to the cardiovascular system) is a proper breathing technique for MVC production.
3) This set of data implies that voluntary breathing imposes a global impact on the motor system by integrating individual elements into coordinated, meaningful movement, i.e., synergy.

REFERENCE

Li, S. and Laskin, J.L. (2006) *Muscle Nerve* 34:651-655

ACKNOWLEDGEMENT

This study was supported in part by an NIH Grant 1R15 NS053442-01A1

INTEGER PROGRAMMING MODELS FOR OPTIMIZING SHOULDER REHABILITATION

Christopher J. Gatti [1], Jason Scibek [2], Oleg Svintsitski [1],
James E. Carpenter [1], Richard E. Hughes [1,*]

[1] Laboratory for Optimization and Computation in Orthopaedic Surgery,
University of Michigan, Ann Arbor, MI
[2] Department of Athletic Training, Duquesne University, Pittsburgh, PA
*E-mail: rehughes@umich.edu, Web: http://www-personal.umich.edu/~rehughes/index.html

INTRODUCTION

Strength restoration is one goal of shoulder rehabilitation following rotator cuff repair surgery. However, the time spent in a physical rehabilitation setting is limited and the effectiveness of shoulder strengthening exercises needs to be maximized. There is little quantitative support for rehabilitation protocols and the prescription of strengthening exercise protocols is currently based on the judgment of the rehabilitation specialist and tradition-based protocols. Our objective was to develop a mathematical model for determining the optimal shoulder rehabilitation exercise protocol to restore normal shoulder strength given a time-constrained rehabilitation session.

METHODS

An integer programming model was developed to determine the optimal exercise protocol to maximize the time spent strengthening the shoulder during rehabilitation. The model is based on three assumptions: (1) strength is proportional to muscle physiological cross-sectional area (PCSA), (2) muscle hypertrophy (increase in PCSA) is proportional to the initial muscle PCSA, and (3) strength increases linearly with the number of sets of an exercise up to four sets.

The dose-response between the strengthening exercises and strength measurements was based on the results of a meta-analysis of strength training literature (Rhea et al., 2002), and was modeled as an increasing linear function from one to four sets of exercise. The strength gain of each muscle was modeled as muscle hypertrophy and was dependent on the contribution of a muscle to each exercise based on biomechanical muscle parameters obtained from using a computational shoulder model (Holzbaur et al., 2005).

Data were collected at the Mayo Clinic on patients having undergone rotator cuff repair as reported by Silver and colleagues (2006), and consisted of 14 different isometric posture-action combinations. Four isometric strengthening exercises were included in the model: abduction (ABD), adduction (ADD), internal rotation (IR), and external rotation (ER). The posture-action combinations of the measurements are all different from those of the exercises, thus there is an indirect transfer of strength from the strengthening exercises to the strength measurements.

The model was tested using two different rehabilitation outcome objective functions: SVM and contralateral. The SVM objective function used a least-squares support vector machine to determine a vector normal to the optimal separating hyperplane between

pathologic and healthy population shoulder strengths (Silver et al., 2006); this vector represents the direction of optimal strength improvement. The optimal exercise protocol was determined by the projection of the strength gain due to strengthening exercises onto the normal vector. The contralateral objective function increased strength with the goal of the contralateral shoulder strength vector. The rehabilitation session time (30-minutes) constrained the number of exercise sets prescribed where 1 set was assumed to last 2-minutes, including a rest period.

RESULTS

The SVM objective function yielded a subject-independent optimal protocol consisting of 4 sets each of adduction and external rotation. The contralateral objective function yielded subject-specific optimal protocols and typically consisted of various set combinations of abduction and internal and external rotation. To illustrate the effects of the contralateral model, strength percentages (relative to the goal) were averaged over similar actions and are shown in Figure 1 for one subject that was prescribed 4 sets each of abduction and internal and external rotation. It is seen that adduction strength improves despite adduction exercises being absent from the optimal exercise protocol.

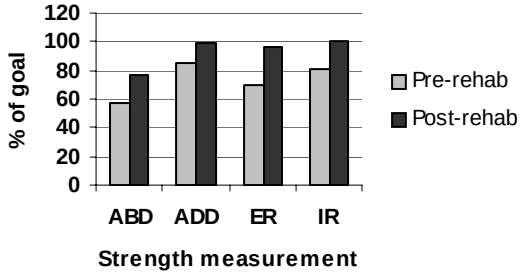

Figure 1. Strength change for one subject.

DISCUSSION

The optimal strengthening protocols are partially consistent with the current practice of shoulder strength restoration. Our model suggests adduction has a place in shoulder rehabilitation.

Our model is limited by a few uncertainties. There is no clearly accepted outcome objective for strength restoration following rotator cuff repair and other objectives, than those tested in the current model, are possible. We represented strength gains as an increase in PCSA; however neural adaptations have been found to play a role in strength gain (Narici et al., 1989).

Future work could include validation and refinement of the current model. Furthermore, shoulder rehabilitation focuses on multiple functional capacities including strength, range of motion, scapular stabilization, muscular endurance, and the individual functional needs of the patient. The current model could be formulated as a multiobjective optimization.

REFERENCES

Rhea MR et al. (2002). *Res Q Exercise Sport* **73**(4):485-8.
Holzbaur KRS et al. (2005). *Ann Biomed Eng* **33**(6):829-40.
Silver AE et al. (2006). *J Biomech* **39**:973-9.
Narici MV et al. (1989). *Eur J Appl Physiol* **59**:310-9.

ACKNOWLEDGEMENTS

We thank the National Institutes of Health for financial support via grant AR048540.

MULTI-SEGMENT FOOT KINEMATICS IN HIGH- AND LOW-ARCHED FEMALES RECREATIONAL ATHLETES DURING WALKING AND RUNNING

Douglas Powell[1], Songning Zhang[2], Clare Milner[2] and Benjamin Long[2]
Biomechanics Lab, The University of Texas of the Permian Basin, Odessa, TX, USA
Biomechanics/Sports Medicine Lab, The University of Tennessee, Knoxville, TN, USA
email: dpowell4@utk.edu, web: web.utk.edu/~Esals/resources/biomechanics_laboratory.html

INTRODUCTION

It has been established that high- and low-arched feet are associated with unique injury patterns (Williams 2001) and several studies have shown kinematic and kinetic differences between high and low arched runners (Williams 2001; Williams et al. 2004). While some studies have examined the inter-segmental motion of the foot using a multi-segment foot model during dynamic activities(Leardini et al. 1999), no data currently exist comparing the inter-segmental foot motion of high- and low-arched feet during dynamic activities. A multi-segment foot model may be more sensitive in detecting arch changes in dynamic activities of high- and low-arched individuals than a traditional single-segment foot model. It may also provide better insight into injury mechanisms and the unique injury patterns associated with each foot type. Therefore, the purpose of this study was to examine inter-segmental foot motions in high- and low-arched females during walking and running. It was hypothesized that high-compared to low-arched subjects will be more rigid and have smaller inter-segmental ranges of motion and excursions.

METHODS

Five high-arched (HA, 1.66±0.09 m and 61.18±4.60 kg) and five low-arched (LA: 1.60±0.06 m and 55.18±5.85 kg) female recreational athletes participated in the study. Each subject performed five barefoot walking and running trials at a self-selected pace with movement conditions randomized. Ground reaction force (GRF, 1200Hz, AMTI) and three-dimensional kinematic data (240Hz, 7-cameras Vicon*PEAK*) were recorded simultaneously. The Leardini model (Leardini et al. 1999) was adopted to model the foot as three segments: rearfoot, midfoot, and forefoot (first ray).

Kinematic variables for the multi-segment foot were calculated using Visual 3D (C-Motion Inc.). Selected variables were analyzed using 2 × 2 (group × movement) repeated measures ANOVAs ($p < 0.05$).

RESULTS AND DISCUSSION

Significant group by movement interactions were present in the walking and running movements. Kinematic variables showing group by movement interactions (Table 1) included rear-midfoot flexion at heel strike (RMF-HS), rear-midfoot flexion excursion (RMF-Exc) and ankle dorsiflexion excursion (Ank Exc).

There were no significant group differences in sagittal, frontal or transverse plane rear-midfoot joint angles between high- and low-arched subjects during walking. A trend did exist, showing that the high- compared to the low-arched subjects were more inverted ($p=0.096$) and internally rotated ($p=0.073$) in the rear-midfoot joint (Figure 1).

No significant differences were observed in the sagittal, frontal or transverse plane

angles in the mid-forefoot joint in walking. High- compared to low-arched subjects were more everted (p=0.053) and externally rotated (p=0.084) at the mid-forefoot joint, however these differences were not statistically significant.

Table 1. Kinematic data with significant group by movement interactions.

	Group	RMF-HS	RMF-Exc	Ank Exc
Walk	LA	4.06 (7.27)	2.18 (3.83)	7.39 (1.48)
	HA	1.57 (2.03)	0.49 (2.93)	4.20 (6.51)
Run	LA	-1.32 (5.06)	7.10 (3.28)	9.45 (5.97)
	HA	3.67 (2.46)	9.21 (2.32)	14.15 (7.03)

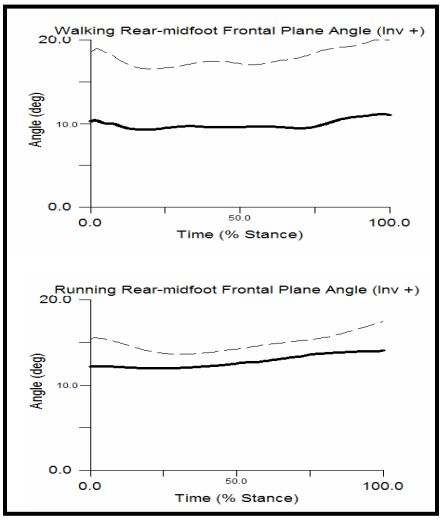

Figure 1. Ensemble frontal plane rear-mid-foot angles during barefoot walking and running in high- (solid) and low-arched (dashed) subjects.

In the running condition, no significant differences were observed in the rear-midfoot joint in the sagittal, frontal or transverse plane. Additionally, no differences were found in the mid-forefoot joint. However, similar trends of rear-midfoot inversion and internal rotation as well as mid-forefoot eversion and external rotation were present (Figure 2).

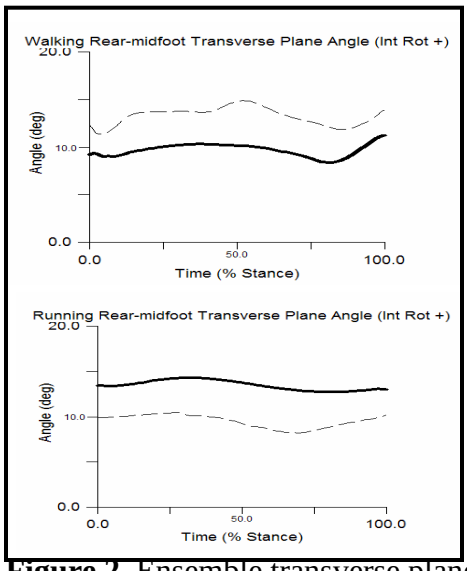

Figure 2. Ensemble transverse plane rear-midfoot angles in high- (solid) and low- (dashed) arched subjects in barefoot walking and running.

CONCLUSIONS

Differences were found between the high- and low-arched groups at the rear-midfoot and ankle joints. Additionally, unique trends were also present between the two groups suggesting meaningful kinematic differences may exist between groups. Furthermore, these trends may be associated with altered kinetic patterns within the foot and the lower extremity. Future research studies should investigate the kinetic patterns within the multi-segment foot in high- and low-arched individuals.

REFERENCES

Leardini, A., et al. (1999). Clin Biomech **14**(8): 528-36.

Williams, D. S., 3rd, et al. (2004). Gait Posture **19**(3): 263-9.

Williams, D. S., McClay, I.S., Hamill, J., Buchanan, T.S. (2001). J Appl. Biomech. **17**: 153-163.

THE EFFECTS OF BOTULINUM TOXIN A INJECTIONS TO THE HAMSTRINGS ON TEMPORAL-SPATIAL GAIT PARAMETERS IN CHILDREN WITH SPASTIC CEREBRAL PALSY

Edward J. Quigley, René van Wieringen, and Pam Versage

Shriners Hospitals for Children-Tampa, Tampa, FL, USA
E-mail: equigley@shrinenet.org
Web: http://www.shrinershq.org/Hospitals/Tampa/services/Motion_Analysis_Lab.aspx

INTRODUCTION

Injection of Botulinum Toxin A (BTX-A) is a common treatment for spasticity in children with cerebral palsy (CP). The efficacy of BTX-A injections to the gastrocnemius muscle has been examined extensively. These studies have included several randomized controlled trials (Corry et al., 1998, Sutherland et al., 1999, Koman et al., 2001). Comparatively, BTX-A injections for treatment of hamstring muscle spasticity and flexed-knee gait in children with CP has received much less attention.

Thompson et al. (1998) studied ten children with CP that walked with crouch gait. A computer model was used to determine the lengths of the hamstrings muscles during gait before and after BTX-A injections. They also measured gait kinematics and reported that knee extension improved by 13 to 15.6 degrees and walking speed increased from 0.60 ms^{-1} to 0.71 ms^{-1}.

Corry et al. (1999) examined ten children with CP before and after BTX-A injections to the hamstrings. They reported an increase in knee extension during stance of 8 degrees; however, this improvement only persisted for 12 weeks. They also noted that mean anterior pelvic tilt increased and the energy cost of walking was unchanged after the injections.

The purpose of this retrospective study was to determine if BTX-A injections to the hamstring muscles improves temporal-spatial gait parameters in children with CP who walk with a flexed-knee gait pattern.

METHODS

A retrospective review of patients examined in the Motion Analysis Laboratory before and after BTX-A injections to the hamstrings was completed. A total of 34 patients with spastic CP who walked with a flexed-knee gait pattern were evaluated. Twenty three of these patients also had injections to the gastrocnemius, two had injections to the rectus femoris, and two had injections to the adductors. The injections were bilateral in all but two of the patients. No surgical procedures were performed on any these patients concurrent with the injections. The mean age (sd) of the patients was 7.6 (3.5) years and the mean time (sd) of post-injection follow-up was 55.8 (17.4) days.

All of the data were captured with an optical motion measurement system (Motion Analysis Corporation) and temporal-spatial parameters were calculated using OrthoTrak gait analysis software. The patients walked at a self-selected speed in bare feet. Twenty one of the patients were also examined while wearing ankle-foot orthoses (AFO). Two-tailed paired t-tests ($p \leq 0.05$) were used to analyze the results.

RESULTS AND DISCUSSION

The pre and post-injection temporal-spatial parameters for barefoot walking and walking with AFOs are shown in table 1. Due to space constraints only data for the right side are reported. There were no substantive differences between the right and left side data. No significant differences before and after the injections were found except for a decrease in cadence after injections for the barefoot condition. Further examination of the data showed that for all parameters approximately half of the patients improved while half of the patients showed no change or worsened. The correlations between time to follow-up and degree of improvement for each parameter were also examined. No significant correlations were found.

SUMMARY/CONCLUSIONS

For this group of patients as a whole, injection of BTX-A to the hamstrings did not result in an improvement in temporal-spatial gait parameters. Examining the data patient-by-patient showed that nearly half of the patients showed improvement while the other half did not change or worsened. The time between the injection and follow-up assessment did not account for the variation in outcomes. It is possible that other factors may be important for determining which patients show a benefit from BTX-A injections to the hamstrings and which do not. These factors may include type and volume of physical therapy, overall functional level, age, body size, and/or injection protocol. Further examination is needed to more fully understand the large variation in patient response to this treatment.

REFERENCES

Corry, I.S. et al. (1998). *Gait & Posture*, **10**, 206-210.

Corry, I.S. et al. (1999). *J Pediatr Orthop*, **18**, 304-311.

Koman. L.A. et al. (2001). *Pediatrics*, **108**, 1062-1071.

Sutherland, D.H. et al. (1999). *Gait & Posture*, **10**, 1-9.

Thompson, N.S. et al. (1998). *Dev Med Child Neurol*, **40**, 622-625.

ACKNOWLEDGEMENTS

The authors gratefully acknowledge the assistance of Susan Angelos, Susan Bailie, Aimee Byrley, Erin Godin, Marilyn Harper, Tristan Seley, and Dionne Vernon.

Table 1: Pre and post injection temporal-spatial data for walking barefoot (n=34) and in AFOs (n=21) (mean± SD).

	Barefoot			AFO		
Parameter	**Pre Injection**	**Post Injection**	**p**	**Pre Injection**	**Post Injection**	**p**
Walking Speed (cm/s)	78.7 ± 22.9	78.0 ± 25.9	0.82	77.7 ± 25.8	74.8 ± 25.4	0.59
Cadence (step/min)	124.0 ± 23.8	116.6 ± 23.5	*0.05*	117.4 ± 17.5	112.2 ± 26.6	0.38
Stride Length (cm)	77.9 ± 21.0	80.6 ± 23.8	0.20	79.5 ± 23.1	79.6 ± 23.3	0.95
Step Length (cm)	39.4 ± 10.5	41.6 ± 16.2	0.33	39.2 ± 12.4	39.4 ± 10.6	0.91
Support (% of cycle)	56.9 ± 5.8	59.0 ± 5.5	0.52	56.8 ± 5.4	57.0 ± 5.9	0.90
Swing (% of cycle)	43.1 ± 5.8	41.0 ± 5.5	0.52	43.2 ± 5.4	43.0 ± 5.9	0.90
Double Support (% of cycle)	7.5 ± 4.2	7.0 ± 5.3	0.63	6.6 ± 4.5	7.1 ± 5.2	0.72

Lower Limb Synergy Patterns of Stroke Subjects While Walking in a Lokomat Robotic Orthosis

Nathan D. Neckel [1,2], Diane Nichols [2], Joseph M. Hidler [1,2]

[1] Catholic University of America, Washington, DC, USA
[2] Center for Applied Biomechanics and Rehabilitation Research (CABRR)
National Rehabilitation Hospital, Washington, DC, USA
E-mail: 06neckel@cua.edu, Web: http://cabrr.cua.edu

INTRODUCTION

Following stroke, some individuals couple joint torques into patterns that can be inappropriate for the desired task [S. Brunnstrom, 1970]. In the lower limbs these couplings, or synergies, are grouped into the extension synergy (hip, knee, and ankle extension, hip, knee, and ankle adduction) and the flexion synergy (hip, knee, and ankle flexion, hip, knee, and ankle abduction) [RL Waters et al, 1982]. In a coordinated multi-joint exercise such as walking, joint torques must be appropriately coupled at certain times throughout the gait cycle. To better understand gait impairments following stroke, the role of the classic flexor and extensor synergy patterns during the gait cycle should be investigated.

Comparing the torque patterns of stroke subjects to control subjects during gait has proven a difficult task due to the inability of many stroke subjects to provide consistent, repeatable, walking patterns in a conventional motion analysis laboratory. The Lokomat robotic orthosis (Hocoma AG, Volketswil, Switzerland) provides a means in which all levels of gait impaired subjects can be guided through an adjustable gait pattern while walking on a treadmill. When the Lokomat is fitted with 6 DOF loadcells and placed over an instrumented treadmill, this setup can be used to calculate the joint torque patterns of stroke and healthy subjects as they walk within the device [Hidler et al 2006].

Presented here is a comparison of how healthy and chronic hemiparetic stroke subjects combine their joint torques into synergy patterns throughout the gait cycle. Special consideration is given to the classic hemiparetic flexion and extension synergies and if their presence can contribute to gait impairments following stroke.

METHODS

Ankle, knee, and hip joint torque patterns in the sagittal and frontal planes were recorded and previously reported in 10 hemiparetic and 5 age matched control subjects as they walked within the Lokomat at 2.5 km/h with minimal body weight support [Neckel et al, 2007]. In order to identify lower-limb synergies, each subject's average joint torque pattern across the gait cycle was expressed as a percentage of that subject's maximum joint torque. This resulted in subject specific profiles of each of the 6 joint torques (e.g. ankle, knee, and hip – frontal and sagittal planes) ranging from 0 to 1 (min to max). Two joints were considered coupled whenever their sum was greater than 1.6 (i.e both torques are at 80% or one torque is at 100% and the second is at 60%). The average joint coupling strategies found in the left leg of healthy subjects was used as a basis to compare the average strategies found in both the impaired and unimpaired limb of the stroke subjects.

RESULTS AND DISCUSSION

Table 1 shows the 15 instances of joint torque coupling, or synergies, found throughout the gait cycle as healthy subjects walked in the Lokomat at 2.5 km/h and whether or not the synergy was found in the impaired or unimpaired limb of the stroke subjects.

Table 1: Synergies while in Lokomat.

Healthy Synergy		% gait cycle	Unimp	Imp
ankle inv	knee ext	17-22		
ankle ev	hip flx	47-52		
knee valgus	hip flx	47-52		
knee valgus	hip abd	17-22		
knee varus	hip add	90-100	✓	
ankle plant	ankle ev	47-52		
ankle plant	knee valgus	47-52		
ankle dorsi	hip ext	3-8	✓	
ankle plant	hip flx	47-52	✓	✓
ankle inv	knee valgus	17-22		
ankle inv	hip abd	17-22		
knee ext	knee valgus	17-22		
knee flx	knee varus	90-100		
knee ext	hip abd	17-22		
knee flx	hip add	90-100		

The first five torque couplings of Table 1 depict the classic flexor and extensor synergies normally associated with hemiparetic stroke. If stroke subjects tend to couple these torques in the impaired limb, even when it is inappropriate, one would expect that they would be present when it is appropriate in the gait cycle. However, as shown in Table 1, these synergies are not present in the impaired limb while stroke subjects walk in the Lokomat. The last ten torque couplings of Table 1 go against the classic flexor / extensor synergy patterns so it is of no surprise that the impaired limbs of the stroke subjects could not match the control subjects. Overall, more than half of the synergies exhibited by healthy subjects include the ankle, implying the significant ankle contributions to walking in the Lokomat. Even with the assistance of the Lokomat, stroke subjects have poor control of the impaired ankle so it may be unreasonable to expect a match with the control subjects in those synergies. Table 1 also highlights the inability of the unimpaired limb to match the synergy patterns employed by the control subjects. It is likely that this difference is due the unimpaired limb having to compensate for the impaired limb.

Synergy patterns employed by the stroke group, but not the control group, were also investigated and are shown in Table 2. It is of no surprise that the lone abnormal synergy pattern in the impaired limb follows the classic flexor /extensor synergy pattern.

Table 2: Abnormal Synergies

Unimpaired Limb		% gait cycle	classic flx/ext
knee flx	hip ext	3-8	
ankle inv	hip flx	47-52	
Impaired Limb			
ankle plant	ankle inv	33-38	✓

SUMMARY/CONCLUSIONS

After screening the torque coupling patterns of healthy and stroke subjects as they walk in the Lokomat it was found that neither the impaired nor unimpaired limbs behave like the healthy limb. This is surprising since the Lokomat promotes symmetric step patterns and offers the subject constant support.

REFERENCES

Brunnstrom, S. (1970). *Movement Therapy in Hemiplegia*. Harper and Row.

Waters, R.L., Frazier, J., Garland D.E. (1982). *J. Bone Joint Surg Am,* **64**, 284-8.

Hidler. J.M., Neckel, N.D. (2006). *Proceedings of IEEE EMBS'06*, 185-188.

Neckel, N.D., Hidler. J.M. (2007). *Proceedings of ICORR'07,* accepted.

EFFECT OF FELT AND RECOGNIZED EMOTIONS ON GAIT KINEMATICS

Melissa Gross[1], Elizabeth Crane[1] and Barbara Fredrickson[2]
[1]University of Michigan, Ann Arbor, MI, USA
[2]University of North Carolina, Chapel Hill, NC, USA
Email: mgross@umich.edu, Web: www.sitemaker.umich.edu/mgrosslab

INTRODUCTION

Although emotion is expressed through multiple physiological channels including voice, face, body, autonomic responses and subjective experience, relatively little is known about the biological expression of emotion in body movements. Typically, the effects of emotion on body movement have been studied in actors portraying emotions, and the emotion-related effects have been described only qualitatively, e.g., "heavy-footed" for angry gait (Montepare 1987). A biological basis for bodily expression is suggested by cross-cultural studies in which emotion is recognized in body movements (Hejmadi 2000) and by fMRI studies in which emotional body positions activate brain regions associated with perception of specific emotions (de Gelder 2006). The purpose of this study was to quantitatively describe the biological effects of felt and recognized emotions on body movements during walking.

METHODS

Forty-two undergraduates (22 female, 20 male; 20.1±2.7 yrs) recalled an experience from their own lives in which they felt two positive emotions (content and joy), two negative emotions (angry and sad), or no emotion at all (neutral). After recalling an emotion, participants walked across the lab (5 m) while video and whole body motion capture data (120 Hz) were acquired. To validate that the emotion was actually felt by the walker and not just portrayed, after each gait trial participants rated the intensity of 8 emotions (4 target; 4 non-target) using 5-item Likert scales. Only trials in which participants felt the target emotion with at least moderate intensity were included in the kinematic analysis.

To determine whether the walkers' felt emotions were recognizable in their body movements, video clips of the walkers with blurred faces were randomized and shown to 60 undergraduates (29 female, 31 male; 20.9±2.7 yrs). After viewing each video clip, observers selected one of 10 emotions (4 target, 4 non-target, neutral/no emotion, and none of the above) that they thought the walker experienced during the trial. A trial was recognized if the felt emotion agreed with the observer-selected emotion. A Chi square test was used to determine if agreement differed from chance levels (10%). A generalized linear mixed model with crossed random effects was used to model the binomial response variable (agreement) with a logit link. Fixed effects of emotion, walker gender, observer gender, and video sequence were tested. A linear mixed model with random walker effects and fixed effect of emotion was used to model the mean and range of motion of joint angles, velocity, stride length and cadence.

RESULTS

Walkers felt and observers recognized the same emotion in 140 of 210 gait trials (67%). Walkers felt the target emotions in more than 97% of trials (Table 1). On average, among the target emotion trials that were felt, sad was most recognized (73.8%)

and anger was least recognized (61.9%). Neutral trials were least felt (69%) because walkers reported feeling content at above-threshold levels in some trials. Recognition rates for each emotion depended on walker. The best recognition rates for individual walkers were 93.3%, 73.3%, 66.7%, 53.3% and 53.3%, for sad, anger, joy, content and neutral trials, respectively.

Gait velocity was greatest in high-activation emotion trials (anger and joy), and least in sad trials (Table 2). Velocity was not different among neutral and low-activation emotion trials (content and sad). Emotion-dependent velocity differences were due primarily to changes in cadence rather than stride length.

Both posture and limb motions changed with emotion. In sad trials, the neck was 6.2, 11.5, 10.6 and 9.7 degrees more flexed than in anger, joy, content and neutral trials, respectively. The shoulders were slightly but significantly elevated in sad compared to content and neutral trials (1.6 and 1.8 deg, respectively). Amplitude of arm swing was significantly reduced in sad trials compared to the other emotions. Shoulder and elbow ranges of motion were significantly less in sad (19.2 and 21.7 deg) than in anger (32.1 and 40.9 deg), content (26.5 and 32.2 deg) and joy (30.7 and 40.1 deg) trials. Hip flexion was slightly but significantly reduced in sad trials compared to anger, content or joy trials (2.6, 1.3, 2.2 deg, respectively).

Amplitude of elbow flexion was also greater in the high-activation emotion trials (anger and joy) than in neutral trials (29 and 3.3 deg, respectively). Among positive emotions, elbow amplitude was significantly less in content than in joy trials (2.5 deg).

CONCLUSIONS

Bodily expression of felt and recognized emotions was associated with emotion-specific changes in gait parameters and kinematics. Knowledge of emotion-related changes in gait provides a basis for better understanding of the biological relationship between emotion and body movements.

REFERENCES

De Gelder B. (2006). *Nature Reviews Neuroscience*, **7**, 242-249.

Hejmadi A., et al. (2000). *Psychological Science*, **11**, 183-187.

Montepare, J.M., et al. (1987). *J. Nonverbal Behavior*, **11**, 33-42

ACKNOWLEDGEMENTS

We thank Brady West for his assistance with the statistical analyses.

TABLE 1: Percent of gait trials that were felt and/or recognized

Trials	Anger	Content	Joy	Neutral	Sad
Felt (%)	100.0	97.6	100.0	69.0	97.6
Recognized (%)	61.9	73.8	66.7	83.3	76.2
Felt and Recognized (%)	61.9	71.4	66.7	57.1	73.8

TABLE 2: Effect of emotion on gait parameters.

Gait Parameter	Anger	Content	Joy	Neutral	Sad
Velocity (m/s)	$1.43^{a,b}$	1.23^{c}	$1.44^{c,d,e}$	$1.19^{a,d}$	$1.07^{b,e}$
Cadence (steps/minute)	$122.2^{a,b,f}$	$111.1^{c,f,g}$	$120.8^{c,d,e}$	$111.6^{a,d,h}$	$104.6^{b,g,e,h}$
Stride Length	1.40	1.33	1.42^{e}	1.28	1.24^{e}

Superscripts indicate significant pairwise differences ($p<0.05$)

OBJECTIVE BIOMECHANICAL MEASUREMENTS INDICATE LONGITUDINAL LEARNING EFFECT IN ROBOT-ASSISTED SURGERY

Irene H. Lee[1], Ka-Chun Siu[1], Bernadette Brown-Clerk[1], Dimitrios Katsavelis[2], Dmitry Oleynikov[2] and Nick Stergiou[1]

[1]HPER Biomechanics Lab, University of Nebraska at Omaha, Omaha, NE, USA
[2]Department of Surgery, University of Nebraska Medical Center, Omaha, NE, USA
E-mail: ilee@mail.unomaha.edu, Web: http://biomech.unomaha.edu

INTRODUCTION

Robot-assisted surgery is slowly changing the way that surgery is performed. Specifically, in 2005 there were more than 300 da Vinci™ robotic surgical systems (dVSS; Intuitive Surgical, Inc., Sunnyvale, CA) worldwide. Robot-assisted surgery is primarily used because it provides various benefits over manual laparoscopic surgery, such as binocularity with 3D visualization, increased precision, and enhanced surgical dexterity (De Ugarte et al., 2003). However, research on quantifying the improvement of surgical dexterity and how novices learn to use these robotic instruments is limited. The aim of this study is to present the longitudinal learning curve throughout the training regimen using objective biomechanical measures to evaluate performance and learning effect for a robotic surgical task. A learning curve provides an assessment tool to examine the improvement of surgical performance (Kaul et al., 2006). We combined this assessment tool with objective biomechanical measures to evaluate training proficiency. In order to measure and specifically describe the smoothness of trainees' movements, we selected the kinematic measures speed and path curvature. Both speed and path curvature have been identified as valid objective measures (Judkins et al., 2005) to quantitatively examine robotic surgical performance.

METHODS

Nine right-handed novice users (1st and 2nd year medical students and graduate students; age of 29.5 ± 7.8) with basic surgical knowledge were recruited to participate in this study on two consecutive days. On both training days, each participant passed a surgical needle through ten designated points ten times. Participants required to pass the needle accurately along an inanimate material in the horizontal plane using two dVSS laparoscopic graspers. The material was flexible and required the participant to stabilize the opposite side with one grasper while passing the needle through the material with the other grasper. This needle passing task mimics an actual laparoscopic skill that requires significant bimanual coordination. Proficiency was evaluated with kinematic measures derived from the dVSS graspers and collected using the Application Programmer's Interface implemented in LabView 8.0 (National Instruments, Inc., Concord, MA). To quantify the nature of the participants' performance, time to task completion, total traveling distance, speed, and path curvature were calculated for each trial using MatLab. Paired t-tests were used to compare the first trial of the first training day and the tenth trial of the second training day (the 20th trial overall) for all objective measurements. Nonparametric statistical analysis with a Wilcoxon signed-rank 2-sided test was used, because we could not assume normality of

the measurements. The significance level was set at $p < 0.05$.

RESULTS AND DISCUSSION

Across all trials, time task to completion decreased significantly between the 1st and 20th trial (Figure 1). Total distance traveled gradually decreased and the difference between the 1st and 20th trial was significant (Figure 2). The average speed significantly increased between the 1st and 20th trial (Figure 3). Since the path curvature was not normally distributed, the medians of the 1st and 20th trial were compared (Table 1). The smaller range of path curvature of the 20th trial indicated that the trainees' movements became straighter and smoother.

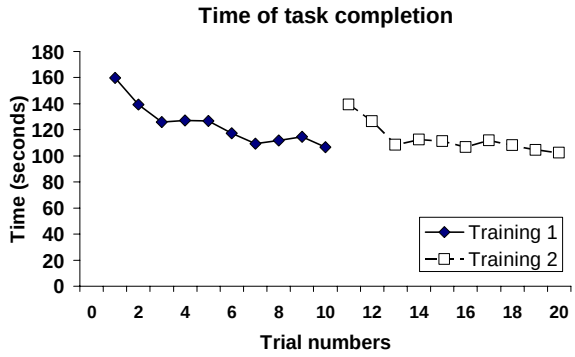

Figure 1: The learning curve for the time of task completion (TTC).

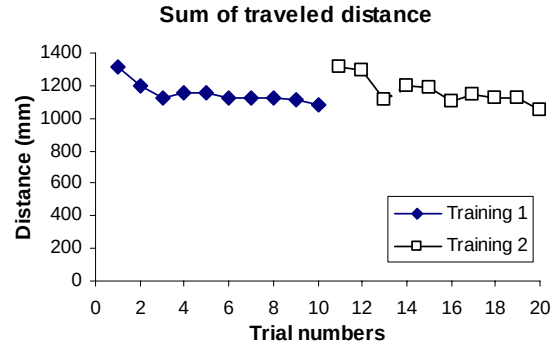

Figure 2: The learning curve for the sum of traveled distance.

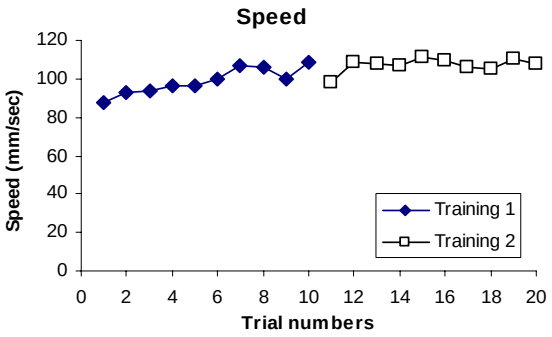

Figure 3: The learning curve for speed.

SUMMARY/CONCLUSIONS

We found that objective biomechanical measures, specifically kinematics, indicate longitudinal training improvements of robotic surgical performance after a short and intensive training program. Such measures can be used to evaluate surgical proficiency and learning of fundamental surgical skills in a robot-assisted environment. These findings provided further evidence of a robotic surgery learning curve which can be used to develop a clinically relevant training evaluation.

REFERENCES

De Ugarte, D. A. et al.(2003). *Surg Endo*, **17**, 960-963.

Kaul S, et al. (2006). *Curr Urol Rep*, **7**, 125-129.

Judkins, T. N. et al. (2005). *Stud Health Technol Inform*, **119**, 243-248.

ACKNOWLEDGEMENTS

This study was supported by the NIH, NIDRR, and the Nebraska Research Initiative.

Table 1: Path curvature (range of the median for nine subjects).

	1st trial	20th trial	***p*-value**
Path Curvature (m^{-1})	92.72 - 297.43	81.12 – 267.28	0.021

A Rigid Body Model of a Lacrosse Shot Underestimates Measured Ball Velocities

Joseph Crisco, Ph.D., Michael Rainbow, B.S., Eileen Wang

Bioengineering Laboratory, Department of Orthopaedics,
Brown Medical School/Rhode Island Hospital, Providence, RI, USA
E-mail: joseph_crisco@brown.edu, Web: www.brownbiomechanics.org

INTRODUCTION

Lacrosse is the fastest growing sport in the U.S. and has seen a revolution in equipment design over the past two decades. Different stick designs have been shown to affect ball speed and angle of release (Livingston, 2006). However, the precise mechanism underlying the shot is not known. The purpose of this study is to determine if ball speed can be fully explained by modeling the stick as a rigid body. Accordingly, we hypothesized that ball speed would equal stick tip speed at release.

METHODS

Three lacrosse shots were collected for each of 15 male lacrosse players (age 21 ± 4 yrs) at skill levels ranging from high school to college varsity in this IRB exempt study. The kinematics of the stick and ball were collected at 250 Hz using a passive, four camera Vicon MX system. A calibration frame was collected on two different stick models: an Assassin (AM) and a Ripper (BM) (Shamrock Lacrosse, East Hanover NJ). Prior to calibration, each stick was outfitted with 7 retro-reflective markers (**Fig 1**). Rigid body transforms were generated from the calibration frame to each shot frame using the method of Soderkvist and Wedin in Matlab (Mathworks, Natick MA). The time of release was the time when the stick tip and ball were closest. Tip and ball velocities were calculated at release by differentiating the position data with respect to time using a central difference technique. The angle of the shaft with horizontal (β), the angle between the ball path and stick shaft (α), and the angle between the tip velocity and stick shaft were also calculated at release (**Fig 2**). A paired t-test was used to evaluate the differences between ball speed and stick tip speed. A two-way RM ANOVA was used to determine the significance of the differences between stick models for variables listed in Table 1.

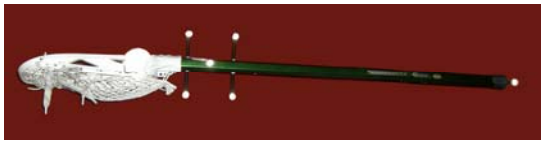

Figure 1: Retro-reflective markers were applied to the top of the head and bottom of the shaft. A 5-marker tracking cluster was rigidly attached to the shaft such that visibility was maximized in the plane of the shot.

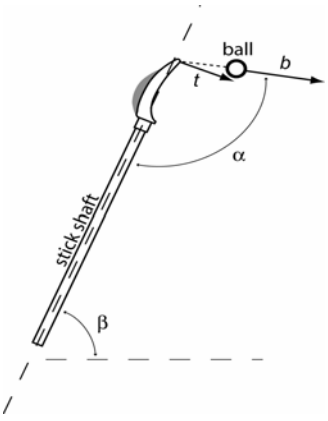

Figure 2: Lacrosse stick variables. *t* = tip velocity vector, *b* = ball velocity vector, α = ball-shaft angle, ß = shaft-horizontal angle.

RESULTS AND DISCUSSION

Ball shot speeds with both sticks were notably and significantly ($P<0.01$) faster than stick tip speed at the time of release. Examining **Fig. 3**, we postulate that at any given stick speed there is an optimal ball

speed, which is stick specific. This postulate arises from the observation that there is a non-normal distribution of ball speeds at each stick speed: data are dense near this optimal ball speed, with a distribution of ball speeds below this value. These lower ball speeds are considered to be shots with sufficient stick speed but with non-optimal stick technique. Ball shot speeds ranged from 55 to 85 mph. In this range, optimal ball speeds with stick AM were approximately 10 mph greater than the stick tip speed, while ball speeds with stick BM were almost 12 mph greater than the stick tip speed.

In comparing the two types of sticks directly (**Table 1**), we found that ball shot speeds with stick BM were significantly ($P < 0.01$) faster than those with stick AM by a mean difference of 2.4 mph. There was no difference in the average stick speed. Shots with stick AM were released on average with the shaft of the stick nearly vertical, while shots with stick BM were released differently ($P<0.01$) at approximately 8 degrees past vertical. Associated with this significant difference in the shaft angle was a significant difference in the angle of the path of the ball with respect to the shaft, by about 4º. The ball path was approximately 90º relative to the shaft of stick AM and approximately 94º relative to the shaft of stick BM. At the time of release the velocity of the tip was not different with stick model and was approx. 77º.

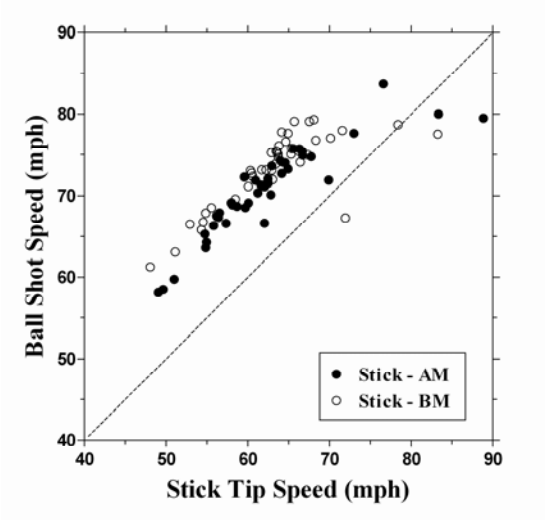

Figure 3: Both sticks shot the ball at speeds significantly greater than the speed of the tip of the stick (dashed line). Ball speeds with stick BM were on average approx. 2.5 mph faster than those with stick AM.

SUMMARY/CONCLUSIONS

This data suggests that the faster shots with stick BM were associated with a release at a later time in the complete shot cycle. Since the target was the same, the ball released at a flatter angle with stick BM. At this time, it is unclear as to why shots with stick BM were faster.

REFERENCES

[1] Livingston L.A. (2006). *J Sci Med Sport*, **Aug,** 299-303

ACKNOWLEDGEMENTS

We gratefully acknowledge Shamrock Lacrosse for providing the lacrosse equipment, Vicon for providing the motion capture system, and US Lacrosse for finical support. The opinions expressed in this abstract are those of the authors and do not necessarily reflect those of US Lacrosse.

Table 1: Average values (± SD) for 85 shots with 15 players. (* significant difference between stick models.)

Stick	**Ball Shot Speed (mph)**	**Stick Tip Speed (mph)**	**Stick Shaft Angle at Release (deg.)**	**Ball - Shaft Angle at Release (deg.)**	**Stick Tip Vel. - Shaft Angle at Release (deg)**
AM	70.8 ± 5.4 *	62.3 ± 7.8	90.3 ± 7.6 *	90.4 ± 5.3 *	76.9 ± 3.0
BM	73.2 ± 4.6 *	63.3 ± 6.8	82.1 ± 9.1 *	94.5 ± 7.2 *	77.4 ± 3.5

CAN INTERVERTEBRAL KINEMATICS PREDICT CLINICAL OUTCOME OF LUMBAR DISCECTOMY?

Soo-An Park, Nathaniel Ordway, Jerry Calabrese, Hansen Yuan, and Amir Fayyazi

SUNY – Upstate Medical University, Syracuse, NY, USA
E-mail: parkso@upstate.edu

INTRODUCTION

Discectomy has been used for the treatment of lumbar disc herniation for more than 50 years, but it still remains controversial due to the residual or recurrent low back pain (LBP) following the surgery. Retrospective clinical studies have suggested some reasons (young patient with preoperatively advanced disc degeneration, postoperatively decreased disc height), but it is not definitive.

Kinematic effects of lumbar discectomy have been investigated *in vitro*. Previous biomechanical studies have demonstrated significant increases in motion when comparing discectomy to an intact spine. However, there is limited clinical information published in the literature to support *in vitro* findings due to the lack of accuracy of standard radiographs.

The purpose of this prospective study was to determine the progress of *in vivo* segmental motions during lumbar sagittal and axial plane movements following discectomy using radiostereometric analysis (RSA) and examine if there was a relationship to clinical outcome.

Two questions were examined with this study: 1) what is the amount of motion that occurs *in vivo* in relation to the lumbar discectomy over time; 2) would this change be related with the clinical outcome?

METHODS

Following approval by the Institutional review board, eight patients (4 males & 4 females, ages: 40.9 ± 5.7 yrs) with lumbar disc herniation were scheduled to undergo lumbar discectomy at either L4/L5 or L5/S1 and enrolled in the study. Informed consent was obtained. The standard lumbar microdiscectomy procedure was performed by the three different surgeons. Following the discectomy, three or four tantalum beads were inserted into the upper and lower vertebrae adjacent to the involved disc.

The patients were followed post-operatively at 1 month (8 patients) and 1 year (4 patients). Standardized standing neutral, flexion, extension, left/right axial rotation biplanar films were collected at each time point of follow-up. Three dimensional segmental motions were determined for each position relative to neutral using RSA. In addition to the kinematic analysis, Oswestry Disability Index (ODI) was collected at each follow-up time point.

The three dependent variables (segmental sagittal rotation (SR), superior/inferior (SIT), and anterior/posterior (APT) translations) for each sagittal motion (neutral (N) to flexion, N to extension, and extension to flexion) were submitted to a 3 × 2 (sagittal motions × time points) MANCOVA with repeated measures on both factors and ODI criteria (ODI at 1 year < 50%, ODI >= 50%) as a covariate. Due to the limited number at follow-up, the three dependent variables (axial rotation, APT, right/left translation) for the right or left

axial motion were submitted to one-way (2 time points) MANCOVA with ODI criteria as a covariate.

RESULTS AND DISCUSSION

MANCOVA and follow-up tests demonstrated that SIT (p=0.001) and APT (p=0.041) significantly decreased from 1 month to 1 year, and SIT from extension to flexion was significantly greater than that from N to extension (p=0.014) (Table 1).

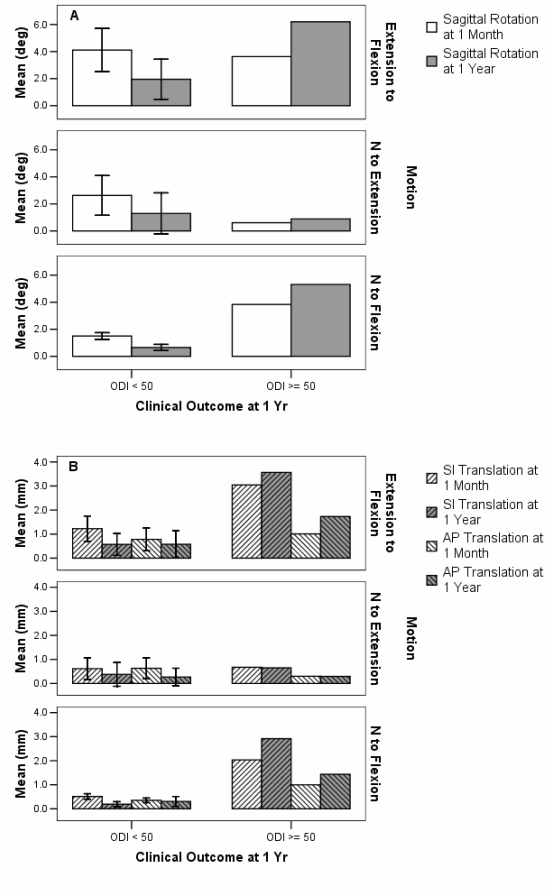

Figure 1: Intervertebral kinematics of lumbar discectomy over time, grouped with ODI at 1 year. **A:** sagittal rotation, **B**: sagittal translations.

There were significant interactions on time × covariate for SIT (p=0.001) and APT (p=0.043) and motion × covariate for SR (p=0.047) and SIT (p=0.015). Contrast procedures identified that SIT and APT decreased at 1 year time point in low ODI group, but those increased in high ODI group (Figure 1). And SR and SIT from extension to flexion were greater than those from N to extension in high ODI group, while those were not in low ODI group.

Analysis of axial rotation showed there was no significant difference over time. Absolute amount of one sided (right or left) axial rotation was measured at 0.2 ± 0.2° at 1 month and 0.3 ± 0.2° at 1 year.

SUMMARY/CONCLUSIONS

In vivo kinematics of the lumbar motion segment following microdiscectomy can accurately be measured using the RSA technique. In our small sized sample, the segmental motion decreased over time up to the 1 year time point following lumbar discectomy. The only exception was in the patient who reported a worse clinical outcome. A larger patient group is needed to conclude the distinct relationship between segmental motion and clinical outcome.

ACKNOWLEDGEMENTS

This study was partially supported by DuPuy Spine, Inc. (Raynham, MA).

Table 1: Dependent variables with significant main effects for time (*) and motion factor (+) (mean ± SD).

Time	1 Month			1 Year		
Motion	**N to Flex**	**N to Ext**	**Ext to Flex**	**N to Flex**	**N to Ext**	**Ext to Flex**
SR (°)	2.1 ± 1.2	2.1 ± 1.6	4.0 ± 1.3	1.8 ± 2.3	1.2 ± 1.3	3.0 ± 2.4
SIT (mm)	0.89 ± 0.77	0.63 ± 0.37^{*+}	1.68 ± 1.01^{*+}	0.87 ± 1.36	0.45 ± 0.43^{*+}	1.32 ± 1.54^{*+}
APT (mm)	0.51 ± 0.33	0.55 ± 0.39*	0.84 ± 0.4*	0.59 ± 0.59	0.28 ± 0.3*	0.87 ± 0.74*

SR (sagittal rotation), SIT (sup./inf. Translation), APT (ant./post. Translation), N (neutral), Flex (flexion), Ext (extension)

EFFECTS OF RETRO LOCOMOTION ON LUMBOPELVIC MOVEMENT AND IMPACT ATTENUATION IN ATHLETES WITH LOW BACK PAIN

Anthony J. House, Janet S. Dufek, Brent C. Mangus, and John A. Mercer

University of Nevada, Las Vegas – Las Vegas, NV
E-mail: housea3@unlv.nevada.edu

INTRODUCTION

The American Academy of Orthopaedic Surgeons (*www.aaos.org* 2006) states that almost every person in our society will have at least one episode of low back pain (LBP) at some time in his or her life. Certified Athletic Trainers have worked with athletes to help alleviate LBP for years. Intervention techniques often include specific therapeutic modalities and techniques which are both costly and not readily available to the patient outside of well-equipped clinics and rehabilitation facilities. Clinicians in many different medical fields have sought alternative solutions to help patients alleviate LBP. Anecdotally, backward walking (retro locomotion) seems to be an effective alternative solution. During retro locomotion, the heel strike associated with ground contact is replaced by initial forefoot contact (Bates and Dufek, 2001), potentially manifesting altered impact attenuation (IA) and lumbopelvic movement to alleviate pain associated with vertebral pressures and gait asymmetries.

The purpose of this investigation was to explore the efficacy of a retro locomotion intervention program on the alleviation of LBP in the athletic population. We hypothesized that the incorporation of retro locomotion as an intervention would reduce patients' self-reported pain measures, increase walking velocity, modify IA characteristics, and increase range of motion (ROM) at the low back/pelvis.

METHODS

Division I athletes experiencing LBP in the past 8 months and electing to allow the LBP to resolve without physician intervention volunteered (n=5, age=21.2±5.1yrs, ht=172.8±7.3cm, wt=68.5±7.7kg). Responding volunteers were asked to report to the Sports Injury Research Center Biomechanics Laboratory, were given verbal and written study participation information and were asked to sign an informed consent to participate form, as approved by the Biomedical Institutional Review Board at the University of Nevada, Las Vegas. Athletes with acute lower extremity injuries or abnormalities (true leg-length discrepancy > 2cm) were thanked and excused. Subjects participated in supervised intervention sessions tri-weekly for three-weeks. Sessions consisted of walking backward on a treadmill at preferred pace for fifteen minutes per session. Data collection was performed pre- and post-intervention while walking backward on a treadmill, at a subject-preferred speed. Pre-post testing included collection of self-reported pain rating (1-10 scale), preferred backward walking velocity, maximum impact acceleration values using uniaxial accelerometers secured bilaterally on the distal anteromedial tibia and on the forehead. The maximum impact values measured with the accelerometers were used to calculate IA [1-(Head Peak/LegPeak) x 100] for 10 right-foot contacts and 10 left-foot contacts. A biaxial electrogoniometer was implemented to collect and calculate

sagittal and coronal ROM of the lumbopelvic region (T12-S2) between right leg strides. Data were collected at a *fs*=1000Hz and smoothed using a 4th-order Butterworth filter with a *fc*=20Hz.

Dependent t-tests were utilized to evaluate pre-post self-reported pain rating, walking velocity, and lumbopelvic ROM. A 2 (pre-post) x 2 (limb) repeated measures ANOVA was utilized to evaluate bilateral IA. Single subject Model Statistic analyses (Bates et al., 2004; Dufek et al., 1991) were also performed to evaluate individual subject's IA and lumbopelvic ROM characteristics for right leg strides. Statistical analyses used a 95% confidence interval.

RESULTS

A significant decrease in self-reported pain rating (pre=3.2±1.3, post=2.0±1.0, p=.004) for the group was identified along with a significant increase in backward walking velocity (pre=1.14±0.13 m/s, post=1.39±0.11 m/s, p=.003). There were no other significant group results observed.

Single subject results identified a significant decrease in IA for 4 of 5 subjects, while a significant increase in sagittal and coronal ROM was observed for 3 of 5 subjects.

SUMMARY/CONCLUSIONS

Results agree with anecdotal reports that a retro locomotion intervention serves as an alternative exercise modality for aiding athletes to cope with LBP. Upon further evaluation, the decrease in IA post-intervention was attributed to an increase in head impact under similar leg impact characteristics. This indirect measure may reflect a decrease in potential impact energy absorbed within the low back and a reduction in potential axial loading of the lumbar spine. Also, subjects with increased lumbopelvic ROM pose an increased potential for opening of facet joints and coincidently a reduction in potential vertebral pressures. It appears that the retro locomotion intervention may relieve LBP and concomitant spinal rigidity associated with the pain-spasm cycle.

It is apparent that individual results may vary based upon specific etiology, illustrated when reviewing results of the group analysis vs. the single subject analysis. Due to a limited number of subjects, varied performance outcomes, and varied responses to the intervention, no significant differences in IA or ROM were demonstrated for the group. However, the single subject analysis detected significant differences. Of note is the fact that during the 3 week retro locomotion intervention, athletes continued regular sport participation and treatment. Retro locomotion was introduced as a supplement to various on-going treatments uncontrolled by the research team. Investing efforts for further research into the therapeutic implications of retro locomotion for LBP is encouraging and is warranted.

REFERENCES

American Academy of Orthopaedic Surgeons website: *www.aaos.org*.

Bates B.T. et al. (2004). Single Subject Analysis. Innovative Analyses of Human Movement, (N. Stergiou, Ed.), 5-28.

Bates, B.T. and Dufek, J.S. (2001). *The Backwards Strides*, 84-86.

Dufek J.S. et al. (1991). *MSSE,* **23**(9): 1062-1067.

ACKNOWLEDGEMENTS

Partial funding provided by a grant from the Far West Athletic Trainers' Association Research and Grants Committee.

CENTER OF MASS AND ANKLE INCLINATION ANGLES DURING WALKING: AN ALTERNATIVE DETECTION OF GAIT INSTABILITY

Chu-Jui Chen and Li-Shan Chou

Department of Human Physiology, University of Oregon, Eugene, Oregon USA
E-mail: chou@uoregon.edu, Web: biomechanics.uoregon.edu/MAL/index.html

INTRODUCTION

Instantaneous inclination angles between the whole body center of mass (COM) and center of pressure (COP) during gait were reported to detect gait instability in the elderly [1]. Accurate calculation of the COP requires a single foot placement on each force plate. However, many studies indicated that older adults, especially fallers, walk with a significantly smaller step than young adults [2,3]. Such gait modification and inter-trial inconsistency of this population greatly increase difficulty in obtaining a clean foot placement on the force plate, which will hinder the calculation of COM-COP inclination angles. Therefore, the purpose of this study was to find an alternative parameter, similar to COM-COP inclination angles, for assessing instantaneous alignment between COM and base of support during gait without the concern of the subject's ability in making proper foot contacts with the force plate. Effectiveness to identify patients with imbalance using the inclination angle formed by the lateral ankle marker and COM during gait was assessed in this study.

METHODS

Eight elderly patients with gait imbalance (mean age = 78.3 ± 5.8) and eight healthy elderly controls (mean age = 77.5 ± 6.2) were recruited for this study. Subjects were asked to walk on a level surface with self-selected pace while barefoot. Whole body motion was captured with an 8-camera motion analysis system (Motion Analysis Corp., Santa Rosa, CA). A total of 29 markers were placed on the subject's bony landmarks [4]. Two force plates (AMTI, Watertown, MA) were used to collect ground reaction forces for the calculation of COP. Inclination angles of the lines formed by the COM and lateral ankle marker as well as by the COM and COP were computed for each frame during the single stance phase of gait. The effect of subject group on the average medial and peak anterior inclination angles during the time period were assessed using the *t*-test with an α level of 0.05.

RESULTS AND DISCUSSION

Representative profiles of the medial and anterior-posterior inclination angles during the single support phase from a patient and a healthy subject were shown in Fig. 1 and Fig. 2. COM-Ankle medial inclination angles were consistently greater than COM-COP inclination angles. Average medial COM-Ankle and COM-COP inclination angles of imbalance patients were 6.4˚ ± 0.8˚ and 4.4˚ ± 0.9˚, respectively. Average medial COM-Ankle and COM-COP inclination angles of healthy individuals were 5.3˚ ± 0.8˚, and 2.6˚ ± 0.9˚. Imbalance patients were found to display a significantly greater medial inclination angle than healthy elderly ($p=0.025$ for COM-Ankle angle; $p=0.002$ for COM-COP angle; Fig.3).

Compared to the medial COM-COP inclination angle, it is reasonable to expect the medial COM-Ankle inclination angle to be greater due to the lateral ankle marker's locations.

Peak anterior COM-Ankle and COM-COP inclination angles of imbalance patients were 18.7˚ ± 3.6˚ and 9.2˚ ± 1.8˚. Peak anterior COM-Ankle and COM-COP inclination angles of healthy individuals were 23.4˚ ± 2.4˚, and 11.6˚ ± 2.9˚. Healthy individuals were found to have significantly greater peak anterior inclination angles than patients ($p \leq 0.001$ for COM-Ankle angle; p=0.002 for COM-COP angle).

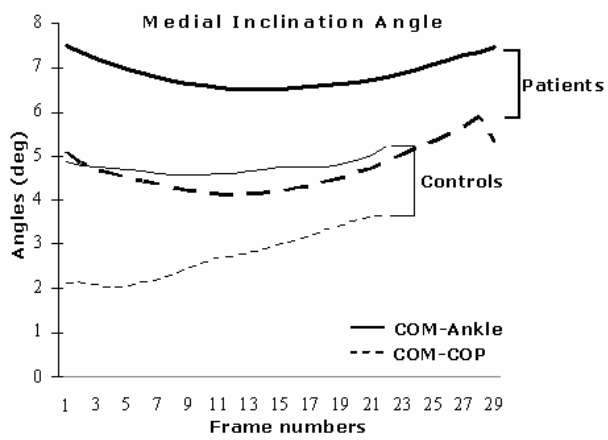

Figure1. Medial inclination angles during the single stance phase.

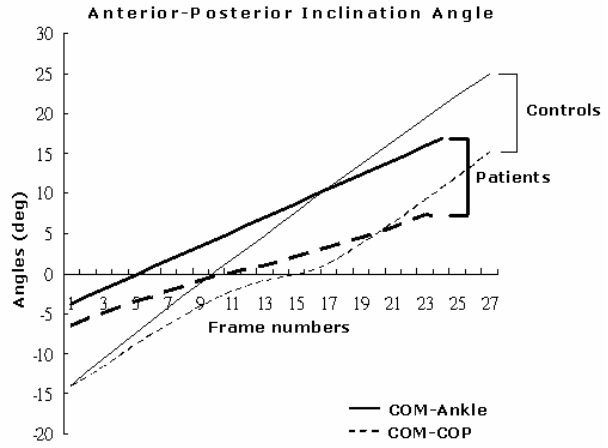

Figure2. Anterior-posterior inclination angles during the single stance phase.

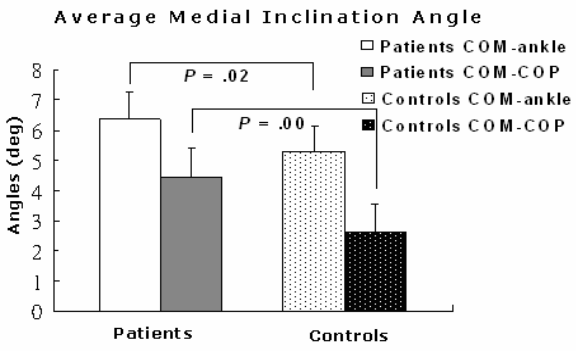

Figure3. Mean medial inclination angles during the single stance phase.

Findings from this study demonstrated that COM-Ankle inclination angles during the single stance phase, similar to the COM-COP inclination angles, could successfully distinguish patients with gait imbalance. Calculation of the COM-Ankle inclination angle will not require the subject's proper foot placement on the force plate, which could be a more suitable assessment to clinical populations.

SUMMARY/CONCLUSIONS

The COM-Ankle inclination angles during single stance phase are effectiveness to identify patients with imbalance.

REFERENCES

Lee, H.J., Chou, L.S. (2006). *APM&R* 87, 569-575.

Judge, J., et al. (1995). *Gait and Posture* 3(2), 81-81(1).

Mbouroua, G.A., et al. (2003). *Gerontology* 49, 21-26.

Hahn, M.E., Chou, L.S. (2004). *J Biomech* 37, 837-44.

ACKNOWLEDGEMENTS

Technical assistance from Vipul Lugade is greatly appreciated.

DECREASED KNEE FLEXION DURING LANDING INCREASES FRONTAL PLANE LOADING OF THE KNEE

Christine D. Pollard[1], Susan M. Sigward[1], and Christopher M. Powers[1]

[1]University of Southern California, Los Angeles, CA, USA
E-mail: cpollard@usc.edu, Web: http://pt.usc.edu/ACLprojectprevent/

INTRODUCTION

Female athletes have been reported to have a 4 to 6 greater chance of tearing their anterior cruciate ligament (ACL) than their male counterparts (Arendt et al., 1995). It has been theorized that the number of ACL injuries in female athletes is due to gender related differences in the performance of athletic activities. Investigations of gender differences in knee joint kinematics have revealed that, when compared to males, females demonstrate decreased knee flexion and increased knee valgus during landing and cutting. Hewett et al. (2005) has found both knee valgus motion and moments to be predictors of ACL injury. In general, the knee joint mechanics exhibited by females are thought to place them at a greater risk of ACL injury.

It has been proposed that females lack the strength and/or neuromuscular control of the sagittal plane musculature (i.e. hip and knee extensors) to effectively decelerate the body center of mass during landing and cutting tasks. More specifically, it is thought that females limit the amount of knee flexion during dynamic tasks, and instead, rely more on their passive restraints in the frontal plane (i.e. ligaments) to control these tasks (Hewett et al., 2002).

The purpose of this study was to examine differences in frontal plane kinematics and kinetics at the knee between females who exhibit "high knee flexion" angles and those who exhibit "low knee flexion" angles during landing.

METHODS

Subjects consisted of 43 healthy female club soccer players ranging in age from 11 to 17 years (average age 13.5 yrs). Three-dimensional kinematics (eight camera Vicon motion analysis system, 250 Hz) and ground reaction forces (AMTI, 1500 Hz) were collected while each subject performed a drop landing task from a height of 46 cm (3 trials). Kinematics and net joint moments at the knee (normalized by body mass) were calculated using inverse dynamics equations (Visual 3D^{TM} software).

In order to compare frontal plane knee kinematics and moments between subjects who utilized "high knee flexion" angles during landing versus those who exhibited "low knee flexion" angles, subjects were divided into groups based on their peak knee flexion angle during the landing task. Subjects who exhibited a peak knee flexion angle 0.5 standard deviation above the overall group average peak knee flexion angle of 92° were assigned to the "high knee flexion" group and those who exhibited a peak knee flexion angle 0.5 standard deviation below the overall group average were assigned to the "low knee flexion" group. Using this criteria 10 subjects were placed in the "high knee flexion" group (average peak knee flexion angle = 110°) and 12 were placed in the "low knee

flexion" group (average peak knee flexion angle = 78°).

Variables of interest included the peak knee valgus angle and peak knee valgus moment during the deceleration phase of landing. Differences between groups were evaluated using independent sample t-tests. Statistical analyses were performed using SPSS statistical software (Chicago, IL). Significance levels were set at $P \leq 0.05$.

RESULTS AND DISCUSSION

On average, subjects in the "low knee flexion" group demonstrated increased peak knee valgus angles (7.0° vs. 2.2°; $P<0.01$) and increased peak knee valgus moments (-0.56 vs. -0.36; $P=0.02$) when compared to subjects in the "high knee flexion" group. (Figure 1).

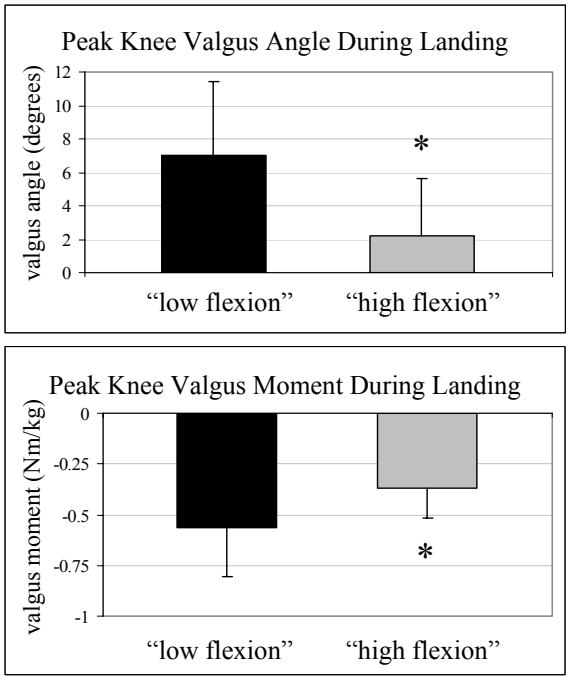

Figure 1: Comparison of frontal plane knee kinematics and kinetics between subjects who demonstrate "low flexion" and "high flexion" knee angles during landing.

Our data indicate that individuals who utilize greater sagittal plane knee motion demonstrate less loading at the knee in the frontal plane. This finding is important since it has been shown that individuals who exhibit increased knee valgus angles and moments are at a greater risk of ACL injury. These results support the premise that females who limit deceleration in the sagittal plane may employ a strategy of absorbing impact in the frontal plane during landing.

The current study provides support for the underlying framework of numerous ACL injury prevention programs which train females to land with increased sagittal plane motion (Hewett et al., 1999). This emphasis may increase sagittal plane strength and control as well as deter individuals from relying on their passive restraints.

SUMMARY/CONCLUSIONS

Individuals who utilize "low knee flexion" angles during landing exhibit increased peak knee valgus angles and valgus moments compared to those who utilize "high knee flexion" angles. Future work is needed to better understand the underlying reason for this particular movement strategy.

REFERENCES

Arendt, E., Dick, R. (1995). *Am J Sports Med,* **23** 694-701.

Hewett, T.E. et al. (1999). *Am J Sports Med,* **27**, 699-706.

Hewett, T.E. et al. (2002). *Clin Orthop,* **402**, 76-94.

Hewett, T.E. et al. (2005). *Am J Sports Med,* **33**, 492-501.

ACKNOWLEDGEMENTS

This study was funded by the National Institutes of Health (R01 AR053073-02).

RELATIONSHIP OF MUSCLE ACTIVITY TO FATIGUE DURING HIGH-POWER EXERCISE

Brian K. Schilling[1], Loren Z.F. Chiu[2], Andrew C. Fry[3], Robyn Karlage[1], George J. Salem[2]

[1] Exercise Neuromechanics Laboratory, The University of Memphis
[2] Biokinesiology and Physical Therapy, The University of Southern California
[3]Health, Sport and Exercise Sciences, The University of Kansas
Email: bschllng@memphis.edu Web: https://umdrive.memphis.edu/g-HSS/TENMDL/

INTRODUCTION

The purpose of this investigation was to study the relationships between neuromuscular phenomena and acute performance responses during resistance exercise. Acutely, resistance exercise results in either a short-term increase (potentiation) or decrement (fatigue) in performance. Physiologically, a number of mechanisms are speculated to contribute to these acute responses. While well-studied in animal models, the relationships between these physiologic mechanisms with potentiation and fatigue are less studied in humans, particularly during complex multi-joint tasks. The frequency spectrum of the electromyogram has been suggested to be an indicator of the fatigue associated with exercise (Bilodeau et al. 2003). Although several mechanisms are suggested, a leftward shift in the frequency spectra could be due to a decreased recruitment of type II motor units as a result of fatigue.

Since the clean and the clean pull are commonly performed by athletes as a training and competition exercise, they are useful for examining the interaction between potentiation and fatigue over the course of an exercise bout.

METHODS

Men (n=9) voluntarily participated in the investigation subsequent to providing written informed consent as approved by The University of Memphis Institutional Review Board. All participants had experience performing the clean and clean pull exercise, and self-reported their one repetition maximum (1 RM) clean, which was verified from competition records and/or training logs. Subjects performed a warm-up consisting of clean pulls at 50%, 70% and 90% of their 85% 1 RM clean followed by three maximal-effort repetitions in the clean pull exercise at 85% 1 RM. These maximal-effort repetitions were repeated for a total of 15 sets, with approximately four minutes between sets. A digital video camera (Model PV-DV203; Panasonic, Secaucus) was positioned perpendicular to the frontal plane, 10 m in front of the lifting platform. Reflective tape was placed around the center of the barbell and the shutter speed set at 1/100 s. Digital video data were collected (60 fields per second) and analyzed using Datapac 2K2 version 3.17 (Run Technologies, Mission Viejo). Reflective markers were automatically digitized to yield XY coordinates. From the vertical coordinates (Y-), average power during the second pull was determined (Garhammer 1993).

During the four minute between-set interims, subjects performed maximal effort isometric pulls in a rack designed to mimic the position in the top part of the clean pull. Force was sampled at 1000 Hz with Datapac 2K2 and low-pass filtered at 50 Hz. Disposable bipolar EMG electrodes were placed bilaterally on the subjects' lateral

gastrocnemius, lateral hamstring, vastus lateralis, and lumbar erector spinae muscles. Muscle electrical activity was recorded using the Myopac EMG System (Runtech; Mission Viejo, CA). EMG data were collected simultaneously with force and digitally band-pass filtered at 20-500 Hz, and Fast Fourier Transformed to obtain mean and median frequency. Mean and median frequencies were summed across all muscle groups.

All data (barbell power, mean & median frequency) were normalized to the first set of exercise and expressed as a percentage. Thus, a value greater than 100% indicated potentiation, whereas a value less than 100% indicated fatigue.

RESULTS AND DISCUSSION

The minimum % value (i.e fatigue) was correlated between barbell power in the second pull with mean (r=0.684; p=0.042 and median EMG frequency (r=0.713; p=0.031) during the rise phase of the isometric force-time curve (Figure 1).

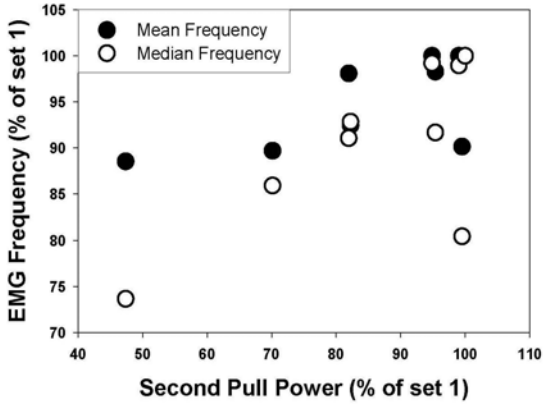

Figure 1. The mean and median frequency versus power for the clean pull.

This suggests that the mechanisms responsible for a leftward shifting of the EMG frequency spectrum possibly contributed to the decline in power output during the clean pulls. The maximum % value (i.e. potentiation) was not significantly correlated between barbell power and mean frequency (r=0.493, p=0.177). However, the shared variance (24%) should not be ignored. The low-pass filtering effect of skin and adipose tissue may dampen a rightward shift of the frequency spectrum, often associated with increasing force (Bilodeau et al. 2003). Fine wire EMG may be required to further investigate this phenomenon.

SUMMARY AND CONCLUSIONS

Clean pull exercise results in fatigue, related to a leftward shift of the EMG frequency spectrum. Further analysis is required to determine the mechanisms responsible for potentiation, and methods by which the two phenomena can be analyzed when occurring simultaneously. The model used herein to examine potentiation/fatigue gives insight to immediate responses to exercise, which may be utilized to better design training programs to enhance strength and power.

REFERENCES

Bilodeau, M. S. Schindler-Ivens, D.M. Williams, R. Chandran, and S.S. Sharma (2003). EMG frequency changes with increasing muscle force and during fatigue in the quadriceps femoris muscle of men and women. *Journal of Electromyography and Kinesiology* 13, 83-92.

Garhammer, J. (1993). A review of power output studies of Olympic and powerlifting: methodology, performance prediction, and evaluation tests. *Journal of Strength and Conditioning Research*, **7**, 76-89.

ACKNOWLEDGEMENTS

The authors would like to thank Corey Lohnes and Andrew Galpin for their assistance in data collection.

SAGITTAL ACL GRAFT ORIENTATION INFLUENCES PASSIVE AND DYNAMIC ANTERIOR TIBIAL TRANSLATION

Sean Scanlan [1], Ajit Chaudhari [2], Katerina Blazek [1], Joshua Schmidt [1], Jason Dragoo [1], and Tom Andriacchi [1,3]

[1] Stanford University, Stanford, CA, USA
[2] The Ohio State University, Columbus, OH, USA
[3] VA Palo Alto Health Care System, Palo Alto, CA, USA
E-mail: sscanlan@stanford.edu, Web: biomotion.stanford.edu

INTRODUCTION

The primary goal of anterior cruciate ligament (ACL) reconstruction is to eliminate instability, restore function, and prevent secondary problems such as premature osteoarthritis. Current surgical recommendations indicate a tibial tunnel placement posterior to the native ACL insertion [Fu, 2000], which prevents impingement but results in an inherently nonanatomic, more vertical sagittal orientation of the graft. A vertical graft would presumably be less efficient at resisting anterior loads, one of the primary functions of the ACL. Supporting this theory, an *in vitro* study reported higher graft forces were required to resist anterior tibial loads at elevated grafts angles [Li, 2006]. Yet, it remains to be seen what effect graft orientation will have on the resultant *in vivo* knee motion during passive clinical exam or under dynamic physiological loads.

The purpose of this study was to test the hypotheses that 1) passive anterior-posterior (AP) stability decreases as the graft becomes more vertical and 2) dynamic AP translation during walking is correlated to the angle of the ACL graft in the sagittal plane.

METHODS

Seventeen subjects with unilateral ACL reconstructions and no other history of serious lower limb injury (avg 30 yrs, 1.7 m, 69 kg, 6 male, 7-170 mo past reconstruction) were recruited for the study after providing IRB-approved informed consent. Static knee laxity was assessed using a KT-1000 arthrometer (MedMetric, San Diego, CA) at manual maximum load. Sagittal-plane MR images (3D-SPGR, 1.5T) were obtained of both knees of each subject lying in a supine, extended position. The proximal tibia was segmented for each knee and a plane was fit to the medial plateau. The angle of the graft in the reconstructed knee and native ACL in the contralateral knee were determined with respect to the medial tibial plateau in the sagittal plane. Each subject also performed three walking trials at a self-selected speed for each limb while being recorded using an opto-electronic motion capture system (Qualisys, Sweden). The 6-DOF kinematic measurements of the tibiofemoral joint were derived from a previously-described point cluster technique [Andriacchi, 1998].

Linear regressions were performed on the seventeen ACL reconstructed patients to determine the correlation of graft angle in the sagittal plane with side-to-side KT-1000 laxity differences and maximum anterior translation during swing phase of walking (α=0.05). The difference in the sagittal angle of the graft and native ACL was tested using paired Student's t-tests (α=0.05).

RESULTS

The results did not support the first hypothesis. The more vertical graft correlated with increased AP stability as indicated by a reduced side-to-side KT-1000 difference ($r = -0.60$, $p=0.01$) (Fig. 1). Similarly, patients with a more vertical graft had less anterior tibial translation during swing phase of normal walking ($r = -0.55$, $p=0.02$) (Fig. 2). The sagittal orientation of the graft (64.2 ± 7.4^{o}) was significantly more vertical than the intact ACL (53.7 ± 4.3^{o}).

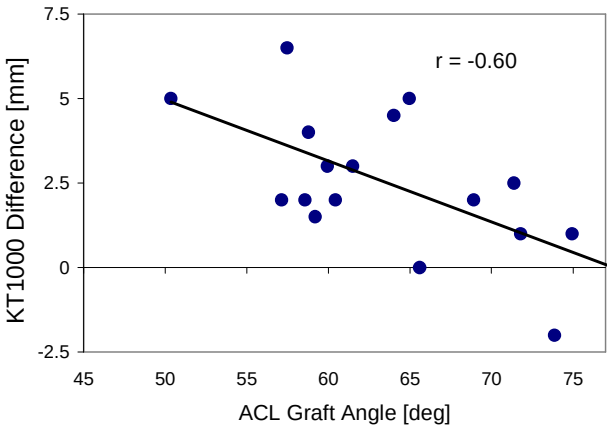

Figure 1. Correlation between KT-1000 side-to-side laxity difference and sagittal plane graft angle.

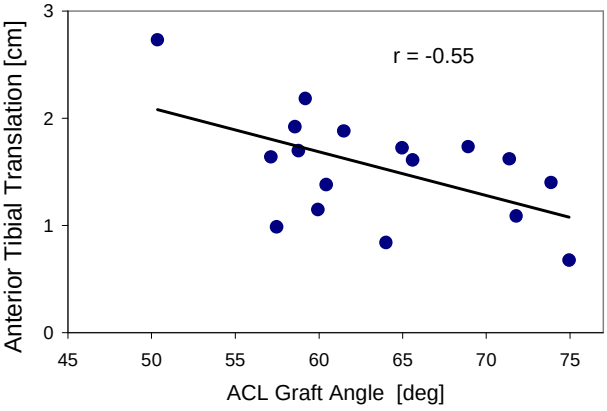

Figure 2. Correlation between anterior tibial translation during swing phase of walking and sagittal plane graft angle.

DISCUSSION

These results suggest that graft angle not only affects the common clinical measurement of static AP laxity, but it also influences knee motion during activities of daily living such as walking. This is an important finding considering that altered knee kinematics have been implicated in the premature development of osteoarthritis following ACL injury [Andriacchi, 2004].

The results of this study are somewhat paradoxical as the more vertical, non-anatomic graft resulted in reduced anterior translation of the tibia. This was unexpected, since a more vertical graft is inherently less efficient at resisting anterior tibial loads. However, this finding may be a consequence of a graft that is up to 1cm shorter in length, and thereby stiffer [Li, 2006], due to a posterior tibial tunnel position [Hefzy, 1986]. Additionally, the results could reflect an increased initial graft tension [Fu, 2000] or elevated dynamic forces in the non-anatomic grafts [Li, 2006].

CONCLUSIONS

The contribution of graft placement to post-operative tibiofemoral motion is an important factor to consider when performing ACL reconstruction.

REFERENCES

Andriacchi TP, et al. (1998). *J Biomech Eng*, **120**, 743-9.

Andriacchi TP, et al. (2004). *Ann Biomed Eng*, **32,** 447-57.

Fu FH, et al. (2000). *Am J Sports Med*, **28**, 124-30.

Hefzy MS and Grood ES. (1986). *J Biomech Eng*, **108**, 73-82.

Li G, et al. (2006). *Acta Orthop*, **77**, 267-74.

ACKNOWLEDGEMENTS

The authors acknowledge the aid of Chris Dyrby and NIH Grant #5R01-AR39421.

IN VIVO KNEE LOADING MEASURED BY AN INSTRUMENTED TOTAL KNEE REPLACEMENT DURING ACTIVITIES OF DAILY LIVING

Chris Dyrby[1,2]Darryl D'Lima[3], Cliff Colwell[3], Anne Mündermann[1,2], Thomas Andriacchi[1,2,4]

[1]Stanford University, Stanford, CA,
[2]Bone and Joint Center, Palo Alto VA, Palo Alto, CA,
[3]Shiley Center for Orthopaedic Research & Education, Scripps Clinic, La Jolla, CA
[4]Department of Orthopedic Surgery, Stanford University Medical Center, Stanford, CA
Email: dyrby@stanford.edu Web: http://biomotion.stanford.edu

INTRODUCTION

The knee sustains large contact forces over a broad range of flexion angles. The flexion angle where the largest forces occur during specific activities is an important consideration for understanding both normal and pathological conditions, since the position of the tibial-femoral contact is related to the activity, the phase of the activity, and knee flexion angle (Dyrby and Andriacchi, JOR 2004, Andriacchi and Dyrby, JBiomech 2005). Variations in the thickness of healthy knee cartilage suggests that in regions of habitual loading, stance phase knee flexion during walking, shows thicker regions of cartilage and thinner regions where it is less likely to be loaded (Andriacchi TP et al. 2004). The relationship between knee loads at high flexion angles is also an important consideration. For example, the incidence of osteoarthritis is substantially higher (15% to 30%) in workers who performed deep knee bends as part of their job, than in the general population (Felson et al. 2000). Thus, when analyzing the influence of knee loading on disease processes or in evaluating design criteria for total joint replacement it is important to consider specific activities. The overall goal of this study was to examine the relationship between activity, load, and flexion angle where maximum load occurs for walking, stair ascending and descending, chair rising and sitting, squatting and golf swing.

METHODS

A custom-designed instrumented knee prosthesis was implanted in the right knee of an 81-yr-old male (170 cm, 633 N). The subject performed a number of activities of daily living: walking, chair sit to stand and stand to sit, ascending and descending stairs, squatting, and a golf swing. Kinematic data were collected using an optoelectronic motion capture system (Qualisys). The knee flexion angle was calculated for the stance phase of each activity. The instrumented knee transmitted the compressive load from 4 uniaxial load cells embedded in the tibial component (D'Lima DD et al. 2005). The total force, the sum of all four load cells, was normalized to body weight (Bw). The range of knee flexion angles when the total compressive force exceeded 1, 1.5, 2 and 2.5BW were identified for each activity. We chose a range of force values based upon commonly seen ranges reported during the activity of walking. The maximum value (2.5 BW) was based upon a sub-maximal force seen during self selected normal walking.

RESULTS AND DISCUSSION

The activities were grouped into three categories based on knee flexion angle at peak loading (Figure 1). First, for habitual loading, walking, there was moderate load-low flexion angles. Next, stair activities and

golf had high load-moderate flexion. Finally, squatting and chair activities had moderate load-high flexion. The maximum compressive load was seen during stair ascent (3.6BW). Max load occurred at considerably different flexion angles, 8.5° for walking to 92° for squat (Figure1).

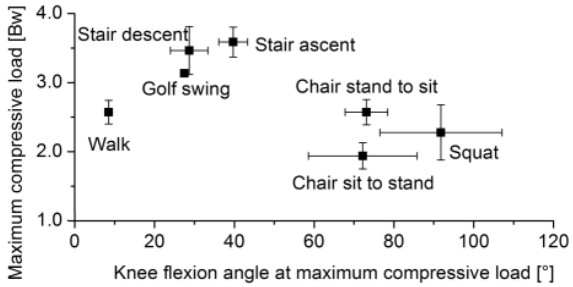

Figure 1: Max compressive load and the knee flexion angles at which they occur for each of the selected activities (± 1 std dev).

The ranges of knee flexion angles for large compressive loads varied for the activities (Figure 2). Activities that produced similarly high loads (2 to 2.5BW) occurred at different flexion ranges. For example, 2BW was produced at flexion range of 8° to 17° for walking while for squatting 2BW occurred over the 55° to 112° range (Figure 2). The results of this study showed that the knee is exposed to a wide range of peak loads and positions. In addition, within each movement, moderate to high loads are observed over substantially different ranges of flexion angles.

The loads and flexion angles can contribute to the limited lifetime of current implant designs. Cultural and activity related requirements to the function of joint replacements even at extreme angles such as squatting have led to the design of newer and improved joint replacements. However, to date joint *in-vivo* loads during these activities were largely unknown.

While the results of this study were based on a single subject, the relative loads across activities and associated flexion angles likely reflect a broader population. These loading conditions at specific angles of flexion give insight into the loading condition that could influence cartilage maintenance (Andriacchi et al 2004, Felson et al, 2000). Similarly, new TKR designs should consider these load-angle relationships for specific activities.

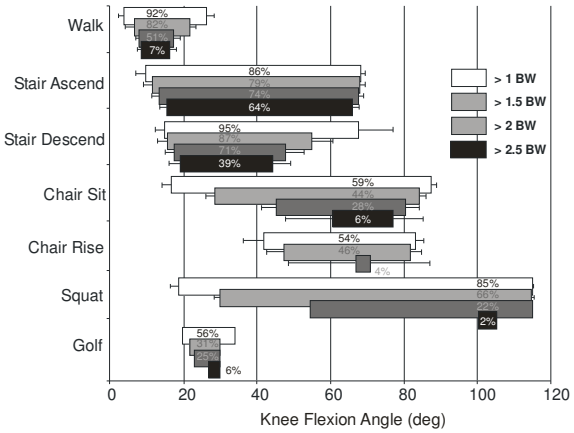

Figure 2: Range of flexion angles for activities with total compressive forces exceeding 1-2.5BW (± 1 std dev). Percentage of stance phase above these values is embedded in each bar.

REFERENCES

Andriacchi TP et al. (2004) Ann. Biomed Eng. **32**(3), 447 -57

D'Lima DD et al. (2005) *Clin Orthop Rel Res* **440**, 45-49.

Dyrby CO and Andriacchi TP (2004) *JOR* **22**(4), 794-800.

Felson DT et al. (2000) Ann. Int Med **133**(8) 635-46

ACKNOWLEDGEMENTS

Lise Worthen-Chaudhari and Jennifer Erhart. NIH Grant AR39421

DETECTING ASYMMETRIES IN BRACED AND UNBRACED LIMBS

K. Alex Shorter, John D. Polk, Karl S Rosengren, and Elizabeth T. Hsiao-Wecksler

[1] University of Illinois at Urbana-Champaign, Urbana, IL, USA
E-mail: ethw@uiuc.edu, Web: mechse.uiuc.edu/research/ethw

INTRODUCTION

Gait function depends on both coordinated motion of the body and the timing of that motion (Perry, 1992). Unfortunately, univariate measurements lack the ability to capture the spatio-temporal complexity of the gait cycle, and provide little information on the behavior of other joints. For example, quantitative assessments of joint ranges of motion are typically conducted at discrete and easily defined points in time (e.g., heel-strike, mid-stance, toe-off) (Vaughan, 1992). Such measures fail to capture the motion that occurs between these discrete temporal events, and fail to assess how problems at one joint affect other joints.

This study introduces two new quantitative metrics to address these limitations. These metrics identify (i) which joint angles are affected by a perturbation, (ii) the timing during the gait cycle when these effects are prominent, and (iii) how a perturbation at one joint affects ipsilateral and contralateral joints. To test these metrics, a data set with known asymmetries was created by restricting joint range of motion using a brace at the ankle or knee. By creating a known and repeatable gait asymmetry in a controlled population, we can better assess how effectively different approaches detect, track, and quantify changes in symmetry. This simulated data set is particularly advantageous because normal gait can be compared directly to perturbed gait. The proposed approach identifies regions of the gait cycle most affected by bracing and provides quantitative metrics that can be used to describe and compare motions.

METHODS

The knee or ankle of the dominant leg was constrained by a brace (DonJoy, Vista, CA) in ten healthy male subjects, mean age 21 ± 2 (SD) yrs. All subjects were experienced treadmill walkers, right leg dominant, and walked at a self-selected speed. Subjects walked on a treadmill without bracing, with the knee braced, and with the ankle braced.

Kinematic data were collected using a six camera motion analysis system at 120 Hz (Vicon, Oxford, UK Model 460) and were used to calculate traditional parameters (TP) and newly developed regions of deviation (ROD) parameters. TP were: joint angle range of motion, step length, single leg support time, foot rotation angle, and step width. Bilateral TP values were used to calculate symmetry indices to quantify asymmetry (Becker, 1999).

The first metric, symmetry regions of deviation (SROD), identifies regions of deviation in bilateral joint angle symmetry.

$$SROD = \begin{cases} \dfrac{\left(\sum_{i=1}^{10} \Delta\theta_i - SNorm\right)}{10} & , \Delta\theta_i > SNorm \\ 0 & , \Delta\theta_i \le SNorm, \quad i = subject \end{cases}$$

$$where: \Delta\theta = \theta_{Right} - \theta_{Left} \quad and \quad SNorm = \Delta\theta_{mean} - \Delta\theta_{SD}$$

The second metric, individual regions of deviation (IROD), identifies regions of deviation in an individual joint angle.

$$IROD = \begin{cases} \dfrac{\left(\sum_{i=1}^{10} \theta_i - INorm\right)}{10} & , \theta_i > INorm \\ 0 & , \theta_i \le INorm, \quad i = subject \end{cases}$$

$$where: \quad INorm = \theta_{mean} \pm \theta_{SD}$$

Paired t-tests were used to compare both univariate gait parameters and the peak SROD and IROD values. Repeated measures ANOVA tests were used with symmetry index values. Significant main effects were further examined by LSD post-hoc comparisons. ($\alpha = 0.05$)

RESULTS AND DISCUSSION

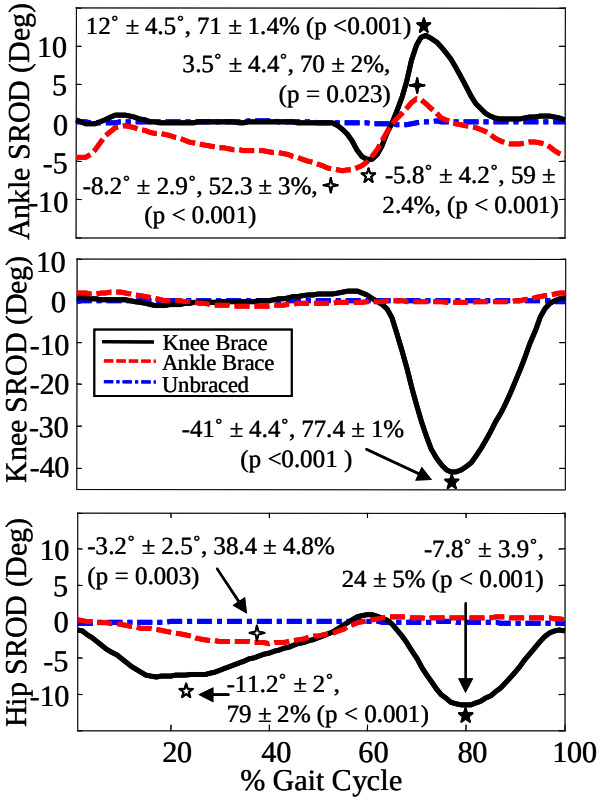

Figure 1: Plots of the average symmetry ROD (SROD) values. Filled five-point stars indicate knee-braced (KB) peak values during swing, and filled four point stars mark ankle-braced (AB) peaks during swing. Unfilled four point stars identify AB peaks during stance, and unfilled five point stars mark KB peaks during stance.

Bilateral values for ankle, knee, and hip joint range of motion and single leg support time showed increased asymmetry in gait due to bracing. Step width was also increased by bracing. The ROD parameters showed that significant asymmetries had been created between joint angle pairs, and that knee bracing increased asymmetries in joint behavior during swing, while ankle bracing tended to affect stance.

Traditional parameters provide gross indicators of asymmetric gait behavior. ROD parameters detect asymmetry, but also identify the phases of the gait cycle with the largest deviations, and give information about the impact of gait perturbation on neighboring joints. This additional information could be used in a clinical setting to identify, track and characterize asymmetric behavior.

SUMMARY/CONCLUSIONS

Gait function depends on both coordinated motion of the body and the timing of that motion. As a result, traditional gait analysis parameters have limited ability to describe the impact of known perturbations on gait function because they do no provide specific temporal information. ROD analysis provides quantitative information on the effect of bracing throughout the gait cycle and how contralateral and ipsilateral joint angular behavior is modified. This new analysis links coordinated limb movement to temporal events in the gait cycle for improved gait analysis.

REFERENCES

Perry, J. (1992). *Gait Analysis: Normal and Pathological Function*. SLACK Inc.

Vaughan, C. L. et al. (1999). *Dynamics of Human Gait.* Human Kinetics Publishers.

Peter Becker, D. R. et al. (1995). *CORR*, **311**, 262-269.

ACKNOWLEDGEMENTS

Mary Jane Neer Research Fund, College of Applied Life Studies, UIUC

ACCURACY OF RADIOGRAPHIC INTERVERTEBRAL KINEMATICS AS A DETERMINANT OF LUMBAR FUSION

Soo-An Park, Nathaniel Ordway, Hansen Yuan, Bruce Fredrickson, Mike Sun, Amir Fayyazi

SUNY – Upstate Medical University, Syracuse, NY, USA
E-mail: parkso@upstate.edu

INTRODUCTION

Multiple fusion techniques are available for reconstruction of lumbar spinal degeneration. In the review of literature, segmental sagittal motion of less than 5 degrees has been reported as an indication for fusion. The appearance of robust fusion mass in the posterolateral gutters and bridging bone in the disc space have also been recognized as indication of solid fusion. Unfortunately, routine radiographs are not sensitive enough to accurately measure the postoperative segmental motion and the quality of fusion mass is best seen on CT scan and can be deceiving on radiographs.

Radiostereometric Analysis (RSA) is a precise technique in measuring segmental motion and can be used to examine kinematics following lumbar fusion. The purpose of this study was to precisely measure the *in vivo* motion of the lumbar spine over time following lumbar fusion procedures with particular interest in changes seen over time as a result of the type of fusion and instrumentation.

METHODS

This study was approved by the institutional review board and all subjects received informed consent. Eight patients (3 males & 5 females, ages: 56.8 ± 12.0 yrs) with lumbar spondylosis were scheduled to undergo lumbar fusion with or without decompression at L3/L4, L4/L5 and/or L5/S1 and enrolled in the study. The patients were followed post-operatively at 1 month, 1 year and 2 year.

Anterior lumbar interbody fusion (ALIF) with posterior facet screw fixation (ALIF/PF), posterior lumbar interbody fusion with posterior pedicle screw fixation (PLIF/PF), posterior lumbar fusion with pedicle screw fixation (PLF/PF), stand alone ALIF (ALIF/NF) and posterior lumbar in situ fusion without fixation (ISF/NF) were performed on this cohort by three spine surgeons. During the operation, 3-4 tantalum beads (0.8 or 1.0 mm diameter) were implanted into each vertebra.

At each post-operative follow-up, biplanar standing (ST)/supine (SU) neutrals and flexion (FL)/extension (EXT) radiographs were obtained and 3-D segmental motions were calculated using the RSA software. At the same time, the plain radiographs were obtained to grade the progress of fusion. Oswestry Disability Index (ODI) was also collected at each time point to determine the clinical outcome.

Sagittal rotation (SR), superior/inferior (SIT) and anterior/posterior (APT) translations were measured for each movement (ST to FL, ST to EXT, ST to SU, and EXT to FL). Twelve dependent variables (the amount of each motion in each movement) were submitted to three different non-parametric median tests with the group based on time category (1 month, 1 year, 2 year), fusion category 1 (Circumferential fusion (CF: ALIF/PF + PLIF/PF), PLF/PF, ALIF/NF, ISF/NF), and

fusion category 2 (ALIF/PF, PLIF/PF, PLF/PF, ALIF/NF, ISF/NF).

RESULTS AND DISCUSSION

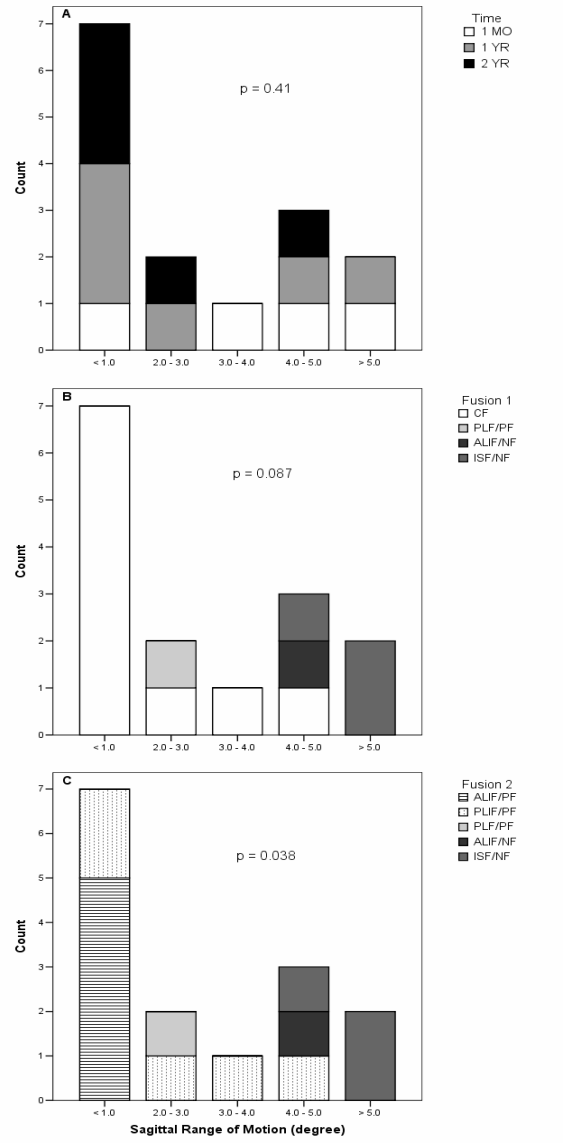

Figure 1: Sagittal ROM (SR from EXT to FL) of each group in time category (A) and fusion category 1 (B) show more even distribution along each degree of motion. However, in fusion category 2, each procedure demonstrated a significantly specific distribution (C).

There was no significant difference in any dependent variables (in frequencies between higher than median and less than median) with respect to time; it appears that the amount of stability provided by the construct at 1 month does not diminish overtime nor is there any additional stability provided with bony fusion up to 2 years in this small cohort.

In fusion category 1, a significant difference was noted with SR from ST to FL ($p = 0.029$). In fusion category 2, there was a significant difference in SR from ST to FL ($p = 0.017$) and ST to SU ($p = 0.008$). Additionally, there was a significant difference noted with SR ($p = 0.038$), SIT ($p = 0.038$), and APT ($p = 0.038$) from EXT to FL.

The amount of motion seemed to be lowest with the ALIF/PF and PLIF/PF although the PLF/PF was slightly more mobile than ALIF/PF. On the other hand, ISF/NF and ALIF/NF allowed the largest amount of motion. PLIF/PF showed more variable distribution than the other techniques. In one case (PLIF/PF), the sagittal ROM was measured to more than 5° despite strong radiographic (AP + Flex/Ext X-rays) evidence of fusion and good clinical outcome.

SUMMARY/CONCLUSIONS

The analysis of our limited data demonstrates that the motion of the fused spinal segment was dependent on the construct. Circumferential fusion seems to be most stiff construct followed by PLF/PF. Longer follow up did not add any additional stability to the spinal segment. A larger cohort is needed to confirm these findings.

ACKNOWLEDGEMENTS

This study was partially supported by DuPuy Spine, Inc. (Raynham, MA).

CORRELATION BETWEEN KNEE ADDUCTION MOMENT AND THE RATIO OF MEDIAL-TO-LATERAL COMPARTMENT COMPRESSION IN SUBJECTS WITH KNEE OSTEOARTHRITIS UNDERGOING HIGH-TIBIAL OSTEOTOMY.

Timothy Bhatnagar[1] Trevor Birmingham[2], and Thomas Jenkyn[1,2]

[1] Biomedical Engineering, University of Western Ontario, London, ON, Canada
[2] Wolf Orthopaedic Biomechanics Lab, Fowler Kennedy Sport Medicine Clinic, London, ON, Canada
Email: tjenkyn@eng.uwo.ca

INTRODUCTION

Patients with knee osteoarthritis (OA) have been shown to experience a larger external knee adduction moment during walking (Andriacchi and Mundermann, 2006). Therefore, an elevated peak knee adduction moment is considered a risk factor for medial compartment OA development and progression (Andriacchi, 1994). Knee adduction moment is also considered a good proxy measure for the magnitude of medial compartment compression (Miyazaki 2002). However, the correlation between these two quantities has not yet been established.

High-tibial osteotomy (HTO) is a common surgical procedure used to correct excessive varus knee alignment. A goal of HTO is to shift compressive loading from the medial to lateral compartment. However, this shifting of load has yet to be quantified in this patient group.

This study developed a numerical model of the internal structures of the knee joint, and used non-linear optimization to calculate the internal loading during walking gait. Of particular interest was the ratio of compression between the medial and lateral compartments. There were two goals of this study. First, determine the correlation between peak external knee adduction moment (KAM) and the ratio of medial-to-lateral compartment compressive loading ratio (MLR) both pre-HTO and post-HTO. Second, to quantify the shift of compressive load from medial to lateral compartments with HTO.

METHODS

30 patients (6 females, 24 males; mean age=50.0 ± 9.4 yrs.; BMI = 30.0±2.8) with clinically diagnosed OA primarily affecting the medial compartment of the knee underwent a medial opening wedge HTO. Walking gait analysis was performed immediately pre-surgery, and at six months post-surgery using optical motion analysis (8 Eagle cameras EvaRT system, Motion Analysis Corp, Santa Rosa, CA, USA) and floor-mounted force plate (OR6, AMTI, Watertown, MA, USA). The external joint kinetics were calculated using inverse dynamics.

The kinematic and forceplate data from the gait analysis also served as input for the internal knee joint model. The anatomical geometry was generic but scaled to patient height and knee alignment. Knee alignment was determined statically with standing full leg x-rays by the surgeon. Structures included in the model were four ligaments (ACL, PCL, LCL, MCL), two compressive contact surfaces (medial and lateral compartments) and 11 muscles (quadriceps, hamstrings, gracilis, sartorius, popliteus and gatrocnemius). Each loading surface was divided into 64 equal-area facets. A loading solution was found to satisfy mechanical equilibrium and minimize the sum of squares of all structural loads. Model output was the ratio of medial-to-lateral compartment compression (MLR).

Paired t-tests compared KAM pre-HTO versus post-HTO, and for peak MLR pre-HTO versus post-HTO. A Pearson R

coefficient was calculated correlating peak KAM to MLR for the all pooled subjects and for both pre-HTO and post-HTO conditions.

RESULTS AND DISCUSSION

The peak KAM decreased from 2.53 ± 1.32 [%BW*ht] pre-HTO to 1.63 ± 0.81 [%BW*ht] post-HTO ($p<0.001$). The peak MLR decreased from 2.81 ± 0.62 to 1.69 ± 0.61 [dimensionless] ($p<0.001$). The MLR is shown for a representative patient in Figure 1 during stance phase of gait for pre-HTO, 6-months post-HTO and 12-months post-HTO A strong correlation was demonstrated between KAM and MLR for the pre-HTO and 6-month post-HTO conditions with the Pearson coefficients $r=0.739$ and $r=0.821$ respectively.

SUMMARY/CONCLUSIONS

These results suggest that adduction moment is a good proxy for quantifying the internal compressive loading in the knee. Even without considering muscle loading and possible co-contraction of antagonists, adduction moment explains nearly three-quarters of the variance in the internal loading. However, further research is required to increase confidence in this proxy measure in a clinical setting.

REFERENCES

Andriacchi, T.P., Mundermann, A. (2006). *Curr Op Rheum,18: 514-8*

Andriacchi, T.P. (1994). *Orthop Clin North Am 25: 395-403*

Miyazaki, T., et al. (2002).*Ann Rheum Dis. 61: 617-22*

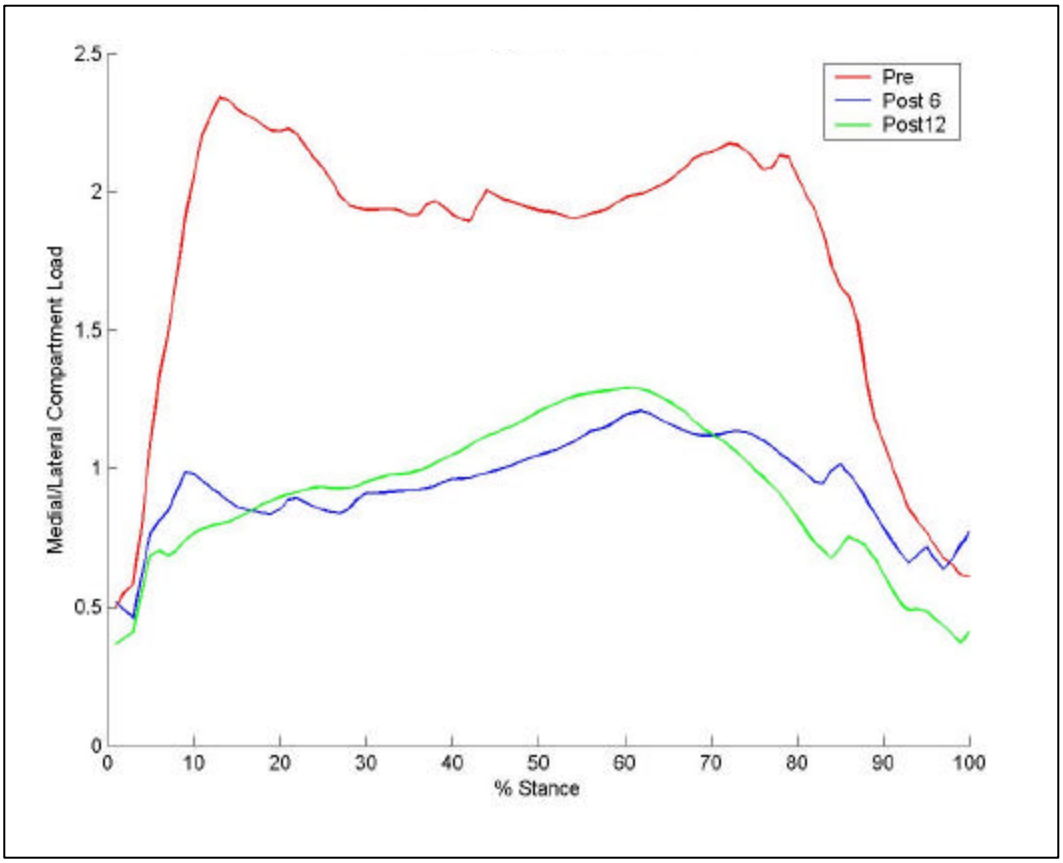

Figure 1: Medial-to-lateral compartment compression ratio (MLR) for a representative knee OA patient. Curves are shown for immediately pre-HTO surgery (Pre: red), 6-months post-HTO (Post6: blue) and 12-months post-HTO (Post12: green). The horizontal is normalized to 100% stance phase.

ESTIMATION OF MYOTENDINOUS JUNCTION DISPLACEMENT USING A CROSS CORRELATION ALGORITHM FOR ULTRA-SOUND IMAGES

Liliam Fernandes de Oliveira, Carolina Carneiro Peixinho, Daniel de Souza Alves, Taian de Mello Martins Vieira

[1] Federal University of Rio de Janeiro, Rio de Janeiro, RJ, Brazil
E-mail: liliam@bridge.com.br, Web: www.eefd.ufrj.br

INTRODUCTION

Ultrasound images have been used to investigate in vivo tendon properties as stress/strain relation, slackness and hysteresis, derived from myotendineous junction (MTJ) displacement (Muraoka, 2002, 2005; Muramatsu, 2001; Kubo, 2005). Although the medial gastrocnemius muscle (MG) MTJ structures are normally well visualized in US images, the quantitative approach often relies on identifying the same point in the beginning and in the end of the movement. which has potential methodological problems. Cross correlation algorithm for tracking an area of interest in US images was reported by Dilley for the median nerve mobilization (2001), and it was showed to be a suitable method for studies of the dynamics of soft tissues.

The aim of this study was to apply a cross correlation algorithm to calculate the displacement of the medial gastrocnemius MTJ during passive and active ankle movements.

METHODS

Images from the MG MTJ of five subjects (62.5 ± 11.62 kg, 168.4 ± 7.8 cm, 21.6 ± 3.84 years) were recorded in two conditions: passive and free active ankle movement from 80 (dorsiflexion) to 110º (plantarflexion). An ultrasound apparatus (EUB-405, Hitachi, Japão) with an electronic linear array probe of 7.5 MHz wave frequency was used to capture images, which were sampled with a rate of 5 frames per second and stored for analysis. A search algorithm was developed in LabView (National Instruments, Dallas, EUA) for estimating the MTJ displacement over the range of motion of the ankle.

The region of interest (ROI) in the first condition (the MTJ boundaries) was defined visually (Fig. 1a). For identifying its position within the frame corresponding to the end of movement, the ROI was cross-correlated iteratively with regions of same dimensions. The searching range changed laterally for each subject (≈200 pixels), and vertically (≈15 pixels), in order to assure MTJ identification. The indexes of the maximum value of the resultant correlation matrix (Fig 2) were multiplied by the spatial resolution (0.11 mm) for determining the MTJ displacement.

To provide some comparisons, a simplest method for the determination of MTJ, developed in LabView, was also applied. It consisted of visually tracing two lines, one over the deep aponeurosis and other over the superficial one. The crossing point P was referred to the MTJ and used to calculate the MTJ displacement, considering it the horizontal difference between the P points in the first and the last images.

Each procedure was repeated three times by the same examiner and the mean value was considered for comparison, using the non parametric Wilcoxon test for paired samples, with a significant level of $p < 0.05$.

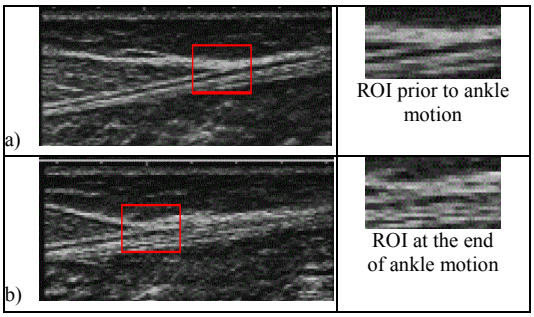

Figure 1: Frame and ROI determination prior to movement (a). ROI identified by the search algorithm after ankle motion (b)

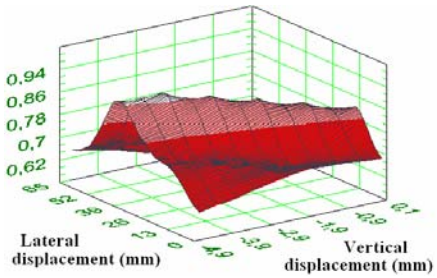

Figure 2: Correlation values for each comparison between ROI and regions over the search range (4.9mm and 65mm for this subject) on the frame corresponding to the end of ankle motion.

RESULTS AND DISCUSSION

Table 1 presents the results for both methods.

Table 1: Mean ± SD for MTJ passive (pass) and active (act) displacements

	Cross-corr	P point
Pass(mm)	16.03 ± 4.25	16.23 ± 2.14 NS
Act (mm)	25.32 ± 3.11*	25.95 ± 2.74 NS

NS between methods
* p = 0,04 between passive and active

The correlations obtained from the method were 0,91 ± 0,07 for passive condition and 0,89 ± 0,05 for the active one.

Results from the literature related to passive MTJ displacement show values of approximately 22-24 mm for ankle angle amplitudes of about 45º (Muraoka, 2002; Kubo, 2005). Our results are lower than that likely because the range of motion adopted was of 30º. When analyzing the specific range used in our study, Kubo's results (2005) were similar to ours (13mm).

The significant higher MTJ displacement during active conditions is reasonable as muscle contraction promotes an additional tension for tendon elongation. It was not found available data for GM free active conditions. The studies that used maximum voluntary isometric contractions with the ankle positioned at 90º report values around 10 mm (Muraoka, 2005; Kubo, 2005), which is acceptable as the displacement was limited to a specific ankle angle.

In relation to the method itself, some limitations have to be pointed out. Although already validated (Dilley, 2001), further validation of the algorithm using phantoms and anatomic pieces must be included, as well as its reproducibility with a higher N. These advances will attest the efficiency of the method in eliciting the calculation of displacements even when images are not sufficiently clear to visualize the *MTJ*.

CONCLUSIONS

The initial results show that cross correlation algorithm seems to be a promising method for studying passive and active elongation of tendinous tissues of human body in vivo.

REFERENCES

Dilley, A. et al. (2001). *Ultrasound in Med & Biol*, **27**, 1211-1218.

Kubo, K. et al. (2005). *Clinical Biomechanics,* **20**, 291-300.

Muramatsu, T. et al. (2001). *J Appl Physiol,* **90**, 1671-1678.

Muraoka, T. et al. (2002). *Cells Tissues Organs,* **171,** 260-168.

Muraoka T. et al. (2005). *J Appl Physiol*, **99,** 665-669.

EXAMINATION OF CUTTING KNEE MECHANICS USING PRINCIPAL COMPONENTS ANALYSIS

Kristian O'Connor and Michael Bottum

Department of Human Movement Sciences
University of Wisconsin-Milwaukee, Milwaukee, WI, USA
E-mail: krisocon@uwm.edu Web: www.chs.uwm.edu/neuromechanics

INTRODUCTION

Several studies have identified a disparity of non-contact anterior cruciate ligament (ACL) injury rates between males and females engaged in similar physical activities. Determining the nature of how interaction of external and internal factors creates a higher likelihood of injury in females has experienced mixed findings. Typical studies have been limited to discrete measures of kinematic and kinetic variables, with lack of consensus on the most relevant set of dependent variables (e.g., Pollard et al., 2004; McLean et al., 2004).

A cutting maneuver may be viewed as a complex coordinated task between multiple musculoskeletal components and the nervous system. Daffertshofer (2004) suggested that multivariate analysis methods, such as principle component analysis (PCA), which examine the entire spectrum of multidimensional waveform data, might more accurately identify embedded patterns of complex movements. Although widely viewed in statistical fields as a powerful data reduction tool, PCA's application to biomechanical problems has been slow to take hold, despite having shown promise in identifying pathological movement (Deluzio et al. 1997) and loading (Wrigley et al., 2006) patterns. PCA, due to its ability to extract modes of variability (principle components, or PCs) from complex data sets, may be better suited to recognize differences between male and female joint dynamics. The purpose of this study was to identify functional differences in knee dynamics during an unanticipated cutting maneuver using principal components analysis.

METHODS

Seventeen male and sixteen female recreationally active individuals participated in this study. Each subject was asked to perform five trials of a randomly cued running and cutting maneuver. Three-dimensional kinematic data were collected using a seven-camera Motion Analysis Eagle system (200 Hz), and force data were collected using an AMTI force platform (1000 Hz). Resulting three-dimensional knee kinematic and kinetic data was time normalized to 100% of stance (101 data points). Touchdown angles, ranges of motion, and peak moments were extracted. For the PCA analysis, each individual trial served as an input to the PCA (33 subjects × 5 trials = 165 trials – 12 discarded trials = 153 total trials). The data were compiled into a 153×101 matrix for each joint variable (3 angles and 3 moments). PCA was performed on each variable in the manner described by Wrigley et al. (2006) using Matlab v7.3. Parallel analysis was used to determine the number of PCs to retain for each variable. Eigenvector scores were calculated for each trial, and a mean of the scores was generated for each subject for each retained PC. Two-tailed t-tests were performed on the discrete measures and on the subject mean eigenvector scores between genders ($p<0.05$).

RESULTS AND DISCUSSION

Parallel analysis revealed four to seven PCs (modes of variation) accounting for 96.8% of the explained variance of each of the six joint variables. In the frontal plane, there were no significant differences between genders for the TD angle, ROM, or peak moments (Figure 1). However, there were significant differences between genders for PC2 for both angle and moment data. PC2 identified a high frequency angle oscillation during early stance (Figure 1). In the sagittal plane, the peak flexion angle differed, which was also captured by PC1. In the transverse plane, TD angle and ROM were different, which was captured by PC1 and PC3. The peak transverse plane moment was not different, but PC2 detected significant differences between genders.

Principal component analysis was able to detect pattern differences between genders that were not always identified by traditional discrete measures. This technique identified significantly greater angle oscillations in the frontal plane for females. These differences may be clinically relevant based on previous findings highlighting the importance of the frontal plane. PCA provides potential in avoiding the need to specify a set of dependent variables a priori and can automatically identify relevant functional patterns.

REFERENCES

Daffertshofer,A. et al. (2004). *Clinical Biomechanics*, **19**, 415-428.

Deluzio,K.J. et al. (1997). *Human Movement Science*, **16**, 201-217.

Pollard et al. (2004). *Clinical Biomechanics*, **19**, 1022-1031.

McLean et al. (2004). *MSSE*, **36,** 1008-1016.

Wrigley,A.T. et al. (2006) *Clinical Biomechanics*, **21**, 567-578

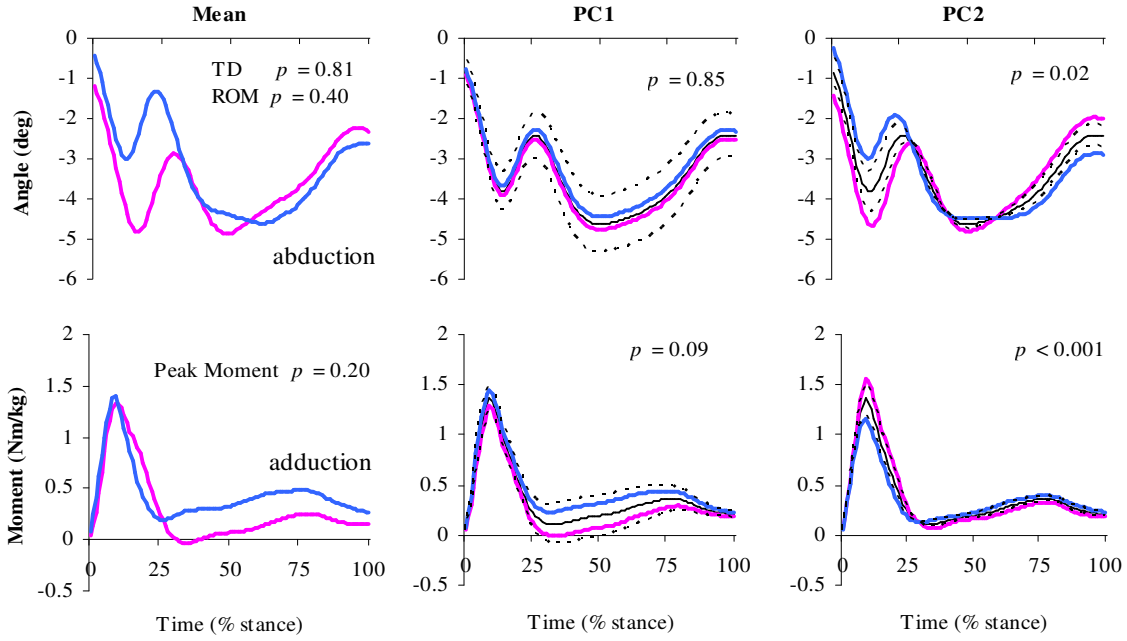

Figure 1: Group mean frontal plane angle and moment data for males (blue) and females (pink) with the p-values of discrete (TD angle, ROM, and peak moment) and PC-score gender comparisons. PC1 and PC2 demonstrate the extracted patterns with the black solid line representing the overall group mean. The dashed lines represent the between-subjects standard deviation of the PC scores' effect on PC coefficients, and the lines for each gender represent their average PC score-coefficient relationship.

Strand-based Simulation of Tendinous Systems

Shinjiro Sueda [1] and Dinesh K. Pai [1, 2]

[1] University of British Columbia, Vancouver, BC, Canada
[2] Rutgers University, Piscataway, NJ, USA
E-mail: pai@cs.ubc.ca, Web: http://www.cs.ubc.ca/~pai

INTRODUCTION

One of the challenges in computational biomechanics is simulation of the musculoskeletal dynamics with tendons and complex routing constraints. Tendons move freely in the axial direction, even in highly constraining configurations. Moreover, tendons that wrap around bones can exert forces on the bones at not only the origin and insertion, but also at intermediate points along its length. A well known example of this effect is demonstrated by the tendinous hood structure of the extensor mechanism of the finger (Wilkinson et al., 2003; Valero-Cuevas and Lipson, 2004).

Previous approaches to dynamic simulation, based on either lines-of-force (Delp and Loan, 2000; Garner and Pandy, 2000) or solid mechanics models (Blemker and Delp 2005), are not well-suited for complex structures like the extensor mechanism, where tendons and bones interact in a subtle, but important way. We propose a framework for simulating tendons using a new dynamic modeling primitive, a "strand," which is based on cubic spline curves, with the following desirable attributes: (1) Conceptually simpler routing mechanism, without the need for idealized wrapping surfaces. (2) Full dynamics of muscles and tendons, resulting in a more accurate exchange of forces between tendons and bones. (3) Efficient to simulate.

METHODS

There are three basic building blocks in our framework – rigid bodies for bones, spline-based "strands" for tendons, and virtual sliding points (Lenoir et al. 2004) for constraining strands to slide along arbitrary spline surfaces. The surface constraint works as follows. If a strand is parameterized by s, and the sliding surface is parameterized by (u, v), then the constraint ensures that a fixed point on the strand, $p(s)$, stays on the sliding surface at some location $p_0(u, v)$. The virtual sliding point, (u, v), on the surface is treated as a generalized coordinate of the system, and is included in the system state, along with the configurations of rigid bodies and strands.

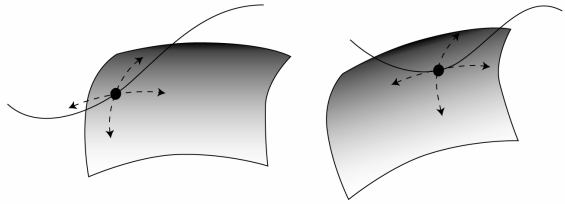

Figure 1: Surface constraint between a strand and an arbitrary rigid surface. The constraint point is fixed to the strand, while it moves freely on the surface.

The final constrained dynamics equation is obtained by discretizing the unconstrained force equations and applying velocity-level constraints (with stabilization) on the generalized coordinates of the system.

$$\begin{pmatrix} M & G^T \\ G & 0 \end{pmatrix} \begin{pmatrix} \Phi^{(k+1)} \\ \lambda \end{pmatrix} = \begin{pmatrix} M\Phi^{(k)} + hf \\ -\mu g \end{pmatrix}.$$

Here, M is the generalized inertia matrix, Φ is the generalized velocity, f is the generalized force, g is the positional constraint, G is the constraint Jacobian, and

λ is the Lagrange multiplier. This sparse linear system is solved at each time step to generate the new generalized velocities, from which we obtain the updated positions of the rigid bodies, strands, and virtual sliding points.

RESULTS AND DISCUSSION

We used a commercial skeleton model (cgCharacter, Adelaide) for the finger bones. The tendon paths were constructed based on standard textbook models in the literature. We then placed the sliding and surface constraints at strategic locations along the tendons so that the penetrations would be minimized across different finger configurations. The PCSA of the tendon was set to $0.123cm^2$ and Young's modulus to 421MPa. The input to the model was a set of tensions for the following 5 tendons: extensor digitorum communis, dorsal interosseous, palmar interosseous, flexor digitorum profundus, and flexor digitorum superficialis. Figure 2 shows some of the poses from the dynamic simulation. The extensor tendons slide smoothly on the bone surface, and during certain configurations, they act as flexors by exerting downward forces on the finger.

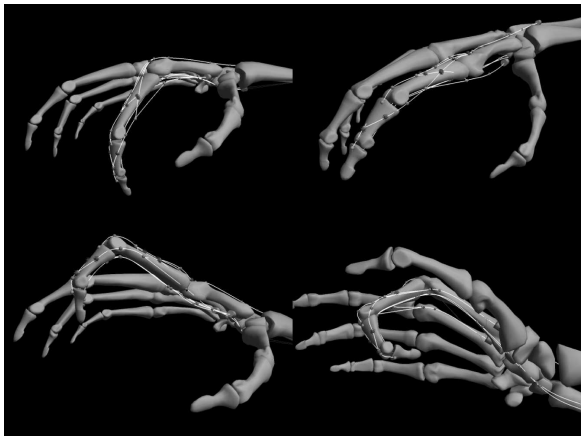

Figure 2: Snapshots from a dynamic simulation of extension/flexion of the index finger.

SUMMARY/CONCLUSIONS

We have developed a new modeling primitive for the simulation of tendinous systems based on the strand model. By using a spline-based approach, our model is able to route tendons efficiently even in complex areas such as the extensor mechanism of the finger. The tendons in our model can, unlike line-based approaches, transmit forces to the bones not only at the origin and insertion, but also at intermediate constraint points on the surface of the bone. We believe that this is important for areas such as the hood of the extensor mechanism and other tendons that span over multiple joints. Our model is computationally much more efficient than solid mechanics models, since it is more suited for the fiber-like structure of tendons.

REFERENCES

Blemker, S. S., Delp, S. L. (2005). Annals of Biomedical Engineering 33 (5), 661–673.

Delp, S. L., Loan, J. P. (2000). Computing in Science & Engineering 2 (5), 46–55.

Garner, B. A., Pandy, M. G. (2000). Computer Methods in Biomechanics and Biomedical Engineering 3, 1–30.

Lenoir, J., Grisoni, L., Meseure, P., Remion, Y., Chaillou, C. (2004). GRAPHITE 2004. ACM Press, New York, NY, USA, 58–64.

Valero-Cuevas, F. J., Lipson, H. (2004). 26th Annual International Conference of the IEEE EMBS. Vol. 2. 4653–4656.

Wilkinson, D. D., Weghe, M. V., Matsuoka, Y. (2003). In: Proceedings of ICRA 2003. Vol 1. 238–243.

ACKNOWLEDGEMENTS

This research was supported in part by a Canada Research Chair.

EFFECTS OF GENDER ON LOWER EXTREMITY MUSCLE ACTIVATION IN CHILDREN PERFORMING A SINGLE-LEG UNANTICIPATED LANDING TASK

Ronald P. Pfeiffer [1,2], Michelle B. Sabick [1,3], David Clark [1], Seth Kuhlman [1], Kevin G. Shea [1,4], Kristof Kipp [1], and Kristin Kipp [1]

[1] Center for Orthopaedic and Biomechanics Research (COBR)
[2] Department of Kinesiology
[3] Department of Mechanical and Biomedical Engineering
Boise State University, Boise, Idaho
[4] Intermountain Orthopaedics, Boise, Idaho
E-mail: rpfeiff@boisestate.edu, Web: http://coen.boisestate.edu/cobr

INTRODUCTION

Although many studies have attempted to identify why anterior cruciate ligament (ACL) injury incidence is higher in female athletes than in males, few studies have investigated differences in muscle activation strategies in very young athletes. The purpose of this study was to compare lower-extremity muscle activation differences between preadolescent boys and girls when performing an unanticipated drop-landing task. The landing task incorporated a visual cue just prior to ground contact that guided the subject to run in one of three possible directions upon landing. The rationale of the unanticipated task was to simulate an actual game situation where an athlete must react to game circumstances while in free-fall.

METHODS

Thirty-eight subjects (17 males, 21 females) were recruited from a local youth soccer league. Anthropometric data are shown below.

Subjects were suspended from a horizontal bar 30.5 cm above the ground (Figure 1). Targets were placed directly in front of the landing area, 30^o to the left, and 30^o to the right, all at a distance of 3.66m. Landing leg was determined before each trial. Subjects were instructed to, upon landing, run as fast as possible toward the illuminated target. Upon verbal command, subjects dropped onto one of two floor mounted force plates, landing on the pre-determined leg. One of the targets was randomly illuminated during free-fall.

Three trials were collected for each running direction and for each landing leg, totaling 18 trials per subject. The resulting three conditions were designated center (C), sidestepping 30^o (SS), and crossover 30^o (XO). The order in which the 9 trials were performed was randomized for each leg.

Muscle activation in the landing leg was monitored using surface electromyography (sEMG). The muscles of interest were the vastus lateralis (VL), vastus medialis (VM),

Table 1: Anthropometric data (mean±SD)

	Age	Height (m)	Weight (N)
Males	10.44±0.63	1.44±0.08	354.53±53.73
Females	10.05±0.69	1.45±0.08	363.93±79.04

Figure 1: Female subject just prior to bar release.

medial hamstring (MH), lateral hamstring (LH), and the medial head of the gastrocnemius (G). Signals were sampled at 1250 Hz and bandpass filtered from 20 to 500 Hz to remove motion artifacts.

Three phases of the landing were analyzed, pre-contact (PC), weight acceptance (WA), and peak push-off (PPO)(Besier et al. 2003). For each landing phase in each trial, maximum sEMG amplitude was determined for each muscle. Those values were then normalized to maximum voluntary isometric contraction (MVIC) data that were collected for the quadriceps and hamstrings groups prior to testing. In addition, all SS and XO trials were normalized to the average maximum sEMG amplitude during the C trials. For each subject, an average normalized sEMG value was calculated from the three trials of each condition during each of the three landing phases. The averaged normalized sEMG values were then compared in the statistical analysis. Differences between males and females were assessed for each variable using independent samples *t*-tests. Alpha level was set at $p<0.05$.

RESULTS AND DISCUSSION

There were no significant differences between genders across all landing phases (PC, WA, PPO) and landing tasks (C, SS, XO) for the VL, MH, LH, and G muscles. However, significant differences between genders were noted at both PC and WA for the VM on all landing tasks (Table 2).

The boys in this study employed a landing strategy that included much higher VM amplitudes than did the girls, during both the PC and WA phases. That outcome may suggest that the males in this study were demonstrating a tendency towards "quadriceps dominance" in their landings as compared to the females, who, based on previous research on older subjects, tend to demonstrate a more "ligament dominant" strategy when landing (Hewett et al, 2002; Ford et al, 2005). Ligament dominant strategies have been identified as potential etiological factors in non-contact ACL injuries (Hewett et al, 2002).

Table 2: Gender comparisons of the sEMG values (% MVIC) for the vastus medialis

Variable	Gender	Mean+ SD	*t*-score	Sig.
PC-C	Male	1.99±1.28	2.501	0.015
	Female	1.36±0.83		
WA-C	Male	2.27±1.77	3.165	0.002
	Female	0.92±0.92		
PC-SS	Male	1.92±1.26	2.374	0.020
	Female	1.33±0.83		
WA-SS	Male	2.06±1.05	2.962	0.004
	Female	1.34±0.99		
PC-XO	Male	2.02±1.19	3.088	0.003
	Female	1.30±0.78		
WA-XO	Male	2.33±1.50	3.835	0.000
	Female	1.26±0.80		

PC=Pre-contact; WA=Weight acceptance; C=center run; SS=Side-step; XO=Crossover step

REFERENCES

Besier, T. F., et al. (2003). *Med Sci Sports Exerc*. **35**, 119-127.

Ford, K. R. et al. (2005). *Med Sci Sports Exerc*. **37**, 124-129.

Hewett, T. E., et al. (2002). *Clin Orthop*. **402**, 76-94.

ACKNOWLEDGMENTS

The authors would like to thank the athletes from Capitol Youth Sports Association, Boise Idaho for their participation in this study.

IN VIVO SARCOMERE LENGTH MEASUREMENT BY MINIMALLY INVASIVE MICROENDOSCOPY

Michael E. Llewellyn[1], Robert P. J. Barretto[2], Mark J. Schnitzer[2,3], and Scott L. Delp[1,4,5]

Departments of Bioengineering[1], Biological Sciences[2], Applied Physics[3], Mechanical Engineering[4], and Orthopaedic Surgery[5]. Stanford University.
Email: llewellm@stanford.edu Web: http://nmbl.stanford.edu/

INTRODUCTION

Knowledge of muscle sarcomere lengths is needed to understand of muscle physiology and disease. Unfortunately, individual human sarcomere lengths have never been measured *in vivo* due their small size (1-4 µm), which is not resolvable with current clinical imaging modalities. We have developed a minimally invasive method capable of imaging individual sarcomeres deep within the muscle of living animals without the use of exogenous dyes. We have used this technique to visualize individual sarcomeres and muscle fibers of mice. Our technique is also applicable to humans, and opens the door to clinical measurement of individual sarcomere lengths.

METHODS

Muscle produces a nonlinear optical signal during a process called Second-Harmonic Generation (SHG), which is thought to originate from the tail region of myosin heavy chain (Plotnikov et al., 2006). We generated a SHG signal in the muscle of anesthetized C57BL/6 mice (Figure 1A and 1B) using a Gradient Refractive Index (GRIN) microendoscope (Jung et al., 2003). For this study, we used microendoscopes whose diameters ranged from 1000 µm to 350 µm (Figure 1C). These microendoscopes produced acceptable fields of view and allowed us to reach depths of several centimeters within the tissue. We imaged both muscle in its passive state and when activated through stimulation of the tibial nerve. We measured average sarcomere lengths by fitting a sine wave to the autocorrelation function of an image.

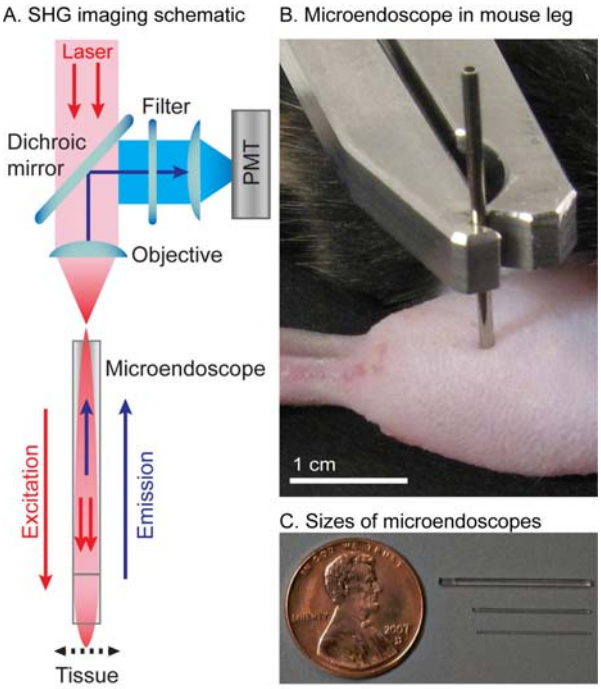

Figure 1: **GRIN microendoscope used to conduct sarcomere imaging.** An infrared pulsed laser is focused by a GRIN microendoscope to excite deep tissue. The same microendoscope collects the emitted SHG signal, which is reflected off a wavelength-specific dichroic mirror through a filter and into a photomultiplier tube (PMT) detector (A). A stainless-steel clad 350 µm microendoscope is inserted in the lateral gastrocnemius of a living mouse (B). The three sizes of microendoscopes (1000 µm, 500 µm, 350 µm diameter.) shown near a coin for scale (C).

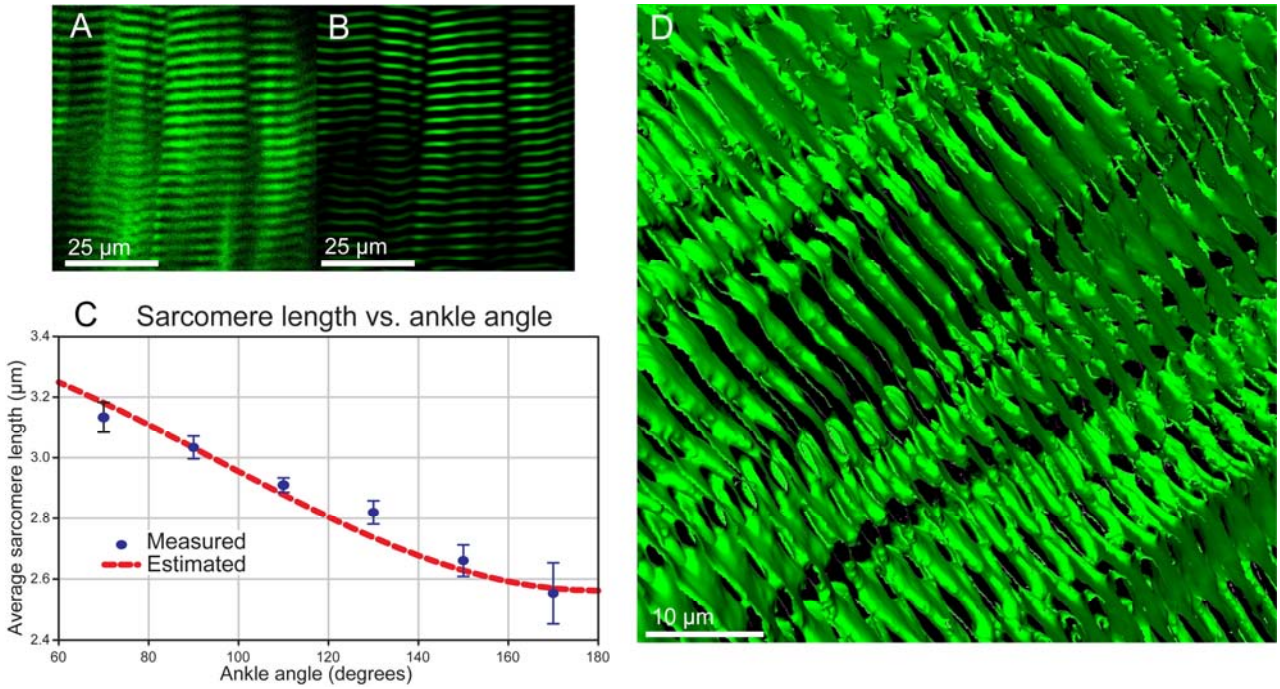

Figure 2: *In vivo* muscles fibers imaged through a 350 µm microendoscope (A). Image A after it has been band-pass filtered for sarcomere lengths between 1-5 µm (B). Measured and estimated sarcomere length vs. ankle angle for the mouse lateral gastrocnemius (n=5); error bars indicate standard error of measurement (C). A benefit of multiphoton imaging is its intrinsic sectioning capability. A 3D rendering of mouse lateral gastrocnemius from a stack of 1µm thick slices (D).

RESULTS AND DISCUSSION

We have demonstrated the feasibility of minimally invasive SHG microendoscopy to measure individual sarcomere lengths *in vivo* without the use of exogenous dyes (Figure 2A and 2B). We were able to measure sarcomere lengths from deep within both passive and active muscle tissue. We measured passive sarcomere length vs. ankle angle (Figure 2C) that is consistent with previous studies (Goulding et al., 1997) and estimates based on measured architectural data such as pennation angle, moment arm, and fiber lengths. Additionally, we were able to create high-resolution 3D models of sarcomeres *in vivo* due to the intrinsic sectioning capabilities of multiphoton microscopy (Figure 2D).

For the first time, there is an imaging modality capable of measuring individual sarcomere lengths *in vivo* with minimal invasiveness, opening the door for researchers to address fundamental questions about muscle physiology. Additionally, because this imaging modality is adaptable to humans, we are looking forward to its use in clinical imaging.

REFERENCES

Plotnikov, S. V., A. C. Millard, P. J. Campagnola et al., *Biophysical journal* **90** (2), 693 (2006);

Jung, J. C. and M. J. Schnitzer, *Optics letters* **28** (11), 902 (2003).

D. Goulding, B. Bullard, and M. Gautel, *Journal of muscle research and cell motility* **18** (4), 465 (1997).

ACKNOWLEDGEMENTS

We would like to thank the NIH and the Stanford BioX program for support.

EFFECTIVE MOMENT ARM ESTIMATION OF INDEX FINGER MUSCLES

Sang Wook Lee[1], Hua Chen[2], Joseph D. Towles[1], and Derek G. Kamper[1,2]

[1] Rehabilitation Institute of Chicago, Chicago, IL, USA
[2]Illinois Institute of Technology, Chicago, IL, USA
E-mail: sanglee2@northwestern.edu

INTRODUCTION

The contribution of muscle-tendon force to joint moment generation is fundamentally affected by its moment arm (MA), defined as the normal distance between the joint center of rotation and the muscle-tendon line of action. One popular technique for estimating the MA is the tendon excursion method, which computes instantaneous MA from the slope of the tendon excursion-joint angle relationship (An et al., 1983). With regard to the fingers, however, the excursion method may not fully explain the effects of tendon forces on the production of joint moments, due to the complex tendinous structure in the finger. The contribution of tendon force to a joint moment is not solely quantified by its geometric MA length, but also by force distribution patterns resulting from multiple tendon insertion sites and from reaction forces across multiple joints.

In this study, we present a novel method to measure the effective moment arm (EMA) of finger tendons. The EMA represents the total effect of tendon force on joint moment production. This technique was employed to examine the effects of finger posture (joint angles) on EMA magnitudes.

METHODS

Three fresh-frozen cadaveric hand specimens, transected midway between the wrist and elbow, were used for the experiment (hand length mean ± SD: 171.7 ± 3.3 mm). The five tendons that compose the extensor apparatus, i.e. extensor digitorum communis (EDC), extensor indicis profundus (EIP), first dorsal interosseous (FDI), first palmar interosseous (FPI), and lumbrical (LUM), were exposed and sutured to nylon cords to allow tendon loading. The cords attached to the intrinsic muscles (FDI, FPI, and LUM) were routed through remaining ligament structures, such as the carpal tunnel, to maintain the anatomical lines of action. Each specimen was mounted on a fixation device (Agee-Wristjack, Hand Biomechanics Lab, Sacramento, CA), and the index fingertip was secured to a 6 degree-of freedom load cell (JR3, Inc., Woodland, CA). Three levels of tendon force (8.3%, 16.7%, 25% of the corresponding muscle's maximal force capability) were applied to each tendon. A set of 9 joint postures, consisting of three pairs of proximal and distal interphalangeal (PIP, DIP) joint angles ((0º, 0º), (30º, 20º), and (45º, 30º)) explored at each of three metacarpophalangeal (MCP) joint angles (0º, 30º, 60º), were tested for each specimen. Joint moment values were calculated from fingertip forces and moments using the transpose of the Jacobian matrix.

The moment produced by tendon forces about joint i (m_i) can be divided into three sub-components:

$$\begin{aligned} m_i &= m_i^{act}\left(\underline{\theta}, \underline{f}\right) + m_i^{sub}\left(\underline{\theta}, \underline{f}\right) + m_i^{pas}\left(\underline{\theta}, \underline{\dot{\theta}}\right) \\ &= \sum_{j=1}^{N_{tendon}} r_{ij}\left(\underline{\theta}\right) \cdot f_j + m_i^{pas}\left(\underline{\theta}, \underline{\dot{\theta}}\right) \end{aligned} \quad (1)$$

where m^{act} denotes the moment generated by active tendon force, m^{sub} the subsequent moment indirectly generated via reaction forces between tendons and segments or pulleys, m^{pas} the passive moment existing regardless of muscle activation, $\underline{\theta}$ joint angle vector, and $\underline{f}$ tendon force vector. From the

given relationship, the EMA r_{ij} of tendon j about joint i in a given static posture was estimated via multiple measurements of joint moments with varying tendon force f_j magnitudes (all f_k=0, $k \neq j$). For a given tendon force-joint moment dataset, the least-square method is applied to fit a line, resulting in the EMA (r_{ij}) as the slope of the line, and m_i^{pas} as its y-intercept. Note that m_i^{pas} remains constant when there's no change in $\underline{\theta}$, since m^{pas} is not a function of f.

RESULTS AND DISCUSSION

For all experimental conditions, tendon forces exhibited a strong linear relationship with joint moments (R^2 mean ± SD = 0.93 ± 0.17).

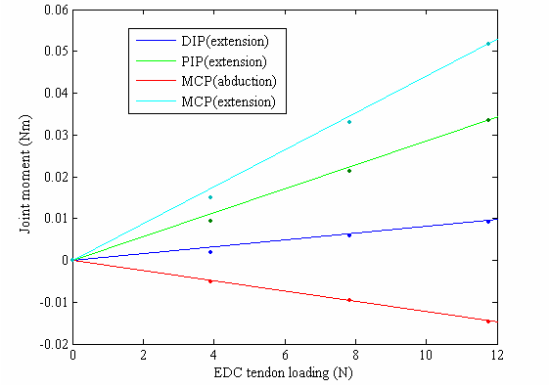

Figure 1: Representative plot of joint moment (<u>with passive moment excluded</u>) vs. EDC tendon force (specimen #1, all joint angles = 0º). R^2 = 0.97 – 0.99 for this case.

Estimated EMA magnitudes were fundamentally affected by postures, primarily by changes in IP angles. Table 1 summarizes the mean ± SD of the estimated EMA values for each IP posture (mean across subjects and MCP angles). Changes in MAs due to MCP flexion were smaller than changes due to IP flexion. MCP angles were found to affect primarily the EMAs for MCP flexion for FPI and LUM; this effect may have resulted from palmar migration of the lines of tendon action.

The EMAs for EDC and EIP at the MCP joint increased when IP angles increased. This may be explained by an increase in the distance between the line of action of the terminal or central slips and MCP joint. Similarly, EMAs for FPI and LUM about the MCP joint increased as the IP joints flexed. Concurrently, their extension EMAs at the PIP joint gradually decreased. This may be attributable to palmar migration of the lateral bands.

Table 1: Estimated EMA (mean ± SD, unit: mm). Positive numbers indicate extension or abduction. (e: extension, a: abduction)

	PIP = 0º, DIP = 0º			
	DIP(e)	PIP(e)	MCP(e)	MCP(a)
EDC	0.8±1.4	1.7±0.9	2.5±1.1	-0.1±0.7
EIP	1.0±1.3	1.9±0.9	2.7±1.2	-1.0±0.6
FDI	1.0±0.6	0.1±0.4	-0.6±0.9	1.4±0.7
FPI	3.3±2.1	1.1±1.1	-0.5±1.3	-2.0±0.9
LUM	2.0±1.7	0.2±0.5	-1.3±1.3	0.8±0.9
	PIP = 30º, DIP = 20º			
EDC	2.6±1.6	3.3±1.0	5.1±1.2	0.1±0.4
EIP	2.3±1.5	3.1±0.9	4.8±1.2	-1.2±0.3
FDI	-0.1±0.8	-0.2±0.6	-0.7±1.0	2.2±0.4
FPI	-1.1±1.2	-0.9±0.8	-2.9±1.4	-2.7±1.4
LUM	-0.7±1.5	-0.7±1.0	-2.5±2.2	1.1±0.6
	PIP = 45º, DIP = 30º			
EDC	2.4±1.2	3.3±0.9	5.1±1.0	0.3±0.2
EIP	2.2±1.2	3.1±0.9	4.8±1.1	-1.3±0.5
FDI	0.1±1.0	-0.1±0.8	-0.8±1.3	2.6±0.7
FPI	-1.1±0.8	-1.1±0.5	-3.5±1.4	-3.0±1.3
LUM	-0.9±1.2	-1.2±1.1	-3.4±2.8	1.4±0.8

It should be noted that estimated EMA values are smaller than the MA values reported in previous studies (An et al., 1993; Buford et al., 2005). Dissection of the extensor hood has led us to surmise that its interactions with ligaments and the joint capsules reduce the net extension/flexion forces applied to the bones. Note also that the EMA values obtained here are valid only for static force exertion – different EMAs are expected to result from free movements.

REFERENCES

An, K. N. et al. (1993). *J Biomech*, **16**, 419-25.
Buford, W. L. et al. (2005). *J Hand Surg [Am]*, **30**, 1267-75.

RELATIONSHIP BETWEEN KNEE FLEXION MOMENT AND EARLY CARTILAGE CHANGES IN THE ACL RECONSTRUCTED KNEE

Sean Scanlan[1], Katerina Blazek[1], Joshua Schmidt[1], Seungbum Koo[1], Ajit Chaudhari[2], Jason Dragoo[1], and Tom Andriacchi [1,3]

[1] Stanford University, Stanford, CA, USA
[2] The Ohio State University, Columbus, OH, USA
[3] VA Palo Alto Health Care System, Palo Alto, CA, USA
E-mail: sscanlan@stanford.edu, Web: biomotion.stanford.edu

INTRODUCTION

Premature knee osteoarthritis (OA) is frequently reported in patients after anterior cruciate ligament (ACL) injury, even in patients who have had an ACL reconstruction [Gillquist, 1999]. While a mechanical etiology for the high prevalence of OA is commonly suggested, there are few studies linking altered ambulatory joint mechanics to morphological changes in the articular cartilage.

A reduction in the external peak knee flexion moment (balanced by net quadriceps moment) walking has been reported in ACL deficient knees and may be a necessary compensation to avoid excessive anterior translation of the tibia in the absence of the anterior-posterior (AP) restraint of the ACL [Andriacchi, 2005]. Following restoration of the AP restraint with ACL reconstruction, patients should presumably reestablish a more normal flexion moment during gait without experiencing AP instability. However, complete restoration of normal flexion moments in ACL reconstructed subjects is not observed during walking [Bulgheroni, 1997]. The impact of this alteration in joint mechanics on the health of the articular cartilage at the knee is unknown. This study tested the hypothesis that early post-operative changes in cartilage morphology are related to the peak knee flexion moment during walking in the ACL reconstructed knee.

METHODS

Nine subjects with unilateral ACL reconstructions and no other history of serious lower limb injury (avg 40 yrs, 1.7 m, 67 kg, 3 male, 3.4 mo injury to reconstruction, 8-48 mo past reconstruction) were recruited for the study after providing IRB-approved informed consent. Subjects underwent bilateral, non-weightbearing MR imaging and a gait test at self-selected walking speed. A force-plate and a previously-described link model were used to estimate the net external forces and moments acting at the joints [Andriacchi, 1997]. The patients were then partitioned into a low and high flexion moment group based on magnitude of the peak external knee flexion moment in the reconstructed limb, with a cutoff at 2.8 %bw*ht. Tibial cartilage in the bilateral knee MR images were segmented and reconstructed into 3D models with thickness maps [Koo, 2005](Fig 1).

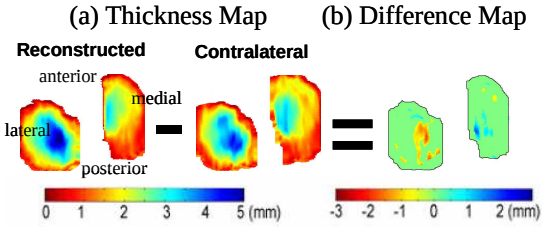

Figure 1. (a) Thickness maps for the ACL reconstructed and contralateral tibial cartilage (b) Difference maps created by subtracting the two thickness maps.

Tibial cartilage regions experiencing thinning or thickening (i.e. swelling) greater than 0.4mm relative to the contralateral, healthy tibia were classified as a region experiencing a measurable morphological change. These affected regions were then quantified as a percentage of the total medial and lateral cartilage area. A Student's t-test (α=0.05) was used to detect differences in the percentage of affected tibial cartilage area between the low and high peak knee flexion moment groups.

RESULTS

Significantly greater ($p<0.05$) early morphological changes in the medial tibial cartilage were observed in ACL reconstructed patients with a low peak external knee flexion moment (17.3±1.5%, n=5) when compared to those with a high peak flexion moment (8.3±2.3%, n=4) (Fig. 2) during walking. There was no relationship between the changes in lateral tibial cartilage and knee flexion moment.

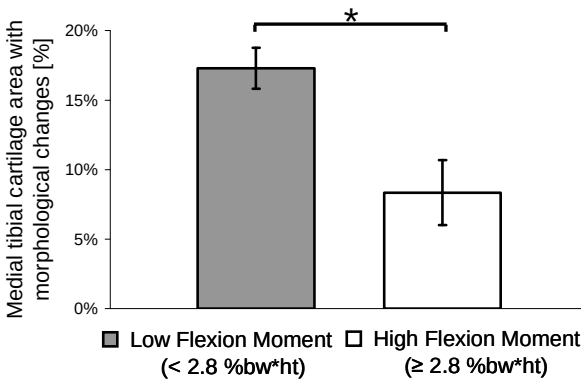

Figure 2. Comparison of percentage medial cartilage area with early morphological changes in the low and high flexion moment groups. * Significant difference ($p<0.05$).

DISCUSSION

The results support the theory that alterations in joint mechanics are associated with early morphological changes in the articular cartilage of the ACL reconstructed knee. While previous studies indicate that compensatory reduction in knee flexion moment may be critical in controlling tibiofemoeral stability in the ACL deficient knee [Andriacchi, 2005], the results of the current study suggest that a reduced flexion moment after ACL reconstruction may have a negative effect on the health of the cartilage. Combined with the altered tibiofemoral kinematics commonly observed in ACL reconstructed patients, a reduced flexion moment may significantly change the stress distribution within the cartilage and initiate a degenerative response. These patterns of early changes to the articular cartilage may be markers of events leading to the initiation of premature OA. Thus, these results support the importance of restoring normal knee mechanics in the ACL reconstructed knee.

CONCLUSIONS

These results suggest that restoration of the knee flexion moment after ACL reconstruction might be an important factor in maintaining the health of the articular cartilage at the knee.

REFERENCES

Gillquist J, et al. (1999). *Sports Med*, **27**, 143-156.

Andriacchi TP, et al. (2005). *J of Biomechanics*, **38**, 293-298.

Bulgheroni P, et al. (1997). *Knee Surg Sports Traumatol Arthrosc*, 5, 14-21.

Andriacchi TP, et al. (1997) *Basic Orthopaedic Biomechanics*, 37-68.

Koo S, et al. (2005). *Osteoarthritis Cartilage*, **13**, 782-789.

ACKNOWLEDGEMENTS

The authors acknowledge the aid of Chris Dyrby and NIH Grant #5R01-AR39421.

ENERGETICS AND BIOMECHANICS OF WALKER ASSISTED GAIT

Jonathon R. Priebe and Rodger Kram

Locomotion Laboratory, Department of Integrative Physiology
University of Colorado, Boulder, CO, USA
E-mail: Priebe@colorado.edu Web: www.colorado.edu/intphys/research/locomotion.html

INTRODUCTION

Nearly 4 million Americans use a "walker" to aid with ambulation. Four-wheeled (4W) and two-wheeled (2W) walkers are pushed from behind and involve a normal bipedal (BP) walking pattern. In contrast, a four-footed (4F) walker must be lifted completely off the ground and requires a special type of walking pattern (gait) referred to as "step-to" (ST). ST walking requires the user to step forward with one foot and then step-to the same position with the other foot.

Previous research report that using a 4F walker increases energetic cost by 212%, but did not offer any biomechanical explanation for the elevated cost (Holder et al., 1993; Foley et al., 1996).

The purpose of this study was to investigate the energetic cost and kinematics of walking unassisted and with three different walkers. We tested two hypotheses: 1) At a fixed speed, walking with a 4F walker, using a ST gait is metabolically more expensive than walking unassisted or with a 2W or 4W walker. 2) The greater cost of using a 4F walker is due to the slower walking speed, cost of lifting the walker, and a disabled inverted-pendulum energy exchange mechanism associated with the step-to gait.

METHODS

Ten (5M, 5F) young, healthy, adult subjects volunteered. We trained the subjects to walk with the three walkers and the ST gait. After training, we measured preferred walking speed (PWS) with each device and unassisted.

The experimental protocol consisted of eight trials: 1. standing, 2. BP at 1.25 m/s, 3. BP at 0.30 m/s, 4. 2W walker BP at 0.30 m/s, 5. 4W walker BP at 0.30 m/s, 6. 4F walker ST at 0.30 m/s, 7. ST unassisted at 0.30 m/s, 8. repeated lifting of 4F walker.

We measured metabolic rate using expired gas analysis. Net metabolic rate = exercise - standing. For the ST trial without walker, subjects matched their step-step-pause pattern to the rhythm used with the 4F walker. The 4F walker lifting trial consisted of lifting the walker forward, with a pause and then backward followed by another pause, matched to the same timing as the 4F walker trial.

We used repeated-measures ANOVA and Tukey post-hoc test with a criterion of $p < 0.05$.

RESULTS AND DISCUSSION

The net metabolic cost for subjects walking with the 4F walker at 0.30m/s was "only" 84% greater than bipedal (BP) walking at the same speed ($p<.001$). Metabolic cost with the 4W and 2W walkers was just 3% and 10% greater than BP walking at the same speed; respectively ($p<.001$; Figure 1).

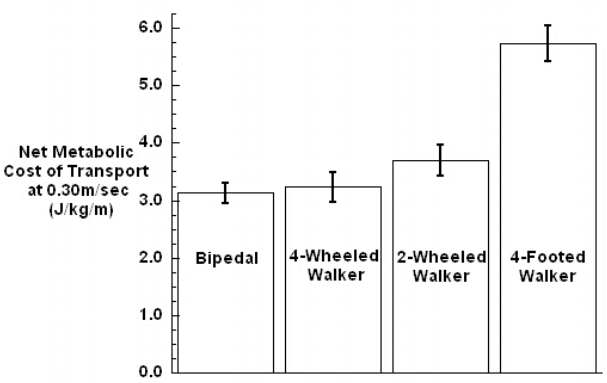

Figure 1: Mean values ± SEM.

Net metabolic power for walking at 0.30 m/s with the 4F walker was not statistically different from the combined metabolic rates for ST walking at 0.30 m/s plus the cost of 4F walker lifting (p=.25, Figure 2).

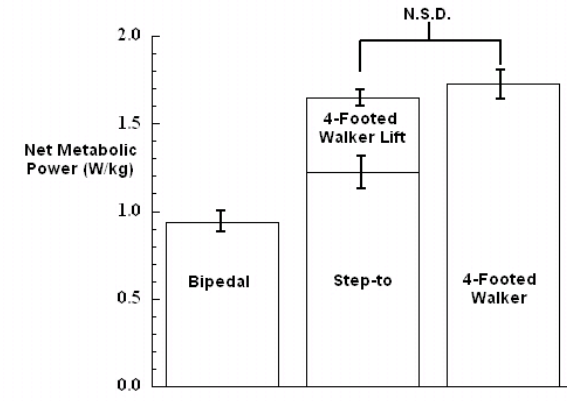

Figure 2: Mean values ± SEM..

Our findings suggest that three principle factors contribute to the greatly elevated metabolic cost of using a 4F walker: slow speed, lifting, and the step-to gait.

The 4F walker involves a dramatically slower preferred walking speed (4F 0.35m/s vs. BP 1.52m/s). The metabolic cost of bipedal walking at 0.30m/s increased metabolic cost per distance by 73% compared to walking bipedally at 1.25m/s.

Lifting the 4F walker comprised 25% of the metabolic rate when using the 4F walker. Reducing the weight of 4F walkers could help mitigate the elevated cost of using these walkers.

The 4F walker requires the user to employ a ST gait. At 0.30m/s, ST walking unassisted was 29% more expensive than BP unassisted.

Using a 4F walker is an aerobically challenging task for elderly people. Using a 4F walker requires 90% of $\dot{V}O_2$ max in 85 year old community dwelling females, which is comparable to elite marathon runners.

Future walker designs should combat the three major problems we have identified. Ideally, such devices should provide the stability of a 4F walker, but allow the users to walk bipedally at a normal speed with no lifting required.

SUMMARY/CONCLUSIONS

Three principle factors contribute to the greatly elevated metabolic cost of using a 4F walker: slow speed, lifting the walker, and the step-to gait.

REFERENCES

Holder, C.G., Haskvitz, E.M., Weltman, A. (1993). Journal of Orthopaedic and Sports Physical Therapy. **18**, 537-542.

Foley, M.P., Prax, B., Crowell, R., and Boone, T. (1996). Physical Therapy. **76**, 1313-1319.

QUANTITATIVE ANALYSIS OF FINGER MOVEMENTS DURING REACHING AND GRASPING TASKS

Jaewon Choi and Thomas J. Armstrong
University of Michigan, Ann Arbor, MI, USA
E-mail: jaewonc@umich.edu

INTRODUCTION

Quantitative assessment of finger movement facilitates modeling of hand motion, which can be used for design of tools and products or for rehabilitation purpose. Many researchers have studied finger movements to investigate the functional synergies (Braido and Zhang, 2002; Santello et al., 1998) or the effect of object properties, but only the aperture change was observed (Jeannerod, 1984; Paulignan et al., 1997). In this study, we defined and observed spatial and temporal variables for reaching and grasping movements. We tested the hypothesis that object size affects both spatial and temporal variables during reaching and grasping movement.

METHODS

Experiments

Sixteen healthy subjects (11 males, 5 females), whose hand sizes ranged from 2% female to 82% male, participated in the experiment. Three sizes of cylindrical handles (diameter: 26 mm, 60 mm, 114 mm) were used. The cylindrical handle was located 30 cm in front of and at elbow height of the subject. Subjects were asked to start with their hands at rest and then to reach for and grasp the handles with power grip at normal speed. Twenty-four markers were attached to all the joints and the tips of the hand. The OptoTrak® motion tracking system was used to track positions of the markers at a 100-Hz sampling rate.

Data Analysis

The data were low-pass filtered with a 5-Hz cut-off frequency. A typical joint angular profile during grasping movement is shown in Figure 1. Initial, open, and final angles were first defined as in Figure 1. A 'start time' ('close time') was defined as a time when the joint angle reached 5% of the difference between initial and open angle (open and final angle). An 'open time' ('final time') was defined as a time when the joint angle reached the open angle (final angle). Time variables were normalized by the duration of hand movement: the time for the hand to reach the handle located 30 cm in front of the subject. One-way ANOVA tests were performed using SPSS® to examine the effects of handle sizes.

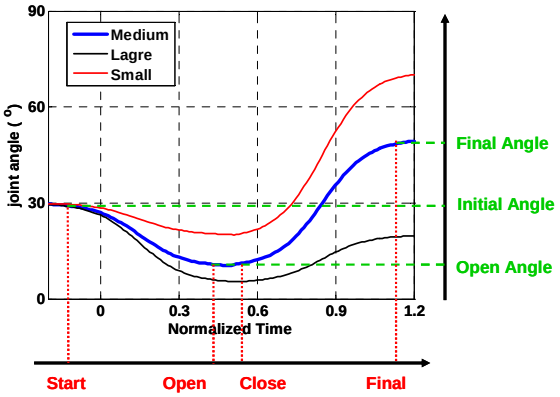

Figure 1. Typical joint angle pattern of grasping task.

RESULTS AND DISCUSSION

The mean hand movement time to reach 30 cm was 1.00±0.23 seconds and was not significantly different over varying handle sizes. The joint angles at rest posture, open angles, final angles, normalized open times, and normalized final times for all joints of the middle finger are shown in Table 1. Both open angles and final angles were significantly affected by the size of handles ($p<0.05$). These results agree well with previous studies that found the dependency

of aperture on the object size (Jeannerod, 1984; Paulignan, 1997) and the sensitivity of final angles to object size (Choi and Armstrong, 2006; Buchholz and Armstrong, 1992). Normalized open times were also affected by the handle sizes significantly at all joints ($p<0.05$). The mean normalized open time was 0.38 for MCP, 0.49 for PIP, and 0.53 for DIP joint. The effect of handle size was significant ($p<0.05$) for normalized final time except for the MCP joint. The mean normalized final time was 1.40 for DIP, 1.31 for PIP, and 1.29 for MCP joint, because all joints required additional increases to complete the grasp after completion of reaching.

Figure 2 shows average angular velocity profile of middle finger during reaching and grasping small, medium, and large handles. The maximum velocity during flexion was largest for the small handle (169, 168, 111 °/s for MCP, PIP, and DIP joint) and smallest in large handle (33, 38, 41 °/s for MCP, PIP, and DIP joint). This explains why normalized final times are smaller in the small handle than in the large handle, even though the angle difference between open angle and final angle is much larger in the small handle. The maximum acceleration during flexion was largest in the small handle (813, 833, 514 °/s^2 for MCP, PIP, and DIP joint) and smallest in the large handle (483, 146, 212 °/s^2 for MCP, PIP, and DIP joint). All these quantitative data can be used to determine the contribution of acceleration and velocity components to actual torques and passive characteristics of each joint in modeling of finger movements. Data for the thumb and other finger joints will be presented.

SUMMARY/CONCLUSIONS

Both spatial and temporal variables were affected by the size of the object in most joints. MCP joint reaches open (final) angle first, and then PIP and DIP joints follow during grasping tasks. Object size also affects velocity and acceleration components during reaching and grasping motions.

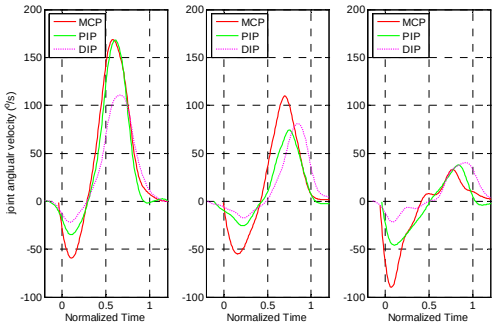

(a) Small (b) Medium (c) Large

Figure 2. Average joint angular velocity vs. normalized time for small to large handles (40 trials for each handle, 16 subjects).

REFERENCES

Buchholz et al., 1992, *J Biomech 25.*

Choi et al., 2006, *16th IEA Meeting.*

Jeannerod et al., 1984, *J Mot Behav 16.*

Paulignan et al., 1997. *Exp Brain Res. 114*

Santello et al., 2002. *J Neuroscience 22*

Zhang et al., 2002, *Human Mov Sci 22.*

ACKNOWLEDGEMENTS

The project was funded by NIOSH (National Institute for Occupational Safety and Health).

Table 1: Rest postures, open angles, final angles, normalized open times, and normalized final time for middle finger [mean (std)].

	Rest Posture(°)	Open Angle (°)			Final Angle (°)			Normalized Open Time			Normalized Final Time		
		Lg	Med	Sm	Lg	Med	Sm	Lg	Med	Sm	Lg	Med	Sm
DIP	13.2 (8.6)	5.1 (2.6)	6.7 (3.8)	7.7 (5.5)	22.8 (8.2)	34.6 (9.6)	51.8 (8.8)	0.55 (0.21)	0.56 (0.15)	0.41 (0.11)	1.49 (0.27)	1.38 (0.23)	1.33 (0.22)
PIP	35.7 (12.2)	17.8 (9.3)	25.4 (10.6)	26.6 (11.9)	28.9 (8.0)	49.0 (7.4)	80.4 (5.8)	0.55 (0.17)	0.50 (0.14)	0.35 (0.07)	1.41 (0.25)	1.30 (0.21)	1.22 (0.18)
MCP	34.0 (12.9)	8.4 (5.4)	12.6 (7.4)	16.7 (8.7)	22.0 (10.8)	49.2 (8.5)	80.0 (5.0)	0.35 (0.15)	0.43 (0.09)	0.32 (0.08)	1.35 (0.26)	1.31 (0.21)	1.23 (0.18)

INFLUENCE OF CYCLING INTENSITY ON RUNNING KINEMATICS AND ELECTROMIOGRAPHY IN WELL TRAINED TRIATHLETES

Javier Mon, Ramón Maañón, Oscar Viana, Jose A. Sánchez, Rafael Martín, Miguel Fernández del Olmo*

Faculty of Sciences of Sport and Physical Education (INEF Galicia)
*E-mail: mafo@udc.es

INTRODUCTION

The sport of triathlon comprises a sequential swim, cycle, and run over a variety of distances. One of the main problems of this sport is the difficulty in run foot after the cycling bout. Compared with an isolated run, the first few minutes of triathlon running induce a variety of physiological changes (VO2 increased, alterations in ventilatory efficient) that lead an increase in the energy cost (Bernard et al., 2003; Millet and Vleck, 2000). These physiological changes have been related with neuromuscular and biomechanics alterations on running pattern (Gottschall and Palmer, 2002; Vercruyssen et al., 2002).

However, for our knowledge there are not studies in which the triathletes are required to keep a continuous and identical velocity after two bouts of different cycling intensities. This approach can be useful to understand which mechanisms are more stables in neuromuscular and biomechanics running pattern.

METHODS

Subjects

14 male triathletes with at least 5 years of racing experience participated in this study. 8 compete in international level and 6 in national level. All athletes gave written informed consent that followed the guidelines of the University of A Coruña Human Research Committee.

Procedures

4 testing sessions in 2 separated days:
Session 1.- a maximum aerobic power incremental test (MAP) in ergocycle, besides to a maximum aerobic speed incremental run test (MAV)
Session 2.- 5 Km isolated run at speed of 85% of MAV (5kmAIS);
Session 3.- 45 min cycling at 55% of MAP followed by 5 Km running at objective speed of 85% of MAV (5kmtB55);
Session 4.- 45 min cycling at 70% of the MAP followed by 5 Km running at objective speed of 85% of MAV (5kmtB70).

EMG activity from the vastus lateralis (VL), bíceps femoris (BF), medial gastrocnemius (MG) and gluteus (GL) muscles of the right leg were continually recorded during the experimental sessions both for the cycling and running bouts. Kinematics data was obtained during the first 50 meters of each lap by video recording at 50 Hz sampling rate. Five video cameras were positioned each 10 meters to record. The stance and swing time was recording by a contact sensors wear in the shoe and connected to the portable EMG data acquisition system (Biometrics DataLog P3X8, Biometrics Ltd, UK) at a 1000 Hz sampling rate.

Statistical analysis

A two way repeated measures ANOVA (Condition * Distance) was performed to analyse the EMG and kinematics parameter during the run for each condition.

RESULTS AND DISCUSSION

The main finding in this study shows that, in the cycle-run conditions, the EMG parameters in the run bout are not affected by the cycling intensity. Compared with the isolated run the results show a significant higher RMS of MG and VL for the cycle-run conditions (figure 1). Surprising the variability of the EMG (calculated as the sum of the variability in all the muscles) was significant lower ($F = 5.68$ $p = 0.01$) for the cycling-run conditions compared with the isolated run.

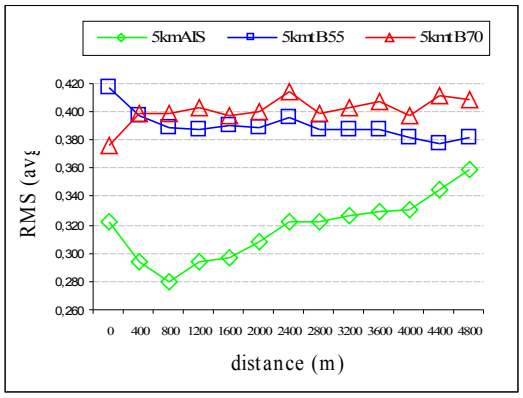

Figure 1: RMS of vastus lateralis for the three different conditions.

The kinematics analysis showed a significant decrease in the sum of the hip, knee and ankle angles during the support phase for the 5kmtB70 compared with the 5kmAIS and 5kmtB55 ($F = 2.33$ $p = 0.019$). This difference was significant during the first 1200 meters (figure 2).

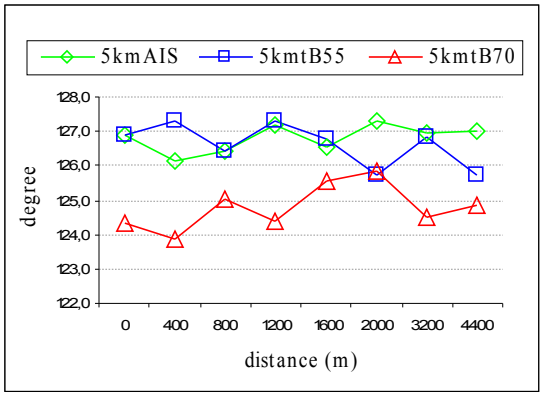

Figure 2: Sum of the hip, knee and ankle angles during the support phase.

SUMMARY/CONCLUSIONS

Our study shows that when the triathletes have to keep a constant running velocity, the cycling intensity can affect the kinematics of the running without affect the EMG parameters. The isolated running in well training triathletes is not the best situation to study their running pattern.

REFERENCES

Bernard, T., Vercruyssen, F., Grego, F., Hausswirth, C., Lepers, R., Vallier, J.M., et al. Effect of cycling cadence on subsequent 3 km running performance in well trained triathletes. Br J Sports Med, XXXVII(2). 2003. 154-158; discussion 159.

Gottschall, J.S., & Palmer, B.M. The acute effects of prior cycling cadence on running performance and kinematics. Med Sci Sports Exerc. XXXIV(9). 2002. 1518-1522.

Vercruyssen, F., Brisswalter, J., Hausswirth, C., Bernard, O., Bernard, T., & Vallier, J. M. Influence of cycling cadende on subsequent running performance in triathletes. Med Sci Sports Exerc, XXXIV(3). 2002. 530-536.

Millet, G.P., & Vleck, V. E. Physiological and biomechanical adaptations to the cycle to run transition in Olympic triathlon: review and practical recommendations for training. Br J Sports Med., XXXIV(5). 2000. 384-390.

ACUTE TORSIONAL FAILURE: DO PHYSIOLOGICAL LOADING RATES EFFECT THE SPINE'S LIMIT?

Janessa DM Drake and Jack P Callaghan

University of Waterloo, Waterloo, ON, Canada
E-mail: jdrake@ahsmail.uwaterloo.ca

INTRODUCTION

In performing many work tasks and daily activities, the lumbar spine is routinely exposed to axial rotational motions and moments. From the anatomical structure of the spine it can be postulated that the facet joints function as the primary resistance of any applied axial rotation/moment. Damage to the facet joints can be one source of pain. However, previous work investigating acute axial rotational failure tolerances of functional spinal units (FSUs) was performed using variable compressive loads and applied moments making evaluation of failure difficult (Adams and Hutton, 1981; Farfan, 1969; Farfan et al., 1970). Yingling et al. (1997) have shown the rate of loading effect the ultimate strength and mode of failure in FSUs in acute compressive failure testing.

Without failure limits it is impossible to contextualize failure results that occur in various loading conditions. Defined limits will also enable the comparison of different experimental outcomes. Therefore, the failure point due to axial rotation needs to be quantified as well as how other factors can mitigate the failure point. The purpose of this study was to investigate how loading rate mitigates acute rotational failure of FSUs in a neutral posture.

METHODS

Eighteen porcine cervical spine FSUs (C3/4) were axial loaded with 1500N of compressive force combined with one of two axial twisting rates, either 2°/s or 6°/s. Specimen preparation involved removal of the surrounding muscle tissue leaving the osteoligamentous structures of the FSUs. The FSUs were secured to aluminum cups via 16-gauge wire and dental plaster (Callaghan & McGIll, 2001). To enable radiographic documentation of the nucleus pulposus, it was injected with approximately 0.7mL of a radio-opaque mixture. The FSUs were mounted into a custom three-axis servo-hydraulic dynamic testing system. The specimens were preloaded with 300N of compression in a neutral posture for 15 minutes to precondition the specimens and counter any swelling that had occurred postmortem. The specimens were then subjected to 1500N of compression and the ranges of motion (RoM) were quantified by flexing-extending just beyond the neutral zone five times at a rate of 0.5°/s, followed by left and right axial twist motions at a rate of 0.7°/s.

The specimens were randomly assigned to loading rate and testing direction groups. Following the RoM testing, failure testing to the right or left was performed. The rest of the protocol involved a second RoM test, failure in the opposite direction, and a final RoM test. The FSUs were X-rayed prior to and following failure testing. Both macroscopic and radiographic damage to the FSU were recorded. Figure 1 exhibits the type of failure data collected. The angle at failure coincides with the time when the peak moment was recorded.

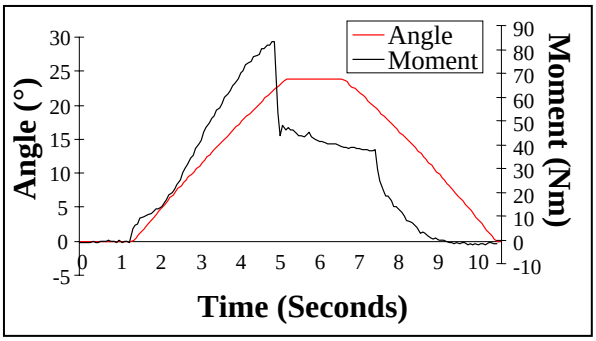

Figure 1: A representative failure curve. Shown is a failure to the right, at a loading rate of 6°/s.

RESULTS AND DISCUSSION

There were no statistical differences between left/right direction of failure for the moment (P=0.811) or angle (P=0.313) as shown in Figure 2. There were also no statistical differences between the failure moment (P=0.506) or angle (P=0.411) for the two loading rates of 2°/s, and 6°/s. The specimens failed at 73.4 ±17.3 Nm and 73.2 ±18.2 Nm of axial moment in the 2°/s, and 6°/s respectively. The peak angle at failure for 2°/s was 20.2 ±3.7° and was 19.9 ± 3.2° for the 6°/s loading rate.

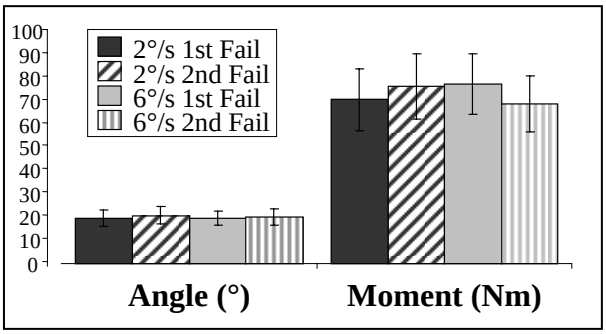

Figure 2: The angle and moment values for the 2°/s and 6°/s rotational loading are subdivided into the first failure (solid) and second failure (striped) for the specimens.

All of the specimens failed at the junction of the laminae with the superior articular facets on the C4 vertebra. The failure occurred when the facet joint was compressed due to the applied rotation. There was no observable disruption of the annular fibres of the intervertebral disc, and there was no movement of the nucleus pulposus.

Farfan (1969) reported that intact FSUs, under approximately 427N, failed with 32.7Nm range 26.0-39.5Nm) of applied axial moment. Based on this data, the porcine specimens in this study would likely be within the range of human FSUs, if they were also loaded with 1500N of compression. The angular displacement at failure reported by Farfan et al. (1970) for human FSUs was 22.6°. The porcine specimens in this study failed at similar angles.

SUMMARY/CONCLUSIONS

There was no effect of physiological loading rate on the failure data or damage observed. This suggests acute torsional failure may not be sensitive to loading rate. This work will be useful in contributing to understanding the mechanical characteristics and injury mechanisms of the spine when exposed to twisting motions/moments of varying rates.

REFERENCES

Adams, M.A., Hutton, W.C. (1981), *Spine*, **6**, 241-248.

Callaghan, J.P., McGill, S.M. (2001) *Clin. Biomech.*, **16**, 28-37.

Farfan, H.F. (1969). *Can. J. Surg.*, **12**, 336-341.

Farfan, H.F. et al. (1970). *J. Bone Joint Surg.*, **52A**, 468-497.

Yingling, V.R. et al. (1997). *Clin. Biomech.*, **12**, 301-305.

ACKNOWLEDGEMENTS

Janessa Drake is supported by a Canadian Institute for the Relief of Pain and Disability (CIRPD)/Canadian Institutes of Health Research (CIHR) Doctoral Research Award.

THE EFFECT OF STROKE LENGTH ON ACTIVE DRAG IN SWIMMING

Bryan J. Morrison [1,2] & Richard N. Hinrichs [2]

[1] Valparaiso University, Valparaiso, IN, USA
[2] Arizona State University, Tempe, AZ, USA
E-mail: bryan.morrison@valpo.edu

INTRODUCTION

The main resistive force in swimming is due to drag on a swimmer's body from the water. There are two forms of drag, one is active drag (F_D), which is the drag encountered while propelling the body through the water. The other is passive drag or the drag encountered while gliding during a push-off after a turn or after entering the water from the start. These different types of drag are both proportional to the frontal area (the projected area that is perpendicular to the direction of travel) and approximately proportional to the square of the swimmer's velocity (Clarys, 1978). Minimizing the frontal area of the body in the water can reduce drag and is achieved both by streamlining and by increasing buoyancy in the water (such that more of the body is out of the water and/or the body is positioned more horizontally) (Kolmogorov et al., 1997). It was also determined that the best swimmers have been able to find a way to minimize active drag. Others have found low passive drag to be a good predictor of performance (Chatard et al., 1990).

The speed at which a swimmer moves through the water can be broken down farther into two components, the stroke length (SL) and stroke rate (SR). Velocity (V) can be calculated by the equation V = SR×SL. When swimming at a constant velocity, reduced drag tends to alter the SL×SR combination selected for that velocity by increasing SL and decreasing SR (Chatard & Wilson, 2003). In other words drag affects the SR×SL relationship chosen for a selected velocity.

Toussaint and colleagues (1989) looked at density changes and found when density is reduced performance is improved due to a reduction in drag. They used a system called the Measurement of Active Drag (MAD) system. The MAD system is composed of equally spaced rigid pads placed beneath the surface of the water that the swimmers push against to propel them through the water. The force applied to each pad is recorded to determine the propulsive force, which on the average is numerically equal to the resistive force when traveling at a constant velocity. The purpose of this study is to investigate the relationship between active drag and SL at a constant velocity. It is hypothesized that there will be a minimum active drag for each swimmer.

METHODS

Subjects were recruited from an NCAA Division I swim team with a mean age of 19.1 ± 1.2 years for the men and 18.6 ± 1.1 years for the women. Ten men and 10 women participated and signed informed consent forms approved by the institutional review board. The mean mass was 79.0 ± 6.9 kg and 69.4 ± 5.2 kg for the men and women, respectively. The mean height of the male subjects was 1.82 ± 0.055 m, while the mean height for the female subjects was 1.73 ± 0.050 m.

A MAD-type system (Toussaint, et al., 1989) was constructed and placed in the water below the swimmers. Three different sets of paddles were used. These paddle sets had a between paddle distance of 1.25 m, 1.35 m, or 1.45 m. Each set of paddles was constructed with 27.4 m of ¼ inch galvanized cable with standard lane line end components. Each swimmer was given as long as needed to become comfortable with the SL and SR for each trial. The order of SL was balanced to remove any learning that may have occurred during the three trials. The SR was chosen to create a velocity of 1.5 m/s and was maintained by using a Tempo Trainer (Finis, Livermore, CA) and checked by looking at the onset of force at each paddle over the entire length. Only lengths with an error of no greater than 5% of the selected SR were analyzed.

RESULTS AND DISCUSSION

The results showed a significant between subjects effect of gender ($p<.05$) as expected from previous studies. Women had a significantly lower drag than men ($p<.05$). The SL manipulation resulted in significant active drag changes ($p<.05$). Both men and women had a within subject effect of active drag. The men and women had a significantly lower active drag for the 1.35 m SL condition compared to the 1.25 m and 1.45 m conditions (Figure 1). Both men and women had a significant quadratic effect ($p<.05$) and minimum active drag force for 1.5 m/s. Each subject had their own SL that resulted in a minimum active drag when the data was fit by a second order polynomial.

These results demonstrate that each swimmer is unique and will have their own active drag-SL relationship. Investigating a large enough sample size would help demonstrate whether ability level is also a factor in the SL that minimizes active drag.

SUMMARY/CONCLUSIONS

Understanding the active drag and SL relationship in freestyle swimming can lead to an improvement in swimming and training techniques. Designing a training program to improve SL at a given velocity's minimum active drag will improve performance in all race distances. Another technique could be to lower active drag at a given velocity and SL. These two techniques could be used to enhance all levels of swimmers from recreational to triathletes to Olympians.

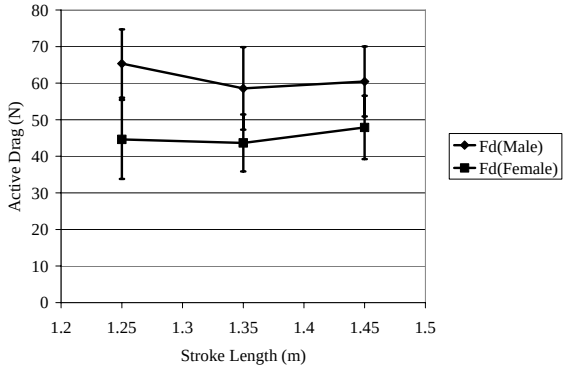

Figure 1: The results of the stroke length manipulations on active drag in freestyle swimming.

REFERENCES

Clarys, J. P. (1978). Human Morphology and Hydrodynamics. Baltimore: University Park Press.

Kolmogorov, S. V., Rumyantseva, O. A., Gordon, B. J., & Cappaert, J. M. (1997). J Appl Biomech, **13**, 88-97.

Chatard, J. C., Lavoie, J. M., Bourgoin, B., & Lacour, J. R. (1990). Int J Sports Med, **11**, 367-372.

Chatard, J. C., & Wilson, B. (2003). Med Sci Sports Exerc, **35**, 1176-1181.

Toussaint, H. M., et al. (1989). Med Sci Sports Exerc, **21**, 325-328.

MECHANICAL VIBRATIONS REDUCE THE INTERVERTEBRAL DISC SWELLING AND MUSCLE ATROPHY FROM BED REST

Nilsson Holguin[1], Jesse Muir[1], Harlan J. Evans[2], Yi-Xian Qin[1], Clinton Rubin[1], Mark Wagshul[1], and Stefan Judex[1]

[1]Department of Biomedical Engineering, State University of New York-Stony Brook, Stony Brook, NY11794
[2]Johnson Space Center, NASA, Houston, TX 77058
E-mail: Nilsson.Holguin@gmail.com

INTRODUCTION

Loss of functional weight bearing, such as experienced during space flight or bed rest (BR), distorts intervertebral disc (IVD) [1] and muscle morphology [2]. IVDs are avascular structures consisting of cells that may derive their nutrition and waste removal from the load induced fluid flow into and out of the disc [3]. A diurnal cycle is produced by forces related to weight bearing and muscular activity, and comprised of a supine and erect posture over a 24 hr period. A diurnal cycle will include a disc volume change of ~10-13%. However, in space there are little or no diurnal changes because of the microgravity, which removes the gravitational load and compressive forces to the back muscles. The BR model and the etiology of the disc swelling and muscle atrophy could provide insight into those subjects confined to bed for chronic disease/injury and aging. We hypothesize that extremely low-magnitude, high-frequency mechanical vibrations will abate the disc degeneration and muscle loss associated with long-term BR.

METHODS

Eighteen normal subjects were recruited. The study, thus far, consisted of 10 males and 8 females (33 ± 7 yrs). Control subjects underwent BR for up to 90d and were scanned by computed tomography (CT) at 0d (n=10), 45d (n=4), or 90d (n=6) and MRI at 0d (n=2), 60d (n=2), 90d (n=2) and 8d after completion of BR (n=2). Experimental subjects (VIBE) were subjected to 90 days of bed rest but received vibrations at 0.3g and 30Hz for 10min/day. The VIBE subjects were scanned by CT at 0d (n=8) and 90d (n=8), and by MRI at 0d (n=8), 60d (n=6), 90d (n=7) and 8d after completion of BR (n=7).

CT scans were taken between T12 and L3 to measure the IVD and back muscle volume. MRI scans were taken between T12 and S1 to measure the IVD and nucleus volume. Tissues volumes were contoured by hand. In all subjects, lean whole body mass was determined by DXA. Differences between groups were assessed by Students' T-test ($p<0.05$).

RESULTS AND DISCUSSION

Effective countermeasures to long term BR are currently not available. Exercise regimes involving walking with and without additional backpacks indicate that conventional mechanical loads applied at relatively low frequencies are unable to return disc volume to normal levels [4]. By increasing the frequency of the mechanical signal, extremely low-magnitude, high frequency whole body vibrations can be anabolic and/or anti-catabolic to muscle [5].

Data from a previous study [6] were used to compare our 90d data groups to 1d of BR. IVD volumes measured by CT scans (Fig.1)

showed that after 90d of BR the volume of the IVD of control subjects increased by 55% in L1-L2 ($p>0.05$) and 60% in L2-L3 ($p<0.05$). In contrast, the superposition of low-level vibrations for 10 min/d mitigated this expansion by 61% ($p<0.01$) in T12-L1, 36% ($p<0.05$) in L2-L3, and 33% ($p>0.05$) in L1-L2. IVD volumes measured by MRI scans showed that mechanical vibrations concomitant to BR abated the IVD swelling at 60d by 150% and 90d by 65%. Eight days after BR, the control group showed a plasticity of 9%, while the VIBE group showed no residual change ($p>0.05$). There was not any difference in the swelling of the nucleus pulposus between the control and VIBE groups.

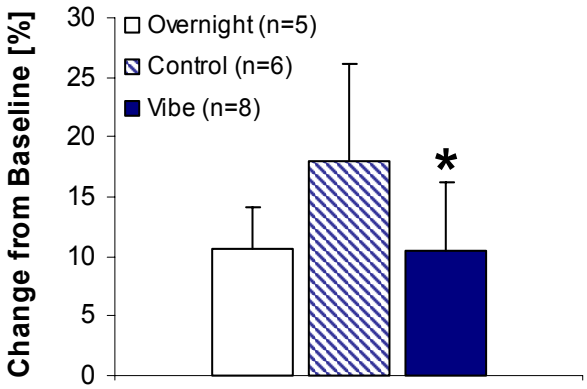

Fig. 1. IVD swelling from baseline (mean + SD), as measured by CT scan in control and VIBE subjects

Mechanical vibrations reduced the back muscle atrophy from long-term BR by 33% ($p>0.05$). Intrinsic back muscle volume was highly correlated with DXA whole body lean mass ($R^2=0.97$). Whole body vibrations reduced the whole body muscle mass loss from -2.1% to -1% ($p>0.05$).

The MRI data showed that the differences between controls and vibrated subjects were associated with changes in the annulus fibrosus, rather than the nucleus pulposus. The plasticity reduction posits that vibrations will not only attenuate the harmful effects of long-term BR during BR but after BR as well.

SUMMARY/CONCLUSIONS

The mechanisms by which whole body vibrations affect soft tissues are yet to be determined. However, considering the additional potential benefits of whole body vibrations on the skeletal and sensorimotor system, these mechanical signals may present a promising non-pharmacologic countermeasure of tissue degeneration both on earth as well as in space

REFERENCES

[1] A. D., LeBlanc, H. J., Evans, V. S., Schneider, R. E., Wendt, 3rd, and Hedrick, T. D. (1994). *Spine*, 19(7), pp. 812-817.

[2] P. E., di Prampero, and M. V., Narici, (2003). *J. Biomech*, 36(3), pp. 403-412.

[3] S., Holm, and A., Nachemson. (1983). *Spine*, 8(8), pp. 866-874.

[4] W. C., Hutton, J. A., Malko, and W. A., Fajman. (2003). *Aviat Space Environ Med.* 74(1), pp. 73-78.

[5] X. J. Musacchia and S. Fagette. (1997). *J Gravit Physiol*, 4(3), pp.49-59.

[6] J.A., Malko, W.C., Hutton, and W.A. Fajman. (2002). *J Spinal Disord Tech*. Apr;15 (2):157-63.

ACKNOWLEDGEMENTS

This research opportunity was funded by the National Space Biomedical Research Institute and NASA.

CAN A PASSIVE DYNAMIC WALKING ROBOT EXHIBIT A DETERMINISTIC NONLINEAR GAIT?

Timothy N. Judkins[1], Chris Arellano[2], Melissa Scott-Pandorf[2] and Max J. Kurz[2]
[1]Dept of PTRS, University of Maryland School of Medicine, Baltimore, MD
[2]Laboratory of Integrated Physiology, University of Houston, Houston, TX, USA
E-mail: tjudkins@som.umaryland.edu

INTRODUCTION

There is a growing body of evidence that nonlinear step-to-step variations are related to how the nervous system controls stable locomotion. However, we still have a limited understanding of how the neuromechanical variables of the locomotive system influence the observed nonlinear structure. Reliable models that closely resemble the nonlinear gait dynamics are required to advance our knowledge in this scientific field. Recently our lab and others have demonstrated that a passive dynamic walking model can have a deterministic nonlinear gait pattern (Garcia et al., 1998; Kurz & Stergiou, 2006). Results from the simulations of these models suggest that it may be possible to build a physical walking robot that has a deterministic nonlinear gait pattern. Here we explored if the results from our simulations can be extended to a physical passive dynamic walking robot, which can provide insight into the nonlinear gait patterns observed in human walking.

METHODS

We built the simplest passive dynamic walking robot that could walk with a stable gait in three dimensions (Fig 1A). The robot had two rigid legs, a pin joint between the hips, and feet that were curved in the sagittal and frontal planes. The foot curvature in the frontal plane allowed for the robot to avoid collisions at mid-stance by slightly rocking to the side. Walking was initiated by positioning the robot at the top of a slightly inclined treadmill and giving it a slight push sideways. The robot would rock over the stance leg, and the opposite leg would swing forward taking a step down the treadmill. At foot-strike the robot would rock onto the opposite foot for the next step of the gait cycle. We evaluated five stable long-term locomotive trials (40-100 steps per trial) from the robot as it walked on the treadmill (Biodex, RTM 400, Shirley, NY). A high speed (60 Hz) three-dimensional motion capture system (Vicon-Peak, Centennial, CO) was used to evaluate the sagittal plane leg kinematics of the robot's gait.

A

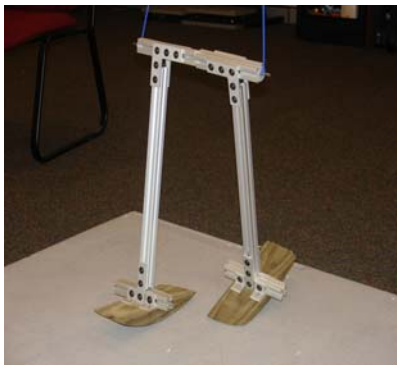

B

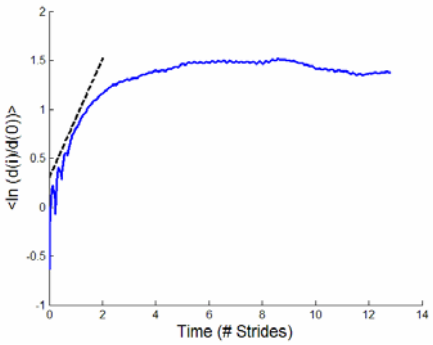

Figure 1: A) Passive dynamic walking robot. B) Divergence curve for the robot's gait. The slope of the best fit line estimates the largest Lyapunov exponent.

State space reconstruction of the locomotive attractor from the leg angle time series was performed using standard embedding techniques (Kantz & Schreiber, 2004). This process involved using an average mutual information algorithm to calculate the time lag, and a global false nearest neighbors algorithm to calculate the number of embedding dimensions.

The largest Lyapunov exponent (λ) was calculated to quantify the nature of the variations in the locomotive attractor. λ quantifies the rate of divergence of neighboring trajectories in the locomotive attractor and the sensitivity of the system to local perturbations. Increases in λ indicate increases in the amount of divergence in the locomotive attractor. The rate of divergence was determined by calculating the Euclidean distances between neighboring trajectories in state space as a function of time (Eq. 1; Rosenstein et al., 1993).

$$y(i) = \frac{1}{\Delta t}\left\langle \ln[d_j(i)\right\rangle \qquad [1]$$

λ was estimated from the slope of the linear region of the divergence curve that exists from zero to two strides (Fig 1B). A pseudo period surrogation (PPS) algorithm was used to determine if the divergence in the reconstructed attractor were deterministic or stochastic fluctuations (Miller et al., 2006). If λ for the surrogate (λ_{surr}) was significantly different from λ for the original data (λ_{orig}), it can be inferred that the variations in the gait pattern were deterministic.

RESULTS AND DISCUSSION

The time lag and embedding dimension used to reconstruct the locomotive attractor were 16 $\pm$ 0.8 and 4, respectively. λ_{surr} was significantly different than the λ_{orig} (λ_{orig}=0.63±0.2; λ_{surr}= 1.14$\pm$0.2; p=0.003). This indicated that the nonlinear variations in the robot's gait pattern were deterministic and possibly chaotic. The deterministic step-to-step variations in the robot's gait were most likely a result of the mechanical coupling of the components of the locomotive system. It is still debatable if the variations in human locomotion are stochastic, deterministic or both. However, the results presented here support the notion that the variations in a locomotive system can have a deterministic pattern. Possibly, the passive dynamics of the locomotive system may play some role in the observed deterministic portion of the step-to-step variations.

SUMMARY/CONCLUSIONS

We were able to build a passive dynamic walking robot that is capable of a deterministic nonlinear gait pattern. This robot will provide a new scientific platform for exploring what neuromechanical variables influence the nonlinear features of gait.

ACKNOWLEDGEMENTS

Research was supported by the Texas Learning and Computational Center Grant awarded to MJK.

REFERENCES

Garcia, M., Chatterjee, A., Ruina, A., Coleman, M. (1998). *J Biomech Eng* **120(2):281-8**.

Kantz, H. & Schreiber, T. (2004). *Nonlinear Time Series Analysis* Cambridge University Press: New York.

Kurz, M.J.. & Stergiou, N. (2005). Bio Cybern **93(3):213-21**.

Miller, D., Stergiou, N., Kurz, M.J. (2006). *J Biomech* **39(15):2873-6**.

Rosenstein, M.T., Collins, J.J. & De Luca, C.J. (1993). *Physica D* **65:117-134**.

METHOD FOR VISUALIZATION AND ANALYSIS OF THE 3D JOINT AXIS COMPLEX

Thomas M. Greiner[1] and Kevin A. Ball[2]

[1] University of Wisconsin – La Crosse, La Crosse, WI, USA
[2] University of Hartford, West Hartford, CT, USA
E-mail:greiner.thom@uwlax.edu

INTRODUCTION

Multidimensional data capture is now routine in the study of biomechanics, yet researchers are still confronted with vexing methodological limitations. There are no established and accepted methods available to utilize and analyze data that describes the coupled relationship between the orientation of an axis and its associated motion. We present a method, illustrated with a simple analysis of the tibiotalar joint, that reduces a joint's multiple axes to a simple shape (the axis triangle) for each joint observation. Visualization of these triangles provides a quick and easy method for appreciating biological variation. Employing the tools of shape analysis also allows for the correct application of multivariate statistical techniques. The axis triangle method provides for an appropriate analysis of the mutually dependent characteristics of joint axis orientation and motion.

METHODS

Figure 1 presents the steps involved in creating an axis triangle. Analogous to the vector-based system of Grood and Suntay (1983), the motion patterns of a joint are evaluated as movements about three non-orthogonal axes. A set of direction cosines describe the orientation of an axis as a vector $\mathbf{e} = (x,y,z)$, where $\|\mathbf{e}\| = 1$. A vector of this form is produced for each axis and is weighted by scalar multiplication of the movement about that axis. These endpoints describe a triangular shape oriented in 3D space. Because this triangle is formed from data derived from kinematic qualities, its shape and orientation serve as a viewable descriptor of those qualities. The growing field of geometric morphometrics provides an analytical perspective to compare these shapes in rigorous fashion using multivariate procedures available in most common statistical packages.

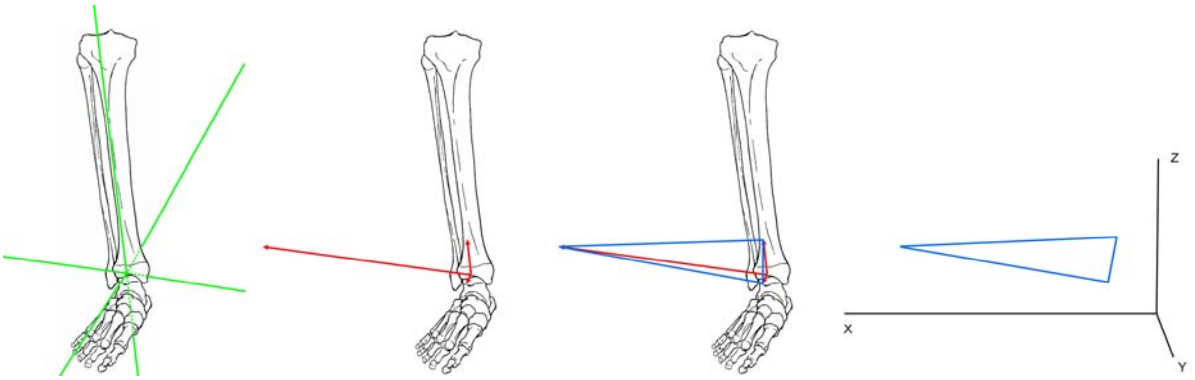

Figure 1. The sequence of forming the axis triangle. Three axes of rotation are identified. Each axis is represented by a vector where its direction corresponds to axis orientation and its length represents the motion about that axis. The end points are connected to form a triangular shape. The shape, size and orientation of this triangle is evaluated as an expression of the joint axis complex.

The data used to illustrate these methods are drawn from a functionally aligned rigid body analysis of the tibia and talus in response to a plantarflexion-dorsiflexion driving motion (Ball, et al., 2004). We demonstrate these data since it is intuitive that plantarflexion-dorsiflexion occurs primarily as rotation about an axis referenced medial-lateral, but lying slightly oblique to the transverse and coronal planes (Inman, 1976). Secondary rotations are less expected. We focus on a comparison of females and males and, for simplicity, analyze total ranges of motion in this demonstration. Coordinate values of the resulting axis triangles are analyzed using the MANOVA procedure within SAS.

RESULTS AND DISCUSSION

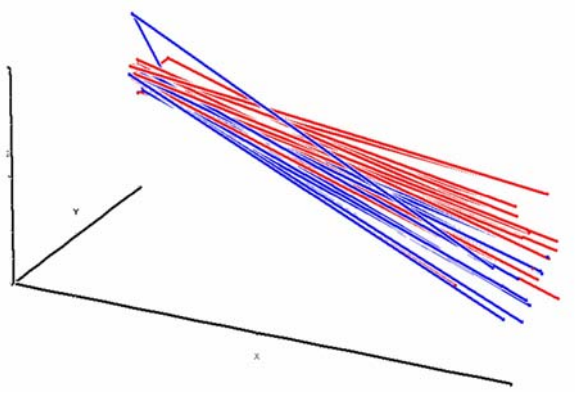

Figure 1. The axis triangles produced to summarize the tibiotalar joint. Blue triangles are the male subjects, red triangles are the females. The figure is rotated so as to maximize the visual appreciation of the differences among the triangles. The axis points referenced to the medial-lateral plane are pointing to the right and slightly down.

Figure 2 shows that both sexes display the predominant influence of the axis referenced to the medial-lateral direction. All triangles are “scalene” but tend towards an isosceles condition with rough equivalence between the points referencing the anterior-posterior and superior-inferior orientations. The female associated triangles appear to be oriented slightly differently than those of the male subjects.

The statistical analysis of the axis triangles produced a Wilks’ λ of 0.2595, an associated F (10,12) of 3.42 with a resulting probability of p=0.0237. Assuming an alpha level of 0.05, these results suggest that the differences between male and female tibiotalar joint axis configurations are statistically significant. *Post hoc* analyses were conducted as a MANOVA evaluation of each axis point in the triangles. The evaluation of the axes referenced to the medial-lateral direction proved to be the sole source of the significant difference between the sexes (p=0.0112). This analysis supports the conclusion that the male and female tibiotalar joint configurations are different. This difference is due to sex specific utilizations of the medial-lateral referenced axis and not to overall joint mobility or to the utilization of secondary axes.

SUMMARY/CONCLUSIONS

The method presented here is one of data transformation that creates an inseparable association between an axis and its associated motion. It provides a means of visualizing relationships based upon complex kinesiological data. It also conditions the data in such a way that it may be analyzed using appropriate multivariate statistical tools.

REFERENCES

Ball, K.A., et al. (2004) *Proceedings of the ISB 3D*, 77-80.

Grood, E.S., Suntay, W.J. (1983) *J. Biomech. Eng.* **105**, 136-144

Inman, V.T. (1976) *The Joints of the Ankle*. Williams & Wilkins

COMPRESSIVE PROPERTIES OF TRABECULAR BONE IN THE DISTAL FEMUR

Travis Burgers[1], Jim Mason[2], Glen Niebur[3] and Heidi Ploeg[1]
[1] University of Wisconsin, Madison, WI, USA
[2] Zimmer Inc., Warsaw, IN, USA
[3] University of Notre Dame, Notre Dame, IN, USA
Email: ploeg@engr.wisc.edu, Web: http://www.engr.wisc.edu/groups/BM/

INTRODUCTION

Early loosening and implant migration are two problems that lead to failures of cementless (press-fit) femoral knee components of total knee replacements. Fehrig et al. (2001) found 27% and 3% of early revision surgeries were a result of implant migration and loosening, respectively. Sharkey et al. (2002) found implant migration to be the cause of 21.2% of early (< 2 years) revisions and 22.2% of late (> 2 years) revisions. They found loosening to be the cause of 16.9% and 34.4% of early and late revisions, respectively. To begin to address these early failures, this study determined the anterior-posterior (AP) mechanical properties of trabecular bone from four locations in the human distal femur.

METHODS

Twenty-eight cylindrical specimens were removed perpendicular to the press-fit surface after the surgical cuts on ten human cadaveric femurs (age 71.5 ± 14.2 years) had been made. The longitudinal axis of each cylinder was approximately in the anterior-posterior direction. These specimens were taken from four locations, shown on the bone and the femoral knee component in Figure 1.

The bone mineral apparent density (BMAD), which is a volumetric density measured using dual energy X-ray absorptiometery, was measured for each specimen. Compression testing was performed utilizing methods to reduce the effects of end-artifacts (Keaveny et al., 1997). The apparent modulus of elasticity, yield and ultimate stress, and yield and ultimate strain were measured.

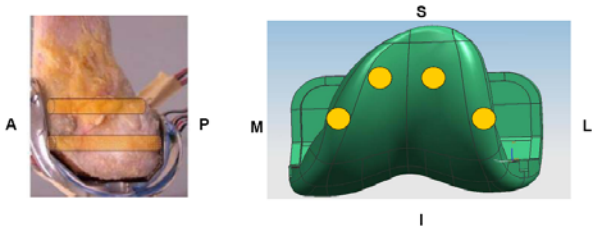

Figure 1: Cores were taken at two locations in the superior-inferior (SI) direction corresponding to the anterior shield, and the intercondylar region of the implant (left). Cores were taken from both medially and laterally at each SI location (right).

RESULTS AND DISCUSSION

An unbalanced two-way analysis of covariance (ANCOVA) was used to determine that the apparent modulus, yield and ultimate stress, and yield and ultimate strain each significantly differed ($p < 0.05$) between the superior and inferior locations. Linear and power law relationships between the mechanical properties and BMAD in each location were determined, as shown in Figure 2. The figure shows that for the same density, the apparent modulus was higher in the inferior region than the superior region. The same result was found for the stresses. These results show that the press-fit fixation characteristics of the femoral knee component differ on the anterior shield and posterior condyles.

SUMMARY/CONCLUSIONS

The significance of this study is the property-density relationship of the distal femur varies as a function of superior and inferior location. This is important for the press-fit fixation of the bone-implant interface because the anterior shield is press-fit in the superior region and the posterior condyles are press-fit in the inferior region.

There are difficulties in comparing the results measured in this study with past studies because BMAD was used here and apparent or quantitative computed tomography (QCT) density has been used in past studies. The power law constants for the superior location (1920 MPa and 0.857) seem to be lower than the previously reported results. But the results of the inferior and pooled locations (16100 MPa and 1.37; 12100 MPa and 1.37) seem to be on the same order of magnitude as the proximal femur multiplicative constant (15010 MPa - greater trochanter) and power constant (1.49 - femoral neck) reported by Morgan et al. (2003).

These property-density relationships will be critical to the assignment of mechanical properties in finite element models for further investigation of the press-fit interface of femoral knee components. Quantifying the loads of this interface will provide a better understanding of the mechanical interaction between the implant and the bone. This research addresses the primary failure mode of femoral knee components and will ultimately lead to improved implant survival rates.

REFERENCES

Fehring et al., 2001. *Clin Orthop Relat Res* **392**, 315-318.

Keaveny, et al., 1997. *J Orthop Res* **1**, 101-110.

Morgan et al., 2003. *J Biomech* **7**, 897-904.

Sharkey et al., 2002. *Clin Orthop Relat Res* **404**, 7-13.

ACKNOWLEDGEMENTS

T. Burgers gratefully acknowledges the support of Zimmer, Inc. for this study and Geoff Piller for his help processing the data.

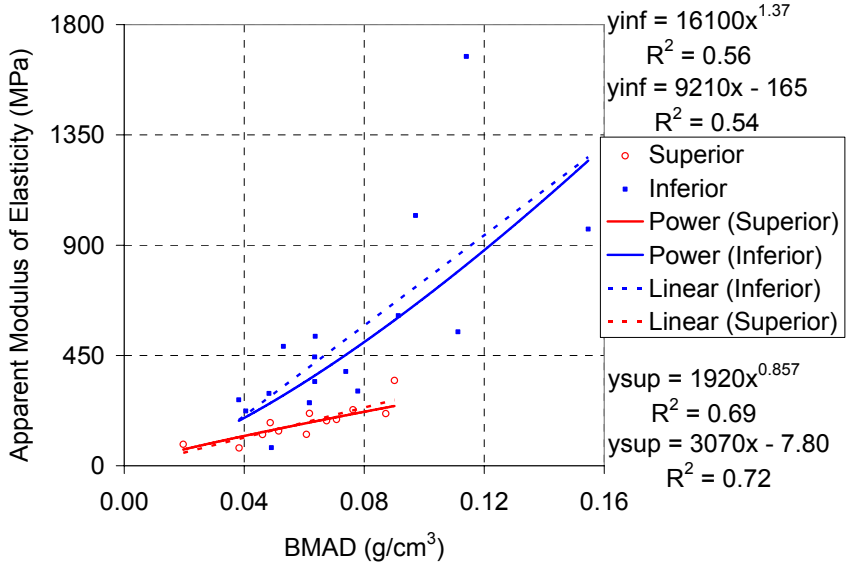

Figure 2: Apparent modulus of elasticity versus bone mineral apparent density. Each of the linear and power coefficients was significantly different for the superior and inferior regions, except the linear constant, which was not significantly different from zero.

Reflex and Nonreflex Characterization of Spasticity in Children with Cerebral Palsy: Dependence of Catch Angle on Velocity

Yi-Ning Wu [1,3] , Hyung-Soon Park[2], Deborah Gaebler[1,2], Jia-Jin Chen[3], and Li-Qun Zhang [1,2]

[1] Northwestern University University, Chicago, IL, USA
[2] Rehabilitation Institute of Chicago, Chicago, IL, USA
[3] National Cheng Kung University, Tainan, Taiwan
E-mail: l-zhang@northwestern.edu

INTRODUCTION

Spasticity, contracture and muscle weakness are commonly seen in children with cerebral palsy. Although it is commonly accepted that spasticity is characterized with velocity-dependent increase in muscle tone, it is not clear whether the commonly measured "catch" is dependent on the movement velocity. Furthermore, convenient and quantitative device/measurement in clinical setting for evaluating children with CP is essential and there is a lack of quantitative and convenient method and device to evaluate spasticity, contracture and muscle weakness in a clinical setting. Hence the aim of this study was to evaluate spasticity, contracture and muscle weakness quantitatively using our custom a Manual Spasticity Evaluator (MSE) and Handheld Tendon Tapper (HTT).

METHODS

Ten children with cerebral palsy with spasticity at the elbow joint, aged between 7 and 16 (mean±std= 10.1±2.8 years old) and a control group of 10 age-matched children, aged from 6 to 15 (mean±std= 11.3±3.2 years old) were recruited for the study.

The children sit upright next to the MSE with the shoulder abducted and flexed at 75˚. The forearm was strapped to the beam of the MSE with the elbow flexion axis aligned with its rotation axis. The arm was secured to a supporting brace. EMG signals were recorded from the biceps and triceps brachii muscles using surface electrodes.

First, different levels of force were applied onto the biceps tendon by the HTT and reflex-mediated EMG and torque responses were measured. Next, the elbow was moved at a slow velocity of 30˚/sec manually, guided by audiovisual feedback to measure the ROM and contracture with controlled terminal torque (0.5, 1 and 1.5 Nm) followed by higher velocities arranged at random order for evaluating spasticity and detecting the catch angle related to stretch reflex. The tapping force, reactive torque τ, joint angle, and EMG signals were sampled simultaneously at 1000 Hz for further analysis.

The reflex torque varies with the tendon tapping force. Hence the gain of the tendon reflex was determined by determining the reflex system impulse response with the corresponding system gain and threshold in tapping force. The catch angle was detected by the abrupt increase of $d\tau/dt$ (Peng et al 2004). Mann-Whitney U test and Spearman rank correlation test were chosen for the statistical analysis.

RESULTS AND DISCUSSION

The gain of the tendon reflex with tapping force and elbow torque as system input and output respectively shows that children with CP had higher tendon reflex gain than the

control subjects (p=.005). The catch angle in children with CP was determined with 4 relevant parameters displayed simultaneously (Fig. 1). The width of the shaded area represented the movement velocity and the gradually narrowed path showed the slow down and choke during the "catch", and the narrowest path occurred after the movement passing through a "hot spot" which stands for the abrupt increase of $d\tau/dt$. The corresponding position of the hot spot was taken as the catch angle (Fig. 1).

The ROM of children with CP was significantly smaller than that of the control subjects at torque limits of 0.5 and 1 Nm ($p<.001$), but showed no difference at 1.5 Nm (p=.058). There was no difference of flexion ROMs between the groups.

The catch angle varied with the velocity considerably (7.17˚±4.37˚) and showed significant correlation with the velocity (correlation coefficient = .25 at α level of .038, Figure 2). In other words, the catch angle occurred later during extension at higher velocities, indicating the increased resistance at higher velocities was also dependent on the position. The $d\tau/dt$ and torque at the catch angle increased significantly with increasing velocity (p=.002 and .005 respectively). Nonetheless the passive torque at the corresponding catch angles at the different velocities was not significantly different.

SUMMARY/CONCLUSIONS

The current results demonstrate that (1) children with CP have higher gain in reflex component, (2) under the controlled terminal torque, the children with CP retain less range of motion toward the extension direction, (3) the sensing of the catch is contributed not only from the reflex component but also the stiffness of the activated muscle when the elbow was moved further at the higher velocities.

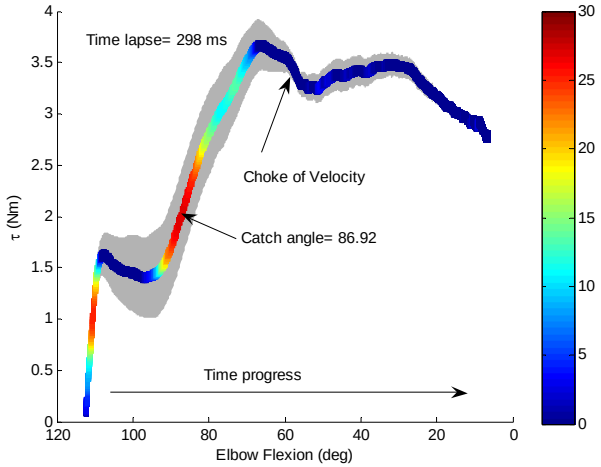

Figure 1: 4-dimensional plot used for catch angle determination. X-axis and Y-axis are the elbow flexion angle and resistance torque of the elbow, respectively. The width of the gray shaded area indicates the stretching velocity by the operator, and the color curve showed the changes of $d\tau/dt$.

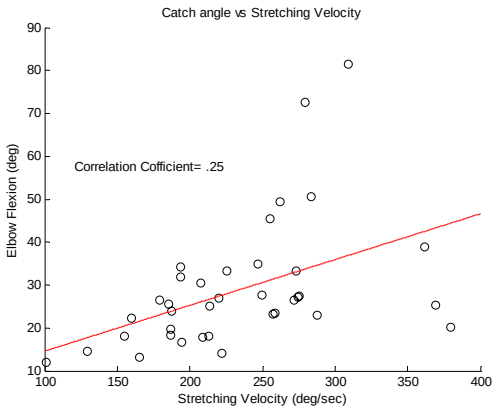

Figure 2: Correlation between the stretching velocity and the catch angle.

REFERENCES

Peng, Q. et al. (2004). *Proceedings of 26th IEEE EMBS'*04,4896-4899

Park, H. et al. (2005). *Proceedings of IEEE 9th ICORR'*05, 303-306

ACKNOWLEDGEMENTS

The authors would like to acknowledge the support of the National Institutes of Health and the National Science Foundation.

ANALYSIS OF STRAINS IN EXTENSOR MECHANISM OF INDEX FINGER

Sang Wook Lee[1], Hua Chen[2], Joseph D. Towles[1], and Derek G. Kamper[1,2]

[1] Rehabilitation Institute of Chicago, Chicago, IL, USA
[2]Illinois Institute of Technology, Chicago, IL, USA
E-mail: sanglee2@northwestern.edu

INTRODUCTION

Understanding of the functional anatomy of the finger extensor mechanism is important for analysis of motor control and facilitation of rehabilitation. Attempts have been made to examine the effects of finger posture on the geometry (Garcia-Elias et al., 1991) and strains of specific components (Hurlbut et al., 1995) of the extensor mechanism. Although these studies provided important information regarding the behavior of the mechanism, the effects of individual tendon forces and the localized response throughout the hood were largely unexplored.

The purpose of this study is thus to provide a thorough examination of the extensor mechanism behavior in response to individual tendon loads. We observed how the entire structure deforms and adapts to each tendon force using a three-dimensional measurement system. Strain and spatial translation of different regions in the extensor hood were examined to provide a comprehensive description of its behavior.

METHODS

Three fresh-frozen cadaveric hands were prepared to examine the behavior of the extensor hood under tendon loading. The distal tendons for the 5 extensor muscles of the index finger, extensor digitorum communis (EDC), extensor indicis profundus (EIP), first dorsal interosseous (FDI), first palmar interosseous (FPI), and lumbrical (LUM), were exposed and sutured to nylon cords to allow tendon loading. Each hand was mounted on a fixation device (Agee-Wristjack, Hand Biomechanics Lab, Sacramento, CA), with the tip of the index finger attached to a clamp with a magnetic base. Strains on the surface of extensor hood were estimated based on the distances between markers attached to the surface of the hood. Fifty-eight markers (diameter: 1.6 mm) were secured to the hood surface (Fig. 1), and their movements were recorded with a three-dimensional motion capture system (DMAS, Spica Technology Corp., Maui, HI). The markers yielded 41 gauge lengths in distal-proximal direction (used to compute longitudinal strain) and 37 in radial-ulnar direction (used to compute lateral strain). The 5 tendons were sequentially loaded at three different postures (Table 1).

Table 1: Experimental conditions

Tendon loading condition					
Tendon	EDC	EIP	FDI	FPI	LUM
Force	1.2kgf	1.2kgf	.9kgf	.9kgf	.6kgf
Postures tested					
P1	MCP: 0º, PIP: 0º, DIP: 0º				
P2	MCP: 30º, PIP: 30º, DIP: 20º				
P3	MCP: 60º, PIP: 45º, DIP: 30º				

(MCP: metacarpophalangeal, PIP: proximal interphalangeal, DIP: distal interphalangeal)

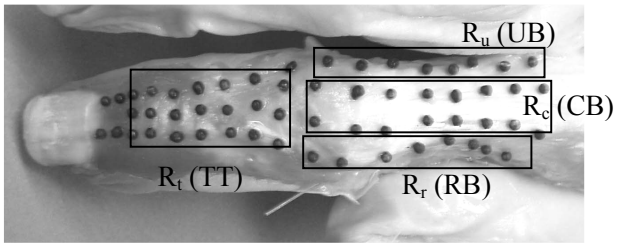

Figure 1: Marker placements on the finger extensor hood and its representative regions (TT: terminal tendon, CB: central band, RB: radial band, UB: ulnar band)

Average lateral and longitudinal strains and spatial translations of four specific regions of the hood surface (Fig. 1) were also examined to capture more global effects.

RESULTS AND DISCUSSION

In EDC and EIP loading, greatest longitudinal strain was observed in R_c (central band) or R_t (terminal tendon) across postures. Negative lateral strain (compression) was observed in most of R_c, R_r (radial band), and R_u (ulnar band), in contrast to zero or small positive lateral strain (stretch) in R_t (Fig. 2(a)).

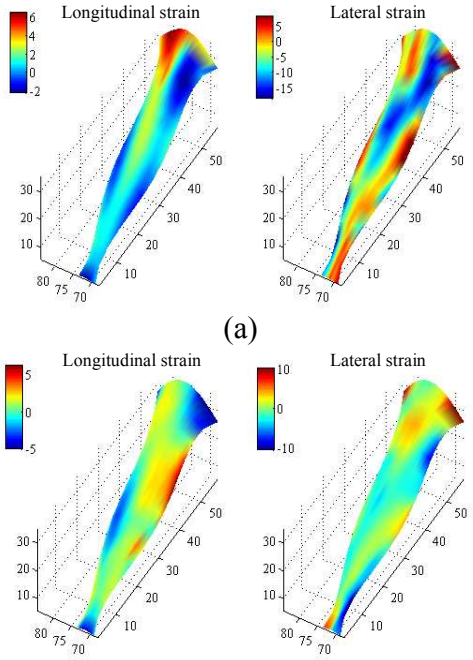

Figure 2: Contour plot of strains in specimen 1 (right hand) (a) EDC (b) LUM

In all specimens, greatest longitudinal strain during LUM loading was observed at R_r near the PIP joint (Fig. 2(b); Table 2). Additionally, large degrees of radial shift of the R_r and R_c regions were observed. In a similar way, in FPI loading, high longitudinal strain at R_u near PIP, and ulnar shift of R_u and R_c resulted (Fig. 3). Spatial translation (ulnar/radial shift), not only deformation, of the hood was found to be an important aspect of its adaptation to tendon forces. In most cases, strains induced by FDI loading were smaller than those induced by other tendons, in accordance with its insertion into the proximal phalanx and transverse or oblique fibers connected to the hood, but not directly into the lateral band as FPI or LUM.

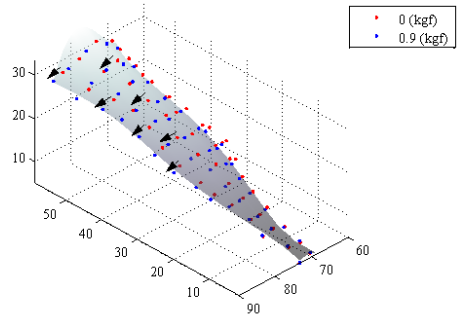

Figure 3: Measured marker movements: ulnar shift of the hood in FPI loading (Specimen 1)

Table 2: Maximum longitudinal strain values (ε_{max}) (%) in all specimens (Posture: P1)

	Specimen 1		Specimen 2		Specimen 3	
	Region	ε_{max}	Region	ε_{max}	Region	ε_{max}
EDC	R_c	6.5	R_c	17.0	R_t	15.8
EIP	R_c	5.5	R_c	7.9	R_u	11.2
FDI	R_r	5.2	R_t	7.3	R_c	4.8
FPI	R_t	9.8	R_u	4.5	R_u	6.5
LUM	R_r	6.2	R_r	6.4	R_r	6.0

Overall, the flexed postures (P2 and P3) displayed deformation patterns similar to those of P1,but with lower strain values; for example, in EDC loading of specimen 2, maximum longitudinal strain values were 17.0, 13.0, and 11.5 (%) in P1, P2, P3 respectively,

It should be noted that the sample size for this study was very small. Further testing is needed to confirm these initial results. Additionally, material testing of the different components of the hood will be performed to assess possible differences in elasticity.

REFERENCES

Garcia-Elias, M. et al. (1991). *J Hand Surg [Am]*, 16, 1130-36.

Hurlbut, P.T., Adams, B.D. (1995). *J Hand Surg [Am]*, 20, 832-40.

EPISODIC SUBLUXATION INCREASES THIRD BODY INGRESS AND EMBEDMENT IN THE THA BEARING SURFACE

Anneliese D Heiner [1,2], Hannah J Lundberg [2,3], Thomas E Baer [1], Douglas R Pedersen [1,2], John J Callaghan [1,2,4], Thomas D Brown [1,2]

[1] Department of Orthopaedics and Rehabilitation, University of Iowa, Iowa City, IA
[2] Department of Biomedical Engineering, University of Iowa, Iowa City, IA
[3] Current Address: Department of Orthopedic Surgery, Rush University, Chicago, IL
[4] Orthopaedics Department, VAMC, Iowa City, IA
E-mail: anneliese-heiner@uiowa.edu Web: poppy.obrl.uiowa.edu

INTRODUCTION

In total joint arthroplasty, third body particles can migrate between the articulating surfaces and result in accelerated wear, by directly abrading the polyethylene liner and by scratching the metal femoral counterface. Third body particles embedded in polyethylene acetabular components are a well-documented finding in total hip retrieval studies, and are suspected of being a major contributor to the variability of wear.

Hip joint subluxation, involving separation between the head and liner subsequent to impingement, is a means by which third body particles could potentially enter the closely conforming articular bearing space. A computational fluid dynamics model has provided theoretical evidence that, during THA subluxation, joint fluid is drawn into the space that opens between the head and liner (Lundberg et al., in press). Third body particles suspended in this fluid would presumably be convected to the articulating surfaces by this mechanism.

The present study was designed to test the hypothesis that occasional events of femoral head subluxation would increase the number of third body particles that enter the bearing space and become embedded in the acetabular liner, as compared to level walking cycles alone.

METHODS

A cemented smooth femoral stem was potted into a femoral fixture at 12° adduction. A metallic acetabular shell was potted into an acetabular fixture at 30° tilt. For each test, a fresh 28mm femoral head and matching fresh UHMWPE acetabular liner were attached to the stem and shell. The specimens were placed in a multi-axis joint motion simulator (Figure 1) mounted in an MTS 858 Bionix. The joint motion simulator allows control of rotations about three axes, as well as control of axial load.

Figure 1: Total hip arthroplasty preparation in a multi-axis joint simulator, with third body particle circulation.

The femoral and acetabular fixtures included rings around which a hip capsule surrogate, consisting of thin plastic sheeting, was secured. The sheeting confined a glycerin-water mixture which served as a (viscosity-matched) surrogate synovial fluid. This fluid was kept circulating through the hip capsule surrogate throughout the test, by means of a peristaltic pump.

Each head-liner pair was first preconditioned by six minutes of level walking cycles. Twenty-five grams of metallic third body particles (CoCrMo beads) were then injected into the system, to circulate along with the surrogate synovial fluid. The walking cycles were then continued for two hours. In five of the ten head-liner pairs tested, twenty flexion subluxation events (Figure 2) were interspersed within the walking cycles. After the test period was completed, the number and location of embedded particles on the acetabular liner were determined.

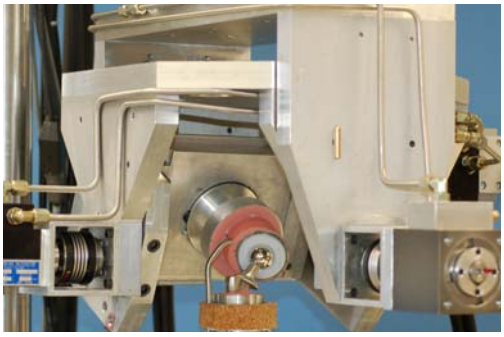

Figure 2: Flexion subluxation motion (hip capsule surrogate removed for clarity).

RESULTS

Subluxation during hip simulator testing dramatically increased the number of third body particles that became embedded in the bearing surface (Figure 3), from an average of 21 particles per liner in the walking-only group, to an average of 334 particles per liner in the walking-plus-subluxation group ($p = 0.007$, 1-tailed Student's t-test). The addition of subluxation also considerably increased the amount of scratching on the femoral heads.

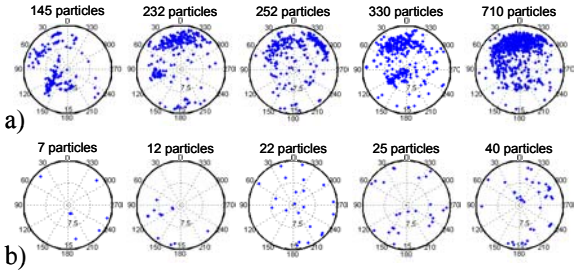

Figure 3: Location and count of embedded third body particles for acetabular liners tested in a hip simulator for a) walking-plus-subluxation cycles, and for b) walking-only cycles. The superior direction is vertical.

DISCUSSION

Subluxation allows third body particles to more easily enter the bearing surface, become embedded into the acetabular liner, and subsequently scratch the femoral head. In contemporary THA, third bodies are a fact of life, due to the supervening desirability of component modularity and non-cemented fixation. Subluxation is also a fact of life, as is demonstrated by retrieval studies showing impingement damage on the majority of acetabular liners. The potent combination of third body particles and hip subluxation therefore needs to be borne prominently in mind when considering mechanisms of accelerated wear.

REFERENCE

Lundberg, H.J. et al. (accepted). *J Biomechanics*

ACKNOWLEDGEMENTS

This study was funded by NIH 5R01 AR047653 and an NSF Graduate Fellowship. DePuy Orthopaedics, Inc., provided the implants.

DETERMINATION OF HEADING FREQUENCY IN YOUTH SOCCER

Erin Hanlon and Cynthia Bir

Wayne State University, Detroit, MI, USA
E-mail: cbir@wayne.edu, Web: www.bioengineeringcenter.org/home/labs/sports

INTRODUCTION

Youth participation in soccer in the United States has increased dramatically, with the American Youth Soccer Organization (AYSO) growing from nine teams in 1964 to 50,000 teams in 2005. This increase in participation has been paralleled with an increase in injuries (Witol 2003). One of the biggest debates surrounding injuries related to youth soccer involves the effects of repetitive heading (Naunheim 2003).

One of the first steps in delineating the effects of repetitive heading is determining an accurate exposure incidence. Currently, there is a lack of on-field data to quantify the incidence of heading in soccer as it relates to player position and age group. The majority of previous studies use a method of athlete reporting. These data are essential to conduct the controlled laboratory experiments needed to ultimately determine the effects of repetitive heading.

The frequent use of athlete reporting in studies relating heading frequency to findings is unreliable and a better method of estimation is required. Therefore, the purpose of this study is to explore the frequency of soccer heading in the youth population across age groups, skill levels and gender.

METHODS

Males' and females' teams ranging in ages from U13 (under 13 years old) to U18 (under 18 years old) were observed during the 2006 Canton Cup Soccer Tournament, a weekend long tournament in Canton, MI. Only teams participating in the top two skill divisions of their age bracket were included in the study. The highest division was given the designation by the tournament of blue and the next highest level was red. A total of 124 teams playing 158 games were observed throughout the tournament. It should be noted that due to the fact that soccer is a spring sport for high school aged females in Michigan, the highest age division for the tournament was U14.

Each header that took place during the game was recorded on a data sheet that contained a grid outline of the soccer field. Both the player number and time of occurrence were noted within the specific area of the grid where the header took place. No personal identifiers were recorded. Different colors were used to denote different teams to allow for a better representation of defensive versus offensive position on the field.

RESULTS AND DISCUSSION

Significant differences between age groups were not noted for either division within the female population. However, for the male population, significant differences were noted between the U12 to U13 and U14 to U15 age groups in the red division. The only significant difference in the male blue division was between the U12 and U15 age groups. A positive linear regression was noted in the male blue division from U12 to U15 (R^2=.9447), however from U15 to U18 there was no significant increase with age.

A similar trend was also noted in the female population (R^2=.9998), but the stabilization effect with age was unable to be assessed due to the lack of data at the older age groups. Significant differences were also reported between the male and female populations across all age groups within each division ($p<0.05$). The male populations were observed to have a higher header/minute ratio than their female counterparts.

Maximum headers in one game by a single player were also monitored to determine the highest exposure incidence. The maximum number of headers in a single game by a player was 13 headers. This was observed in a U14 male blue division game. The range of maximum headers in one game by one player was from 4 to 13 headers.

The current study is limited by the fact that data was collected over a weekend long tournament and that a maximum of three games were observed for each team. Even with these limitations, important trends in the amount of headers players are experiencing and their age.

SUMMARY/CONCLUSIONS

A positive correlation was established between age and headers/minute within the higher skill levels. This occurs up until the age division of U15 at which point a plateau occurs. Although there is currently no data available for the same divisions of the female population, it is expected that there would be a similar trend based on the data available for the U12-U14 age groups. These trends are most likely due to both development of the player and comfort level with the skill. After a certain level is achieved, the overall incidence of heading stabilizes.

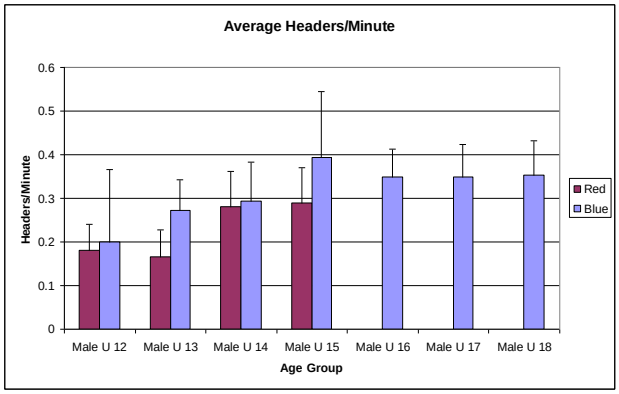

Figure 1: Number of headers/minute for the male population.

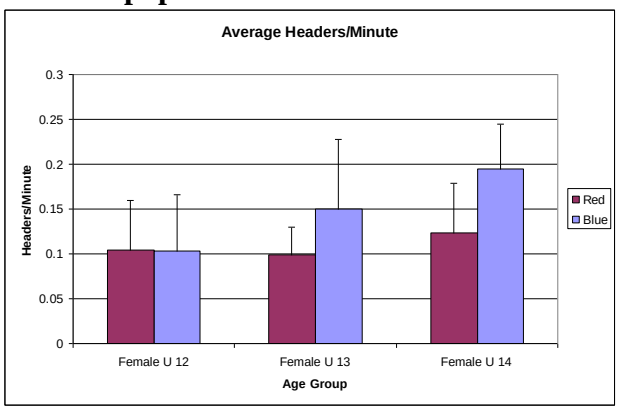

Figure 2: Number of headers/minute for the female population.

REFERENCES

Naunheim, R. S., et al. (2003). *Med Sci Sports Exerc* **35**: 1406-12.

Witol, A. D. and F. M. Webbe (2003). *Arch Clin Neuropsychol* **18**: 397-417.

ACKNOWLEDGEMENTS

This study was funded by the National Operating Committee on Standards for Athletic Equipment (NOCSAE). The authors would also like to acknowledge Daniel Jammoul, Sarah Stojsih, Demario Tucker, Charlene Schreiner, and the monitors from the Canton Soccer Club.

VALIDATION OF TRI-AXIAL ACCELEROMETER FOR THE CALCULATION OF ELEVATION ANGLES

Tal Amasay[1], Keely Zodrow[1], Laurel Kincl[2] and Andrew Karduna[1]

[1]Orthopaedic Biomechanics Lab, University of Oregon, Eugene, OR, USA
[2]Labor Education and Research Center, University of Oregon, Eugene, OR, USA
E-mail: tamasay@uoregon.edu

INTRODUCTION

One of the main issues in occupational studies focusing on musculoskeletal disorders of the upper extremity is to quantify workers' exposures to risk factors during a workday. It has been shown that workers are more susceptible to shoulder injuries when they have a high lifetime exposure to arm elevation above 90° (Svendsen et al. 2004). For whole day ambulatory recordings, body-mounted transducers, in combination with data loggers are used. It has been shown that accelerometers with a DC response can measure static acceleration and therefore can detect orientation relative to the line of gravity (Hansson et al. 2001). However, most of these devices are clumsy, complicated to mount, not self-contained and not commercially available. The Virtual Corset™ (Microstrain Inc, Williston, VT) is a battery powered tri-axial accelerometer with an integrated data logger, all contained within a pager casing with no cables, intended to measure 2 planes of trunk motion, flexion and lateral bending. The purpose of the study was to derive an equation to convert accelerometer data to shoulder elevation angles and to validate this equation with data collected with the Virtual Corset™.

METHODS

The first step was to derive an equation to convert accelerometer data to elevation angles. In a Cartesian coordinate system the angle θ between a vector (x y z) and its projection on the XY plane represents the elevation angle of the vector relative to that plane (figure 1).

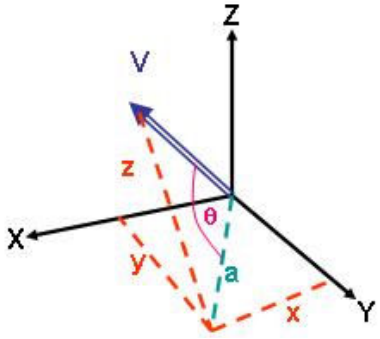

Figure 1: Vector projection on the XY plane.

To find the angle θ we first solve for the length a:

$$a = \sqrt{x^2 + y^2} \qquad (1)$$

Next θ, is given as:

$$\theta = \tan^{-1}\left(\frac{z}{a}\right) \qquad (2)$$

Combining equations 1 and 2 yields equation 3, which solves for the elevation angle as a function of x, y and z:

$$\theta = \tan^{-1}\left(\frac{z}{\sqrt{x^2 + y^2}}\right) \qquad (3)$$

When measuring acceleration with a tri-axial accelerometer (x y z are the component of the acceleration) in static position the resultant vector is the gravitational acceleration, thus, equation 3 can be used to calculate the elevation angle at different orientation of a tri-axial accelerometer relative to gravity.

To validate equation 3, the Virtual Corset™ was mounted on a vise which can be rotated through 360° of elevation and 90° of axial rotation (figure 2), where 0° of axial rotation represents shoulder abduction and 90° of axial rotation is shoulder flexion. A PRO 3600 digital protractor (Macklanburg Duncan, OK), with a reported accuracy of 0.1°, was attached to the vise to identify the elevation angles. The vise was rotated through 360° of elevation in 10° increments. At each elevation angle, the axial rotation was varied from 0° to 90° in 15° increments. Each position was held for 10 seconds and the x y z accelerometer data were recorded and averaged. Elevation angles were calculated using equation 3. This procedure was repeated two different days for the Virtual Corset™.

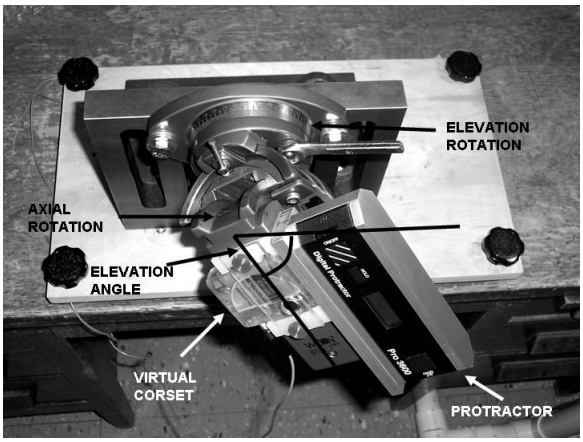

Figure 2: Test setup

The root mean square (RMS) error was calculated for each position between the known inclination angles and the calculated elevation angles.

RESULTS AND DISCUSSION

The RMS error of the calculated elevation angles, for the whole range, was found to be less than 1° for both trials (figure 3). The maximum difference between the calculated and the actual elevation angles was less than 2°. The Virtual Corset™ manufacture reports a typical accuracy of ± 0.5° of projection angles which are limited to 360° of trunk flexion and ± 70° of trunk lateral bending; not reporting angles accuracy when the movement occurs in different planes. Our results showed that the calculated angles error was similar in the different axial rotation angles that were tested.

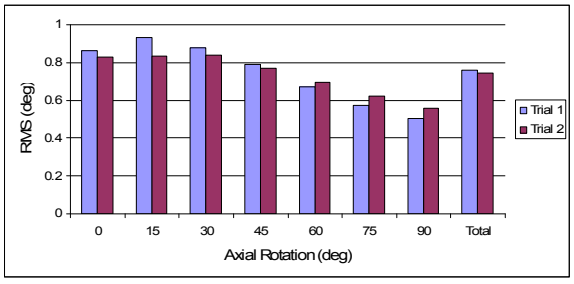

Figure 3: RMS error of elevation angles at different axial rotation in two different trials

SUMMARY/CONCLUSIONS

The tri-axial accelerometer (Virtual Corset™) can be used to accurately reconstruct elevation angles. Future studies will be conducted to measure the elevation angle during dynamic conditions and in-vivo scenarios for the upper extremity.

REFERENCES

Hansson, G. A., et. al., 2001. *Med Biol Eng Comput* 39, 405-13.

Svendsen, S. W., et. al., 2004. *Occup Environ Med* 61, 844-53.

ACTIVE AND PASSIVE SCAPULAR KINEMAITCS IN PATIENTS WITH ROTATOR CUFF TEARS

Olutola Akiode[1], David Suprak[2] and Andrew R. Karduna[1]
[1] University of Oregon, Eugene, Oregon, USA
[2] University of Colorado, Colorado Springs, Colorado, USA
Email: tolakiode@yahoo.com WEB: http://biomechanics.uoregon.edu/obl/

INTRODUCTION

The incidence of rotator cuff tears has been demonstrated to be as high as 40% in people over the age of 40 years. This makes the condition an important one in terms of productivity because of days lost from work and workers' compensation claims from disability. Alterations in scapular kinematics have previously been demonstrated in patients with cuff tears. Most studies demonstrated greater scapular upward rotation in shoulders with rotator cuff tears as compared to normal shoulders in order to achieve the same degree of humeral elevation (Paletta Jr, G.A. et al 1997, Yamaguchi K. et al 2000 and Mell A.G. et al 2005). The aim of the present study was to further examine these kinematic relationships in both an active and passive model.

METHODS

Twenty-two subjects with full thickness rotator cuff tears volunteered to take part in the study. The inclusion criterion was a full thickness tear involving both the supraspinatus and infraspinatus tendons that had been diagnosed by either MRI or ultrasound. Exclusion criteria were previous surgery on the involved shoulder, orthopaedic or neurological disorders of the cervical spine, any neurological condition believed to affect neurological innervation of the shoulder muscles and local steroidal injections in the past 30 days.

During the course of the study, 18 asymptomatic control subjects with no history of shoulder dysfunction were also recruited that matched the patients with cuff tears on the basis of gender and age ($\pm$ 5 years).

Three-dimensional *in-vivo* kinematics of the shoulder was collected using the Polhemus Fastrak (Colchester, VT). A thoracic receiver was placed over T2 with double sided tape and a humeral receiver was mounted on a molded cuff strapped to the distal humerus. A scapular tracker was mounted over the scapular. The tracker had been validated in a previous study (Karduna et al 2001). Surface Electromyography (EMG) data were collected using the Myopac Jr system (Run Technologies, Mission Viejo, CA). Kinematic and EMG data were collected simultaneously. EMG data were normalized to a maximum voluntary contraction (MVC) for each muscle. Active and passive elevation in the coronal planes was performed. In order to minimize the resistance to motion, passive trials were performed on a table with the subject prone and the upper limb supported on a trough connected to an adjustable pole which swung on hinges secured on the ceiling. Passive trials were accepted if the EMG readings were less than 20% MVC.

RESULTS AND DISCUSSION

Data was analyzed for 17 subjects and 18 healthy controls that were able to elevate the arm to 95^0. Mean ages were 73.3 ± 8.4 years for subjects and 71.9 ± 11.8 years for controls. The general trend was similar in both groups during active and passive trials (see figure below).

A

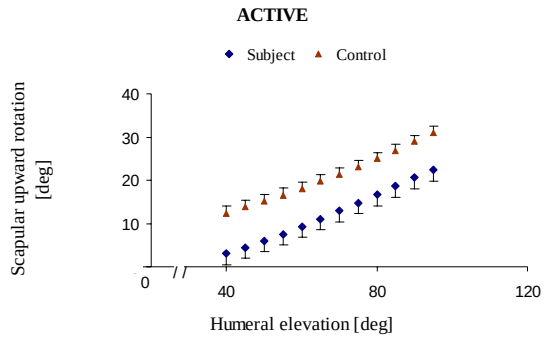

B

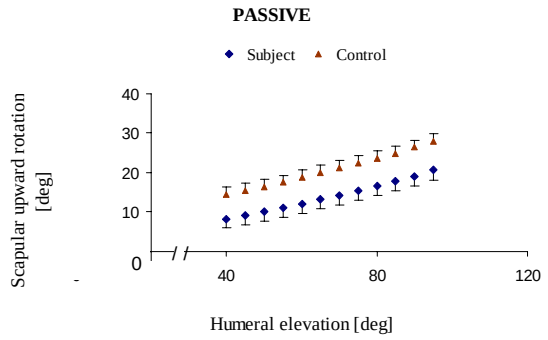

Figure: Mean +/- SEM of scapular upward rotation during humerothoracic elevation in the coronal plane.

The control group started humeral elevation at a higher degree of scapular upward rotation than the subjects with rotator cuff tears, although the change in upward rotation per degree of humeral elevation was similar for both groups.

These results are in contrast with previous studies which demonstrate greater upward rotation in subjects with rotator cuff tears when compared to healthy controls (Paletta et al 1997, Yamaguchi et al 2000 and Mell et al 2005). It has also been shown that some subjects with full thickness rotator cuff tears have normal shoulder kinematics (Yamaguchi et al 2000). These were however asymptomatic individuals. We made no distinction between asymptomatic and symptomatic cuff tear subjects. Several methodological differences between the present study and these previous studies might account for the discrepancy such as plane of motion, age of the subjects, sensor placement and data analysis. There was greater upward rotation per degree of humeral elevation in the active trials compared to passive in both cuff tear subjects and control. This was more evident in the cuff tear subjects between 40^0 and 80^0.

SUMMARY/CONCLUSIONS

Differences in scapular kinematic patterns between patients with rotator cuff tears were found to be less than has been previously reported. Further analysis and additional measurements need to be pursued in order to reconcile these inconsistencies.

REFERENCES

Paletta Jr, G.A. et al. (1997) *J Shoulder Elbow Surg* ,**6**, 516-527

Yamaguchi, K. et al (2000). *J Shoulder Elbow Surg*, **9,** 6-11.

Mell A.G. et al (2005). *J Shoulder Elbow Surg*, **14**, 58S-64S.

Karduna, A. et al. (2001). *Journal of Biomechanical Engineering*, **123,** 184-90.

A NEW METHOD FOR STUDYING THE ANABOLIC EFFECTS OF VIBRATIONAL LOADING OF BONE: CONSTRAINED TIBIAL VIBRATION IN MICE

Blaine A Christiansen, Philip V Bayly, and Matthew J Silva

Washington University, St. Louis, MO, USA
E-mail: bac2@wustl.edu

INTRODUCTION

Vibrational loading has been shown to initiate the formation of new trabecular bone as well as to prevent bone loss commonly associated with disuse, ovariectomy, or menopause in both animal models and humans. Such methods are potentially useful for the treatment of osteoporosis or age-related bone loss. Studies investigating vibrational loading have typically used whole-body vibration (WBV) as their loading method. However, WBV has limitations in small animal studies because transmissibility of vibration is highly dependent on the posture of the subject. In the current study we propose constrained tibial vibration (CTV) as an experimental method for vibrational loading of mice under controlled conditions, and characterize the vibrational behavior of a mouse leg loaded by CTV.

METHODS

Accelerometers were used to measure the transmissibility of vibration through a mouse lower leg *in vivo* during CTV at frequencies from 20-150 Hz (Fig. 1). First, we examined the frequency response of the mouse tibia to CTV loading at input vibrational magnitudes from 0.1-0.5 g maximum acceleration. Second, we used an elastic finite element model of the tibia/fibula to predict the vibrational response of the tibia during CTV loading. Using this model, we were able to predict the spatial distribution of longitudinal strain, as well as investigate the relationship between the magnitudes of transmissibility and strain. Finally, strain gages were used to validate the relationship between transmissibility and strain predicted by the

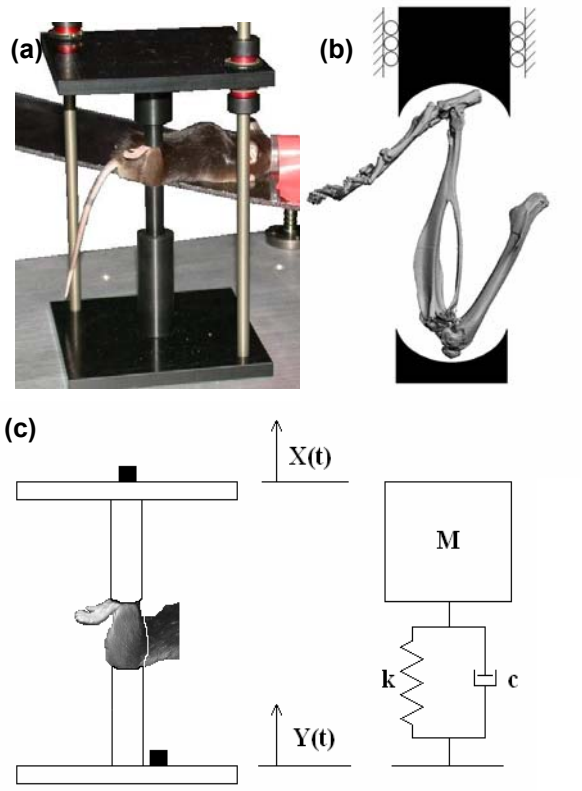

Figure 1: (a) A mouse in the CTV device. (b) MicroCT reconstruction of the orientation of a mouse leg in the CTV device. (c) The CTV device modeled as a one degree-of-freedom vibrational system. M represents the mass of the upper platform (125 g), which is supported by the leg, and is free to slide vertically. Transmissibility is defined as the magnitude of acceleration recorded at the top platform divided by the magnitude of acceleration at the bottom platform.

finite element model, and to determine the absolute magnitude of cortical bone strain experienced during CTV as a function of input frequency.

RESULTS AND DISCUSSION

We found that an *in vivo* mouse leg in the CTV system behaves similarly to a one degree-of-freedom vibrational system. Additionally, it exhibits a nonlinear response to loading magnitude, as increasing the magnitude of vibration from 0.2 g – 0.5 g caused the natural frequency of the system to shift from 75 Hz to 60 Hz. Using the FE model, the locations of maximum strain during CTV were predicted (Fig. 2a), and peak transmissibility was predicted to occur at the same frequency as peak cortical strain (Fig. 2c). Strain gage data confirmed the FE data (Fig. 2d), and showed that the maximum peak-to-peak tibial strain during CTV *in vivo* is approximately 330 με and occurs at 60-70 Hz.

SUMMARY/CONCLUSIONS

This study presents a comprehensive mechanical analysis of constrained tibial vibration (CTV), which we propose as a model for studying the skeletal effects of vibrational loading under highly controlled conditions. We showed a clear dependence of CTV on vibrational frequency and magnitude. These parameters, along with the mass of the top platform of the system, could be altered in future loading studies to control the amount of bone strain experienced during CTV. This loading model will be used in future *in vivo* studies, and may become an important research tool to understanding the mechanisms behind the osteogenic response of bone to vibration.

ACKNOWLEDGMENTS

NIH AR47867

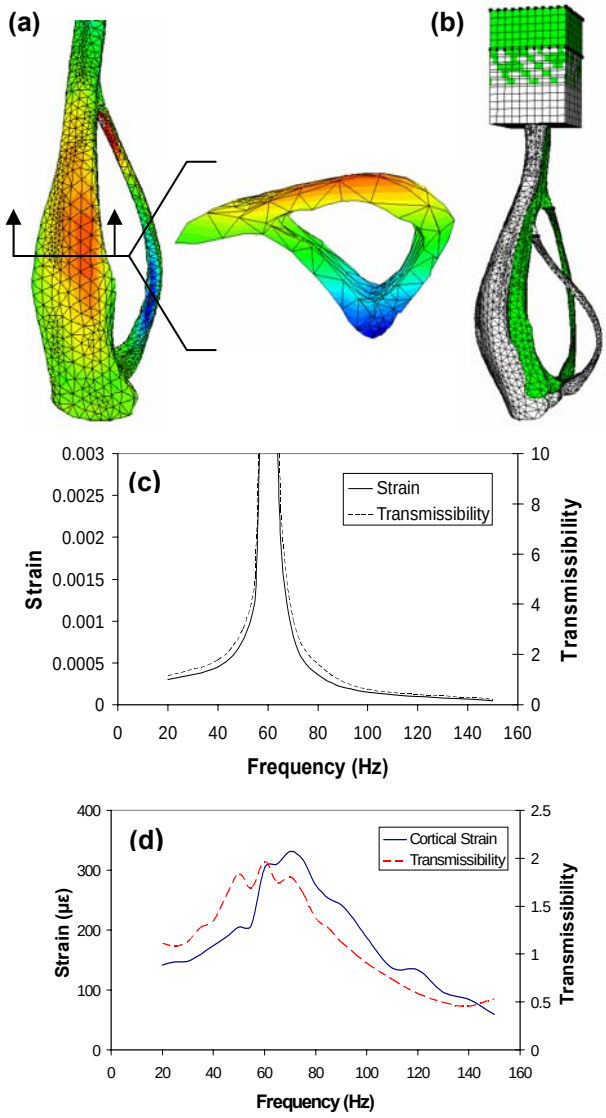

Figure 2: (a) Distribution of longitudinal strain during CTV loading as predicted by the finite element model. The peak tensile strain was located on the anterior-medial surface of the tibia, while the peak compressive strain was located on the interosseous crest of the tibia. (b) Deformational mode of the first natural frequency of the system, showing the deformed (white) and undeformed (green) condition. (c) Plot of the frequency response of transmissibility and longitudinal strain predicted by the finite element model. (d) Experimentally determined frequency responses of transmissibility and cortical strain. Estimated natural frequency was 60-70 Hz for both factors.

ANGULAR MOMENTUM CONTROL OF FORWARD DYNAMIC WALKING

Alexandre Ledoux [1], Bradford Bennett [1,2], Pradip Sheth [1], Shawn Russell, and [1]Mark Abel[2]

University of Virginia, Charlottesville, VA, USA
[1] Department of Mechanical and Aerospace Engineering
[2] Department of Orthopedic Surgery
E-mail: bcb3a@virginia.edu

INTRODUCTION

Stable walking, in particular the balance and postural stability during gait, has been widely studied in robotics. However, only a few studies have used angular momentum about the center of mass (CoM) to create stable bipedal gait (Goswami 2004). Popovic(2004a) demonstrated the regulation of angular moment of the full body around its CoM and presented a control strategy where the system angular momentum was explicitly controlled (2004b). This strategy was however only presented for the single support phase of walking.

In this present study, we demonstrate the feasibility of stable walking simulations using angular momentum about the CoM as a control. Subject-specific human models were run in forward dynamics mode by applying controlled torques. Proportional and Derivative (PD) gain at each joint minimized the errors between individual segment's desired and simulated angular momentum about the CoM. Simulations included the determination of the ground reaction forces using a developed contact model between the foot and the floor.

METHODS

Clinical gait kinematics of 3 test subjects without history of lower extremity pathology were used to develop/validate the patient specific models. All kinematics were collected using Vicon motion analysis system (Oxford, UK).

From this data the angular momentum about the CoM for each body segment was calculated and averaged for each subject. This data was used to populate the 19xN angular momentum matrix [A] where N is the number of data points over a gait cycle.

For each subject, a full body model was created in MSC.Adams (MSC.Software) using LifeMod (Biomechanics Research Group, Inc). Models were made patient-specific using subject anthropometric data. The models were composed of 19 segments and 16 joints representing a full body in three dimensions though motion was constrained to the sagittal plane for these simulations. A contact model (foot/floor interaction) is used to compute the ground reaction force when the foot is in contact with the floor and Coulomb friction is applied between the foot geometries and the floor. Contact parameters (i.e. stiffness and damping) were optimized for better match to measured ground reaction force if experimental force plate data was available for one trial. However, this optimization process is not mandatory.

Forward dynamic simulations were run using the angular momentum about the CoM of each segment, [A], as a negative feedback control. At each subsequent time point, 1,2,…N, in the gait cycle standard proportional and differential (PD) feedback gain were used to determine individual joint torques applied during the simulation to minimized error between desired and simulated angular momentum.

RESULTS/VALIDATION

Forward dynamic simulations were successfully completed using the subject-specific human model, foot/floor contact model, and PD control for both the single and double support phases of gait. Figure 1 shows agreement between the clinically measured joint angles and the forward dynamic solution for a single subject. Figure 2 shows the degree of agreement between measured and computed ground reaction forces for the same subject. Results for the other subjects were similar.

Analysis also found that angular momentum computed from the kinematics data collected experimentally show invariance with walking speed. These results are consistent with the ones published by Popovic(2004b) and should allow computation of different walking speeds with the same angular momentum control.

CONCLUSIONS

Stable walking patterns are simulated using angular momentum about the full body CoM as high level control. The trajectories produced using PD controllers (tracking reference angular momenta) correlate with the reference trajectories.

The subject specific models make no assumptions with regard to symmetry and the entire gait cycle is computed. Thus this methodology is applicable to subjects with gait pathology. Our research has found that children with cerebral palsy have angular momentums with patterns similar to a typical walker. Extension of this work to pathologic gait is underway.

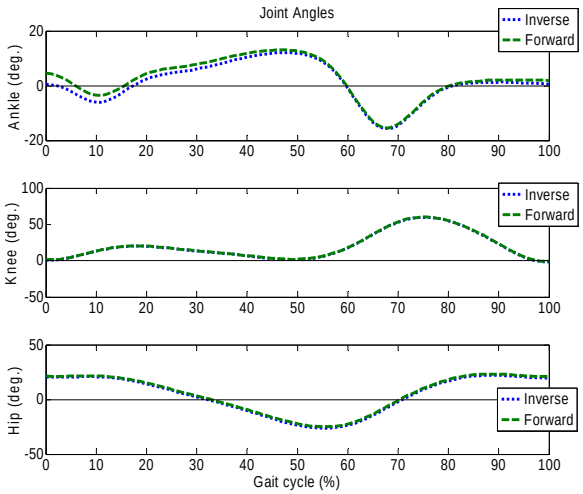

Figure 1: Ankle, knee, and hip angles during inverse and forward simulation.

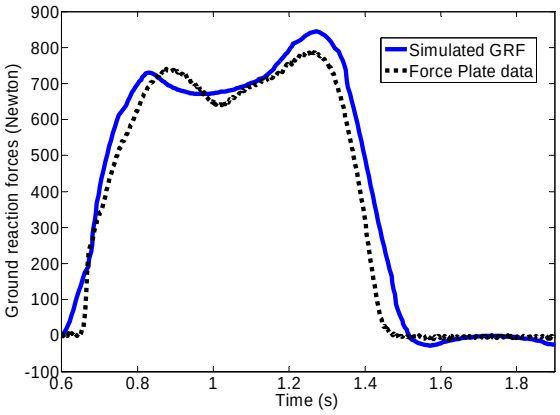

Figure 2: Simulated and experimental ground reaction forces.

REFERENCES

Goswami, A., Kallen, V. (2004). *Proc IEEE ICRA'04*, 3785-3790

Popovic, M. et al. (2004a). *Proc IEEE ICRA'04*, 2405-2411

Popovic, M. et al. (2004b). *Proc IEEE/RSJ IROS'04*, 1685-1691

ACKNOWLEDGEMENTS

The authors would like to thank the staff at the Gait and Motion Analysis Lab, Kluge Children's Rehabilitation Center at the University of Virginia, where experiments are conducted. This work was supported in part by NSF grant 0503256.

GROUND REACTION FORCES BETWEEN RUNNING SHOES, RACING FLATS AND DISTANCE SPIKES IN RUNNERS

Suzanna Logan, Iain Hunter, Brent Feland, Ty Hopkins, Allen Parcell

Brigham Young University, Provo, UT, USA
E-mail: iain_hunter@byu.edu Web: http://biomech.byu.edu

INTRODUCTION

During distance running, ground reaction forces (GRF) of more than two times a person's body weight are typical. Attenuation of GRF has been a major concern for shoe designers and manufacturers, as one of the primary roles for running shoes is to provide shock absorption. Additionally, in competitive shoes such as racing flats and spikes, the weight of the shoe has been reduced to improve performance. In comparison to most regular running shoes, spikes and racing flats have less cushioning and a thinner heel.

Several studies have looked at the reduction of GRF in running shoes, but there is a lack of data on the GRF in competitive footwear. Studies comparing barefoot and shod running have found significantly increased loading rates and greater vertical impact peaks in the barefoot condition (De Wit, 2000).

The objective of this study was to compare how GRF are influenced while running in training shoes, racing flats and spikes at a given speed, and therefore provide meaningful information that could influence the timing and frequency of the use of competitive footwear in runners.

METHODS

Twenty subjects (10 male, 10 female) from the Brigham Young University track/cross-country teams ran across a Kistler force plate (Type 9287BA, Amherst, NY) embedded into the track at 6.7m/s for males, and 5.7m/s for females. Two valid trials were obtained for each subject in each of three types of shoes – training shoes (Nike® Air Pegasus™ 2005), racing flats (Nike® Zoom Waffle Racer™ 2005), and distance spikes (Nike® Zoom Miler™ 2005). Forces were normalized to body weight in Newtons.

Only subjects who had a heel strike were included in the data analysis (n=18). Impact peak (BW), loading rate (BW/s), peak braking and propulsive force (BW), peak vertical force (BW), stance time (s), and vertical stiffness (BW/m) were subjected to a repeated-measures ANOVA and Tukey's post-Hoc test ($p<0.05$).

RESULTS AND DISCUSSION

Impact peak and vertical stiffness significantly increased between running shoes and spikes. Differences between stance time and loading rate approached significance with trainers being lower (Table 1). Loading rate and impact peak in the flats and spikes were expected to be higher, given similar results from previous studies comparing barefoot and shod running (DeWit, 2000), and could be explained by the decreased cushioning in flats and spikes, which would affect the negative acceleration of the foot at impact. The increased vertical stiffness is attributed to the decreased cushioning in the spikes causing a greater

negative vertical acceleration at ground contact.

Higher vertical stiffness is usually correlated to increased peak forces coupled with smaller lower extremity excursions, which leads to increased loading rates (Butler, 2003). Increases in these variables have been associated with potential increased risk of bony injuries (Ferber, 2002; Williams, 2004).

Whether or not increased GRF raises injury risk has been a topic of debate in research. In this study, the amplified loading rate, stiffness, and impact peak demonstrate that running in spikes and flats produces a greater external load on the body. The initial impact between the foot and the ground are directly transmitted to the leg and can potentially be an influential factor in injury risk (Hewett, 1999). However, there may also be an osteogenic effect when wearing the less-cushoined shoes.

Stance time in spikes and flats bordered on being significantly lower than in training shoes. The importance of decreased stance time is mostly from a performance standpoint, as shorter stance times have been correlated with higher running speeds (Munro, 1987). The lighter shoe should also improve running economy.

SUMMARY/CONCLUSIONS

The external load placed on the body during running is significantly increased in competitive footwear compared to regular running shoes. The differences are evident in the larger impact peak and vertical stiffness (in the spikes condition), as well as in the shorter stance time. These data can be used to better inform competitive runners, coaches, and trainers of the risks and performance benefits, when determining the frequency and duration of the use of competitive footwear in training.

REFERENCES

Butler, R.J., Crowell, H.P. III, McClay-Davis, I.M. (2003). *Clinical Biomechanics,* 18, 511-517.

DeWit, B., De Clercq, D., Aerts, P. (2000). *J. Biomechanics,* 33, 269-78.

Ferber, R., McClay-Davis, I., Hamill, et al. (2002). *Med. Sci. Sports and Exercise,* 34, S5.

Hewett, T.E., Lindenfeld, T.N., Riccobene, J.V., et al. (1999). *American J. of Sports Med.*, 27, 699-706.

Williams, D.S. III, McClay-Davis, I.M., Scholz, J.P., et al. (2004). *Gait and Posture,* 19, 263-269.

Table 1: Results where significant differences were observed (mean± SD). Superscripts (A,B,C) denote differences between groups $p < 0.05$ for impact peak and vertical stiffness. Superscripts (A,B,C) denote differences approaching significance between groups $p < 0.10$ for loading rate and stance time.

Condition	Impact Peak (BW)	Loading Rate (BW/s)	Stance Time (s)	Vertical Stiffness (BW/m)
Trainers (A)	2.3 ± 0.44^{BC}	151 ± 56.9^{BC}	0.162 ± 0.013^{BC}	63 ± 26.4^{C}
Racing Flats (B)	2.7 ± 0.71^{A}	206 ± 113.3^{A}	0.156 ± 0.008^{A}	101 ± 77.3^{A}
Spikes (C)	2.9 ± 0.51^{A}	214 ± 131.8^{A}	0.156 ± 0.01^{A}	138 ± 106.7^{A}

DISINTEGRATING THE METABOLIC COST OF HUMAN RUNNING: WEIGHT SUPPORT, FORWARD PROPULSION, AND LEG SWING

Erin M. Warddrip and Rodger Kram

Locomotion Lab, Integrative Physiology Dept. University of Colorado, Boulder, CO USA
E-mail: erin.warddrip@colorado.edu Web: www.colorado.edu/intphys/research/locomotion.html

INTRODUCTION

Running is a natural, intuitive motion. Analytically however, running is a composite of specific tasks including weight support, forward propulsion, leg swing, braking, arm swing, and balance. Our previous studies have inferred the metabolic cost of separate tasks by using assistive devices to reduce the metabolic cost (Chang and Kram 1999, Moed and Kram 2005, Teunessen et al. in review). However, we have not accounted for synergies between the tasks.

The purpose of this study was to ascertain the energetic costs of three individual tasks that comprise running, i.e. weight support, forward propulsion, and leg swing. We applied combinations of assistive devices to runners, measured the subsequent decreases in metabolic rate and deduced the cost of normally performing each task.

METHODS

Five healthy, fit, adult runners (3M, 2F) volunteered. We measured metabolic rate via expired gas analysis during standing, running at 3.0 m/s normally, and with combinations of assistive devices. We calculated net metabolic rate as (running – standing). The first assistive device provided weight support (WS) via a waist harness (Figure 1A). To assist with forward propulsion, a device pulled with an aiding horizontal force (AHF) at the waist (Figure 1B). A third device provided leg swing assist (LSA), by applying a forward pulling force to the feet during the first half of the swing phase (Figure 1C). We tested 12 combinations of these assistive devices over two sessions. Guided by previous experiments, these trials consisted of 4 levels of body weight (100, 75, 50 and 25%) combined with AHF values of 10% of effective weight and LSA of 2% of normal body weight.

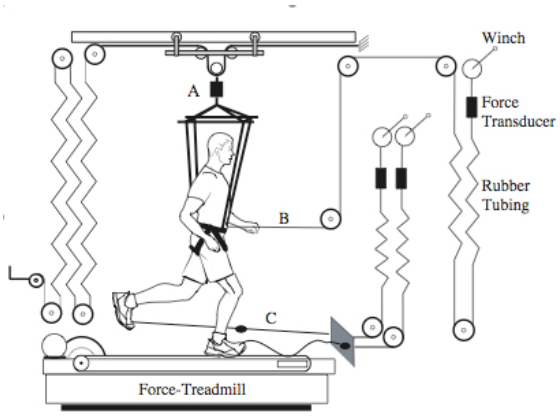

Figure 1: Schematic of Setup

RESULTS AND DISCUSSION

We calculated mean net metabolic rates for each trial (Table 1). We then normalized metabolic rates as a percentage of the metabolic rate of the normal running trial.

With weight support, we found a linear decrease in metabolic rate that was less than directly proportional to body weight (Figure 2). Extrapolating the WS line in Figure 2 to 0% body weight, the intercept is 69% lower than the value for the normal weight running trial. We therefore deduce that weight

support comprises 69% of the net cost of running, consistent with Teunissen et al.

Providing AHF further reduced the metabolic rate during running (Figure 2, middle line). We calculated the difference between the WS line and the (WS + AHF) line in Figure 2 expressed as a % of the WS only value. We averaged these values for each level of WS. This calculation suggests that forward propulsion comprises 29% of net running cost. That value is slightly lower than our previous estimates of the cost of forward propulsion (Chang and Kram 1999), perhaps due to synergies.

Providing LSA caused a fairly consistent absolute decrease in the metabolic rate at each WS level (Figure 2, bottom line). At 100% of normal weight, the difference between the (WS + AHF) and the (WS + AHF + LSA) lines in Figure 2 was 0.66 W/kg which is ~7% of the net cost of normal running (9.76 W/kg). That value is also a bit lower than our previous estimates of the cost of leg swing (Moed and Kram 2005), again possibly due to synergies.

Our assistive devices did not completely eliminate the cost of running. Extrapolating the (WS + AHF + LSA) line to 0% body weight reveals an intercept of 0.97 W/kg which is 10% of the normal running net cost. That remaining value may reflect the metabolic costs of arm swing, balance, increased ventilation and cardiac work.

By another method of accounting, WS comprises 69% of the net cost of normal running, forward propulsion 29% and leg swing 7%. The sum of those values is 105% which indicates that our methods were able to nearly disintegrate the costs of running.

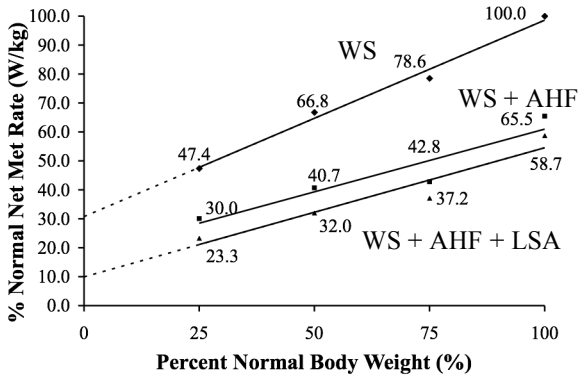

Figure 2: Percent normal net metabolic rate versus percent normal body weight for combinations of running assistive devices at 3.0m/s

SUMMARY/CONCLUSIONS

The energetic costs of running can be inferred by combining assistive devices and measuring the corresponding reductions in metabolic cost. Weight support, forward propulsion, and leg swing are the major energy consuming processes.

REFERENCES

Chang, Y. H., Kram, R. (1999). *J. of Appl. Physiol.*, **86**, 1657-1662.

Moed, B. and Kram R. (2005) Proceedings of XXIX ISB Congress, Cleveland, OH.

Teunissen L.P.J., Grabowski A., Kram R. In review *J. Exp. Biol.*

Table 1: *Mean Net Metabolic Rate (W/kg) (SEM)*

%BW	**25**	**50**	**75**	**100**
WS only	4.63 (0.34)	6.52 (0.55)	7.67 (0.54)	9.76 (0.31)
WS + AHF	2.93 (0.39)	3.97 (0.63)	4.18 (0.55)	6.39 (0.60)
WS + AHF + LSA	2.27 (0.39)	3.13 (0.43)	3.63 (0.39)	5.73 (0.62)

Lateral falls after a slip are affected by medial/lateral slipping foot displacement

Karen L. Troy[1], Stephanie J. Donovan[1], Mark D. Grabiner[1]
[1]Department of Movement Sciences, University of Illinois at Chicago, Chicago IL
Email: grabiner@uic.edu

INTRODUCTION

Falls are a major source of injury in older adults, and over 90% of all hip fractures are sustained after a fall (Grisso et al, 1991). Laterally directed falls in particular expose the hip to impact, placing a person at high risk for fracture. During normal gait, friction between the stance foot and the ground contributes to a moment about the hip, which arrests and reverses lateral trunk motion. During a slip this hip moment can be considerably reduced. We have recently observed a high incidence of laterally directed falls following a slip (Troy et al, *in review*). The purpose of the present study was to determine what factors contributed to this phenomenon.

METHODS

Twenty-one independent and community-dwelling older adults (8 males, age 70.9±5.1 years, height 165.6±10.9 cm, mass 72.2±13.2 kg) participated in this institutionally approved study and provided written informed consent prior to participation. Subjects were screened by a physician for exclusion factors that included neurological, musculoskeletal, and cardiovascular disorders. During testing they wore an instrumented safety harness that precluded contact of the hands, knees, or buttocks with the ground in the event of a fall. Subjects walked through a motion capture volume and over a 2.4 x 1.2 m Plexiglas sheet, the surface of which was coated with a film of water soluble lubricant allowed to dry. Several control trials during which the subject knew there was no threat of slipping were recorded both with and without the safety harness. Immediately prior to the slipping trial and without the subjects' knowledge, the Plexiglas was sprayed with a mist of water, causing the lubricant to become very slippery. Each subject was only slipped once. Because most subjects slipped with their left foot, the data for those who slipped with their right foot were mirror-imaged so that comparisons between all subjects could be made. Data will be referenced to slip foot side or recovery foot side.

Data were recorded at 60 Hz from 22 passively reflecting markers, used to construct a 13 segment rigid body model. From motion capture data (Motion Analysis, Santa Rosa, CA) the onset of the slip and the instant of recovery (the instant the non-slipping foot contacted the surface) were identified. The following variables were calculated for each subject: heel-to-hip distance of the slipping foot in the mediolateral direction at heel strike, mediolateral foot displacement from heel strike to recovery, lateral displacement of the recovery foot from the body center of gravity, and trunk angle and angular velocity in the sagittal and frontal planes 133 ms after recovery. This time point was chosen to examine the effectiveness of the recovery response and because no subject had yet engaged the safety harness.

Subjects were classified as fallers if they were completely and continuously supported by the harness after losing their balance due to the slip. Fall direction was quantified using trunk position and angular velocity 133 ms after the instant of recovery. Subjects were classified as backwards fallers if their trunk was in extension and had an extension velocity of greater than 50 deg/s. Subjects were classified as lateral fallers if at recovery their trunk was laterally flexed and had a lateral flexion velocity of greater than 50 deg/s in the same direction (left/right).

For each group (lateral fallers and non-lateral fallers), Pearson correlations were

calculated for all variables. T-tests were used to compare lateral to non-lateral fallers.

RESULTS AND DISCUSSION

Eighteen of the 21 older adults fell after being slipped. Of the 18 who fell, 10 were classified as lateral fallers, 10 were classified as backwards fallers, 3 fell diagonally, and 1 had no rapid trunk motion (other than vertically down).

Two variables were significantly different between lateral and non-lateral fallers: frontal plane trunk velocity at rec_{+133} (lateral fallers: 88°±28°, non-lateral fallers: 32°±23°, $p<0.001$) and M/L slip distance (2.45±6.47 cm of medial displacement vs. 5.74±7.04 cm of lateral displacement, $p=0.03$). Only two of the eight subjects who did not fall laterally experienced medial foot displacement.

Table 1 Summary of Pearson correlation results.

	M/L slip displ	heel-to-hip dist	lateral dist recov. foot to body COG	frontal plane angle
Lateral Fallers				
heel-to-hip dist	0.59			
lateral dist recov. foot to body COG	0.02	-0.40		
frontal plane angle	-0.69*	-0.80**	0.21	
frontal plane ang veloc	-0.76*	-0.77**	0.06	0.93**
Non-Lateral Fallers				
heel-to-hip dist	-0.82*			
lateral dist recov. foot to body COG	0.13	-0.18		
frontal plane angle	-0.81*	0.57	-0.09	
frontal plane ang veloc	-0.18	0.52	-0.10	0.37

*p<0.05, **p<0.01 (2-tailed)
+ ML slip displ. Indicates the foot has moved laterally
+ angle/velocity indicates a tilt towards the slip foot
+ heel-to-hip dist. indicates the heel is lateral to the hip

For subjects who fell laterally, the more lateral the M/L foot displacement, the larger the trunk angle and angular velocity away from the slipping foot (Table 1). In this group of subjects heel-to-hip distance at heel strike was strongly associated with both frontal plane trunk angle and angular velocity. For the eight subjects who did not fall laterally heel-to-hip distance predicted M/L slip distance, which was associated with larger trunk angles but not angular velocity. Interestingly, heel-to-hip distance was negatively correlated with M/L slip distance in non-lateral fallers, but was positively correlated in lateral fallers ($p=0.075$).

As expected, six out of the seven individuals who fell laterally towards the slip foot side experienced medial slipping foot motion, whereas two of the three who fell away from the slip foot side experienced lateral foot motion.

To our knowledge this is the first report of laterally-directed falls after slips during forward walking. Nearly 86% of older adults fell after being slipped and over half of them experienced laterally-directed falls.

Many factors including trunk position and velocity in the frontal plane at heel strike, step width, ab- and adductor strength, and upper extremity motion may contribute to medial/lateral foot motion during the slip. However, the data suggest that medial slips may more frequently result in falls to the side than lateral slips, possibly because of the difficulty of executing a more medially placed recovery step requiring a backwards crossover step. Medial displacement of the foot during a slip may be influenced by foot placement and whole body kinematics at slip initiation. The data further highlight the importance of allowing unconstrained motion of the slipping foot (Troy and Grabiner, 2006) and trunk during and after laboratory slips.

ACKNOWLEDGEMENTS

Funding provided by NIH R01AG16778

REFERENCES

Grisso et al. N Engl J Med 1991 May 9; 324(19): 1326-31

Troy et al. Injury Prev. *in review*

Troy and Grabiner, Gait Posture 2006 Dec;24(4): 441-7

Prospective Study of Kinetic Factors Associated with Tibial Stress Fractures in Runners

Michael B Pohl [1], Irene S Davis [1,2] and Joseph Hamill [3]

[1] University of Delaware, Newark, DE, USA
[2] Drayer Physical Therapy institute, Hummelstown, PA, USA
[3] University of Massachusetts, Amherst, MA, USA
E-mail: pohl@udel.edu

INTRODUCTION

Tibial stress fractures are a common overuse injury found in female runners. In a study of 1076 female runners, the incidence of tibial stress fracture and stress syndrome were reported to be 3 and 5% respectively (Taunton et al., 2002). A stress fracture is one of the most serious injuries given they require up to eight weeks of rest from high impact activities such as running. The risk of re-injury is high and if left untreated they can progress to a macrofracture.

A number of kinetic loading variables have been associated with the incidence of tibial stress fractures in cross-sectional studies. Impact peak (IPEAK), vertical instantaneous load rate (VILR), vertical average load rate (VALR), vertical impact peak (IPEAK) and peak positive tibial acceleration (PPA) were found to be greater in subjects who had suffered a previous stress fracture when compared to controls (Milner et al., 2005). In addition, the adduction freemoment (ADDFM) has been reported to be greater in stress fracture subjects (Milner et al., 2006). Hence high loading in both vertical and longitudinal directions may be risk factors in runners obtaining a tibial stress fracture.

Although greater loading has been identified as risk factors for stress fractures, it remains unclear whether this is a cause or consequence of the injury. Prospective studies are required to gain further insight into this relationship. The aim of this study, therefore, was to compare pre-existing loading mechanics in a group of female runners who went on to develop a tibial stress fracture/reaction versus healthy controls. It was hypothesised that IPEAK, VILR, VALR, PPA and ADDFM would all be higher in subjects who demonstrated a prospective tibial stress fracture/syndrome.

METHODS

The data are part of an ongoing prospective study of females currently running a minimum of 20 miles per week. An instrumented baseline gait analysis was performed at the commencement of the study when subjects were free from injury. Participants ran overground at 3.7 ms^{-1} along a 25m runway containing a force plate. Retroreflective markers were attached to the lower extremity and an accelerometer mounted on the distal medial aspect of the tibia. Kinematic data were collected at 120Hz using a 6 camera Vicon system (Oxford, UK). Kinetic data from the force plate and accelerometer were sampled at 960Hz. Three-dimensional kinematics and kinetics of five trials were calculated for both lower extremities.

Participants then reported their subsequent running mileage and injuries on a monthly basis for a period of two years. To date, fourteen subjects (22±8 y, 22±8 mpw) have gone on to sustain a tibial stress fracture/reaction. A tibial stress reaction

was operationally defined as tibial pain and tenderness located over a diffuse bony area of several centimeters. Stress reactions have been included in the injury group since it has been shown to be part of a continuum of bony injury leading to a stress fracture (Anderson et al., 1997). Comparisons were made between the injured group (TSF) and 14 age and mileage (24±7 y, 24±8 mpw) matched control (CON) runners. Statistical analyses were not conducted due to the small sample size. Instead a 15% difference between groups was defined as being clinically relevant.

RESULTS AND DISCUSSION

Table 1: Differences in loading variables between PTSF and CON groups.

	CTRL	PTSF	%diff
IPEAK (BW)	1.6	1.8	11.8
VILR (BW/s)	80.9	81.9	1.2
VALR (BW/s)	69.7	69.4	0.6
PPA (g)	4.8	5.6*	16.4
ADDFM ($x10^{-3}$)	4.6	6.3*	36.3
IMP (s) ($x10^{-3}$)	0.1	0.5*	338.0

* Greater than 15% difference between PTSF and CON.

A comparison of the variables of interest is shown in Table 1. As hypothesized, PPA was more than 15% greater in the PTSF group compared to controls. Given the repetitive nature of running, even small increases in loading may be magnified over thousands of consecutive foot strikes. The fatigue limit of bone is dependent on the magnitude of the load per cycle and the number of cycles over which this loading is performed. An increase in PPA would result in an increase in the load per cycle placed on the bone. Hence, this would increase the chance of exceeding the fatigue limit of the bone, thus resulting in a stress fracture.

The remaining vertical loading variables, IPEAK, VILR and VALR were not found to be different between groups. This is in contrast to the results of Milner et al. (2005), who found these loading variables to be elevated in subjects who had previously suffered a stress fracture. However, their study was retrospective and it is possible that IPEAK, VILR and VALR were altered as a result of the stress fracture injury.

Both ADDFM and IMP were greater in the PTSF group. A greater peak ADDFM implied there was a greater resistance to toe-out in runners who went on to develop a stress fracture/reaction. The elevated impulse signifies that this increased resistance to toe-out was evident throughout the stance phase. Hence, increased torsional loads in the tibia may also increase, thereby elevating an individual's risk of developing a stress fracture

SUMMARY

Results from this prospective study suggest that runners who go on to develop a tibial stress fracture/syndrome exhibit greater vertical and torsional mechanical loads. This suggests that interventions to reduce these loads during running may decrease the risk of sustaining a stress fracture.

REFERENCES

Anderson, M.W. et al. (1997). *Radiology,* **204**, 177-180.
Milner, C.E. et al. (2006). *J.Biomech,* **39**, 2819-2825.
Milner, C.E. et al. (2005). *MSSE,* **38**, 323-328.
Taunton, J.E. et al. (2002). *Br.J.Sp.Med,* **36**, 95-101.

ACKNOWLEDGEMENTS

Supported by Dept of Defense grant DAMD17-00-0515

RUNNING STABILITY IS ENHANCED BY A PROXIMO-DISTAL GRADIENT IN JOINT MECHANICS

Monica A. Daley[1] and Andrew A. Biewener[2]

University of Michigan, Ann Arbor, MI, USA[1]
Harvard University, Bedford, MA, USA[2]

E-mail: abiewener@oeb.harvard.edu

INTRODUCTION

Animals and humans regularly encounter uneven and unexpected changes in terrain properties. Consequently, their locomotion requires stabilization to deal with perturbations to steady movement. Past work has examined how humans respond to unexpected changes in substrate stiffness (Ferris et al. '99) and substrate damping (Moritz & Farley '04). These studies suggest that humans adjust their overall leg stiffness to rapidly respond to changes in substrate properties.

In this study, we examine how bipedal running guinea fowl respond to an unexpected change in substrate height. In a previous study (Daley et al. '06) we found that guinea fowl display robust stabilization of their center of mass (CoM) energy when subjected to an unexpected change in substrate height equal to ~40% of their hip height (stumbling only once in 74 trials). Guinea fowl displayed to main stabilization modes. In 63% of perturbation trials, running guinea fowl stabilize by converting the decrease in CoM potential energy (PE) to kinetic energy (KE), speeding up to stabilize their running (KE_H mode). In 37% of trials, guinea fowl absorbed the loss of CoM PE through negative work (or damping) done by limb muscles during the perturbed step (E_{COM} mode).

Here we use inverse dynamics to examine the underlying patterns of joint moment dynamics during each of these substrate height stabilization responses, compared with steady level running. We test the hypothesis that proximal muscles and joints operate under feedforward control, showing little change in performance following the perturbation; whereas, distal muscles and joints exhibit force and length-dependent feedback to adjust joint dynamics to operate as springs or to absorb energy, depending on whether the animals adopt the KE_H or E_{COM} stabilization mode.

METHODS

Five adult guinea fowl (*Numida meleagris* 1.95±0.28 kg) were used in this study. Animals ran (2.5 – 3.4 ms^{-1}) down a runway over a Kistler (9281A) force platform and were filmed in lateral view at 250 fps using a high-speed Redlake PCI-500 video camera. Animals were subjected to unexpected breakthrough drop perturbations of 8.5 cm (~40% hip height) by raising the runway and disguising the force-plate opening with white tissue paper to match the white runway surface (Fig. 1). Tissue breakthrough required 3.5±2.3N with the limb being unloaded prior to making contact with the force-plate as weight support was re- established to varying degrees.

Figure 1. *Unexpected breakthrough trial.*

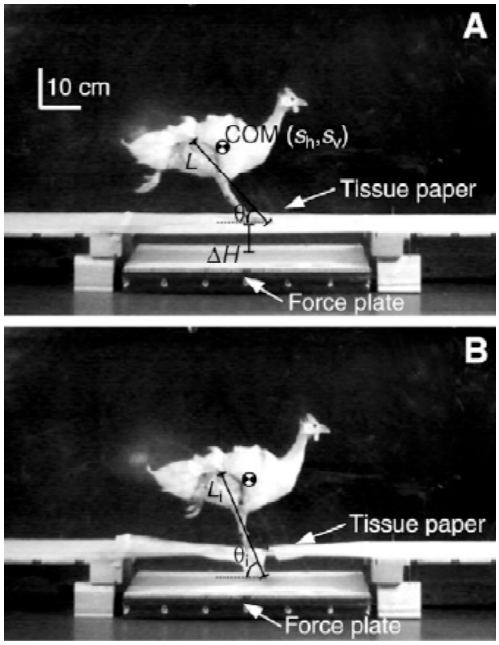

Segment masses and inertia were obtained from one animal and adjusted to match the weight and size of the other individuals, to enable inverse joint dynamics analysis.

RESULTS AND DISCUSSION

Although, limb contact times were reduced during the perturbed step, guinea displayed no significant change in net work performed at the hip and knee joints (Fig. 2). In contrast joint work at the ankle and TMP joints varied significantly depending on stabilization mode. Whereas the ankle behaved as a spring-like joint during level steady running, it absorbed a small amount of energy during the KE_H mode trials and substantial energy during the E_{COM} trials. Whereas, the TMP joint absorbed energy during steady level running, it behaved more spring-like during KE_H mode trials, but absorbed energy during E_{COM} trials.

These results support our hypothesis of feedforward control (at the joint mechanics level), as neither the hip or knee altered its mechanical function in response

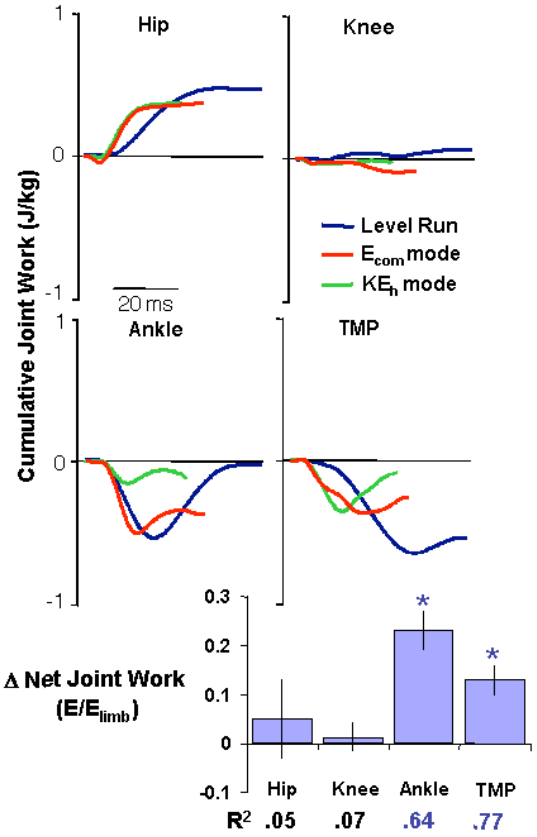

Figure 2. *Cumulative joint work based on inverse dynamics analysis for level running vs two stabilization strategies.*

to the rapid unexpected change in substrate height. The ankle and TMP joints however appear to respond by adjusting their absorption of energy relative to operating with spring-like behavior, depending on whether than animals stabilize by speeding up or absorbing CoM energy. Future work needs to examine the behavior of muscles operating at proximal and distal joints.

REFERENCES

Daley, M.A. et al. (2006). *J. Exp. Biol.* **209**, 171-187

Ferris, D.P. et al. (1999). *J. Biomech.* **32**, 787-794.

Moritz, C.T., Farley, C.T. (2004). *J. Appl. Physiol.* **97**, 1313-1322.

(supported by NIH **AR047679)**

COMPARISON OF KINEMATIC METHODS FOR DETERMINING FOOTSTRIKE AND TOE-OFF DURING OVERGROUND RUNNING

Rebecca E Fellin [1] and Irene S Davis [1, 2]

[1] University of Delaware, Newark, DE, USA
[2] Drayer Physical Therapy Institute, Hummelstown, PA, USA
Email: fellin@udel.edu

INTRODUCTION

The study of gait often requires the identification of footstrike and toe-off. This is typically accomplished with the use of force plates, an instrumented walkway or footswitches. However, when these devices are not available, an alternative method is needed.

Several kinematic methods to determine footstrike and toe-off have emerged in the literature. For running Hreljac and Stergiou (2000) used sagittal plane foot and shank angular velocities. The timing of peak knee extension has been used to separated running strides (Dingwell et al, 2001). In addition the vertical position of the ankle marker (Alton et al, 1998) and the vertical velocity and displacement of the foot markers (Schache et al, 2001) have also been used to define stance. A study by Zeni et al. (2007) suggested using relative displacement between the sacral and foot markers to determine stance during walking. However, to date these methods have not been compared to each other. Therefore, the purpose of this study was to compare these kinematic methods of determining footstrike and toe-off with a force platform. We hypothesized the Hreljac and Stergiou method would be the most accurate method since it was the only running method validated with force platform data.

METHODS

This is an ongoing study of recreational runners ages 18-45, running at least 10 mpw. To date, two female and three male runners (31.8 ± 7.1 years and rearfoot strikers) have been studied. Retroreflective markers were applied to the right lower extremity. Subjects ran at 3.35m/s along a 25m runway striking a force plate at the center. Kinematic data sampled at 120 Hz with a VICON (Oxford, UK) system and filtered at 12Hz. Kinetic data were sampled at 1080 Hz with a Bertec (Ohio, USA) force plate and filtered at 50 Hz. Five trials were averaged for each subject.

Stance was first determined using the force plate data (FP). Footstrike was identified when the vertical ground reaction force exceeded 10 N. Toe-off was determined when the force dropped below 10N. Stance was then determined using 5 kinematic methods reported in the literature.
1. *Angular Velocity Method (ANGV)* Footstrike was defined as the time coincident with the local minimum of sagittal plane foot angular velocity. Toe-off was defined as the local minimum of the shank angular velocity. 2) *Peak Knee Extension (PKEXT)* The time of peak knee extension was used to identify footstrike, while the second peak knee extension was used to identify toe-off. 3) *Foot Vertical Displacement (FPOSZ)* The minimum vertical position (z) of the distal heel marker was used to identify footstrike. The minimum vertical position (z) of the 2nd metatarsal head marker was used to find toe-off. 4) *Foot Vertical Velocity (FVELZ)* The change in vertical velocities from negative to positive of the distal heel and second

metatarsal head markers to determine footstrike and toe-off, respectively. 5) *Foot-Sacrum Y Displacement (FSDISY)* Footstrike was defined at the time of maximum positive displacement in the direction of progression (y) between the sacrum and distal heel marker: $T_{hs}=(Y_{heel} - Y_{sacrum})_{max}$. Toe-off was defined as the minimum displacement in y between the second metatarsal head marker and the sacrum marker: $T_{to}=(Y_{toe} - Y_{sacrum})_{min}$

Absolute and rms errors (in ms) were computed for each subject and averaged across subjects.

RESULTS AND DISCUSSION

The absolute and rms errors are presented in Table 1 and Figure 1, respectively. Based on these preliminary results, footstrike was most accurately determined using the FVELZ method which, on average, was determined within 1.33 ms (rms = 5 ms) of that measured with the force plate. However, the FPOSZ method also accurately determined footstrike, within 3.83 ms (rms = 6.67 ms) of the force plate time. In general, there was more error in determining toe-off. However, the PKEXT method identified it within 1.67 ms (rms= 6.33 ms) of that of the force platform. In all of these cases, footstrike and toe-off were identified within one video frame (8.33ms) of the force plate data.

Interestingly, the ANGV method resulted in the greatest amount of error. The angular acceleration curves had multiple minima, some occurring in the middle of stance, which caused toe-off to be detected consistently early. Both PKEXT and FSDISY methods consistently detected footstrike about 5 frames early. This is most likely due to people fully extending their leg shortly prior to footstrike and then flexing their leg slightly before footstrike.

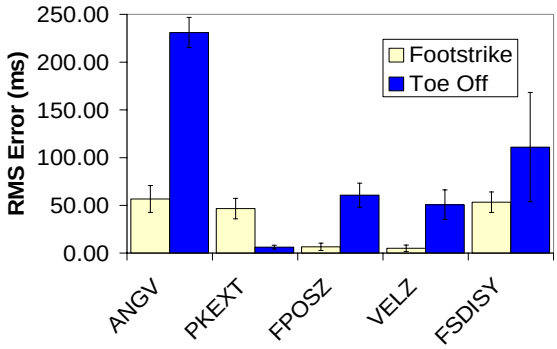

Figure 1: Stance determination RMS errors

These results begin to suggest utilizing different kinematic methods to accurately determine footstrike and toe-off during running may be best.

SUMMARY/CONCLUSIONS

The distal heel marker vertical velocity was the most valid measure for determining footstrike. However, toe-off was best determined by the peak knee extension method.

REFERENCES

Hreljac, A., Stergiou, N. (2000). *Med. Biol. Eng. Comput.*, **38**, 503-506.

Zeni, J.A. et. al. (2007) *International Society for Posture and Gait Research*.

Dingwell, J.B. et. al. (2001). *J. Biomech. Eng.* **123**, 27-32.

Alton, F. et. al. (1998). *Clin. Biomech*. **13**, 434-440.

Schache, AG et. al. (2001). *Clin. Biomech.* **16**, 667-680.

Table 1: Absolute error (in ms) of stance determination methods (mean ± SD)

Event	ANGV	FSDISY	PKEXT	FPOSZ	FVELZ
Footstrike	-47.33 ± 14.1	-52.00 ± 10.8	-46.67 ± 10.8	3.83 ± 6.0	1.33 ± 5.8
Toe-off	-231 ± 15.8	111 ± 150.7	1.67 ± 3.6	-60.67 ± 12.7	-50.67 ± 15.5

Negative values indicate early event estimation, positive values indicate late event estimation

PREDICTION OF JOINT MOMENTS USING AN EMG-DRIVEN MODEL ON STROKE PATIENTS

Qi Shao, Daniel N. Bassett, Kurt Manal, Thomas S. Buchanan

Center for Biomedical Engineering Research
University of Delaware, Newark, DE, USA
E-mail: buchanan@udel.edu, Web: www.cber.udel.edu

INTRODUCTION

Abnormal kinematic and kinetic patterns are associated with disability following stroke. The estimation of internal forces and moments during movements is important for developing better rehabilitation regimens for this population. In this study, we used an EMG-driven model to estimate muscle forces and joint moments for stroke patients, and compared the results of prediction on joint moments using different calibration protocols. Although such models have been used in healthy people, this is the first study to model post-stroke patients.

METHODS

Two stroke patients who gave informed consent were included in this pilot study. EMGs from major muscles, joint positions, and force plate data were collected from 4 walking trials on stroke subject #1 and 3 walking trials on stroke subject #2. Maximum voluntary contraction trials were collected for normalization of EMG.

Our model used EMG and joint kinematics as input to estimate individual muscle forces and joint moments (Buchanan et al., 2004). The lower limb anatomical model was developed using SIMM (Delp, et al., 1990).

The EMG were first high-pass filtered, rectified, normalized, then low-pass filtered. A recursive filter and a non-linearizing process were then employed to transform the filtered EMG to muscle activation.

A modified Hill-type muscle model was used to calculate individual muscle forces. Muscle tendon length and activation data were used as input to the muscle model, and then muscle fiber lengths were calculated by forward integration of the fiber velocities obtained from the equilibrium between tendon and muscle fiber force. Once individual muscle forces were estimated, they were multiplied by muscle moment arms to determine the total joint moment.

Subject specific muscle parameters used as inputs to the model are difficult to obtain. We used Simulated Parallel Annealing (Higginson et al., 2005) to calibrate/tune the model parameters to minimize the difference between the joint moments calculated from our model and those from inverse dynamics. After the model was calibrated, it could be used to predict novel trials.

Different calibration protocols were used in this study, including tuning to 1, 2 and 3 walking trials. The calibrated models were then employed to predict the other trials, focusing on the stance phase of gait.

RESULTS AND DISCUSSION

The predicted ankle joint moment matched the inverse dynamic joint moment, as shown in Figure 1. Similarly, the predicted knee joint moment was close to the inverse dynamic joint moment, as shown in Figure 2. The coefficients of determination (R^2) between the predicted and the inverse

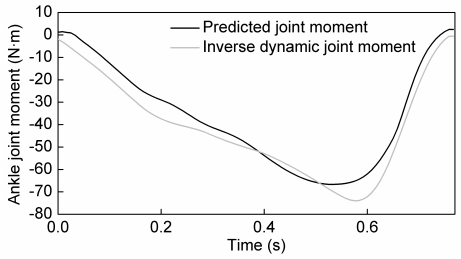

Figure 1: Ankle joint moment of subject 1, tuning the model using data from trial 1 and predicting trial 2. (Positive joint moment indicates dorsiflexion)

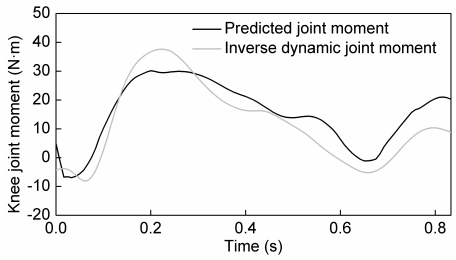

Figure 2: Knee joint moment of subject 1, tuning the model using data from trial 3 and predicting trial 4. (Positive joint moment indicates knee extension)

dynamic joint moments for all trials and subjects are shown in Figures 3 & 4. The R^2 values for the ankle joint were about 0.9, which showed a good prediction. The R^2 values for the knee joint were smaller. This may be related to the more complicated anatomical structure on the knee and abnormal EMG and kinetic patterns of stroke patients. Calibrating the model to more trials generated better results on prediction, especially for the knee joint.

Since the model can be used to predict novel trials, it may be employed to calculate the muscle activation patterns for a stroke patient to achieve a desired healthy joint moment profile. The calculated patterns may be used as guideline during functional electrical stimulation (FES) interventions for stroke patients. This model can also be used to estimate individual muscle forces and joint moments revealing the underlying

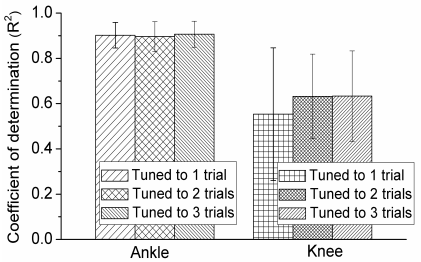

Figure 3: Coefficients of determination between the predicted and inverse dynamic joint moments for subject 1.

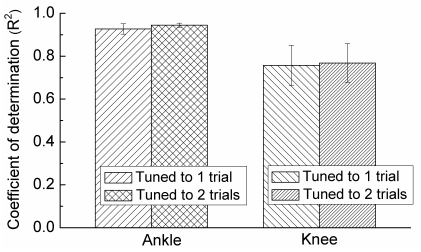

Figure 4: Coefficients of determination between the predicted and inverse dynamic joint moments for subject 2.

neuromuscular principles for clinicians and physical therapists.

SUMMARY/CONCLUSIONS

Our EMG-driven model could be used to predict novel walking trials of post-stroke patients. Calibrating to more trials improved the accuracy of prediction. This model may be used in the study of post-stroke patients, providing insights for clinicians and physical therapists.

REFERENCES

Buchanan, T.S. et al. (2004). *J Applied Biomechanics,* 20, 367-395.

Delp, S.L. et al. (1990). *IEEE Trans Biomed Eng.,* 37, 757-67.

Higginson, J.S. et al. (2005). *J Biomech.*, 38, 1938-1942.

ACKNOWLEDGEMENTS

NIH R01-HD38582 and P20-RR1645.

CONTRIBUTIONS OF PASSIVE-TENSION VS INERTIAL EFFECTS ON GRAVITY CORRECTION FOR STRENGTH TESTING

Laura Frey Law, Andrea Laake, and Colleen Delmonaco

Virtual Soldier Research Program, University of Iowa, Iowa City, IA, USA
E-mail: laake@engineering.uiowa.edu

INTRODUCTION

The value of gravity correction for isokinetic strength testing has been debated in the literature over the years. Many now concur that gravity correction improves the accuracy of strength estimates (Iossifidou and Baltzopoulos, 1998, Pincivero, et al., 1997) However there still exist multiple methods to assess gravity correction factors, without a comprehensive understanding of the relative contributions of inertial effects versus potential soft-tissue passive tension. The underlying assumption has been to estimate gravity correction based almost solely on inertial effects. Thus, once the torque due to passive limb weight is known at one angle, it can then be estimated as a cosine function for every other position within the range of motion (ROM). However, this estimate may not be accurate at the end ranges of motion. Our goal was to better determine the role of inertial versus soft-tissue passive tension on passive torque, and ultimately to determine the most accurate method for gravity correction.

METHODS

This study was a sub-analysis for a larger study involving 22 subjects: 12 males (25.0 $\pm$ 4.7 yrs, 183.1 $\pm$ 5.6 cm, 85.7 $\pm$ 6.5 kg) and 10 females (22.9 $\pm$ 3.3 yrs; 169.2 $\pm$ 6.1 cm; 66.1 $\pm$ 12.3 kg). Written-informed consent, as approved by our Institutional Review Board, was obtained prior to all testing. The subjects warmed-up on a cycle ergometer (5 min) prior to all strength testing. Passive joint torques were measured using an isokinetic dynamometer (Biodex System 3, New York, USA) with the recommended Biodex standard positioning. Range of motion (ROM) limits were set from full knee extension (~0º) to 120º knee flexion.

Passive torque was measured at 5 randomly-ordered positions: 15, 35, 55, 75, and 100º of knee flexion. At each position, subjects were instructed to relax while the raw torque, position and velocity data were sampled at 1000 Hz and further analyzed using Matlab (The Math Works Inc, Natick, MA, USA). Additionally, passive torque of the dynamometer arm alone was recorded at each angle using 0° as the horizontal.

Estimates of passive torque were calculated from one mid-range measure of passive torque (55°) for both the subject data and the isolated dynamometer arm. Percent error determinations were calculated for each remaining angle, 15, 35, 75, and 100°. Repeated Measures Analysis of Variance (ANOVA) were used to compare errors between men and women, across angles, and to assess linear versus a cosine representations of the passive torques curves ($p \leq 0.05$).

RESULTS AND DISCUSSION

Both the linear and the cosine functions provided equally accurate estimates for gravity correction across the range of motion. Some subjects produced passive torque curves that closely approximated a linear relationship (see example shown in

Figure 1). Other subjects exhibited the traditional curvilinear (cosine) passive torque curve (see example shown in Figure 2). This suggests that while for some individuals the inertial influences dominate, others may have increased soft-tissue stiffness at the end-ranges. For these subjects, the passive torque deviated substantially from the traditionally expected cosine relationship. This occurred near full extension in particular with % errors ranging from 1.7% to 38.1% (mean 14.3%).

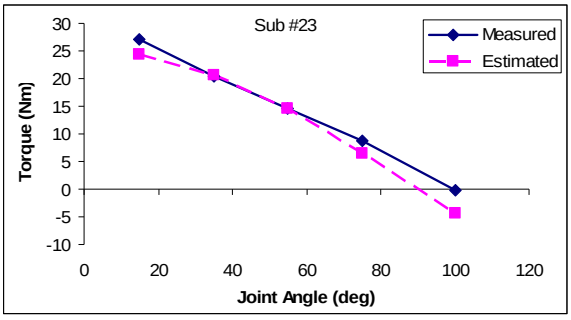

Figure 1. Example of one female subject with a linear passive torque curve.

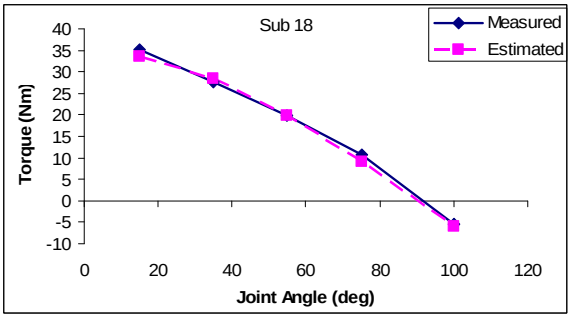

Figure 2. Example of one female subject with a curvilinear passive torque curve.

Previously, it was suggested that to best correct for gravity correction errors, adding 15° to knee angle helps explain the discrepancies seen between estimated and measured passive torque (Keating and Matyas, 1996). While this may provide a partial correction, it does not fully account for the difference in shape between the subjects with more curvilinear versus linear passive torque curves. Figure 3 shows excellent agreement at the more flexed positions (55 deg by definition is identical) for the linear and simple cosine estimate. This is likely to be partially a result of the linear nature of the cosine function across this region. However, adding 15° to the knee flexion angle did not improve the accuracy of the gravity correction estimate. No significant differences between genders were noted. Further the errors observed at the more extended knee positions suggest hamstring stiffness may be a dominant factor to consider in some individuals.

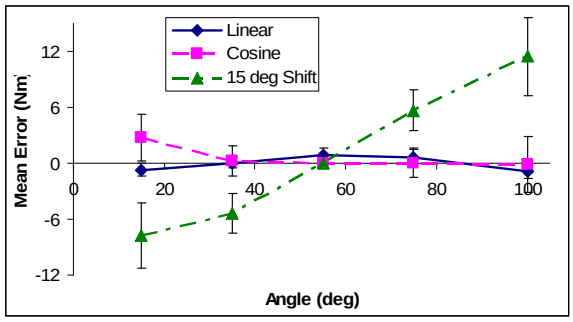

Figure 3. Mean (SD) errors using: linear estimate, cosine estimate, and cosine estimate with a 15° shift from horizontal.

SUMMARY/CONCLUSIONS

Gravity correction has become a standard for isokinetic testing, however multiple methodologies remain in use. We suggest that due to individual differences in soft-tissue stiffness, measured passive torque at several positions through the range of motion provides the most accurate estimation.

REFERENCES

Iossifidou, A. N., et al. (1998). *Int J Sports Med* **19**, 567-73.

Keating, J. L., et al. (1996). *J Orthop Sports Phys Ther* **24**, 142-53.

Pincivero, D. M., et al. (1997). *Int J Sports Med* **18**, 113-7.

MOMENT ARM MEASUREMENT TO VALIDATE A CLOSED-LOOP FEEDBACK-CONTROLLED ELBOW JOINT SIMULATOR

Laurel Kuxhaus [1,2], Pat Schimoler [1,2], Angela M. Flamm [2], Jeffrey S Vipperman [1], Mark E. Baratz [2] and Mark Carl Miller [1,2]

[1] University of Pittsburgh, Pittsburgh, PA, USA
[2] Allegheny General Hospital, Pittsburgh, PA, USA
E-mail: mcmiller@wpahs.org

INTRODUCTION

To have a complete understanding of a joint's function, one must understand both the anatomic parameters and how the brain controls the joint's actuation. Accurate measurements of anatomical parameters are critical to nonlinear biomechanical modeling, to control, and to a clinical understanding of orthopaedic reconstruction. Likewise, the study of neuromuscular control contributes to our understanding of joint structure and function. Towards the goals of understanding and improving human elbow joint control, a physiologic elbow joint simulator which operates completely under closed-loop control has been constructed in our laboratory. The closed-loop force control also permits measurement of moment arms in cadaveric elbow specimens. We hypothesized that this approach is valid in the sense that it yields comparable moment arms to previously-reported values (cf. Magnusen, 2002.)

METHODS

The hardware design has been previously developed and described (Magnusen, 2002.) Briefly, four servoelectric actuators (BE series, Parker-Hannifin, Rohnert Park, CA) are attached via high-tension cable to each of the major muscles that act across the elbow joint: the *biceps brachii*, *triceps brachii*, *brachialis* and *pronator teres*. Custom pulleys preserved the physiologic lines of action of these muscles. In-line load cells (Model 31, Honeywell Sensotec, Columbus, OH) monitored muscle forces which were used as feedback to the ACR8020 (Parker-Hannifin, Rohnert Park, CA) controller. For this study, a proportional only controller maintained constant force on each actuator. Custom mounts held potentiometers aligned with both the flexion/extension (f/e) and pronation/supination (p/s) axis (P1401a, Novotechnik, Southborough, MA.)

An axis finder, modeled after Hollister *et al.* (1992), was used to ensure proper potentiometer alignment. High-tension cable (80lb, Stren, Spirit Lake, IA) was sutured to the tendons of the fresh-frozen cadaveric elbow specimen with Krackow whip stitches. Knots in the cable were reinforced with cyanoacrylate adhesive. Minimal tissue was excised from the specimen to preserve its inertial properties.

Once secured to the simulator's frame, each tendon was loaded to a minimum of 22.24 N. Equal forces in all muscles were not possible due muscle redundancy and low static friction in the system. With the cylinders operating in force control to maintain constant tension in the lines, the elbow was manually actuated. Six cases were studied: f/e motion with the p/s angle of 1) neutral, 2) fully pronated, 3) fully supinated, and p/s motion with the f/e angles held constant at 4) 30°, 5) 60°, and 6) 90°.

To maintain constant force, the cylinders moved as prescribed by the controller, thus cylinder travel was equivalent to tendon excursion. Data were recorded at 20 Hz. A minimum of three motion cycles of each type was collected.

Subsequent analysis was completed using MATLAB (The MathWorks, Natick, MA, USA.) Fourth-order polynomial curves were fit to both the potentiometer (joint angle, θ) and cylinder travel (tendon excursion, r.) These curves were differentiated and the moment arms were calculated using the following equation:

$$M.\ A. = dr/d\theta \quad (1)$$

RESULTS AND DISCUSSION

The computed moment arms for the *brachialis* (Figure 1) compare well with previously-reported results and our design intent (Magnusen, 2002; Kuxhaus 2005.) As expected, the f/e moment arms do not vary much with changes in p/s angle. The moment arms in flexion differ slightly from those in extension due to controller lag and movement direction. A PI controller and correction for friction may reduce this effect. Figure 2 also compares well with established moment arm values (Bremer *et al.*, 2006) and shows that for the *biceps brachii*, the p/s moment arms vary systematically with f/e angle. Slight changes (<6°) in the f/e angle during measurement caused the variability in the f/e=90° case. The minimum R-squared value for all fitted curves is >0.99.

SUMMARY

The measured muscle moment arms agree with established values. This validates one aspect of the elbow simulator's design and illustrates the feasibility of this new technique. Future work will refine this technique for use in a system identification process and model-reference control scheme.

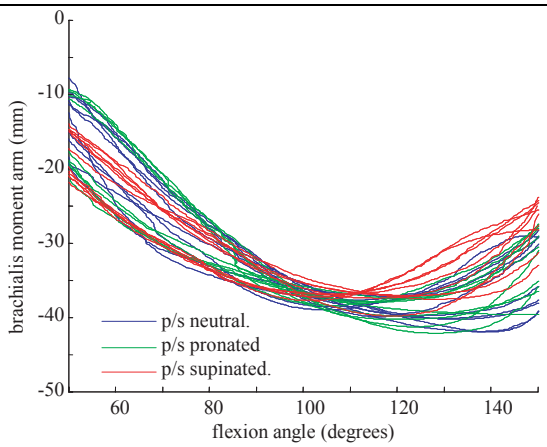

Figure 1: Brachialis f/e moment arms at varying p/s angles.

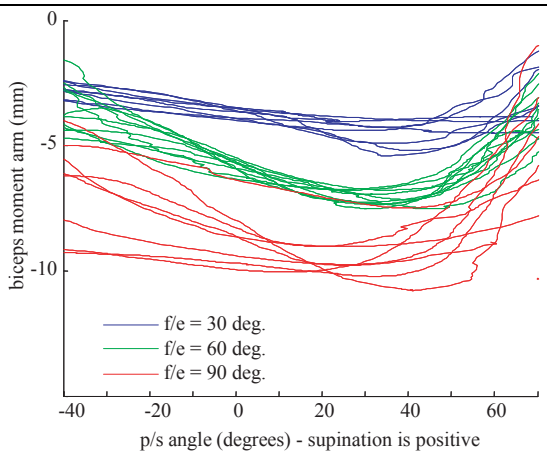

Figure 2: Biceps p/s moment arms at varying f/e angles.

REFERENCES

Bremer, A.K. et al. (2006). *Clin Biomech* **21**, 683-691.

Hollister, A. et al. (1992). *J Orthop Res* **10**(3), 454-60.

Kuxhaus et al. (2005) ASB, Cleveland, OH.

Magnusen, J.P. (2002) MS Thesis, University of Pittsburgh.

ACKNOWLEDGEMENTS

U. Pittsburgh's Provost Development Fund (LK) and Am. Soc. Surg. Hand.

BIOMECHANICS OF THE PRODISC ARTIFICIAL DISC USING FINITE ELEMENT ANALYSIS

Yabo Guan, Frank A. Pintar, Narayan Yoganandan,
Jiangyue Zhang, Dennis J. Maiman

Department of Neurosurgery, Medical College of Wisconsin
VA Medical Center, Milwaukee, Wisconsin

INTRODUCTION

Surgical treatments for degenerative disc disease can be grouped into two categories: fusion (arthrodesis) and total disc replacement (arthroplasty). Because fusion limits motion of the fused segments, it is believed that fusion may induce or accelerate degenerative change at adjacent levels. As an alternative to interbody fusion, an artificial disc serves to replace the degenerated disc and restore the functional biomechanical properties of the motion segment. The objective of this study is to develop an experimentally validated three dimensional nonlinear finite element (FE) model of lumbosacral spine to provide useful information for artificial disc designers and examine the effects of surgical treatment on the structure for clinicians.

METHODS

An intact 3D L4-S1 lumbosacral spine nonlinear FE model was used. The 3D geometrical details for FE model were obtained from computed tomography (CT) images of a human cadaver. CT data were imported into Mimics and geometrical surfaces of the lumbosacral spine were generated. The exported IGES files from the Mimics software were inputted to TrueGrid to create a hexahedral finite element mesh. The model included intervertebral discs, vertebral bodies, ligaments, and facet joints. The model was validated against the experimental data in flexion and extension, left and right lateral loadings[2]. Then the model was modified to implant a Prodisc artificial disc into L5-S1 level (Figure 1). The disc consists of two cobalt-chrome alloy end plates that are plasma sprayed with titanium and have two vertical keels for fixation in the vertebral bodies and a polyethylene inlay. The material properties used for the disc are shown in Table 1. The elements representing the L5-S1 disc and anterior longitudinal ligament were removed at L5-S1 level. Posterior longitudinal ligament remained unchanged. The contact between the plate and vertebral body was simulated using a tie constraint. A surface-based contact was used to simulate the sliding between upper metallic plate and polyethylene inlay. The coefficient of friction between plate and inlay was assigned as 0.05. All nodes on the inferior surface of S1 were constrained in all degrees-of-freedom. A pure moment up to 4.0 Nm was applied through a coupling element which is coupled with all nodes on the superior surface most of the entire L4 vertebra. Flexion and extension loading conditions were used. The intersegmental sagittal rotations under flexion and extension bending moments were obtained. The contact pressure on the interface between cobalt-chrome endplate and polyethylene inlay were obtained.

RESULTS

The rotation-moment response curves for both intact (no surgery) and Prodisc model at unimplanted level (L4-L5) are shown in Figure 2(a). The intersegmental rotations under flexion were 3.3^0 and 3.4^0 for intact and Prodisc, respectively. Under extension, these values became the same at 3.2^0. The rotation-moment response curves at implanted level (L5-S1) are shown in Figure 2(b). The intersegmental rotations under flexion were 4.50 (intact) and 3.40 (Prodisc), respectively. Under extension, these values became 3.3^0 (intact) and 7.3^0 (Prodisc). The history of contact pressure occurred on the surface of inlay was shown in Figure 3.

DISCUSSION / CONCLUSIONS

The rotation-moment response curves imply that the implantation of Prodisc does not affect the motions at adjacent level under both flexion and extension. At implanted level, the rotation decreased by 24% under flexion and increased by 120% under extension. High value of rotation predicted under extension was mainly caused by the complete annulotomy and can be explained as following. When the anterior longitudinal ligament was removed, there is no motion restraint under extension except for the

contact constraint between superior plate and inlay. Other FE studies have shown that reconstruction of anterior longitudinal ligament may restore the biomechanical function[1,3]. Preserving the posterior portion of annulus or the lateral annulus may improve stability. Secondly, without the compressive preload, after certain amount of pure moment, the superior plate no longer contacted the inlay. This can be demonstrated by the abrupt motion change under extension shown in Figure 2(b). The history of contact pressure on inlay also indicated that superior plate detached from the inlay after 2.0 Nm moment was applied. Although the body weight can produce compressive loading to alleviate this scenario, the predication from computer model may suggest that excessive extension should be avoided for patients implanted with artificial disc.

Under flexion, the contact pressure increased constantly with the increase of moment and reached the largest at the moment of 3.0 Nm. The contact was occurred at the anterior region of polyethylene inlay (Figure 4). Contact pressure is much lower during extension due to the mechanism mentioned above. These results indicated that anterior region of inlay may be the most likely worn.

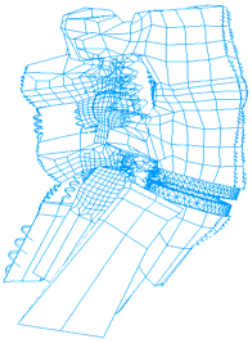

Figure 1: L4-S1 FE model with Prodisc implanted at L5-S1.

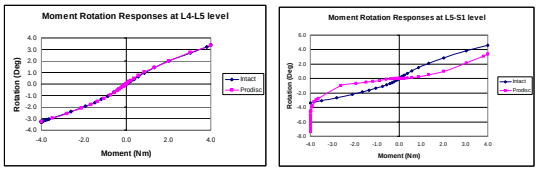

(a) (b)

Figure 2: Moment-rotation responses at (a) L4-L5 level and (b) L5-S1 level.

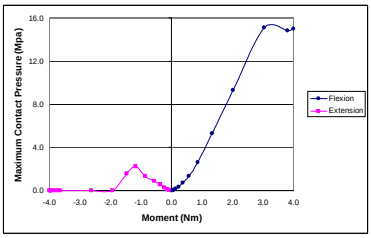

Figure 3: History of contact pressure on the inlay.

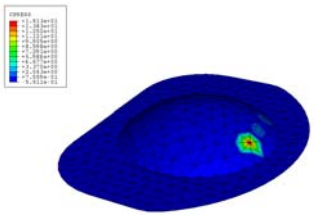

Figure 4: Contact pressure contour under flexion when highest value reached.

Table 1. Material properties used for Prodisc.

	Young Modulus (Mpa)	Poisson's Ratio
cobalt-chrome alloy plate	220,000	0.32
polyethylene inlay	1,000	0.49

REFERENCES

1. Dooris AP, Goel VK, Grosland NM, et al. Load-sharing between anterior and posterior elements in a lumbar motion segment implanted with an artificial disc. Spine 2001;26:E122-9.
2. Guan Y, Yoganandan N, Zhang J, et al. Validation of a clinical finite element model of the human lumbosacral spine. Med Biol Eng Comput 2006;44:633-41.
3. Rohlmann A, Zander T, Bergmann G. Effect of total disc replacement with ProDisc on intersegmental rotation of the lumbar spine. Spine 2005;30:738-43.

ACKNOWLEDGEMENTS

The study was supported in part by a grant from Synthes Spine, L.P.

.

EFFECTS OF REPETITIVE DROP JUMPS ON LOWER EXTREMITY LANDING MECHANICS

Joshua T. Weinhandl[1], Jeremy D. Smith[1], W. Holmes Finch[2], and Eric L. Dugan[1]

[1] Biomechanics Laboratory, Ball State University, Muncie, IN, USA
[2] Education Psychology, Ball State University, Muncie, IN, USA
E-mail: jtweinhandl@bsu.edu, Web: http://www.bsu.edu/biomechanics/

Fatigue, which can be defined as a decreased capacity of muscle fibers to absorb energy and produce force, might be a contributing factor in musculoskeletal injuries during prolonged activity. Several studies have focused on the effects of fatigue on landing kinematics and kinetics. Chappell et al. (2005) reported that fatigue resulted in decreased knee flexion at impact during a stop-jump. Pappas et al. (2007) found no change in knee flexion angle, but did report an increased peak VGRF at impact during a 0.4 m landing task after fatigue. Devita & Skelly (1992) reported an increase in work performed at the ankle and a decrease at the hip and knee as landing stiffness increased.

An increase in VGRF during landings in a fatigued state may reflect the inability to efficiently absorb the impact. Minimizing peak VGRF is thought to be a more optimal landing strategy since increased VGRF potentially increases injury risk (Dufek & Bates, 1991; Pappas et al., 2007). The purpose of this study was to assess the effects of fatigue on peak VGRF, lower extremity joint posture at initial contact, and lower extremity joint work during the impact phase of landing using a repetitive drop jump protocol.

METHODS

Nine recreationally active college students (4 females and 5 males, age = 22$\pm$2 yrs, mass = 77.3$\pm$22.3 kg) participated in the study. Participants were excluded if they were not physically active 2-3 times per week for at least 30 minutes, if they had participated in varsity athletics or had a lower extremity injury within the past 18 months. Prior to testing, informed consent was provided and the general testing procedures were approved by the university's Institutional Review Board.

Motion (240Hz) and ground reaction force data (2400Hz) were captured while subjects completed drop jumps. Drop jumps were performed from a box height equal to their maximal countermovement jump height every 20 seconds. The fatigue protocol continued until subjects were unable to reach 80% of their initial rebound height for five consecutive drop jumps or had completed 200 drop jumps. Landing mechanics of the dominant leg were analyzed.

Joint angular positions, moments, and powers were calculated using Vicon's PlugIn-Gait model. Net joint work was calculated as the integral of the joint powers at the ankle, knee and hip respectively. A normalization scheme was used to standardize the number of jumps performed during the fatigue protocol to 100 equally spaced trials. Four repeated-measures ANOVAs ($p<0.05$) were used to identify significant changes in rebound jump height, joint angular positions at initial contact, peak VGRF, and net work performed at each joint during the impact phase. The impact phase was defined as the first 100 ms following initial ground contact, which is consistent with Devita & Skelly (1992).

RESULTS AND DISCUSSION

Results for the initial and final 10% of the fatiguing protocol are reported. Rebound jump height significantly decreased for all subjects ($p<0.001$). Net work increased at the ankle ($p<0.001$), decreased at the knee ($p<0.001$), and remained unchanged at the hip ($p=0.708$). There was a significant increase in ankle, knee, and hip extension at initial ground contact ($p<0.001$). However, there was no significant change in peak VGRF during the impact phase, 20.2 N/kg vs. 19.5 N/kg ($p=.909$).

The increase in net work performed at the ankle and decrease in net work at the knee suggests an increased reliance on the ankle plantarflexors to absorb the impact forces during fatigue. These findings are consistent with Devita & Skelly (1992) who reported an increased contribution of the ankle plantarflexors and decreased contribution of the knee extensors as initial knee extension increased during drop landings. Devita & Skelly (1992) suggest that this redistribution in energy absorption may predispose the lower extremity skeletal structures to greater stresses. The VGRF results are not consistent with Pappas et al. (2007) who reported an increase in VGRF after fatigue. This may be due to the nature of the task. In Pappas' study the subjects were not required to perform a subsequent jump after the initial landing. This is in contrast to the current study, where subjects performed a jump for maximal height immediately after landing.

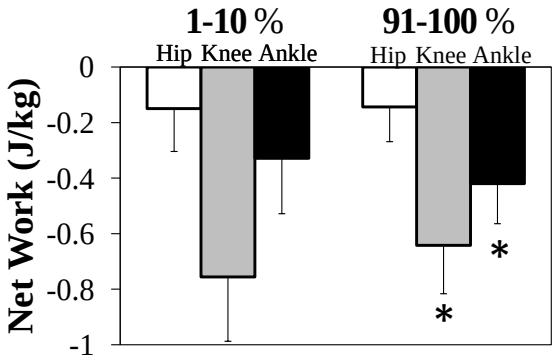

Figure 1: Net work values for the first 10% and last 10% of the fatigue protocol. * indicates final 10% was significantly different from initial 10%.

SUMMARY/CONCLUSIONS

These subjects displayed a more extended posture at ground contact with fatigue. However, this did not result in an increase in peak VGRF. This might be a result of the subjects' increased reliance on the ankle plantarflexors to absorb the impact force. More work is needed to determine whether this response to fatigue increases injury risk at either the ankle or the knee.

REFERENCES

Chappell, J. D., et al. (2005). *Am J Sports Med*. **33(7)**, 1022-1029.

Devita, P., & Skelly W. A. (1992). *MSSE*. **24(1)**, 108-115.

Dufek, J. S., & Bates, B. T. *MSSE*. **22(2)**. 370-377.

Pappas, E., et al. (2007). *JSSM*. **6**, 77-84.

Table 1: Joint position at initial contact at 0% and 100% of the fatigue protocol (mean±SD). * indicates final 10% was significantly different from initial 10%. Zero degrees represented full extension at the hip and knee and neutral at the ankle. Positive angles reflect flexion at the hip and knee, and dorsiflexion at the ankle.

	Hip	**Knee**	**Ankle**
1-10%	40.0±7.9 deg	19.3±8.1 deg	-13.2±11.2 deg
91-100%	*35.4±7.9 deg	*12.3±6.2 deg	*-23.8±7.6 deg

MENISCAL INJURY IN CONJUNCTION WITH ACUTE AND CHRONIC ACL TEARS INCREASE PEAK CARTILAGE STRESSES

Nathan A Netravali [1] and Thomas P Andriacchi [1]

[1] Stanford University, Stanford, CA, USA
E-mail: nan4@stanford.edu, Web: biomotion.stanford.edu

INTRODUCTION

Anterior cruciate ligament (ACL) injury is frequently associated with an increased incidence of premature knee osteoarthritis (OA) (Daniel et al. 1994). In conjunction with acute ACL ruptures, meniscal tears are typically found in the lateral meniscus while the medial meniscus usually remains intact. Yet, in chronic cases of ACL ruptures, the medial meniscus shows degeneration in most subjects while damage to the lateral meniscus does not progress (Cipolla et al. 1995). The rotational kinematic changes along with the high loads during the initial phase of the gait cycle have been suggested as one possible mechanism for the initiation of cartilage breakdown after ACL injury (Andriacchi et al. 2004). Yet, the combined effect of these rotational changes with lateral meniscal damage on cartilage stress has not been examined. This study sought to compare the effects of both a typical acute and chronic ACL deficiency on the peak stresses in the tibial articular cartilage in the neutral position of the knee as well as changes in the locations of these peak stresses relative to a healthy knee.

METHODS

The geometry for the femur, tibia, femoral and tibial articular cartilage, and menisci were derived from segmented magnetic resonance (MR) images to build 3-D models of the bones, cartilage, and menisci. (Koo et al. 2005) and solid meshes were created using MSC Patran (MSC Software, Santa Ana, CA). The model consisted of 30,311 nodes and 15,294 elements. Bone was assumed to be rigid relative to the soft tissue and modeled using rigid 2D elements. The cartilage was discretized into 8-noded brick elements while the meniscus was discretized into 10-noded tetrahedral elements. The cartilage was assumed to behave as a linear elastic, isotropic solid with a modulus of 10 MPa and a Poisson's ratio of 0.46 (Haut Donahue et al. 2002). The menisci were modeled as linearly elastic, transversely isotropic with radial and axial moduli of 20 MPa and a circumferential modulus of 140 MPa (Yao et al. 2006). The in-plane Poisson's ratio was 0.2, while the out of plane Poisson's ratio was 0.3. A previous method was used (Haut Donahue et al. 2002). to model the meniscal horns.

The anterior (ACL) and posterior (PCL) cruciate ligaments and medial (MCL) and lateral (LCL) collateral ligaments were modeled using nonlinear tension-only springs with a constant, k, of 1500. Contact was modeled between the femoral cartilage and the meniscus, the meniscus and the tibial cartilage, and the femoral and tibial cartilage for both the medial and lateral sides resulting in six contact pairs with a coefficient of friction of .00001 between all contact pairs. An ACL-deficient knee was modeled by removing the ACL spring elements and rotating the tibia 5º internally from the normal knee. A lateral longitudinal meniscal tear was introduced by removing elements from the posterior portion of the lateral meniscus. Medial meniscal

degeneration was simulated by removing approximately 20%, by volume, of the elements in the posterior third of the medial meniscus. The medial-lateral load ratio at the instant of the first peak adduction moment during gait was used (Schipplein et al.1991). This resulted in a 5.15:1 medial-lateral load ratio, which was distributed as a 700 N (1 body weight) load. The femur was only constrained to maintain full extension while the tibia was held fixed in all six degrees of freedom. Model predictions (ABAQUS 6.5 (HKS Inc., Pawtucket, RI) of stress distributions and contact areas were tested by comparing the location of peak stresses to the location of peak contact pressure found in cadavers using pressure-sensitive film (Ihn et al. 1993).

RESULTS AND DISCUSSION

The results support the hypothesis that the shift in the location of the contact regions post ACL injury could result in high loads on cartilage that cannot adapt to withstand these loads. Introducing an ACL-deficiency (ACLD) with a rotational offset resulted in increased peak von Mises stresses in the lateral plateaus (Fig 1) in every case. The ACLD in all cases resulted in an anterior shift of the peak stresses on the lateral side and a posterior shift medially (Fig 2). This could result in degenerative changes to the cartilage initiating the early stages of OA.

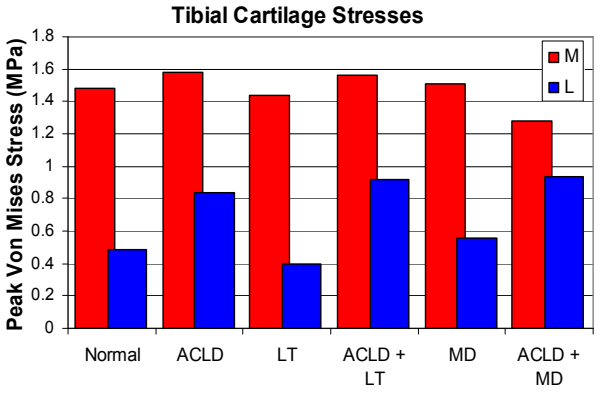

Fig 1. Peak von Mises stresses in medial (M) and lateral (L) tibial plateaus.

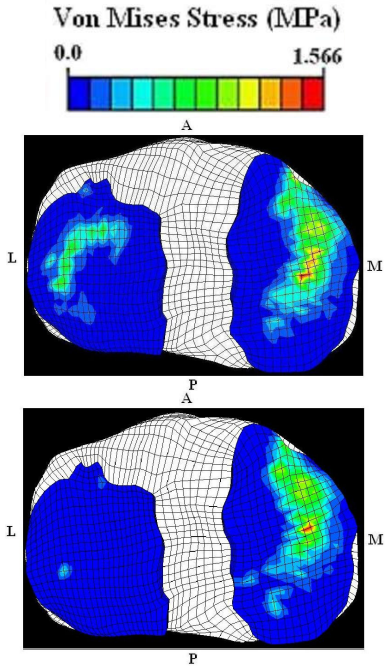

Fig 2. Distribution of peak von Mises stresses on the tibial plateau for normal (top) and ACLD+LT (bottom).

While the simplifications in this study likely influenced the magnitudes of stresses predicted by this model, the conclusions regarding the relative increases between the ACL deficient knee and the healthy knee seem consistent with the clinical observation that kinematic changes associated with ACL injury can lead to premature OA in this population.

REFERENCES

Andriacchi, T.P., et al. (2004). *Ann. Biomed. Eng,* **32,** 447-457.

Cipolla, M., et al. (1995). *Knee Surg. Sports. Traum. Arthrosc.*, **3,** 130-134.

Daniel, D.M., et al. (1994). *Am. J. Sports Med*, **22**, 632-644.

Haut Donahue, T.L., et al. (2002), *J. Biomech. Eng.,* **124**, 273-280.

Ihn, J.C., et al. (1993) *Int.Orth*, **17,** 214-218.

Koo, S. et al. (2005). *Osteoarth. Cart.*, **13**, 782-789.

Schipplein, O.D. et al. (1991) *J Orthop. Res.*, **9,** 113-121.

Setton, L.A. et al. (1999). *Clin. Orth. & Rel. Res*, **367S**, S254-S272.

Yao, J. et al. (2006). *J. Biomech. Eng.,* **128**, 135-141.

CHANGING THE DEMAND ON SPECIFIC MUSCLE GROUPS AFFECTS THE WALK-RUN TRANSITION SPEED

Jamie L. Bartlett and Rodger Kram

Locomotion Lab, Department of Integrative Physiology
University of Colorado, Boulder, CO, USA
E-mail: bartletj@colorado.edu
www.colorado.edu/intphys/research/locomotion.html

INTRODUCTION

Some have proposed that local, muscle specific factors trigger the walk-run transition. Hreljac (1995) suggested that overexertion of the ankle flexor muscles during fast walking triggers the walk-run transition. Similarly, Prilutsky and Gregor (2001) determined that swing-phase (flexor) muscles influence the walk-run transition speed. Contrary to the flexor muscle overexertion hypotheses, Neptune and Sasaki (2005) proposed that impaired force production in the ankle extensors makes fast walking less effective. They suggested that running at and above the preferred transition speed allows for an improved contractile state of the muscles.

Our purpose was to determine if changing the demand on the "trigger" muscles alters the preferred walk-run transition speed. We hypothesized that decreasing the demand on trigger muscles would increase the transition speed and conversely, increasing the demand on trigger muscles would decrease the transition speed.

METHODS

On 20 volunteers, we first determined the normal preferred walk-run transition speed (PTS) on a motorized treadmill using a step-wise protocol with a randomized speed order. We then determined PTS while subjects walked with external devices that decreased or increased the demand on specific muscles. We concurrently measured the electromyographic (EMG) activity of several lower leg muscles at each speed and condition.

One external device applied a horizontal force near the subject's center of mass (Figure 1a). This force can pull the person forward, providing an aiding horizontal force (AHF) that decreases the need of the propulsive muscles (ankle extensors) during walking. Additionally, this device can pull the person backward, providing an impeding horizontal force (IHF) that increases the need of the ankle extensors during walking (Gottschall and Kram 2003). A leg swing assist (LSA) device applied forward pulling forces at the feet (Figure 1b), effectively

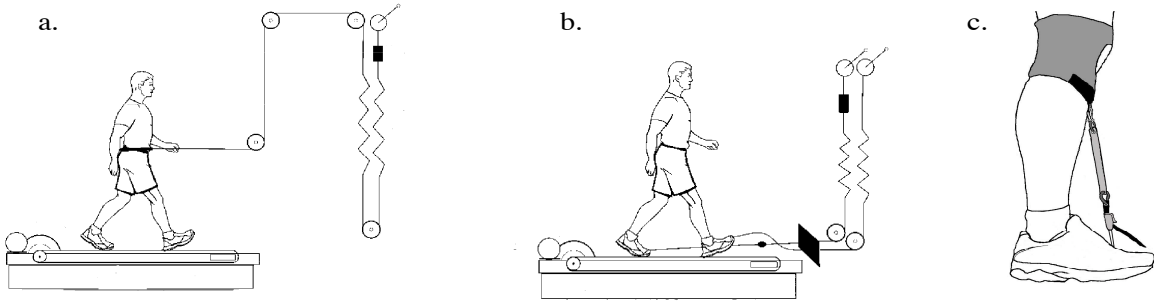

Figure 1. External assist devices: a) aiding horizontal force, b) leg swing assist, c) dorsiflexor assist.

aiding the leg muscles (hip flexors) during swing (Modica and Kram 2005). For this study, we developed a dorsiflexor assist (DFA) device (Figure 1c) that reduced the demand on the ankle flexor muscles. The DFA externally exerts a torque that reduces activity in the ankle flexor muscles during the first half of swing and at heel strike.

RESULTS AND DISCUSSION

When muscle demand was decreased (AHF, DFA and LSA), the preferred walk-run transition speed significantly, but modestly, increased ($p < 0.001$). When the muscle demand was increased (IHF) the preferred walk-run transition speed significantly, but modestly, decreased ($p < 0.001$).

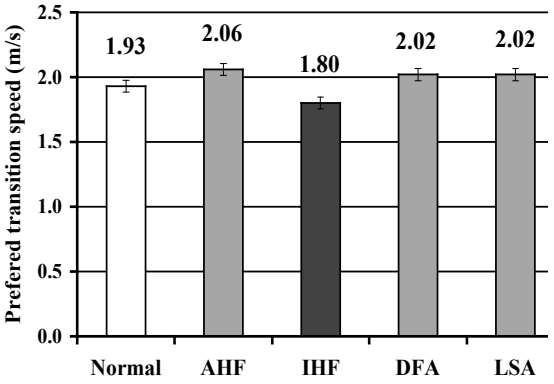

Figure 2. The preferred transition speed when walking normally and with external devices.

Compared to normal walking at the PTS, activity of the ankle extensor muscles (Figure 3a) was significantly less when walking with the aiding horizontal force (AHF) and significantly greater with the impeding horizontal force (IHF). Activity of the tibialis anterior muscle, an ankle flexor (Figure 3b), was significantly less during walking with the dorsiflexor assist (DFA). Rectus femoris (hip flexor) EMG decreased while walking with the leg swing assist (not shown).

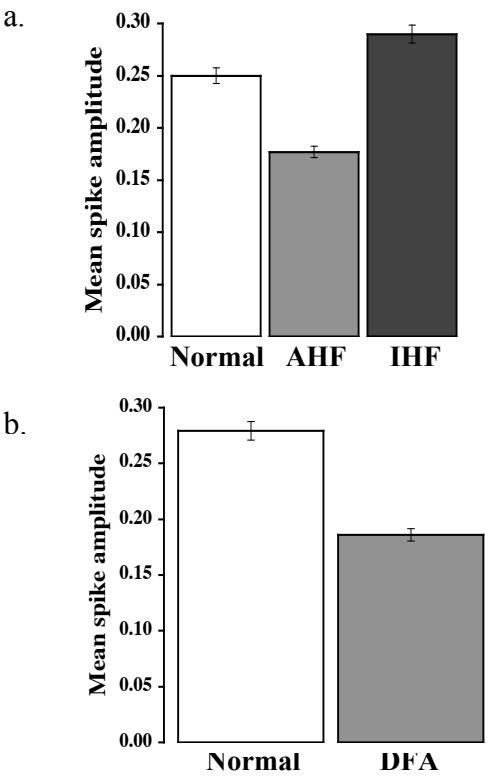

Figure 3. EMG activity of the medial gastrocnemius (a) and tibialis anterior (b) while walking at PTS normally and with external devices. Mean ±SEM.

SUMMARY AND CONCLUSIONS

Changing the demand on specific muscle groups can alter the walk-run transition speed, supporting the idea that local, muscle specific factors trigger the walk-run transition.

REFERENCES

Gottschall, J.S., Kram, R. (2003). *J Appl Physiol,* 94:1766-72.

Hreljac, A. (1995). *J Biomech,* 28:669-77.

Modica, J.R., Kram, R. (2005*). J Appl Physiol,* 98:2126-31.

Neptune, R.R.,Sasaki, K. (2005). *J Exp Biol*, 208: 799-808.

Prilutsky, B.I.,Gregor, R.J. (2001). *J Exp Biol,* 204:2277-87.

FEEDFORWARD POSTURAL CONTROL IN STANDING: ROLE OF LATERAL MUSCLES AND BODY ORIENTATION

Marcio Santos and Alexander Aruin

University of Illinois at Chicago, Chicago, IL, USA
santosmj@uic.edu

INTRODUCTION

The central nervous system (CNS) uses anticipatory activation of the trunk and leg muscles to minimize planned postural perturbations (Aruin & Latash, 1995a). The majority of previous studies of anticipatory postural adjustments (APAs) investigated the activation of the ventral and dorsal trunk and leg muscles prior to different types of perturbations (Aruin & Latash, 1995b). Only a few studies investigated APAs in muscles that maintain lateral stability of the body.

METHODS

Healthy young subjects (n=10) were required to stop a moving pendulum with their right or left arms while standing. The pendulum was released and stopped in 5 different positions: lateral on the right and left sides ($+90^o$ and -90^o, respectively), oblique (intermediary position between frontal and saggital planes) on the right and left sides ($+45^o$ and -45^o, respectively), and frontal (0^o) planes. The pendulum, attached to the ceiling, was adjustable (1.1 to 1.4 meters) to match the subjects' shoulder height and had a load (1.36 kg) attached next to its foam covered handlebar. The subjects were required to watch the pendulum as it was released by an experimenter from the same distance (0.8 m), and directed toward the subject's hand which was held extended at the shoulder level.

Electrical activity of muscles (EMG) was recorded bilaterally from the following muscles groups: rectus femoris (RFR and RFL), biceps femoris (BFR and BFL), rectus abdominis (RAR and RAL), external obliques (EOR and EOL), erector spine (ESR and ESL), and gluteus medius (GMR and GML). The ground reaction forces were measured using a force platform (AMTI, USA). To register the moment of the impact, an accelerometer (PCB, USA) was attached to the handlebar of the pendulum. The EMGs were aligned using the accelerometer signal (T_0), and then averaged. Anticipatory EMG changes were quantified by integrating the signals during the 100ms time window before T_0 ($\int EMG_{100}$). The $\int EMG_{100}$ was further corrected by the $\int$EMG of the baseline activity from 500ms to 450ms before To ($\int EMG_{50}$) as described below:

$$\int EMG = \int EMG_{100} - 2\int EMG_{50}$$

The $\int$EMGs were then normalized with respect to the highest value for each muscle and subject individually. Multiple repeated measures ANOVAs were used to compare the $\int$EMGs between the conditions for each side and Post hoc analysis was also performed. Statistical significance was set at $p < 0.05$. A paired T-test was used to compare each condition between sides.

RESULTS

The overall results showed anticipatory activations of the ventral (RFR, RFL, RAR and RAL) and lateral muscles (EOR, EOL, GMR, and GML). During the same time period, dorsal muscles (BFR, BFL, ESR, and ESL) predominantly demonstrated anticipatory inhibition. For all positions, the external oblique muscles responded with anticipatory activations.

The ∫EMG indices were greater in the oblique positions at the side of the perturbations. For EOR, the ∫EMGs at +45° were significantly greater than the ∫EMGs at -45° and +90° (p = 0.03 and p = 0.005, respectively). The anticipatory activation of the EOL at -45° was significantly greater than at +90° (p = 0.005) (Figure 1).

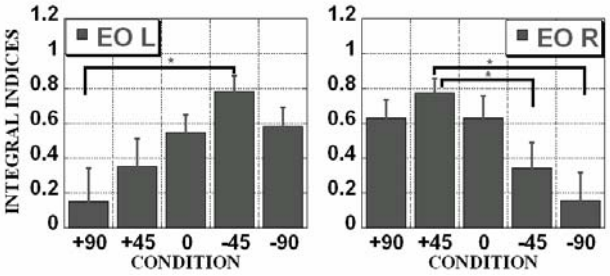

Figure 1 - ∫EMG means and standard error bars for the left (EO L) and right (EO R) external oblique muscles. * denotes the principal significant differences. Conditions are in degrees.

Although the overall activation patterns of the gluteus medius were anticipatory in nature, they were greater in the lateral and oblique planes on the contralateral side of the perturbations. For both sides, the anticipatory activations in the frontal plane were smaller (Figure 2). The ∫EMGs for GMR at 0° were significantly smaller when compared to the -45° position (p = 0.02). The GML ∫EMGs in both positions, +45° and +90°, were significantly greater than those at 0° (p = 0.02 and p = 0.03, respectively). At the same time, the lateral muscles (EOR, EOL, GMR, and GML) did not show significant differences between sides.

DISCUSSION

The current study demonstrated a well defined pattern of APAs of the lateral muscles (GM and EO). Past studies showed that the reactions of GM to the sideways pushing are critical to maintain the postural stability (Gilles *et al.*, 1999). The present experiment showed that the GM muscles also play an important role in APAs while counteracting either lateral or forward perturbations.

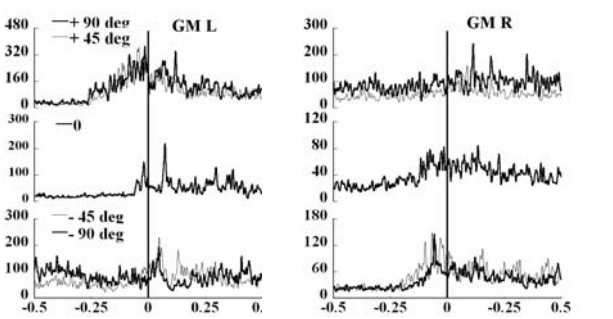

Figure 2 – EMG profiles of the right (GM R) and left (GM L) gluteus medius muscles of a representative subject during the 5 conditions. The vertical lines correspond to T_0.

As GM muscles are responsible for lateral pelvis stability, their anticipatory activation was more marked during lateral perturbations (±90), especially on the contralateral side (Figure 2). At the same time, contrary to the pattern of activation of GM muscles, the EO activations, which contribute to trunk rotation and side bending, were more pronounced when the perturbations occurred in the oblique plane (±45), primarily on the same side as the perturbations.

CONCLUSION

Similar to the patterns reported in the ventral and dorsal muscles, the CNS seems to employ the same strategy of anticipatory activation in the lateral muscles prior to a predictable external perturbation. Additionally, the APA magnitudes in the lateral muscles depend on the direction of the perturbations.

REFERENCES

Aruin, A. S., Latash, M. L. (1995a). *Exp Brain Res,* **103**(2), 323-332.

Aruin, A. S., Latash, M. L. (1995b). *Exp Brain Res,* **106**(2), 291-300.

Gilles, M., et. al.(1999). *Exp Brain Res,* **124**(2), 137-144.

EFFECT OF VISUAL UNCERTAINTY ON ADAPTATION TO ANKLE PERTURBATIONS

Timothy N. Judkins[1,3], Lewis A. Wheaton[1,3], J.C. Mizelle[1], Hermano I. Krebs[2,4,5], Richard F. Macko[2,3], and Larry W. Forrester[1,2,3]
[1]Deptartments of Physical Therapy and Rehabilitation Science and [2]Neurology, University of Maryland School of Medicine. Baltimore, MD
[3]Baltimore VA Medical Center and GRECC, Baltimore, MD
[4]Mechanical Engineering Department, Massachusetts Institute of Technology, Cambridge, MA
[5]Department of Neurology and Neuroscience, Weill Medical College of Cornell
Email: tjudkins@som.umaryland.edu, web: http://pt.umaryland.edu

INTRODUCTION

The human nervous system is capable of adapting to a wide variety of environmental perturbations such walking over ice or rough terrain. In the case of reaching, the brain adapts to these unknown dynamics by making adjustments to motor commands to achieve desired hand or tool position [1]. It has been shown that errors made while perturbed in a velocity-dependent conservative force field are well predicted using memory of the previous movement error as well as estimates of current and previous perturbations [2, 3]. This short-term motor adaptation occurs during reaching in many environments, but has remained virtually unexplored in the lower extremity. The objective of this study is to determine how visual feedback affects sensorimotor integration during simple ankle movements in randomly perturbed force fields

METHODS

Following Institutional Review Board requirements, informed consent was obtained from seven healthy volunteers who had no known history of neurological events, no significant visual problems and were able to move the ankle freely through a range of variable stiffness settings. For testing, subjects were seated with a two

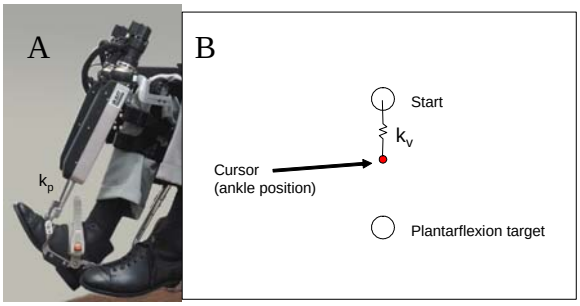

Figure 1: A) The anklebot produces a spring-like load (k_p). B) A virtual spring (k_v) is applied to the cursor. Subjects were instructed to make "down-and-up" movements to a plantarflexion target in 0.5 seconds.

degree-of-freedom ankle robot (Anklebot; Interactive Motion Technologies, Cambridge, MA) attached to their left leg. A table blocked direct view of the subject's legs at all times, and a cursor representing the subject's ankle position was displayed on an LCD (Figure 1). Ankle and cursor position data were collected at 200 Hz.

Subjects performed "down-and-up" ankle movements in the sagittal plane against a spring-like load generated by the Anklebot. The subject was instructed to plantarflex to a target (-3.5º) and return to the start location (3.5º) in 0.5 sec. The stiffness of the robot varied randomly from trial-to-trial. Three visual feedback conditions were studied: veridical vision and proprioception (**V=P**), no vision (**PO**), and stochastic vision (**V≠P**). During **PO**, the cursor was not displayed. During **V≠P**, a randomly varying, virtual

stiffness was applied to the cursor. Movement extent errors were modeled using an autoregressive model:

$$\varepsilon_p^{\,i} = \beta_0 k_p^{\,i} + \alpha_1 \varepsilon_p^{\,i-1} + \beta_1 k_p^{\,i-1} + \gamma_0 \varepsilon_v^{\,i} + \delta_0 k_v^{\,i} + \gamma_1 \varepsilon_v^{\,i-1} + \delta_1 k_v^{\,i-1} \quad [1]$$

where $\varepsilon_p^{\,i}$ is current trial proprioceptive movement error, $\varepsilon_p^{\,i-1}$ is previous trial proprioceptive error, $\varepsilon_v^{\,i}$ is current trial visual error, $\varepsilon_v^{\,i-1}$ is previous trial visual error, $k_p^{\,i}$ is current trial physical stiffness, $k_p^{\,i-1}$ is previous trial physical stiffness, $k_v^{\,i}$ is current trial virtual stiffness, and $k_v^{\,i-1}$ is previous trial virtual stiffness. A one-way Analysis of Variance (ANOVA) was used to compare the standardized coefficients of the model across conditions for all subjects.

RESULTS AND DISCUSSION

As expected, current trial perturbation strength had the most influence over movement errors, and there were no significant differences between conditions (Figure 2). Subjects relied on prior proprioceptive errors the most when only proprioception information was available (**PO**), and the least when there was conflicting visual information (**V≠P**). Subjects relied on prior perturbation strength more in the **PO** and **V=P** conditions compared to **V≠P**. These results suggest that there is context-dependent weighting of sensory information depending upon the availability and consistency of the information.

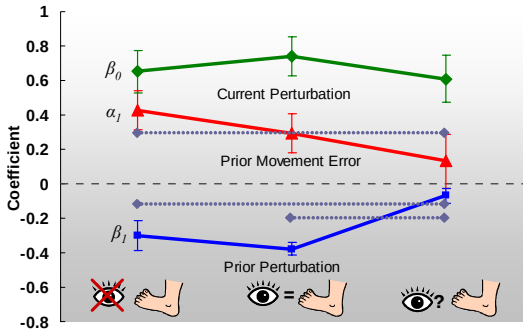

Figure 2: Standardized coefficients for each term in the short-term adaptation equation (Eq. 1). Horizontal bars indicate $p<0.05$ between conditions.

SUMMARY/CONCLUSIONS

This study clearly demonstrated that the availability and consistency of visual information modulates sensory weighting for motor adaptation at the ankle. However, it remains unclear how ankle motor adaptation may be affected by sensorimotor deficits. Future studies will investigate sensorimotor integration for ankle motor control in neurologically impaired populations such as stroke and peripheral neuropathy.

REFERENCES

1. Thoroughman, K.A. and Shadmehr R. (2000) *Nature*. **407**, 742-7.
2. Scheidt, R.A., et al. (2005) *J Neurophysiol*. **93**, 3200-13.
3. Scheidt, R.A., et al. (2001) *J Neurophysiol*. **86**, 971-85.

ACKNOWLEDGEMENTS

This research was funded by the VA Center of Excellence in Exercise and Robotics (B3688R) and the NIH (T32-HD041899-01A1

VARIABILITY OF JOINT COUPLING WITHIN THE LOWER EXTREMITY IN RUNNERS WITH PATELLOFEMORAL PAIN DURING A PROLONGED RUN

Tracy A. Dierks[1], Irene S. Davis[2,3], John P. Scholz[2], and Joseph Hamill[4]

[1]Department of Physical Therapy, Indiana University, Indianapolis, IN, USA
[2]Department of Physical Therapy, University of Delaware, Newark, DE, USA
[3] Drayer Physical Therapy Institute, Hummelstown, PA, USA
[4]Department of Exercise Science, University of Massachusetts, Amherst, MA, USA
E-mail: tdierks@iupui.edu; http://www.shrs.iupui.edu/pt/content/bios/dierks.php

INTRODUCTION

Runners with patellofemoral pain (PFP) syndrome have been reported to exhibit less variability in continuous relative phase (CRP) joint coupling patterns at the transition periods of heel-strike and toe-off when compared to uninjured runners (Hamill et al, 1999). Variability within a biological system is believed to provide a mechanism of plasticity that allows for greater flexibility and adaptation to constantly changing task constraints (Goldberger, 1991). Thus, Hamill et al. (1999) concluded that runners with PFP were more susceptible to repetitive CRP coupling patterns resulting in a decreased ability to vary the distribution of repetitive loading forces, which may be associated with PFP. However, too much variability may result in decrement of performance. This might then imply that there is a window of variability that is optimal for performance while minimizing the risk for injury.

The mechanisms that contribute to PFP remain relatively unclear. The knee pain experienced by runners with PFP is generally not present at the beginning of a run, with the onset of pain being subtle and progressively worsening throughout the run. However, no studies have examined joint coupling variability in runners with PFP at the end of a prolonged run, where knee pain is present. Therefore, the purpose of this study was to investigate lower extremity CRP variability in runners with PFP over the course of a prolonged run. It was hypothesized that the PFP group would exhibit less CRP variability compared to uninjured runners, and the CRP variability would further decrease at the end of the run.

METHODS

The runners that participated in the study included 20 with PFP and 20 uninjured. All were between the ages of 18 and 45 and ran at least 10 miles per week. Each subject performed a prolonged run on a treadmill at a self-selected pace. 3D kinematic data (120 Hz) of the leg with the most painful knee (random for uninjured) were collected for 20 consecutive footfalls at the beginning and end of the run. The prolonged run ended when one of three events occurred: 1. 85% heart rate maximum was reached, 2. 17 was reached on the rating of perceived exertion scale, and 3. for the PFP group, 7 was reached on a visual analog pain scale.

The CRP relationships of interest included: 1. rearfoot eversion/inversion and tibial internal/external rotation ($RF_{(ev/in)}$-$T_{(rot)}$), 2. $RF_{(ev/in)}$ and knee flexion/extension ($RF_{(ev/in)}$-$K_{(f/e)}$), and 3. $RF_{(ev/in)}$ and knee internal/ external rotation ($RF_{(ev/in)}$-$K_{(rot)}$). To calculate the CRP, for each joint motion a phase plot was constructed by plotting angular position against angular velocity, and phase angles were then calculated. The CRP was calculated as the difference between corresponding phase angles throughout stance (Hamill et al, 1999). CRP measurements were assessed within four relatively equal periods of stance based on vertical ground reaction force events. Finally, variability was calculated as the within-subject standard deviation of the

mean CRP measure for each period of stance. A two-factor ANOVA for each period of stance (group by time) was used to assess each CRP measure with a Tukey post-hoc for follow-up comparisons at $p \leq 0.05$ and trends were noted at $0.05 \leq p \leq 0.10$.

RESULTS AND DISCUSSION

No interactions were noted and thus only main effects will be discussed. A trend towards a group difference was observed in the $RF_{(ev/in)}$-$K_{(rot)}$ relationship during periods 1 and 2, where the PFP group was more variable (Table 1). This is contrary to the idea that overuse injury may be associated with less variable CRP coupling patterns (Hamill et al, 1999). Our results suggest that the PFP group exhibited a more flexible system than the controls. However, this may have been a compensation for pain.

Over time, both groups displayed an increase in variability during period 4 for all relationships at the end of the run (only significant for $RF_{(ev/in)}$-$T_{(rot)}$ relationship). Increased variability is thought to be associated with a decrease in the stability of the system, suggesting new coupling patterns may be emerging (Scholz, 1990). Therefore, these results may indicate that as the runner fatigues, new CRP coupling patterns were beginning to emerge throughout the entire lower extremity at push-off. This may be related to muscle fatigue in the invertors of the foot, which has been reported to alter rearfoot motion during running (Christina et al, 2001). As the lower extremity progresses to an unloaded state during period 4, it may be easier to alter CRP coupling patterns, resulting in increased CRP variability. For the runners with PFP, this may have influenced patellofemoral mechanics via the kinematic chain. However, this too may have been a compensation for pain.

The findings of this study may have been limited by the nature of treadmill running. As the treadmill speed was constant throughout the run, minimal deviations in stride length, and subsequently, joint angles and velocities were likely to occur. Thus, it may have been difficult for the runners to exhibit large changes in CRP variability.

SUMMARY/CONCLUSIONS

These findings demonstrate that runners with PFP displayed atypical knee rotation CRP coupling pattern variability during the first half of stance when compared to uninjured runners during a prolonged run. In addition, CRP variability within the entire lower extremity increased at toe-off at the end of the run. It is unclear at this time whether these differences were a cause of, or a compensation for, the PFP.

REFERENCES

Christina, KA et al. (2001). *Hum. Mov. Sci.*, 20, 257-276.

Goldberger, AL (1991). *News Physiol. Sci.*, 6, 87-91.

Hamill, J et al. (1999). *Clin. Biomech.*, 14, 297-308.

Scholz, JP (1990). *Phys. Ther.*, 70, 827-843.

Table 1. Group means by periods of stance for CRP variability (within SD) at the beginning and end of the run. PFP is patellofemoral pain group, UNJ is uninjured group.

CRP Relationship	Period 1		Period 2		Period 3		Period 4	
$RF_{(ev/in)}$-$T_{(rot)}$	PFP	UNJ	PFP	UNJ	PFP	UNJ	PFP	UNJ
Begin	16.1	16.4	12.8	10.0	7.6	7.3	13.4	10.9
End	15.7	12.8	12.0	10.9	7.9	8.1	14.7^^	13.0^^
$RF_{(ev/in)}$-$K_{(f/e)}$								
Begin	15.7	14.9	13.2	10.1	7.9	7.3	14.8	11.7
End	16.1	13.3	12.8	11.1	7.6	8.1	15.2^	13.4^
$RF_{(ev/in)}$-$K_{(rot)}$								
Begin	19.1	18.8*	18.3	13.6*	12.2	10.8	23.5	21.4
End	20.9	15.3*	18.3	14.9*	12.5	12.1	26.1^	23.6^

^^Significant time effect, $p<0.05$. ^Trend towards significant time effect, $p<0.10$.
*Trend towards significant group effect, $p<0.10$.

A STOCHASTIC BIOMECHANICAL MODEL FOR OF THE RISK AND RISK FACTORS FOR NON-CONTACT ACL INJURY

Bing Yu [1], Chengfeng Lin [2], Chuanshu Ji [1], Pual S. Weinhold [1], Michael T. Gross [1], Darin A. Padua [1], and William E. Garrett [3]

[1] University of North Carolina at Chapel Hill, Chapel Hill, NC, USA,
[2] National Cheng Kong University, Tainan, Taiwan
[3] Duke University Medical Center, Durham, NC, USA
E-mail: byu@med.unc.edu

INTRODUCTION

Anterior cruciate ligament (ACL) injury is one of the most common injuries in sports. The majority of ACL injuries are non-contact injuries. To prevent non-contact ACL injuries, modifiable risk factors have to be identified. Although tremendous efforts have been made in the last decade to identify risk factors for non-contact ACL injuries, little scientific evidence have been revealed to support any proposed risk factors. The limited progress in research on ACL injury preventions is largely due to limitations in traditional epidemiological research methods that are expensive and labor intensive, and lack ability to establish cause-and-effect relationship between injury and associate factors. Stochastic biomechanical modeling is a method of studying the random outcome of human movements. This method has been successfully applied in many studies on musculoskeletal system injury preventions. The purpose of this study was to develop and validate a stochastic biomechanical model for studying the risk and risk factors of sustaining non-contact ACL injury.

METHODS

An ACL loading model was instrumented to a Monte Carlo simulation to express the risk of sustaining non-contact ACL injury in a stop-jump task as a function of selected sagittal plane and non-sagittal plane biomechanical factors. The total ACL loading at the peak posterior ground reaction force was decomposed as the loadings from sagittal and non-sagittal plane biomechanics. ACL loading from sagittal plane biomechanics was expressed as an inverse dynamic function of knee flexion angle, posterior ground reaction force, tibial tilting angle, the location of center of pressure relative to ankle joint center, and hamstring and gastrocnemius forces. Lower extremity anthropometry data were obtained from literature and normalized to standing height and body weight. ACL loading from non-sagittal plane biomechanics was expressed as a regression function of knee valgus-varus and internal-external rotation moments. The relationships of the ACL loadings with non-sagittal biomechanics were determined using the *in vitro* ACL loading data. The density distribution of each independent variable was determined from the *in vivo* data of 40 male and 40 female college aged recreational athletes in a stop-jump task. A non-contact ACL injury was defined as the peak ACL loading was greater than 2250 N for males and 1800 N for females. Monte Carlo simulations were performed to determine non-contact ACL injury rate for each gender. Each Monte Carlo simulation had 100,000 iterations. Ten Monte Carlo simulations were

performed for each gender. Female-to-male non-contact ACL injury rate ratio was determined and the contributions of sagittal and non-sagittal plane biomechanics to ACL injury loading in each simulated injury case were recorded.

RESULTS AND DISCUSSION

The female-to-male non-contact ACL injury rate predicted by the stochastic biomechanical model was 4.96 to 1, which was essentially the same as the injury rate ratio of 4.59 to 1 in the basketball players reported in literature using traditional epidemiological methods. The stop-jump task is frequently performed in the sports of basketball. Non-conntact ACL injuries frequently occur in the stop-jump and similar tasks. The similarity of the predicted and reported relative injury rates supports the validity of the stochastic biomechanical model developed in this study.

The validity of the stochastic biomechanical model developed in this study was also supported by some predicted biomechanical characteristics of non-contact ACL injuries. The predicted knee flexion angle at the peak ACL loading in the simulated injury trials was 22.0 ± 8.0 degrees for male subjects and 24.9 ± 5.6 degrees for female subjects, which were consistent with those reported in literature. The predicted contribution of the sagittal plane biomehanics to ACL injury loading was 1839.86 ± 894.81 N for males and 1773.27 ± 603.83 N for females, which were also consistent with the literature if ACL elevation angle is considered in the literature as this study did.

The mean contribution of sagittal plane biomechanics to ACL injury loading were 1839.86 ± 894.81 N for males and 1773.27 ± 603.83 N for females, respectively. The mean contribution of non-sagittal plane biomechanics to ACL injury loading were 926.83 ± 666.45 N for males and 501.20 ± 388.81 N for females. These results suggest that the contribution of sagittal plane biomechanics to ACL injury loading was 82% of the strength of the ACL for males and 99% for females, while the contribution of non-sagittal plane biomechanics to ACL injury loading was 41% to the strength of the ACL for males and 28% for females. These results indicate that the sagittal plane biomechanics alone can generate sufficient force to injure the ACL while the non-sagittal plane biomechanics alone may not be able to in the stop-jump task.

SUMMARY/CONCLUSIONS

A stochastic biomechanical model has been validated and applied to predict the relative risk and risk factors for the non-contact ACL injury in the stop-jump task. Although most of the non-conntact ACL injuries involve both sagittal and non-sagittal plane biomechanics, sagittal plane biomechanics may play a major role in the risk for non-contact ACL injury in the stop-jump task. Future studies are needed to apply the stochastic biomechanical model to quantify the effects of detailed risk factors on the risk for non-contact ACL injury.

REFERENCES

Agel et al. (2005). Am J Sports Med, 33:524-530.

Markolf et al. (1995). J Orthop Res, 13: 930-935.

McLean et al. (2003). Clin Biomech, 19: 828-838.

Olsen et al. (2004). Am J Sports Med, 32: 1002-1012.

Stapleton et al. (1998). Am J Sports Med, 26: 442-445.

SENSITIVITY OF FUNCTIONAL HIP JOINT CENTER LOCATION TO BODY MASS INDEX, MOVEMENT PATTERN AND MARKER CLUSTER

Annegret Mündermann [1,2], Stefano Corazza [1], Priyanshu Gupta [1], Valentina Camomilla [3], Chris O. Dyrby [1,2], Thomas P. Andriacchi [1,2]

[1] Stanford University, Stanford, CA, USA
[2] Bone and Joint Research Center, VA Palo Alto, Palo Alto, CA
[3] Istituto Universitario di Scienze Motorie, Rome, Italy

E-mail: amuender@stanford.edu Web: biomotion.stanford.edu

INTRODUCTION

Resultant moments and forces in joints of the lower extremity play a critical role in diseases of the musculoskeletal system including osteoarthritis or osteoporosis (Miyazaki et al. 2002). The quality of standard gait analysis relies mainly on the capability of the investigator to identify anatomical landmarks. This can be especially challenging in patients who suffer from these diseases as they are often elderly and overweight. The hip joint center location is usually determined using anatomical measures and regression equations and is particularly prone to errors introduced by palpation mainly due to the lack of accessibility of medial landmarks. Several methods have been proposed to determine the hip joint center functionally by moving the thigh segment through its range of motion and associate it with the center of a sphere fitted to the marker trajectories (Camomilla et al. 2006). Simulation studies (Camomilla et al. 2006) have shown that the functional hip joint center location is sensitive to the movement pattern applied and the location and size of the marker cluster on the thigh segment. The purpose of this study was to experimentally determine the sensitivity of the functional hip joint center location to body mass index, movement pattern and choice of marker cluster.

METHODS

Ten normal weight subjects (7 male, 3 female; age: 46.9 ± 16.9yrs; BMI: 22.9 ± 1.2kg/m^2) and 10 overweight subjects (4 male, 6 female; age: 53.1 ± 10.7yrs; BMI: 30.9 ± 2.2kg/m^2) participated in this study after giving informed consent. None of the subjects had previously been treated for any clinical lower back or lower extremity condition or had any activity-restricting medical or musculoskeletal condition. Reflective markers were placed on anatomical landmarks on the pelvis (bilateral ASIS, bilateral PSIS), hip joint (proximal aspect of greater trochanter). A nine-marker cluster was attached to the anterior-lateral aspect of the thigh (Andriacchi et al. 1998). Subjects performed a star arc pattern consisting of flexion-extension, abduction –adduction and circumduction of the lower extremity with a fully extended knee and minimal pelvis motion while standing on the contralateral limb and being recorded with a standard ooptoelectronic system. They were allowed to hold on to a rail with the contralateral hand to maintain balance. The hip joint center location was computed following the Bell and Andriacchi methods (Bell et al. 1989; Andriacchi & Strickland 1985) and the S4 method (Halvorsen 2003) for T, arc, star and stararc patterns using the six most proximal markers and all cluster markers. Deviation from the Bell method was

calculated for each method, subject, movement pattern and marker cluster and averaged across subject groups. Significant differences between methods, groups, movement patterns and marker clusters were detected using independent and paired Student's t-tests ($\alpha = 0.01$).

RESULTS AND DISCUSSION

The largest deviation between methods was observed for normal weight subjects between the functional hip joint center location and the Bell method in the medio-lateral direction (Figure 1). The functional hip joint center location in normal weight subjects was also significantly more lateral than in obese subjects in relation to the Bell method. However, the accuracy of these differences remains to be interpreted after a direct measure of the actual hip joint center location is obtained. In general, the average functional hip joint center location in obese subjects was within one standard deviation of both the Bell and Andriacchi methods. In contrast to the modeled data reported by Camomilla et al. (2006), small differences were observed between movement patterns and marker clusters (Figure 1). While the average hip joint center location in overweight subjects was similar between methods, movement patterns and marker clusters, a larger standard deviation in this group was observed. Therefore, a validation and an improvement of the functional method in this population is especially important for accurate calculations of joint kinematics and kinetics to determine mechanical factors that may predispose subpopulations of overweight or obese persons to musculoskeletal diseases such as osteoarthritis or osteoporosis.

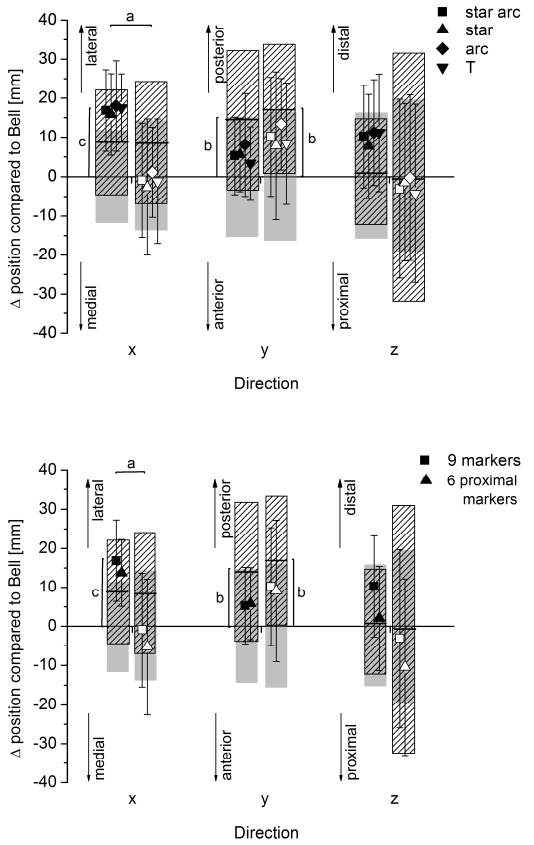

Figure 1: Average (± 1 std. dev.) deviation of the functional hip joint center location (symbols) and the Andriacchi joint location (lined boxes) compared to the Bell method. Grey boxes: ±1 std. dev. Bell method; closed symbols – BMI < 25kg/m^2; open symbols – BMI > 28kg/m^2. significant differences ($P < 0.01$): a – overweight vs. normal weight; b – Andriacchi vs. Bell method; c – functional vs. Bell method.

REFERENCES

Andriacchi, T.P., Strickland, A.B. (1985) *NATO Series*, 83-101.

Andriacchi, T.P. et al. (1998) *J Biomech Eng* **120**, 743-749.

Bell, A.L. et al. (1989) *Hum Mov Sci* **8**, 3-16.

Camomilla, V. et al. (2006) *J Biomech* **39**, 1096, 1106.

Halvorsen, K. (2003) *J Biomech* **36**, 999-1008.

Miyazaki, T. et al. (2002) *Ann Rheum Dis* **61**:617-622.

Schipplein, O.D., Andriacchi, T.P. (1991) *J Ortho Res,* **9**, 113-119.

ACKNOWLEDGEMENT

VA grant # A05-4076P.

EFFECTS OF AREA SELECTION CHOICE ON QUANTIFYING PROXIMAL TIBIA BONE DENSITY

Todd Royer and David Hudson

University of Delaware, Newark, DE, USA
E-mail: royer@udel.edu

INTRODUCTION

Previous research on osteoarthritic gait has demonstrated an important link between abnormal joint loading and bone mineral density (BMD). Patients with medial compartment knee osteoarthritis (OA) have large knee abduction moments and elevated proximal tibia BMD (Wada et al., 2001). There is an associated link between increased BMD and osteoarthritis, however the causative relationship is not clear (Hurwitz et al., 2001). Osteoarthritis is a degradation of articular cartilage, nonetheless, Radin and Rose (1986) have suggested that OA is initiated by or prompted to progress by increased density of subchondral bone. Therefore, quantifying bone mineral density may be important to understanding the progression of OA.

Hurwitz and colleagues (1998) reported a strong link between medial/lateral distribution of proximal tibia BMD and internal knee abduction moment, where larger abduction moments (representing larger medial joint forces) are associated with larger medial/lateral BMD ratios. Hurwitz et al (1998) used the midline of the proximal tibia to separate the medial and lateral compartments. However, it is conceivable that using the midline as a medial/lateral divider may result in the bone density quantification to over or underestimate the distribution of knee joint load. Therefore, the purpose of this study was to assess choice of proximal tibia bone mineral density quantification (three medial/lateral width and two height techniques) and subsequent correlations with internal knee abduction moment during walking.

METHODS

Fourteen males and 18 females (M_{age} = 39.1 ± 15.3 yrs; M_{height} = 172.9 ± 10.6 cm; M_{mass} = 76.0 ± 15.1 kg) with asymptomatic knees served as subjects. Gait and BMD data were obtained from both legs (n=64) for analysis.

To obtain data used in calculating gait mechanics, lightweight reflective markers were placed bilaterally on the legs and feet of the subject using the Helen Hayes marker set. Motion analysis cameras captured three-dimensional position data (60Hz) of these markers and a force platform captured ground reaction force data (480Hz) as the subject walked at their freely chosen speed overground along a 20-meter walkway. Peak net internal abduction moments for the knee (MK_{abd}) of both legs were determined using an inverse dynamics approach and normalized to body mass (Orthotrak software, Motion Analysis Corporation).

BMD of the knee was measured bilaterally via dual energy x-ray absorptiometry (Hologic Delphi W). Medial and lateral compartments of the proximal tibia were divided using three methods: 1) 50% medial, 50% lateral, 2) 40% medial, 20% middle, 40% lateral, and 3) 33% medial, 33% middle, 33% lateral. The middle region's BMD was not quantified. Height of the compartment area was quantified using two

methods: 1) full height – from tibial plateau to the superior surface of the fibular head, and 2) half height – the proximal half of the full height. BMD ratio was calculated as medial BMD/lateral BMD for a total of six areas (3 medial/lateral methods by 2 height methods).

Pearson product moment correlations were calculated between MK_{abd} and each of the six BMD ratios.

RESULTS AND DISCUSSION

The mean MK_{abd} was 0.43 (sd=0.15) Nm/kg. Med/lat BMD ratios ranged from 1.16 (sd=0.08) for the 40% med/lat full height method to 1.26 (sd=0.14) for the 33% med/lat half height method. This range of BMD ratios is consistent with published data of asymptomatic knees, measured with the 50% width technique (Hurwitz et al., 1998).

The strongest correlation between knee abduction moment and proximal tibia medial/lateral BMD was 0.357, associated with the 40% med/lat full height method (Table 1). This method disregards the middle 20% of the proximal tibia, which may be susceptible to "cross-over" effects, where medial joint forces could potentially affect the lateral aspect of the tibia near the midline, and vice versa. Our correlation of 0.357 was smaller than the 0.556 correlation reported by Hurwitz et al. (1998).

The differences in correlations among the different medial/lateral quantification methods were smaller than the correlation differences between height techniques. Furthermore, our data suggest the full height area technique yields greater correlations.

SUMMARY/CONCLUSIONS

Our study demonstrated minor sensitivities in the selection of the proximal tibia medial/lateral compartment area when calculating the BMD ratio. Disregarding a small 20% middle portion of the proximal tibia when quantifying BMD may prove beneficial when conducting follow-up testing, where identifying the exact midline for the 50% med/lat method may be more prone to error.

REFERENCES

Hurwitz, D.E., et al (1998a) *J Biomech*, **31**, 423-30.

Radin, E.L. & Rose, R.M. (1986). *J Orthop Res*, **2**, 221-234

Wada, M. et al. (2001). *Rheumatology*, **40**, 499-505.

ACKNOWLEDGEMENTS

Support from the University of Delaware Research Foundation and NIH-RR16548 (Tom Buchanan, PI) is acknowledged.

Table 1: Pearson product moment correlations (p value) between MK_{abd} and each proximal tibia medial/lateral BMD ratio method (n=64 legs).

medial/lateral method	**50% med/lat**	**40% med/lat**	**33% med/lat**
height method			
full	0.326 (p=0.008)	0.357 (p=0.003)	0.317 (p=0.010)
half	0.231 (p=0.065)	0.238 (p=0.057)	0.213 (p=0.089)

MUSCLE ACTIVATION, JOINT POSITION AND MUSCLE MASS DISTRIBUTION: CONSIDERATIONS FOR MUSCULOKELETAL MODELING AND MOVEMENT SIMULATION

Timothy Clark and David Hawkins
Human Performance Laboratory, University of California, Davis, CA, USA
E-mail: dahawkins@ucdavis.edu

INTRODUCTION

During human movement, muscle-tendon (MT) lengths change and masses are redistributed throughout the corresponding limb segments. These alterations affect limb inertial properties of the segment, including segment center of mass location and moments of inertia. Current musculoskeletal models and movement simulation software packages such as SIMM (Software for Interactive Musculoskeletal Modeling; Musculographics, Inc.) utilize static quantities to describe these inertial parameters (Delp and Loan, 1990; Delp, et al., 1995). It is not known how muscle mass redistribution within a limb affects limb inertial properties or the errors created in movement simulations by using static limb inertial models.

The objectives of this study were (1) to quantify how physiological alterations of MT geometry affect limb inertial properties, and (2) to determine how such changes affect dynamic simulations of human movement.

METHODS

A digital leg model (DLM) (Figure 1) provided the foundation from which to determine the effects of MT length changes on limb mass distribution and inertial properties. The DLM was constructed from a previous digital model of the human leg (Barr and Hawkins, 2001) and was based on high resolution images obtained from the National Library of Medicine's Visual Human Male Project. The DLM was modified to allow the geometry of individual MT structures of the DLM to be altered, thus providing a representation of how these structures would likely exist for a given muscle activation and joint configuration (Figure 2). Because of its broad use and widespread acceptance in musculoskeletal modeling and movement simulation, SIMM was used to identify muscle length changes associated with muscle activation and various joint angle changes.

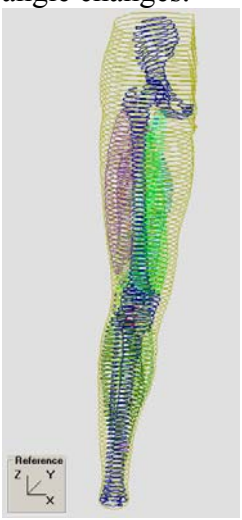

Figure 1: Visual representation of the Digital Leg Model (DLM). The DLM slice resolution is 1 mm, but shown here with 1 cm slice resolution for clarity. A subset of the DLM structures is illustrated.

Using DLM software algorithms, limb segment inertial parameters were calculated for specific muscle activation levels and joint angle configurations. Newtonian equations of motion were used to estimate the effects of muscle length changes and corresponding mass redistributions on

simulated limb dynamics. Also, to relate results back to commercial dynamic simulation software packages, SIMM was used to quantify how accounting for muscle mass redistribution during movement could affect simulated movement dynamics.

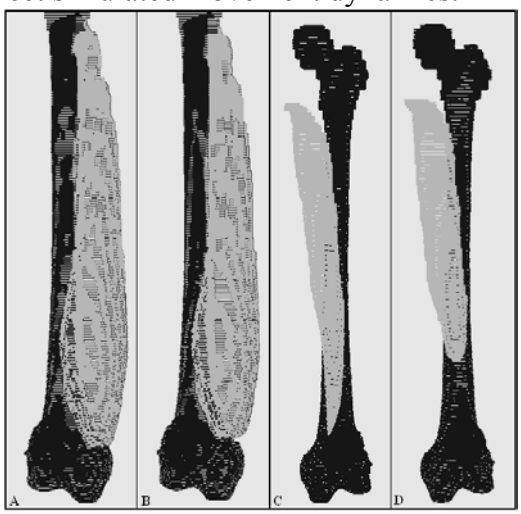

Figure 2: (A) Anterior view of vastus medialis muscle (light gray) in the baseline leg, passive condition. (B) Vastus medialis muscle; 100% isometric activation at 0° knee flexion (straight leg). (C) Posterior view of semimembranosus muscle (light gray) in the baseline, passive condition. (D) Semimembranosus muscle; 100% isometric activation at -90° of knee flexion.

RESULTS AND DISCUSSION

Muscle activation and limb movement altered limb segment center of mass and moments of inertia by less than 0.04 cm and 1.12%, respectively. The physiological variations in limb inertial properties resulted in less than 0.01% change in maximum angular velocity for a simulated straight-leg hip flexion task.

With varying joint angle positions, alterations in leg segment center of mass locations caused by agonist muscles are likely offset by the lengthening of antagonist muscles on the opposite side (i.e. anterior/posterior) of the segment. In the cases of joint angle changes from baseline, the minimal differences in inertial properties may be the result of counteracting length and mass distribution changes of antagonist muscle groups.

The underlying goal of the current project was to determine if assumptions inherent in current commercially-available dynamic simulation software packages (such as SIMM) regarding fixed inertial parameter values of the lower limb segments are valid, as no studies have been conducted to determine how mass is redistributed within a limb segment during limb movement and muscle activation, and how this mass redistribution affects limb inertial parameters. Upon examination of differences between limb inertial properties at baseline conditions and extreme joint angle configurations at varying levels of muscle activation, MT length changes and accompanying alterations in mass distribution were shown to have a minimal effect on limb segment center of mass locations and moments of inertia.

SUMMARY/CONCLUSIONS

These data demonstrate that to assume static quantities for limb segment center of mass and moments of inertia in movement simulations appears reasonable and induces minimal errors in the movement dynamics.

REFERENCES

Barr, A., Hawkins, D.A. (2000). *J Appl. Biomech,* **16**, 301-308.
Delp, S.L., et al. (1990). *IEEE Trans Biomed Eng*, **2**, 46-55.
Delp, S.L., Loan, J.P. (1995). *Comp. Biol Med*, **25**, 21-34.

STABILITY CRITERIA REDUCE NEUROMUSCULAR REDUNDANCY IN POSTURAL CONTROL

Nathan E. Bunderson [1], Thomas J. Burkholder [1], and Lena H. Ting [1,2]

[1] Georgia Institute of Technology, Atlanta, GA, USA
[2] Emory University, Atlanta, GA, USA
E-mail: nbunderson@gatech.edu

INTRODUCTION

Postural control requires the coordination of multiple muscles to achieve both endpoint force production and postural stability. Since biomechanical constraints do not uniquely determine the pattern of muscle activation the system is redundant, and any particular activation pattern that can produce the desired force may or may not be stable.

The goal of this project was to determine the contribution of intrinsic muscle properties to limb stability during isometric force generation. It has been debated to what level intrinsic properties contribute to postural stability (Hasan, 2005, Morasso & Sanguineti, 2002, Richardson et al., 2005, Winter et al., 2001) and their contributions influence the role of higher neural control centers such as reflexes and descending commands in postural control.

We therefore hypothesize that the choice of muscles used by the nervous system for posture is influenced by intrinsic stability properties of muscles. Further, by using a stability criterion, we predict that the neuromuscular redundancy in selection of muscle activation patterns will be reduced. We examined the role of stabilizing muscle length-tension relationships, and stabilizing or destabilizing muscle moment arm changes with joint angle (Young et al., 1992) in a 3D, anatomically redundant musculoskeletal model of the cat hindlimb (Burkholder & Nichols, 2004) (Fig. 1).

METHODS

The cat hindlimb model includes 31 Hill-style muscles, a fixed pelvis, seven axes of rotation, and a metatarsophalangeal joint pinned to ground, resulting in a total of four kinematic degrees of freedom. We evaluated the stability of the model associated with a large set of muscle activation patterns, each producing the same stance-like endpoint force (F_{EP}) at the nominal limb posture. Random activation sets that produced F_{EP} were generated by quadratic programming.

We used dynamic stability analysis to quantify limb stability for each activation pattern. Limb equations of motion were linearized for each pattern and eigenvalues and eigenvectors were calculated for each linearized system. The stability of the limb was quantified by the real component of the eigenvalues (λ), identifying stable ($\lambda < 0$) and unstable ($\lambda > 0$) activation sets.

"Influential" muscles (those having the greatest influence on limb stability), were identified by correlating eigenvalues to muscle activation levels. We then examined whether the stabilizing/destabilizing nature of these influential muscles was attributable to intrinsic muscle stability at a joint.

RESULTS AND DISCUSSION

30% of all activation patterns produced a limb stable in all four modes corresponding to the four degrees of freedom. Three of the

four modes were dominated by non-sagittal joint motion and were stable for 83-100% of the activations patterns. The ankle extension mode (AE) was the only mode dominated by sagittal plane joint motion and was stable for 35% of the activation patterns. The inherent stability of the non-sagittal modes suggests that the limb may be structured to minimize the demands of neural control or to allow the nervous system to focus on propulsive tasks.

Four primary influential muscles were identified for the AE mode. Three were stabilizing: medial gastrocnemius (MG), vastus lateralis (VL) and extensor digitorum longus (EDL), and one was destabilizing: flexor hallucis longus (FHL) (Fig. 1). These effects were due primarily to moment arm changes. These results predict FHL should be inactive during quiet standing.

The stability of the limb may also depend on the *combination* of muscles comprising an activation set. Of the four muscles with the greatest intrinsic stability in ankle extension, only two were identified as influential muscles: EDL and MG. Moreover, VL (a knee extensor muscle) is also an influential muscle for the ankle extension mode. This suggests that the combination of muscles activated across the limb, and not just the local intrinsic stability are important in determining limb stability.

SUMMARY/CONCLUSIONS

We have shown that limb stability during isometric force production depends on the muscle activation pattern. Moreover, the set of stable solutions represent a reduced set of potential patterns for producing a given endpoint force. We have also shown that stabilizing activation patterns are comprised of muscles with stabilizing intrinsic contributions, but also depend on the combination of muscles activated.

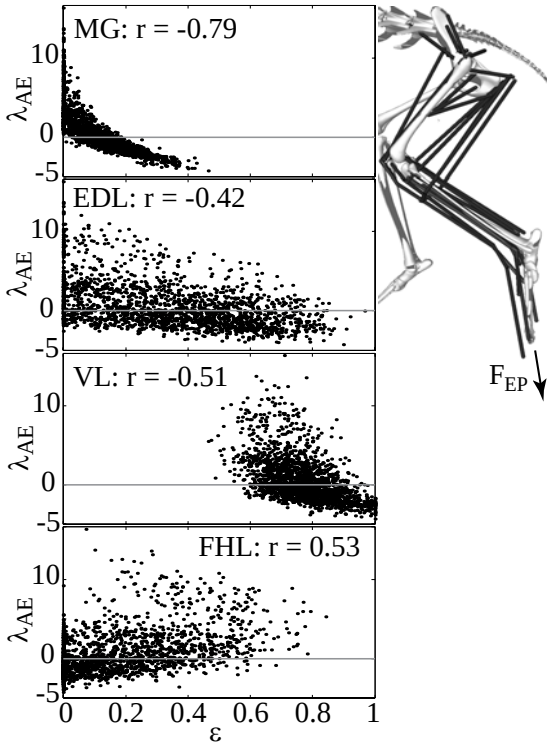

Figure 1: Left: Ankle extension mode stability (λ_{AE}) versus normalized activation level ($0 < \varepsilon < 1$) for MG, EDL, VL and FHL. Increasing activation of MG, EDL, and VL is stabilizing. Increasing activation of FHL is destabilizing. Correlation coefficients (r) are positive for destabilizing muscles, and negative for stabilizing muscles. Right: model diagram

ACKNOWLEDGEMENTS

NIH HD46922

REFERENCES

Burkholder, T.J., Nichols, T.R. (2004). *Journal of Morphology*, **261,** 118-129.

Hasan, Z. (2005). *J Mot Behav*, **37,** 484-93.

Morasso, P.G., Sanguineti, V. (2002). *J Neurophysiol*, **88,** 2157-62.

Richardson, A.G. et al. (2005). *J Neurosci*, **25,** 3181-91.

Winter, D.A. et al. (2001). *J Neurophysiol*, **85,** 2630-3.

Young, R.P. et al. (1992). *Neurosci Lett*, **145,** 137-40.

PATIENT-SPECIFIC FRACTURE ANALYSIS IN OSTEOGENESIS IMPERFECTA (OI)

Jessica M Fritz [1], Zeifang Fan [2], Peter A Smith [3], and Gerald F Harris [2, 3]

[1] Marquette University, Milwaukee, WI, USA
[2] Orthopaedic and Rehabilitative Engineering Center (OREC), Milwaukee, WI, USA
[3] Shriners Hospitals for Children, Chicago, IL, USA
E-mail: gerald.harris@mu.edu

INTRODUCTION

Osteogenesis imperfecta (OI) is an inherited connective tissue disorder characterized by skeletal deformities and brittle bones. A prevalence of 1 in 5,000 to 1 in 10,000 has been suggested (Beyers 1992). It is affects an estimated 20,000 to 50,000 people in the United States (Cleveland Clinic 2006). OI is clinically classified into four types (I-IV). OI type I is the mildest and most common form of OI. The bones of type I patients have little or no deformation and a mildly short stature. Patients with type I average about 40 prepubescent fractures, but very few post-puberty (Cleveland Clinic 2006). OI type II is the most severe form of the disease. It affects 10 percent of the OI patient population. It is marked by severe bone fragility and long bone deformation. Often patients with type II die at or shortly after birth. Type III is the most severe form of OI among children and young adults. It affects 20 percent of the OI population. Persons with OI type III often experience about 100 prepubescent fractures. Type IV falls between types I and III in terms of severity. Patients exhibit mild to severe bone fragility, moderately deforming bones and variable short stature (Beyers 1992). Across all types, the poor bone quality poses major orthopaedic and rehabilitation challenges. Patients are often restricted in their physical activities. Three treatment options are available to OI patients: 1) non-surgical (conservative), 2) surgical and 3) drug therapy (Cleveland Clinic 2006). All are performed with the goal of maximizing function, minimizing deformity, maintaining patient comfort, and allowing for independent living. Treatment strategies are generally personalized based on motor function, functional needs, and fracture risk. However, fracture risk assessment is difficult to evaluate and is very clinician dependent. The goal of this project is to create a reliable patient-specific model for fracture prediction using finite element analysis (FEA), kinetic gait data and bone material property data gathered from unique nanoindentation tests.

METHODS

OI bone material properties are input as isotropic linear elastic solid with a Young's modulus and a Poisson's ratio based on previous and continued nanoindentation testing of children and young adults (Fan 2006). OI bone specimens are analyzed with the Triboindenter® (TriboIndenter, Hysitron, Inc., Minneapolis, MN) system at the University of Memphis/University of Tennessee. The fracture prediction models are created and analyzed in ABAQUS/CAE (ABAQUS, Inc., Providence, RI) using tetrahedral elements. The femur model originated from the standard femur, which was available through the International Society of Biomechanics (ISB) website (Viceconti 1996). The standard femur is altered through nodal manipulation to match a specific OI type I patient's right femur morphology based on a coronal plane X-ray. Boundary and loading conditions are based on gait kinematics and muscle loading data.

Initial stance, mid-stance, and terminal stance are used as three critical femur loading points of the gait cycle based on the hip and knee moment and power and joint reaction moment graphs of the patient's gait analysis. Muscle forces as a percentage of body weight also contribute to the overall boundary conditions of the FEA model (Polgár 2003). The muscle insertion locations are based on femoral anatomy. With all the patient-specific parameters input into the model, it is then analyzed to look at stress and strain distributions and maximums as well as von Mises stresses.

RESULTS AND DISCUSSION

The femur model shows that altered morphology leads to increased stress concentrations in the femur as well as higher strain values along the medial aspect. The altered material properties of OI bone also contribute to increased fracture risk. The higher femoral Young's modulus of 19 GPa causes the bone to potentially fracture under the loading of a routine gait cycle.

The results of the model are consistent with increased fractures seen clinically in OI patients. The increased Young's modulus noted with nanoindentation is representative of increased brittleness in OI bone as compared to normal bone. This often means that activities of daily living for a healthy person could cause fracture in OI patients. It is hoped that future models will include automated methods for image detection and morphology alteration. Another potential improvement is the use of bi-planar X-rays (sagittal/coronal) with stereo-photogrammetry and advanced image processing to convert the two orthogonal planar images into a representative 3-D solid model. While CT scans allow a 3-D reconstruction, the amount of radiation is a concern for OI patients who, due to numerous fractures, are frequently exposed to imaging radiation. The validity of the current model appears to be suitable for continued application. We estimate that approximately 50% of the enrolled subjects will experience some type of fracture during a two year time course.

CONCLUSIONS

A patient-specific model with material properties from nanoindentation and applied loading based on physiologic conditions and gait analysis offers an improved method for predicting fracture in OI. Improved fracture prediction in turn may allow more effective clinical intervention including activity modification and assistive device recommendations. Ultimately, the proposed FEA model could offer a more reliable tool to enhance the clinician's ability to effectively treat OI.

REFERENCES

Beyers, P.H., Steiner, R.D. (1992). *Annu Rev Med*, **43**, 269-282.

Cleveland Clinic Osteogenesis Imperfecta. (2006). Retrieved from: http://www.clevelandclinic.org/health/health-info/docs/2600/2610.asp?index=9500

Viceconti, M., et al. (1996). *J. Biomech*, **29**, 1241.

Fan, Z., et al. (2006). *J Biomed Mater Res*, **part A**, 71-77.

Polgár, K., et al. (2003). *Proc Instn Mech Engrs, Part H: J Eng in Med*, **217**, 173-189.

ACKNOWLEDGEMENTS

Funding provided through the Department of Education, National Institute for Rehabilitation Research (NIDRR), H133G06052. and Shriners Hospitals for Children.

PASSIVE AND ACTIVE CONTRIBUTIONS TO JOINT KINETICS IN ELDERLY GAIT

Amy Silder, Bryan Heiderscheit, Ben Whittington, and Darryl G. Thelen
University of Wisconsin, Madison, WI, USA
Email: silder@wisc.edu

INTRODUCTION

Aging is associated with a shift in the source of joint power generation during walking. Older adults tend to exhibit reduced ankle power accompanied by increased power generation about the hip (DeVita and Hortobagyi, 2000). It is possible that hip flexion contractures in older adults may contribute to this redistribution of joint powers. Hip flexor tightness may inhibit hip extension in late stance, thereby reducing the effectiveness of plantarflexor push-off (Kerrigan, et al., 2003) while passively increasing net hip power (McGibbon and Krebs, 2004). The purpose of this study was to evaluate this hypothesis by investigating the effect of age on the passive and active contributions to hip and ankle powers during walking.

METHODS

Twenty healthy older (7 males, 13 females; age, 72±5y) and 20 healthy young (9 males, 11 females; age, 26±3y) adults participated in this study. All subjects performed a series of five walking trials across a 10m walkway at 80, 100, and 120% of preferred speed. Three-dimensional whole body kinematics were recorded at 100Hz using an 8 camera motion capture system. Ground reaction forces were synchronously collected for two successive foot strikes using three imbedded force plates. Inverse kinematics and inverse dynamics were used in conjunction with a scaled whole body model to estimate joint angles, moments, and powers throughout the gait cycle.

Passive joint moment-angle relationships about the hip, knee, and ankle were characterized for each subject (Silder, et al., 2006). Individuals were positioned side-lying with their dominant leg supported on a table via low-friction carts (Fig. 1). The lower limb was slowly manipulated through full ranges of hip, knee, and ankle motion using two 3D load cells over a series of 15 unique trials. Lower extremity EMG signals were monitored to ensure the muscles were relaxed such that passive properties were obtained. Kinematics and load cell forces were simultaneously measured and used to calculate joint angles and passive joint moments.

The passive joint moment-angle relationships were represented by a set of exponential functions that accounted for the stretch of both uni-articular tissues and bi-articular muscles (Silder, et al., 2006). Model parameters were estimated on a subject-specific basis using a least squares fitting routine. Joint angles measured during walking were then used in conjunction with the models to estimate passive joint moments and powers during walking. Active contributions were defined as the net power minus the passive contribution. Powers were integrated to estimate the work attributable to active and passive structures.

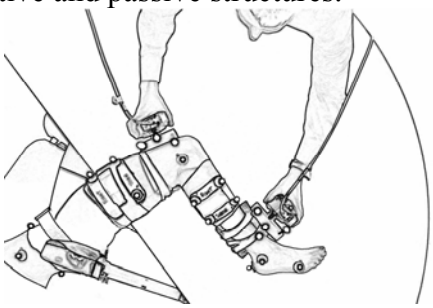

Figure 1: Passive joint moments were measured with the subject sidelying while the lower extremity was manipulated with two hand-held load cells (top view).

RESULTS

There were no significant differences between older and young adults with respect to walking speed, step length, or cadence (Table 1). Nevertheless, the older adults in this study exhibited greater peak hip extensor power (H3) and reduced peak ankle plantarflexor power (A2). This resulted in the older adults doing significantly more net work at the hip but less net work at the ankle at all walking speeds ($p<0.01$) (Table 1).

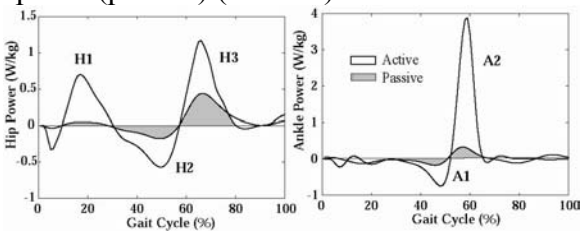

Figure 2: Representative plots of net and passive hip and ankle powers.

Passive structures about the hip provided an energy storage and return mechanism for both groups by contributing substantially to the negative hip power during late-stance (H2) and positively during initial swing (H3) (Fig. 2). Passive energy storage and return also occurred at the ankle during the A1 and A2 power bursts respectively, though the magnitudes were not as large as the hip. The work done by passive structures at the hip and ankle were not significantly different between groups at any of the speeds tested (Fig. 3).

CONCLUSIONS

Healthy older adults did not exhibit an increased reliance on the use of passive structures during walking when compared to young adults, suggesting that healthy older adults are more likely generating additional hip power actively rather than passively. Further research is needed to determine if these results extend to older adults who exhibit more pronounced impairments. We conclude that there must be alternative, underlying causes of the distal to proximal shift in joint power production seen in the gait of healthy older adults, which may include distal weakness, impaired sensory function, and/or balance concerns.

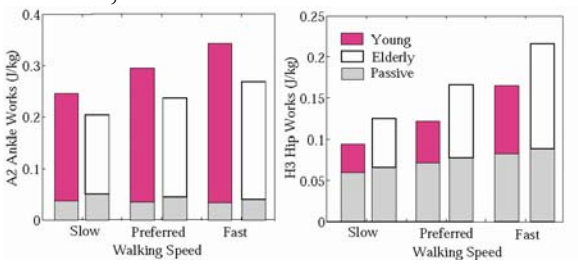

Figure 3: Passive and active work done during the A2 and H3 power bursts.

REFERENCES

DeVita, P., and Hortobagyi, T., (2000). *J Appl Physiol,* **88,** 1804-1811.

Kerrigan, C. et al, (2003). *Arch Phys Med Rehabil,* **84**, 1-6.

McGibbon, C. and Krebs, D., (2004). *J Appl Physiol*, **96**, 149-160.

Silder, A. et al, (2006). *J Biomech,* (in press).

ACKNOWLEDGEMENTS

NIH AG24276, NSF pre-doctoral fellowship (AS), Jane Mahoney, MD

Table 1: Temporal gait characteristics and net works (mean±SD) done at the ankle and hip during the A2 and H3 power bursts, respectively (*denotes significant group difference $p<0.01$).

	Young Adults			Older Adults		
	Slow	**Preferred**	**Fast**	**Slow**	**Preferred**	**Fast**
Speed (m/s)	1.06±0.10	1.33±0.13	1.59±0.14	1.06±0.10	1.32±0.13	1.58±0.16
Step Length (m)	0.75±0.06	0.83±0.07	0.90±0.07	0.75±0.06	0.82±0.06	0.90±0.08
Cadence (steps/min)	99±10	112±10	122±10	100±6	115±7	125±8
A2 Work (J/kg)	0.24±0.07*	0.29±0.07*	0.34±0.09*	0.20±0.07*	0.23±0.08*	0.27±0.09*
H3 Work (J/kg)	0.09±0.04*	0.12±0.04*	0.17±0.05*	0.13±0.04*	0.17±0.04*	0.22±0.05*

DISEASE SEVERITY INFLUENCES TRUNK SWAY AND KNEE LOADING DURING WALKING IN PATIENTS WITH MEDIAL COMPARTMENT KNEE OA

Annegret Mündermann [1,2], Jessica L. Asay [1], Thomas P. Andriacchi [1,2]

[1] Stanford University, Stanford, CA, USA
[2] Bone and Joint Research Center, VA Palo Alto, Palo Alto, CA
E-mail: amuender@stanford.edu Web: biomotion.stanford.edu

INTRODUCTION

Osteoarthritis (OA) of the knee affects a large portion of the population. The load distribution at the knee, as estimated dynamically by the external knee adduction moment, has been associated with the presence, severity and rate of progression of the disease (Sharma et al. 1998; Miyazaki et al. 2002; Mündermann et al. 2004). It has been suggested that patients with less severe knee OA adopt a gait pattern to reduce the adduction moment while patients with more severe knee OA have higher knee adduction moments. The less severe patients appeared to reduce their knee adduction moment by increasing their medio-lateral trunk sway (reflected in altered hip abduction and adduction moments) (Mündermann et al. 2005). Recently, a novel method for reducing the knee adduction moment has been proposed. Following this method, medio-lateral trunk sway was increased and substantial reductions in the knee adduction moment were observed in a healthy population (DeMarre et al. 2006). This study tested the hypothesis that disease severity in patients with knee OA is an important factor in using medio-lateral trunk sway as a mechanism to reduce the knee adduction moment during walking.

METHODS

Fourteen patients with radiographically diagnosed medial compartment knee OA (6 female, 8 male; age: 59.3 ± 7.7yrs; height: 170.4 ± 9.8cm; mass: 80.4 ± 16.2kg) and 25 physically active adults (13 female, 12 male; age: 53.1 ± 11.6yrs; height: 171.1 ± 12.5cm; mass: 76.1 ± 15.3kg) participated in this study. None of the healthy subjects had previously been treated for any clinical lower back or lower extremity condition or had any activity-restricting medical or musculoskeletal condition. Patients were grouped into a less (KL grade ≤ 2; n = 6) and a more severe (KL grade ≥ 3; n = 8) OA group based on their Kellgren Lawrence (KL) grade (Kellgren & Lawrence 1963). Subjects performed walking trials at a self-selected slow, normal and fast speed in their own low top, comfortable walking shoes, and one trial was identified for each subject with walking speed closest to 1.2m/s. The external knee moment was calculated from the position of skin markers, ground reaction force measurements, and limb segment mass/inertia properties and normalized to body weight and height (% Bw·Ht) (Schipplein and Andriacchi 1991). Medio-lateral trunk sway was calculated as the angle of the upper trunk segment relative to the vertical axis (Figure 1; d). Medio-lateral trunk sway phasing [%] was calculated as the time of heel-strike relative to time of peak medial and lateral position of the upper trunk segment(b/(a+b)*100). A significant difference in demographic variables and gait variables were detected using two-way ANOVAs. A relationship between the knee adduction moment and trunk sway amplitude within each group was detected using linear regression analysis ($\alpha = 0.05$).

RESULTS AND DISCUSSION

Reduced knee adduction moments in patients with less severe knee OA correlated with increased trunk sway (Figure 2). In contrast, the knee adduction moment in more severe patients did not correlated with trunk sway amplitude. Similarly, no relationship between these variables was observed for control subjects ($R^2 = 0.021$; P = 0.500). It is important to note that as a group patients with knee OA walked with a 22.7% higher knee adduction moment than healthy control subjects (P = 0.47) when walking at 1.2m/s. However, after stratifying patients patients based on their severity, only patients with more severe knee OA had greater than normal knee adduction moments. The results of this study support the hypothesis that only patients with less severe knee OA who walk with greater medio-lateral trunk sway do experience smaller knee adduction moments and is similar to earlier reports of successful gait adaptation via altered hip joint moments and the potential of lowering the adduction moment in patients with less but not with more severe knee OA (Mündermann et al. 2004, 2005). Thus, gait interventions that mimic or amplify natural gait compensations may be an effective yet non-invasive method for the prevention and treatment of knee OA.

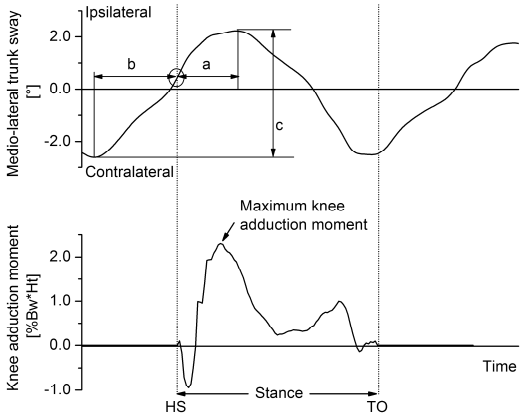

Figure 1: Illustration of variables describing the knee adduction moment and medio-lateral trunk sway.

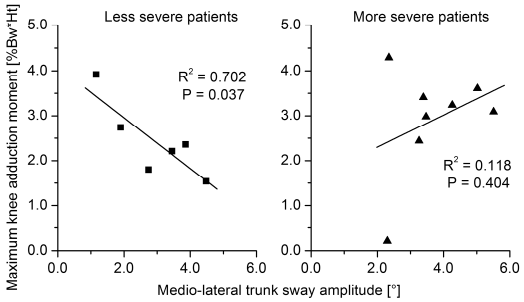

Figure 2: Less (more) severe patients had a negative (positive) correlation between the knee adduction moment and trunk sway amplitude.

REFERENCES

DeMarre, J.L. et al. (2006) *Proceedings of ASB'06*.

Kellgren, J.H. Lawrence, J.S. (1963) *Atlas of standard radiographs*. Blackwell.

Miyazaki, T. et al. (2002) *Ann Rheum Dis* **61**:617-622.

Mündermann, A. et al. (2004) *Arthritis Rheum*, 50, 1172-1178.

Mündermann, A. et al. (2005) *Arthritis Rheum*, **52**, 2835-2844.

Schipplein, O.D., Andriacchi, T.P. (1991) *J Ortho Res,* **9**, 113-119.

Sharma, L. et al. (1998) *Arthritis Rheum*, **41**, 1233-1240.

Table 1. Average variable differences in between patients with less (KL ≤ 2; N = 6) and more (KL ≥ 3; N = 7) severe medial compartmental knee OA and matched control subjects (N = 25). *P < 0.05.

Variable	Δ KL ≤ 2 vs. control	Δ KL ≥ 3 vs. control	Δ all KL vs. control
Maximum knee adduction moment [%]	7.4	28.6	19.5*
Trunk sway amplitude [°]	-1.5*	-0.7	-1.0
Trunk sway phasing [%]	4.1	-19.2	-9.2*

HEIGHT ESTIMATION OF AN OBSTACLE IS SCALEABLE TO TOE ELEVATION AT OBSTACLE CROSSING

Chris K. Rhea and Shirley Rietdyk
Purdue University, West Lafayette, IN, USA
E-mail: crhea@purdue.edu

INTRODUCTION

Obstacle negotiation is a part of everyday life. While researchers have studied how the sensory components of the nervous system contribute to successful obstacle negotiation (Patla, 1998; Rhea & Rietdyk, 2007; Courtine et al., 2007), little is understood about how visual information available before the task influences the actual task performance. To assess performance during gait, measures of foot placement while approaching the obstacle and toe clearance/elevation while crossing the obstacle are commonly examined. To better understand how visual information available before the task is integrated into the task of adaptive gait, a height estimation task can be used to capture a subject's visual perception of obstacle height.

Toe clearances have been shown to decrease with multiple exposures to a common obstacle height (Rhea & Rietdyk, 2005). However, little is know about the role of subjects' perception of the obstacle's height before acting on the obstacle. This project compared subjects' perceived height of an obstacle with their toe elevation at obstacle crossing. It was hypothesized that subjects would accurately perceive the obstacle's height and their height estimation of the obstacle would positively correlate to their toe elevation at obstacle crossing.

METHODS

Six subjects (age: 23.1 ± 4.6 yrs; mass: 65.2 ± 10.8 kg; height: 1.71 ± 0.07 m) participated in the study and gave informed consent. Four infrared emitting diodes (IREDs) were placed on the subject's toe and heel on the lateral aspect of their right foot and medial aspect of their left foot. Displacement data was collected at 120 Hz with two Optotrak 3020 sensors (Northern Digital, Inc.).

A 10 cm obstacle was placed in the middle of an eight meter walkway. Prior to walking over the obstacle, subjects were told to stand approximately three steps from the obstacle and raise and lower their toe 20 times to their perceived height of the obstacle (Figure 1). Subjects then crossed the same obstacle for 50 consecutive trials.

The dependent variable was toe elevation during the height estimation task and while the foot was directly over the obstacle during crossing. Toe elevation was measured as the vertical displacement of the toe from the ground. Toe clearance decreases with increased exposure to an obstacle (Rhea & Rietdyk, 2005), so only the first five trials of obstacle crossing were used in this analysis.

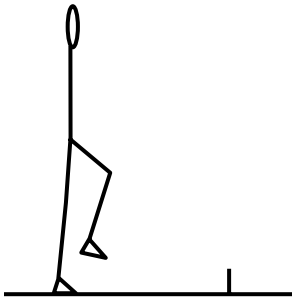

Figure 1. Static assessment of obstacle height.

RESULTS AND DISCUSSION

Height estimation values ranged from 4.0-16.3 cm with a mean of 10.6 cm. A significant ($p < .01$) positive correlation of .95 was found between toe elevation during the height estimation and the obstacle crossing tasks. The toe elevation during the obstacle crossing task was an average of 15.5 cm greater than the toe elevation during the height estimation task (Figure 2). A trendline was fitted to the data and had a slope of 1.08.

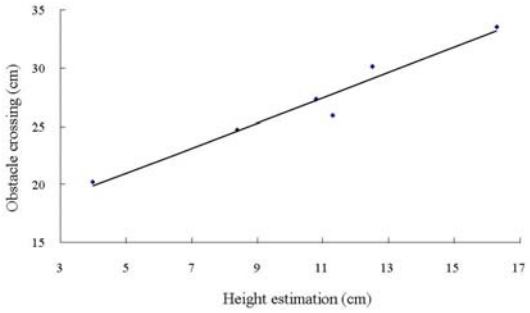

Figure 2. Toe elevation during the height estimation and obstacle crossing tasks.

Using the height estimation task as a measure of perception, this provides direct evidence that perception and action are coupled during an obstacle avoidance task.

Although the subjects perceived the obstacle to be taller or short than it actually was, their toe elevation at obstacle crossing was 15.5 cm greater than their perception of the obstacle's height. This shows that variability in toe clearance is dependent on the individual's perception of the obstacle height.

SUMMARY/CONCLUSIONS

There is a direct relationship between the perceived height of an obstacle and toe elevation at obstacle crossing. Crossing an obstacle safely is achieved by adding 15.5 cm to the perceived height of the obstacle.

REFERENCES

Courtine, G., et al. (2007) *Journal of Neurophysiology*, 97(1), 772-779.

Patla, A.E. (1998) *Ecological Psychology*, 10(3-4), 287-304.

Rhea, C.K. & Rietdyk, S. (2005) *Proceedings of the XX Congress of the International Society of Biomechanics*.

Rhea, C.K. & Rietdyk, S. (2007). *Neuroscience Letters*, in press.

STATIC POSTURAL STABILITY OF INDIVIDUALS WITH MENTAL RETARDATION BEFORE AND AFTER WEIGHT AND BALANCE TRAINING

Courtney A. Haynes[1] and Thurmon E. Lockhart, PhD[2]

Virginia Polytechnic Institute and State University, Blacksburg, VA, USA
[1] School of Biomedical Engineering and Sciences
[2] Grado Department of Industrial and Systems Engineering
Email: chaynes7@vt.edu

INTRODUCTION

Mental retardation (MR) occurs in 2.5–3 percent of the general population and is the most common developmental disorder (CDC 2005). As of the year 2000, there were approximately 6–7.5 million Americans living with MR while another 60 million suffer from some level of developmentally related cognitive impairment (ADA 2000). Individuals with MR are known to be at an elevated risk of falls (Sherrard 2001). The annual morbidity and mortality rates due to accidental injuries of people with MR have been reported as 55.6/1000 and 150/100,000, respectively (Sherrard 2001). Falls were reported to be the most common cause of accidental injury.

Implementing weight and balance training can increase static postural stability (Hess 2006). Postural stability measurements provide a quantification of deviations of a person's center of pressure (COP). Increasing postural stability can reduce the risk of falling and thus the associated cost, both emotional and financial, of suffering a fall accident. The objective of this study was to determine whether the static postural stability of individuals with MR can be improved with weight or balance training. Specifically, an increase in postural stability would be indicated by a decrease in mean COP, anteroposterior (AP) and medial-lateral (ML) sway range, or mean COP velocity.

METHODS

Sixteen participants (12 males, 4 females, 39±9.9 years old) with varying degrees of MR were used in this study. The experiment employed a three group pretest-posttest design. Participants were randomly assigned to one of three training groups: control (C), weight training (N), or balance training (B). Each group performed a balance test before and after the training.

The balance test consisted of standing in the center of a force plate (BERTEC #K80102, Type 45550-08, Bertec Corporation, Columbus, OH) for 30 seconds. Two trials were recorded for each of two experimental conditions: eyes open and eyes closed. Force plate data was sampled at 1200 Hz. The weight-training group completed Nautilus training three times a week while the balance training group performed balance exercises three times a week using foam Thera-band therapy pads. After 8 weeks of training, the participants repeated the balance tests.

To determine the effect of training on static postural stability, a 2-way repeated measures ANOVA was used. The test conditions of 'eyes open' and 'eyes closed' were used as blocking variables. A mixed-model design of training type (C, N, B) x training time (pre, post) was used, with training group as a between-subjects factor and training time as a within-subjects factor. All levels of

significance were set to 0.05. The dependent variables of interest were the mean COP, mean velocity of COP, and the range of AP and ML sway.

RESULTS AND DISCUSSION

No significant differences were found between pre- and post-training effects for mean COP, mean COP velocity, and the range of AP and ML sway.

Despite the fact that no significant differences were found, an observation of data trends suggests that balance training may cause a slight decrease in the mean velocity of COP for both the eyes open and, more markedly, the eyes closed condition. The balance training appears to have also elicited a small decrease in mean COP as well as in AP and ML range again for the eyes closed condition. Table 1 presents the results of pre- and post-training with eyes closed for the balance training group.

Table 1: Group (B), eyes closed (mean±SD)

Eyes-Closed Stability Parameter	**Training Group: B**	
	Pre-	**Post-**
Mean COP (cm)	1.52±0.28	1.22±0.32
AP Range (cm)	7.22±1.55	6.70±1.69
ML Range (cm)	6.77±3.17	6.44±3.47
Mean COP Vel (mm/s)	32.9±6.13	17.2±6.71

In comparison with the published postural stability parameters of healthy people, the data collected in this study illustrates the magnitude of the deficits in stability caused by MR. In a study published by Maki et al. (1990), healthy and elderly subjects of both genders were measured to have sway ranges in either direction of a few centimeters. The sway measures reported for the MR subjects in the present study were often greater than 10 cm. Also, the mean COP velocity for the subjects in the Maki study were reported as less than 10 mm/s whereas the subjects in the current study exhibited mean COP velocities greater than 20 mm/s. Thus, even though the results of this study did not report statistically significant changes in postural stability after training, knowledge was gained in that relative magnitudes of stability for the MR population were quantified.

SUMMARY/CONCLUSIONS

It was the objective of this study to quantify postural stability of subjects with MR and to assess whether a balance and weight training regimen could successfully improve these measures. No statistical significance was found due to the training effects, but this study provides a quantification of the deficits in postural stability that are present in individuals with MR. More subjects would be needed to definitively determine whether or not weight or balance training can affect the stability of individuals with MR and whether it can be an effective intervention for reducing fall accidents.

REFERENCES

Americans with Disabilities Act, 2000.

Centers for Disease Control and Prevention, 2005.

Hess, J.A. et al. (2006). *Aging Clin Exp Res*, **18(2)**, 107-15.

Maki, B.E. et al. (1990). *JAGS*, **38**, 1-9.

Sherrard, J. et al. (2001). *Injury Prevention*, **7**, 56-61.

ACKNOWLEDGEMENTS

I would like to thank Virginia Tech and the State of Virginia for funding this research as well as the staff at the Southwestern Virginia Training Center (SWVTC) for their cooperation. Additionally, Niti and Jian for help in data collection.

ESTIMATION OF KNEE JOINT COMPRESSION FORCE IN SUBJECTS WITH MEDIAL COMPARTMENT KNEE OSTEOARTHRITIS

Joseph A. Zeni, Jr [1] and Jill S Higginson [1,2]

[1] Biomechanics and Movement Science Program, University of Delaware, Newark, DE, USA
[2] Department of Mechanical Engineering, University of Delaware, Newark, DE, USA
E-mail: jzenijr@udel.edu

INTRODUCTION

Determination of individual muscle force contributions during walking is limited by the problem of redundancy in the motor system. While it is possible to determine external joint moments using an inverse dynamics approach, there are significant limitations to determining actual intersegmental contact forces. The role of these contact forces in pathologies such as knee osteoarthritis (OA) is not well understood, but may play a role in disease progression.

Previous authors have used optimization techniques to estimate intersegmental contact force at the knee (Anderson and Pandy 2001). We have developed a two-dimensional static optimization technique for estimating knee contact force that can be applied to pathological gait. The purpose of this investigation is to determine if the optimization technique produces results that are physiologically meaningful for individuals with knee OA, as well as to serve as a foundation on which future optimization parameters in this subject population can be established.

METHODS

Ten subjects (4 males) with bilateral knee OA voluntarily took part in the investigation. Radiographic grading of the severity of knee OA was based on the Kellgren-Lawrence scale and subjects were divided into groups based on the OA severity (Grade 1 = mild, 2-3 = moderate, 4 = severe). All data were collected on a split belt treadmill capable of collecting vertical and horizontal ground reaction forces (Bertec Corp., Columbus, OH, USA). Subjects walked at 0.8 meters/second to decrease differences in joint loading that may be associated with different self-selected walking speeds. EMG, 3D motion analysis and kinetic force plate data were obtained during 30 second walking trials.

Joint angles, external joint moments and joint reaction forces derived from kinematic and kinetic data were determined using OrthoTrak v.6.3.3 (Motion Analysis, Santa Rosa, CA, USA). Moment arms and muscle orientations for each subject were exported at each point in the gait cycle using SIMM software (Delp and Loan 1995).

Custom written Matlab code was used to determine the uni- and bi-articular muscle forces required to achieve joint moments in the sagittal plane for the ankle, hip, and knee. To overcome muscle redundancy, muscle forces to minimize net muscle stress were determined (Crowninshield and Brand 1981). Individual muscle force contributions were limited to 85% of their maximum force generating capabilities (Challis 1997).

The plots of individual muscle forces during the gait cycle for each subject were then compared to the EMG recorded during the walking trial. Bilateral maximal knee

contact force was computed as the vector sum of muscle and joint reaction forces.

RESULTS AND DISCUSSION

Maximal knee contact force derived from the optimization procedure ranged from 1.69 body weight (BW) to 3.00 BW (mean = 2.15 BW). Non-normalized maximal values for knee contact force ranged from 1230 N to 2838 N (mean = 1870 N). These results correspond well to experimental measures of knee contact force by Taylor et al. (2001) who used telemetered force data from an implanted total knee device. At one year post-op, they reported walking on a treadmill at speeds similar to ours resulted in about 2.1 BW, nearly identical to our results.

When analyzed on the basis of OA grade, the severe group showed the highest averaged non-normalized intersegmental force, 1971 N (SD = 330.1). The mild group showed the lowest average force, 1621 N, a difference of 350 N (p=0.067).

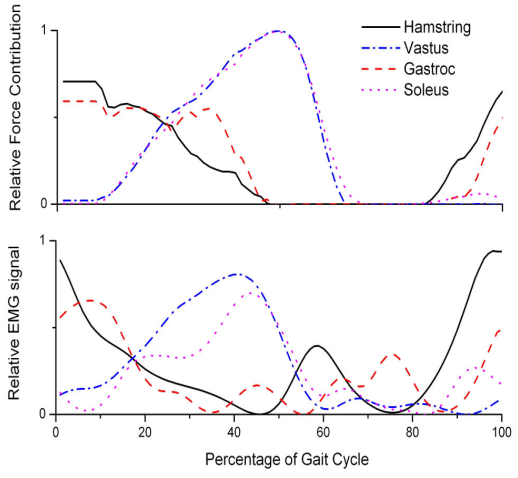

Figure 1: Theoretically derived relative force contributions (top) closely matched the relative experimentally obtained EMG signal (bottom) from a representative subject during a gait cycle (HS to HS).

When the predicted forces were compared to the EMG activation patterns (Fig. 1), the results were very similar. On/off times as well as peak activation times coincided closely with the predicted muscle forces.

SUMMARY/CONCLUSIONS

The static optimization techniques utilized here provide force data that matches the activation patterns from experimentally determined EMG. The maximal intersegmental contact forces are also similar to previous reports that have obtained the data experimentally (through instrumented knee prostheses) and mathematically (static and dynamic optimization procedures). The results from the maximal knee contact force in the mild and severe OA group suggest that differences in knee joint loading do exist depending on OA severity.

Future research using this technique will include frontal and coronal plane moments to determine differences in knee joint loading in subjects with knee OA. We will also determine whether an alternate choice of cost functions, such as minimization of joint compression, will provide even more clinically relevant information.

REFERENCES

Anderson, FC and Pandy, MG. (2001) *J Biomech*, **34**, 152-161.

Challis, JH (1997). *Med Eng Phys*, **3**, 253-61.

Crowninshield, RD and Brand, RA. (1981) *J Biomech*, **9**, 655.

Delp, SL and Loan, JP. (1995) *Comput Biol Med*, **1**, 21-34.

Taylor, SJG and Walker, PS. (2001) *J Biomech*, **34,** 839-848.

ACKNOWLEDGEMENTS

NIH P20-RR16458

EFFECT OF PARKINSON'S DISEASE ON STEP RESPONSE TO A BACKWARDS PULL

Molly A. McVey [1,2], Antonis P. Stylianou [1,2], Carl W. Luchies [1,2], Kelly E. Lyons [1], Rajesh Pahwa[1], Stephen D. Jernigan[1]

[1] University of Kansas Medical Center, Kansas City, KS, USA
[2] University of Kansas, Lawrence, KS, USA
E-mail: luchies@ku.edu, Web: www2.kumc.edu/coa

INTRODUCTION

Postural instability leading to falls is one of the most disabling symptoms of Parkinson's disease (PD). The consequences of a fall can have severe physical, psychological, and economic impacts including fractures, fear of falling, and loss of independence (Balash, Y. et al. 2005, Tinetti, M.E. et al. 1994). The response to a large balance perturbation often involves a step response to reconfigure the base of support, which must be done quickly and appropriately in order to prevent a fall. Differences in the step response strategy, kinetics, and kinematics have been shown in older adults who also have an increased risk of falling. Therefore, this study sought to investigate the step response in terms of response strategy, ankle plantarflexion angle, and impulse at landing for the first step taken during the response.

METHODS

Five subjects with idiopathic PD (age: 75 ± 4.5 yrs, mild severity: H&Y 2) and four healthy controls (HC) (age: 74 ± 5.1 yrs) participated in the in the protocol approved by the institution's human subject committee.

Task: Participants stood in an upright, relaxed position, with arms crossed at the chest. A rigid waist harness was attached to a cable and weight-drop mechanism, which when released, delivered a posterior waist pull to the subject. The subject was asked to respond naturally to the disturbance.

The weight-drop device was loaded with a weight equal to 20% of body weight and pulled the subject backwards a distance equal to 8.7% of waist height, corresponding to a 5º equivalent disturbance angle (Luchies et al. 1994).

Data Collection: Force plate data were collected using three AMTI (Advanced Medical Technology Inc.; Watertown, MA) six-component force plates sampled at 1080 Hz. Kinematic data were collected at 120 Hz using reflective markers and a six camera Vicon 512 (Vicon Peak, Lake Forest, CA) motion analysis system. Markers were placed bilaterally on the 2nd metatarsal, ankle, heel, calf, and lateral femoral condyle. All responses were video taped.

Data Analysis: The consistency of the response was determined by analyzing video taken during the trials. An inconsistent response was defined as a change in the stepping limb for the first step across the multiple trials. Ankle plantarflexion (PF)/dorsiflexion (DF) angles were determined for the leg used during the first step in the response. Ankle angle from beginning of the trial to liftoff and from liftoff to landing of the first step was determined from the kinematic analysis within an inverse dynamics model (Vaughan, C.L. et al. 1992). The first step

landing impulses in the A-P, M-L, and vertical directions were determined from force plate data. T-tests ($p<0.05$) were used to assess group differences.

RESULTS AND DISCUSSION

All subjects responded to the waist pull by taking at least one step backwards. HC were more consistent in the choice of stepping limb than PD (HC: 100%, PD: 60%). HC went into PF prior to liftoff of the first step. In contrast, PD tended to go into DF prior to liftoff. Figure 1 shows the mean normalized ankle angle both prior to liftoff and from liftoff to landing of the first step. At liftoff time, PD were in DF (-5.7º ± 9.7º) while HC were in PF (8.4º ± 2.7º). The initial angle is different between the groups because of the stooped posture that the PD tended to have when standing flat footed. The different angle prior to liftoff may indicate different muscle activations affecting the ankle joint. During the step and at landing, both groups show a similar pattern into DF, but PD tend towards deeper DF (PD: 15.4º±13.9, HC: 4.5º±2.2º). Table 1 shows the landing impulse for the first step. PD and HC showed similar A-P and M-L impulse at landing. PD showed higher, although not significantly different vertical impulse compared to HC.

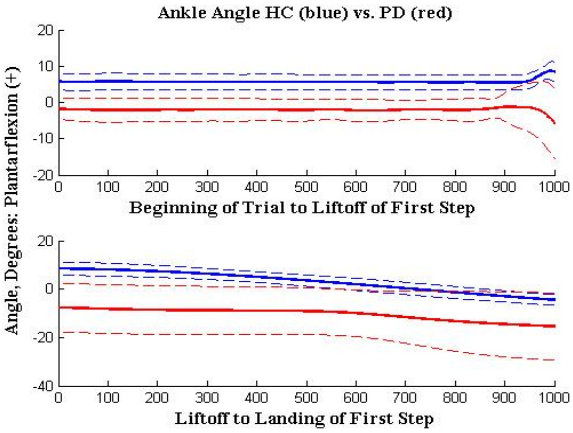

Figure 1: Mean (solid) ± SD (dashed) of mean normalized ankle PF/DF angle prior to (top) and during (bottom) the first step for the two groups (HC: blue, PD: red).

Table 1. Impulse at Landing (N-s/kg)

	HC	PD	t-test
A-P	1.666± 0.083	0.170 ± 0.089	0.94
M-L	0.122 ± 0.020	0.170 ± 0.116	0.45
Z	2.045 ± 0.444	2.928 ±1.183	0.20

SUMMARY/CONCLUSIONS

The results indicate that PD subjects respond differently to a balance disturbance. They were less consistent in the choice of stepping limb, and responded with a different strategy in that they did not respond to the pull by plantarflexing at the ankle before liftoff of the first step in the response. Even though the impulses at landing are similar, the ankle angle configuration at landing may have an effect in restoring postural control.

REFERENCES

Balash, Y. et al. (2005). *J Neurol* **252,** 1310-5.

Luchies, C.W. et al. (1994). *J Am Geriatr Soc*, **42**, 506-512.

Tinetti, M. E. et al. (1994). *J Gerontol* **49**, M140-7.

Vaughan, C.L. et al. (1992).*Dynamics of Human Gait.* Human Kinetics.

ACKNOWLEDGEMENTS

We gratefully acknowledge support from the Landon Center on Aging and the Self Graduate Fellowship.

SPINAL MECHANICS DURING DROP LANDING: EFFECTS OF GENDER AND LANDING TECHNIQUE

Soo-An Park [1] John W. Chow [2], and Mark D. Tillman [2]

[1] SUNY – Upstate Medical University, Syracuse, NY, USA
[2] University of Florida, Gainesville, FL, USA
E-mail: parkso@upstate.edu

INTRODUCTION

The mechanics of spine during activities that demand vigorous spinal movements has rarely been studied. The purpose of this study was to determine the effects of gender and landing techniques on spinal column kinematics and loads to the lumbosacral (L/S) and cervicothoracic (C/T) junctions during drop landings.

METHODS

Thirteen male (21.4 ± 1.3 yrs) and 13 female (21.1 ± 1.3 yrs) healthy individuals participated in this study. A sagittal plane 5-segment (3 lower extremity and 2 spinal segments) mechanical model was used. A set of reflective markers was placed on the lower extremity, pelvis and trunk, and another set was placed on skin over selected spinous processes to track the kinematics of different spinal regions (Figure 1).

Data were collected using a 3-D motion capture system (Motion Analysis Corp., Santa Rosa, CA) and a Bertec forceplate. Each subject performed 3 drop landings using his/her own landing technique (NL) and 3 soft landings with instruction (SL). During each trial, the subject descended from a 50- cm high platform and landed on a forceplate with the left foot at the center of forceplate. Assuming bilateral symmetry in lower extremity mechanics, GRFs were doubled when applied to the model.

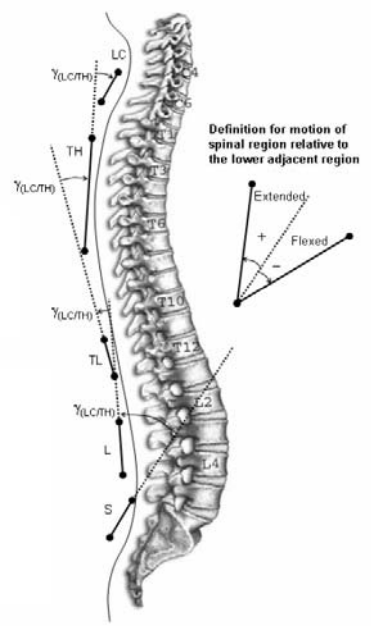

Figure 1: Ten markers on the spine were used to define different spinal regions – sacral (S), lumbar (L), thoracolumbar (TL), thoracic (TH), and lower cervical (LC) regions.

Dependent variables were divided into 5 groups. One group of landing variables was peak vertical GRF, time for landing phase, touchdown angles and flexion ROMs of knee and hip joints after touchdown. Two groups of spinal kinematics included touchdown (TD) angle and initial extension ROM of different spinal regions. The angle of a spinal region was defined as the angle between the spinal region and its lower adjacent region. Two groups of spinal kinetics included joint resultants at L/S and C/T junctions computed using an inverse dynamics approach. The 5 groups of dependent variables were submitted to 5 separate 2 × 2 (Gender × Landing type) MANOVAs with repeated measures on the last factor and follow-up univariate analyses of variance were conducted when appropriate.

RESULTS AND DISCUSSION

MANOVA and follow-up univariate tests revealed that, when going from NL to SL condition, significant increases in the landing phase (0.22±0.08s to 0.36±0.14s, $p<0.001$), TD angles (knee: 7.3±6.8° to 10.5±6.4°, $p<0.001$; hip: 61.5±12.0° to 66.6±12.3°, $p<0.001$), flexion ROMs of knee (53.0±10.4° to 69.9±14.2°, $p<0.001$) and hip (33.3±13.7° to 51.2±10.8°, $p<0.001$) joints, extension ROMs in TH (4.6±3.7° to 8.0±5.1°, $p<0.001$) and LC (10.3±7.8° to 16.3±10.4°, $p=0.006$) regions, and decreases in peak vertical GRF (23.91±3.87 $N \cdot kg^{-1}$ to 15.77±3.03 $N \cdot kg^{-1}$, $p<0.001$) and all joint resultants for L/S ($p<0.001$) and C/T junctions ($p<0.001$) were observed (Table 1.A).

Females exhibited significantly greater TD angle of TL region ($p=0.003$), flexion ROM of hip ($p=0.001$) and extension ROM of TH region ($P=0.012$) than males across both landing conditions. Greater TL TD angle means that TL region was extended and increased the lumbar lordosis by the definition of variable. The significant interaction in TH TD angle between gender and landing type ($p=0.032$) means that males demonstrated more flexed TH region at TD from NL to SL condition, while females did not (Table 1.B).

The model used in this study showed reasonably matched values of spinal kinetics and kinematics comparing with the landing variables. Spinal kinetics during drop landing significantly decreased from NL to SL in each gender, but some gender differences were shown in kinematics. Females demonstrated extended TL region and increased lordosis at TD and compensated for it by using greater motion at the hip joint and TH region during the landing phase, whereas males showed more flexed TH posture at TD from NL to SL condition.

SUMMARY/CONCLUSIONS

Gender differences in spinal kinematics at TD and compensatory motions during drop landing (an activity demands vigorous spinal movements) may be one of the reasons for the gender disparity in knee joint injury. Regardless of gender, the increased motions of TH and LC regions from NL to SL, in addition to the increased motions of lower extremity joints, suggest that the spinal column is actively involved in energy absorption during drop landings.

Table 1: A. Spinal kinetics with significant main effect for landing type. B. Dependent variables showed significant gender main effect (*) and interaction (+). (mean ± SD)

A		**AxF** ($N \cdot kg^{-1}$)	**ShF_{ant}** ($N \cdot kg^{-1}$)	**ShF_{post}** ($N \cdot kg^{-1}$)	**FlxM** ($N \cdot m \cdot kg^{-1} \cdot BH^{-1}$)	**ExtM** ($N \cdot m \cdot kg^{-1} \cdot BH^{-1}$)
L/S	NL	20.91 ± 6.04	3.24 ± 1.60	21.75 ± 7.29	2.72 ± 0.90	7.06 ± 2.30
	SL	13.97 ± 3.84	1.84 ± 1.03	10.16 ± 4.92	1.84 ± 0.88	3.91 ± 1.40
C/T	NL	21.95 ± 8.23	10.35 ± 3.99	10.35 ± 3.99	5.65 ± 1.68	6.94 ± 2.66
	SL	9.75 ± 5.04	8.70 ± 3.49	8.70 ± 3.49	4.11 ± 1.62	3.64 ± 1.33

B		**TD angle of TL/L (°)***	**TD angle of TH/TL (°)+**	**Ext ROM of TH/TL (°)***	**Flx ROM of Hip (°)***
Male	NL	7.6 ± 5.1	-23.1 ± 6.2	3.3 ± 2.8	24.8 ± 11.5
	SL	7.2 ± 6.1	-25.1 ± 8.2	5.4 ± 3.9	47.0 ± 7.2
Female	NL	16.1 ± 7.8	-20.7 ± 7.6	6.0 ± 4.2	41.7 ± 10.2
	SL	16.7 ± 8.4	-20.1 ± 6.9	10.6 ± 4.9	55.5 ± 12.3

Note: A positive TD angle indicates the spinal region is in an extended state or extension motion relative to the lower adjacent region (see Figure 1). Abbreviations: AxF (axial force), ShF (shear force), FlxM (flexion moment), ExtM (extension moment)

FORWARD DYNAMICS SIMULATIONS OF HUMAN GAIT USING NEUROMUSCULOSKELETAL TRACKING

Ajay Seth[1], Hyung Joo Kim[2], and Marcus G. Pandy[2]

[1] Stanford University, Stanford, CA, USA
[2] University of Melbourne, Melbourne, Australia
E-mail: aseth@stanford.edu

INTRODUCTION

Forward dynamic simulations are needed to understand muscle function in human walking. However, accurate forward simulations of gait are difficult to generate for a number of reasons. First, acceleration estimates from experiments are prone to errors due to skin movement. Second, simulating foot-ground interaction presumes that an accurate model of the foot is available, which is a major challenge in itself. Third, neuromusculoskeletal models are highly non-linear dynamical systems that are inherently unstable, and so some form of balance control is required. While control-systems tracking is more efficient for simulation than parameter optimization (Anderson and Pandy, 2001), current methods ignore ground contact dynamics by applying experimental ground reaction forces (GRFs) and moments directly to modeled feet (e.g., computed muscle control (CMC), Thelen and Anderson, 2006). This is satisfactory when input kinematics are accurate and if forward simulations independent of the experimental data are not needed. If, however, a novel movement is to be simulated, then the model will be required to reproduce GRFs as well as kinematics obtained from a gait experiment in order to have confidence in that model. In this study, neuromusculoskeletal tracking (NMT, Seth and Pandy, 2007) was applied as a way of synthesizing the complete dynamics of gait in a forward simulation. Tracking of the center of pressure (COP) and marker kinematics were added in an attempt to improve foot-contact timing and movement stability in the model.

METHODS

Data from thirty markers and two force-plates were recorded from three healthy males walking at their self-selected speeds. GRFs for a full gait cycle cannot be recorded using two force plates; thus, marker kinematics and GRFs were recorded simultaneously for 85% of the gait cycle. A 23 degree-of-freedom, 54 muscle-actuated model (Anderson and Pandy, 2001) was used to track the experimental data. The fore-aft and medio-lateral ground springs were replaced with purely viscous (velocity-dependent) elements and a continuous friction model (Seth, 2007). Segment lengths, joint axes, and joint angles were calculated such that virtual markers affixed to the model segments tracked subject markers with a mean RMS error of less than 5 mm using a least-squares optimization approach.

The NMT method consists of two stages. Stage 1 applies feedback linearization (FBL) to linearize the multibody and contact dynamics of the model. A linear feedback controller is then used to compute the net joint moments according to model tracking error with respect to measurements of COP, marker positions, joint angles, and GRFs obtained from the gait experiments. Stage 2 also applies FBL to linearize the neuromuscular activation and contraction dynamics, but, here, an optimal linear quadratic tracker is formulated to compute an optimal set of neural excitations such that muscles produce the required joint moments while minimizing the integral of the square of all muscle forces over the gait cycle.

RESULTS

The NMT method required 320 secs on a desktop 2.2 GHz Pentium IV PC to track 85% of the gait cycle corresponding to contra-lateral toe off (cTO) to heel strike (HS). The forward simulation closely tracked both the kinematics and GRFs obtained from experiment (Fig. 1). The calculated muscle activations (Fig. 2) also compared closely with EMG data presented in the literature (Winter, 1987).

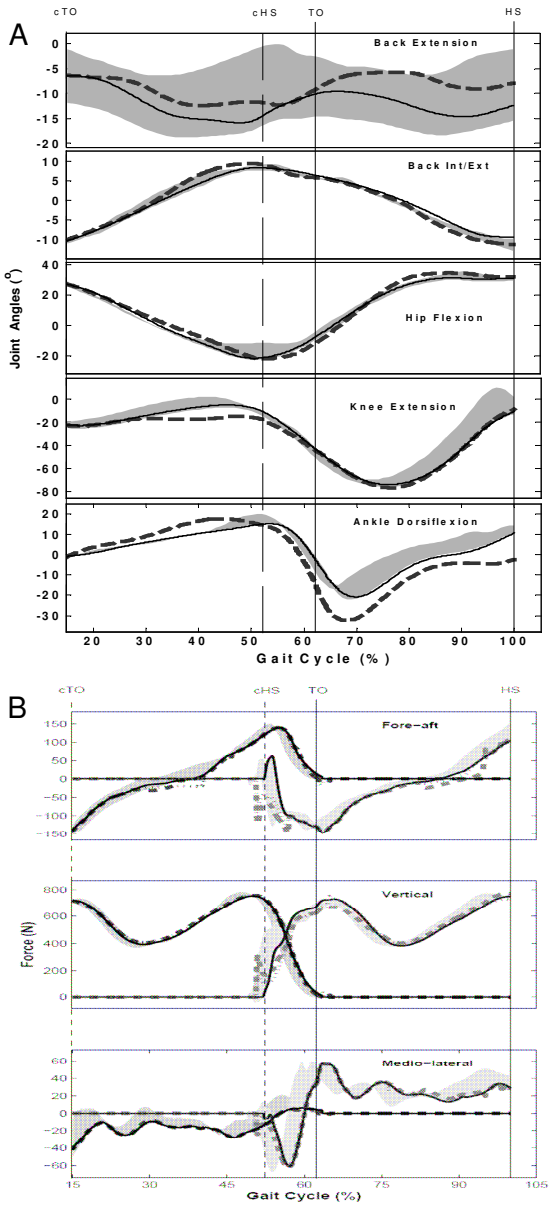

Figure 1: Model (dashed), median of experimental trials (solid) and mean ± 1SD (shaded) kinematics (A) and GRFs (B) for one subject.

CONCLUSIONS

By modifying a model of ground contact and including marker and COP kinematics in the tracking framework, we have shown that the NMT method can dynamically reproduce the kinematics and kinetics of human walking, and still produce muscle activation patterns that are consistent with EMG data. Furthermore, the NMT method is 4 orders of magnitude faster than the simulations derived using parameter optimization (Anderson and Pandy, 2001).

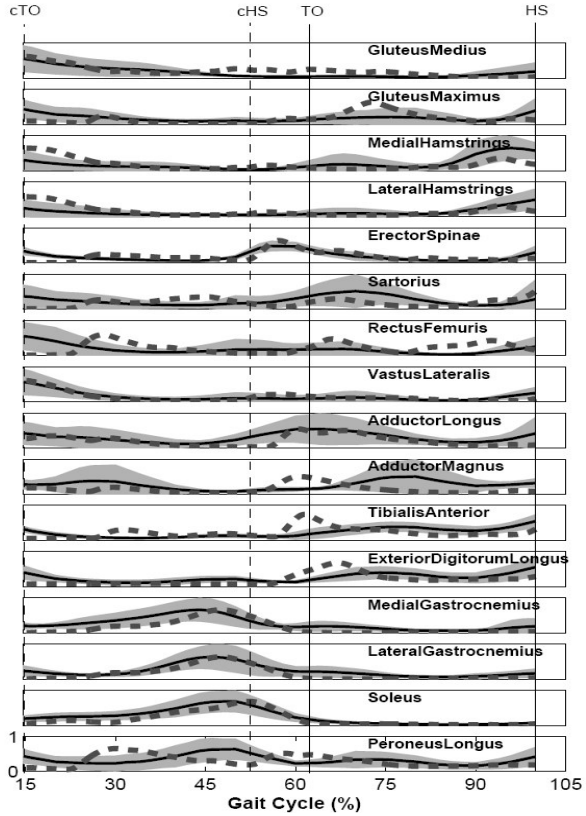

Figure 2: Model muscle activity compared to EMG from subjects by Winter (1987).

While the CMC method is computationally efficient, it does not synthesize the GRFs during a movement simulation, nor does it resolve muscle forces dynamically. Thus, a particularly valuable feature of the NMT method is that it can be used to validate complex musculoskeletal models intended for performing what-if-type simulations.

REFERENCES

Anderson , F.C., Pandy, M.G. (2001). *J. Biomech. Eng.,* **23**, 63-74.

Seth, A., Pandy, M.G. (2007). *J. Biomech.,* **40**, 356-366.

Seth, A. (2007). PhD thesis, U. Texas at Austin.

Thelen, D.F., Anderson, F.C. (2006). *J. Biomech.,* **39** , 1107-1115.

Winter, D. A. (1987). *Biomechanics & Motor Control of Human Gait*. U. Waterloo Press.

ACKNOWLEDGEMENTS

Support was provided by NASA grant #NNJ04HI99G, UT Continuing Fellowship to AS, and a VESKI award to MP.

RAMBLING-TREMBLING DECOMPOSITION IN TWO DIMENSIONS

Thomas Robert [1], Vladimir M Zatsiorsky [1], Marcos Duarte [2] and Mark Latash [1]

[1] The Pennsylvania State University, University Park, PA, USA
[2] Universidade de Sao Paulo, Sao Paulo, SP, Brazil
E-mail: rut12@psu.edu, Web: http://www.kinesiology.psu.edu/research/laboratories/mcl/

INTRODUCTION

Rambling-trembling decomposition of the center of pressure (CoP) trajectory (Zatsiorsky, Duarte 1999, 2000) is based on the idea that during quiet standing the body sways for two reasons: the migration of the reference point with respect to which the equilibrium is maintained (rambling, R) and the deviation away from that point (trembling, T). So far, the RT decomposition was performed in only one plane, either anterior-posterior (AP) or medio-lateral (ML). The technique of the RT decomposition is based on determining the so-called instant equilibrium point (IEP), the CoP position at the instance when the horizontal ground reaction force (GRF), either F_{AP} or F_{ML}, equals zero. The IEPs for the AP and ML body sway usually do not coincide and it is not clear how the RT decomposition can be performed for the CoP trajectory on the supporting surface.

The goals of this study are: (1) To develop a method of the RT decomposition of the CoP trajectory in the plane. (2) To study the relations between the R and T fractions of the CoP trajectory in the plane and the shear ground reaction forces. Note, that when RT decomposition is performed in either AP or ML direction the involved variables (forces, displacements) are scalars. When the analysis is performed in the plane the forces and displacements are 2-D vectors.

METHODS

Seven subjects (3 males, 4 females) participated in this study. Their age was 29.4±7.5 years, their height 173±6 cm and their mass 70±18 kg. None of these subjects has any known historical postural disorder. Subjects were asked to stand on a force plate (model AMTI OR6-7-1000), with a comfortable feet width, and to maintain their posture during one minute. Subjects were barefoot and with eyes open. The ground reaction forces were recorded at a sampling frequency of 200 Hz on a personal computer using a 12 bit AD board. A low pass Butterworth filter (4^{th} order, zero lag, cut off frequency = 8 Hz) was applied to the ground reaction forces (Zatsiorsky, Duarte 1999). The CoP coordinates were computed from these data (Zatsiorsky, Duarte 2000).

The following definition was accepted: the IEP is a CoP position on the plane at the instant when the norm of a horizontal force vector is zero. The IEPs were identified as the points where the magnitude of the shear force was in a local minimum, under 5% of the maximal shear force recorded during the trial. The R trajectory was estimated by interpolating the IEP points, using 3D cubic cardinal splines (2 coordinates and the time). The T component was defined as the 2D vectors of the deviation of the CoP from the R trajectory.

A canonic correlation procedure was used in order to investigate the correlation between the shear forces and the T trajectory, which are both 2D variables (vectors). The principle was to study the correlation between two uni-dimensional canonic variables (F and T), made by linear combinations of the elements of the original

two-dimensional variables (F_x, F_y and T_x, T_y, respectively):

$$F=a1\cdot F_x+b1\cdot F_y;\ T=a2\cdot T_x+b2\cdot T_y;$$

The coefficients of the linear combinations are adjusted in order to find the highest correlation between the two canonic variables. In this case, in order to go back to the original vectors variables, the set of coefficients {ai,bi} that corresponds to the highest correlation has been interpreted as angles: $\alpha i=\text{atan2}(bi,ai)$. Thus, the difference $\alpha 1-\alpha 2$ indicates the orientation of the T vectors relative to the shear forces vector obtained for the highest canonical correlation. The same procedure was applied to study the correlation between the shear force and the R vectors.

RESULTS AND DISCUSSION

Figure 1 illustrates the results obtained for a typical subject. The R trajectory is, as expected, well smoother than the CoP trajectory. Note the similarity of the shear force and the T vectors. The results of the canonical correlation, displayed in the Table 1, confirm this visual impression. The shear force and the T component are highly correlated. Moreover, their preferential orientation is not different of zero, which means that the vectors are aligned. On the other hand, the correlation between the shear force and the T component is relatively poor.

Table 1: Canonical correlation between the shear force vectors and the T and R vectors.

	T trajectory	R trajectory
correlation	**0.84** ± *0.06*	**0.26** ± *0.06*
$\alpha 1-\alpha 2$ (°)	**1.0** ± *10.6*	**177.7** ± *27.0*

The results of the planar RT decomposition extend previously obtained data for the unidirectional decompositions. They confirm the idea that the CoP trajectory is composed by the migration of an attracting point (rambling) and the oscillations around the R trajectory (trembling).

The results also indicates that the loops typically observed in the CoP trajectories (cf. numbers displayed in Figure 1) are mainly due to the trembling component, that are commonly considered as arising due to elastic restoring forces.

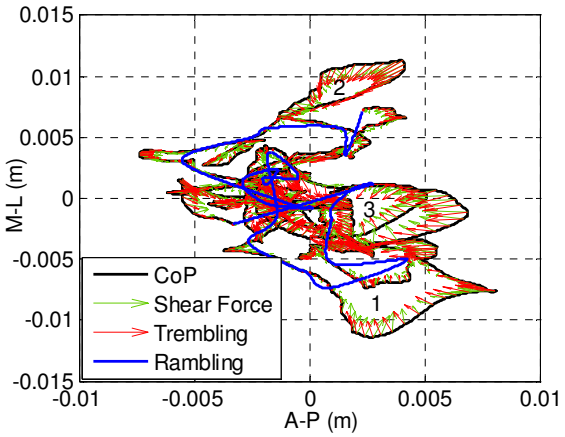

Figure 1: 2D representation of the CoP trajectory, the Rambling trajectory, and the Trembling and shear forces vectors for a typical subject.

SUMMARY/CONCLUSIONS

This study proposes an extension of the decomposition of the CoP into the Rambling and Trembling components to a 2-D case. A high correlation between the trembling component of the CoP migration and the shear forces (both of them are vectors) was observed.

REFERENCES

Zatsiorsky V. M., Duarte M. (1999). *Motor Control,* **3**, 28-38.

Zatsiorsky V. M., Duarte M. (2000). *Motor Control,* **4**, 185-200.

ACKNOWLEDGEMENTS

This study was supported by NIH grants NS035032 and AR048563.

POSITIONAL AND DIRECTIONAL PATTERN OF WRIST RANDOM MOTION

Jie Tang, Zong-Ming Li
Hand Research Laboratory, Department of Orthopaedic Surgery
University of Pittsburgh, Pittsburgh, PA
Email: zmli@pitt.edu, Web: http://www.pitt.edu/~zmli/handlab/

INTRODUCTION

The motion at the wrist joint complex results from interplay among the complex and irregularly shaped carpal bones, the highly developed ligament network, and synergistic muscle action. Most previous studies about wrist motion focused on the maximal motion ability (Ryu et al. 1991; Li et al. 2005), yet the wrist functions in a subset of its attainable motion region during common manual activities (Ryu et al. 1991). The purpose of this study was to examine the wrist movement during its random, submaximal and comfortable movement. Specifically, we would (1) compare the wrist workspace in random motion with respect to the maximum motion ability; and (2) analyze the wrist positional and directional pattern in the apparently random motion.

METHODS

Fifteen young male subjects (age 29.5 ± 7.2 years) without any musculoskeletal disorders in the upper extremity participated in the study. Reflective markers were attached to the dorsal side of the right forearm and hand to establish two local coordinate systems (Li et al. 2005). To maintain a constant finger posture, the subject loosely held a 25 mm diameter cylindrical light tube while perform the tasks. Each subject was instructed to perform two wrist motion tasks: circumduction and random motion. The circumduction task required moving the wrist circumferentially in a clockwise direction (viewed from proximal to distal) to explore the maximum motion envelope. Five cycles were performed at self-selected paces. During the random motion task, the subject was instructed to move the wrist "aimlessly" and continuously in a self-preferred comfortable manner for 60 seconds.

Wrist motion was recorded using a motion analysis system (VICON 460, Oxford, UK) at a frequency of 100 Hz. Euler angles were calculated to quantify flexion/extension (FE), radial/ulnar deviation (RUD), and pronation/supination angles for the wrist joint complex. In this study, we focused on the angular data in FE and RUD. The maximum envelope for a circumduction was constructed by the convex hull of the FE-RUD angle data; and the data from the random motion was fitted by an ellipse which included 95% of samples along each axis using a principal component analysis. The density distribution of the positional data was calculated. To characterize the directional pattern of wrist motion, a vector field was derived from the angle-angle positional data, and the histogram of the vector orientation was analyzed. Paired t-tests were used to assess the differences between workspaces of the circumduction and that of the random motion ($\alpha = 0.05$).

RESULTS

An example of the angular positions during random motion relative to circumduction by the same subject is shown in Figure 1. The ranges of motion (ROM) in FE and RUD during random motion were significantly smaller than that in circumduction ($p < 0.001$), with the ratio of 54.8% and 63.6%, respectively. The relative area of the fitted ellipse during random motion was 43.5% of

the area of the convex hull of circumduction. The major axis of the fitted ellipse has a slant angle of 14.5° ± 12.4° with respect to the direction of wrist extension. The wrist positions during the random motion demonstrated a highest density at the 30° extension and 10° ulnar deviation (Figure 2). A plot of the vector field showed a motion flow pattern oriented towards northeast or southwest (Figure 3). A rose plot of the vector orientation showed the highest frequency distributions in 15° and -195° with respect to the direction of wrist extension (Figure 4).

DISCUSSION

We found that the wrist had a subset of motion range that is about 60% of its maximal movement capability. The ROM during random motion in this study agreed with previous report (Ryu et al. 1991) that the functional ROM during activities of daily living were about 80° of FE and 40° of RUD. The random motion tends to locate in the region of extension and ulnar deviation, which corresponds to the functional neutral position of the wrist. The positional data cluster has an overall orientation that combines extension and radial deviation. The vector field of the positional data showed a similar directional preference. This motion pattern is consistent with previous report on the coupling between flexion and ulnar deviation and the coupling between extension and radial deviation during instructed flexion-extension or radial-ulnar deviation tasks (Li et al. 2005). Our findings of the wrist random motion are useful for ergonomic workspace design and wrist rehabilitation protocols.

REFERENCE

Li ZM, et al. (2005). *Clin Biomech*, **20**, 177-183.

Ryu JY, et al. (1991). *J Hand Surg [Am]* **16,** 409-419.

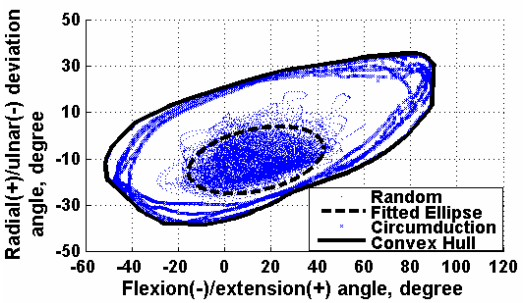

Figure 1: An example of angle-angle plot wrist positions in FE and RUD in random motion relative to circumduction trajectories.

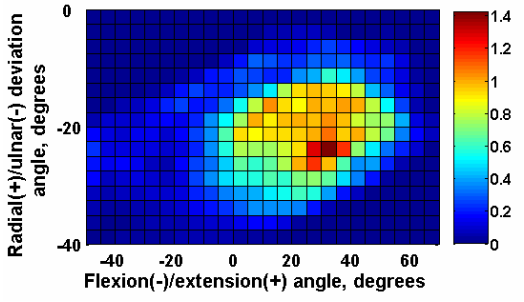

Figure 2: Density distribution of wrist position during random motion (data from all subjects).

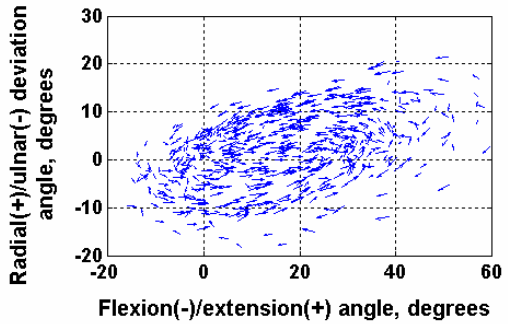

Figure 3: An example of the vector field of the FE and RUD angular data.

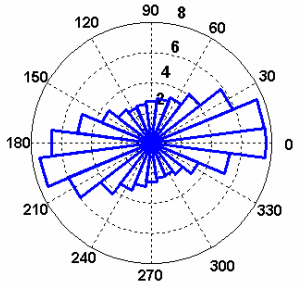

Figure 4: A rose plot for the angular histogram of the orientation angles of the vector field (data from all subjects).

EFFECTS OF LABRUM THICKNESS AND MODULUS ON GLENOHUMERAL CAPSULE AND LABRUM STRAINS

Ben Ellis [1], Nick Drury [2], Richard Debski [2], and Jeff Weiss [1]

[1] University of Utah, Salt Lake City, UT, USA
[2] University of Pittsburgh, Pittsburgh, PA, USA
E-mail: ben@sci.utah.edu, Web: mrl.sci.utah.edu

INTRODUCTION

The shoulder is the most often dislocated joint in the body, and 80% of the dislocations occur in the anterior direction. The primary regions of the glenohumeral capsule that provide anterior stability in abduction and external rotation are the Anterior (AB-IGHL) and Posterior (PB-IGHL) Bands of the Inferior Glenohumeral Ligament, and the Axillary Pouch (AP). Previously, we developed and validated a subject-specific finite element model of the glenohumeral capsule (Moore, 2006). The model did not explicitly represent the labrum, which serves as an insertion site for the capsule (Eberly, 2002) and deepens the glenoid socket. The model predicted an area of high strain concentration near the insertion of the AP to the glenoid during a simulated diagnostic exam (Fig. 1, left). However, labrum strains were not validated experimentally and the effects of the labrum on capsule mid-tissue strains are unknown. The objective of this study was to investigate the effects of labrum thickness and modulus on mid-tissue and labrum strains using a finite element model of the glenohumeral capsule.

METHODS

Our previously validated finite element model of the glenohumeral capsule was modified to explicitly include the labrum. The labrum utilized similar shell elements and constitutive model as the capsule. A baseline model was created with labrum moduli equal to the corresponding capsule region (i.e. 2.05, 2.73, 4.92, 2.12, and 2.12 MPa for the AB-IGHL, PB-IGHL, AP, antero-superior, and posterior regions, respectively), and a thickness set to the capsule thickness of 2.0 mm (Fig 1, left). A previous study (Howell, 1989) was used to assign the labrum of the baseline model a depth of ~3.0 mm (dimension from glenoid to capsule). As per our validation studies, the models were driven by kinematics that simulate a simple translation test for anterior instability: a 25 N anterior load was applied to the joint at 60° of glenohumeral abduction and 60° of external rotation.

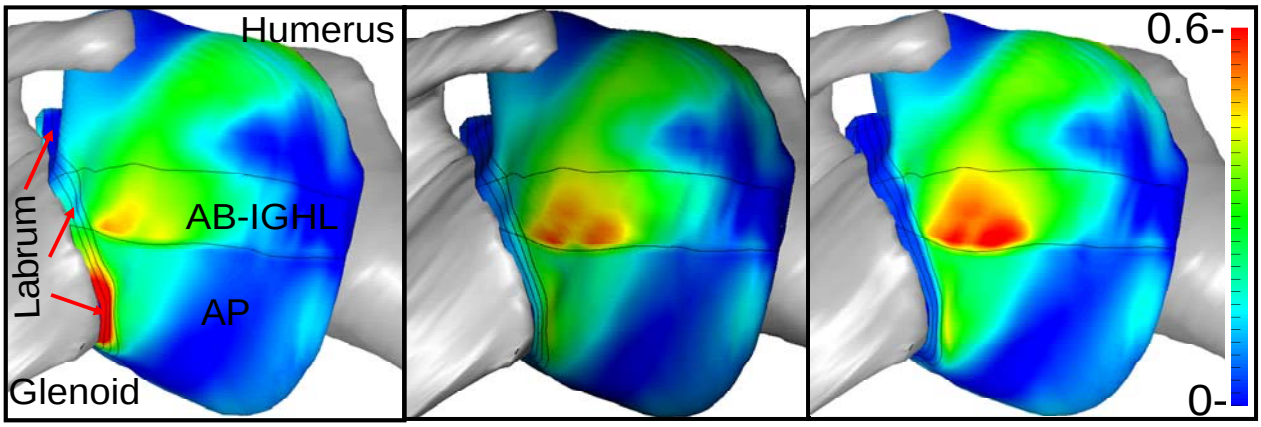

Figure 1. Left) Nominal model. Middle) Model with 6 mm thick labrum. Right) 5X modulus model.

Four models were created for a labrum thickness sensitivity study. Inspection of cadaveric samples demonstrated that the labrum tapers from glenoid to capsule, so the thickness was tapered from 3.0, 4.0, 5.0, and 6.0 mm, respectively, down to 2.0 mm. These thickness values were based on published data (Carey, 2000).

Based on an animal study (Ferguson, 2001), the labrum modulus was varied with respect to its corresponding capsule region modulus. Three models were created for the labrum modulus sensitivity study, with labrum moduli 50%, 2X, and 5X higher than the respective capsule region moduli (with nominal model thickness).

Average regional Green-Lagrange 1st principal strains from the described models were calculated for the mid-tissue regions that were previously used to validate the capsule model. Qualitative assessment of labrum strains was also conducted for each model.

RESULTS

Stiffening the labrum by increasing the thickness or the modulus slightly increased mid-tissue strains, but substantially decreased labrum strains (Fig. 1). The models that had labrum thicknesses of 3.0, 4.0, 5.0, and 6.0 mm had average capsule mid-tissue strain increases of 2, 3, 3, and 4%, respectively. Increasing the labrum modulus by 50%, twice, and five times increased capsule mid-tissue strains an average of 3, 4, and 5%, respectively. Except for the model with a 6 mm thick labrum, all of the average mid-tissue strain increases due to thickening the labrum were within the repeatability of our experimental strain measurements (±3.5%). Increasing the labrum modulus had a slightly greater effect with the 2X and 5X moduli models causing increases in average mid-tissue strains larger than the experimental repeatability. The mid-tissue strain increases were largest near the labrum for both methods of increasing the labrum stiffness.

DISCUSSION

The results of this study demonstrate that increased labrum stiffness, either through increased thickness or modulus, has a larger effect on labrum strains than on capsule mid-tissue strains. Tapering the labrum from its thickest point at the glenoid to its thinnest point where it connects to the capsule, was supported by the cadaver's anatomy and seems more realistic than the large stiffness gradient caused by increasing the entire labrum modulus. Since the labrum acts as an interface between the relatively soft capsule and bone, the labrum could stiffen from capsule to glenoid to decrease stress risers at the interface. This construct stiffening probably occurs through both an increase in modulus and thickness and further research is needed to ascertain exactly how these parameters change throughout the labrum.

REFERENCES

Moore, SM. (2006). Thesis Document. Univ. of Pittsburgh.

Carey, J, et al. (2000). *J Biomed Mater Res,* **51**:711-16.

Howell, SM.(1989). *Clin Orthop*,**243**:122-5.

Ferguson, SJ, et al. (2003). J Orthop Res, **19**: 887-96.

Eberly, V., et al. (2002).*Clin Orthop*,**400**:26-31.

ACKNOWLEDGEMENTS

Financial support from NIH #AR-050218 is gratefully acknowledged.

KINEMATICS OF CERVICAL BILATERAL FACET DISLOCATION

Manohar M. Panjabi, Andrew K. Simpson, Paul C. Ivancic,
Adam M. Pearson, Yasuhiro Tominaga, and James J. Yue

Biomechanics Research Laboratory, Yale University School of Medicine, New Haven, CT, USA
E-mail: paul.ivancic@yale.edu

INTRODUCTION

Bilateral facet dislocation (BFD) is a devastating consequence of cervical spine trauma, occurring most often during motor vehicle collisions, diving accidents, and falls. Standard guidelines for cervical stabilization following reduction of BFD do not exist. The use of numerous treatment modalities such as halo vest immobilization, anterior plating, posterior fusion with plates or wires, or a combination of anterior and posterior fusion, indicates that the optimal treatment regimen has yet to be established. These controversies may be due to poor understanding of the high-speed facet motions during dislocation. The purpose of this study was to determine the BFD kinematics using a functional spinal unit model with muscle force replication.

METHODS

Four fresh-frozen human cervical spines were dissected of all non-osteoligamentous soft tissues and partitioned into 10 functional spinal units (C3/4, C5/6, and C7/T1). Each functional spinal unit was mounted in resin at the upper and lower vertebrae. Motion tracking flags, each with three non-collinear markers, were rigidly fixed to both mounts. The lower mount was rigidly fixed to a 55° extension wedge on a sled apparatus. A 3.3 kg mass with sagittal, horizontal, and frontal plane moments of inertia of 0.019, 0.014, 0.015 kg m^2, respectively, was rigidly attached to the upper mount. The functional spinal unit and mass were stabilized using simulated compressive muscle forces. Horizontal acceleration of increasing severity was applied to the lower mount with frontal impact using the sled apparatus until BFD was achieved. High-speed cameras recorded the spinal motions at 500 frame/sec.

Intervertebral rotations of flexion (+RX), extension (-RX), left (+RY) and right (-RY) axial rotation, and left (-RZ) and right (+RZ) lateral bending were expressed in the endplate coordinate system (**Figure 1A**). For facet translations, two points were defined on each inferior facet of the upper vertebra: A-R and P-R were the anterior and posterior corners of the right facet, respectively (**Figure 1B insert**), and, similarly, there were points A-L and P-L for the left facet. The translations of these points were calculated relative to respective points on the superior facets of the lower vertebra using the rotation data, vertebral flag marker translations, and geometrical rigid body relationships (Ivancic et al., 2006). The facet translations were left (+Tx) and right (-Tx) lateral shear, axial separation (+Ty) and compression (-Ty), and anterior (+Tz) and posterior (-Tz) sliding, expressed in the facet coordinate system.

Single factor, non-repeated measures ANOVA ($P<0.05$) and Bonferonni pair-wise post-hoc tests were used to determine differences in the average peak facet translations (anterior and posterior, left and right facet corners) and rotations (RX, RY, and RZ). Occurrence times of the motion peaks were also determined.

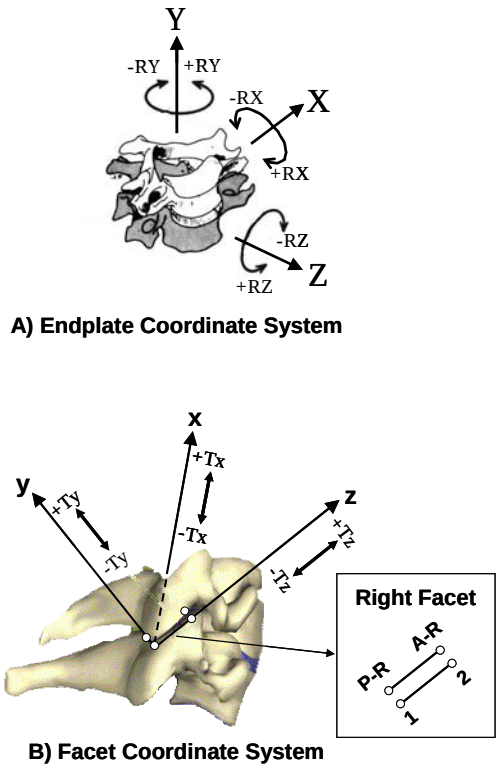

Figure 1. The coordinate systems and nomenclature for motions.

RESULTS

Average of 10 Specimens. Peak +RX of 63.1° significantly exceeded all other rotation peaks. The highest peak +Tz of 22.0 mm occurred in the posterior edge of the left facet and could not be statistically differentiated from the other +Tz peaks. The +Ty peak, reaching 7.9 mm at the posterior edge of the left facet, was significantly greater than the +Ty peaks at the anterior facet edges. The -Ty peaks reached 9.9 mm and 7.4 mm at the anterior and posterior edges of the left facet, respectively. The greatest +Tx and -Tx peaks were 2.0 mm and 3.6 mm, respectively.

The temporal analysis of the sagittal motions at the right facet joint during BFD is illustrated in **Figure 2**. Peak axial separation occurred first, greater at the posterior facet corner, as compared to anterior, as the upper facet slid anteriorly relative to the lower facet and flexed (**Figure 2B**). Peak flexion rotation occurred next, as the upper facet continued to slide anteriorly, axial separation at the posterior facet corner decreased, and compression occurred at the anterior facet corner (**Figure 2C**). Peak anterior sliding was then observed as axial separation at the posterior facet corner continued to decrease (**Figure 2D**). Lastly, peak axial compression occurred, greatest at the anterior corner (**Figure 2E**).

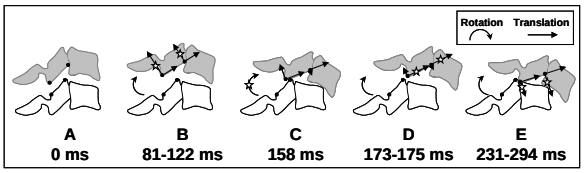

Figure 2. Temporal analysis of sagittal motion peaks during BFD. Not to scale.

DISCUSSION AND CONCLUSIONS

BFD in the cervical spine causes neurological symptoms in greater than 90% of patients. Ours is the first study to provide comprehensive three-dimensional facet translations and intervertebral rotations during high-speed BFD of a human functional spinal unit model with muscle force simulation. During BFD, the main sagittal motions included facet separation, flexion rotation, anterior sliding, followed by compression, however, non-sagittal motions also existed. These motions indicated that unilateral dislocation may precede BFD.

REFERENCES

Ivancic, P.C.et al. (2006). *Traffic Inj Prev*, **7**, 81-87.

ACKNOWLEDGEMENTS

This research was supported by a grant from the Cervical Spine Research Society.

FINITE ELEMENT SIMULATION OF NANOINDENTATION TESTS FOR CORTICAL BONE USING A DAMAGED PLASTIC MODEL

X. Neil Dong, Satya P. Paruchuru, Xiaodu Wang

University of Texas at San Antonio, San Antonio, TX, USA
E-mail: xuanliang.dong@utsa.edu, Web: http://engineering.utsa.edu/~bioeng

INTRODUCTION

Finite element analyses have been used to interpret the experimental data of nanoindentation tests for cortical bone (Tai et al., 2005). However, a simple perfect plastic model cannot take into consideration the damage accumulation which is an important part of the material behavior in bone tissue. In this study, a damaged plastic model was proposed to simulate indentation tests of cortical bone.

METHODS

A semi-empirical constitutive model of cortical bone tissue behavior was developed (Leng et al, 2007). Prior to yielding, the initial elastic modulus of bone (E_0) was constant and the bone tissue followed the linear elastic behavior. After yielding, the relationship between the instantaneous strain (σ_i) and stress (ε_i) was described by the following equation

$$\varepsilon_i = \frac{\sigma_i}{E_0} e^{m\left(\varepsilon_i - \sigma_y / E_0\right)} + k\left(\varepsilon_i - \frac{\sigma_y}{E_0}\right) \qquad (1)$$

where m was a material constant related to the sensitivity of bone to the damage accumulation; σ_y was the yield stress; and k was the parameter indicating the capability of bone to sustain permanent deformation.

The simulation of nanoindentation tests was conducted using a general purpose finite software ABAQUS. The model contained a bone sample and a Berkovich indenter, which was represented by an equivalent conical indenter with an effective angle of 70.3° (Figure 1). The indenter was modeled as an analytical rigid body without deformation. Axis-symmetric quadrilateral elements (CAX4R) were used to simulate bone tissue. A refined mesh was formed directly beneath the indenter tip whereas the rest of the model had a relatively coarse mesh.

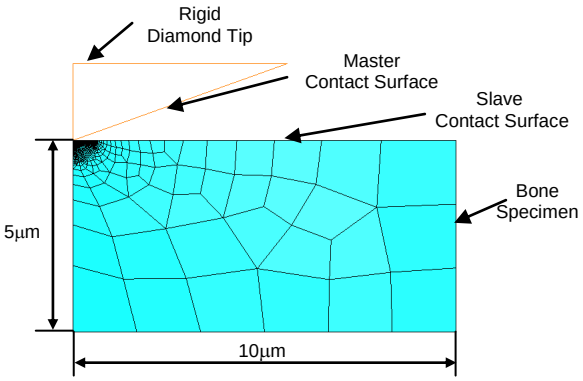

Figure 1. Schematic illustration of an axis-symmetric finite element model

The contact interaction between the pyramidal tip and the bone specimen was represented by a master surface and a slave surface, respectively (Figure 1). A velocity-independent Coulomb friction model was used to describe surface interactions.

A shear damage criterion was used to describe the damage initiation of bone tissue. Once damage was initiated, a damage evolution law was used to delineate the progression of damage until failure in bone tissue. The failure of bone tissue was defined by a material parameter relevant to fracture energy dissipation.

RESULTS AND DISCUSSION

Experimental data about the nanoindentation test of bovine cortical bone were obtained

from the literature (Tai et al., 2005). The results from the damaged plastic model were consistent with experimental data (Figure 2). The elastic modulus and yield stress of bone tissue from the damaged plastic model were 16 GPa and 180 MPa, respectively. However, a perfect plastic model with the same elastic modulus and yield stress produced an indentation load about 10% greater than the experimental data.

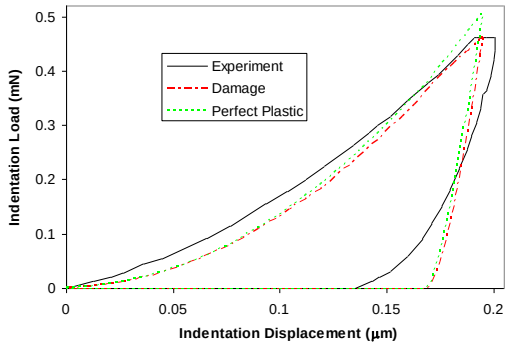

Figure 2. Comparison between experimental data and finite element simulations of nanoindentation tests for cortical bone.

For a perfect plastic model, stresses in bone beneath the indenter tip reached the yield stress for all elements (Figure 3a). However, there was a damage area directly under the tip for the damaged plastic model. In the damage area, the von Mises stress was less than the yield stress.

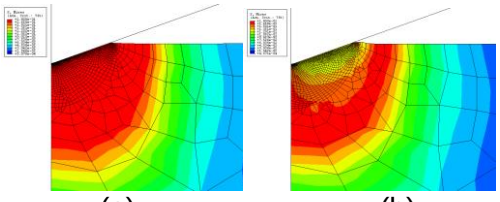

(a) (b)

Figure 3. Comparison of von Mises stresses in bone tissue for a perfect plastic model (a) and a damaged plastic model (b).

The damaged plastic model took into consideration the failure strain of bone tissue while the perfect plastic model did not consider the failure of bone tissue and bone tissue continued to deform at a high stress level.

In the study from Tai et al., the elastic modulus (E_0=9GPa) was underestimated and the yield stress (σ_y=240MPa) was overestimated. The elastic modulus and yield stress calculated from the damaged plastic model are in agreement with experimental data in the literature (Martin et al., 1998). It indicates that an appropriate constitutive model for bone tissues is required to simulate nanoindentation tests for cortical bone.

There are some limitations in this study. First, the viscoplastic behavior of bone tissue is not considered. Second, the anisotropic behavior of bone tissue is not examined. In addition, microstructures and ultrastructures of cortical bone have not been taken into consideration.

SUMMARY/CONCLUSIONS

A damaged plastic model is a realistic representation for bone tissue. It can be used to extract more accurate information about material properties of bone tissue from nanoindentation tests than a perfect plastic model.

REFERENCES

Leng et al. (2007) Proceedings of the ASME Bioengineering Summer Conference.

Martin et al. (1998) Skeletal Tissue Mechanics. Springer Press.

Tai, K. et al. (2005) *J Mater Sci Mater*, **16**, 947-59.

ACKNOWLEDGEMENTS

This work was supported by NIH grants and DST SR/BY/E-38/05, Gov. of India

STRAINS IN THE BICEPS BRACHII DURING DYNAMIC ELBOW FLEXION SHOW CONCENTRIC, ECCENTRIC AND ISOMETRIC BEHAVIOR SIMULTANEOUSLY

John E. Novotny, Brian A. Knarr, and Hehe Zhou

University of Delaware, Dept. of Mechanical Engineering, Center for Biomedical Engineering Research, Newark, DE, USA
E-mail: novotny@udel.edu, Web: www.me.udel.edu

INTRODUCTION

Skeletal muscles are complex, dynamic structures whose primary function is the application of force to their bony origins and insertions. There are various models of muscle function which generally assume a uniform behavior from origin to insertion during force generation. It is understood that skeletal muscles deform non-homogeneously but how is not clear. Changes in these internal mechanics could be important to understanding normal function and dysfunction with fatigue, pathology or aging (Pappas *et al.*, 2002). We have developed methods to quantify internal muscle mechanics using cine phase-contrast magnetic resonance imaging (CPC-MRI) and post-processing algorithms (Zhou and Novotny, 2006) and have described Lagrangian finite strains during cyclic motion in the supraspinatus and biceps brachii. The purpose of this paper is to define the overall uniformity of deformation within the normal biceps brachii during elbow flexion by observing frequency distributions of the finite Lagrangian and principal strain magnitudes. Areas within the muscle may be acting concentrically, eccentrically and isometrically simultaneously during overall contraction. The assumption of muscle incompressibility can also be assessed.

METHODS

MRI images were collected for 8 normal subjects (one female, seven males; age 24-34). Scans were performed with a clinical scanner (GE 1.5 Tesla, Milwaukee, WI). MRI images through the mid-plane of the biceps brachii (34×34 cm^2 FOV, 256×128, TR=24ms, flip angle=30°, V_{ENC} = 10cm/s) were collected during cyclic flexion-extension of the elbow at 24 equally spaced time frames. The arm moved from full extension to ~120° flexion. A resistive force was applied through an elastic band to a maximum of ~5% MVIC. We derived finite strain fields from the CPC-MRI data. The first frame at full extension and minimal resistive force was the zero strain reference. Longitudinal strain (SY), transverse strain (SX), shear strain (SXY), maximum principal strain (PS1), minimum principal strain (PS2) and maximum in-plane shear strain (PSXY) were calculated for 0.2×0.2 pixel triangular meshes at each frame for the distal half of the muscle. The percent areas of each muscle at various incremental ranges of strain magnitude were calculated and frequency distributions across the 24 time frames created and averaged across subjects.

RESULTS AND DISCUSSION

Mean frequency distributions of percent area at various strain increments are seen in Figures 1-4 for PS2 and PS1, averaged across subjects, at 150° and 120° flexion during muscle shortening. Due to space limitations, other strains will not be discussed. Contraction velocity was highest at 150° and near zero at 120° as the forearm slowed to change direction. Resistance force was intermediate at 150° and highest at 120°. In Fig. 1, PS2 values were generally negative showing shortening, with a peak around -15%, and a negative

maximum near -40%. Surprisingly, portions showed positive PS2, or pure elongation, up to 25%. In Fig. 2, the distribution shifted to higher values of negative strain with a peak near -30%. There were lower standard deviations and less percent area with positive strains. For PS1 in Fig. 3, the distribution showed a peak near 20%, which was expected if the material was behaving incompressibly. A long tail to the distribution, though, extended upward from the peak to values of 250%. In Fig. 4, the peak area decreased in magnitude and shifted to more positive values, and the percent area at 50 to 100% strain increased. Standard deviations decreased also. Thus, as the overall muscle contracted, areas within the muscle underwent very complicated deformations, some being stretched eccentrically, some straining very little and some exhibiting Poisson's values much different than 0.5.

SUMMARY/CONCLUSIONS

These results indicate the possibility of compartmentalized muscle function within the biceps brachii, even during this simple motion and relatively low loads and velocities. Non-uniformity could be a function of non-uniform activation, material properties or fiber type and contractibility. Future work should focus on how these distributions change with fatigue, pathology or ageing, and aim to describe mechanisms. Other muscles' behaviors will be investigated. Results will aid in building models of internal muscle mechanics.

REFERENCES

Pappas, G.P. et al. (2002) *J Appl Physiol*, 92, 2381-2389.

Zhou H, Novotny JE (2006) *J Magn Reson Imaging*, Jan; 25(1):175-84.

ACKNOWLEDGEMENTS: American Radiological Services, Newark, DE.

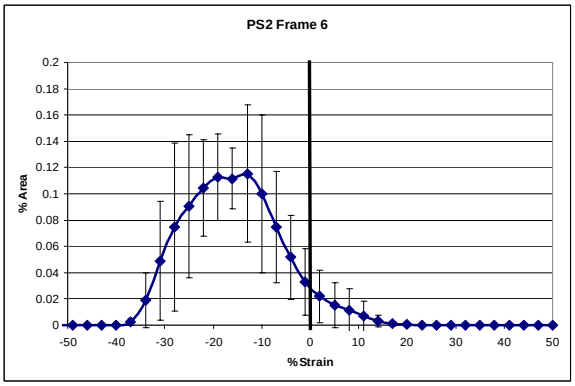

Figure 1. Mean percent area at various PS2 values over 3% strain ranges for 150°elbow flexion (with SD).

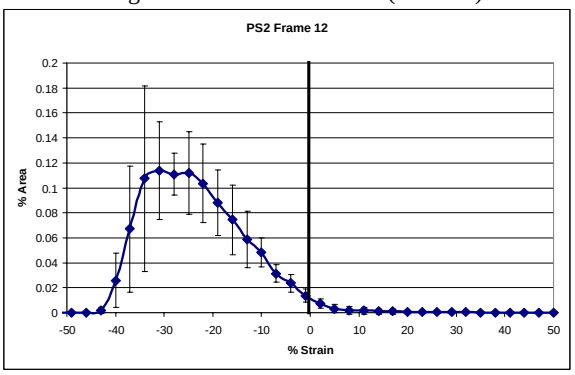

Figure 2. Mean percent area at various PS2 values over 3% strain ranges for 120°elbow flexion (with SD).

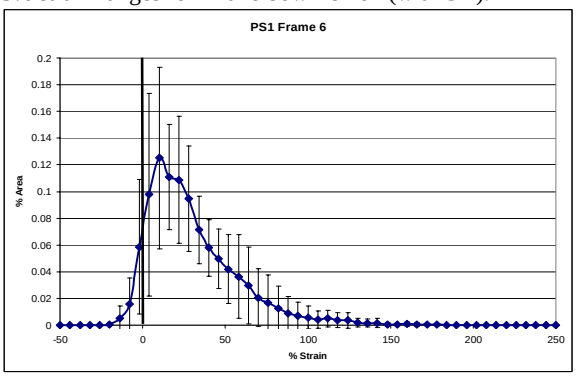

Figure 3. Mean percent area at various PS1 values over 6% strain ranges for 150°elbow flexion (with SD).

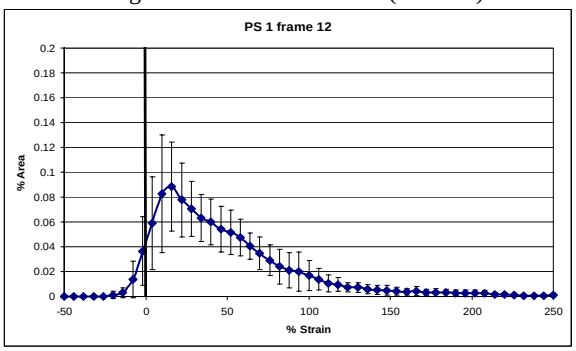

Figure 4. Mean percent area at various PS1 values over 6% strain ranges for 120°elbow flexion (with SD).

THE INFLUENCE OF STRIDE LENGTH ON IMPACT SHOCK AND METABOLIC COST DURING WALKING IN OBESE WOMEN

Elizabeth Russell, Joseph Hamill
Biomechanics Laboratory, University of Massachusetts, Amherst, MA, USA
E-mail: jhamill@kin.umass.edu

INTRODUCTION

Obesity is associated with many health risks, including knee osteoarthritis (KOA) (Felson et al., 1988). KOA is a degenerative joint disease involving the breakdown of articular cartilage, and develops when the tissues cannot handle the mechanical stresses they undergo (Radin et al., 1982). A higher body weight results in repetitive, high-force loading at the knee that can initiate or progress KOA. The pain and discomfort associated with KOA limits mobility, thus inhibiting weight loss.

At heel strike during walking the body undergoes a rapid deceleration which may be reduced at the knee joint through an alteration in gait kinematics. A decrease in stride length (SL) has been shown to reduce impact shock during locomotion (Hamill et al., 1995). Also, at a constant speed, an increase in SF (decrease in SL) increases the metabolic cost of locomotion (Holt et al., 1991).

The purpose of this study was to investigate the effects of a decreased SL on the impact shock and metabolic cost of walking in obese women. We hypothesized that, at a constant S, a decrease in SL and increase in SF from the preferred walking gait will decrease the impact shock and increase the metabolic cost.

METHODS

Ten (N=10) obese (BMI $\geq$ 30 kg·m^{-2}) females participated in this study. Kinetic (1200Hz) measures were taken using an AMTI force platform and uni-axial accelerometer tightly strapped to the distal tibia to record impact shock. Measured variables included impact shock, net impact shock, peak impact force and rate of force loading. A metabolic cart used indirect calorimetry to measure steady state VO_2.

During the preferred condition, subjects walked at a self-selected pace 10 times across 10m of track with a centrally-located force platform. Preferred S, SL and SF were recorded. Mean SF was increased by 15% using a metronome to pace gait. Markings on the floor defined the decreased SL during which locomotor S remained the same as at the preferred SL. All subjects wore the same make and model of footwear.

Preferred treadmill speed (PS) was found by increasing and decreasing speed until the subject consistently selected the same speed. PSF was measured and subjects achieved a steady state VO_2 at the preferred SF and the preferred SF +15%.

Ground reaction force (GRF) and accelerometer data were filtered with a Butterworth low-pass filter with a cutoff of 50 Hz. Impact shock was defined as the peak deceleration value at impact from the accelerometer. Net shock was the product of each subject's mean impact shock and SF for a given condition. Peak impact force was defined as the maximum vertical GRF value during the first 50% of stance and rate of loading was calculated from 10-80% of peak GRF. Steady state VO_2 measures were the

average of the final two minutes of steady state.

A repeated measures ANOVA of means assessed differences between two SL conditions. Criterion for significance was set at $P<0.05$. Effect sizes were calculated as per Cohen (1990).

RESULTS AND DISCUSSION

Mean age and BMI were 25.3 ± 9.8 years and 33.1 ± 4.2 $kg \cdot m^{-2}$, respectively. PS, SL and SF were 1.33 ± 0.08 m/s, 0.75 ± 0.06 m and 106.61 ± 4.83 steps/min, respectively. Effect sizes for impact shock and metabolic cost were 0.49 and 0.38, respectively.

A decrease in SL (increase in SF), relative to the preferred gait, did not significantly decrease impact force and impact shock during walking in obese women. It is possible that an increase in SF (and subsequent decrease in SL) greater than 15% is necessary to elicit the expected decrease in the variables negatively affecting the knee joint during locomotion. Previous work investigating the effects of a decreased SL and increased SF used a running gait and a 15% increase in SF during running would likely be a much greater magnitude of increase than during walking. GRF and rate of force loading values were not significantly different between the preferred and experimental conditions.

Steady state VO2 increased significantly ($p>0.05$) with a 15% increase in SF. Therefore, more calories were utilized for the same walking speed as the preferred gait.

The results of this study do not support taking shorter, quicker steps to reduce the risk of developing or progressing KOA in obese women. If altering the kinematics of walking by decreasing SL can reduce the magnitudes of impact shock and impact force, SF must increase by more than 15%. Since decreasing SL did not affect impact shock, net impact shock was significantly greater ($p<0.05$) during the experimental condition when more steps were taken to accomplish the same distance. Therefore, the repetitive loading on the joints was increased. Nevertheless, the results of this study do support using an increased SF to increase the number of calories expended during walking.

SUMMARY/CONCLUSIONS

Impact with the ground may cause injury unless impact forces and accelerations are reduced. Altering the kinematics of walking by increasing the SF 15% (decreasing the SL) while remaining at a constant speed does not appear to decrease the impact shock during initial heel contact with the ground, but does increase the caloric expenditure of walking. However, since more frequent impacts are necessary to accomplish the same distance, the deleterious variables associated with foot contact are increased.

REFERENCES

Cohen, J. (1990) Statistical Power Analysis for the Behavioral Sciences (2nd Ed.). Erlbaum, New Jersey.

Felson, D.T. et al. (1988) Obesity and knee osteoarthritis: The Framingham study. *Ann Int Med*, **109**, 18-24.

Hamill, J. et al. (1995). Shock attenuation and stride frequency during running. *Human Movement Sci*, **14**, 45-60.

Holt, K.G. et al. (1991). Predicting the minimal energy costs of human walking. *Med Sci Sports Exerc*, **23**(4), 491-498.

Radin, E.L. et al. (1982) Effect of prolonged walking on concrete on the knees of sheep. *J Biomech*, **15**(7), 487-492.

Gait Adaptability in People with Unilateral Trans-tibial Amputations in Response to Variable Walking Speed and Body Weight Support

Clinton J. Wutzke[1], Nicholas Stergiou[2], Iraklis I. Pipinos[3],
Jason M. Johanning[3], A. Joseph Threlkeld[1]
[1]Rehabilitation Science Research Laboratory, Creighton University, Omaha, NE, USA
[2] HPER Biomechanics Laboratory, University of Nebraska at Omaha, Omaha, NE, USA
[3]VA Nebraska Western Iowa Medical Center, Omaha, NE, USA
Corresponding Author: joethrelkeld@creighton.edu; Website: http://cures.creighton.edu

INTRODUCTION

Lower limb amputations reduce the number of muscle receptors, proprioceptors and plantar sensory receptors (Dietz, 2002). Visual cues combined with modified somatosensory information revise the motor output thus influencing gait adaptability and safety (Kavounoudias et al, 2005). Residual sensory receptors may be further compromised by dysvascular conditions.

Changes in walking speed challenge individuals with amputations to utilize residual sensory input to efficiently maneuver the prosthesis during gait (Dingwell et al, 1996). Body weight support (BWS) combined with treadmill gait at selected speeds allows the assessment of multiple strides while varying sensory input from the periphery (Threlkeld et al, 2003)

Our purpose was to assess motor adaptability of people with trans-tibial amputations by evaluating kinematic responses to changes in walking speed and body weight support vs. matched controls. We also compared a small subset of people with unilateral trans-tibial dysvascular amputations vs. traumatic amputations.

METHODS

All volunteers read, understood and signed an IRB approved informed consent. Six people with unilateral trans-tibial amputations (3 dysvascular amputations, 3 traumatic amputations; $\bar{x}$ age 57.1 yrs, $\bar{x}$ ht. 176.3 cm, $\bar{x}$ wt. 83.3 kg) and eight group matched controls participated in the study.

Subjects walked on a treadmill at three speeds (0.36, 0.8, and 1.07 m/s) at each of three BWS levels (0%, 30%, and 50%) while wearing a harness attached to a commercial BWS system (NeuroVigor II). Joint kinematics were captured at 60 Hz. with a MotionAnalysis system and normalized to percentage of gait cycle (%GC) using OrthoTrak software.

Temporal (cadence, initial double support, total support, total swing) and kinematic (knee and ankle) variables were compared using Repeated Measures ANOVA ($p \leq 0.05$): controls vs. both the intact and the amputated limb; dysvascular vs. traumatic.

RESULTS AND DISCUSSION

Changing walking speeds and BWS caused significant gait changes in all subjects ($p<0.001$). **Tab. 1**

As walking speed decreased and as BWS levels decreased, all subjects increased the %GC spent in double limb support and total support. Compared to controls, people with amputations devoted a larger %GC on the prosthetized limb to initial double support ($p<0.001$) and total support ($p=0.038$) at all speeds and BWS levels. **Tab. 1**

Average knee flexion during the early swing (first 1/3) was significantly greater in controls compared to the amputated limb of people with prosthetics (p=0.012) but controls were the same as the intact limb of people with amputations (p=0.589). **Tab. 1**

Subjects with dysvascular amputations had markedly less average knee flexion of the intact limb during early swing compared to subjects with amputations from trauma ($p<0.016$). Differences ranged from 27.5^o at 0.36m/s @ 0%BWS to 17.7^o at 1.07m/s @50%BWS but there were no differences when comparing the prosthetized sides.

CONCLUSIONS

All subjects displayed temporal and kinematic adaptability to changing walking speed and BWS level. The increased %GC in initial double support and total support on the prosthetized limb of people with amputations allows greater time to transfer weight from the intact to the amputated limb; a compensation that increases gait stability and is consistent with compromised somatosensory feedback mechanisms.
In normal gait, early swing knee flexion with ankle dorsiflexion ensures foot clearance and avoids tripping. Increased mean early swing knee flexion on the prosthetized side of subjects with trans-tibial amputations was likely a compensation for the prosthetic ankle. There was a marked reduction in mean early swing knee flexion in the intact limb of people with dysvascular amputations versus subjects with traumatic amputations possibly reflecting diminished compensatory adaptability in people with dysvascular amputations.

REFERENCES

Dietz, V. (2002). *Nat Rev Neurosci, 3*(10), 781-90.
Dingwell, J. B.et al (1996). *Prosthet Orthot Int, 20*, 101-110.
Kavounoudias, A. et al (2005). *Arch Phys Med Rehab, 86*, 633-640.
Threlkeld, A. J. et al (2003) *Gait Posture*, 17(3):235-245

Table 1: Measures of Interest from Control (**Ctrl**) Subjects and the Prosthetized Limb of Subjects with Unilateral Trans-tibial Amputations (**Amp Prost**).

Speed (m/s)		0.36			0.8			1.07		
BWS (%BW)		0 $\bar{x}$ (s.d.)	30 $\bar{x}$ (s.d.)	50 $\bar{x}$ (s.d.)	0 $\bar{x}$ (s.d.)	30 $\bar{x}$ (s.d.)	50 $\bar{x}$ (s.d.)	0 $\bar{x}$ (s.d.)	30 $\bar{x}$ (s.d.)	50 $\bar{x}$ (s.d.)
Initial Double Limb Support (%GC)	Cntl	21.4(1.4)	20.2(1.0)	16.0(1.6)	14.6(2.5)	14.4(2.7)	13.5(2.4)	12.9(1.3)	13.5(1.1)	12.2(0.9)
	Amp Prost	25.2(2.2)	25.1(1.4)	23.3(4.5)	18.2(2.3)	18.0(2.0)	17.5(2.1)	15.0(1.9)	15.3(1.8)	15.0(1.4)
Total Support (%GC)	Cntl	72.0(1.1)	71.1(1.6)	65.9(2.1)	65.3(2.7)	64.9(3.0)	64.1(2.4)	63.9(1.4)	63.7(1.3)	62.7(1.0)
	Amp Prost	73.9(1.4)	72.5(3.7)	72.1(3.1)	66.6(2.2)	66.2(1.8)	65.7(1.9)	64.5(2.5)	63.9(2.2)	63.6(1.8)
Early Swing (%GC)	Cntl	43.3(2.6)	42.1(3.5)	43.5(3.5)	46.6(4.4)	46.8(4.9)	45.4(4.3)	51.3(3.0)	49.0(3.5)	46.9(3.6)
	Amp Prost	26.5(11.6)	34.5(12.1)	33.5(10.2)	38.1(11.3)	34.1(7.9)	37.3(11.5)	43.4(9.5)	42.9(9.6)	43.2(9.7)

CARPAL CARTILAGE THICKNESS MAPPING USING μCT

Jane A. Casey, Douglas C. Moore, and Joseph J. Crisco
Department of Orthopaedics, Brown Medical School/RI Hospital, Providence, RI, USA
E-mail: douglas_moore@brown.edu

INTRODUCTION

CT image-based computer modeling is increasingly being used to investigate the normal bony articulations in the wrist, as well as the consequences of conformational changes that develop after wrist injury (e.g. scapholunate advanced collapse, or SLAC wrist). The inclusion of cartilage on the CT-generated bone surfaces is necessary to maximize the clinical and biomechanical relevance of these techniques.

This study was performed to evaluate the application of 3-D μCT-generated cartilage thickness maps to carpal bone models generated using a clinical CT scanner. In particular, we evaluated μCT/CT bone congruence, the scalability of cartilage thickness with bone volume, and cartilage penetration at different wrist positions.

METHODS

Clinical CT Scanning and Kinematics Four fresh-frozen cadaver forearms (2M, 2F, ages 66, 69, and 62, 62 respectively) were CT scanned at various positions of flexion, extension, radial and ulnar deviation (pure and combined), and the kinematics of the capitate, lunate, and scaphoid were determined via markerless bone registration (Crisco 1998). The scans were performed at 120 kVp and 80 mA, yielding 3-D volume images with a *z*-axis resolution of 1 mm and an in-plane resolution of 0.3 mm x 0.3 mm (neutral) or 0.9 x 0.9 mm (other positions).
μCT Imaging Following clinical CT imaging, the capitate, lunate, scaphoid and radius were removed via careful dissection. High-resolution (60 μm isotropic voxel size) 3-D images of each bone were generated using a Scanco μCT 40 (Scanco Medical AG, Bassersdorf, Switzerland). The bones were scanned in air (to facilitate cartilage segmentation) using the following settings: 55 kVp, 145μA, 250 ms integration time.
Generation of Bone/Soft Tissue Volumes 3-D bone and soft tissue volumes (cartilage + ligament) were generated via simple thresholding and manual editing (Mimics, Materialise, Ann Arbor, MI).
Alignment of μCT Volumes Each μCT-generated bone was aligned with the corresponding clinical CT-generated bone using Geomagic Studio (Geomagic, Durham, NC). The resulting transforms were then applied to the soft tissue volumes to align them in the same coordinate system.
Assessing μCT and CT Bone Congruence Congruence of the μCT and CT-generated bone models was assessed by comparing the distance between the surfaces of the registered bones, their centroid locations, inertial axes, and calculated bone volumes.
Carpal Cartilage Thickness Quantification The individual cartilage facets on each bone (i.e. the lunate facet on the scaphoid), were manually defined on the soft tissue volumes using Geomagic Studio and then saved as separate surfaces. The shortest distance from the μCT bone surfaces to each of the cartilage facet surfaces was quantified using Geomagic Qualify. Scaling was assessed by regressing the average cartilage thickness for each bone against μCT bone volume.
Assessing Cartilage Penetration The aligned μCT bones and cartilage facets were visualized in nine positions of flexion, extension, radial and ulnar deviation using

the CT-derived kinematic transforms. Penetration was reported on a scale of 0 (no cartilage contact) to 3 (bone penetration).

RESULTS

μCT to CT Congruence The fidelity of the μCT and CT-generated bones was high. On average, the CT-generated bone surface fell outside the μCT-generated bone surface by 0.178 mm, though the regions where one model was larger than the other were randomly distributed (Fig. 1). The centroids were almost identical (Δ = 0.283 mm), while the direction of the inertial axes differed at most by 4.5°. The CT-generated bones were on average 196.0 mm^3 larger than the μCT-generated bones.

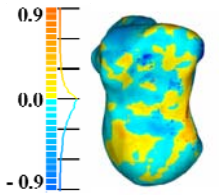

Figure 1 Distance Map, μCT to CT

Scaling of Carpal Cartilage Thickness The average *per bone* carpal cartilage thickness ranged from 0.48 - 1.16 mm and was independent of bone volume (Fig. 2).

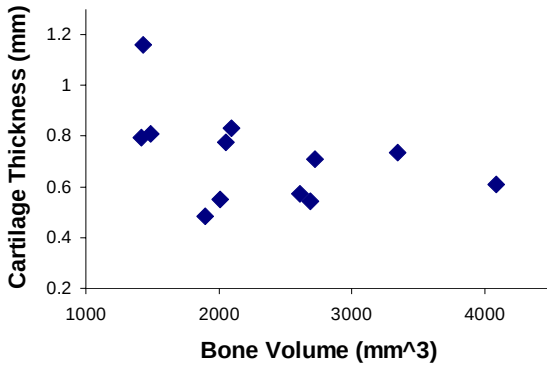

Figure 2 Average cartilage thickness plotted as a function of bone volume (each point is one scaphoid, lunate or capitate)

Cartilage Penetration Cartilage penetration was smallest in the neutral wrist position for all articulating surfaces. Otherwise, penetration was least at the scapho-lunate articulation (Table 1).

Table 1: Average measure (n= 4) of cartilage penetration in various positions

	Cap-Lun	Cap-Sca	Lun-Sca	Lun-Rad	Sca-Rad
Neutral	0.3	1.0	0.1	1.5	1.4
40° F	0.6	1.1	0.5	1.8	1.4
40° E	1.6	1.9	0.1	1.8	2.6
10° R	1.0	0.6	0.3	1.6	1.4
30° U	1.5	0.9	0.1	1.3	1.3
40° F + 30° U	0.9	1.0	0.0	1.5	1.1
40° E + 30° U	2.0	1.9	0.0	1.8	1.9
40°E + 10° R	1.8	1.8	0.3	2.0	2.8
40°F + 10° R	0.6	0.6	0.5	1.4	1.5

DISCUSSION

This study was performed to evaluate the application of μCT-generated cartilage surfaces to clinical CT-generated carpal bone models. Our technique yielded μCT-generated cartilage surfaces that fit the CT-generated bone surfaces with good fidelity, as assessed by μCT and CT-generated bone surface congruence. We were surprised that carpal cartilage did not scale with bone volume, given that the dimensions of the carpal bones increase isometrically with increasing bone volume (Crisco, 2005). We were also surprised by the amount and extent of cartilage-cartilage and cartilage-bone penetration generated using this technique, though they are not unreasonable given the error inherent in aligning the μCT and CT bone models, and the errors associated with calculating kinematics using markerless bone registration, which are on the order of 0.5 mm and 0.5° (Neu 2000).

REFERENCES

Crisco *et al*. (1999). *JOR*, **17**, 96
Crisco *et al*. (2005). *J Hand Surg*, **30A**, 35
Neu *et al*. (2000). *J Biomech*, **122**, 528

ACKNOWLEDGEMENTS

Funded by NIH grant HD052127. Special thanks to Jason Machan Ph.D., Ryan Calfee M.D., Evan Leventhal, and Mike Rainbow.

STABILIZATION OF LOCOMOTION BY A MUSCULOSKELETAL MODEL OF CAT HINDLIMBS WITH HILL-TYPE ACTUATORS

Alexander N. Klishko[1] and Boris I. Prilutsky

Georgia Institute of Technology, Atlanta, GA, USA
[1]Permanent address: Institute of Mathematical Problems of Biology, Puschino, Russia
E-mail: aklishko3@gatech.edu, Web: www.ap.gatech.edu/prilutsky

INTRODUCTION

Animals during locomotion are able to withstand sudden external perturbations (Jindrich and Full, 2002). This could be achieved by both reflex responses and intrinsic mechanical properties of the musculo-skeletal system (Jindrich and Full, 2002). The contribution of the latter to locomotion stabilization is difficult to assess experimentally. The aim of this study was to investigate inherent stabilizing effects of a musculoskeletal model of cat hindlimbs with Hill-type actuators (no short-range stiffness) using forward dynamics simulations.

METHODS

For forward dynamics simulations we used a 2D, 10-DOF model of cat hindlimbs with the trunk (for details see Ivashko et al., 2003). Each hindlimb was actuated by 9 muscles with the force-length-velocity properties and pennation of the muscle fibers and the force-length properties of the tendon and passive parallel structures; these data were taken from the literature. Muscle dynamics was described by a Hill-type model similar to one of He et al., 1991. Muscle force was computed as a function of muscle activation, fiber length, velocity, acceleration, and pennation angle. The ground reaction forces were computed from horizontal and vertical displacements of the feet contact points on the ground which was modeled as a viscoelastic material.

In order to simulate normal, unperturbed cat locomotion, we used as input low-pass filtered EMG profiles of 9 hindlimb muscles during walking recorded and/or published previously. The equations of hindlimb motion and muscle dynamics were integrated over one complete walking cycle using the second-order Runge–Kutta method with a constant 0.025-ms step starting with recorded (Prilutsky et al., 2005) generalized coordinates and velocities at the beginning of left leg swing. To minimize the difference

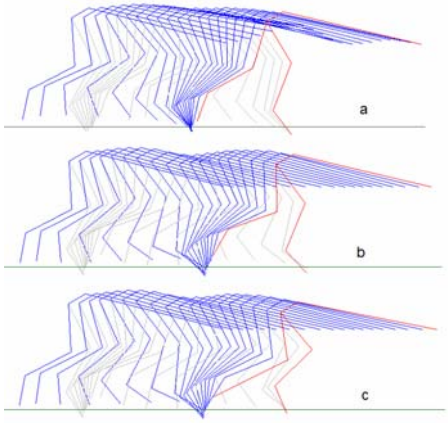

Figure 1: Stick-figures of experimental non-perturbed walk (**a**), simulated non-perturbed walk (**b**), and simulated perturbed walk (**c**; perturbation: t=0%, Δt=7.5 ms, F=0.1 N); the maximum deviation of the hip vertical coordinate from unperturbed hip trajectory (D2) was 14% (considered unstable walk).

in joint angles and ground reaction forces between the experiment and simulation, we used a simulated annealing optimization algorithm to adjust the muscle excitation patterns by tuning three pattern parameters per muscle until the difference between the experimental and simulated kinematics and ground reaction forces was within 10% (e.g. Neptune and Sasaki, 2005). Such a solution was found (see stick-figures in Fig. 1b and

compare them with the experiment, Fig. 1a). Normal walking was perturbed by applying a single rectangular force impulse to the left leg in either horizontal or vertical direction. The impulse was defined by 3 parameters which were varied in simulations: onset time (t: 0-90% cycle), duration (Δt: 0-37.5 ms) and magnitude (F: 0.01-10 N). The ability of the model to resist perturbations was estimated using 2 measures D1 and D2. D1 was the mean normalized deviation of the generalized coordinates from those of simulated unperturbed walking, computed over 15 ms from perturbation onset. The model was considered to loose balance if the deviation of the hip vertical coordinate one cycle after the perturbation (D2) was 14% or higher (Fig. 1c).

RESULTS AND DISCUSSION

Perturbations with durations up to 37.5 ms, applied at the cycle onset, destabilized locomotion (D2≥14%) if perturbation magnitude exceeded 0.02 N for vertical impulses (Fig. 2, left), and 0.01 N for horizontal. The two measures of stability (D1 and D2) were closely related for perturbations at cycle onset (Fig. 2, right).

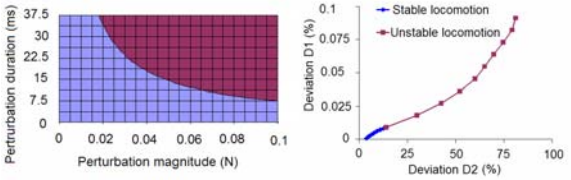

Figure 2: Left: Areas of stable (D2<14%; blue) and unstable (D2≥14%; brown) walking after vertical perturbations (Δt=0-37.5 ms, F=0-0.1N) at cycle onset (t=0). **Right**: Relationship between stability measures D1, D2 after above perturbations.

Thus the model was considered to loose balance if D1 ≥ 0.01% which corresponded to D2≥14%. Vertical impulses of Δt=7.5 ms, for example, applied at any cycle instance, did not destabilized locomotion (D1<0.01%)

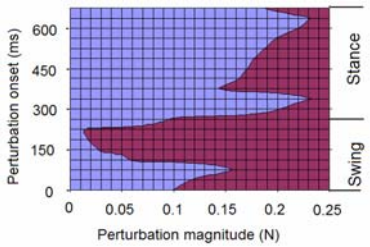

Figure 3: Areas of stable (D1<0.01%; blue) and unstable (D1≥0.01%; brown) walking after vertical perturbations (t=0-37.5 ms, Δt=7.5 ms, F=0-10N).

if F< 0.01 N (Fig. 3). The model was substantially more resistant to destabilizing perturbations in vertical direction compared to horizontal and during stance than in swing (Fig. 3). The most destabilizing effects had perturbations applied at 75% of the swing phase (Fig. 3).

SUMMARY/CONCLUSIONS

Overall, this musculoskeletal model with Hill-type actuators seems unable to withstand even small perturbations applied to the foot during locomotion. Thus, reflexes and short-range stiffness should be taken into account to explain locomotion stabilization in animals.

REFERENCES

He, J. et al. (1991). *IEEE Trans. Automat. Control*, **36**, 322-332.

Ivashko, D.G. et al. (2003). *Neurocomputing* **52–54**, 621 – 629.

Jindrich, D. L., Full R. J. (2002). *J. Exp. Biol.*, **205**, 2803–2823

Neptune, R.R., Sasaki, K. (2005). *J Exp Biol.*, **208**, 799-808.

Prilutsky et al. (2005) *J. Neurophysiol*., **94**, 2959-2969.

ACKNOWLEDGEMENTS

This work was supported by NIH grant NS048844.

TEMPERATURE-DEPENDENT MECHANICAL PROPERTIES OF HUMAN TYPE-I MUSCLE FIBERS

Sampath K. Gollapudi[1] and David C. Lin[1, 2, 3]

[1]Dept. of Mechanical and Materials Engineering, [2]School of Chemical and Bioengineering, [3]Dept. of Veterinary and Comparative Anatomy, Pharmacology and Physiology, Washington State University, Pullman, WA, USA
Email: sampath@vetmed.wsu.edu

INTRODUCTION

Crossbridge muscle models have been used successfully to study the basic mechanisms of contraction in skeletal muscles. However, they have not been used to analyze whole muscle function. The development of fiber-specific (slow vs. fast) crossbridge models is an important step to bridging this gap because a whole muscle model could be formed from a heterogeneous population of single fiber models.

As part of this development, we aim to experimentally record the variations in the force-velocity (F-V) properties from type-identified single fibers and fit the parameters from Huxley's 1957 two-state crossbridge model. However, because single fiber experiments tend to degrade at elevated temperatures (>28 ^{o}C), our strategy is to record F-V properties from 4-28 ^{o}C and estimate the model parameters at each temperature. Once we identify the temperature-dependant relationship of each model parameter within this temperature range, the *in vivo* (37 ^{o}C) function of each fiber type can be estimated by using extrapolation techniques.

METHODS

Single fibers were chemically skinned and dissected free from biopsies of human *lateral gastrocnemius* muscle. Fibers glued to aluminum clips were attached between the force transducer and motor hook. This improved technique allowed better tracking of sarcomere pattern, especially at higher temperatures. Each fiber was maximally activated in a Ca^{++} solution at a specific test temperature (12, 20, and 28 ^{o}C); sarcomere length was set to 2.5 µm and a perturbation was then applied as a linear change in force (force ramp) for both lengthening and shortening contractions to measure the F-V behavior. Each fiber was later analyzed by gel electrophoresis for myosin heavy chain type. For this study, a total of 12 type I fibers have been measured.

RESULTS AND DISCUSSION

Figure 1 shows the averaged F-V curves for human type-I fibers during lengthening and shortening contractions across all trials at 12 ^{o}C (n=4), 20 ^{o}C (n=3) and 28 ^{o}C (n=5). These F-V curves clearly demonstrate that the mechanical properties of both shortening and lengthening contractions are quite temperature sensitive. Particularly, crossbridge kinetics were faster at higher temperatures thereby having a direct impact on the shortening velocities. For lengthening trials greater than 20 ^{o}C, the F-V behavior did not show a steady behavior especially at higher strain levels suggesting the need to consider more complicated crossbridge models to explain this behavior.

Figure 2 shows the averaged Power-Velocity (P-V) curves during shortening and lengthening trials for the above set of fibers. The shortening P-V curves revealed that

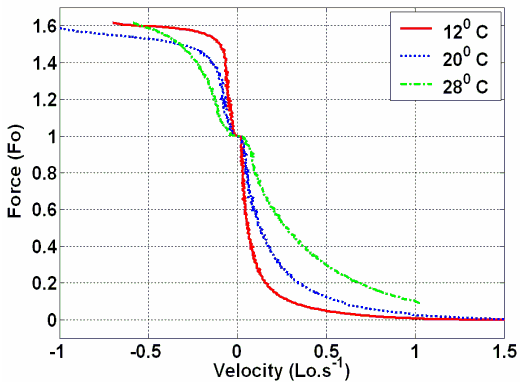

Figure 1: Averaged F-V curves at 12 ^{o}C, 20 ^{o}C and 28 ^{o}C. F_o, L_o are isometric tension and length.

optimal velocity (where work is maximum, V_{opt}) and optimal power (W_{opt}), which determine *in vivo* function, are temperature-dependent (Table 1). Though the trends in these properties compare with the results from Bottinelli et al. (2000), the magnitude of temperature dependence was not as great. Our studies also showed no predefined temperature-dependent relationships among these properties during lengthening trials.

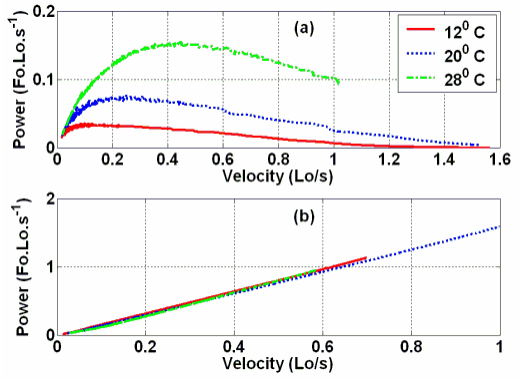

Figure 2: Averaged P-V curves at 12 ^{o}C, 20 ^{o}C and 28 ^{o}C (a) Shortening (b) Lengthening

By simulating the Huxley's crossbridge model for similar ramp pertubations, it is also possible to estimate the model parameters. These analyses provide valuable information about how crossbridge kinetics at the microscopic level influences the behavior at macroscopic level. Also, these data at lower temperatures can be used to extrapolate *in vivo* function at physiological temperature (37 ^{o}C). A similar study can be extended for type-II fibers and these results can be integrated to understand the whole muscle function *in vivo.*

SUMMARY

Mechanical properties (F-V and P-V) of human type I muscle fibers are found to be highly-temperature sensitive. These data will be used with a simplified crossbridge model to tie the temperature controlled biophysical experimental data to macroscopic force predictions. A need to further extend this study to *in vivo* temperatures is also justified in order to understand the differences in contractile properties among various fiber types.

REFERENCES

Huxley, A. F. (1957), Prog. Biophys. Biophys. Chem., 7, pp. 257–318.

Bottinelli, R. et al. (2000), Journal of Physiology, 495.2, pp. 573-586.

ACKNOWLEDGEMENTS

Support provided by Whitaker Foundation and WSU Bioengineering Research Center.

Table 1: Mechanical Properties during Shortening

Temperature	12 ^{o}C	20 ^{o}C	28 ^{o}C
V_{opt} (Lo/s)	0.09013	0.25127	0.44958
W_{opt} (Fo Lo/s)	0.035767	0.076248	0.15470
F_{opt} (Fo)	0.3968	0.30345	0.344119

IS A PASSIVE ELEMENT RESPONSIBLE FOR THE ENHANCEMENT OF ISOMETRIC MUSCLE FORCE FOLLOWING ACTIVE STRETCH?

Sharon R. Bullimore and Walter Herzog

Human Performance Lab, Faculty of Kinesiology, University of Calgary, Canada.
Email: sbullimore@kin.ucalgary.ca. Web: www.kin.ucalgary.ca/HPL/.

INTRODUCTION

For over 50 years, it has been recognised that steady-state isometric muscle force is higher following an active stretch, than during a purely isometric contraction at the same muscle length ('force enhancement' or FE). This phenomenon is not predicted by the widely-accepted cross-bridge model of muscle contraction and the underlying mechanism is unknown. It has been proposed that some or all of the extra force may be generated by a passive structure which is engaged upon activation and elongated during stretch (Edman et al., 1982; Herzog, 2001). If this is the case, it would be expected that subsequent shortening of the muscle would reduce the elongation of this structure, and so decrease the amount of FE, and that shortening the muscle back to its original length would eliminate the FE altogether. Our goal was to determine whether FE exhibits these characteristics. We obtained FE by actively stretching a muscle fibre, and then applied a rapid drop in length. We tested two hypotheses: 1) the amount of FE remaining after the drop will decrease as drop size increases; 2) FE will be eliminated by drops equal to or greater than the stretch distance.

METHODS

Intact single muscle fibres were dissected from the lumbrical muscles of the frog, *Xenopus laevis*, and mounted in the experimental apparatus. A force-length relationship was obtained to determine optimal length (L0). Contractions (3s) were performed in sets of three (Fig. 1) in the following order: 1) 'iso-drop': the fibre was activated at 1.2L0 and then rapidly shortened by the prescribed drop distance 1.5s after activation; 2) 'pure-iso': the fibre was activated and held isometric at the final length of the preceding iso-drop contraction; 3) 'stretch-drop': the fibre was activated at 1.15L0, actively stretched to 1.2L0 and then rapidly shortened by the prescribed drop distance 1.5s after activation. Drop distances of 25, 50, 75, 100, 150 and 200% of stretch distance were used.

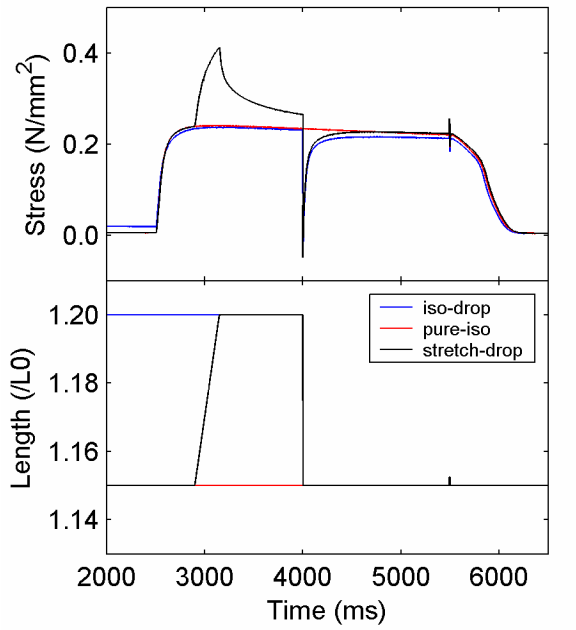

Figure 1: Raw stress-time and length-time traces for one set of 3 contractions (see 'methods' for details of the types of contraction). In this example, drop distance was 100% of stretch distance. Note that the force enhancement persists after the drop.

The FE remaining after the drop was calculated as the percent difference between the forces in the stretch-drop and iso-drop contractions 1.44s after the drop. The force depression (FD) induced by the drop was calculated as the percent difference between the forces in the pure-iso and iso-drop contractions 1.44s after the drop.

RESULTS AND DISCUSSION

The amount of FE remaining after the drop decreased as drop distance increased (Fig. 2), as predicted by hypothesis 1. However, in contradiction with hypothesis 2, FE was not eliminated by a drop of 100% stretch distance, and continued to decrease up to the maximum drop of 200% stretch distance. Therefore, we conclude that FE does not exhibit the characteristics that would be expected if it were generated by elongation of a passive element.

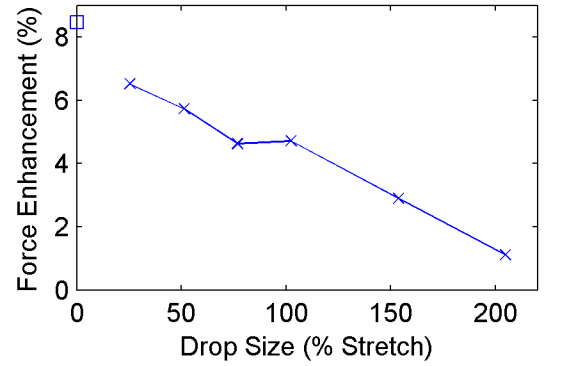

Figure 2: The force enhancement remaining after a rapid drop in length decreased as drop size increased, even beyond a drop size corresponding to 100% of stretch distance. □ indicates the force enhancement present without a drop.

In all cases, FD was observed after the rapid drop in length (Fig. 3). This was unexpected because FD is not thought to be induced by unloaded shortening (Marechal and Plaghki, 1979), and the drops in the current study were at least 50 times the expected maximal shortening velocity of the fibres, and thus must have been unloaded. This observation is not consistent with the theory that FD arises from stress-induced inhibition of cross-bridge attachment (Marechal and Plaghki, 1979) because unloaded shortening would be expected to release the stress on the myofilaments.

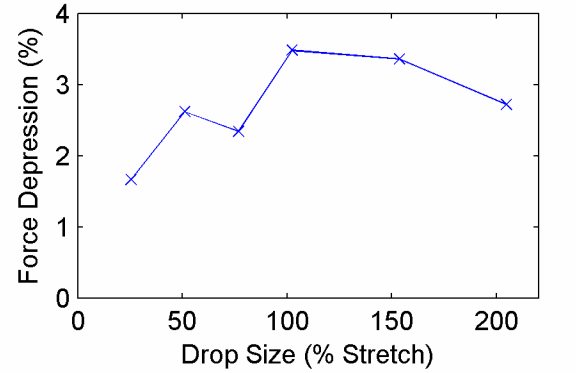

Figure 3: Force depression was consistently induced by the rapid drops and did not show a clear relationship to drop size.

CONCLUSIONS

The characteristics of FE do not seem to be consistent with the theory that it is caused by elongation of a passive element. Therefore alternative mechanisms should be considered; for example, an increase in the force generated by the cross-bridges.

REFERENCES

Edman, K.A.P. et al. (1982). *J. Gen. Physiol.*, **80**, 769-784.

Herzog, W. (2001). *Eur. J. Sport Sci.*, **1**, 1-14.

Marechal, G., Plaghki, L. (1979). *J. Gen. Physiol.*, **73**, 453-467.

ACKNOWLEDGEMENTS

Canada Research Chairs Program, AHFMR, NSERC.

SWITCHING CONTROL TO ACTUATE ELBOW MOTION

Pat Schimoler [1,2], Jeffrey S. Vipperman [1], Laurel Kuxhaus [1,2], Daniel D. Budny [1], Angela M. Flamm [2], Mark E. Baratz [2], and Mark Carl Miller [1,2]

[1] University of Pittsburgh, Pittsburgh, PA, USA
[2] Allegheny General Hospital, Pittsburgh, PA, USA
E-mail: mcmiller@wpahs.org

INTRODUCTION

Injuries and trauma to the elbow can lead to difficulty with activities of daily living. Two particular clinical issues provide the impetus for developing a controlled elbow joint motion simulator (JMS) for cadaveric specimens. First, insertion of a radial head prosthesis may be necessary after an unreconstructable, comminuted radial head fracture and second, ulnar collateral ligament (UCL) injuries are common among athletes. To quantify effects after surgical intervention, it is useful to have a system that actuates the arm in a repeatable, physiologic manner. (Johnson *et al.*, 2000) We propose that a switching algorithm can successfully control both flexion-extension (F-E) with a constant pronation-supination (P-S) angle and P-S while maintaining a constant flexion angle.

METHODS

The JMS has four major components: the frame, controller, actuators, and sensors. The frame constrains the elbow, supports the motors and provides physiologic lines of action for the applied forces which simulate muscle tension. (Magnusen, 2002, Kuxhaus et al., 2005) Full controllability of the elbow's two degrees of freedom is available via the *brachialis* (flexion), *triceps* (extension), *biceps* (flexion, supination), and *pronator teres* (pronation). The controller, drives, and motors (ACR8020, Gemini GV, and BE Series, Parker Hannifin, Rohnert Park, CA) apply loads to replicate muscle tension. Displacement feedback is provided by two potentiometers (P1401a, Novotechnik, Southborough, MA) powered by a DC power supply (HP6284A, Hewlett Packard, Palo Alto, CA). Force feedback is supplied by load cells (Model 31, Honeywell Sensotec, Columbus, OH) conditioned by strain gage conditioners (Model 3270, Daytronic, Dayton, OH). 80lb line connects tendons to the actuators (Super Braid, Stren, Spirit Lake, IA).

Two similar algorithms control motion based on a logical switching algorithm, both driven with discrete PI controllers. The first controls F-E for UCL testing. The arm's inertia combined with the unidirectional, cable actuation can cause slack in the agonist during high speed movements. Joint stability is compromised, propelling the load-controlled antagonist into a sudden movement to reestablish joint stiffness possibly causing travel overshoot problems. The first algorithm overcomes this instability at higher speeds by switching primary movers between the *brachialis* for flexion and *triceps* for extension.

The second algorithm controls P-S through the *biceps* and *pronator teres* as above while maintaining a fixed flexion angle. EMG measurement has shown that constant flexion angle is maintained by tapering the *brachialis* force while the *biceps'* activation increases. (Naito, 2004) This effect can be recreated with a JMS by modulating the *brachialis* according to the arm flexion angle. As the *biceps* apply tension for

supination, the added flexion moment is countered by sufficiently reducing *brachialis* tension. Due to the cable/tendon actuation, it is necessary to maintain a minimum load on the *brachialis* to prevent slack and ensure stability because no compressive load may be applied. If, in an effort to maintain flexion angle, the *brachialis* tension falls below a minimum load level, *triceps'* activation provides the equalizing moment.

The controller was validated on a mechanical elbow with physiologic dimensions and insertions. The mean error, standard deviation and system precision were used to determine the system's tracking abilities. The mean error and standard deviation measure accuracy with regard to the difference between the reference and actual position after removing the control system lag which is determined through a cross correlation computation. System precision is found from averaging the standard deviation of three trials at each sample point.

RESULTS AND DISCUSSION

Figures 1 and 2 show the tracking error and the force modulation. The system tracks a sinusoidal input (Fig. 1) at an average error of 0.44° (P-S) and 0.12° (F-E). The average deviations between the reference and actual position are 1.05° (P-S) and 0.81° (F-E). The precision is on average 1.40° (P-S) and 0.21° (F-E). Figure 2 shows the change in forces during supination. The accuracy and precision results indicate that the algorithms can successfully control both P-S and F-E.

SUMMARY

The switching control algorithm to actuate cadaveric elbow specimens is accurate and repeatable. Future work will include studies of radial head prostheses, ligament strain measurement, and controller refinements.

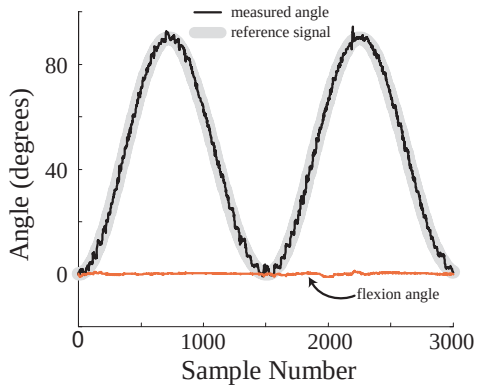

Figure 1: Sinusoidal P-S motion holding flexion constant.

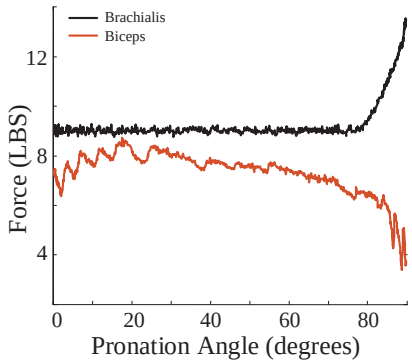

Figure 2: *Biceps* and *brachialis* force during pronation. *Brachialis* is set to provide a minimum of 9 lbs.

REFERENCES

Johnson, J.A. et al. (2000). *J. Biomech.*, **33**, 635-639.

Kuxhaus et al. (2005). ASB, Cleveland, OH.

Magnusen, J.P. (2002). MS Thesis. University of Pittsburgh.

Naito, A. (2004). *Anatomical Science International*, **79**, 11-20.

ACKNOWLEDGEMENTS

Partial funding from Am. Soc. for Surgery of the Hand

BONE SURFACE TRACKING FOR STANDING KNEE MRI: A VALIDATION STUDY

Peter Barrance[1], Michael Pohl[2], Brian Noehren[2], Joaquin Barrios[2] & Irene Davis[2]

[1] Kessler Medical Rehabilitation Research & Education Center, West Orange, NJ, USA
[2] University of Delaware, Newark, DE, USA
E-mail: pbarrance@kmrrec.org, Web: www.kmrrec.org

INTRODUCTION

Accurate measurements of the relative positions of the bones in the knee are important when studying disorders and treatments of the tibiofemoral and patellofemoral joints. The strong influence of joint loading has been recognized in the development of methods to measure kinematics under physiological conditions, such as weightbearing. Joint kinematics can be tracked by registering bone surfaces between serial MRI scans (Fellows et al., 2005). The purpose of the current study was to assess the accuracy of a surface-based kinematic matching method using MRI data collected in a vertically open scanner.

METHODS

Specimen preparation: One left female cadaveric lower extremity was disarticulated at the hip and ankle and dissected of all overlying tissue to leave only the bones and passive connecting structures of the knee joint present. Nylon screws were inserted in holes that were drilled in the cortices of the femur, tibia, and patella. A hollow spherical marker covered with retro-reflective tape was glued to the head of each screw (Fig. 1A). Prior to MRI scanning, a Vicon 512 motion analysis system was used to collect the 3-D positions of each marker.
MRI scanning: Before MRI scanning, the specimen was placed into a large plastic bag which was filled with vegetable oil - a fluid selected for its MRI imaging characteristics. Sagittal scans of the specimen were acquired in the vertically open Fonar Upright 0.6T MRI. This scanner was chosen to allow for future imaging of subjects during weightbearing positions. Sampling parameters included: TE 10 ms, TR 328 ms, slice thickness 3.5 mm, matrix 416x416, FOV 300 mm, time 4:05. Two positions were measured: **Q1** – in extension, and **Q2** – after manual repositioning into approximately 10º flexion (Fig. 1B, C).

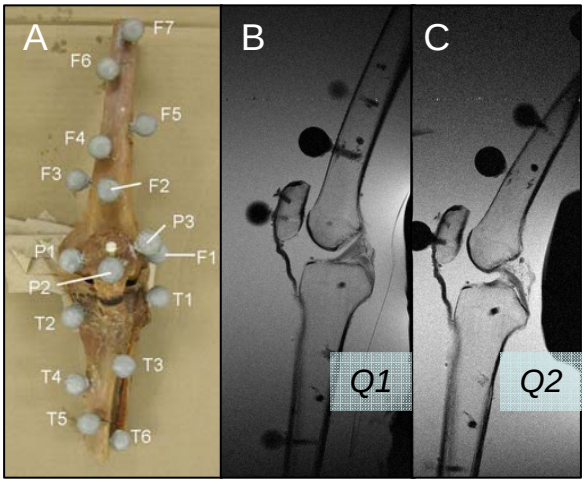

Figure 1: (A) Cadaveric knee with markers attached; (B, C) MRI images in extension *(Q1)*, and flexion *(Q2)* positions; the hollow markers appear as dark circles within the contrast fluid.

Digitization of bone and marker outlines: Images were transferred to laboratory workstations and reformatted, after which the external cortical surface of each bone and the periphery of each marker were digitized manually. The operator followed an instruction to digitize only the peripheries that could be defined with confidence. The coordinates of all digitized points were then transformed into 3-D spatial coordinates using the positional information in the scan images.

Marker based transformations: A least squares algorithm was used to fit a sphere to the points digitized on the marker outlines in the images. The distances between the computed centers of sets of markers attached to each bone were compared with those measured from the motion analysis system; the difference between those methods was found to be 0.94±0.93 mm (mean±SD). Coordinate systems were assigned based on the markers attached to each bone, and their positions were computed at Q1 and Q2. A relative transformation matrix ${}^{Q1\text{-}Q2}T_{mkr}$ between positions was calculated for each bone.

Surface based transformations: The method used to compute changes in positioning in vivo is based on matching the bone surface points in different positions. A surface fitting procedure (Hoppe et al., 1994) was first used to interpolate Q2 bone points on a 1.0 mm grid. Trimmed Iterative Closest Point matching (Chetverikov et al., 2002), a procedure that finds an optimal transformation to match a moving set of points to a target set, was used for each bone to compute the transformations ${}^{Q1\text{-}Q2}T_{TICP}$ from the moving Q1 point set to the fixed Q2 point set.

Validation comparison: We used the MRI-marker system as a comparison measure for evaluating the surface tracking method. We assigned anatomically based coordinate systems relative to landmarks digitized in the Q1 position, and we used ${}^{Q1\text{-}Q2}T_{mkr}$ and ${}^{Q1\text{-}Q2}T_{TICP}$ to calculate the positions of those systems in the Q2 position. We then calculated and compared joint displacement parameters for the tibiofemoral and patellofemoral joints at the Q2 position for a measure of the accuracy of the surface based matching in calculating joint positions.

RESULTS AND DISCUSSION

Errors were <=1.5° for all angles and <1.7 mm for all displacements (Table 1). These are similar levels of error to those found in the validation of an MRI-based method used to measure patellofemoral kinematics in supine subjects (Fellows et al., 2005). We are currently collecting these MRI data from weightbearing subjects; subjects have been able to hold this position in both symmetrical flexion and single leg stance for the imaging time used in the validation study. Minimizing subject motion is critical to maintaining accuracy, and, we have therefore worked to develop a faster scanning sequence (3 minutes).

SUMMARY/CONCLUSIONS

This method can measure knee kinematics with similar accuracy to other MRI methods, with the added advantage of allowing weightbearing scanning.

REFERENCES

Chetverikov D, et al. (2002). *International Conference on Pattern Recognition*.
Fellows RA, et al. (2005). *J Biomech*, **38**, 1643-52.
Hoppe H, et al. (1994). *SIGGRAPH*.

ACKNOWLEDGEMENTS

We gratefully acknowledge John Greenhalgh, Ph.D. (Fonar Corporation) for the development of MRI sequences for this study, and Laura Shultz for contributions to data processing methods.

Table 1: Errors and excursions for the tibiofemoral and patellofemoral joints

Degree of freedom:	Sagittal rotation (º)	Frontal rotation (º)	Axial rotation (º)	Med/lateral (mm)	Ant/post (mm)	Superior (mm)
Tibiofemoral error/excursion:	0.65/9.8	0.51/-0.5	0.60/0.0	1.48/-0.45	0.66/-0.24	0.49/3.43
Patellofemoral error/excursion:	1.50/7.63	0.65/-1.38	0.42/-0.41	1.63/1.32	0.65/-2.05	0.72/3.47

DISPLACED SOFT TISSUE VOLUME AS A METRIC OF COMMINUTED FRACTURE SEVERITY

Thaddeus Thomas, Donald D Anderson, J Lawrence Marsh, and Thomas D Brown
The University of Iowa, Iowa City, IA, USA
E-mail: thaddeus-thomas@uiowa.edu

INTRODUCTION

The assessment of injury severity in a highly comminuted fracture (one with many fragments) is a crucial prelude to treatment, guiding surgical decisions and signaling potential complications. Complexities such as the degree of comminution, axial malalignment and fragment dispersal preclude a reliable and reproducible human-based assessment of injury. Variable injury severity is a substantial confounder in multi-center studies of treatment and outcome for specific fracture types. New validated CT-based methodologies have yielded an objective fracture severity metric [1], opening the door to studies aimed at improving patient outcomes.

While the CT-based fracture severity metric agrees well with expert clinician opinion, its value is limited since it only accounts for the degree of fracture comminution. Comminution is a principal component of injury severity, but there are other factors that also have significant implications for treatment and potential complications. The current study addresses this limitation, by developing techniques to explicitly quantify fragment displacement and dispersal.

METHODS

CT studies were obtained from 20 tibial pilon fracture cases. The intact and the fractured tibias were segmented using a semi-automated algorithm[2]. The mirror image of the healthy contralateral tibia provided a reference template from which fracture fragment displacement and dispersal were assessed.

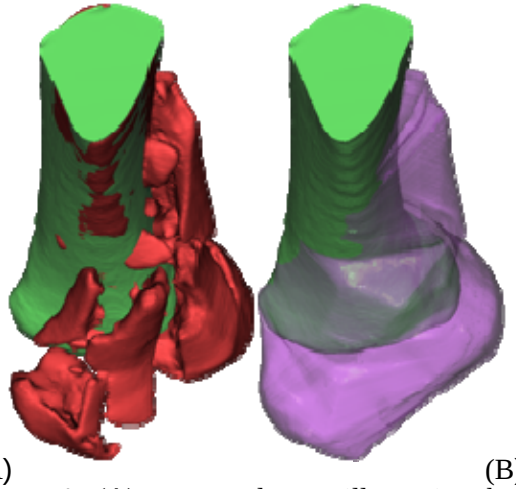

(A) (B)

Figure 1. (A) an example case illustrating the intact geometry aligned proximally with the fractured base fragment. (B) The corresponding convex hull encasing the displaced tissues.

The CT data from the fractured tibias contain a proximal intact segment (base fragment). Using the reverse engineering software, Geomagic Studio (Raindrop Geomagic, Research Triangle Park, NC), the fractured bone base fragment was registered in space relative to its intact contralateral mirrored template using an iterative closest point algorithm (Figure 1).

Once aligned, the fragment displacement was stratified by calculating the volume of tissue displaced during the fracture event. In each slice, a convex hull (the smallest convex polygon circumscribing an object) of the aligned tibias was generated (Figure 2). The difference in circumscribed volumes between the intact limb and aggregate intact/fractured convex hulls reflects the amount of radiating fragment dispersion and

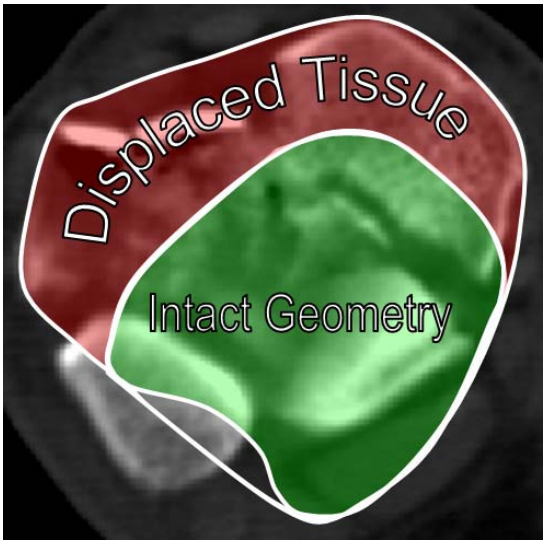

Figure 2. The intact geometry and circumscribing convex hull are projected onto the fractured CT slice. The displacement metric is based upon their areal difference, i.e. the displaced tissue.

axial malalignment in a single aggregate displacement metric.

Cases were rank ordered with increasing injury severity based upon the judgment of three experienced orthopaedic clinicians. Cases were also rank ordered according to fracture energy and displacement measurements. To assess the clinical relevance of the CT based metrics, their agreement to that of the clinicians was evaluated by concordance.

RESULTS/ DISCUSSION

The severity rankings of the raters were in good agreement with the displacement metric (concordance values of 0.82, 0.87 and 0.89). The clinicians' subjective assessments were validated with a 0.89 average inter-rater concordance. While the fracture energy metric was shown to have acceptable agreement (average concordance of 0.77), fragment displacement offered an improved method to quantitatively capture the clinicians' perception of injury severity (Figure 3).

CONCLUSIONS

The ability to perform objective injury assessments using information obtained solely from standard-of-care CT images is a step toward advancement in the treatment of intra-articular fractures. Future work will include the application of displacement measures to a larger series of cases, and examination of their correlation with fracture treatment and outcome.

REFERENCES

1. Anderson D, et al. 50th ORS Meeting, 29, 488, 2004.
2. Anderson DD, Muehling VL, Marsh JL, Brown TD. Computer Aided Surgery, 9(3):116, 2004.

ACKNOWLEDGMENTS

This research was supported by NIH AR048939,the AO Research Fund, and the Orthopaedic Trauma Association.

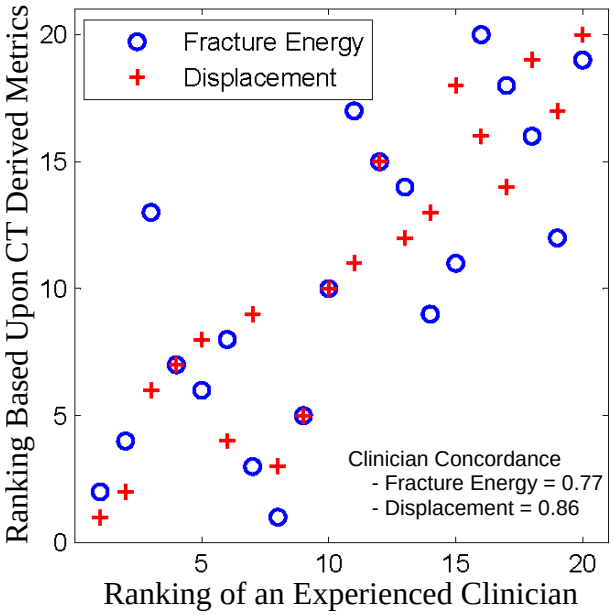

Figure 3. Rank ordering comparison of 20 tibial pilon cases based upon clinician assessment and CT-based methods.

METABOLIC COSTS AND WALKING SYMMETRY OF TRANS-TIBIAL AMPUTEES ARE INFLUENCED BY PROSTHETIC MASS DISTRIBUTION

Jeremy D Smith [1] and Philip E Martin [2]

[1] Ball State University, Muncie, IN, USA
[2] The Pennsylvania State University, University Park, PA, USA
E-mail: jeremysmith@bsu.edu

INTRODUCTION

Unilateral, trans-tibial amputees expend 20% to 30% more metabolic energy than non-amputees walking at the same speed (Gailey et al., 1994). Reasons for these higher costs are not fully understood. The use of lighter weight prostheses is thought to reduce walking metabolic cost, but empirical results have been equivocal. For example, Lehmann et al. (1998) increased prosthesis mass of trans-tibial amputees from approximately 40% to 70% of intact leg mass without significantly altering cost. Gait asymmetries are also common in unilateral amputees. Asymmetrical walking patterns have been thought to contribute to increased joint loading of the intact leg, which may lead to early degenerative joint disease (Royer and Wasilewski, 2006).

Based on the effects different inertia configurations had on the half-period of oscillation of a simple pendulum, we altered prosthetic leg inertia with the intent of increasing, decreasing or not changing swing time of the prosthetic leg. We hypothesized that adding mass proximally to the prosthetic leg (i.e., near the thigh center of mass) would improve walking symmetry and reduce metabolic costs during walking.

METHODS

Six unilateral, trans-tibial amputees (age: 47±16 yrs, mass: 104±10 kg, height: 175±8 cm) participated in this study. All were fully ambulatory, used energy storing prostheses, and maintained some degree of physical activity in their vocational or daily activities.

Inertial properties of each participant's prosthesis were measured using oscillation and reaction board techniques. Seven load conditions were studied (2 loads x 3 positions) plus an unloaded baseline condition (NL). 100% and 50% of the estimated mass difference between the intact and prosthetic legs were added at each of the following load positions: a) near the prosthetic ankle, b) near the prosthesis center of mass, and c) near the prosthetic leg's thigh center of mass. Participants walked at their measured preferred velocity for all walking conditions. Temporal and metabolic data were measured while participants completed 10 min treadmill walking trials under each load condition. In a separate session, kinematic data were measured while participants walked overground under the same load conditions.

Symmetry indices (SI) were computed for stance time, swing time, and knee and thigh angular positions and velocities to determine the effects of the loading configurations on walking symmetry:

$$SI = \frac{(P - I)}{0.5 * (P + I)} * 100$$

where P and I refer to prosthetic and intact legs. Nine planned contrasts were used to statistically identify significant ($p < 0.05$) effects due to the different load configurations.

RESULTS AND DISCUSSION

Metabolic cost increased significantly compared to NL regardless of load position (Figure 1). Cost increased to a greater extent for more distally positioned loads. Our results do not support previous findings (Selles et al., 2004a) of a reduced muscular cost for proximally positioned masses. Adding mass distally to the prosthetic leg also increased stance and swing time asymmetries. However, adding mass to the prosthesis COM or thigh COM had little or no effect on temporal asymmetries (Figure 1). Increased stance time asymmetries were due primarily to increased stance time of the intact leg, whereas increased swing time asymmetries were due primarily to increased swing time of the prosthetic leg. Temporal walking symmetry did not improve with any of the load configurations. Thigh kinematics of the prosthetic leg exhibited the greatest effects due to load, which was consistent with previous findings (Selles et al., 2004b). Specifically, thigh angular velocity of the prosthetic leg was reduced by adding mass; distally positioned loads had the greatest effect on thigh angular velocity.

SUMMARY/CONCLUSIONS

Adding mass proximally to the prosthetic leg did not improve walking symmetry or reduce metabolic cost during walking. It appears that the use of lightweight prostheses minimize metabolic costs and walking asymmetries.

REFERENCES

Gailey, R. S. et al. (1994). *Prosthet Orthot Int*, **18,** 84.

Lehmann, J. F. et al. (1998). *Arch Phys Med Rehabil*, **79,** 162.

Royer, T. D., and Wasilewski, C. A. (2006). *Gait Posture*, **23,** 303.

Selles, R. W. et al. (2004a). *Disabil Rehabil*, **26,** 694.

Selles, R. W. et al. (2004b). *Arch Phys Med Rehabil*, **85,** 2046.

ACKNOWLEDGEMENTS

Funding was provided by grants from the American Society of Biomechanics and the International Society of Biomechanics.

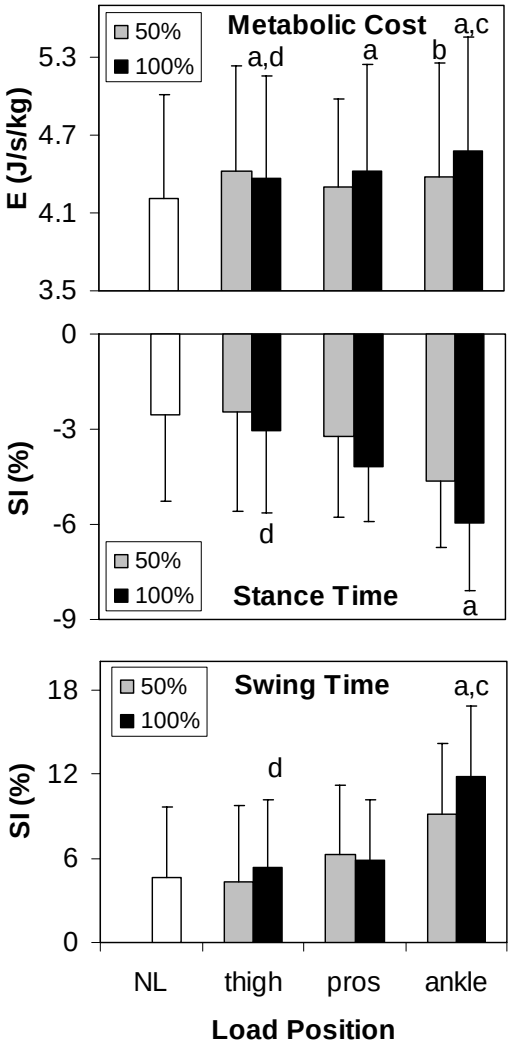

Figure 1: Load effects on metabolic cost, stance time symmetry, and swing time symmetry (means ± SD).
a – NL vs 100% mass for load position
b – 50% vs 100% mass for load position
c – 100% ankle vs 100% pros
d – 100% ankle vs 100%

EFFECT OF FACET ARTHROPLASTY ON THE BIOMECHANICS OF THE LUMBAR SPINE – A FINITE ELEMENT STUDY

Sasidhar Vadapalli, Jorge A. Ochoa, and David M. Rosler
Archus Orthopedics Inc., Redmond, WA
E-Mail: svadapalli@archususa.com, Web: www.archususa.com

INTRODUCTION

Spinal stenosis is due to the encroachment of the spinal neural foramina by hypertrophic facets and displaced soft tissues, which compress the nerve roots, often resulting in functional impairment due to neurological symptoms in the legs. Surgical decompression with instrumented fusion, which restricts mobility of the spine at the operated level, is the current standard of care. The incidence of reoperation post-decompression due to adjacent level disease can be as high as 20% [Gillet, P., 2003].

The Total Facet Arthroplasty System® (TFAS®) (Archus Orthopedics Inc., Redmond, WA) is a novel device designed to treat spinal stenosis. TFAS® allows a comprehensive decompression by complete removal of the facets and lamina. TFAS® is intended to stabilize the spine and reinstate proper segmental biomechanics. We hypothesize that TFAS® will: (1) maintain the physiological range of motion at the operated level and (2) will not overload the disc at the operated or adjacent levels. TFAS® is currently undergoing clinical trials in the United States.

METHODS

A 3-dimensional, nonlinear finite element (FE) model of an intact (Intact) adult human lumbar spine (L1-Sacrum) was developed (Figure. 1A). The geometry was derived from the MRI scan of a single subject. The intact FE model was validated by comparing the range of motion (ROM) calculated after applying pure flexion/extension (+8.0/-6.0 Nm), unilateral bending (6.0 Nm) and unilateral rotation (5.0 Nm) moments to equivalent experimental results generated on a cadaveric spine simulator [Phillips, F.M. et al., 2006].

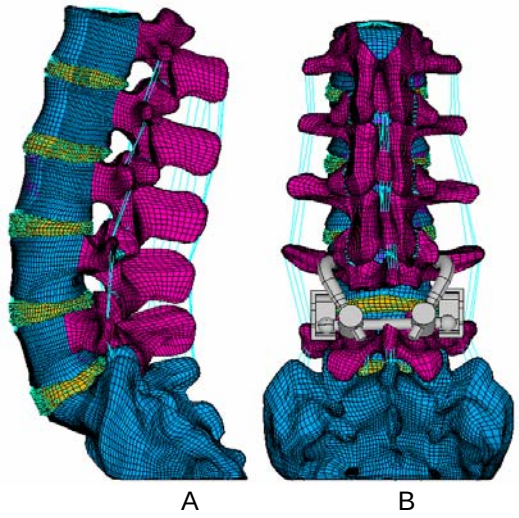

Figure 1: (A): Intact and (B): TFAS models

The intact model was modified to include the TFAS® at the L4-L5 level (TFAS) (Figure 1B). The TFAS® surgical technique was simulated by removing all of the supraspinous and interspinous ligaments, ligamentum flavum and facets across L4–L5 and the majority of the L4 spinous process and lamina. Interactions of the natural facets and TFAS® bearings were defined as nearly frictionless generalized contact between deformable bodies. Finally, the model was modified to simulate a posterior fusion (Fusion) with instrumentation at the L4-L5 level. The TFAS® and fusion hardware were rigidly anchored at the pedicles. All models were rigidly constrained at the sacrum and pure moments

were applied to L1. The analysis was performed using ANSYS v10.0 FE software.

Each loading mode was analyzed at its loading limits at the operated and immediately adjacent levels for: (1) peak ROM and (2) strain energy density (SED) in the disc. These measurements were used to evaluate how the different treatment modalities affected the segmental kinematics and load sharing of the intervertebral discs.

RESULTS AND DISCUSSION

The TFAS® replicated the intact ROM at the instrumented segment (L4L5) in all loading modes, while the Fusion model reduced ROM (Figure. 2).

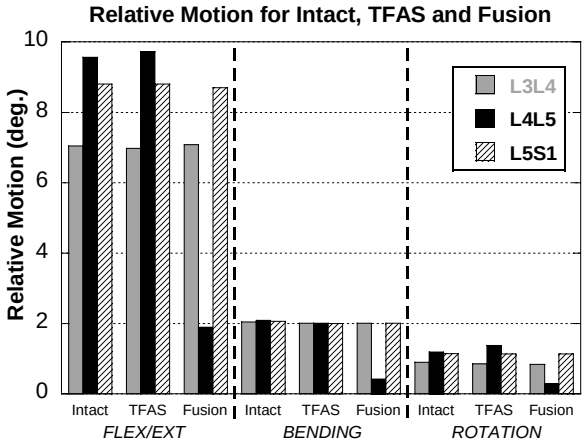

Figure 2: ROM for Intact, TFAS and Fusion at instrumented and adjacent levels.

For Fusion, the SED (Table 1) in the L4-L5 disc was reduced in all loading cases, indicating an unloading of the disc tissue.

The TFAS model generally replicated intact disc tissue SED's at the operated and adjacent levels. The strain energy in the disc at the adjacent levels (L3-L4, L5-S1) for fusion did not change compared to Intact, which is counter-intuitive and requires further investigation.

SUMMARY/CONCLUSIONS

The inclusion of TFAS® at the L4-L5 segment maintained the mobility of the spine at the operated level with no effect on the motion at the adjacent levels. Additionally, the loading of the intervertebral disc at the operated level was more akin to the intact condition with TFAS® than with fusion.

To better understand the effect of fusion on adjacent levels, a loading protocol where the moments applied to the Fusion model are varied until their overall angular motion is equal to that of the intact case (hybrid approach [Goel, V.K. et al., 2005]) may provide a more relevant comparison of pre-and-post fusion function of the spine.

REFERENCES

Gillet, P. (2003). *J Spinal Disord Tech*, vol. **16:4**, pp. 338–345.

Phillips, F.M., Voronov, L.I. et al. (2006). *The Spine Journal*, vol. **6:5** (Supplement), p. 137S.

Goel, V.K., Grauer, J.N. et al. (2005). *Spine*, vol. **30:24**, pp. 2755–2764.

Table 1: Comparison of SED (Joules·mm^{-3}) of the disc under load for Intact, TFAS and Fusion.

Disc Level	FLEX/EXT			BENDING			ROTATION		
	Intact	TFAS	Fusion	Intact	TFAS	Fusion	Intact	TFAS	Fusion
L3-L4	604	602	603	180	181	182	48	47	47
L4-L5	686	829	37	236	225	10	76	95	6
L5-S1	960	964	953	158	158	158	78	77	76

OPTIMALITY OF ANTAGONIST CO-CONTRACTION

Manoj Srinivasan
Princeton University, Princeton, NJ, USA
E-mail: msriniva@princeton.edu, Web: www.tam.cornell.edu/~ms285

INTRODUCTION

I ask you to close your eyes and hold your hand out. I then inform you that I will hit your hand at some uncertain time. Your goal is to keep your hand as still as possible. What do you do? You stiffen your hand in anticipation of the impulsive perturbation.

Stiffening or co-contraction of nominally antagonist muscles is a well-known stabilizing mechanism. By such co-contraction, we take advantage of the force-length, force-velocity, and possibly other history-dependent intrinsic properties of skeletal muscles to create a fast-responding (often) stable system.

On the other hand, co-contraction is reasonably characterized as muscles fighting against each other, and is therefore considered wasteful of metabolic energy. While energy optimization has proven relatively successful in predicting muscle coordination in a variety of tasks, it cannot predict co-contraction in simple tasks since strategies involving co-contraction are typically energetically sub-optimal.

Hogan (1984) derived co-contraction of antagonist muscles as an open-loop solution to a stochastic optimal state regulator problem of trying to keep an arm vertical (an unstable position) in the presence of random Gaussian perturbations.

Here I elaborate this idea to the Bayesian setting (Koerding and Wolpert, 2004) described in the first paragraph here: you want to resist an external force about which you have some but not all information.

METHODS

I consider the simplest setting in which these questions can be reasonably analyzed: a one degree-of-freedom system that can be visualized as a single-link arm with two uni-articular muscles or a single mass connected two antagonist muscles, as shown in Figure1. The two muscles have simple (linear and identical) force-length and force-velocity properties. The activation to these muscles can be any arbitrary function of time.

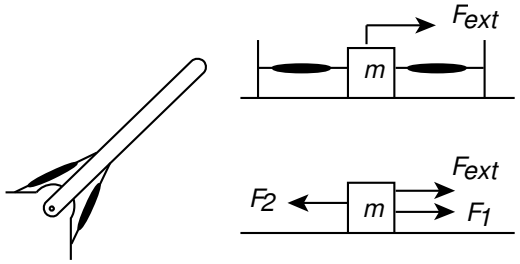

The mass is subject to a possibly uncertain time-varying external force $F_{ext}(t)$. The timing and magnitude of this external force is drawn from a Gaussian or a uniform probability distribution about a certain mean. The variance of the timing and the magnitude determines the amount of uncertainty in the external force.

The objective is to keep the mass (or the arm) as still as possible in an averaged sense given the uncertainty and not waste too much energy in the process.

We numerically solve a variety of stochastic optimal control problems: with and without state feedback, with varying amounts of noise an delay in the feedback, and with

varying amounts of prior uncertainty in the external force, and with varying relative weights for the cost of position error (task) versus the metabolic cost (here, integral of squared muscle forces). We assume for simplicity that muscles are noiseless actuators, unlike in Todorov (2002).

RESULTS AND DISCUSSION

When there is no uncertainty in $F_{ext}(t)$, the external force can be exactly cancelled by the muscle forces. However, there are infinitely many open-loop solutions that exactly cancel the external force, since there are two muscles. The solution that minimizes energy from among these position-error minimizing solutions consists of muscle-2 exactly canceling the external force and muscle-1 producing no force at all: $F_2(t) = F_{ext}(t)$ and $F_1(t) = 0$.

As soon as a small amount of uncertainty is introduced into the external force timing, we find that the open-loop energy-minimizing solutions from among the position-error minimizing solutions have substantial co-contractions. Not surprisingly, we find that there is co-contraction observed is not wasteful, but is rather anticipatory – the muscles co-contract only when there is likely to be an external force.

Finally, when there is substantial temporal uncertainty in the prior knowledge of the external force, the optimal open-loop response seems essentially to co-contract both muscles completely and to nearly equal extents (with F_1 a little less than F_2).

Some preliminary observations on the effect of feedback: the limit of perfect state-feedback in absence of any prior knowledge of the external force approaches, in performance, of open-loop limit in the presence of perfect prior knowledge of the external force. As the state-feedback is made noisy and delayed with no prior information about the external force, we approach the limit of open-loop control, also with no prior information about the external force.

SUMMARY/CONCLUSIONS

I have presented a theory of co-contraction in a simple context – a theory that agrees overall with our expectations of what such a theory must predict. This theory can be extended to many degree-of-freedom systems. It can also be modified to reflect noise in muscle activation (Todorov and Jordan, 2002). Current work is aimed at understanding in greater detail the effects of various noise effects in the presence of feedback.

The simple problem here has close connections to a variety of contact problems, such as leg contacting the ground with some uncertainty during legged locomotion and a finger contacting a surface during manipulation. The primary utility of the simple example, however, is to understand the various simple things that can happen in the presence of uncertainty in a biomechanical system without much of the attendant dynamical complexity.

REFERENCES

Hogan, N. (1984) *IEEE Transactions on Automatic Control*, AC-29, 681-690.

Todorov, E. and Jordan, M. (2002). *Nature Neuroscience,* 5, 1226-1235.

Koerding, K.P., Wolpert, D.M. (2004) *Nature,* 427, 244-247.

ACKNOWLEDGEMENTS

This research was supported by NSF FIBR grant **0425878**.

FUNCTIONAL HETEROGENEITY WITHIN AND BETWEEN HIND LIMB MUSCLES DURING RUNNING IN GUINEA FOWL

Timothy E. Higham and Andrew A. Biewener

Harvard University, Bedford, MA, USA
E-mail: thigham@fas.harvard.edu

INTRODUCTION

Terrestrial vertebrates employ limb muscles to control movements of the skeletal system or to counterbalance loads (Biewener and Gillis, 1999). The complex activation patterns within muscles have long been identified using electromyography (e.g. English, 1984) and, in recent years, some of the complex patterns of *in vivo* muscle length changes have been elucidated using techniques such as Magnetic Resonance Imaging (Pappas et al., 2002), geometric modeling (Gregor et al., 2006), and sonomicrometry (Soman et al., 2005).

Muscles are often heterogeneous, exhibiting spatial variation in recruitment, fiber type composition, and force generation. Unequal shortening within a muscle can be due to several factors including, for example, muscle architecture (Pappas et al., 2002) and fiber type regionalization (Chanaud and Macpherson, 1991). Understanding how this heterogeneity in muscle shortening translates into overall muscle function is imperative for understanding how the musculoskeletal system can adapt to changes in demand placed upon the locomotor system.

Muscle synergists, such as the lateral (LG) and medial (MG) gastrocnemius muscles of terrestrial vertebrates, can also vary considerably in fiber type composition, architecture and recruitment patterns. Having multiple muscles acting at the same joint provides flexibility with regards to optimal function. For example, one of the muscles might be optimized for ballistic movements while another might be optimized for slow, steady movements. Understanding the differences in function between synergists will provide insight into the role of redundancy in the musculoskeletal system.

The goals of this study are to address the following two questions using guinea fowl: 1) Do the proximal and distal regions of the MG exhibit similar fascicle strain and activation patterns? 2) Do the MG and LG exhibit similar fascicle strain, activation and force patterns?

METHODS

Adult guinea fowl (*Numida meleagris*) were used in this study, and data were collected from four individuals. Each individual was trained to run on a motorized treadmill. Muscle activation patterns were quantified by inserting fine-wire bipolar EMG hook electrodes into the proximal and distal regions of the LG and MG. Muscle length patterns were quantified by inserting 2mm sonomicrometry crystal pairs into the two muscles. One pair was implanted into the LG and two pairs (proximal and distal locations) were implanted into the MG. The two crystals of a pair were separated by approximately 1cm. Forces exerted on the tendons of each muscle were measured using E-type stainless steel tendon buckle force transducers. One high-speed Photron camera (250 frames per second) was used to capture hind limb movements of the guinea fowl during the experiment.

In order to alter the demand placed upon the locomotor system, each bird ran on a level and uphill surface, and at speeds ranging from 0.5 m/s to 2.5 m/s. Following each experiment, the bird was euthanized and the location of the electrodes and crystals were verified. Several morphological measurements were recorded for the muscles and tendons.

RESULTS AND DISCUSSION

Activation of the LG and MG preceded the onset of force, which occurred at the beginning of the stance phase of the stride. The onset of force generation in the LG was coincident with footfall, whereas the MG began generating force after the LG by an average of 6.6±0.8 ms (Fig. 1). The MG and LG differed in the amount of force generated relative to the amplitude of their fascicle strain patterns, indicating that work output differed between these muscles.

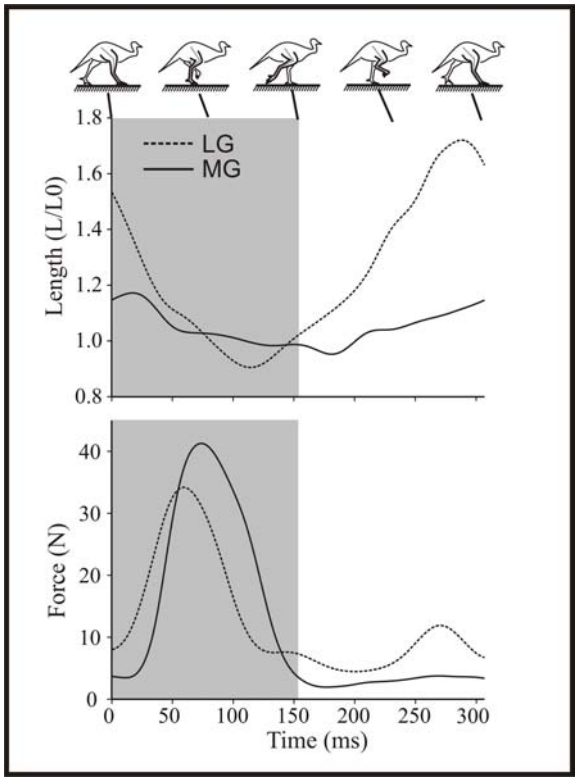

Figure 1: *Relative length (upper panel) and force (lower panel) from the lateral (LG) and medial (MG) gastrocnemius muscles for a guinea fowl running on a level treadmill at a speed of 2 m/s. Note that the shaded area indicates the stance phase of the stride.*

Fascicle strain was greater in the proximal MG compared to the distal MG at all speeds and inclines. For example, when running on a level surface at a speed of 2 m/s, the proximal and distal MG shortened at the beginning of stance by 17±0.4% and 1±0.1%, respectively. This suggests that the proximal portion of the MG is doing more work and contributing more to power production at the ankle than the distal portion of the MG. The decrease in strain along a proximal-distal axis appears to be a common theme within muscles as well as within limbs of terrestrial vertebrates.

REFERENCES

Biewener, A.A., Gillis, G.B. (1999). *J. Exp. Biol.*, **202**, 3387-3396.

Chanaud, C.M., Macpherson, J. M. (1991). *Exp. Brain Res.*, **85**, 271-280.

English, A.W. (1984). *J. Neurophysiol.*, **52**, 114-125.

Gregor, R. J. et al. (2006). *J. Neurophysiol.*, **95**, 1397-1409.

Pappas, G. P. et al. (2002). *J. Appl. Physiol.*, **92**, 2381-2389

Soman, A. et al. (2005). *J. Exp. Biol.*, **208**, 771-786.

ACKNOWLEDGEMENTS

This research was supported by NIH Grant AR047679. We thank Pedro Ramirez for animal care.

THE OPTIMAL RELEASE ANGLES OF ELITE DISCUS THROWERS

Steve Leigh[1], Hui Liu[2], and Bing Yu[1]

[1] The University of North Carolina at Chapel Hill, USA
[2] Beijing University of Sports, Beijing, China
E-mail: stvleigh@email.unc.edu, Web: www.med.unc.edu/ahs/physical/ctrhmschome.htm

INTRODUCTION

The official distance achieved by a discus thrower has three components: the vacuum flight distance, the aerodynamic distance, and the distance lost at release. The vacuum flight distance is dependent on discus release characteristics: the resultant release velocity, and the release angle and height. The release angle significantly affects the vacuum flight distance, the aerodynamic distance (however this relationship may be non-linear), and, therefore, the official distance (Bartlett, 1992; Hay & Yu, 1995).

Optimal release angles have been determined from elite athletes' data and wind tunnel testing (Bartlett, 1992). These optimal angles were based on two assumptions: (1) release angle and resultant release velocity are independent, and (2) the optimal release angle is the same for all throwers. These two assumptions have not been validated. The optimal angles currently recommended may contain significant errors.

The purposes of this study were to determine the relationships between the release angle and the resultant release velocity, and between the release angle and the aerodynamic distance, and to determine the optimal release angle for single athletes.

METHODS

Two video camcorders were used to record 3 female and 3 male elite discus throwers' performances in actual competitions with a setup for the DLT procedure. At least 10 trials by each athlete were analyzed. Twenty-one body landmarks and the discus center were digitized for each trial (Hay & Yu, 1995). 3-D coordinate data were obtained using the DLT procedure (Abdel-Aziz & Karara, 1971). Release parameters were reduced for each trial (Hay & Yu, 1995).

Multiple regression analyses were performed to express the resultant release velocity and the aerodynamic distance as functions of the release angle for each subject. A forward selection procedure was used to determine the power of the best regression equation for each subject. The vacuum flight distance was estimated from the resultant release velocity and the release angle. The official distance was calculated as a sum of the estimated vacuum flight distance, the aerodynamic distance, and the distance lost at the release (Hay and Yu, 1995). The regression equations were applied to express the official distance as a function of the angle of release for each subject. A computer simulation was performed to determine the official distances within a range of release angles (30°-50°). The release angle corresponding to the longest official distance was considered the optimal release angle for a given subject.

RESULTS AND DISCUSSION

All subjects had linear relationships between the resultant release velocity and the angle of release. The regression coefficients for the release angle and resultant release velocity relationship varied among subjects.

The regression coefficients tended to show that the resultant release velocity decreased as the angle of release increased. The regression determinant for the resultant release velocity as a function of the release angle varied from 0.28 to 0.51 ($p < 0.01$). These results demonstrate that the resultant release velocity was affected by the angle of release for individual throwers. Increasing the angle of release resulted in a decrease in the release velocity. This indicates that increasing the vertical release velocity of the discus may result in a disproportionate decrease the horizontal release velocity because of the limited strength and power of the thrower. The dependency of the resultant release velocity on the release angle does not support the first assumption in the determination of optimal release angles from aerodynamic data alone. The relationship between the resultant release velocity and the release angle may depend on the physical and technical characteristics of an athlete. Further research is necessary to determine these physical and technical characteristics and how they relate to the optimal release angle.

Five of the throwers had linear relationships between the aerodynamic distance and the angle of release. The regression coefficients for the release angle and aerodynamic distance relationship varied among subjects. For four of the six throwers, the regression coefficients suggest that the aerodynamic distance increased as the angle of release increased. The regression coefficient for one subject suggests that the aerodynamic distance decreased as the angle of release increased. The regression determinants of the aerodynamic distance as a function of the release angle varied from 0.18 to 0.65 ($p < 0.01$) for five throwers. These results suggest that the aerodynamic distance is correlated with the release angle for most of the subjects. Our results, which show that increasing the release angle would increase the aerodynamic distance, are consistent with wind tunnel data. Aerodynamic data is important when calculating optimal release angles. Our results show that the relationship between the release angle and the resultant release velocity affects the optimal angle calculations.

The simulated official distance had a single maximum, which occurred with a release angle between 30° and 50° for all subjects. The optimum release angle varied among subjects, which does not support the second assumption in the determination of optimal release angles from aerodynamic data alone. The simulated optimal release angles for four subjects were similar to the mean release angles of elite discus throwers in the current literature. The simulated optimal release angles for two subjects were significantly greater than range of optimal release angles reported in the current literature. These results indicate that the release angles used by elite discus throwers are not necessarily optimal for a given individual elite discus thrower.

CONCLUSIONS

The optimal release angle for a given thrower is affected by both aerodynamic factors and their physical and technical characteristics. All these factors and characteristics should be carefully considered when determining the optimal release angle for a given athlete.

REFERENCES

Abdel-Aziz YI and Karara HM (1971). *ASP Symposium on Close Range Photogrammetry,* ASP, Falls Church, VA.

Bartlett, R.M. (1992). *Journal of Sports Sciences,* **10**, 467-510.

Hay, J.G. and Yu, B. (1995). *Journal of Sports Sciences,* **13**, 125-140.

SHOULDER MECHANICS: ANALYTICAL MODELING AND VALIDATION

Sarah R. Sullivan [1], Noshir A. Langrana [1], and Sue Ann Sisto [2]

[1] Rutgers University, Piscataway, NJ, USA
[2] Human Performance and Movement Analysis Laboratory (HPMAL), Kessler Medical Rehabilitation Research and Education Corporation (KMRREC), West Orange, NJ, USA
E-mail: sarsulli@eden.rutgers.edu

INTRODUCTION

In the US, more than 10,000 spinal cord injuries are reported each year. This population depends upon their upper limbs to provide a means of locomotion. Upper limb pain and pathology is common among manual wheelchair users due to this dependency on upper limbs. This study focuses on two-issues: 1.) Develop and refine a computational model using the AnyBody Modeling System (Damsgaard, 2006) that quantifies the contribution of various muscles on shoulder joint forces (Sullivan 2005); 2.) Generate confidence in this model by validating the computational Modeling System used in this study (Damsgaard, 2006).

METHODS

Part I: Our Shoulder Model

A computational biomechanical model of the shoulder was constructed as previously reported (Sullivan, ASME 2005) (Figure 1). The resulting shoulder joint forces were calculated via inverse dynamics in the AnyBody Modeling System, and the joint force profiles were analyzed.

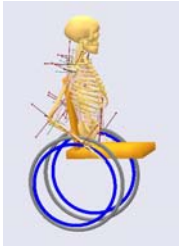

Figure 1: Model Set-up

Part II: Validation

Two models of varying complexity were created to validate the mathematics within the software. A two-dimensional (Figure 2a) and three-dimensional (Figure 2b) musculoskeletal model of a two-segment arm-complex doing a bicep curl was created using the AnyBody Modeling System (Damsgaard, 2006). Segment and muscle properties were based on the data and modeling assumptions of the Dutch Shoulder Model (van der Helm, 1992). The elbow joint was held in 90^{o} flexion with the upper arm perpendicular to the ground, while the distal end of the lower arm statically held a 5-pound dumbbell. An inverse-dynamics analysis was run, and the resulting muscle and joint forces for both 2D and 3D scenarios were compared to the results from long-hand calculations.

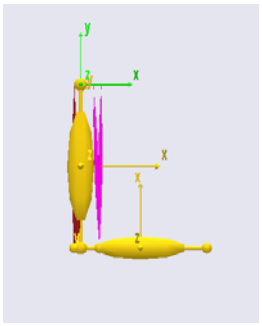

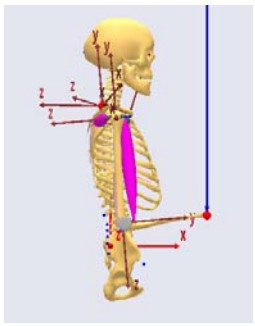

Figure 2a (left): Initial rigid-body 2-segment model
Figure 2b (right): 3-D skeleton

RESULTS

Part I:

Previous studies have reported peak glenohumeral (GH) joint forces during the push phase to be between 800 and 1400 N, with quasistatic push phase forces being upwards of 2000 N (Van der Helm 1996, Veeger 2002). Our shoulder model produced

feasible results with maximal GH reaction forces falling within this range (Figure 3).

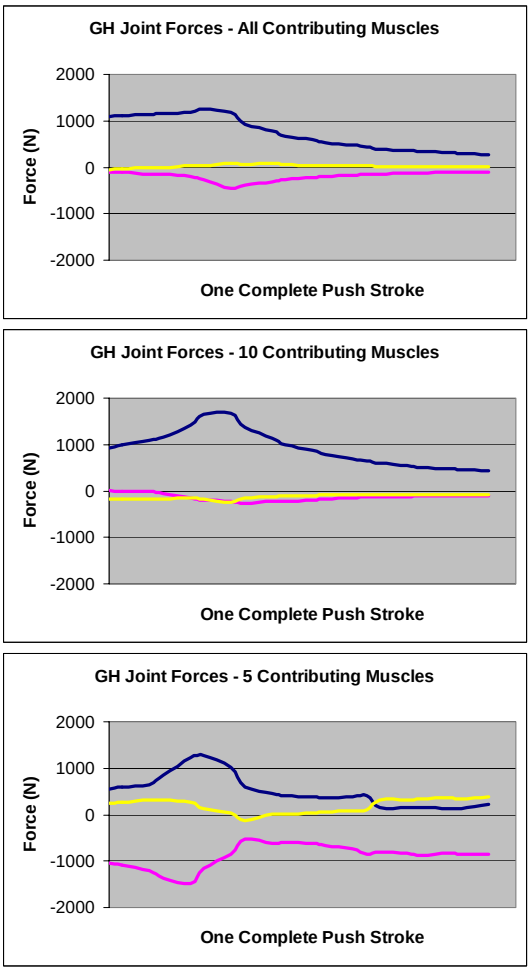

Figure 3: Resulting joint reaction forces based on muscle-input into the model (x-dir: blue, y-dir: pink, z-dir: yellow - ISB). Top: all upper-body musculature. Middle: only coracobrachialis, infraspinatus, latissimus dorsi, levator scapula, rhomboids, serratus anterior, subscapularis, supraspinatus, and teres major and minor. Bottom: Only pectorals, deltoids, biceps, triceps, and trapezius.

Part II:

Muscle and joint reaction force results were comparable to those calculated analytically from force and moment equations. Results were as follows (Newtons): B (biceps) =103.9; T (triceps) =12.4, Fx=-5.3, Fy=-248.6, Fx'=2.8, Fy'=-156.7. Based on PCSA, B and T contributions were factored as follows: B_B(breve)=103.9; B_L(long)=107.6; $T_{LA\ 1\&2}$(lateral)=12.4; $T_{ME\ 1\&2}$(medial)=23.5; $T_{LH\ 1\&2}$(long)=0. These results are identical to the muscle and joint reaction outputs calculated by AnyBody.

SUMMARY

Varying the muscle contributions in the model has a profound effect on the resulting shoulder joint reaction forces calculated by AnyBody (Figures 3). Confidence in these results can be established through multiple validations. By completely validating simple, and then more complicated physiologically-representative models through analytical equations, confidence in the mathematics within AnyBody software can be obtained. The fact that there was parity in muscle forces between AnyBody outputs and long-hand calculations validated the mathematics within the software. This will, in turn, lend confidence to future patient-specific modeling results.

REFERENCES

Damsgaard M, et al. (2006). *Simulation Modelling Practice and Theory*, **14**, 1100.

Sullivan S, et al. (2005). *The Proceedings of ASME IDETC/CIE*.

Sullivan S, et al. (2006). *The Proceedings of BMES Conference.*

Van der Helm FC, et al. (1992). *J. Biomech.* **25**, 129-144.

Van der Helm FC, et al. (1996). *J. Biomech.* 29: 39-52.

Veeger, HEJ, et al. (2002). *Clin. Biomech.* **17** (3): 211-8.

ACKNOWLEDGEMENTS

Funding and lab resources provided by NSF GK-12 Fellowship, KMRREC, and HHK.

MAGNETIC RESONANCE IMAGE SEGMENTATION FOR BIOMECHANICAL MODELING OF THE ORBIT

Qi Wei [1, 2] , Joseph L. Demer [3], Joel M. Miller [4], and Dinesh K. Pai [1, 2]

[1] Rutgers University, New Brunswick, NJ, USA
[2] University of British Columbia, Vancouver, BC, Canada
[3] Jules Stein Eye Institute and Department of Neurology, David Geffen Medical School at University of California, Los Angeles, USA
[4] Smith-Kettlewell Institute, San Francisco, CA, USA
E-mail: pai@cs.ubc.ca, Web: www.cs.ubc.ca/~pai

INTRODUCTION

It is difficult to understand the mechanical and neural contributions of the extraocular muscles (EOMs) and connective tissues to eye movement without simulating a realistic, biomechanically complete model. We present a semi-automatic method to acquire 3D functional models of the orbit from magnetic resonance (MR) images with the orbit in different gazes. Having structural models, we mechanically model each EOM by several *strands* (Sueda and Pai 2007), that are physically-based dynamic cubic spline curves with mass. The resulting strand can be computationally simulated. Efficient and accurate reconstruction of patient-specific orbital models has important applications in clinical diagnosis and realistic surgical planning.

METHODS

Previous approaches to orbit reconstruction have been based on time consuming manual image segmentation. Our approach combines deformable model fitting to dense point clouds and adaptive feature selection. We first build a template of the orbit including the orbital wall, the globe, the optic nerve, and the extraocular muscles. Since the topological relationship of these structures is fixed and the geometric variation of these structures over gazes and among subjects is small, we could fit this carefully constructed template to new image data by deforming it to fit the detected features. Using the template to define a prior probability that encodes background knowledge of orbital anatomy, estimating new models is more efficient and robust.

Each structure is represented by a cubic B-Spline surface, which can be deformed smoothly and locally by moving its control points. It is an efficient yet powerful modeling primitive. To fit a mesh to a new set of feature points, a total least-square optimization is performed to compute the new positions of the control points such that the total distance of the data points to the resulting surface is minimized (Hoschek and Lasser, 1993). In order to deal with the nonuniform distribution of the points and the difficulty of detecting EOM tendons, two quadratic regularization terms are introduced to the objective function.

$$\min_x \left(\|Ax - P\|_2^2 + \alpha F_{smoothness} + \beta F_{self} \right)$$

Given a new subject, we first apply an affine registration method to align the template with the data in the primary gaze. A subject-specific template is then generated by fitting the registered template to the primary gaze using the techniques described in the following. Multiple structures appear in the images. It is not a trivial problem to classify the features into different objects (see Figure 1). We propose to use 3D spatial information and 2D image intensity information adaptively and iteratively to

select features and perform surface fitting.

For each structure, features are first pruned based on their 3D distances to the B-Spline mesh. Feature points far away are discarded. The remaining points are selected incrementally such that the polygonal region formed in the image shows similar intensity distribution to what EOM shows in MR images. Kullback Leibler distance is used as the similarity measurement. This is repeated several times to improve robustness. After features are selected for all objects, B-Spline surface fitting is performed for each of them by computing new positions by least-squares optimization. We apply feature selection and fitting alternatively until the template converges to the data.

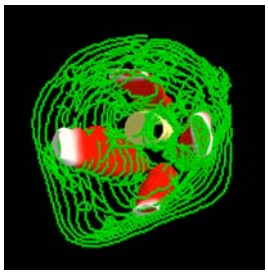

Figure 1. The subject template consists of four rectus muscles and the optic nerve, all represented by B-Spline surfaces. The feature points in abduction are shown in green and are computed by applying Canny edge detection on the images.

To simulate the model using the strand-based simulator, we represent each EOM by one or more strands. Using multiple strands, larger muscles can be realistically modeled. The orbital and global layers of EOMs can also be considered. We have developed an approach to generate multiple strands with reasonable configurations given the geometry by solving a quadratic constrained linear programming problem (QCLP) and inverse freeform deformation (IFFD).

RESULTS AND DISCUSSION

Each data set contains 18 coronal MR images. The image and slice resolutions are 0.315^2 mm and 2 mm, respectively. The models in Figure 2 can be used in simulation and many other applications.

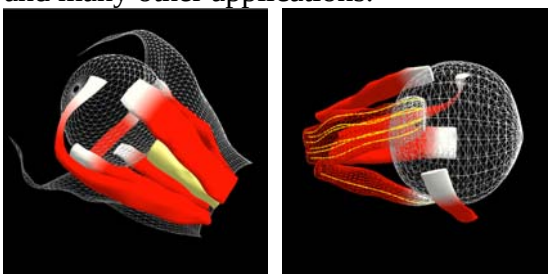

Figure 2. Reconstruction a right orbit in central gaze. Various numbers of strands (shown as yellow curves in the figure on the right) can be used to model EOMs for various simulation requirements.

SUMMARY/CONCLUSIONS

We present a semi-automatic computational framework to generate subject-specific biomechanical models of the human orbit efficiently and robustly. It can be extended to other reconstruction applications. Combining axial strain estimation method based on volume preservation (Wei, et al. 2007), mechanically correct functional models can be generated.

REFERENCES

Sueda, S., Pai, D.K. (2007). Strand-based Simulation of Tendonous Systems. American Society of Biomechanics Abstract (submitted).

Hoschek, J., Lasser, D. (1993). Fundamentals of Computer Aided Geometric Design. A. K. Peters.

Wei, Q. et al. (2007). Strain Estimation in Muscles, Tendons, and other Incompressible Generalized Cylinders. To be submitted.

ACKNOWLEDGEMENTS

This research was supported in part by a Canadian Research Chair and NIH grant R01NS050942, U.S. Public Health Service, National Eye Institute grant EY08313.

EVALUATION OF THE ASSESMENT OF SYMMETRY DURING GAIT

Daniel J. Gales [1,2] and John H. Challis [1]
[1] Biomechanics Laboratory, Department of Kinesiology, The Pennsylvania State University, University Park, PA, USA
[2] Lock Haven University of Pennsylvania, Lock Haven, PA, USA
E-mail: djg153@psu.edu

INTRODUCTION

Asymmetry between the two sides of the body during gait has been associated with musculoskeletal disorders (Sadeghi et al., 2000). A number of different methods have been used to quantify gait symmetry. For example, Herzog et al. (1989) utilized a symmetry index (SI), computed as percentage of the difference between the two sides relative to the mean of the two sides in some gait parameter. Others have used statistical methods for assessing the presence of asymmetry including correlation coefficients and coefficients of variation (Sadeghi et al., 2000). To eliminate the influence of the magnitude of the variable when computing an index based on a ratio, Zifchock and Davis (2006) utilized a symmetry angle (SA) to assess symmetry in gait parameters.

Researchers examining ground reaction force symmetry during running have reported contrasting results. Hamill et al. (1984) used 10 footfalls from each leg to examine ground reaction force symmetry in 10 subjects. They used the SI, and concluded during walking and running that there was symmetry in the ground reaction force parameters. Munro et al. (1987) used six footfalls from each leg to examine ground reaction forces in running in 20 subjects. They identified right-left asymmetries.

Zifchock and Davis (2006) showed that two different normalization procedures can result in alternative interpretations regarding gait symmetry. They argued that the symmetry index can artificially inflate results and introduced a new method for assessing symmetry, the symmetry angle.

All studies to date have only analyzed a limited number of footfalls when assessing gait symmetry; the validity of this approach has not been examined. The purpose of this study was therefore twofold, first to examine the differences between the symmetry index and the symmetry angle for assessing gait symmetry, and secondly to assess if this number of footfalls analyzed influences the assessment of gait symmetry.

METHODS

Eight healthy young adult subjects with mean age 24.6 years ± 3.5, and body weight 627.0 N ± 61.8 voluntarily participated in this study. All subjects were experienced runners with no known musculoskeletal or neurological pathology.

The subjects ran on a treadmill for 1662.6 steps ± 79.4 at their self-selected preferred velocity of running (3.48 m/s ± 0.9) for 600 seconds. The treadmill was a Kistler Gaitway Instrumented Treadmill, which has two force plates beneath the treadmill belt. From these force plates, vertical ground reaction force (VGRF) and center of pressure (COP) data were collected at 250 Hz. These data were filtered with a 2nd order Butterworth filter with a cut-off of 30 Hz. The start and end of footfalls were identified using a 30 N threshold and data below this value were assumed to be noise.

From the force and COP two parameters were selected for further analysis: step time and peak impact VGRF. To quantify the symmetry two symmetry measures were computed. The symmetry index (SI) was computed using the following equation:

$$SI = \frac{(X_R - X_L)}{0.5(X_R + X_L)} * 100$$

The symmetry angle (SA) was computed using the following equation:

$$SA = (45 - \arctan(X_L / X_R)) / 90 * 100)$$

where X_R, X_L are gait parameters measured for the right or left limb respectively. For each subject from their 600 seconds of collected data 10 footfalls were selected at random and the gait symmetry computed using the subsequent four footfalls per foot, giving 10 estimates for each subject of gait symmetry.

RESULTS AND DISCUSSION

Table 1 indicates the number of times for each subjects the SI and SA indicated they were right or left asymmetrical for their step times and peak impact VGRF. For step times there were inconsistencies between the two measures of symmetry, and across trials in how each subject was classified (i.e., either right or left asymmetrical). For the peak impact VGRF the SI and SA were identical indicating these measures produced similar indicators of symmetry for this gait parameter. There were for the majority of subjects inconsistencies across trials of how symmetry was classified.

For step time, consider for example subject 5, depending on what portion of the complete data set is analyzed this subject could be classified as right or left asymmetrical. These results indicate that four footfalls per leg are not sufficient to classify gait symmetry, and that alternate methods of measuring symmetry do not overcome this weakness. There needs to be further research to both identify suitable measures of gait symmetry, and the appropriate number of footfalls with which to assess gait symmetry

REFERENCES

Hamill, J. (1984). *Res Q Exerc Sport, 55*(3), 289-293.

Herzog, W., et al. (1989). *Med Sci Sports Exerc, 21*(1), 110-114.

Munro, C.C.F., et al. (1987). *J Biomech, 20*(2), 147-155.

Sadeghi, H., et al. (2000). *Gait Posture, 12*(1), 34-45.

Zifchock, R, & Davis, I. (2006). Poster presentation, *ASB Conference*, Blacksburg, Virginia.

Table 1: Number of times each foot showed dominance in step time and peak impact vertical GRF when measured using symmetry index (SI) and symmetry angle (SA)

Subject	Step Time				Peak Impact Vertical GRF			
	Right SI	***Left SI***	***Right SA***	***Left SA***	***Right SI***	***Left SI***	***Right SA***	***Left SA***
1	10	0	9	1	9	1	9	1
2	1	9	1	9	10	0	10	0
3	7	3	6	4	10	0	10	0
4	4	6	3	7	7	3	7	3
5	5	5	4	6	1	9	1	9
6	6	4	5	5	9	1	9	1
7	10	0	10	0	1	9	1	9
8	5	5	5	5	10	0	10	0

ADAPTIVENESS OF DISTAL POSTURAL CONTROL LEARNING

Manuel E. Hernandez MS[1,3], James Ashton-Miller PhD[1,2], and Neil B. Alexander MD[2,3,4]

[1]Biomechanics Research Laboratory, [2]Institute of Gerontology,[3]Mobility Research Center, Division of Geriatric Medicine, Department of Internal Medicine, The University of Michigan, [5]VA Ann Arbor Health Care System Geriatric Research, Education and Clinical Center, Ann Arbor, Michigan.

E-mail: manueleh@umich.edu Web: www.med.umich.edu/geriatrics/moblab/

INTRODUCTION

Balance is an integral part of daily living. The ability to maintain Center of Mass (COM) stability during tasks such as reaching or stooping reduces the risk of falling and suffering injury. Balance control requires accurate and rapid control of the Center of Pressure (COP), upon the detection of a loss of balance (LOB). A loss of balance occurs when the Center of Mass (COM) falls outside of the basis of support and is not actively accelerating towards a state of equilibrium (i.e. stable gait).

Fitt's law introduced a theoretical framework for the trade-off between accuracy and speed in upper extremity reaching tasks, such as reciprocal tapping (Fitts, 1954). These principles have not been well characterized in whole body movement (Danion, 1999). We propose to examine the effect of gender on the learning of a 1-DOF distal postural control (DPC) task, and hypothesize movement time (MT) changes due to inertial properties (e.g., height, and weight), while controlling for accuracy.

METHODS

Subjects. Healthy young males (mean±SD, age 23.3±4.5, N = 6) and females (age 22.8±3.4, N = 5) were recruited from the local community. Table 1 includes a summary of measured characteristics.

Protocol. In order to determine the relationship between learning effects in a novel DPC task and gender, a modification to the Functional Base of Support (FBOS) test was used (King et al., 1994, Fitts 1954). Participants stood upright and then leaned forward and backward, to determine their FBOS. FBOS was defined as the limits between the maximal forward and backward excursion of the COP from a steady upright stance. Learning is evaluated by asking participants to shift their COP signal as accurately as possible, so as to achieve 10 consecutive correct trials, within a 60 second trial, with the use of visual feedback. Target width (TW) and COP movement amplitude (MA) (2x2 full factorial) were tested in 4 randomized blocks. MT is calculated for the first subset of trials with 5 consecutive correct trials. To control for musculoskeletal properties, isometric peak torque measurements of ankle dorsiflexion and plantarflexion were evaluated using an isokinetic dynamometer (Biodex v.2.0), using 2 trials of 3 seconds each.

RESULTS AND DISCUSSION

Changes in the mean MT of correct reciprocal movements during the performance of the distal postural control task are shown in Figure 1. Correlations between MT and gender were significant ($r = -.187$, $p < .05$). To further explore the effect of gender, a repeated-measure

MANOVA on MT was performed, to control for TW, MA, and block order. Multivariate tests indicated statistically significant effects of MA ($p<.05$), TW ($p<.01$), and block ($p<.01$). Significant interaction effects (block*TW, $p<.05$) and slight effects (block*gender, $p<.10$) were observed. Further within-subject contrasts demonstrated significant block*gender interactions between only the first and second block ($p<.05$).

Table 1: Characteristics of males and females. Isometric strength measurements were normalized by body weight [N] and height [m]. (*: $p < 1.0$,**:$p<0.5$)

Characteristics:	**Males**	**Females**
Height (m)**	1.81±.09	1.68±0.05
Weight (kg)*	76.1±16.9	59.1±8.6
FBOS (cm)	17.0±2.7	17.4±3.2
Mean Movement Frequency (Hz)	0.99±0.41	1.09±0.46
Normalized Ankle DF (%)	2.1±0.9	1.9±0.4
Normalized Ankle PF (%)	6.3±1.9	8.4±1.9

Key: DF – dorsiflexion, PF – plantarflexion

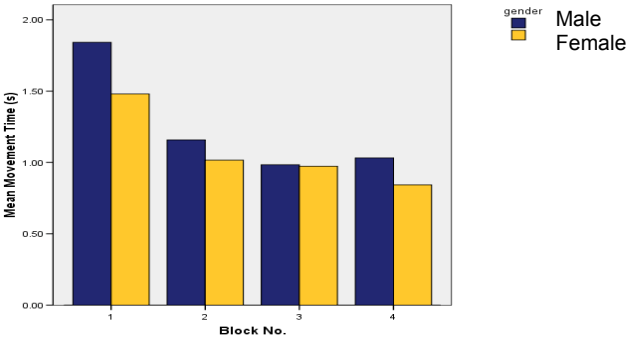

Figure 1: Mean Movement Time of Reciprocal Movements in the Distal Postural Control Task across repeated trials (blocks 1-4). First bar indicates males, and second bar indicates females.

Differences in inertial properties may explain the higher movement times observed in males, when compared to females. The lower height and decreased weight of females would lead to decreased moments of inertia. As expertise in this DPC task is attained, gender differences are nullified, and both groups achieve similar MTs. This capacity to overcome intrinsic differences in inertial properties might be explained by the use of a common controller.

SUMMARY/CONCLUSIONS

Preliminary findings suggest that COP movement time may depend on gender during the early stages of learning a novel DPC task. Further analysis should be undertaken to find the mechanism responsible for the differences observed. Also, in order to evaluate the effects of aging, older controls should be used to compare against young adults.

REFERENCES

Danion, F., Duarte M., Grosjean, M. (1999). *Neuroscience Letters,* **277**, 131-133.

Fitts, P.M. (1954). *J. Exp Psychol,* **47**, 381-91.

King, M.B., Judge, J.O., Wolfson, L. (1994). *J. Gerontol,* **49**, M258-63.

ACKNOWLEDGEMENTS

We would like to thank the following collaborators, which provided us assistance in collecting data: Brad Grincewicz, Eric Pear, and Pooja Desai. We are grateful to the National Institutes of Health for NRSA Grant Number 1 F31 AG024689-01, which supports this project.

DIFFERENCE IN BIOMECHANICAL PROPERTIES BETWEEN A CERVICAL PEDICLE SCREW CONSTRUCT AND LATERAL MASS CERVICAL FIXATION

Hyung Soon Park[1,2], Brad Dunlap[2], Eldin E. Karaikovic[2], and Li-Qun Zhang[1,2]

[1] Rehabilitation Institute of Chicago, Chicago, IL, USA
[2] Northwestern University, Chicago, IL, USA
E-mail: l-zhang@northwestern.edu

INTRODUCTION

Posterior cervical spine fixation with lateral mass screws has traditionally been used (An, 1991). There are concerns of inadequate fixation in cases with poor bone quality or large defects in the posterior elements due to fracture or post laminectomy. In patients with poor bone quality who require multi-segmental fixations, the current dorsal stabilization procedures in the sub-axial cervical spine using lateral mass screws are often insufficient.

Cervical pedicle screw fixation has been suggested as an alternative procedure (Abumi, 1994), but there are still limited data available on the biomechanical differences between pedicle screw and lateral mass fixation. Prior work has indicated that cervical pedicle screws had higher screw pullout strength (Jones, 1997; Johnston, 2006), and increased stability (Kothe, 2004).

The purpose of our study was to measure the residual load in the adjacent discal surfaces and facet joints for two different posterior fixation constructs (lateral mass screw and pedicle screw), and to investigate whether there was any difference in biomechanical properties between the two constructs.

METHODS

Two different posterior cervical fixation systems (pedicle screw-rod vs. lateral mass screw-rod constructs) were used in order to determine if there was any biomechanical advantage of one over the other.

Two motion segments (C4-5 and C6-7, each instrumented with one type of instrumentation) from five cervical cadaver spines (for a total of ten motion segments) were used for testing. Bone mineral density was determined using DEXA scan. Radiographs and CT scans were used to exclude the presence of fractures or other pathologic conditions. Lateral mass screws and pedicle screws were then installed at one and the other segment of a specimen. The instrumentation method for a segment was chosen randomly so that each spine would contribute one motion segment to each group, and it would serve as its own internal control.

A pressure sensor (Tekscan Inc.) was placed through a slit in the annulus at the junction of the inferior end plate/superior surface of an intervertebral disc. The pressure sensor measured pressure values and distribution during axial loading.

The motion segments were securely clamped and mounted into a jig and tested with a non-destructive physiologic load (Fig. 1). Uniplanar axial load was applied with a maximum load of 90 Newtons for 200 cycles as previously described (Johnston, 2006). The jig was designed so as to align the vertical axis of loading with the center of flexion axis (Fig. 1). By using a force sensor (Transducer Techniques Inc), a high precision linear motor (8.5 μm resolution by Physik Instruments) was controlled so that the constant loading/unloading rate (22.5 N/sec) was maintained during the cyclic loading between 0 to 90 Newtons.

Once the type of screw is chosen randomly, a specimen was preloaded by 40 cycles of loading between 0 to 40 Newtons. Then the specimen was loaded at two conditions; without instrumentation and with the screws fixed to the rods.

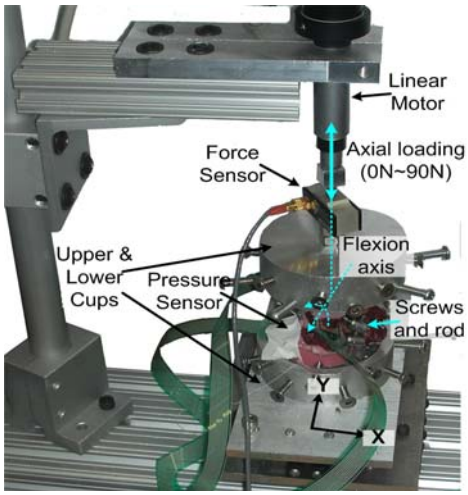

Figure 1. Experimental setup. The specimen was clamped into a jig which was designed so as to align the vertical axis of loading with the center of flexion axis.

RESULTS

For data analysis, average pressure, peak pressure, and contact area under 90 Newton load were measured at the sensor area (about 200mm^2). The pressure reduction at disc area before and after the instrumentation was then compared between the two types of instrumentation methods: lateral mass screw-rod and pedicle screw-rod.

The pedicle screw instrumentation reduced significantly larger amount of average pressure, peak pressure, and force (P-value < 0.05) at the disk area than did the lateral mass screw (Fig. 2).

DISCUSSION

In addition to the significantly higher pullout strength (Johnston, 2006) and higher stability to lateral bending (Kothe, 2004), the results from this study showed that the pedicle screw reduced larger amount of pressure at the disc area and took more load than did the lateral mass screw.

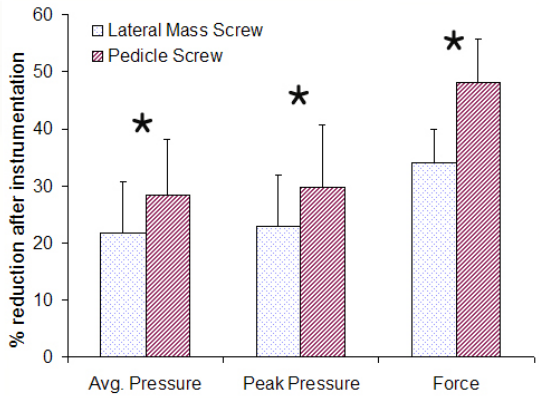

Figure 2. The difference between the two constructs. Average and peak pressures, and force at the disc area were measured under 90N loading over 200 cycles for without and with the instrumentation. The % reduction in those parameters after instrumentation were then calculated and compared. Pedicle screw showed significantly higher reduction ratio for the three parameters. * P<0.02

Due to proximity of neurovascular structures and small pedicle size, some authors have expressed concerns of potential iatrogenic injury with cervical pedicle screws (Kowalski, 2000). However, our results showed that pedicle screws provided more rigid constructs which are needed in cases of comminuted vertebral body fractures or destructive flexion-extension cervical spine injuries.

REFERENCES

Abumi, K. et al. (1994). *J. Spinal Disord.*, **7**, 19-28.

An, H.S. et al. (1991). *Spine*, **16**, 548-51.

Johnston, T.L. et al. (2006). *Spine J.*, 6, 667-72.

Jones, E.L. et al. (1997). *Spine*, **22**, 977-82.

Kothe, R. et al. (2004). *Spine*, **29**, 1869-75.

Kowalski, J.M et al. (2000). *Spine*, **25**, 2865-67.

RAPID SHOULDER FLEXION AFTER A SLIP MAY ASSIST FALL AVOIDANCE

Stephanie J. Donovan, Karen L. Troy, Mark D. Grabiner
University of Illinois at Chicago, Email: grabiner@uic.edu

INTRODUCTION

Falls and fall-related injuries are the leading cause of accidental death in older adults over 75 years [1]. Up to 50% of fall-related injuries result from slipping accidents [2]. Reestablishing dynamic stability is a complex task that seems to become more difficult with age. Identifying successful slip recovery mechanisms may be helpful for the design of intervention programs aimed at modifying slip responses.

Several biomechanical studies have identified mechanisms necessary to regain dynamic stability after a slip. Most recently, emphasis has been placed on segmental coordination for a successful recovery, including hip extensor in the unperturbed leg and knee flexion in the perturbed leg [3,4]. Rapid and symmetric upper extremity elevation may counteract the trunk extension velocity (TEV) induced from the slip by causing an anterior shift of the body's center of mass (COM) [3,5]. Here, we aim to identify age-related shoulder and trunk kinematic differences and quantify the biomechanical contribution of the upper extremities in recovery from an unconstrained slip.

METHODS

Thirty-five young (17 males, age 24.9±5.0 years, 172.2±10.6cm, 151.3±31.6 kg) and 21 independent and community-dwelling older adults (8 males, age 70.9±5.1 years, height 165.6±10.9 cm, mass 72.2±13.2 kg) participated in this institutionally approved study. Older subjects were screened by a physician for exclusion factors that included neurological, musculoskeletal, and cardiovascular disorders.

All subjects wore a safety harness which protected the subject from ground impact. Subjects walked through a motion capture volume that included a Plexiglas sheet (2.4 x 1.2m). Immediately prior to the slipping trial and without the subjects' knowledge, the Plexiglas was coated with a thin film of mineral oil or a water-based lubricant allowed to dry and activated with a mist of water. All data are referenced to slip foot or recovery foot (unperturbed foot). Only one slip trial was attempted for each subject.

The motion capture data (Motion Analysis, Santa Rosa, CA) of 22 passive reflective markers was recorded at 60 Hz. The onset of the slip and the instant of recovery (unperturbed foot contacted the ground) were identified. Analysis included slip onset to 133ms after recovery (rec_{+133}) because slip-induced trunk extension was reversed within 133 ms following recovery or subjects who fell had not yet engaged the safety harness. Shoulder and trunk position and velocity were calculated at recovery, rec_{+133} and peak values. Slips were categorized as backwards-directed if the trunk was in >2° extension and was still extending with a velocity of >50°/s at rec_{+133}. Ten older adults who fell and the 24 young adults who recovered were classified as backwards fallers and were further analyzed here. Data was log transformed and a repeated measures ANOVA was performed to evaluate differences in shoulder flexion angles and velocities between young and older groups.

A simple two-segment sagittal plane model of the upper extremities and trunk was developed using the conservation of angular momentum. It was assumed that both arms moved symmetrically and simultaneously. The model calculated the shoulder flexion velocity required to decrease a given TEV by a desired percentage. This algorithm was

then used to estimate the percent decrease in TEV due to shoulder flexion for each subject. To fit the assumption of symmetry, peak flexion velocity was averaged for each of the subjects' shoulders and used as an input for the model algorithm.

RESULTS AND DISCUSSION

Although the young adults achieved a larger peak shoulder flexion velocity, peak shoulder flexion angles were not different between young and older groups (Table1). However, the young subjects achieved larger shoulder flexion angle and velocity at the time of recovery (Table 1). Both groups attempted a recovery step 200-300ms after heel strike on the slippery surface.

The two-segment mathematical model indicated that rapid, symmetric shoulder flexion can be effective in decreasing TEV during a slip. The shoulder flexion velocity required to decrease TEV by a specific percentage increases linearly as slip-induced TEV increases (Figure1). For example, a 20% decrease of a peak TEV of 100 deg/sec requires a shoulder flexion velocity of approximately 253 deg/sec. Alternatively, a 20% decrease of a peak TEV of 150 deg/sec requires a shoulder flexion velocity of 380 deg/sec. On average, the model estimates young adults were able to decrease TEV by 43%±47, but older adults only by 20%±9 (p=0.011).

Rapid shoulder flexion may contribute to the recovery from a slip by aiding in control of TEV, thus reducing the backward velocity of the trunk COM. Although older adults who fell were able to achieve large peak shoulder flexion velocities, young non-fallers were more effective at using their arms to reduce TEV. If the arms are to play a role in the recovery of a slip, they must be rapidly elevated by the time of the recovery before the COM has shifted posterior to the base of support. These findings indicate that interventions aimed at training older adults to avoid falling after a slip may be more beneficial if rapid elevation of the upper extremities is included as a training goal.

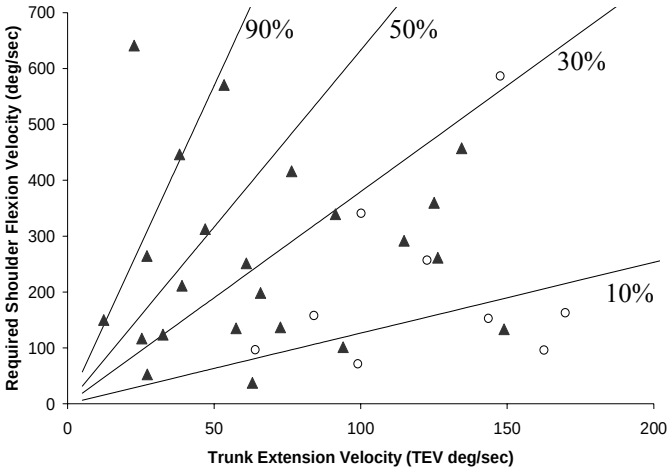

Figure 1 Each line represents a calculated percent decrease in TEV caused by shoulder flexion velocity. Plotted points represent individual subject data (open circles older adults, filled triangles young adults).

REFRENCES

[1] Lilley, J. M., T. Arie, et al. (1995). Age Ageing **24**(4): 346-65. **[2]** Courtney, T. K., G. S. Sorock, et al. (2001). Ergonomics **44**(13): 1118-37. **[3]** Marigold, D. S., A. J. Bethune, et al. (2003) J Neurophysiol **89**(4): 1727-37. **[4]** Troy, K.L., Donovan S.J., et al. Injury Prev. in review. **[5]** Tang, P. F. and M. H. Woollacott (1998) J Gerontol A Biol Sci Med Sci **53**(6): M471-80.

Table 1 Comparison of young and old shoulder kinematics

Variables	Young (n=24)		Old (n=10)		p-Value
	Slip-Side	Recovery-Side	Slip-Side	Recovery-Side	Young vs. Old
Shoulder Flexion Angle at Recovery LN(deg)	2.41±1.31	2.15±1.18	1.74±1.41	0.78±1.31	0.02*
Shoulder Flexion Velocity at Recovery LN(deg/sec)	1.88±4.36	1.84±3.70	-1.89±4.50	-0.02±4.19	0.05*
Peak Shoulder Flexion Angle LN(deg)	3.19±0.91	3.13±0.96	2.70±0.97	2.82±0.65	0.555
Peak Shoulder Flexion Velocity LN(deg/sec)	5.40±0.66	5.08±1.04	5.40±0.66	5.68±0.98	0.05*

Data reported as log transformed, Values are means ± SD, *significant difference $p \leq 0.05$

SUBJECT SPECIFIC GEOMETRY RECONSTRUCTION OF KNEE BONES

Anthony G Au [1], Darren Palathinkal [1], Adrian B Liggins [2], V James Raso [2], Jason Carey [1], Robert G Lambert [1], Alidad Amirfazli [1]

[1] University of Alberta, Edmonton, AB, Canada
[2] Capital Health Authority, Edmonton, AB, Canada
E-mail: a.amirfazli@ualberta.ca, Web: http://www.mece.ualberta.ca/staff/alidad/

INTRODUCTION

Accurately predicting mechanical stresses in knee bones is critical in the design of total knee replacement (TKR) implants. Subject specific finite element (FE) models can be particularly helpful in developing implants for individuals requiring non-conventional implants. Capturing the complex 3D knee bone geometry is a crucial first step in generating such FE models. Such geometry can be reconstructed from computed tomography (CT) images using voxel mesh techniques (Keyak et al., 1990). However, the subsequent models contain jagged edges and lack a clearly defined endosteum, potentially compromising the accuracy of stress predictions. Alternatively, surfaces can be reconstructed by skinning with NURBS surfaces. However, problems have been encountered with bifurcating geometry such as in the femoral condyles (Viceconti et al., 1999).

Knee bone border extraction methods have not been well examined. Manual identification of borders is too cumbersome for subject specific modeling, but automated methods via thresholding and local pixel intensity analysis lack accuracy and repeatability, and may not perform well on poorly contrasted CT images from TKR candidates (Testi et al., 2001).

The present study introduces a semi-automatic procedure to reconstruct distal femur and proximal tibia geometry from CT images using a combination of edge extraction and CAD surface generation. Particular emphasis will be placed on reconstructing the often overlooked endosteum. A novel solution is proposed to overcome bifurcation problems during skinning. Validation of this technique will also be presented. Consequences of reconstructing surfaces using voxel mesh versus NURBS will also be discussed.

METHODS

CT images were obtained for the left knee of a 47-year-old male (resolution: 512 x 512 pixels; thickness: 1.25 mm). Solid models were reconstructed using two methods. The commercial method employed a voxel mesh technique from Simpleware (Exeter, UK). Cortical bone in each image was identified by manually thresholding with a range of attenuation values. The surface was generated by stacking the thresholded images.

The in-house method employed a 6-step edge extraction process performed by a customized MATLAB (Mathworks, Natick, MA) program. CT images were smoothed and convolved with a Sobel gradient operator to accentuate two rings of high attenuation change (Fig 1). Images were thresholded by analyzing attenuation histograms to eliminate soft tissue for more effective edge extraction.

The periosteal interface was identified by tracing the outer ring of the bone, with pixels containing the strongest gradient

tracked in a clockwise direction (Fig 1). The endosteum was often not clearly defined due to subtle attenuation changes between cortical and cancellous bone, therefore the above tracing operation was not effective. A more effective method was to analyze a line of pixels intersecting the endosteum and identify the interface point from the gradient profile (Fig 1). Cubic splines were used to fit the interface points to produce smoother edges.

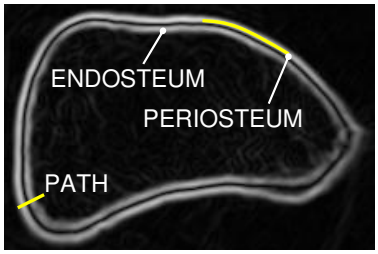

Figure 1: Gradient-operated image of femoral shaft displaying rings representing endosteum and periosteum (overlapped with a partial trace). PATH illustrates a line of pixels used to generate a gradient profile.

A Pro/Engineer (PTC, Needham, MA) CAD surface encompassed all transverse curves, but excluded the femoral condyles due to their bifurcation. Reconstructing the condyles required creating a second surface based on curves extracted from sagittal images (processed identically to the transverse images) and combining it with the transverse image constructed surface.

The accuracies of the two techniques were measured by reconstructing composite and *ex vivo* bovine knees and comparing with surface data obtained using a coordinate measuring machine (CMM) and laser scans.

RESULTS AND DISCUSSION

Validation revealed commercial and in-house periosteal surfaces had mean errors of 0.6 mm and 0.5 mm, respectively. This is on the order of magnitude of the image resolution (0.3 mm/pixel) and laser scanned models (0.5 mm). The sagittal surface used to overcome bifurcating geometry did not compromise accuracy.

The voxel model showed a slightly jagged surface due to the thin CT slices, but the endosteum representation was poor. The condyle cortex thickness was greatly overestimated because the technique required thresholding of entire CT images, which compromised precise definition of the endosteal interface since no single attenuation value clearly distinguished cortical from cancellous bone. The in-house technique analyzed gradients local to the endosteum rather than applying a global threshold value, resulting in a more representative interface (Fig 2). Additionally, this technique accommodates poorly contrasted images by estimating the cortical thickness from better-defined surrounding bone, a feature that has not been available to date.

Figure 2: Sectioned proximal tibia showing periosteal and endosteal surfaces.

REFERENCES

Keyak, J., et al. (1990). *J Biomed Eng*, **12**, 389-397.

Viceconti, M., et al. (1999). *Comput Methods Programs Biomed*, **59**, 159-166.

Testi, D., et al. (2001). *Comput Methods Programs Biomed*, **65**, 175-182.

DETERMINING SITE-SPECIFIC BONE LOSS IN MICE

Brandon J. Ausk, Philippe Huber, Sundar Srinivasan, Ted S. Gross
University of Washington, Seattle, WA, USA
E-mail: bjausk@u.washington.edu, Web: depts.washington.edu/osl

INTRODUCTION

The development of high-resolution micro-CT scanners capable of small animal in vivo scanning enables exploration of bone adaptation over time. However, despite registration algorithms that allow superpositioning of sequential images (1), a severe constraint on this approach lies in that surface registration landmarks are altered when bone morphology is altered. Thus, the biological response under study confounds the ability to accurately register serial images. Recently, we developed a murine disuse model in which right hindlimb muscle function is transiently inhibited by intramuscular injection of botulinum neurotoxin A (2). When both the quadriceps and calf muscles are paralyzed, trabecular bone loss in the distal femur and proximal tibia ranges from 43 to 54% and cortical bone loss at the tibia mid-diaphysis reaches 15% by 3 wk (2). Subsequent studies have indicated that the bone loss in this model, unlike other rodent models of disuse, is driven almost entirely by osteoclastic bone resorption (3). Bone loss at cortical sites in this model is therefore characterized by an unchanged periosteal (outer) surface, which enables assessment of image registration. We therefore hypothesized that site-specific bone loss (i.e., around a given cross section of cortical bone) could be accurately assessed via serial high-resolution μCT scanning.

METHODS

To assess the variability of our approach, six female C57B6 mice underwent two high-resolution μCT scans separated by 24 hr. For the in vivo study, ten female C57B6 mice (16 wk) received IM injections of Botox (2.0 units/100 g) in the right calf (no quadriceps injection) immediately following a μCT scan (Day 0). Following 3 wk of free cage ambulation, a second μCT scan (Day 21) was obtained for all mice. Each scan was conducted by anesthetizing the mouse with isoflurane, using a custom apparatus to secure the mouse and lower limb, and scanning 2 mm of the tibial shaft centered 2.4 mm proximal to the tibia-fibula junction (Scanco μCT 40; 11 μm voxel).

Image processing was conducted identically for the validation and in vivo studies. The pre- and post-scans of individual mice were superimposed using a recently developed vendor supplied 3-D image registration program (Scanco IPL Registration Command). This software enables alignment of serial images through identification of translation parameters that must be applied to the secondary image to fit it to the primary image. To accomplish this, stepwise trial translations and rotations are identified (using a combination of simplex and Powell's search methods) that minimize comparison errors in both the centers of mass and moments of inertia along the long axis of the scan volumes (using periosteal envelopes as registration landmarks). The procedure is repeated until no further improvement in image registration is obtained. Following alignment, 2-D cross-sections located 1.4 mm proximal to the tibia-fibula junction were exported to custom image processing software (Matlab) and converted to grayscale. Within the grayscale image, bone present in both pre- and post-scan images was colored gray (G)

and bone present only in the pre-scan was colored white (W; representing resorption area). Subsequently, image-filtering techniques were used to remove 'phantom' W-pixels that occur due to edge-line roughness errors associated with pixelated images in both the control and in vivo studies. Finally, the resulting image was partitioned circumferentially into 16 equal angled sectors originating from the center of mass of the Day 0 scans (Fig 1A) and percent bone loss in each sector, as well as for the entire cross section, computed using pixel color identification (100*W/(W+G)). For the variability assessment, error was determined as the percentage of cortical area that was not aligned. For the in vivo study, 1-way ANOVA with a Tukey follow-up test was used to explore the non-uniformity of bone loss across sectors.

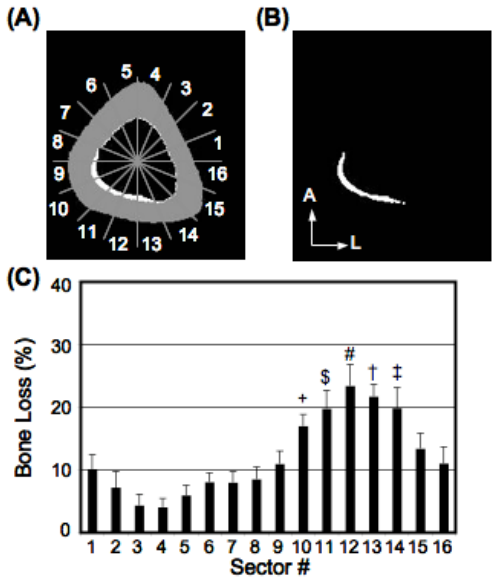

Fig 1. Superimposed μCT images pre and post transient calf paralysis (A, gray represents common cortical area) shows bone loss (B, white) occurs non-uniformly (C; mean + SE, n=10). Significant differences noted ($p \leq 0.05$; + vs sectors 3-4, $ vs sectors 2-7, # vs sectors 1-9 and 16, † vs sectors 1-8, ‡ vs sectors 1-7).

RESULTS AND DISCUSSION

Our approach produced accurate superpositioning of two volumetrically identical serial μCT scans (0.6 ± 0.06% error in whole cross section). Mapped images of Botox treated mice showed substantial bone loss (12.1 ± 1.5%) due entirely to endocortical expansion. Within individual cross sections, bone loss was highly non-uniform around the circumference (Fig 1B). Sectors located on the posterior surface showed significantly higher rates of bone resorption than sectors located on the anterior surface (Fig 1C).

SUMMARY/CONCLUSIONS

Cortical bone loss in this study was nearly identical to that previously observed in calf only injected mice (12%; 4). We found that the error in our serial scanning/image registration and assessment was very low at the assayed cortical bone site (<1%). As a result, we were able to accurately identify focal bone resorption in the in vivo study. This observation is suggestive of either directed osteoclast chemotaxis or focal inhibition of osteoclast attachment. In conclusion, these data validate our serial imaging approach in this model and thereby enable a variety of experiments to explore the biological mechanisms underlying focal osteoclastic resorption. Further, it should be possible to extend this technique to examine trabecular alterations in the same bones.

REFERENCES

(1) Boyd, S.K., et al. (2006). *Ann Biomed Eng*, **34,** 1587-1599. (2) Warner, S.E. et al. (2006a). *Bone,* **38**, 257-564. (3) Warner, S.E. et al. (2006), *Proceedings of ORS'06*, 42. (4) Warner, S.E. et al. (2006). *28th Am Soc Bone Miner Res.*

ACKNOWLEDGEMENTS

Supported in part by NIAMS (AR45665, TSG; AR053596, SS).

An Unconstrained Workloop Approach to Study Stability in Frog Muscle *In Vitro*

Kartik Sundar[1], Stephen P. DeWeerth [1], and Lena H. Ting [1,2]
[1] Georgia Institute of Technology, Atlanta, GA, USA
[2] Emory University, Atlanta, GA, USA
E-mail: ksundar@neuro.gatech.edu

INTRODUCTION

In the face of uneven terrain and environmental uncertainty, the ability of a muscle to produce a consistent amount of power is important in animal locomotion. Intrinsic muscular properties may help stabilize power production reducing the importance of higher neural centers in responses to small mechanical perturbations. Previous studies suggest that the physiology of *in vivo* frog muscle is optimized to produce maximum power (Lutz and Rome, 1994). Because muscle power is near maximal for a range of loads (Hill, 1938), muscles may also be optimized for stability at high power.

Traditional workloop methods constrain the muscle by predetermining the muscle trajectory (Josephson, 1985), and therefore the effect of mechanical perturbations cannot be studied. In this study we developed an *unconstrained* workloop method to investigate the dynamics of work production in the frog plantaris longus (PL). We *hypothesize* that muscle work is robust to mechanical perturbations when loaded near the peak of the power-load relationship.

METHODS

To test our hypothesis we measured the mechanical work that the frog PL generates when working against several different loads (Fig. 1). To asses the stability at each load we quantified the change in work between a perturbed and unperturbed condition.

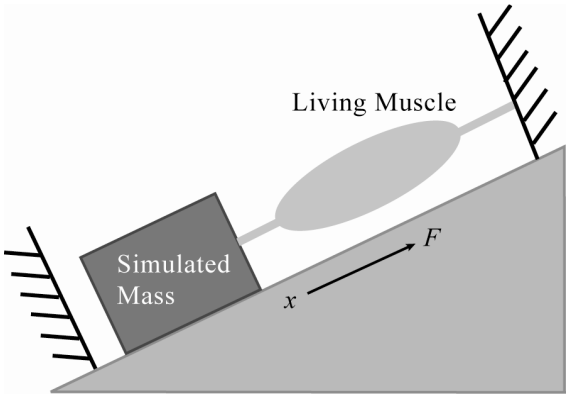

Figure 1: Schematic of the experimental design. We use a novel *in vitro* approach to connect living muscle to virtual mechanical devices.

We developed a system that allows a living *in vitro* frog muscle to be connected to a simulated mechanical device. Traditional muscle physiology experiments usually fix or predetermine one of the muscle states (force, length, velocity) such that it is independent of the other states. Our unconstrained approach relates all of the muscle states together creating a virtual connection between a living muscle and a simulated mechanical system. Here, muscle length is dependent on the force of gravity, the force that the muscle produces, and the inertial properties of the mass.

The PL was maximally activated for 100 ms and the muscle force and length were measured. Immediately after the activation was completed, force impulses (-0.1 N, 100 ms) were administered for the perturbed condition (pushing the load down the hill).

RESULTS AND DISCUSSION

When activated, the muscle contracted and performed work on the load (pulling the mass up the hill). Larger loads resulted in higher forces and smaller changes in length (Fig. 2). The applied perturbations altered the shape of the workloop and changed the total work generated (shaded region).

The change in work due to a mechanical perturbation decreased as the muscle produced more work (Fig. 3). At a load of 1 N, approximately 30% of the maximal isometric tension (P_0), the muscle produced a maximal amount of work, and the mechanical perturbation had little effect on the total work produced. Conversely, at lower work levels, which occurred for either small loads or large loads, perturbations had a much larger influence on the total work produced.

SUMMARY/CONCLUSIONS

We used an unconstrained workloop to study the power generating capabilities of the frog PL. Unlike traditional methods, this approach will allows us to study *in vitro* muscle during more natural dynamic conditions.

Optimizing muscle performance for peak power production may also increase stability because of the shape of the power-load relationship. This biological property is in contrast to engineered systems where a power-stability tradeoff is typically encountered.

ACKNOWLEDGEMENTS

This work is supported in part by the National Science Foundation IBN-0349042.

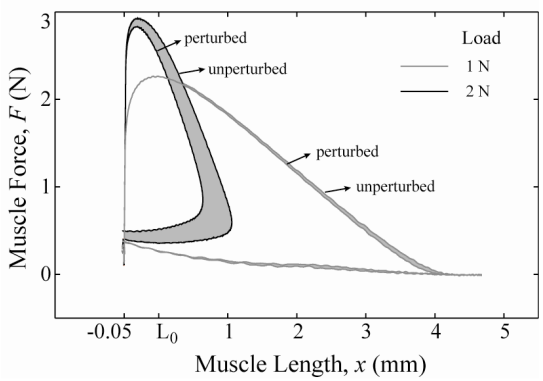

Figure 2: Two unconstrained workloop examples. The shaded region indicates the difference in work between the perturbed and unperturbed trials. In both examples shown, the perturbed system generated less work.

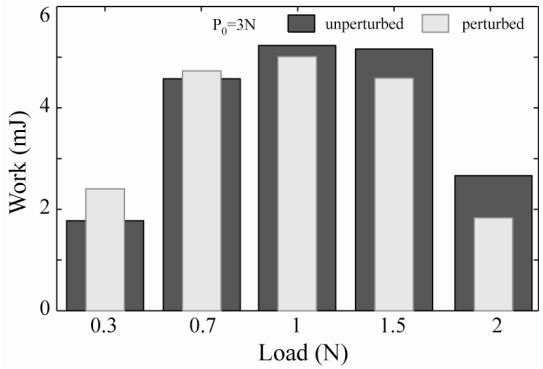

Figure 3: Work is robust to perturbations when the muscle is operating at loads near $0.3P_0$ (1 N). At small loads, the mechanical perturbation increased the work produced.

REFERENCES

Hill, A.V. (1938). Proc. of the Royal Soc. of London B: Biological Sciences, **126**, 136-195.

Josephson, R.K. (1985). *J. Experimental Biology*, **114**, 493-512.

Lutz, G.J., Rome, L.C. (1994). *Science*, **263**, 370-372.

EFFECT OF SURFACE COMPLIANCE ON STEPPING RESPONSES TO TRUNK PERTURBATIONS

Manuel E. Hernandez MS[1,3], and James Ashton-Miller PhD[1,2]

[1]Biomechanics Research Laboratory, [2]Institute of Gerontology, [3]Mobility Research Center, The University of Michigan, Ann Arbor.

E-mail: manueleh@umich.edu Web: www.med.umich.edu/geriatrics/moblab/

INTRODUCTION

A disproportionate increase in falling injuries as people age has been well documented during walking (Woolley, 1997). Dynamic balance on a narrow beam has been found to be hindered by walking with thick, soft soles (Robbins *et al*., 1992). Compliant surfaces have been frequently used to challenge balance during upright stance, and thus would be expected to decrease the ability to maintain dynamic balance during walking.

To model walking, a trunk segment was added to a planar passive dynamic walker (McGeer, 1990). In addition to the legs modeled in the original model, the addition of trunk allows for the observation of trunk stability on overall system performance, and provided a rigid body with significant inertia to perturb.

This simulation explores the behavior of a passive dynamic walker after trunk perturbations in the sagittal plane, given different surface compliances that range from concrete to rubber mats.

METHODS

Model. The model consists of a four degree of freedom (4-DOF) passive walking system, which includes four point masses: one on each leg, one on the trunk, and one on the ground contact to model the mass of the ground segment underneath the body. The model was created in Matlab (Mathworks), using the equations of motion that were derived by Kane's Method in Mathematica (Wolfram Research), and utilizing non-dimensional parameters for the segment masses, moment of inertias, and lengths. The compact form of the equations of motion can be expressed as:

$$M(\phi)\ddot{\phi} = V(\phi,\dot{\phi}) + G(\phi) + T \qquad (1)$$

where the mass matrix, velocity vector, gravity vector, and torque vector are used, with respect to the segment angles. The stabilization of the trunk is achieved by assuming a 2-DOF system with damping and spring stiffness, whose parameters are determined from rough, experimental measurements. Perturbations are introduced by the use of a step input at the onset of a swing and are applied through the full duration of the step.

RESULTS AND DISCUSSION

Modeling Trunk Perturbations. The results of increasing positive torque or increase of negative force led to very similar segment characteristics behavior. Similarly, the increase in positive force was similar to the increase in negative torque (Figure 1). However, parameter studies revealed that an 8:10 relationship between torque and force ratios above at an initial torque magnitude of -0.3 consistently led to the highest energy losses during heelstrike.

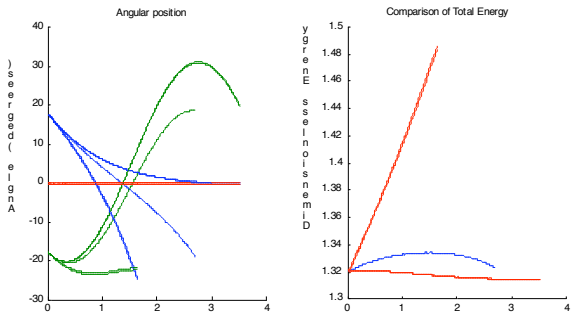

Figure 1: Segment kinematics and system energetics based on the limits of force/torque perturbations. All simulations considered a non-compliant surface.

Surface Compliance. The results from the comparison of surface compliance on system behavior during a step revealed the most significant effect in swing leg trajectory, in comparison with the stance leg (25% difference in swinging leg angle vs. 18% difference in stance leg angle). The total energy of the system demonstrated significant increases in energy fluctuation as the surface compliance increased, given the unperturbed condition (Figure 2).

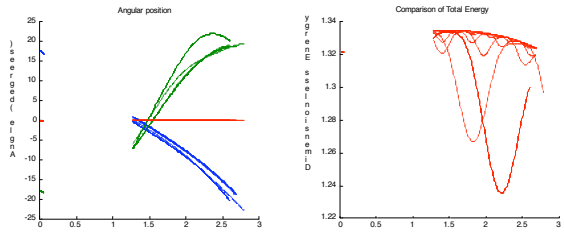

Figure 2: Effect of surface compliance on unperturbed system on segment kinematics and system energetics. Surface stiffness, K, values range from 4376 Nm to 14.4 Nm.

SUMMARY/CONCLUSIONS

The effect of either torque or force trunk perturbations were very similar on the boundary values of a normal gait, yet demonstrated subtle variations within a fixed range of perturbations. With respect to the local minima derived from the parameter study, the conditions that arise to produce an increase in the energy loss at heel strike makes intuitive sense, since those perturbation combinations both contribute to an increase in angular momentum during a forward step. The increased observed effect of angular momentum perturbations suggests that perturbations that lead to trunk bending could be more dangerous during walking. This effect can be physically explained by the increase in hip torques necessary to maintain trunk stabilization, which when acting on the stance leg would prompt a torque about the foot contact point and accelerate the stance leg forward toward the ground.

The addition of surface compliance led to significant changes in energy losses, yet revealed changes of less than 10% in the maximal angle deviations during an unperturbed gait. Similarities in segment trajectories under varied surface compliance conditions suggests that the body is capable of passively maintaining a desired center of mass trajectory, and therefore suggests that gait changes might be best explained by active control.

REFERENCES

McGeer, T. (1990) *International Journal of Robotics Research* **9**(2), 62-82.

Robbins S.E., Gouw G.J., and McClaran J. (1992) *J Am Geriatr Soc* 40, 1089-1094.

Woolley, S.M., Czaja, S.J., Drury, C.G. (1997). *J. Gerontol.* **52A**, M80-87.

ACKNOWLEDGEMENTS

We are grateful to the National Institutes of Health for NRSA Grant Number 1 F31 AG024689-01, which support this project.

EXPERIMENTAL EVALUATION OF MODEL-BASED LOWER EXTREMITY INDUCED ACCELERATIONS

Betsy V. Hunter[1], Darryl G. Thelen[2], and Yasin Y. Dhaher[1]

[1]Northwestern University, Evanston, IL, USA
[2]University of Wisconsin-Madison, Madison, WI, USA
E-mail: b-hunter@northwestern.edu

INTRODUCTION

Following neurological pathologies such as stroke, impaired motor control may result in detrimental gait abnormalities. Hence, there is increasing interest in establishing rehabilitation interventions to improve locomotion (Daley, 2004; Johnson et al. 2004). These treatments, outcomes of which are highly variable, are primarily based on an anatomical perception of muscle function and may not incorporate effects of dynamic coupling. In order to target three-dimensional multi-joint abnormalities, improvement of these intervention strategies will likely require integration of a more extensive definition of muscle function.

In recent years, Induced Acceleration Analysis (IAA) has been used to provide a direct correlation between a system's kinetics and kinematics. Using IAA with musculoskeletal modeling, an individual muscle's contribution to the movement of multiple joints can instantly be determined. However, IAA-based simulation techniques lack substantial experimental validation of muscle-specific results. Therefore the goal of this study is to determine if model-based predictions of muscle contributions would emulate observed functions under a **well-controlled experimental paradigm**. We hypothesize that three-dimensional acceleration directions obtained in gait simulations will be observed experimentally under identical conditions. We propose that findings will facilitate the interpretation of dynamic muscle function in cross-planar movements that occur following stroke.

METHODS

The experimental framework uses individual muscle stimulation of the biceps femoris (BF), rectus femoris (RF) and vastus lateralis (VL) to isolate each muscle's contribution to movement. Ten healthy subjects were positioned in four static multi-joint configurations ranging from toe-off to heel strike of gait (figure 1). Series elastic elements placed between the orthosis and the limb allowed for small movements while counterbalancing gravity. As each muscle was delivered a 60ms pulse train, spring forces and limb movements were recorded. Joint angles were differentiated twice to obtain experimentally observed accelerations.

Figure 1: Experimental setup with limb in static posture. Series elastic elements allow for stimulation induced joint movements.

The experiment was simulated using a three segment, two-dof model. Inputs included muscle force (representing the stimulation) and external forces applied to the femur and tibia (measured spring forces). The resulting

induced accelerations at the hip and knee were calculated.

RESULTS

The simulations predicted all three muscles to accelerate the hip into extension, the RF and VL to knee extension, and BF to knee flexion in the first 3 configurations and knee extension near heel strike. As shown in figure 2, most subjects were consistent in the acceleration direction predicted by the model (averaging hip and knee: 65%, 81%, 83% of subjects for BF, RF and VL, respectively).

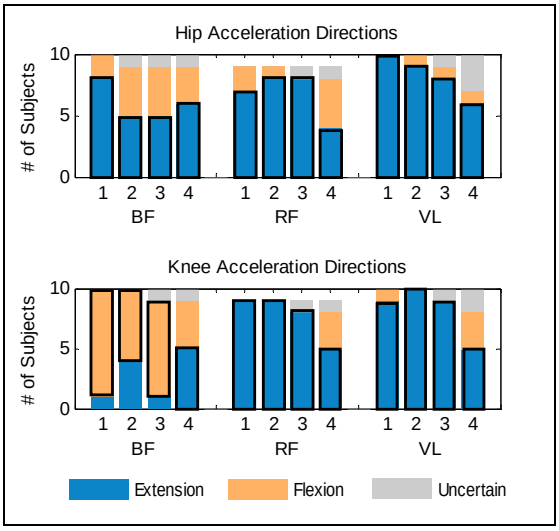

Figure 2: Subject distribution of hip and knee sagittal acceleration directions for each muscle in four postures. Regions outlined in black indicate directions predicted by model.

In the frontal plane, our simulations predicted BF and VL to accelerate the hip into adduction and RF in abduction. In preliminary three-dimensional experiments, the majority of acceleration directions are consistent with model predictions. On average, frontal plane accelerations are 1/2, 2/3 and 1/6 the size of sagittal plane accelerations for BF, RF, and VL, respectively.

DISCUSSION/CONCLUSIONS

Muscle stimulation has been shown to be an effective strategy for observing individual muscle behavior. The non-intuitive behaviors observed in RF (hip extension) and BF (knee flexion) are contrary to what their anatomical structure suggests and indicate that biarticular muscles can indeed accelerate joints in the opposite direction of their static torque generation capability (Zajac, 1993). Additionally, the hip movement observed following VL stimulation indicates that uniarticular muscles can produce movement of distant joints due to system dynamics (Zajac, 1993).

Preliminary data of three-dimensional muscle induced accelerations indicate that dynamic out-of-plane contributions of these muscles are larger than perceived by static moment arm values (3/10 and 1/4 the size of sagittal plane accelerations for BF and RF, respectively). Therefore, sagittal plane muscles groups targeted in current rehabilitation interventions may have a significant and unanticipated contribution to frontal plane movement and thus may hinder the success of these intervention strategies.

REFERENCES

Daly et al. (2004). *JRRD*, **41,** 807-820.
Johnson et al. (2004). *Arch Phys Med Rehabil*. **85,** 902-909.
Zajac, F.E (1993). *J. Biomech.*, **26,** 109-124.

ACKNOWLEDGEMENTS

We would like to acknowledge Winsean Lin for his assistance in data collection. Research is supported by NIDRR Field Initiated # H133A990008 and NSF Graduate Research Fellowship.

EVIDENCE OF GENDER SPECIFIC MOTOR TEMPLATES TO RESIST A VALGUS PERTURBATION AT THE KNEE

Martha Cammarata[1,2], Tobey DeMott [2], and Yasin Dhaher [1,2]
[1] Department of Biomedical Engineering, Northwestern University, Chicago, IL, USA
[2] Sensory Motor Performance Program, Rehabilitation Institute of Chicago, Chicago, IL, USA
E-mail: m-cammarata@northwestern.edu

INTRODUCTION

The incidence of anterior cruciate ligament (ACL) injuries in female athletes is up to six-fold higher than in their male counterparts (Agel et al. 2005). A prospective study implicated abnormal abduction loading at the knee during a jump landing as the primary predictor for ACL injury risk in female athletes (Hewett et al. 2005). Indeed, females tend to assume postures conducive to high abduction loading at the knee during sport maneuvers (Ford et al. 2005). This may suggest that the mechanisms of knee joint stability in this plane differ between genders.

While males have greater passive knee stiffness than females in the frontal plane (Bryant and Cooke 1988), it is not known if there exist differences in reflexively mediated muscle activation. Previous work has demonstrated that reflexive muscle activation can be elicited via a valgus perturbation at the knee in male subjects (Dhaher et al. 2003). These muscle contractions were shown to significantly increase knee joint valgus stiffness by 25% on average. (Dhaher et al. 2005). However, it remains to be seen if a valgus perturbation triggers a similar muscular response in female subjects. Accordingly, in this study, we sought to compare the properties of valgus induced muscle contractions between genders.

METHODS

Five males and nine females with no history of neurological or musculoskeletal disorders participated in the study. Female subjects were tested within 3 days of menses to reduce the potential confounding factor of hormonal variations between subjects.

Subjects were seated in an experimental chair with the right knee fully extended. The right ankle was placed in a cast and connected to a servomotor via a rigid cantilever beam. Brackets were secured around the knee to prevent medial/lateral translation. To eliminate mechanical delay, the knee joint was pre-loaded in the abduction direction (3° or 4°). Then, abduction positional perturbations, ranging from 5° to 7°, were applied to the knee at a loading speed of 60°/s. At least 4 trials at each amplitude were performed on each subject. Surface electrodes recorded EMGs from quadriceps [rectus femoris (RF), vastus lateralis (VL), vastus medialis (VM)] and hamstring [semitindinosus (ST), and biceps femoris (BF)] muscles.

Data was filtered online with an 8^{th} order low-pass Butterworth filter with a 220 Hz cutoff and sampled at 1000 Hz. EMG signals were then rectified and filtered again with the same digital filter at a 120 Hz cutoff. Valgus induced muscle activity was considered significant if the rectified EMG activity, averaged over 70ms and 500ms after the onset of movement (t_o, see Figure 1), was greater than the mean plus one standard deviation of the background EMG signal calculated between 10ms and 110ms prior to t_o. For each subject, the probability that a given perturbation would result in firing of a muscle was computed as the ratio of trials where a significant EMG response occurred to the total number of trials performed at that angular perturbation on the

same subject. The proportions were averaged for each muscle and gender and then compared between genders.

RESULTS AND DISCUSSION

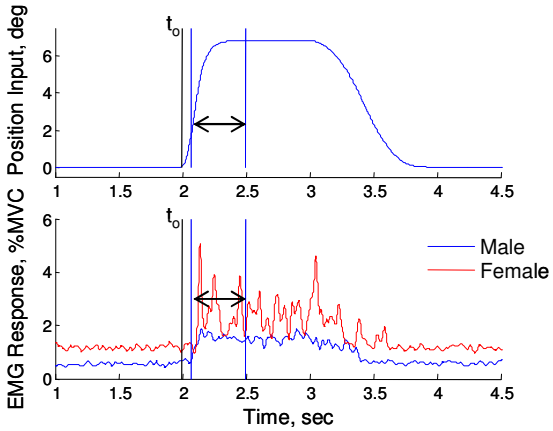

Figure 1. Seven degree position input signal (top) and resulting EMG activity in the ST muscle, normalized by MVC (bottom). The arrows specify the time window used to calculate perturbation induced EMG activity.

Reflex muscle activation in response to a valgus perturbation was observed much more frequently in males than females at all perturbation amplitudes (Table 1). In females the ST muscle displayed the largest probability of firing. For the 7° valgus perturbation reflex firing of ST was consistent across trials in 3 female subjects resulting in a firing probability of 0.36. The onset latency of the muscular responses averaged 102 +/- 22 ms for females and 94 +/- 19ms for males, which is less than the onset latency of a volitional triggered response (182 +/- 34ms).

Based on the firing probabilities, it appears that females rely more on hamstring muscles than quadriceps. Also, both genders showed a preferential firing of medial muscles (RF, VM, ST) over lateral muscles (VL, BF), which would be optimal to resist the lateral perturbation.

SUMMARY/CONCLUSIONS

Our preliminary results indicate that the probability that a valgus perturbation will elicit a neuromuscular response is much greater in males than females. While a larger sample size is warranted, these results may indicate that there exist gender differences in the motor control template used by the CNS to maintain joint stability in the frontal plane. It remains to be seen if such motor templates are modifiable via proprioceptive training paradigms designed specifically to reduce the prevalence of ACL injury in the female population.

REFERENCES

Agel J et al. (2005), *Am J Sports Med,* **33**(4): 524-30.

Bryant JT, Cooke DT. (1988), *J Orthop Res,* **6**(6):863-70.

Dhaher YY et al. (2003), *J Biomech*, **36**(2): 199-209

Dhaher YY et al. (2005), *J of Neurophysiology,* **93**(5):2698-709.

Ford KR et al. (2005), *Med Sci Sports Exerc,* **37**(1):124-9.

Hewett TE et al. (2005), *Am J. Sports Med,* **33**(4):492-501.

ACKNOWLEDGEMENTS

This work was supported by the National Institute of Health (1-R01-AR049837-01)

Table 1: Probability that a valgus perturbation will elicit a reflex response at each amplitude.

		Overall		RF		VL		VM		ST		BF	
		M	F	M	F	M	F	M	F	M	F	M	F
5	Mean	0.89	0.09	0.87	0.06	0.70	0.03	0.87	0.00	0.95	0.13	0.93	0.21
	SD	(0.25)	(0.19)	(0.30)	(0.17)	(0.48)	(0.08)	(0.18)	(0.00)	(0.10)	(0.22)	(0.15)	(0.31)
6	Mean	0.87	0.16	0.83	0.16	0.73	0.14	0.77	0.09	1.00	0.29	0.83	0.15
	SD	(0.24)	(0.22)	(0.33)	(0.26)	(0.33)	(0.19)	(0.28)	(0.20)	(0.21)	(0.28)	(0.33)	(0.24)
7	Mean	0.91	0.15	0.92	0.05	0.83	0.11	0.81	0.06	1.00	0.36	0.92	0.23
	SD	(0.23)	(0.27)	(0.17)	(0.10)	(0.33)	(0.25)	(0.38)	(0.11)	(0.13)	(0.41)	(0.17)	(0.31)

ADAPTATIONS TO TASK MECHANICS ALTER STRETCH REFLEX GAIN BUT NOT INTERMUSCULAR COORDINATION

Eric J. Perreault [1] Kuifu Chen [2], and Gwyn Lewis [3]

[1] Northwestern University, Evanston, IL, USA
[2] China Agricultural University, Beijing, China
[3] Aukland University of Technology, Auckland, NZ
e-mail: e-perreault@northwestern.edu

INTRODUCTION

The human motor system regulates arm mechanics to produce stable postures during interactions with different physical environments. This regulation occurs partly via involuntary mechanisms, including stretch sensitive reflexes. For example, single joint studies have demonstrated that reflex sensitivity increases during interactions with more compliant environments, suggesting that reflex gain increases to enhance limb stability when that stability is not provided by the environment (Dietz et al. 1994). Although such studies demonstrate the adaptability of stretch reflexes to changes in environmental mechanics, they have focused on individual joints. In contrast, most functional tasks require the coordinated activity of multiple joints within a limb, and it remains unclear how reflexes coordinating actions of muscles throughout the limb are modulated by the mechanical requirements of a task.

The purpose of this study was to quantify multijoint stretch reflexes as humans use their arms to interact with stiff and compliant environments. Our hypothesis was that stretch reflex sensitivity increases within muscles throughout the limb during interactions with compliant environments. In addition, we quantified reflex coordination across muscles to determine if any observed sensitivity changes were accompanied by changes in muscle recruitment patterns.

METHODS

Data were collected from 8 subjects. Reflexes were elicited by perturbing the dominant arm with a 3 degrees of freedom (DOF) robotic manipulator. [HapticMaster; FCS Control Systems]. The robot was configured as a critically damped 2nd order system with an isotropic stiffness of 10 N/m (compliant) or 10kN/m (stiff) to determine how reflexes were altered by the mechanical properties of the human-environment interface. Randomly occurring perturbations with an amplitude of 30mm and a velocity of 500mm/sec were applied along the three axes illustrated in Fig. 1. Perturbation amplitude and velocity were matched in the stiff and compliant environments. Subjects exerted constant, voluntary flexion or extension forces during each experimental trial (±0, 5, 10% MVC; X-axis).

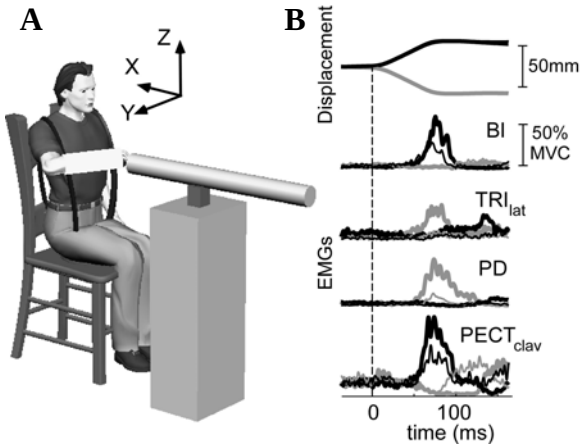

Figure 1: Experimental setup and typical reflexes elicited by Y-axis perturbations.

Electromyograms (EMGs) were recorded from 8 muscles representing the major elbow and shoulder muscles accessible via surface EMG: brachioradialis (BRD), biceps (BI), triceps long head (TRI_{long}), triceps lateral head (TRI_{lat}), anterior, middle and posterior deltoid (AD, MD, PD) and clavicular pectoralis ($PECT_{clav}$). Reflex magnitude was quantified by the average rectified EMG 50-100ms after perturbation onset. Reflex coordination was assessed using independent components analysis (ICA) to look at common muscle activations across all tasks (Tresch et al. 2006).

RESULTS AND DISCUSSION

Stretch reflex sensitivity increased during interactions with the compliant environment. Typical subject responses are shown in Fig. 1B. Thin traces correspond to data collected in stiff environment and thick traces to data from compliant environment. Color corresponds to perturbation direction, as shown in first row. Increased reflex sensitivity in the compliant environment occurred in all muscles and all subjects ($p<0.05$), and was not due to changes in background muscle activity.

Similar reflex coordination patterns were observed during interactions with stiff and compliant environments. Fig. 2 shows the coordination patterns estimated using ICA performed on data from a single subject; 4 ICs accounted for > 90% of the reflex variance in all subjects. Each group of 8 bars shows a single coordination pattern (one IC). Bar height indicates relative activation of each muscle. Coordination patterns estimated from stiff environment (left) are similar to those from compliant environment (right) for this subject. Cross-validation was used to assess similarity of the ICs estimated from data in each environment. Across all subjects, there was no significant difference in the accuracy of the reflexes predicted from ICs in either environment ($p>0.15$).

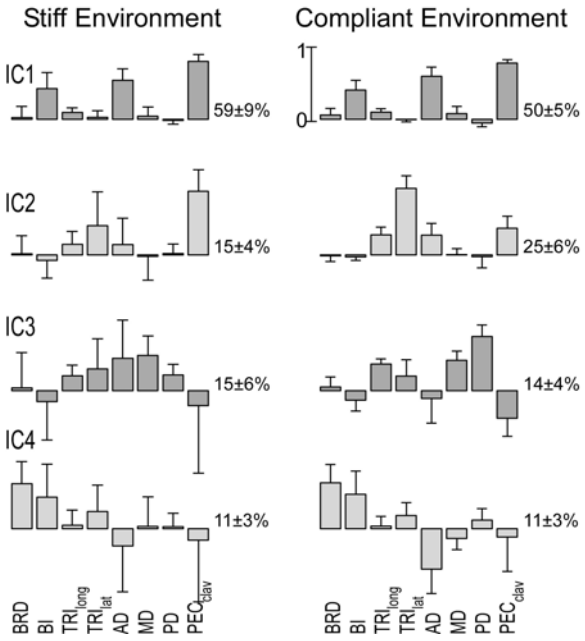

Figure 1: Single subject reflex coordination patterns. Numbers give relative IC variance.

SUMMARY/CONCLUSIONS

Our results are the first to demonstrate stretch sensitive reflexes throughout the arm modulate with the mechanical requirements of a task. The observed modulation did not represent a change in reflex coordination, suggesting that modulation for this task occurred through altered use of fixed muscle coordination patterns rather than through a change in the strategy of coordination.

REFERENCES

Dietz V et al. (1994) *Electroencephalogr Clin Neurophysiol* **93**: 49-56

Tresch MC et al. (2006) J Neurophysiol **95**: 2199-2212

ACKNOWLEDGEMENTS

This work was supported by NIH grants K25 HD044720 and R01 NS053813.

DTI-Based Fiber Tracking Reveals A Multifaceted Alteration Of Pennation Angle In Tibialis Anterior Muscle Upon Muscle Lengthening

Anneriet M. Heemskerk, Tuhin K. Sinha, Zhaohua Ding, Bruce M. Damon

Radiology and Radiological Sciences and Institute of Imaging Science, Vanderbilt University, Nashville, TN, USA
E-mail: a.m.heemskerk@vanderbilt.edu, Web: http://vuiis.vanderbilt.edu/

INTRODUCTION

Diffusion-tensor magnetic resonance imaging (DTI) offers great potential for understanding structure-function relationships in skeletal muscle (Sinha (2006), Lansdown (2007)). The basis for these studies is that the diffusion of water is greater along the long axes of muscle fibers than along their transverse axes. This anisotropy can be characterized using the diffusion tensor, with the orientation of the principal eigenvalue corresponding to the long axis of the muscle fiber. These local, voxel-based directions can be combined by a fiber tracking algorithm to reconstruct the whole-muscle architecture. The fiber tracking data can be used to characterize important muscle architectural parameters, such as pennation angle (θ), fiber length, and physiological cross-sectional area. These parameters influence the mechanical behavior of the muscle and are altered upon active or passive muscle lengthening or shortening. The goal of this study was to determine how θ changes in three dimensions upon muscle lengthening.

METHODS

DTI and anatomical MR images were acquired of the tibialis anterior (TA) of 6 subjects with the foot in 0˚ of plantarflexion (anatomical position), +15˚ of plantar flexion, and at 0˚ on a different day. Data were obtained with a 3T scanner using a double flexible surface coil covering the length of the TA. For anatomical reference a T_1 weighted scan was obtained: FOV=192×192 mm^2, matrix size=256×256, slice thickness =3 mm, 112 slices, TR=0.5 s, TE=18.6 ms. DTI images were acquired in 5 stacks, using an EPI sequence with the same geometric parameters, 128×128 reconstructed matrix, 4 excitations, TR= 5 s, TE=46 ms, b=500 s/mm^2, and diffusion weighting in 6 directions specified according to Jones (1999).

Image registration was performed of 1) the diffusion weighted images to the b=0 image, 2) the DTI stack to the adjacent stack, and 3) DTI set to the anatomical image set. From the anatomical images, the borders of the TA were traced and the position of the central aponeurosis was digitized. A 3D mesh reconstruction of the aponeurosis was defined with 280 rows × 100 column density and the points of intersection were used as seed points for fibertracking. Fibertracking was performed by following the direction of greatest diffusion from the seed points along each of the deep and superficial aspects of the TA's aponeurosis. For each fiber tract, position vectors were formed between the seed point and each of its first five points. For each point, the angle was calculated as the angle between the position vector and the plane tangent to the seed point from which that fiber tract emerges. θ was calculated as the mean of these 5 points. The mean θ was calculated for 50 evenly spaced segments along the aponeurosis (10 rows and 5 columns).

A 3-way repeated measures ANOVA was performed on the difference between the two foot positions with compartment, rows and columns as factors.

RESULTS AND DISCUSSION

Example of fibertracking results are displayed in Figure 1. The mean pennation angle was larger in the deep compartment than in the superficial compartment (Figure 2) ($p=0.044$), as was demonstrated before (Lansdown (2007)). The pennation angle was larger proximally than distally. θ did not differ in any location along the aponeurosis when the 0˚ measurement was repeated.

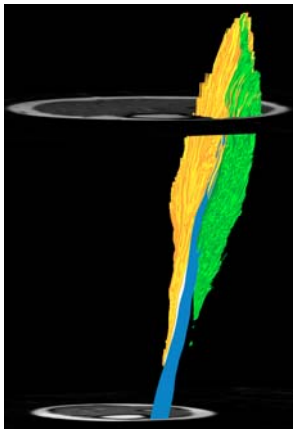

Figure 1: Example of fibertracking results. Fiber tracts from the deep compartments are indicated as gold-shaded lines and from the superficial compartment as green-shaded lines. The aponeurosis is indicated in blue.

The change in θ was larger in the proximal portion of the muscle than in the distal portion ($p=.003$), which is to be expected as the distal part of the aponeurosis is known to be more stiff. There was a tendency for the θ change to be greater in the posterior portion of the muscle ($p=0.069$), which might arise from a larger axial displacement of this part of the aponeurosis. This tendency was greater in the proximal part of the muscle than in the distal part of the muscle (columns × rows interaction, $p=.047$). Also, this interaction occurred to a different extent for both compartments (compartment×rows ×columns $p<0.0005$), with the change in angles being larger and more heterogeneous

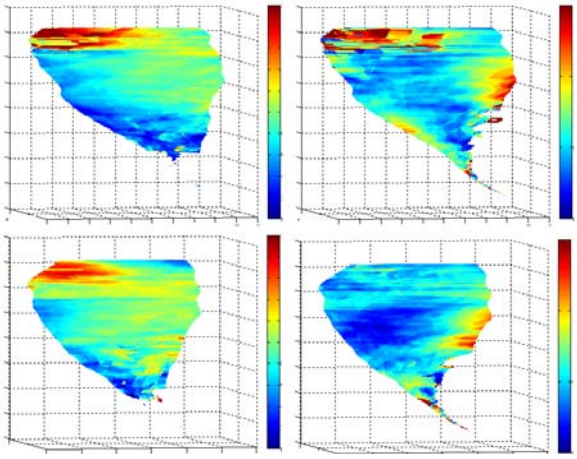

Figure 2: Distribution of pennation angles along the aponeurosis. Left: superficial compartment, right: deep compartment. Upper row: foot at 0˚, bottom row: foot at 15˚. Color bars indicate θ in degrees (left: 0-20˚, right 0-15˚)

in the superficial compartment than in the deep compartment. Therefore, upon muscle lengthening a 3D alteration of the muscle's pennation properties occurs.

CONCLUSIONS

DTI-based fibertracking enables the 3D reconstruction of a multifaceted alteration of pennation angles upon muscle lengthening. These data can be used to improve the understanding of structure-function relationships in muscle.

REFERENCES

Jones, D.K., Horsfield, M.A., Simmons, A. (1999). *Magn. Reson. Med.* **42(3).** 515-25

Lansdown, D.A. et al. (2007) *submitted to Journal of Applied Physiology*.

Sinha, S., Sinha. U., Edgerton. V.R. (2006). *J. Magn. Reson. Imaging,* **24(1)**, 182-90.

ACKNOWLEDGEMENTS

Support: NIH/NINDS R01 NS034834
NIH/NIAMS AR050101
NIH/NCRR M01 RR 00095

MEASUREMENTS OF *IN VIVO* PATELLOFEMORAL JOINT KINEMATICS WITH REAL-TIME MRI

Christine Draper [1], Thor Besier [1], Juan Santos [1], Garry Gold [1], Gary Beaupre [1,2], Scott Delp [1]

[1]Stanford University, Stanford, CA
[2]VA Rehabilitation Research and Development Center, Palo Alto, CA
email:cdraper@stanford.edu; website: http://nmbl.stanford.edu

INTRODUCTION

Accurate measurements of *in vivo* joint kinematics are needed to understand normal and pathological joint mechanics. Methods to quantitatively measure joint kinematics enable us to better identify abnormal motion and to evaluate treatments for certain musculoskeletal disorders.

Current methods of measuring *in vivo* joint motion include bi-plane radiography (Tashman, 2003) and cine-phase-contrast MRI (Sheehan, 1998). Recent advances in MRI technology have resulted in the implementation of real-time image acquisition (Kerr, 1997). Real-time MRI is non-ionizing and allows measurement of bone and soft tissue motion during dynamic, weight-bearing activities.

The purpose of this study was to determine the feasibility of measuring patellofemoral joint kinematics during upright, weight-bearing knee extension using real-time MRI.

METHODS

We examined the patellofemoral joints of six healthy control subjects. All subjects were female, between the ages of 20 and 30, and had no history of knee injuries. Real-time MR images of their knees were obtained using a 0.5T Signa SP open-MRI scanner (GE Healthcare) and the following scan parameters: field-of-view: 16cm, spatial resolution: 1.88mm, frame rate: 6 frames/s, 6 acquisitions/frame, 16ms readout trajectory. A custom-built backrest stabilized subjects in an upright, weight-bearing posture. Subjects performed continuous squatting movements in the scanner from 0° to 60° of knee flexion and back at a rate of 6°/s. An oblique-axial plane through the widest portion of the patella was imaged.

To evaluate whether the measurements obtained from real-time MRI are consistent with other methods of measuring joint alignment, we used quasi-static MRI (FOV: 20cm, matrix size: 128x128, slice thickness: 5mm, resolution: 1.6mm, TE: 5.6ms, flip angle: 70, # slices: 1) to obtain axial images at five knee flexion angles (0°, 15°, 30°, 45°, 60°). Subjects performed quasi-static knee flexion, holding each position for about 15 seconds.

Clinical measurements of patellar motion were estimated by manually identifying bony landmarks in each image frame. Bisect offset describes the medial/lateral position of the patella and is reported as the percentage of the patella lateral to the midline of the femur. Patellar tilt is a measure of the angle between the patella and the posterior femoral condyles (Figure 1).

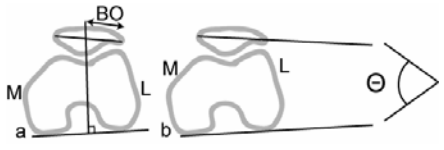

Figure 1: Diagram of bisect offset (BO) (a) and patellar tilt (Θ) (b) measurements.

For each subject, the measured kinematics from two real-time MRI trials were averaged and smoothed with a Hamming window filter.

To assess the precision of our estimates, we measured bisect offset and patellar tilt three times on the same set of real-time MR images and found the measurements to be repeatable (average RMS difference of 3.0% for bisect offset and 1.0° for patellar tilt).

RESULTS AND DISCUSSION

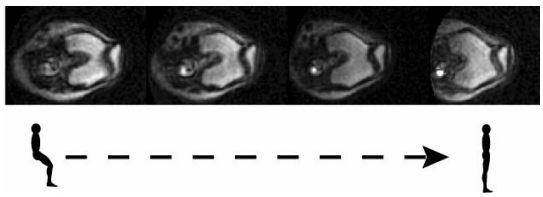

Figure 2: Sample real-time MRI frames during weight-bearing knee extension.

The measurements from the real-time MR images are within one standard deviation of the mean measurements obtained from the quasi-static images for most knee flexion angles (Figure 3). There are differences in the measurements of bisect offset at 45° and 60° and in patellar tilt at 30° of knee flexion. However, it is not known whether the kinematics occurring during a dynamic squat will necessarily equal those measured from quasi-static images. In future studies, we will analyze more subjects to identify whether the knee joint kinematics are different during a dynamic task.

Real-time MRI enables continuous measurements of joint kinematics to be obtained during dynamic, weight-bearing tasks. The techniques developed in this study may improve the diagnosis and treatment of subjects with patellofemoral pain. Abnormal motion of the patella relative to the femur is thought to be one cause of pain. However, it is unclear whether the clinical observation of altered patellar motion correlates with the kinematics occurring during the functional, weight-bearing activities that cause pain. We plan to use real-time imaging techniques to address this question. We will quantify the knee joint kinematics during dynamic, weight-bearing knee extension in subjects with patellofemoral pain and compare them to the measurements obtained in this study.

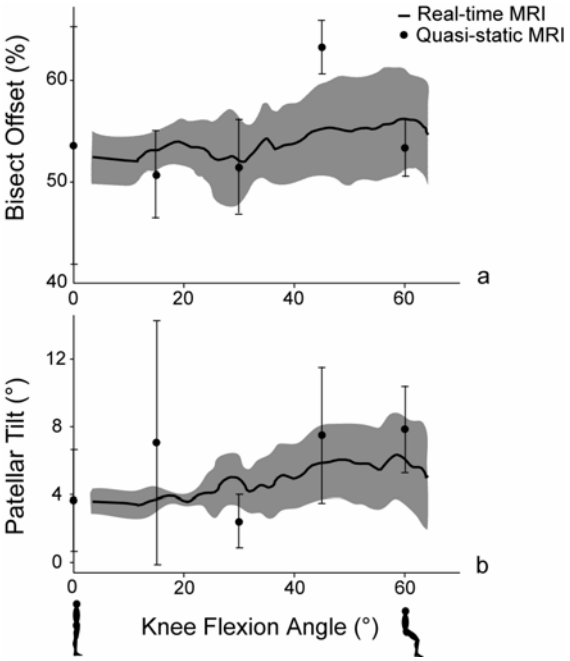

Figure 3: Relationship between knee flexion angle and (a) the percentage of the patella lateral to the midline of the femur (bisect offset) and (b) patellar tilt angle. The solid line is the mean ± SD of the measurements from real-time MRI. The circles are the mean ± SD of measurements from the quasi-static images.

REFERENCES

Tashman, S. and Anderst, W. (2003), *J Biomech Eng*, **125**, 238-245.

Sheehan,F.,et al.(1998),*J Biomech,***31,**21-26.

Kerr, A., et al. (1997), *Magn Reson Med*, **38**, 355-367.

ACKNOWLEDGEMENTS

VA Rehabilitation R&D Service (#A2592R), the NIH (EB002524-01, EB005790-01), the NSF, and SGF.

DYNAMIC POSTURAL STABILITY DURING SIT-TO-WALK TRANSITIONS IN THE HEALTHY YOUNG AND HEALTHY ELDERLY

Thomas A. Buckley[1], Chris J. Hass[2] and Chris Pitsikoulis [3]

[1] Georgia Southern University, Statesboro, GA, USA
[2] University of Florida, Gainesville, FL, USA
[3] Teachers College Columbia University, New York, NY, USA
E-mail: Tom.Buckley@DC.edu

INTRODUCTION

The study of transitional movements such as gait initiation (GI) and sit-to-stand (STS) has provided valuable insights into the control of dynamic postural stability in the elderly. The study of GI and STS has clearly been valuable in understanding dynamic postural stability within common activities of daily living (ADL); however, little attention has been paid to the functional task of initiating gait from the seated position, or Sit-to-Walk (STW). This is surprising since the initiation of gait from a seated position is a common ADL and it represents a complex transitional task that imposes challenges to both the locomotor and postural control systems.

In healthy young adults (HYA), STW is a merged task based on the coincidental timing of seat-off and gait initiation (Magnan 1996, Kerr 2004). Healthy older adults (HOA) perform STW slower than HYA (Kerr 2006), however no detailed biomechanical analysis of STW in the elderly has been performed. Thus, the purpose of this study was to biomechanically evaluate STW in the HOA population and compare the performance of the HOA to the HYA.

METHODS

Twelve healthy older adults (age: 63 $\pm$ 8y.o., ht: 169.8 $\pm$ 10cm, wt: 79.2 $\pm$ 15.5kg, BMI: 25.5 $\pm$ 3.4) and twelve healthy young adults age: 29 $\pm$ 3y.o., ht: 170.6 $\pm$ 7.6cm, wt: 76 $\pm$ 14.8kg, BMI: 25.9 $\pm$ 3.1) participated in this study. Kinematic data was collected at 120Hz with 41 retro-reflective markers attached. Kinetic data from 2 forceplates were sampled at 1560Hz.

Each subject performed 5 trials of STW. Trials began with the subject seated on a backless and armless adjustable height stool (40 – 58cm) such that the subject's knees were flexed to approximately 105º. In the initial starting position, subjects were seated so that their greater trochanter was located near the front edge of the stool. The feet were placed comfortably on the force platforms and the position was recorded and subsequently standardized throughout the experiment by placing tracings on the force platform. Potential intersubject differences due to movement of the upper limbs were minimized by requiring the subjects to sit with the palmar aspect of their hands resting on their stomach, just inferior to the xiphoid process.

Phases of STW were identified as previously described (Kerr 2004). In addition, spatiotemporal characteristics, COP-COM separation, and COM momentum were calculated. In pilot work we were unable to replicate Kerr's (2004) definition of GI, therefore initial swing leg heel-off was used as a marker to identify the initiation of gait within STW.

Three separate MANOVA's were used to analyze the STW task. A 2 (group) x 2 (task) repeated measures ANOVA was used to compare between tasks.

RESULTS AND DISCUSSION

The HYA moved quicker through each phase of STW except phase I as seen in the table below.

Phase	Description	HYA (s)	HOA (s)	p-value
I	Mvmt initiation to seat off	0.48	0.50	0.389
II	Seat-off to peak vertical velocity	0.39	0.51	0.022
III	Gait initiation to swing toe off	0.12	0.16	0.006
IV	Swing Toe Off to Stance Toe Off	0.47	0.54	0.007
Total	Total Task Time	1.46	1.82	0.001

Table 1. Temporal durations of each phase of the STW task.

The HYA took significantly longer steps ($p<0.001$) at significantly faster velocities ($p<0.001$) than the HOA. There was no difference in the initial step width between groups.

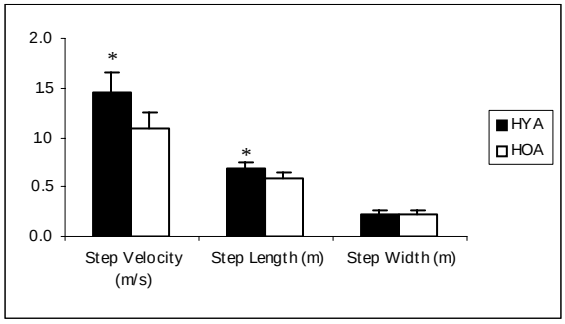

Figure 1. Spatiotemporal characteristics of the groups during the STW task. * indicates significant difference between groups

The HOA initiated gait after a significantly longer delay from seat-off ($p<0.001$) and while standing significantly more erect ($p=0.002$) than the HYA. While the HYA merged the two tasks shortly after seat-off, the HOA delayed the initiation of gait until they were nearly fully upright.

Additionally, the HYA produced significantly greater peak horizontal momentum ($p=0.005$), peak horizontal momentum prior to seat-off ($p=0.020$), and peak vertical momentum ($p=0.044$) during STW. It is likely this increased generation of momentum resulted in the HYA having a greater COP-COM separation ($p=0.001$) at the conclusion of the single support phase of the initial step during STW.

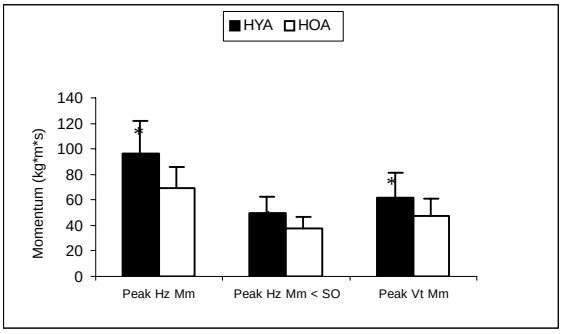

Figure 2. Horizontal and Vertical momentum generated during the STW task. * indicates significant difference between groups

CONCLUSIONS

HOA are unable to successfully fully merge the STW task around seat-off, however the tasks were not distinct as the initiation of gait occurred while still rising. This suggests the HOA utilized a more conservative postural strategy of performing STW. Conversely, and in agreement with previous literature (Magnan 1996, Kerr 2004), the HYA successfully merged the two tasks around, or shortly after, the point of seat-off.

REFERENCES

Kerr A, et al. (2006) *Gait Posture*, **epub** August.

Kerr A, et al. (2004) *Clin Biomech* (**19**), 385-390.

Magnan A, et al. (1996) *Gait Posture* (**4**), 232-241.

A GENETIC ALGORITHM APPROACH TO SINGULARITY AVOIDANNCE IN THE ANALYSIS OF WEIGHT LIFTING PERFORMANCE

Amir H. Javadi[1,2], Ahmed R. Arshi[1,2], Elham Shirzad[1,2], and Manssour Moeinzadeh[3]

[1] Amir Kabir University of Technology, Tehran, Iran
[2] National Olympic Academy of Iran, Tehran, Iran
[3] University of Illinois at Urbana-Champaign, USA
E-mail: manssour@uiuc.edu, Web: http://www.iese.uiuc.edu/

INTRODUCTION

The existing publications on biomechanics of weight lifting tend to concentrate on injury prevention or performance evaluation through various kinetic or kinematic evaluation of the athletes (GAR98, CAR04). An analytical model could prove effective in an individualized approach to performance enhancement. The athlete can be represented by a planar 6 degrees of freedom robotic manipulator where the barbell trajectory is an input to an inverse kinematics problem. Closed form approach and many iterative solutions face a major upheaval in avoiding singularities and thus find it difficult to ensure a smooth motion of the resulting configurations. The convergence potentials of GAs through an efficient search in such large and complex solution spaces are theoretically and empirically exhibited in a number of articles (GOL89, JAV03 and HUA06). A genetic algorithm approach is therefore adopted in determination of a near optimum solution to a highly redundant inverse kinematics problem. Implementation of GA is taken place through adoption of two categories of constraints, the first of which defines the barbell trajectory and the second containing two sets of physiological and kinesiological constraints. The physiological constraints are defined by joint torques and the kinesiological constraints represent joint angles and velocities.

METHODS

Modeling and comparative data are obtained through motion analysis using WINAnalyze using a single digital camera placed at right angles to the sagittal plane recorded the motion at 125fps. The athlete is modeled as a planar 6 degrees of freedom manipulator. The model is fixed on one base (toes). GA is used to solve the trajectory tracking of the barbell during the motion of the athlete's snatch lift. The generated series of configuration is optimized for minimum total displacement of COM for preserving the maximum stability, and minimum total consumed energy in each joints, so the lesser the fitness value, the better the onfiguration. Torque is calculated using recursive Newton-Euler method (SHI06).

The variables of the problem are joint angles as shown in Fig. 1. Initial joint angles are given by vector below,

$$\underline{\Theta_s} = \{\Theta_{s1}, \Theta_{s2}, \Theta_{s3}, \Theta_{s4}, \Theta_{s5}, \Theta_{s6}\}.$$

So GA uses vector shown below, except for the initial configuration,

$$\Delta\underline{\Theta_s} = \{\Delta\Theta_{s1}, \Delta\Theta_{s2}, \Delta\Theta_{s3}, \Delta\Theta_{s4}, \Delta\Theta_{s5}, \Delta\Theta_{s6}\}$$

in which $\Delta\Theta_{si}$ for $i = 1..6$ is less than 5°.

The population size is set to 100. The genetic operators are uniform crossover and mutation, which are applied with probabilities of 1.00 and 0.01 respectively. The selection method used is tournament selection, with tourney-size 15.

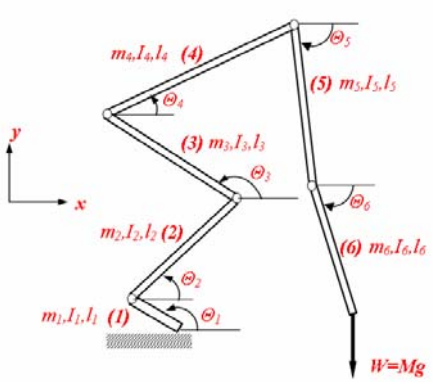

Figure 1: Body model. Illustrating a manipulator with 6-DOF.

RESULTS AND DISCUSSION

The mean value of fitness of the population in each generation is gradually improved in each generation. One configuration generated by GA is shown in Fig. 2, where the obtained configuration is presented at the end of the second pull phase of snatch. Red points represent the discrete barbell trajectory and green crosses show variations of center of mass of the body-weight system.

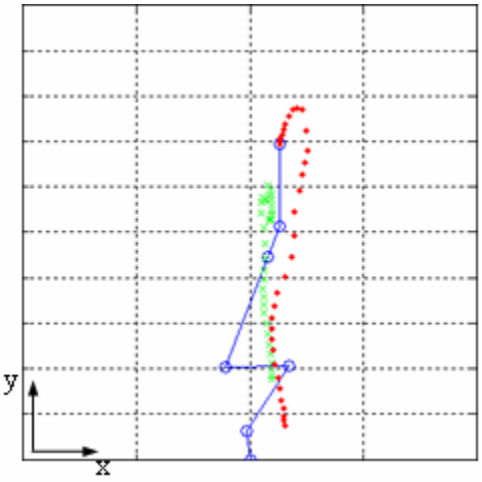

Figure 2: The resulting configuration of body model using GA.

The resulting configuration obtained through implementation of genetic algorithm indicates an enhancement in performance by suggesting an alternative technique where joint torques are lower and thus the consumed energy is reduced.

SUMMARY

This paper has aimed at establishing the Genetic Algorithm as a useful tool in formulation of an individualized analytical model towards performance enhancement and injury prevention in weight lifting by providing the athlete and the coach with a more effective alternative weightlifting technique.

REFERENCES

Carlock, J.M. et al (2004). *The relationship between vertical jump power estimates and weightlifting ability: A field-test approach*. J. Strength Cond. Res. 18(3):534–539.

Goldberg, D. E. (1989). *Genetic Algorithms in Search, Optimization, and Machine Learning*. Addision-Wesley Publishing.

Garhammer, J. (1998). *Weightlifting performance and techniques of men and women. International Conference on Weightlifting and Strength Training*. K. Ha¨kkinen, ed. Lahti, Finland: Gummerus Printing, 89–94.

Huang, P. et al. (2006). *Global Minimum-Jerk Trajectory Planning of Space Manipulator*, International Journal of Control, Automation, and Systems, vol. 4, no. 4, pp. 405-413, August.

Javadi, A.H., and Mojabi, P. (2003). *Team learning via decentralized conflict resolution through utilizing GA in path planning*, in proc. of 9th European conference of the international society for terrain vehicle systems, ISTVC03, England.

Shirzad, E. et al. (2006). *Mathematical modeling and computer simulation of weightlifting sport, phase 1: pull phases in snatch technique*, International journal of scientific research, vol. 16, pp. 323-327.

LOAD-MODIFYING FOOTWEAR INTERVENTION LOWERS KNEE ADDUCTION MOMENT, REDUCES PAIN, AND IMPROVES FUNCTION IN SUBJECTS WITH MEDIAL COMPARTMENT KNEE OSTEOARTHRITIS

Jennifer Erhart [1,2], Nicholas J. Giori [1,2,3], and Thomas P. Andriacchi [1,2,3]

[1] Department of Mechanical Engineering, Stanford University, Stanford, CA, USA
[2] Bone and Joint Center, Palo Alto VA, Palo Alto, CA, USA
[3] Department of Orthopedic Surgery, Stanford University, Stanford, CA, USA
E-mail: jerhart@stanford.edu Web: www.stanford.edu/group/biomotion

INTRODUCTION

A high maximum adduction moment at the knee during walking has been associated with an increased rate of progression (Miyazaki et al. 2002) and worse treatment outcome (Andriacchi 1994) of medial compartment osteoarthritis (OA) of the knee. Consequently, many interventions for knee OA attempt to reduce the maximum knee adduction moment. Wedged inserts have been shown to reduce the knee adduction moment in healthy and osteoarthritic populations (Krenshaw et al. 2000, Kerrigan et al. 2002). However, randomized control studies of laterally wedged insoles in subjects with medial compartment knee OA have failed to show reductions in pain compared to control after both 6 and 24 months of use (Maillefert et al. 2001, Pham et al. 2004). Variable-stiffness shoes with greater lateral sole stiffness than medial sole stiffness have also been shown to reduce the knee adduction moment in healthy individuals (Fisher et al. 2007). However, it is not known if this reduction occurs in an osteoarthritic population, or if this reduction is associated with a decrease in pain. The purpose of this study was to test the following hypotheses: (1) the knee adduction moment will be reduced in subjects with medial compartment knee osteoarthritis after six months of variable-stiffness shoe wear (2) the reduction in knee adduction moment will be accompanied by a reduction in pain and improvement in function.

METHODS

24 subjects with symptoms of medial compartment knee OA participated in this prospective placebo-control study after giving written consent in accordance with the Institutional Review Board. At an initial visit, subjects were randomly assigned to either a constant-stiffness control shoe (12 subjects; 5 male, 7 female; age: 63.3 ± 8.5 yrs; height: 1.66 ± 0.08; mass: 73.6 ± 16.1 kg) or a variable-stiffness intervention shoe (12 subjects; 5 male, 7 female; age: 65.5 ± 11.3 yrs; height: 1.71 ± 0.08; mass: 85.1 ± 15.4 kg) to wear as their main walking shoe (at least 4 hours of wear per day) for 6 months. Subjects were blinded as to their shoe type. The variable-stiffness intervention shoe has a lateral sole stiffness 2.5x greater than the medial sole stiffness, which is equal to the stiffness of the control shoe sole. Subjects also completed WOMAC functional improvement-based patient ratings specific to osteoarthritis to assess pain and function (Bellamy et al. 1988). At the 6 month time point, subjects again completed WOMAC questionnaires and performed 3 walking trials at a self-selected normal speed in their study shoe (control or intervention) and their own personal walking shoe (comfortable walking shoe used by the patient).

Kinematic and kinetic data were collected using an 8-camera optoelectronic motion capture system (Qualisys) and reflective markers. External inter-segmental forces and moments were calculated for the lower limb

using previously described methods (Andriacchi et al. 2004). The first peak knee adduction moment was calculated for each trial. Average values for each shoe and subject were determined for each subject's more affected leg (determined by self-reported pain), and paired two-tailed Student's T-tests were used to compare the different shoes (α=0.05). Paired two-tailed Student's t-tests (α=0.05) were also used to compare the functional-improvement based ratings at the initial and 6 month time points.

RESULTS AND DISCUSSION

The knee adduction moment of the subjects' more affected leg was significantly reduced for the intervention group ($p<0.01$) with the variable-stiffness shoes versus the subjects' own personal walking shoes after 6 months of wear, with an average reduction of 6.4%. For the constant-stiffness control shoe group, there was no significant difference in knee adduction moment with the control shoes versus the subjects' own personal walking shoes after 6 months of wear.

For the intervention group, there was a significant improvement in WOMAC score ($p<0.01$) from the initial to 6 month time point, with an average absolute reduction in WOMAC score of 31 points. For the control group, there was no significant change in WOMAC score from the initial to the 6 month time point (Figure 1).

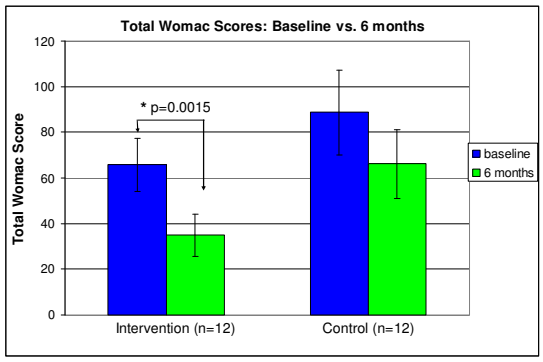

Figure 1: Average WOMAC scores (±SEM) at the initial and 6 month time points for the intervention and control groups.

SUMMARY/CONCLUSIONS

The use of a variable-stiffness shoe significantly reduces pain and improves function after 6 months of shoe wear. This finding is in contrast to studies of lateral wedges, which did not find reductions in pain after long-term use. It is possible that the dynamic action of the variable-stiffness shoe is more effective at reducing pain and improving function than the fixed foot position of a lateral wedge. Furthermore, the reduction in pain is accompanied by a reduction in knee adduction moment; thus the variable-stiffness shoes provide both reduced load and reduced pain, and may slow the rate of progression of medial compartment knee OA.

This study supports the conclusion that wearing a variable-stiffness shoe can reduce the knee adduction moment, significantly reduce pain and improve function, and possibly slow the progression of knee osteoarthritis, in patients with symptoms of medial compartment knee osteoarthritis.

REFERENCES

Andriacchi TP et al. (1994) *Orthop Clin North Am* **14**, 289-295.

Andriacchi TP et al. In *Basic Orthopaedic Biomechanics*, 3rd ed., 91-121, 2004.

Bellamy N et al. (1988) *J Rheumatol* **15**,1833-1840.

Crenshaw SJ et al. (2000) *Clin Orthop* **375**, 185-192.

Fisher DS et al. (2007) *J Orthop Res* **25(4)**, 540-546.

Kerrigan DC et al. (2002) *Arch Phys Med Rehabil* **83**, 889-893.

Maillefert JF et al. (2001) *Osteoarthritis Cartilage* **9**, 738-745.

Miyazaki T et al. (2002) *Ann Rheum Dis* **61**, 617-622.

Pham T et al. (2004) *Osteoarthritis Cartilage* **12**, 46-55.

ACKNOWLEDGEMENTS

Study supported by VA grant # A02-2577R.

TORQUE COUPLING POST STROKE: IMPLICATIONS FOR GAIT

Theresa Hayes, MS [1,2], Yasin Dhaher, PhD [1,2]

[1]Northwestern University, Chicago, IL, USA
[2]Rehabilitation Institute of Chicago, Chicago, IL USA
E-mail: t-hayes3@northwestern.edu Web: www.smpp.northwestern.edu

INTRODUCTION

Investigations of post-stroke gait have reported abnormal swing phase joint kinematics, including circumduction (lateral movement of limb) and stiff-knee (reduced peak knee flexion) (Kerrigan et al. 2000). In addition, two patterns of tightly coupled motions at adjacent joints have been observed in the hemiparetic limbs of stroke subjects. These behaviors consist of knee flexion with hip abduction, flexion, and external rotation and knee extension with hip adduction, extension and internal rotation (Brunnstrom 1970). It has been suggested in the upper limb that coupled movements are manifestations of an abnormal motor template that can be identified during isometric torque generation tasks (Levin 1996). However, the clinically observed lower limb coupled movements are obtained in the supine position, making it difficult to determine their potential contribution to the observed gait abnormalities. Therefore the goal of this study was to investigate the presence of torque coupling in functionally relevant, load-bearing postures in the chronic stroke population. Given that post-stroke gait abnormalities involve the hip frontal plane and knee sagittal plane kinematics, we hypothesize that abnormal across-joint torque coupling between the hip frontal and knee sagittal plane torques will be observed in the stroke group. Consistent with clinical observations, we further hypothesize that this coupling will be dependent on limb posture.

METHODS

Twenty-four ambulating stroke subjects who suffered a monohemispheric CVA no less than 12 months prior and 15 age-matched control subjects were tested. Subjects' lower limbs were secured in a computer–controlled, instrumented exoskeleton that measures the interaction forces/moments between the subject and the orthosis. The pelvis was also fixed to the exoskeleton and body-weight support of 30-40% body weight was provided via a harness. The experimental protocol was performed at two postures: "toe-off" (hip 15^o extension, knee 45^o flexion) and "mid-swing" (hip 10^o flexion, knee 65^o flexion). It consisted of measuring the maximum voluntary hip torques (MVHT) in the abduction and adduction directions and target-matching at 50% of the MVHT, while receiving real-time visual feedback. Subjects were instructed to produce the hip target torque and hold for 200ms.Meanwhile, subjects were unaware that the knee flexion/ extension torque measurements were recorded simultaneously. The distributions of the knee torque (flexion or extension) produced during each frontal plane hip torque task (abduction and adduction) were tested for differences between groups using a Chi-square test. To address the specific differences in group behaviors, one sample non-parametric t-tests on the knee torques were also performed.

RESULTS AND DISCUSSION

The frequency of the knee torque direction was dependent on subject group only during

the hip adduction task at the toe-off position ($p<0.05$), see Table 1. Specifically, the stroke group coupled hip adduction with knee extension torque, see Figure 1.

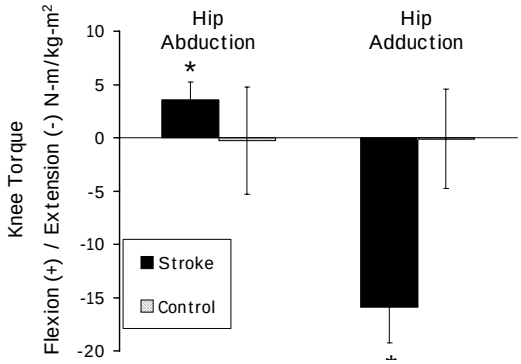

Figure 1: Knee torque during hip abduction and adduction tasks in the toe-off position. * significant knee torque($p<0.05$).

Moreover, while no significant differences in the knee torque distribution were observed between groups during the abduction task at toe-off, significant knee flexion torque was produced by the stroke group, see Figure 1. The change in posture from toe-off to mid-swing reduced the intensity of the stroke group knee torque as well as eliminated the difference in the knee torque distribution between groups during hip adduction.

SUMMARY/CONCLUSIONS

The torque coupling between hip adduction and knee extension at the toe-off posture suggests that abnormal across-joint behavior may contribute to impaired swing-phase kinematics. These findings are consistent with earlier reports of higher extension torque prevalence than flexion torque coupling in neurologically-impaired populations (Sawner 1992.) Moreover, this coupling was not observed in the midswing posture, despite the larger net knee extension moment arm predicted by musculoskeletal models (SIMM, Musculographics, Inc.) Taken together, these findings suggest a change in the neural template following stroke is potentially responsible for the observed behaviors. By clarifying these underlying impairments, more efficacious methods of improving post-stroke gait performance may be developed.

REFERENCES

Brunnstrom S. (1970) Movement therapy in hemiplegia. A neurophysiological approach. New Your: Harper & Row.

Kerrigan DC, Frates EP, Rogan S, Riley PO. (2000) Hip hiking and circumduction: quantitative definitions. *Am J Phys Med* Rehabil. 79(3):247-252.

Levin MF. (1996) Interjoint coordination during pointing movements is disrupted in spastic hemiparesis. *Brain.* 119:281-93.

Sawner K, J. L. (1992) *Brunnstrom's movement therapy in hemiplegia: a neurophysiological approach.* 2nd ed. Philadelphia: JB Lippincott.

ACKNOWLEDGEMENTS

Funding for this project was provided by the American Heart Association and NIDRR.

	Toe-off				Mid-swing†			
	Hip Adduction*		Hip Abduction		Hip Adduction		Hip Abduction	
	Stroke	Control	Stroke	Control	Stroke	Control	Stroke	Control
Knee Flexion	3	10	16	8	10	7	15	7
Knee Extension	21	5	8	7	12	7	7	7
Total	24	15	24	15	22	14	22	14

Table 1: Frequency of knee torque direction. * Significant group effect ($p<0.05$), degrees of freedom =3. †Two stroke and one control subject only completed the toe-off testing.

A MUSCULOSKELETAL MODEL OF THE RAT HINDLIMB

Will L Johnson[1], Devin L Jindrich[2], Roland R Roy[1], V Reggie Edgerton[1]

[1] UCLA, Los Angeles, CA, USA
[2] Arizona State University, Tempe, AZ, USA
E-mail: johnsonw@ucla.edu

INTRODUCTION

As a first step towards developing a dynamic musculoskeletal model of the rat hindlimb, we measured muscle origin and insertion coordinates relative to bony landmarks and characterized joint center locations. Using these measurements, we analyzed muscle moment arms as a function of joint angle for most muscles of the hindlimb.

Development of this model required us to answer the following questions: Can joint centers of the hindlimb be approximated by simple functions dependent on joint angles? Secondly, can muscle attachment sites be approximated by curves and are the centroids of those curves sufficient to describe the attachments? We used the model to test the hypothesis that postural change alone, and particularly the transition from quadrupedal to bipedal posture, is sufficient to alter the function of selected muscles of the leg.

METHODS

Muscle origin and insertion coordinates were quantified using stereophotogrammetry. Muscles were successively dissected away from the bones, and photographs taken. Each photographic frame contained the feature being measured and three pin landmarks. A commercial stereophotogrammetry program and landmark pin-defined rotations were used to find 3-D coordinates of each origin and insertion in a bone coordinate system (BCS) defined to closely coincide with the human joint coordinate system recommended by the International Society of Biomechanics.

In a second experiment, joints were moved through their natural range while photographs were taken. Pin coordinates were found in the BCS in accordance with the process described above. Instantaneous joint centers were found using a method derived from Woltring (1985). We modeled each joint as a moving point dependent on joint angle; a first-order function was used to describe this dependence.

Given the coordinates of a particular muscle's origin and insertion and the coordinates of the joint center, we were able to calculate the moment arm of that muscle for arbitrary joint angles.

RESULTS AND DISCUSSION

Measurement of musculoskeletal anatomy in the rat hindlimb allowed us to determine appropriate functions for joint center movement and the attachment sites. The resulting model demonstrated that limb posture can substantially affect muscle mechanics. While existing joint models can provide adequate kinematic descriptions, modeling the joint as a moving point allows more realistic modeling of joint dynamics. However it requires the approximation that at any given joint angle, differential rotations in any direction will be about the same point. We consider this approximation reasonable since it is equivalent to requiring the center location function to be continuous. Relative er-

rors less than 7% indicate that this method can accurately model moving joint centers.

To reduce the error inherent in estimating the attachment area centroid, we selected points on the margin of and spanning the attachment area. Because such a span of points does not follow a normal distribution, their mean is not appropriate to describe the attachment centroid. Instead, we described muscle attachment sites as second-order curves. The length of the fit parabola and standard errors in the orthogonal directions give an estimate of muscle attachment sizes. These relative sizes are consistent with observations of attachment size made during dissection.

Most muscles have moment arms with a large range across the physiological domain of joint angle, but their moment arms peak and vary little within the stance domain. The small variation in moment arms during stance simplifies the neural control requirements during this phase. This is in contrast to variable movements which require control over a larger range of moment arms and may impose greater control burdens than required during quadrupedal locomotion.

The moment arms of a number of muscles crossed zero as angle varied. Pectineus and the obturators switch function as the hip transitions between angles within the stance domain of quadrupedal locomotion (Fig. 1). Because a zero crossing in the negative direction indicates an intrinsically stabilizing muscle (Young, Scott, et al. 1983), these muscles are likely primarily responsible for hip stabilization. However in the domain of hip angles encountered during bipedal locomotion, the moment arms of these muscles do not cross zero and thus are no longer intrinsically stabilizing. Eight muscles have intrinsically stabilizing moment arms about the hip, indicated by a negative-slope zero crossing. Interestingly, no muscles were observed to have intrinsically stabilizing moment arms in adduction/abduction about the hip or ankle.

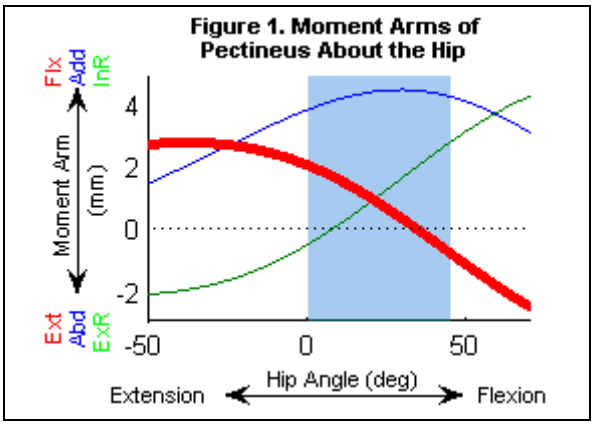

SUMMARY/CONCLUSION

This study investigated the morphological properties of the rat hindlimb necessary for determination of muscle moment arms throughout the physiological range of motion. We found that muscle function is largely determined by the change in moment arm with joint angle, which may produce an intrinsically stabilizing arrangement or reduce the control burden. Furthermore, muscle function changes dramatically with transition from quadrupedal to bipedal posture.

REFERENCES

H. J. Woltring, R. Huiskes, et al. (1985). *Journal of Biomechanics* **18**: 379-89.

R. P. Young, S. H. Scott, et al. (1983). *Experimental Brain Research* **V96**: 141-51.

ACKNOWLEDGEMENTS

Supported by NIH grant PO 1 NS 16333

DEVELOPMENT OF A LOWER EXTREMITY BIOMECHANICAL MODEL WITH INTEGRATED MULTISEGMENTAL FOOT MOTION

Jason T Long, Mei Wang, and Gerald F Harris
Orthopaedic and Rehabilitation Engineering Center
Marquette University/Medical College of Wisconsin, Milwaukee, WI
Email: jlong@mcw.edu; Web: www.orec.org

INTRODUCTION

Current methods of conducting gait analysis in the clinical environment are limited by the biomechanical models used for the measurement. The standard clinical model is limited by its means of calculating the location of the hip joint center and by its method of modeling the foot as a single rigid segment. Commonly used predictive methods for calculating hip joint center (HJC) are based on anthropometric measurements and regression equations. Recent studies (Leardini, 1999; Piazza, 2004) have suggested that a functional method of HJC location, involving special calibration trials and spherical fitting algorithms, may provide a better approach.

The foot is a complicated structure, and a single-segment representation of its several sections is a simplification which masks the true nature of many walking problems. Gait analysis with such a single-segment model is of limited use for patients with foot-specific pathology. Several models specific to the foot and ankle have been published in the literature (Kidder, 1996; MacWilliams, 2003; Kitaoka, 2006; Simon, 2006; Leardini, 2007), but none of these provides information proximal to the tibia. A means of simultaneously analyzing lower extremity motion (pelvis, hip, and knee) and multisegmental foot/ankle motion is not currently available in the clinical environment. Our group has previously developed and validated the Milwaukee Foot Model (MFM); this unique four-segment model is capable of indexing the motion of surface markers to the underlying bony anatomy via radiography (Kidder, 1996; Myers, 2004).

The purpose of this study was to design a lower extremity biomechanical model with two unique capabilities: HJC location calculated via the functional method, and integrated assessment of multisegmental foot and ankle kinematics.

METHODS

The model was developed using Matlab v7.1 (The Mathworks, Inc.; Natick, MA). Data is provided by a Vicon 524 Motion Analysis System (Vicon Motion Systems, Inc.; Lake Forest, CA), which includes 15 video cameras capturing data at 120 Hz. Segmental kinematics are calculated from the position coordinates of reflective markers placed on specific anatomical segments of walking subjects; measures of bony orientation are taken from weightbearing radiographs and entered separately to index foot marker motion to the bony anatomy. All testing and processing takes place in the OREC Motion Analysis Lab, located at the Medical College of Wisconsin.

To date, ten healthy adults have been recruited and undergone testing. Each subject underwent plane film radiography to collect weightbearing A/P, lateral, and coronal plane x-rays of the foot and ankle. Each data collection session was comprised of instrumentation, calibration, and motion testing. Instrumentation involved the application of reflective markers to the body at specific anatomical landmarks. Calibration involved the capture of marker

position data by the Vicon system during a quiet standing ("static") trial, and also during several trials involving sagittal and coronal plane motion of the hip joint ("HJC calibration trials", following the protocol described by Piazza (Piazza, 2004)). Motion testing involved the capture of various activities followed. Joint kinematics calculated with the proposed model will be compared to output from standardized models, and measures of within- and between-day variability will be calculated using the coefficient of multiple determination. The effect of xray indexing will also be assessed with a perturbation study of the tibia-calcaneus offset angle.

RESULTS AND DISCUSSION

Preliminary results are available from the foot portion of the new model. The most apparent differences are a temporal shift in motion patterns and slightly shifted measures of hindfoot and forefoot kinematics. The temporal shift can likely be explained by filtering methods used in the MFM; these methods are not duplicated in the new model. Shifted kinematics are likely due to differences in methods of calculating bone-based axes for the hindfoot segment; the MFM employs an iterative optimization approach for aligning axes, while the new model uses a series of sequential rotations matched to global projection angles.

REFERENCES

Leardini, A., et al., 1999. Validation of a functional method for the estimation of hip joint centre location. *Journal of Biomechanics* **32**, 99-103.

Piazza, S.J., et al., 2004. Assessment of the functional method of hip joint center location subject to reduced range of hip motion. *Journal of Biomechanics* **37**, 349-356.

Kidder, S.M., et al., 1996. A system for the analysis of foot and ankle kinematics during gait. *IEEE Transactions on Rehabilitation Engineering* **4**, 25-32.

MacWilliams, B.A., et al., 2003. Foot kinematics and kinetics during adolescent gait. *Gait & Posture* **17**, 214-224.

Kitaoka, H.B., et al., 2006. Foot and ankle kinematics and ground reaction forces during ambulation. *Foot & Ankle International* **27**, 808-813.

Simon, J., et al., 2006. The Heidelberg foot measurement method: Development, description and assessment. *Gait & Posture* **23**, 411-424.

Leardini, A., et al., 2007. Rear-foot, mid-foot and fore-foot motion during the stance phase of gait. *Gait & Posture* **25**, 453-462.

Myers, K.A., et al., 2004. Validation of a multisegment foot and ankle kinematic model for pediatric gait. *IEEE Transactions on Neural Systems & Rehabilitation Engineering* **12**, 122-130.

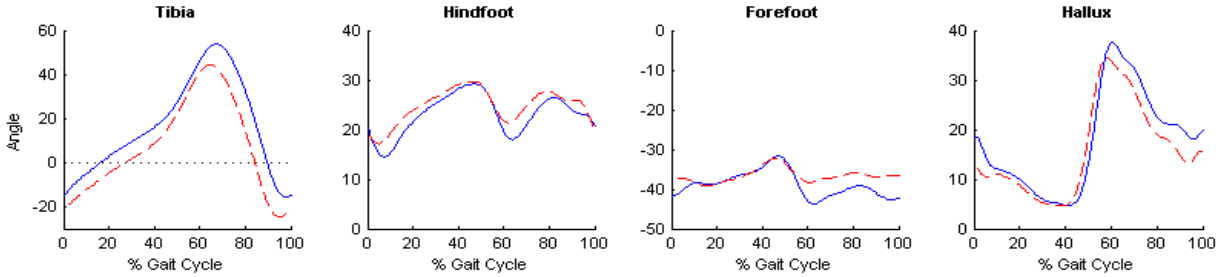

Figure 1: Sagittal plane output of new model (blue solid) and Milwaukee Foot Model (red dash). Composite average data are plotted for seven walking trials by a single subject. Positive values indicate forward motion (tibia) and relative dorsiflexion (hindfoot, forefoot, hallux).

CRITICAL TIME-TO-CONTACT AFTER POSTURAL PERTURBATIONS

C.J. Hasson, C. Gariépy, G.E. Caldwell, R.E.A. Van Emmerik, and W.J. McDermott
University of Massachusetts, Amherst, MA, USA; E-mail: cjhasson@kin.umass.edu

INTRODUCTION

During quiet stance, stability requires keeping the body center of mass (CoM) above its base of support. An external force applied to the upper back will accelerate the CoM towards the front stability boundary. By developing ankle torque with the plantarflexor muscles, the ground reaction force center of pressure (CoP) moves in front of the CoM to stabilize and counteract the forward sway.

At a given instant, the projected time for the CoM or CoP to contact a stability boundary is known as *time-to-contact* (TtC). During quiet stance, mean TtC has been viewed as a global measure of overall stability, while minimum TtC values have been thought to represent points of instability (Van Wegen et al., 2002). During a perturbation with acceleration towards the anterior stability boundary, the CoM TtC indicates the degree of impending danger of falling forward (Riccio, 1993). If TtC becomes too small, the ankle musculature may have insufficient time to produce the angular impulse needed to reverse the CoM before it reaches the stability boundary.

In this study we examined CoM and CoP motion and TtC after external perturbations of increasing magnitude. We expected the minimum TtC for the CoM to decrease as the perturbing force increased, and sought to identify a critical TtC value associated with a subject's decision to step forward as the perturbation became unmanageable with ankle plantarflexor torque alone.

METHODS

A pendulum of constant mass instrumented for angular position and impact force was used to deliver perturbation impulses of known magnitude at 78% standing height (Fig. 1). Five subjects (27 ± 2 yrs, 77 ± 11 kg, 178 ± 6 cm) stood on a force plate while strapped to a lightweight wooden backboard that distributed the force of the impact and constrained motion to sagittal plane rotation about the ankle joint only. Subject and backboard kinematics were captured at 200 Hz with an 8-camera Qualysis system. Ground reaction forces (GRFs) were sampled at 1000 Hz.

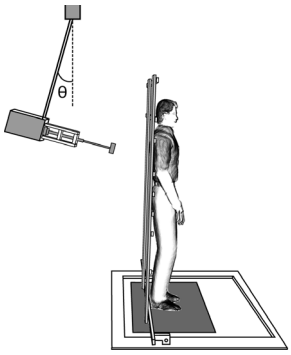

Fig 1. Apparatus.

In each trial, subjects were instructed to stand quietly, resist the perturbation, and return quickly to quiet stance. They were to step only when necessary to prevent a fall. Pendulum release occurred at a random time 2 to 5 s after a "ready" light. Subjects wore earphones with white noise to mask the pendulum release. A series of trials with increasing perturbations was performed, with an initial pendulum release angle (θ) of 10º (Fig. 1). The release angle was increased by 5º increments in subsequent trials until the subjects stepped. Perturbation magnitude was quantified by the peak pendulum angular velocity prior to impact (PP_{VEL}).

The CoP position was computed from low-pass filtered GRFs, and the CoM position from segmental kinematics. The CoM TtC to the anterior (toes) and posterior (heel) stability boundaries was calculated using methods developed by Slobounov et al. (1997). This required the solution of two quadratic equations of the form

$$\frac{1}{2}a\tau^2 + v\tau + (p - p_X) = 0$$

where p, v, and a are the positions, velocities, and accelerations of the CoM, p_x is the anterior-posterior (AP) location of the toe (or heel) markers, and τ is the TtC.

RESULTS AND DISCUSSION

In a typical perturbation response, the CoM accelerated towards the toes, followed by rapid forward motion of the CoP that placed it in front of the CoM (Fig. 2, Top).

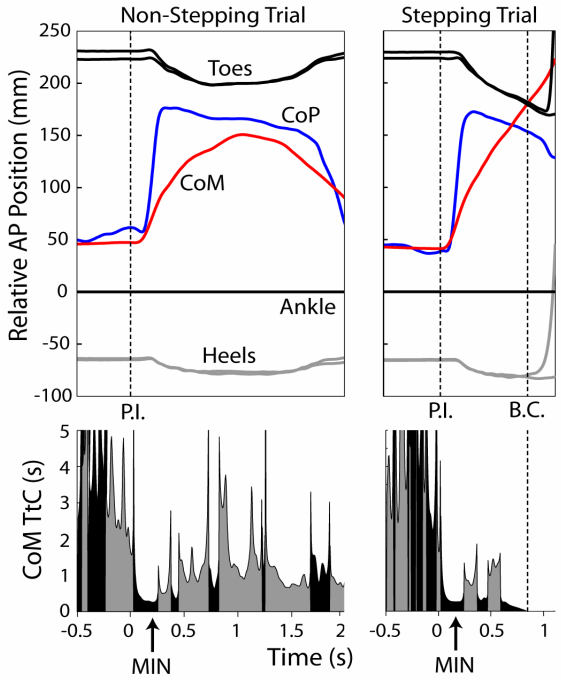

Fig. 2. Non-stepping (Left, PP_{VEL}=129°/s) and stepping (Right, PP_{VEL}=155°/s) trials for one subject. Top: AP displacement of the CoM, CoP, and toe/heel markers referenced to the ankle joint center. Bottom: CoM TtC; toe and heel trajectory contact indicated by black and grey shading, respectively. P.I.: Pendulum Impact; B.C.: Boundary Contact.

Except for the smallest perturbations, the CoP moved quickly to an initial position of 27 ± 7 mm (mean ± s.d.) from the toes. The time that the CoP remained in this forward position increased with perturbation level. In all trials, the minimum TtC occurred during the initial acceleration of the CoM towards the toes (MIN in Fig. 2, Bottom). As PP_{VEL} increased, the minimum TtC decreased (Fig. 3). As expected, more massive subjects required higher perturbation levels to elicit a step response than less massive subjects. In the stepping trials, the range of minimum TtC values was much smaller than the range of PP_{VEL} values (9.4% vs. 37.7% of total range; Fig. 3, brackets). Regardless of subject mass or absolute impact magnitude, there appeared to be a threshold TtC (~0.25 s) that dictated whether subjects stepped.

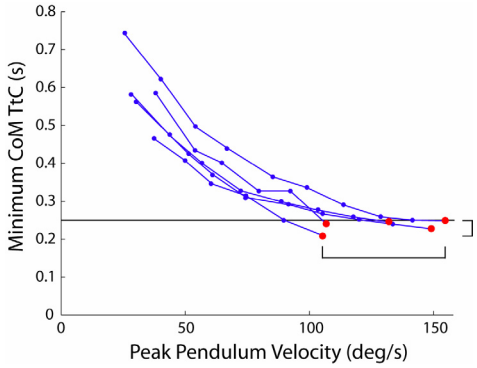

Fig. 3. Minimum CoM TtC as a function of peak pendulum angular velocity (PP_{VEL}) for 5 subjects. Last point (enlarged circle) in each line is the stepping trial. Horizontal line indicates possible threshold TtC of ~ 0.25 s. Brackets indicate range of TtC and PP_{VEL} for stepping trials.

CONCLUSIONS

During a perturbation, the body could use TtC information to predict whether it will be possible to reverse the CoM direction before a stability boundary is reached. It appears that the postural control system initiates a step response when TtC values fall below a critical threshold of ~0.25 s, invariant of body mass or perturbation magnitude.

REFERENCES

Riccio GE (1993) In: Variability and Motor Control (pp. 317-357), Human Kinetics.

Slobounov SM, et al. (1997) *J. Mot. Behav.*, **29**, 263-281.

Van Wegen EE, et al. (2002) *Hum. Mov. Sci.*, **21**, 61-84.

ACKNOWLEDGEMENTS

Funded by NIH grant R03AG026281-01A1.

DETERMINATION OF FACTORS AFFECTING THE ACCURACY OF AREA MOMENT OF INERTIA CALCULATIONS FOR LONG BONES FROM CT SCANNED IMAGES

-Ameet Aiyangar, Heidi-Lynn Ploeg
Department of Mechanical Engineering, University of Wisconsin-Madison
Email: aiyangar@cae.wisc.edu

Introduction

The area moment of inertia (MI) is an important measure of the bending resistance of long bones, besides the elastic modulus. There is not yet a significant appreciation of the effect of ignoring the deviations from standard symmetric beam bending theories as applied to homogeneous materials, while interpreting data from bending tests. As a consequence, a standard method to accurately compute the area moment of inertia, taking into account the heterogeneities in the bone structure and irregular geometrical shape, has not been clearly established. Accurately computing MI for bone is more complicated as a composite model needs to be employed. This can be accomplished by using grayscale variations in computed tomography (CT) images, which correlates with the elastic modulus *[Bhatavadekar et al, 2006]*. Nevertheless, the optimum number of "materials" that constitute bone and a way to determine the different "materials" and their respective geometries still needs to be established.
One also needs to evaluate the sensitivity of the calculations to other factors such as choice of threshold value used for segmenting the CT data and the effect of scanning slice thickness. Furthermore, the effect of slight variations in orientation of the bone between CT scanning and the actual mechanical bending test, characterized by tilt and rotation angles also needs to be evaluated. The tilt angle is the angle made by the long axis of the bone with the CT scan table. Rotation angle is a rotation about the long axis of the bone as shown in figures 1 and 2.

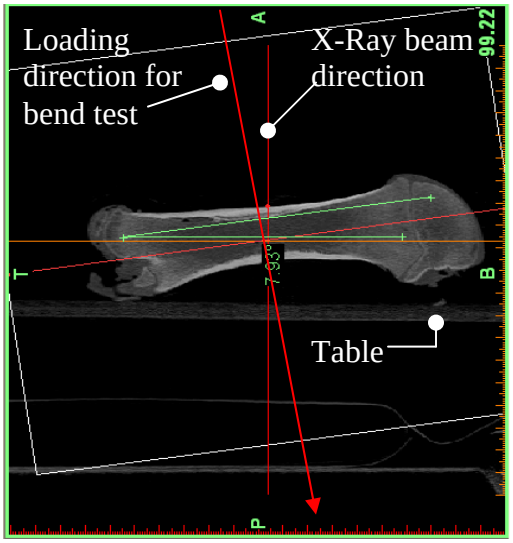

Figure 1: Tilt Angle

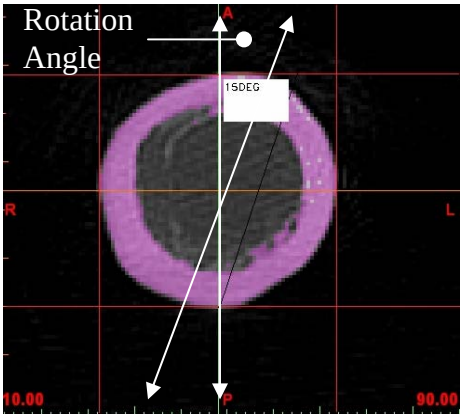

Figure 2: Rotation Angle

Methods

A 2^5 un-replicated full factorial statistical experiment was conducted to determine the effect of five factors, tabulated below, on the MI calculation of a porcine femur bone using segmented CT image data. Segmented CT data of the cross-sectional area of a

single slice at the center of a porcine femur bone was used for the study. Mimics 10.0 software (Materialise, Ann Arbor MI) was used to segment the CT data. A custom-written MATLAB function was used to compute the MI for all combinations of the factors mentioned above, using a composite materials model. The statistical analysis was performed using Minitab and a custom-written program, which used Yates' algorithm and Dong's method *[Dong, 1993]* to identify the significant effects at a 90% confidence level.

Results

Analysis of the data revealed that the threshold effect (Factor C) was extremely large and was overwhelming the effects of the other variables. In order to get a better understanding of the effects of the remaining variables, the data was divided into two sets according to the level of factor C, and each set was analyzed again separately as a 2^4 un-replicated full factorial experiment. This analysis revealed that, for a low threshold value, the tilt angle, the rotation angle and the number of materials used in the significantly affected the computed value of MI. A two-factor interaction between tilt and rotation was also found to be significant. In addition, factor D, the slice thickness, was found to be significant when the data at the high threshold value was analyzed. The regression models are given below:

High(+) Level of C:

$$\hat{y} = \eta + \frac{A}{2}x_1 + \frac{B}{2}x_2 + \frac{D}{2}x_4 + \frac{E}{2}x_5 + \frac{AB}{2}x_1x_2$$

Low (-) Level of C:

$$\hat{y} = \eta + \frac{A}{2}x_1 + \frac{B}{2}x_2 + \frac{E}{2}x_5 + \frac{AB}{2}x_1x_2 \quad ; \quad \varepsilon = y - \hat{y}$$

Conclusions

The study suggests that the low threshold value should be used while using segmented CT data for calculation of MI. The need to use a composite materials model to describe the bone structure also emerges as a significant factor. Further tests need to be conducted to determine the optimum number of "materials" that should be used to model the bone structure.
The findings also suggest that care should be taken to ensure that the CT data is re-sliced in order to match the orientation with that maintained during the bending tests, before computing MI.

References

1. Bhatavadekar, N.B. et al. (2006). Am J Phys Anthropol, **131**, 243-251.
2. Dong F, (1993). Statistica Sinica, **3**, 209-217.

Acknowledgements:

We thank T. D. Crenshaw, Animal Science Department, University of Wisconsin-Madison, for providing porcine femur bones for this study.

Table 1: Factors with the respective high and low levels for the factorial experiment

	Factor	Variable	Low Level (-)	High Level(+)
1	A	Tilt Angle	0^0	8^0
2	B	Rotation Angle	0^0	15^0
3	C	Windowing Threshold Value	230HU	600HU
4	D	Slice Thickness	0.625mm	1.25mm
5	E	# Of Materials	5	20

Enhanced Inter-Joint Reflex Coupling May Contribute to Impaired Coordination in Hemiparetic Stroke

James Finley[1,2], Eric Perreault[1,2], and Yasin Dhaher[1,2]

[1] Department of Biomedical Engineering, Northwestern University, Chicago, IL, USA
[2] Sensory Motor Performance Program, Rehabilitation Institute of Chicago, Chicago, IL, USA
E-mail: j-finley@northwestern.edu, Web: http://sulu.smpp.northwestern.edu

INTRODUCTION

The dynamics of hip frontal plane and knee saggital plane movements, which can normally be disassociated, are intrinsically coupled following stroke. This coupling is manifested during gait by excessive hip circumduction and a reduction in knee flexion during the swing phase (Kerrigan *et al.*, 2000). Although previous studies have characterized the dynamics of this coupling, the neural mechanisms contributing to this impaired coordination are unknown.

It has been suggested that abnormal coordination following stroke may be due to altered descending commands (Luft *et al.*, 2005) or altered processing of sensory information in the spinal cord (Dietz, 1997). While most studies have focused on the influence of descending control, the purpose of this work is to determine if there is evidence for altered processing of afferent information that may contribute to abnormal coupling seen following stroke.

Evidence from feline models has shown that heteronymous reflexes, which involve excitation of a muscle via afferents from another muscle, result in coordinated activation of muscles across multiple joints in the hind limb (Nichols *et al.*, 1999). To date, no studies have investigated the presence of these heteronymous stretch reflexes in the human lower limb and how these reflexes change following stroke.

The goal of this study is to investigate whether the dynamic coupling between the hip frontal plane and knee saggital plane degrees-of-freedom following stroke is also evident at the muscular level through heteronymous reflexes. Given the abnormal across-joint movement pattern, we hypothesized that activity in the quadriceps is facilitated by spinal circuits which couple activation of the adductors to activation of the quadriceps.

METHODS

Eighteen subjects were recruited for this study including 10 with hemiparesis resulting from stroke and 8 unimpaired, age-matched controls. Subjects from the stroke population were recruited if they had a unilateral stroke, presented right side hemiparesis, and had no cognitive deficits that would prevent them from performing the experimental protocol.

A computer-controlled servomotor was used to apply a randomized sequence of ramp and hold perturbations to both the hip and knee joints in separate sessions. EMG activity was recorded in the quadriceps, hamstrings and the hip adductors using bipolar surface electrodes. Perturbation amplitude, velocity, and the level of background activity in the adductors and quadriceps were varied during the experiment and a linear mixed-effect model was developed to determine which experimental parameters had a significant influence on the homonymous and heteronymous reflex amplitudes.

RESULTS AND DISCUSSION

Hip abduction perturbations produced stretch reflexes in the adductors (AM) for both subject populations. Additionally, stroke subjects had heteronymous reflexes in rectus femoris (RF), shown in Figure 1, which ranged in amplitude from 3.2-12.5% of the maximum voluntary contraction (MVC). This pattern of activation is the same as the as the coupling between these muscles during hemiparetic gait. While the amplitude of RF activity may seem small, it is comparable to the maximum amplitude of 17±11% of MVC measured during gait in subjects with stroke (Turnquist *et al.*, 2007).

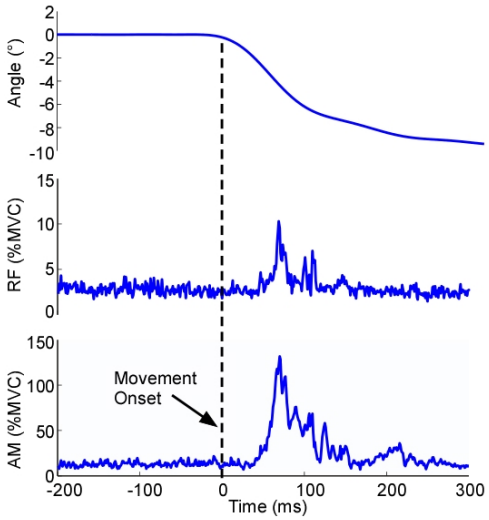

Figure 1: Hip abduction stretches elicited excitatory responses in AM and in RF.

Knee flexion perturbations provided additional evidence for a heteronymous reflex connection between RF and AM in subjects with stroke. These perturbations elicited heteronymous reflexes in the AM (Figure 2) with an average amplitude of 5.1±3.8% of MVC across all subjects.

SUMMARY/CONCLUSIONS

We observed a bi-directional, reflex-mediated coupling between rectus femoris and the hip adductors in subjects with hemiparetic stroke. This suggests that changes in the excitability of spinal networks may contribute to the abnormal inter-joint coordination patterns seen following stroke. Further studies will be necessary to quantify how this reflex coupling contributes to limb mechanics and if interventions targeted at reducing this coupling will result in improved rehabilitation outcomes.

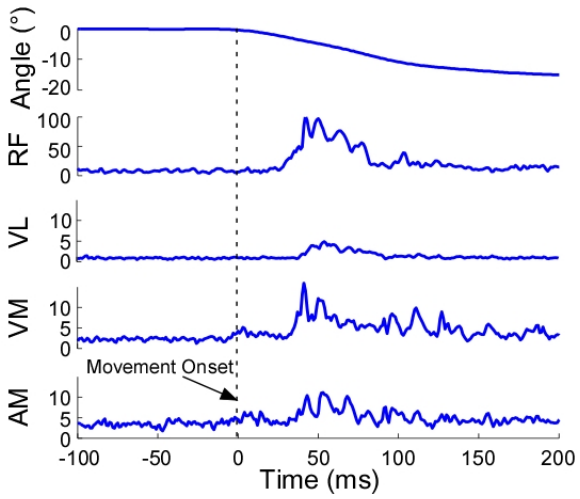

Figure 2: Knee flexion perturbations elicited heteronymous reflexes in AM. EMG is expressed as a percentage of MVC.

REFERENCES

Dietz (1997). *Electroencephalogr Clin Neurophysiol* **103**, 333-355

Kerrigan et al. (1998). *Am J Phys Med Rehabil* **79**, 247-252.

Luft et al. (2005). *Neuroimage **26**, 184-194*

Nichols et al. (1999). *Exerc Sport Sci Rev* **27**, 255-84.

Turnquist et al. (2007). *GCMAS Conf Proc, Springfield, MA 2007*

ACKNOWLEDGEMENTS

Supported by NIDRR grant #H133G04006 and an NSF Graduate Research Fellowship

DEFORMATION AT BRANCH POINTS IN HUMAN CEREBRAL ARTERIES

Joshua H. Smith[1], Louis Y. Cheng[2], Geoffrey T. Manley[1], and Kenneth L. Monson[1]

[1] Department of Neurological Surgery, University of California, San Francisco, CA, USA
[2] Applied Biomechanics, Alameda, CA, USA
E-mail: kenneth.monson@ucsf.edu

INTRODUCTION

Head injury frequently involves damage to the cerebral blood vessels. Even when the vessels are not damaged, they may contribute to the overall response of the brain (Zhang et al., 2002). While previous work in our laboratory has focused on the mechanical properties of unbranched segments of cerebral vessels (Monson et al., 2003, 2005), the cerebrovascular network contains many branch points.

To our knowledge, the only study testing the susceptibility of human cerebral branch points to failure considered the effects of internal pressurization only (Mitchell and Jakubowski, 2002). We have recently compared the response of human branched arterial vessels to axial deformation with that of unbranched segments. Only 3 of the 12 vessels tested failed in branch regions, but none of the specimens failed at midsection locations not associated with a branch. Non-branch failure always occurred at the attachment points of the vessel to the testing apparatus, indicating the likelihood of tissue damage during the vessel attachment process.

We have investigated our experimental observations further through the use of a finite element model of a branched cerebral vessel. The data reported here characterize the behavior of an idealized branched vessel to axial deformation comparable to that used in our experimental testing.

METHODS

The non-linear finite element solver LS-DYNA (LSTC, Livermore, CA) was used for the finite element analysis of the branched vessel. Geometry and mesh were constructed using TrueGrid (XYZ Scientific Applications, Livermore, CA). Following an approach similar to that of Thubrikar et al. (1990), the arterial branch was modeled as the intersection of two cylindrical tubes. The nodes near the intersection were modified to create a transition region between the branch and the main vessel using two methods (denoted A and B).

The radius r_m and thickness t_m of the main vessel were taken from experimental measurements. The radius r_b and angle θ of the branch were varied to test the sensitivity of stress concentrations at the branch point to these factors. Because of the large displacement applied to one end of the main vessel, a neo-Hookean strain energy function was assumed with material properties taken from previous studies (Monson et al., 2006; Zhang et al., 2002). Following our experimental testing, idealized branched vessels were simultaneously subject to an axial stretch of 1.4 and an internal pressure of 20 kPa.

RESULTS AND DISCUSSION

Figure 1 shows the maximum principal stress contours for the case when $r_m / r_b = 2$ and $\theta = 45°$. There is an increase in the stress on the inside of the vessel wall in the

transition region between the main vessel and the branch. Furthermore, there is a stress concentration on the outside of the main vessel, probably due to the thinning of the vessel wall in that area resulting from our algorithm to generate the smooth transition region. This outer stress concentration is not observed in specimens with branches that are more perpendicular to the main vessel, but is larger than the internal stress concentration in vessels with branches of 30°.

Figure 2 shows the maximum principal stress as a function of the branch angle and the branch radius. For branches that are relatively perpendicular to the main vessel, we see that the maximum principal stress actually increases as the size of the branch decreases. This is contrary to both our experimental observations and simulations of non-branched vessels having a simple hole of various sizes in its wall. Furthermore, changes in transition geometry specifically designed to reverse the unexpected branch-size trend were only partially successful.

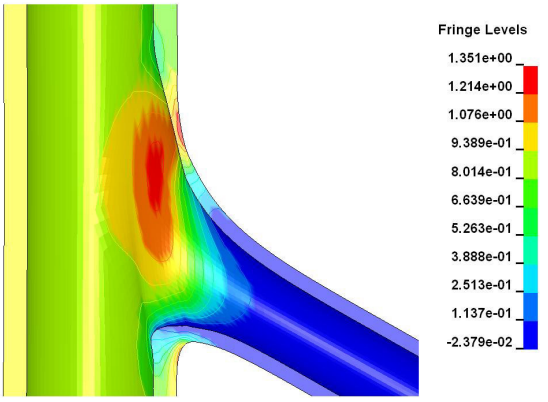

Figure 1: Maximum principal stress (MPa) in a 45° branched vessel under an internal pressure of 20 kPa and axial stretch of 1.4.

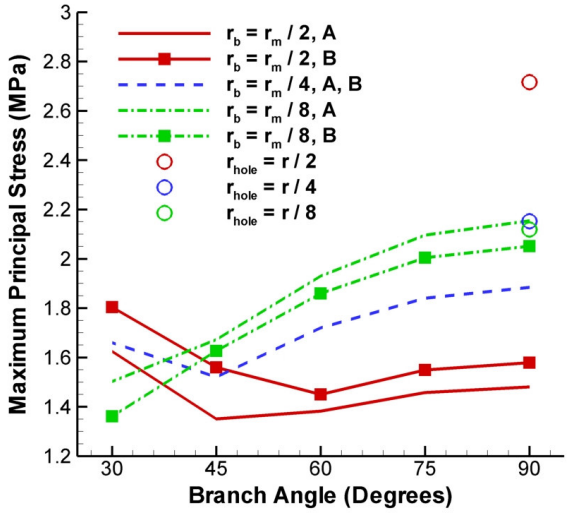

Figure 2: Maximum principal stress in a branched vessel as a function of branch angle and transition region geometry and in a non-branched vessel with a hole.

SUMMARY/CONCLUSIONS

The stress concentration at branch points is sensitive to the geometry of the transition region between the main vessel and its branch, suggesting that more study of the geometry is necessary. The fact that geometry changes do not resolve differences in simulated trends in comparison to experimental findings suggests that material properties may also vary across the transition region.

REFERENCES

Mitchell, P., Jakubowski, J. (2002). *Brit. J. Neurosurg.*, **16**, 578—582.

Monson, K.L. et al. (2003). *J. Biomech. Eng.*, **125**, 288—294.

Monson, K.L. et al. (2005). *J. Biomech.*, **38**, 737—744.

Monson, K.L. et al. (2006). *Proceedings of 2006 ASB Annual Conference.*

Thubrikar, M.J. et al. (1990). *J. Biomech.*, **23**, 15—26.

Zhang, L. et al. (2002). *Stapp Car Crash J.*, **46**, 145—163.

ACKNOWLEDGEMENTS

This work was supported by a grant from the CDC (R49 CE000460).

STAIR DESCENT KNEE POWER CHANGES FOLLOWING MINIMALLY INVASIVE COMPUTER NAVIGATED TOTAL KNEE ARTHROPLASTY

John McCamley[1], Kristine Csavina[1], M. Wade Shrader[1,2], David J. Jacofsky[1,2]
[1] SHRI-CORE Orthopedic Research Labs, Sun City West, AZ, USA
[2] The CORE Institute, Sun City West, AZ,USA
E-mail: john.mccamley@thecoreinstitute.com , Web: www.thecoreinstitute.com

INTRODUCTION

Falls on stairs are a leading cause of injury in older adults with most accidents occurring during stair descent (Starzell, et al., 2000). Studies have shown that stair descent moments at the knee are three times those moments measured during level walking (Andriacchi, et al., 1980). Knee flexion angles required to successfully descend stairs are greater than the angles necessary for level walking (McCamley, 2007). The higher demands placed on the knee joint during stair descent can limit the ability of patients with joint deficiencies from performing this activity.

Osteoarthritis causes pain that limits the loads applied to the knee joint. Total knee arthroplasty (TKA) relieves this joint pain. Minimally invasive and computer navigated surgery is becoming an increasingly common form of TKA. This type of surgery produces less disruption to the soft tissues surrounding the knee joint providing the potential for faster recovery than conventional surgery.

The aim of this study was to measure the differences in knee power absorbed during stair descent in patients before and four months after TKA and compare these data with those measured for a group of healthy age-matched individuals.

METHODS

Eleven TKA patients (5 males, 6 females; 73 ± 8.1 years) volunteered to participate in the study. Data were also collected from sixteen healthy age-matched volunteers from the same community (5 males, 11 females; 68 ± 5.8 years).

Motion analysis data were collected using a ten camera motion capture system (Motion Analysis Corp., Santa Rosa, CA) with lower body limb segments defined by 28 reflective markers. The stair system consisted of three steps mounted on two force platforms (AMTI, Watertown, MA) in such a manner that forces could be recorded for all three steps. Data were recorded while the patients and control subjects descended the stairs in a reciprocating manner. A minimum of three trials were recorded for each subject. Mean values for patients prior to and after surgery where compared using a paired t-test. Post surgery values for patients where compared to controls using an unpaired t-test (α = 0.05)

RESULTS

Peak knee power absorbed occurs immediately prior to contralateral foot strike when the stance limb is supporting the full weight of the body while in a flexed position. Table 1 lists the average cadence, peak knee angle, moment and power for the patients prior to, and after surgery, and for the control group. The graphs shown in figure 1 represent the average of values for

the subjects in each group at time points in the normalized gait cycle. Analysis of the data shows that while cadence improved significantly following surgery it remained significantly different to the control group. Significant variations in knee angle are not possible due to the need to position the foot within a defined area on each step. The changes in sagittal plane kinematics following surgery were not significant. There were significant differences between the knee power absorption measured for the control group and the patient group prior to surgery. The results show that while there are improvements in knee motion following TKA these improvements do not immediately restore the ability of patients to descend stairs.

CONCLUSIONS

In another study, measurements of knee power for these same patients while walking were not significantly different from that for the control group (McCamley, 2007). Stair descent is more challenging and provides an opportunity to measure differences not seen while performing other less demanding tasks. Understanding the limitations TKA causes in patients may help in the rehabilitation of these persons enabling them to become more independent sooner after surgery. Further study is necessary to determine if more time is needed for knee kinematic parameters to reach levels similar to those measured in healthy subjects.

REFERENCES

Andriacchi, T.P. et al. (1980). *J. Bone & Joint Surg.* **62-A**, 749-757.

McCamley, J.D. (2007) Unpublished M.S. thesis, Arizona State University, AZ.

Startzell, J.K., et al. (2000). *J. Am. Geriatrics Society* **48**, 567-580.

Table 1: Mean (SD) for Pre-op, Post-op and Control groups; A: paired t-test, pre-op – post-op, B: unpaired t-test, post-op - control.

	Pre-Op n = 11	Post-Op n = 11	Control n= 16	T-test significance A	B
Cadence Steps/minute	42.34 (13.05)	60.15 (8.28)	79.43 (10.03)	**<0.001**	**<0.001**
Knee flexion angle at toe off	86.8 (6.8)	89.3 (5.1)	91.7 (12.6)	0.112	0.609
Peak knee moment (N-m/kg)	0.91 (0.33)	1.04 (0.20)	1.20 (0.22)	0.066	0.079
Peak knee power Abs. (Watts/kg)	-2.06 (0.52)	-2.23 (0.42)	-2.90 (0.61)	0.684	**0.012**

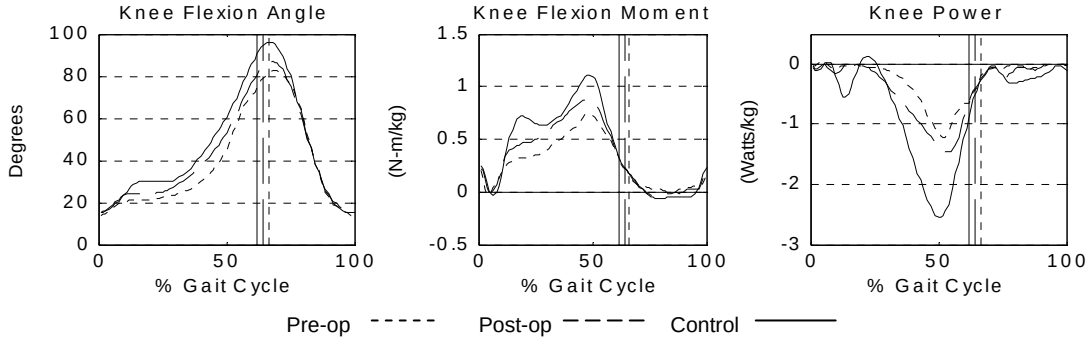

Figure 1: Average knee sagittal angle, moment, and power for the patients' injured knee pre- and post-surgery, and for control subjects over a normalized gait cycle.

EFFECTS OF WHEELCHAIR PROPULSION TRAINING ON PUSHRIM KINETICS

Alicia Koontz, Ian Rice, Rachel Cowan, and Michael Boninger
Human Engineering Research Laboratories, VA HealthCare System, Pittsburgh, PA, USA
University of Pittsburgh, Pittsburgh, PA, USA
E-mail: akoontz@pitt.edu Web: www.herlpitt.org

INTRODUCTION

Upper limb pain is very common in manual wheelchair users (MWUs) with spinal cord injury (SCI) (Sie et al., 1992). While much has been published identifying the prevalence of upper limb pain in individuals with SCI, very little has been published on its treatment and even less on its prevention. Propulsion research (Boninger et al., 2005) and substantial ergonomics literature (Steering Committee…, 1995) have identified specific biomechanical parameters associated with risk of injury to the upper limb. Based on these conclusions we designed a propulsion training program aimed to reduce cadence and increase push angle. Increasing push angle while maintaining a constant velocity should cause a reduction in forces at the pushrim as work remains constant. We are currently conducting a randomized control trial (RCT) to evaluate the effectiveness of the training program with MWUs who have been using a wheelchair for at least two years. The purpose of this study was to examine the intervention groups thus far to determine if training impacts pushrim kinetics. We believe that if this program proves to modify technique, it will result in a simple intervention that leads to a significant reduction in upper limb pain and injury.

METHODS

Subjects: Eleven MWUs provided informed consent in a study approved IRB. Eight MWUs (6 men and 2 women) were randomly assigned to an intervention group (group 1-training video or group 2 - video and biofeedback). The others (n=3) were randomized to a control group (group 3). Only data from the interventional groups combined were analyzed since fewer subjects have been tested as controls. Six subjects had a SCI (3 thoracic and 3 cervical) and two subjects had spina bifida (SB). They were an average of 37 ± 8 years old, 20 ± 13 years since SCI or years since birth (if SB), and weighed 77.2 ± 22.3 kg.
Experiment protocol: Subjects own personal wheelchairs where secured to a wheelchair dynamometer that simulated propulsion over smooth, level ground. No changes to their wheelchair setup were made. The wheelchairs were fitted on the non-dominant side with a SMART^{Wheel} (Three Rivers Holdings, Inc., Mesa, AZ) which measures three-dimensional forces and moments. Three sets of data were collected: baseline, post-training, and followup. *Baseline:* Subjects were instructed to propel at a comfortable pace (CP) with no velocity feedback and a constant speed of 2 m/s (with velocity feedback on a 17" computer screen). After acclimating to the dyno, 20 seconds of data were collected after reaching steady-state (240 Hz) for each speed trial. *Training:* After baseline testing, all eight subjects viewed an instructional video that emphasized reaching back, matching the speed of the hand to the speed of the pushrim, taking long strokes, and smoothly releasing the pushrim. Three subjects also received real-time feedback that directed them to minimize cadence and maximize push angle. Training consisted of practicing the techniques from the video while propelling at CP and 2m/s and (for 3 subjects) with alternating biofeedback (10 sec on/15 sec off) during four 1-minute blocks that were separated by rest breaks. At completion, 20 seconds of data were collected after reaching steady-state CP and

2 m/s. *Follow-up:* Subjects were asked to practice at home the techniques that they learned in the training program. They returned back to the lab and repeated the biomechanics testing an average of 18.2 ± 7.4 days later.

Data analysis: The propulsion cycle was divided into two phases, push or recovery phase based on the presence or absence of pushrim forces. Variables included: number of strokes per second (cadence), push angle, average resultant force (FR), average wheel torque (Mz), mechanical effective force (MEF), and average velocity. MEF was defined as Ft^2/FR^2, where tangential force (*Ft*) was calculated by dividing wheel torque by the radius of the wheel. These values were determined from the first ten cycles and a mean was computed. Repeated measures ANOVA ($\alpha < 0.1$) with Bonferroni corrected post hoc tests were used to examine differences between baseline and post-training data.

RESULTS AND DISCUSSION

Subjects used significantly fewer strokes after training to propel at a comfortable pace (Table 1). At 2 m/s, cadence also significantly decreased immediately after training and at followup (*baseline* = 1.34 ± 0.24; *post* = 0.97 ± 0.16; *follow up* =1.16 ± 0.28, p=0.004). It was interesting to find that MEF increased significantly in the CP trial and in the 2m/s trial (trend: p=0.15). Neither the instructional video nor the biofeedback incorporates any information about force optimization. Redirecting the forces more tangentially appears to have been a strategy chosen to lower stroke cadence and increase push angle while maintaining a chosen speed. In both speed trials, we saw a mean increase in the push angle at followup (2 m/s trial *baseline* = 110 ± 30; *follow up* =121 ± 33 degrees, p=0.167). The large variability perhaps due to a heterogeneous sample of MWUs and combining the two training groups made it difficult to detect statistical differences.

SUMMARY/CONCLUSIONS

This preliminary analysis indicates that our training program can modify the propulsion techniques of long-time MWUs and that the program was effective in the retention of learned techniques. We intend to validate these findings against those of a control group of MWUs with similar user characteristics as those in the training groups. Both training programs, especially the instructional video alone, are simple enough to execute in the clinic allowing for an easy intervention that could preserve upper limb function and extend the duration of pain-free manual wheelchair use.

REFERENCES

Sie, I.H. et al. (1992) *Arch Phys Med Rehabil,* **73,** 44-48.

Boninger, M.L. et al. (2005) *J Rehabil Rehab Dev*, **42(3)**, 9-20.

Steering Committee…(1999) *Work-related MusculoSkeletal Disorders: a Review of the Evidence,* National Academy Press, Washington D.C.

ACKNOWLEDGEMENTS

NIH 1-R03-HD049735-01A1 and VA RR&D Service

Table 1: Temporal and Pushrim Kinetics Data for the Comfortable Pace Trial (mean± SD).

Trial	Average FR (N)	Average Mz* (N*m)	Velocity (m/sec)	Push Angle (degrees)	Cadence** (strokes/sec)	MEF**
Baseline	52.8 ± 21.4	9.0 ± 3.3[A]	1.3 ± 0.3	114.5 ± 30.6	1.09 ± 0.24[B,C]	0.31 ± 0.13[D]
Post	54.7 ± 16.0	10.5 ± 3.7[A]	1.2 ± 0.3	112.5 ± 27.0	0.89 ± 0.09[C]	0.38 ± 0.15[D]
Follow up	48.9 ± 12.7	8.6 ± 2.2	1.3 ± 0.3	124.5 ± 22.1	0.91 ± 0.17[B]	0.34 ± 0.15

Main **p<.05, *p<0.1; Paired A: (p=0.083), B: (p=0.014), C: (p=0.096), D: (p=0.008)

THE SHORT-TERM EFFECT OF WHOLE BODY VIBRATION TRAINING ON COLLEGIATE SPRINT ATHLETES

Brad Roberts, Iain Hunter, Robert Thiebaud, Mike Bishop

Brigham Young University, Provo, UT, USA
E-mail: iain_hunter@byu.edu Web: http://biomech.byu.edu

INTRODUCTION

Whole body vibration (WBV) training has been the subject of a great amount of debate and research towards improving athletic performance. Whole body vibration is done with the subject standing on a vibrating platform typically with the subject at a slightly flexed position at the knee and hip while the platform oscillates at 20-40 Hz through an amplitude of 1-5 cm (Figure 1).

Figure 1: Positioning used during vibration.

Whole body vibration has been described to produce forces similar to those of power and strength training and has been reported to improve muscular power of the upper and lower musculature, changes to hormonal profile, and increases in cardiovascular responses. (Cochrane, 2004)

Studies have shown over 30% increases in maximal explosive strength, as well as increases in maximum dynamic force, maximum isometric force, and a debatable amount in isometric endurance (Issurin, 2006).

With previous results on acute increases in explosive performance, the purpose of this study was to investigate the effects of short term WBV on sprint starts among collegiate track athletes.

METHODS

Eleven subjects from the Brigham Young University track team were randomly assigned to either a non-vibration or vibration group for testing day number one. Force measurements were taken using a force plate (Kistler 9287BA, Amherst, NY) embedded under the track surface where the starting blocks were placed. Each subject completed three trials with medio-lateral, anterior-posterior, vertical, and resultant forces being measured. Each group did either a non-vibration or a vibration testing day, and then completed the other condition one week later. Participants subjected to vibration were vibrated for 60 s at 26 Hz with an amplitude of 4mm on a Galileo 2000 vibration platform (Orthometrix, White Plains, NY). Following the vibration, approximately two minutes passed before the sprint start. Peak resultant force for non-vibration trials were compared to vibration trials using repeated measures ANOVA.

RESULTS AND DISCUSSION

Peak resultant force was 6% greater when the vibration platform was utilized prior to the start (p=0.013).

One theory behind whole body vibration studies is that, through vibration, the muscle spindle's sensitivity can be increased. This would occur through vibration induced increases in firing of the alpha sensory and gamma motor neurons resulting in a quicker trained response from the muscle spindle giving a more rapid response to changes in muscle length ultimately ending in a quicker and stiffer (and thus stronger) muscle response. The inhibitory response from the GTO complex is also depressed.

While peak forces were greater in this study for the treatment group, the time of force production must also be considered. Greater peak forces typically result in greater impulses; however, further research with a larger or multiple force plates is required to answer the question of impulse. Impulse could not be measured in this study since the hands did not fit on the force plate. Peak forces were measured correctly here since the hands were off the ground when peak force was attained.

Table 1: Peak resultant force while in contact with the starting blocks (p=0.013).

Condition	Peak Force (BW)
Vibration	2.41 ± 0.20
Control	2.28 ± 0.19

Another possible benefit of WBV could be a decrease in injury risk. The increase in peak forces following WBV could be due to an increase in muscle spindle fiber sensitivity and stretch-reflex loop sensitivity (Cardinal, 2003). As the muscle spindle and stretch-reflex loop become more sensitive, the muscle could adapt quicker to forces that may cause musculotendon injury. Also, another study found that flexibility in elite female field hockey athletes increased after WVB use (Cochrane, 2005). An increase in flexibility could allow greater range of motion before the muscle would be torn. Therefore, a possible decrease in injury risk could be seen by applying WBV to individuals before competition.

SUMMARY/CONCLUSIONS

Greater forces can be generated in the sprint start following whole body vibration. However, further research is needed to determine whether any meaningful differences in velocity of the start exist. Although greater forces were applied, the practicality of using a platform before competitions needs to be considered. Platform portability may be difficult due to its size, and restrictions at venues may limit their use. Thus, use of the platform in training may be the best application of these findings.

REFERENCES

Cardinal, M., Bosco, C. (2003). *Exerc. Sport Sci. Rev*., **31**, 3-7.
Cochrane, D., Stannard S. (2005). *Br. J. Sports Med*., **39**, 860-865.
Issurin V.B. (2005). *J. Sports Med. Phys. Fitness,* **45**, 324-336

IDENTIFICATION OF RISK FACTORS FOR TENDON OVERUSE INJURIES

Katie Antle and David Hawkins

Human Performance Laboratory, University of California, Davis, CA, USA
E-mail: dahawkins@ucdavis.edu

INTRODUCTION

The Achilles tendon is an extremely important tendon for human locomotion and if injured can severely affect a person's movement capability and quality of life (Mazzone and McCue, 2002). People of all ages can sustain tendon injuries, but people between 30 and 50 years of age appear to be particularly susceptible to tendon injuries. Very little data exist regarding muscle-tendon properties in-vivo and their association with the risk for tendon injury.

Because of the clinical importance of Achilles tendon injuries and our ability to quantify Achilles tendon force and deformation in-vivo, we used the Gastrocnemius-Soleus-Achilles-Tendon Complex as a model to study basic muscle-tendon properties and their association with tendon injury. We hypothesized that the risk of sustaining an Achilles tendon injury increases (1) as the stiffness ratio of active muscle to tendon increases, (2) as the tendon stress and strain during a maximum isometric ankle plantar flexion increases, and (3) as the passive ankle plantar flexion/dorsiflexion range of motion (ROM) deviates by more than 1 standard deviation relative to normative ROM values.

METHODS

Ultrasound and joint testing methods, developed previously in our laboratory (Figure 1), were used to obtain the data needed to test the hypotheses. Two groups of physically active subjects, 30-50 years of age, were tested. One group had no prior history of Achilles tendon injury. The other group experienced pain in the midsubstance of the Achilles tendon in one leg during and after physical activity within the past year.

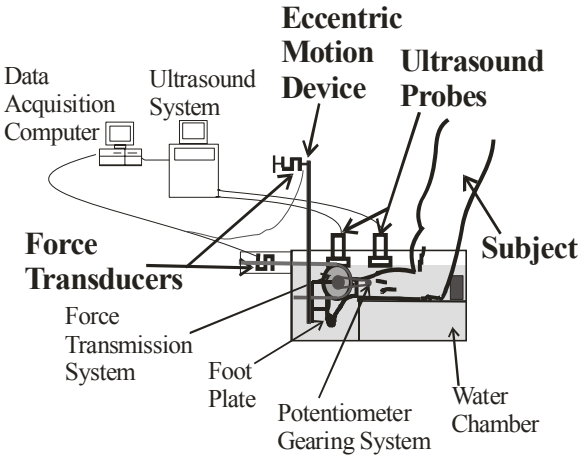

Figure 1: Testing Chamber Schematic. The subjects placed their leg in the water chamber. A force transducer and gearing system allowed quantification of ankle plantar flexion torque. Dual ultrasound probes allowed quantification of tendon length.

Subjects placed their leg in a water chamber and pressed against an instrumented foot pedal that quantified ankle plantar flexion torque. The foot plate was held stationary for isometric trials but could rotate freely for eccentric trials. Ultrasound probes were placed over the calcaneal osteotendinous junction (OTJ) and either the soleus muscle-tendon junction (MTJ) or gastrocnemius MTJ. Data were collected during maximum isometric plantar flexion efforts and

eccentric actions at 60% of isometric maximum voluntary contraction (MVC). Force transducer data and ultrasound images were collected simultaneously. At the end of testing, one ultrasound probe was rotated 90 degrees and a cross-sectional image of the Achilles tendon was recorded. Ankle plantar/dorsiflexion ROM was determined using a manual goniometer and passive manipulation.

Ultrasound and force data were combined to determine muscle and tendon stiffness, tendon elastic modulus, and tendon stress and strain during maximum isometric plantar flexion efforts and eccentric actions at 60% of isometric MVC. The calcaneal OTJ, the soleus MTJ, and the gastrocnemius MTJ were digitized in the ultrasound images using Image J (National Institutes of Health) and the distances between these anatomical landmarks were used to quantify tendon deformation. Tendon stiffness was determined from the slope of the tendon force-deformation curves obtained from the maximum isometric ankle plantar flexion trials. Muscle stiffness was estimated from the muscle force-deformation data obtained during the eccentric trials. Stress and strain were calculated from the force-deformation data, tendon cross sectional area (obtained by digitizing the cross-sectional ultrasound images), and resting tendon length.

ANOVA was used to determine if significant differences existed in the data between contralateral limbs of uninjured individuals, and between uninjured individuals and the asymptomatic side of injured individuals.

RESULTS AND DISCUSSION

Testing and data analysis are on-going with initial data demonstrating similar values between contralateral sides of the uninjured group and different values between the uninjured group and the asymptomatic leg of the injured group. Data demonstrate differences between the uninjured and injured groups relative to stress and strain at maximum isometric ankle plantar flexion efforts, muscle to tendon stiffness ratio, and dorsiflexion ankle ROM. These initial results suggest that there are differences in muscle-tendon mechanical properties between uninjured subjects and the asymptomatic leg of subjects who have experienced tendon injury.

SUMMARY/CONCLUSIONS

Tendon overuse injuries can significantly impact a person's way of life, hindering normal function, making it an important clinical issue. We hypothesized that a person's susceptibility to tendon injury may relate to the basic properties of their muscle tendon unit. Initial results support this hypothesis. Understanding how basic mechanical properties of muscle-tendon complexes relate to tendon injury is an important first step in developing effective screening processes that can be used to identify individuals at risk for tendon injury and training programs to reduce tendon injury susceptibility.

REFERENCES

Mazzone, M.F., McCue, T. (2002). *Am. Family Physician*, **65**, 1805-1810.

ACKNOWLEDGEMENTS

This project was partially funded through the UCD and Humanities fellowship.

THE INFLUENCE OF PATELLAR LIGAMENT INSERTION ANGLE ON QUADRICEPS USAGE DURING WALKING IN ACL RECONSTRUCTED SUBJECTS

Choongsoo S. Shin [1], Ajit M. Chaudhari [2], Chris O. Dyrby [1,3], and Thomas P. Andriacchi [1,3]

[1] Stanford University, Stanford, CA, USA
[2] Ohio State University, Columbus, OH, USA
[3] Veterans Administration Palo Alto Health Care System, Palo Alto, CA, USA
E-mail: scslove@stanford.edu, Web: www.stanford.edu/group/biomotion

INTRODUCTION

It has been theorized that reduced quadriceps contraction is an adaptation to prevent anterior tibial translation in ACL-deficient (ACL-D) knees (Berchuck, 1990) and consequently the quadriceps reduction during walking is proportional to the patellar ligament insertion angle (PLIA) (Figure 1). This theory has been supported by a recent study that reported the peak net quadriceps moment was correlated with the PLIA for ACL-D knees, but not in contralateral knees (Shin, 2007). In addition, the PLIA of ACL-D knees is significantly smaller than the PLIA of their uninjured contralateral knees (Shin, 2007), most likely as a consequence of the loss of tension in the ACL. At present it has not been shown whether ACL reconstruction (ACL-R) restores the PLIA and if the PLIA is restored if the quadriceps reduction previously observed in ACL-D knees disappears.

This study tested the following hypotheses: (1) The PLIA of ACL-R knees is not different from the PLIA of uninjured contralateral knees; (2) Peak external knee flexion moment during walking (balanced by net quadriceps moment) is not correlated with PLIA in ACL-R knees.

METHODS

24 unilateral ACL-R subjects (33.6 ±9.2 years, 9 males, 1.69±0.08 m, 69.1±10.2 kg, BMI 24.2±3.1kg/m^2, 3.6±3.2 years post injury, 2.8±2.8 years post surgery) were tested after IRB consent. Sagittal-plane MRIs (3D-SPGR) were taken in a supine, non-weight-bearing, fully extended position. PLIA of the both knees were measured as the angle between the patellar ligament and the tibial shaft, as described previously (Figure 1) (Shin, 2007). Hypothesis 1 was tested using a paired two-tailed paired Student's t-test ($\alpha = 0.05$, power=0.9). Kinetics was measured using an opto-electronic motion capture system (Qualisys, Gothenburg, Sweden) using a previously-described 6-marker link protocol (Andriacchi, 1980). All subjects walked at three self-selected speeds (fast, normal, slow), three trials each. Peak external knee flexion moments (% body weight * height) corresponding to the average walking speed (1.35m/s) were estimated from each individual's speed vs. peak knee flexion moment regression equation, since peak knee flexion moment is known to be strongly correlated with walking speed (R^2=0.73) (Lelas, 2003). The difference in peak knee flexion moment between ACL-R and contralateral knees was examined using a paired two-tailed Student's t-test (α=0.05). Linear regression analysis was performed to study the relationship between PLIA and the peak knee flexion moment (Hypothesis 2).

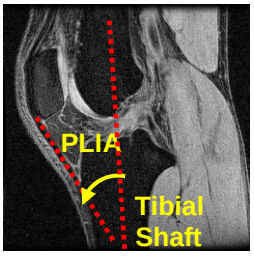

Figure 1: Measurement of patellar ligament insertion angle (PLIA) relative to tibial shaft

RESULTS AND DISCUSSION

ACL reconstruction restored the PLIA to normal values. The PLIA of the ACL-R knee was not different from the contralateral knee (p=0.18, power=0.985). In addition, peak knee flexion moment (balanced by net quadriceps moment) was not correlated with the PLIA following ACL reconstruction (R^2=0.012, power=0.99) (Figure 2).

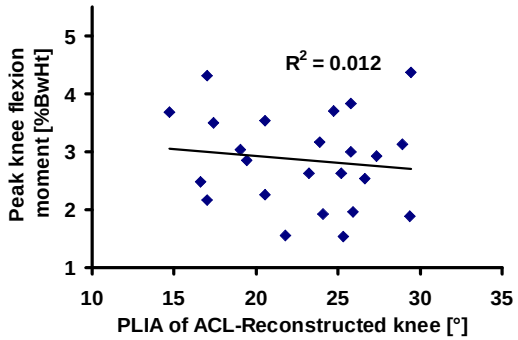

Figure 2: In ACL–R knee, no correlation was observed between peak external knee flexion moment and PLIA

These results on ACL-R knees show an important difference to a previous study (Shin, 2007), which reported ACL-deficient subjects with a large PLIA reduced their quadriceps usage proportionately to the PLIA. The combined results of these studies further support the theory that a reduced quadriceps moment in an ACL deficient population is an adaptation to reduce the anterior tibial translation associated with quadriceps contraction when the knee is near full extension.

It should be noted that while the peak knee flexion moment was not correlated with PLIA in ACL-R knees, the magnitude of the knee flexion moment in patients following ACL reconstruction was significantly lower than the peak knee flexion moment in the contralateral knees for almost every subject. This reduced quadriceps moment (Figure 3) is similar to previous studies for ACL-D knees and is consistent with previous findings that quadriceps reduction remains several years post surgery and rehabilitation (Devita, 1998). It remains unknown why quadriceps reduction adaptations persist in ACL-R knees, but this persistent adaptation may result in altered tibiofemoral contact kinematics that may lead to early onset of osteoarthritis.

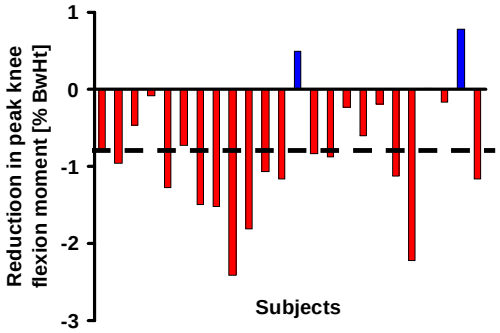

Figure 3: Most subjects show reduced peak knee flexion moment (red bars). Mean reduction was 0.83% BwHt (black dashed line).

In summary, this study has shown that the PLIA of ACL-R knees returned to normal after surgery and that patients no longer adapt their gait in response to the PLIA. However, quadriceps function did not return to normal levels during walking following ACL reconstruction, which may partially explain the increased incidence of osteoarthritis in this population.

REFERENCES

Berchuck, M. et al. (1990). *J. Bone Joint Surg. Am.*, **72**, 871-77.

DeVita, P. et al. (1998). *Med. Sci. Sports. Exerc*, **30**, 1481-1488.

Shin, C.S., et al. (2007). *J. Ortho. Res. Accepted for publication*

Andriacchi, T. P. et al. (1980). *J. Bone Joint Surg. Am.,* **62**, 749-757.

Lelas, J.L. et al. (2003). *Gait Posture*, **17**, 106-112.

ACKNOWLEDGEMENTS

Partial support form NIH R01-AR39421

GAIT STABILITY FOLLOWING TOTAL HIP REPLACEMENT

Vipul Lugade[1], Li-Shan Chou[1], Virginia Klausmeier[1], Brian Jewett[2] and Dennis Collis[2]

[1] Department of Human Physiology, University of Oregon, Eugene
email: chou@uoregon.edu, web: biomechanics.uoregon.edu,
[2] Orthopaedic Healthcare Northwest, Eugene, OR

INTRODUCTION

The prevalence of osteoarthritis among the aging community has resulted in 250,000 primary hip arthroplasties being performed annually in the United States (Lindemann et al., 2006). Total hip replacement (THR) has been reported to be a cost effective procedure that can improve mobility and the quality of life for suffering patients (Ethgen, et al., 2004; Lindemann et al., 2006).

The purpose of this study was to examine the effectiveness of the anterior and lateral THR. Gait stability in the medio-lateral and anterior-posterior directions was investigated during walking (Lee and Chou, 2006). It was hypothesized that both THR approaches would allow patients to ambulate in a safe and stable manner 16 weeks after surgery.

METHODS

Thirty adults were recruited for this study and were divided into three groups: 12 subjects with THR utilizing anterior approach (7 males/5 females; age = 56.9 ±3.3 years; mass = 92.8 ±15.0 kg; height = 170.4 ±8.0 cm), 8 subjects with THR utilizing a lateral approach (7 males/1 female; age=57 ±7.6 years; mass = 98.1 ±14.9 kg; height = 175.5 ±9.2 cm) and 10 control subjects (5 males/5 females; age = 59.9 ±5.3 years; mass = 74.7 ±15.1 kg; height = 168.1 ±7.2 cm). Prior to surgery all patients were evaluated for hip function, with similar Harris hip scores of 52.8 ±12.7 and 58.7 ±11.8 reported for the anterior and lateral groups, respectively. All patients had the same un-cemented Zimmer hip implants and underwent similar physical therapy.

Subjects who underwent THR were tested at 3 different times: pre surgery, 6-weeks and 16-weeks post surgery. Control subjects were tested during two separate visits.

During each visit, whole body motion analysis was performed using an eight-camera motion analysis system. Whole body center of mass (CoM) position was calculated using a 13-segment model with the weighted sum method (Hahn and Chou, 2004). The center of pressure (CoP) position was calculated using the ground reaction forces/moments measured with force plates. Instantaneous sagittal and frontal CoM-CoP inclination angles were calculated (Figure 1; Lee and Chou, 2006). A mixed model analysis of variance with repeated measures was used to compare the effects of group and time period. Gait parameters and CoM-CoP inclination angles were used as dependent measurements, with the significance level set at 0.05.

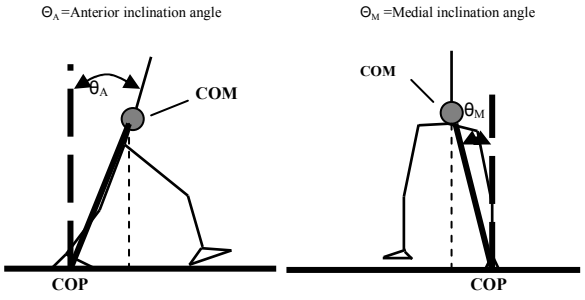

Figure 1: CoM-CoP inclination angles in the sagittal and frontal planes.

RESULTS AND DISCUSSION

Compared to pre surgery, significant increases in gait velocity and stride length were observed in the anterior group after surgery (See Table). Such significant changes were not witnessed in the lateral group, though significant group effects were seen among both surgical groups when compared to the control group. By 16 weeks post surgery, no group differences were seen between the surgical groups and the control group.

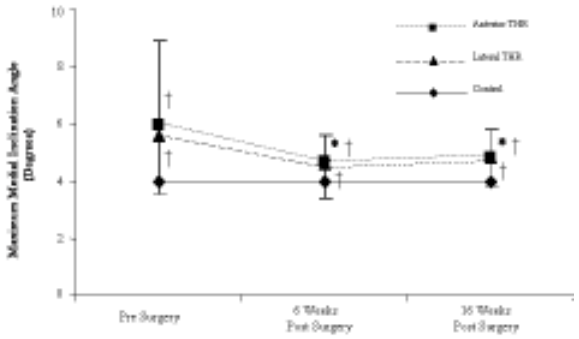

Figure 2: Medial Inclination angles

Results of the maximum CoM-CoP inclination angles are presented in Figures 2-3. Compared to pre surgery, the anterior group displayed a significant decrease in their medial inclination angle post surgery. No significant decrease was seen in the lateral group. Both groups, when compared to controls, showed significantly greater medial inclination at all time points. When compared to the control group, both surgical groups displayed significantly smaller anterior inclination angles.

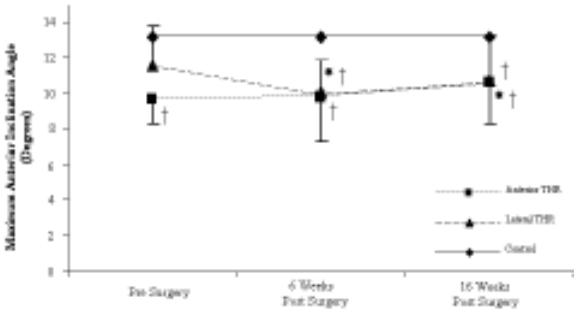

Figure 3: Anterior inclination angles

SUMMARY/CONCLUSIONS

Results from this study highlight the improvements in gait performance of patients following THR. Though improvements are seen in medial inclination angles after surgery, differences still exist between patients and controls 16 weeks post surgery. Improvements among both surgical groups highlight the benefits of THR for those patients who suffer from osteoarthritis of the hip.

REFERENCES

Ethgen, O., et al. *J Bone Joint Surg Am* **86-A**, 963-74, 2004.

Lindemann, U., et al. *Clin Rehabil* **20**, 413-20, 2006.

Lee, H.J. and L.S. Chou. *Arch Phys Med Rehabil* **87**, 569-575, 2006.

Hahn, M.E. and L.S. Chou. *J Biomech* **37**, 837-4, 2004.

	Controls	Anterior THR			Lateral THR		
		Pre surgery	6 weeks post surgery	16 weeks post surgery	Pre surgery	6 weeks post surgery	16 weeks post surgery
Gait Velocity (m/s)	1.28 (0.17)	0.94 † (0.26)	1.08 *† (0.20)	1.19 * (0.17)	1.09 (0.26)	1.02 † (0.26)	1.19 * (0.16)
Stride Length[a]	0.80 (0.08)	0.61 † (0.13)	0.69 *† (0.07)	0.73 * (0.07)	0.69 † (0.14)	0.65 † (0.14)	0.73 (0.08)
Step Width[b]	0.36 (0.07)	0.44 † (0.11)	0.42 † (0.07)	0.40 (0.09)	0.42 (0.06)	0.45 † (0.07)	0.42 (0.05)

* Time significance within a group, compared to pre-surgery ($p < 0.05$); † Group significance, compared to control group ($p < 0.05$); [a] Normalized to body height; [b] Normalized to ASIS width.

QUANTIFYING STRETCH REFLEX CONTRIBUTIONS TO MULTIJOINT COORDINATION FOLLOWING STROKE

Randy D. Trumbower [1], Vengateswaran J. Ravichandran [2], Eric J. Perreault [1, 2, 3]

[1] Rehabilitation Institute of Chicago, Chicago, IL, USA
[2] Biomedical Engineering, Northwestern University, Chicago, IL, USA
[3] Physical Medicine and Rehabilitation, Northwestern University, Chicago, IL, USA
E-mail: r-trumbower@northwestern.edu

INTRODUCTION

Multijoint coordination is impaired following stroke and restricted by abnormal muscle coactivation patterns. Previous studies have demonstrated that stretch reflexes about a single joint are enhanced following stroke and have suggested that this enhancement contributes to the abnormal activation patterns during voluntary arm movements. However, these prior investigations have not addressed reflex contributions to multijoint coordination, even though this coordination is necessary for most functional tasks.

There is evidence that abnormal constraints on muscle coordination between activation of elbow flexors and shoulder abductors increases with increased voluntary muscle activity opposing gravity (Beer et al. 2004). Beer et al. (1999) showed that increased elbow flexion torque occurred with increased shoulder abduction torque. Altered spinal function may contribute to this abnormal flexor synergy pattern. Hence, quantifying stretch-related reflex role in impaired coordination is essential for understanding the neural constraints imposed on arm function post-stroke.

The purpose of this study was to quantify multijoint stretch reflexes following stroke to determine if the patterns of reflex coordination mirror those during voluntary activation. We focused on reflex activity during changing levels of voluntary arm support in persons post-stroke.

METHODS

Six chronic stroke (Fugl-Meyer (FM) scores 20-64) and 3 age-matched control subjects were seated with the paretic (stroke) or dominant (control) arm positioned in 60° of shoulder abduction, 40° of shoulder flexion, and 90° of elbow flexion. Forearm was supported in pronation and hand was rigidly attached to a 3 degrees-of-freedom (DOF) robotic manipulandum (Figure 1A). We used a 4 DOF arm support device (Rahman et al. 2001) to vary support against gravity from 15N of shoulder adduction to 15N of shoulder abduction (Figure 1A); a maximum of 13 levels were tested per subject. The robot provided a sequence of randomly timed ramp-and-hold perturbations along 3 orthogonal directions. Perturbations displaced the hand 25mm at 400mm/s while subjects maintained arm posture. Surface electromyography (EMG) was used to measure reflexes from brachioradialis (BRD), biceps (BI), triceps longus (TRI_{long}), triceps lateralis (TRI_{lat}), anterior (AD),

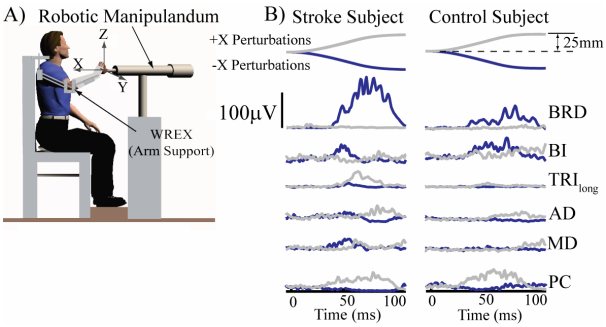

Figure 1. A) Experimental Setup, B) Typical multijoint reflexes from a stroke and an age-matched control subject during active support.

middle (MD), and posterior (PD) deltoids, and clavicular head of pectoralis (PC). Only times within 100ms after perturbation onset were considered.

RESULTS AND DISCUSSION

Multijoint stretch reflexes during active arm support were larger in the stroke subjects than controls at all levels of activation (Figure 1B). For example, during 15N of active arm support, the BRD activity of stroke subjects (76±33μV) was over twice the age-matched controls (29±20μV). The exaggerated reflexes may contribute to compromised multijoint coordination.

Reflex coordination patterns were similar across 5 of 6 stroke subjects, and these were significantly different from those of the age-matched controls. We quantified differences in reflex patterns between groups using independent component analysis (ICA) (Tresch et al. 2006). Independent components (ICs) were used to characterize reflex patterns across all conditions. Each IC shows a single coordination pattern of relative muscle activation as indicated by bar height (Figure 2). We used group ICs to predict reflex patterns of individual stroke subjects. The stroke within-group prediction accuracies were high (R^2=0.86±0.04) compared to the predictions made using the control group ICs (R^2=0.72±0.08). Only the least impaired stroke subject (FM=64) did not fit this pattern, but rather was more similar to the control group.

Reflex coordination patterns for the stroke group indicated a flexor bias that was significantly different from the control group. An average of 4 ICs accounted for >90% of the EMG variance. Between group correlations were computed for each IC (IC_1=0.79, IC_2=0.94, IC_3=0.58, and IC_4= -0.23). High relative variance and between-group correlation for IC_2 suggests a reflex pattern common to both groups during the studied tasks. However, the pattern for IC_1 consisted of strong elbow flexion (BRD activity) which accounted for a relative variance of >43% in the stroke group. This was more than twice the variance accounted for by the most similar coordination pattern estimated form the control data. IC_2 and IC_4 also showed elbow and shoulder reflex patterns mostly during abduction that was consistent with a flexion bias.

SUMMARY/CONCLUSIONS

This study quantified the coordination of stretch reflex patterns across a broad range of active arm support conditions in persons with stroke. Reflex activation patterns were consistent with previous evidence that abnormal synergies of shoulder and elbow muscles emerge during volitional tasks following stroke.

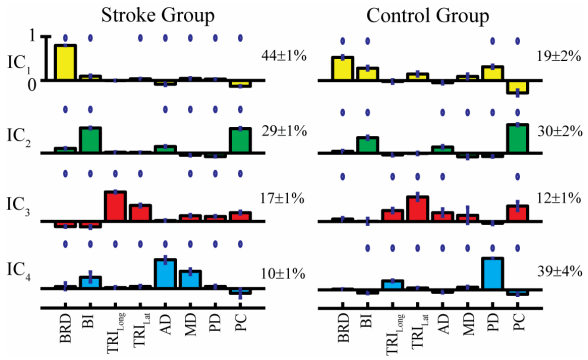

Figure 2. Muscle synergies identified by ICA applied to the muscle stretch reflexes collected during 13 arm support conditions (• p<0.05). Numbers correspond to relative variance of ICs.

REFERENCES

Beer, R.F., et al. (2004) *Exp Brain Research* **156**: 458-470.

Beer, R.F., et al. (1999) *Arch Phys Med Rehabil* **80**: 766-772.

Rahman, T.W., et al. (2001). *Int of Assist Tech in the Inform Age*: 31-36.

Tresch, M.C., et al. (2006). *J Neurophysiol* **95**: 2199-212.

ACKNOWLEDGEMENTS

This work was supported by NIH grants K25 HD044720 and R01 NS053813.

VIRTUE OF BOUNDARY ELEMENT METHOD IN CALCULATION OF PRESSURE DISTRIBUTION ON BOUNDARY BASED SEGMENTED MEDICAL IMAGES

Ali Pashaee [1,2] , and Nasser Fatouraee [2]

[1] Young Researchers Club, South Branch of Azad University, Tehran, Iran
[2] Amirkabir University of Technology (Tehran Polytechnic), Tehran, Iran
E-mail: nasser@aut.ac.ir, Web: http://bme.aut.ac.ir/biofluids

INTRODUCTION

Conventional methods for non-invasively estimation of pressure distribution in the cardiovascular flow domain use the differential form of governing equations. Here we use the integral form in these calculations. The most appropriate equation relating the velocity data of flow imaging devices (such as ultrasound, MRI and CT) to the pressure distribution is the Pressure-Poisson Equation (PPE) which is obtaining by simply taking divergence of Navier-Stokes Equation.

The aim of this study is to evaluate the advantage of using concepts of Boundary Element Methods (BEM) for extraction of pressure map from flow images. The motivation is the facilities provided with the boundary integral form of governing equations specially in boundary based segmented medical flow images. In this type of segmentation, continuous splines are fitting to the edge of interested field. These provided boundary segments could be switched directly to computational boundary elements to avoid further assumptions associated with the construction of computational nodes and elements which are used in other methods. These splines could also be used for extraction of boundary normal vectors required for applying Neumann boundary conditions. As an exclusive characteristic, using BEM concepts, pressure map with arbitrary resolution or at single arbitrary points could be calculated.

On the other hand image data naturally contaminated with different measurement resources noise which according to the computational method will affect the pressure distribution [Pashaee et al]. It is expecting that the integration feature of BEM may lead to reduction of the noise induced pressure map fluctuations.

METHODS

In order to provide a checking tool for this method, we used a divergence free mathematical Couette flow domain to provide artificial PC-MR images. Flow domain in provided image is segmented using quadratic Bezier curves. The spline functions are modified to obtain the boundary normal vectors. The required boundary elements are constructed on these spline curves. Constant variable elements are considered in this analysis. At the imaging domain with the described method, the calculation of pressure in the domain needs pressure data on boundary elements. Here first we derive the pressure distribution on boundary elements and then to obtain the pressure data in every point in the domain. The integral form of governing equation came from Green theorem. The discretization of integral equation and calculation of related terms are presented. Also the analytic solution of integral constants in the singularity points is presented. A domain integral term is appearing in the governing PPE, so we employ image pixels as the domain

elements. Gauss theorem is used for deriving the internal pixels of the segmented domain. Domain pressure gradient (which is obtaining from the Navier-Stokes Equations using velocity data) are concentrated on discrete internal pixels positions. For accurate calculation of pressure gradient on the arbitrary boundary element points, a distributed approximation approach is used. This method approximates the value of pressure gradient from the adjacent pixel values. Applying the obtained equation on all boundary elements obtains a linear system of equations which could be solved using the available numerical methods to obtain the boundary pressure data. At the second step, as a post-processing procedure, the pressure data at every arbitrary point in the domain could be calculated using the boundary data.

RESULTS AND DISCUSSION

In order to evaluate the potentials of this method versus the conventional methods, a common differential based method [Song et al] is applied to the test image. The pressure distribution from the BEM and conventional method are compared with the analytic values in Figure 1. This figure depicts the accuracy provided from this method.

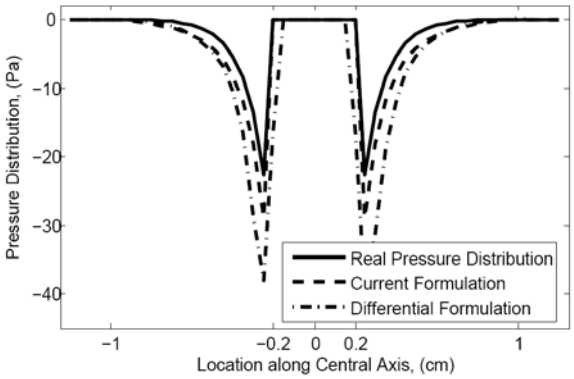

Figure 1: A comparison of pressure data obtained from the integral and differential form of governing equation.

For comparison of the effect of spatial noise on the calculated pressure domain from both the current and conventional methods, an artificial white Gaussian noise with SNR=10 is added to the velocity data of test flow domain to provide an artificial noisy image. The resulted image is analyzed by both methods. Figure 2 shows the resulted pressure domain and their comparison with the analytic one. As shown, the distribution from the BEM is considerably smoother than the conventional method. This denotes the robustness of described method to noise.

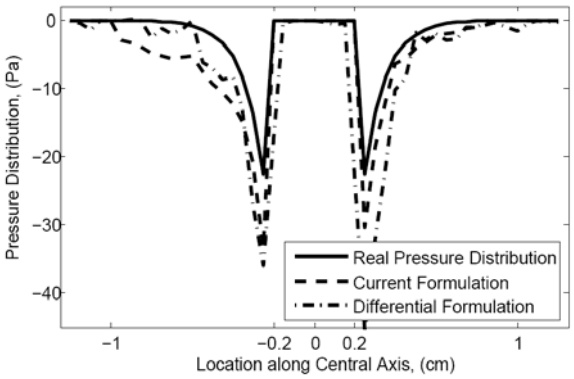

Figure 2: Comparison of pressure data obtained from noisy flow image.

SUMMARY/CONCLUSIONS

BEM for estimation of pressure domain from non-invasive flow image provides the following characteristics: reduce the computational domain to 1 dimensional; execute flexible calculation of pressure data in arbitrary points or at finer spatial resolutions; is more robust to presence of noise; less consideration on stability and compatibility is necessary; it is accurate and needs less meshing attempt.

REFERENCES

Pashaee, A. et al. (2005). *Proceedings of ICBME 2005*, 543-1 to 543-4

Song, S.M. et al. (1994). *IEEE Trans. Med. Imaging*, **13**, 386-397

Sex differences in neuromuscular activation strategies during anticipated and unanticipated jump landing tasks.

Tyler Brown[1], Scott McLean[1], and Riann Palmieri-Smith[1]

[1] University of Michigan, Ann Arbor, MI USA
E-mail: tynbrown@umich.edu

INTRODUCTION

Anterior cruciate ligament (ACL) ruptures are a common and traumatic sports related injury, occurring far more frequently in females compared to males (Arendt, 1995). This sex disparity in injury rate is typically viewed to stem from underlying differences in neuromuscular activation strategies. Recent studies have evaluated neuromuscular behaviors during more sports relevant factors, but the effects of unanticipated movements on neuromuscular control strategy, remains unclear. This study aimed to determine the effects of anticipation and sex on resultant lower limb muscle activation times during anticipated and unanticipated landing tasks.

METHODS

Six subjects (3 male and 3 female) were recruited to participate and required to perform 30 successful jump landings, comprised of three specific tasks. The randomly ordered landing response was governed by the activation of a light stimulus (L1, L2 and L3). Activation of L1 required subjects to land on their left foot and jump laterally to the right. Activation of L2 required the subjects to jump off the right foot, laterally to the left. When L3 was activated, subjects landed on both feet, one foot on each force plate, and jumped vertically as high as possible. Each jump was further labeled as either anticipated (AN) or unanticipated (UN) event. For AN trials, the light stimulus was activated approximately 5 seconds prior to the subject initiating the jump. For UN trials, the stimulus was automatically triggered via a light-beam switch broken following take-off, such that the subject received it approximately 350 ms prior to ground contact.

Muscle activity during the dynamic landing tasks was recorded by active surface electromyography (EMG) electrodes (Delsys, Boston, MA) placed over the muscle bellies of the medial hamstring (MH), lateral hamstring (LH), vastus lateralis (VL), rectus femoris (RF) and vastus medialis (VM). Raw signals were collected at 1080 Hz, band pass filtered (10-500 Hz), processed using a root mean square algorithm with a 15msec moving window and normalized to a maximum voluntary isometric contraction. EMG variables of interest were then calculated including, average muscle pre-activity (mean amplitude 100 ms prior to initial ground contact), average muscle re-activity (mean amplitude from ground contact to the peak ground reaction force) and muscle onset times. Onset times were defined explicitly as the point when the respective muscle's EMG amplitude was 3 standard deviations above resting EMG amplitude for 50 ms. Muscle co-contraction ratios, defined as the simultaneous activation of antagonistic muscles (VL/LH and VM/MH), were also calculated using the pre- and re-activity RMS EMG of each muscle via the formula: [(less active muscle/more active muscle) x (sum of the integrated activity of both muscles)] (Rudoloph et al., 2001). A repeated-measures analysis of variance

(ANOVA) was used to determine for the main effects and potential interactions between sex and movement (AN and UN) (alpha = < 0.05).

RESULTS AND DISCUSSION

Only findings presenting with statistical significance are reported in Table 1. The mean amplitude of the VM was significantly (p=0.022) larger during the pre-activity phase of UN compared to AN movements. The LH (p=0.024) demonstrated significantly larger re-activity phase mean amplitudes in UN compared to AN. While not statistically significant a trend of earlier muscle onset times was also observed in each muscle during UN compared to AN movements. Differences were also observed in muscle co-contraction ratios according to sex. Specifically, VM/MH ratio was significantly greater in males for both the pre- (p=0.016) and re-activity (p=0.019) phases during AN and UN jump landings (Figure 1).

The findings of this study contradict current theory and indicate that UN jump landings precipitate earlier and larger muscle activations compared to AN movements (Besier et al., 2001). The implications of this phenomenon are unclear, and we will address these explicitly in our ongoing research.

The significant gender difference of the co-contraction ratio of the VM/MH muscle pair may be an important contributing factor to the sex disparity in injury rates. Specifically, the altered ratio observed in females likely induces increased knee abduction loading during the landing, which is a known ACL injury risk factor.

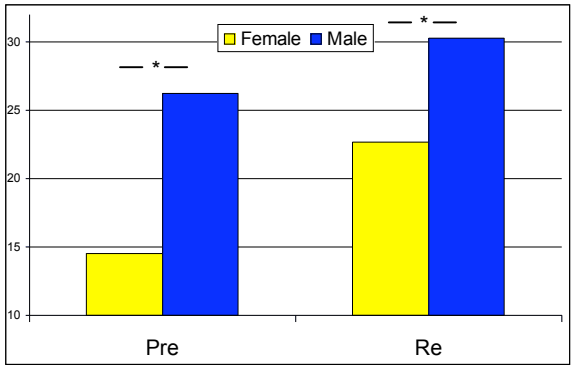

Figure 1: The co-contraction ratio of the muscle pair VM/MH during the pre- and re-activity phases. * alpha (p = <0.05)

SUMMARY/CONCLUSIONS

Unanticipated landings induce different neuromuscular strategies compared to anticipated tasks, suggesting they may implicate within the ACL injury mechanism. Also, the assessment of resultant joint load states, in conjunction with unanticipated effects, within even more realistic sports environment (eg., fatigue) may provide further insight to ACL injury mechanisms.

REFERENCES

Arendt, E., Dick, R. (1995). *Am. J. Sports Med.* **23**, 694-701.

Besier T.F. et al., (2001). *Med. Sci. Sports Ex.* **33**, 1176-1181.

Rudolph, K.S., et al (2001). *Knee Surg. Sports Traumatol. Anthrosc.* **9**, 62-71.

Table 1: Mean EMG onset time and amplitude for anticipated and unanticipated jump landings.

	Re-Activity			**Re-activity**		
	Onset (s)	Pre	React	Onset (s)	Pre	React
VM	0.16 (.11)	7.50 (1.77)	16.95 (5.41)	0.26 (.21)	12.01 (5.04)*	22.43 (8.33)
LH	0.22 (.27)	11.86 (13.37)	10.48 (6.48)	0.30 (.33)	11.88 (6.28)	26.93 (18.90)*

* alpha (p = < 0.05)

FEMALE NECKS ARE NOT UNIFORMLY SCALED VERSIONS OF MALE NECKS

Anita N. Vasavada [1] Jonathan Danaraj [1], and Gunter P. Siegmund [2,3]

[1] Washington State University, Pullman, WA, USA
[2] MEA Forensic Engineers & Scientists, Richmond, BC, Canada
[3] University of British Columbia, Vancouver, BC, Canada
E-mail: vasavada@wsu.edu

INTRODUCTION

Females have an increased incidence of whiplash injury (Harder *et al.*, 1998) and neck pain (Mäkelä *et al.*, 1991). Biomechanical analyses of these gender differences has been limited by the lack of an accurate model of the human female neck. It is not known whether female models can be developed by simply scaling male neck geometry, or if it is necessary to develop a unique model of the female neck.

The goal of this study was to quantify differences in head and neck geometry and neck strength in male and female subjects size-matched for height and neck length. We hypothesized that women have smaller external head and neck dimensions, smaller vertebral dimensions, and lower neck strength than men. If these hypotheses are true, it will necessitate the development of a gender-specific musculoskeletal model for females.

METHODS

Fourteen pairs of men and women with differences in standing height and neck length (vertical distance from the C7 spinous process to the tragus) within ±0.5 cm were selected for paired analysis.

Lateral and anterior-posterior cervical spine radiographs were digitized to calculate vertebral dimensions. Maximum isometric flexion and extension strength were measured with the subject lying down, using a hand-held dynamometer. Neck strength measurements were corrected for the weight of the head (Clauser et al., 1969).

Because muscle moment is the product of its force (proportional to neck muscle cross-sectional area) and moment arm, we predicted that the ratio of female to male neck strength would be related to neck and vertebral dimensions in the following way:

$$\frac{NS_F}{NS_M} = \frac{[NW_F * ND_F - VW_F * VD_F] * MA_F}{[NW_M * ND_M - VW_M * VD_M] * MA_M},$$

where *NS*=neck strength, *NW*=neck width, *ND*=neck depth, *VW*=average vertebral width, *VD*=average vertebral depth, *MA*=moment arm (average distance from the posterior-inferior corner of the vertebra to the tip of the spinous process), and the subscripts *M* and *F* denote male and female.

Paired *t*-tests were used to test for differences, with a significance level of p=0.05.

RESULTS AND DISCUSSION

Head and neck anthropometric parameters (other than height and neck length) were significantly smaller in females compared to males (Table 1). Differences in neck anthropometry (9 to 16%) were larger than differences in head anthropometry (3 to 6%). Females had significantly smaller vertebrae in the anterior-posterior (AP) dimension, but not in the medial-lateral (ML) dimension. Vertebral heights were significantly smaller in females for vertebrae C3-C5, but these differences were generally

less than the differences in vertebral depths or spinous process lengths (Figure 1).

Table 1: Anthropometric dimensions in height-matched men and women (mean and S.D.). *indicates $p < 0.05$.

	Male	Female
Height (cm)	169 ± 3	169 ± 3
Weight (kg)*	74 ± 9	66 ± 9
Head circ. (cm)*	57.7 ± 1.3	56.2 ± 1.5
Head width (cm)	15.3 ± 0.8	14.8 ± 0.8
Head depth (cm)*	19.9 ± 0.8	19.0 ± 0.6
Head height (cm)*	19.7 ± 1.5	18.4 ± 0.8
Neck length (cm)	10.8 ± 0.5	10.7 ± 0.5
Neck circ. (cm)*	39.4 ± 2.2	33.1 ± 2.0
Neck width (cm)*	11.7 ± 1.1	10.6 ± 0.7
Neck depth (cm)*	12.3 ± 0.7	10.3 ± 0.5

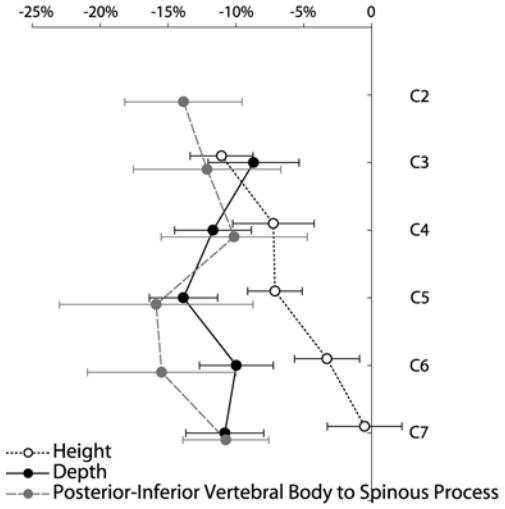

Figure 1: Percent difference (female-male)/male for cervical vertebral dimensions. Horizontal bars indicate S.E.M.

Female neck strength (corrected for head weight) was significantly lower (68 ± 25% and 80 ± 31% of male neck strength for flexion and extension respectively). Based on the anthropometry and radiology measures, the neck strength of females was predicted to be 71 ± 12% of males, which was not significantly different from the experimental neck strength ratios.

SUMMARY/CONCLUSIONS

In this sample of men and women who were matched by standing height and neck length, women had significantly smaller head and neck external dimensions, smaller vertebral size in the anterior-posterior dimension, and lower neck strength. We predicted a ratio of female to male neck strength based purely on differences in external neck and vertebral geometry, which corresponds well to the ratios measured experimentally. These findings support our hypothesis and demonstrate that male and female necks are not geometrically similar; further, geometric differences can explain much of the gender difference in neck strength.

The results of this study show that female necks are not simple scaled versions of male necks. Scaling the male neck based on one linear dimension (e.g., standing height) cannot be used to construct a model of the female neck musculoskeletal system. Therefore, female-specific models will be necessary to evaluate the biomechanical factors that lead to gender differences in neck-related disorders.

REFERENCES

Clauser, C.E. *et al*. (1969). *Weight, volume, and center of mass of segments of the human body*.

Gordon, C.C. *et al*. (1989). *1988 anthropometric survey of U.S. army personnel: methods and summary statistics*.

Harder, S., *et al*. (1998). *Journal of Clinical Epidemiology*, **51**, 377-84.

Mäkelä, M., *et al*. (1991). *American Journal of Epidemiology* **134**, 1356-1367.

ACKNOWLEDGEMENTS

We thank Richard Lasher, Linda Rico, Liying Zheng, Darin Porter and Helen Schiebe. This work was funded by the Centers for Disease Control (R49 CE000660-01).

POWER REQUIRED TO MAINTAIN BALANCE ON A MOVING PLATFORM

Venkata Gade[1], Nitin Moholkar[1], Jerome Allen[1], David Tung[2], and W. Thomas Edwards[1]

[1] Kessler Medical Rehabilitation Research and Education Center, West Orange, NJ, USA
[2] University of Medicine and Dentistry of New Jersey, Newark, NJ, USA
E-mail: vgade@kmrrec.org Web: www.kmrrec.org

INTRODUCTION

The measure of Center of pressure (COP) has been conventionally used to describe posture and balance and give a measure of effort. Movement response to a platform translating sinusoidally in the anterior posterior direction can be used to understand balance. Prior studies have demonstrated that maintaining balance on a translating platform involves choosing a balance strategy depending on the frequency of platform translation. It is believed that at all frequencies; subjects tend to select strategies that minimize the motion of the head and the upper body. Does the selection of strategy also reduce the effort required to maintain balance? The objective of this study was to quantify the effort in maintaining balance on a moving platform using the power spectrum analysis for COP movement in anterior posterior direction.

METHODS

Fifteen healthy adult individuals participated in the study. The subjects were free of neurological, audiological, opthalmological and internal pathologies, and medications affecting balance. All the participants gave their informed consent for participation.

A NeuroCom Research Balance Platform consisting of two independent AMTI force plates provided the anterior-posterior translations and gathered the ground reaction forces. Subjects stood on the platform with their feet shoulder width apart with one foot on each forceplate. Motion data along with the forceplate information was collected using a six camera Vicon system. The platform translated sinusoidally with fixed frequencies (0.1, 0.25, 0.5, 0.75, 1.0, and 1.25 Hz) with a peak to peak amplitude of 6 cm. Each translation frequency was repeated three times with both eyes open and closed conditions. Subjects were protected from falling in the event of loosing balance using a safety harness system.

The effort required for maintaining balance during a trial was quantified by the average power calculated from the power spectrum of the COP movement. Power spectrum was calculated from the Fast Fourier transform of zero-mean COP trajectory. The average power, $P_{ave}(t)$, of a signal in time series by definition is:

$$P_{ave}(t) = 1/T \int |x(t)|^2 \, dt \qquad (1)$$

The integral of power spectral density across all frequencies, $P_{freq}(f)$, is proportional to the average power of the signal.

$$P_{freq}(f) \alpha P_{ave}(t) \qquad (2)$$

We confirmed that the integral of power spectrum was scaled properly to match the calculated average power. The integral of power spectrum across all frequencies was divided by the constant of proportionality, calculated from equation-1, to obtain the average power for COP movement. The

average power was calculated for each platform frequency and averaged across all the subjects to quantify the effort required to maintain balance.

RESULTS AND DISCUSSION

Figure-1 shows the power spectrum for a translation frequency of 0.75 Hz, eyes open condition for a representative subject. As expected the power spectrum is dominated by the peak at the platform translation induced frequency.

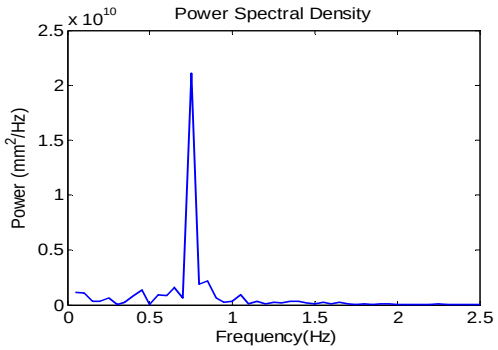

Figure 1: Power spectrum for a 0.75 Hz frequency trial showing the power content for frequencies up to 2.5 Hz.

Several trends were observed with respect to the frequency of oscillation and eyes open or closed condition.

- At each frequency, subjects tend to select a strategy that minimize the motion of the head and the upper body and that reduces effort, power.
- Across all frequencies, the average power calculated from the power spectrum of COP, P_{ave} (t), shows an increase in its value at increased translation frequency.
- In general, all the subjects showed a higher average power, P_{ave} (t), in eyes closed conditions when compared to the same frequency eyes open trial. Two subjects showed more average power for eyes open when compared to eyes closed trials.

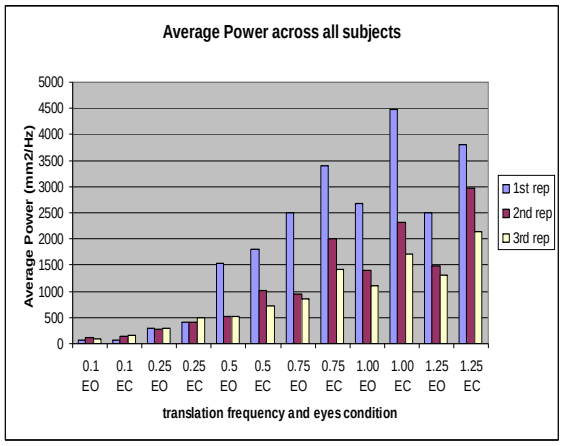

Figure 2: Average power across the subjects for the COP movement. Each translation frequency repeated for three times with eyes open followed by eyes closed condition.

SUMMARY/CONCLUSIONS

This study, for the first time demonstrates the effort required to maintain balance on an oscillating platform. These results suggest that under different dynamic conditions there are postural control strategies that enhance stability and reduce effort. It is hoped that new diagnostic and treatment techniques can be derived from these studies and applied in rehabilitation using whole body oscillations and other balance therapies.

REFERENCES

Buchanan, J.J., Horak, F.B. (1999). *J Neurophysiol.*, **81**, 2325-39.

Corna, S., et al. (1999). *Exp Brain Res.*, **124**, 331-3441.

Rocchi, L., et al. (2004). *Med Biol Eng Comput.*, **42**, 71-79.

Roy, M., H., (2002). *Principles of Random signal analysis and low noise design*.

ACKNOWLEDGEMENTS

Support by the Henry H. Kessler Foundation

Changes in leg stiffness and sprint characteristics during the acceleration phase of running in top sprinters

Kai Kobayashi[1], Shigeo Iso[1], Kazuyuki Kanosue[1], Hiroyasu Tsuchie[2], Tetsuo Fukunaga[1], Yasuo Kawakami[1]

[1] Waseda University, Tokorozawa, Saitama, Japan

[2] Josai University, Sakado, Saitama, Japan

E-mail: k-kai@toki.waseda.jp

INTRODUCTION

When runners sprint, they repeat contact and aerial phases, and their legs behave like a single linear spring. Leg elasticity in the eccentric phase during the first half of contact phase has been estimated by leg stiffness based on a spring-mass model. There are a few studies reporting the influence of running velocity on the leg stiffness (Arampatizis et al. 1999, Farley et al.1996, Kuitunen et al. 2002, McMahon et al. 1990). However, changes in leg stiffness during the acceleration phase of sprint have not been reported. The purpose of this study was to investigate changes in leg stiffness and sprint characteristics during the acceleration phase of running in top sprinters.

METHODS

Five top sprinters and five athletes (control) (Table 1) performed repeated the maximal start dash along a 100m linear indoor track. Cinematographic recordings of sprint were obtained from 12 infrared cameras (VICON system; VICON Motion Systems, 120 Hz), and ground reaction force was also obtained from 6 force platforms (90cm×60cm, Kistler-9287A; Kistler). The markers were placed on the lateral surfaces of the joints. Force was measured at 600 Hz. Running velocity was calculated by multiplying stride frequency and stride length. The leg stiffness was calculated from the ratio of the change in ground reaction force to the displacement of the center of mass. The vertical leg stiffness was calculated from the ratio of the change in vertical component of the ground reaction force to the vertical displacement of the center of mass.

RESULTS AND DISCUSSION

During the acceleration phase, the running velocity increased that was accompanied by an increase in the stride length ($P<0.01$) while the stride frequency remained unchanged. Within the stride length, the aerial length was increased significantly ($P<0.01$). These results indicate that the increase in the running velocity during the acceleration phase is influenced by the aerial length rather than the stride frequency.

The leg stiffness of top sprinters was constant throughout the acceleration phase, but their vertical leg stiffness increased ($P<0.05$) with increasing running velocity (Fig. 1). However, leg stiffness and vertical leg stiffness of control athletes were not

increased over the entire acceleration phase. Top sprinters ran with smaller displacements of the center of gravity and greater vertical ground reaction force compared with control subjects. As a result, the vertical leg stiffness of top sprinters increased during the acceleration phase of running but that of control athletes did not. A significant correlation between the maximal stride length and the vertical leg stiffness was found (Fig. 2). These results indicate that the vertical leg stiffness significantly influences the aerial stride length during the acceleration phase of running.

CONCLUSIONS

The main finding of this study was that the better running performance during the acceleration phase of running is related with larger stride (aerial) length, which is due to the greater vertical leg stiffness.

REFERENCES

- Arampatzis A., Bruggemann G. P., Metzler V.：The effect of speed on leg stiffness and joint kinetics in human running. J Biomech. 32(12)：1349-1353. 1999
- Hunter J.P., Marshall R. N., McNair P.J. Segment-interaction analysis of the stance limb in sprint running. J. Biomech. 37：1439-1446, 2004
- Kuitunen Sami, Komi P. V., Kyrolainen Heikki：Knee and ankle joint stiffness in sprint running. Med Sci Sports Exerc34(1)：166-73, 2002

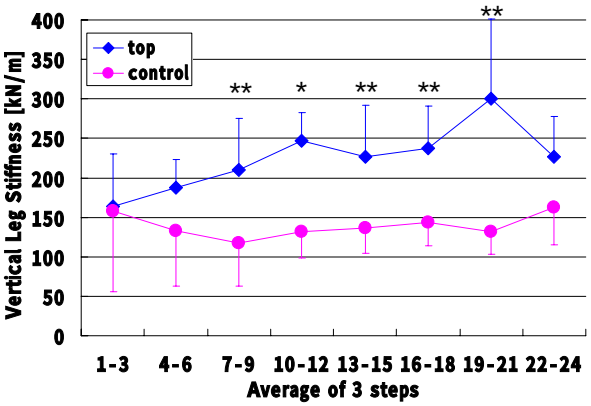

Figure 1: The vertical stiffness change during the acceleration phase of running (*P<0.01, **P<0.05).

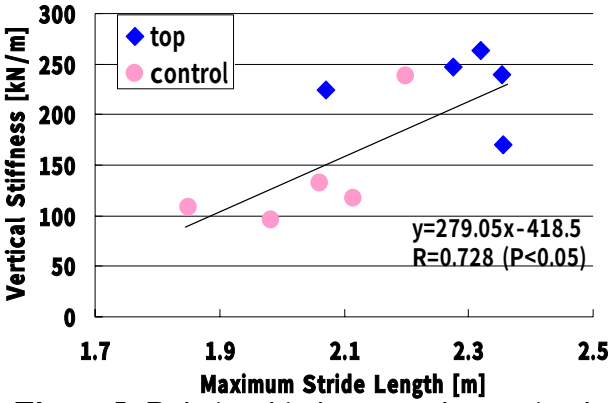

Figure 2: Relationship between the maximal stride length and the vertical leg stiffness.

Table 1: Physical characteristics of the subject groups.

subject group	height[cm(±SD)]	weight[kg(±SD)]	100m personal best[sec(±SD)]
top sprinter	175.4(±2.9)	70.7(±3.2)	10.23(±0.14)
control	168.9(±3.0)	60.4(±3.2)	11.38(±0.19)

Determination of the psoas major muscle thickness by B-mode ultrasonography

Yoichi Katsumata [1], Yohei Takai [1], Yasuo Kawakami [2] and Tetsuo Fukunaga [2]

[1] Graduate School of Sport Sciences, Waseda University, Saitama, Japan
[2] Faculty of Sport Sciences, Waseda University, Saitama, Japan
E-mail: kats.yo1@fuji.waseda.jp

INTRODUCTION

The main functions of the psoas major muscle (PM) are to flex the hip joint and to increase spine stability. Some studies have reported that the cross-sectional area (CSA) of PM is related to sport performance and lower-back pains. (Hoshikawa et al.,2006; Dangaria and Naesh). At present, CT and MRI are used to measure CSA of PM (Hoshikawa et al., 2006; Masuda et al., 2002). However, these methods are costly and time consuming, and are not applicable in field research on large numbers of subjects. In contrast, the brightness mode (B-mode) ultrasonography has the same advantages as that of CT or MRI in visualizing muscle tissues without any radiation exposure, and is more suitable for field use. However, the validity of muscle thickness measurement of PM by B-mode ultrasonography as a representative of PM CSA has not been estabilished. This study aimed to develop the method of assessing the PM thickness using a B-mode ultrasonography and to compare it with the MRI-measured CSA.

METHODS

Sixteen healthy collegiate students were recruited in the study (14.3±0.8 years, 1.73 ±0.05m, 67±7kg, mean ± SD). The cross-sectional images of PM were obtained from the position 5cm to the right and left sides of the fourth lumbar vertebrae (L4) -L5 level with a B-mode ultrasonographic apparatus (SSD-6500, Aloka, Japan) and a linear scanner (scanning frequency; 7.5 MHz). During the measurements, the subjects remained in a supine position with their arms and legs relaxed in an extended position. In the calibrated image muscle thickness (MT) of PT of each side was measured. The repeatability was assessed on two separate days with 9 of 16 subjects.

The CSA of PM on both sides was obtained using MRI with a body coil (Signa 1.5T, GE Electronics, USA). T1-weighted, fast spin-echo, and Axial-plane imaging were performed with the following variables: TR (repetition time), 500 ms; TE (echo time), 10.7 ms; matrix, 192 × 192; field of view, 240m; and slice thickness, 10 mm. Three axial images were obtained around the L4-L5 levels. During the measurement, the subjects were in the identical condition to that of ultrasonography. The mean value was calculated from three axial images.

RESULTS &DISCUSSION

The intraclass correlation coefficient for the test-retest of MT was r=0.990 for right side, r=0.970 for left side. The difference in MT values of the first and second measurements was less than 2mm and was not significant.

The CSA of this study (16.6±2.5 cm^2 for right side, 16.6±2.5 cm^2 for left side) was similar in size to those of previous researches (Hoshikawa et al.,2006; Dangaria and Naesh). Both for the right and left sides, MT were significantly correlated to CSA (r=0.899 for right side, r=0.845 for left side, p<0.05, Fig. 1). These results show that our method has good reproducibility and is useful for assessing PM size.

Future studies on a large population covering different age groups, genders, body composition, and athletic background will clarify the influence of PM size on physical performance and lower-back pain.

REFERENCES

- Hoshikawa Y et al. (2006). Med Sci Sports Exerc. 38(12):2138-43.
- Takahashi K et al. (2006). J Musculoskelet Neuronal Interact. 6(2):201-5
- Dangaria TR and Naesh O. (1998). Spine.15;23(8):928-31.

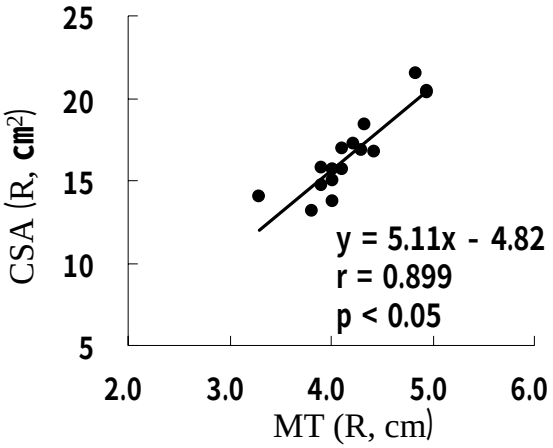

Fig. 1 Relationship between MT and CSA

R: right side MT: muscle thickness

RELATIONSHIP BETWEEN FAILURE PROGRESSION IN A LUMBAR DISC AND MANUAL LIFTING - A POROELASTIC FINITE ELEMENT MODEL STUDY

R.N Natarajan (1,2),S.A Lavender (3), H. An (1), G. B J Andersson (1)

(1) Rush University Medical Center, Chicago, Illinois. (2) University of Illinois at Chicago, Chicago, Illinois, (3) Ohio State University, Columbus, Ohio
E-mail: raghu_natarajan@rush.edu

INTRODUCTION

The degenerative process of the intervertebral disc is a cascading event which is often attributed to cumulative damage. Macroscopic autopsy studies have shown that nuclear clefts form first later followed by annular tears. Repetitive loading advances this damage process since the cyclic loadings does not allow the time necessary for discs to recover between load applications thereby leading to cumulative damage. Understanding how motion segments react to cyclic loading is important to understand the initiation and progression of the failure processes. The aim of the current paper was to develop a non-linear poro-elastic finite element model that included the physiological parameters such as osmotic pressure and the effect of change in permeability in the disc due to strain and use it to predict the failure initiation and progression in a lumbar disc due to repeated loadings that corresponded to three different commonly occurring lifting activities. It is hypothesized that failure progression in a lumbar disc will be fastest under lifting that involves lateral bending of the trunk.

METHODS

An existing model of the L4-L5 motion segment was modified to include the physiological parameters such as swelling pressure P_{swell} in the disc tissues and the effect of change in permeability of the disc tissue due to strain $P_{permeability}$ (1). To accommodate the variation in concentrations of proteoglycan as well as the porosity, permeability and aggregate modulus with in the disc, regional variations of the tissue properties were included in the analyses. Failure initiation and progression under cyclic loading was monitored using a custom-written failure rule. Failure at any point in a single element was predicted to occur if the internal stress at that point exceeded an assumed failure stress value. The elastic material property at the failure location was reduced by a percentage of the intact elastic modulus for subsequent analyses thus controlling the growth of failure progression in the model.

The loading conditions used in this investigation involved lifting a box weighing 30 pounds (Natarajan, 2004) from mid-shank level to elbow height simulating trunk extension from flexed to upright posture (task 1), (2) lifting the box from elbow height on the right side and placed on the left side simulating trunk twisting posture (task 2) and (3) lifting the box from a maximally lateral flexed posture up to waist level simulating trunk lateral bending motion (task 3). The time history data of spinal loads during the three lift modes were input into the poro-elastic finite element model to determine the corresponding biomechanics of the disc.

RESULTS

The lifting activity that required lateral bending of the trunk (task 3) produced largest disc translational and rotational

motions. Task 3 produced a disc compression of 6.4 mm while task 1 and 2 produced 5.6 mm and 3.1 mm compression respectively. Shear motion of the disc directed along right lateral direction was 4.0 mm for task 3 while a much smaller shear motion was seen during the other two lift activities (2.0 mm for task 1 and 1.8 mm for task 2). A flexion motion of 10^0 was seen during task 3, while task 1 and task 2 produced 5.8^0 and 3.6^0 of flexion respectively. Twisting motion to the right as well as lateral bending rotation was highest for task 3 (4.4^0 and 4.0^0 respectively). The largest von Mises stress of 6.5 MPa was observed in the right lateral quadrant of the annulus during task 3. Both the superior and the inferior end plates experienced a maximum von Mises stress of 12 MPa during the lateral lift task.

In all the three lift cases, failure in the endplate was observed even in the first cycle (Figure 1) with maximum failure occurring under task 3 (4.5% of endplate volume). As the load cycle progressed, endplate failure volume increased. Highest rate of endplate failure volume was observed during task 3. The failure volume reached a plateau quickly under task 2 (5 cycles) while under task 3 it took 15 cycles to reach a maximum endplate failure volume of 8%.

CONCLUSIONS

The analyses conducted here showed that of all the three lift conditions considered in the current study, task 3 produced greatest motions in all the three principal directions as well as largest stresses in the disc tissues leading to highest failure volume due to repeated loading. This conclusion agrees well with those obtained by Schmidt et al., (Schmidt, 2006) who with the help of a finite element model study showed that the risk of disc failure mostly occur in the posterior annulus under a load combination of lateral bending + axial rotation. Costi et al., (Costi, 2006) also showed from their studies on cadaver specimens that lateral bending produced highest motions that induced high physiological maximum shear strain that place the disc at greatest risk for failure and injury. These conclusions agree very well with the results from the current study which showed that task 3 which involved lateral bending of the trunk produced largest motions in the disc, induced largest disc tissue stresses and as a consequence produced largest volume of failure in the disc tissues.

REFERENCES

Natarajan et al., SPINE, 2004, **29(23)**, 2733-2741.
Schmidt et al., ORS, 2006, Poster **1032**.
Costi et al., 2006, J. Biomech, **11.006**.

ACKNOWLEDGEMENTS

NIH: AR48152-02.

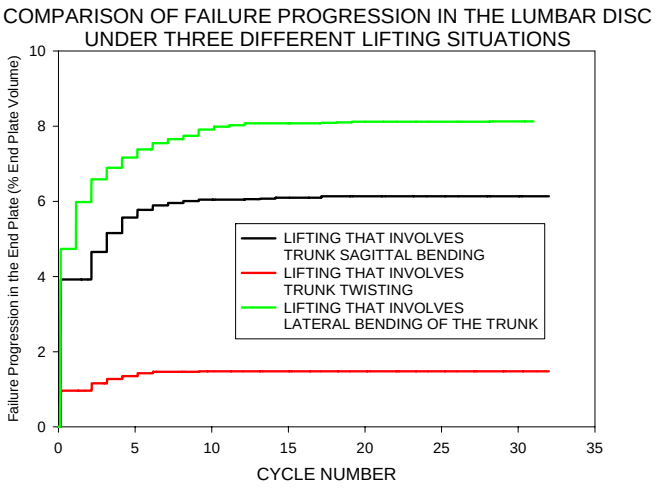

Figure 1: Failure progression in a lumbar disc under three different lifting modes.

Modeling static force generation of rat hindlimb muscles by direct stimulation

Matthew Tresch [1] Sang Hoon Yeo [2], and Dinesh Pai [2]

[1] Northwestern University, Chicago, IL, USA
[2] University of British Columbia, Vancouver, BC, Canada
E-mail: m-tresch@northwestern.edu

INTRODUCTION

Musculoskeletal models are generally created from the bottom up: researchers first measure various parameters of muscle function, then put these parameters into a structural model to predict muscle actions (Delp and Loan, 2000). Although these methods have clearly been greatly successful, it can be difficult to assess the validity of these models.

We describe here a complementary method of creating a musculoskeletal model from the top down: starting with measurements of the true actions of muscles, then building a model to account for these measurements (Loeb et al. 2000). Although the resulting model is structurally similar to that used in bottom up approaches, it is constrained to predict the true action of muscles. This method can potentially help inform traditional muscle modeling procedures, helping to improve the accuracy and utility of musculoskeletal models.

METHODS

We characterized the actions of individual hindlimb muscles in the rat by direct stimulation. The hip was immobilized by posts placed in the pelvis and the distal tibia attached to a 6 degree of freedom force transducer (ATI). Bipolar electrodes were implanted into the muscle at its motor point. Muscles were stimulated using trains of biphasic constant current pulses (70-100Hz, 0.2ms, 0.5-1s train duration). Insulation was placed as necessary to prevent current spread to adjacent muscles. The limb was fixed in a configuration, the muscle stimulated, and the evoked forces and moments recorded. This procedure was repeated for 10-12 configurations of the limb, characterizing the configuration dependence of the muscle. The response at each configuration was summarized as the peak evoked response and converted to joint torques using the measured limb Jacobian.

We then used this isometric data to fit a parametric model of static muscle actions. This model comprises the static component of standard lines-of-force models, consisting of an anatomical model of the muscle path and moment arm and a model of the force generating characteristics of the muscle. Although such models are commonly used, choosing a muscle path can often be difficult, especially for muscles with broad insertions or origins. Our approach provides a way to empirically determine the best approximation. We assumed that the muscle path was fully described by point insertion and origin. This model can be described by the following set of equations:

$$l = f(\theta \mid x_o, y_o, z_o c);$$

$$\tau = R(\theta)^T \cdot F_M\left(l \mid L_{opt}, F_{opt}\right)$$

where τ are the joint torques, θ are the joint angles, R is the moment arm of the muscle, l is the effective muscle length, and the function F_M characterizes the force generating properties of the muscle. The free parameters x_o, y_o and z_o specify the origin of the muscle, c is the insertion point

of the muscle along the tibia, L_{opt} is the optimal muscle length, and F_{opt} is the force produced by the muscle at its optimal length. We approximated the active force length function as a simple Gaussian, with mean L_{opt}. We then fit the model parameters using the measured muscle force data. We chose initial parameters based on the known anatomy (Greene, 1963), then used optimization to update these parameters.

RESULTS

We started with a simple version of the model described above, characterizing the action of the muscle in the sagittal plane. The measured action of semitendinosus is shown in the open arrows of Figure 1. Note that the direction and magnitude of the force are systematically altered as a function of the limb configuration. We attempted to fit the parameters of the structural model described above. The resulting model is shown in Fig. 1 in the overlaid filled arrows. The force vector indicated with a circle at the base was not used for the model fit but represents a generalization prediction of the model. As can be seen in the figure, the paramaterized model fit does a very good job of characterizing the observed muscle action. Across muscles (n = 6) and rats (n = 6), we have found that these models were able to predict approximately 95% of the variance in the observed muscle action.

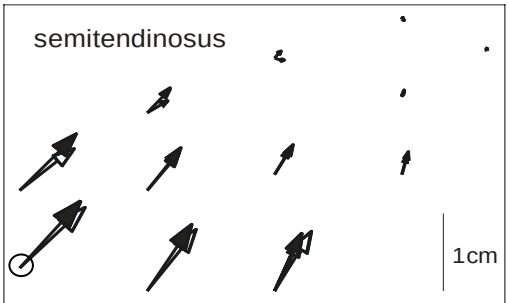

Fig 1 Results of parameterized model fits to force field data, showing the fit (filled arrows) to the force field from ST (indicated here with the open arrows).

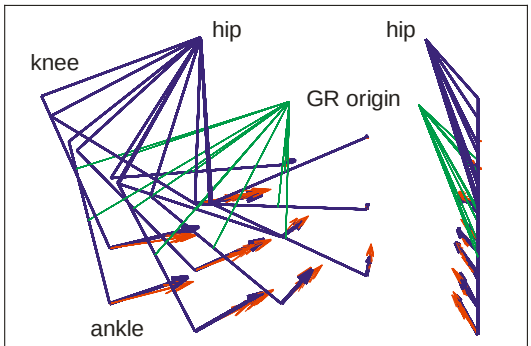

Fig 2 3D parameterized model fit. Blue lines show the limb, green shows the predicted muscle path. Red vectors are measured forces, blue vectors are predicted forces.

Figure 2 shows the extension of this approach to predict the full 6 dimensional action of gracilis (GR). In this case, the measurement of muscle action was repeated 8 times (red arrows). This data was then used to fit the model (blue arrows). Overlaid on the plots are the limb configurations and predicted muscle paths. As can be seen in the figure, the model did a good job of predicting the muscle action and the predicted anatomical path corresponds to the known anatomy of this muscle.

CONCLUSIONS

We have described an approach to muscle modeling based on directly measured muscle actions and demonstrated its utility. We are currently evaluating this approach in further detail, comparing the models created by this approach to those created by measuring muscle parameters directly. By combining information from the two approaches, we hope to continue to refine and improve our rat hindlimb model.

REFERENCES

Delp, S.L. and J.P. Loan (2000), *Computing in Science and Engineering*, **25**(1): 21-34

Loeb, E.P., et al.(2000), *J Cogn Neurosci*, **12**(1): 78-97.

Greene, E.C. (1963), *Anatomy of the Rat.*, New York: Hafner.

Effect of Wrist and Forearm Muscle Architecture on Wrist Radial-Ulnar Deviation and Forearm Pronation Supination Moment

John Ramsay and Roger V. Gonzalez

LeTourneau University, Longview, TX, USA
E-mail: rogergonzalez@letu.edu

INTRODUCTION

To estimating muscle fiber operating ranges in muscles across the human wrist during forearm pronation/supination (P/S) and radial/ulnar deviation (R/D), a existing geometric model of the human elbow, forearm and wrist, comprised of 14 muscles was enhanced using Software for Interactive Musculoskeletal Modeling (SIMM).

METHODS

Previously, muscle wrap points and surfaces were developed (Hunt and Gonzalez, 2004) to calculate musculotendon lengths and moment arms. Maximum isometric moments generated by each muscle during pronation-supination and radial-ulnar deviation were calculated as the product of each muscle's isometric force and the moment arm, assuming full muscle activation. Net isometric joint moment was calculated by summing all muscles which had a concentric moment contribution throughout the range of motion.

Ten of fourteen muscles used in the model were determined to aid in both P/S and R/D. A factor of 65 N-m^{-2} was used to linearly scale their PCSA values to F_o^m, and 50 N-m^2 was used for the remaining muscles P/S muscles (BIC, BRD, PRO, SUP). Since all wrist deviators also created moment during P/S, their scaled values were chosen to fit the experimental R/D, and the remaining muscles for P/S were scaled to fit the experimental data as close as possible. Using these calculated values for F_o^m, the net moment was found in P/S and R/U over their respective ranges of motion, and compared to experimental data (Wisher, et al, 2007). In accordance with experimental data, the model's elbow was flexed 90° and in a neutral wrist position. Figures 1 and 2 show the scaled comparisons.

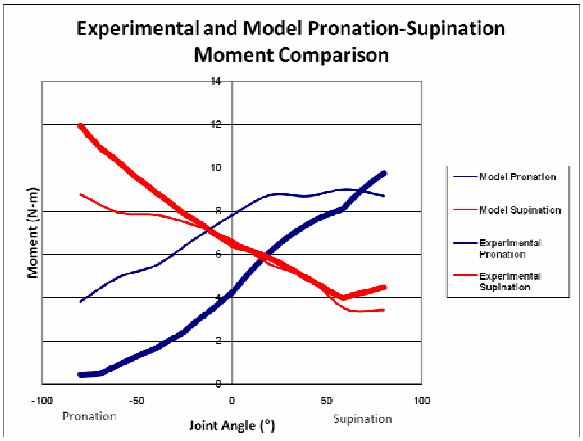

Figure 1. Comparison between model pronation-supination moment arm and experimental values.

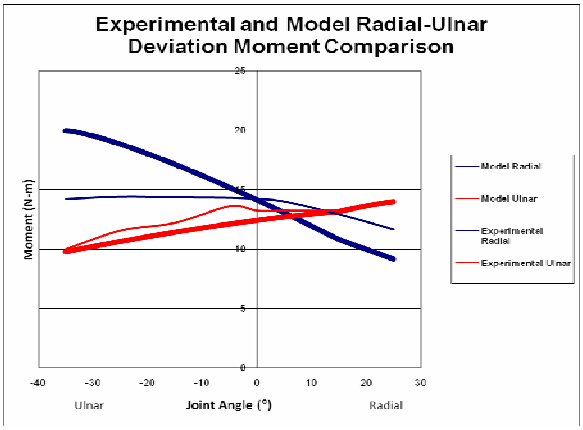

Figure 2. Comparison between model radial-ulnar deviation and experimental values.

Operating ranges for each of the 14 muscles were found by plotting normalized active force vs. normalized fiber length (Fig 3 and

4). Each muscle's active force was normalized to its peak isometric force (F_o^m) and individual muscle fiber lengths were normalized to (l_o^m, Gonzalez, et al, 1997) Muscle moment arms estimated by the model in P/S have been shown to be consistent with experimental data (Hunt and Gonzalez, 2004).

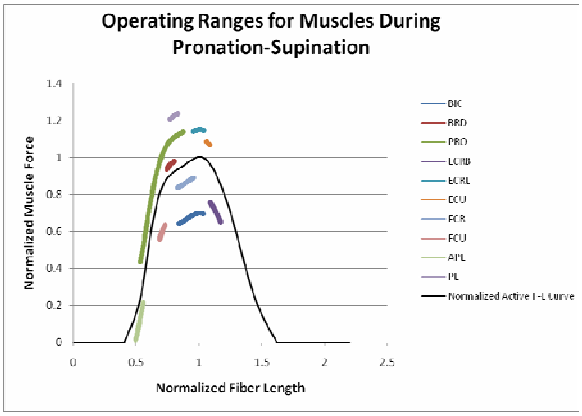

Figure 3: Muscle fiber operating ranges during forearm pronation in a wrist neutral position with the elbow flexed 90°.

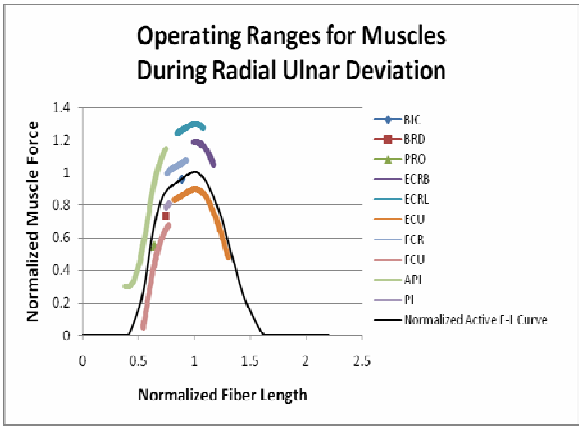

Figure 4: Muscle fiber operating ranges during ulnar deviation with no wrist flexion or extension, neutral pronation-supination and elbow flexed 90°.

RESULTS AND DISCUSSION

The model replicated the minimum pronation moment at full pronation and peaked at full supination. Peak supination moment was at full pronation, and decreased toward full supination and also compared favorably with experimental data (Fig 3).

Similarly, Fig 4 shows that the model's R/U isometric moment also compared favorably to experimental data with peak radial deviation moment at full ulnar deviation, and decreasing toward full radial deviation. Peak ulnar deviation moment occurred at full radial deviation and decreased toward full ulnar deviation. By summing all the pronation and supination moment arms separately, the slope of each resembles the trends of the moment.

While many muscles act on the plateau region of the force length curve, a few appear to operate on the ascending or descending region (Figs 3 & 4). For example, the PRT descends down the ascending portion of the F-L curve during pronation, and similarly the APL and FCU in wrist deviation. During pronation, the model indicates decreasing PRT force and moment, which results in a decreased moment contribution.

SUMMARY/CONCLUSIONS

Additional research is needed to determine the effect of scaling PCSA on pronation-supination and wrist deviation moments, specifically for all deviator muscles during pronation-supination. Also, model R/U moment arms need to be experimentally verified. In general, the model has replicated experimental trends, and provides an approximation of muscle fiber operating ranges during the respective movements.

REFERENCES

Gonzalez, R. et al. (1997) *J. Biomech.* 30(7), pp. 705-12.

Hunt, B. and Gonzalez, R. (2004) *ASME National Congress*.

Wisher, M. and Gonzalez, R. (2007) *24th Houston Soc Eng Med Bio*, p 71.

A NON-LINEAR ANALYSIS OF KINEMATIC VARIABILITY DURING CYCLIC REACH-AND-POINT MOVEMENTS

David P. Heller [1] and Robert W. Gregory [2]

[1] University of Kansas, Lawrence, KS, USA
[2] United States Military Academy, West Point, NY, USA
E-mail: robert.gregory@usma.edu, Web: www.usma.edu/dpe/

INTRODUCTION

Human voluntary movements are highly variable. For example, the most reproducible feature of the trajectories of multi-joint reaching movements is the lack of reproducibility (Latash, 1988). Variability exists at multiple levels of movement organization and is a result of the degrees-of-freedom coordination problem formulated by Bernstein (Latash, 1988).

Variability during reaching movements has been examined to provide insight into movement planning, execution, and outcome. This variability has typically been quantified using traditional statistical methods (e.g., Abend et al.; 1982; Atkeson and Hollerbach, 1985). Unfortunately, traditional methods of statistical analysis can skew or even mask the degree of variability involved in skilled movements (Stergiou, 2004). Therefore, the use of non-linear analytical techniques to provide a more complete analysis of kinematic variability during reaching movements is necessary.

The purpose of this study was to use a non-linear approach to examine kinematic variability during reach-and-point movements. While Burdet et al. (2006) used non-linear tools to assess variability during discrete, two-dimensional reach-and-point movements, the present study was the first to analyze variability during cyclic, three-dimensional reach-and-point movements using a non-linear time series analysis.

METHODS

Twelve healthy, right-arm dominant individuals (6 males, 6 females) between 20-40 years of age participated in this study.

After undergoing informed consent procedures, participants were seated in front of a target grid oriented in the frontal plane. The center of the target grid was placed at 75% of maximum reach distance and aligned with the center of the shoulder joint for all individuals. The 3-cm diameter targets were positioned 25 cm apart to allow the subjects to perform point-to-point reaching movements with their dominant arm in two directions (horizontal and vertical) at two frequencies (1.0 and 2.0 Hz). A motion capture system (Visualeyez VZ3000, PhoeniX Technologies) was used to record the three-dimensional position of the fingertip for 30 movement cycles. The 4 conditions (2 directions × 2 frequencies) were presented in random order.

Kinematic variability was quantified by calculating the Lyapunov exponent (LyE) for consecutive trajectories in time-delay phase space. The LyE values were calculated using Chaos Data Analyzer software (Version 1.0, Physics Academic Software). A factorial ANOVA design was used to assess the effects of movement direction and movement frequency on kinematic variability for all three axes (medial-lateral [M-L], anterior-posterior [A-P], and superior-inferior [S-I]) of motion.

RESULTS AND DISCUSSION

A non-linear analysis of kinematic variability during cyclic reach-and-point movements yielded several key findings. First, the main effect of movement direction on LyE values was not significant ($F_{1,11}$ = 1.30, P=0.28); variability did not differ between the horizontal and vertical movement directions (see Table 1). This contrasts with the finding of increased variability during vertical movements using traditional linear methods (Abend et al., 1982; Atkeson and Hollerbach, 1985).

Second, the main effect of movement frequency on LyE values was significant ($F_{1,11}$ = 65.32, P<0.0001); variability was greater during the 2.0 Hz conditions than the 1.0 Hz conditions (see Table 1). This also contrasts with the finding of velocity profile invariance using traditional linear methods (Abend et al., 1982; Atkeson and Hollerbach, 1985).

Third, the main effect of movement axis on LyE values was significant ($F_{2,12}$ = 224.77, P<0.0001). The fingertip trajectories along the primary movement axis (M-L and S-I axes for the horizontal and vertical movement directions, respectively) exhibited less variability than the fingertip trajectories along the secondary movement axes (A-P/S-I and M-L/A-P axes for the horizontal and vertical movement directions, respectively).

SUMMARY

Kinematic variability during cyclic, three-dimensional reach-and-point movements was assessed using the LyE, which is a measure of local dynamic stability (Burdet et al., 2006). Since local dynamic stability is critical for successful movement execution and this information cannot be assessed through traditional linear methods for quantifying kinematic variability, the use of non-linear analysis is necessary to identify the true structure of variability during reaching movements. The results of this study provided a more complete analysis of kinematic variability during reaching movements than that obtained through the use of traditional linear methods. Future research will focus on the functional role of kinematic and kinetic variability and the characterization of mechanisms by which humans ensure local dynamic stability during cyclic movements.

REFERENCES

Abend, W. et al. (1982). *Brain*, **105**, 331-348.

Atkeson, C.G., Hollerbach, J.M. (1985). *J. Neuroscience*, **5**, 2318-2330.

Burdet, E. et al. (2006). *Biological Cybernetics*, **94**, 20-32.

Latash, M.L. (1998). *Neurophysiological Basis of Movement*. Human Kinetics.

Stergiou, N. (2004). *Innovative Analyses of Human Movement*. Human Kinetics.

Table 1: LyE values (mean ± SD) for consecutive trajectories in time-delay phase space along the M-L, A-P, and S-I axes of movement as a function of movement frequency and movement direction during cyclic reach-and-point movements.

Movement Frequency	Movement Direction	Movement Axis		
		M-L	A-P	S-I
1 Hz	Horizontal	0.066±0.021	0.238±0.081	0.203±0.072
	Vertical	0.231±0.035	0.223±0.037	0.079±0.011
2 Hz	Horizontal	0.141±0.031	0.293±0.095	0.276±0.068
	Vertical	0.315±0.023	0.308±0.037	0.128±0.013

ARCHITECTURE OF THE FIRST DORSAL INTEROSSEOUS MUSCLE

Benjamin W. Infantolino [1], Daniel J. Gales [1,2], and John H. Challis [1]

[1] Biomechanics Laboratory, Department of Kinesiology, The Pennsylvania State University, University Park, PA, USA
[2] Lock Haven University of Pennsylvania, Lock Haven, PA, USA
E-mail: bwi100@psu.edu

INTRODUCTION

The architectural characteristics of a muscle, such as muscle and tendon cross-sectional areas, indicate how the muscle may function in vivo. Muscle architecture has important implications for both clinical applications such as tendon transfers (e.g., Lieber, 1993), as well as accurate musculoskeletal models (e.g., Klein Horsman et al., 2007). The first dorsal interosseous muscle abducts the index finger and is of interest as it is the only muscle responsible for this action. The current data on this muscle is limited, for example Brand et al. (1981) only measured muscle fascicle length and muscle volume in 15 muscles. The purpose of this study was to quantify the architecture of the first dorsal interosseous; the resulting data will have implications clinically and for musculoskeletal models.

METHODS

The first dorsal interosseous muscle from each hand of 5 cadavers was dissected yielding 10 muscles (cadaver height: 171 cm ± 10). The mass of each muscle was determined upon removal; after dissection the mass of the tendons were determined. The overall muscle-tendon length (Lmt), tendon length (Lt), and muscle belly length (Lmb) were measured. The muscle has two heads, and the pennation angle was measured in each head (θ_1, θ_2). The muscle was carefully dissected to expose the internal portion of the tendon or aponeurosis, its length was then measured (Lti).

After these measures were taken two fascicles from each head of each muscle were removed and placed in a solution of 20% nitric acid to digest the connective tissue. Once the connective tissue was sufficiently removed a portion of a muscle fiber was dissected using a dissecting stereomicroscope and fine forceps. The fiber was placed on a slide and images of the fiber at 400x magnification were obtained. (figure 1) Scion Image (NIH Image, version Beta 4.0.2, National Institutes of Health, Bethesda, MD, USA) was used to count the number of sarcomeres along each fiber. Optimum fiber length (Lfopt) was then computed using the optimal sarcomere length from Walker and Schrodt (1974).

For each muscle the physiological cross-sectional area (PCSA), and the tendon cross sectional area (TCSA) were computed. The following ratios were computed to provide insight into the functional role of the muscle: PCSA/TCSA, and Lt/Lfopt.

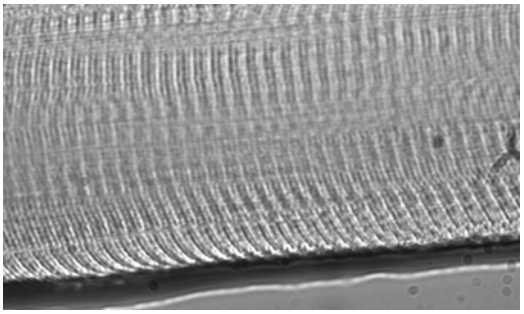

Figure 1: Muscle fiber at 1000x magnification.

RESULTS

The architectural parameters of 10 first dorsal interosseous muscles are presented in table 1.

Table 1: Means and standard deviations (SD) of the architectural parameters of ten first dorsal interosseous muscles.

Parameter	Average	SD
Lmt (mm)	67.3	16.9
Lt (mm, n = 6)	9.2	13.7
Lmb (mm)	58.1	8.2
θ_1 (degrees)	8.9	2.7
θ_2 (degrees)	6.9	3.1
Lti (mm)	28.4	3.1
Lfopt (mm, n = 9)	27.0	4.3
PCSA (mm^2)	1.74	0.59
TSCA (mm^2)	0.05	0.04

In addition to the above architectural parameters various ratios were calculated (table 2). For this analysis only five muscles were analyzed.

Table 2: The means and standard deviations (SD) of the ratios of muscle to tendon cross sectional area (PSCA/TCSA), and fiber optimum to tendon length (Lfopt/Lt).

Parameter	Average	SD
PCSA/TCSA	44.8	28.7
Lfopt/Lt	3.5	4.0

DISCUSSION

There was considerable variability for the lengths and sizes of the ten analyzed first dorsal interossi. The muscles only had small pennation angles, sufficiently small that the influence of muscle pennation can be ignored in models of this muscle (Otten, 1988). The current data adds to the existing data on the first dorsal interosseous and provides data that can be used in future models.

The data exhibits a large amount of variability, even when normalizing the data (ratios of PCSA/TCSA, and Lt/Lfopt). Such variability presents problems when using generic muscle models. Variability is known to exist in other aspects of the musculoskeletal system, for examples in the locations of muscular attachments (Duda et al., 1996), as well as for a specific muscle the portion of the force-length curve used in vivo by different subjects (Herzog et al., 1991). The variability in the data in the present study indicates that generic musculoskeletal models are not appropriate for subject specific interventions and research. More research in the area of muscle architecture is required to provide a better understanding of the architectural variability that exists, of the first dorsal interosseous and other muscles.

REFERENCES

Brand, P. W., et al. (1981). *J. Hand Surg.* **6**(3): 209-219.

Duda, G. N., et al. (1996). *J. Biomech.* **29**(9): 1185-1190.

Herzog, W., et al. (1991). *Med. Sci. Sports Exerc.* **23**(11): 1289-1296.

Klein Horsman, M. D., et al. (2007). *Clin. Biomech.* **22**: 239-247.

Lieber, R. L. (1993). *J. Hand Ther.* **6**(2): 105-113.

Otten, E. (1988). *Exerc Sport Sci Rev, 16*, 89-137.

Walker, S. M. and G. R. Schrodt (1974). *Anat. Rec.* **178**(1): 63-81.

SIMULATION INSIGHTS INTO EXPERIMENTAL TECHNIQUES FOR ESTIMATING WALKING STABILITY

James A. Norris, Anthony P. Marsh, and Kevin P. Granata

School of Biomedical Engineering & Sciences, Wake Forest University – Virginia Tech
E-mail: granata@vt.edu, Web: www.biomechanics.esm.vt.edu

INTRODUCTION

To understand stability of walking, researchers have recently applied techniques for quantifying stability of dynamic systems (Dingwell and Marin, 2006; England and Granata, 2007; Hurmuzlu and Basdogan, 1994). These techniques originated from analytical derivations where the governing dynamic equations are known and the system evolves absent from disturbances.

For human walking, however, the governing dynamic equations are not known. Furthermore, as we walk we are constantly subjected to small disturbances, or experimental noise. Thus, we assume that we are experimentally measuring data that may be used to accurately reconstruct the dynamics of walking and that noise will not overshadow the ability to quantify the stability of the underlying dynamic system.

The objective of this work was to determine if measures of walking stability based on dynamic systems theory differentiate between a passive and an active forward dynamic model of biped walking in the presence of noise. We hypothesized that the active model would exhibit greater stability in the presence of noise.

METHODS

Passive model. The passive model explored in this paper is the familiar 2D compass biped with point feet (Garcia *et al.*, 1998). It consists of two mass-less legs connected at the hip, a mass at the hip and at each foot. This model passively "walks" down a sloped surface driven by gravity. Walking includes a swing-phase, where the stance foot behaves like a pin joint, and an instantaneous double-stance phase when the swing foot strikes the ground. Swing-phase is governed by four first-order equations, $\dot{\mathbf{s}} = \mathbf{F}(\mathbf{s})$, where $\mathbf{s}$ includes angles and velocities of the swing and stance legs. At foot-strike, an inelastic collision brings the swing foot to rest, and the state after foot-strike is calculated from angular momentum conservation $\mathbf{s}^+ = \mathbf{H}(\mathbf{s}^-)$.

Active model. The active model is identical to the passive model, but with the ability to generate stance ankle and hip torques. These torques are a nonlinear function of the state, $\mathbf{Q}(\mathbf{s})$. Thus, the swing-phase equations remain autonomous and may be expressed as $\dot{\mathbf{s}} = \mathbf{F}(\mathbf{s}) + \mathbf{Q}(\mathbf{s})$. The function $\mathbf{Q}(\mathbf{s})$ was specified such that the passive walking cycle, $\mathbf{s}_{eq,}$ remains unaffected by $\mathbf{Q}(\mathbf{s})$, i.e. $\mathbf{Q}(\mathbf{s}) = \mathbf{0} \; \forall \; \mathbf{s}_{eq}$, and if $\mathbf{s}$ is disturbed from $\mathbf{s}_{eq}$ it is attracted back to $\mathbf{s}_{eq}$. Thus, the active model is inherently more stable than the passive model.

Analytical stability. Local and orbital stability were calculated from the governing dynamic equations. Local stability was quantified by the full Lyapunov exponent spectrum (Wolf *et al.*, 1985). Orbital stability was quantified by Floquet multipliers (Hurmuzlu and Basdogan, 1994).

Noise. Each walker took 600 steps over the same 5 "bumpy" downhill slopes, which enforced they matched step heights. The nominal downhill slope was 0.01 radians

and the bumps were uniformly distributed random heights **U**([–0.0001,+0.0001]) expressed as a fraction of leg length, *L*.

Stability in the presence of noise. The time dependent state vectors for 600 continuous steps were analyzed by calculating the maximum Lyapunov exponent and Floquet multipliers that have been used for experimental analysis of walking stability.

RESULTS AND DISCUSSION

Analytical stability. A system is only as stable as its least stable dimension. Thus, analytical stability measures in Table 1 are organized from least to greatest stability. The active model exhibited greater local and orbital stability as confirmed by a more negative maximum Lyapunov exponent and Floquet multipliers with smaller magnitudes.

Table 1: Analytical stability calculations.

	Passive	Active
Lyapunov exponents	-0.13 -0.44	-0.21 -0.34
Magnitude of Floquet multipliers	0.61 0.18	0.19 0.15

Stability in the presence of noise. Average divergence of initially close points in the state-space, **s**, is shown in Figure 1. The maximum Lyapunov exponents were positive for both models, indicating local instability (Table 1). The active model was more stable as indicated by a significantly smaller maximum Lyapunov exponent and smaller Floquet multipliers.

Table 2: Stability in the presence of noise, mean ± sd for the 5 bumpy surfaces.

	Passive	Active
Max Lyapunov exponent (1e-5)	143.3±5.4	7.3±0.4
Magnitude of Floquet multipliers	0.73±0.02 0.73±0.02 0.67±0.04 0.42±0.04	0.64±0.03 0.64±0.03 0.62±0.04 0.04±0.01

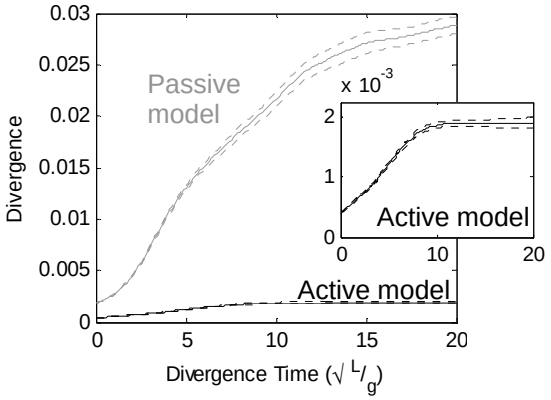

Figure 1: Divergence of initially close trajectories. Dotted lines show ± sd for the 5 bumpy surfaces. A typical step was 3.9 $\sqrt{L/g}$.

CONCLUSIONS

Although the stability measures calculated after the model walked over a noisy surface did not agree with the stability calculated from the undisturbed dynamic equations, they did correctly identify that the active model was more stable; confirming our hypothesis. Ultimately, we are interested in understanding stability of the underlying dynamic control system. Combined modeling and experimental approaches will be essential in identifying stability of the control system from experimental measures.

REFERENCES

Dingwell,J.B., Marin,L.C. (2006). *Journal of Biomechanics,* **39**(3), 444-452.

England,S.A., Granata,K.P. (2007). *Gait Posture,* **25**(2), 172-178.

Garcia,M. et al. (1998). *J.Biomech.Eng,* **120**(2), 281-288.

Hurmuzlu,Y., Basdogan,C. (1994). *J Biomech.Eng,* **116**(1), 30-36.

Wolf,A. et al. (1985). *Physica D: Nonlinear Phenomena,* **16**(3), 285-317.

ACKNOWLEDGEMENTS

This work was supported by the Wake Forest University Claude D. Pepper Older Americans Independence Center (P30-AG21332).

Mechanics and energetics of level walking with powered ankle exoskeletons

Gregory S. Sawicki[1] and Daniel P. Ferris[1]

[1]Human Neuromechanics Laboratory, University of Michigan, Ann Arbor, MI, USA
E-mail: gsawicki@umich.edu

INTRODUCTION

Humans can rapidly learn to walk with a unilateral powered ankle exoskeleton controlled by their own muscle activity (Gordon et al., 2007). Over two thirty-minute practice sessions, individuals alter their soleus muscle activation to command distinct bursts of exoskeleton power during the push-off phase of walking. Substituting biological muscle work with artificial muscle work could reduce energy expenditure during gait. The goal of this study was to determine how much a robotic ankle exoskeleton could reduce the metabolic cost of walking. Muscles produce positive mechanical work with an efficiency of ~25% (Hill, 1938). Therefore, we hypothesized that for every 1 Joule of positive exoskeleton work, the user should save 4 Joules of metabolic energy.

METHODS

Nine healthy subjects walked on a treadmill at 1.25 m/s with bilateral powered ankle exoskeletons under proportional myoelectric control (**Fig. 1**). During three practice sessions, subjects walked with exoskeletons unpowered for 10 minutes, powered for 30 minutes and unpowered for 15 minutes. We recorded (1) O_2 and CO_2 flow with a metabolic cart (2) artificial muscle forces from series load transducers (3) joint kinematics using reflective markers and (4) electromyography (EMG) from surface electrodes at the beginning and end of each session.

To establish baseline joint mechanics, we collected five overground walking trials at 1.25 m/s with exoskeletons unpowered. We used inverse dynamics to calculate the average ankle, knee and hip joint powers over a stride. To quantify exoskeleton mechanical assistance, we used artificial muscle forces and moment arm lengths, along with ankle joint angular velocity, to compute the average mechanical power delivered by exoskeletons over a stride. To assess energy expenditure, we converted gas flow rates using the Brockway equation and subtracted the energy required for quiet standing to calculate net metabolic power. To quantify muscle activity, we rectified and high pass filtered (4th Order Butterworth, f_c=20Hz) EMG data and computed the root mean square (RMS) average over the stride. All EMG was normalized to unpowered walking data.

We used a repeated measures ANOVA to determine if there were differences in net metabolic power and soleus RMS EMG between unpowered and powered walking conditions.

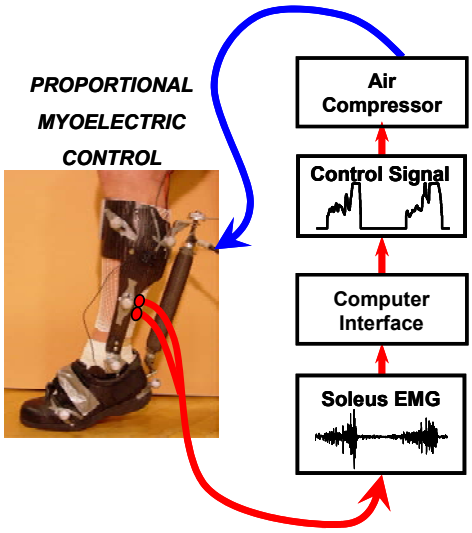

Figure 1. Artificial muscle drives ankle extension using a command from subjects' own soleus EMG

RESULTS AND DISCUSSION

Initially subjects walked with increased ankle plantar flexion, but kinematics returned close to normal with practice (**Fig. 2A**). Soleus EMG was 24% lower in the powered condition (ANOVA, $p < 0.001$) (**Fig. 2B**). Exoskeleton average mechanical power was 0.23 ± 0.02 W/kg (mean ± s.e.); 65% of ankle positive work and 22% of summed joint positive work **(Fig. 2C).** Net metabolic power was significantly lower (-13%) with exoskeletons powered (2.91 ± 0.13W/kg) versus unpowered (3.36 ± 0.13W/kg) ($p < 0.001$) (**Fig. 2D**).

Reductions in net metabolic power (13%) were not proportional to decreases in summed joint mechanical power (22%) from powered ankle assistance. Furthermore, for every 1 Joule of exoskeleton work, the user saved only 1.9 Joules of metabolic energy.

CONCLUSIONS

These results suggest that the ankle plantar flexors perform mechanical work during walking with remarkably high efficiency (~51%). Achilles tendon elastic energy storage and return likely contributes to the high apparent efficiency (Ishikawa, 2005). Our findings will be useful in designing powered ankle orthoses and prostheses for improving mobility and reducing metabolic cost in both healthy and patient populations.

REFERENCES

Gordon, K.E., Ferris, D.P. (2007). *J Biomech,* In Press.

Hill, A.V. (1938). *Proc Royal Soc Bio Sci,* B126:136-195.

Ishikawa, M., Komi, P.V. (2005). *J Appl Physiol,* 99:603-608.

ACKNOWLEDGEMENTS

Supported by NSF BES-0347479 to *DPF*.

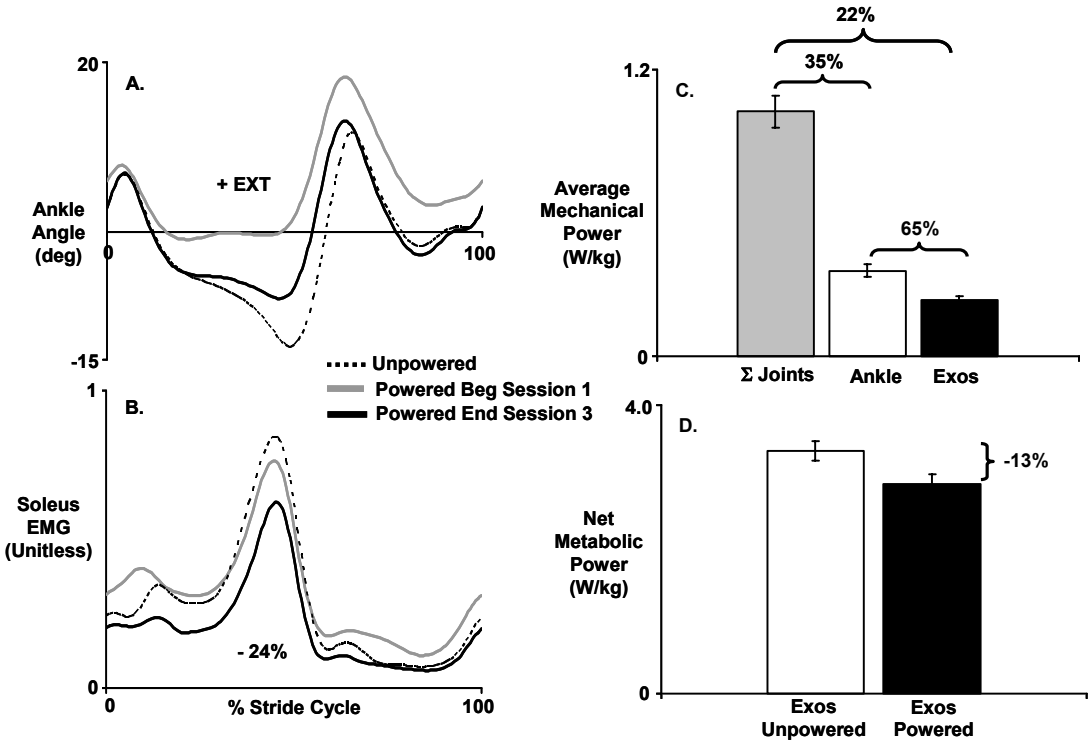

Figure 2. (A) Stride cycle average (heel strike to heel strike) ankle kinematics and (B) normalized linear enveloped (low pass=6Hz, high pass=20Hz) soleus EMG over the practice sessions. Soleus RMS was 24% lower in the powered condition by the end of session 3. (C) Stride average positive mechanical power for ankle joint (white) and ankle+knee+hip joints (gray) during unpowered walking and exoskeletons (black) during powered walking. Brackets indicate right bar as % of left bar. (D) Average net metabolic power for unpowered walking (white) and powered walking (black) during last 3 minutes of practice session 3. Bracket shows % difference. All power values are normalized to subjects' body mass and are mean ± s.e. for 9 subjects.

Presentation of target torque level and error information enhance maximal voluntary elbow flexion torque

[1]Makoto Fukuda, [1]Yohei Takai, [2]Yasuo Kawakami and [2]Tetsuo Fukunaga

[1] Graduate School of Sports Sciences, Waseda University, Saitama, Japan
[2] Faculty of Sport Sciences, Waseda University, Saitama, Japan
E-mail: makoto.fukuda@moegi.waseda.jp, Web: http://www.f.waseda.jp/fukunaga/

Introduction

Maximal voluntary contraction (MVC) is influenced not only by structural factors such as the cross-sectional area and fiber types of muscle but also by functional factors such as brain activation (Ikai & Steinhaus, 1961). MVC force exerted with the performer's shout exceeds that without shout, which suggests the possibility of controlling psychological suppression that limits muscle force (Ikai & Ishii, 1961). It has also been shown that subjects improve their performance and brain activation with a feedback of the error from the target task (Kawashima et al, 2000). The maximal long jump distance is enhanced when the goal is visually presented to the subject (Sadamoto & Ohtsuki, 1977). We hypothesized that visual feedback of exerted torque with the error information (VFB) increases brain activation and muscle force. We tested this hypothesis by investigating the relationship between neural activity and MVC enhancement with VFB.

Methods

Thirteen male and two female subjects (23.9±1.8yrs 162.7±24.9cm , 68.5±32.1kg, mean ± SD) volunteered to participate in this study. The subject was seated on a chair with their dominant forearm in neutral position and their wrist fixed onto a custom-built device (Static Torque Model Vte-002R, Vine, Japan). The maximal voluntary isometric elbow flexion torque (MVT) was measured with the elbow flexed at 90°. A value of 110% MVT was calculated and shown on an oscilloscope as a target that was visually fed back to the subject. The subject was instructed to exceed the target value by using torque feedback. For non-visual feedback condition (nVFB), the subjects performed the same MVT task without VFB. Surface electromyographic signals (EMG) were recorded from the biceps brachii (BB) and brachioradialis (BR) muscles.

Results

Figure 1 shows MVT of the subjects with and without VFB. Thirteen out of 15 subjects increased MVT by VFB. Both the peak and mean torque for 5seconds were significantly higher for VFB ($p<0.05$). The mean EMG amplitude of BB and BR during VFB condition was significantly higher than those in nVFB. Figure 2 shows the relationship between MVT and EMG amplitude of BB in VFB. The EMG amplitude of BB was correlated positively with MVT ($p<0.05$).

Discussion

Our results suggest that VFB condition enhanced the subject's brain activation. It is possible that the brain activation is enhanced due to increasing motivation (Ikai & Steinhaus, 1961). Since the EMG signal is the final form of motor command, it is suggested that increasing MVT with VFB is due to the increased motor command to BB. It has been suggested that the right prefrontal cortex is related to the motivation in depressed

patients (Elliot et al, 1997). Activation of the primary motor area that controls muscle activity is correlated with muscle force (Thickbloom et al, 1998). Based on these findings, it is suggested that the VFB condition increased activation of the right prefrontal cortex that augmented activation of the primary motor area for BB.

References

Elliot, R. et al. (1997). Psychological Medicine. 27: 931-942.

Ikai, M. and A.H. Steinhaus. (1961). J. Apply. Physiol. 16: 157-169.

Ikai, M. and Ishii, K. (1961) Japan J. Phys. Educ. Hlth. Sport Sci. 5: 154-165.

Kawashima, R. et al. (2000). Neuroimage 12: 698-706.

Sadamoto, T. and Ohtsuki, T. (1977). Japan J. Phys. Educ. Hlth. Sport Sci. 22: 215-229.

Thickbroom, G.W. et al. (1998). Exp Brain Res. Jul; 121(1):59-64.

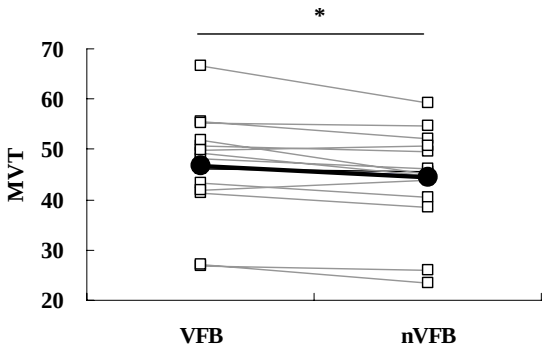

Figure 1: Mean maximal voluntary elbow flexion torque (MVT) of all subjects in VFB (left) and nVFB (right). MVT in VFB was significantly higher than nVFB ($p<0.05$).

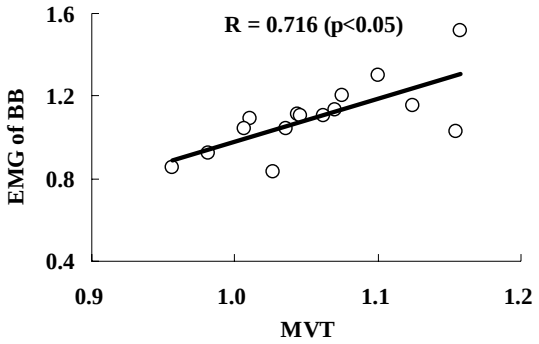

Figure 2: The relationship between relative MVT and EMG activity. The MVT and EMG amplitude in VFB condition was normalized to those in nVFB.

PROCESSING EFFECTS ON JOINT MOMENTS DURING IMPACT LANDINGS

Scott C. White & Jeffery T. Podraza

Dept. of Exercise & Nutrition Sciences, School of Public Health & Health Professions
University at Buffalo, Buffalo, NY
Email: swhite@buffalo.edu

INTRODUCTION:

Joint loads calculated from rigid body, inverse dynamic models provide unrealistic estimates of active moments generated by muscles during impact (Gruber et al, 1998). The moments oscillate (McNitt-Gray, 1993) and the magnitudes may be overestimated (Gruber et al, 1998). Recent evidence suggests that errors are introduced when segment position data and ground reaction forces (GRFs) are processed differently (Bisseling & Hof, 2006). Filtering segment position at lower cut-offs than the GRF data attenuates equalizing segment acceleration moments in the inverse dynamic equations. A cut-off frequency of 20 Hz for both has been recommended when assessing knee moments during impact (Bisseling & Hof, 2006). Given the interest in joint loads during impact, selecting appropriate filter cut-offs is important. We propose that filter selections should be based on a frequency analysis of the GRFs. This study presents information on predominate frequencies for different impact-like scenarios and shows how three different processing methods change the calculated joint moments.

METHODS:

Six subjects performed five impact-like movements typically reported in the literature. Three involved an acceleration over a 1.5 meter distance to a sudden stop (L1), a plant and push off to the left (L2) and a plant and cross over to the right (L3). In each case GRFs were measured for the right foot landing. The fourth movement was a drop landing from a 20 cm height (L4) and the fifth involved stepping down and out from a 10 cm height to land in single leg support (L5) Vertical and shear forces were measured (Kistler force plate) and digitally sampled at 2400 Hz. The frequency content for GRFs during landing were determined (~1.0 Hz resolution) using a Fast Fourier Transform sampled to the nearest power augmented with zero endpoint padding. The 98^{th} percentile frequencies for the GRFs were determined from the cumulative sum of the integrated power-frequency spectrum.

Joint moments were calculated for L5 with each subject modeled as a two dimensional, sagittal plane, three segment, rigid body. Segment position coordinates were digitized (60 Hz) from video. In the first method (SM), joint moments were calculated using inverse dynamics (Winter, 1990) with unfiltered GRFs and filtered position data at cut-offs based on Jackson's method (Jackson, 1979). In the second technique (RM), moments were calculated after filtering the position and the force plate data based on the 98^{th} percentile of GRFs. In the third approach (AM), moments were filtered (98^{th} percentile) after they had been calculated with no filtering of the position and the force plate data. A zero-lag, fourth order, Butterworth filter was used for each.

RESULTS AND DISCUSSION:

The 98^{th} percentile frequency was highly variable both within and between subjects

for the five impact-like movements (Table 1). A common 20 Hz filter cut-off for forces and position data would not be suitable for all impact-type movements. Filtering data is always a compromise between removing noise and signal; therefore, it is recommended that filter cut-offs be selected based on an objective criterion such as frequency analyses of GRFs.

Knee and hip moments calculated with the standard processing method (SM) were greater than those calculated by the RM or AM methods; they also peaked early after impact (0.517 s; Fy = 22 N) and oscillated at the knee (Fig. 1) and at the hip. In agreement with others, filtering GRFs and marker coordinates with a common filter cut-off reduces "artifacts" when calculating net joint moments during impact (Bisseling & Hof, 2006). Gruber et al (1998) attributed these moment "errors" to rigid body assumptions and proposed wobbling-mass models to account for soft tissue effects. Magnitude and timing errors can be attributed to inconsistencies in data processing; therefore, the relevance of soft tissue motion on joint kinetics should be revisited.

Much of the literature has used SM processing approaches to calculate and compare lower limb joint kinetics (McNitt-Gray, 1993; Cowling & Steele, 2001). The magnitude and timing of joint moments may have been affected by inconsistent processing of input data. Future analyses of impact-like activities need to consider these effects on joint moment values.

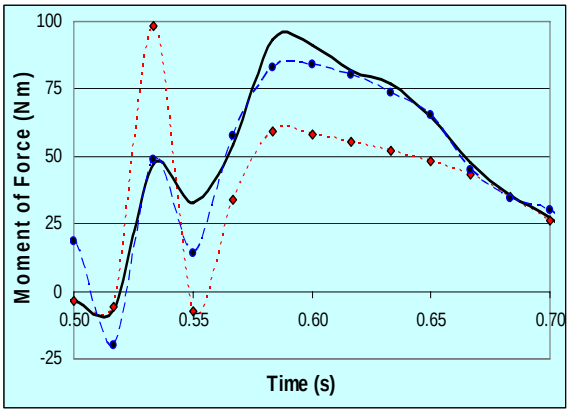

Fig. 1: Knee moment calculate with AM (solid black) SM (dashed-diamond red), RM (dashed-circle blue).

REFERENCES:

Bisseling, R & Hof, A. (2006) *J Biomechanics* **39**,2438-2444.

Gruber, K et al. (1998) *J Biomechanics* **31**,439-444.

Jackson, K. (1979) *IEEE Trans Biomed Eng* **BME-26**,122-124.

McNitt-Gray, J. (1993) *J Biomechanics* **26**, 1037-1046.

Cowling E & Steele, J. (2001) *Electromyogr Kinesiol* **11**,263-268.

Winter, DA. (1990) *Biomechanics and Motor Control of Human Movement* 2nd ed. John Wiley & Sons, Inc.

Table 1: 98th percentile frequency (Hz).

Landing	Fx	Fy	Fz	Fx, Fy Range
L1	26 (19)	17 (12)	39 (7)	7 – 50
L2	18 (8)	10 (6)	10 (8)	2 – 28
L3	23 (15)	8 (6)	7 (4)	2 – 39
L4	27 (9)	11 (3)	39 (16)	9 – 59
L5	19 (9)	12 (7)	24 (11)	8 – 38

Notes: L1 to L5 = different impact-like landings. Fy = vertical, Fx = anterior-posterior, Fz = medial-lateral. "( )" = standard deviation.

INTERLIMB COMPARISON OF COMPENSATION STRATEGIES FOR GLOBAL KINEMATIC VARIABLES IN TWO-LEGGED HUMAN HOPPING

Arick Auyang[1], Young-Hui Chang[1]
[1]Comparative Neuromechanics Lab, School of Applied Physiology, GeorgiaTech, Atlanta, GA, USA
Email: arick.auyang@gmail.com Web: www.ap.gatech.edu/chang/cnlyhchang.html

INTRODUCTION

Recent research has shown evidence for asymmetric control strategies between dominant and non-dominant arm during dynamic upper extremity tasks (1, 2). Considering the symmetrical gait patterns observed in the legs during locomotion, little has been done to investigate the symmetry of control strategies in lower extremity tasks. Human hopping in place is a bilaterally symmetrical task in which both legs must perform similarly. It is also a form of locomotion that has been extensively studied (3). Furthermore, the dynamics of human hopping can be simplified but accurately described using a low degree of freedom spring-mass system which has clearly identifiable global kinematic control variables such as leg length and leg orientation (4, 5). The Uncontrolled Manifold (UCM) concept is a hypothesis that the neuromechnical system exploits neuromuscular redundancy by allowing noise to control specific local variables within a null space that stabilizes a specific global variable (6). Our objective is to determine whether global compensation strategies such as leg length and leg orientation are symmetrical between the two legs during human hopping in place. We hypothesized that 1) leg length would be symmetrically controlled throughout the entire hopping cycle and 2) leg orientation would also be symmetrically controlled throughout the entire hopping cycle.

METHODS

Subjects hopped on two legs at frequencies of: 2.2, 2.8, and 3.2Hz. Three trials for each condition were collected in a randomized order for 30 seconds each. Hops with joint angle trajectories outside 1 standard deviation were discarded.

Sagittal plane joint kinematics data (120Hz) were collected on healthy, right leg dominant subjects (N = 7, ages 21-30) using a six-camera Vicon system. Leg length and orientation were calculated as a function of four segment angles (foot, shank, thigh, and pelvis.

Each hypothesis was tested with a corresponding Jacobian matrix that related small changes in the local joint angles to small changes in the global control variable being tested with the UCM analysis (for review of UCM analysis see ref. 6).

The variance of the local joint kinematics that was located within the null space (the UCM) tended to stabilize the global variable (e.g., leg length or leg orientation) and is referred to as the Goal-Equivalent Variance (GEV). The local variance that lay outside of the UCM is referred to as Non-Goal-Equivalent Variance (NGEV). A **UCM RATIO** (**GEV:NGEV)** was also calculated for each subject at every 1% of the hopping cycle and averaged across all subjects **(Figure 1)**. If **UCM RATIO** > 1, i.e. **GEV** > **NGEV**, we considered the global control variable to be **CONTROLLED** by a non-random structuring of the local joint variance.

RESULTS AND DISCUSSION

We did observe no asymmetries for leg-length control throughout the hopping cycle and across the different frequencies. However, we found that leg-length was

controlled only minimally throughout the contact phase with increased control during the aerial phase (Figure 1).

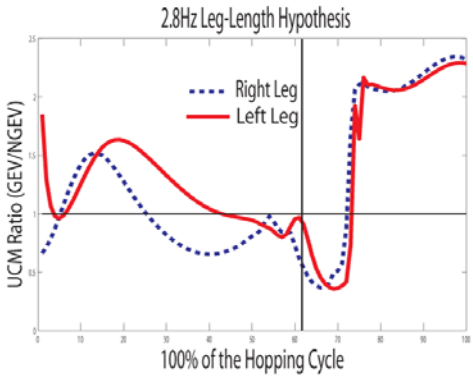

Figure 1 UCM ratio (GEV:NGEV) of leg-length during 100% of the hopping cycle starting with foot contact (contact and aerial phases separated by vertical line). Horizontal line indicates UCM Ratio=1. Representative data are from one subject.

Leg orientation was controlled throughout the entire hopping cycle. Surprisingly, leg orientation appeared to be asymmetrical controlled during the contact phase, but not during the aerial phase (Figure 2).

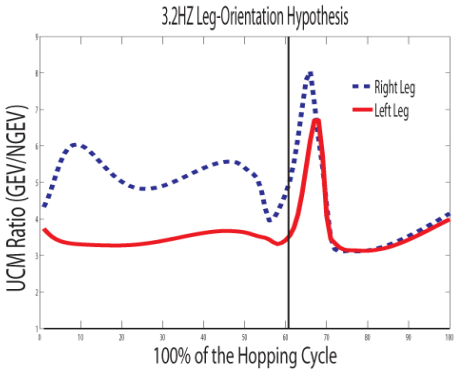

Figure 2 UCM ratio (GEV:NGEV) of leg orientation during 100% of the hopping cycle starting with foot contact (contact and aerial phases separated by vertical line). Vertical scale begins with UCM Ratio=1 since leg orientation was always controlled. Representative data are from one subject.

SUMMARY

Reminiscent of upper extremity tasks, we observed some differences in control strategies between the dominant and non-dominant limb during a locomotor task. Although this may be intuitive for arm control where use is heavily dependent on dominance, this is particularly surprising for leg control for human locomotion where stereotyped movements are achieved with bilaterally symmetrical performance.

The duration of leg orientation control throughout the entire hopping cycle is consistent with our previous results from one-legged hopping (7). Similarly, the duration of of leg-length control in the contact is also consistent with our previous findings (7).

During the aerial phase, joints were close to full extension, mechanically constraining the local and global variability, thus potentially structuring the variance passively into a "controlled" state for both global variables.

This study provides interesting insight on the influence of limb dominance on limb control and compensation strategies during bilaterally symmetric lower extremity tasks such as locomotion.

REFERENCES

1. Sainburg, Kalakanis (2000). *J. Neurophysiol.* **83**, 2661-2675.
2. Sainburg (2002). *Exp Brain Res*. **142**, 241-258.
3. Farley et al. (1991). *J. Appl Physiol.* **71,** 2127-32.
4. McMahon, T.A., Cheng, G.C. (1990). *J. Biomech.* **23 Suppl 1**, 65-78.
5. Blickhan, R. (1989). *J. Biomech.* **22**, 1217-27.
6. Scholz, J.P. and G. Schöner. *(1999). Exp Brain Res.*. **126**(3): p. 289-306.
7. Auyang, A.G. and Y.-H. Chang. (2006). Proc. Soc. Neurosci. Atlanta, GA.

BIOMECHANICS OF ADJACENT SEGMENTS WITH NUMBER OF INTER-BODY BONE GRAFTS AND SPINAL INTRUMENTATIONS FOR A MULTI-LEVEL FUSION CONSTRUCT USING A FINITE ELEMENT MODEL

Mozammil Hussain [1], Ahmad N. Nassr [3], Raghu N. Natarajan [1,2], Gunnar B.J. Andersson [1], Howard S. An [1]

[1] Rush University Medical Center, Chicago, IL, USA
[2] University of Illinois at Chicago, Chicago, IL, USA
[3] University of Pittsburgh, Pittsburgh, PA, USA
E-mail: hussmoz@iit.edu

INTRODUCTION

Cervical fusion is a traditional procedure for the treatment of single- and multi-level spondylotic myleopathy or radiculopathy. The stand-alone graft has been shown to be less effective in providing the stability to construct especially with multi-level decompression. Additional stabilization of stand-alone grafting with anterior instrumentation (plate and screws), posterior instrumentation (rods and screws) or a combination of anterior and posterior instrumentation helps in achieving better fusion rates and reduces the possibility of graft dislodgement or subsidence. With the addition of spinal instrumentation and increase in the stiffness of the construct level, the adjacent levels are subjected to increased motion. In spite of previous *in vivo* and *in vitro* studies, the biomechanics of degeneration of adjacent segments after a multi-level fusion procedure is poorly understood. To date, no study exists in the literature showing the influence of number of inter-body grafts and instrumentations used for multi-level cervical decompression on the biomechanics of adjacent segments.

The objective of the present study was to compare the biomechanical response of the levels adjacent to the multi-level fusion construct by varying the number of inter-body grafts (corpectomy and/or discectomy) and spinal instrumentations (anterior and/or posterior). The rotational motion, stresses in the disc, and loads on the articulating facets of the adjacent levels were studied.

METHODS

A three-dimensional finite element (FE) model of a C3-T1 segment of the cervical spine was developed from the CT scan of a 38-year old normal female subject. The intact model was previously validated with the published specimen studies. Five surgical fusion models from C4 to C7 were developed from the intact model – discectomy with anterior fixation, corpectomy-discectomy with anterior fixation, corpectomy with anterior fixation, corpectomy with posterior fixation and corpectomy with anterior-posterior fixation. The discectomy fusion was performed with three inter-body grafts placed at C4-C5, C5-C6 and C6-C7 levels. The corpectomy fusion was performed with a single strut graft placed in between C4 and C7. The corpectomy-discectomy fusion was built with two grafts (C4-C6 corpectomy and C6-C7 discectomy). The grafts were centrally placed covering up-to 50% endplate area. The anterior fixation was created by using an anterior plate with rigid screw trajectory from C4 to C7. Two uni-cortical screws each at the cephalad and caudal ends of the anterior plate were placed parallel to the endplates. The posterior fixation was built by using a vertical rod with rigid screw

trajectory from C4 to C7. Two uni-cortical screws at each segment were placed in the posterior lateral mass. The anterior-posterior fixation was built by using an anterior screw-plate together with the posterior screw-rod system. The anterior and lateral mass screws of 16 mm long with an outer and inner diameter were 3.5 and 2.5 mm were used. The material properties of the spinal structures and instrumentations were adopted from the literature. The physiologic rotations based on literature data were prescribed on the C3 vertebra (flexion=45°, extension=35°, axial rotation=20°, lateral bending=25°). The inferior surface of the T1 vertebra was fixed. A constant pre-load of 73.6 N was applied using two isotropic truss elements connecting each of the lateral edges of the vertebral bodies to mimic the follower load technique. The analysis was performed using the commercially available FE code, ADINA.

RESULTS AND DISCUSSION

The results of the present study showed an increased motion of the adjacent levels with surgical interventions as compared to the intact case (Figure 1). Also, the stresses in the discs and loads on the facets of the levels adjacent to the fusion construct were higher than the intact values.

By decreasing the number of inter-body grafts for multi-level fusion (discectomy to corpectomy-discectomy to corpectomy) and increasing the number of spinal instrumentations (anterior to posterior to anterior-posterior) for stabilizing the construct, an increased motion was observed at the adjacent segments (Figure 1). Previous studies have reported a similar increase in the motion at levels adjacent to fusion construct. The same trend was seen with the stresses in the discs and loads on the facets of the adjacent non-operated levels. Lee *et al*[1] and Yang *et al*[2] observed increased stresses in the discs and facet loads at the levels adjacent to the fusion level when the posterior instrumentation was used as compared to the anterior fixation.

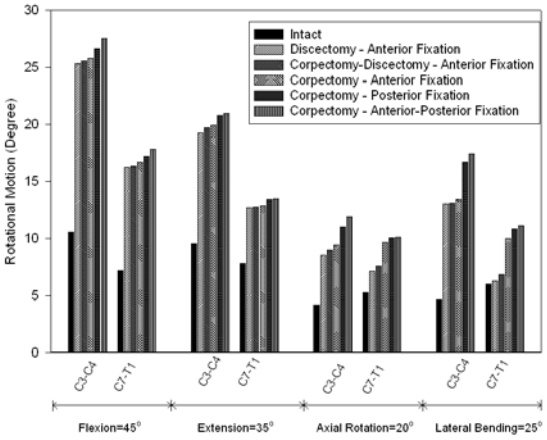

Figure 1: Rotational motion of adjacent segments with various fusion procedures added with different fixation techniques

SUMMARY

The levels adjacent to the multi-level fusion construct were affected by the number of inter-body grafts and the type of fixation technique used. The results of this study should help surgeons to appropriately choose the fusion procedure and the type of fixation to avoid the degeneration of adjacent segments and at the same time, to achieve a better fusion at the construct level.

REFERENCES

Lee, C.K., Langrana, N.A. (1984). *Spine*, **9**, 574-581.

Yang, S.W., Langrana, N.A. et al. (1986). *Spine*, **11,** 937-941.

ACKNOWLEDGEMENTS

This study was supported by the Department of Orthopedic Surgery, Rush University Medical Center, Chicago, Illinois.

EXPLORING THE IMPULSE RESPONSE OF THE POSTURAL CONTROL SYSTEM

Pilwon Hur, Brett A. Duiser, Elizabeth T. Hsiao-Wecksler

University of Illinois at Urbana-Champaign, Urbana, IL, USA
Email: ethw@uiuc.edu Web: mechse.uiuc.edu/research/ethw

INTRODUCTIONS

Investigating how individuals respond to disturbances to balance is essential to improving our understanding of the etiology of falls. We were particularly interested in the response of the postural control system after a transient perturbation. Previous studies of dynamic postural control have focused mainly on using persistent perturbations, such as continuous translations or rotations of a moving platform (e.g., Ishida, 1997). However, real-life loss of balance is sudden, such as a slip while walking or a bump while standing on a bus. Therefore, it is important to understand how balance and postural control mechanisms are utilized in response to unexpected and transitory disturbances. While impulse response and its associated characteristics are rudimentary concepts in engineering control theory, these issues have not been explored from a rigorous controls perspective in the postural control literature. In this investigation, the impulse loading and impulse response control-theory paradigm were used to examine the postural response to a mild, quick-release tug at the pelvis.

METHOD

Subjects

Thirty healthy adult subjects divided into three age groups (n=10 per group) were each tested during a single session. Age groups were young adults (20-30 years, YA), middle-aged adults (42-53 years, MA), and older adults (71-79 years, OA).

Experimental Protocol

Twenty randomized trials were conducted: 10 quiet standing trials and 10 perturbed trials, all 30s in duration. The subject was instructed to maintain a quiet, upright posture throughout the recording. The subject stood on a force plate (AMTI, BP600900) with arms crossed at the chest and eyes open (Fig. 1). During perturbed trials, the weight was released, causing a brief mild tug. During quiet-stance trials, no action was taken. Anterior-posterior (AP) ground reaction forces and center of pressure (COP) data were recorded. Tug force was recorded with a load cell (PCB Piezotronics, 208C02). Data were sampled at 1000 Hz.

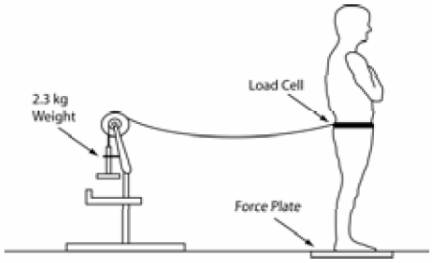

Fig. 1. Experimental setup.

Data Processing

From the perturbed trials, descriptive parameters of the AP COP, such as the maximum posterior displacement (*MaxDisp*), max displacement normalized by body weight, tug force and tug height (*NormMaxDisp*), difference between max and min displacements (*Range*), and time from peak tug force to MaxDisp (*Latency*) were calculated.

To further examine the postural control system impulse response, spectral analysis system identification (Peterka, 2002) was used to develop a model of the perturbed postural control system as a single-link inverted pendulum modulated by active and passive torques generated by a time-delayed proportional-derivative controller and a spring-damper compensator at the ankle (Fig. 2).

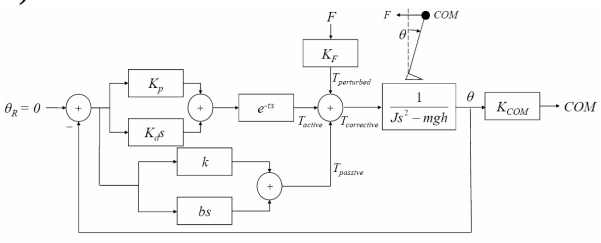

Fig. 2. Block diagram of control system

To compute the pendulum lean angle (*q*), the horizontal displacement of the center of mass (COM) was derived from AP force and COP data using a modified gravity-line projection method (Zatsiorsky, 2000). A constrained nonlinear optimization algorithm was used to identify model parameters which best fit the experimental data.

We quantified the robustness of each age group by examining the maximum of the sensitivity function (*MaxSens*) of the modeled systems. The sensitivity function describes how sensitive a system is to small perturbations in the system; larger values indicate reduced robustness or decreased relative stability of the system.

RESULTS AND DISCUSSION

Parameter	YA	MA	OA	p-val
Peak Force (lb)	6.54 (0.48)	6.75 (0.70)	6.40 (1.29)	0.68
MaxDisp (mm)	20 (8)	18 (5)	23 (6)	0.22
NormMaxDisp	0.28 (0.09)	0.27 (0.07)	0.35 (0.08)	0.08
Range (mm)	29 (7)	26 (4)	32 (9)	0.19
Latency (ms)	183 (35)	157 (34)	157 (22)	0.11
MaxSens (dB)	9.31 (1.49)	8.66 (1.63)	10.9 (1.94)	0.02

Table 1. Average (standard deviation) descriptive and spectral analysis parameters for each age group.

No significant differences were found between the age groups for any of the descriptive response parameters (Table 1, ANOVA). However, significant age-related differences were found for *MaxSens*. OA were found to have significantly larger *MaxSens* values than both YA and MA (Tukey HSD post hoc test). This result suggests that while conventional descriptive parameters may not be able to detect age-related response differences, the sensitivity function may be a useful parameter to assess the relative stability of the postural control system.

SUMMARY AND CONCLUSIONS

This study investigated the postural sway response to an impulsive perturbation and examined how this response varies with age. We applied a mild backward tug to three different age groups. Descriptive measures did not detect any age-related differences in sway response. Maximum sensitivity values from spectral analysis, however, showed significantly larger values for older adults than young or middle-aged adults. Thus maximum sensitivity may be a useful parameter for measuring relative stability or robustness of the postural control system to external perturbation.

REFERENCES

Ishida et al., IEEE Trans Biomed Eng 44:331-336, 1997

Zatsiorsky et al., Motor Control 4, 185-200, 2000

Peterka, *J Neurophysiol* 88: 1097-1118, 2002

AKNOWLEDGEMENTS

This study is funded by the Center for Advanced Studies and the Campus Research Board at the University of Illinois at Urbana-Champaign.

TRADE-OFFS IN PERFORMANCE ASSOCIATED WITH MUSCLE FIBER TYPE COMPOSITION

Brian R. Umberger

University of Massachusetts, Amherst, MA, USA
E-mail: umberger@kin.umass.edu, Web: http://people.umass.edu/umberger/

INTRODUCTION

Muscle fiber type composition is believed to influence both maximal and submaximal human performance. This can be inferred from power athletes tending to have a high percentage of fast twitch (FT) muscle fibers, while endurance athletes tend to have a high percentage of slow twitch (ST) fibers (Komi et al., 1977). In addition, there are positive correlations between the percentage of FT muscle fibers and jump height (Fry et al., 2003), and between the percentage of ST muscle fibers and gross pedaling efficiency (Coyle et al., 1992). However, isolating the effects of muscle fiber type on performance using experimental techniques is difficult, due to power and endurance athletes differing in strength, body mass, and training history (Komi et al., 1977). Computer modeling and simulation techniques provide an alternative means for directly investigating the effects of muscle fiber composition. This can be achieved by varying model parameters related to muscle fiber type, independent of all other model parameters. Therefore, the purpose of this study was to use a musculoskeletal model to determine how muscle fiber type composition affects both maximal and submaximal human performance.

METHODS

Simulations of maximum-effort vertical jumping and submaximal pedaling were generated using a two-dimensional musculoskeletal model (Umberger et al., 2006) (Figure 1). For jumping, the foot-ground interface was modeled using visco-elastic springs, and for pedaling, the feet were rigidly affixed to the pedals. The model was actuated by nine muscle groups that were controlled by specifying the magnitudes of a set of neural control nodes for each muscle. The values of the control nodes that produced a maximum height jump and submaximal (200 W, 80 rpm) pedaling were found using numerical optimization. Differences in muscle fiber type composition were simulated by scaling the values of the Hill constants and the activation time constants, by the proportion of FT muscle fibers. Three sets of fiber type proportions were considered that defined a standard (Std) condition (42% FT : 58% ST), a FT condition (60% FT : 40% ST), and a ST condition (24% FT : 76% ST) (Umberger et al., 2006). Other than the muscle model constants specifically being varied for a particular condition, all other model parameters were maintained at the Std values. This analysis allowed the effects of muscle fiber type composition to be investigated in isolation from other confounding factors.

Figure 1: Musculoskeletal model used to simulate jumping (left) and pedaling (right).

RESULTS AND DISCUSSION

Muscle fiber type composition had a substantial effect on maximal and submaximal performance, independent of any other factors that might also differ between power and endurance athletes (Figure 2). Jump height was 9% higher for the FT model than for the Std model, but gross pedaling efficiency was 10% lower. For the ST model, jump height was 13% lower than for the Std model, but gross efficiency was 12% higher. Further analysis revealed that jump height was most strongly influenced by the way in which muscle fiber type composition affected the muscle force-velocity relation. Submaximal efficiency, on the other hand, was determined primarily by the manner in which muscle fiber type influenced the metabolic cost of activating the muscles.

Muscle fiber type composition, therefore, represents a clear trade-off between explosive movement capacity and economy of movement. Fiber type distribution is genetically-determined, and our current fiber type profile reflects evolutionary pressures experience by early human ancestors. The transition to a hunter-gatherer existence over 2 million years ago would have selected for a combination of FT and ST fibers, to provide a reasonable compromise between endurance and explosive ability. This is likely why humans, as a whole, do not exhibit extreme fiber type distributions, as are found in some other species, like the lion (mostly FT) and skunk (mostly ST) (Burke, 1994).

SUMMARY/CONCLUSIONS

These simulation results demonstrate that muscle fiber type composition is an important, independent determinant of human performance, and also illuminate the trade-offs associated with having a particular fiber type composition. For example, having a high proportion of FT muscle fibers will improve explosive movement potential, but this will come at the cost of higher energy utilization during submaximal activities.

REFERENCES

Burke, R.E. (1994). *Myology*. McGraw Hill.

Coyle, E.F. et al. (1992). *Med. Sci. Sports Exer.*, **24**, 782-788.

Fry, A.C. et al. (2003). *J. Strength Cond. Res.*, **17**, 746-754.

Komi, P.V. et al. (1977). *Acta Physiol. Scand.*, **100**, 107-114.

Umberger, B.R. et al. (2006). *J. Biomech.*, **39**, 1472-1479.

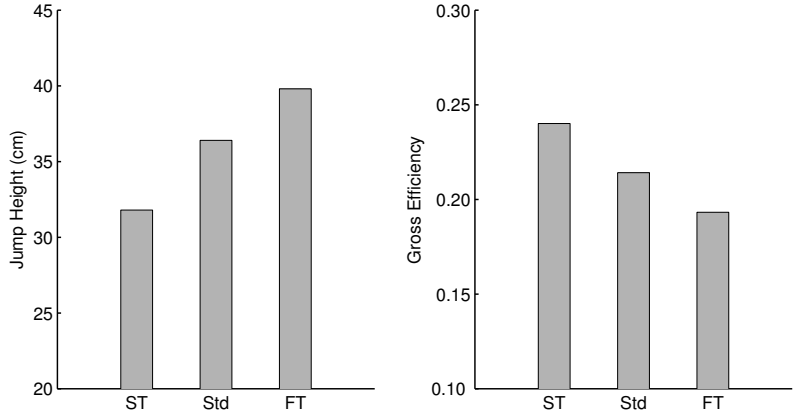

Figure 2: Maximum jump height (left panel) and gross pedaling efficiency (right panel) for the three fiber type conditions. Jump height increased and gross pedaling efficiency decreased as the percentage of FT fibers increased.

COACTIVATION OF HAND MUSCLES AND MOVEMENT FLUCTUATIONS IN OLD ADULTS

Minoru Shinohara [1], Adam R. Marmon [2], and Roger M. Enoka [2]

[1] Georgia Institute of Technology, Atlanta, GA, USA
[2] University of Colorado, Boulder, CO, USA
E-mail: shinohara@gatech.edu Web: www.ap.gatech.edu

INTRODUCTION

Neural strategies for motor tasks often differ between young and old adults. For example, old adults tend to coactivate antagonist muscles in a variety of motor tasks, presumably to stabilize the limb or finger to achieve a specific task force or trajectory (Seidler-Dobrin et al. 1998, Spiegel et al. 1996). Despite these expectations, coactivation has not been demonstrated to improve the performance of steady motor tasks by old adults.

Fluctuations in force or acceleration during steady contractions are often greater in old adults compared with young adults. Mechanisms that influence steadiness include the discharge characteristics of motor units and the distribution of agonist muscle activity (Enoka et al. 2003). The functional role of antagonist coactivation for steadiness was questioned because previous findings have indicated that there is no association between the amount of antagonist activity and steadiness in old adults (Burnett et al. 2000).

Recently, Shinohara et al. (2006) and Yoshitake et al. (in press) provided experimental evidence suggesting that the temporal association in muscle activity between agonist muscles plays a role in steadiness. If there is a temporal association between activity in agonist and antagonist muscles, therefore, the characteristics of the temporal association may influence the fluctuations in net torque about a joint.

The purpose of the current study was to re-examine the influence of coactivation on steadiness by investigating the temporal association between activity in agonist and antagonist muscles during steady contractions performed by old adults.

METHODS

Twelve healthy, right-handed old adults were tested (6 men and 6 women, 77.3 ± 6.6 yrs). The subject performed steady contractions with the first dorsal interosseus muscle in the left hand. An inertial load corresponding to 10% of the maximal voluntary contraction force was supported by the index finger of the subject.

There were three contraction modes: isometric, shortening, and lengthening. In isometric contractions, the subject maintained the index finger in a neutral position for 12 s. For the shortening and lengthening contractions, the subject steadily moved the index finger through 10-degrees of motion in 6 s. These contractions were performed with and without visual feedback of index finger displacement. After completion of these tasks, the subject repeated the tasks while intentionally increasing and decreasing coactivation of the antagonist muscle (second palmar interosseus).

Acceleration of the index finger was recorded in the abduction-adduction plane. Intramuscular recordings of the electromyogram (EMG) were obtained for

the first dorsal interosseus (agonist) and the second palmar interosseus (antagonist) muscles. In addition, surface EMG was recorded from the first dorsal interosseus muscle.

Data were analyzed for the middle 10 s for isometric contractions and for the middle 4 s of the shortening and lengthening contractions. The standard deviation (SD) of acceleration was determined after the linear trend was removed. Average amplitude of EMG (aEMG) was obtained for the same period and normalized to the EMG recorded during maximal voluntary contractions. The coactivation ratio was calculated as the normalized aEMG of antagonist muscle divided by the normalized aEMG of the agonist. Furthermore, a cross-correlation function was calculated with the rectified and low-pass filtered (50 Hz) EMGs of the two muscles.

RESULTS AND DISCUSSION

The coactivation ratio derived from intramuscular EMGs was 0.83 ± 0.64 (collapsed across feedback conditions and contraction modes) when no instructions were provided for coactivation. When the subject intentionally altered the level of coactivation of the antagonist muscle, the coactivation ratio increased to 1.41 ± 1.34 ($P < 0.01$) and decreased to 0.56 ± 0.73 ($P < 0.05$), respectively, during the two conditions. There was no interaction between feedback conditions or mode of contraction. Similar changes were observed for the coactivation ratio using the surface EMG for the first dorsal interosseus muscle.

The SD of acceleration was 0.16 ± 0.09 m/s^2 (collapsed across feedback conditions and contraction modes) when no coactivation instructions were provided. There were no significant changes in the SD of acceleration (0.17 ± 0.10 m/s^2) when the antagonist coactivation was intentionally increased or decreased (0.17 ± 0.11 m/s^2). There were no significant interactions between feedback conditions or contraction mode.

There were no significant peaks in the cross-correlation function between the antagonist and agonist (intramuscular or surface) EMGs for any condition or contraction mode.

CONCLUSIONS

Although subjects were able to alter the coactivation ratio intentionally, the modulation of EMG activity was not related and there was no change in the measure of steadiness (SD of acceleration) across conditions.

REFERENCES

Burnett, R.Y. et al. (2000) *J Appl Physiol*, **89**, 61-71.

Enoka, R.M. et al. (2003) *J Electromyogr Kinesiol*, **13**, 1-12.

Seidler-Dobrin, R.D. et al. (1998) *Motor Control*, **2**, 314-330.

Shinohara, M., et al. (2006) *Exp Brain Res*, **169**, 15-23.

Spiegel, K.M., et al. (1996) *Exp Physiol*, **81**, 805-819.

Yoshitake, Y. et al. (in press) *Muscle Nerve*, DOI: 10.1002/mus.20764.

ACKNOWLEDGEMENTS

This work was supported by NIH grant AG09000 awarded to RME. We thank Brandon Mai for help with data collection and Ashley Johnson and Shikhar Vohra for help with data analysis.

NON-RIGID REGISTRATION OF DEFORMABLE SHAPE MODELS PRODUCES A SUPERIOR NORMATIVE FEMUR MODEL

Weidong Luo[1,2], Steven Stanhope[1], Frances Sheehan[1]
[1]Physical Disabilities Branch, NIH
[2]Catholic University of America
E-mail:wdluo@yahoo.com, Web: http://pdb.cc.nih.gov

INTRODUCTION

Quantifying shape variation for anatomical structure is a complicated task. In general, it requires an accurate shape description, registration of shapes and an ability to study shape variation on both a global and a local scale. Usually, a statistical normative shape needs to be generated first as the reference. Early studies of creating normative femoral shapes were mainly based on rigid registration methods using surface landmarks. Recently, non-rigid registration has been used to create normative shapes, but most of them were limited in their ability to interpret shape variations or lack anatomical meaning (Tang 2005). In order to better describe both local and global variations between bones, a multiple vector bursts (MVB) method was created that could describe shape in a hierarchical way with integrated anatomical meaning. Using non-rigid registration to fit the MVB into individual shapes, the local variation was described by first quantifying and then removing the global variation.

The purpose of this study was to compare the normative femoral shapes generated based on rigid and non-rigid method.

METHODS

17 legs of 17 volunteer subjects with no injuries or illness affecting their lower extremities were scanned with a T1-weighted spin echo MRI sequence in axial plane with 15mm slices at the main shaft and 4mm slices at the distal and proximal femur. The in-plane resolution was 0.94 mm for all images. Geometric femoral models were segmented from the MRI data. All femurs were aligned and scaled based on mean palpable length. First, a 49 vector burst (VB) MVB model created from a randomly selected femoral shape based on a central axis that was extracted using the maximal sphere theory. Second, in order to generate a rigid normative femoral shape, this MVB model scaled its vectors to fit within the individual femurs, generating 17 MVB models. These models were averaged to create an initial average model. To remove the influence of the femur selection, a new MVB model was created for this initial average model and was then used to generate the final rigid normative femoral shape. In order to generate a non-rigid normative femoral model, non-rigid registration was applied to the MVB model, created from rigid normative femoral shape, and the MVB was deformed to fit within the individual femurs, generating 17 MVB models. The non-rigid normative femur was created by averaging these MVB models.

Four global shape parameters were automatically defined from the MVB model and compared to values available in the literature: 1) PAA (pseudo-anteversion angle): the projection into the axial plane of the angle connecting the femoral head vector burst origin (VBO) to the central greater trochanter VBO and a line connecting the lateral and medial condylar VBO; 2) SAA (standard anteversion angle); 3) PD (proximal distance): the distance measured from the femoral head VBO to the central greater trochanter VBO; 4) FSC (Femoral Shaft Curvature): the radius of the best fit circle of all VBOs in the main shaft. To

validate the MVB methodology's ability to quantify local shape variation, the deviation in the average femoral surface was quantified and compared between the rigid and non-rigid normative femoral shape. In order to validate the accuracy of the non-rigid registration, a synthetic model with artificial deformation was used.

RESULTS AND DISCUSSION

The goal of this work was to develop a new methodology that could accurately quantify shape on a hierarchical scale from global to local variations. The rigid normative femoral shape had higher surface standard deviations and underestimated values of normative shape as compared to the non-rigid method (Fig 1). Thus, the MVB methodology, based on non-rigid registration provided an improved method for determining local shape variations.

Global shape parameters produced values that matched with previous studies, but typically had a smaller standard deviation (Table 1). The pseudo-anteversion angle, defined within this study, had a smaller variability than the standard anteversion angle due to its use of more stable interior feature points than surface landmarks.

The synthetic model demonstrated that PAA measurement based on a MVB model was consistent with the true value, only slightly higher (0.2 degrees or 4%) and that a small surface deformation could be detected. This further demonstrated that non-rigid registration of the MVB method was accurate in quantifying both global and local shape deformation.

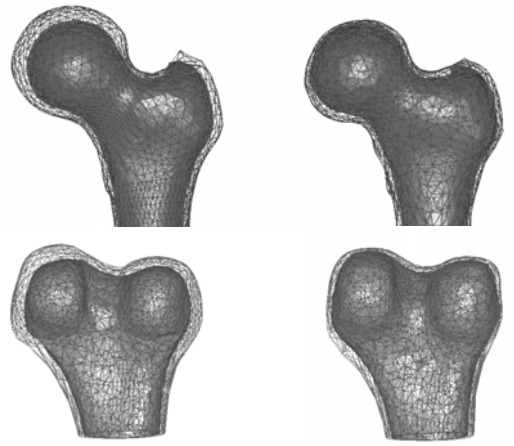

Figure 1: Local shape variation at proximal femur and distal femur. The solid model was the normative femoral shape (left: rigid normative, right: non-rigid normative) and the mesh was the one SD plus model. The standard deviation was higher and the normative model was smaller for rigid normative femoral shape as compared to the non-rigid normative femoral shape.

REFERENCES

Tang, T.S (2005). Ellis,R.E. *Med. Image Comput. Comput. Assist. Interv. Int. Conf.* 8, 223-230

Sugano,N.et. al. (1998) *J. Comput. Assist. Tomogr.* 22, 610-614

Demissie,S. *et al.* (2007) *Bone* 40, 743-750

Egol,K.A. et. al.(2004) *J. Orthop. Trauma* 18, 410-415

Measure	Current Mean	Current SD	Past Study	N	Mean	SD
PAA (deg)	19.2	8.3	(not available)			
SAA (deg)	19.6	10.8	Sugano et al	30	19.8	9.3
PD (mm)	50.1	6.7	Demissie et al	346(M) /592(F)	54.0/46.0	8.0/7.0
FC (cm)	114	28.3	Egol et al	948	120	36

Table 1: For each measure the mean and SD are provided for the current study (column 2&3) and past studies (column 6&7). Column 5 provides the number of subjects.

DOES WEIGHT INFLUENCE LOCOMOTIVE STABILITY?

Christopher J. Arellano, Charles S. Layne, Daniel P. O'Connor, Melissa Scott-Pandorf and Max J. Kurz

Laboratory of Integrated Physiology, University of Houston, Houston, TX, USA
E-mail: carellano@uh.edu

INTRODUCTION

The amount of weight carried by the locomotive system appears to influence locomotive strategies used by the neuromuscular system. For example, obese individuals have slower gait patterns, shorter step lengths, increased step widths, and altered lower extremity kinematics compared to their lean counterparts (DeVita & Hortobagyi, 2003). These changes in the gait kinematics may be related to neuromuscular strategies that ensure stability. However, limited efforts have been made to explore how increasing weight influences gait stability, and the neuromuscular strategies used for a stable gait. The purpose of this study was to explore the influence of weight on the dynamic stability of human locomotion.

METHODS

Twenty-three subjects (height = 1.7 ± .1 m, weight = 63.9 ± 8.7 kg, age = 23.8 ± 4.5 yrs) walked on an treadmill for three minutes at a self-selected speed while carrying an additional 10%, 20%, and 30% of their body weight. An increase in weight was accomplished by symmetrically adding thin lead strips to a customized hip belt worn by the subject. The right lower extremity joint kinematics were recorded in the sagittal plane with a high-speed (120 Hz) three-dimensional motion capture system.

The state vector (**x**) of the locomotive system was used to evaluate the stability and neuromuscular strategies. **x** was defined by the joint position and velocity of the hip, knee, and ankle at heel-contact. Figure 1 depicts an example first-return map for the hip joint component of **x** over successive gait cycles. Shifts of the equilibrium point (**x***) along the diagonal were assumed to reflect changes in the neuromuscular strategies used for ensuring gait stability.

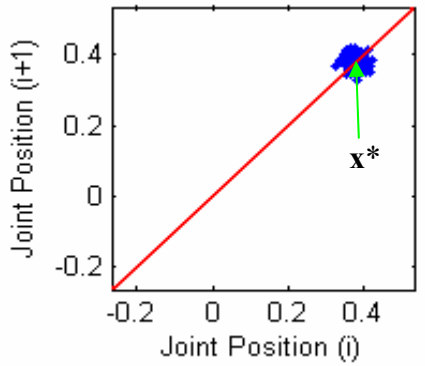

Figure 1: First -return map for the hip joint. x* represents the hip joint's equilibrium point.

Floquet analysis was used to quantify the dynamic stability of the gait pattern (Hurmuzlu et al., 2001). This involved linearizing the first-return map about **x*** to satisfy the following relationship

$$\delta x^{n+1} = \mathbf{J}\,\delta x^{n}$$

where δ denotes the deviation about **x*** at each n^{th} step, and **J** is a 6 x 6 constant coefficient matrix that represented the Jacobian. δx^{n} and δx^{n+1} were defined as

$$\delta x^{n} = [x_{n} - x^{*}, x_{n+1} - x^{*}, x_{n+2} - x^{*}, \ldots]$$

$$\delta x^{n+1} = [x_{n+1} - x^{*}, x_{n+2} - x^{*}, x_{n+3} - x^{*}, \ldots]$$

A least squares algorithm was used to solve for **J** (Tedrake, 2004).

$$J = \left[\left(\delta x^{n+1}\right)\left(\delta x^{n}\right)^{T}\right]\left[\left(\delta x^{n}\right)\left(\delta x^{n}\right)^{T}\right]^{-1}$$

The largest eigenvalue (β) was computed from **J** and was used to quantify the stability of the gait pattern. A β value further away from zero signified a less stable gait.

RESULTS AND DISCUSSION

The value of β did not significantly change ($p > 0.05$) across the various conditions of increased weight (Figure 2). This suggested that the subjects were able to maintain a stable gait pattern while carrying additional weight around their waist. Exploration of **x*** (Table 1) suggested that neuromuscular strategies at the hip ($p < 0.05$) and knee ($p < 0.05$) may have changed to ensure a stable gait, while the ankle joint strategy was unchanged ($p > 0.05$). Hence, our results indicate that the neuromuscular system can adapt to acute changes in weight. The neuromuscular strategies used by obese individuals are presumably a result of a chronic adaptation to additional weight. It is unknown if the neuromuscular strategies seen here are similar to the gait stability strategies used by obese individuals. Based on our current findings, our future investigations are directed towards exploring if obese individuals have similar or different strategies to maintain gait stability.

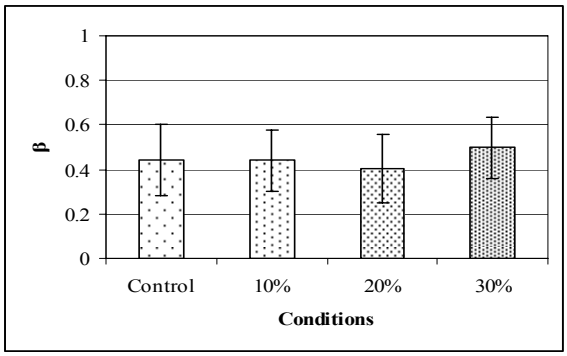

Figure 2: β values across conditions (mean ± SD).

SUMMARY/CONCLUSIONS

The human locomotive system is capable of maintaining stability while being subjected to acute changes in weight. Our results suggest that adaptations in the hip and knee joints are primarily responsible for maintaining the gait stability while carrying additional weight.

REFERENCES

DeVita, P. & Hortobagyi, T. (2003). *J. Biomech.*, **36**, 1355-1362.

Hurmuzlu, Y. B., et al. (2001). *ASME J. Biomech. Eng.,* **118**, 405-411.

Tedrake, R., et al. (2004). *Proc. IEEE ICRA.,* **5**, 4656-4661.

ACKNOWLEDGEMENTS

Funding provided by the Texas Learning and Computational Center grant awarded to MJK.

Table 1: Equilibrium point (radians) generated at heel strike: mean ± SD.

Joint	Control	10%	20%	30%
Hip	0.433 ± 0.065	0.459 ± 0.058	0.471 ± 0.059	0.489 ± 0.065
Knee	0.024 ± 0.061	0.047 ± 0.078	0.065 ± 0.092	0.099 ± 0.110
Ankle	-0.046 ± 0.059	-0.038 ± 0.051	-0.047 ± 0.052	-0.043 ± 0.055

IN VIVO EXAMINATIONS OF MEDIAL GASTROCNEMIUS: CHANGE OF FORCE-GENERATING CAPACITY IN STROKE SURVIVORS

Fan Gao[1] and Li-Qun Zhang[1,2]

[1] Rehabilitation Institute of Chicago, Chicago, IL, USA
[2] Northwestern University, Evanston, IL, USA
E-mail: l-zhang@northwestern.edu

INTRODUCTION

Spasticity, contracture and muscle weakness are commonly observed in patients post stroke, which affect patient's mobility considerably. Although spasticity and contracture have been investigated intensively, it is not clear how muscle properties, such as force generating capacity, muscle architecture are altered in patients post stroke. A better understanding of changes in muscle properties could help us gain insight into the mechanisms underlying spasticity, contracture and muscle weakness and provide us guidance to effective stroke rehabilitation.

We hypothesized that spasticity, contracture, and muscle weakness at the ankle joint in stroke is associated with significant changes of plantar muscle biomechanical properties. The purpose of this study was to evaluate the force-generating capacity of the medial Gastrocnemius muscle. A programmable electrical stimulator was used to activate the Medial Gastrocnemius (MG) selectively at a constant intensity across joint configurations and muscle force length relationship at the fascicle level was compared between stroke and control populations.

METHODS

Ten stroke survivors (55±8 yr, height, 1.76±.06 m) and ten age and gender-matched healthy subjects (52±5 yr, height, 1.75±.05 m) without neuromuscular injury participated in the study, with an informed consent approved by the IRB committee of Northwestern University.

Subjects were seated upright with thigh strapped to the seat and the knee and ankle joints were aligned to the centers of the corresponding JR3 force/torque sensors (JR3, Inc.), which were mounted on a custom leg-foot linkage. Four knee configurations, starting from full extension with an increment of 30° in flexion, were tested. Ankle angle was also systematically varied with an increment of 10° in dorsi-flexion and 15° in plantar flexion within the ankle range of motion.

A Compex™ electrical stimulator was used to produce trains of biphasic pulses with pulse width of 300 μs and frequency of 40 Hz. The duration of each electrical train was 2s and the interval between two consecutive electrical pulse trains was 3s. Each stimulation trial lasted 50 seconds and there were around 10 contractions induced in each trial.

All ultrasound images were collected using a B-mode ultrasonography scanner (GE LOGIQ-9, Waukesha, WI). Longitudinal scan of MG using LogiqView were conducted as the muscle was activated. The moment arm of MG around ankle joint was obtained from SIMM (MusculoGraphics, Inc.) and scaled to the individual subjects. The muscle force was calculated from the joint torque and moment arm. For each subjects, the force-generating capacity was established by relating muscle force and muscle fiber length using the model proposed by Kaufman et al., (1989). Peak

point of the fitted curved was identified as the optimal point on the force-length curve (Figure 1). The width of the fitted curve was measured at various normalized tension levels, ranging from 0.1 to 0.5 with a step of 0.1.

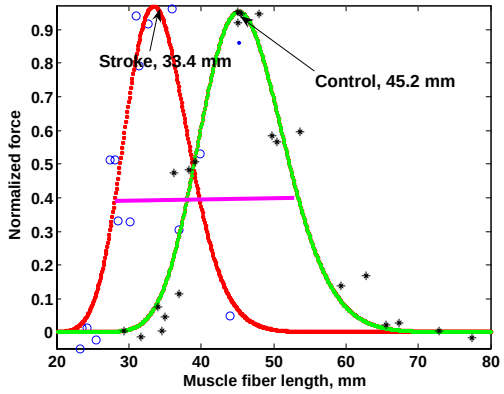

Figure 1. Typical curve-fitting of force-generating capacity with optimal point and sample spanning width marked.

Student T-test (SPSS, Inc.) was used to compare the optimal length and spanning width between stroke survivors and healthy subjects. Statistical significance was set as $P<0.05$.

RESULTS AND DISCUSSION

Stroke survivors showed a shifted force-length relationship and the optimal fiber length was significantly shorter compared to that of healthy control. The optimal fiber length was 46.6±4.0 mm and 33.6±2.0 mm (mean±SD) for the normal control and stroke survivors, respectively ($P=0.001$). The stroke survivors also had significantly smaller spanning width ($P<0.05$ at all evaluated force levels, Table 1). For instance, the spanning widths were 26.2 ± 2.8 and 13.3 ± 2.1 mm for control and stroke respectively at a tension level of 40%. The narrower force-length curve in stroke indicates that compared to normal control, the muscle fiber length operated in a significantly reduced range.

The force-length curve at the sarcomere level can be established by using the number of sarcomeres in series of human MG reported by Huijing (n = 17,600) (1985). The optimal sarcomere length of 2.6 –2.8 μm (Walker and Schrodt, 1974) correspond to fascicular length between 46 and 49 mm in the GM muscle. The results of the current study suggest that the GM of healthy subjects operated around the optimal region and the GM of stroke patients had an average sarcomere length of 1.9 μm. However, the shortening of the muscle fibers could be associated with reduced number of sarcomeres in series. Further study at the sarcomere level is being conducted to clarify the issue.

SUMMARY

Spasticity, contracture and muscle weakness around the ankle joint in stroke may be associated with changes of plantar flexor muscle properties, specifically, muscle fiber length, range of fiber length change during functional activities, number of sarcomere in series, and force-generating capacity may be changed considerably in stroke.

REFERENCES

Huijing, P.A. et. al. *Acta Anat* (Basel), 1985. 123(2): p. 101-7.

Kaufman, K.R. et. al. *J Biomech*, 1989. 22(8-9): p. 943-8.

Walker, S.M. and G.R. *Schrodt, Anat Rec*, 1974. 178(1): p. 63-81.

Table 1: Spanning widths (mean± SE, mm). * indicates significant difference

Tension level:	**10%**	**20%**	**30%**	**40%**	**50%**
Control	41.9 ± 3.8*	35.4 ± 3.8*	30.2 ± 3.2*	26.2 ± 2.8*	22.6 ± 2.4*
Stroke	21.5 ± 3.5	17.7 ± 2.9	15.3 ± 2.5	13.3 ± 2.1	11.5 ± 1.9

TRADITIONAL VS CONTINUOUS DATA COLLECTION FOR GAIT EVALUATION

Peter M. Quesada [1,2], James E. Doane [1,2], Ann M. Swank [2], and Robert V. Topp [2]

[1] Department of Mechanical Engineering, University of Louisville, Louisville, KY, USA
[2] Exercise Physiology Laboratory, University of Louisville, Louisville, KY, USA
E-mail: peter.quesada@louisville.edu

INTRODUCTION

In human movement laboratories where clinical gait evaluations are performed, subjects are commonly instructed to stand still just prior to collection of each walking trial. Upon being prompted, subjects then walk through a calibrated capture volume. This process is repeated until a desired number of trials have been recorded.

Guidelines have been suggested regarding desired distances between initial starting positions and data capture areas. Such guidelines are predicated on the notion that a few (commonly regarded as 2-3) gait cycles are required before a subsequent cycle is representative of an individual's typical gait. These guidelines, however, do not address the issue of whether the gait achieved, within a few cycles from a static position, is indicative of the gait that would be achieved following a larger number of cycles. Consequently, this paper presents an assessment of whether gait variables obtained following a few cycles are representative of values obtained after a more substantial walking duration.

METHODS

The present study's sample was drawn from a larger project involving individuals who had undergone or were scheduled for a total knee arthroplasty (TKA). Consequently, these individuals represented a patient population for whom clinical gait evaluation might be desired. Six subjects were approximately 3 months post-TKA, while the remaining subjects were approximately 1 month pre-TKA. The subjects had overall mean age, height and mass of 63±8 years, 173±11 cms and 93±22 kgs, respectively.

Each subject was instructed to take an initial standing position outside a calibrated capture volume. The capture volume was positioned along a straight section of a marked stadium track shaped path. The path length was approximately 35 meters. Upon being prompted, subjects were directed to walk through the capture volume, where motion tracking and ground reaction data were obtained with an 8-camera Hawk system (Motion Analysis Corp.) and a force plate (Bertec, Inc.), respectively. Consequently, this initial walking trial represented a "traditional" gait evaluation trial. However, subjects did not stop at the end of the capture volume and return to the starting point. Rather, each subject continued walking for several laps around the marked path. Subsequent "continuous" trials were obtained each time a subject passed through the capture volume.

For each subject, a set of common kinematic and kinetic measures were computed for the traditional and two continuous trials. The computed kinematic and kinetic variables consisted of: walking speed, stride length, maximum knee flexion angle, maximum hip flexion angle, maximum ankle plantar flexion angle, maximum knee extension moment, maximum hip flexion moment, and maximum ankle plantar flexion moment.

These variables were used to assess whether gait obtained a few (typically two or three) gait cycles after initiation (i.e. during a traditional trial) were representative of values obtained after a much larger number of gait cycles (i.e. during continuous trials).

For each gait variable of each subject, the average absolute difference between the traditional and continuous trials was determined, as was the absolute difference between the continuous trials. The signed differences between these absolute values were then computed. For each gait variable signed differences were compared with an expected distribution, based upon a null hypothesis that for a given individual traditional and continuous trials were members of the same population of trials.

RESULTS AND DISCUSSION

Kinematic variables for which traditional trial values were not representative of continuous trial values were walking speed, maximum knee flexion angle, and maximum hip flexion angle. Kinetic variables for which traditional trial values were not representative of continuous trial values were maximum knee extension moment and maximum ankle plantar flexion moment.

As an example the figure on the right shows maximum ankle plantar flexion moments (normalized by body weight and height) for the traditional trial and continuous trials of each subject. These results demonstrated that traditional trial plantar flexion moments generally fell outside the continuous trial values far more often, and by significantly greater amounts than would be predicted by random chance if traditional trial plantar flexion moments were representative of continuous trial values.

Amounts by which traditional trial values may diverge from continuous trial values could be affected by particular patient types. For example, individuals who might "loosen up" after a moderate walking duration might exhibit more divergence between traditional and continuous trial values.

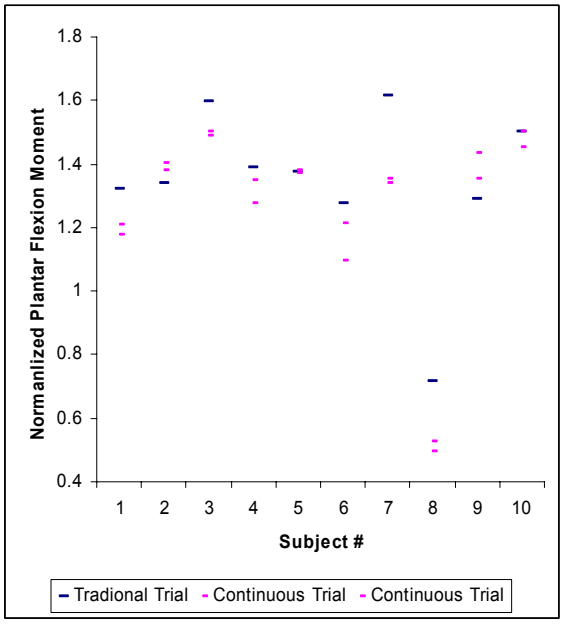

Figure: Ankle plantar flexion moments for traditional and continuous walking trials.

SUMMARY/CONCLUSIONS

For the majority (5 of 8) of variables that were examined, values obtained during traditional trials were generally not representative of continuous trial values. Facilities, limited by spatial constraints to the traditional approach, should consider how gait characteristics obtained from an individual might diverge from those that occur during continuous walking.

ACKNOWLEDGEMENTS

This work received support from the National Institute for Nursing Research (Grant # 1RO1 NR080).

INDEPENDENT EFFECTS OF WEIGHT AND MASS ON MUSCLE ACTIVITY DURING WALKING

Craig P. McGowan [1, 2], Richard R. Neptune [2] and Rodger Kram[1]

[1] University of Colorado, Boulder, CO, USA
[2] University of Texas, Austin, TX, USA
E-mail: mcgowac@colorado.edu, Web: www.colorado.edu/intphys/research/locomotion.html

INTRODUCTION

There have been differing reports of which muscles contribute to forward propulsion of the body during normal walking (e.g., Gottschall and Kram, 2003; Neptune et al., 2001). Further, load carrying studies have measured the relative metabolic cost of weight support to estimate the contribution of muscle groups to support. However, simply adding a load to the body not only increases the weight that must be supported, but also increases the mass that must be accelerated and decelerated over the gait cycle. Therefore, relative changes in muscle activity during loaded/unloaded conditions cannot be used to distinguish between a muscle's contribution to body support versus propulsion. Recent studies have shown that both of these tasks contribute to metabolic cost during locomotion and thus likely require significant contributions from various muscle groups (Grabowski, et al., 2005).

Simulation studies have suggested that both the soleus (SOL) and gastrocnemius (GAS) provide both body support and forward propulsion (e.g., Liu et al, 2006; Neptune et al., 2001). However, during the propulsion phase while providing body support, SOL acts to accelerate the trunk forward, whereas GAS acts to accelerate the leg into swing (Neptune et al, 2001). Thus, while both muscles are likely to be sensitive to changes in body weight, SOL is more likely to be sensitive to added mass.

In the present study, we tested the hypothesis that SOL plays a primary role in providing forward propulsion by employing a combination of trunk loading and weight support in order to produce independent manipulations of body weight (gravitational forces) and body mass (inertial forces).

METHODS

Ten healthy subjects walked on a dual-belt motorized force-treadmill at 1.3 m/s with combinations of added mass and/or weight support. In addition to a control trial, subjects walked with added trunk loads equal to 25 and 50% of body weight (BW), and with 25 and 50% weight support. In addition, subjects also walked with simultaneous added load and weight support equal to 25 and 50% BW, effectively increasing mass without changing weight.

We measured muscle activity using surface electrodes placed over SOL and medial GAS of the right leg. The EMG amplifier had a gain of 1700 and bandpass filtered (16-500Hz) the raw data, which were recorded at 2000Hz. We determined muscle activity level from the time integrated area of the rectified EMG signals calculated during the stance phase. We calculated within subject mean muscle activity from 15 strides and normalized the data relative to control trials.

RESULTS AND DISCUSSION

Below, we present results for the group means during each condition. The data

support our hypothesis that the SOL plays a primary role in providing propulsion. Muscle activity in SOL increased in a similar manner when both weight and mass were added (Fig 1A), and when only mass was added (Fig 1B). SOL activity decreased somewhat during weight support trials, but there was no progressive effect with greater levels of weight support (Fig 1C). In contrast, GAS activity decreased during weight support trials and increased during added weight trials (Fig 1A, C). However, GAS activity was not significantly different from the control condition during added mass only trials (Fig 1B).

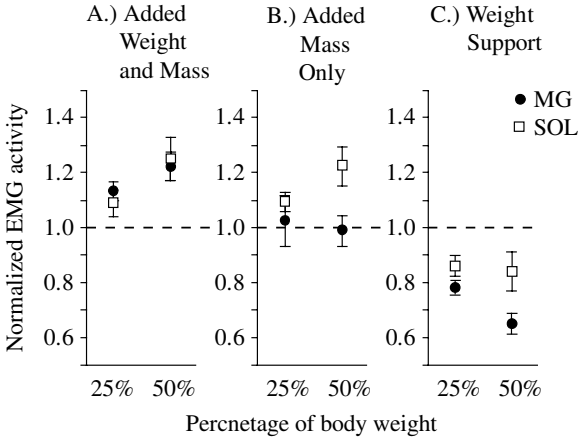

Figure 1. SOL (□) was predominately affected by changes in mass (A,B), whereas GAS (●) muscle activity showed a clear relationship with changes in weight (A,C). EMG activity was normalized to control trials (dashed line).

The experimental design of this study enabled the evaluation of muscle activity effects due to independent changes in body weight and body mass. Our rationale was that if SOL accelerates the trunk to provide propulsion, it would be sensitive to increases in body mass, but not sensitive to decreases in body weight due to weight support, since body mass does not change. In general, this rationale was supported. SOL activity increased when mass was added to the trunk, independent of body weight. In addition to providing propulsion, SOL also plays a role in weight support, thus a decrease in activity during the weight support trials is not surprising. However, SOL activity is likely constrained from decreasing further by its need to provide propulsion.

Neptune et al. (2001) suggested that in addition to providing body support, GAS primarily acts to accelerate the leg into swing, which explains why GAS was unaffected by increasing trunk mass (Fig. 1B). Further, Browning et al. (2007) showed that GAS activity increased when mass was added to the feet. Thus, because the primary role of GAS is body support and swing initiation, GAS is able to decrease its activity when weight support is provided.

SUMMARY/CONCLUSIONS

Through novel experiments, we provide empirical evidence for the functional role of individual ankle extensors during normal human walking. Our conclusion that SOL is the primary contributor to trunk forward propulsion in late stance is in agreement with previous simulation based studies (e.g., Neptune et al., 2001).

REFERENCES

Browning, R., Modica, J., Kram, R., Goswami, A. (2007), *Med. Sci. Sports Exerc.* 39**,** 515-525.

Gottschall, J, Kram, R. (2003). *J. Appl. Physiol,* **94**, 1766-1772.

Grabowski, A, Farley, C., Kram, R. (2005). *J. Appl. Physiol,* **98**, 579-583.

Liu, M., Anderson, F., Pandy, M., Delp, S. (2006). *J. Biomech.*, **39**, 2623-2630.

Neptune, R., Kautz, S., Zajac, F. (2001). *J. Biomech,* **34**, 1387-1398.

ACKNOWLEDGEMENTS

This work is supported by NIH grant F32-AR054245-01 to C.P.M.

SWING PHASE INTERRUPTION IN A SLIP: ACTIVE OR PASSIVE RESPONSE?

Rakié Cham, PhD
Department of Bioengineering, University of Pittsburgh, Pittsburgh, PA, USA
E-mail: rcham@pitt.edu

INTRODUCTION

Prevention of slip-precipitated falls requires an understanding of postural reactions to such perturbations. Prior slips/falls gait research has, to a large extent, focused on the leading/slipping leg, while the dynamics of the trailing leg have not been often examined. In Moyer et al. (2007), four types of trailing leg response, termed *minimum*, *foot-flat* (FF), *mid-flight* (MID), and *toe-down* (TD) were identified. Trailing foot toe off occurs in all four patterns. The swing phase is interrupted in FF, MID and TD responses, the focus of this analysis (Fig 1).

(a) FF ***(b) MID*** ***(c) TD***

Figure 1: Trailing leg responses to a slip involving a swing phase interruption. (a) FF: entire foot sole contacts ground near leading/slipping foot. (b) MID: forefoot contacts ground behind leading/slipping foot. (c) TD: most severe slips; tip of forefoot contacts ground immediately (~50 ms) after toe off. *Adapted from (Moyer et al., 2007).*

It may be argued that the swing phase interruption is not an active postural strategy but rather a consequence of the passive dynamics of the fall. Indeed, Tripp et al. (2004) suggested that the direction of the step cannot be modulated after foot lift-off. Thus, the goal of this analysis is to compare the latency of the muscles in the trailing leg with foot floor contact time to determine if the swing phase interruption is an active or passive response. Net joint moments computations revealed that simultaneous hip extension and knee flexion reactions in the trailing limb cause the interruption of the swing phase, lowering the leg onto the ground and decelerating knee extension (Moyer *et al.*, 2007). Thus, compared to normal gait, it is expected that during the slip the magnitude of the hamstring will be greater than that of the vastus lateralis, but that the knee extensors activity will be non-negligible to prevent limb collapse as body weight is transferred from the leading/slipping leg to the trailing leg.

METHODS

Ten healthy adults walked at a self-selected pace, while ground reaction forces and whole body motion were sampled at 1080 and 120 Hz, respectively. EMGs were also collected from major muscle groups in both legs at 1080 Hz. Subjects were informed that the first few trials would be dry to ensure normal walking (dry condition). Then, without the subjects' knowledge, glycerol was applied on the floor to initiate a slip at heel contact of the leading/left leg. Only EMG data collected from the medial hamstring and vastus lateralis in the trailing/right leg were analyzed here.

All EMGs (dry and slip) were rectified, low-pass filtered at 50 Hz using a zero-phase filter, time normalized to stance duration (leading leg) of normal walking and magnitude normalized to the peak value collected during normal walking. EMG data collected in the dry trial prior to the slip were subtracted from the EMGs recorded

during the slip. The resulting time series was used to determine muscle latency post slip initiation using a threshold of two standard deviations above the (slip – dry) difference prior to slip initiation. In addition, this threshold was exceeded for a minimum of 30 ms for a point to be picked as the latency. Latency data were visually confirmed.

RESULTS

The latency of the hamstring and vastus lateralis ranged from 140 to 200 ms (Fig 2). For the most severe slips, e.g. TDs and few MIDs, the muscle response in the trailing leg started prior to toe off. As expected, in general, the relative magnitude of the hamstring activity was greater than that of the vastus lateralis.

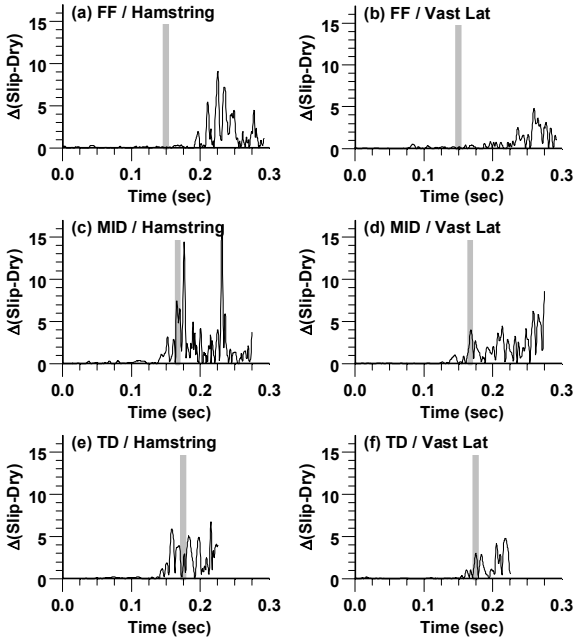

Figure 2: Typical difference in hamstring (left) and vastus lateralis (right) activity between dry and FF (a-b) /MID (c-d) /TD (e-f) slip. All EMGs are divided by the peak value recorded during normal gait before the (slip–dry) difference is computed. Time "0" = heel contact of leading leg onto slippery floor. Vertical gray line = time of trailing leg toe off. Data are chopped at time of trailing foot floor contact.

The hamstring and vastus lateralis activity was initiated prior to foot contact in all MID/FF slip patterns (Fig 2 a-d, Table 1). In contrast, the latency of these muscles were detected prior to foot floor contact time in only one of two TD slip patterns (Fig 2e-f, greater variability is reflected in Table 1).

Table 1: Mean (SD) of within-subject difference between latency of trailing leg muscle response and trailing foot floor contact time. A negative number indicates the muscle response occurred prior to foot floor contact time in the trialing leg.

Latency – contact time (ms)	***Hamstring***	***Vastus lateralis***
FF (N=4)	-108 (14)	-90 (16)
MID (N=4)	-129 (8)	-126 (7)
TD (N=2)	52 (196)	31 (144)

DISCUSSION AND CONCLUSIONS

In summary, the latency of the muscles in the upper trailing leg is detected prior to trailing foot floor contact in FF/MID slip patterns. These findings suggest that the swing phase interruption is an active reaction in FF/MID responses. The findings also confirmed that the activity of the trailing leg's hamstring and vastus lateralis plays a role in slip-initiated recovery efforts.

The argument of an active swing phase interruption strategy may not hold in TD slip patterns. While the muscular response in the trailing leg may be initiated early, it is likely that the severity of the slip may not allow time for effective active responses, resulting in the fall driving the dynamics of limb collapse.

REFERENCES

Moyer, B.E. et al. (2007). *J of Biomech*, submitted.

Tripp, B.P. et al. (2004). *IEEE Trans Neural Syst Rehabil Eng* **12,** 140-152.

ACKNOWLEDGEMENTS

NIOSH R03-OH007533/R01-OH007592. Many thanks to Dr. J Furman for screening subjects.

EFFECTS OF AN ELASTIC KNEE ORTHOSIS ON UNILATERAL HOPPING

Michael S. Cherry [1,2], Sridhar Kota [1], and Daniel P. Ferris [2]

[1] Compliant Systems Design Laboratory, [2] Human Neuromechanics Laboratory
The University of Michigan, Ann Arbor, MI, USA
E-mail: mscherry@umich.edu

INTRODUCTION

When hopping on elastic surfaces, humans compensate by increasing leg stiffness to keep combined leg-surface stiffness constant (Ferris & Farley 1997). Similarly, humans adjust biological ankle stiffness when a spring is placed in parallel with the ankle via an ankle brace, keeping total ankle stiffness constant (Ferris et al., 2006). The purpose of this study was to determine if human hoppers also adjust biological knee stiffness when a spring is placed in parallel with the knee. We hypothesized that subjects would decrease biological knee stiffness to compensate for parallel spring stiffness and maintain a constant overall leg stiffness.

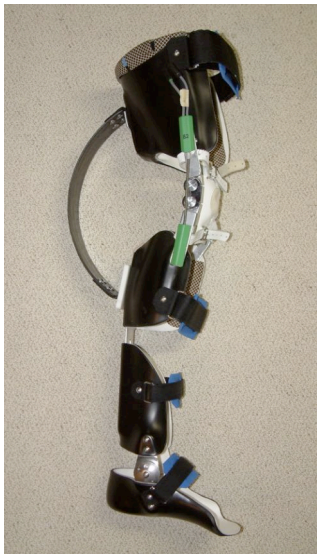

Figure 1: Knee orthosis with carbon composite leaf spring on posterior side for energy storage during knee flexion. Ankle joint is free-moving and passive.

METHODS

Six human subjects [mass: 89.5 (SD 9.8) kg, age: 25 (SD 4.0) yr] hopped in place on their left leg at their preferred frequency. Subjects hopped while wearing the orthosis (Figure 1), both with and without the spring attached (Spring and No Spring conditions, respectively). The brace provided 31.5% (SD 7.3%) of the total knee stiffness in the Spring condition.

We collected kinematics and kinetics for the left leg and torso and electromyography (EMG) for the left tibialis anterior, soleus, medial gastrocnemius, lateral gastrocnemius, vastus medialis, vastus lateralis, rectus femoris, and medial hamstrings. We calculated EMG root-mean-squared (RMS) amplitudes and normalized by the mean RMS value in the No Spring condition for each subject. We created EMG linear envelopes by low-pass filtering with a 6 Hz cut-off frequency and normalizing by the peak value in the No Spring condition.

We calculated leg stiffness using vertical ground reaction force and center of mass displacement obtained by twice integrating the force data. We calculated joint stiffness using joint torques and displacements in the sagittal plane during the ground contact phase. The results presented in this study represent twenty hops per subject per condition.

RESULTS AND DISCUSSION

Contrary to our hypothesis the total knee stiffness and leg stiffness increased during

the Spring condition (see Table 1). Subjects also increased hop frequency during the Spring condition (p=0.02). The preferred frequencies for hopping were 1.93 (SD 0.16) Hz and 2.03 (SD 0.14) Hz for the No Spring and Spring conditions, respectively.

Biological knee stiffness decreased significantly and ankle stiffness did not change significantly. The decrease in biological knee stiffness appears to be a result of decreases in knee extensor muscle activation during stance (Figure 2). Corresponding decreases in EMG RMS amplitudes for VM, VL, and RF were 18.9% (SD 16.1%), 28.7% (SD 16.3%), and 27.8% (SD 20.7%), respectively (p<0.02 for all). No other muscle groups had significant EMG changes (p>0.3 for all).

The knee was more flexed at ground contact in the Spring condition compared to the No Spring condition [27.4º (SD 8.9º) and 25.4º (SD 8.4º) respectively, p<0.01] but underwent less flexion during stance [23.2º (SD 5.6º) Spring vs. 26.7º (SD 5.4º) No Spring, p=0.01]. There was no significant difference in ankle angle at ground contact or range of motion during stance (p>0.3).

SUMMARY/CONCLUSIONS

Subjects hopped at a greater frequency when wearing a brace with an elastic spring in parallel with the knee. Leg stiffness and total knee stiffness also increased, while biological knee stiffness decreased, presumably as a result of decreased knee extensor activation. These results indicate that an elastic lower-body exoskeleton could likely decrease the metabolic cost of locomotion with bouncing gaits.

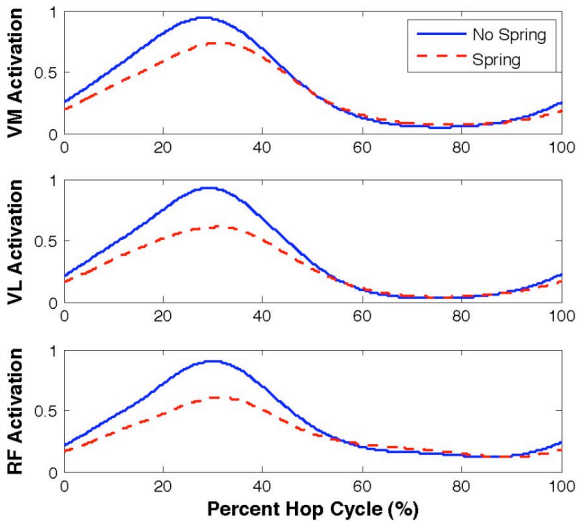

Figure 2: EMG muscle activation for major external knee extensors. Percent hop cycle begins at ground contact and ends at ground contact for the subsequent hop. VM – vastus medialis, VL – vastus lateralis, RF – rectus femoris.

REFERENCES

Ferris, D.P. and Farley, C.T. (1997). *J Appl Physiol*, **82**, 15-22.

Ferris, D.P., et al. (2006). *J Appl Physiol*, **100**, 163-170.

ACKNOWLEDGEMENTS

This research is supported by NSF BES-0347479 and an NSF Graduate Research Fellowship.

Table 1: Stiffness values for the leg, knee, and ankle. *Significant difference detected.

	No Spring	Spring	*p* Value
Leg Stiffness:	13400 ± 2800 N/m	14700 ± 2600 N/m	0.03*
Total Knee Stiffness:	9.8 ± 1.7 N·m/rad	12.0 ± 2.5 N·m/rad	0.01*
Biological Knee Stiffness:	9.8 ± 1.7 N·m/rad	8.3 ± 2.3 N·m/rad	0.03*
Ankle Stiffness:	6.0 ± 1.6 N·m/rad	5.6 ± 1.8 N·m/rad	0.19

STRESSES ON MOVABLE CORE AND LOADS ON FACETS ARE HIGHER BY IMPLANTING A CERVICAL ARTIFICIAL DISC PROSTHESIS AS COMPARED TO BONE GRAFTING FUSION TECHNIQUE – A FINITE ELEMENT MODEL STUDY

Mozammil Hussain [1], Raghu N. Natarajan [1,2], Gunnar B.J. Andersson [1], Howard S. An [1]

[1] Rush University Medical Center, Chicago, IL, USA
[2] University of Illinois at Chicago, Chicago, IL, USA
E-mail: hussmoz@iit.edu

INTRODUCTION

The fusion technique is a common procedure adopted by many surgeons in the treatment of various kinds of degenerative disc pathologies. It has been shown that the fusion grafting is good for decompressing the degenerative level and better fusion results are achieved at the expense of increased construct stiffness. At the same time, the increased flexibility and intra-discal pressures of the non-operated segments raised more concerns about the degeneration of adjacent levels. Recent advancements have shown that by using a movable core between endplates at the degenerative segment restores the motion, both at the operated and non-operated levels. Previous studies have compared the biomechanical response of the adjacent levels after fusion bone grafting and artificial disc placement showing better motion preservation by adopting the later technique. More in depth understanding is still required on the biomechanics of operated level that how the motion, stresses on the core and loads on the facets correlate with the stability of the surgical construct. Many investigators have emphasized the motion preservation by using the artificial disc but to the best of our knowledge, no study exists in the cervical spine literature showing the stresses on the movable core between the endplates and the load on the facets at the implanted level.

The objective of the present study was to compare the biomechanics of the operated level with bone grafting fusion and artificial disc prosthesis. The rotational motion, stresses on the implant, and loads on the articulating facets were studied.

METHODS

A three-dimensional finite element (FE) model of a C3-T1 segment of the cervical spine was developed from the CT scan of a 38-year old normal female subject. The intact model was previously validated with the published specimen studies. Three surgical models with the implant at C5-C6 level were developed from the intact model – discectomy with stand-alone graft, discectomy with anterior fixation, artificial disc prosthesis (movable core between endplates). The discectomy fusion was performed by using an inter-body graft. The discectomy with anterior fixation was built with the bone graft and stabilizing the anterior column with a plate (titanium) having rigid screw trajectory. The artificial disc prosthesis consisted of a movable core (polyethylene) between endplates (cobalt-chrome). The grafts were centrally placed covering up-to 50% endplate area. Two uni-cortical screws (titanium) each at the cephalad and caudal ends of the anterior plate were placed parallel to the endplates. The screws of 16 mm long with an outer and inner diameter of 3.5 and 2.5 mm were used. The artificial disc prosthesis was centrally placed with a diameter of 10 mm and

thickness of 4 mm. The material properties of the spinal structures and implants were adopted from the literature. The physiologic rotations based on literature data were prescribed on the C3 vertebra (flexion=45°, extension=35°, axial rotation=20°, lateral bending=25°). The inferior surface of the T1 vertebra was fixed. A constant pre-load of 73.6 N was applied using two isotropic truss elements connecting each of the lateral edges of the vertebral bodies to mimic the follower load technique. The analysis was performed using the commercially available FE code, ADINA.

RESULTS AND DISCUSSION

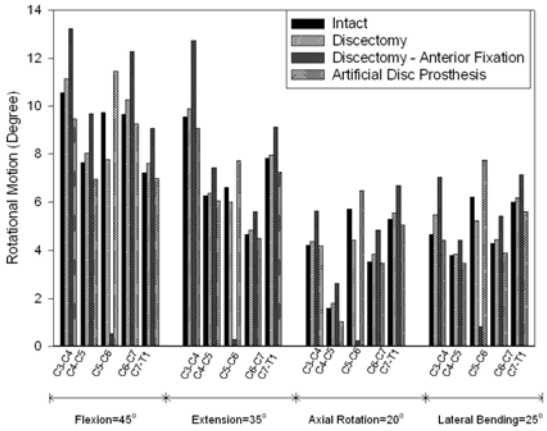

Figure 1: Inter-segmental rotational motion from C3 to T1 with bone grafting fusion (without and with anterior fixation) and artificial disc prosthesis at C5-C6 level

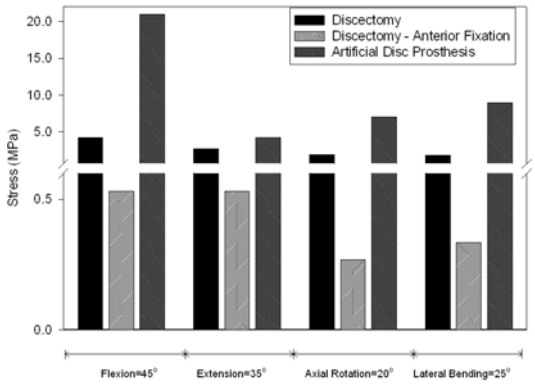

Figure 2: Stresses on the implant at C5-C6 level

The results of the present study showed a decrease in the motion of operated level and an increase in the motion of non-operated levels with fusion grafting (without and with anterior plate fixation) as compared to the intact case (Figure 1). When using the artificial disc prosthesis, an increased motion at the implanted level and a decreased motion at the adjacent segments were observed. The inter-segmental rotational motions of the model with artificial disc prosthesis were much closer to the intact values as compared to the models with bone graft. This finding agreed well with the previous studies in the literature.

Figure 2 shows the stresses on the implant – bone graft and polyethylene. The yield stress of the polyethylene is about 12-15 MPa. The stresses on the polyethylene core were too high (exceeding or close to the yield point) as compared to the stresses on the bone graft. Also, the loads on the facets at operated segment were found to be much higher by using the polyethylene core than bone graft. Furthermore, the stresses in the discs and loads on the facets of the adjacent segments were lower by implanting polyethylene core (values close to intact) as compared to the bone graft at C5-C6 level.

SUMMARY

The present study showed that even though the motion was preserved at all levels by using the artificial disc prosthesis than the traditional fusion grafting technique, the higher stresses on the core and loads on the facets at operated level could lead to further wear of core and degeneration of facets.

ACKNOWLEDGEMENTS

This study was supported by the Department of Orthopedic Surgery, Rush University Medical Center, Chicago, Illinois.

A HYBRID METHODOLOGY USING ULTRASONOGRAPHY AND MOTION ANALYSIS FOR ESTIMATION OF ACHILLES TENDON MOMENT ARMS *IN VIVO*

Justin D. Cowder, Nicole Chimera, Thomas S. Buchanan and Kurt Manal

University of Delaware, Department of Mechanical Engineering, Center for Biomedical Engineering Research, Newark, DE, USA
E-mail: manal@udel.edu, Web: www.cber.udel.edu

INTRODUCTION

Current techniques for computing musculotendon moment arms (MA) include the center of rotation and tendon excursion methods (Maganaris 2004; Ito et al., 2000). Both methods require an angular change in joint position and a change in musculotendon length or its line of action and thus require 4 measurements to compute the MA at a given joint angle. Errors associated with these measurements are difficult to ascertain when data are collected in vivo and therefore the effect of such errors on MA accuracy cannot be determined. One way to improve MA estimates is to reduce the number of measurements necessary to derive the MA. In this paper we present a hybrid methodology using ultrasonography and video-based motion analysis to estimate Achilles tendon moment arms for the ankle joint in the sagittal plane. Two values at each joint angle are needed to compute the MA. One is the spatial location of the joint center and the second is the distance from the transducer to the midline of the tendon. The technique was validated using an animal model and used to estimate Achilles tendon moment arm for a single subject in vivo.

METHOD

Overview: The sagittal plane MA for the Achilles tendon is the perpendicular distance from the ankle joint center (J) to the midline of the tendon (T) (see Figure 1). The joint center is assumed to lie at the mid-point between the medial and lateral malleoli. The spatial location of retro-reflective markers over the malleoli and 2 markers attached to the top of the ultrasound probe were tracked using a motion analysis system. The markers on the probe were used to define a line (V). The distance (P) from (J) to the perpendicular intersection with (V) was computed and the distance (L) to the distal wand marker was determined. The depth of the midline of the tendon (T) from the top of the sonogram was measured at a distance (L) from the distal edge of the image. The depth is depicted by (D) and is represented by the dashed portion of the line from (J) to (V). The moment arm is then:

$$MA = P - D - offset \ ,$$

where *offset* is a constant value from (V) to the recording surface of the transducer.

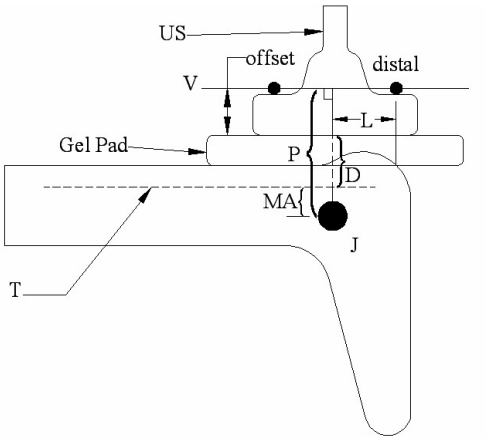

Figure 1: Ultrasound probe (US), joint center (J), tendon midline (T) and moment arm (MA). A gel standoff pad (G) was placed between the shank and the probe. See text for other label definitions.

Validation: A 6 camera Qualysis motion analyis system was used to record the position of markers attached to the medial and lateral malleoli of a lamb shank and markers on the US probe. Ultrasound images were acquired using a 60 mm linear transducer (Aloka SSD-5000, Tokyo, Japan) in B-mode setting at 10 MHz. A gel standoff pad was used to maximize coupling between the probe and the shank. Marker data and US images were synchronized using a contact switch fixed to the image save button on the US console. Five trials were collected and MAs were computed using the hybrid method (MA_{hybrid}). Additional trials were collected using a digitizing pointer as shown in Figure 2. The pointer was used to digitize the midline of the tendon on either side of the joint. The perpendicular distance between a line connecting the digitized points and the joint center is the sagittal plane moment arm ($MA_{measured}$) and was used to validate the MA_{hybrid} method.

Figure 2: Lamb shank with marker over lateral malleolus. Markers on pointer are used to digitize points on the tendon.

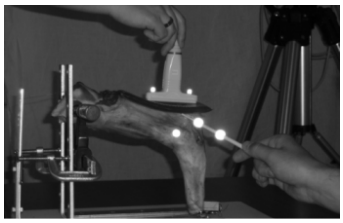

Figure 3: MA_{hybrid} setup with subject at rest in a neutral ankle angle. A Biodex was used to monitor joint angle.

***In Vivo* MA:** The hybrid method was used to estimate Achilles tendon MA for a single subject at rest and MVC with the ankle in maximum dorsiflexion (DF) and at a neutral angle. Two trials for each condition were collected. The experimental setup is seen in Figure 3.

RESULTS AND DISCUSSION

The average $MA_{measured}$ for the lamb specimen was 38.8 mm (SD = 0.05) and 37.5 mm (SD = 0.5) using the MA_{hybrid} method. This corresponds to a 3.3% difference. *In vivo* estimates of human Achilles tendon moment arm are listed in Table 1. The MAs were smaller with the ankle in a dorsiflexed position.

Table 1. *In vivo* Achilles tendon moment arms reported in millimeters (SD). The knee was in 115 degrees of flexion (Figure 3).

Ankle Angle	Rest	MVC
Neutral	36.5 (0.0)	39.0(0.7)
21° DF	34.5 (1.6)	35.1 (2.3)

SUMMARY/CONCLUSIONS

The hybrid method requires fewer error prone measurements than other techniques and therefore may be a more accurate estimate of Achilles tendon MA *in vivo*. Excellent agreement between the hybrid approach and measured values for the lamb shank was observed and therefore we conclude the method is accurate. Although our *in vivo* values were smaller than MAs reported by Maganaris et al., the values seem appropriate based on anthropometric measurements for our subject. Both *in vivo* studies showed a reduction in Achilles tendon moment arm with dorsiflexion.

REFERENCES

Maganaris, C.N. (2004). *Eur J Appl Physiol*, **91**, 130-139.

Ito, M. et al. (2000). *J. of Biomech*, **33**, 215-218.

ACKNOWLEDGEMENTS

NIH P20-RR16458 & R01AR048212

REFERENCE HAND CONFIGURATIONS DURING GRIP FORCE ADJUSTMENTS

Sun Wook Kim, Vladimir M. Zatsiorsky, Mark L. Latash
Penn State University, University Park, PA USA
E-mail: mll11@psu.edu

INTRODUCTION

Grip force shows feed-forward adjustments to expected changes in the load force during movement of hand-held objects (Johansson and Westling 1984). In particular, during vertical movement of a vertically oriented handle, a special role is played by the glabrous skin receptors, especially those of them that are responsible for the perception of tangential force and object slipping (Johansson and Westling 1984).

Following the equilibrium-point hypothesis, we view changes in the grip force as consequences of neural control signals that change reference hand configuration (Feldman and Levin 1995). Experimental observations of reference configurations have been elusive so far. The main purpose of this study has been to observe and characterize reference hand configurations during quick motion of a hand-hold object.

METHODS

Five healthy right-handed male and female volunteers participated in the experiment (on average, 27.6 years of age, 73 kg of weight, and 1.72 m of height).

An aluminum handle built of two horizontal bars and two vertical pillars was used in this study. Five six-component transducers (four Nano-17 and one Nano-25 ATI industrial Automation, Gerner, NC) were attached to the handle to measure the forces along three orthogonal axes and the moments of force about the center of the contact surface about the three axes (Fig. 1).

Four ProReflex cameras (Qualisys, Gothrnburg, Sweden), with the sampling frequency of 200 Hz were used to measure movement kinematics.

Spherical retro-reflective makers (3 mm in diameter) were attached to the dorsal aspects of identifiable and palpable surface landmarks such as the finger tip (FT), distal interphalangeal, proximal interphalangeal, and metacarphalangeal joints, styloid process of radius, styloid process of ulna, and at a point between the last two markers.

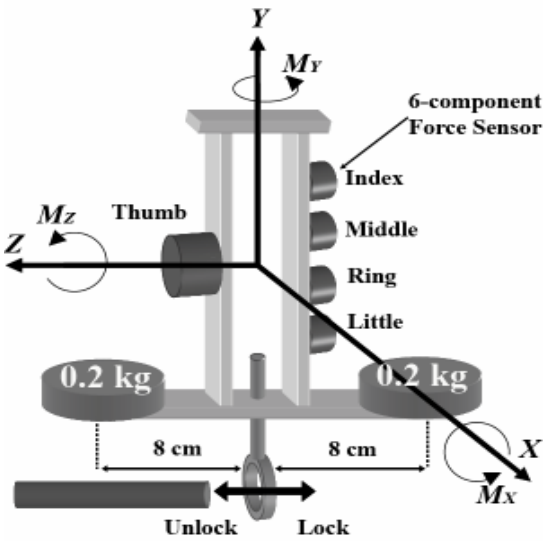

Figure 1: Experimental setup.

During the experiment, the subject sat on a chair and positioned the right forearm on the table. The tips of the digits were placed over the center of the sensors mounted on the handle. Two 0.2 kg loads were used, either placed symmetrically along the horizontal attachment to the handle or both loads on one of the two endpoints. The subjects were instructed to lift rapidly the handle up to a visually presented target in a self-paced manner. In

catch trials (on average, every 10-th trial), the handle could be locked to the table using a rod that the subject could not see or feel (Fig. 1). Prior to each trial, the subjects grasped the handle that rested on the table with the thumb normal force of 10 N. The subjects were instructed not to correct their hand action in cases of perturbations but "to let the hand move the way it wants".

In the transducer-centered reference frame, the grip force (normal force) was along the z-axis. The vertical (load) force was along the y-axis. The apparent stiffness was estimated as $K_{app} = \Delta F_Y / \Delta Y$ for each of the digit tips in the Y-direction.

RESULTS AND DISCUSSION

In regular trials, the subjects showed feed-forward changes in the grip force. In catch trials, when the subjects moved the handle with balanced loads, the hand overshot its target position and the digits flexed with the fingertips and the thumb tip moving towards each other. Figure 2 illustrates the trajectory of an unperturbed movement (thin solid), its acceleration (dashed), the grip force (thick, solid), and the grip force in a catch trial (dotted). In catch trials, the grip force dropped (the slip started) about 80-90 ms after the grip force change initiation and the hand movement started about 80 ms later than in non-catch trials.

The digit configuration in the catch trials was different for the unbalanced loads leading to hand rotation into pronation (when the load was to the right of the subject) and into supination (when the load was to the left). Apparent stiffness for all digits depended on the load location. It ranged from 0.24 to 1.86 N/m.

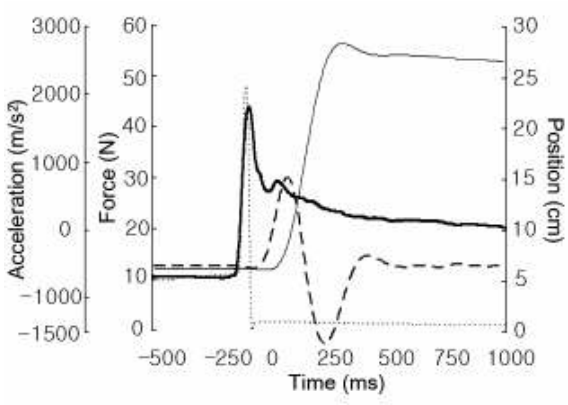

Figure 2: The trajectory of the handle in the vertical direction, its acceleration (dashed) and the grip force (normal thumb force).

SUMMARY/CONCLUSIONS

Grip force adjustments may be described using the framework of the equilibrium-point hypothesis as changes in the reference hand configuration. These changes may be observed and quantified experimentally. They depend on the external rotational moment of inertia and external torque.

REFERENCES

Johansson, R.S., Westling, G. (1984). *Exp Brain Res 56*: 20-30.

Feldman, A.G., Levin, M.F. (1995). *Behav Brain Sci . 18*: 723-806.

ACKNOWLEDGEMENTS

AG-018751, NS-035032, and AR-0485

EFFECT OF ORIENTATION ON FAILURE CRITERIA FOR LUMBAR S INE SEGMENTS

Naira Campbell-Kyureghyan, Sai Vikas Yalla, and David Burnett

University of Louisville, Louisville, KY, USA
E-mail: nhcamp01@louisville.edu

INTRODUCTION

Many studies have been performed to determine the compressive failure limits of spinal segments. The majority have used force as the criterion and the results show significant scatter from 1.5 kN to 10 kN (Chaffin, 1999). A number of factors are known to influence the failure strength including bone density, age, size, and orientation. The failure results are typically reported in non-normalized terms such as force or deformation, and the tests were virtually all performed without considering the orientation of the specimens. Although some recent studies have correctly orientated the segments (Lindsey, 2005), they did not compare the values to non-oriented test results. Stress distribution is affected by orientation (Campbell-Kyureghyan, 2005), but current biomechanical model failure limits are based on non-oriented test results. This study examines the failure behavior of lumbar spine segments under compression loading considering the effect of (1) spinal segment orientation; (2) normalization; and (3) a proposed new criterion of energy density.

METHODS

Motion segments, consisting of one intervetebral disc and the adjacent pair of vertebral bodies, were removed from four fresh intact lumbar spines (L_1-L_5) from human cadavers (3 males, 1 female, age range 58-71 years) with no spinal pathologies. Lumbar segments were DXA scanned from both the lateral and anteroposterior projections. Geometric properties of the vertebral bodies and the discs were measured and the segments were tested in accordance with a protocol approved by the institutional Human Tissue Committee.

During testing, the motion segments were orientated at either the neutral Harrison angle (normal standing human body posture – Table 1) (Harrison, 2001) or in-line axially (non-oriented).

T e 1: Harrison angles for lumbar region.

Level	Mean	SD	Level	Mean	SD
L1/L2	-1	6.3	L2/L3	-6.8	4.4
L3/L4	-10.9	4.5	L4/L5	-15.9	5.1

After a 15 minute static preload of 350 N, an axial compressive load was applied at a rate of 4 mm/hr. Force and axial deformation were collected at 100 Hz. Failure was determined by a drop in sustained force. The force and deformation were normalized to stress and strain values using the measured geometric properties.

RESULTS AND DISCUSSION

Results for force, stress, strain, energy, and energy density for both oriented and non-oriented specimens are reported in Table 2. Orientating the lumbar specimens in the neutral position decreased their failure force by 25%. Failure stress was also computed and the stress for lumbar segments oriented in the neutral position was 7% lower than in non-oriented segments, a statistically significant (80%CI) difference. Failure

strain was found to be 35% higher in the oriented segments.

Energy dissipation and energy density (normalized to disc volume) in the intervertebral disc were calculated. An average failure energy (SD) of 4769 (2318) KJ was found for the oriented specimens and 4054 (2516) KJ for the non-oriented specimens. The oriented segments had approximately 30% higher energy density at failure compared to the non-oriented segments.

Bone mineral density (BMD) ranged from 0.827 to 1.249. In agreement with previous research (Hansson, 1980) a linear correlation with failure force (R^2=.89) and stress (R^2=.88) were found. Interestingly, strain and energy density were not correlated with BMD. This is due to the influence of the disc response on these criteria.

SUMMARY CONCLUSIONS

Orienting the motion segment varies the distribution of forces and mode of deformation, and therefore failure. The oriented lumbar spine segments failed at lower force and stress than non-oriented specimens, while undergoing larger strains. One possible explanation of these results is that the non-oriented specimens had more contact in the posterior regions with the resulting bone-to-bone interaction leading to the higher forces and lower deformations.

The variability in *in i o* segment alignment may explain a portion of the subject specificity regarding injury tolerances and ignoring orientation when determining failure limits can lead to over prediction of lumbar spinal strength.

This study provides a clear indication of the effect of segment orientation on the failure properties. Application of reported failure values must consider the testing orientation. Normalization of the results removes the effects of specimen size and reduces the scatter in the data. In addition, normalized values are more easily compared between studies. Finally, energy density shows promise as a failure criterion and incorporates both force and deformation.

REFERENCES

Campbell-Kyureghyan, N.H. et al. (2005). *Clinical Bio echanics*, , 455-464.

Chaffin, D.B., et al. (2006). *ccupational Bio echanics.* John Wiley and Sons, Inc.

Hansson, T. et al. (1980). *pine*, **5**, 46-55.

Harrison DE., et al. (2001). *pine*, **6**, E235-42.

Lindsey, D.P. et al. (2005). *pine*, , 645-649.

ACKNOWLEDGEMENTS

This research was supported in part by a grant from the University of Louisville and the Department of Orthopedic Surgery.

T e : Mean (SD) of failure criteria for oriented and non-oriented lumbar spine segments.

	F r e N	**S re M**	**S r i**	**E erg**	**E erg De i**
Oriented	2.6 (0.7)	1.7 (0.5)	23 (11)	4769 (2318)	0.25 (0.14)
Non-Oriented	3.3 (1.4)	1.8 (0.5)	15 (1.1)	4054 (2516)	0.17 (0.05)

A BIOMECHANICAL COMPARISON OF AN ALL-LOCKED VS. HYBRID SCREW CONFIGURATION OF PROXIMAL TIBIAL PLATES

Chris Estes [1], Kristine R. Csavina[2] , David J. Jacofsky [1,2] , M. Wade Shrader[1,2]

[1] The CORE Institute, Sun City West, AZ, USA
[2] SHRI-CORE Orthopedic Research Labs, Sun City West, AZ, USA
E-mail: wade.shrader@thecoreinstitute.com, Web: www.thecoreinstitute.com

INTRODUCTION

Locking-plate technology has dramatically changed internal fixation techniques for many fractures. The locking plate technique has evolved from using all-locked screws with a non-anatomically contoured plate to a newer concept of using a "hybrid plate": a mixture of locked and AO-type non-locked screws with a more anatomically contoured plate. This construct permits the utilization of compression screws, which enhance fracture reduction and interfragmentary compression, while retaining the biomechanical advantages of locking screws. Studies have shown that hybrid plates allow the flexibility to use a compression technique for the simple fracture and fixed angle locking technique for comminuted portions (Messmer P, 2003; Gautier, 2003). Many theorize that the benefits of locked technology in conjunction with the benefits of traditional fixation will optimize construct strength.

However, despite the options a combination plate offers, it has been advised that different types of screws should not be used in the same fracture fragment (Perren, 2001). The biomechanics integral to compression and locking screw constructs produces an environment for either primary (endosteal) or secondary (enchondral) bone formation, respectively. The mixture of two different biomechanical principles into a single construct may not achieve the stability required for either type of healing (Egol, 2004).

Although the technique of combining screw types is increasingly more common in orthopedic practice today, no study to date has biomechanically compared the strength of hybrid plates to pure locking screw constructs. Therefore, the aim of this study was to compare the biomechanical properties of combination plates instrumented with an all-locked screw construct to a hybrid locked/non-locked screw configuration for simulated proximal tibia fractures.

METHODS

Specimen: Biomechanical testing was performed on five matched pairs of human tibias. Fresh tissue was vacuum-sealed, wrapped in saline-soaked towels, and stored at -20º C. Average age was 63.7 yrs (ranging from 47–78 yrs, all males).
Fracture Replication: A metaphyseal osteotomy was created to replicate a high energy proximal tibia fracture with medial bone loss (AO 41-A3.2).
Plate/Screw Instrumentation: Fractures were reduced and instrumented with the Peri-Loc proximal tibia plating system (Smith & Nephew, Memphis, TN). Tibia pairs were randomly assigned fixation constructs. Both constructs had 5.7mm locking screws in holes 1, 2, & 3 with 4.5mm locking cortex screws in holes 7, 9, & 11. The all-locked construct had locking cortex screws instrumented in hole 4 & 6, while the hybrid construct had non-locking cortex screws instrumented first to compress the plate to the bone. Hole 5 was located over the

osteotomy line and left open. All screws were sized and selected for bicortical purchase. The tibias were potted in a neutral position with Labstone (Dentsply, York, PA) in a stainless steel fixture.

Figure 1: Locked vs. Hybrid Plate

Loading: Loading tests were conducted using a uniaxial servo-hydraulic load frame (Shore Western, Monrovia, CA). The femoral interface consisted of the femoral condylar component of a total knee arthroplasty (TKA) prosthesis that rotated about an anterior-posterior axis to ensure symmetrical loading of the medial and lateral tibial condyles throughout the test. Vertical fracture site displacement was measured on the medial cortex with a cable-extension position transducer (Celesco, Chatsworth, CA), accurate to 0.02 millimeters.

Cyclic loading was used in order to measure irreversible (subsidence) and reversible (deflection) vertical displacement of the medial cortex relative to an applied load. Ascending maximal loads were applied and increased in step-wise fashion every tenth cycle. The F_{max} per load level began at 200 N and increased by 100 N increments; at 1000 N, the F_{max} was increased to 1200 N and each subsequent load was increased in 400 N increments until complete wedge gap closure or catastrophic failure. Each cycle was generated in a sinusoidal pattern at a rate of 0.5 Hz. All data were recorded at a rate of 500 Hz. The primary outcome measure was vertical subsidence and deflection at each axial load level. The subsidence was obtained from the peak displacement at the end of each resting period between load levels. Deflection was obtained from the maximum change in displacement within each cycle of load application.

RESULTS AND DISCUSSION

There was no difference in the bone mineral density in any of the tibia pairs ($p=0.45$). The all locked group showed a trend towards increased plastic deformation at failure (5.8 mm) when compared to the hybrid group (3.8 mm), (NS, $p=0.06$). There were no statistical differences in elastic or total deformation, or in varus collapse of the construct between the two groups.

SUMMARY/CONCLUSIONS

Since there were no differences in the deformation the plating constructs in a proximal tibia fracture model, this study suggests that the surgical technique of all-locked screws may be biomechanically equivalent to the hybrid screw concept. The introduction of combination screw plates has allowed the surgeon more freedom to utilize the unique biomechanical strengths of either non-locking or locking screws into the same construct. The combination of screws can be used to treat two different fractures with a single plate or to utilize the strengths of both screws in a single complex fracture.

REFERENCES

Messmer P, et al. (2003). *Ther Umsch.* **60(12)**,762-7.

Gautier E, Sommer C. (2003). *Injury*. **34(2)**, B63-76.

Perren SM. (2001). *Injury*. **32(2)**, B10-4.

Egol KA, et al. (2004). *J Orthop Trauma*. **18(8)**, 488-93.

LOW DIMENSIONAL MOTOR CONTROL AND MUSCLE SYNERGIES

Max Berniker [1] Emilio Bizzi [2], and Matthew Tresch [1]

[1] Northwestern University, Chcicago, IL, USA
[2] M.I.T., Cambridge, MA, USA
E-mail: mbernike@csail.mit.edu

INTRODUCTION

A number of recent studies have suggested that the central nervous system reduces the complexity of motor control by using a low dimensional control strategy. In this hypothesis, complex behavior results from the combination of a small number of 'muscle synergies'. Each muscle synergy specifies a particular balance of activation across a set of muscles, such that within a given synergy, the activation of muscles will covary. To produce movements, the CNS can simply specify the scaling and timing of these synergies, thereby greatly simplifying motor control.

Several questions regarding this hypothesis remain unclear. For example, why are particular muscles within a given synergy? More basically, can muscle synergies actually produce effective control of complex behaviors? The present study evaluates one principle for the specification of muscle synergies: that they are chosen to allow for the most effective control of the limb.

METHODS

All analyses are based on a physiologically realistic model of the frog hindlimb (Kargo et al. 2002). Our goal was to create a low dimensional representation of this high dimensional, non-linear dynamic system. This representation should capture the significant input-output dynamics of the system, i.e. it should succinctly summarize how control inputs are transformed into motor outputs. To find this representation we used a recently developed technique for empirical balancing for non-linear systems (Lall et al. 2002). This technique attempts to find a transformation from the original state, x (here a 17 dimensional vector consisting of hip and knee joint angles, joint velocities and 13 muscle activation states) to a reduced order state, z. With this transformation we can then find a reduced order model of the original system,

$$\left\{\begin{array}{c}\dot{x} = f(x,u)\\ y = g(x)\end{array}\right\} \Rightarrow \left\{\begin{array}{c}\dot{z} = A_k z + B_k u\\ \hat{y} = C_k z\end{array}\right\}$$

The equations to the left define the original high dimensional system, with state x, control input u, and output y. The equations to the right define the reduced order model with state z and estimated output, $\hat{y}$. The subscript k denotes the dimension of the reduced order system; here we consider k=6. Since the dimension of u (here 13, one motor command for each muscle) is greater than k, B_k has a null space. We can therefore define a set of low dimensional motor commands, analogous to muscle synergies. Further, since empirical balancing captures the significant dynamics of the original system, these synergies will be those that are most effective for controlling the frog hindlimb. To evaluate the performance of these synergies defined using empirical balancing (referred to BAL synergies), we compared them to a set of synergies defined according to a different principle. These synergies simply spanned the space of end point forces (referred to as FS synergies).

RESULTS AND DISCUSSION

We first found that the reduced order model of the frog hindlimb was able to capture the input-output dynamics very well, explaining more than 94.5% of the variance in limb trajectories. We then compared the MOR and FS synergies to those found experimentally a range of frog behaviors (Cheung et al. 2005). We found that each of the 6 MOR synergies was significantly correlated with at least one experimental synergy ($p < .05$). In contrast, only 3 of the 6 FS synergies were significantly correlated to an experimental synergy. The synergies used during natural behaviors are therefore similar to the synergies which are most effective for control.

We then evaluated whether these synergies could in fact be used to produce a range of behaviors. We considered 3 cases of control: using the MOR synergies, using the FS synergies, and using commands without restriction. This last case represents the best possible solution for the frog hindlimb. Commands for each case were found using optimal control techniques. An example movement for each case is shown in Figure 1. Although there were qualitative differences between some trajectories (see Fig. 1A), on average, both the MOR and FS synergies produced output trajectories close to the best possible (correlations of 0.99±0.02 and 0.96±.03, $p>.05$). However, the commands used to produce these trajectories were very different ($p < .01$; Fig. 1B). The commands found using the MOR synergies were very similar to the best case without restriction on commands (correlation of 0.89±.10), whereas the commands using the FS synergies were quite different (correlation of 0.51±0.15). As a consequence, the total control cost (a combination of trajectory error and control effort) was substantially higher when using the FS synergies ($p < .01$). On average, the ratio of MOR cost to optimal cost was 2.06±1.01, whereas for the FS synergies this ratio was 16.69±8.53. These results show that movements using MOR synergies allow for near optimal control. Further, this near optimal performance is not a feature of any set of synergies, but is a special aspect of the synergies identified according to the principle outlined here.

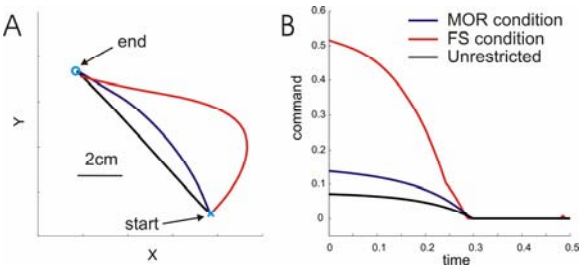

Figure 1. A. Example endpoint trajectories, starting at the x and ending on the circle. The three conditions are MOR (blue), FS (red) and unrestricted (black). B. Three muscle commands from the same movement.

CONCLUSIONS

These results suggest that the nervous system uses muscle synergies that allow for the most effective control of the limb. Such a strategy might allow for simplification of control while still allowing for a range of behaviors.

REFERENCES

Kargo et al. (2002) *J. of Exp. Biology*, 205, 1683-1702.
Lall et al. (2002) *Int. J. Robust and Nonlinear Control*, 12, 519-535.
Cheung et al. (2005) *J. Neuroscience*, 25, 6419-6434.

THREE-DIMENSIONAL HYPERELASTIC MODEL OF THE HUMAN KNEE: A PARAMETRIC SENSITIVITY STUDY

Qunli Sun and Yasin Dhaher

Northwestern University and Rehabilitation Institute of Chicago, Chicago, IL, USA
E-mail: y-dhaher@northwestern.edu

INTRODUCTION

Finite element (FE) models of articular joints have proven to be highly useful for understanding their functions in normal and pathological states. However, the degree to which the model accurately represents the complexity of a biological system is open to question. The accuracy of model predictions is a complex function of the accuracy of each component in the model (material properties, for example), and the importance of each component is likely to be dependent upon the use of the model. There are no general guidelines as to how each component of a model contributes to its accuracy during these uses. The goal of this study was to develop 3D and coupled hyperelastic FE model of human knee joint and investigate the effect of variations in material properties on the model-based predictions of the global (joint kinematics) and local (contact stresses and locations) mechanical variables.

METHODS

The articular geometries as well as the origin and insertion of muscles and ligaments were derived from digitized MRI images of a healthy subject and a 3D FE mesh was generated (Fig.1). The FE model included bones (femur, tibia, patella, and fibula) and major soft constraints (articular cartilages, quadriceps tendon, menisci, and patellar ligament (PL), anterior and posterior cruciate ligaments (ACL and PCL), medial and lateral collateral ligaments (MCL and LCL), and medial and lateral patellofemoral

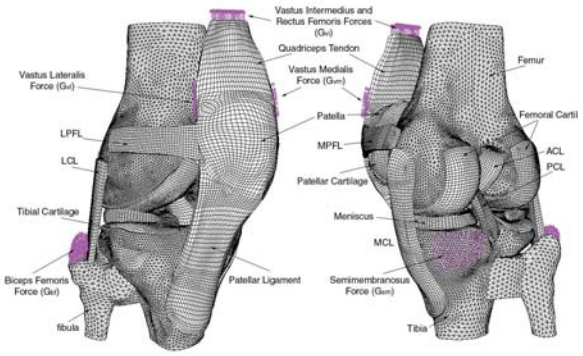

Fig.1 FE Model of the Knee

ligaments (MPFL and LPFL)). The bones were modeled as rigid bodies while the soft tissues were modeled as Neo-Hookean hyperelastic (ligaments and tendon) or linear elastic continuum (cartilages and menisci). Fifteen pairs of contact were set in the model. ABAQUS/Explicit formulation (ABAQUS 2004) was employed to solve the problem. In our simulations, the material parameters were assumed or estimated based on literature. Specifically, the Neo-Hookean parameter C_{10} of ligaments was assumed to take any value within their ranges in published data (for instance, 20.5~125.9 MPa for the patellar ligament). A targeted in vitro experimental data of joint mechanics (Wilson et al. 2000) were used to fine tune the FE model and identify the optimal set of material parameters. This was achieved using an in-house optimization technique that was integrated with ABAQUS. The FE model of the joint was exposed to loadings similar to the ones used in Wilson et al.'s study, namely, passive knee flexion.

Once an optimal set of parameters were identified, a parametric sensitivity study was conducted. In this study, we will present simulation outcomes resulting from changes

in the material properties of one of the passive tissues included in the model. Specifically, C_{10} of the patellar ligament was varied between + 30% to -30% of its optimal value. Simulations were conducted to illustrate the differential effect of varying material parametric on the estimates of the global and local variables.

RESULTS AND DISCUSSION

The optimal values of C_{10} were 24, 15, 22, 15, 65 MPa for ACL, PCL, MCL, LCL, and PL, respectively. The overall kinematics of the tibia was fairly in agreement with the experiment data when the optimal set of material parameters was employed in this model (Fig. 2).

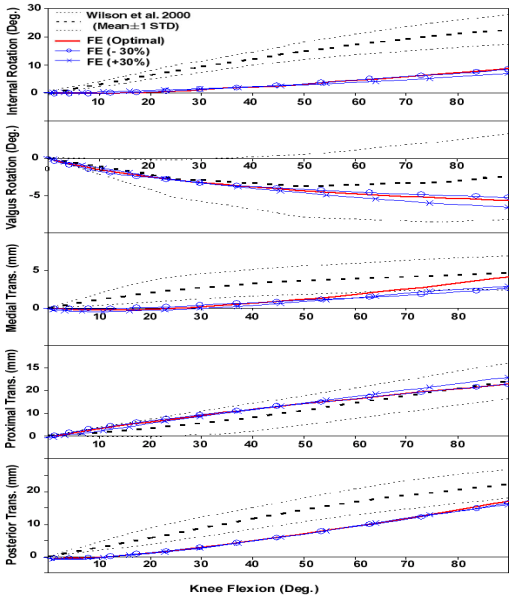

Fig. 2 Tibial movements: FE and experimental data. The ±30% in the figure represented the cases in which PL's C_{10} was increased or decreased by 30%

The sensitivity of the tibial motions to the material parameter C_{10} in the FE model was then examined. Our sensitivity analysis indicated that changes in the ligament stiffness in virtually did not significantly change the estimated global kinematics of the tibia-femoral joint during the passive flexion task (Fig. 2). Substantial changes were, however, observed in the local variables as defined in the stress levels in the meniscus and patellar cartilages during the same task (Fig. 3).

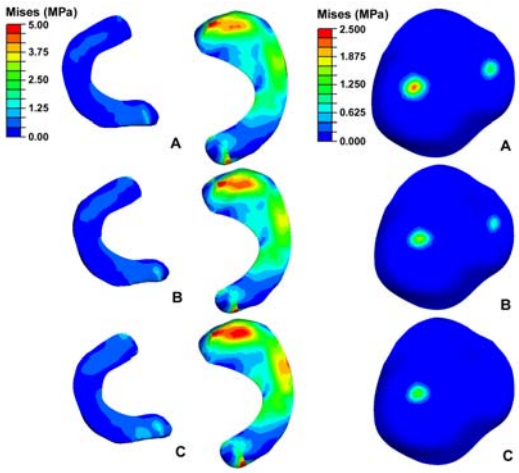

Fig. 3 Stress distribution of menisci (left) and patellar cartilage (right) at 20° flexion. B: Optimal parameter set was used. C and A: PL's C_{10} was varied by ±30%.

SUMMARY/CONCLUSIONS

A comprehensive 3D FE model of human knee joint was developed. The study has shown the feasibility of the model in predicting the global knee kinematics. Further efforts are being made to study the knee kinematics and local stress distribution with the FE model under various loads and muscle tone.

REFERENCES

ABAQUS (2004). ABAQUS Analysis User's Manual. ABAQUS, Inc.

Wilson, D. R. et al. (2000). J. Biomech. 33(4), 465-73.

ACKNOWLEDGEMENTS

This work was supported by the National Institute of Health (1-R01-AR049837-01).

MUSCULAR ACTIVATION DURING HOPPING TASKS: COMPARISON OF SURFACE VS. FINE-WIRE ACTIVATION PATTERNS

Nicole Chimera[1], Daniel Benoit[2], and Kurt Manal[1]

[1]Center for Biomedical Engineering Research, University of Delaware, Newark, DE
[2]School of Rehabilitation Sciences, University of Ottawa, Ottawa, ON
Email: chimera@udel.edu, web: http://www.cber.udel.edu/

INTRODUCTION

Neuromuscular activation strategies may provide the dynamic stability necessary to protect against ACL injury (Hewett et al., 1999). Walking and running are relatively simple tasks for many knee ligament injured patients. Because of the high demands of sport and an understanding of ACL injury mechanics, neuromuscular activation patterns during more strenuous tasks such as hopping may lend insight into joint stabilization strategies. When recording muscle activation patterns, surface electrodes are used more often than fine-wire; most likely due to the simplicity of use, little discomfort to patients, and fairly good reproducibility (Kadaba et al., 1985, Komi & Buskirk, 1970). There are characteristics of surface electrodes however that should be considered. For example, they sample from a larger tissue volume than fine-wire electrodes (Jacobsen et al., 1995). Additionally, muscle fibers may shift with respect to the skin/surface electrode with changes in joint angles (Farina et al., 2001). Thus, choice of electrode type may influence the timing and shape of the activation profile, especially during dynamic activities.

EMG is used during functional tasks to determine muscle onset and time to peak activation; two variables which may contribute to dynamic stability (Rudolph et al., 2001). Muscle onset and time to peak may be influenced by choice of electrode and therefore it is important to understand the influence electrode type has on these timing variables. Previous studies have shown that muscle activation patterns during manual muscle testing, walking and running are similar, and that timing measures are not different when using surface and wire electrodes (Perry et al., 1981; Jacobson et al., 1995).

However hopping tasks, reported to decrease the incidence of knee ligament injuries (Hewett et al., 1999), have yet to be considered. The purpose of this investigation was to compare surface and fine-wire neuromuscular activation patterns during hopping.

METHODS

Seven healthy male subjects participated in this study. EMG activity for the medial and lateral gastrocnemius, soleus, and tibialis anterior were collected using surface and fine-wire electrodes simultaneously while the subjects performed three walking, single leg hopping, and hop and stop (hopped, landing held) trials. The EMG signals were full-wave rectified and low pass filtered using a 4^{th} order Butterworth digital filter with a cut-off frequency of 6 Hz. Dynamic EMG data were normalized to the maximal activation recorded during isometric plantar flexion or dorsiflexion contractions using the surface or fine-wire EMG signals respectively.

Muscle onset was defined to occur when EMG activity reached 2.5 times above baseline. Correlation coefficients were used to evaluate similarity between surface and fine-wire muscle activation patterns, and paired t-tests to determine if onset and time to peak were significantly different when using surface and fine wire electrodes.

RESULTS AND DISCUSSION

No significant differences were detected in muscle activation onset (Table 1) or time to peak activity (Table 2). Furthermore, correlation analysis revealed that surface and fine-wire EMGs were highly correlated for most muscles and across tasks (Table 3). For walking, hopping, and hop and stop trials the surface and fine-wire electrodes exhibited

no differences in average muscular activation profiles and timing variables (Figure 1).

Table 1. Activation onset difference between surface and fine-wire electrodes. No statistical differences ($p > 0.05$) were detected.

	Gait (ms)	Hop (ms)	Hop Stop (ms)
Soleus	6*	6	4*
Med Gas	2*	1	5*
Lat Gas	4*	2	2
Ant Tib	0*	0	20*

"*" indicates onset detected by wire before surface

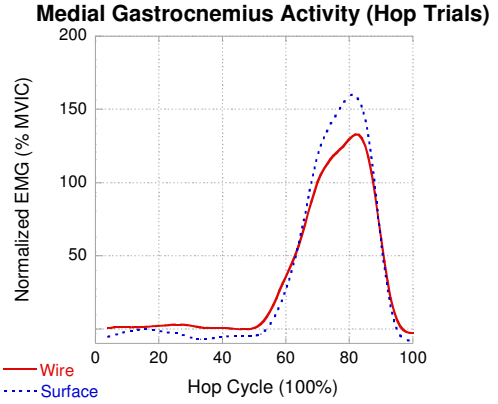

Figure 1: Representative subject's ensemble averaged surface and fine-wire electrode

SUMMARY/CONCLUSIONS:

During dynamic hopping tasks onset of muscle activation, time to peak muscle activation, and muscle activation patterns recorded using surface and fine-wire electrodes were similar. Thus, the use of non-invasive surface electrodes provides an adequate representation of timing variables for the muscles tested and the dynamic hopping tasks examined in this study. This suggests that surface electrodes can be used to determine these timing variables during hopping tasks and that making rehabilitation recommendations based on these variables may be appropriate.

Table 3. Averaged correlation coefficients for muscle activation patterns recorded using surface and fine-wire electrodes.

	Gait	Hop	Hop Stop
Soleus	.70	.86	.95
Med Gas	.96	.88	.88
Lat Gas	.76	.75	.82
Ant Tib	.87	.74	.80

REFERENCES

Hewett, T.E. et al. (1999). *Am J Sports Med*, **27(6)**, 699-705.

Farina, D. et al. (2001). *IEEE Eng Med Biol,* **20**, 62-71.

Jacobson, W.C. et al. (1995). *J. Electromyogr Kinesiol,* **5(1)**, 37-44.

Kadaba, M.P. et al. (1985). *J. Orthop Res,* **3**, 350-359.

Komi, P.V., Buskirk, E.R. (1970). *Electromyogr,* **4**, 357-367.

Perry, J. et al. (1981). *Phys Ther,* **61(1)**, 7-15.

Rudolph, et al. (2001). *Knee Surg Sports Traumatol Arthrosc*, **9**, 62-71.

ACKNOWLEDGEMENTS

NIH P20-RR16458

Table 2. Time to peak muscle activity detected by surface and fine-wire electrodes. P-value > 0.05 for all muscles and across all tasks.

	Gait (ms ± SD)		Hop (ms ± SD)		Hop Stop (ms ± SD)	
	Wire	Surface	Wire	Surface	Wire	Surface
Soleus	65 ± 5	62 ± 11	65 ± 6	60 ± 13	99 ± 0	99 ± 0
Med Gas	64 ± 3	66 ± 3	66 ± 6	63 ± 11	82 ± 5	98 ± 3
Lat Gas	55 ± 8	70 ± 4	68 ± 18	62 ± 13	98 ± 4	99 ± 0
Ant Tib	16 + 0	2 + 0	48 + 31	58 + 25	81 + 6	98 + 4

HAMMERING AND DART THROWING ARE KINEMATICALLY DIFFERENT

Patrick F Curran, Michael J Rainbow, Douglas C Moore, and Joseph J Crisco

Department of Orthopaedics, Brown Medical School/RI Hospital, Providence, RI, USA
E-mail: joseph_crisco@brown.edu

INTRODUCTION

Wrist motion is conventionally described in terms of flexion (F), extension (E), ulnar (U) and radial (R) deviation, based on the classical orthogonal anatomic planes. However, more often than not normal wrist motion involves combinations of these motions. One important combined motion involves movement of the wrist along a path from radial extension (RE) to ulnar flexion (UF). This oblique motion is generically referred to as the "dart thrower's motion" and is used for both physically demanding tasks and those that require fine motor control (Palmar 1985). Despite the apparent importance of this motion, it has received relatively little formal investigation.

This study was performed to quantify the range of motion (ROM) of the wrist during maximum flexion-extension (FE) and ulno-radial deviation (UR), and to investigate the functional coupling of wrist FE and UR during three tasks: dynamic hammering (DH), slow/static hammering (SH), and dart throwing (DT). We hypothesized that functional coupling of FE/UR occurs with these tasks, but that the degree of coupling would not differ amongst them.

METHODS

Acquisition

Eleven healthy male subjects (age = 26.3± 10.6 years) with no history of recent upper extremity injury were recruited after IRB approval and informed consent. Wrist motion was recorded using two small, state-of-the-art MTx inertial measurement units, or IMUs (Xsens Technologies B.V., Netherlands). The IMUs were tightly affixed to the subjects' dominant hands and distal forearms via custom-formed rigid splints (Orthoplast, DePuy International Inc., Raynham, MA). The output of the IMU motion sensors was sampled at100 Hz, combined, and stored to a PC using the Xsens Xbus Master software.

Each subject performed four trials of the following tasks:1) Maximum ROM in F, E and UR deviation, 2) DH: Three hammer strikes driving a 3" nail into a wooden block, 3) SH: Five slow, steady simulated hammering strikes, with the hammer moved parallel to a vertical reference plane, 4) DT: Six dart tosses at an eye level-mounted dartboard, 2.4 m away

Analysis

Raw data were converted to rotation matrices for analysis. Rotation of the hand (**H**) with respect to the distal forearm (**F**) was calculated in the IMUs' global coordinate system via

$$\mathbf{R}_{GCS} = \mathbf{F}_0\mathbf{F}_1^{-1}\mathbf{H}_1\mathbf{H}_0^{-1} \quad \text{(Neu 2001)}$$

Rotation in the global coordinate system **($\mathbf{R}_{GCS}$)** was transformed to motion in a wrist-based coordinate system ($\mathbf{R}_{JCS}$) using a similarity transform

$$\mathbf{R}_{JCS} = \mathbf{J}_{wr}^{-1}\,\mathbf{R}_{GCS}\,\mathbf{J}_{wr}$$

where $\mathbf{J}_{wr}$ is the vector description of the wrist-based coordinate system. $\mathbf{J}_{wr}$ was derived by: 1) averaging the F and E helical axes from the ROM trials, 2) crossing this average with the average of the R and U

axes, and 3) crossing this result with the average of the F and E helical axes:

$$\mathbf{J}_{wr} = [(\mathbf{n}_{FE} \times \mathbf{n}_{UR}) \ \mathbf{n}_{FE} \ \{(\mathbf{n}_{FE} \times \mathbf{n}_{UR}) \times \mathbf{n}_{FE}\}]$$

The strike portions of the paths of motion were analyzed and compared using a one-way repeated measures ANOVA to determine if the ROM in F, E, U, and R differed as a function of task DH, SH and DT. The back-swings were ignored. Differences in the functional coupling of FE and UR during each task were evaluated by comparing regression slopes.

RESULTS AND DISCUSSION

In all directions of wrist motion, there was significantly less ($P<0.01$) wrist ROM with dynamic hammering than with the dart throw (Fig. 1). Interestingly, during dynamic hammering the wrist remained extended, flexing on average $\leq 7^{o}$ of extension. The ROM during static hammering was greater than that during dynamic hammering (Fig. 1).

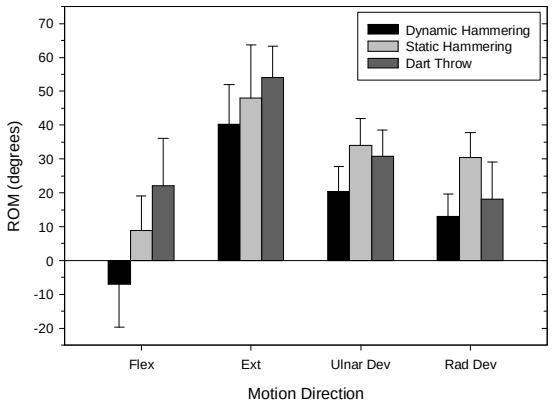

Figure 1. Wrist ROM with each task completed by n=11 subjects.

All directions of wrist motions were employed to accomplish each of the three evaluated tasks, with clear functional coupling between FE and UR (Fig. 2). Dynamic hammering involved nearly equal contributions of FE and UR (0.9 ± 0.3), with a linear RMSE of 3.8 ± 1.6º. On average, the dart throw involved significantly less UR deviation than FE (1.6 ± 0.7), and it also had a higher RMSE (9.05 ± 3.5º). FE and UR coupling during static hammering (0.7 ± 0.2) was similar to the coupling of dynamic hammering.

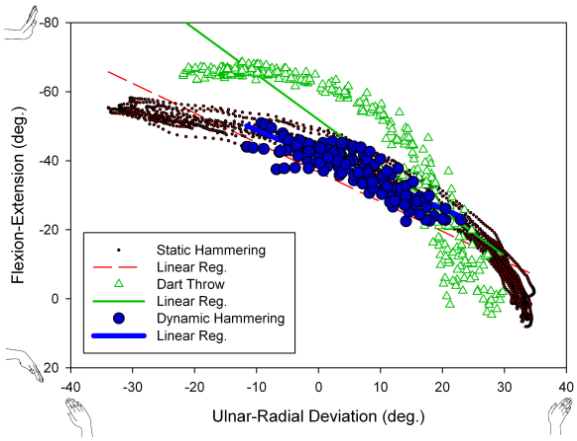

Fig 2. Wrist motion during each task consisted of coupled wrist motions.

SUMMARY/CONCLUSIONS

Dynamic hammering, static hammering and the dart throw employ combinations of flexion, extension, ulnar and radial deviation. Importantly, the amount of functional coupling for dynamic hammering was nearly 1:1, which was significantly differs from that of the dart throw, which was 1.6:1. This finding clearly demonstrates that the hammering and the dart throw are kinematically different tasks. Our finding that coupling is similar in static and dynamic hammering suggests that static positioning can be used to approximate dynamic hammering (e.g. for CT image-based analysis of wrist kinematics during hammering).

REFERENCES:

Palmer et al. (1985) J Hand Surg.[Am.], **10**, 39-46.
Neu et al. (2001). J Biomech, **34**, 1429-38.

ACKNOWLEDGEMENTS

Supported by NIH AR053648

PATIENT-SPECIFIC ORTHOPAEDIC SURGICAL PLANNING: IMAGE DATASETS TO FE MODELS

Srinivas C Tadepalli, Kiran H Shivanna, Vincent A Magnotta, Nicole M Grosland

The University of Iowa, Iowa city, IA, USA
E-mail: stadepal@engineering.uiowa.edu Web: www.ccad.uiowa.edu/mimx/

INTRODUCTION

Computational simulations of surgical procedures are of significant interest in orthopaedic-related research. Over the years, the finite element method has emerged as a viable means to determine the stresses and strains in implants and their interaction with the host bone. Very few surgical planning studies, however, have been performed on patient-/subject-specific models. Toward that goal, we have made advancements in automating the patient-specific bony geometry definitions from CT and/or MR image datasets and toward automating the development of corresponding patient-specific finite element (FE) mesh definitions via a custom-written software package, IA-FEMesh (Shivanna, 2006). The objective of this project is to advance these efforts by introducing tools to simulate a variety of surgical procedures, thereby interactively incorporating implants into such models. These models may then accommodate the implant under consideration. One day, such models may aid the surgeon in preoperative planning, ultimately resulting in an improved clinical outcome.

METHODS

As a proof of concept, the preoperative planning techniques are introduced in a proximal phalanx bone, representative of any long bone. Our procedure for FE mesh generation initiates with a source image set (i.e. CT and /or MR) and involves a series of interdependent steps initiating with image processing/segmentation, surface generation and identification, followed by the nodal/finite element definitions(Figure 1).

Once the 3D models of the bony structures are created, operative techniques such as a cut required of an osteotomy or the introduction of a drill hole to accommodate the insertion of a screw can be performed either at the level of 3D surface representation (to be meshed thereafter) or directly in the pre-meshed bone.

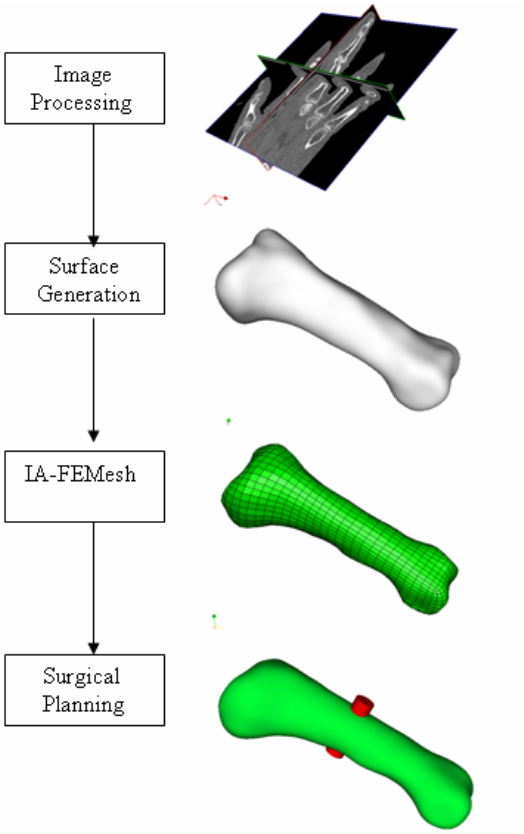

Figure 1: Model development Flow chart.

In the former method, the bony surface is clipped with a cylinder where the hole is to be created. Since the surface, by definition is hollow, we create a cylindrical surface joining the two circular contours bounding the through hole, thereby creating a cylindrical hole as shown in Figure 2b. Thereafter, the bounding box mesh definitions afforded by IA-FEMesh are used to create a mesh with a desired mesh seeding. In a pre-meshed bone, a cylindrical surface with the desired diameter is created and the elements inside the cylindrical surface are removed followed by a constrained smoothing operation. The operator has the ability to interactively position (i.e. translate and rotate) the cutting and drill guides prior to introducing the desired cut/hole.

RESULTS AND DISCUSSION

Figure 2 illustrates the resulting surface/ finite element models. These models provide orthopaedic surgeons a wide range of modeling tools for surgical planning.

SUMMARY/CONCLUSIONS

We have developed 3D models of proximal bone from CT/MR images. Hexahedral finite element meshes of these models are created automatically. The same methods can be extended to other parts of the body for patient specific analysis. In conclusion this method appears to be a feasible and practical tool for simulation and planning of difficult procedures commonly performed in orthopaedics. Further developments of the system are proceeding with the objective of automating the interactive preprocessing steps.

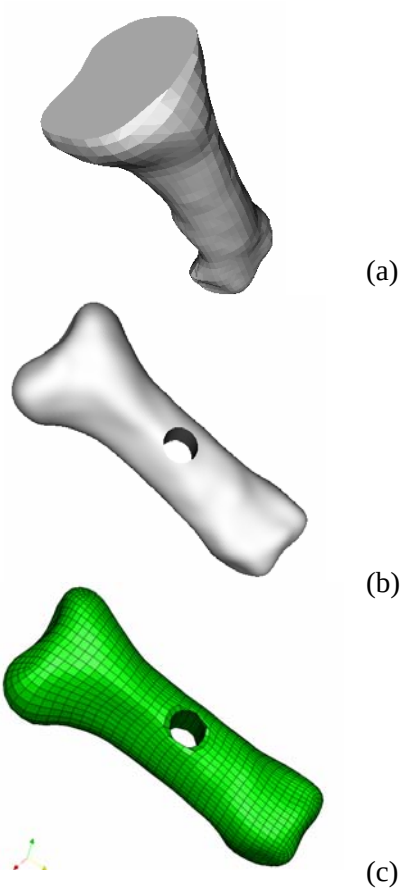

Figure 2: Surgical preparation procedures (a) simulated osteotomy and a drill hole introduced (b) in the surface, and (c) in the meshed model.

REFERENCES

Shivanna K.H., *et al*. (2006) Automating patient-specific finite element model development. 9th MICCAI Conference.

REFINEMENTS IN MODELING THE MECHANICAL PROPERTIES OF LARYNGEAL SOFT TISSUE

Eric J. Hunter [1], and Ingo R. Titze[1,2]

[1] National Center for Voice and Speech, Denver, Colorado, USA
[2] NCVS, Dept. Speech Pathology and Audiology, University of Iowa, Iowa City, IA, USA

E-mail: ehunter@dcpa.org; www.ncvs.org

INTRODUCTION

Significant advances have occurred in our understanding of the structure and function of the human laryngeal system, whose main functions are airway protection, respiration, and phonation. Nevertheless, there is still much to learn and apply; for this to happen, the composition of the larynx (geometry and properties) must be accurately defined. Of particular importance are the vocal folds, the primary sound generator of the human voice, as well as a source of airway protection.

The kinetics of the vocal folds can be classified into two parts; vocal fold vibration with (small and relatively fast deformations at 100 – 1000 Hz or more) and vocal fold posturing (large and relatively slow deformations at frequencies of <1 – 10 Hz which occurs when the vocal folds are positioned for prephonation, pitch change, inhalation, and airway closure). Vocal fold posturing is powered primarily by the laryngeal muscles, with passive contributions by the vocal ligament, laryngeal muscles not in contraction, and surrounding cartilages and joints.

The purposes of this report were to measure more accurately and quantify in greater detail the passive properties of the canine LCA, IA, and PCA by using Titze's adaptation of the Kelvin model (Titze, 1996, Hunter, 2004). New details of the hysteresis of the vocal ligament's stress-strain curve were also presented. A summary of all five intrinsic laryngeal muscles (using canine tissues), in addition to the human vocal ligament and mucosa, was given in terms of the tissue model parameters. This paper then provides the mathematical model and parameters to simulate the dynamic longitudinal stress-strain response of the five laryngeal muscles, vocal ligament, and vocal fold mucosa.

METHODS

The tissue data used in the current study was collected as part of several previous experiments on human and canine laryngeal tissue conducted at the National Center for Voice and Speech at the University of Iowa (Alipour, 2005, Min, 1995). To obtain the passive properties of the tissues, samples were stretched and released by applying a 1-Hz sinusoidal signal (approximating the rate of vocal fold posturing and similar to other comparable studies). Sample freshness was maintained in a warmed, oxygenated, Krebs-Ringer solution.

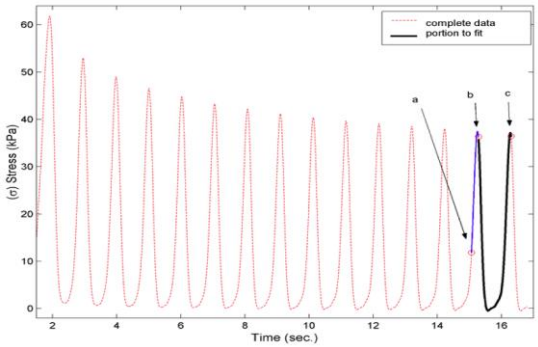

Figure 1. Stress from a sinusoidal (1 Hz) elongation of a PCA muscle. Stress in time

with the solid line between Points **b** and **c** is the portion of the data modeled.

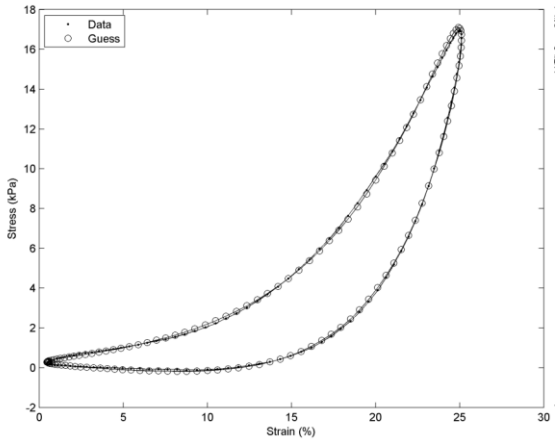

Figure 2. A good fit of the model to stress-strain data from a PCA muscle. Notice that there is little difference between the data points (dots) and the modeled stress (circles).

Stress-strain data from fifteen canine laryngeal muscle samples and eight human vocal ligaments were used to find parameters of a modified Kelvin model; a bounded Nelder and Mead Simplex method was the technique used to fit the parameters.

RESULTS AND DISCUSSION

Parameter optimization was used to obtain parameter values. As the modified Kelvin model was nonlinear, average parameter results are not always useful; therefore, a method of obtaining mean stress curve parameters was used to get the most representative parameters.

SUMMARY/CONCLUSIONS

Passive parameters of the modified Kelvin model were summarized for the vocal ligament, mucosa and all five laryngeal muscles. Results suggest that the LCA, PCA and IA muscles are functionally different from the TA and CT muscles in their load-bearing capacity. Further, the LCA, PCA and IA have a much larger stress-strain hysteresis effect than has been previously reported for the TA and CT or the vocal ligament. The variation in this effect suggests that the connective tissue within the TA and CT muscles is somehow similar to the vocal ligament but different from the LCA, PCA or IA muscles. The grouping of abductor/adductor muscles vs. pitch control muscles is in general agreement with the histology and muscle fiber-type found in the laryngeal muscles where abductor and adductor muscles are described as "allotypically different" and "kinetically faster than the fastest limb myosin heavy chain". Further demonstrating the potential significance of grouping tissues in the laryngeal system by functional groups was the unique finding that, over their working elongation range, the LCA and PCA were nearly as exponentially stiff as the vocal ligament (in the healthy functional range of each tissue). Finally, from the optimized parameters and related information, have helped increment the ability to apply this knowledge to realistic laryngeal models using computational simulations and laboratory experiments.

REFERENCES

Titze IR. (1996). In: *Vocal fold physiology: controlling complexity and chaos*, Singular Publishing Group. 47-62.

Hunter EJ, Titze IR, Alipour F. (2004). *J Acoust Soc Am* **115**: 1747-1759.

Alipour F, Titze IR, Hunter EJ, Tayama N. (2005). *J Voice* 19: 350-359, 2005.

Min YB, Titze IR and Alipour-Haghighi F. (1995). *Ann Otol Rhinol Laryngol* **104**: 563-569.

ACKNOWLEDGEMENTS

Muscle data was collected with support from DC004347 (NIDCD). The analysis and modeling were conducted also supported by the NIDCD (DC006801).

ASSESSMENT OF FUNCTION OF AN ORTHOTIC BRACE CONTROL MECHANISM

Peter M. Quesada [1], Stephen C. Anderson [1], Jessica Hagan [1],
William P. Hnat [1], John H. Lilly [2], and Kenneth A. Mook [3]

[1] Dept. of Mechanical Engineering, University of Louisville, Louisville, KY, USA,
[2] Dept. of Electrical and Computer Engineering, [3] Div. of Physical Medicine and Rehab.
E-mail: peter.quesada@louisville.edu

INTRODUCTION

Low load prolonged stretch (LLPS), in a number of forms, has been applied to manage muscle contractures associated with spasticity and hypertonia. Such musculo-skeletal complications can stem from acute onset and chronic pathologies including cerebral vascular accident, traumatic brain injury, cerebral palsy and others (Yarkony & Sahgal 1987, Roper 1987). Contractures associated with spasticity and hypertonia can dramatically impair function, and substantially detract from quality of life.

Many LLPS devices have the form of a flexible orthotic brace. These devices employ passive elastic components that generate restorative load, which increases as deformation increases. No currently available orthotic braces, for applying LLPS, employ any control mechanisms that adapt dynamically to an individual wearer.

Pneumatic muscle actuators (PMAs) can generate active load and exhibit variable elastic behavior. These PMA characteristics can be readily modified by changing their air pressure. The investigators have incorporated PMAs in a prototype orthotic LLPS device, and have developed a control mechanism that is intended to dynamically adapt the device to the wearer.

The aim of this work was to assess the function of the prototype orthotic brace control mechanism. The device's control mechanism was evaluated with respect to its ability to switch appropriately between an operating mode that controls joint position and a mode that controls PMA load. The device should engage joint position control mode when a spastic activity event is not occurring, and it should switch to joint load control mode during a spastic activity event. This study used healthy participants, in whom muscle spasticity was simulated, to determine whether the control mechanism appropriately switches between modes.

METHODS

Ten healthy individuals participated in this investigation. Subjects were healthy adults with no muscle spasticity or hypertonia. Electrode patches were placed on the skin surface above the biceps muscle of each subject. The prototype orthotic brace was then placed on each subject's arm, such that upper and lower arms were each contained in one of the braces two segments, and such that the elbow joint was aligned with the joint connecting the brace segments.

After the brace was placed, the desired brace position was set to 15º of flexion, and the control mechanism was engaged in joint position control mode. A small battery-operated TENS device was used to deliver electrical stimulation through the electrodes, in order to cause the elbow flexor muscles to contract. This action simulated occurrences of a spastic muscle activity event.

During simulated episodes of spastic muscle activity, joint position, pneumatic muscle

actuator tension and pneumatic muscle air pressure were collected with a 12 bit data acquisition card (Daqcard-6062E; National Instruments). This card also provided analog output, through which the control system functions were performed.

Recorded data were used to determine whether, during simulated spastic activity events, the control mechanism appropriately switched to load control mode, and whether it appropriately switched back to joint position control mode when electrical stimulation ended. The cycle of turning electrical stimulation on and off was repeated approximately 10 times per subject.

RESULTS AND DISCUSSION

The results shown in Figures 1 & 2 were typical across subjects. Upon initially establishing a reference angle for the joint position control mode the device achieved the desired joint position within 2 seconds (Figure 1). The upper threshold for switchover from position to force control mode was set at 23 lbs, while the lower switchover threshold was set at 20 lbs. This threshold difference mitigated unwarranted oscillation between modes.

Upon initiation of a simulated episode of spastic activity, the pneumatic muscle actuator tension increased until the upper threshold was crossed (Figure 2). The device then successfully transitioned into force control mode, and the pneumatic muscle actuator tension remained near the upper threshold. Joint angle was permitted to increase during this mode. Upon termination of the episode, PMA tension decreased below the lower threshold, and position control mode was re-initiated. It was noted that joint angle tracking between simulated episodes was somewhat less consistent. It was thought that this result was due to the subjects being healthy and not actually having a true baseline of joint contracture.

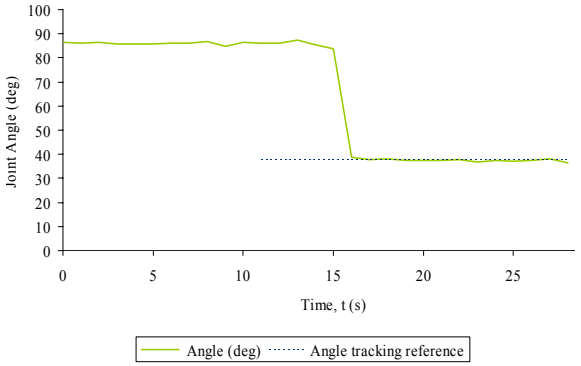

Figure 1. Joint position at initiation of position control mode for a typical subject.

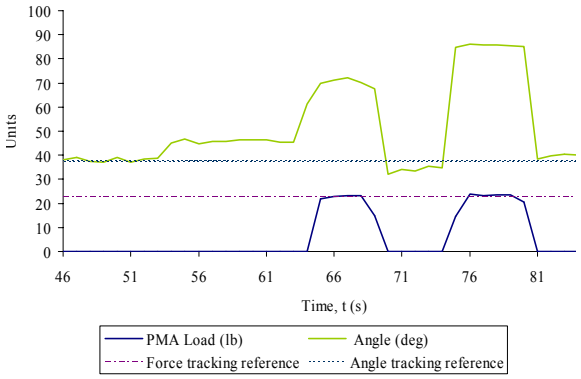

Figure 2. Joint position and PMA load during simulated episodes of spastic activity.

SUMMARY/CONCLUSIONS

The control mechanism was determined to function in the manner that was intended. Consequently, it was further determined to proceed to actual patient testing with the prototype orthotic device.

REFERENCES

Roper B.A. (1987). *Clin. Orthop.* 219:78-86.
Yarkony G.M., Sahgal, V, (1987). *Clin. Orthop.* 219:93-96.

ACKNOWLEDGEMENTS

Work was supported by NSF (#0503117).

The Effect of Screw Diameter on a Lateral Tibial Plateau Fracture: A Comparison of 4.0mm vs. 6.5mm Cannulated Screws

Anjali Gupta[2], M. Wade Shrader[1,2], Kristine Csavina[2], David J. Jacofsky[1,2]

[1] The CORE Institute, Sun City West, AZ, USA
[2] SHRI-CORE Orthopedic Research Labs, Sun City West, AZ, USA
E-mail: wade.shrader@thecoreinstitute.com, Web: www.thecoreinstitute.com

INTRODUCTION

Tibial plateau fractures represent about 1% and comprise 8% of fractures in the elderly (Cooper, 2002). These fractures more commonly affect the lateral plateau, accounting for about 70% to 80%, in comparison to a 10% to 23% fracture rate of the medial plateau (Koval, 2002). Few studies have evaluated lag screw fixation on the Type I split fracture. A few studies on this fracture showed that the addition of a third screw (Koval, 1996, Parker,1999) or a buttress plate (Koval, 1996) did not offer further advantage in stabilizing the fracture.

Clinically larger screw diameters are used for treatment though smaller diameter screws make for easier placement at the tibial plateau. Orthopedic surgeons prefer the smaller diameter screws especially when plating the fracture. The purpose of this study was to evaluate the failure loads of two 4.0mm cannulated screws compared with two 6.5mm cannulated screws.

METHODS

Samples: Seven unembalmed, matched pairs of human tibias were thawed to room temperature and kept moist with constant saline solution throughout preparation and testing. Prior to testing, specimens were dual-energy x-ray absorptiometry (DEXA) scanned for bone mineral density to assure density correlation within matched pairs. The fractures were created at approximately 22.5 degrees off the vertical plane starting at the most medial portion of the lateral plateau.

Screw Instrumentation: All tibia pairs were reduced by one orthopedic surgeon and randomly assigned an internal fixation technique of either two 4.0mm cannulated screws or two 6.5mm cannulated screws. A Peri-Loc proximal tibia plate (Smith & Nephew, Memphis, Tennessee) was placed against the lateral aspect of the proximal tibia to approximate the insertion of the lag screws. This area was first marked onto the surface of the bone, secured with a K-wire, and finally fixated with the cannulated screws. The tibias were potted in Labstone (Dentsply, York, Pennsylvania) and positioned upright with the long axis of the bone vertical in both the antero-posterior and lateral plane similar to Parker et.al. (Parker,1999).

Loading: Axial loading tests were conducted using a uniaxial servo-hydraulic load frame (Dynamic Testing Systems, Phoenix, Arizona). To ensure symmetrical loading and to more closely represent physiological conditions, a femoral component of a total knee prosthesis was used to load the tibial plateau (Karunakar MA, 2002). Fracture site displacement was measured with a cable-extension position transducer (Celesco, Chatsworth, California), accurate to 0.02 millimeters, positioned along the vertical. An axial preload of 50N was applied to the tibia to stabilize the construct, and then a load of 25N/s was applied to the lateral plateau until

clinical failure, defined as displacement greater than 2mm.

RESULTS AND DISCUSSION

No significant differences were noted in the bone mineral density or tibial plateau widths of the paired tibias. The average failure strength of the tibias instrumented with two 4.0mm cannulated screws was 1243 ± 516 N while the average load for those instrumented with two 6.5mm cannulated screws was 1876 ± 762 N. The Wilcoxon signed pairs test showed a p=0.091 indicating that there was no statistical significance between the two fixation types.

The stiffness was also calculated using linear regression on the most linear portion of the failure strength vs. displacement graphs for each tibia. The average and standard deviations for the stiffness of the tibias fixated with 6.5mm and 4.0mm were 969 ± 389 N/mm and 545 ± 227 N/mm, respectively. There was no statistical significance in the stiffness between the two screw sizes. The small sample size of this study may have contributed to the variability in the data. Additionally, no correlation was found between the load at failure, stiffness and bone mineral density. Radiographs taken after tibial loading indicated that the screws did not exhibit bending or pull-out.

The average body weight taken from an older population in another study at the SHRI-CORE labs was 175 lbs. Using this weight, walking loads were estimated at 940N (1.2 time body weight). Average failure loads of the two 4.0mm cannulated screws, approximately 1240 N, were greater than this estimated average load at walking, though two individual tibia failed below 940N and one failed at 990N. All of 6.5mm instrumented tibias failed well above 940N. Since patients may not be compliant with non-weight bearing instructions during early fracture healing, patient weight and activity level should be considered when selecting screw size. Additional testing should include additional tibia pairs and fatigue testing to determine early loosening of the screws.

SUMMARY/CONCLUSIONS

The purpose of this study was to evaluate and compare the failure loads of two 4.0mm and two 6.5 mm cannulated screws used in reducing a lateral tibial plateau fracture. No statistical difference was found in failure loads when specimens were under a ramped loading condition. This study suggests that 4.0mm screws should be considered for lateral plateau fracture fixation since the average failure load for these screws was above the average walking loads. Patient's weight and adherence to standard clinical management should be considered.

REFERENCES

Cooper HJ, et al. (2002). *Bull Hosp Joint Dis* **60**, 72-75.

Koval KJ, Zuckerman JD (2002). *Lower extremity fractures and dislocations. Handbook of Fractures.* Springer.

Koval KJ, et al. (1996). *J Orthop Trauma* **10**, 304-308.

Parker PJ, et al. (1999) *J Bone Joint Surg [Br]* **81B**, 478-480.

Karunakar MA, et al. (2002). *J Orthop Trauma* **16**, 172-177.

SURGICAL RECESSION OF THE GASTROCNEMIUS FOR ISOLATED CONTRACTURE: A CASE STUDY

Nicole Chimera[1], Michael Castro[2] & Kurt Manal[1]

[1]University of Delaware, Department of Mechanical Engineering, Center for Biomedical Engineering Research, Newark, DE, USA
[2]Pennsylvania Orthopaedic Foot & Ankle Surgeons, Philadelphia PA.

E-mail: manal@udel.edu, Web: www.cber.udel.edu

INTRODUCTION

The inability to achieve normal ankle dorsiflexion is known as equinus. Isolated gastrocnemius contracture (IGC) is an equinus in which there is normal ankle dorsiflexion with the knee flexed however there is less then a 5° (DiGiovanni, 2002) or 10° (DiDomenico, 2005) of dorsiflexion with the knee fully extended. The inability to achieve normal dorsiflexion during the stance phase of gait can result in early heel-rise and may be associated with elevated fore-foot pressure (Hill, 1995); which may provide insight into why decreased ankle dorsiflexion range of motion is associated with numerous foot injuries (DiGiovanni et al, 2002). Surgical intervention may be indicated if conservative treatment fails to resolve gastrocnemius tightness and symptoms persist. One surgical option is the Strayer procedure (gastrocnemius recession) which involves division of the gastrocnemius tendon distal to the muscle bellies. We are unaware of any study reporting quantitative biomechanical analysis of pre- and post- gastrocnemius recession for treatment of IGC in neurologically intact subjects. The purpose of this case study is to report kinematic and foot pressure measurements pre and post-operatively for a healthy, active 62 year old female subject clinically diagnosed with bi-lateral ICG.

METHODS

The subject participated in two data collections. The first collection took place one week prior to surgery and the second approximately 3 months following right gastrocnemius recession. Motion analysis data were collected pre and post operatively and foot pressure recordings for the right and left feet were sampled post-op.

Kinematics: A 7 camera Qualisys motion analysis system was used to track markers attached to the right foot, shank and thigh of the subject. The subject performed 5 walking trials at a self selected speed. Marker trajectories were sampled at 100 Hz and filtered using a 4th order Butterworth digital filter with a low-pass cut-off frequency of 6 Hz. Joint kinematics were computed using Visual3D. The interval of interest was limited to the stance phase of gait. The same tester applied the markers pre and post-operatively to minimize potential differences due to marker placement.

Foot Pressure Recordings: Foot pressures were measured using a high-resolution pressure mat (Tekscan Inc.). Five walking trials at a self-selected speed were collected for the right and left feet. Foot pressures were sampled at 50 Hz and stored for later analysis. Left foot data were collected and used as a surrogate for the right foot prior to surgery. Note the patient had IGC of the left leg at the time of testing. The surrogate data may actually be a conservative estimate of right foot loading because the right

gastrocnemius was the tighter of the two prior to surgery.

RESULTS AND DISCUSSION

The patient had a 15 degree increase in dorsiflexion range of motion upon clinical examination following surgery. This increase is similar to an 18 degree gain reported by Pinney et al., (2002). Figure 1 shows that the clinically observed increase in dorsiflexion was used during walking.

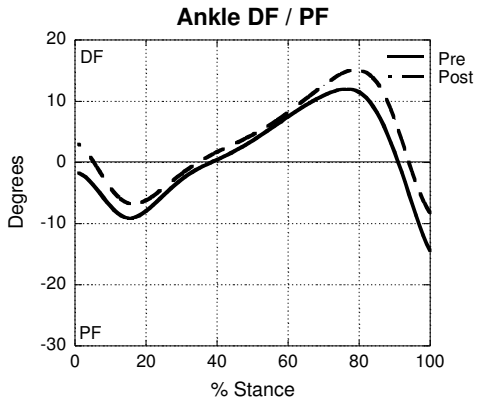

Figure 1. Ankle joint angle pre and post surgery. Note the subject had greater dorsiflexion (DF) post-op.

The foot pressure findings were consistent with our a priori expectation that left gastrocnemius tightness would result in early heel rise. Recall the subject had left gastrocnemius tightness at the time of testing. The left heel rose 12% of stance earlier than the right foot after gastrocnemius recession (Figure 2). The right and left pressure maps were temporally-aligned so that both feet in the image were at the same percentage of stance. The left heel lifted off the ground at 65% of stance and the right at 77%. Stance duration for the right and left feet were almost identical.

SUMMARY/CONCLUSIONS

The gastrocnemius is a two-joint muscle and when tight cannot accommodate normal

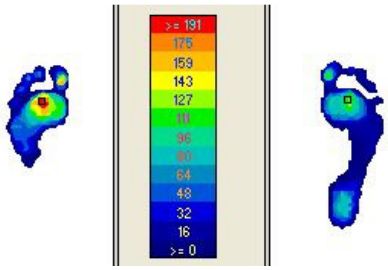

Figure 2. Right and left foot pressures at 65% of stance. Note the elevated fore-foot pressure on the left side.

knee extension and dorsiflexion during mid to late stance. Subjects with IGC lift the heel off the ground early to compensate for loss of ankle dorsiflexion. Early heel rise will cause the forefoot to be loaded for a greater proportion of stance resulting in elevated plantar pressures. This chain of events was exhibited by our subject. The patient reported her outcome as excellent with no foot pain on the right side during activities that were painful pre-surgery. She has elected for left gastrocnemius recession and we will continue to follow her progress. Gastrocnemius recession improves patient function, normalizes joint kinematics and reduces forefoot pressure. Gastrocnemius recession may be a consideration for patients with chronic, non-healing mid- and forefoot ulcers secondary to diabetic neuropathy. This will be the focus of future work.

REFERENCES

DiDomenico, L.A., et al. (2005). *J Am Podiatr Med Assoc,* **95(4):** 410-413.
DiGiovanni, C. W., et al. (2001). *J Rehabil Res Dev,* **38(3):** 335-340.
Hill, R. S. (1995). *J Am Podiatr Med Assoc,* **85(6):** 295-300.
Pinney, S. J., et al. (2002). *Foot Ankle Int,* **23(1):** 26-29.

ACKNOWLEDGEMENTS

NIH P20-RR16458

ASYMMETRY OF WHEELCHAIR PUSHRIM BIOMECHANICS OVER VARYING SURFACES

Melissa M.B. Morrow, Kai-Nan An, and Kenton R. Kaufman

Mayo Clinic College of Medicine, Department of Orthopedic Research, Rochester, MN, USA
E-mail: Kaufman.Kenton@mayo.edu

INTRODUCTION

The association between wheelchair use and upper extremity injuries has been recognized as a significant issue for many years. Despite that fact, our basic understanding of wheelchair propulsion has been restricted by technological limits to the rather artificial setting of the laboratory.

Technological advancements have improved the ability to collect and analyze the biomechanics of wheelchair propulsion. Past studies have used a variety of stationary systems to simulate propulsion. While useful, these systems have a distinct disadvantage in that the user is not subjected to the types of surfaces that are usually traversed during activities of daily living, most notably sidewalk cross-slopes in the outdoor environment.

As studies expand to include the users' natural environment, it will be important to document if there are any differences in biomechanical variables collected between the left and right wheels. This is especially true in the outdoor environment where we expect users to be more asymmetrical in their propulsion due to the unevenness of surfaces. There has been no study published that has focused on this issue. We hypothesize that the force variables will not differ significantly between the wheels during collection over indoor level surfaces, but will differ when propelling over the uneven terrain encountered outdoors.

METHODS

Ten subjects were recruited for this study. These individuals had an injury level below the T4 level and at least six months' experience in wheelchair propulsion.

Subjects used their own wheelchair for all testing. Both rear wheels were removed and replaced with SmartWheels (Three River Holdings, LLC, Mesa, AZ). The SmartWheel has a precision of 2N and a resolution of 0.2N. All data was collected at 240 Hz . Use of these wheels did not necessitate changes in seat alignment, wheel camber, or axle position.

The mobility course consisted of two indoor routes and one outdoors. The ten-meter indoor routes were over (1) smooth level tile and (2) level low-pile carpet. The 500-meter outdoor course was over both smooth and aggregate sidewalk surfaces and contained level, mild ascent and descent grades, and cross-slopes, typical of paved sidewalks.

For each route, the SmartWheels recorded three pushrim force components (F_x, F_y, F_z) and three moments (M_x, M_y, M_z) about the hub for the duration of each trial. The fraction effective force (FEF) was calculated as the tangential force divided by the resultant force (van der Woude, 2001). This study focused on the mean left and right push cycle propulsion moment (M_z) and FEF for each course. Asymmetry was calculated as the absolute value of the differences between mean values of each side for M_z and FEF, ΔM_z and ΔFEF,

respectively. The Δ variables were investigated for each subject and as a population. A repeated measures ANOVA was performed with the statistical significance set at $p < 0.05$.

RESULTS AND DISCUSSION

The left and right population mean values of the FEF and M_z over each ground condition are shown in Figures 1 and 2. The subject ΔFEF values across ground conditions were significantly different, indicating differing levels of FEF asymmetry over each surface. Further, the population ΔFEF of the outdoor course was significantly greater than both the tile and carpet surfaces. As expected, the levels of carpet and tile FEF asymmetries did not differ statistically.

The subjects propelled with a similar level of M_z asymmetry over all surfaces. There was no statistically significant difference for the subject or population ΔM_z quantities between the three ground conditions.

The varied FEF levels with no observed change in M_Z may be indicative of differences in individual techniques. Further analysis is required to determine if these differences are related to hand dominance. However, these findings point to the value of collecting propulsion forces bilaterally.

SUMMARY/CONCLUSIONS

In conclusion, the results suggest that wheelchair propulsion out of the laboratory is an asymmetrical exercise. This asymmetry creates different demands between upper limbs. This study highlights the importance of using realistic surfaces that adequately mimic the mechanics of manual wheelchair propulsion outside of the lab setting.

REFERENCES

van der Woude, L.H.V. et al. (2001). *Med Eng & Phys*, **23**, 713-733.

ACKNOWLEDGEMENTS

The authors would like to thank Diana Hansen, Kathie Bernhardt, and Brian Kotajarvi for their help in data collection and analysis. Funding was gratefully provided by NIH R01 HD 48781.

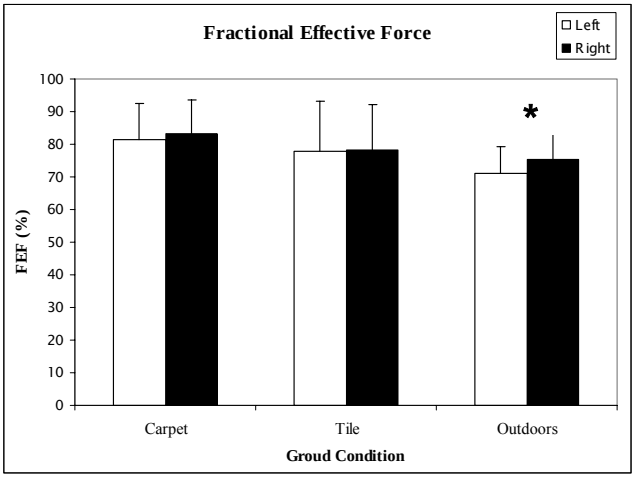

Figure 1. Left and right FEF (mean + std) over each ground condition (n=10). The star indicates a significantly greater left-to-right asymmetry in the outdoor course than in the indoor courses ($p<.05$).

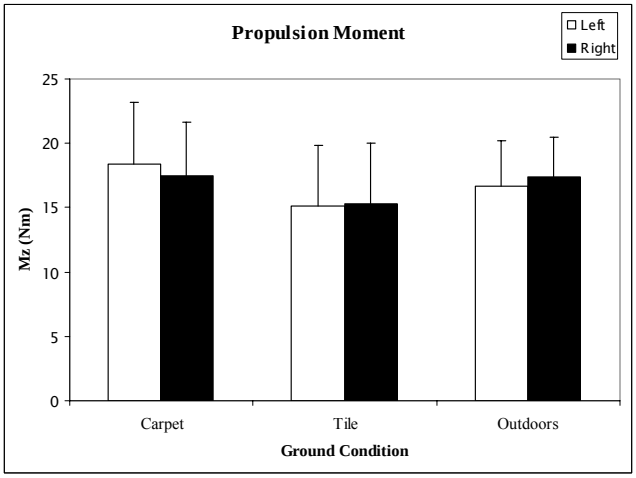

Figure 2. Left and right M_Z (mean + std) over each ground condition (n=10).

FINITE HELICAL AXES OF ACL-DEFICIENT AND ACL-RECONSTRUCTED KNEES DURING WALKING

Bo Gao, Nigel Zheng
University of Florida, Gainesville, Florida USA,
Email: nigelz@ufl.edu

INTRODUCTION

Anterior cruciate ligament (ACL) injury has been associated with knee osteoarthritis and ACL reconstruction is often performed to restore the joint stability (Daniel et al, 1994). As a quantitative approach to describe the kinematics of knee joint, finite helical axis (FHA) has been used to analyze the stability of knee joints during non-ambulation activities, including ACL-deficient (ACL-D) and ACL-reconstructed (ACL-R) (Montgomery et al, 1998; Moorehead et al, 2001; Dennis et al, 2005). These non-ambulation activities included seated flexion/extension, deep bending, etc. However, walking is the most used daily activities and has different kinematics than non-ambulation activities (Dyrby et al, 2004). This study evaluated the FHA characteristics of healthy, ACL-D, and ACL-R knees during level walking.

METHODS

Thirty five subjects were recruited and tested using an IRB approved protocol, including 15 healthy subjects, 10 subjects with unilateral ACL-R knees and 10 with unilateral ACL-D knees. At the time of the test, ACL-R and ACL-D subjects were 3 months to 2 years after injury or surgery. Eighty nine retro-reflective markers were attached to the major joints and lower extremities (Fig. 1) and an 11-camera motion analysis system (MAC, Santa Rosa, CA) was used to collect the motion during level walking at 60 Hz (Zheng et al, 2007).

Figure 1: Marker placement on a tested subject.

Instantaneous helical axis of the knee joint was calculated between every 1/15 second and expressed as femur relative to tibia (Spoor et al, 1980). The origin of tibial coordinate system was defined as the middle point between the tibial epicondyles; Z axis was defined as the unit vector from middle point of malleoli to the origin; Y direction was defined as the cross product of the Z axis and the vector from heel to the second toe; thus X was the cross product of Y and Z axes. The helical axes of the femur were analyzed by examining their intersection points with the sagittal plane (Y=0), frontal plane (X=0), and transverse plane (Z=10 mm) in the tibial coordinate system. The median position (median values in both directions) and the interquartile range (between the 3rd and 1st quartile in each direction) of these intersection points on each plane during a gait cycle were selected as quantitative variables to evaluate the knee axis position as well as the joint stability. Differences between ACL-D, ACL-R and healthy groups were tested using one-way analysis of variables (SPSS, Chicago, IL).

RESULTS AND DISCUSSION

Figure 2 illustrates the median positions of the intersection points of FHA in the three planes. In the sagittal plane, there was significant difference of the intersection positions between ACL-D and healthy groups along the anterior/posterior (AP) direction. Rotation axes of the ACL-D knees shifted posteriorly compared with

those of healthy knees (about 7.0 mm, $p<0.05$). That was resulted form the anterior shifting of the tibia. The trend of this shifting could still be noticed for ACL-R group although the difference was not significant. In the frontal plane, the intersection positions of rotation axes shifted laterally for ACL-R groups compared with those of the healthy group ($p<0.05$). In the transverse plane, no significant difference was found in either direction.

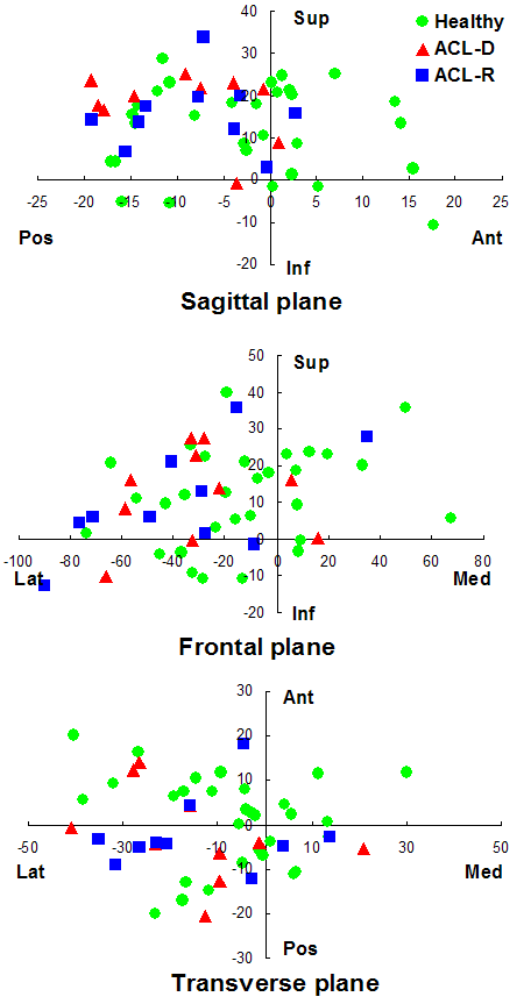

Figure 2: Median positions of intersection points of helical axes with three planes during walking (units: mm).

Figure 3 shows the interquartile ranges of the intersection points of FHA in the sagittal plane during walking. The ACL-D knees showed significant larger range of axis shifting compared with those of healthy knees in both AP and superior/inferior directions. The trend also existed for FHA of ACL-R knees, especially in AP direction ($p<0.05$). No significant differences were found for the interquartile ranges in the other two planes.

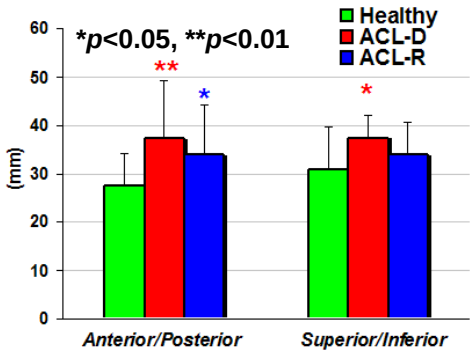

Figure 3: Interquartile range of FHA shifting in the sagittal plane during walking.

SUMMARY/CONCLUSIONS

Results of this study revealed that the ACL-D knees had altered kinematics of the FHA and were less stable in sagittal and frontal planes compared with the healthy joints. Differences in the FHA kinematics were found between the ACL-R and healthy knees.

REFERENCES

Daniel DM. et al. (1994). *Am J Sports Med* **22**, 632-44.

Montgomery SC. et al. (1998). *The Knee* **5**, 289-295.

Moorehead JD. et al. (2001). *IEEE Transactions on Biomed Eng.* **48**, 384-393.

Dennis DA. et al. (2005). *J Biomech.* **38**, 241-253.

Dyrby CO. et al. (2004). *J. Orthop Res.* **22**:794-800.

Zheng N. et al. (2007). *ORS paper 164.*

Spoor CW. et al. (1980). *J Biomech*, **13**, 391-393.

EMG-BASED ESTIMATES OF PENNATION ANGLE FOR THE PRIMARY ANKLE DORSI AND PLANTARFLEXORS DURING ISOMETRIC CONTRACTIONS

Kurt Manal, Dustyn P. Roberts and Thomas S. Buchanan

University of Delaware, Department of Mechanical Engineering, Center for Biomedical Engineering Research, Newark, DE, USA
E-mail: manal@udel.edu, Web: www.cber.udel.edu

INTRODUCTION

Fiber pennation angle is an important functional characteristic of muscle. Pennation changes with muscle contraction intensity and fiber length (Maganaris et al., 1998; Narici et al., 1996), and thus such changes should be considered when using musculoskeletal models to estimate muscle force. In this study we examined how pennation angle for the primary ankle dorsi and plantarflexor muscles (TA, LG, MG and SOL) changed with increasing contraction effort. Real-time ultrasonography and muscle activity were recorded over a full range of muscle contraction intensities (rest to MVC). We hypothesized that there is a relationship between EMG and pennation angle. The goal of this work was to identify if such a relationship exists and to provide the equations that characterize how pennation angle changes with increasing contraction effort.

METHODS

Eight male and female subjects were seated in a Biodex dynamometer and performed a series of isometric dorsiflexion and plantarflexion contractions. Muscle activity and ultrasound images for the primary ankle dorsi and plantarflexor muscles (TA, LG, MG and SOL) for the right and left legs were tested near optimal fiber length—the length at which the muscle generates the greatest force. This was approximated using a lower extremity biomechanical model of the leg (Delp et al., 1990). The TA was tested in 30 degrees of plantarflexion and triceps surae in approximately 20 degrees of dorsiflexion. Surface electrodes were used for the TA, MG, LG, and fine wire electrodes for the SOL to minimize cross-talk from adjacent muscles. The root mean square amplitudes of the EMG and moment signals for 2 seconds of each contraction were taken as representative signals. EMG for each muscle was normalized to the peak value recorded during MVC. Ultrasound images were collected using a linear 10 MHz transducer (Aloka SSD-5000, Tokyo, Japan). Pennation angles were measured off-line using methods described elsewhere (Manal et al., 2006).

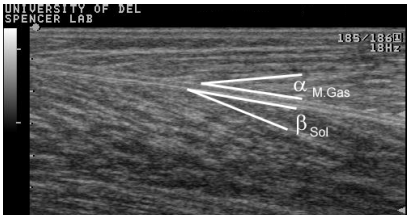

Figure 1. Pennation angle for the medial gastrocnemius ($\alpha_{M.Gas}$) and SOL (β_{SOL}).

Exploratory regression was undertaken to determine the best fitting relationship between normalized EMG and pennation angle for each muscle. Pennation angle at rest and MVC were included in the analysis to account for gender differences. We used subject specific pennation angle at rest and MVC for each subject. Group average pennation angles are listed in Table 1.

RESULTS AND DISCUSSION

A significant positive linear relationship ($p < 0.05$) between normalized EMG and

pennation angle for each muscle was observed when pennation angle at rest and MVC were included in the analysis. The coefficient of determination, R^2, ranged between 0.76 for the TA to 0.87 for the SOL. The relationship between measured and regression estimated pennation angle for the soleus is illustrated in Figure 2.

Table 1. Pennation angle estimated from normalized EMG and pennation angle at rest (θ_{rest}) and MVC (θ_{MVC})

	Regression Equations	R^2
SOL	$\theta_{EMG} = -10.52 + 16.10(EMG) + 0.43(\theta_{REST}) + 0.63(\theta_{MVC})$	0.87
MG	$\theta_{EMG} = -7.42 + 13.15(EMG) + 0.56(\theta_{REST}) + 0.50(\theta_{MVC})$	0.82
LG	$\theta_{EMG} = -3.18 + 6.54(EMG) + 0.52(\theta_{REST}) + 0.51(\theta_{MVC})$	0.82
TA	$\theta_{EMG} = -1.80 + 3.59(EMG) + 0.63(\theta_{REST}) + 0.40(\theta_{MVC})$	0.76

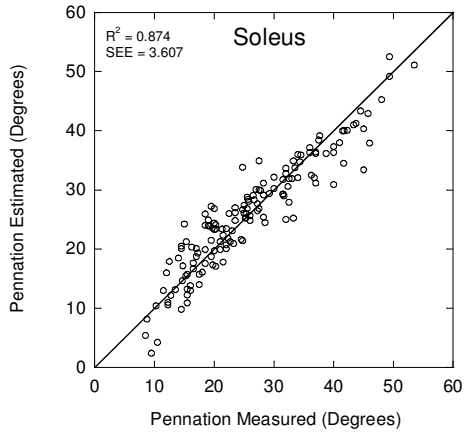

Figure 2. Regression estimated and measured pennation angles for the soleus.

Average values for pennation angle at rest and MVC for male and female subjects are reported in Table 2. Average values can be used with the equations in Table 1 when subject specific values are not possible to obtain. Table 3 shows the increase in error when using average values.

Table 3. Differences between regression estimated pennation with subject specific (sub) values at rest and MVC compared to group average values (group). Errors reported in degrees (SD).

	SOL	MG	LG	TA
Sub	0.9 (0.7)	1.9 (1.9)	2.4 (1.8)	2.7 (2.3)
Group	1.4 (1.2)	4.0 (3.9)	3.8 (3.1)	5.6 (3.7)

SUMMARY/CONCLUSIONS

Since pennation angle and EMG for the triceps surae have such a strong correlation, incorporating this relationship into a model may better represent the architecture of these large muscles which dominate ankle plantarflexion. The results of this study establish the regression equations necessary to predict pennation angle from EMG. The equations are easy to implement and can improve musculoskeletal force estimates for the primary dorsi and plantarflexors.

REFERENCES

Delp , S. et al. (1990). *IEEE Trans on Biomed Eng,* **37,** 757-767.

Maganaris, C. et al. (1998). *J. of Physiology,* **512 (Pt 2),** 603-614.

Manal, K. et al. (2006). *J. of App Biomech*, **22,** 255-263.

Narici, M.V. et al. (1996). *J. of Physiology,* **496 (Pt 1),** 287-297.

ACKNOWLEDGEMENTS

NIH P20-RR16458 & R01AR048212

Table 2. Average pennation at rest and MVC

	Tib Ant (TA)		Lat Gast (LG)		Med Gast (MG)		Soleus (SOL)	
	Male	**Female**	**Male**	**Female**	**Male**	**Female**	**Male**	**Female**
Rest	9.4 (1.8)	8.7 (1.0)	14.1 (4.8)	11.8 (3.2)	18.6 (2.9)	15.8 (1.8)	20.0 (5.8)	15.2 (3.8)
MVC	14.3 (2.2)	12.1 (1.4)	22.4 (8.7)	16.7 (4.7)	34.6 (6.6)	27.4 (5.5)	39.7 (7.3)	27.1 (7.4)

ELECTROMYOGRAPHIC CORRELATES OF INTERNAL MODELS OF TARGET REACHING TASKS IN RANDOMIZED FORCE FIELDS

Mukul Mukherjee [1] Wen Liu [1]

[1] University of Kansas Medical Center, Kansas City, Kansas, USA
E-mail: mmukherjee@kumc.edu

INTRODUCTION

It is believed that our ability to perform motor tasks in diverse environments expertly emerges from our capacity to store internal models of tasks, tools and environments in our memory.[1-2] Electromyography (EMG) has been shown to provide physiological correlates of such internal models since motor adaptation to a new dynamic environment would require changes in the activation patterns of the involved muscles.[3]

Healthy human subjects have been shown to be capable of learning a motor task in a randomly changing dynamic environment.[4] We believed that such an adaptation would stem from discrete changes in the activation patterns of the principle muscles involved in this task. Based on a past study that showed distinct EMG changes during early and late phases of learning a motor task[3], we hypothesized that learning a motor task in a randomly changing dynamic environment subjects would not only involve reduction of the EMG onset time and the EMG integrated activity of the prime mover but also demonstrate a shift in the directional bias of EMG spatial activity.

METHODS

Nine neurologically healthy right-handed subjects (27.67 ± 4.27 years) made 15cm center out target reaching movements with the dominant hand in a randomized dynamic environment while being seated on a chair. This was performed while holding the manipulandum of a two-joint robotic arm. The start, target and instantaneous hand positions were displayed to the subject on a computer monitor kept in front of the subject. Subjects performed 2 blocks of practice trials and 1 block of baseline trials without the force field being applied. The force field was applied in 5 blocks of reaching trials for a total of 200 movements. The randomized dynamic environment was created using velocity dependent viscous curl fields which was always orthogonal to the hand velocity and formed a counterclockwise circulating pattern. The amplitude of the perturbing force varied randomly from one trial to the next. EMG of the biceps brachii, long head of triceps and the anterior & posterior deltoid muscles were recorded. Repeated measures ANOVA was used to find statistical significance for the following dependent variables – EMG onset and integrated EMG activity. The independent variables were muscle (4 levels), target direction (8 levels) and muscle action type (agonist or antagonist).

RESULTS AND DISCUSSION

Late training had significantly earlier onset of EMG activity than baseline or early training trials ($p<0.005$). This is shown in figure 1 for one subject. This finding had been demonstrated in the past in non-randomized dynamic environments.[3,5]

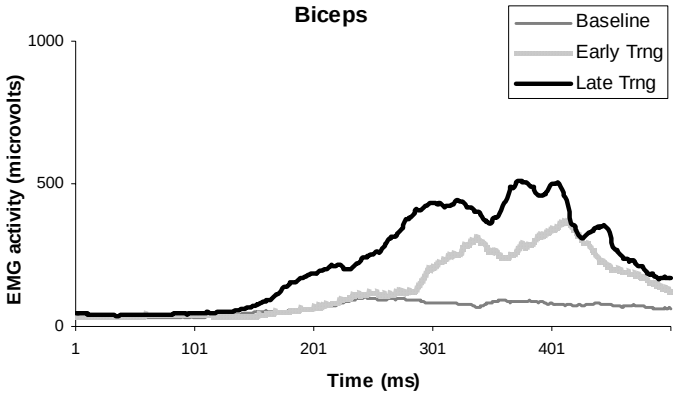

Figure 1. The EMG time series of the biceps muscle in one subject in baseline, early and late training during performance of the reaching movement in the 315˚ target (from the positive x-axis).

There was a significant reduction in integrated EMG activity after training ($p<0.05$). Past literature has shown that dynamic tasks require finer control than increased co-contraction and end point stiffness.[3,6] The direction of optimal activity for muscles involved in dynamic tasks demonstrates rotation with motor learning.[3,5] In presence of unpredictable dynamic environments, the directional bias of the muscles show reversal of rotation ($p=0.012$) between baseline to early and early to late training (figure 2).

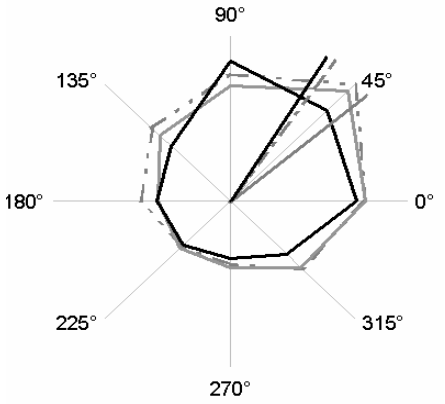

Figure 2. The directional effect of the integrated EMG activity as a polar plot for the anterior deltoid muscle. Resultant vectors of the integrated EMG activity in the 8 directions are shown by dashed and dotted grey lines for baseline, solid grey lines for early training and solid black lines for late training.

SUMMARY/CONCLUSIONS

Electromyographic correlates of motor adaptation in an unstable dynamic environment were shown. These include an earlier onset of EMG and a significantly reduced integrated EMG activity with training. An initial rotation of the EMG bias during early training reversed and rotated back to the baseline in late training. Future studies involving electrophysiological and neurophysiological data from the higher centers of the central nervous system may provide a clearer picture of internal models in randomized force fields.

REFERENCES

1. Wolpert, D.M. et al. (1995). *Science*. 269:1880-1882.
2. Kawato, M. et al. (2003). *Prog Brain Res*. 142:171-188.
3. Thoroughman, K.A., Shadmehr, R. (1999). *J Neurosci*. 19:8573-8588.
4. Scheidt, R.A. et al. (2001). *J Neurophysiol*.86:971-985
5. Li, C.S. et al. (2001). *Neuron.*;30:593-607.
6. Burdet, E. et al. (2001). *Nature*. 414:446-449

ACKNOWLEDGEMENTS

This work was partially supported by a research grant from the National Science Foundation (BES-0302466)

STRESSES IN THE L2 VERTEBRA UNDER DIFFERENT LOADING CONDITIONS

Ibrahim Erdem [1], Eeric Truumees [2], and Marjolein C. H. van der Meulen [1]

[1] Cornell University, Ithaca, NY
[2] William Beaumont Hospital and the Beaumont Comprehensive Spine Center, Royal Oak, MI
E-mail: mcv3@cornell.edu

INTRODUCTION

The low bone mass that characterizes osteoporosis renders the skeleton, particularly the spine, susceptible to fracture under physiological loads. Better means of risk assessment may reduce the considerable morbidity and mortality with which these injuries are associated. Finite element (FE) models may improve clinical predictions of loading effects on vertebrae, especially stresses and strains produced in the tissues that cannot be measured experimentally. To date, FE methods have been used to identify vertebrae at high risk for fracture. However, these models' accuracy and reliability depend on the geometry, material and boundary conditions selected and have been based on simplified loading or material properties (eg, Crawford et al. 2003; Guo et al. 2005). Our objective was to examine the effect of increasing anatomic fidelity in the boundary conditions and material properties of FE-based predictions of L2 vertebral stresses under loading.

METHODS

Computed tomography (CT) images from a 55 year old female cadaver were used to generate the exact geometry of the L1 and L2 vertebrae. First, surface geometry was extracted from 1mm thick axial CT slices with an in-plane voxel size of 0.453 mm (Mimics, Materialise, Belgium). Then the surfaces (STL-format) were converted to surface splines (Studio, Raindrop Geomagic, NC). Finally, the surface model (NURBS format) was converted to a FE mesh (Truegrid, XYZ Scientific Applications, CA).

Two FE models were created. The first model included only the L2 vertebra with loads applied through steel plates on the superior and inferior endplates of L2. The second FE model was an L1-L2 spinal motion segment including the intervertebral disc and structurally relevant ligaments and the facet joints (Fig.1). The vertebrae were modeled with 8-noded solid elements. For each model, two bone material conditions were simulated: a homogeneous elastic modulus of 1000 MPa, or a heterogeneous modulus assigned based on an exponential density-elasticity relationship (Morgan et al. 2003). The facet joints were modeled as frictionless contact surfaces braced with capsular ligaments.

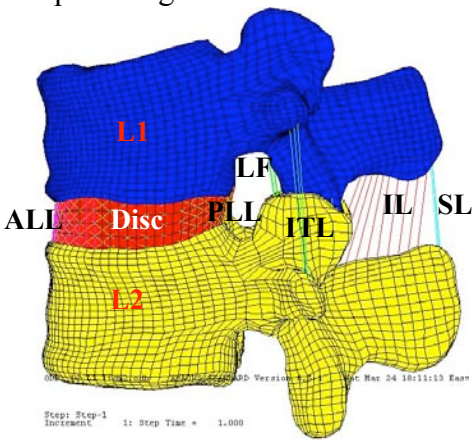

Figure 1: FE model of the spine segment

The disc model included the nucleus pulposus and the anulus fibrosis, represented as four layers of stiff fibers (Table 1) embedded in soft matrix (E=4.2 MPa). The nucleus, comprising ~40% of total disc volume, was modeled as a nearly incompressible solid with low stiffness (E=0.2 MPa). The ligaments and disc fibers

were modeled as tension-only axial elements. Locations, areas and material properties were obtained from the literature (Table 1) (eg, Goel et al. 1988; Shirazi-Adl et al. 1984).

Both models were fixed at the inferior-most endplate. Uniform compression (500 N) or flexion (7.5 Nm) loads were applied to the superior endplate. Stresses were calculated in L2 (ABAQUS, Hibbitt, Karlsson & Sorensen, Inc, RI).

Table 1: Ligament and fiber properties

	A	E		A	E
ALL	64	20	CL	40	20
PLL	20	20	Fiber1	0.35	550
ITL	10	50	Fiber2	0.30	475
SL	30	15	Fiber3	0.25	400
IL	40	10	Fiber4	0.20	360
LF	40	20			

A: Cross sectional area in mm^2, E: Elastic modulus in MPa, ALL: Anterior longitudinal ligament, PLL: Posterior longitudinal ligament, ITL: Inter-transverse ligament, SL: Supraspinous ligament, IL: Interspinous ligament, LF: Ligamentum flavum, CL: Capsular ligament, Fiber1: Outer most anular fiber layer, Fiber4: Innermost anular fiber layer

RESULTS AND DISCUSSION

Heterogeneity of bone substantially altered the distributions of von Mises stresses in the midtransverse section of L2 for both compression and flexion (Fig. 2,3). The stress distributions changed markedly when a more physiological loading was applied to L2 through L1 and the disc, ligaments, and facets (Fig. 2,3). Stress magnitudes differed most in the cancellous tissue. The mid-centrum stresses differed up to 450% in flexion and –15% in compression across the four models. The stress differences were less in the posterior (-67% in flexion and +11% in compression) and anterior (-21% in flexion and -68% in compression) cortices.

CONCLUSIONS

Accurate heterogeneity of the bone and physiological loading are critical to accurate stress predictions in the L2 vertebra. We expect these models to better assess vertebral fracture risk and treatment outcome.

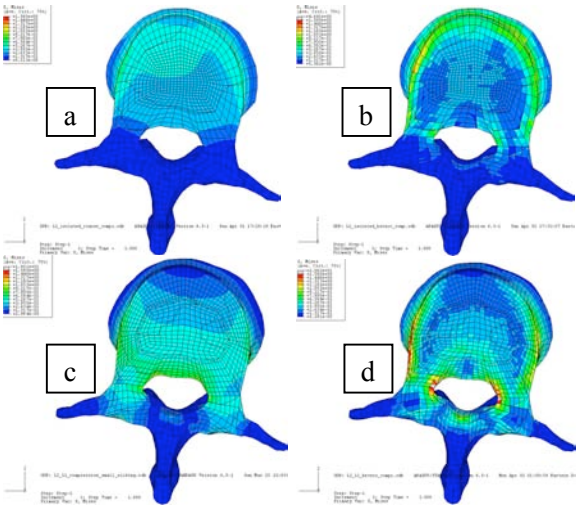

Figure 2: Stresses due to compression for a) homo- and b) heterogeneous L2 alone; c) homo- and d) heterogeneous L1-L2 segment

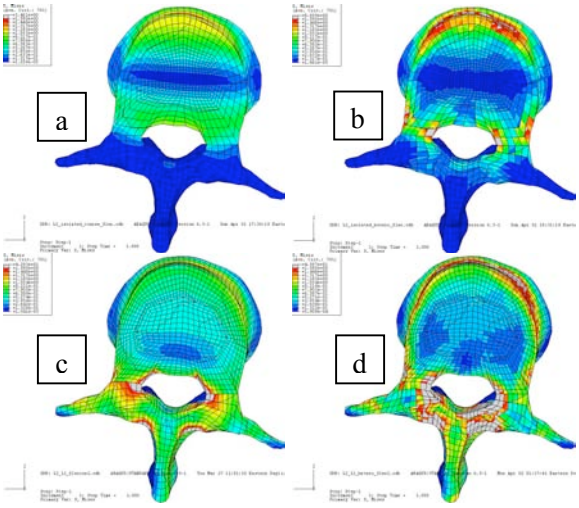

Figure 3: Stresses due to flexion for a) homo- and b) heterogeneous L2 alone; c) homo- and d) heterogeneous L1-L2 segment

REFERENCES

Crawford *et al.* (2003) *Bone* **33**, 744-750.
Goel *et al.* (1988) *Spine* **13**, 1003-1011.
Guo *et al.* (2005) *Spine* **30**, 631-637.
Morgan *et al.* (2003) *J Biomech* **36**: 897-904.
Shirazi-Adl *et al.* (1984) *Spine* **9**, 120-134.

McConnell Taping in Patellar Maltracking: A 3D *in vivo* Knee Joint Kinematic Study

Aditya Derasari[1] Timothy Brindle[2] Katharine E. Alter[2], and Frances T. Sheehan[2] and

[1] University of South Florida, Tampa, FL, USA
[2] National Institutes of Health, Bethesda, MD, USA
E-mail: fsheehan@cc.nih.gov Web: pdb.cc.nih.gov

INTRODUCTION

Patellofemoral pain, often associated with patellar maltracking, is a common condition presenting to physiotherapist and sports medicine practices. McConnell taping, which aims to improve patellar tracking within the femoral sulcus groove, is a popular practice among clinicians in treating patellofemoral pain whose suspected source is patellar maltracking. Past research has been limited in its ability to quantify the affects of interventions, such as taping, on knee joint kinematics due to the lack of three dimensional techniques that could accurately track the *in vivo* 3D patellofemoral and tibofemoral kinematics during volitional activities. A previous static study showed no change in medial-lateral patellar displacement with taping in healthy women (Pfeiffer et al. 2004). Thus, this study set out to test the effect of McConnell taping upon medial-lateral patellar displacement in patients with patellar maltracking associated with patellofemoral pain using fast-PC MRI technique. In addition all other translational and rotational degrees of freedom of the patellofemoral (PF) tibiofemoral(TF) joint were studied. This is the first study to investigate the effectiveness of McConnell taping to correct patellar tracking under dynamic conditions in a population of patients diagnosed with patellar maltracking.

METHODS

Four subjects diagnosed patellar maltracking associated with anterior knee pain were referred to the study. For all subjects both knees were examined. To be included within the study the subject had to exhibit one of the following symptoms at that knee: 1) Q-angle≥15º, 2) a positive apprehension test, 3) lateral hypermobility (≥ 10 mm) of the patella, 4) a positive 'J sign', or 5) a history of patellar subluxation. Subjects were placed supine in within the 1.5-T MR imager (LX-9.1M4; GE Medical Systems, Milwaukee, WI, USA). Data were acquired using dynamic imaging sequences (fast-PC MRI) while subjects cyclically extended and flexed their knee through a comfortably attainable range of motion at 35 cycles/ minute.

By integrating the 3D velocity acquired using the fast-PC MR, the 3D kinematic translations and rotations were quantified (Sheehan 2007) for the PF and TF joints. For consistency in comparing subject data, all translational data were scaled by the average epicondylar width (77.3mm) of the 34 knees in the able-bodied knee joint kinematic database and the individual subject's epicondylar width.

RESULTS AND DISCUSSION

All knees, but one met one or more of the patellar-maltracking criteria. The one that did not was excluded from the analysis. Interestingly, the McConnell taping resulted in both a lateralization and a medialization of the patella in this cohort of patients. For 4/7 final knees, the average PF displacement during extension was more medial with taping (values maximum and minimum average changes throughout extension

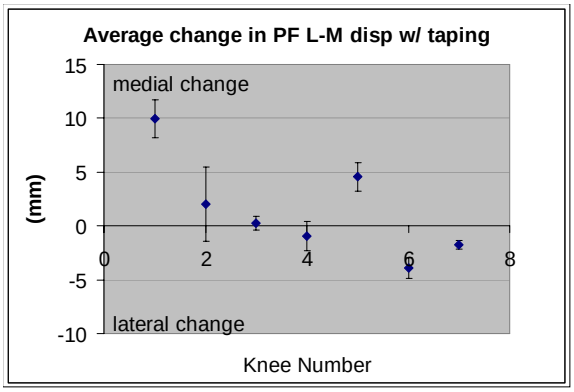

Figure 1: Alteration in PF Medial Shift with Taping. The average medial shift in PF displacement throughout extension (with 1 SD error bar) is provided for each knee

ranging from 0.2mm to 9.9mm increase in medial displacement) and for 3/7, the average PF displacement was more lateral with taping (-0.9mm to -3.00mm).

Surprisingly, large changes in PF tilt, PF flexion-extension and TF internal-external rotation were also seen with taping (Fig 2). With taping, PF extension was increased (1.3 to 9.5) in 5/7 knees and decreased (-.07 to -5.8) in 2/7 knees with taping; patellar medial tilt was increased (2.2º to 11.2º) in 4/7 knees and decreased (-1.0º to -12.0º) in 3/7 knees; and tibial internal rotation was increased (5.4º to 15.2º) in 4/7 knees and decreased (-0.2º to -2.4º) in 3/7 knees with taping. No single degree of freedom demonstrated a consistent direction of change with taping across all knee.

Interestingly, the knee (#1: Fig 1) with the largest medial change in PF displacement with taping had the shallowest femoral sulcus groove while the subject with the smallest absolute value of medial change with taping (#3: Fig 1) had the steepest groove. Thus, the effectiveness of McConnell taping may not be entirely due to alteration of patellar alignment, but may also be influenced by other factors, such as bone shape.

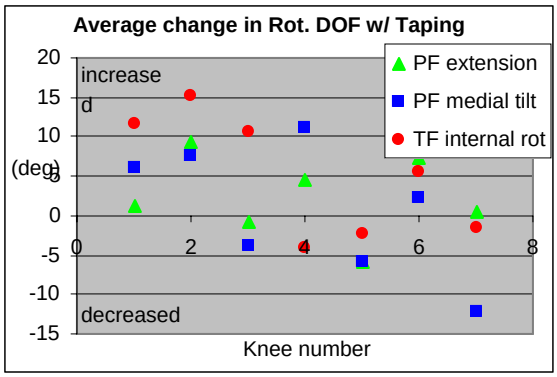

Figure 2: Alteration in Rotational Degrees of Freedom w/ Taping. A positive value for a triangle, square, and circle indicates increased PF extension, PF medial tilt and TF internal rotation, respectively, throughout extension with taping.

SUMMARY/CONCLUSIONS

McConnell taping altered knee kinematics in all degrees of freedom during volitional movement. Patellar position was not uniformly medialized with taping and no consistent pattern of change was found. Taping resulted in differing amounts and directions of change in all the degrees of freedoms. The alterations due to taping on specific degrees of freedom also differed across knees.

This preliminary study is limited by the small number of subjects. As a greater cohort is studied, a more consistent pattern of change may be elucidated and associations between altered kinematics and clinical findings can be better assessed.

REFERENCES

Pfeiffer, R.P. et al. (2004). *Am J Sports Med.*, **32**, 622-628.

Sheehan (2007) *J. Biomechanics* 40:5,1038-1047

OPENSIM: AN OPEN-SOURCE PLATFORM FOR SIMULATING AND ANALYZING MUSCULOSKELETAL DYNAMICS

Frank C. Anderson[1], Eran Guendelman[1], Peter Loan[2], Ayman Habib[1], Chand John[1], Allison Arnold[1], Darryl Thelen[3], and Scott Delp[1]
[1] Stanford University, Stanford, CA, USA
[2] Musculographics Division, Motion Analysis Corporation, Santa Rosa, CA, USA
[3] University of Wisconsin, Madison, WI, USA
E-mail: fca@stanford.edu, Web: www.simtk.org/home/opensim

INTRODUCTION

Muscle-actuated simulations allow one to study how the elements of the neuromusculoskeletal system function together to generate movement. Although the value of simulation is broadly recognized and individual investigators have made elegant contributions, the field remains fragmented. Many laboratories develop their own custom simulation software, making it difficult for a simulation to be reproduced, evaluated, and used outside the laboratory where it was developed. In addition, since software tools are not freely accessible for assisting in the development and analysis of musculoskeletal simulations, researchers typically must spend a great deal of time implementing each new simulation and creating tools to analyze it. As a result, many laboratories cannot dedicate the resources needed to generate their own simulations. These conditions create a major barrier to advancing simulation technology and achieving the scientific potential of musculoskeletal simulation.

We have established a freely available open-source simulation platform, called OpenSim, to accelerate the development and sharing of simulation technology and to integrate dynamic simulations into the field of movement science.

METHODS

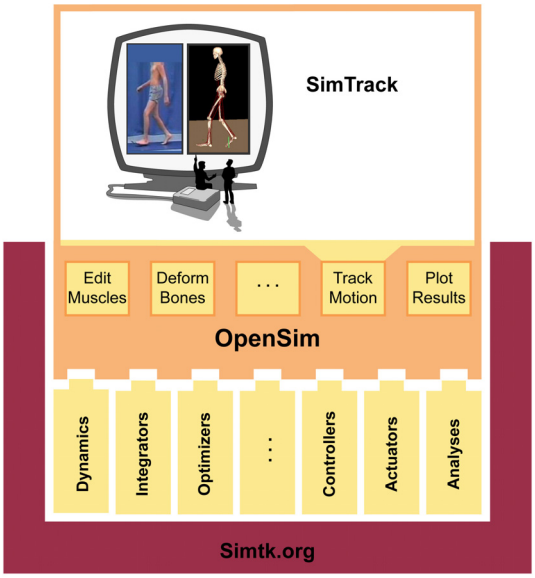

Figure 1: Schematic of OpenSim.

OpenSim is an object-oriented software platform written in C++ for modeling, simulating, and analyzing the musculoskeletal system (Fig. 1). It is built on computational components that allow one to derive equations of motion for dynamical systems, perform numerical integration, and solve constrained non-linear optimization problems. Users can extend OpenSim by writing their own plug-ins for specialized controllers, analyses, actuators, and contact forces. A graphical user interface, written in Java, allows users to view models, edit muscles, and plot results. SIMM models (Delp et al., 1990) can be imported and analyzed. SimTrack, a set of tools in

OpenSim, enables muscle-driven simulations to be generated that accurately represent the dynamics of individual subjects (Delp et al., *in press*). By using computed muscle control (Thelen and Anderson, 2006), rather than traditional optimal control, SimTrack dramatically reduces the computer time needed for generating simulations. OpenSim is being developed and maintained on simtk.org.

RESULTS AND DISCUSSION

OpenSim provides a platform on which the biomechanics community can build a library of models and simulations that can be exchanged, tested, analyzed, and improved through multi-institutional collaboration. Currently, there are about 30 collaborators from 12 different institutions working together on simtk.org to develop and improve OpenSim.

The architecture of OpenSim encourages users to extend functionality by developing their own muscle models, contact models, controllers, and analyses. For example, there are currently more than ten analysis plug-ins, authored by different users, available in OpenSim. These analyses compute muscle moment arms and lengths, joint forces, muscle-induced accelerations, and other variables. Although these analyses were developed for different models, they have general applicability and can be used with any OpenSim model. The plug-in architecture of OpenSim thus provides a means of rapidly disseminating new functionality to the biomechanics community.

Historically, optimal control has been used to generate muscle-actuated simulations. Even with parallel computing, generating these solutions has been extremely costly (e.g., Anderson and Pandy, 2001). Recent advances have made it possible to generate simulations in minutes. With SimTrack, it is now practical to generate simulations on a per-subject basis, opening up new possibilities for the use of simulation, including, for example, using simulation to assist in identifying the causes of a movement abnormality and evaluating potential treatments for an individual.

We believe the adoption of a community-owned open-source software platform for simulating and analyzing the musculoskeletal system will accelerate research. A common platform means that models can be evaluated and simulations can be reproduced. When a simulation is developed, it can be posted on simtk.org, and then anyone can download, evaluate, analyze, and extend it. Having access to the source code means that the mathematics underlying musculoskeletal models can be critically reviewed and improved. OpenSim has been seeded with an initial set of capabilities. Our hope is that the broader biomechanics community will not only use OpenSim, but also engage in its development by extending its functionality, building new models, and contributing new simulations.

REFERENCES

Anderson, F.C., Pandy, M.G. (2001). *J. Biomech. Eng.*, **123**, 381-390.

Delp, S.L., et al. (1990). *IEEE Trans. Biomed. Eng.*, **37**, 757-67.

Delp, S.L., et al. (*in press*). *IEEE Tans. Biomed. Eng*.

Thelen, D.G., Anderson, F.C. (2006). *J. Biomech.*, **39**, 1107-15.

ACKNOWLEDGEMENTS

NIH Roadmap for Medical Research U54 GM072970, HD33929, and HD046814.

Measurement of Ground Reaction Force in Single Limb Support through Markerless Motion Capture

Stefano Corazza [1] and Thomas P. Andriacchi [1,2]

[1] Stanford University, Stanford, CA, USA
[2] Bone and Joint Research Center, VA Palo Alto, Palo Alto, CA
E-mail: stefanoc@stanford.edu, Web: biomotion.stanford.edu

INTRODUCTION

The study of the mechanics of normal and pathological human movement is enhanced by an analysis of intersegmental forces and moments. In fact extrinsic measures of musculoskeletal loading play a major role in the identification of both injury mechanisms during sport and risk factors of diseases such as osteoarthritis. Direct measurement of the ground reaction force using a force plate is common practice for the calculation of intersegmental forces and moments. While this type of measurement is certainly very accurate, it is difficult to implement in a natural environment outside motion analysis laboratory. Previous studies [Bobbert, 1992] have demonstrated that is possible to accurately calculate the normal component of the ground reaction force when kinematics together with an accurate biomechanical model of the subject are available.

This work presents a method for the calculation of the human body kinematics together with the vertical component of the ground reaction force that can be implemented in a natural environment in a completely unencumbered way, i.e. without the use of force measurement devices or marker-based motion capture methods.

METHODS

In the present work we calculated the vertical component of the ground reaction force from the movement of the instantaneous center of mass of the subject during single limb support, using subject specific inertia information obtained through a Markerless Motion Capture method based on visual hull reconstruction. The Markerless Motion Capture (MMC) method used in this study is the one described in [Corazza, 2006] and is based on the reconstruction of a 3D representation of the subject defined as visual hull [Laurentini, 1994] (Figure 1, left). Eight 75 Hz (Basler) VGA cameras were used to capture the motion of subjects while running. Visual hulls were reconstructed with a 2 cm cubic voxel size. The visual hulls obtained from volume intersection techniques applied to a multiple camera arrangement are a locally convex approximation of the subject's body outer surface. The accuracy of the visual approximation of the subject's real volume increases as the number of cameras increases [Mündermann, 2005].

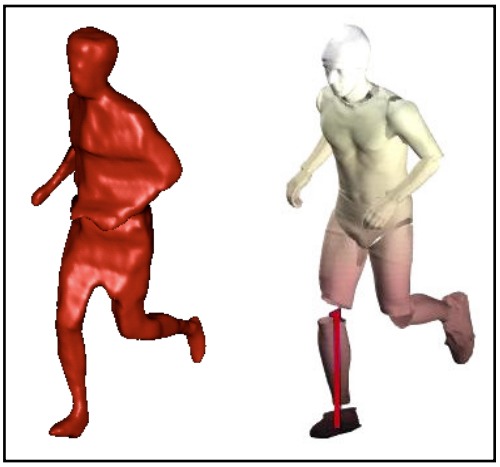

Figure 1: Running trial. Left: visual hull reconstruction of a subject using 8 (Basler) VGA cameras. Right: matched model representation, with the ground reaction force.

Under the assumption of uniform density of the human body the center of the visual hull volume can be considered a good approximation of the subject's center of mass. By solving the equations of motion of an equivalent lumped mass, the vertical component of the ground reaction force was calculated and compared with the measurement coming from a force platform (Bertec, USA). The acceleration of the center of mass (COM) was obtained performing the derivation of the COM trajectory after lowpass filtering and B-spline fitting. The frequency of the lowpass filter was set to 15Hz for best results, according to [Bobbert, 1992]. For the MMC data, heel strike detection was based on kinematic data and was used as boundary condition for the calculated vertical force (GRF equal to zero until heel strike occurs).

The presented method also offers the possibility of accurately calculating the ankle moments, in an inverted pendulum model hypothesis. In fact the contribution to the ankle moment calculation due to the variation over time of the inertia tensor of the body, usually neglected, is now provided. This is because it is possible to calculate the instantaneous inertia tensor of the body of the subject in every frame by using the visual hull data and summing up the contribution of the every single voxel.

RESULTS AND DISCUSSION

The comparison between the vertical components of the ground reaction force calculated using MMC data and measured through a force plate showed good agreement (Figure 1). The high frequency initial peak in the force plate data likely occurred at too high a frequency to be detected by the motion capture system sampling at 75Hz. The two curves compared well with a relative error below 8% on the main force peak measurement.

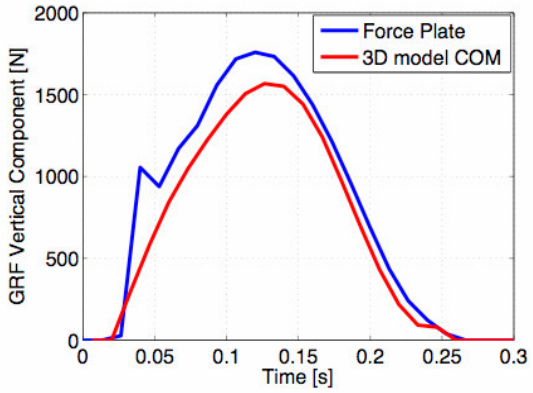

Figure 2: Vertical component of the ground reaction force measured with the force plate (blue) and calculated from MMC data (red).

SUMMARY/CONCLUSIONS

The novel method presented represents a first step towards addressing the calculation of intersegmental forces using subject specific accurate inertia information instead of direct measurement of external forces. The accuracy of the method could be improved by increasing the sample rate of the motion capture system as well as increasing the number of cameras. This is a well-conditioned problem for single limb support that can lead to a framework for the direct calculation of intersegmental forces and moments from MMC kinematic data and subject specific inertial properties. The method can be used in natural environments both indoor and outdoor since it only requires the setting up of video cameras on the surrounding perimeter.

REFERENCES

Bobbert et al. (1992). *J Biomech.*, ***34****(6), 1019-1029.*

Corazza et al. (2006). *Annals Biomed. Eng.,* ***34****(6), 1019-1029.*

Laurentini (1994) *PAMI,* ***16****(2),150-162.*

Mündermann (2005) *IS&T/SPIE,* ***5665****.*

ACKNOWLEDGEMENTS

NSF#03225715 and VA#ADR0001129.

VARIABILITY IN SECONDARY MOTIONS OF THE KNEE FOLLOWING TOTAL JOINT REPLACEMENT

Valentina Ngai [1] and Markus A. Wimmer [1]

[1] Rush University Medical Center, Chicago, IL, USA
E-mail: valentina_ngai@rush.edu, Web: http://www.ortho.rush.edu/tribology/

INTRODUCTION

Total knee replacement (TKR) surgery is a successful procedure, providing patients with pain relief and restoration of functional mobility. However, many patients outlive their prosthesis, ultimately requiring costly and distressful revision surgery. The most prevalent mechanism of implant failure is polyethylene wear of the tibial liner (Sharkey et al., 2002), causing technical failure of the implant, observed through major delamination and fragmentation of the component. Wear simulators are, therefore, an essential tool for pre-clinical evaluation.

We have previously reported (Ngai et al. 2006) that motion input profiles defined in the standard protocol for knee prostheses wear testing (ISO 14243-3), developed by the International Standards Organization (ISO), do not reflect the kinematics of TKR patients. Prior speculations that simulator testing was not completely representative of in vivo through wear scar analyses of retrieved components versus simulated components of the same implant design (Schwenke et al. 2005) were therefore supported. Bigger and more variable wear scarring of retrievals may be due to motion variability from patient to patient; however, simulators replicate one set of parameters only, simulating one possible patient. The variability between patients (interpatient variability) may be much greater than the variability expressed within one patient (intrapatient variability). Therefore, the purpose of this study was to examine and compare the inter- and intrapatient variabilities for primary and secondary knee motions of TKR patients during one complete cycle of walking.

METHODS

Ten TKR patients (6M/4F, 76years±4.9) were recruited and underwent gait analysis. All subjects had well-functioning Miller-Galante II (MGII) type prostheses (affected side L/R=4/6) with an average in-situ time of 12± 0.5years. Subjects were tested during normal level walking using the previously described point cluster technique (PCT) (Andriacchi et al, 1998) to obtain the primary motion, flexion-extension (FE) and the secondary motions, internal-external (IE) rotation and antero-posterior (AP) translation of the tibia with respect to the femur. An optoelectronic camera system (Computerized Functional Testing Corporation, Chicago, IL) was used to record the 3-dimensional motions for 3 separate walking trials per subject. Intrapatient variability was assessed based on the data obtained for the 3 walking trials per subject. Interpatient variability was based on the walking trials for all subjects.

Intrapatient and interpatient coefficients of variation (COV) were calculated separately for each motion. For FE, COV were calculated at the midstance and swing peak flexion angles (Figure1). COV for secondary motions, IE rotation and AP translation, were calculated based on the relative ranges within a data set. For IE rotation, the difference between the minimum tibial internal rotation during

midstance and the maximum tibial external rotation during swing (Figure2) was determined. This range was then utilized as the parameter for COV calculations. Similarly, ranges were also determined for AP translations and utilized for COV calculations. Range 1 denoted the maximum AP travel during midstance and Range 2 represented the maximum AP travel during swing phase (Figure3).

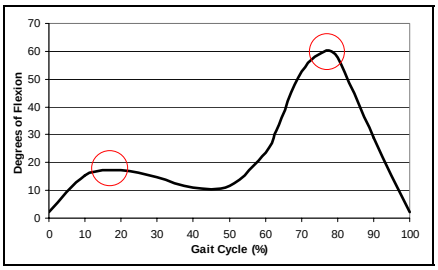

Figure1: Peak flexion angles for COV

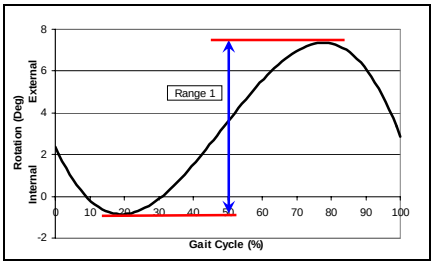

Figure2: Range of IE rotation for COV

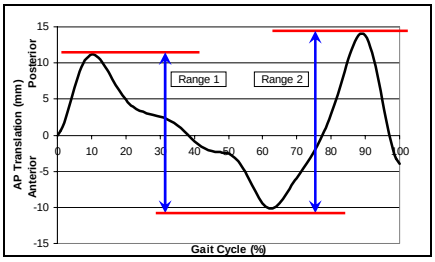

Figure3: Ranges of AP translation for COV

RESULTS AND DISCUSSION

All patients exhibited similar motion patterns, with an internal rotation and posterior translation of the tibia with respect to the femur following heel strike followed by tibial external rotation and anterior tanslation into toe-off. Interpatient COV for all motions were considerably larger than intrapatient COV (Table1), suggesting the observed gait variations between patients cannot be technique related. Patient specific gait can therefore be quite variable, even among the same implant design. Variability observed in wear scars are then possibly related to individual gait adaptations.

Table1: Avg. intra and interpatient COV

	Midstance		Swing	
Motion	**Intra COV (%)**	**Inter COV (%)**	**Intra COV (%)**	**Inter COV (%)**
FE	7.292*	26.254	1.921*	7.872
	Range 1		**Range 2**	
Motion	**Intra COV (%)**	**Inter COV (%)**	**Intra COV (%)**	**Inter COV (%)**
IE Rot	21.367*	57.205	NA	NA
AP Trans	12.120*	71.610	11.248*	42.536

*p <0.001(one-sample t-test)

SUMMARY/CONCLUSIONS

Knee motion variability between patients was greater than the variability within a single patient, suggesting that a single profile for knee wear testing is not reflective of the TKR population. The most representative motion patterns have yet to be identified to better forecast the in vivo situation and provide more viable data for prosthesis evaluation.

REFERENCES

Andriacchi et al. (1998) *J Biomech Eng*, **120**, 743-749.

ISO14243-3 (2002) *Implants for surgery*, International Standards Organization.

Ngai, V. et al (2006) *Proc 5th WCB*, **7464**.

Schwenke, T. et al (2005)*TransORS*,**30**,835.

Sharkey, PF. et al (2002) *ClinOrtho&Rel Res*, **404**, 7-13.

ACKNOWLEDGEMENTS

Thank-you to Dr. K. Foucher, I. Rojas, R. Trombley and NIH R03 ARO520.

Posturographic Analysis Is Possible Without Ground Reaction Forces Measurement Through Markerless Motion Capture

Stefano Corazza [1] and Thomas P. Andriacchi [1,2]

[1] Stanford University, Stanford, CA, USA
[2] Bone and Joint Research Center, VA Palo Alto, Palo Alto, CA
E-mail: stefanoc@stanford.edu, Web: biomotion.stanford.edu

INTRODUCTION

Posturographic analysis is a commonly used non-invasive clinical assessment technique which quantifies the central nervous system control of posture and balance. The movement of the center of mass (COM) movement in antero-posterior and medio-lateral directions while standing still for a fixed time has been used to identify neurological pathology. However, direct measurement of the trajectory of the COM has not been practical since it requires measuring the COM of each body segment and summing their weighted contribution to the overall COM. Thus, the most common and widespread alternative is to measure the center of pressure (COP) by means of a force plate and then performing a double integration to obtain the COM [Zatsiorsky and King, 1998]. [Morasso, 1999]

The purpose of this work was to develop and validate a simple inexpensive fully automatic, three dimensional video based approach to measure the postural movement of the COM without the need of a force plate. A 3D markerless motion capture (MMC) method was implemented to measure the COM and calculate the COP from the direct measurement of the center of the body volume of the subject.

METHODS

The MMC system utilized in the study was equipped with 8 (Basler) VGA cameras. The MMC method used was the one described in [Corazza, 2006] and provided for every captured frame a 3D representation (visual hull, 1 cm voxel size) of the subject which is an approximation of the body outer surface and inner volume. Thus, the calculation of the center of the body volume, and under the assumption of homogeneous density the center of mass, is straightforward. From the projection of the COM on the ground plane (vector $\mathbf{u}_{COM}$ in (1)) it is possible, under the quasi-static motion and small angles θ (see Figure 1) assumptions, to calculate the COP by solving equation (1), where k_s is a shape factor that we can calculate from MMC data.

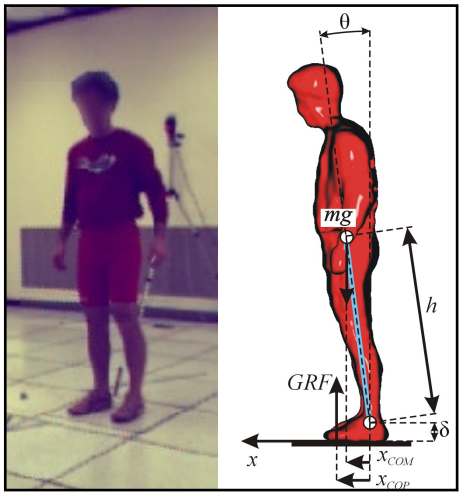

Figure 1: Left: video frame of a subject from one of the 8 (Basler) VGA cameras of the MMC system. Right: visual hull of the subject in the same frame, with in evidence the center of mass and the ankle joint center; the analysis was 3D, sagittal view is shown.

$$\mathbf{u}_{COP} = \mathbf{u}_{COM} - \frac{(hk_s + \delta)}{g}\ddot{\mathbf{u}}_{COM} \qquad (1)$$

To properly perform the derivation of the COM trajectory a Kalman filter and a B-

spline fitting method were used at every derivation step. Using the same equation it was also possible to calculate the COM from the measurement of the COP obtained from a force plate. To validate our new method a comparison over 3 subjects (3 trials each) was performed between i) the calculated MMC COP and the measured COP from the force plate, ii) the measured MMC COM and the calculated COM from the force plate data. All calculations were performed under the same assumptions described in [Morasso, 1999]. Differently from recent studies [Goffredo, 2006] the method is fully automatic, three dimensional, generates subject specific models and was validated against force plate data for both COM and COP.

RESULTS AND DISCUSSION

The mean absolute deviations for the COM between the two methods were 1.0 mm (0.7) mm) and 1.2 mm (1.0 mm) in the antero-posterior and medio-lateral directions, respectively.

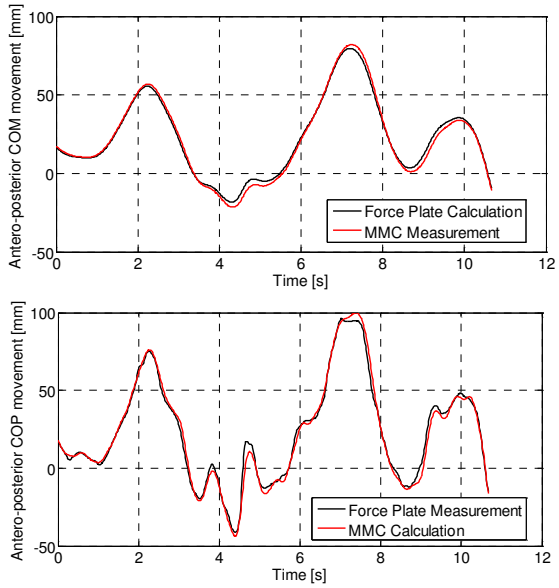

Figure 2: COM (top) and COP (bottom) trajectories along the antero-posterior axis as obtained from the force plate (black) or the MMC method (red).

For the COP they were 1.9 mm (2.3 mm) and 1.4 mm (2.2 mm). Figure 2 shows how the two set of results coming from MMC and force plate line up almost perfectly. By tracking the captured sequences it is possible to locate the ankle joint and segment the foot from the rest of the body, thus excluding it from the calculations in the (1) accordingly to the postural biomechanical model assumptions [Morasso, 1999]. Nevertheless very similar results were obtained either including or excluding the mass of the foot from the calculations, making the tracking process unnecessary and thus the implementation of the method even simpler and faster.

SUMMARY/CONCLUSIONS

A novel method was presented which allows the accurate measurement of COM and COP using only kinematic data through MMC method and without the need of a force plate or pressure mat. The method operates directly on visual hulls and thus does not even require the tracking of the subject through the captured sequence nor the previous definition of a model for it. Effectiveness and accuracy of the method was demonstrated, showing its efficacy and ease of use for clinical applications.

REFERENCES

Corazza et al. (2006). *Annals Biomed. Eng., **34**(6), 1019-1029.*

Goffredo et al. (2004) *Med. Eng.& Physics **28**, 719-726.*

Morasso et al. (1999) *Human Mov. Sci. 1019-1029.*

Zatsiorsky and King, (1998) *J Biomech. **31**(2), 161-164.*

ACKNOWLEDGEMENTS

NSF#03225715 and VA#ADR0001129

EFFECT OF THE KNEE JOINT CONTACT PATH ON THE QUADRICEPS EXTENSION MOMENT DURING GAIT

Hannah J. Lundberg [1], Andrea Swanson [1], Valentina Ngai [1], and Markus A. Wimmer [1]

[1] Rush University Medical Center, Chicago, IL, USA
E-mail: hannah_lundberg@rush.edu, Web: www.ortho.rush.edu/tribology

INTRODUCTION

During passive knee flexion, tibio-femoral contact moves posteriorly on the tibial plateau in the natural knee joint (e.g. Nisell et al., 1986). Rolling motion predominates in early flexion, while sliding becomes dominant after 30 degrees of flexion (Draganich et al., 1987). Previous musculoskeletal models of the lower limb have used this motion pattern when modeling movement of contact between the tibia and the femur (Delp et al., 1990).

During walking or other activities of daily living, the motion pattern is more complex and movement of the femur on the tibia in a purely posterior direction is not representative. This is particularly true for total knee arthroplasty (TKA) where implant design and the condition of soft tissue constraints could affect motion. A different path of tibio-femoral contact results in altered total knee kinetics and kinematics.

It was hypothesized that a tibio-femoral contact path for TKA patients would alter the mechanical efficiency of the quadriceps when compared to the historic, simplified contact paths from the literature. This would in turn influence the contact force and could account for differences seen in the wear patterns from knee simulator wear tests and retrieved implants.

To test the above hypothesis, an average contact path for TKA patients was implemented into a musculoskeletal model of the knee joint. The resulting quadriceps moment was compared with moments generated from a contact path obtained from the literature and that of a fixed point of contact on the tibia.

METHODS

A musculoskeletal model of the knee joint was created using SIMM (Software for Musculoskeletal Modeling v4.1.1, MusculoGraphics Inc., Chicago, IL). The model was modified from that reported by Hurwitz et al. (2003) to allow different contact paths between the tibia and the femur. The quadriceps complex was modeled as four discrete muscles: rectus femorus, vastus medialis, vastus intermedialis, and vastus lateralis. The SIMM knee joint model was used to calculate the moment arm of these four muscles throughout the stance phase of gait. The hip and knee flexion angles (Figure 1A) applied to the knee model were the averages from 10 TKA patients (Ngai et al., 2006) measured using the 6-marker technique for the hip angle, and the point cluster technique (PCT) (Andriacchi et al., 1998) for the knee angle.

The antero-posterior movement of the contact point of the femur on the tibia was obtained for 10 TKA patients from PCT data. This path of contact was averaged and converted to kinematic inputs for the knee joint SIMM model using the method described by Delp et al. (1990). Three different contact paths were implemented: average tibio-femoral contact of 10 TKR patients, the contact path described by Nisell

et al. (1986), and a contact point fixed at ~37% (from posterior) of the sagittal tibial plateau length (Figure 1B). The location on the tibia for the fixed contact point was chosen as the mean throughout stance of the contact path for the TKA patients. The quadriceps moment about the knee was compared for the stance phase of gait and normalized by the maximum moment from the literature based contact path.

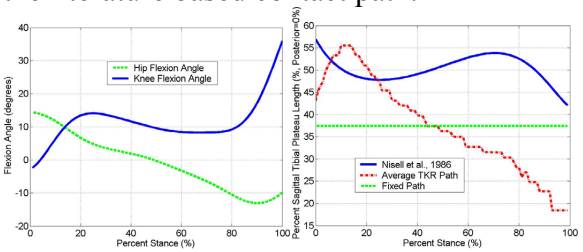

A. **B.**

Figure 1: A. Hip (green) and knee (blue) angle applied to the knee model representing the average kinematics during the stance phase of level walking for 10 TKA patients. B. Contact path movement of the femur on the tibia during the stance phase of gait as reported by Nisell et al. (blue), the average of 10 TKA patients (red), and fixed throughout the stance phase (green).

RESULTS AND DISCUSSION

The normalized extension moment about the knee generated by the quadriceps was lower through most of stance for the TKA patients than for the contact path reported by Nisell et al. (Figure 2). The maximum change was 30% at 82% through the stance phase between the contact path reported by Nisell et al. and the average contact path for the TKA patients. The maximum difference between the fixed contact path and the contact path reported by Nisell et al. was 22% at 3% through the stance phase.

SUMMARY/CONCLUSIONS

The quadriceps moment generated for tibio-femoral contact of TKA patients was lower during the initial period of stance, but higher during mid- and terminal stance than a contact path described in the literature. Since the quadriceps muscles are active during midstance of gait to balance the external flexion moment, the actual contact path allows a more efficient force transfer. With knowledge of the actual contact path a more realistic knee contact force could be calculated using mathematical models of the knee joint. This may lead to more realistic inputs for knee wear simulation.

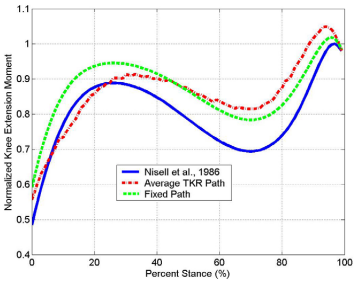

Figure 2: Normalized knee moment during the stance phase of level walking for contact paths according to Nisell et al. (blue), the average of 10 TKA patients (red), and a fixed contact point (green).

REFERENCES

Andriacchi T.P. et al. (1998). *J. Biomech. Eng.*, **120**, 743-749.

Delp S. et al. (1990). *IEEE T. Bio.-Med. Eng.*, **37**, 757-767.

Draganich L. F. et al. (1987). *J. Orthop. Res.*, **5**, 539-547.

Hurwitz D.E. et al. (2003). *J. Biomech.*, **36**, 113-119.

Ngai, V. et al. (2006). *Proceedings of the 5th World Congress of Biomechanics*, 7464

Nisell, R. et al. (1986). *Acta. Orhop. Scand.*, **57**, 41-46.

ACKNOWLEDGEMENTS

Funding provided by a grant from the NIH (R03 AR052039). Dr. Kharma C. Foucher provided invaluable technical assistance.

DEVELOPMENT AND VALIDATION OF A VERSITILE INTRA-ARTICULAR PRESSURE SENSING ARRAY

J.W. Welcher[1,3,4], J. M. Popovich, Jr.[2,3], T.P. Hedman[1,2,5] and Wafa Tawackoli[3]

[1]Department of Biomedical Engineering, USC, Los Angeles, CA
[2]Department of Biokinesiology and Physical Therapy, USC, Los Angeles, CA
[3]Department of Surgery, Cedars-Sinai Medical Center, Los Angeles CA
[4]Biomechanical Research & Testing, LLC, Long Beach, CA
[5]Orthopeutics, L.P., Stevenson Ranch, CA
E-mail: Welcher@usc.edu

INTRODUCTION

Many studies attest to the high frequency of back complaints in society with 60–85% of all people having back pain at some time in life (Andersson, 1997). The etiology of low back pain remains controversial; however, the relationship between anatomical structures, including the lumbar facet joints, and pain clearly exists. In fact, one study of chronic spinal pain (Manchikanti, et al., 2004) found a 31% prevalence of facet joint pain in patients with chronic lumbar spine pain.

The facet joints are the major load bearing elements in the lumbar spine posterior column. . They also share the vertebral column loads and help control the amount and type of motion available in the lumbar spine.

Very little research has been performed examining intra-articular facet joint loads. Of the research that has been conducted, technology such as externally mounted strain gauges (Suezawa, et al., 1980), pressure sensitive films, or force sensitive resistors (FSR's) have been utilized (Hedman, 1992). These measurement methods are either indirect or are lacking in temporal or spatial specificity.

Previous researchers have affixed strain gauges to the external bony surfaces of the facet joints. This method only provides the total forces in the facet without any information on the spatial distribution of these forces. Additionally, it requires that specimen specific Young's Modulus be determined by post test destructive testing on each specimen.

In this study, we are evaluating alternative technologies and a new method for measuring both the temporal and spatial pressure distribution relative to the unique design requirements of the lumbar facets.

METHODS

Numerous existing technologies were investigated to determine their potential feasibility. Criteria for utilization included sensor thickness less than 0.8 mm, steady state response, linear response, minimal or correctable errors associated with curvature, and durability. Each system was independently evaluated depending on their progressive meeting of the criteria.

Inability of the commercially available technology to meet our design criteria necessitated the construction of a custom made system. As shown in Figure 1, this new system consisted of an array of miniature pressure sensors (0-500psi range) arranged in various spatial distributions and embedded in electrically resistant durable Kapton tape.

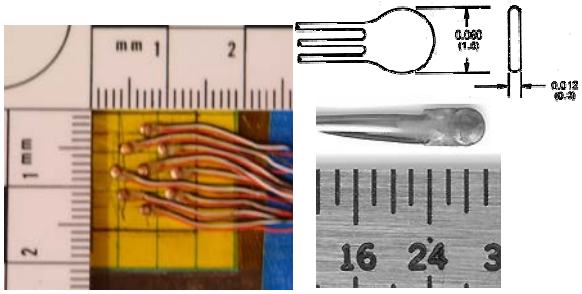

Figure 1: Pressure sensor geometry and sample configurations.

Validation was conducted in a pressure vessel with a hermetically sealed 30-wire pass through (500 psi rated) on one end and an Omega Engineering PX35 High Accuracy (NIST traceable) pressure transducer and pressure regulator on the other. Initial sensor validation data was collected on a 16-bit resolution TDAS-Pro data acquisition system certified to the NHTSA, FAA, ISO 6487 and SAE J211 data acquisition practices.

RESULTS AND DISCUSSION

All of the commercially available systems were found unsuitable for typically two or more reasons. The most common rejection factor was excessive sensor thickness.

As shown in Figure 2, the new sensors were able to capture the appropriate signal power over a range of physiologically relevant frequencies.

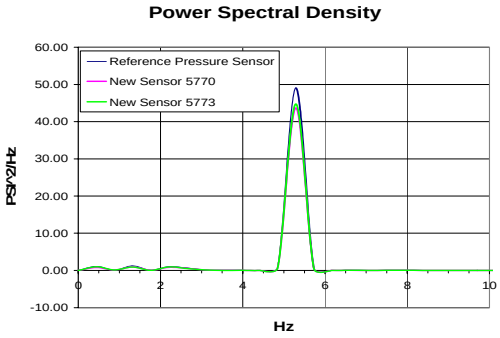

Figure 2: Sensor power spectral density analysis.

Sensor hysteresis was found to be 0.631% +/-0.358% and total combined system and sensor signal-to-noise ratio was approximately 50 dB. Analysis of various other sensor characteristics such as thermal drift and sensitivity to curvature were evaluated and found to comply with our utilization criteria. Embedding the sensors in the Kapton tape did change the supplied calibration values. All subsequent testing was conducted with the corrected calibration values. The combined tape-sensor-tape construct was approximately 0.6 mm thick..

SUMMARY/CONCLUSIONS

Based on our selected criteria, none of the commercially available systems were found to be suitable.

Our new sensor system satisfied all the design requirements with sensor thickness well below 0.8 mm, a linear and steady state response, they can be configured to eliminate curvature effects, are reasonably durable and they can be connected to standard, off-the-shelf, non proprietary data acquisition systems.

REFERENCES

Andersson GBJ. (1997). In: Frymoyer JW, ed. The Adult Spine: Principles and Practice, 2nd ed. Raven Press.

Andersson, GBJ. (1999). *Lancet*, 354, 581-585. .

Hedman TP. (1992). *Journal of Biomechanics*, **25**, 69-80.

Manchikanti, L, et. al. (2004). *BMC Musculoskeletal Dis*, **5**, 15.

Suezawa, Y, et. al. (1980). *International Orthopaedics*, **4**, 205-209.

Automatic Generation of a Subject Specific Model for Accurate Markerless Motion Capture and Biomechanical Applications

Stefano Corazza [1] , Emiliano Gambaretto [2], Lars Mündermann [1] and Thomas P. Andriacchi [1,3]

[1] Stanford University, Stanford, CA, USA
[2] Politecnico di Milano, Italy
[3] Bone and Joint Research Center, VA Palo Alto, Palo Alto, CA

E-mail: stefanoc@stanford.edu, Web: biomotion.stanford.edu

INTRODUCTION

Markerless motion capture (MMC) has received increasing attention in the biomechanical field in recent years as it offers the promise of expanding the applicability of human movement capture, minimizing patient preparation time, and reducing experimental errors caused by, for instance, inter-observer variability. Accurate markerless motion capture facilitating the study of the biomechanics of normal and pathological human movement can be achieved through the use of subject-specific models consisting of detailed morhphological and kinematic information [Mündermann 2006, Corazza 2006]. However, generating a subject-specific model requires dedicated hardware (e.g. laser scan) and extensive manual time to set up the model. The purpose of this work was to develop and validate a method for the automatic generation of subject-specific biomechanical models for MMC that incorporates full body information including a seamless shape (surface mesh), inertial properties of the anatomical segments and joint centers locations.

METHODS

Subject-specific models were created by identifying optimal shape parameters and joint center locations over a subject's laser scan and/or visual hull (3D representation from multiple images) using a continuous space of human shapes [Anguelov 2005], a space of kinematic models and an iterative pose-shape registration algorithm.

The space of human shape was controlled using 20 principal components expressing the most relevant variation in human body shape across a population of 35 subjects. The kinematic model space was characterized by 12 joints with each joint having 6 degrees of freedom. A training set was generated through manual and virtual palpation of bony landmarks using regression equations to identify the optimal location of the joint centers with respect to the surface mesh.

In the shape registration step the 20 shape parameters were varied in order to minimize the sum of the square distances between couples of closest points in the model and the data mesh being either a laser scan (Fig. 1a) or a visual hull (Fig.1b). In the pose registration step an articulated model made of 13 segments was registered to the data mesh through a linearized optimization solved using Levenberg Marquardt (1),

$$\underset{(\delta\omega,\delta t)}{\arg\min} \sum_P \left\| \sum_B -{}_d\hat{P}\,\delta\omega_d + \delta t_d - (C_P - P) \right\|^2 \quad (1)$$

where ω_d and t_d are two vectors representing respectively the rotational and translational degrees of freedom of segment *d*. *B* is the set of body segments linking point *P* to the root segment, ${}_d\hat{P}$ is the skew symmetric matrix associated to the vector which connects point *P* with the origin of

the frame coupled with segment *d*. Typically 5 pose-shape iterations were sufficient to reach convergence. Once optimal pose and shape were identified, the optimal location of the joint centers was calculated as a linear combination of the coordinates of the joint closest mesh vertexes. The optimal linear combination parameters were learned from the training set.

A k-off cross validation was performed on the joint centers locations. The experimental validation compared mean absolute deviations for the knee joint angles between the manually generated model from the laser scan and the automatically generated model from the visual hull (using video cameras).

RESULTS AND DISCUSSION

The method successfully created subject specific models from visual hulls obtained from 8 VGA cameras (Figure 1b) showing an average absolute generalization error of 23.3 mm and 27.5 mm across lower limb and upper limb joints, respectively. The accuracy of sagittal and frontal plane knee joint angles calculated from experiments [Mündermann 2006, Corazza 2006]

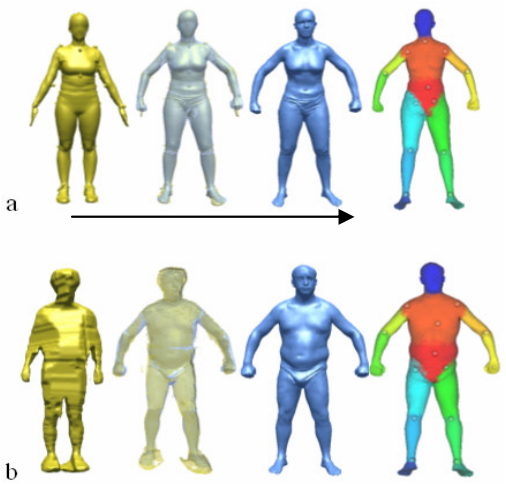

Figure 1: The model generation. The original mesh (left), the pose registered data mesh overlaid with the shape model, the hape model (blue) and the complete kinematic-anatomic model (right).

was 1.1° (0.9°) and 1.6° (1.2°) for flexion and adduction, respectively (Figure 2).The mean absolute deviations in the determination of the knee joint centers were 4 mm, 3 mm and 4 mm in the medio-lateral, vertical and antero-posterior directions, respectively. Similar results were obtained for the ankle and hip joints.

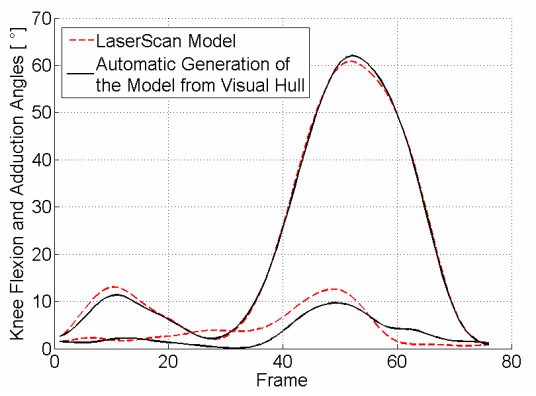

Figure 2: Deviations on knee joint angles during a gait trial on a subject not included in any of the training sets.

SUMMARY/CONCLUSIONS

The method presented here provides a fully automatic approach that eliminates the need for tedious manual intervention and expensive laser scan hardware for setting up a subject-specific model for MMC. Validation results showed deviations similar to the ones found in markerless vs marker-based validations. This work represents an important step towards the expanded application of MMC and its integration with biomechanical modeling.

REFERENCES

Moeslund (2001). *Comp. Vision and Image Understanding,* ***81****(3), 231-268.*

Mündermann (2006). *J.Neur.Rehab.,* **3**(6).

Corazza et al. (2006). *Annals Biomed. Eng.,* ***34****(6), 1019-1029.*

Anguelov et al. (2005). *SIGGRAPH Proc.*

ACKNOWLEDGEMENTS

NSF#03225715 and VA#ADR0001

CONSTITUTIVE EQUATIONS OF FEMALE HUMAN PELVIC FLOOR MUSCLES

Dejun Jing [1] Kuo-cheng Lien[1] James Ashton-Miller[1] , and John O. Delancey [2]

[1] Biomechanics Research Lab, Department of Mechanical Engineering
[2] Department of Obstetrics & Gynecology, Woman's Hospital
University of Michigan, Ann Arbor, MI, USA
E-mail: djing@umich.edu, Web: http://me.engin.umich.edu/brl/

INTRODUCTION

Good constitutive equations of female human pelvic floor muscles are vital for finite element study of vaginal delivery and birth induced muscle injuries. Unfortunately, such kind of material property data are still not available so far, and it is not surprising that existing published pelvic floor models "borrowed" material properties from other soft tissues, such as cardiac tissue (d'Aulignac 2005) and tongue muscle (Lee 2005).

The purpose of this study is to derive constitutive laws of female human pelvic floor muscles required by finite element modeling. To measure the properties of these muscles, we developed a tension test system which is capable of doing both unaxial and biaxial tests on soft tissues. Since the deformations of pelvic floor muscles are generally time-dependent, finite and nonlinear, derivation of constitutive equations was based on the theory of hyper-viscoelasticity.

METHODS

Fresh specimens of pubovisceral muscle (PVM), iliococcygeal muscles (ICM) and perineal bodies (PB) were collected for uniaxial tension tests. Each specimen was preconditioned first with 5 cyclical stretches up to 30% strain under a stretching rate of 0.1mm/second. After a 15-minute rest for recovery, the specimen was stretched in the "ramp-and-hold" mode (first linearly stretched up to 100% strain at a 0.5mm/second stretch rate, followed by being held at fixed length for at least one hour), while the values of stress and strain were recorded simultaneously to the computer.

Based on the Quasi-Linear Viscoelasticity (QLV) theory (Fung 1972), the constitutive equations of the tissues take the form of

$$\mathbf{S}(t) = \int_0^t G(t-\tau)\frac{\partial \mathbf{S}^e(\mathbf{C}(\lambda))}{\partial \tau} d\tau$$

where $\mathbf{S}$, $\mathbf{S}^e$, $\mathbf{C}$ and G are the second Piola-Kirchhoff (P-K) stress tensor, instantaneous elastic P-K stress response, right Cauchy-Green tensor, and reduced relaxation function. Mooney-Rivlin model was used to characterize the elastic stress response $\mathbf{S}^e$,

$$W = C_{10}(I_1 - 3) + C_{01}(I_2 - 3) + C_{11}(I_1 - 3)(I_2 - 3)$$

where I_1 and I_2 are invariants of right Cauchy-Green tensor $\mathbf{C}$. The reduced relaxation function takes the form of Prony series

$$G(t) = g_\infty + \sum_{i=1}^{3} g_i e^{-t/\tau_i}$$

with constraints of

$$\tau_i > 0$$

$$g_\infty + \sum_{i=1}^{3} g_i = 1 \quad \text{and} \quad g_\infty, g_i > 0$$

A nonlinear optimization code using Matlab was developed to curve-fit the experimental data to extract material constants C_1 , C_2 , g_i and τ_i .

RESULTS AND DISCUSSION

Figure 1 shows curve-fitting of tissue stiffness data using Mooney-Rivlin model. With the 2nd-order term being included, Mooney-Rivlin model can reasonably characterize the elastic response of tissues in both small and large strain regions.

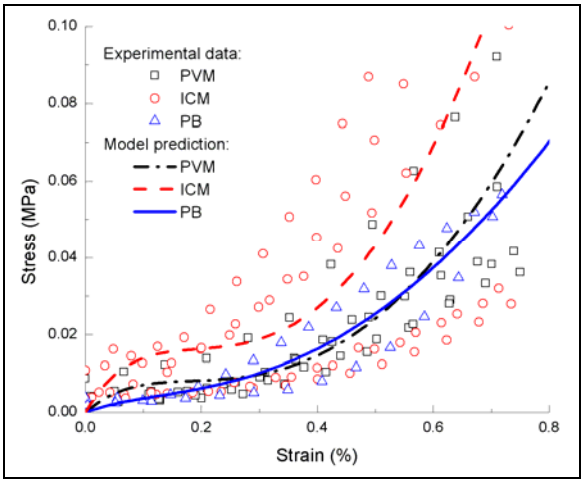

Figure 1: Instantaneous elastic responses of PVM, ICM and PB (experimental data vs. prediction from Mooney-Rivlin equation).

Figure 2 shows curve-fitting of reduced relaxation function. The short- and long-term relaxation behaviors were well modeled with 3-term Prony series.

CONCLUSIONS

Female pelvic floor muscles were tested and the hyper-viscoelastic constitutive equations were derived, which can be directly applied to FE modeling. Even though the results presented here are just preliminary data based on uniaxial tests, to out knowledge, this is the first publication of property data of human pelvic floor muscles so far. Currently, more rigorous biaxial tests on these tissues are on the way in our lab.

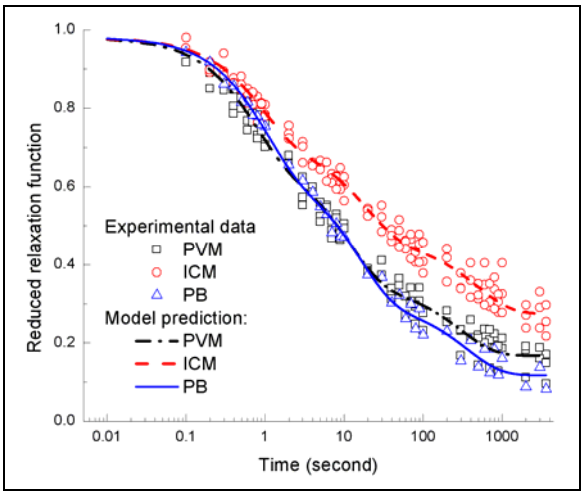

Figure 2: Reduced relaxation function of PVM, ICM and PB (experimental data vs. prediction from Prony-series equation).

REFERENCES

D' Aulignac D et al. (2005). *Compt. Meth. Biomech Biomed Eng*, 8(5), 339-47.

Lee S.L. et al. (2005) *Med Image Comput Comput Assist Interv Int Conf Med Image Comput Comput Assist Interv*, 8, 360-7

Fung Y.C. (1972) *Biomechanics- Its foundations and Objectives*. Prentice Hall, 181-207

ACKNOWLEDGEMENTS

This research was supported by PHS grant 1 P150 HD 044406.

Table 1: Material constants obtained from curve-fitting on test data

	C_{10}	C_{01}	C_{11}	g_∞	g_1	g_2	g_3	τ_1	τ_2	τ_3
PVM	-0.106	0.129	0.038	0.168	0.325	0.308	0.179	11.39	0.708	297.99
ICM	-0.20	0.244	0.069	0.275	0.25	0.265	0.19	18.40	0.907	483.47
PB	-0.03	0.04	0.019	0.118	0.346	0.335	0.183	15.397	0.968	357.05

* Specimen number: PVM=5, ICM=6, PB=2

REGIONAL VARIATIONS IN THE DEPTH-DEPENDENT STRAIN DISTRIBUTION IN THE TIBIAL PLATEAU

Sanchez, GN[1], Bevill, SL[1] ,Briant, PL[1,2], and Andriacchi, TP[1,2]
[1]Stanford University, Stanford, CA
[2]VA Palo Alto RR&D, Palo Alto, CA
gnsanch@stanford.edu

INTRODUCTION

The topological variations in cartilage matrix organization and composition across the tibial plateau suggest local adaptations to regional loading. These local topological variations have important implications for understanding the causes of osteoarthritis [Andriacchi et al, 2004], as well as the mechanical integrity of tissue engineered constructs. While it has been shown that the compressive strain distribution through the depth of articular cartilage is highly non-uniform [Shinagl et al.1997, Wang et al. 2002], it is not known if this depth-dependent strain distribution varies regionally in a manner similar to that described above for the superficial zone.

The purpose of this study was to analyze the effect of matrix organization on the axial strain distribution through the thickness of the tissue. It was hypothesized that the depth-dependent strain distribution varies among the different (central and peripheral) topographical regions of the tibia.

METHODS

Full-depth osteochondral plugs were removed from the central (not covered by the meniscus) and peripheral (covered by the meniscus) regions of porcine lateral tibial plateaus (n =3). Cylindrical samples, 6mm in diameter, from each region were halved longitudinally to provide a flat surface for imaging during mechanical testing and incubated in medium until experiments were performed.

Chondrocytes were fluorescently labeled with a live/dead stain consisting of 5μM calcein-AM and 5μM propidium-iodide, respectively, for 30 minutes. The plugs were then immersed in fresh medium and placed in a custom compression device affixed to a confocal microscope. Images of the unloaded plugs were taken and the cartilage thickness was estimated with the microscope viewer software. A bulk strain of approximately 10% was applied and a second image was taken after allowing sufficient relaxation time. Corresponding chondrocytes were then located between the two images.

Custom code written in MATLAB R14 was used to record each chondrocyte's original location as well as its displacement due to loading. Linear triangular elements were constructed from nodes placed at the chondrocyte locations with a Delaunay triangulation algorithm. The measured displacements were applied as boundary conditions, and the axial compressive strains in each element were calculated.

The local strains were normalized by the bulk strain and the resulting strain profile in each plug was visualized using ABAQUS v6.5 (Figure 1). The average normalized strains in the superficial (upper 20%), transitional (20-40%), and deep (lower 60%) zones were then calculated and compared between specimens of the two regions.

RESULTS AND DISCUSSION

The results support the hypothesis in that the peripheral region had higher strain in the superficial and transitional zones and lower

strain in the deep zone than in the corresponding zones of the central region (Figure 2). Interestingly, the transitional zone strains were higher in the peripheral region than in the central region.
The axial strain distribution was non-uniform in the peripheral region, with strains of approximately 1.5 times the bulk strain in the superficial and transitional zones, while the deep zone experienced less than 0.65 times the bulk strain. In contrast, the average strains in the central region were nearly uniform.

The topological variations agree with previous findings concerning cartilage matrix organization and composition. It has been shown that superficial tissue in the central region has more random fiber orientation while the peripheral cartilage exhibits a thick, well-defined superficial zone of tangentially oriented fibers [Briant, 2006]. In addition, it has been demonstrated that collagen, which resists tensile loads, is most abundant in the peripheral region while proteoglycans, which resist compressive loads, are most abundant in the central region [Appleyard, 2003].

The results of this study suggest that cartilage in the central region (cartilage-on-cartilage loading) has a more uniform strain distribution than cartilage in the peripheral region (protected by the meniscus). Likewise tissue with an organized matrix (central region) has a more uniform strain distribution than cartilage with random matrix organization (peripheral region).

In conclusion, the results of this study support the theory that cartilage health can be highly sensitive to kinematic changes in joint loading. Shifts in the locations of high joint loads during ambulation may result in very different cartilage deformation due to the different matrix structures. This supports the potential for accelerated OA progression following an injury which results in altered gait kinematics such as traumatic injury to the ACL [Andriacchi, 2004].

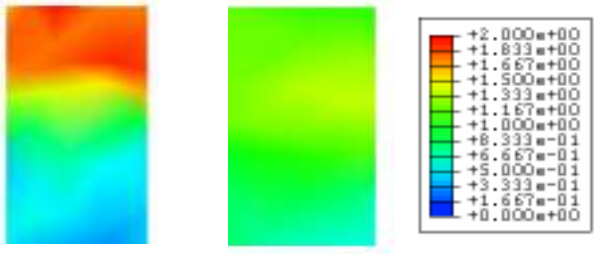

Figure 1: Example contour plots of the normalized axial strain in the peripheral (left) and central (right) regions of the knee.

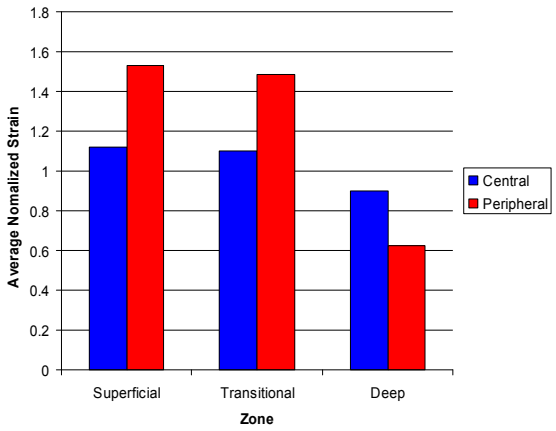

Figure 2: Average normalized strain in histological zones for the central and peripheral regions.

REFERENCES

Andriacchi, T.P. et al. (2004). *Ann Biomed Engr.*, **32**, 447-57.
Appleyard, R.C. et al. (2003). Osteo and Cart., **11,** 65-77
Briant, P.L. et al. (2006). *ASME Sum Bioeng Conf Amelia Island Florida.,*
Schinagl, R., et al. (1997). *J Orthop Res.*, **15**, 499-506
Seonghun, P. et al. (2003). *J Biomech.,* **36**, 1785-1796
Wang, CC, et al. (Oct, 2002). *J Biomech Eng.,*

ACKNOWLEDGEMENTS

This study was funded in part by NIH grant AR049792-01

A HEXAPEDAL JOINTED-LEG MODEL FOR INSECT LOCOMOTION IN THE HORIZONTAL PLANE

Raghavendra Kukillaya and Philip Holmes

Princeton University, Princeton, NJ, USA
E-mail: rkukilla@princeton.edu

INTRODUCTION

We develop an actuated hexapedal jointed-leg model, with agonist-antagonist pair of Hill-type muscles at each joint, to describe cockroach locomotion in the horizontal plane. This is part of our bigger objective to build a neuromechanical model of insect locomotion including body mechanics, muscles, motoneurons, central pattern generator (CPG), and the sensory system.

Schmitt and Holmes (2000a, 2000b) show that a conservative passively-elastic lateral leg spring (LLS) bipedal model can be stable, supporting the suggestion of Brown and Loeb (2000) that, in rapidly running insects, neural feedback might be partially or wholly replaced by largely mechanical feedback. Our model is based on the principles of LLS, but a little closer to reality and an extension of our work in Kukillaya and Holmes (2007).

MODEL AND ANALYSIS

The insect is modeled as a 2-D object with mass, m, yaw moment of inertia, I, and six legs, their mass being ignored. Each leg, comprising a "thigh" and a "shank" segment, is morphologically similar to the cockroach leg. The "hip" and "knee" joints are actuated by agonist-antagonist pair of Hill-type muscles. With this model, we study insect's double tripod gaits with 50% duty cycle.

The actuation is purely feedforward in the form of spike-train input to the muscles.

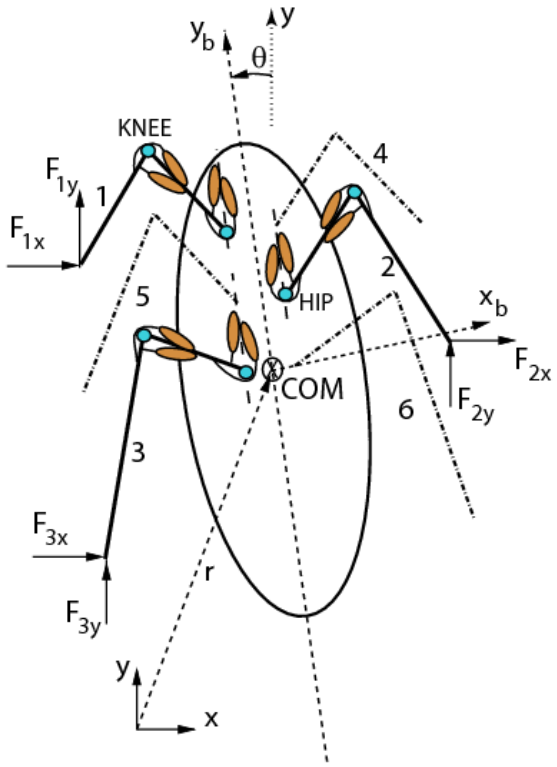

Figure 1: Schematic dorsal view of the insect model. For clarity, the muscles are shown only for the legs in left stance (1-2-3). Right stance corresponds to the 4-5-6 tripod being on the ground. The swing phases are ignored in the present model.

Proprioceptive feedback is implicitly present only as liftoff (LO)/touchdown (TD) signals. LO is purely time based (fixed stride frequency) and at each TD, the feet are kept at prescribed positions with respect to the body. Muscle parameters have been obtained by fitting Hill-type model outputs to experimental data (Ahn and Full (2002), Ahn et al. (2006)).
Time-based sinusoidal approximations of experimental foot-force data provide

necessary joint torques and equivalently the muscle input parameters (inter-spike interval, spike onset time, muscle force scaling). Thus, we obtain a three degree-of-freedom dynamical system driven by feedforward spike-train inputs. We search for periodic gaits of this system and study their stability.

RESULTS

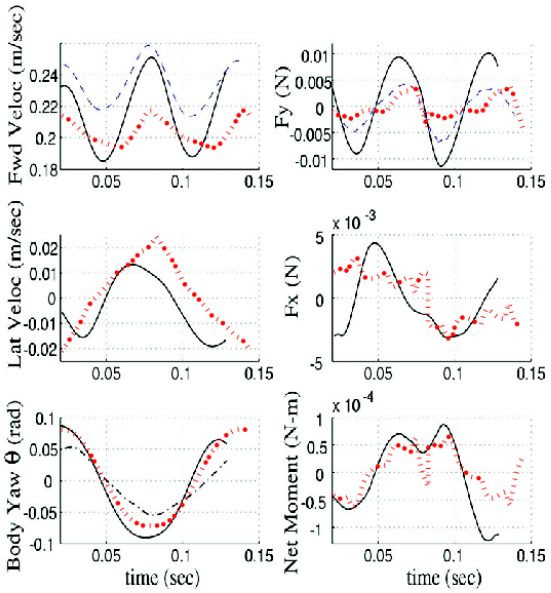

Figure 2: Experimental data (Full et al. (1991), Kram et al. (1997), Full and Tu (1990)) are shown in black; model results are shown as thick dotted red lines.

A stride-to-stride Poincaré map is defined, fixed points of which correspond to periodic gaits of the full system. Stability can be determined by numerically solving for the eigenvalues of the map. Stable and unstable solutions correspond to the insect model running along a straight line and moving in circles, respectively. Figure 2 shows a comparison of the model gait characteristics with experimental data, for a stable periodic gait (running along y axis).

The data is shown for one full stride (left and right stance). It is to be noted that the model results are shown for a different average forward speed ($V_y \approx 0.2$ m/s) and stride frequency than those for the experiment. The model and insect gaits match closely in all the variables.

CONCLUSIONS

The present model with Hill-type muscles exhibits stable periodic gaits which has good comparison with the insect gait. We want to do a complete stability analysis for the model in the insect's typical speed range (0.1-0.6 m/s). Further, we hope to study the robustness of these stable gaits by applying impulsive lateral force perturbations and randomizing the foot touchdowns.

REFERENCES

Ahn, A., Full, R. (2002). *J. of Exp. Biology,* **205**, 379-389.

Ahn, A. et al. (2006). *J. of Exp. Biology,* **209**, 3370-3382.

Brown, I., Loeb, G. (2000). *Biomechanics and neural control of movement*, pages 148-163, Springer Berlin Heidelberg NY.

Full, R. et al. (1991). *J. of Exp. Biology,* **158**, 369-390.

Full, R., Tu, M. (1990). *J. of Exp. Biology,* **148**, 129-146.

Kram, R. et al. (1997). *J. of Exp. Biology,* **200**, 1919-1929.

Kukillaya R., Holmes, P. (2007). submitted to *Biological Cybernetics,* in review.

Schmitt. J., Holmes, P. (2000a). *Biological Cybernetics,* **83(6)**, 501-515.

Schmitt, J., Holmes, P. (2000b). *Biological Cybernetics,* **83(6)**, 517-527.

ACKNOWLEDGEMENTS

We thank Shai Revzen for providing us with the TD foot position data.

Background: Architectural data form an integral part of mathematical models that have been developed to study skeletal muscle; however, human muscle architectural data are often incomplete, based on sampling of a small number of fiber bundles, from selected areas within a muscle belly. We have developed a method using digitization and 3D computer reconstruction to determine the architectural parameters throughout the volume of a human muscle. Purpose: To compare the architectural characteristics and physiological cross sectional area (PCSA) of the extensor carpi radialis longus (ECRL) and brevis (ECRB). Method: Eight cadaveric specimens were serially dissected, digitized and reconstructed in 3D using Maya™. The fiber bundle length of 180-250 fiber bundles and their angles of pennation and the total muscle volume were computed and PCSA calculated, for the muscle as a whole and for the architecturally distinct regions. Results: Architectural parameters vary regionally in ECRL and ECRB both from superficial to deep and medial to lateral. Although the PCSA of ECRL was significantly greater than ECRB, regional differences in PCSA also varied significantly. Conclusion: The architecture is non-uniform throughout the volume of ECRL and ECRB. Implications: Detailed architectural studies may lead to the development of muscle models that can more accurately predict their force generating capabilities and how it relates to muscle pathophysiology.

A CHECK OF MESH QUALITY

Nicole M Grosland[1], Curtis Lisle[2], Kiran H. Shivanna[1],
Steve Pieper[2], Vincent A Magnotta[1]

[1]The University of Iowa, Iowa city, IA, USA
[2]Isomics, Inc., Cambridge, MA USA
E-mail: nicole-grosland@uiowa.edu Web: www.ccad.uiowa.edu/mimx/

INTRODUCTION

The accuracy of finite element calculations is dependent upon the quality of the mesh. Degenerate elements with small volumes in conjunction with large displacements of the associated nodes may lead to large local errors of the solution. The worst scenario results in an insolvable system of equations.

Even if a mesh is valid and all of the elements are approximately the same size, the quality, as measured by parameters such as aspect ratio, skew, and Jacobian quality metrics, may be poor. Theoretically, the FE solution should approach the exact solution as the size of the largest element approaches zero. It has been demonstrated, however, that if dihedral angles approach π as the element size decreases, convergence to the exact solution may fail. ABAQUS, for example, checks the distortion of each element through the angle between isoparametric lines of each element. In general, the criterion set for this test consists of verifying whether the angle is greater than 45º or less than 135º in order to reduce the influence of the element distortion on the accuracy of the numerical integration.

An assessment of mesh quality using ABAQUS, for example, is conducted during the pre-processing phase. In an effort to couple a check of mesh quality with our custom-written meshing software (IA-FEMesh), we have developed a stand alone application.

METHODS

A goal of the stand alone viewer is to make the mesh generation process more efficient by providing rapid, visual feedback to the user (Figure 1). Our mesh quality application (Figure 2) utilizes the open-source VERDICT library to analyze element quality according to several metrics that have been proposed in the literature (Knupp 2000, Knupp 2001, and Knupp 2003). In addition to readily identifying zero-volume elements, the user is allowed to choose between a number of mesh quality metrics: including volume, Jacobian, scaled Jacobian, edge-ratio, and the Frobenius aspect.

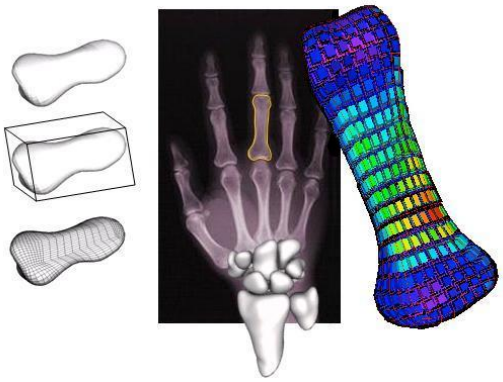

Figure 1. Contours illustrate the mesh quality on an element-by-element basis.

The Jacobian calculates the partial derivatives of the hexahedron shape functions with respect to the Cartesian coordinate system. The edge ratio provides the ratio of the longest to the shortest edge in each hexahedron. The Frobenius measures the average condition number of

the transformation matrix from an isosceles configuration for each of the 8 corner tetrahedra of a hexahedron. A scaled Jacobian is also available that scales the resulting Jacobian between +1 and -1. Quality values are assigned per element and visualized using the VTK library. The user can interact with the mesh and change the mesh quality metric in real-time using the VTK pipeline architecture.

Since datasets generally contain a large number of elements, interactive tools have been developed that allow users to isolate and examine both individual elements and element groupings. A user may dynamically position "cutting planes" within the dataset to expose the internal mesh. Furthermore, the elements may be scaled (shrink option) for improved visualization (Figure 1). The surface normals may also be displayed (Figure 2).

RESULTS AND DISCUSSION

Figures 1&2 illustrate the mesh quality tool applied to a phalanx bone of the hand. The most distorted elements (Jacobian metric) are highlighted in red (Figure 2). Elements of poor quality can quickly be identified, and if need be a new mesh generated, before importing the resulting mesh into a finite element package such as ABAQUS.

We assert the uniqueness of our work not in the development of specific mesh quality metrics. Instead, our contribution comes from providing a framework to couple these individual techniques together into a simple, timesaving stand-alone application.

Algorithmic extensions to the VERDICT mesh quality library are being developed to mirror the angle and edge length constraints imposed by FE solvers, such as ABAQUS.

SUMMARY/CONCLUSIONS

A mesh quality visualization tool has been developed to facilitate the generation of high quality finite element mesh definitions. The current tool was developed initially to support hexahedral meshes. The tool supports the ability to display a number of mesh quality metrics and to interact with the mesh to explore mesh quality before importing the mesh into a finite element package for analysis.

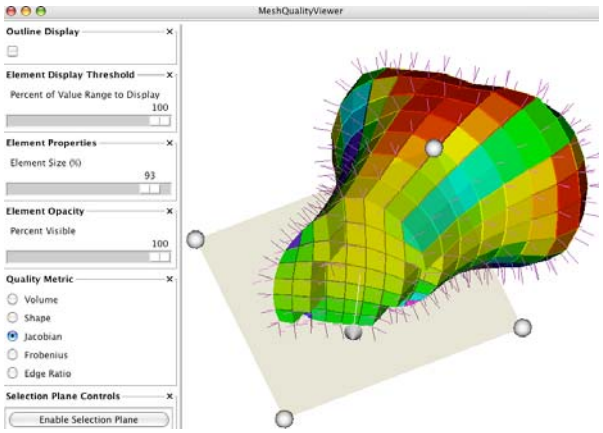

Figure 2. Mesh quality check user interface

REFERENCES

Knupp P.M., (2000). *Int. J. Numer. Meth. Engng*, **48**,1165-1185.

Knupp P.M. (2001). *Siam J. Sci. Comput. _* **23**, 193–218, 2001.

Knupp P.M. (2003). *Finite Elements in Analysis and Design*, **39**, 217–241

ACKNOWLEDGEMENTS

The authors gratefully acknowledge the financial support provided by NIH Awards EB005973 and U54 EB005149.

EFFECTS OF AGE AND LOSS OF BALANCE DIRECTION ON THE KINEMATICS OF THE THRESHOLD OF BALANCE RECOVERY

Alessandro Telonio and Cécile Smeesters

Research Center on Aging, Sherbrooke QC, Canada
Human Performance and Safety Laboratory (PERSEUS), Sherbrooke QC, Canada
Department of Mechanical Engineering, Université de Sherbrooke, Sherbrooke QC, Canada
E-mail: Cecile.Smeesters@USherbrooke.ca Web: http://www.usherbrooke.ca/gmecanique

INTRODUCTION

It is only recently that studies have focused on postural perturbations at the threshold of balance recovery, i.e., postural perturbations large enough that balance recovery is not always possible and a fall can occur. The knowledge at the threshold of balance recovery is thus very limited. Moreover the effects of age and loss of balance direction on the threshold of balance recovery have not been quantified, despite evidence of their importance during small and medium postural perturbations (Hsiao, Robinovitch, 2001; Maki et al., 1996). Understanding the effects of age and loss of balance direction are particularly important given that case controlled studies have shown that sideways falls, compared to other fall directions, increase hip fracture risk (Greenspan et al., 1998; Hayes et al., 1993; Nevitt, Cummings, 1993). Therefore, the purpose of this study was to quantify the effects of age and loss of balance direction on the kinematics of the threshold of balance recovery.

METHODS

Balance recovery following sudden release from an initial lean was performed by ten healthy younger adults (21.8±3.7yrs) and ten healthy older adults (66.1±2.4yrs) with an equal number of males and females in each group. The maximum lean angle that these healthy adults could be released from and still recover balance using a single step was determined for i) forward, ii) dominant side, iii) non-dominant side and iv) backward leans. The lean angle was sequentially increased until the subjects failed twice at a given angle and the lean directions were randomly ordered. Initial lean angles, reaction times, weight transfer times, step times, step lengths and step velocities were measured using force platforms (AMTI, Newton, MA) and a motion measurement system (Optotrak, NDI, Waterloo, ON). Two-way analyses of variance with repeated measures were used to determine the effects of age and lean direction.

RESULTS AND DISCUSSION

Both age ($p<0.001$) and lean direction ($p<0.001$) significantly affected the maximum lean angles that healthy adults could be released from and still recover balance using a single step (Figure and Table). There was also a significant interaction between age and lean direction ($p=0.027$). Moreover, at the maximum lean angles, age and lean direction also significantly affected several of the other kinematics variables (Table).

At lean angles larger than their maximum, participants failed to recover balance. Younger adults were more likely to sustain harness failures than stepping failures in all lean directions. However, older adults were more likely to sustain stepping failures than harness failures in all lean directions.

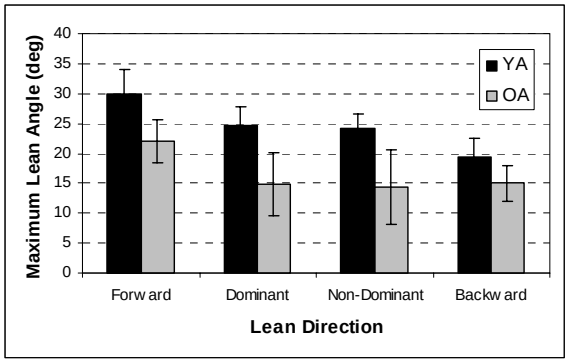

Figure: Effects of age ($p<0.001$) and lean direction ($p<0.001$) on the maximum lean angle that younger (YA) and older (OA) adults could be released from and still recover balance.

Finally, crossover steps were rare. At lean angles smaller than their maximums, only one younger male and two older females used crossover steps. However, at the maximum lean angles, only one older female used crossover steps.

CONCLUSIONS

Results have shown that lean direction significantly affects the postural disturbance younger and older adults could sustain. Moreover, the age-related reduction in maximum lean angles is more important for dominant (40%) and non-dominant (41%) leans than for forward (26%) or backward (23%) leans. It is thus conceivable that different mechanisms could be responsible for balance recovery in different directions.

At lean angles larger than their maximum, older adults were more likely to take multiple steps. However, crossover steps, typically seen during small and medium postural perturbations (Hsiao and Robinovitch, 2001; Maki et al., 1996), were only rarely seen at the threshold of balance recovery.

REFERENCES

Hsiao, E.T., Robinovitch, S.N. (2001). *J. Gerontol.*, **56**(1), M42-47.

Maki, B.E., et al. (1996). *J. Biomech.*, **29**(3), 343-353.

Greenspan, S.L., et al. (1998). *Am. J. Med.*, **104**(6), 539-545.

Hayes, W.C., et al. (1993). *Calcif. Tissue Int.*, **52**(3), 192-198.

Nevitt, M.C., Cummings, S.R. (1993). *J. Am. Geriatr. Soc.* **41**(11), 1226-1234.

ACKNOWLEDGEMENTS

We gratefully acknowledge the assistance of Benjamin Huneault, Véronique Lalancette, Éric Giguère and Mathieu Hamel along with the support of the Junior I Research Fellow Grant of an FRSQ (Fonds de la Recherche en Santé du Québec) Centre 6391 and 5393 from the Research Centre on Aging to Cécile Smeesters.

Table: Effects of age and lean direction on kinematics variables

Lean Direction	Age	Max Lean Angle (deg) *** ††† ‡	Reaction Time (s) †††	Weight Transfer Time (s) *** †††	Step Time (s)	Step Length (m) ** †††	Mean Step Velocity (m/s) ** †††	Maximum Step Velocity (m/s) * ††† ‡‡‡
Forward	**OA**	22.1±3.5	0.065±0.008	0.196±0.024	0.212±0.025	0.836±0.068	3.99±0.65	5.57±0.83
	YA	29.9±4.1	0.068±0.015	0.128±0.026	0.197±0.019	0.961±0.078	4.90±0.65	6.97±1.09
Dominant	**OA**	14.8±5.2	0.088±0.011	0.185±0.057	0.223±0.091	0.557±0.122	2.79±0.98	3.86±1.19
	YA	24.7±3.1	0.084±0.009	0.141±0.052	0.206±0.041	0.758±0.122	3.75±0.52	4.96±0.61
Non-Dominant	**OA**	14.3±6.2	0.090±0.010	0.165±0.023	0.219±0.071	0.606±0.096	2.92±0.70	3.92±0.82
	YA	24.1±2.4	0.083±0.010	0.133±0.028	0.204±0.026	0.737±0.091	3.65±0.43	4.79±0.52
Backward	**OA**	15.0±2.9	0.097±0.015	0.108±0.030	0.248±0.029	0.654±0.126	2.69±0.69	4.04±0.80
	YA	19.4±3.1	0.085±0.010	0.083±0.013	0.221±0.029	0.778±0.127	3.54±0.42	5.05±0.73

* $p<0.05$, ** $p<0.01$, *** $p<0.001$ for age: Younger Adults (YA), Older Adults (OA).
† $p<0.05$, †† $p<0.01$, ††† $p<0.001$ for lean direction.
‡ $p<0.05$, ‡‡ $p<0.01$, ‡‡‡ $p<0.001$ for age * lean direction.

CHANGES IN THE POSTURAL CONTROL SYSTEM FOLLOWING LOCALIZED MUSCLE FATIGUE: A TIME-DELAYED STABILITY ANALYSIS

Bradley S Davidson, Michael L Madigan, and Maury A Nussbaum

Virginia Polytechnic and State University, Blacksburg, VA, USA
E-mail: bsd@vt.edu, Web: www.biomechanics.esm.vt.edu

INTRODUCTION

Despite the growing support for localized muscle fatigue (LMF) increasing postural sway (Gribble and Hertel 2004), the mechanism behind this increase in sway remains unclear. Some have speculated that LMF introduces inaccuracies in proprioceptive feedback (Lundin et al. 1993). It is also possible that LMF elicits changes in the postural control system itself. Therefore, the purpose of this study was to develop a feedback-controlled model of the postural control system that accurately reproduces body kinematics during small postural perturbations, and investigate changes in gain parameters and time-delay stability with LMF.

METHODS

Participants included 16 older (62.2±5.1) and 16 younger (19.4±1.4) adults. During the experimental session, small magnitude postural perturbations were administered before and after fatiguing the lumbar extensor muscles.

Padded ballistic pendulums were used to administer five randomly-timed gentle forward perturbations (6 N·s) at the inferior margin of the scapulae. During the perturbations, participants stood with feet together and eyes closed, with hands clasped behind their back. Following an initial set of unfatigued perturbations, the lumbar extensors were fatigued to 70% of the unfatigued maximum voluntary contraction with repeated isotonic contractions (Davidson et al. 2004). Immediately after the exercise, a series of five fatigued perturbations were administered in the same manner as before the exercise. Kinematics during response to perturbations were recorded using reflective markers.

A feedback-controlled dynamic model of upright stance was created to simulate the experimentally recorded data. The 2-D model consisted of an inertially correct body segment with passive ankle stiffness and damping. Input to the model was the experimentally recorded pendulum force, $F(t)$, and the controlling ankle torque, $T_A(t)$, was composed of time-invariant proportional and differential feedback gains operating on the time-delayed state. An arbitrary reference angle was included to simulate the naturally occurring forward lean (Figure 1).

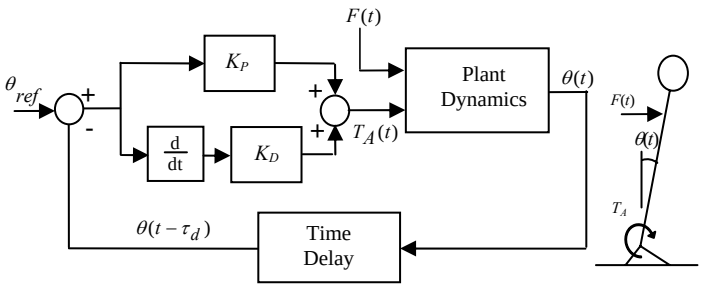

Figure 1: Schematic and free body diagram of controlled dynamic system

The linearized time-delayed equations of motion in 1st order form are given as:

$$\dot{x}(t) = A_0 x(t) + A_1 x(t - \tau_d) + (g + bF(t))$$

where x is the state vector, $(g + bF(t))$ is a vector containing the constant and transient torques due to pendulum force and body mass, and A_0 and A_1 represent the non-delayed and delayed state matrices, respectively. Simulations began at the instant of pendulum contact using the recorded initial conditions, and continued for two seconds.

After determining system parameters, system stability was quantified by the delay margin (the maximum time-delay a system can encounter before it becomes unstable). In short, the delay margin was calculated with a frequency-sweeping method (Gu et al. 2003) that solves the generalized eigenvalue problem containing the non-delayed and delayed state matrices from above. The delay margin of the system relative to the identified time-delay was calculated. A two-way repeated measures analysis was used to test for effects of LMF and age on K_P, K_D, and τ_{rel}.

RESULTS AND DISCUSSION

In general, the parameterized simulations performed well in modeling the experimental data (R^2=0.823±0.154). Statistical analysis revealed no significant (p<0.05) changes with LMF or age (Figure 2). However, the differential gain, K_D, demonstrated a trend towards a significant age effect (p=0.0808). These differences in age are consistent with findings with respect to quiet stance (Maurer and Peterka, 2005).

One other important trend occurred in the relative delay margin, τ_{rel}, with LMF (p=0.0941). Following the fatiguing exercises, mean τ_{rel} decreased from 398 to 365 msec (8.3%). A decreasing delay margin indicates a diminishing region of stability with respect to time-delay. LMF did not produce an unstable postural control

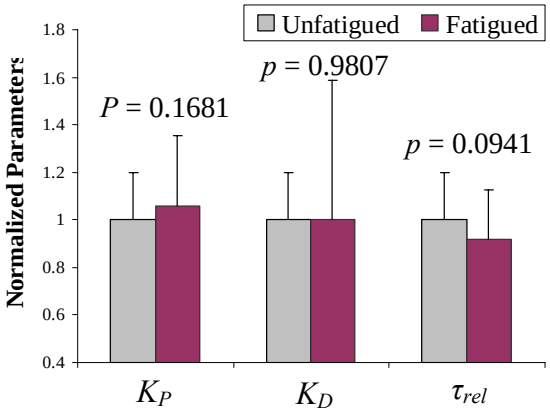

Figure 2: Plot of variables with LMF

system. Instead, these results imply that the fatigued system is less robust to noise, inaccurate or conflicting afferent information, and other sources of variance.

CONCLUSIONS

In summary, a feedback-controlled dynamic model was created that can accurately simulate the response to small perturbations to upright stance. This model was used to identify postural control gains, and was combined with a novel time-delayed stability analysis to identify possible LMF-induced changes in postural stability.

REFERENCES

Davidson, B.S. et al. (2004). *Eur. J. Appl. Physiol.*, **93**, 183-189

Gribble, P.A., Hertel,J. (2004). *Arch. Phys. Med. Rehabil.,* **85**, 589-592.

Gu, K., et al. (2003). *Stability of Time-Delay Systems*. Birkhäuser.

Lundin, T.M. et al. (1993). *J. Appl. Biomech.,* **9**, 191-201.

Maurer, C., Peterka, R.J. (2005). *J. Neurophysiol.* **93**, 189-200

ACKNOWLEDGEMENTS

This research was supported by R01 OH07882-02 (to MAN).

ACL Injury Prevention Using a Novel Pivoting Elliptical Machine

Yupeng Ren[1-2] , Hyung soon Park[1-2], Yining Wu[1-2], Alison Chang[2], Joel Press[1-2], and Li-Qun Zhang[1-2]

[1] Rehabilitation Institute of Chicago, Chicago, IL, USA
[2] Northwestern University, Chicago, IL, USA, E-mail: l-zhang@northwestern.edu

INTRODUCTION

Anterior cruciate ligament (ACL) is the most commonly injured knee ligament in sports-related activities, especially in pivoting sports. The highest incidence is in individuals 15 to 25 years old who participate in pivoting sports (Griffin et al., 2000). ACL injury biomechanics, including the factors contributing to the higher incident rate in female athletes than their male counterparts are still unclear. There is a lack of convenient and effective devices for training athletes, especially females, to improve neuromuscular control in tibial rotation and to potentially better prepare them for pivoting sports. A pivoting elliptical exercise machine is developed to carry out the training which generates perturbations to the feet/legs in tibial rotations during sagittal plane elliptical movement. Training based on the pivoting elliptical machine addresses the specific issue of movement control in pivoting and potentially better prepare athletes for pivoting sports. Training outcome can also be evaluated in multiple measures using the pivoting elliptical machine.

METHODS

A special pivoting elliptical machine is designed to help subjects improve neuromuscular control in tibial rotation (and thus reduce the risk of ACL injuries in pivoting sports). Practically, isolated pivoting exercise is not closely related to functional activities and may not be effective in the training. Therefore, in this study, pivoting training is combined with sagittal plane stepping movements to make the pivot training practical and functional.

Training in pivoting control can be done under the motor control in the following ways: (1) The footplate is perturbed back and forth in tibial rotation (pivoting) torque during the sagittal plane elliptical stepping movement. The subject is asked to resist the foot/tibial rotation torque and keep the foot pointing forward while doing the sagittal plane elliptical movements. The tibial rotation perturbation torque amplitude, frequency, and waveform can be adjusted. (2) The footplate is made free to rotate (through back-drivability control which minimizes the resistance torque at the rotating disks or by simply releasing the cable driving the rotating disk) and the subject needs to maintain stability and keep the foot straight during the elliptical stepping exercise. Both modes are used to improve neuromuscular control in tibial rotation (Fig 1.).

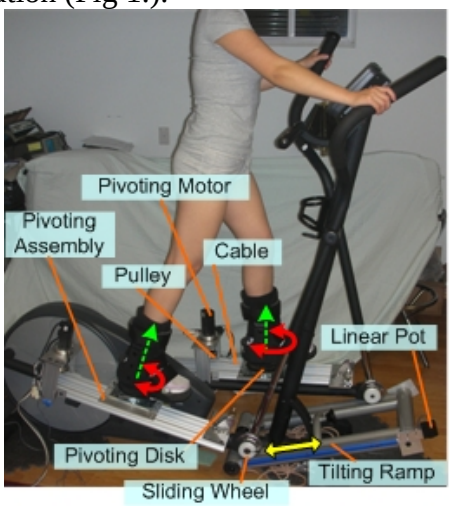

Fig. 1. A special elliptical machine (called “Pivoting elliptical machine”) The EMG measurement is optional.

RESULTS AND DISCUSSION

The subjects easily got used to the elliptical movement with rotational perturbations at both feet and performed the pivoting elliptical movement naturally. The rotational perturbations resulted in stronger muscle activities in the targeted lower limb muscles. The hamstrings and gastrocnemius activities are increased considerably during forward elliptical movement *with the pivoting perturbation* (Fig. 2).

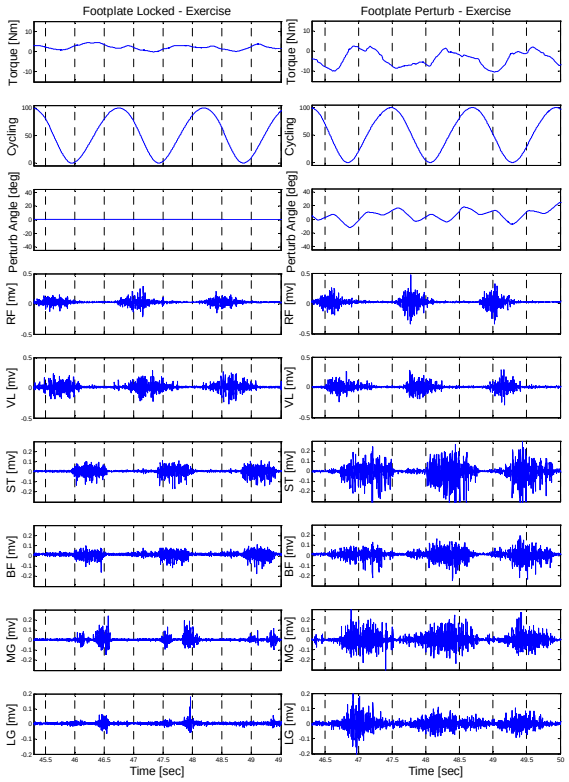

Fig. 2. The footplates were perturbed by a series of torque pulses which rotate the footplates back and forth. The subject was asked to perform the elliptical movement while maintaining the foot pointing forward.

Improvement in sensory-motor performance through the pivoting elliptical training is observed. Over five 30-minute training sessions, subjects showed marked improvement in controlling tibial rotation, as shown in the reduced rotation instability (variation in rotation) (Fig. 3a). The pivoting disks were made free to rotate and the subject was asked to keep the feet stable and pointing forward during the elliptical movements. Standard deviation of the rotating angle during the pivoting elliptical exercise was used to measure the rotating instability, which was reduced markedly after the training (Fig. 3a), and the instability reduction was obvious for both left and right legs (Fig. 3b).

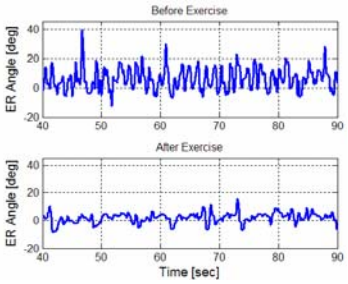

Fig. 3a

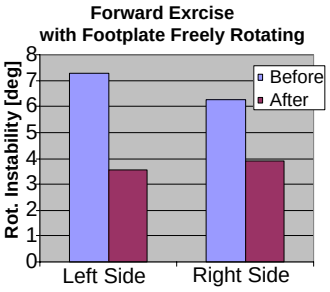

Fig. 3b

Similar improvement was observed for rotation instability measured under external perturbation of the footplate by the motor, as shown in Fig. 4, the increased stability following the training may be related to improvement in tibial rotation muscle strength, which was increased after the training of multiple sessions.

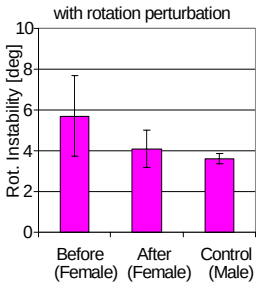

Fig. 4

SUMMARY/CONCLUSIONS

The proposed pivot training has significant potential for injury prevention. 1) it target major underlying mechanisms of ACL injury associated with pivoting. 2) combining tibial rotation with sagittal plane elliptical movements makes the training simple and practical. 3) training-induced neuromuscular changes in tibial rotation can be quantified by strength, laxity, stiffness, proprioception, reaction time, and stability in tibial rotation.

REFERENCES

Griffin et al. Noncontact ACL injuries: Risk factors and prevention strategies. J. AAOS. 8, 141-150, 2000

THE EFFECT OF LOADING RATE ON PORCINE LUMBAR SPINAL SEGMENTS: AN IN-VITRO BIOMECHANICAL STUDY

J.M. Popovich, Jr.[1,3], J.W. Welcher [2,3], K. Kulig [1], G. Pelled [3], D. Gazit [3], and W. Tawackoli [3]

[1] Biokinesiology & Physical Therapy, University of Southern California, Los Angeles, CA, USA
[2] Biomedical Engineering, University of Southern California, Los Angeles, CA, USA
[3] Stem Cell & Biomechanics Laboratory, Cedars-Sinai Medical Center, Los Angeles, CA, USA
E-mail: popovich@usc.edu

INTRODUCTION

The lumbar spine consists of varying tissues, including bone, cartilage, fibrocartilage, nucleus pulposus, and ligaments. As such, the viscoelastic properties of the lumbar spine are represented by a combination of these different tissue properties. The biomechanical characteristics of spinal specimens are dependent on many factors, including the loading profile, loading history and direction of load application (Chow, et al., 2004). Recommendations for in-vitro biomechanical testing have been established and serve as general guidelines for testing spinal implants (Wilke, et al., 1998).

In order to investigate the effects of spinal implants and therapeutic technologies on spine biomechanics, it is necessary to determine proper testing protocols specific to the specimens being utilized. That is, the mechanical properties are highly dependent upon the specimen being tested (Wilke, et al., 1998). While loading rate of spinal specimens has been studied (Myers, et al., 1991, Adams and Dolan, 1996, and Wilke, et al., 1998), biomechanical variables measured and specimens included do not provide data specific to porcine specimens. Therefore, the purpose of this investigation was to determine the effect of loading rate on the biomechanical properties of porcine functional spinal units (FSU). We hypothesized that increases in loading rate would result in detectable viscoelastic changes.

METHODS

Three fresh frozen porcine lumbar FSUs were dissected and used for biomechanical testing. Specimens were free of any gross morphologic deformity or pathology. Wood screws were inserted into the cranial and caudal vertebra of the FSU to assist in anchoring the specimen in two-part polyurethane potting solution. Specimens were submerged into the potting solution at the level of the vertebrae midline, parallel to the corresponding intervertebral disc. To ensure adequate hydration, each specimen was sprayed with isotonic saline solution.

Potted specimens were thawed at room temperature and tightly secured into the fixtures of an eight-axis Bose Kinematic Spine Tester (Bose Corporation, ElectroForce Systems Group, Eden Prairie, MN). The testing protocol consisted of five loading cycles of continuous pure bending moment in each flexion/extension, bilateral, and 45 off-axis, while maintaining a 0N axial load. Loading rate was randomly performed at four angular velocities of 0.25°/sec, 0.5°/sec, 0.75°/sec, and 1.0°/sec, with a load limit set to ± 7.5Nm. Time between each loading period was two minutes.

Kinematic and kinetic data were recorded at a sampling rate of 10Hz. Data analysis was performed using Matlab version R2006a (The Mathworks, Inc., Natick, MA). The fourth bending cycle was used to calculate

total range of motion (ROM), hysteresis, and neutral zone (NZ) range.

RESULTS AND DISCUSSION

A representative load-deformation curve demonstrating changes at different loading rates is displayed in Figure 1.

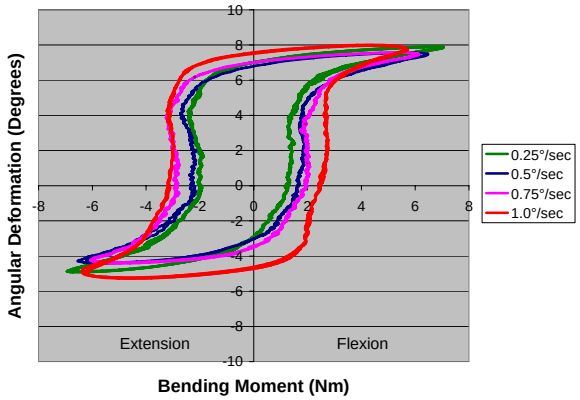

Figure 1: Load-deformation curve of porcine functional spinal unit.

Descriptive statistics including total ROM, hysteresis, and NZ range are summarized in Table 1. Total ROM and NZ range did not change considerably following each loading rate condition (less than 19%); however, there was a pattern of overall decrease in total ROM at greater loading rates, while there was an increase in NZ range at greater loading rates. Hysteresis demonstrated greater changes (range: 15% – 52%) associated with differing loading rates. These patterns existed across all three loading directions.

SUMMARY/CONCLUSIONS

Upon observation of biomechanical testing, changes in loading rate from 0.25°/sec to 1.0°/sec had minimal effect on total ROM and NZ range in porcine lumbar specimens. However, due to the viscoelastic properties of the porcine spinal specimens, hysteresis did demonstrate differences between loading rate conditions in all three loading directions. Future work will include a larger sample size, increased loading rates, and further statistical analysis.

REFERENCES

Adams, M.A., Dolan, P. (1996). *Clinical Biomechanics*, **11**, 194-200.

Chow, D.H.K., et al. (2004) *Clinical Biomechanics*, **19**, 99-106.

Myers, B.S., et al. (1991). *Journal of Biomechanics*, **24**, 811-817.

Wilke, H.J., et al. (1998) *European Spine Journal*, **7**, 148-154.

Wilke, H.J., et al. (1998) *The Anatomical Record*, **251**, 15-19.

Table 1: Variables measured at four loading rates for each bending direction (mean ± s.d.).

	Flexion/Extension			
Loading Rate:	**0.25°/sec**	**0.5°/sec**	**0.75°/sec**	**1.0°/sec**
Total ROM [°]:	13.9 ± 0.9	13.5 ± 1.0	12.8 ± 1.4	12.6 ± 1.0
Hysteresis [Nm°]:	50.8 ± 5.5	60.2 ± 9.1	68.0 ± 13.3	77.3 ± 6.0
Neutral Zone [°]:	9.9 ± 1.3	11.3 ± 1.3	11.3 ± 1.7	11.7 ± 1.0
	Bilateral Bending			
Total ROM [°]:	12.8 ± 1.5	12.2 ± 1.5	11.8 ± 0.9	11.4 ± 1.1
Hysteresis [Nm°]:	48.0 ± 8.2	55.2 ± 10.2	62.1 ± 11.0	69.8 ± 9.8
Neutral Zone [°]:	10.1 ± 1.3	10.2 ± 1.5	10.4 ± 1.1	10.5 ± 1.1
	45° Off Axis/Oblique Bending			
Total ROM [°]:	13.6 ± 0.8	12.8 ± 0.5	12.5 ± 0.7	12.3 ± 0.3
Hysteresis [Nm°]:	50.5 ± 5.1	58.4 ± 6.8	67.0 ± 7.8	76.7 ± 9.7
Neutral Zone [°]:	10.5 ± 0.4	10.8 ± 0.6	11.0 ± 0.6	11.4 ± 0.5

POST-TKA EFFECTS OF PREHABILITATION ON STANDING KNEE KINETICS

Peter M. Quesada [1,2], James E. Doane [1,2], Ann M. Swank [2],
Claudia A. Angeli [3], John Nyland [4], and Robert V. Topp [2]

[1] Dept. of Mechanical Engineering, University of Louisville, Louisville, KY, USA,
[2] Exercise Physiology Laboratory, [3] Frazier Rehab Institute, [4] Dept. of Orthopaedic Surgery
E-mail: peter.quesada@louisville.edu

INTRODUCTION

Osteoarthritis (OA) at the knee is among the most common chronic joint pathologies (Brady et al.). Knee OA is often quite debilitating, and substantially affects activities of daily living, such as standing from a chair (Felson et al.), which can have substantial knee joint loading demands. Conservative treatments for knee OA are often limited in the level of relief that they can provide. Consequently, TKA is often indicated when conservative approaches become ineffective.

Persons with better fitness often demonstrate greater capacity for recovery following various forms of bodily trauma. Consequently, it is anticipated that a program of prehabilitation prior to TKA may improve preoperative function, and could lead to better outcomes following postoperative rehabilitation.

The ultimate success of a TKA is not fully determined until following an individual's post-surgery rehabilitation. Prior to surgery, however, patients are often sedentary. In the present study the effects of a prehabilitation program on standing knee joint kinetics following TKA were investigated.

METHODS

The sample for the present study consisted of ten subjects who underwent TKA for severe knee OA. Five individuals (1 males & 4 females, with mean age, height, and weight of 66 years, 165 cm, and 89 kg, respectively) were randomly assigned to participate in a prehabilitation program (resistive strength and balance training) prior to TKA. The remaining subjects (2 males & 3 females, with mean age, height, and weight of 65 years, 169 cm, and 84 kg, respectively) were instructed to not modify their activity levels. Following TKA all subjects in both groups participated in a standardized, post-surgery rehab.

All subjects completed testing sessions approximately 4-6 weeks prior to TKA, and 12 weeks after TKA. At both sessions motion tracking data were obtained with an optoelectronic system. Two stand/sit trials were performed at each session. The first was performed with the unaffected limb on a force platform, and the affected limb on the ground. Foot placements were reversed for the second trial. For the second trial, subjects were instructed to perform as many stand to sits in 30 seconds as they were able. They were also instructed to perform the first trial at the same pace as the second one, but for a single repetition. Only the first stand/sit of the second trial was considered here. For each trial, peak vertical ground reaction, peak knee extension moment, and peak knee power generation were obtained.

RESULTS AND DISCUSSION

The total subject pool, at session 1 (prior to interventions), exhibited lower normalized peak vertical ground reaction forces, peak knee extension moments, and peak knee

power generation (Figure 1); although statistical significance was not quite attained for the latter measure ($p = 0.07$). Thus asymmetry ratios (i.e. affected/unaffected) for these measures were considerably less than unity at initial testing. No significant improvements in asymmetry ratios, however, were seen for either group. For the total subject pool these kinetic measures continued to be lower for the affected limb at the testing session 12 weeks following TKA (Figure 2), with statistical significance attained for each measure.

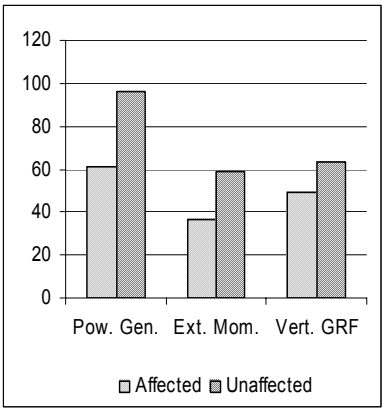

Figure. 1: Normalized peak knee power generation, peak vertical ground reaction, and peak knee extension moment for unaffected and affected limbs at session 1.

Overall functional measures, such as number of stand/sit cycles in 30 seconds, do not evaluate mechanisms with which activities are performed. The ground reaction force, knee extension moment, and knee power generation deficits at each session are indicative of compensations being employed by individuals to cope with functional deficits. Although complaints of pain may be mitigated following TKA, such compensations could result in deterioration of a "good" knee and, subsequently, lead to a second TKA if such functional deficits are not further addressed.

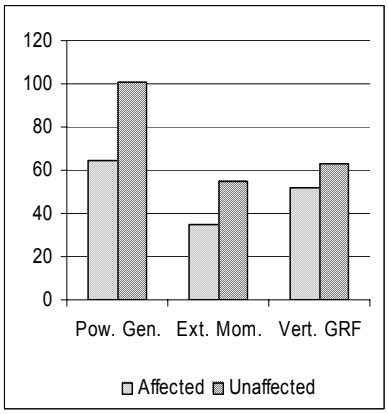

Figures. 2: Asymmetry ratio changes (session one minus session two) for prehabilitation and non-prehabilitation

SUMMARY/CONCLUSIONS

In the present study pre-surgery knee joint kinetic measures during standing were lower for the operative limb. Following TKA, these surgical limb deficits persisted for both the control and prehabilitation groups. Consequently, the prehabilitation protocol may not be affecting the mechanisms by which these individuals stand. However, the sample size is small at this time, and subject recruitment is continuing.

REFERENCES

Brady, O., et al. (2000): *Can. Med. Assoc. Journ.*, 163(10), 1285-1291.

Felson, D. T., et al. (1987): *Arthr. Rheum.*, 30, 914-918.

ACKNOWLEDGEMENTS

This work received support from the National Institute for Nursing Research (Grant # 1RO1 NR080).

COMPARISON OF FINGER FORCE ENSLAVING AND SHARING BETWEEN MVF AND OSCILLATORY FINGER FORCE PRODUCTION TASKS

Qi Li, Marcio A. Oliveira, Jae Kun Shim
University of Maryland, College Park, MD, USA
E-mail: qili@umd.edu Web: www.hhp.umd.edu/KNES/faculty/jkshim/neuromechanics

INTRODUCTION

Finger interaction indices such as finger enslaving calculated from experiments of multi-finger maximum voluntary force (MVF) production task have been used to model the inter-connections between finger forces and the central nervous system (CNS) commands to the fingers. However, it has not been studied whether different finger force production tasks would induce different inter-connections. This study aimed to investigate the effects of force production patterns (maximum force production and oscillatory force production) and finger force direction (flexion and extension) on the finger interaction indices, such as force enslaving (FE; involuntary force of non-task fingers), and force sharing (FS; percentage contributions of finger forces to the total force during a four-finger force production task).

METHODS

Apparatus Four two-directional (tension and compression) force sensors with amplifiers (Models 208 M182 and 484B, Piezotronics, Inc.) were used to measure isometric finger flexion and extension forces. The frame was attached to an aluminum panel with a vertical slit. C-shaped aluminum thimbles were attached on the bottom of each sensor. The frame was tilted at 25^{o} with respect to the antero-posterior axis such that all finger joints were slightly flexed when the distal phalanges were positioned inside the thimbles. The forearm and hand was fixed in a brace.

Procedure Sixteen healthy and right handed young adults (8 females and 8 males) were asked to insert each finger tip of the right hand into a thimble and were instructed to produce two main tasks: (a) maximum flexion and extension isometric force with one finger (I- index, M-middle, R-ring, and L-little) and all four fingers (IMRL) at a time over several seconds; (b) fast and slow oscillatory (flexion and extension) finger force production (oscillation task) following a auditory feedback metronome (60 and 120 bpm) with one finger (I, M, R, L) and all four fingers (IMRL). The forces produced in either direction were 20% of the task finger's MVF. The conditions lasted 20 seconds (for a total of 20 cycles).

The forces of both instructed finger and non-instructed fingers were recorded (Figure 1). Indices of digit interaction such as FE and FS were computed for the MVF tasks. For the oscillation tasks, gain of frequency-response function (input: task finger force, output: non-task finger forces) was used as indices of finger interaction.

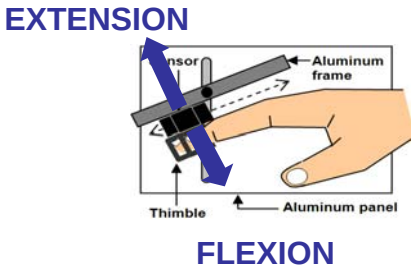

Figure 1: Experimental setup

RESULTS

When compared two force production patterns (peak and oscillatory), FE during MVF task was greater than both conditions of oscillation tasks (60 and 120bpm). While FE was not significant different between two oscillatory conditions (Figure 2), FE in extension direction was in general greater than in flexion direction. No significant differences for FS were found when compared force production patterns (peak and oscillatory) and directions (flexion and extension). The middle finger showed higher contribution during four-finger task (Figure 3).

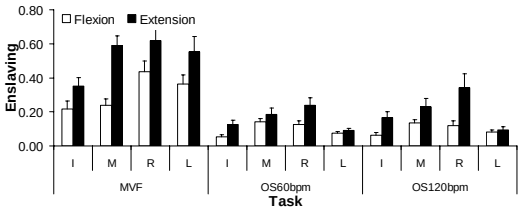

Figure 2: Force enslaving during flexion and extension in MVF, 60bpm and 120bpm oscillation tasks

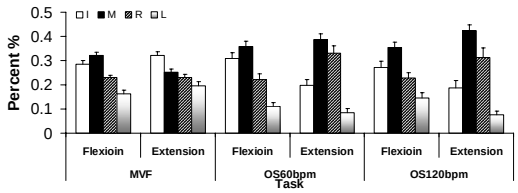

Figure 3: Force sharing during flexion and extension in MVF, 60bpm and 120bpm oscillation tasks

CONCLUSIONS

Our results showed that the FE indices are affected by force production pattern and by the finger force direction. We suggest that different inter-finger matrix (enslaving matrix) should be used for modeling of different finger force production tasks.

REFERENCES

Jae Kun Shim, et al.(2007). *Exp Brain Res*, 176, 374-386,.

Minoru Shinohara, et al.(2003).*Appl Physiol*, 94, 259-270,.

Table 1: Force Enslaving ratio

	MVF				OS60bpm				OS120bpm			
	I	M	R	L	I	M	R	L	I	M	R	L
Flexion	0.22± 0.05	0.24± 0.04	0.43± 0.06	0.36± 0.05	0.05± 0.01	0.14± 0.02	0.13± 0.02	0.07± 0.01	0.06± 0.02	0.13± 0.02	0.12± 0.03	0.08± 0.01
Extension	0.35± 0.05	0.59± 0.06	0.62± 0.09	0.55± 0.09	0.12± 0.03	0.18± 0.04	0.24± 0.04	0.09± 0.01	0.17± 0.04	0.23± 0.05	0.34± 0.08	0.10± 0.02

Table 2: Force Sharing ratio

	MVF		OS60bpm		OS120bpm	
	Flexion	Extension	Flexion	Extension	Flexion	Extension
I	0.285±0.014	0.321±0.015	0.308±0.025	0.198±0.023	0.272±0.026	0.186±0.031
M	0.321±0.014	0.252±0.011	0.358±0.021	0.387±0.024	0.354±0.021	0.423±0.024
R	0.230±0.009	0.230±0.013	0.223±0.023	0.330±0.030	0.227±0.023	0.314±0.039
L	0.164±0.014	0.197±0.015	0.111±0.016	0.085±0.016	0.147±0.021	0.077±0.015

BIDIRECTIONAL NEURAL COUPLING BETWEEN UPPER AND LOWER LIMBS

Helen J. Huang [1] and Daniel P. Ferris [1]

[1]Human Neuromechanics Laboratory, University of Michigan, Ann Arbor, MI, USA
E-mail: hjhuang@umich.edu

INTRODUCTION

Humans have neural connections between their upper limbs and lower limbs that influence muscle activation patterns. For example, during human walking upper limb muscles are activated to swing the arms in coordination with lower limb movement (Hinrichs 1990). In addition, upper limb muscle activation can facilitate lower limb muscle activation during passive locomotor-like movements of the lower limbs (Ferris et al 2006; Huang & Ferris 2004).

The purposes of this study were to determine a) if lower limb muscle activation facilitates upper limb muscle activation during passive locomotor-like movement of the upper limbs, and b) if simultaneous upper and lower limb muscle activation results in a change in electromyography (EMG) amplitude compared to just upper or just lower limb muscle activation in healthy subjects. Based on our previous work, we hypothesized that lower limb activation would increase muscle activation in the passive upper limbs. We also hypothesized that simultaneous maximum upper limb and lower limb activation would result in decreased muscle recruitment compared to independent maximum upper limb or lower limb activation. This is contrary to what we have demonstrated for passive limb movement but it is in agreement with other studies showing a bilateral deficit with simultaneous activation of the upper limbs (Ohtsuki 1983).

METHODS

Six healthy subjects performed recumbent stepping (Figure 1) using four different combinations of upper and lower limb effort (active-A or passive-P).

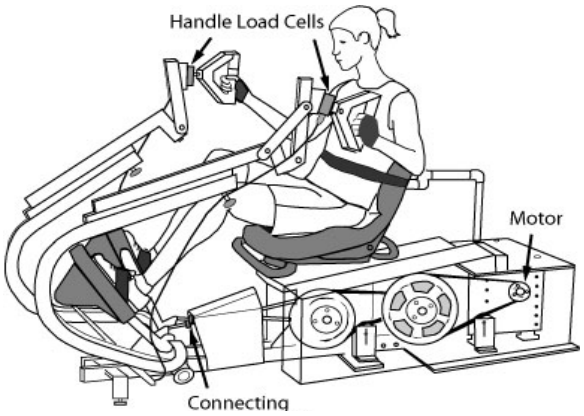

Figure 1: Recumbent stepping machine with real-time computer controlled resistance and force and position sensors. (Modified from TRS 4000, NuStep Inc, Ann Arbor, MI). The machine provided smooth consistent stepping regardless of subject effort through a custom designed position control of a prescribed sine wave stepping profile.

For active effort, we instructed subjects to use maximal effort. For passive effort, we instructed subjects to relax and exert minimal effort. The four conditions were a) passive upper & passive lower, PU-PL b) passive upper & active lower, PU-AL c) active upper & passive lower, AU-PL, d) active upper & active lower, AU-AL. Velcro gloves and pedal straps secured subject's hands and feet to the handles and pedals, respectively. A torso strap helped minimize torso movement. The stepping frequency

was 75 BPM, 1.25 Hz. After each trial, subjects rested for at least 30 seconds.

We collected EMG and joint kinematics from upper and lower limbs. We calculated limb forces from load cells on the handles and pedals. For each condition and muscle, we calculated the root-mean-square (RMS) EMG for the three strides with the greatest subject work. We normalized the RMS amplitudes to the maximum AU-PL RMS EMG for the upper limb muscles and likewise, to the maximum PU-AL RMS EMG for the lower limbs for each subject. To determine differences between conditions for each muscle, we used a repeated measures ANOVA and Tukey-Kramer Honestly Significant Difference (HSD) post-hoc tests.

RESULTS AND DISCUSSION

Lower limb muscle activation resulted in greater muscle activation of passive upper limb muscles (Fig. 2A *conditions). PU-AL RMS amplitudes were significantly greater than PU-PL amplitudes for the anterior deltoid, posterior deltoid, biceps, and triceps muscles. Similarly, upper limb muscle activation facilitated muscle activation of passive lower limbs (Fig. 2B * conditions). AU-PL amplitudes were significantly higher than PU-PL amplitudes for the vastus medialis, medial hamstrings, and tibialis anterior muscles. During simultaneous upper and lower limb muscle activation, EMG amplitudes were significantly lower compared to just upper limb activation or just lower limb activation for the posterior deltoid, vastus medialis, tibialis anterior, and soleus muscles (Fig 2, **conditions)

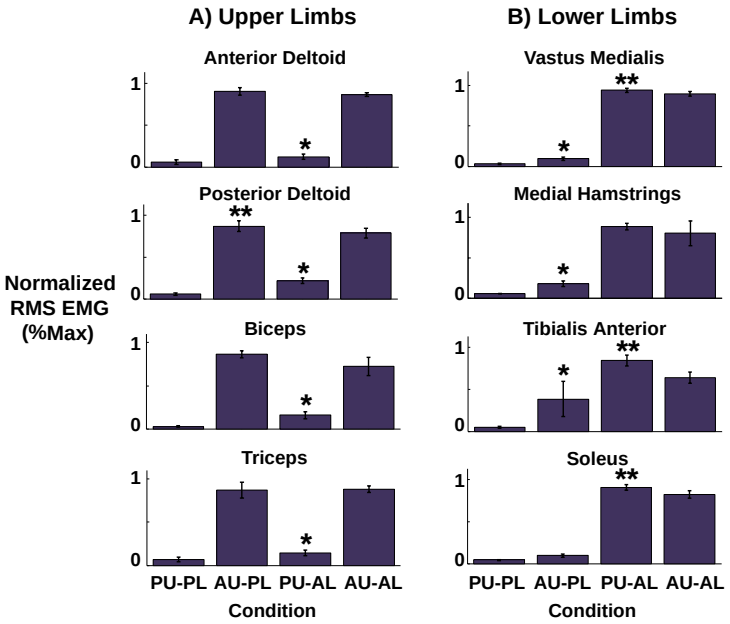

Figure 2: Averaged normalized RMS EMG with standard error bars for all subjects and strides. *Significantly different from PU-PL condition. **Significantly different from AU-AL condition.

SUMMARY / CONCLUSIONS

These results suggest that neural coupling between upper limbs and lower limbs is bidirectional during locomotor-like movements in healthy subjects. This bidirectional neural coupling facilitates muscle activation of passive limbs but hinders muscle activation of active limbs. Bidirectional upper-lower neural coupling could have implications for rehabilitation of interlimb coordination after neurological injury.

REFERENCES

Hinrichs, R.N. (1990). *Multiple Muscle Systems.* Springer-Verlag. 694-705.

Ferris, D.P. et al. (2006). *Exerc Sport Sci Rev*, **34**(3), 113-120.

Huang, H.J. and Ferris, D.P. (2004). *J Appl Physiol*, **97**, 1299-1308.

Ohtsuki, T. (1983). *Behav Brain Res*, **7**, 165-178

ACKNOWLEDGEMENTS

This project was supported by PVA SCRF and an NIH NRSA.

POINT MARKERS VERSUS CLUSTER TRIADS: MULTI-SEGMENT FOOT MODEL PERFORMANCE IS INSENSITIVE TO THE ARCHITECTURE OF THE REFLECTIVE MARKERS USED IN OPTICAL MOTION ANALYSIS

Kiersten Anas[1], Shawn Robbins[2], Colin Dombroski[2], and Thomas Jenkyn[1,2]

[1]Biomedical Engineering, University of Western Ontario, London, ON, Canada
[2]Wolf Orthopaedic Biomechanics Lab, Fowler Kennedy Sport Medicine Clinic, London, ON, Canada
Email: tjenkyn@eng.uwo.ca

INTRODUCTION

Clinical gait analysis commonly treats the foot as a single rigid segment, which does not allow kinematic information to be collected for the joints within the foot. These joints are susceptible to injury and dysfunction (Hunter and Prentice, 2001) and would benefit from quantification with gait analysis. A number of clinical tests assess foot function under static conditions (Hunter and Prentice, 2001), but a weak correlation has been demonstrated between the static and dynamic function of the foot. Several kinematic models in the literature address this problem by defining separate segments within the foot (Carson, et al., 2001; Kidder, et al., 1996; Leardini, et al., 1999). However, there is no consensus on the architecture of the skin-mounted markers for tracking these kinematic models; whether to use individual point markers or rigid clusters of markers.

This study compares the performance of a multi-segment kinematic foot model (Jenkyn and Nicol, 2007) tracked using point markers versus triad clusters of markers.

METHODS

30 healthy subjects (21 females, 9 males; mean age=27.7, range 19 to 53 years; mean height=170.8, range 157 to 193 cm; mean weight=67.6, range 44 to 104 kg) with no clinically diagnosed foot or ankle dysfunction, performed barefoot level walking at a self-selected speed. Gait analysis was performed using an optical motion tracking system (8 Eagle camera EvaRT system, Motion Analysis Corp, Santa Rosa, CA, USA) and floor-mounted force plate (OR6, AMTI, Watertown, MA, USA) using passive reflective markers in a modified Helen Hayes marker setup for all but the right foot.

The hindfoot, midfoot and medial and lateral forefoot segments of the right foot were tracked with either 7 point markers (Figure 1A) or with 4 triad clusters (Figure 1B). The hallux was tracked with a triad cluster in both cases.

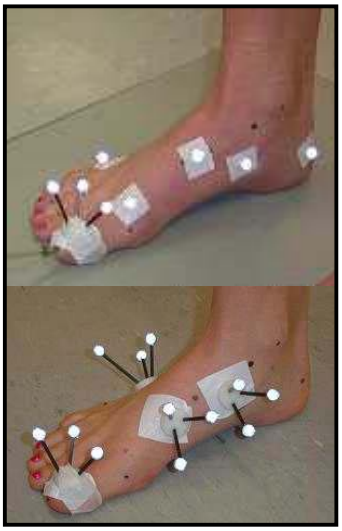

Figure 1: A) Point markers attached to the segments of the foot (one on hindfoot and one on midfoot not shown)

B) Triad clusters attached to the segments of the foot (one on hindfoot not shown).

Marker trajectories markers in both cases were post-processed to calculate the same four joint motions: hallux dorsi-plantarflexion (HA), forefoot frontal plane supination-pronation (FFA-frontal), hindfoot frontal plane supination-pronation (HFA-frontal) and medial longitudinal arch height-to-length ratio (MLA). These measures

were compared between cases using intraclass correlation coefficients using a two-way mixed model of absolute agreement.

RESULTS AND DISCUSSION

The agreement between the point marker and the triad cluster methods of tracking the multi-segment foot model is shown in Table 1. Four kinematic measures are compared: medial longitudinal arch (MLA) height-to-length ratio, hallux (HA) dorsi-plantarflexion, forefoot (FFA) supination-pronation twist in the frontal plane and hindfoot (HFA) supination-pronation in the frontal plane. The mean and standard deviation (SD) are shown for each measure for each marker type. The intraclass correlation coefficient (ICC) and its 95% confidence interval are also given. For all measures except for HA the 95% confidence interval of the ICC spanned zero, showing no significant difference between marker architecures. Only the hallux angle (HA) was significantly different between architectures. This is likely due to a different definition of the long axis of the medial forefoot segment between cases yielding a shift in the absolute magnitude of hallux dorsi-plantarflexion angle without changing the shape of the angle curve.

SUMMARY/CONCLUSIONS

The results of this study demonstrated that the performance of the multi-segment kinematic model of the foot was unaffected by the architecture of the passive reflective markers used with optical motion analysis; whether individual point markers or triad clusters. Since each method carries advantages and disadvantages, researchers should be confident in choosing whichever marker architecture is more convenient without fear of compromising the measured kinematics.

REFERENCES

Carson M.C., et al. (2001) *J Biomech* 34(10): 1299-1307

Hunter S., Prentice W.E. (2001) *Techniques in Musculoskeletal Rehabilitation.* McGraw-Hill.

Jenkyn T.R. and Nicol A.C. (2007) *J Biomech* epublished

Kidder S.M., et al. (1996) *IEEE Trans Rehab Eng* 4(1): 25-32.

Leardini A., et al. (1999) *Clin Biomech* 14(8): 528-536

Table 1: Agreement between the point marker and the triad cluster methods of tracking the multi-segment foot model. Four kinematic measures are compared: medial longitudinal arch (MLA) height-to-length ratio, hallux (HA) dorsi-plantarflexion, forefoot (FFA) supination-pronation twist in the frontal plane and hindfoot (HFA) supination-pronation in the frontal plane. The mean and standard deviation (SD) are shown for each measure for each marker type. The intraclass correlation coefficient (ICC) and its 95% confidence interval are also given. Only the hallux angle (HA) was significantly different between conditions.

	POINT		CLUSTER		ICC	95% CI	
	Mean	SD	Mean	SD		Lower	Upper
MLA (dimensionless)	0.0060	0.0091	0.0049	0.0176	-0.19	-0.54	0.21
HA (degrees)	-10.85	6.16	-8.47	6.45	0.54	0.22	0.75
FFA-frontal (degrees)	0.08	1.19	0.56	4.70	-0.029	-0.41	0.35
HFA-frontal (degrees)	-0.19	2.02	1.36	3.73	0.22	-0.11	0.53

Effect of Neuromuscular Resistance Training on Multi-Finger Synergy

Jeffrey Hsu, Sohit Karol, Jae Kun Shim
University of Maryland, College Park, MD
E-mail: jefhsu@umd.edu Web: http://www.hhp.umd.edu/KNES/faculty/jkshim/

INTRODUCTION

The hand and fingers are one of the main tools humans use to interact with the external world. Multiple fingers are required for many everyday manipulative tasks. For example, while holding a glass of water, the central nervous system (CNS) must control and coordinate the fingers dexterously to avoid spilling the water and breaking the glass. Previous studies have suggested that for manipulative dexterity, it is critical for the CNS to be capable of coordinating groups of hand digits (i.e., multi finger synergy (Shim et al. 2005) and controlling individual digits (i.e., individual finger independency (Schieber & Poliakov 1998).

Previous studies have employed neuromuscular resistance training (NMRT) of the hand and fingers with simultaneous training of all digits or one digit training. The studies showed that NMRT can cause neuromuscular changes including adaptations in neural control of finger muscles and increases in hand and finger strength. However, these studies lacked the examination of NMRT on multiple-effector systems.

The objective of this study was to propose a NMRT protocol that embellishes the principle of training specificity which examines whether specific training protocols, designed to change force stabilizing synergy or moment stabilizing synergy, could induce the intended adaptations in multi-finger coordination strategies.

METHODS

Thirty-three young adults (23.0±2.9 yrs) participated in this experiment. The subjects were assigned into three experimental and one control group such that the four-finger isometric maximum voluntary force was similar for all groups. The control group (G0; n=8) received no intervention. The first experimental group (G1; n=7) trained with four fingers simultaneously with no restrictions. The second experimental group (G2; n=8) trained individual fingers without constraints on the non-training fingers. The third experimental group (G3; n=10) trained individual fingers with restricted movements on non-training fingers.

The training setup consisted of a simple pulley system where a load was hung vertically and an aluminum thimble was attached to the opposite side to be pulled horizontally by the training fingers. Four thimbles were attached for G1 and one thimble was attached for G2 and G3.

Subjects in G1, G2 and G3 were trained three sessions per week for six weeks at 70% of the measured one repetition maximum (1-RM). One repetition was defined as concentric flexion and eccentric extension about the metacarpal-phalangeal joint.

The experimental setup included four one-dimensional pizeo-electric sensors (for the 2nd-5th digits) attached to a customized aluminum frame which has four slits for the sensor positions to match the individual hand sizes of subjects. C-shaped thimbles were attached inferior to the sensor for subjects to insert their finger tips (Figure 1). Signals from the sensors were amplified, conditioned and digitized at 1000 Hz with a 16-bit A/D Board and a customized LabVIEW program. MatLab programs were written to process and analyze data.

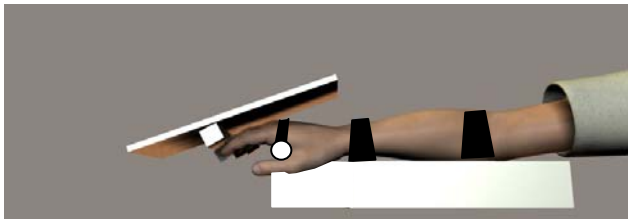

Figure 1. Experimental setup

All subjects sat facing a computer with the forearm resting in a customized wrist-forearm brace. The subjects were instructed to perform two tasks- maximal voluntary forces (MVF) production with five conditions (index- I, middle-M, ring-R, little-L, and four finger- IMRL) in flexion and an accurate force production task following a ramp template. Subjects were tested bi-weekly for the 1-RM, MVF task, and accurate force production task, starting from the first day of participation for a total of four testing sessions (S0, S1, S2, and S3).

Synergies were tested within the framework of the Uncontrolled Manifold Hypothesis. Delta variance was used to calculate the force (ΔV_{force}) and moment (ΔV_{moment}) stability. Constant Error (CE) was a measure of accuracy.

RESULTS

The results showed that moment stabilizing synergies increased with training for G1, while force stabilizing synergies increased for G3. For all groups, finger independence (FI) and CE values decreased significantly and the MVF increased (not shown in Figures).

CONCLUSION

UCM results suggested that adaptations of multi-finger neuromuscular system were specific to the training protocols- yielding changes of different multi-finger synergies (i.e., specificity of training for multi-finger synergies). This result implied that the NMRT protocols should be carefully designed for specific target coordination. Increase in finger strength and decrease in FI suggest that these two indices might be related to each other. A strength-dexterity equivalence hypothesis was proposed, explaining the relationship between the increases in strength and performance after the training, as opposed to the previously reported, strength-dexterity tradeoff (Shinohara, 2002)

REFERENCES

Schieber MH, Poliakov AV (1998). J Neursci, **18**, 9038-45

Shim JK, Latash ML, Zatsiorsky VM (2005) *J Neurophysiol* **93**: 3649-3658

Shinohara et al., (2002). J Appl Physiol, **94**, 259-70

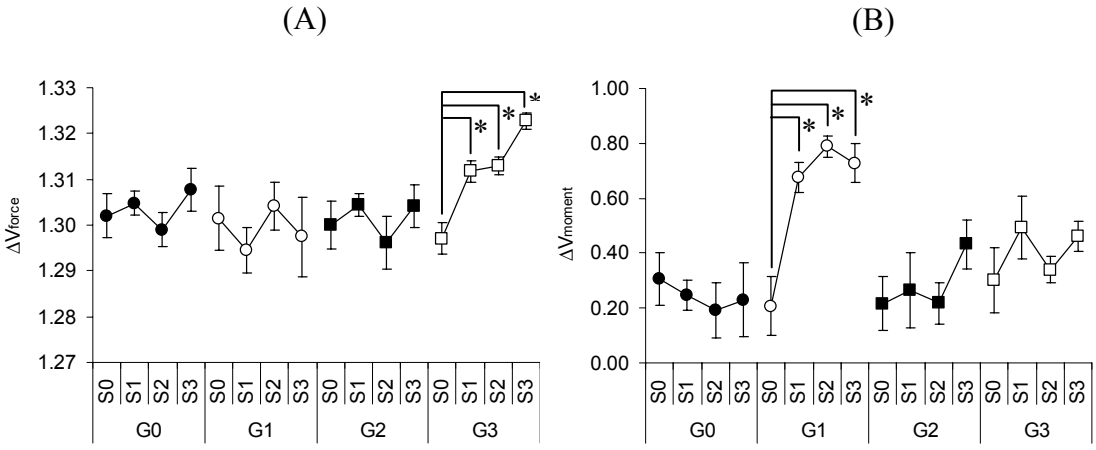

Figure 2. (A) ΔV_{force} and (B) ΔV_{moment} during all finger pressing tasks. G0, G1, G2, G3 represent the control group, the group of four-finger simultaneous training, the group of individual finger training without restriction, and the group of individual finger training with restriction to non-training finger movements, respectively. S0, S1, S2, and S3 stand for consecutive test sessions with two-week intervals. * Signifies significant ($p<.05$) differences of ΔV between sessions.

SOLUTIONS OF A REDUNDANT MOTOR TASK WITH SUB-TASK CONFLICT

Jaebum Park[1] and Jae Kun Shim[1]

[1]University of Maryland, College Park, MD, USA
email: jbpark@umd.edu web: http://www.hhp.umd.edu/KNES/faculty/jkshim

INTRODUCTION

Although robotic researchers often try to create biologically inspired grippers, the control strategies used by the human central nervous system (CNS) to solve mechanically challenging problems have not been throughly studied. In this study we employed a two-finger manipulation task with a mechanical redundancy and investigated how the human CNS solves the problem of the mechanical redundancy during multi-digit manipulation (Shim et al. 2005). In addition, the manipulation task had two sub-tasks (i.e., controlling resultant force and resultant moment) which had a control conflict between them. For example, when a task is to achieve a static position of a hand-held object, the CNS is required to control both translational and rotation position of the object, but performing stable translation and rotation require negative and positive covariations of finger forces, respectively, which cause a conflict sub-task control between them (Latash et al. 2001). The aim of this study was to investigate CNS control strategies when a task has conflicting sub tasks.

METHODS

Eight right-handed males participated as the subject, and the subjects were asked to press two six-component sensors equally distanced on a horizontal panel using index and middle fingers. A fulcrum was positioned between two sensors at the midway of a flat panel (Fig 1). For each trial, the subjects pressed the sensors while maintaining a constant level of force (i.e., force control) and keeping balance (i.e., moment control). Subjects performed the task under four conditions: two different pressing force magnitudes (i.e. 10N & 20N) and two moment arms (i.e., 1.4cm & 2.8cm).

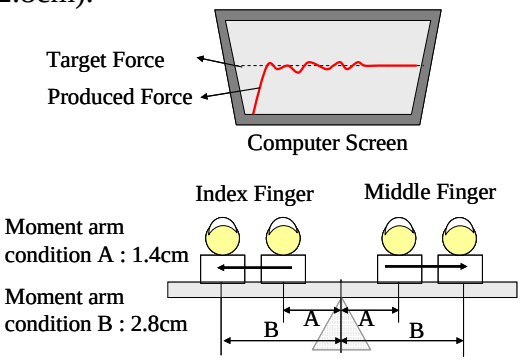

Figure1: Experimental set-up.

The following analysis was performed.

Principal Component Analysis (PCA)

For each condition, a set of variables (Index and middle finger forces, moment of normal forces) were grouped, and coefficient of correlation between variables were computed. This matrix was used to perform a principal component analysis (PCA).

Uncontrolled Manifold (UCM) analysis:

Two variances were calculated in 2-dimensional force or moment space and divided by the numbers of degrees of freedom for each variance: one variance along the task space (V_{UCM}) and the other variance orthogonal to the task space (V_{ORT}).

RESULTS & DISCUSSION

Principle component analysis

The PCA on a set of variables (index and middle finger normal forces, tangential force, and moments of normal forces) indicated three PCs accounted for 92.46 ± 2.07% of the total variances.

Table 1: Loadings of principal components (PC1 to PC3). Loadings in table are the averaged values across all 4 conditions.

	PC1	PC2	PC3
F_n^{Index}	**-0.93**	0.08	-0.09
F_n^{Middle}	**0.79**	-0.06	0.27
F_t^{Index}	0.12	**-0.56**	0.26
F_t^{Middle}	0.25	**0.84**	0.20
M_n^{Index}	**0.64**	0.05	-0.15
M_n^{Middle}	0.09	0.19	**0.95**

The normal forces of index, middle fingers had large loading showing different signs in the same PCs while small loading in other PCs (Table.1). The increase in F_n^{index} is accompanied by a decrease in F_n^{middle} so that there is a negative covariance between them. This is typical CNS strategy for the force stabilization. The tangential forces of both fingers were in the second PC showing large loadings. The negative covariance was shown between two fingers tangential forces. This means that the resultant moment of tangential force would be close to zero moment because the moment arms of tangential forces are constant in this task. Therefore, the tangential forces acted for the moment stabilization even though the moment of tangential force is the part of total moments in this task. The loading of M_n^{Index} was large in PC1 where the large loading of F_n^{index} and F_n^{middle} were shown. Especially, an increase in F_n^{index} is accompanied by a decrease in M_n^{Index}. This implies that an increase in F_n^{index} is coupled with a lot of decrease in moment arm (d_n) of F_n^{index}. M_n^{Index} and d_n are independent each other due to the movement of finger tips. M_n^{middle} had a large loading solely in the third PC. This finding means that CNS control M_n^{middle} independently. On the other hands, moment arm of F_n^{middle} (d_n^{middle}) was independent to F_n^{index} and F_n^{middle}.

Uncontrolled Manifold (UCM) analysis

For the force control hypothesis, V_{UCM} was always greater than V_{ORT} increasing the target force levels and decreasing given moment arm conditions. However, V_{ORT} was almost equal (F1) or greater (F2) than $V_{UCM.}$ Therefore, an increased in target force caused CNS explore broadly along task space accompanying large error variances in force control. However, the variance in force control hypothesis decreased with the length of moment arm, implying that CNS explores small task space with longer moment arm condition. In the moment control hypothesis, an increase in the target force needs an increase in a variance along task space as well as the error variance. In addition, the moment control strategy is changed with an increase in the moment arm under the increased target force (F2).

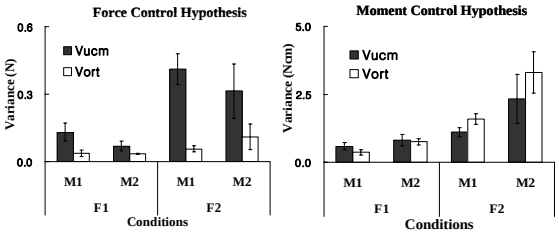

Figure3: V_{UCM} and V_{ORT} of force and moment control hypothesis. Averaged variances across subjects were represented for each condition.F1 and F2 represent 10N and 20N as target force levels, respectively. M1 and M2 are given moment arm conditions. (i.e, M1:1.4cm, M2:2.8cm)

CONCLUSIONS

When the task requires the control of force and moment simultaneously, the moments of finger force were more stabilized than the finger forces. Especially, if the moment arm is increased, the variance along task space is decreased in force control hypothesis while increased in moment control hypothesis. PCA results show that normal forces behave to stabilize the resultant force while the tangential forces act to stabilize the resultant moment.

REFERENCES

Latash ML, Scholz JF, Danion F, Schoner G (2001) *Exp Brain Res* **141**: 153-165

Shim JK, Latash ML, Zatsiorsky VM (2005) *J Neurophysiol* **93**: 3649-3658

MUSCLE SYNERGIES FOR HUMAN POSTURAL CONTROL ARE ROBUSTLY USED ACROSS MULTIPLE POSTURAL CONFIGURATIONS

Gelsy Torres-Oviedo[1,2] and Lena H. Ting[1,2]

[1] Georgia Institute of Technology, Atlanta, GA, USA
[2] Emory University, Atlanta, GA, USA
E-mail: lting@emory.edu, Web: http://www.neuro.gatech.edu/groups/ting/

INTRODUCTION

Recent studies provide evidence that the nervous system does not control muscles independently during complex, natural behaviors such as standing postural control. A few neural commands activating fixed patterns of muscle activation, or muscle synergies, account for a range of postural responses in cats (Ting and Macpherson 2005; Torres-Oviedo et al. 2006).

We hypothesize that muscle synergies observed in one postural condition represent *preferred* patterns of muscle activation used by each individual's nervous system. Therefore, we predict that the same set of muscle synergies is used when the biomechanical context of the postural task changes. The implications of such a finding would be that the nervous system chooses to use a consistent set of muscle synergy patterns over a range of postures, even if they may not be optimal in a purely biomechanical sense.

METHODS

To test our hypothesis, we randomly interspersed different balance perturbation directions and biomechanical contexts. Subjects stood at 6 biomechanically distinct stance conditions – narrow, normal, wide, very wide, one-leg and crouched stance – yielding a total of 72 different perturbation direction and stance combinations. Nine healthy subjects (5 females and 4 males, aged 18-31) stood on a platform that translated in 12 directions evenly distributed in the horizontal plane. We analyzed the spatial, temporal, and inter-trial variability in 16 leg and lower back muscles of each subject's right side before and during automatic postural responses, characterized by three consecutive 75-ms time bins starting 100 ms after perturbation onset.

Nonnegative matrix factorization was used to identify muscle synergies, W_i, in a single postural task. These muscle synergies were subsequently used to reproduce postural responses in all other stance conditions by modulating the synergy activations, C_i. Task-specific muscle synergies, W^{test} were extracted from the remaining variability in the test conditions that were not well-reproduced by the muscle synergies from the control condition.

RESULTS AND DISCUSSION

In all subjects, 4 to 6 muscle synergies were required to reproduce the postural responses in the control condition (Figure 1A, normal stance).

This same set of muscle synergies accounted for the modulation of muscle activity when the distance between the feet was varied. Narrow stances evoked high levels of muscle activity, while wide stances evoke low levels of muscle activity. These variations were characterized (>92%) by changing the activation levels C_i of each muscle synergy (Figure 1B).

In one-legged stance, an additional, *task-specific* muscle synergy was required to reproduce the variability in muscle activity (Figure 1C). This task-specific muscle

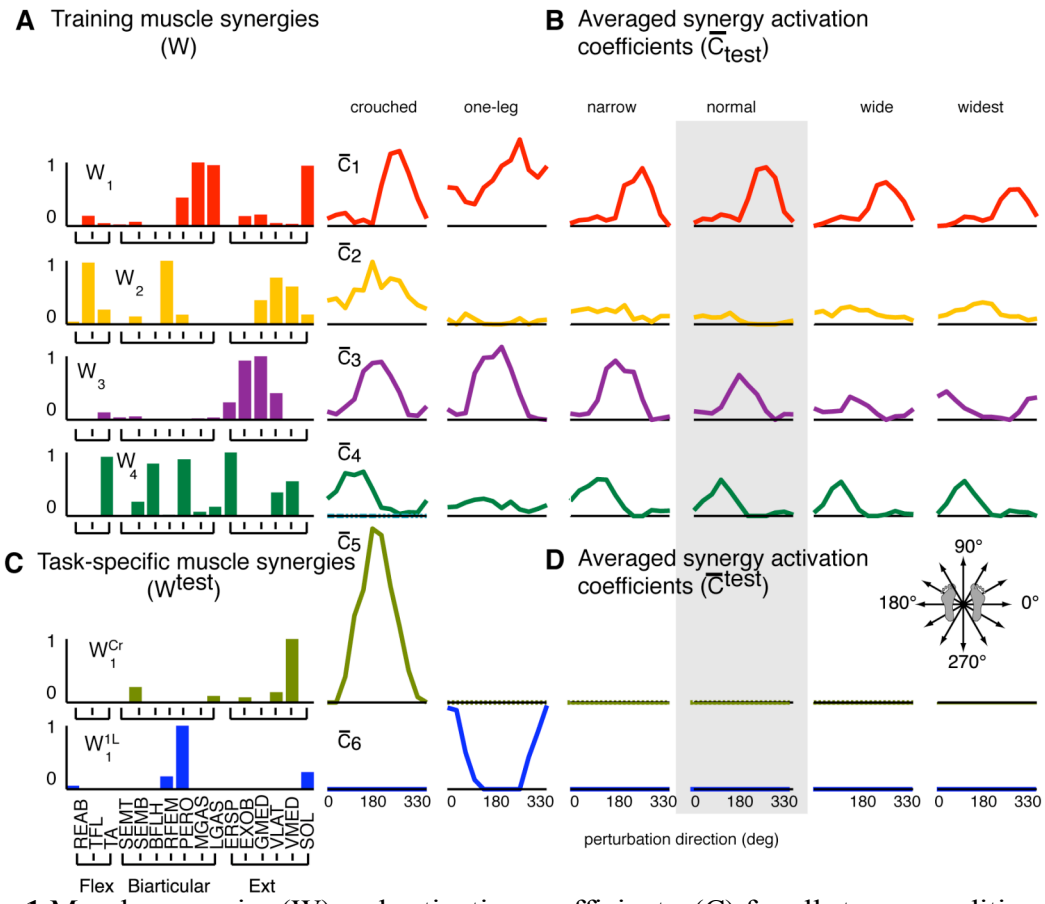

Figure 1 Muscle synergies (W) and activation coefficients (C) for all stance conditions and perturbation directions in one subject.

synergy activated ankle evertors which provide the ankle stability required for maintaining single-leg balance.

In the crouched condition, an additional task-specific muscle synergy was also necessary. However, this synergy activated only one single quadriceps muscle (Figure 1C). The same muscle is also activated by one of the *general* muscle synergies over the same range of perturbations (Figure 1A, W_2). This may reflect a nonlinear activation of muscles within a muscle synergy, which might occur via modified afferent inputs associated with large changes in joint angles.

CONCLUSIONS

In face of different environmental contexts, the nervous system simplifies muscle coordination by modulating the contribution of a *general* set of muscle synergies. When an additional biomechanical function is necessary, such as the need to generate medially-directed forces in one-legged stance, task-specific muscle synergies may be recruited.

ACKNOWLEDGEMENTS

NIH HD046922 and NS053822.

REFERENCES

Ting L.H., Macpherson J.M. (2005) *J Neurophysiol,* 93:609-613.

Torres-Oveido, G., Macpherson J.M. Ting L.H.*(2006) *J Neurophysiol,* 96:1530-1546

CHARACTERIZING HAMSTRINGS MUSCLE DYNAMICS DURING KNEE FLEXION-EXTENSION USING REAL-TIME MRI

Niccolo Fiorentino[1], Jonathan Lin[2], Michael Guttman[2], Andy Derbyshire[2], Dimitru Mazilu[2], Nicholas Evoy[2], Elliot McVeigh[2], and Silvia Blemker[1]

[1] Department of Mechanical & Aerospace Engineering, University of Virginia
[2] Laboratory of Cardiac Energetics, NHLBI, National Institutes of Health
Email: niccolo@virginia.edu

INTRODUCTION

The hamstrings muscles are highly susceptible to strain injuries and are commonly injured during running and sports-related activities. In order to understand the mechanisms for muscle tissue injury, we must characterize the local tissue strains during knee motion. While dynamic magnetic resonance imaging (MRI) has been previously used to study musculoskeletal motion (Asakawa et al., 2003), local hamstring muscle tissue strains during large knee flexion-extension motions have not been characterized *in vivo* due to limitations in scanner bore size. The goal of the current work is to develop an experimental approach to characterize hamstring muscle tissue strains in real time during loaded dynamic knee flexion-extension motion.

METHODS

Four volunteers were placed in the left lateral position to allow for a large range of knee angles inside a wide bore (70 cm), 1.5T Siemens Espree scanner (Figure 1). The wide bore scanner permitted knee angles ranging from 40 degrees at full extension to 140 degrees at full flexion. A real-time pulse sequence developed for interventional MRI (Guttman et al., 2003; McVeigh et al., 2005) was modified to apply and image a parallel line-pattern of temporary magnetic fiducial markers (or tags) on thigh muscles during knee flexion-extension. Tag application and image acquisition were initiated by a trigger pulse sent to the MRI scanner by a LabView control program. The LabView control program monitored leg movement via a position encoder connected to the foot by a rope with a counter balance on the opposite end to provide a controlled amount of resistance during the flexion-extension motion. LabView sent a trigger pulse to the scanner when the knee reached full flexion or extension. Position encoder values were calibrated based on direct measurements of knee angle made from a set of real-time dynamic images at the knee joint (Fig. 2A)

Because tag movement reflects underlying tissue movement (McVeigh, 1996, Ozturk et al., 2003), we calculated muscle tissue strains based on the distance between adjacent tags at the start of and during knee flexion/extension. Percent strain (S) was calculated according to the formula $S = 100*(l_f - l_o)/l_o$, where l_f is the current distance between tags and l_o is the initial distance. Strain measurements were obtained at 6 locations in the biceps femoris long head (Fig 2B).

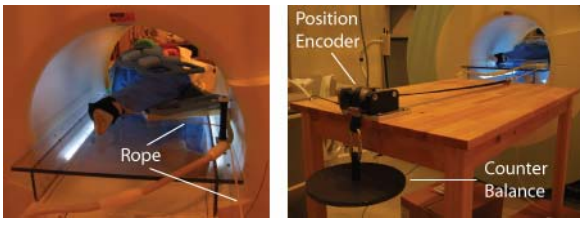

Figure 1: Volunteer in MRI scanner, and position encoder with counter balance attached to foot.

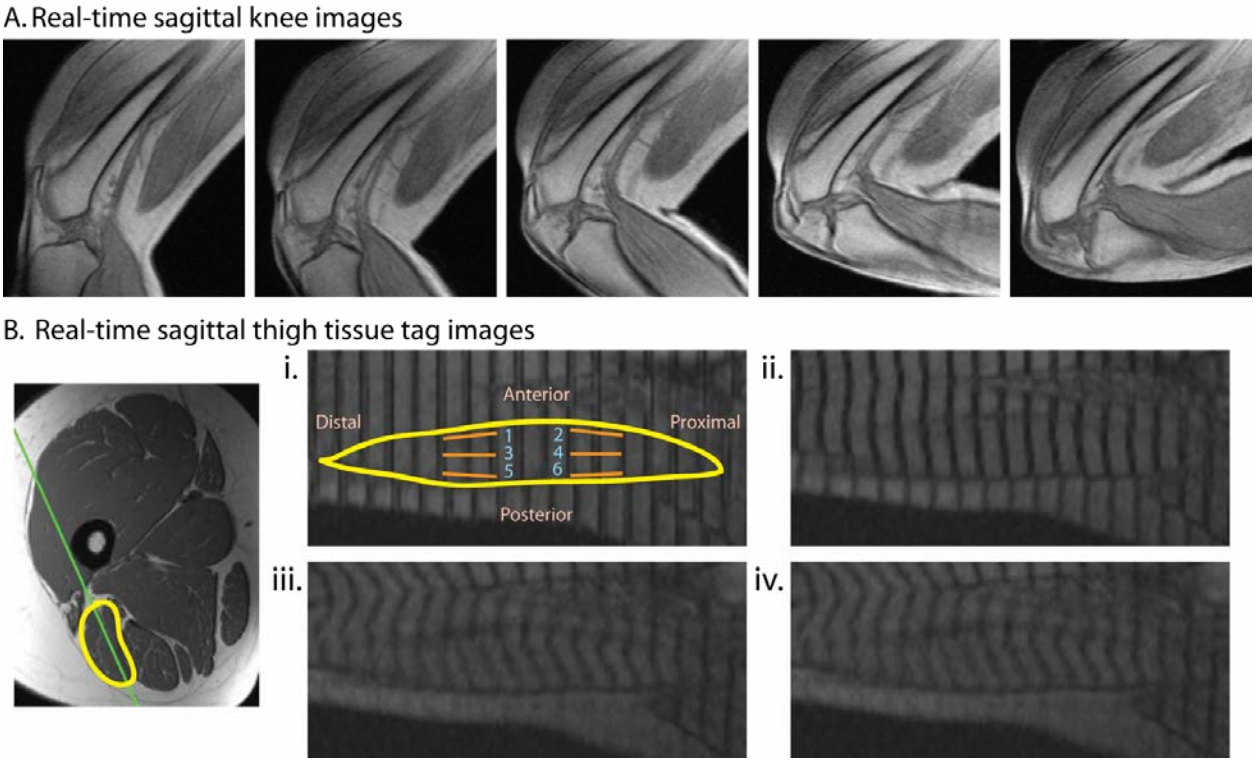

Figure 2: Real-time sagittal MR images demonstrating large knee flexion-extension angles (A), high-resolution axial image highlighting imaging plane in green for the biceps femoris muscle (B), circled in yellow, and four successive tagged images starting with undeformed tag lines (i-iv). Strain measurement regions are indicated by numbered line segments.

RESULTS AND DISCUSSION

Joint angles calculated from the calibrated position encoder compared favorably to a separate set of angles measured directly. For two sets of measurements made by the same user the angles calculated from the encoder differed from direct measurements by 4.78 ± 3.33 degrees and 5.92 ± 4.90 degrees (mean ± standard deviation).

Analysis of the tagging data (Fig. 2B) collected during active dynamic knee flexion revealed that some regions within the biceps femoris long head lengthen while others shorten. For example, for the 4 subjects imaged in this study, minimum strains (across 6 regions within the muscle) ranged from -11.48% to -3.90% and maximum strains ranged from 2.61% to 4.33% (these values correspond to approximately 30 degrees range of knee flexion; negative values indicate shortening, and positive values indicate lengthening). These results highlight the complex behavior of the hamstrings during dynamic knee motion. Further refinements in this technique will allow for a detailed exploration of tissue strains during large ranges of dynamic active knee motion and reveal new insights into the mechanisms for hamstrings strain injury.

REFERENCES

Asakawa, D.S. et al. (2003). *Semin Musculoskelet Radiol*, **18,** 287-95.

Guttman, M.A. et al. (2003). *Circulation*, **108**, 429.

McVeigh, E.R. et al. (2005). *Acad Radiol*, **12**, 1121-1127.

McVeigh, E.R. (1996). *Magn Reson Imaging*, **14**, 137-150.

Ozturk, C. et al. (2003). *Proc. IEEE*, **91**, 1627-1648.

A FUNCTIONAL METHOD FOR LOCATING THE SUBTALAR JOINT AXIS: *IN VIVO* ASSESSMENT OF ACCURACY

Gregory S. Lewis[1], Andrea R. Seisler[2], Tamara L. Cohen[1],
Kevin A. Kirby[3], Frances T. Sheehan[2], Stephen J. Piazza [1]

[1] The Pennsylvania State University, University Park, PA, USA
[2] National Institutes of Health, Bethesda, MD, USA
[3] California School of Podiatric Medicine, Oakland, CA
E-mail: *steve-piazza@psu.edu;* Web: *www.biomechanics.psu.edu*

INTRODUCTION

The subtalar (talocalcaneal) joint is located distal to the ankle (tibiotalar) joint and is the primary joint involved in frontal-plane motion and posture of the hindfoot. Abnormal subtalar joint mechanics play a significant role in producing frontal-plane deformities of the foot in cerebral palsy, adult flatfoot, and other conditions. Measurement of the subtalar joint moments produced by muscles and the ground reaction force would be an important first step toward understanding subtalar joint mechanics and toward producing more effective treatments for foot and lower extremity pathologies (Kirby, 2001). This would require knowledge of the subtalar joint axis location, but this axis has long been known to vary considerably across subjects (Inman, 1976), making application of a generic axis problematic.

Functional methods for locating joint centers and axes for the hip, knee, and shoulder from measured joint motion have received much recent attention but no such method for the subtalar joint has had its accuracy confirmed *in vivo*. Previous cadaver testing in our laboratory has shown that it may be feasible to move the foot of a patient about the subtalar joint with minimal ankle motion such that markers over the calcaneus and tibia can be used to estimate the subtalar joint axis (Lewis et al., 2007). In the present work, errors in a subtalar joint axis location protocol were assessed *in vivo* using magnetic resonance (MR) imaging to track bone motions.

METHODS

Subtalar joint axes were located in four healthy subjects (2 M, 2F; 23 – 29 y) using a custom-designed apparatus to apply foot movements. Each subject was placed in the supine position and a plastic plate was attached to the plantar surface of the foot. While a constant dorsiflexing load was applied to the plate, a pair of cords were used to move the foot in pronation-supination cycles. The directions along which the cords pulled were determined using a three-dimensional rigid-body dynamic model constructed in SD/FAST (Symbolic Dynamics; Mountain View, CA). Generic joint locations and segment inertial properties for the model were specified based on previously-reported measurements (Lundberg and Svensson, 1993). Ratios of the angular acceleration of the subtalar joint to that of the ankle joint was computed as the point of application and direction of the force applied to the foot was varied, and the parameters corresponding to the highest such ratio were applied in the subject tests.

Passive pronation-supination motion cycles were applied by a tester while fast-phase-contrast MR images of the tibia, talus, and calcaneus were collected in a quasi-coronal plane. Two different testers applied motions with two trials per tester per subject. The three-dimensional positions and orientations

of the three bones at 24 instants during movement were determined by integration of the MR-determined velocity data. A least-squares fit helical axis was determined for both the calcaneus-tibia and the calcaneus-talus (true subtalar) kinematics. The difference in orientation and the minimum distance between the calcaneus-tibia axis and the true subtalar axis were then computed.

RESULTS AND DISCUSSION

Subtalar joint location errors, averaged across all subjects, testers, and trials, were 5.7 ± 3.8° (Figure 1) and 1.5 ± 0.9 mm. Two-way repeated measures ANOVA indicated that the results were insensitive to tester and trial. (all $p > 0.263$).

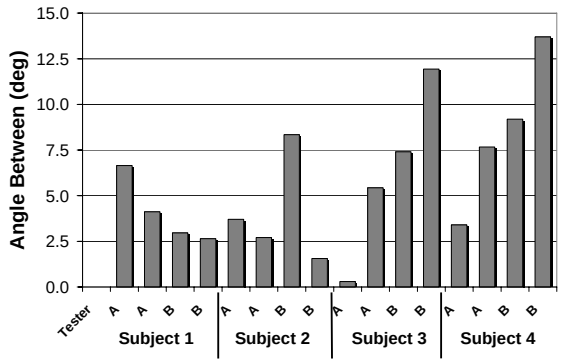

Figure 1: Angular errors in locating the subtalar axis. Angles shown are those between calcaneus-tibia axes and the true subtalar (calcaneus-talus) axes.

The range of motion at the subtalar joint, which was limited by space constraints in the bore of the MR scanner, was 14° on average (range: 11° to 18°). Motion at the ankle joint, undesirable if the subtalar axis is to be calculated from tibiocalcaneal motion, was only 3° on average (1° to 5°).

The joint axis location errors found in the present study are satisfactory when judged in the context of the previously-measured variation in axis location across subjects (Figure 2). With an intersubject range of over 40°, location errors of 6° should produce much more accurate estimates of subtalar joint moments than would be possible using generic joint axes.

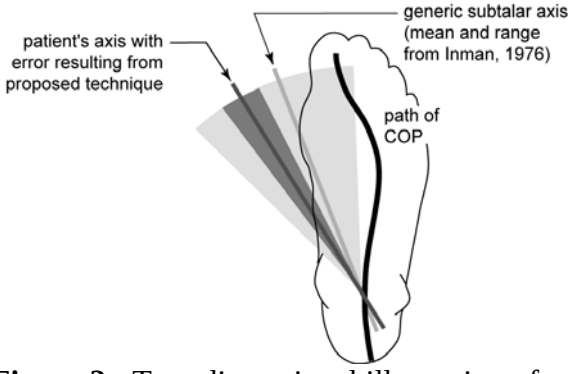

Figure 2: Two-dimensional illustration of the potential benefits of locating a patient-specific subtalar axis using the proposed technique. A hypothetical patient's axis placed 1 s.d. away from the mean from cadaver tests (Inman, 1976) and a range indicating 6° of axis location error is shown.

SUMMARY/CONCLUSIONS

The results of these tests support the feasibility of functional determination of the subtalar joint axis location, with average errors of about 6° and 1.5 mm. Further assessments of the repeatability of the method when applied using skin-mounted markers are planned.

REFERENCES

Inman, V.T. (1976). *The joints of the ankle.* Williams and Wilkins.

Kirby, K.A. (2001). *JAPMA,* **91**, 465-488.

Lewis, G.S. et al. (2006). *J Biomech Eng,* **128**,596-603.

Lewis, G.S. et al. (2007). *Gait & Posture,* **25**, 63-69.

Lundberg, A., Svensson, O.K. (1993). *Foot,* **3**, 65-70.

ACKNOWLEDGMENT

This work was supported by NSF BES-0134217

A FINITE ELEMENT ANALYSIS OF FEMORAL STRESSES IN A SIMULATED FALLING ON THE HIP CONDITION

Miranda N. Shaw [1], Dan M. Dragomir-Daescu [1], Mark E. Bolander [2], Kevin E. Bennet [1], Sean McEligot [1], Michael J. Burke [1], and Geraldine K. Bernard [1]

[1] Mayo Clinic Division of Engineering, Rochester, MN, USA
[2] Mayo Clinic College of Medicine Orthopedic Research, Rochester, MN, USA
E-mail: dragomirdaescu.dan@mayo.edu

INTRODUCTION

With increased incidence of hip fracture risks in osteoporotic patients, it is important to develop preventive treatment options including bone strengthening implants. Analytical and experimental techniques are used to optimize material and design of orthopedic implants. In the current study, the finite element (FE) method was used to evaluate the stress distributions in the proximal region of a femur in a simulated falling on the hip condition. The model used is the standardized femur introduced by Viceconti et al. The simulations were performed using the original, intact model as well as models with implants made of PMMA, Cortoss, and 316L stainless steel.

METHODS

Numerical simulations (FE) using cylindrical implants integrated in the neck region of the standardized femur model (Viceconti 1996) were performed (Figure 1). The analyses were performed using ANSYS 11.0 finite element software to simulate the falling on the hip condition.

Polymethyl methacrylate (PMMA) has been successfully used to augment vertebral bodies, but has several shortcomings including a short working time, radiolucency, and large heat generation (80-124°C) (Erbe 2001). Cortoss synthetic bone filler has been developed more recently to overcome these disadvantages, primarily less heat generation (58-68°C), and provide superior bone integration than PMMA (Erbe 2001, Heini 2003). Also, type 316L stainless steel is widely used in a variety of orthopedic implants.

In the current work, three implant designs were evaluated. The implant was modeled as a cylinder 1, 1.5, and 2 cm in diameter and approximately 8.5 cm in length (Figure 1). Implant material properties were simulated using Simplex P for PMMA and the reported material properties for Cortoss and type 316L stainless steel, respectively. Literature data for femoral bone mechanical properties were used (Table 1). To more closely mimic the anatomical femur, the cortical shell and trabecular bone were modeled. The trabecular bone was modified from the standardized femur to create a hollow femoral shaft.

Boundary conditions were applied to the model to simulate falling on the hip. A frictionless support was applied to the femoral head, and forces of 1000N, 4000N, and 8000N were applied to the greater trochanter. The distal femoral shaft was constrained allowing only rotation perpendicular to the femoral shaft, as shown in Figure 1. The femur was meshed with tetrahedral elements and the implant meshed with hexahedral elements. Meshes with around 900,000 elements were used.

Table 1: Material property data for the standardized femur model and implants.

	Young's Modulus (GPa)	Poisson's Ratio
Cortical	14.2	0.30
Trabecular	1.0	0.30
PMMA	2.828	0.29
Cortoss	5.8	0.29

RESULTS AND DISCUSSION

Maximum von Mises stresses in the femur were recorded in the subcapital and intertrochanteric neck regions for all implant designs. Maximum stresses occur in the cortical bone and decrease as implant diameter increases. Bone stresses are greater with the PMMA implant than the Cortoss and 316L implants. Therefore, it can be deduced that trabecular bone will be stressed more with a less stiff implant such as PMMA and Cortoss than with a stiff metal implant.

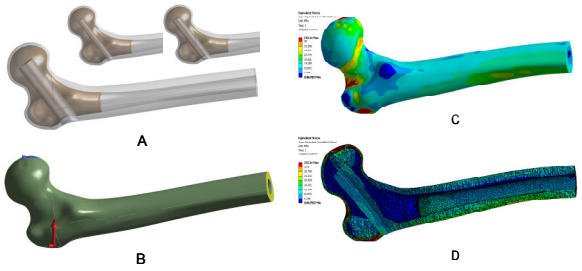

Figure 1: (A) FE model geometry; (B) Boundary conditions applied to simulate falling on the hip; (C) Maximum von Mises stress plot; (D) Internal von Mises stresses.

The total femoral deformation with PMMA and Cortoss implants is similar to normal bone deformation (1.2% maximum difference); however, a stainless steel implant decreases the total deformation by 4.2%. The relatively small deformations resulted from the FE analysis lead to the conclusion that the standard femur model with elastic modulus close to that of bone is too stiff to detect changes due to different implant materials. Therefore, it is important to design implants using FE models derived from CT scans of bones. With such models, patient based FE models can be developed to evaluate if the proposed implant will be beneficial or to optimize the implant mechanical properties.

SUMMARY/CONCLUSIONS

FE analyses of stresses resulted from falling on the hip condition at 1KN, 4KN, and 8KN impact forces were performed. The intact standardized femur model and models with proximal implants made of PMMA, Cortoss, and stainless steel were simulated. The results show that the stresses in the cortical bone decrease when the stiffness of the implant increases and when the diameter of the implant increases. The opposite is true for the trabecular bone: the stresses increase with stiffer implants. Although the standard femur can offer an initial model to study different implantation methods more refined models based on CT scans of osteoporotic patients must be used to select the required material and geometry of an effective implant.

REFERENCES

Currey, J.D. (2002) *Bones: Structure and Mechanics*. Princeton University Press.

Erbe, E.M. et al. (2001) *Eur. Spine J.*, **10**, S147-52.

Heini, P.F. et al. (2003) *49th Ann. Meeting Ortho. Res. Soc.*, Poster 1248.

Viceconti, M. et al. (1996a) *J. Biomech.*, **29**, 1241.

Table 2: Maximum von Mises stress (MPa) in subcapital and intertrochanteric regions of the femur due to a 4000 N force on the greater trochanter.

Bone Stress Region	Normal	Implant Size (cm)	Implant Material		
			PMMA	Cortoss	316L
Subcapital	22.9	**1.0**	22.2	21.7	18.3
		1.5	21.7	20.4	16.8
		2.0	20.4	18.5	14.8
Intertrochanteric	36.9	**1.0**	36.1	36.0	30.4
		1.5	36.1	34.2	25.8
		2.0	35.2	33.3	22.3

AN INNOVATIVE DIAGNOSTIC TOOL FOR REDUCING TRAUMATIC KNEE INJURIES

Kristian M. O'Connor[1], Brian S. R. Armstrong[2], Stephen R. Watts[2], Mustafa M. A. Farrah[2], and Michael C. Bottum[1]

[1] Department of Human Movement Sciences
[2] Department of Electrical Engineering
University of Wisconsin-Milwaukee, Milwaukee, WI, USA
E-mail: krisocon@uwm.edu Web: www.chs.uwm.edu/neuromechanics

INTRODUCTION

Research efforts toward reducing ACL injury have focused on anatomical, hormonal, and neuromuscular factors that may contribute to increased risk. A variety of possible discriminators have been investigated (e.g., strength imbalances, static misalignment, etc.), but the method that has proved most successful is 3-D motion analysis of dynamic activities (Hewett et al., 2005). This study was performed within the confines of a traditional motion capture laboratory, but an ideal large scale 3-D motion analysis screening tool for ACL injury risk would be able to record outside of the laboratory with a single camera, requiring little or no calibration and little technical expertise for the user. Further, this system would generate nearly instantaneous feedback to the clinician and athlete, and would be relatively inexpensive. No technology currently exists on the market that can meet these criteria. The Retro-Grate Reflector (RGR) is such a system. The RGR is a new, single-image 6-DOF optical motion-tracking technology (Armstrong et al., 2002). An RGR target is constructed by applying artwork on the front and back of a transparent substrate, such as a glass or plastic plate (Figure 1).

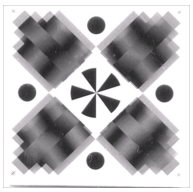

Figure 1: RGR target. Moiré patterns change as orientation of target changes.

The three-layer structure of substrate and artwork produces moiré patterns, which are seen as light and dark fringes. The moiré patterns respond to changes in orientation. Small rotations produce moiré-pattern displacements that are visible to the eye. Because the phase angle of each moiré pattern is detected by averaging over many pixels, RGR orientation measurement is extremely accurate. Armstrong et al. (2002) reported ± 0.0082 deg RMS error over a 54° measurement range. With the out-of-plane rotations revealed by the moiré patterns, the RGR system is able to determine 6-DOF pose from a single camera image. The remaining degrees of freedom are measured from the image using standard photogrammetric techniques.

RGR motion tracking addresses the high-cost and specialized facility, calibration and training requirements of existing human motion capture systems by incorporating only one camera, - eliminating multi-camera calibration - and detecting RGR targets with automated image processing software. This technology was developed on an optical bench, and the initial goal of this project is to adapt the technology for use under conditions suitable for human subjects testing. The purpose of the current study was to establish the ability of RGR technology to replicate 6-DOF measurements recorded by a multi-camera motion capture system.

METHODS

A 5-inch square RGR target was mounted on a block with four retro-reflective markers (Figure 2). Its pose was recorded simultaneously by a Motion Analysis 7-camera Eagle system (Santa Rosa, CA) and a Basler A501k (Ahrensburg, Germany) 1.3 MPixel camera. The camera was placed ~3 m from the measurement volume. Eleven static positions were recorded where position and orientation were manipulated. Pose was determined separately using, 1) the four markers recorded by the Eagle system, and 2) the RGR target imaged by the Basler camera. The RGR coordinates were co-registered with the Eagle system inertial frame. Translation and rotation variables from the 11 positions were correlated between the measurement systems for each DOF.

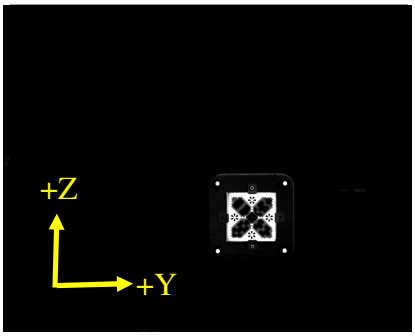

Figure 2: RGR target mounted with four reflective markers for simultaneous RGR and Eagle collection. Target displayed in capture volume (position 3) with assignment of inertial coordinate system displayed.

RESULTS AND CONCLUSIONS

The RGR system successfully replicated the orientation and position reported by the multi-camera system (Figures 3 and 4). The correlations between measurement systems were all greater than 0.99. This initial test establishes that RGR is a viable motion capture tool, with the next phase to adjust target design and tracking algorithms to track continuous motion. This technology has great promise as a field deployable 3-D motion capture tool.

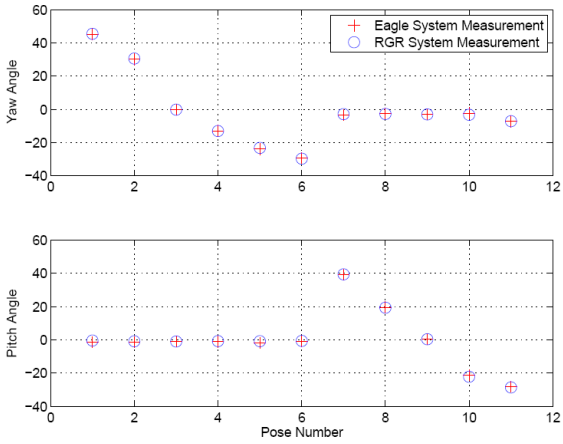

Figure 3: Comparison of pitch (Y axis) and yaw (Z axis) rotations determined by Eagle and RGR Systems for each position. All angles correlated greater than 0.99 between systems.

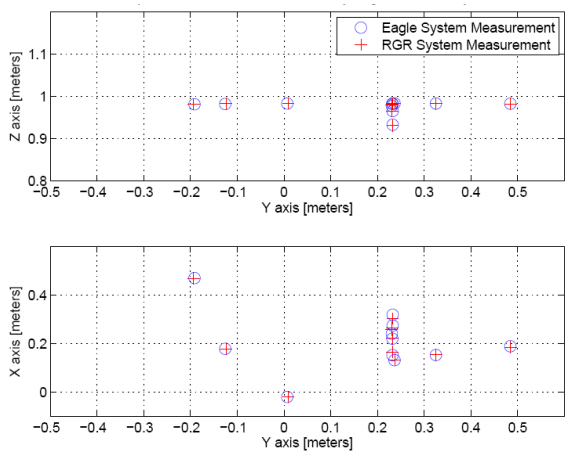

Figure 4: Comparison of X, Y, and Z positional data determined by Eagle and RGR systems. All three displacements correlated greater than 0.99 between systems.

REFERENCES

Armstrong, BSR (2002). In *Proc. 2002 Int. Conf. on Robotics and Automation*. IEEE.

Hewett, TE *et al*. (2005). *American Journal of Sports Medicine*, **33**, 492-501.

ACKNOWLEDGEMENTS

The authors would like to thank the UWM Research Growth Initiative for its financial support of this project.

THE EFFECT OF FATIGUE ON SHEAR FORCES IN THE KNEE DURING A JUMP LANDING TASK

Mindy Bennett[1], Chad Harris[1], Kristof Kipp[2], Mark DeBeliso[1], Kathy Berg[3]

[1]Boise State University, Boise, ID.
[2]Oregon State University, Corvallis, OR.
[3]University of Vermont, Burlington, VT
Email: Mindy.Bennett@gmail.com

INTRODUCTION

Sports involving repetitive sprinting and jumping (e.g. basketball and soccer) have been identified as high risk sports for knee injury in females. These activities create the potential to induce fatigue in the muscles of the lower extremity. It has been suggested that fatigue may affect the dynamic stability of the knee, specifically its ability to prevent excessive shear forces. Loss of stability has been implicated as a contributing factor in the mechanism of knee injury. The purpose of this study was to determine if sprinting induced fatigue alters jump landing kinetics during a jump landing task.

METHODS

Female collegiate soccer players (n=13, Age: 19.6 ± 0.9 yrs, Wt: 62.2 ± 7.4 kg) performed 10 trials of jump landings (JL). The JL required subjects to jump horizontally a distance that was ½ of their maximal standing broad jump, and reach a height vertically in the middle of their horizontal jump that was ½ of their maximal vertical jump. The first five trials were performed following a brief warm up and were in a non-fatigued condition (NF). The next five trials were performed in a fatigued condition (F) following a protocol which included: a timed T-test (TT), a timed 274 meter shuttle run (SR), a repeated sprint test consisting of 12-20m sprints departing every 20 seconds (RS), and continuous TT until attainment of fatigue criteria (90% of predicted maximum heart rate and RPE ≥ 17). Rest times between TT, SR, and RS were 30 seconds as was the time from the last TT to the first JL during the F conditions. Landing kinetics were collected on flush mounted Kistler force plates at 1250 Hz. The resultant shear forces were normalized to body weight and calculated for both the dominant leg and non-dominant leg. A one-way analysis of variance was performed with significance set at $p = .05$.

RESULTS

All subjects attained the fatigue criteria (% HRmax = 91.0 ± 0.0, RPE = 17.6 ± 0.7). For forces in the X-direction leg dominance did not have a significant effect on the amount of shear force in either the fatigued or non-fatigued state ($p=.2186$). For forces in the Y-direction leg dominance did not have a significant effect on shear forces in fatigued or non-fatigued state ($p=.2783$).

CONCLUSION

Fatigue has been suggested as a mechanism of knee injury. However, it

does not appear that fatigue alters the magnitude or direction of shear forces in either the dominant or non-dominant leg during a jump landing task. Further research is warranted to investigate whether fatigue alters lower limb kinematics between dominant and non-dominant legs during jump landings.

VALIDATION OF ORTHOPAEDIC RELATED IMAGE SEGMENTATION TECHNIQUES

Nicole A. DeVries, Esther E. Gassman, Nicole A. Kallemeyn, Kiran H. Shivanna, Vincent A. Magnotta, Nicole M. Grosland

The University of Iowa, Iowa City, IA, USA
E-mail: nicole-grosland@uiowa.edu, Web: www.ccad.uiowa.edu/mimx

INTRODUCTION

Three-dimensional anatomic models often rely on image datasets for their geometric definitions. Several image segmentation techniques are commonly implemented to define the structural boundaries, including: threshold techniques, edge-based methods, region-based routines, and connectivity-preserving relaxation methods. Regardless of the technique, a means to validate the method is mandatory for its successful implementation. Unfortunately, a reference standard is oftentimes unattainable. Ideally, one would like to obtain a reference standard that is independent of the image acquisition process and provides a high resolution representation of the structure of interest (Warfield, 2004).

METHODS

Five arms (5 donors), amputated at the elbow, were obtained from the Anatomy Gifts Registry located in Hanover, Maryland. The donor set was comprised of five female specimens with a mean age of 71.8 years.

For each specimen, images were obtained on a Siemens Sensation 64 CT scanner (matrix = 512x512, KVP = 120) with an in-plane resolution of 0.34mm and a slice thickness of 0.4mm. Following image acquisition, the data was processed using the BRAINS2 software (Andreasen, 1992). The images were spatially normalized and resampled to 0.2-mm^3 voxels such that the third metacarpal was aligned vertically. The images were cropped to contain only the phalanges for ease of data management.

Two trained technicians (referenced as Tracer1 and Tracer2) manually traced 5 distal, middle, and proximal phalanx bones of the index fingers using the BRAINS2 software. In order to ensure minimal inter-rater variability, a study was conducted to compare the performance of the two tracers by determining their relative overlap.

The distal, middle, and proximal phalanx bones were dissected from the index finger of each hand. Care was taken during the dissection and denuding procedures to avoid any tooling marks that may introduce potential errors in the resulting surface measurements. Once completely denuded, the bones were degreased via a soapy water solution, dried thoroughly, and due to the natural color and porous texture of the bone, coated with a thin layer of white primer. While the thickness of the single coat of primer was negligible, it improved the scanner's ability to detect the bony surface. Three-dimensional surface scans of each physical specimen were acquired using a Roland LPX-250 3D laser scanner (0.2 mm resolution).

RESULTS AND DISCUSSION

The tracers demonstrated a high degree of reliability for the manually defined regions

of interest. The average relative overlap computed between Tracer1 and Tracer2 was 0.89 for all the bones. The proximal, middle, and distal phalanges had overlaps of 0.91, 0.90, and 0.87, respectively. This suggests that the manual raters were able to define the regions of interest even in the presence of abnormal anatomy.

To validate the tracers' accuracy and reliability, the manual traced unsmoothed surfaces were compared to the physical surface scans. Table 1 summarizes the mean Euclidean distance between the two surfaces for the bones of each specimen. The distal phalanx had the largest mean distance (0.08 mm), while the middle and proximal bones each resulted in a mean distance of 0.06 mm. It should be noted that the mean percentage of points within the original in-plane image resolution (0.34 mm) was greater than 95% for each of the specimen (Figure 5a). Over 99% of the points for specimens MD05010306R, MD05021815R, and SC05030303R were within the voxel limit.

This study was conducted on a range of cadaveric specimens that included several pathological conditions including arthritis of the hand and osteoporosis. Even given these conditions, the manual definitions were very similar to the true anatomical shape.

SUMMARY/CONCLUSIONS

The validation and characterization of image segmentation techniques has been an ongoing challenge in the research field. This study examines the validity of image-segmented bony structures, initiating with the phalanx bones of the human hand. Computed tomography datasets of five index fingers from cadaveric specimens were manually segmented and the regions-of-interest converted to surface representations. These surfaces were than compared to physical surface scans, finding the average distance between the surfaces was 0.06 mm. Thus, this study shows that manual segmentation techniques applied to define bony structures from CT images can accurately represent the true surface geometry.

REFERENCES

Warfield, S.K., Zou, K. H., Wells, W. M. (2004). *IEEE Trans. Med. Imaging*, **23**, 903-921.

Andreasen, N.C., et al. (1992) *J Neuropsychiatry & Clinical Neurosciences*, **4**, 125-133.

ACKNOWLEDGEMENTS

The authors gratefully acknowledge the financial support provided by NIH Awards EB001501.

Table 1. Average Euclidean distance and standard deviation between the manually traced unsmoothed surfaces and the physical surface scans.

Finger ID	Proximal Phalanx (mm)	Middle Phalanx (mm)	Distal phalanx (mm)	Finger Average (mm)
CA05042125L	0.07 (0.09)	0.09 (0.11)	0.13 (0.14)	0.10
MD0510306R	0.04 (0.06)	0.04 (0.07)	0.05 (0.07)	0.04
MD05021815R	0.05 (0.07)	0.05 (0.06)	0.06 (0.08)	0.05
MD05042226L	0.08 (0.11)	0.08 (0.11)	0.09 (0.16)	0.08
SC05030303R	0.04 (0.05)	0.05 (0.07)	0.05 (00.06)	0.05
Bone Average	0.06	0.06	0.08	

ESTIMATING LEAN ANGLE THROUGH APPLICATION OF THE GRAVITY LINE PROJECTION ALGORITHM

Pilwon Hur[1], Seiji Naito[2], Elizabeth T. Hsiao-Wecksler[1]

[1]University of Illinois at Urbana Champaign, Urbana, IL, USA
[2]Nagoya University, Nagoya, Japan
Email : ethw@uiuc.edu Web : mechse.uiuc.edu/research/ethw

INTRODUCTIONS

To understand the human postural control system, control models that represent the upright body as a single link inverted pendulum are frequently used. These models usually output the lean angle of the pendular body and use the desired lean angle as a reference input. Lean angle is defined as the angle between vertical and a line connecting the ankle and body center of mass (COM). In some experimental situations, it is not possible to collect kinematic data to estimate the location of the COM. In this study, we were interested in assessing the accuracy of estimating the location of the COM using only force plate data, rather than kinematic data from a motion capture system.

Numerous methods have been proposed to estimate the displacement of the COM (Lafond, 2004). Among those, we used zero-point to zero-point double integration, or gravity line projection, (GLP) method (Zatsiorsky and Duarte, 2000), which is robust and independent of standing conditions; furthermore, it only requires force plate data. In this study, we compared lean angles computed using either estimates of COM location based on (1) kinematic data from a motion capture system and (2) the GLP method.

METHOD

Subjects. Eight young adult subjects (7 males, 1 female; age 24±2.7 yrs, height 175±10 cm, and weight 77±15 kg) were tested.

Experimental Protocol

Subjects were tested in two conditions: 3 quiet standing trials, 3 voluntary sway trials in the AP direction, all 30s in duration. For both conditions, subjects were instructed to stand with arms at their side and eyes open, looking at a large stationary picture placed at eye level and 3m away. Ground reaction force and COP were recorded with a force plate (AMTI, BP600900). We collected kinematic data to compute the location of the body COM using a motion capture system (Vicon 460) with a 34-marker set placed on the head, torso, arms, and legs. All data were sampled at 120 Hz.

Data Processing

1. Lean angle from kinematic data via motion capture system (Gold-standard lean angle): We estimated the location of the COM through the segmental method, where the body's COM was derived from a 12-segment model of the body (Vaughan et al., 1999). Lean angle was then calculated from the average of the ankle joint centers to this COM position. We used these data as the reference data for verification.

2. Lean angle from GLP algorithm: We used the modified GLP algorithm (Zatsiorsky and Duarte, 2000) to compute the location of the COM. Since the GLP method

can only estimate the horizontal location of the COM, to calculate the body lean angle, we also needed the distance between the ankle and COM. We approximated this distance as 58.71% of body height for males and 57.48% of body height for females according to King and Zatsiorsky (1997).

Data Analysis

We used the root mean square error (RMSE) and cross-correlation between the two calculation methods to quantify how closely the GLP-derived lean angle compared to the gold standard lean angle derived from the kinematic motion capture data. We also checked robustness to the uncertainty generated due to estimating the ankle to COM distance by varying body height up to ± 20%.

RESULT AND DISCUSSION

Average RMSE for the eight subjects was 0.036 ± 0.008 deg for quiet stance and 0.287±0.094 deg for voluntary AP sway (Fig 1). Average cross-correlation was 0.985 ± 0.014 for quiet stance and 0.992 ± 0.006 for voluntary AP sway. Average RMSE and cross-correlation values for the cases when body height was varied ± 20% were 0.057 ± 0.01 deg and 0.985±0.014, respectively, for quiet stance and 0.276±0.11 deg and 0.992±0.006, respectively, for voluntary AP sway. These results suggest that using the GLP method to compute the location of the COM along with approximating the length of the pendulum is a good method for estimating body lean angle.

SUMMARY AND CONCLUSIONS

In this study, we investigated whether it was possible to calculate lean angle with only force plate information. By applying the modified GLP algorithm to estimate the horizontal displacement of the body COM, the results suggest that estimating lean angle with only force plate data is a viable approach, especially when kinematic motion capture data are not available.

REFERENCES

King and Zatsiorsky, *Gait Posture* 6, 27-38, 1997

Lafond et al., *J Biomech* 37, 1421-1426, 2004

Vaughan et al., *Dynamics of Human Gait; 2nd Ed*. Kiboho Publishers, 1999

Zatsiorsky and Duarte, *Motor Control* 4, 185-200, 2000

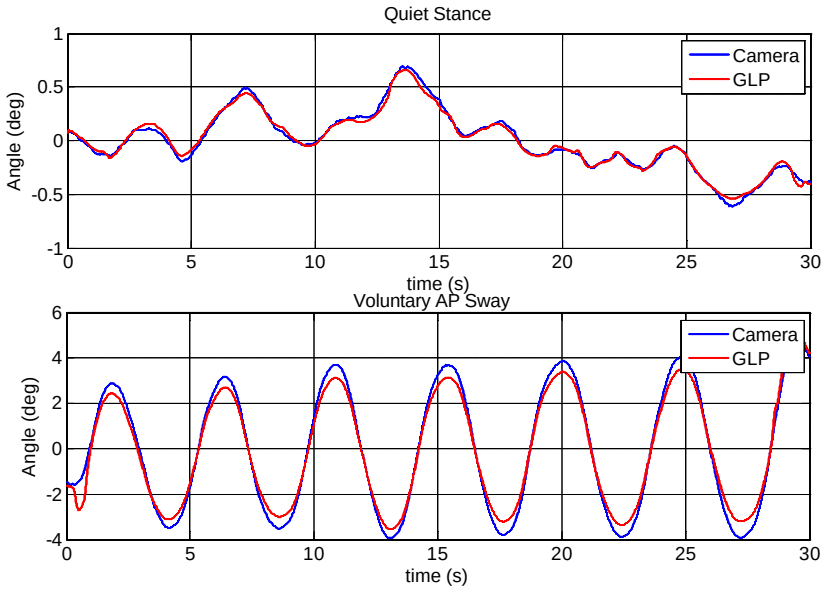

Figure 1. Sample body lean angles during quiet standing and voluntary sway. Lean angles were derived from kinematic data collected on a motion capture (camera) system versus application of the gravity line projection (GLP) method.

A COMPARISON OF FORCE-VELOCITY PROPERTIES OF SINGLE MUSCLE FIBERS OBTAINED UNDER DYNAMIC AND STEADY-STATE CONDITIONS

David C. Lin and Sampath K. Gollapudi

Washington State University, Pullman, WA, USA
Email: davidlin@wsu.edu

INTRODUCTION

The force-velocity (F-V) relationship of skeletal muscle is used for identifying optimal function and estimating muscle model parameters. Although accurate measurement of F-V properties is important, methods in which specific forces or velocities are used in a series of activations can lead to inconsistent results because of variability in the repeated activations.

An alternative method is to use a force ramp (F-R), which is linear decrease in force over time [1]. The F-R method is appealing because only one activation is necessary for recording the F-V curve. Theoretically, a constant rate of change in force should produce a constant velocity in a linear series-elasticity component. The estimated F-V curve would then be the F-V curve of the contractile element plus a constant velocity. Furthermore, differences between the isotonic and F-R loads in the mechanical history preceding each measurement in the F-V curves may lead to discrepancies due to force depression/enhancement mechanisms.

The aim of this study is to determine the differences in the F-V curves obtained from isotonic and F-R loads in single fibers. We hypothesize that the differences in the F-V curves can be accounted for by an offset in velocity and by the amount of preceding work, which is related to the amount of force depression/enhancement [2]. The significance of these results is that the F-R method could provide more consistent F-V measurement in muscle ranging from human *in vivo* studies to single fiber preparations.

METHODS

Rat soleus single fibers were prepared by a chemical skinning solution and mechanical separation. The fiber ends were glued to clips, and the clips were attached to a force transducer and motor. Sarcomere length was set to 2.6 μm by laser diffraction. Fibers were maximally activated at 12ºC in a high calcium solution (pCa=4.4), and one of the following randomized loads were applied: a F-R load or an isotonic load of magnitude 10, 20, 50, or 75% of isometric force (F_o) (Figures 1 and 2). Force and fiber and sarcomere lengths were recorded. Each fiber was typed by electrophoresis.

Because sarcomere inhomogeneity is a problem with skinned single fibers, data from fibers which showed changes greater than 10% in F_o across the experimental trials were not used. Second, if the plot of fiber versus sarcomere strains did not have a slope equal to one, indicating sarcomere inhomogeneity, the data were not analyzed. Fiber length data were differentiated and lowpass filtered at 50 Hz to calculate velocity. F-V plots from the F-R data were generated by plotting the force (normalized by F_o) and velocity (normalized by L_o) at each point in time. F-V plots for the isotonic data were plotted as discrete points.

The velocity difference between the F-R F-V curve and isotonic points was calculated

for each fiber. Next, the isotonic F-V points were adjusted as a linear function of the difference in the amount of work between the two protocols [2]. The velocity offset was recalculated after this modification.

RESULTS AND DISCUSSION

Experimental data with minimal sarcomere inhomogeneity have been obtained from 10 type I fibers. Data obtained in one fiber for the F-R and isotonic loads are shown in Figures 1 and 2, respectively.

The F-V curve for the F-R data in Figure 1 could be described by a hyperbolic function (Hill's equation) with an additional velocity offset (Figure 3). At higher forces (75 and 50% of F_o), the F-V curve from the F-R method was faster than the corresponding isotonic points and well approximated by a constant offset. At the lower forces (20 and 10% of F_o), this was not the case, as the velocity became nearly equal to the corresponding isotonic points.

Modification by the difference in the amount of work most affected the lower forces of the isotonic data (Figure 3). The modified isotonic F-V points were slower than F-R F-V curve, and the difference in the F-V data were better approximated with a constant velocity offset.

SUMMARY

F-V data were collected from rat soleus single fibers using isotonic and F-R loads. Differences in the curves could be explained by a velocity offset and modification of force by the differences in the amount of work. Thus, with one activation under nonsteady-state force conditions, it is possible to obtain a F-V curve that is approximate to one obtained with traditional methods using multiple activations.

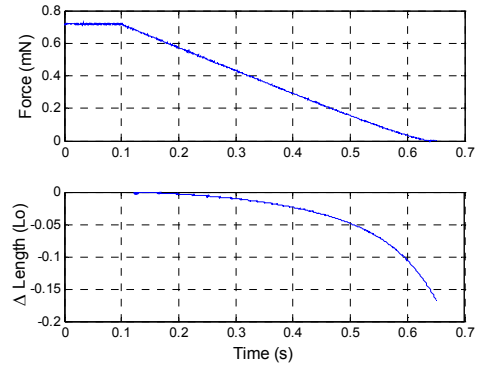

Figure 1. Mechanical response of a single fiber to an F-R (left) and isotonic (right) loads.

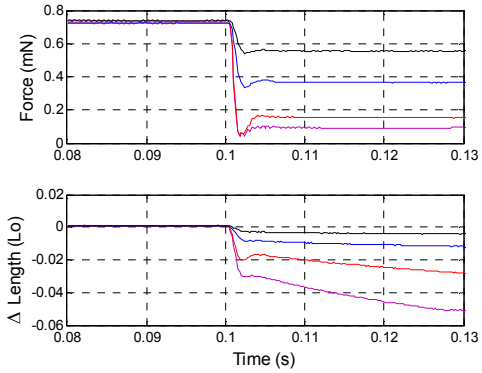

Figure 2. Mechanical response of a single fiber to an F-R (left) and isotonic (right) loads.

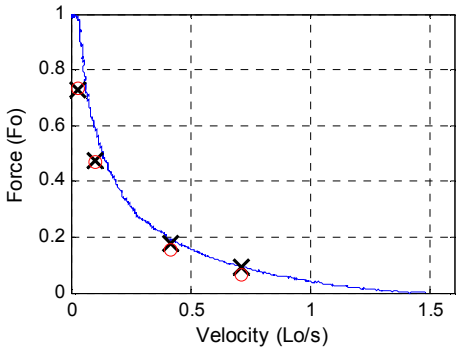

Figure 3. F-V curves from F-R (line) and isotonic data (**x**) and modified isotonic data (○).

REFERENCES

[1] Lin, D.C. and Nichols, T.R. (2003). *ASME J. Biomech. Eng.*, **125**, 132-140.

[2] Herzog, W. *et al.* (2000). *J. Biomech.*, **33**, 659-668.

ACKNOWLEDGEMENTS

Support from the Whitaker Foundation.

FUNCTIONAL GAIT OUTCOMES AFTER INTERTROCHANTERIC HIP FRACTURE

Kimberly Yarnall[1,3], Ellen Boeke[1], M. Wade Shrader[2,3], Kristine Csavina[1,3]

[1]SHRI-CORE Orthopedic Research Labs, Sun City West, AZ USA
[2]The CORE Institute, Sun City West, AZ USA
[3]Harrington Department of Bioengineering Arizona State University, Tempe, AZ USA
email: kim.yarnall@thecoreinstitute.com

INTRODUCTION

According to the American Academy of Orthopedic Surgeons, 352,000 hip fractures occur each year, and by the year 2050 it is estimated that the number will have escalated to 650,000 hip fractures per year. Despite these numbers, very few studies have extensively evaluated the post-operative walking capacity of these patients. Previous studies evaluated maximal vertical force to determine how much reliance was placed on walking aids and analyzed the single-leg support phase to determine what percentage of the gait cycle was spent on the injured leg versus the uninjured leg. Two studies have extensively evaluated these parameters for intertrochanteric hip fractures, but neither was a full motion analysis study. Additionally, competing conclusions were published in regards to the significance of fracture healing in the improvement of walking capacity. (Barrios, 1993, Walheim 1990) These studies were limited in the number of gait parameters evaluated, and the conflicting conclusions support the fact that studies performed without complete gait analysis offer inconclusive results. The purpose of this study was to quantify gait parameters for level walking after hip fractures and compare this data to age matched controls.

METHODS

All patients were treated for intertrochanteric hip fractures by orthopedic surgeons at The CORE Institute between October 2006 and early December 2006. This study was approved by the Sun Health Institutional Review Board and all subjects signed the Informed Consent and HIPPAA Authorization forms prior to participation in the study. Exclusion criteria were defined as an inability to walk short distances without assistive devices, dementia, neuropathies, and unrelated gait disorders. The seven patients who fit these criteria and were willing to participate, included four females and three males (age 82.71±8.9) Control subjects were individuals previously recruited and tested in the SHRI-CORE Motion Analysis Lab. The group of seven age and sex-matched control subjects consisted of four males and three females (age 79.43±6.7).

Three dimensional kinematic and kinetic data were recorded using a passive marker 10-camera Eagle 4.0 system (Motion Analysis Corp., Santa Rosa, CA) and four AMTI OR6-6 forceplates (AMTI, Watertown, MA). At least six consistent walk trials were gathered to ensure three clean right foot strikes and three clean left foot strikes. All data was taken using the modified Helen Hayes marker set and was processed using Motion Analysis Software (Santa Rosa CA), EVaRT 5.0.1 and OrthoTrak 6.2.8.

Single leg support, stride length, minimum hip flexion in stance, maximum hip moment in stance, max power generation, and max power absorption in stance for injured versus uninjured were compared using a paired t-test and then both limbs were compared to controls using an unpaired student t-test assuming equal variance. Significance was defined as $p<0.05$.

RESULTS AND DISCUSSION

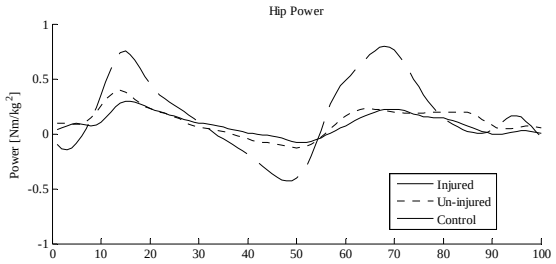

Figure 1: Hip Powers exhibited during level walking.

No statistical differences were found between the injured limb and the uninjured limb for any of the gait parameters evaluated. However, all gait parameters for injured and uninjured legs were statistically different than controls. Figure 1 illustrates the significantly lower power generation and absorption capacity of patients after hip fracture. After hip fracture these patients were still walking with reduced hip flexion angles and moments in the stance phase indicating that full recovery is not achieved between 4 and 6 months post operation. Additional patients should be evaluated to better understand the gait outcomes of hip fracture patients.

REFERENCES

Barrios, C et al., *Clinical Orthopaedics and Related Research* **294**, 187-192, 1993.

Walheim, G et al., *Journal of Orthopaedic Trauma* **4(2)**, 137-143, 1990.

Table 1: Temporal/Spatial and Hip Kinematic and Kinetic Results (*statistically different from control ($p<0.05$))

	Single Leg Support	Stride Length (cm)	Min Hip Flexion in Stance	Max Hip Moment in Stance	Max Power Generation in Stance	Max Power Absorption in Stance
Injured Leg	68.9 ± 5.5	72.3 ± 18.1*	12.2 ± 8.9*	0.39 ± 0.17*	0.38 ± 0.28*	-0.12 ± 0.15*
Uninjured Leg	69.9 ± 6.5	72.4 ± 18.4*	10.4 ± 6.1*	0.44 ± 0.18*	0.45 ± 0.24*	-0.15 ± 0.18*
Controls	-	110.4 ± 8.0	2.2 ± 6.1	0.58 ± 0.1	0.79 ± 0.29	-0.47 ± 0.13

BICYCLE SEAT DESIGN AND GENDER EFFECT ON SEAT AND HANDLEBAR PRESSURE DURING NON-STATIONARY CYCLING

Eadric Bressel [1] and John Cronin [2]

[1] Utah State University, Logan UT, USA
[2] Edith Cowan University, Perth, Australia
E-mail: ebressel@cc.usu.edu

INTRODUCTION

Some bicycle seats may not reduce pressure effectively and may increase the risk of perineal discomfort or injury, which seems to be a common occurrence among cyclists (e.g., Anderson & Bovin, 1997). Studies have reported insightful information on how seat design influences seat and handlebar pressure (Lowe et al., 2004) and internal perineal compression (Gemery et al., 2007), yet factors that interact with seat design such as gender have not been included in these analyses.

An additional shortcoming in this area is the failure to account for balance needed whilst cycling on a non-stationary bicycle. Previous researchers (Lowe et al., 2004) used stationary ergometers and therefore arm and leg muscles did not have the additional task of steering or balancing which presumably changes a persons ability to unload the seat and decrease seat pressure.

In view of these shortcomings, it was the purpose of this study to examine the effect of various bicycle seat designs on seat and handlebar pressure in male and female cyclists during non-stationary bicycling.

METHODS

Thirty participants, comprising male (n = 17; M_{age} = 32.1 ± 11.5 yrs) and female (n = 13; M_{age} = 29.8 ± 11.3 yrs) recreational cyclists, pedaled a road bicycle at 118 W over a 350 m flat course under three different saddle conditions illustrated in Figure 1.

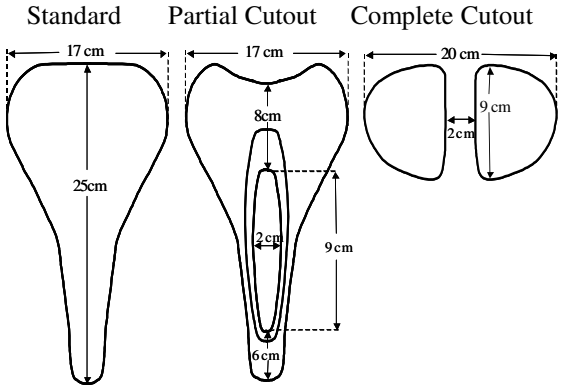

Figure 1: A top view of the three saddle designs and their physical dimensions.

Seat pressures were sampled at 5 Hz via a remote interface module attached to the subject's waist and connected to a pressure-sensing mat designed for bicycle seats (FSA, Vista Medical Ltd). The 1.0 mm thick mat contained a matrix of 768 piezoresistive sensors. The mat was systematically positioned over the seat using methods described by Bressel & Cronin (2005).

Mean pressure (i.e., average of all sensors) was calculated for the total (or overall), anterior, posterior seat, and handlebar interfaces. Mean differences and interactions were assessed using a repeated-measures analysis of variance with gender as a between subjects factor. Probability of Type I error was set at .05.

RESULTS AND DISCUSSION

Although no interactions were observed, the gender effect indicated that overall seat and handlebar pressure values were 51% greater for males than females ($P < 0.05$). Because pressure is the distribution of force over an area, the greater pressure values are likely related to greater mean body weights in the male subjects.

The seat design analysis indicated that anterior seat pressure values for the complete cut-out seat were significantly lower than values for the standard (68%, $P = 0.001$) and partial cut-out (62%, $P = 0.001$) seats (Figure 2). These results support those reported by Lowe et al. (2004) and suggest that saddle design effects seat pressure similarly during non-stationary and stationary cycling. Since the perineal cavernous spaces that house penile vasculature are compressed maximally below the pubic symphysis (Bressel et al., 2007), it would seem logical to reduce pressure over the anterior seat region.

The complete cut-out seat seems to reduce anterior seat pressure near the pubic symphysis, yet it inadvertently leads to significantly greater pressure over the posterior seat and handlebars (Figure 2).

In conclusion, our results indicate that males and females respond similarly to different seat designs and that the choice of saddle design should be dictated by where the user wants pressure reduced since overall pressure was not different between seats (Figure 2).

REFERENCES

Anderson, K. V. & Bovin, 6. (1997). *Acta Neurol Scand,* **95**, 233-240.

Bressel, E. & Cronin, J. (2005). *J Biomech,* **38,** 1325-1331.

Bressel, E. et al. (2007). *J Biomech,* **40**, 198-202.

Gemery, J. M. et al. (2007). *BJU Int,* **99**, 135-140.

Lowe, B. D. et al. (2004). *Med Sci Sports Exerc,* **36**, 1055-1062.

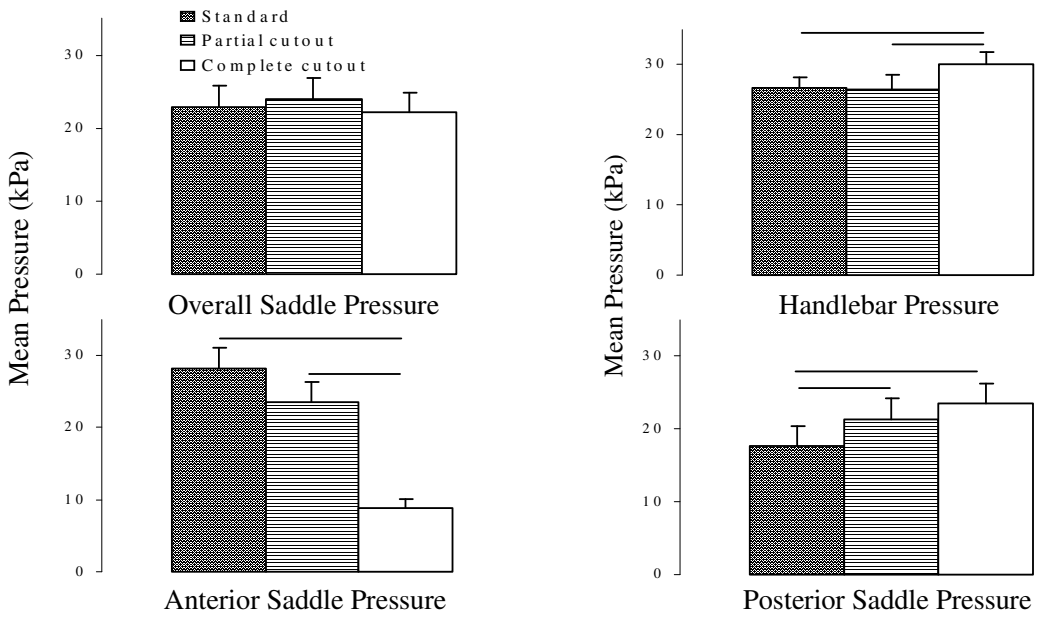

Figure 2: Pressure values (mean ± SEM) for the standard, partial cutout, and complete cutout saddle conditions. Horizontal bars signify groups that are significantly different ($P < 0.05$).

Changes in Patellofemoral Contact Pressure due to Imbalance of the Knee Extensors

Andrew Sawatsky, Doug Bourne Azim Jinha, Walter Herzog
University of Calgary, Calgary, AB Canada
E-mail: aj_sawatsky@hotmail.com

INTRODUCTION

Muscle imbalance in the knee extensor muscles has been associated with problems in patellofemoral tracking (Powers, 2000), joint pain, and osteoarthritis. Changes in patellar tracking and pressure distribution are suspected to cause patellofemoral pain (PFP). The main region of pain is the lateral aspect of the patellofemoral joint. Weakness of the vastus medialis (VM) relative to the vastus lateralis (VL) is the usual imbalance associated with PFP (Cowan et al., 2002; Lefebvre et al., 2006). The fibers of VM are aligned about 50° to 55° medially, and this structural arrangement has been thought to pull the patella medially while the vastus lateralis has been assumed to provide the corresponding lateral balance.

A commonly used treatment for PFP is exercises directed at increasing the strength of the VM in the hope to balance the lateral tensions. Although the idea that muscle imbalance causes maltracking of the patella and so causes pain makes intuitive sense and has clinical and anecdotal support, it has not been tested scientifically.

The purpose of this study was to create an animal model of quadriceps imbalance and to test the effect of extreme imbalances on patellofemoral contact pressures. Muscle imbalance was produced by eliminating the action of VM by cutting it in mid-belly. We hypothesized that the elimination of VM causes a lateral shift of the patellofemoral contact pressures, and might cause lateral patellar subluxation.

METHODS

All experiments were performed on knees (n=9) of six months old New Zealand white rabbits (mass 4.9-5.9kg). Measurements of patellofemoral contact pressures were performed before and after VM transection at a variety of force levels. Experiments were approved by the Animal Ethics Review Committee of The University of Calgary.

In order to assess changes in patellofemoral contact pressures, low grade and medium grade pressure sensitive film (Fuji) was used. Prior to measurement, rabbits were placed into a stereotaxic frame with only the tibia and foot of test limb being mobile. The film was inserted into the joint through bilateral, retinacular, 20-25mm incisions while the joint was fully extended. The tibia was then placed behind a tibial restraining bar at a knee angle of approximately 90°, as determined with a hand held goniometer. The tibial restraining bar measured knee extensor forces. Patellofemoral contact pressures were measured while stimulating the knee extensor muscles through the femoral nerve at supra-maximal currents and frequencies of 200, 60, 50, 40, and 30Hz. Contact pressures were always measured with the low grade film (range = 1-16Mpa). When the low grade film was saturated, measurements were also made using the medium grade film (range = 18 - 52MPa). Contact area measurements were all determined from the low grade film, while peak and average pressures were determined from the low and medium grade films.

Contact area was calculated by integrating across the low grade Fuji film. Peak pressure was obtained as the maximal pressure in an area of at least 0.25mm^2. Average pressure

was calculated as the total contact force divided by the total contact area.

RESULTS AND DISCUSSION

Peak pressures before and after VM transection were similar in each animal and remained similar when averaged across all animals (figure 1). Average pressure increased with increasing knee extensor forces and remained the same before and after VM transection (figures 2). Contact area size and shape also remained virtually identical before and after VM transection, and so did the pressure distribution (results not shown).

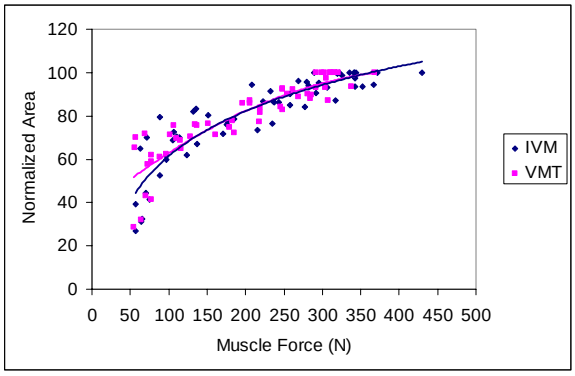

Figure 1 Change in normalized area as a function of muscle force. Across all Rabbits in both hind limbs for IVM and VMT

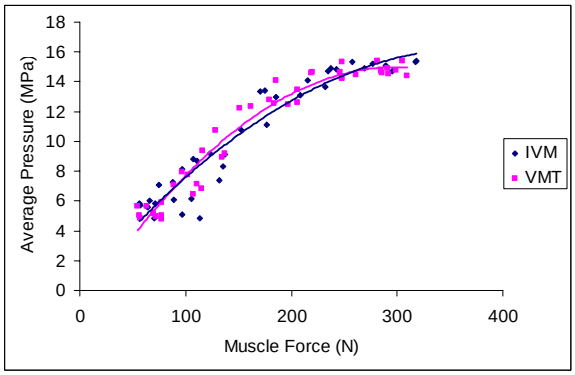

Figure 2 Average pressures as a function of knee extensor forces across all animals with the VM intact (VM) and transected (VMT)

Clinical and anecdotal evidence has led to the common notion that knee extensor imbalance is a cause for PFP associated with changes in patellofemoral contact pressure distribution. One common treatment for PFP is the strengthening of the VM because it has been assumed implicitly that weakness of VM relative to VL is the primary cause of the joint pain. Specific strengthening of the VM is supposed to correct this muscle imbalance, thereby equalizing the medial and lateral forces acting on the patella, allowing for proper patellar tracking in the femoral groove (Cowan et al., 2002). However, here we found that extreme changes in knee extensor imbalance produced by complete elimination of the VM by transection had no visible and consistent effect on patellofemoral contact pressure distributions and contact areas in the New Zealand White rabbit. Although these results may not translate directly to the human condition, it questions the clinical assumption that muscle imbalance causes changes in patellofemoral pressure distributions and joint pain.

References

Cowan, S.M., et al., 2002. *Med SciSport Exerc* **34**:1879-1885

Goh, J.C., et al., 1995. *Brit edit soc bone jt surg*. **77**-B:2:225-231

Lefebvre, R.,et al., 2006. *J manip physiol therap*. **2**:139-144

Powers, C.M., 2000. *Physic Therap* **80**:10:956-964

GAIT ADAPTATIONS AND RECOVERY RATES FOLLOWING MINIMALLY INVASIVE TOTAL HIP REPLACEMENT

Robert M. Trombley, Kharma C. Foucher, Richard A. Berger, and Markus A. Wimmer

Rush University Medical Center, Chicago, IL, USA
E-mail: Markus_A_Wimmer@rush.edu, Web: www.ortho.rush.edu/Gait/

INTRODUCTION

Minimally invasive surgical (MIS) techniques for total hip replacement (THR) are becoming more common; to minimize recovery time compared to conventional THR approaches. Most studies to date have focused on perioperative factors such as blood loss and hospital stay. There are few studies analyzing objective measures of function such as gait kinematics and kinetics. The objective of the present study was to examine the rate of recovery during the first postoperative year, and to test the hypothesis that gait returns to normal after two-incision MIS THR.

METHODS

Participating in a larger randomized study, thirteen subjects with primary hip osteoarthritis (OA) were assigned to receive a THR with a two-incision approach. These 8 men and 5 women were 58±8.48 years old. A gender and age-matched group of 24 normal subjects with no evidence of hip osteoarthritis was chosen for comparison.

Kinematics and kinetics of walking were measured using published techniques (Andriacchi et al., 1997) at five different time points – preoperatively, three weeks, three months, six months, and one year after surgery. Motion of six retro-reflective markers was captured using a four-camera optoelectronic system. A multi-component force plate was used to collect the ground reaction forces. Inverse dynamics were used to calculate external moments. All moments were normalized to percent body weight * height (%BW * ht) to minimize differences due purely to body size (Moisio et al., 2003). Since speed has a significant effect on some external moments during gait, trials for adjacent time points were speed matched as closely as possible.

Paired t-tests were used to assess rate of recovery within five time points. Student's t-tests were used to determine whether there were significant differences between normal subjects and MIS THR subjects. A significance level of less than 0.05 was used throughout.

RESULTS AND DISCUSSION

All THR subjects were able to walk in the gait lab without assistive devices three weeks after surgery. Rate of recovery was assessed by examining dynamic range of motion and external moments at all four postoperative time points (Figure 1). All significant improvements occurred within three months of surgery. Preoperative and three week postoperative extension and abduction moments were significantly different ($p=0.05$, $p=0.005$ respectively). Changes in dynamic range of motion and internal rotation moment between three weeks and three months after surgery were highly significantly different ($p<0.002$).

Although there was improvement over time, patients did not return to normal after surgery. Significant differences were still seen between gait of normal subjects and

that of THR subjects one year after surgery (Figure 2).

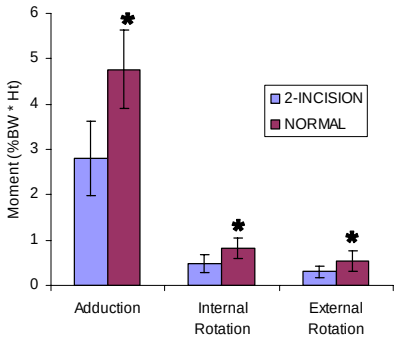

Figure2. Peak adduction, external rotation, and internal rotation comparison of two-incision subjects to normal subjects after one year postoperative gait testing. Significant improvements are indicated with star (*).

Peak external adduction, internal rotation, and external rotation moments were significantly reduced compared to normal ($p=0.001$, $p=0.001$, and $p=0.05$ respectively).

SUMMARY/CONCLUSIONS

Functional recovery of subjects with MIS THRs occurred within the first three months of surgery. No further significant improvements were seen after this time point. While improvements have been made, even after one year following surgery gait kinematics and kinetics did not reach normal values. The chronically reduced recruitment of hip muscles stabilizing the external hip moments may be related to hip muscle weakness which developed over time over time during progression of OA at the hip. A focused hip muscle strengthening program might favorably alter such conditions.

REFERENCES

Andriacchi T.P., et al. (1997). In *Basic Orthopaedic Biomechanics* 2nd ed. Eds. VC Mow and WC Hayes.

Moisio, K.C., et al. (2003). *J. Biomechanics*, **36**(4), 599-603.

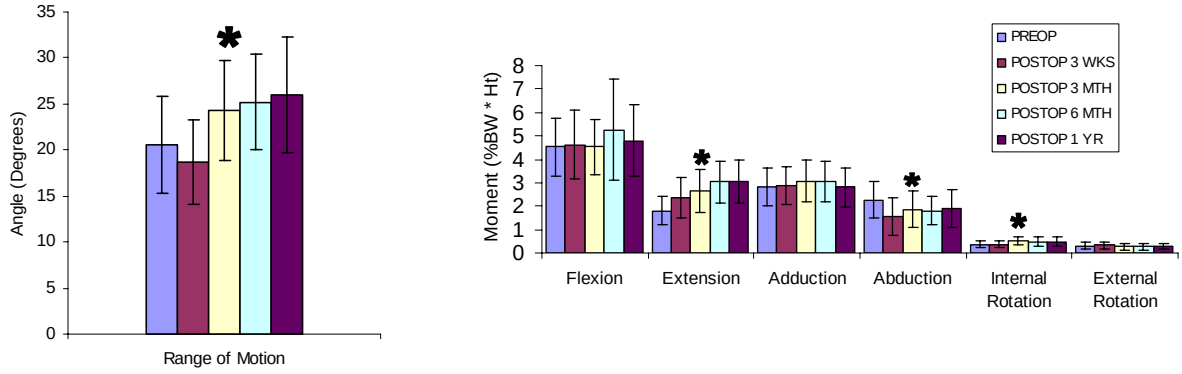

Figure 1. Hip range of motion and moments for five time periods from preoperative gait testing to one year postoperative gait testing. Significant improvements are indicated with star (*).

A CALIBRATION METHOD FOR STEREO FLUOROSCOPIC IMAGING SYSTEMS

J. Erik Giphart [1], Bart L. Kaptein [2], Kevin B. Shelburne [1], Michael R. Torry [1]
[1] Steadman-Hawkins Research Foundation, Vail, CO, USA
[2] Leiden University Medical Center, Leiden, The Netherlands
E-mail: erik.giphart@shsmf.org , Web: www.shsmf.org

INTRODUCTION

Stereo fluoroscopic motion analysis systems provide the highest precision and accuracy in measuring *in vivo* joint motion. Calibration of these systems is necessary to: 1) correct for the significant image distortion in the image intensifiers; 2) determine the x-ray focus position for each fluoroscopy system relative to its image plane; and 3) determine the spatial relationship between the two fluoroscopy systems.

This study focuses on the determination of the focus position. Previous calibration methods include using the manufacturer's specification of the focus position (Li et al., 2004) and the use of accurately machined calibration boxes with fiducial and control planes (Garling et al., 2005). The accuracy of the manufacturer's specification may be questioned, while calibration data collection with large boxes can be difficult and limiting to the setup. The purpose of this study was to validate a new calibration method which uses a relatively inexpensive fiducial plate and small cube while preserving calibration accuracy.

METHODS

Equipment Two Philips BV Pulsera fluoroscopy systems were used in Digital Exposure mode to collect all images. An acrylic calibration box with 317 fiducial and 21 control markers was built with the control plane distance from the fiducial plane of 400 mm. An aluminum fiducial plate was machined with 406 holes. Both fudicial planes had a squared pattern with 15mm distance between the holes/markers. Lastly, a foam cube with 15 markers was built and average marker positions were determined from RSA recordings with the cube in 3 different orientations. Data analysis was performed using Model-based RSA software (Medis Specials, BV, The Netherlands)

Calibration Three calibration methods were implemented to find the focus positions.
• Method 1: Using the Fiducial-Control plane method (Garling et al., 2005).
• Method 2: Using a fixed position at 1000mm from the image center.
• Method 3: Using a new nested optimization algorithm: the inner optimization loop determined the error of the best match of the foam cube markers given a focus position; the outer optimization loop searched for the focus position that minimized the matching error from the inner optimization loop.

Image distortion was corrected using the fiducial plane markers of the box (Method1) or the fiducial plate (Method2,3). The relative positions of the two fluoroscopy systems were always based on the foam cube data.

Data collection and analysis First, a caliper instrumented with two markers was recorded in three configurations (closed; opened 25.4mm, opened 50.8mm) in three poses each. Second, a box with 16 markers was attached to a micromanipulator which could displace the box along two perpendicular axes with an accuracy of 5µm. Ten displacements of 1mm each were

applied to the box and measured with the fluoroscopic motion analysis system using the 3 calibration methods.

RESULTS

Means and standard deviations (Std 1-3 below) for the 3 caliper configurations were calculated. The difference between the means was compared with the 2 successive 1" (25.4mm) displacements applied to the caliper (Error 1-2 below).

Table 1. Standard deviations (mm) and errors (mm) of measured caliper configurations across the three calibration methods.

	Method1	Method2	Method3
Std1	0.0444	0.0286	0.0243
Std2	0.1893	0.0640	0.0102
Std3	0.0792	0.0463	0.0199
Error 2.5cm	-0.0189	0.0343	0.0252
Error 5.0cm	0.0714	0.0694	0.0837

The mean and standard deviations of the differences between the measured and micromanipulator applied displacements were calculated (i.e., bias and error) as well as of the absolute differences. The root-mean-squared (RMS) error is also presented.

Table 2. Error measures (mm) based on ten micromanipulator displacements across the 3 calibration methods.

	Method1	Method2	Method3
Mean	-0.0086	0.0030	0.0002
Std	0.0178	0.0185	0.0153
Mean (abs)	0.0150	0.0125	0.0098
Std (abs)	0.0123	0.0133	0.0113
RMS	0.0190	0.0178	0.0145

DISCUSSION

The caliper results show that the new calibration method (Method3) had the highest and most consistent precision (lowest std) of 18.1µm (average of the 3 measures). The micro-manipulator results show that the new calibration method has the lowest bias (0.2 µm) and highest accuracy (15.3 µm) as well as the lowest RMS error of 14.5 µm.

Simply assigning the focus position to the manufacturer's specification (Method2) also provided good results. Precision is 2.6 times less (46.3 µm) compared to new calibration method, but the accuracy is only 21% less while the bias is limited to 3 µm.

The Fiducial-Control plane method (Method1) demonstrated the poorest results in the experiments with reduced precision and increased bias. The accuracy was similar compared to the other methods.

The primary limitation of this study was that the acrylic calibration box was not manufactured with the same tolerance as the fiducial plate. We hypothesize that the resulting reduced accuracy of the distortion correction in Method1 caused the reduced calibration performance rather than the focus position determination. A second limitation of this study is that the Direct Linear Transform (DLT) method was not included (You et al., 2001).

CONCLUSION

The new calibration method is equal to or better than the two currently reported calibration methods that were tested.

REFERENCES

Garling, E.H. et al. (2005). *J. Biomech*, **38**, 893-901.
Li, G. et al. (2004). *Trans ASME*, **126**, 314-318.
You, B. et al. (2001). *IEEE Trans Med Imag*, **20**, 514-525.

ACKNOWLEDGEMENT

Supported in part by the Steadman Hawkins Research Foundation and the Stravos Niarchos Foundation

FUNCTIONAL GAIT OUTCOMES IN STAIR CLIMBING AFTER INTERTROCHANTERIC HIP FRACTURE

Kimberly Yarnall[1,3], Ellen Boeke[1], M. Wade Shrader[2,3], Kristine Csavina[1,3]

[1]SHRI-CORE Orthopedic Research Labs, Sun City West, AZ USA
[2]The CORE Institute, Sun City West, AZ USA
[3]Harrington Department of Bioengineering Arizona State University, Tempe, AZ USA
email: kim.yarnall@thecoreinstitute.com

INTRODUCTION

According to the American Academy of Orthopedic Surgeons, 352,000 hip fractures occur each year, and by the year 2050 it is estimated that the number will have escalated to 650,000 hip fractures per year. Despite these numbers, very few studies have extensively evaluated the post-operative walking capacity of these patients and no studies have assessed the ability of these patients to climb stairs. Previous studies evaluated maximal vertical force to determine how much reliance was placed on walking aids and analyzed the single-leg support phase to determine what percentage of the gait cycle was spent on the injured leg versus the uninjured leg. (Barrios, 1993, Walheim,1990) The purpose of this study was to quantify gait parameters for stair ascent after hip fractures and compare this data to age-matched controls.

METHODS

All patients were treated for intertrochanteric hip fractures by orthopedic surgeons at The CORE Institute between October 2006 and early December 2006. This study was approved by the Sun Health Institutional Review Board and all subjects signed the Informed Consent and HIPPAA Authorization forms prior to participation in the study. Exclusion criteria were defined as an inability walk without assistive devices, inability to ascend stairs, dementia, neuropathies, and unrelated gait disorders. The four patients who fit these criteria and were willing to participate, included two females and two males (age 80±6.7) Control subjects were individuals previously recruited and tested in the SHRI-CORE Motion Analysis Lab. The group of six age-matched control subjects consisted of four males and two females (age 78±6.1) from the same community.

Three dimensional kinematic and kinetic data were recorded using a passive marker 10-camera Eagle 4.0 system (Motion Analysis Corp., Santa Rosa, CA) and four AMTI OR6-6 forceplates (AMTI, Watertown, MA). At least six consistent walk trials were gathered to ensure three clean right foot strikes and three clean left foot strikes. All data was taken using the modified Helen Hayes marker set and was processed using Motion Analysis Software (Santa Rosa CA), EVaRT 5.0.1 and OrthoTrak 6.2.8.

Single leg support, minimum hip flexion in stance, maximum hip moment in stance, max power generation in stance and max power generation in swing for the injured leg versus the uninjured leg were compared using a paired t-test and then both limbs were compared to controls using an unpaired student t-test assuming equal variance. Significance was defined as $p<0.05$.

RESULTS AND DISCUSSION

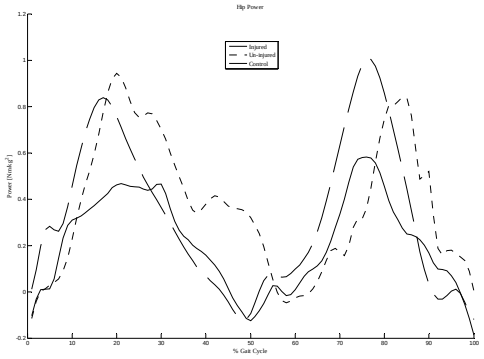

Figure 1: Hip Powers exhibited during stair ascent.

Statistical differences in this study were found for minimum hip flexion in stance, single leg support time, and maximum power generation in swing when comparing the injured leg to the uninjured leg. Figure 1 illustrates the decreased power generation in swing for the injured leg. No statistical differences were apparent when comparing intertrochanteric hip fracture patients to age-matched controls. This could be due to the limited number of patients enrolled in this study. These preliminary results indicate that they are still favoring their uninjured legs and compensating for their injured leg as noted in the significant differences between the injured and uninjured legs.

REFERENCES

Barrios, C et al., *Clinical Orthopaedics and Related Research* **294**, 187-192, 1993.

Walheim, G et al., *Journal of Orthopaedic Trauma* **4(2)**, 137-143, 1990.

Table 1: Temporal/Spatial and Hip Kinematic and Kinetic Results (*statistically different from control, **injured statistically different from uninjured ($p<0.05$))

	Single Leg Support (%)	Min Hip Flexion in Stance	Max Hip Moment in Stance	Max Power Generation in Stance	Max Power Generation in Swing
Injured Leg	67.2 ± 7.83**	27.0 ± 8.0**	0.6 ± 0.28	0.82 ± 0.46	0.77 ± 0.30**
Uninjured Leg	72.9 ± 6.5	24.1 ± 9.0	1.02 ± 0.75	1.23 ± 0.98	1.24 ± 0.20
Controls	-	21.6 ± 3.4	0.67 ± 0.22	1.06 ± 0.44	1.15 ± 0.37

AN ALGORITHM FOR AUTOMATED TRACKING OF TENDON EXCURSION FROM ULTRAOUND IMAGES

Sabrina S.M. Lee, Gregory S. Lewis, and Stephen J. Piazza

The Pennsylvania State University, University Park, PA, USA
E-mail: *sul167@psu.edu*

INTRODUCTION

One commonly-used method for measuring muscle moment arm is the tendon excursion method, in which moment arm is calculated as the first derivative of the displacement of the tendons with respect to the joint angular displacement (An et al., 1983). This method has been used to estimate moment arms in cadaver specimens through direct attachment of transducers to tendons (e.g., Brand et al., 1975). It has also been applied *in vivo* through ultrasound imaging of tendon displacement (e.g., Maganaris et al., 2000), but this technique usually requires manual digitization of landmarks on each frame of the image sequence. An automated method for tracking the tendon would provide a time-efficient means for evaluating muscle moment arms in clinical and research settings. The purposes of this study were to develop a novel automated tendon tracking algorithm that incorporates the Lucas-Kanade algorithm for calculating optical flow (Lucas & Kanade, 1981) and to test the accuracy of the algorithm using phantom, cadaver, and *in vivo* experiments.

METHODS

Automated tracking was implemented using an algorithm which computes pixel velocities based on spatial and temporal image brightness which is assumed to be constant from frame-to-frame. A pyramidal approach with increasing resolution from top to bottom allows for large pixel velocities to be calculated. By adding the average of the five greatest pixel velocities within a region around the selected landmark to the initial selected pixel, the pixel location in the subsequent frame can be estimated. Three experiments were conducted for validation: (1) a wire "phantom" was moved through three nominal distances (approx. 5 mm, 10 mm, and 20 mm) while ultrasound images of the wire were captured. The wire excursion estimated using automated tracking was compared to direct measurements made with a cable extensometer attached to the wire; (2) *in vitro* excursion of the lateral gastrocnemius tendon estimated using manual tracking were compared to direct measurements of tendon excursion made using a cable extensometer in a fresh-frozen lower-leg cadaver specimen; (3) i*n vivo* excursions of lateral gastrocnemius tendon estimated using automated tracking were compared to excursions estimated using manual landmark identification in five subjects (Figure 1).

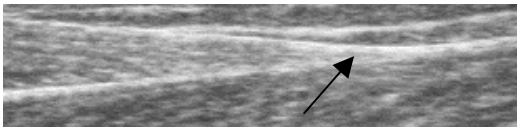

Figure 1. Ultrasound image of lateral gastrocnemius. The arrow indicates the musculotendon junction as the tracking landmark.

This three-tiered approach for validation was implemented because the automated tracking algorithm did not perform consistently on cadaver ultrasound images, perhaps because of tissue degradation due to dehydration, freezing, and thawing.

Ultrasound images were acquired at 30 Hz using an Aloka 1000 scanner operating in B-mode with a 7.5 MHz probe. Root-mean-squared errors (RMSE) were computed for comparisons of wire or tendon excursion measured by either the cable extensometer, manual tracking, or automated tracking as described above.

RESULTS AND DISCUSSION

RMSE between direct measurement and automated tracking of the wire for the phantom experiment averaged across ten trials were 0.2 ± 0.1 mm, 0.4 ± 0.1 mm, and 0.9 ± 0.2 mm for mean excursions of 5.1 mm, 8.9 mm, and 19.3 mm, respectively (Figure 2a). RMSE between manual tracking of ultrasound and direct measurement in the cadaver model, averaged across five trials, were found to be 2.30 ± 0.7 mm for sagittal plane movements and 0.30 ± 0.1 mm for frontal plane movements (Figure 2b). RMSE between manual tracking and automated tracking measured in vivo averaged across five trials were found to be 1.1 ± 0.3 mm for sagittal and frontal plane movements, respectively (Figure 2c).

Good agreement was found between direct and automatically tracked measurements of wire excursion, between manually-tracked and direct measurements of tendon excursion in cadaver specimens, and between manually-tracked and automatically tracked tendon excursion *in vivo*. Relative to the total tendon excursion which was about 17-30 mm for sagittal plane motions and 2-7 mm for frontal plane motions, the RMSE found in this study suggest that errors in moment arms computed from automated tracking of tendon excursion would amount to less than 10%.

SUMMARY/CONCLUSIONS

These small errors and ease of use of the automated tracking method suggest that the method could be a useful, effective, and time-efficient clinical tool for assessment of moment arms of superficial muscles.

REFERENCES

Brand, P.W. et al. (1975). *J Bone Joint Surg Am*, **57**, 779-784.

Lucas, B.C. and Kanade, T.. (1981). *Proc. DARPA*, 121-130

Maganaris, C.N. (2000). *J Biomech*, **33,** 375-379.

ACKNOWLEDGMENTS

The authors would like to thank Sohaib Khan for contributing a MATLAB implementation of the Lucas-Kanade algorithm. This work was supported by NSF BES-0134217.

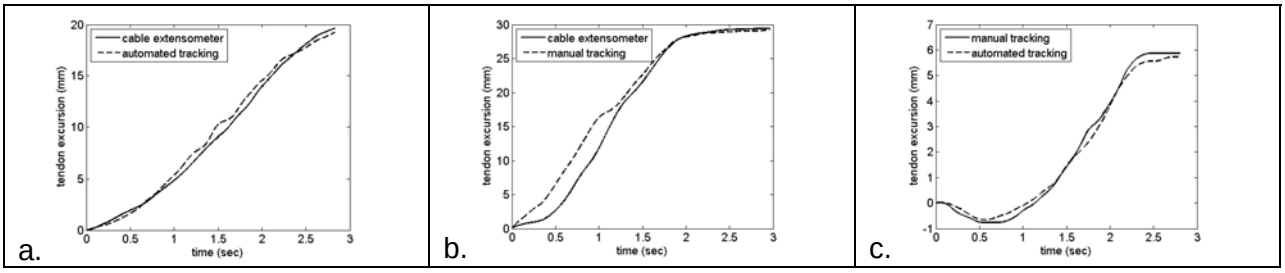

Figure 2. Typical examples of a) phantom measurements by direct measurements versus automated tracking (RMSE = 0.77 mm), b) *in vitro* measurements by direct measurements versus manual tracking (RMSE = 2.21 mm), c) *in vivo* measurements by manual tracking versus automated tracking (RMSE = 0.21 mm).

MINIMAL MUSCLE ATROPHY DURING HIBERNATION IN CAPTIVE BROWN BEARS

John D. Hershey, Charles T. Robbins, O. Lynne Nelson, and David C. Lin

Washington State University, Pullman, WA USA
E-mail: davidlin@wsu.edu

INTRODUCTION

Previous studies on wild black bears (*Ursus americanus*) have shown skeletal muscle morphology, composition and overall force generating capacity do not differ drastically between late fall and early spring [1, 2]. These findings are surprising in that prolonged inactivity during hibernation should cause significant amounts of atrophy, leading to decreased maximal force and a shift toward faster fiber types.

The amount and characteristics of the seasonal variations in skeletal muscle were not consistent in the previous studies in that the variation in muscle properties ranged from no significant change to a 23% change. Moreover, measurements were made in the late fall, when muscle strength may already be compromised and in the early spring, when physiological changes to regain muscle strength may have already started.

The goals of this study were to confirm that the amount of muscle atrophy in captive brown bears (*U. arctos)* is minimal, similar to that observed in wild black bears. This study will extend previous studies by examining muscle samples between mid-summer (peak activity) and mid-winter (peak inactivity) and characterize twitch dynamics as part of the atrophy measurements.

METHODS

Six captive brown bears from the Washington State University Bear Research Center were studied. The bears hibernated each winter from late October to late March. All protocols were approved by the Institutional Animal Use and Care Committee.

Samples from the *biceps femoris* muscle were collected during the summer and winter. Each sample was connected to a force transducer and fixed hook within an experimental chamber circulating an aerated physiological solution at 37°C. To elicit isometric twitches, a pair of plate electrodes provided field stimulation at a supramaximal voltage. Ten consecutive twitches were recorded. After 5 minutes of rest, twitches were again recorded and this procedure was repeated for a total of three twitch trains. Individual twitches were analyzed for half rise time, time to peak, half decay time, and total twitch time.

After the electrical stimulation recordings, the sample was flash frozen in liquid nitrogen. A piece of the sample was processed for total protein concentration by a standard Bradford method. Another piece was sectioned and stained for ATPase activity. The sections were digitally photographed at a low magnification. Four hundred random fibers were classified as type I or type II by staining intensity. Each fiber's cross-sectional area was measured.

Statistical analysis was performed with a two-tailed, non-parametric, Wilcoxon Signed Rank test for seasonal differences. Significance was accepted at the $p<0.05$ level.

RESULTS AND DISCUSSION

Satisfactory twitch data was obtained from summer and winter samples in five bears (Figure 1). Although all values in winter were higher than the corresponding summer values (Table 1), only half rise time was statistically different ($p = 0.043$).

Average protein concentration was 194.2±7.8 mg/g in the summer and decreased to 178.2±7.6 mg/g during hibernation ($p = 0.028$). Slow and fast fiber percentages were 48.0 and 52.0±9.9% respectively in summer and 47.7 and 52.3±7.7% in winter, indicating no seasonal difference. Cross-sectional area showed no significant differences between summer (10074±2618 μm^2) and winter (9125±958 μm^2) for slow fibers and between summer (9450 ±1774μm^2) and winter (9421±1870 μm^2) for fast fibers.

These results agreed with a study which showed minimal skeletal muscle atrophy between seasons in wild black bears. For example, the time to half maximal force in the twitch contractions increased in winter relative to summer samples. This is in contrast to the faster twitch dynamics in muscle undergoing disuse atrophy [3]. Our results also shows that skeletal muscle in bears does not change between the periods of peak use and of peak disuse.

SUMMARY/CONCLUSIONS

We measured the amount of atrophy between mid-summer and mid-winter in muscle samples from six captive brown bears and found minimal seasonal differences. In fact, the twitch dynamics were slightly slower in winter, opposite to that expected from muscle that does not have much weight-bearing activity. These findings merit further investigation as to the mechanisms behind this intriguing ability of hibernating bears.

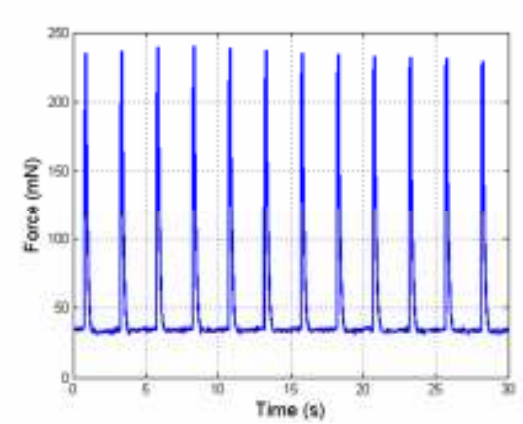

Figure 1: Isometric twitches from a bear *biceps femoris* sample.

REFERENCES

[1] Tinker, D.B. et al. (1998). *Physiol. Zool.,* **71**, 414-424.
[2] Harlow, H.L. et al. (2001). *Nature,* **409**, 997.
[3] Shields, R.K. (2002). *J. Orthop. Sports Phys. Ther.*, **32**, 65-74.

ACKNOWLEDGEMENTS

Funding provided by the Autzen Foundation

Table 1: Average twitch characteristics for 5 bears.

Season	Half Rise Time(s)	Time to peak (s)	Half Fall Time(s)	Total Twitch Time(s)
Summer	0.019	0.067	0.126	0.392
Winter	0.029	0.081	0.132	0.429

IN VIVO MEASUREMENT OF THE INVERSION-EVERSION MOMENT ARMS OF GASTROCNEMIUS AND TIBIALIS ANTERIOR

Sabrina S.M. Lee, Stephen J. Piazza

The Pennsylvania State University, University Park, PA, USA
E-mail: *sul167@psu.edu*

INTRODUCTION

Identifying the muscles that contribute to frontal-plane deformities such as hindfoot varus and hindfoot valgus is a difficult task because of ambiguity in the frontal plane actions of those muscles. Electromyography, gait analysis, and visual observation may be useful for identifying abnormal kinematic, kinetic, and muscle activity patterns, but none of these techniques will characterize the action of a potentially offending muscle. One way to quantify a muscle's action is to measure its moment arm; a muscle with a greater moment arm will produce more moment about a joint axis for a given force. Inversion-eversion moment arms of extrinsic foot muscles have been measured previously in cadavers (Hintermann et al. 1994; Klein et al. 1996; Piazza et al. 2003), but *in vivo* measurements have not been reported. The purposes of this study were: 1) to use ultrasound imaging to measure the inversion-eversion moment arms of lateral and medial gastrocnemius (LG and MG), and tibialis anterior (TA) in healthy subjects; 2) to investigate the influence of plantarflexion and muscle activity on moment arm; and 3) to correlate the moment arms with anthropometric variables.

METHODS

Moment arms of LG, MG, and TA were measured in ten healthy subjects (5 m, 5 f, 21-32 y) who gave informed consent prior to testing. Nine anthropometric measures were taken: 1) height, 2) shank length, 3) foot length, 4) calcaneal tuberosity to 1^{st} metatarsal head, 5) 1^{st} to 5^{th} metatarsal head, 6) intermalleolar width, and the heights of the 7) lateral and 8) medial malleoli, and 9) medial arch.

Tendon excursion was measured using B-mode ultrasonography (Aloka 1100; transducer: SSD-625, 7.5 MHz) and inversion-eversion angle was measured using a potentiometer-instrumented rotating foot platform. With the subject in a seated position and the foot on the foot platform, the ankle was rotated from 15° eversion to 20° inversion. Three levels of muscle activity (rest, light, and maximum voluntary contraction) and three sagittal plane positions (0°, 15°, and 30° plantarflexion) were tested. Moment arm was calculated by evaluating the analytical derivative of a second-order polynomial fit to tendon excursion versus angle data at 15° eversion, neutral position, and 20° inversion. Three-way repeated measures ANOVAs (muscle, muscle activity, plantarflexion angle) were conducted for each frontal plane angle (15° eversion, 0°, and 20° inversion), followed by Tukey post-hoc tests when appropriate. Best-subset and stepwise regression were used to determine correlations between anthropometric variables and moment arm.

RESULTS AND DISCUSSION

The moment arms of all three muscles significantly varied with frontal plane angle (all $p < 0.001$) (Table 1). LG and TA muscles exhibited evertor moment arms and MG exhibited a slight invertor moment arm

when the ankle was everted and all became greater invertors with progressive inversion. The moment arms of the gastrocnemius muscles showed differences throughout the frontal plane range of motion: 1) at 15° eversion, LG exhibited a significantly larger evertor moment arm than MG ($p < 0.001$); 2) at neutral position, MG was a significantly greater invertor than LG ($p = 0.001$); and 3) at 20° inversion, the moment arm of LG appeared to be greater than of MG, but not significantly ($p = 0.083$). Muscle activity had a significant effect on inversion-eversion moment arms of LG and MG (all $p = 0.005$); as muscle activity increased, LG and MG invertor moment arms became greater invertors and evertor moment arms became significantly greater evertors. However, muscle activity did not have a significant effect on the TA moment arm (15° eversion, $p = 0.805$; 0° = 0.287; 20° inversion, 0.240). The effect of sagittal plane ankle position seemed to differ across subjects, as there were significant subject-plantarflexion-muscle activity interactions ($p < 0.01$) and there was not a main effect of sagittal plane on moment arm (15° eversion, $p = 0.212$; 0° = 0.130; 20° inversion, 0.214).

Multiple regressions involving a subset of four of the nine predictors best explained moment arm variance across the experimental conditions tested. Better fits were obtained under light contraction ($p = 0.001$, 0.198, 0.007) for all three angles, respectively, rather than during maximal contraction. Regression residuals were smaller than 2 mm and 4 mm across plantarflexion angles for the light and maximum contraction condition, respectively.

SUMMARY/CONCLUSIONS

This study has shown that the frontal plane moment arms of the gastrocnemius and TA differ across the frontal plane range of motion in healthy individuals and this quantification of muscle action can improve the understanding and preoperative planning of treatment for frontal plane ankle deformities.

REFERENCES

Hintermann, B. et al. (1994). *Foot Ankle Int,* **15,** 386-395.

Klein, P. et al. (1996). *J Biomech,* **29**, 21-30.

Piazza, S.J., et al. (2003). *J Bone Joint Surg Am,* **85-A,** 858-865.

ACKNOWLEDGMENTS

The authors would like to thank Tamara Cohen for her assistance with data collection. This work was supported by NSF BES-0134217.

Table 1: Inversion-eversion moment arms measured at different frontal plane foot positions and muscle activity levels (mean and s.d.). Moment arm values are averaged across three trials and three sagittal-plane foot positions. Positive moment arms indicate muscles that are invertors.

Frontal Plane Angle	Muscle activity	Mean moment arm (mm) (SD)		
		LG	MG	TA
15 ° eversion	At rest	-2.9 (2.2)	-0.8 (2.1)	-1.6 (3.2)
	Light contraction	-2.3 (2.7)	0.3 (2.4)	-1.1 (4.3)
	MVC	-1.9 (2.6)	0.2 (2.7)	-1.3 (3.7)
0°	At rest	0.8 (1.6)	2.3 (1.7)	2.8 (2.0)
	Light contraction	1.6 (1.9)	3.5 (1.9)	3.6 (2.5)
	MVC	1.8 (1.9)	3.6 (2.5)	3.4 (2.6)
20 ° inversion	At rest	5.9 (1.8)	6.5 (2.1)	8.6 (2.9)
	Light contraction	6.8 (2.3)	7.7 (3.6)	9.8 (3.3)
	MVC	6.7 (2.2)	8.0 (4.3)	9.7 (4.5)

THE EFFECT OF HAND POSITION ON SUBSCAPULARIS FORCE DURING THE BELLY-PRESS TEST

Takashi Yanagawa [1], Michael R Torry [1], Kevin B Shelburne [1], Marcus G Pandy [2]
[1] Steadman Hawkins Research Foundation, Vail, CO, USA
[2] The University of Melbourne, Melbourne, VIC, AUS
E-mail: takashi.yanagawa@shsmf.org, Web: www.shsmf.org

INTRODUCTION

The "belly-press test" is often used to help diagnose a subscapularis muscle tear in the clinic. A patient is asked to place his or her hand on the abdomen and press that region by rotating the arm internally with the elbow positioned anterior to the coronal plane. If the elbow is moved posterior to that plane, the test is considered positive (Gerber et al, 1996). If the patient is obese with an extended abdomen, the humerus must be flexed to obtain the starting hand and elbow position of the belly press test. It is unknown whether the flexed position of the humerus compromises the validity of the test. The purpose of this study was to calculate the force in the subscapularis during the belly-press test and compare the value to that calculated when the humerus is flexed.

We hypothesized that flexion of the humerus would reduce the force in the subscapularis.

METHODS

An upper extremity computer model (Garner and Pandy, 2001) was used to calculate the muscle forces in the shoulder. Nineteen muscles including upper and lower portions of the subscapularis were included in the model. To simulate the force of the hand on the abdomen, a 10N force was applied to the hand that pushed the hand anterior to the abdomen (Figure 1). Muscle forces were calculated by solving a static optimization problem that minimized the stress in the muscles. Three belly-press conditions were simulated: First, a normal belly-press was simulated with the hand placed on the abdomen of the model. Then, to represent obesity, the hand was moved 5 cm and 9.4 cm anteriorly, which added 10° and 20° of extra humeral flexion to the normal belly-press position, respectively (Figure 1).

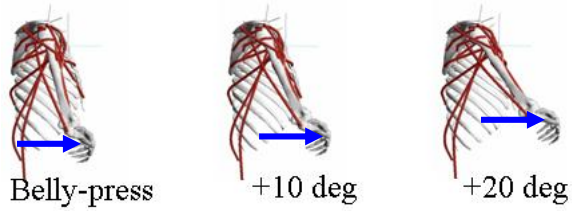

Figure 1: Belly-press test and its variations with extra flexion of 10° and 20°.

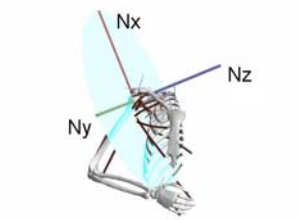

Figure 2 An external force frame was placed on the plane that is parallel to the external force of the abdomen.

The torque produced by the shoulder muscles was calculated about an axis that was perpendicular to the plane created by the glenohumeral joint and the external force (Figure 2). This way, the torque produced by each muscle could be compared to the torque produced by the belly-press force.

RESULTS

The lower subscapularis produced the largest force (Figure 3) and the most torque among the rotator cuff muscles in all the conditions (Figure 4). As the humerus was flexed, and the hand was placed further anterior to the body, both upper and lower subscapularis forces decreased (Figure 3).

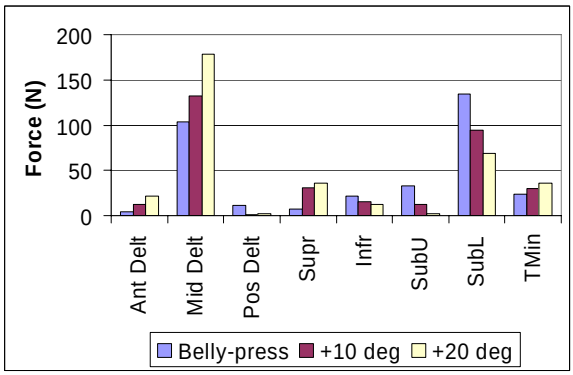

Figure 3: Muscle forces with increasing flexion of the humerus.

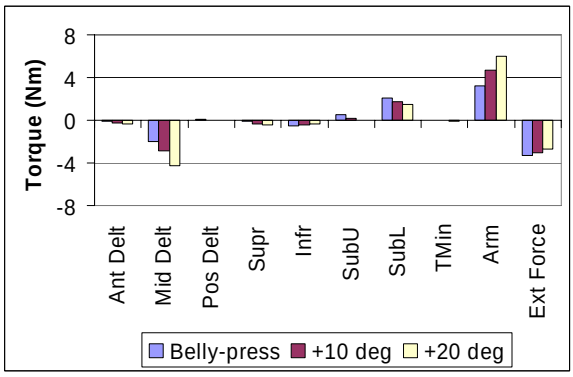

Figure 4: Muscle torques about Nz, arm weight and external force in the external force frame.

The sum of all the positive torques increased, as the hand moved away from the belly region (Figure 5). However, most of the increase came from the weight of the arm. Subscapularis torque decreased as a percentage of the total positive torque from 42% to 19%.

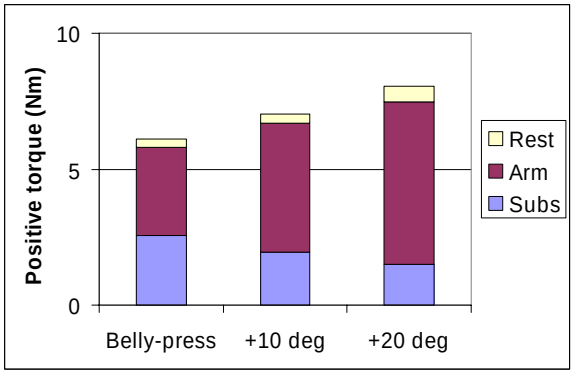

Figure 5 Positive torque about the Nz axis.

DISCUSSION

These results indicate that the belly-press test with extra flexion would rely less on the subscapularis muscle force. As arm flexion increased, the torque needed to press the belly with 10N of force was increasingly composed of the weight of the arm. Thus, the test with extra flexion may not be as effective as the normal belly-press position.

SUMMARY

Subscapularis force decreased with increasing flexion of the humerus. With the humerus flexed, torque was dominated by the weight of the arm. Therefore, the utility of the belly press test in the obese may be diminished.

REFERENCES

Garner. B.A., Pandy M.G. (2001). *Comput Methods Biomech Biomed Engin,* **2,** 107-124.

Gerber C, et al. (1996). *J Bone Joint Surg Am,* **78,** 1015-23.

ACKNOWLEDGEMENT

Supported in part by the Steadman Hawkins Research Foundation and the NFL Charities

GLENOHUMERAL JOINT REACTION FORCES FOLLOWING LATISSIMUS TENDON TRANSFER

Takashi Yanagawa [1], Peter J Millett [2], Michael R Torry [1], Kevin B Shelburne [1], Marcus G Pandy [3]

[1] Steadman Hawkins Research Foundation, Vail, CO, USA
[2] Steadman Hawkins Sports Medicine Clinic, Vail, CO, USA
[3] The University of Melbourne, Melbourne, VIC, Australia
E-mail: takashi.yanagawa@shsmf.org, Web: www.shsmf.org

INTRODUCTION

Massive rotator cuff tears often produce superior migration of humeral head and limit shoulder function. For irreparable cuff tears, latissimus tendon transfer is an option to restore shoulder function (Gerber, 1992). Margermans et al. (2004) calculated moment arms of the transferred latissimus muscle and compared different attachment sites. However, they did not report glenohumeral joint reaction forces (GHJRFs), which mainly determine the stability of the humeral head in the glenoid. Thus, the purpose of this study was to compare the GHJRFs between the intact shoulder, the shoulder with a rotator cuff tear, and shoulder with the rotator cuff tear following latissimus tendon transfer. We hypothesized that the shear forces at the glenohumeral joint would decrease following latissimus transfer in the rotator cuff torn shoulder.

METHODS

Measured 3D clavicular, scapular, and humeral positions during abduction were applied to a 3D model of the upper extremity (Garner and Pandy, 1999, Yanagawa et al. in review). A static optimization problem was solved to compute the muscle forces needed to abduct the arm in four muscle conditions: 1) normal, 2) rotator cuff tear (RCT), 3) tendon transfer to the supraspinatus insertion (Supr), 4) tendon transfer to the infraspinatus insertion (Infr). In the rotator cuff tear condition, no force was transmitted in the supraspinatus and infraspinatus muscles. To simulate muscle weakness, the tendon transfer calculations were repeated with the strength of the remaining cuff muscles, subscapularis and teres minor, reduced to 20% of maximum. Stability ratios (shear force divided by compression force) as proposed by Fukuda et al. (1988) were calculated to show the effect on glenohumeral stability

RESULTS AND DISCUSSION

The resultant GHJRF increased in the RCT condition (Figure 1). Transfer of the latissimus tendon to either the supraspinatus or the infraspinatus insertion reduced the resultant GHJRF closer to, but below, normal levels.

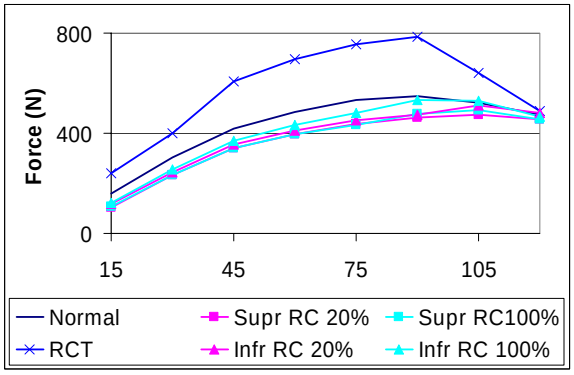

Figure 1: Resultant joint reaction force during abduction from 15° to 120°.

The magnitude of compressive component of the GHJRF was higher than the anterior

or superior components in any condition (Figure 2). The tendon transfer conditions (Supr and Infr) produced lower compression forces than those of the normal and RCT conditions (Figure 2). Because of the low compressive force and high shear force, anterior and superior stability ratios tended to be higher for the Supr and Infr conditions compared to those of the normal shoulder for most of the angles (Figure 3 and Figure 4).

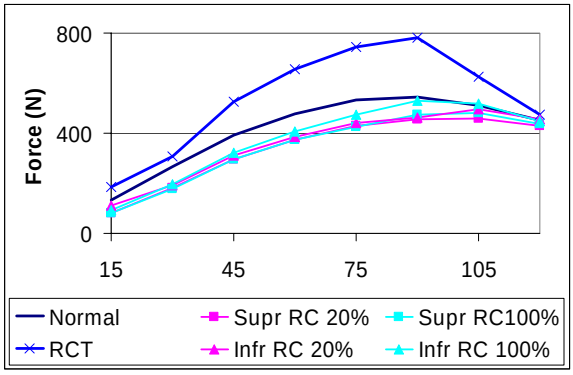

Figure 2: Glenohumeral joint compression force during abduction.

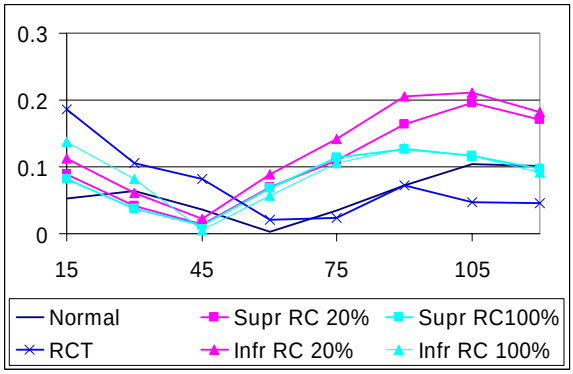

Figure 3: Anterior stability ratios.

When the remaining rotator cuff muscles were weakened to 20% of their normal strengths, the anterior stability ratios tended to be larger than normal (Figure 3). This suggests that retaining the potential strength of subscapularis and teres minor would assist in centering the glenohumeral joint in the fore-aft direction.

CONCLUSIONS

The goal of the latissimus tendon transfer surgery is to restore shoulder function. In this study, the tendon transfer to either the Supr or Infra locations produced near normal magnitudes of resultant. However, the stability ratios of the tendon transfers were higher than normal. Thus, the shoulder with tendon transfer may be less stable than the normal shoulder. The anterior stability ratios were even higher when the remaining rotator cuff muscles were weakened to 20%. As suggested by Gerber (1992), this indicates that the success of the surgery may depend on the strength of the subscapularis and teres minor muscles.

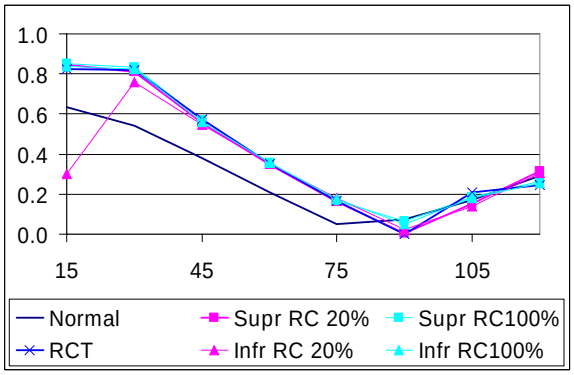

Figure 4: Superior stability ratios.

REFERENCES

Fukuda K et al. (1988). *Orthopedics*, **11,** 141-9.

Garner B.A, Pandy M.G. (2001). *Comput Methods Biomech Biomed Engin.* **4,** 93-126.

Gerber, C. (1992). *Clin Orthop Relat Res*, **275**, 152-160.

Magermans D.J. et al. (2004) *Clin Biomech.* **19**, 350-7.

Yanagawa et al. (in review). *J Biomech Eng.*

ACKNOWLEDGEMENTS

Funded in part by the NFL Charities, and the Steadman Hawkins Research Foundation.

Regulation of Reaction Forces During the Impact Phase of Landings

Joseph M. Munaretto [1], Jill L. McNitt-Gray [1,2,3], and Henryk Flashner [4]
[1]Department of Biomedical Engineering, [2]Kinesiology, [3]Biological Sciences
[4]Aerospace and Mechanical Engineering
University of Southern California, Los Angeles, CA, USA
E-mail: munarett@usc.edu

INTRODUCTION

Human motion is representative of the continuous interaction between the musculoskeletal system, the nervous system, and the environment. When humans perform movements involving large external reaction forces, task-specific control strategies are implemented to regulate the magnitude and direction of the force relative to body. Modeling observed system dynamics during landing movements requires that the control-logic accurately represents the control strategies implemented by the individual in preparation for foot-first interaction with the environment.

Previous simulations of drop landings have shown the sensitivity of peak vertical ground reaction forces (VGRF) to initial kinematics at contact (Munaretto et. al 2006), but did not incorporate a foot segment nor the effects of torque modifications to accommodate different landing conditions. In this study we hypothesized that modifications in lower extremity joint torques can help explain differences in reaction forces observed between landing tasks.

METHODS

Experimental drop landings were performed by a subject (n = 1) from a height of 0.7 m. The subject was instructed to land as soft as possible and as hard as possible. Three trials of each task were performed. Opto-electric cameras (110 Hz) and software was used to reconstruct 3-D coordinates of reflective markers placed on the subject to describe segment kinematics. Sagittal plane motion was determined from the 3-D coordinates. Ground reaction forces (600 Hz, Kistler) were also recorded.

A four segment dynamic model of the human body was created using a dynamic simulation software package (MSC ADAMS). Segments for the foot, shank, thigh, and torso were represented as rigid bodies connected by revolute joints. A foot-ground surface model was implemented to describe the vertical and horizontal ground reaction forces (Gruber et al. 1998).

Toe-first drop landings were simulated using experimental kinematics observed at contact. Segment angles, angular velocities, as well as horizontal and vertical velocities at contact were input as initial conditions for both soft and hard landing conditions. Vertical ground reaction forces (VGRF) were computed and kinematics of the system were compared between tasks.

The effect of joint torque control on peak vertical reaction forces was determined by performing soft and hard landing simulations using kinematics at contact as initial conditions and feedback laws based on joint displacement, angular velocity, and angular acceleration.

RESULTS AND DISCUSSION

Experimental VGRF-time curves demonstrated the ability of a recreational athlete to reduce the magnitude of the peak vertical reaction force by 50% by simply choosing to land as hard or as soft as possible (Figure 1). Differences in segment motion between hard and soft landings were observed prior to and during contact.

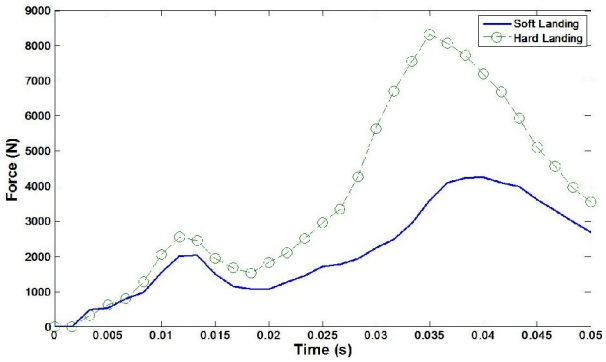

Figure 1: Experimental VGRF for 2 landing conditions

Simulated peak vertical forces using observed kinematics at contact were comparable to experimental results (Figure 2). Reduction of peak force in the soft landing compared to the hard landing was about 30%. Modifications in initial kinematics affected VGRFs, but did not explain the entire difference in VGRF between tasks (50% reduction). The simple addition of a damping ankle joint torque was found to further reduce simulated peak VGRFs (50%). These results emphasize the need to consider multiple mechanisms individuals may use to regulate reaction forces during the impact phase of landings.

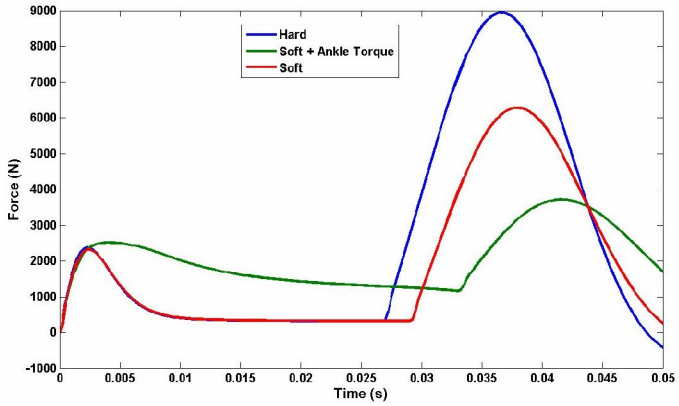

Figure 1: Simulated VGRF using only initial kinematics at ground contact

SUMMARY/CONCLUSIONS

Modifications in flight phase and impact phase joint level control helped explain task-dependent differences in experimental peak VGRF and joint torques. Future work will explore how task and subject specific control laws are modified to regulating reaction forces and segment motion during a range of landing tasks.

REFERENCES

Munaretto, J.M., McNitt-Gray, J.L., Flashner, H.(2006). *Proceedings of ASB'06*

Gruber, K. Ruder, H., Denoth, J., Schneider, K. (1998). *Journal of Biomechanics* 31, 439-444.

ANALYSIS OF MECHANISM OF UNDER CUT SER ICE IN SOFT TENNIS

Tsubasa Sugimoto[1], Keizo Yamamoto[2], Takako Hatakeyama[3], Shieko Hareyama[3]

[1]Graduate School of Hokusho University, [2]Hokusho University, [3]Hokusho College
Ebetsu, Hokkaido, JAPAN
E-mail: kyamamoto@hokusho-u.ac.jp, Web: http://www.hokusho-u.ac.jp/

UR OSE

The purpose of this study was to analyze the mechanism of under-cut (UC) service in soft-tennis. Soft-tennis is a tennis-like sport that uses a hollow rubber ball (66 mmϕ, 30 or 31g). A court size is same and a rule is about the same as general tennis. Rackets are lighter and its face is smaller than tennis. In comparison with tennis, there are fewer injuries. It is popular in Japan as a sport for all ages and they can enjoy even up to advanced ages.

The serves in soft-tennis are basically the same as in tennis, but there are special serves utilizing the different characteristics of the ball. The UC serves is one of the services peculiar to soft-tennis and the soft ball. This service has the advantages of a low bounce and an irregular movement after bouncing. Recently, This service has been used in the game frequently, but the mechanism has not yet been elucidated.

METHOD

The experiment was performed in a gymnasium with a wood floor. Seven female competitive soft-tennis players (age 19.1±0.8 yrs, height 159.5±3.8 m, weight 53.1±4.9 kg) performed three UC services each, so a total of 21 services were performed.

The swinging motion of the racket and the trace of the ball were recorded with two synchronized cameras at 60fps each, and analyzed three dimensionally with a motion analysis software (FrameDias II, DKH Co.,Ltd.). In addition, the movement of the ball just after impact was recorded by a high-speed video camera (250fps).

From the experiment mentioned above, we measured the following four items: the swinging velocity of the racket at an impact (v), the angle between the racket's face and its direction of movement at an impact (impact angle, θ, Fig.1), the rotating speed of sidespin of the ball just after impact (ω) and the bounce ratio (h). The bounce ratio was calculated by dividing the height of a bounce by the height of the drop from its azimuth after serve.

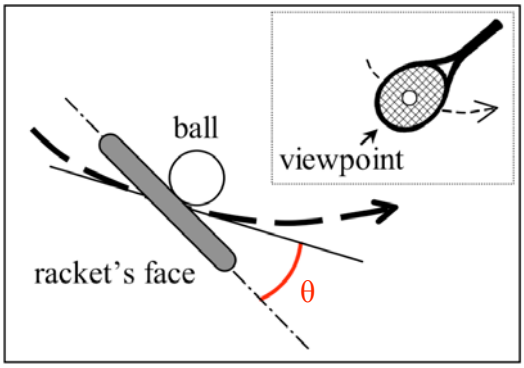

Figure 1: Illustration of impact angle (θ). The broken line and the thin solid line indicate the racket's direction of movement and tangential line of the direction at an impact respectively.

In this study, we treated the bounce ratio as an index of the performance of an UC service. Regression analyses were used to examine relations between each analysis items.

RESULTS AND DISCUSSION

The ratio of height of bounce (h) decreased as the rotating speed of the ball (ω) increased (r = -0.89, Fig.2). The rotating speed (ω) increased as the swinging velocity of the racket (v) increased (r = 0.59) and the impact angle (θ) decreased (r = -0.82). In the present study, a small impact angle (θ) means that the racket's face brushes around the side of the ball, and then a ball spins. In addition in a multiple regression analysis, the swinging velocity of the racket and the impact angle were independently associated with increased the rotating speed of the ball (r = 0.84).

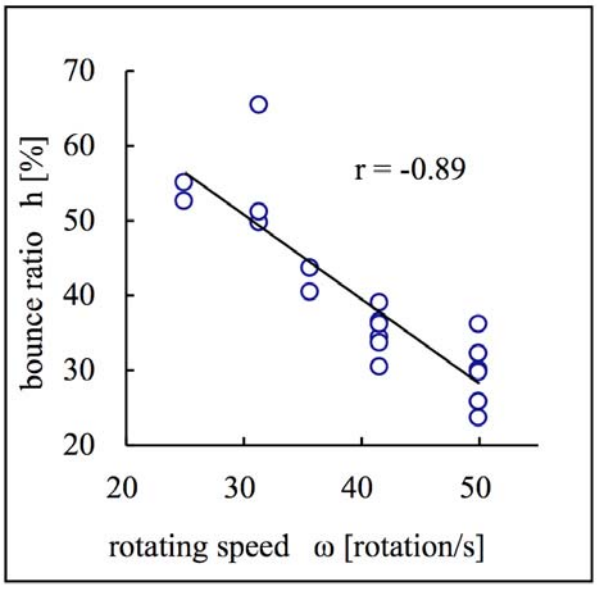

Figure : Relationship between the bounce ratio and rotating speed.

CONCLUSIONS

The results indicated that the performance of an UC service was dramatically affected by the rotating speed of the ball in sidespin. According to the results, to make the ball spin (i.e. to serve the UC service), players should make the impact angle small and make the swinging velocity big at the impact.

MUSCLE FORCES AT THE KNEE DURING WALKING AND RUNNING IN ATIENTS WITH ATELLOFEMORAL AIN

Thor Besier [1] Gary Beaupré [2] Garry Gold [1] Michael Fredericson [1] and Scott Delp [1]

[1] Stanford University, Stanford, CA, USA
[2] VA Rehabilitation Research and Development Center, Palo Alto CA, USA
E-mail: besier@stanford.edu, Web: http://nmbl.stanford.edu

INTRODUCTION

It is commonly believed that stresses placed on the patellofemoral (PF) joint are responsible for eliciting a pain response and the development of PF pain syndrome. Testing this hypothesis requires knowledge of the articulating geometry of the PF joint as well as the forces acting on the patella.

Quadriceps muscle forces play a crucial role in determining the medial-lateral force balance of the patella and the associated contact force and pressure distribution (Elias et al., 2006; Dhaher & Kahn, 2002). However, direct measurement of muscle forces in a subject population is not currently feasible, so it remains to be seen if the distribution of muscle forces in a group of patients with PF pain is different to those who are pain-free.

The purpose of this study was to use an electromyographic (EMG)-driven musculoskeletal model of the knee (Lloyd & Besier, 2003) to estimate muscle forces in a group of patients with PF pain and compare these with a group of pain-free controls. Of particular interest were the individual contributions from the quadriceps to the knee extension moment during walking and running.

METHODS

Twenty-seven individuals with PF pain (16 female; 11 male) and 16 pain-free controls (8 female; 8 male) participated in this study. Subjects performed various tasks in a motion capture laboratory, including walking and running, stair climbing, and static and dynamic squatting. Segmental kinematics and ground reaction force data were collected and inverse dynamics used to calculate the net flexion-extension (FE) moment at the knee joint. Surface EMG recordings were taken from the following muscles: vastus lateralis, vastus medialis, rectus femoris, biceps femoris, semimembranosus, medial and lateral gastrocnemius.

Joint kinematics and EMG were input to an EMG-driven model of the knee (Figure 1). Muscle tendon lengths and FE moment arms were calculated for each task using a scaled anatomical model (Delp et al., 1990). A modified Hill-type muscle model was used to estimate muscle forces.

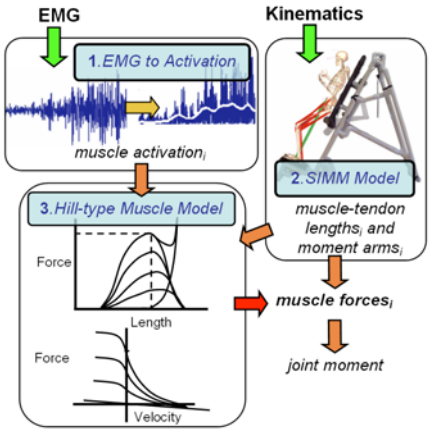

Figure 1 Schematic of the EMG-driven model.

Subject-specific models were calibrated by adjusting muscle and activation parameters to improve the model estimates of the net joint moment during a walk, run, and static

squat trial. Following calibration, muscle forces were normalized using each muscles maximum isometric force to enable comparison across groups. The contributions from each of the quadriceps muscles to the total extension moment produced were then calculated.

RESULTS AND DISCUSSION

Following calibration, the EMG-driven model estimated FE joint moments close to those estimated using inverse dynamics (walking: r^2=0.81±0.09 & running: r^2=0.89±0.07). Normalized muscle force profiles were similar between PF pain and control subjects, during both walking and running, with no difference in the magnitude of normalized forces across groups.

During walking and running, the quadriceps produced an extension moment at the knee greater than the net joint moment (Figure 2a). This was due to the moments produced by the hamstring and gastrocnemii muscles during stance. The magnitude of the peak difference between the quadriceps moment and the net joint moment was similar across PF pain and control groups, suggesting similar levels of co-contraction for a given joint moment.

The contribution from each quadriceps muscle were also similar across subjects for walking and running, although patients with PF pain displayed slightly greater standard deviations than controls. During early stance, or weight acceptance (WA) and at peak knee extension (PKE), vastus lateralis provided the largest contribution (~45±10%), followed by vastus intermedius (~29±3%), and vastus medialis (~26±7%). Rectus femoris contributed only ~5±2%. These relative contributions were consistent across the stance phase during walking and running (Figure 2).

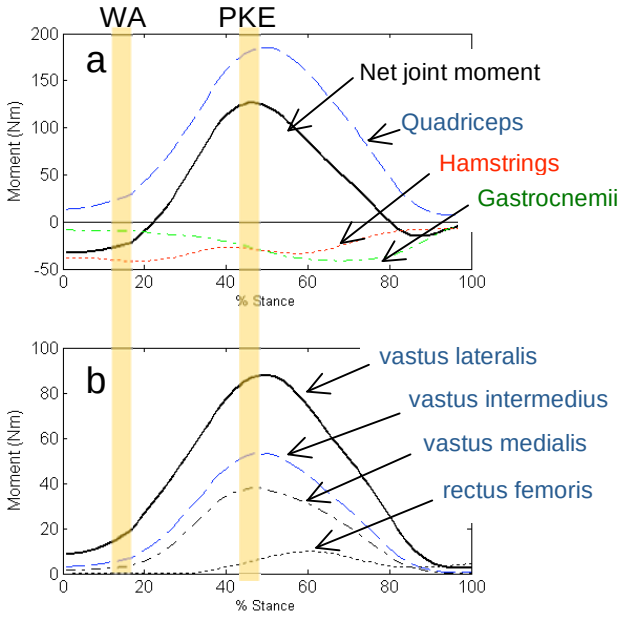

Figure Knee joint moments produced by muscles during a run. Note the extension moment produced by the quadriceps exceeds the net joint moment, due to co-contraction of the hamstrings and gastrocnemii (a).

SUMMARY CONCLUSIONS

Relative to the net knee joint moment, patients with PF pain appear to produce the same magnitude and distribution of forces as those who are pain-free during walking and running.

REFERENCES

Delp et al. (1990). EEE Trans Biomed Eng. ***37,*** 757-67.

Dhaher & Kahn (2002). *J. Biomech. Eng,* ***124,*** 758-767.

Elias et al. (2006). *J. Biomechanics,* ***39,*** 865-872.

Lloyd. D.G. & Besier, T.F. (2003). *J. Biomechanics,* ***36,*** 765-776.

ACKNOWLEDGEMENTS

Stanford Regenerative Medicine (1R-90DK071508), VA Rehab R&D (A2592R) and the NIH (EB005790-01).

Regulating Shoulder Net Joint Moments During Wheelchair Propulsion

Shashank Raina[1], Jill L. McNitt-Gray[1, 2, 3], Philip S. Requejo[2, 4]
[1]Depts. of Biomedical Engineering, [2]Kinesiology, [3]Biological Sciences, USC, Los Angeles, CA
[4]Pathokinesiology Laboratory, Rancho Los Amigos National Rehabilitation Center, Downey, CA
E-mail: sraina@usc.edu

INTRODUCTION

Wheelchairs play an important role in maintaining the independence of its users. Wheelchair propulsion requires that repetitive forces be applied to the rim of the wheels. Repetitive loading imposed on the upper extremity during wheelchair propulsion often leads to pain or injury of the shoulder (Mercer, 2006; Koontz, 2002).

The purpose of this study was to identify factors that contribute to the magnitude of the shoulder net joint moments during different phases of the propulsion and determine how these factors are modified during self-selected slow and fast propulsion conditions in user populations with thoracic or cervical level spinal cord injury.

METHODS

Ten wheelchair users volunteered to participate in this study (n=5 cervical level injury (C6 or C7); n=5 thoracic level spinal injury) in accordance with the Institutional Review Board at the Ranchos Los Amigos Medical Center, Downey, CA. The average age of the participants was 43(9) years, average mass was 75(11) kg and average height was1.71 (0.04) m.

Reflective markers were used to monitor the 3D motion of the hand, forearm, upper arm, and trunk segments. Three markers were also placed on the right wheel to track wheel rotation (Vicon® marker tracking system). The force applied to the wheelchair during propulsion was measured using force transducers mounted along the spokes of the wheel. A four-segment 3D upper extremity model was generated using segment kinematics (Visual3D). Net joint moments at the time of the first and second peak rim force were determined and compared within subject across speeds. The first peak force occurred immediately after contact with the wheel and the second peak occurred during the push phase (Fig. 1).

RESULTS

The magnitude of the shoulder net joint moments were dependent on the force applied to the rim, the relative angle between the proximal and distal net joint forces and the forearm and upper arm segments, and the magnitude of the elbow net joint moment. Users had comparable net joint moments at the elbow during slow and fast propulsion (Fig.2). During fast propulsion, user with paraplegia experienced lower shoulder net joint moment than user with cervical level injury (Fig. 2).

User with paraplegia applied a higher force to the rim yet had a smaller relative angle between the segments and the reaction forces than the user with cervical level injury (Fig.1).

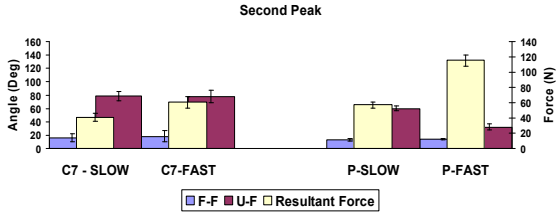

Figure 1: Relative angle between forearm and the reaction force (F-F), upper arm and reaction force (U-F) and the magnitude of the resultant force applied to the rim for exemplar users (C-Cervical, P-Paraplegia).

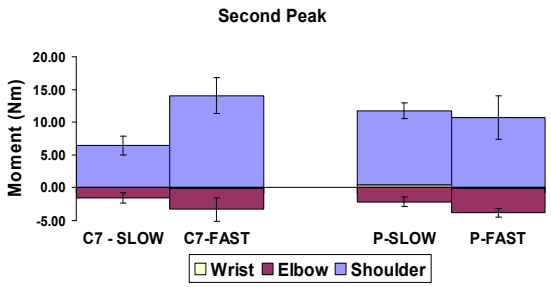

Figure 2: The wrist, elbow and shoulder NJMs during the push phase (flexor moment (+), extensor moment (-) for exemplar users (C, P) across speeds (slow, fast).

DISCUSSION

Net joint moments at the shoulder were regulated either by controlling the relative angle between the force and the segments or by regulating the force itself. Both the cervical and paraplegic user showed a change in the elbow moments direction from flexor to extensor when going from first peak (contact) to the second peak (push). An extensor moment at the elbow during the push phase assists flexor moment at the shoulder thereby contributing to a reduction in shoulder net joint moment magnitude.

Despite having larger reaction forces during fast propulsion, users with paraplegia had smaller shoulder NJMs than users with cervical level injury. These observed differences in shoulder NJM magnitudes for users with paraplegia were related to smaller relative angles between the reaction force and segment angles than those observed for users with cervical level injury. No significant changes in the relative angle between the reaction force and upper extremity segments were observed across speeds for users with cervical level injury.

These observed differences in shoulder moment magnitudes may be associated with the ability of users with paraplegia to control their trunk rotation. Control of trunk rotation allows the user to orient his trunk so that the upper arm can be more aligned (~ 30°) with the reaction force vector thereby leading to smaller NJMs at the shoulder.

SUMMARY

Increases in rim forces do not necessarily translate into larger NJMs at the shoulder. Users with cervical level injury used the same technique between slow and fast propulsion. In contrast, users with paraplegia applied greater force to the rim during fast propulsion yet tended to reorient their trunk thereby reducing the magnitude of the shoulder NJM. Future studies will investigate techniques used by wheelchair users with different control deficits to determine mechanisms specific populations use to distribute the mechanical demand imposed on the upper extremity.

REFERENCES

Mercer, J.L. et al. (2006). *Clinical Biomechanics*, **21,**781-789.

Koontz, A.M. et al. (2002). *J. Rehabilitation Research and Development*, **39(6)**, 635-650

ROBUST CONTACT SPRING PLACEMENT USING TRIMMED NURBS SURFACES FOR SIMULATION OF ARTICULAR CONTACT

Ryan L. Landon, Stephen J. Piazza

The Pennsylvania State University, University Park, PA, USA
E-mail: *steve-piazza@psu.edu*, Web: *www.biomechanics.psu.edu*

INTRODUCTION

Musculoskeletal modeling of the total knee replacements (TKR) has allowed analysis of knee implant designs under realistic loading conditions. Rigid-body spring modeling (RBSM) is a common method used for contact force calculations in simulations of TKR motion. This method requires an evenly-distributed placement of springs on the surface of the tibial implant, and this has been accomplished for cruciate-retaining (CR) implants by projecting rays vertically from an even grid onto the articulating surface (Bei and Fregly, 2004). A posterior-stabilized (PS) tibial implant, however, has a post with surfaces that are roughly parallel to the projected rays. This causes unevenly-spaced points that can lead to erratic contact behavior because large sections of the post will go unrepresented in the contact model.

Design software packages define solids as non-uniform rational b-splines (NURBS) surface patches trimmed and sewn together. NURBS map two-dimensional <*u*,*v*> and one-dimensional <*u*> objects to three-dimensional patches and curves that trim those patches. Solving the spring-placement problem by triangulating the surfaces results in unsatisfactory results because the springs are concentrated where the <*u*,*v*> isolines in parameter space are close together.

This paper presents a method for taking advantage of NURBS, while allowing points to be placed independently of Cartesian coordinates and achieve even spring placement. Sensitivity of model outputs to spatial spring density is reported.

METHODS

Five separate simulations were run, each with a different spring spacing. Surfaces were divided into sections no greater than 10 mm by dividing the surface equally first in the *u* then the *v* direction. A second pass was made to divide these smaller bins into regions no larger than 1, 2, 3, 4, and 5 mm for each of five runs, respectively. The surface area of each bin was approximated using triangles linking the bin's corners to its spring at the center. Then each spring was assigned stiffness proportional to the area it represented. Once the springs were placed, springs outside the trimming curve were eliminated.

Determining whether a point was within the valid surface region is problematic in three-dimensions. However, projecting the curve as a two-dimensional problem results in misinterpretation of complex geometries when the surface patch wraps back on itself (Figure 1).

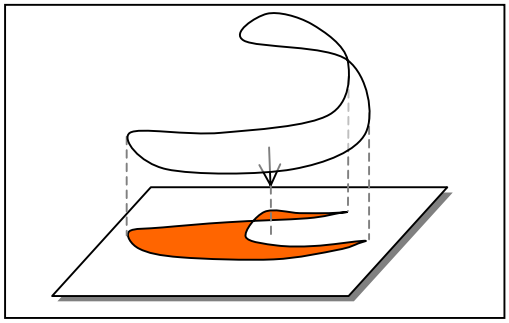

Figure 1: Trimming curve ambiguity when determining if points are within bounds.

Trimming curve ambiguity was overcome and boundary check efficiency achieved by projecting the curve onto the surface patch

normal to the surface and then converting it to a polygon in <*u*,*v*> coordinates.

Springs and surface patches most likely to come in contact were checked first using linked lists and bounding boxes based in the NURBS surface's coordinate frame. Then the spring's force was determined using the Kelvin-Voigt damped-spring model.

The lower-extremity model of Delp et al. (1990) was fitted with TKR models that employed this contact algorithm to perform a dynamic simulation of a supine range of motion test commonly performed by a surgeon during and after TKR. The model included ten muscles and three ligament groups. Knee kinematics were determined by the contact forces and by passive muscle and ligament forces as the ankle was moved toward the hip. Ankle positions were chosen such that the knee flexed from 20° to 150°.

RESULTS AND DISCUSSION

Springs were placed evenly over all surfaces of the PS implant, including the post (Figure 2). When the kinematics of the patella for spring spacings of 2, 3, 4, and 5 mm were compared to the 1 mm spacing results, the positional RMS error ranged between 1.0 and 1.2 mm. The rotational RMS error was between 0.6° and 0.7° for 2, 3, and 4 mm spacing, but 2.7° for 5 mm.

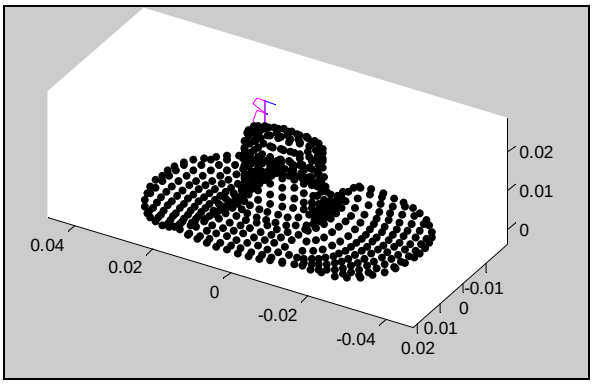

Figure 2: Even point placement with three millimeter spacing on a PS tibial implant.

Simulation run time dropped 62% from 1 mm to 2 mm spacing, 23% from 2 mm to 3 mm, and rose 2% from 3 mm to 4 mm (Figure 3). With 5 mm spacing, the simulation became unstable at 130 degrees flexion. Two additional simulations with spring spacing of 2.5 mm and 3.2 mm were run to confirm these trends.

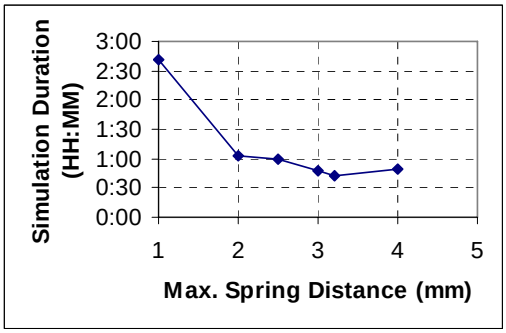

Figure 3: Run time decreased for 2, 3, and 4 mm spring spacings, but stability was compromised at higher spring spacings.

SUMMARY/CONCLUSIONS

In conclusion, springs were placed evenly on a PS knee implant. Simulation outputs for this type of spring placement were not sensitive to spring density for springs placed closer than 4 mm apart. This method for contact force determination is robust when confronted with complex geometric distortions, and should aid in future implementations of RBSM contact modeling.

REFERENCES

Bei, Y., Fregly, B.J. (2004). *Med. Eng. Phys.*, **26**, 777-789.

Delp, S.L., Loan, J.P., Hoy, M.G., Zajac, F.E., Topp, E.L., Rosen, J.M. (1990) IEEE Trans. Biomed. Eng., **37**, 757-67.

ACKNOWLEDGMENTS

This work was funded in part by Stryker Orthopaedics, Inc.

CRITERIA FOR WRAPPING SURFACE PARAMETERS FOR SPINAL MUSCLES

Anita N. Vasavada, Richard A. Lasher, Travis E. Meyer

Washington State University, Pullman, WA, USA
E-mail: vasavada@wsu.edu

INTRODUCTION

Curved muscle paths have been represented in musculoskeletal models of limbs by wrapping over geometric surfaces (Garner and Pandy, 2000; Arnold *et al*., 2000). However, the process for selecting and validating wrapping surface parameters is not well defined for musculoskeletal models of the spine, where muscles cross multiple vertebral joints, and muscle paths are not obviously constrained by a single anatomical structure.

The goal of this study was to develop a set of criteria to guide in the definition of wrapping surfaces for spinal muscles. Specifically, objective methods and an error metric were defined to select and evaluate the shape, size and location of geometric constraints that approximate the centroid paths of muscles obtained from MRI scans.

METHODS

Axial proton density-weighted MR images were obtained from the base of the skull to T2 in 6 mm intervals in one male subject with a 55^{th} percentile neck circumference (Gordon et al., 1989). The subject was scanned with the head in neutral, 30^o flexion, 30^o extension, 30^o axial rotation, 20^o lateral bending, 6 cm protraction and 5 cm retraction.

Eighteen neck muscle volumes were outlined, and their centroids calculated on each slice. The muscle centroid path was defined by a line connecting each centroid point, and the straight path by a line between the first and last centroid points. An error metric, defined as the average distance between the modeled path and the centroid path over all slices, was used to compare the modeled straight and wrapped paths to the centroid paths.

Wrapping surfaces were defined based on the following criteria:
1. The *need* for wrapping surfaces was based on the value of the error metric (straight vs. centroid path). If the error metric was less than 6 mm (5% of the average neck diameter), wrapping surfaces were considered unnecessary.
2. The *direction* in which the wrapping surface should constrain the muscle was determined by whether the centroid path was farther from the vertebral center than the straight line path (convex), or whether the centroid path was closer to the vertebral center (concave).
3. The *shape* of the wrapping surface was spherical for convex wrapping and cylindrical for concave wrapping.
4. The *size* of the wrapping surface and *position* relative to the vertebra was chosen such that the surface of the wrapping object was at the same distance horizontally from the vertebral center as the centroid path.
5. The *vertebral level* to place the wrapping surface was selected using the error metric (wrapped vs. centroid path). If error metrics were not significantly different among vertebral levels, we selected the level where the muscle was farthest from the bone for convex paths or closest to the bone for concave paths.

Wrapping surface parameters were defined for muscle paths using data from the neutral position and validated in the other postures.

RESULTS AND DISCUSSION

For most neck muscles, the error metric between centroid and straight paths was greater than 6 mm, indicating that wrapping surfaces would improve their representation. Two examples are presented: the sterno-mastoid (SM) segment of sternocleidomast-oid with a convex path, and the semispinalis capitis (SC) with a concave path.

For the SM, a spherical wrapping surface was centered at the vertebral body (Figure 1). We evaluated wrapping surfaces from C2-C6 because surfaces at C1 or C7 would include the muscle endpoints. The error metric decreased from 8.9 mm for a straight path to 6.3 mm for wrapping surfaces at C2 or C3. The vertebral level chosen for the wrapping surface did not make a significant difference in the error metric. Because the centroid path was farthest from the vertebral body at C2 for all postures, C2 is a good choice of wrapping surface level for SM.

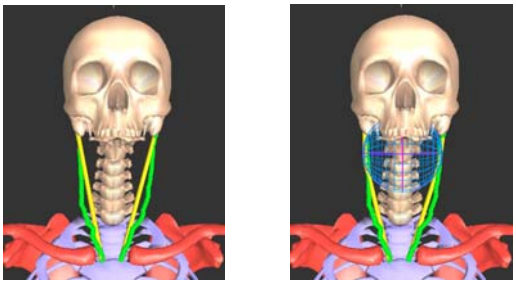

Figure1. A. SM centroid and straight paths. B. SM centroid and wrapped path with surface at C2.

For the SC, cylindrical wrapping surfaces were evaluated at C3-C6 (muscle endpoints would be within wrapping surfaces at C1, C2 or C7). The error metric decreased from 16.1 mm for a straight line to 6.3 mm for a wrapping surface at C3 or 6.4 for a wrapping surface at C4. Although there were no significant differences in error metrics among the vertebral levels, the wrapping surface at C4 had the lowest error metric when averaged over all postures. The centroid path was also closest to the C4 vertebral body in the neutral posture, making C4 a good choice for the placement of the SC wrapping surface (Figure 2).

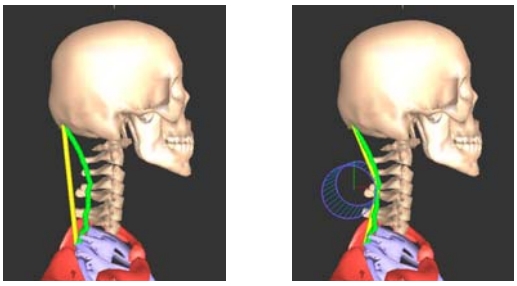

Figure 2. A. SC centroid and straight paths. B. SC centroid and wrapped paths with surface at C4.

SUMMARY/CONCLUSIONS

We have developed objective methods for the selection and validation of wrapping surfaces for spinal muscles. These methods may also be applied to other multi-joint systems. For the sterno-mastoid and semispinalis capitis, wrapping surfaces decreased the error metric to just over 6 mm, our threshold below which a straight path was considered not to need improvement by wrapping. The vertebral level chosen for wrapping surfaces did not significantly affect the accuracy of the modeled muscle path. For these muscles, selecting wrapping surfaces based on the minimum or maximum distance to the vertebra is a good criterion to choose the vertebral level for wrapping surfaces.

REFERENCES

Arnold, A.S. et al. (2000). *Computer Aided Surgery*, **5**, 108-119.

Garner, B. and Pandy, M.G. (2000). *Comp Methods Biomech Biomed Eng*, **3**, 1-30.

Gordon, C.C. et al. (1989). *1988 anthropometric survey of U.S. army personnel: methods and summary statistics*.

ACKNOWLEDGEMENTS

We thank Patrick Gavin, Jean Cloran, Rob Houston, and Christopher Robinson. Funded by the Whitaker Foundation.

REDUCED SHOE-SURFACE FRICTION CAN INCREASE THE RISK OF NON-CONTACT ACL INJURY DURING CUTTING MOVEMENTS

Ariel Dowling [1], Stefano Corazza [1], Lars Mündermann [1], Todd Alamin [1], Thomas Andriacchi [1,2] and Ajit Chaudhari [3]

[1] Stanford University, Stanford, CA, USA
[2] Veteran's Administration Palo Alto Health Care System, Palo Alto, CA, USA
[3] The Ohio State University Medical Center, Columbus, OH, USA
E-mail: adowling@stanford.edu Web: biomotion.stanford.edu

INTRODUCTION

Non-contact injuries to the anterior cruciate ligament frequently occur during cutting maneuvers and are most likely to occur when the planted limb is not in a neutral alignment but instead is in valgus alignment [Chaudhari, 2006]. It has been suggested that in healthy subjects, increased valgus loading (abduction moment) of the knee during cutting is an indicator of increased risk for an ACL injury [Hewett, 2005] and when ACL-D subjects complete an anticipated side step cutting maneuver, they exhibit both lower knee flexion angles and knee moments [Houck, 2007]. Changing the coefficient of friction of the shoe-surface interface has been suggested as a risk factor for ACL injury, since anticipation of the surface friction can influence the loading and posture of the body at foot contact, a critical time for non-contact ACL injury [Heiden, 2006].

This study examined the hypotheses that the position of the center of mass and the kinetic (abduction moment) and kinematic (knee flexion angle) risk factors for ACL injury in sideways cutting are altered by the changing the coefficient of friction of the shoe-surface interface, using a markerless motion capture system (MMC).

METHODS

Five healthy subjects (three male, two female) with no prior knee, hip, or ankle injuries were evaluated. Subjects performed a 60° cut on three different surfaces in random order at a constant speed: a rubber pad (high friction), a vinyl tile floor surface (moderate friction), and surgical booties placed over the subject's shoes with the vinyl floor surface (reduced friction). The coefficient of friction (μ) was determined for each subject based on the shoes worn; on average, the high friction μ was 0.83, moderate friction was 0.67, and reduced friction was 0.45. The speed was self-selected for safety in the reduced-friction condition.

A previously-described MMC system [Corazza, 2006; Mündermann, 2006] was used to measure full-body kinematics and the subject's center of mass (COM) from the center of the volume of MMC data. A full body laserscan was taken of each subject to create a subject-specific model fitted to the image sequences. A force plate was used to measure ground reaction forces. An inverse dynamics approach was used to estimate joint reaction forces and moments. Data was analyzed using two-tailed paired t tests ($\alpha = 0.05$) to determine if the low friction trials were significantly different than the moderate and high friction trials.

RESULTS AND DISCUSSION

There was a greater abduction moment during low friction trials relative to the moderate and high friction conditions. The peak abduction moment during stance,

center of mass (COM) at heelstrike, and knee flexion angle at heelstrike (Figure 1) were significantly different. The combined influence of the reduced μ indicates that the subject has valgus loading at the knee and therefore is at a greater risk for an ACL injury during cutting [Hewett, 2005] when friction is reduced. The kinetics during the low friction trials resemble the abnormal loading displayed by ACL-D subjects.

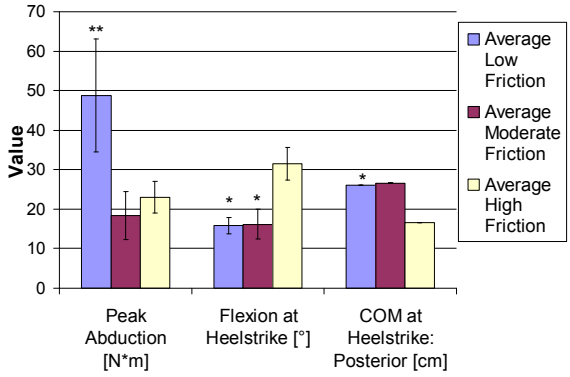

Figure 1: Averaged values for key variables by trial type for all subjects. ** denotes significant difference compared with Moderate and High friction ($p < 0.05$) * significant difference compared with High friction ($p < 0.05$)

In addition, the position of the COM and the amount of flexion of the knee during heelstrike in the low friction condition suggest that the subject is more at risk for an ACL tear (Figure 2). These results also suggest that subjects orient limb position in anticipation of the perceived surface friction.

During the high friction trials, the COM is more aligned over the ankle in a neutral alignment in the coronal plane; additionally the knee flexion angle is statistically larger. During the low friction trials the COM is more posterior with respect to the ankle joint and the knee flexion angle is smaller.

The more neutral alignment during heelstrike of the high friction trials is indicative of normal kinetics. Conversely, the valgus loading, anterior COM, and decreased knee flexion angle at heelstrike exhibited during the low friction trials suggest abnormal kinetics and an increased risk for ACL injury. These results suggest that future improvements in shoe and/or surface design that improve traction may help reduce ACL injury rates.

SUMMARY/CONCLUSIONS

Differences in the peak abduction moment, position of the COM at heelstrike, and the knee flexion angle at heelstrike suggest that there is a greater risk for an ACL injury during sideways cutting on low friction surfaces.

REFERENCES

Chaudhari et al. (2006) *J. Biomech.* **39**(2), 330-8.

Corazza et al. (2006) *Annals Biomed. Eng.* **34**(6), 1019-1029.

Heiden et al. (2006) *Gait Pos.* **24**(2), 237-46.

Hewett et al. (2005) *Am. J. Sports. Med.* **33**(4), 492-501.

Houck. et al. (2007) *J.Orthop.Sports.Phys.Ther.* **37**(2), 56-64.

Mündermann et al. (2006) *J.Neuroeng.Rehab.* **3**(6).

ACKNOWLEDGEMENTS

Funding provided by NSF #03225715. Thanks to Erica Holland, Melissa Makar, and Vijay Agarwal for their assistance.

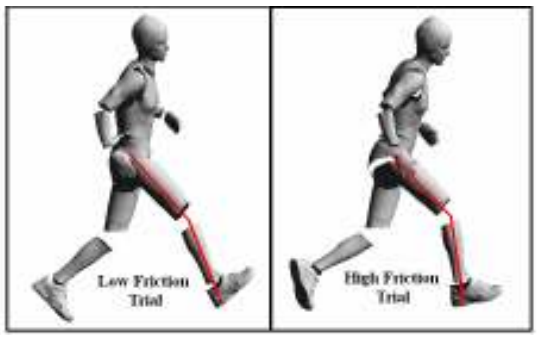

Figure 2: Knee Flexion angle at heelstrike

A NEW METHOD FOR QUANTIFYING FOOT BONE-TO-BONE POSITIONS

William R. Ledoux,[1,2,3] Michael J. Fassbind,[1] Eric S. Rohr,[1] Yangqiu "Patrick" Hu,[4]
David R. Haynor,[4] Bruce J. Sangeorzan[1,3]

[1]RR&D Center of Excellence, VA Puget Sound, Seattle, WA, USA
Departments of [2]Mechanical Engineering, [3]Orthopaedics & Sports Medicine and [4]Radiology,
University of Washington, Seattle, WA, USA
E-mail: wrledoux@u.washington.edu, Web: www.seattlerehabresearch.org

INTRODUCTION

There are many means of quantifying foot shape, including arch indices, X-rays, static hindfoot alignment devices and computed tomography (CT) scans. However, each of these has some inherent difficulties. For a more detailed review, please see Ledoux (2006). Briefly, arch indices typically have a subjective component and do not provide information on specific bones. X-rays are two-dimensional (2D) and have a subjective component (someone must draw the lines). Hindfoot alignment devices only describe part of the foot and require an operator to position them. CT scans are three-dimensional (3-D), but also typically require a user to draw lines. Our own group has developed an objective, 3-D method of quantifying foot bone-to-bone position from CT scans (Ledoux, 2006). However, this method, which consisted of embedding coordinate systems in each bone by assuming uniform density and calculating the inertial matrix, was not without problems. Namely, the orientation of the embedded coordinate system was due to the nothing but the shape of the particular bone. This worked well (i.e., well aligned neutral coordinate systems) for some bones (e.g., the talus), but other bones (e.g., the calcaneus) had coordinate systems that were askew. Consequently, although meaningful data were collected for some bone-to-bone relationships (first metatarsal to talus), it was not sensitive enough to measure differences in hindfoot eversion/inversion (i.e., calcaneus relative to talus) between different foot types. Therefore, the purpose of this study was to develop a means of objectively quantifying foot bone-to-bone position in 3D with a method sensitive enough to measure hindfoot trends across pes cavus (high arched), neutrally aligned (normal arch) and pes planus (flat arched).

METHODS

We performed partial weightbearing (20% body weight) CT scans on subjects between the ages of 18 and 75 with pes cavus (n = 10 subjects, 14 feet), neutrally aligned (n = 10, 20), asymptomatic pes planus (n = 10, 18) and symptomatic pes planus (n = 10, 13) (Ledoux, 2006). Pes planus were split into two groups based on the presence of pain; both feet were included on subjects that had the same foot type bilaterally. The CT data were segmented using *Multi-Rigid*, a custom software package for modeling the morphology and tracking the movement of multiple articulated bones/joints simultaneously via medical imaging (Hu, 2006). *Multi-Rigid* was also used to automatically and objectively determining the embedded coordinate systems for the foot bones. By consensus, three 'experts' constructed a coordinate system for each bone in a template set (i.e., the gold standard) by identifying several prominent feature points on the bone surface, which were used to embed a coordinate system. These points (and the corresponding coordinate systems) were then mapped onto

subject datasets through non-rigid image registration (i.e., 'warped' via affine transformation and B-spline deformation). Each bone in each foot had an objective, 3-D, well aligned coordinate system. The only subjective component was the gold standard. Preliminary work found that the mean distances between the computed points and those picked by the experts were close to the mean distances between the points picked by different experts, suggesting that our method was comparable to the experts (<4 mm). The Cardan angles (alpha, beta and gamma, in the sagittal, frontal and transverse planes respectively) between the bones of interest were calculated. Here we report one relationship that was significant with our previous methods (first metatarsal to talus) and one that was not (calcaneus to talus).

RESULTS

All data have been collected, but only 7 pes cavus, 12 neutrally aligned, 8 asymptomatic pes planus and 5 symptomatic pes planus have been analyzed. There were significant differences ($p<0.05$) across foot types for all six angles that are reported (Table 1). (Numerous other relationships were also different, but are not reported here.) The relationship of the hindfoot, from inverted pes cavus to everted symptomatic pes planus can been seen qualitatively (Figure 1).

DISCUSSION

We have successfully developed a new method of objectively embedding foot bone coordinate systems that was sensitive to position of the hindfoot (i.e., subtalar joint).

REFERENCES

Ledoux, W. R., et al., (2006). *J Orthopaedic Research*, **24**, 2176 - 2186.

Hu, Y., et al., (2006). *SPIE,* **6141**, 133 - 142.

ACKNOWLEDGEMENTS

Dept. of Veterans Affairs grant A3030R.

Table 1: The M1Ta and CaTa angles in degrees (mean ± SD) for the four foot types.

Foot type	M1Ta Alpha (sagittal)	M1Ta Beta (frontal)	M1Ta Gamma (transverse)	CaTa Alpha (sagittal)	CaTa Beta (frontal)	CaTa Gamma (transverse)
Pes cavus	59.0 ± 9.2	-4.4 ± 9.3	-36.5 ± 10.3	16.2 ± 5.6	12.0 ± 5.7	2.3 ± 3.6 [a,b]
Neutrally aligned	24.3 ± 6.3	-20.5 ± 11.4 [a]	-25.4 ± 3.8	7.6 ± 4.0 [a,b]	-4.8 ± 3.5 [a]	4.2 ± 2.6 [a,c]
Asymptomatic pes planus	11.1 ± 6.1 [a]	-28.2 ± 6.3 [a,b]	-9.6 ± 4.8	6.6 ± 3.6 [a,c]	-8.4 ± 7.3 [a]	4.7 ± 3.1 [b,c]
Symptomatic pes planus	-0.1 ± 11.2 [a]	-34.6 ± 5.6 [b]	0.6 ± 7.3	1.7 ± 6.4 [b,c]	-16.2 ± 6.7	10.1 ± 4.8

M1Ta = first metatarsal relative to talus, CaTa = calcaneus relative to talus, Alpha + = plantar flexion, - = dorsi-flexion; Beta + = inversion, - = eversion; Gamma + = external rotation, - = internal rotation, [a,b,c] = no significance

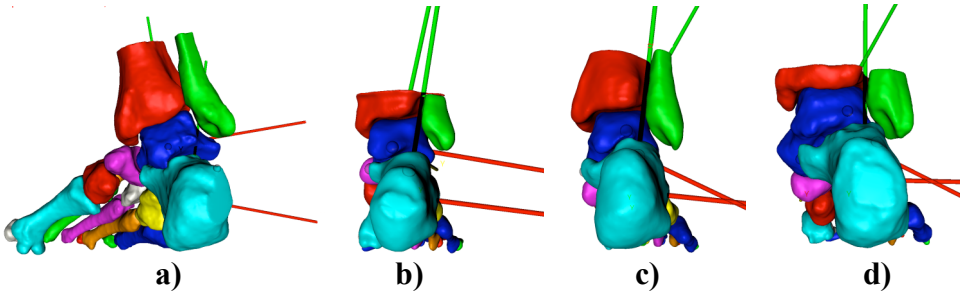

a) **b)** **c)** **d)**

Figure 1: Representative frontal plane hindfoot positions for the following foot types: a) pes cavus, b) neutrally aligned, c) asymptomatic pes planus and d) symptomatic pes planus.

FACTORS AFFECTING LUMBAR KINETICS DURING DEPENDENT TRANSFERS ON AN AIRCRAFT

Brian Higginson, Lisa Welsh, and Michael Pavol

Oregon State University, Corvallis, OR, USA
E-mail: mike.pavol@oregonstate.edu

INTRODUCTION

Air travel by people with disabilities poses many challenges to both airport personnel and travelers. Of greatest concern is the potential for injury during the process of transferring a traveler with disabilities between a wheelchair and an aircraft seat. Dependent transfers on board an aircraft are typically performed using a "front-and-rear" technique (Pelosi & Gleeson, 1988), in which the rear transferor bears an estimated 65-75% of the traveler's weight. This places the rear transferor at high risk of a disabling low back injury. To better understand these risks, this study determined the effects of aircraft spatial constraints, transferee weight, and direction of transfer on the lumbar forces and moments in the rear transferor during dependent transfers on an aircraft.

METHODS

Thirty-three pairs of men (n = 42) and women (n = 24) worked to transfer two anthropometric dummies between a wheelchair and an airplane seat using the "front-and-rear" technique. The mean ± SD age, height, and mass of the rear transferors were 23.6 ± 4.2 yr, 178.0 ± 7.7cm, and 78.0 ± 13.7 kg. Informed consent was provided.

The transfers were performed in a laboratory simulation of an aircraft interior. A standard economy-class airplane seat was mounted to the floor with the armrests raised. An aircraft aisle wheelchair was placed side-by-side with the seat. A small (mass: 57 kg; height: 165 cm) and a large (mass: 78 kg; height: 178 cm) anthropometric dummy served as the transferee. Removable frames were used to simulate the spatial constraints imposed by the surrounding rows and aisles of seats and the overhead bins.

After instruction, warm-up, and practice, subjects transferred each dummy once for each transfer direction (wheelchair-to-seat, seat-to-wheelchair) under constrained and unconstrained conditions. Transfer positions were self-selected and remained unchanged. The movements of the rear transferor were recorded using a motion capture system. Reaction forces on the feet and thigh were collected using two force plates mounted behind the aircraft seat, flush with the floor, and a custom-built force plate mounted to the aircraft seatback.

Resultant lumbar joint forces and moments were calculated at the level of L_3/L_4 using a bottom-up, three-dimensional inverse dynamics approach. These resultant joint forces and moment were then normalized by body weight (BW) and body weight and height (BWxHT), respectively.

Dependent measures consisted of peak lumbar compressive forces (i.e. lumbar loading) and peak lumbar moments about the three principal axes of motion. Three-way repeated measures ANOVA were used to test the effects of dummy size, constraint, and transfer direction on the dependent variables. Pearson correlations to body weight were also computed. Effects were considered significant at $\alpha < .05$.

RESULTS AND DISCUSSION

Transferee size had the most notable influence on lumbar kinetics during the dependent transfers (Table 1). Transfers of the large transferee resulted in greater lumbar loading, as well as increased extension, bending, and twisting moments ($p<0.001$). On average, the lumbar loading was 14% BW greater while transferring the large dummy compared to the small dummy.

The constraints imposed by the interior of the aircraft had relatively little effect on lumbar kinetics, resulting in only a slight decrease (0.5% BWxHT) in bending moment during the transfers (Table 1). This decrease in bending moment of the rear transferor may be related to the inability of the front transferor to shift laterally during the transfer under constrained conditions.

The direction of transfer appeared to have no influence on lumbar moments, whereas increased lumbar loading occurred during outboard transfers (~ 4% BW). It may be that, during inboard transfers, the high seatback provides support during initiation of the transfer, decreasing lumbar loading.

Lumbar loading was inversely related to the body weight of the individual performing the transfer (Figure 1; $R^2=0.53$, $p=0.001$). Lighter transferors experienced larger loading, possibly due to the fact that the weight of the transferee represents a greater proportion of the transferor's body weight.

SUMMARY/CONCLUSIONS

These results indicate that transfers of larger individuals put the rear transferor at greater risk of low back injury during a dependent transfer on an aircraft, whereas surrounding spatial constraints and the direction of transfer have little effect. The potential for injury also appears to be greater during transfers performed by smaller transferors.

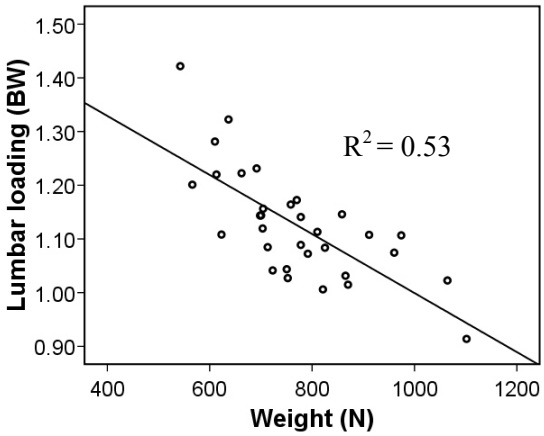

Figure 1: Relationship between lumbar loading and transferor weight.

REFERENCES

Pelosi, T., Gleeson, M. (1988). *Illustrated transfer techniques for disabled people.* Melbourne: Churchill Livingstone.

ACKNOWLEDGEMENTS

Funded by grant H133E030009 from the U.S. Dept. of Education, NIDRR.

Table 1: Influence of transferee size, constraint, and direction of transfer on lumbar loading (F_c), and extension (M_{ext}), bending (M_{bend}), and twisting (M_{twist}) moments (mean ± SD). Lumbar loading and moments are expressed as %BW and %BWxHT, respectively. *p<0.001; †p<0.01

	Size		Constraint		Direction	
	Small	Large	Constrained	Unconstrained	Inboard	Outboard
F_c	109.2 ± 14.7 *	123.2 ± 20.9	116.5 ± 18.7	115.8 ± 17.0	114.2 ± 18.7 *	118.1 ± 17.0
M_{ext}	18.0 ± 2.8 *	21.2 ± 5.1	19.7 ± 4.0	19.4 ± 4.0	19.5 ± 4.0	19.5 ± 4.0
M_{bend}	3.8 ± 1.1 *	5.1 ± 1.1	4.2 ± 1.1 †	4.7 ±1.1	4.5 ± 1.1	4.3 ± 1.1
M_{twist}	2.9 ± 1.1 *	3.8 ± 1.1	3.4 ± 1.1	3.3 ± 1.1	3.4 ± 1.1	3.3 ± 1.1

CRUCIATE LIGAMENT FORCE DURING THE WALL SQUAT AND ONE-LEG SQUAT

Rafael F. Escamilla[1], Naiquan Zheng[2], Alan Hreljac[3], Rodney Imamura[3], Toran D. MacLeod[1], William B. Edwards[4], Glenn S. Fleisig[5], Kevin E. Wilk[6]

[1]Department of Physical Therapy, California State University, Sacramento, USA
[2]Orthopaedics and Rehabilitation Program, University of Florida, Gainesville, FL, USA
[3]Kinesiology and Health Science Department, California State University, Sacramento, USA
[4]Department of Health and Human Performance, Iowa State University, Ames, Iowa, USA
[5]American Sports Medicine Institute, Birmingham, AL, USA
[6]Champion Sports Medicine, Birmingham, AL, USA
e-mail: rescamil@csus.edu

INTRODUCTION

One leg squat and wall squat exercises are used in both athletic training and during knee rehabilitation programs. However, it is currently unknown how cruciate ligament tensile force change among one leg and wall squat exercises as a function of knee angle. The purpose of this study was to compare PCL/ACL tensile forces as a function of squat exercises and knee angle (0-90° during knee flexing phase and 90-0° during knee extending phase, where 0° = full knee extension). It was hypothesized that PCL tensile forces would increase as knee flexion increased and would be greater in the wall squat long (feet further from wall and knee not translating beyond the toes at maximum knee flexion) compared to the wall squat short (feet closer to wall) and the one leg squat, both exercises in which the knee translates beyond the toes at maximum knee flexion.

METHODS

Eighteen subjects (9 males and 9 females) were used with an average age, mass, and height of 29±7 y, 77±9 kg, & 177±6 cm for males and 25±2 y, 60±4 kg, & 164±6 cm for females. Each subject performed the wall squat long (knees over ankles at maximum knee flexion) and the wall squat short (knees translate beyond toes at maximum knee flexion). A one leg squat was also performed, in which the knees also translate beyond toes at maximum knee flexion. Intensity was normalized for each exercise by having each subject their 12 repetition maximum intensity, which were 55±9 kg for males and 36±9 kg for females for the wall squat and 15±3 kg for males and 10±3 kg for females for the one leg squat. Surface electrodes were placed over the vasti muscles, rectus femoris, medial and lateral hamstrings, and gastrocnemius. Reflective markers were positioned over landmarks on the foot, ankle, knee, hip, and shoulder.

Video (60 Hz), EMG & force platform (960 Hz) data were collected during 3 repetitions of each exercise (0-90° knee flexion) and averaged. EMG data were normalized by maximum voluntary isometric contractions (MVIC).

Cruciate ligament tensile forces were calculated using a biomechanical knee model (Zheng et al., 1998) with input variables consisting of resultant knee forces and moments and the muscle force function $F_{m(i)} = {}_ik_iA_i\sigma_{m(i)}[EMG_i/MVIC_i]$, where k_i was a muscle force-length variable, A_i was physiological cross sectional area (PCSA) per muscle, $\sigma_{m(i)}$ was MVIC force per unit PCSA, EMG_i and $MVIC_i$ were EMG window averages, and c_i was a weight factor adjusted in a computer optimization program. Cruciate ligament tensile force as a function of exercise (wall squat long, wall squat short, one leg squat) and knee angle (every 10° from 0-90° and 90-0°) were assessed by a two-way repeated measures analysis of variance ($p < 0.01$).

RESULTS AND DISCUSSION

Cruciate ligament tensile forces for the wall squat long, wall squat short, and one leg squat are shown in Figure 1. Between 0-60° during the

knee flexing phase, PCL tensile force was significantly greater in the wall squat long compared to the wall squat short and one leg squat, and significantly greater in the wall squat short compared to the one leg squat. Low ACL tensile forces (<50 N) were generated in the one leg squat between 0-40° during the knee flexing phase. Between 70-90° during the knee flexing phase, PCL tensile force was significantly greater in the wall squat long compared to the wall squat short and one leg squat. Between 90-50° and 10-0° during the knee extending phase, PCL tensile force was significantly greater in the wall squat long compared to the one leg squat. Between 90-70° during the knee extending phase, PCL tensile force was significantly greater in the wall squat short compared to the one leg squat. At 70° and between 40-0° during the knee extending phase, PCL tensile force was significantly greater in the wall squat long compared to the wall squat short.

It is interesting that PCL tensile force was lower and ACL tensile force was higher in the one leg squat and wall squat short compared to the wall squat long. In the wall squat short and one leg squat the knees translated beyond the toes at maximum knee flexion. Increased anterior translation of the knees appears to decrease PC tensile force and increase ACL tensile force.

SUMMARY/CONCLUSIONS

PCL tensile force was greater during the wall squat long compared to the wall squat short and one leg squat throughout most of the knee flexing and knee extending phases. In addition, PCL tensile force was greatest at maximum knee flexion for all exercises. Low ACL tensile force was generated during the one leg squat between 0-40° knee flexion.

REFERENCES

Zheng et al. (1998), *Journal of Biomechanics*, **31**, 963-967.

ACKNOWLEDGEMENTS

The authors would like to thank Lisa Bonacci, Toni Burnham, Juliann Busch, Kristen D'Anna, Pete Eliopoulos, & Ryan Mowbray for all their assistance during data collection and analyses.

Figure 1. Mean (SD) PCL tensile force during the one leg squat and the wall squat.

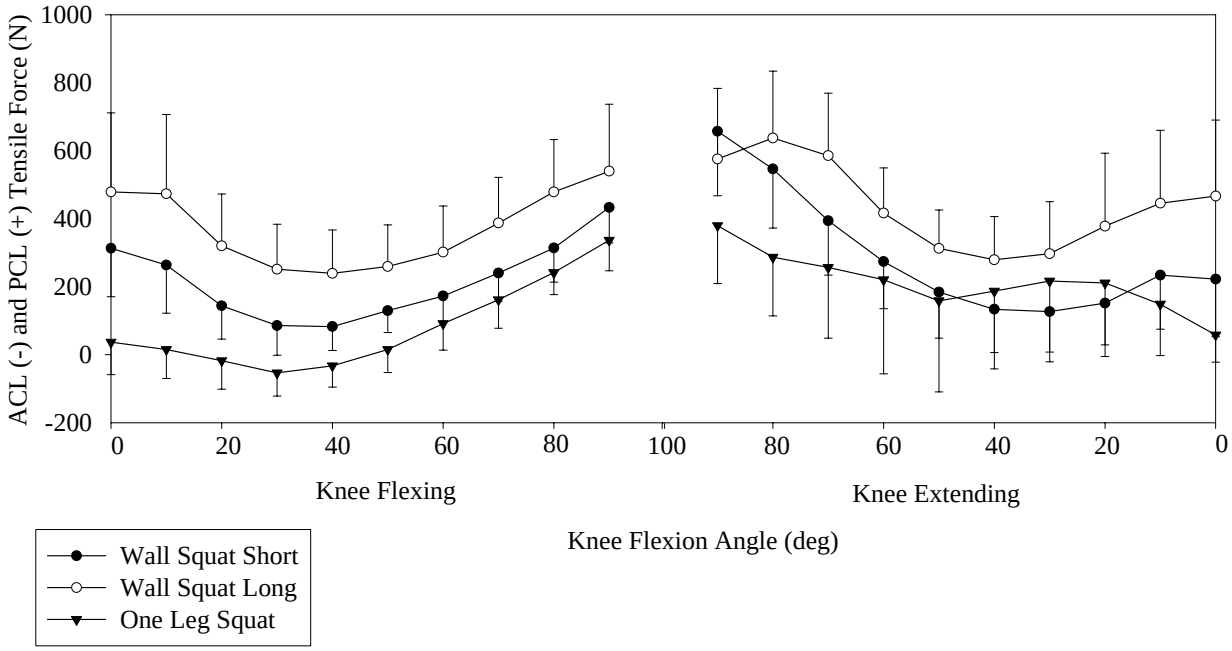

Musculo-Skeletal Modeling Software (MSMS) for Biomechanics and Virtual Rehabilitation

Mehdi Khachani, Rahman Davoodi, and Gerald E. Loeb

Alfred Mann Institute and Department of Biomedical Engineering
University of Southern California, Los Angeles, CA, USA
E-mail: khachani@usc.edu, Web: http://ami.usc.edu

INTRODUCTION

We have developed a new software for modeling human and prosthetic limbs and simulating them to analyze prosthetic, FES, and natural movement control systems. It provides tools to assemble and customize multi-body systems, actuators and sensors, and controllers and to simulate their dynamics. We have also developed a virtual reality environment (VRE) where these models can be simulated with the subject in the loop to evaluate the feasibility of prosthetic control systems and train the patients to operate them.

METHODS

MSMS mainly consists of graphic user interface (GUI), modeling, simulation, and database units [1]. MSMS is implemented using the Java programming language. Dynamic simulations are implemented in Simulink and C programming languages. Standard libraries such as Open-GL are used whenever possible. The basic components and tools have been built, tested and are in use but we anticipate incremental enhancements to both, so we have established an iterative rather than top-down development process.

RESULTS

At the current stage of development, MSMS provides a GUI for building and editing models. The user can edit component properties while visualizing the 3D model from different points of view. The animation feature in MSMS allows animating the model using either live simulation data sent via UDP or using motion files. In addition to animating the joints, the user can change the attributes of objects in the model such as their size and color in run-time. A new feature supports various technologies for 3D displays such as goggles and shutter glasses.

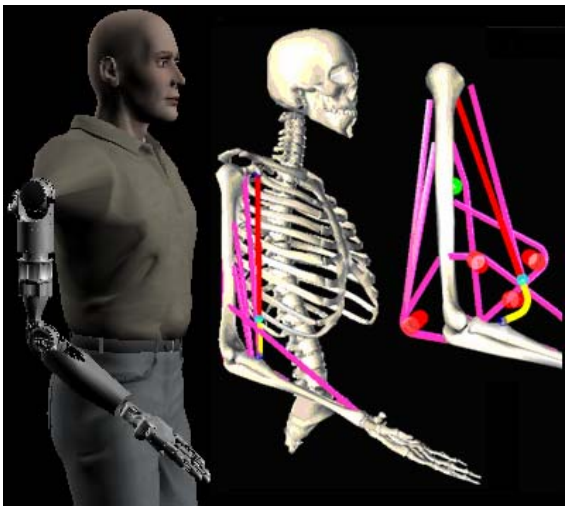

Figure 1: Prosthetic and musculoskeletal limb models in MSMS.

Building an accurate musculoskeletal plant relies on the fidelity of its elementary components. The complex mechanical properties of muscles and tendons are implemented using the ‘Virtual Muscle’ mathematical model [2]. Wrapping algorithms are used to calculate the path of the muscle from its origin to its insertion constrained by bony surfaces (spherical and cylindrical). The components of mechatronic prosthetic limbs are also

available. In addition to modeling biological and prosthetic limbs, MSMS includes models of the environment that consist of objects, external forces and torques, lights and cameras that are essential for simulations of complete rehabilitation tasks.

Models built in MSMS use the eXtensible Markup Language (XML) as a standard format to define musculoskeletal and prosthetic limb models. The database structure is flexible enough to allow for the possibility of establishing a modeling standard. To take advantage of existing models, MSMS can import models developed in popular modeling software including SIMM (Musculographics Inc., USA), and SolidWorks (SolidWorks Corp., USA).

An MSMS model can automatically be exported to dynamics engines such as SimMechanics, which is currently used by MSMS. The C-code representing its mechanical properties is wrapped in a Simulink block where it can be interfaced with controllers built from Simulink and Matlab toolkits. For real-time simulations, models of complete systems are compiled in C and downloaded to a target PC. Real time execution allows for patient-in-the-loop simulations. The subject generates voluntary commands (e.g. EMG or cortical signals) to control the simulated limb while using a stereoscopic display of the virtual arm from his point of view as visual feedback [3]. The patient's central nervous system learns to correct movement based on vision, as it would with the real prosthetic system. This VRE is an efficient and safe platform for testing designs for prosthetic systems. It can also be used to train patients with disabilities. We have developed models of real rehabilitation tasks in the VRE such as grasping and moving objects.

APPLICATIONS

MSMS is currently been used in several laboratories to study prototypes of neural prosthetic systems. In our laboratory, we are using MSMS and VRE to develop FES controllers for quadriplegic patients. These controllers use the residual voluntary movements of the upper arm to drive the synergistic movement of the paralyzed lower arm. Different control strategies are tested in VRE to determine their feasibility before clinical deployment.

Recent work at Caltech consists of testing cortical control of prosthetic limbs by nonhuman primates. Cortical signals are used to control in real time a virtual prosthetic arm that is modeled and visualized in MSMS. At the Rehabilitation Institute of Chicago, EMG signals from re-innervated chest muscles are used to provide motor commands to control the virtual prosthetic limb.

SUMMARY/CONCLUSIONS

MSMS and VRE provide a comprehensive framework for virtual prototyping of neural prosthetic systems for paralyzed and amputee patients. Tools to simulate contact and mechanical interaction with objects are still under development. These are computationally demanding tasks and in some complex applications we may have to trade off accuracy for execution speed while waiting for faster processors.

REFERENCES

[1] Davoodi, R. et al. (2007). *IEEE Trans. Biomedical Eng.*, in press.
[2] Cheng, E et al. (2000). *J. Neuroscience Methods*, **101**, 117-130.
[3]Hauschild, M. et al. (2007). *IEEE Trans. Neural Systems and Rehabilitation Engineering*, **15**,9-5.

WALKING IN SIMULATED HYPER-GRAVITY

Stephen M Cain[1] and Daniel P Ferris[1]

[1]Human Neuromechanics Laboratory, The University of Michigan, Ann Arbor, MI, USA
E-mail: smcain@umich.edu

INTRODUCTION

The relationship between human walking mechanics and metabolic cost is remarkably elusive. Grabowski et al. (2005) used added mass and simulated reduced gravity to examine how bodyweight and body mass independently affect the metabolic cost of walking. They found that adding mass without bodyweight (via reduced gravity) resulted in about 45% of the increased metabolic cost found with just added mass. They concluded that normal load carriage increases metabolic cost due to both increasing forces to support bodyweight and increasing forces to redirect the center of mass at step-to-step transitions.

We studied humans walking in simulated increased gravity to determine if metabolic cost of walking in hyper-gravity would result in smaller increases in metabolic cost than load carriage. Because subjects in hyper-gravity would likely not experience the increased collision costs associated with added mass, we hypothesized that the metabolic cost of walking in hyper-gravity would be lower than the metabolic cost of walking with increased weight. In addition, we used inverse dynamics to determine if joint mechanical work increased in proportion to gravity.

METHODS

Three healthy adult subjects (1 male, 2 female, mean body mass 56.1 kg) walked at 1.25 m/s under five different gravity levels (1G, 1.1G, 1.2G, 1.3G, and 1.4G). The order of the trials was randomized and each trial lasted 7 minutes.

Hyper-gravity was simulated by applying a near-constant downward force to the subject using a custom designed hyper-gravity simulator (Fig. 1). We supplied force by stretching lengths of rubber tubing with a hand winch. The tubing was stretched far enough to make small length changes negligible, keeping tubing tension nearly constant. We transferred the force to the subject by connecting the tubing to aircraft cable, routing the cable through low friction pulleys, and attaching the cable to a belt worn by the subject. Each subject wore a backpack hip belt designed to comfortably transfer vertical loads to the pelvis without interfering with gait. The cable was attached to both the left and right sides of the hip belt to provide a balanced downward force. The cable providing the downward force to the right side was connected to the cable connected to the left side, allowing the subjects to move freely to the right and left without experiencing centering forces.

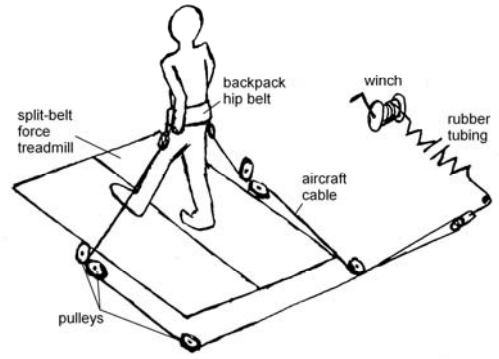

Figure 1: The hyper-gravity simulator.

We collected joint kinematics, electromyography (EMG), metabolic cost, and ground reaction forces while subjects

walked on a custom split-belt force treadmill. We recorded electromyography (EMG) of 8 lower limb muscles. We calculated root-mean-squared (RMS) values for the EMG signals for stance phase. Using the kinematic and kinetic data, we used inverse dynamics to calculate joint moments, powers, and works. We used the Brockway (1987) equation to calculate metabolic rates and subtracted standing metabolic rate from each trial to determine net metabolic rate.

RESULTS AND DISCUSSION

Contrary to expectations, we found that the metabolic cost of walking in hyper-gravity was similar to the metabolic cost of walking with load carriage (Fig. 2). The respective sums of the positive and negative joint powers (ankle, knee, and hip together) increased proportionally with gravity (Fig. 3). However, the increased work was not distributed evenly across the joints. Positive work rates of the ankle and hip and negative work rate of the hip increased greater than gravity (a 40% increase in gravity resulted in a >40% increase in work rate). The work rate at the knee did not change. As gravity level increased, vastus medialis, vastus lateralis, and rectus femoris muscles showed increased activity just after heel strike and just before push off. EMG RMS of these muscles increased linearly with gravity (a 40% increase in gravity resulted in a 100% increase in RMS).

SUMMARY/CONCLUSIONS

The results indicate that increases in metabolic cost due to hyper-gravity cannot be explained by increases in joint work rates alone. It is likely that the cost of generating force to support body weight is significant during walking in hyper-gravity.

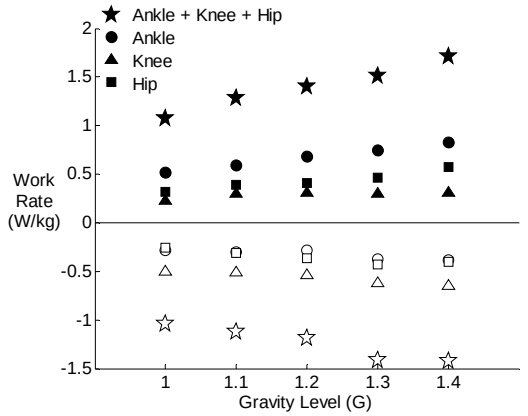

Figure 2: Average positive (filled symbols) and negative (unfilled symbols) work rates for the ankle, knee, and hip of both legs over one complete stride (left heel strike to left heel strike) for different levels of simulated gravity.

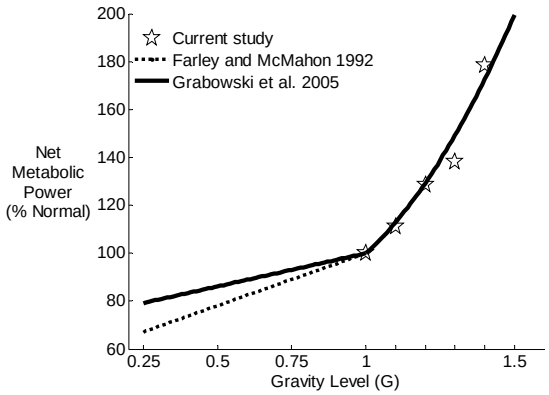

Figure 3: Net metabolic power (as a percentage of normal, 1G) versus gravity level. Results from Farley and McMahon (1992) and Grabowski et al. (2005) are included for comparison. The data from Grabowski et al. for gravity levels >1G are the metabolic cost of walking with load carriage, not the effect of only increased gravity.

REFERENCES

J. M. Brockway, *Hum Nutr Clin Nutr* **41**, 463 (Nov, 1987).

C. T. Farley, T. A. McMahon, *Journal of Applied Physiology* **73**, 2709 (1992).

A. Grabowski, C. T. Farley, R. Kram, *J Appl Physiol* **98**, 579 (Feb, 2005).

ACKNOWLEDGEMENTS

Supported by NSF.

EFFECTS OF UHMWPE SURFACE ROUGHNESS AND LUBRICATION ON THE FRICTIONAL PROPERTIES OF TOTAL KNEE REPLACEMENTS

Ryan C. Lucking, Ryan L. Landon, Stephen J. Piazza

The Pennsylvania State University, University Park, PA, USA
e-mail: *steve-piazza@psu.edu*

INTRODUCTION

Polyethylene wear and aseptic loosening due to wear particles are two of the primary failure modes seen in total knee replacements (TKR) (Sharkey, 2002). Computational tools developed to study the wear behavior of knee replacements have sometimes included friction, although the friction behavior of TKR is not well understood. A great deal of work has been done to quantify changes in wear rate due to factors such as load, counter-face roughness, and kinematics (McGloughlin, 2000), but the connection between these wear variables and friction remains unclear.

Because frictional behavior is not well defined, in many knee models coefficients of friction are tuned to match experimental results. Changes in friction properties caused by wear of ultrahigh molecular weight polyethylene (UHMWPE) are generally not considered in such models. To successfully predict the kinematics, kinetics, and wear behavior of knee replacements with computer models, a better understanding of friction in TKR is needed.

The purpose of this study was to explore the frictional properties of knee replacements under various conditions of lubrication and surface roughness. It was hypothesized that frictional losses in a pendulum test would be reduced with lubrication (as opposed to under dry conditions) and for smooth UHMWPE (rather than roughened samples).

METHODS

A pendulum tester was designed to reproduce the rolling and sliding motion of TKR (Figure 2). A cobalt-chrome femoral component (Triathlon; Stryker Orthopaedics) was fixed in a test frame in an inverted position. Rotating against the femoral component was a hollow steel cylinder lined with a 1 mm thick layer of UHMWPE on its interior. The radius of the cylinder was 80 mm, consistent with the radius of curvature of a typical tibial insert. A 110 N weight was hung from the cylinder to provide compressive loading across the joint.

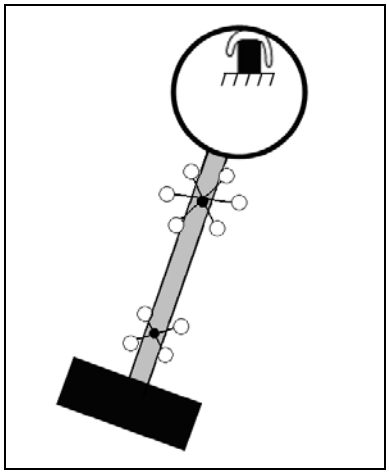

Figure 1: Schematic diagram of pendulum tester with reflective markers.

For trials with lubrication, room temperature water was sprayed from a single low-flow mister nozzle placed between the condyles of the femoral component. Three levels of UHMWPE surface roughness were tested: smooth, rough, and very rough. Smooth samples were untreated while rough and very samples were prepared using 180 and 60 grit sandpaper, respectively. The

sandpaper was applied parallel to the direction of motion to be consistent with anteroposterior scratches found in retrieved tibial inserts (Hood et al., 1983).

The pendulum was set in motion from rest from the same initial angle for each trial. Pendulum angle was recorded at 100 Hz using a three-camera video-based motion analysis system to track markers attached to the pendulum. Six trials were performed for each testing condition. A single UHMWPE sample was used to test the dry and wet conditions for each roughness.

Because viscous friction effects were observed in the pendulum decay, an exponential function of time was fit to the peaks of the decay (Figure 2). Two-way ANOVA was used to assess differences in the time constants caused by lubrication and surface condition.

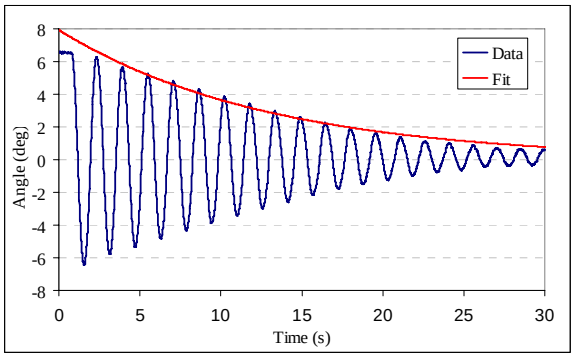

Figure 2: Pendulum angle versus time for a single trial with smooth UHMWPE and lubrication.

RESULTS AND DISCUSSION

Under dry conditions, smooth differed significantly from rough and very rough trials ($p < 0.001$) and the rough trials did not differ significantly from each other ($p = 0.779$). Under wet conditions, very rough UHMWPE was significantly different from both smooth and rough (both $p < 0.007$). However, smooth did not differ significantly from rough when wet ($p = 0.959$). Most notably, the dry-smooth trials had a mean time constant that was almost seven times greater than dry-wet.

Contrary to our expectation, more rapid energy loss was observed under wet conditions. More sliding behavior was observed in wet trials and this sliding perhaps led to greater energy loss than that which resulted from rolling in the dry trials. Surface roughness also appeared to influence frictional loss, but the manner in which this occurred seemed to depend on the lubrication condition.

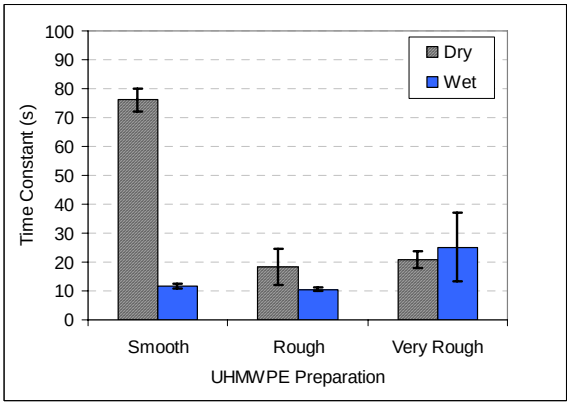

Figure 3: Time constants averaged across trials from exponential fits of pendulum decay. Error bars indicate ±1 SD.

SUMMARY/CONCLUSIONS

This study demonstrated that frictional effects in TKR may be counterintuitive. Ongoing research, including computer modeling of the pendulum test rig will help to explain the complex surface interactions found in TKR for varied lubrication and surface roughness conditions.

REFERENCES

Hood et al. (1983). *Journal of Biomedical Materials and Research*, **17**, 829-842

McGloughlin, T.M. et al. (2000). *Proc Inst of Mech Eng*, **214**, 349-359.

Sharkey, P.F. et al. (2002). *Clin Orthop and Related Research*, **404**, 7-13.

TRANSVERSE DAMAGE AND FAILURE BEHAVIOR OF TRABECULAR BONE

Constance L. Slaboch,[1*] Jacqueline G. Keitly,[1,2] and Glen L. Niebur[1,2]

Tissue Mechanics Laboratory, [1]Dept. of Aerospace and Mechanical Engineering
[2]Interdisciplinary Bioengineering Program
University of Notre Dame, Notre Dame, IN
*E-mail: cslaboch@nd.edu, Web: bones.ame.nd.edu

INTRODUCTION

Osteoporosis is a disease involving trabecular bone that affects many elderly people and is a growing health problem. Many patients are confined to a nursing home for six months or more after treatment of an osteoporotic fracture. Most fractures occur during falls and at anatomic sites where trabecular bone is the major load-bearing element. Therefore, trabecular bone strength during off-axis loading is important for understanding the mechanisms of clinical hip fractures. This information will help identify patients at risk of fracture and develop treatments.

Microdamage is present *in vivo* in trabecular bone in humans, but its role in bone failure is not clear. Recent studies in cortical bone found that higher levels of microdamage were consistent with increased fatigue life. Microdamage has been shown to decrease the modulus of trabecular bone samples loaded along the principal elastic direction. However, the damage behavior for loading along other mechanical axes has not been characterized.

Trabecular bone could be damaged during falls or other off-axis loads, leading to diminished mechanical properties and increased fracture risk. The goal of this research was to determine how microdamage affects the failure behavior of trabecular bone under off-axis compressive loading. Specifically, 1) microdamage was induced to two different levels and 2) changes in the modulus failure properties were quantified.

Ten bovine tibial trabecular bone samples were prepared from eight tibiae. Five samples were randomly assigned to either the low or high damage group. Cylindrical samples, approximately 8 mm in diameter and 30 mm long were prepared with the stiffest principal elastic direction perpendicular to the cylindrical axis. The samples were embedded in brass endcaps for testing.

The initial elastic modulus of the samples was measured by loading to 0.5% compressive strain. The modulus was taken as the slope of a quadratic curve fit at 0 stress, and was averaged from three load cycles. Samples were then damaged by loading to either 1.5% (low) or 2.5% strain (high). Following the damaging load, the modulus was measured a second time. All specimens were then loaded to 10% strain and the ultimate stress and strain were measured (Fig. 1). To compare between samples, the ultimate stress was divided by the initial modulus.

RESULTS

On average, the orientation of the principal elastic direction was 84 ± 06° from the cylinder axis.

The elastic modulus decreased following the damaging loads. The initial elastic modulus for the samples was 411 ± 234 MPa. The damaged modulus for the low damage group decreased by 21 ± 9.7% in comparison to the high damage group which decreased by 43 ± 29% ($p > 0.17$, Student's t-test, Fig. 1).

Neither the ultimate stress nor strain (Fig. 2) was significantly different between the two damage groups, after compensating for dependence on modulus.

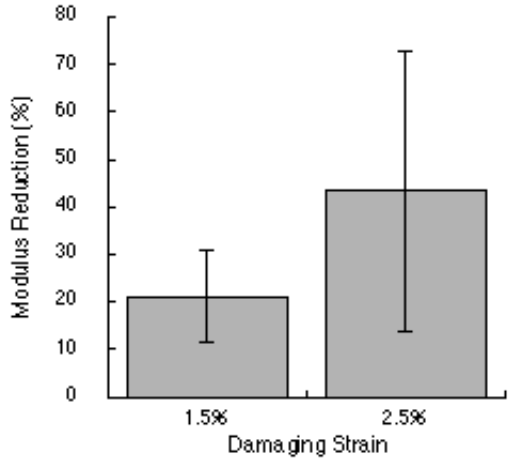

Figure 1: The elastic modulus decreased by similar percentages for samples strained to 1.5% strain and 2.5 % strain ($p > 0.17$). Error bars are one standard deviation (N=5).

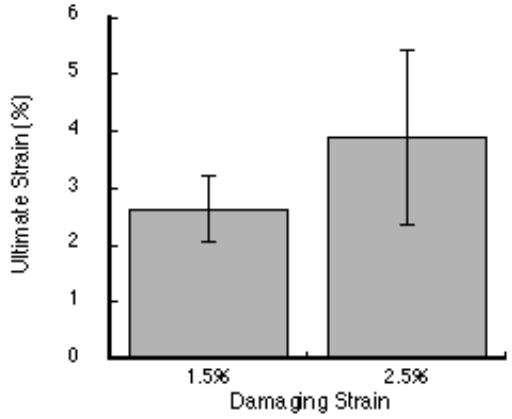

Figure 2: The ultimate strain on the final loading did not differ between the two groups ($p > 0.12$). Error bars are one standard deviation (N=5).

DISCUSSION

The transverse damage behavior of trabecular bone was studied for ten samples loaded to two different damaging strains. Damage to the samples occurred in both cases, with significant modulus reductions for both groups. However, the sample sizes were too small to identify differences in the damage levels between groups. The ultimate properties were also similar between the two groups. As such, this data would suggest that increased levels of damage are not detrimental to the overall failure properties of trabecular bone. However, the number of specimens tested was small, resulting in weak statistical comparisons.

REFERENCES

Braithwaite, RS*, et al.* (2003). *J Am Geriatr Soc* **51**(3): 364-70.

Keaveny, TM*, et al.* (1994). *J Biomech* **27**(11): 1309-1318.

Mori, S*, et al.* (1997). *Bone* **21**(6): 521-6.

Parkkari, j*, et al.* (1999). *Calcified Tissue International* **65**: 183-187.

Sobelman, OS*, et al.* (2004). *J Biomech* **37**(9): 1295-1303.

Wang, X*, et al.* (2004). *J Biomech Eng* **126**(1): 122-125.

AKNOWLEDGMENTS

NIH AR052008

A THREE-DIMENSIONAL MODEL OF THE SUPRASPINATUS MUSCLE

Joshua Webb[1], Silvia Blemker[2], and Scott Delp [1]

[1] Stanford University, Stanford, CA, USA
[2] University of Virginia, Charlottesville, VA, USA
E-mail: joshwebb@stanford.edu, Web: nmbl.stanford.edu

INTRODUCTION

The rotator cuff is an important group of muscles that dynamically stabilizes the glenohumeral joint. Each of these muscles has a complex and specialized structure. For example, the supraspinatus muscle wraps around several structures, has a broad attachment site, and has varied fiber orientation within the muscle. How do these features of the muscle's structure influence its function?

Previous models typically represented this muscle as a collection of line segments (van der Helm, 1994). This approach employs methods such as geometric primitives to represent wrapping around underlying structures and assumes all fibers within the muscle function uniformly. The purpose of this project is to create a three-dimensional finite element model of the supraspinatus muscle that represents its complex fiber geometry and the mechanics of its interaction with surrounding structures, allowing for exploration of the relationship between fiber geometry and fiber behavior.

METHODS

A 3D finite element model (Fig. 1C) of the supraspinatus muscle and tendon was developed from magnetic resonance images. The muscle and tendon were modeled using a hyperelastic, transversely isotropic constitutive relationship between stress and strain. The representation for the 3D fiber orientations (Fig. 1B) within the muscle was created by morphing a fiber template to the finite element mesh (Blemker and Delp, 2005).

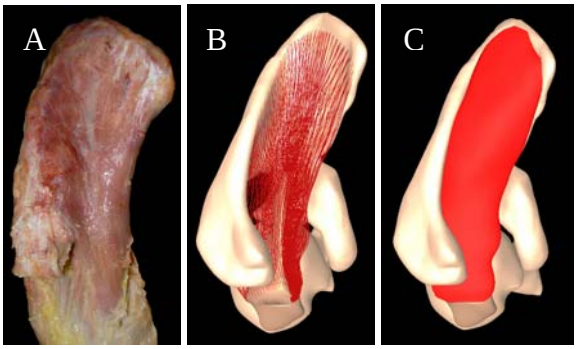

Figure 1: Superior view of cadaver supraspinatus muscle (A), fiber representation of the model (B), and finite element model with fibers and mesh(C)

Finite element simulations were run in NIKE3D (Puso et al., 2001), an implicit finite element solver. The bones were assumed to be triangulated rigid bodies and a penalty formulation was used for resolving bone-muscle and bone-tendon contact. Input boundary conditions were specified bone displacements and muscle activation. Regression equations (de Groot and Brand, 2001) were used to prescribe the motions of the scapula and clavicle as functions of humerus orientation.

The model was tested by comparisons of its fiber moment arms with experimental data (Langenderfer et al., 2006) and with moment arms computed using a model of the upper extremity that represents supraspinatus as a set of line segments (Holzbaur et al., 2005).

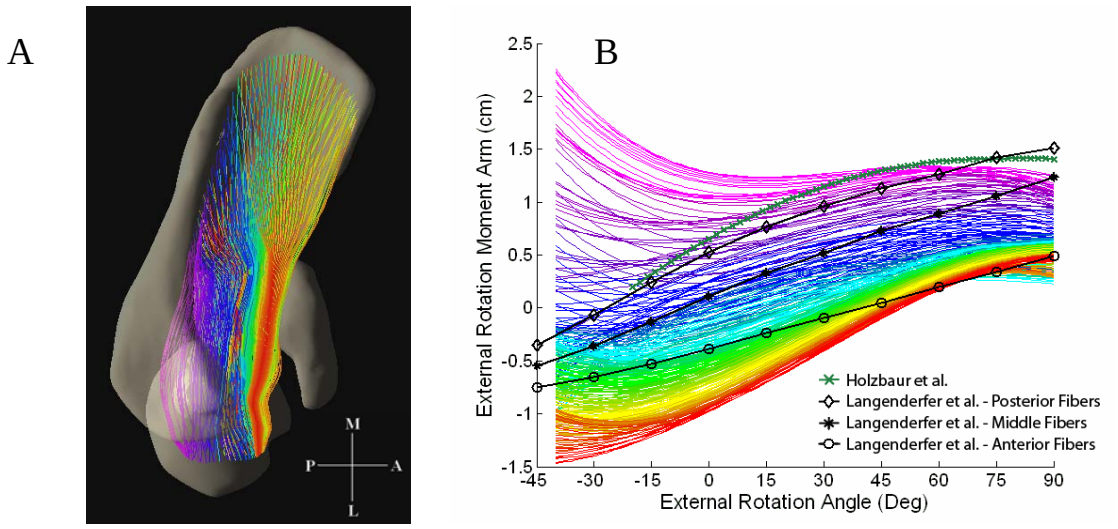

Figure 2: Fiber trajectories within the supraspinatus muscle (A) and external rotation moment arms as a function of external rotation angle (B). External rotation moment arm curves were determined with the joint at 10 degrees of glenohumeral elevation and compared to experimental data (Langenderfer et al., 2006) and a model of shoulder muscles (Holzbaur et al., 2005). Consistent coloring of fibers shown in (A) and fiber moment arm curves shown in (B) illustrates how fiber moment arms vary spatially throughout the muscle.

RESULTS AND DISCUSSION

External rotation moment arms were found to vary primarily with the anterior-posterior location of the fibers. The anterior and middle fibers (red, yellow and green fibers in Fig. 2) are internal rotators at internally rotated positions but switch to weak external rotators at external rotation angles greater than 50 degrees. The posterior fibers (purple fibers) are external rotators at all values of rotation angle. The 3D model predicted a broad range of moment arms across the individual fibers especially at internally rotated positions.

Fiber geometry influences the external moment produced in different regions of the supraspinatus muscle. Calculated moment arms and lengths indicate that the fibers experience different excursions and do not behave uniformly. Modeling that includes this level of detail will give improved understanding of rotator cuff mechanics by more accurately calculating muscle behavior and allowing for a more detailed understanding of structure and function.

REFERENCES

Blemker, S.S., Delp, S.L. (2005). *Annals of Biomed. Eng.*, **33**, 661-673(5).

de Groot, J.H., Brand, R. (2001). *Clin. Biomech.*, **16**, 735-743(9).

Holzbaur et al. (2005). *Annals of Biomed. Eng.*, **33**, 829-840(6).

Langenderfer et al. (2006). *J. Ortho. Res.*, **24**, 1737-1744(8).

Puso et al. (2002). *Lawrence Livermore Natl. Labs Tech. Report*, UCRLMA-105268.

van der Helm, F.C.T. (1994). *J.Biomech.*. **27**, 551-569(5).

ACKNOWLEDGEMENTS

Garry Gold, Kate Holzbaur, NSF

YOUNG ADULTS ADAPT TO PREVENT FALLS FROM UNPREDICTABLE BALANCE DISTURBANCES

Lisa R. Welsh and Michael J. Pavol

Oregon State University, Corvallis, OR, USA
E-mail: mike.pavol@oregonstate.edu

INTRODUCTION

Falls, particularly those due to slips, constitute a major health risk for older adults (Gabell et al., 1985; Luukinen et al., 2000). Effective interventions for fall prevention are therefore needed. Notably, past research has found that individuals can learn not to fall through repeated exposure to the same slipping perturbation (Pavol et al., 2004). Slips can be unpredictable, however. This study determined whether reactive response adaptations would occur in young adults for repeated slips in unpredictable directions.

METHODS

A pneumatically-driven sliding platform was used to cause 30 healthy, consenting, young adults (24 ± 4 yrs; 18 women) to repeatedly lose their balance in different directions during a simulated lifting task. Trials began with participants standing on the platform, secured in a safety harness, with their feet in a standardized position, and holding a foam rod with both hands. Participants were to squat down while keeping their back and elbows straight, touch the rod to a mark on the distal thigh, and then stand back up at a specified, practiced rate. During slip trials, a slip in one of 5 directions was automatically triggered when the computed center of mass had risen from its lowest point by 2% of its descent distance. In inducing a slip, the platform translated 30 cm forward, backward, or diagonally in 0.34 s, or 20 cm right or left in 0.17 s. Participants could not identify the slip direction in advance.

After four no-slip trials, a forward slip was induced on the fifth trial, without warning or practice, causing a backward balance loss. Participants were then informed that a slip might occur in any direction in subsequent trials and they were to try not to fall. Trials 6-29 included four to six each of forward, backward, right, left, and no slip trials, in the same, unpredictable order. After a diagonal slip, trials 31-35 were forward slips. Three-dimensional kinematics of the participants, ground reaction forces, and the force on the safety harness were recorded using a motion capture system, force plate, and load cell.

The first ("unexpected"; trial 5), second (trial 10), and fifth (trial 28) unpredictable forward slips and the last, "predictable" forward slip (trial 35) were analyzed. A trial was classified as a fall if the average safety harness force exceeded 10% of body weight over any 1-s period. Balance control was quantified by the anteroposterior (AP) position (in foot lengths (fl)) and velocity (as a Froude number) of the body center of mass (COM) relative to the rear of the base of support. Weight support was quantified by the vertical height and velocity of the hip midpoint (normalized to body height (bh)). These were determined at slip onset and at liftoff and touchdown of the first recovery step. Time to step liftoff, step time, and AP step length (in %bh) were also determined.

For each variable, participants were grouped by the outcome of the first slip in a group by trial repeated-measures ANOVA. Effects were considered significant at $p < 0.005$.

RESULTS AND DISCUSSION

Eight participants fell upon the first slip. Fallers exhibited a more posterior COM at step liftoff and took a shorter recovery step, placing the foot less posterior to the COM (Table 1). Fallers' hips were also descending faster at step liftoff, leading to a lower hip height at step touchdown.

Fallers adapted rapidly; no participant fell after the first slip trial, despite an inability to predict the needed response. Adaptations between the first and second forward slips by those who initially fell included a less posterior COM and higher and more slowly descending hips at step liftoff, and a greater hip height at touchdown (Table 1). Fallers thus reduced the extent of their slip-induced balance loss and improved their weight support to become like those who recovered.

Those who initially recovered also adapted their reactive response. Like those who fell, they exhibited a less posterior COM at step liftoff and a greater hip height at touchdown upon the second forward slip. Both groups also had a faster response time to step liftoff. By the fifth forward slip, both groups had a longer step time and more posterior stepping foot placement relative to the COM (Table 1). The "predictable" slip differed from the fifth, unpredictable forward slip only by the presence of proactive adjustments; both groups were moving their COM forward faster at the onset of the "predictable" slip.

One variable that did not change was step length. For all slips analyzed, those who fell initially took a shorter step backward than those who recovered (19 ± 5 %bh vs. 27 ± 6 %bh), leading to a foot placement less posterior to the COM. Reactive stepping may thus be a highly stereotyped behavior.

CONCLUSIONS

Young adults adapt their reactive responses employed for balance control and weight support with repeated exposure to slips of unpredictable direction, and rapidly learn how to avoid a fall from these slips. These results may have application to the design of fall prevention programs.

REFERENCES

Gabell, A., et al. (1985). *Ergonomics,* **28**, 965-975.

Luukinen, H., et al. (2000). *Osteoporos Int,* **11**, 631-634.

Pavol, M.J., et al. (2004). *J Gerontol Med Sci,* **59A**, 494-502.

ACKNOWLEDGEMENTS

Funded by the Ringe Faculty Excellence Fund for Life Quality and Longevity.

Table 1: Mean ± SD COM position and hip height at step liftoff (LO) and step touchdown (TD) across the four forward slips analyzed, as a function of the outcome of the 1st slip (Group)

		Forward Slip			
Variable (units)	Group	1st	2nd	5th	"Predictable"
COM at LO	Recover	-0.36 ± 0.12	-0.18 ± 0.15 †	-0.11 ± 0.22 †	-0.11 ± 0.28 ‡
(fl anterior to heel)	Fall	-0.58 ± 0.15 *	-0.26 ± 0.08 †	-0.07 ± 0.23 †	0.03 ± 0.22 ‡
COM at TD	Recover	0.64 ± 0.42	0.83 ± 0.43	0.94 ± 0.37 †	1.03 ± 0.37 ‡
(fl anterior to heel)	Fall	0.11 ± 0.36 *	0.33 ± 0.32 *	0.71 ± 0.40 *†	0.53 ± 0.57 *‡
Hip Height at TD	Recover	53.3 ± 1.7	54.1 ± 1.9 †	53.8 ± 1.6 †	53.3 ± 1.9 ‡
(%bh)	Fall	47.2 ± 1.9 *	54.0 ± 1.6 †	54.6 ± 1.4 †	55.7 ± 1.3 *‡

* $p < 0.005$ vs. Recover; † $p < 0.005$ for 2nd or 5th vs. 1st slip; ‡ $p > 0.05$ for Predictable vs. 5th slip

LOWER EXTREMITY KINEMATIC CONSEQUENCES DURING VERTICAL TO HORIZONTAL MOMENTUM REDIRECTION

Laura Held, Jill L. McNitt-Gray, and Henryk Flashner
Biomechanics Research Laboratory
Departments of Biomedical Engineering, Biological Sciences, and Kinesiology
University of Southern California, Los Angeles, CA, USA
E-mail: held@usc.edu

INTRODUCTION

During landings, insufficient control of shank and thigh motion can result in excessive multi-axis rotation of the knee. As the complexity of tasks increases, the control system must organize its available resources to achieve the performance specifications without introducing loading conditions that put the system at risk for injury. The outcome of the control strategy is reflected in the lower extremity joint torques and the interaction forces with the environment, whereas the kinematic consequences are reflected in the degree of lower extremity joint alignment.

Factors contributing to insufficient control of the knee during foot contact are poorly understood, particularly when tasks are performed in realistic contexts. Previous studies have focused on knee flexion range of motion and knee valgus angles during drop landings as indicators for risk of injury. Lower extremity alignment measurements during task that require horizontal momentum redirection during 3D, sport-specific movements have been limited to 45˚ cutting and cross-over step tasks.

The goal of this study was to determine the kinematic consequences of control strategies used during landings requiring a secondary horizontal momentum redirection task. We hypothesized that the alignment of the lower extremity joint axes during both the impact and push phases of ground contact would be affected by task-specific control strategies.

METHODS

In this pilot study, one female, collegiate volleyball player performed a standing block jump immediately followed by horizontal redirection parallel to (Go Left) or perpendicular to (Go Back) the net. A maximum vertical jump (MVJ) landing was used as a basis of comparison for kinematic results.

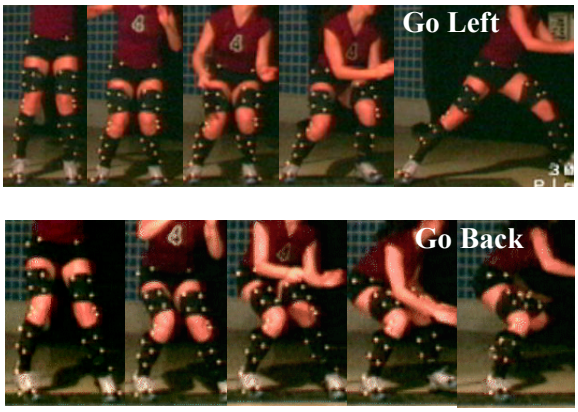

Figure 1. Subject-selected techniques for performing the Go Left and Go Back tasks.

High speed video from three camera views (NAC, 200 Hz) was used to obtain 3-D locations (Motus, Vicon) of four tracking markers on each segment (pelvis, thigh, shank, foot) during a calibration frame and throughout each task. All coordinates were filtered (fourth order Butterworth, 6 Hz cutoff) and imported into Matlab (The Mathworks Inc, MA) for processing. Joint coordinate systems were defined based on palpated bony landmarks (greater trochanter, femoral condyles, fibular head, malleoli).

A quaternion parameterization (Kim et al., 2001) was used to quantify segment orientations. Functional knee joint axes were calculated for each frame using the thigh and shank quaternions and reported using the anatomically-defined axes.

RESULTS

The degree of out of plane knee motion during the impact phase (touchdown to first local minimum of vertical ground reaction force (GRFv)) and the push phase (last local minimum of GRFv to toe off) increased as the direction of the horizontal Go task changed from MVJ to Left to Back (Figure 2a). External rotation of the thigh on the shank at touchdown increased across tasks as the subject modified her foot position at contact (Figure 1). During the push phase, the knee transitioned into internal rotation as the knee extended for both Left and Back. Peak knee valgus increased across tasks.

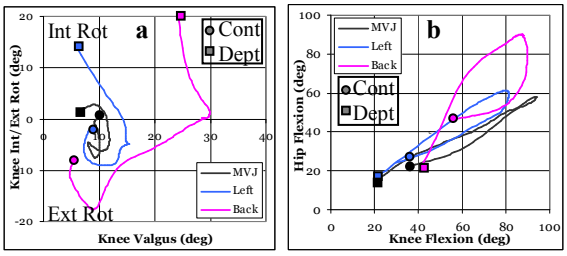

Figure 2: Angle-angle diagrams of the ground contact phase of representative trials of each task.

Sagittal plane knee and hip ranges of motion were also task dependent. When horizontal Go tasks were added to the block jump, maximum knee flexion angle decreased and maximum hip flexion increased (Figure 2b).

Similarly, the degree of off-axis rotation during both the impact and push phases was task dependent. While both Go tasks showed increases in knee valgus throughout the movement, the increase occurred mostly during the impact phase for Left and during the push phase for Back (Figure 3).

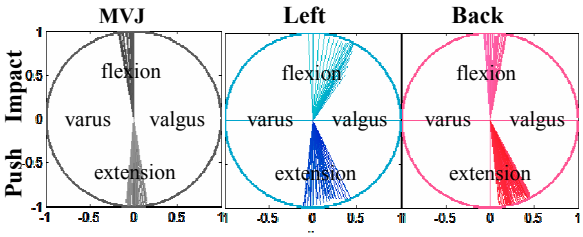

Figure 3. Knee axes of rotation for each time step for each trial. Deviations from vertical (flex (+) and ext (-)) indicate off-axis rotations toward varus (-) or valgus (+). Wider fan spread indicates increased variability over time.

DISCUSSION/CONCLUSIONS

These results indicate that the subject employed different control strategies during the impact and push phases of the Land and Go tasks depending on the required horizontal direction. Both Go tasks resulted in differences in frontal and transverse plane knee kinematics as compared to a simple vertical jump landing. As horizontal direction deviated from Left to Back, out of plane knee motion increased in both planes simultaneously. The coordination between the knee and hip also changed based on the secondary task requirements.

Realistic landing tasks with varied secondary horizontal momentum redirection requirements provide a more complete representation of the kinematic consequences of an individual's control strategies than a standardized MVJ task. Realistic movements that result in sustained axis mal-alignment may require targeted intervention programs that consider control requirements at the whole body and local subsystem level.

REFERENCES

Kim, I. et al. (2001). *AAS* **01-142**, 571-586.
Kuipers. (1999). *Quaternions and Rotation Sequences*. Princeton University Press.

CRUCIATE LIGAMENT FORCE BETWEEN THE FORWARD LUNGE LONG AND SHORT WITH AND WITHOUT A STRIDE

Rafael F. Escamilla[1], Naiquan Zheng[2], Alan Hreljac[3], Rodney Imamura[3], Toran D. MacLeod[1], William B. Edwards[4], Glenn S. Fleisig[5], Kevin E. Wilk[6]

[1]Department of Physical Therapy, California State University, Sacramento, USA
[2]Orthopaedics and Rehabilitation Program, University of Florida, Gainesville, FL, USA
[3]Kinesiology and Health Science Department, California State University, Sacramento, USA
[4]Department of Health and Human Performance, Iowa State University, Ames, Iowa, USA
[5]American Sports Medicine Institute and [6]Champion Sports Medicine, Birmingham, AL, USA
e-mail: rescamil@csus.edu

INTRODUCTION

It is currently unknown how cruciate ligament tensile force change among forward lunge exercises as a function of knee angle both with a stride forward (then back to starting position) and without a stride (performed in stationary position) and using a long lunge (knees over ankle at maximum knee flexion) and short lunge (knees translate beyond toes at maximum knee flexion). The purpose of this study was to compare PCL/ACL tensile forces as a function of lunge exercises and knee angle (0-90°). It was hypothesized that PCL tensile forces would increase as knee flexion increased, would be greater in the forward lunge long compared to the forward lunge short, and greater with a stride than without a stride.

METHODS

Eighteen subjects (9 males and 9 females) were used with an average age, mass, and height of 29±7 y, 77±9 kg, & 177±6 cm for males and 25±2 y, 60±4 kg, & 164±6 cm for females. Each subject performed the forward lunge long and short with and without a stride. Intensity was normalized by having each subject their 12 repetition maximum intensity, which were 49±10 kg for males and 32±7 kg for females. Surface electrodes were placed over the quadriceps, hamstrings, and gastrocnemius, and reflective markers over landmarks on the foot, ankle, knee, hip, and shoulder.

Video (60 Hz), EMG & force platform (960 Hz) data were collected during 3 repetitions of each exercise (0-90° knee flexion) and averaged. EMG data were normalized by maximum voluntary isometric contractions (MVIC).

Cruciate ligament tensile forces were calculated using a biomechanical knee model (Zheng et al., 1998) with input variables consisting of resultant knee forces and moments and the muscle force function $F_{m(i)} = {}_ik_iA_i\sigma_{m(i)}[EMG_i/MVIC_i]$, where k_i was a muscle force-length variable, A_i was physiological cross sectional area (PCSA) per muscle, $\sigma_{m(i)}$ was MVIC force per unit PCSA, EMG_i and $MVIC_i$ were EMG window averages, and c_i was a weight factor adjusted in a computer optimization program. Cruciate ligament tensile force as a function of exercise (forward lunge long with stride, forward lunge short with stride, forward lunge long without stride, and forward lunge short without stride) and knee angle (every 10° from 0-90° and 90-0°) were assessed by a two-way repeated measures analysis of variance ($p < 0.01$).

RESULTS AND DISCUSSION

Cruciate ligament tensile forces for the forward lunge long and short without a stride are shown in Figure 1, while cruciate ligament tensile forces for the forward lunge long and short with a stride are shown in Figure 2. Between 0-80° during the knee flexing phase and 80-0° of during the knee extending phase, PCL tensile force was significantly greater in the forward lunge long compared to the forward lunge short. Both with and without a stride, the forward lunge short generated low PCL tensile force and approached ACL tensile loads at knee flexion angles between 0-40°. There was generally no significant differences in PCL tensile forces between with and without a stride.

It is interesting that PCL tensile force was lower and ACL tensile force was approached during the forward lunge short, which resulted in the knees translating forward beyond the toes at maximum knee flexion. Increased anterior translation of the knees appears to

result in a decrease in PCL tensile force and approaching ACL tensile force.

SUMMARY/CONCLUSIONS

PCL tensile force was greater during the forward lunge long compared to the forward lunge short throughout most of the knee flexing and knee extending phases. In addition, PCL tensile force was greatest at maximum knee flexion for all lunge exercise variations. PCL tensile force was low and ACL tensile force was approached during the forward lunge short between 0-40° knee flexion.

REFERENCES

Zheng et al. (1998), *Journal of Biomechanics*, **31**, 963-967.

ACKNOWLEDGEMENTS

The authors would like to thank Lisa Bonacci, Toni Burnham, Juliann Busch, Kristen D'Anna, Pete Eliopoulos, & Ryan Mowbray for all their assistance during data collection and analyses.

Figure 1. Mean (SD) cruciate ligament tensile force between forward lunge long and short without a stride.

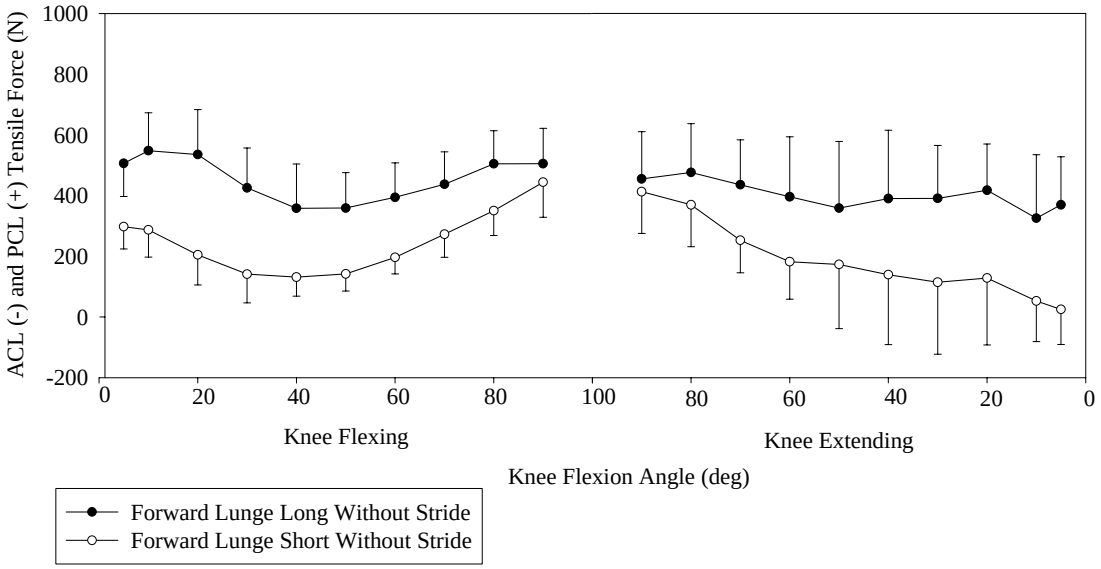

Figure 2. Mean (SD) cruciate ligament tensile force between forward lunge long and short with a stride.

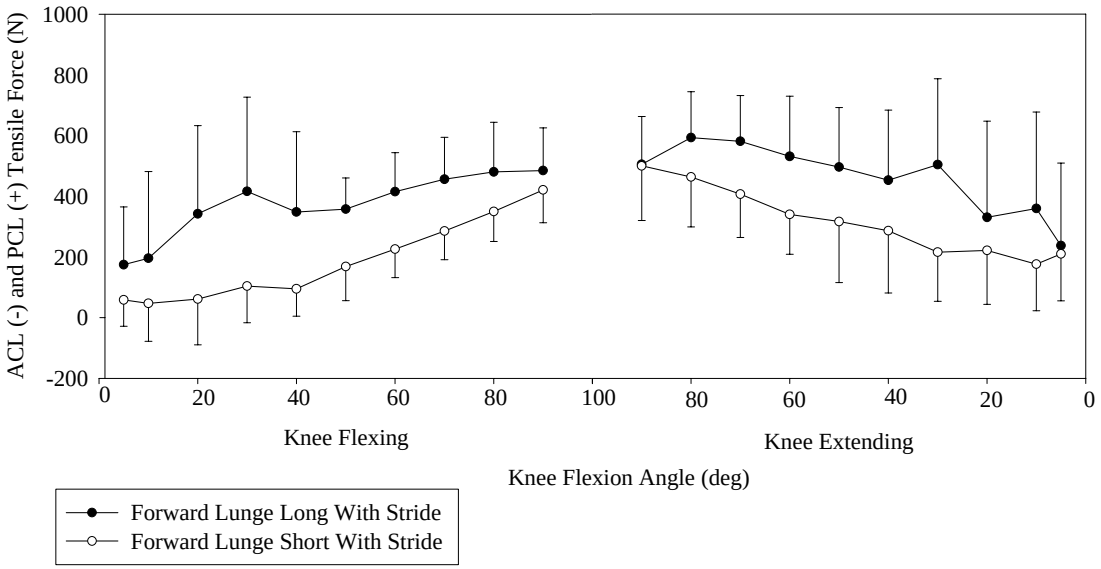

BIRTH OF THE SUPER PEN: AN INNOVATIVE APPROACH TO STUDYING HANDWRITING KINETICS

Alexander W. Hooke and Jae Kun Shim

University of Maryland, College Park, MD USA
Email: ahooke@umd.edu
Web: http://www.hhp.umd.edu/KNES/faculty/jkshim/neuromechanics/index.html

INTRODUCTION

The seemingly simple act of handwriting is one of many marvels of the central nervous system. Whether writing a word or drawing a basic shape, we are able to generate a sort of code that is both universally recognizable, yet individually unique. Many previous researchers have investigated the kinematic aspects of handwriting with objectives ranging from understanding handwriting motor control to searching for a reliable quantification of various neuropathies. Instrumentation limitations have prevented these studies from being extended to the kinetic aspects of the motion (Latash et al. 2003). More specifically, the physical size of even the smallest force transducers inhibits the ability to cluster them at the grip site while maintaining a realistic and comfortable writing grip. The goal of this study was to resolve this issue by designing a "super pen," capable of measuring the individual forces between each individual contact of the hand with the writing utensil.

INSTRUMENT DESIGN

This "super pen" contains four, six-component sensors (Nano-17, ATI Industrial Automation, Garner, NC, USA) countersunk into the pen's body. Each sensor is equipped with a moment arm running along the long axis of the pen such that its only contact point with the body of the pen is at its attachment point on the sensor. At the writing end the pen, each moment arm has a rounded grip pad. Each grip pad corresponds to a single, unique contact point with the hand. The four points making contact with the pen were the tip of the thumb, the tip of the index finger, the lateral surface of the middle finger's distal phalanx, and the webbing between the metacarpophalangeal (MCP) joints of the thumb and index finger. The moment arms are made of titanium and aluminum and are very rigid, withstanding bend under forces

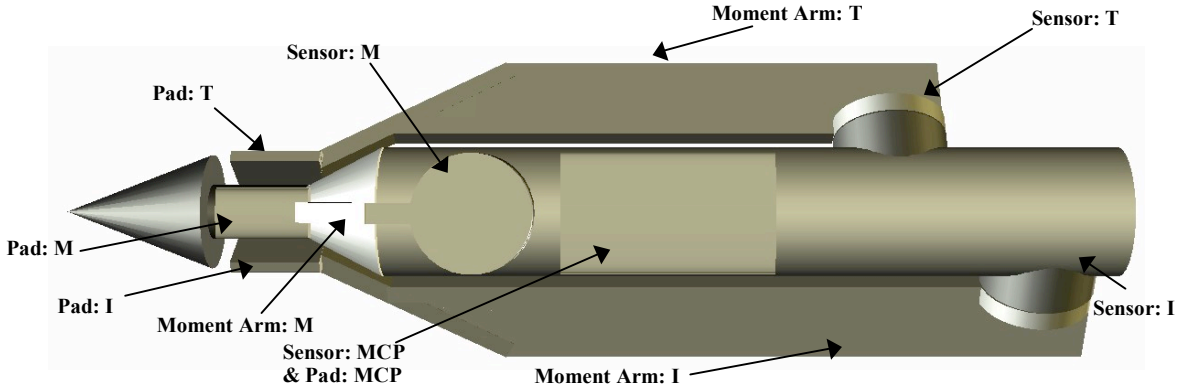

Figure 1: Schematic of pen with sensors, moment arms, and grip pads labeled by contact point. T = thumb, I = index, M = middle, MCP = metacarpophalangeal webbing

used in normal handwriting. Because each moment arm has only two contact points, one at the sensor and one at the sensor's respective digit, the reading detected by the sensors represents the forces of each contact point, individually, at its respective grip site.

The reference systems are aligned locally at each sensor such that z-axis is normal to the surface, the x-axis is tangential to the curve of the pen's body, and the y-axis is tangential to the pen's body along its long axis.

The mass of the pen with all of the sensors attached is 155g. The body is approximately 1.75cm in diameter and 18cm in length. The writing implement is interchangable with plastic, brass, and working ink stylus attachments.

METHOD

The pen was dissembled such that only a single moment arm remained. The pen's body was then fastened in place such that one of the three local axes of the sensor in use was parallel to gravity. A series of 20 different masses were hung from the moment arm such that the force of gravity pulled exclusively along the single, desired axis. This process was repeated for each of the axes on each of the moment arms. The force at the grip pad measured by the sensor was then compared to the actual force graphically, as seen in Figure 2.

RESULTS

In the case of the thumb sensor, the measured values had a nearly one-to-one linear relationship with the actual forces, as seen by the example figure in which of the slope of the thumb sensor's F_y values of 0.9749. This also showed a high linear correlation with an R^2 value of 0.9998. The linearity of the other force components was similar both across and within sensors.

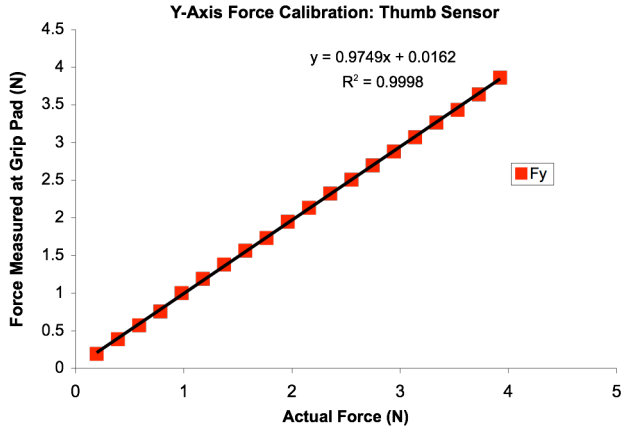

Figure 2: A sample calibration graph comparing the force measured at the thumb's grip pad to the actual force along the y-axis.

CONCLUSIONS

As seen in the results, this new super pen is capable of reliably measuring the individual contact forces between the hand and the writing utensil. The deviations between the different axes' slopes was likely caused by minor flexion in the moment arms, however this does not have a large impact on the instrument's capabilities due the still present strong linear relationship between the measured and known forces.

As we become more familiar with this tool's capabilities, there are a plethora of possible directions to study further. A few we plan to specifically investigate are possible synergies between the different contact points on the pen itself as well as between the pen and the writing surface.

REFERENCES

Latash ML, Danion F, Scholz JF, Zatsiorsky VM, and Schoner G. Approaches to analysis of handwriting as a task of coordinating a redundant motor system. *Hum Mov Sci* 22: 153-171, 2003.

Mechanics and energetics of incline walking with powered ankle exoskeletons

Gregory S. Sawicki[1] and Daniel P. Ferris[1]

[1]Human Neuromechanics Laboratory, University of Michigan, Ann Arbor, MI, USA
E-mail: gsawicki@umich.edu

INTRODUCTION

Our previous results indicated that when bilateral ankle exoskeletons produce ~65% of ankle joint power, the metabolic cost of level walking decreased by 13% (Sawicki et al., 2007). Because level, steady speed walking requires no net mechanical work over a stride, substituting biological muscle work with artificial muscle work may yield larger reductions in energy expenditure during locomotor tasks that require substantial positive muscle work. The objective of this study was to determine the effects of increasing surface incline on the metabolic cost of walking with robotic exoskeletons. We hypothesized that as surface gradient increased, ankle exoskeletons would deliver more mechanical power and users would save more metabolic energy.

METHODS

Nine healthy subjects walked on a treadmill at 1.25 m/s with bilateral powered ankle exoskeletons under soleus proportional myoelectric control (**Fig. 1**). After three thirty-minute practice sessions on level ground, subjects completed 7 minute bouts of unpowered and powered walking at four surface inclines (0%, 5%, 10% and 15% gradient) in a random order. Subjects rested for 3 minutes between trials. We recorded oxygen and carbon dioxide flow rates using a metabolic cart, artificial muscle forces from series load transducers, and joint kinematics using reflective markers.

To quantify exoskeleton mechanical assistance, we used artificial muscle forces and moment arm lengths along with ankle joint angular velocity to compute the average mechanical power delivered by the exoskeletons over a stride. To assess energy expenditure, we converted gas flow rates from minutes 4-6 of each trial using the Brockway equation and subtracted the energy required for quiet standing to calculate net metabolic power. Theoretically, if exoskeletons directly replaced positive muscle work, reductions in metabolic cost should be four times the amount of delivered exoskeleton positive power (i.e. muscular efficiency of 25%). To evaluate exoskeleton performance, we multiplied changes in net metabolic power by 0.25 and then divided by average exoskeletons positive mechanical power. A performance index of 1.0 would indicate that exoskeletons directly replaced biological muscle work.

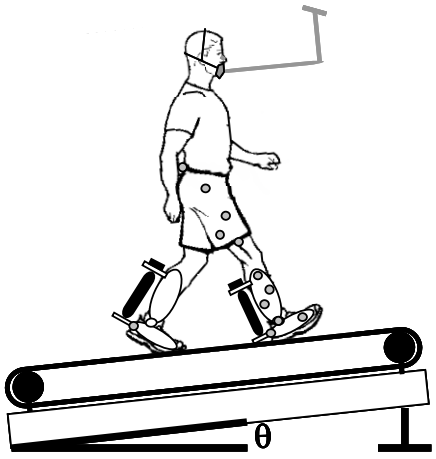

Figure 1. Subjects walked at 1.25 m/s on four different surface inclines while wearing powered bilateral ankle exoskeletons controlled by their own soleus muscle activity.

We used a repeated measures ANOVA to test for differences in positive exoskeleton power across gradients, and net metabolic power between unpowered and powered walking.

RESULTS AND DISCUSSION

Net metabolic power was significantly lower in the powered walking trials for each level of surface incline (**Fig. 2**) (ANOVA, $p < 0.001$). The decrease was between 10% and 13% for all gradients. Exoskeleton average positive mechanical power was significantly higher across surface gradients (0.23 ± 0.19 W/kg (mean ± s.e.) at 0% grade and 0.37 ± 0.03 W/kg at 15% grade) ($p<0.001$) (**Fig. 3A**). As a result, absolute decreases in net metabolic power were larger on steeper slopes and reached a maximum of -0.98 ± 0.12 W/kg at 15% grade (**Fig. 3B**). Exoskeletons performance index increased from 0.47 for level walking to ~0.65 at the two highest grades (**Fig 3C**).

These findings indicate that although powered ankle exoskeletons perform greater mechanical work during incline walking than during level walking, the relative savings in metabolic cost is similar across gradients. However, the increase in exoskeleton performance index indicates that added mechanical power replaces a larger proportion of biological muscle work at higher inclines. The explanation for this discrepancy is likely that the hip and/or knee musculature performs a greater percentage of the total external mechanical work on inclines than on the level.

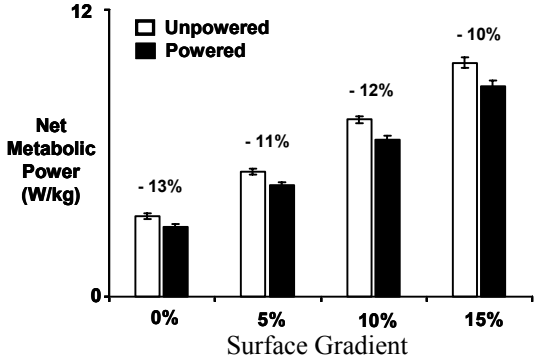

Figure 2. Net metabolic power normalized by subjects' body mass for exoskeleton walking at four different surface gradients (0-15%). Numbers above bars indicate percentage reductions due to mechanical assistance.

CONCLUSIONS

As the demand for positive mechanical power increases with surface gradient, robotic ankle exoskeletons replace a larger proportion of ankle extensor work. However, because of the reduced importance of the ankle on inclines, relative metabolic savings remains independent of surface gradient.

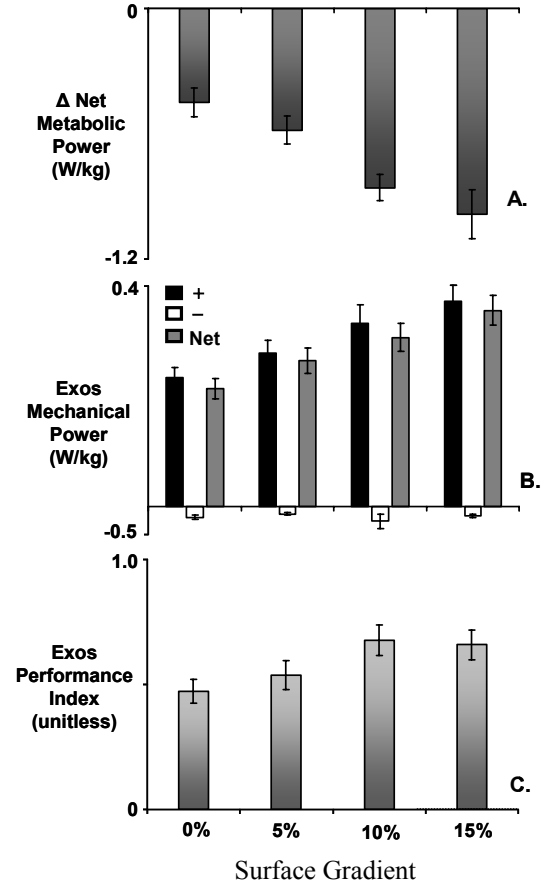

Figure 3. (A) Reduction in net metabolic power (B) exoskeletons average mechanical power (+ black; – white, net gray) and (C) exoskeletons performance index for powered walking at the four surface gradients. All power values are normalized by subject mass. Bars are mean ± s.e.m. A performance index of 1.0 indicates reductions in net metabolic cost that are four times the average positive mechanical power delivered by exoskeletons.

REFERENCE

Sawicki, G.S., Ferris, D.P. (2007). *Proceedings of 31st Annual Meeting of American Society of Biomechanics*.

Supported by NSF BES-0347479 to *DPF*.

STROKE RESUMPTION FOLLOWING FLIP TURNS IN SWIMMING

Bethany Larsen and Richard Hinrichs
Arizona State University, Tempe, AZ, USA
e-mail: hinrichs@asu.edu

INTRODUCTION

Flip turns have become a crucial determinate in the outcome of a swimming competition, constituting up to one third of the total time in some event distances (Blanksby et al., 1996). Recent studies suggest that there is an optimal relationship between glide distance, kick resumption speed, vertical rise path, and stroke resumption speed (Lyttle et al., 1998, 2000). However, these articles make no mention about the form of transition from gliding or kicking to stroke resumption (defined as the initial movement of the hand from the glide position). In front-crawl swimming some swimmers push off on their side and initiate the first pull with the shallow arm (S). Others push off on their side but pull first with their deep arm (D). Still others attain a prone position before pulling with either arm (P).

The purpose of the study was to determine if there was a measurable difference in performance among the three types of stroke transition, as measured by time to, and instantaneous velocity at, 5 m from the turning wall. This study also aimed to identify the influence, if any, each type of transition would have on the other aspects affecting the glide phase of turn; specifically, the glide distance and the vertical ascent from push-off depth to free-swimming depth.

METHODS

Thirty-eight participants (22 currently competitive swimmers and 16 formerly competitive swimmers with an average of 3.65 years since their last competition) volunteered to participate in this study. There were 19 males and 19 females ranging in age from 19 to 56 years with an average age of 29.9 years. All participants provided written informed consent as approved by the ASU Institutional Review Board. An underwater video camera (60 Hz) was used to record the flip turn performances using a two-dimensional version of Challis' (1995) multiphase DLT method. The videos were analyzed to compare the kinematic aspects of the D, S, and P types of transition out of a turn. One point on the body was digitized (mid-hip) per video field using a Motus Motion Measurement System (Peak Performance Technologies, Englewood, CO). The raw data were filtered following the method of Challis (1999). Velocity at 5 m (V_5) was calculated using central differences (Winter, 1990). Time from toe off to 5 m (T_5) was determined from the video to the nearest video field.

Swimmers performed turns under both swimming (subscript S) and gliding (subscript G) conditions. In the swimming condition swimmers transitioned into swimming after the turn. In the gliding condition swimmers glided past 5 m. Following three practice trials of each type, the six different conditions (D_S, D_G, S_S, S_G, P_S, and PG) were performed in random order with one trial per condition per subject. The subjects were to simulate 100-m race pace. If for any reason the swimmer was not satisfied with his or her performance or performed the wrong type of transition, that particular trial was repeated.

The glide and swim trials were entered separately into different two-way MANOVAs with repeated measures (gender × transition type) with transition type as the

repeated measures condition using SPSS v. 13 for Windows (Mapinfo, Troy, NY). Significant main effects were followed up with separate ANOVAs for each measure and subsequent post-hoc t-tests were conducted, and effect sizes analyzed, to compare the individual means.

RESULTS AND DISCUSSION

The MANOVAs revealed no significant gender × transition interactions for any of the dependent variables. Therefore, data from the three transition types were pooled when the genders were compared (see Table 1) and data from both genders were pooled when the three types of transition were compared (see Table 2).

Table 1. Main effects for gender

Variable	Males	Females
T5 glide (s)	2.65 ± 0.52*	3.01 ± 0.49
T5 swim (s)	2.32 ± 0.20*	2.69 ± 0.26
V5 glide (m/s)	0.91 ± 0.27	0.83 ± 0.27
V5 swim (m/s)	1.35 ± 0.26*	1.18 ± 0.21

*males significantly different than females $p<.05$

Table 2. Main effects for condition

Variable	Deep	Shallow	Prone
T5 glide (s)	2.85±0.51	2.85±0.56	2.81±0.56
T5 swim (s)	2.48±0.30	2.50±0.30	2.54±0.29*
V5 glide (m/s)	0.86±0.51	0.82±0.23	0.93±0.29*
V5 swim (m/s)	1.27±0.28	1.24±0.21	1.29±0.26

*prone significantly different than other two, $p<.05$

Males were found to reach 5 m in significantly less time than the females in both the glide and swim trials. There was no significant difference in instantaneous horizontal velocity (V_5) between males and females in the glide trials although there was a trend for males to have higher values. V_5 was significantly higher in the males than females in the swim trials. Instantaneous velocity was significantly higher at 5 m for the P_G than for the D_G and S_G turns, and trended that way for the swim conditions, despite non-significance. There were no significant differences in T_5 between the glide conditions. T_5 was significantly longer for the P_S turn than for the D_S and S_S turns, however this was believed to be a result of participant bias.

SUMMARY/CONCLUSIONS

The prone transition may be superior to the deep and shallow transitions due to a suspected decrease in drag generation as the participant rotates and rises from push-off to free-swimming depth. Deep and shallow transitions arm may be disadvantageous if initiated early after the turn because they would tend to bring the swimmer up to the surface too soon and increase wave drag. Teaching a prone transition offers a cue for swimmers to gauge the "appropriate" amount of time to remain at push-off depth before initiating stroke resumption; effectively reducing wave drag and enhancing velocity once the swimmer reaches the surface.

REFERENCES

Blanksby, B.A. et al. (1996). *Journal of Swimming Research, 11*, 40-45.

Challis, J.H. (1995). *Journal of Applied Biomechanics, 11*, 351-358.

Challis, J.H. (1999). *Journal of Applied Biomechanics, 15*, 303-317.

Lyttle, A.D. et al. (1998). *Journal of Swimming Research, 13*, 15-22.

Lyttle, A.D. et al. (2000). *Journal of Sports Sciences, 18*, 801-807.

Winter, D.A. (1990). *Biomechanics and motor control of human movement*. NY:Wiley.

DESIGN OF SAFE SKI JUMP LANDING SURFACES

Mont Hubbard

University of California, Davis, CA, USA
E-mail: mhubbard@ucdavis.edu, Web: mae.ucdavis.edu/~biosport/

INTRODUCTION

Skiing has slowly evolved in the USA since its strong growth began after WWII. The introduction of snowboards and the move to shorter, more maneuverable skis in the late 1980's have led to the capacity for, and a trend toward, more athletic and acrobatic manifestations of the sport. Terrain parks, including jumps and other man-made features, as opposed to merely groomed slopes, are among the most recent results of this evolution.

With the evolution in style and technique has come a parallel evolution of the types and severity of skiing/snowboard injuries. The snowboard injury rate was more than double that of skiers (Ekeland, et al. 2000) and is probably even higher today. More upper extremity, head and neck trauma exists today and there has been a significant increase in spinal cord injuries (SCI), (Seino, et al. 2001). Although the overall injury rate could still be considered low by some measures, the overall societal costs of SCI's remain very high (Jackson, et al., 2004)

Terrain park features, including jumps, tend to be fabricated. Yet few, if any, standards exist for their construction and at US ski resorts virtually none are designed, in the engineering sense of the word. A few guidelines and rules of thumb occur in industry publications, but no efforts have been made by the industry to consider quantitatively the safety of jumps that already have been made, or to incorporate quantitative considerations into their design.

This work approaches ski jump landing slope design from a fundamental point of view, using a particle dynamic model and neglecting aerodynamic forces in flight.

METHODS

Before the landing surface design can be considered, some measure of (skier or snowboarder) jumper safety must be chosen. One measure commonly used (OSHA, 2007) is *equivalent fall height*, defined as the height corresponding to an impact velocity v acquired in a vertical fall through h in a gravity field of strength g

$$h = \frac{v^2}{2g}$$

Because the coefficient of friction of skis on snow is so small ($\mu \sim 0.05$), when impact occurs between the jumper and landing slope, about 20 times more impulse is imparted to the jumper normal to the slope as along it. This normal impulse, which annuls the component of jumper velocity v_n normal to the slope, generally has the larger capacity for injury and is what must be designed against. The equivalent fall height is then related to v_n by

$$v_n = \sqrt{2gh}$$

Jumps generally have takeoff (the beginning of flight) at the end of an upward linearly sloping takeoff ramp at angle θ_o relative to horizontal. Safe landing slopes are those which limit the equivalent fall height (or equivalently v_n) at impact by choosing the angle ϕ of the landing surface nearly equal

to that of the flight path angle at impact θ according to

$$v_n = \sqrt{2gh} = -v\sin(\theta - \phi) \qquad (1)$$

where v is the speed at impact.

Since the slope of the landing surface is given by $y_s' = \tan(\phi)$ and using the projectile equations to relate conditions at impact to those at takeoff, the landing slope shape $y_s(x)$ can be shown to satisfy a first order ordinary differential equation (ode) of the functional form

$$y_s' = f(y_s, x, \theta_o, g, h) \qquad (2)$$

Solutions result in impact with the slope corresponding to an arbitrarily chosen (safe) equivalent fall height h, for a given a takeoff angle θ_o and for *all* initial velocities v_o. These must be calculated by integrating the ode numerically.

RESULTS AND DISCUSSION

Because any point x,y_s can be a landing point and can be made safe through choice of the landing slope according to (1), the solutions to (2) densely fill the xy plane. Several such solutions are shown in Fig. 1 for equivalent fall height h=1 m and takeoff angle θ_o=25 deg.

Typical safe landing surfaces have monotonically decreasing slopes as a function of x. The ubiquity of the solutions can be used to find good design candidates for a given terrain. The takeoff angle can also be used as a design variable. Although the landing can be made as safe as desired, some tradeoffs must be made with exhilaration, loosely taken to be velocity, flight time, or maximum air height above the surface. The latter two appear to be mostly a roughly linear function of distance jumped on safe slopes.

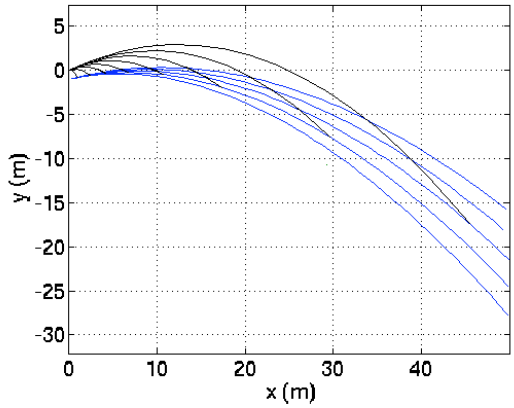

Figure 1: Blue curves are example safe landing slopes $y_s(x)$ with equivalent fall height h = 1 m and takeoff angle θ_o = 25 deg. Black curves are jumper paths for various takeoff velocities v_o.

SUMMARY/CONCLUSIONS

Ski jump landing surfaces can be designed to be arbitrarily safe in the sense that the impact equivalent fall height can be specified. Safe landing surfaces have monotonically decreasing slopes, densely fill the xy plane, and can be used as the basis of a safe landing surface design procedure.

REFERENCES

Ekeland, A. et al. (2005) *J. ASTM Int.*, **2**(5),31-39.

Seino, H. et al. (2001) *Spine*, **26**(11):1294-1297, June 1.

Jackson, A.B. et al. (2004) *Arch. Phys. Med. Rehabil*, **85**(11):1740-1748.

OSHA (2007) http://www.osha.gov/pls/oshaweb/owadisp.show_document?p_table=STANDARDS&p_id=10922

ACKNOWLEDGEMENTS

The author gratefully acknowledges help of, and conversations with, John Kockelman.

EFFECT OF GLUTATHIONE DEPLETION AND AGE ON SKELETAL MUSCLE PERFORMANCE DURING A CHRONIC STRETCH-SHORTENING CONTRACTION EXPOSURE

Robert G. Cutlip, Brent A. Baker, Melinda Hollander, and Michael Kashon
National Institute for Occupational Safety and Health, Morgantown, WV, USA
E-Mail: rgc8@cdc.gov

INTRODUCTION

The age distribution of the workforce in the United States is predicted to shift to older workers (Bureau of Labor Statistics, 1999). We have recently shown in a rat model that aging has a profound effect of the ability of skeletal muscle to adapt to repetitive mechanical loads (Cutlip et al., 2006). Oxidative stress production following high-intensity mechanical loading has been suggested to lead to negative changes in force production (McArdle et al., 2001), especially with aged skeletal muscle. Modulating the oxidative stress profile and quantifying the resulting adaptive response would prove beneficial in broadening our understanding with respect to repetitive-loading induced adaptations.

Glutathione is a major antioxidant in the cell and serves various functions such as directly acting as a reducing agent and recycling radicals generated from other antioxidant molecules. Glutathione depletion can be accomplished using L-Buthionine Sulfoximine (BSO), which is an irreversible inhibitor of γ-glutamylcysteine synthase (GCS). BSO has been well-documented both physiologically and biochemically to chronically deplete levels of glutathione, and animals dosed with BSO would be expected to be more vulnerable to mechanical loading-induced oxidative stress and performance deficits.

The effect of age and glutathione depletion on the ability to adapt to a chronic exposure of stretch-shortening cycles (SSCs) has not been studied. We hypothesized that age and glutathione depletion negatively affects the ability to adapt to repetitive exposures of SSCs.

METHODS

All testing was performed on male Fischer Brown Norway Hybrid rats (F344 x BN F1, N = 32) obtained from the National Institutes on Aging colony. Young adult (N=16, 330g ± 28 g SD, 12 weeks of age) and old (N= 16, 588g ± 32 g SD, 30 months) rats were housed in an AAALAC accredited animal quarters. Young adult (N=8) and old (N=8) animals were dosed with 10mM of BSO in drinking water. The response of the dorsiflexor muscles to isometric and stretch-shortening contractions (SSC) were quantified *in vivo*. Young and old rats underwent exposure to 8 sets of 10 SSCs, 3 times/week, for 4.5 weeks duration. Performance was assessed by isometric testing and dynamic muscle function testing via a single SSC (Table 1).

Table 1. Experimental Protocol

Step	Young BSO and Vehic(N=16)	Old BSO and Vehic (N=16)
1	Isometric Test (90 deg)	Isometric Test (90 deg)
2	1 Stretch-Shortening Contraction **70°-140°-70° ankle angle @ 500 deg/s**	1 Stretch-Shortening Contraction **70°-140°-70° ankle angle @ 500 deg/s**
3	8 sets of 10 intermittent Stretch-Shortening Contractions at **90°-140°-90° ankle angle @ 60 deg/s**	8 sets of 10 intermittent Stretch-Shortening Contractions at **90°-140°-90° ankle angle @ 60 deg/s**
4	Isometric Test (90 deg)	Isometric Test (90 deg)
5	1 Stretch-Shortening Contraction **70°-140°-70° ankle angle @ 500 deg/s**	1 Stretch-Shortening Contraction **70°-140°-70° ankle angle @ 500 deg/s**

The performance parameters used to evaluate the force changes were isometric force, Fmax (i.e, the maximum force

achieved in the eccentric contraction), and negative work (eccentric work). These parameters were generated from the pre-test isometric (step 1) and the pre-test SSC (step 2).

RESULTS AND DISCUSSION

The isometric force of both the young BSO and vehicle group improved over the 4.5 week exposure while the old groups remained static (Fig 1). The peak eccentric force (Fmax) and negative work both showed similar patterns as the isometric force (Figs 2 and 3).

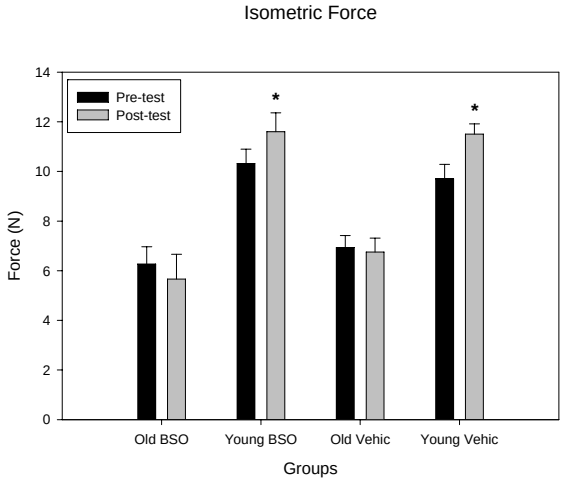

Figure 1: Isometric Force of the old and young BSO and vehicle treated groups.

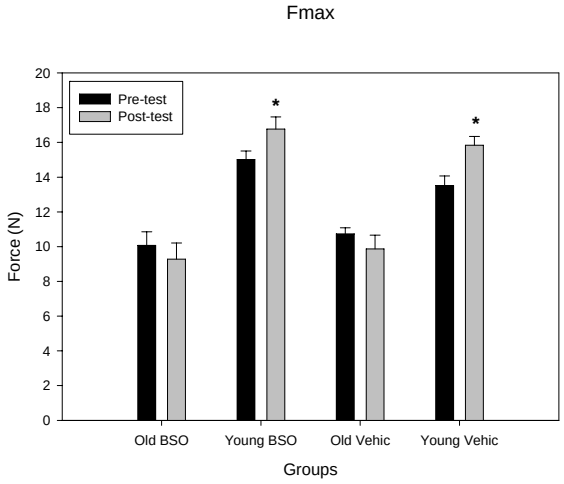

Figure 2: Peak eccentric force of the old and young BSO and vehicle treated groups.

SUMMARY

The young BSO and vehicle groups adapted positively to the chronic exposure while the old animals did not. Glutathione depletion did not have a negative effect on performance in either age group. These results suggest that compensatory mechanisms are age-dependent and allow for adaptation to repetitive mechanical loads even when the glutathione pathway is compromised.

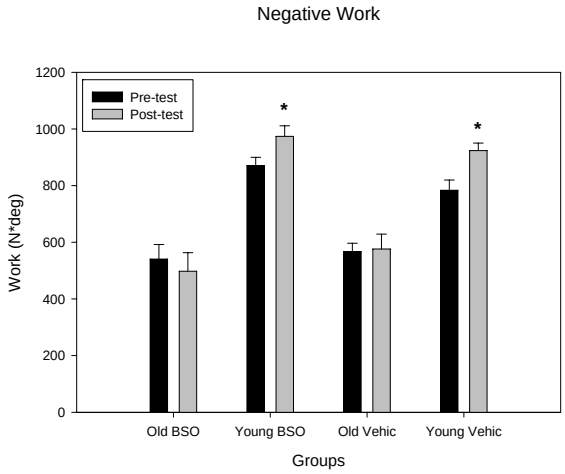

Figure 3: Negative Work of the old and young BSO and vehicle treated groups.

DISCLAIMER

The findings and conclusions in this report are those of the authors and do not necessarily represent the views of the National Institute for Occupational Safety and Health.

REFERENCES

Cutlip RG et al. (2006). Applied Physiology, Nutrition and Metabolism, **31(5),** 573-587.

McArdle A et al. (2001). Am J Physiol Cell Physiol, **280**, 621-627.

Statistics BoL. (1999). [cited; Available from: http://stats.bls.gov/news release/empsit.t12.htm.

KINEMATIC CORRELATES OF THE FREE MOMENT AND COMBINED LOADS DURING RUNNING

Stacey A. Meardon[1], W. Brent Edwards[1], and Timothy R. Derrick[1]

[1] Iowa State University, Ames, IA, USA
E-mail: smeardon@iastate.edu Web: www.hhp.hs.iastate.edu

INTRODUCTION

Stress fractures account for up to15.6% of injuries sustained by runners (Taunton *et al.*, 2002). Recent work has uncovered key biomechanical variables associated with stress fracture in runners. Understanding the relationship between the kinetics and kinematics will aid in the identification of surrogate tests and measures for population based studies.

The free moment is the torsional force about a vertical axis due to friction between the foot and the ground. This moment has been used as an estimate of torsion in the lower extremity and the vertical ground reaction force has been used to estimate axial loads. Both peak absolute free moment and impact peak magnitude have been positively associated with stress fractures in runners (Milner *et al.*, 2005 and 2006).

Combined axial and torsional loads are present during human locomotion (Muller *et al*., 2003) and appear to be more in-phase during the midstance phase of running when compared to the impact phase (Meardon *et al*., 2007). According to recent animal studies, in-phase axial and torsional loads cause a seven-fold decrease in bone's fatigue life (George and Vashishth, 2005).

Altered dynamic hip and knee kinematics have also been reported in persons with a history of stress fracture (Milner *et al*., 2005). The purpose of this study was to identify the key kinematic correlates associated with the free moment and the phase angle of the combined load of the vertical ground reaction force:free moment during impact and midstance phases of running.

METHODS

Four male and three female (22 ± 1.5 years) recreational runners participated in this study. None of the subjects had lower extremity abnormalities that would affect their ability to participate in this study.

Three dimensional kinematic data were collected using a 120 Hz eight-camera motion capture system (Vicon Peak, Centennial, CO). Twenty-three retro-reflective markers were secured on both legs. Ground reaction forces and moments were collected at 1200 Hz.

Participants completed ten trials, striking the force platform with the right limb. All subjects ran at a self-selected 5k race pace and were required to maintain this self-selected pace during each trial (average speed: 3.72±0.34 m/s). Data were exported to Matlab 7.0.4. and smoothed using a low-pass Butterworth filter with a cutoff frequency of 8 Hz for kinematics and 50Hz for kinetics. Three dimensional joint angles of the ankle, knee and hip were calculated using a flexion, adduction, internal rotation order of rotations. Continuous relative phase angles were calculated between the free moment and the vertical ground reaction force at the impact (0-20% stance)

and midstance (40-60% stance) phases of running.

Backward selection regression analyses were performed to identify key kinematic correlates of the free moment and the phase angle of ground reaction force:free moment for both impact and midstance phases of running.

RESULTS AND DISCUSSION

Variables predicted to be associated with the four variables of interest are reported in Table 1. Kinematic variables overall correlated well and accounted for a large portion of the variance of the free moment both at impact and midstance. Univariate analysis revealed that of the predictors in the model summary for in-phase loading in midstance, hip internal rotation had the strongest correlation (0.56). However, a larger portion of the variance associated with in phase loading during impact remains unexplained. Inclusion of velocities or acceleration would most likely improve prediction.

Key kinematic variables associated with stress fracture in female distance runners reported by Milner *et al*. (2005) included hip adduction, knee abduction, and knee internal rotation. The current data indicate that all of these joint angles, with the addition of hip flexion, are strong predictors of the free moment during midstance (Figure 1). Of these joint angles, knee abduction and internal rotation had the highest correlation with the free moment in midstance (0.712, 0.680). Thus, these may be key variables to consider in the development of clinical tests and measures to be used for population studies and in risk factor screening.

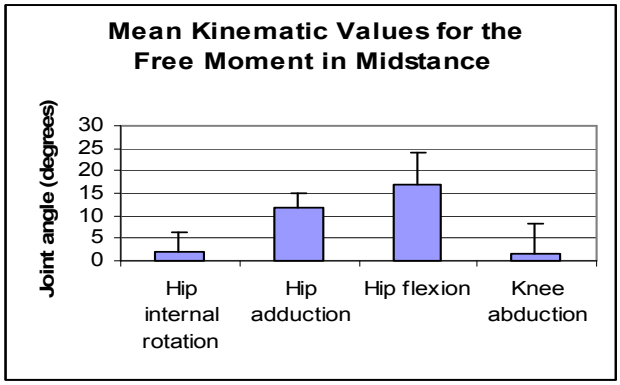

Figure 1.

REFERENCES

Taunton, J. E. *et al.* (2002). *Br. J. Sports Med.,* ***36***(2), 95-101.

Milner, C.E. *et al.* (2006). *Med. Sci. Sports Exer.*, **38**(2), 323-328.

Milner, C.E. *et al.* (2005). *J. Biomech.*, **39**(15), 2819-25.

Milner, C.E. et al. (2005). *Med. Sci. Sports and Exer.*, **37**(5), S346.

Muller, J.A. *et al.* (2003). *Transactions of the 50th Annual Orthopaedic Research Society*, *2004*.

George, W.T. & Vashishth, D. (2005). *J. Biomech.*, **38** , 819–825.

Meardon, S.A. *et al*., (2007). *Combined Sections Meeting of the APTA, 2007*.

Table 1. Backward regression model summaries with associated correlation coefficient (R) and the amount of variance accounted for by the model (R^2) for the outcome variable of interest.

	Model Summary	R	R^2
Peak free moment during impact	peak hip flexion, hip adduction, knee flexion	0.74	0.55
Peak free moment during midstance	peak knee internal rotation, hip adduction, hip flexion, knee abduction	0.89	0.78
Mean phase angle during impact	average knee abduction, hip internal rotation	0.40	0.16
Mean phase angle during midstance	average hip internal rotation, knee flexion, knee abduction	0.62	0.38

INFLUENCE OF LOADING ON KNEE EXTENSOR MECHANICS IN TOTAL KNEE REPLACEMENT: A COMPUTER SIMULATION STUDY

Michael W. Hast, Ryan L. Landon, Stephen J. Piazza
The Pennsylvania State University, University Park, PA, USA
E-mail: *mwh151@psu.edu*

INTRODUCTION

The purported efficiency of the knee extensor mechanism is often used as a benchmark for total knee replacement (TKR) performance. The antero-posterior movement of the tibiofemoral contact points is often taken to be an indicator of knee extensor moment arm, with various authors suggesting that posterior 'rollback' of the femur on the tibia results in reduced demands on the quadriceps (Draganich et al., 1987; Ostermeier et al., 2006). The contact point is equivalent to the center of rotation, however, only in pure rolling contact. The true knee extensor moment arm will depend upon the axis of rotation between the femur and tibia and the geometry of the extensor mechanism (D'Lima et al., 2001). The purpose of this study was to use a computational model to investigate how knee extensor moment arm and the location it the center of rotation vary under different loading conditions.

METHODS

A 12-degree-of-freedom model of a lower extremity with a TKR was placed in three configurations. The first was a supine range of motion (SROM) test in which the ankle was moved toward the hip as passive forces developed in the quadriceps and knee ligaments. The second was a simulated 'Oxford Rig' (OXF) benchtop test in which knee flexion proceeded with a 15 kg mass at the hip and guided by a quadriceps actuator controller, and the third was the same as the second but with a 30 kg mass. A cruciate-retaining knee replacement (Triathlon; Stryker Orthopaedics) was introduced into the model and contact between the components was modeled using a rigid body spring model.

For 'Oxford Rig' simulations, control of quadriceps muscle force was accomplished using a modified version of the computed muscle control (CMC) algorithm presented by Thelen et al. (2003). Quadriceps force was computed using a simplified, two-dimensional, hinged model of the leg along with the CMC control law.

Knee joint angles were computed following the convention of Grood and Suntay (1983). Extensor moment arm length was found by dividing the change in muscle length by the change in joint angle throughout each simulation. Finite helical axes were calculated for each trial in ten degree increments.

RESULTS AND DISCUSSION

Knee extensor moment arms were found to be greatest in near extension and to decrease with knee flexion for all loadings (Figure 1). This pattern is consistent with moment arms measured in natural knees by several previous investigators (e.g., Draganich et al., 1987). The load carried during OXF

simulations did not affect moment arm, but moment arms for SROM were slightly smaller than those measured for OXF at higher flexion angles.

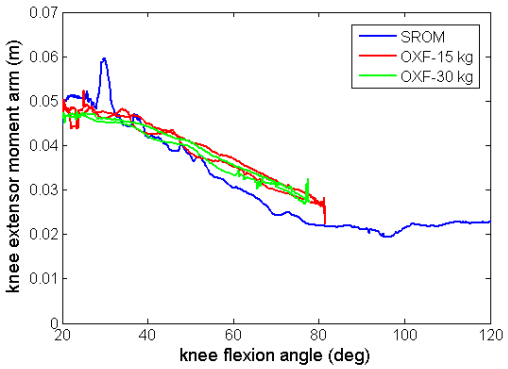

Figure 1: Knee extensor moment arm plotted versus knee flexion angle for all three loading conditions.

Finite helical axes were generally oriented mediolaterally, but the locations of the finite helical axes were found to vary somewhat with flexion angle. As flexion increased, the axis moved posteriorly, especially in the SROM configuration (Figure 2), and the axis moved inferiorly with flexion (Figure 3), again with greater axis movement in the lightly-loaded SROM tests. This movement of the knee's axis of rotation is consistent with the reduced moment arm seen in the SROM simulation (Figure 1): When the knee is flexed, inferior and posterior motion of the axis of rotation will bring the axis closer to the extensor mechanism.

SUMMARY/CONCLUSIONS

Investigations of the determinants of knee extensor efficiency are important for improving knee implant designs and functional outcomes following TKR. Modeling tools may be valuable for predicting the influence of implant design upon knee extensor mechanics, especially when evaluated under varied loading conditions.

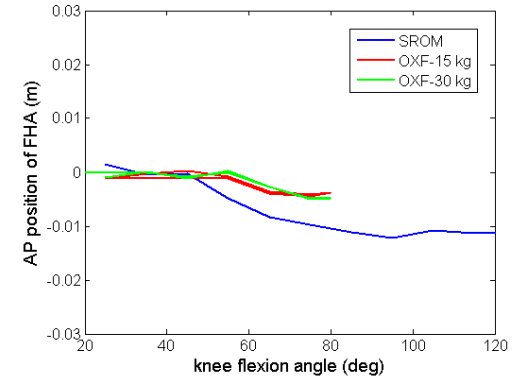

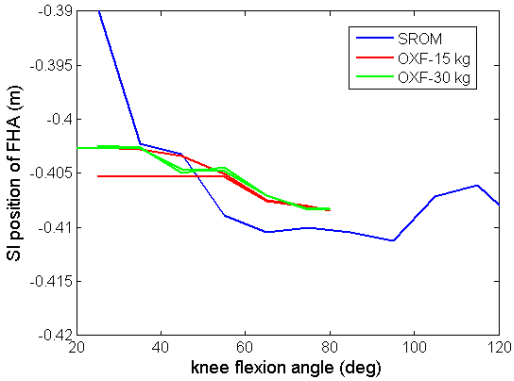

Figure 2 and 3: Location of the finite helical axis plotted versus knee flexion angle.

REFERENCES

Dranganich LF, et al. (1987). *J. Orthop Res,* **5(4),** 539-47.

Ostermeier S, et al. (2006). *Knee*, **14,** 934-39.

D'Lima DD, et al. (2001). *CORR,* **392,** 213-20.

Thelen DG, et al. (2003). *J. Biomech,* **36,** 321-28.

Grood ES, Suntay WJ. (1993). *J. Biomech Eng,* **105,** 136-44.

ACKNOWLEDGMENTS

This work was supported in part by Styker Orthopaedics.

COMPARISON OF THE PLANTARFLEXION MOMENT ARMS OF LATERAL GASTROCNEMIUS BETWEEN SPRINTERS AND NON-SPRINTERS

Sabrina S.M. Lee and Stephen J. Piazza

The Pennsylvania State University, University Park, PA, USA
E-mail: *sul167@psu.edu*

INTRODUCTION

Effective sprinting requires high ankle power and faster ankle rotation which may be facilitated by differences in Achilles tendon moment arm between sprinters and non-sprinters. Elite sprinters often exhibit initial contact with the forefoot (Novacheck et al., 1998) ad it may be the case that musculoskeletal adaptations occurring in response to sprint training are similar to those accompanying equinus gait in cerebral palsy or stroke. Sagittal plane moment arms have been measured previously in the sagittal plane in healthy individuals (Maganaris et al., 1998a,b; Rugg et al., 1990), but have not been investigated in other populations, such as sprinters.

The purpose of this study was to investigate the differences in sagittal-plane Achilles tendon moment arm between sprinters and non-sprinters. Because it has been shown that Achilles moment arms may depend on the level of muscle activity (Maganaris et al., 1998), measurements were made with the subjects at rest and with the triceps surae contracted.

METHODS

Moment arms of the lateral gastrocnemius were measured in 8 male collegiate sprinters and 8 height-matched male non-sprinters who gave informed consent prior to testing. Tendon excursion was measured using B-mode ultrasonography (Aloka 1100; transducer: SSD-625, 7.5 MHz) and plantarflexion-dorsiflexion angle was measured using a potentiometer-instrumented rotating foot platform. Tendon excursion and ankle angle were measured as the foot was rotated from 15° dorsiflexion to 30° plantarflexion. Two levels of muscle activity, rest and light contraction were tested. Moment arm was calculated by evaluating the analytical derivative of a first-order polynomial fit to tendon excursion versus angle data (Figure 2). Two-way ANOVA was performed, with factors of subject group and muscle activity level. Tukey post-hoc comparisons were made to determine if significant differences in mean moment arm existed between groups and muscle activity levels.

RESULTS AND DISCUSSION

Significant differences were found between the sagittal-plane moment arms of sprinters and non-sprinters ($p < 0.001$) (Figure 1). In addition, moment arms were significantly different between rest and light contraction for both sprinters and non-sprinters ($P < 0.001$) (Figure 1). Post-hoc mean comparisons indicated that in non-sprinters, moment arms under light contraction were significantly greater than those found at rest ($p = 0.001$) and were significantly greater than those of the sprinters at rest and light contraction ($p < 0.001$ and $p = 0.001$).

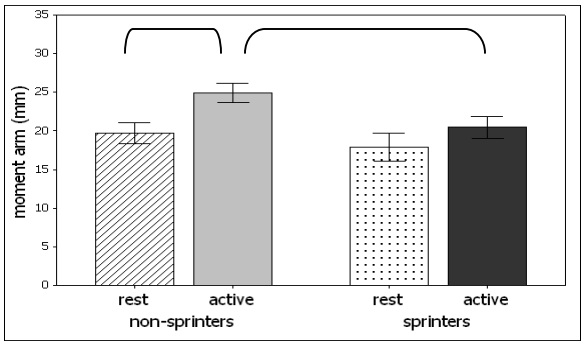

Figure 1. Mean moment arms of non-sprinters and sprinters at rest and at light contraction. Error bars indicated plus and minus one standard error. Asterisks indicate significant differences ($p < 0.05$).

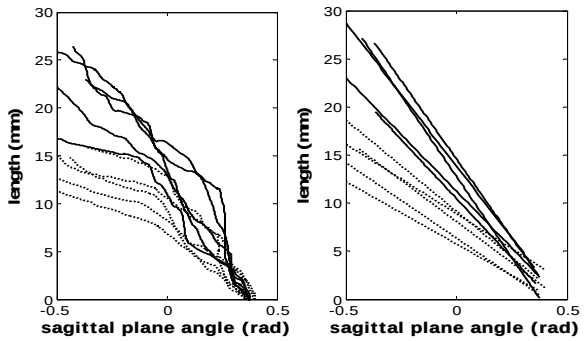

Figure 2. Typical a) raw length-angle data and b) fit data for ten trials of one subject. Solid lines indicate trials with the muscle at rest and dotted lines indicate trials with muscle lightly contracting. Positive angle indicates dorsiflexion.

The reasons for the moment arm differences between sprinters and non-sprinters are unclear, but may be related to musculo-skeletal adaptations in response to sprint training or may be a manifestation of increased tendon slack length in sprinters. Smaller plantarflexor moment arms may permit sprinters to produce rapid forefoot movement at push-off without large changes in muscle fiber length.

Differences in Achilles tendon moment arm between rest and contraction have been attributed to increased thickness of the plantarflexor muscle mass with contraction which shifts the Achilles tendon posteriorly (Maganaris et al., 1998a, 1998b). This theory may not explain the moment arm differences found in this study, however, as it is likely that the sprinters would have larger gastrocnemius muscles than non-sprinters and this have larger moment arms in the active condition. An alternate explanation may be that there is anterior excursion of the center of rotation with contraction as suggested by Maganaris et al. (1998a). It is possible that in non-sprinters this excursion is larger than in sprinters, which may explain the larger difference between moment arms at rest and during contraction.

SUMMARY/CONCLUSIONS

The sagittal plane moment arms of lateral gastrocnemius were smaller in sprinters than non-sprinters. These differences may be indicators of musculoskeletal adaptations that enhance sprint performance, but further work is necessary to minimize the influence of confounding factors.

REFERENCES

Maganaris, C.N. et al. (1998). *J Physiol*, **510**, 977-985.

Maganaris, C.N. et al. (1998b). *J Physiol*, **512,** 603-614.

Novacheck, T.F. (1998) *Gait and Posture*, **7,** 77-95.

Rugg, S.G. et al. (1990). *J Biomech*, **23,** 495-501.

ACKNOWLEDGMENTS

The authors would like to acknowledge Tamara Cohen for help with data collection. This work was supported by NSF BES-013421

ANALYTICAL EXPRESSION OF MUSCULOTENDON MODEL INCLUDING VISCOELASTIC PROPERTIES OF TENDON

Miloslav Vilimek [1]

[1]Czech Technical University in Prague, Prague, Czech Republic;
E-mail: Miloslav.vilimek@fs.cvut.cz Web: www.biomechanics.cz

INTRODUCTION

This paper presents a musculotendon model for muscle force calculation based on Hill type model including viscoelastic properties of tendon. Usually the two approaches for expression the tendon behavior during tension are being used. One of them is the linear model of stress-strain curve without both the toe region and the upper part of the curve with macroscopic failures. Second usual way is to use analytical equation for describing the length tension curve given from experiments (Delp et al., 1995 and Buchanan et al., 2004). These models are usually independent on velocity of loading, which means it does not describe the different length-tension curves in different velocity of muscle shortening.

METHODS

The three-part Poynting-Thomson model of viscoelastic behavior of material, (Figure1), was used for uniaxial tension, (1). From the stress-strain curves of tendons, from the stress-strain data measured during creep and relaxation respectively, the viscous, η, and elastic parameters, E_1 and E_2, of the model were calculated. This equation was arranged into the expression with time derivative tendon force and time derivative tendon length dependency (2). The A, B, C are viscoelastic constants of the model (3).

$$\frac{\eta}{E_1}\cdot\frac{d\sigma}{dt}+\sigma\cdot\left(1+\frac{E_2}{E_1}\right)=\eta\cdot\frac{d\varepsilon}{dt}+E_2\cdot\varepsilon \quad (1)$$

$$\frac{dF^T}{dt}=\frac{A^T\left(L^T-L_s^T\right)}{L_s^T}\cdot A+F^T\cdot B+\frac{dL^T}{dt}\cdot\frac{A^T}{L_s^T}\cdot C \quad (2)$$

$$A=\frac{E_1E_2}{\eta};\quad B=-\frac{\left(E_1+E_2\right)}{\eta};\quad C=E_1 \quad (3)$$

$$\frac{dL^T}{dt}=\frac{dL^{MT}}{dt}-\frac{dL^M}{dt}\Big/\cos(\alpha) \quad (4)$$

$$F^T=F_0^M\left(f_v f_L^a f_{act}+f_L^p\right)\cdot\cos(\alpha) \quad (5)$$

$$f_v \Rightarrow \frac{dL^M}{dt} \quad (6)$$

The other musculotendon parameters are tendon crossectional area, A^T, and tendon slack length, L^T_s. The F^T express tendon force acting into the bone and L^T is instantaneous tendon length.

The equation (4), express the dependency between velocity of tendon elongation, dL^T/dt, velocity of elongation of musculotendon, dL^{MT}/dt, and velocity of muscle shortening/lengthening, dL^M/dt. The parameter α is the pennation angle. The musculotendon length, L^{MT} (velocity, dL^{MT}/dt), is the measuredable parameter between muscle attachments into the bone.

The velocity of muscle shortening dL^M/dt can be obtained from equation (5) including force-velocity factor, f_v (6), (Zajac, 1989). The f_L^a is the active force-length factor, the f_{act} express muscle activation. The f_L^p is the passive force-length factor of the muscle. The parameter tendon slack length is

difficult to measure and for first approach can be theoretically calculated, for example from (Vilimek, 2006).

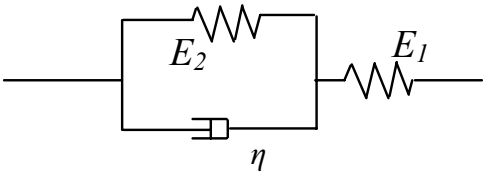

Figure 1: The Poynting-Thomson model of viscoelastic behavior of tendon. From the stress-strain curves of tendons the viscous, η, and elastic parameters, E_1 and E_2, of the model, were obtained experimentally.

RESULTS AND DISCUSSION

The Poyting-Thomson model do not assumes relaxation of material. For a musculotendon modeling it can be used because it is assumed that during 'normal' locomotion the tendons do not relax and have extension up to the 4-5% of strain. This model of tendon appears to be dependent of strain rate during locomotion. The musculotendon model, (2) and (5), including the viscoelastic properties of tendons need experimentally set up the constants A, B, C and cross-sectional area, A^T, tendon slack lengths, L^T_s, of each tendon. The knowledge of muscle belly parameters is also mandatory.

This musculotendon model (2) to simulation of pedaling was applied. The lower extremity musculoskeletal model including 31 muscles was used for this application. The shapes of obtained muscular forces were smoother than muscular forces obtained by muscular model without tendon dynamics. The maximum differences between the both models are in start and end of movement, where velocity of pedaling was significantly changed.

Also in elbow flexion/extension movement simulations the model including tendon dynamics was used. As well as the pedaling simulation the shapes of musculotendon forces are smoother.

Very interesting is using this model for studying the muscular forces during isometric and eccentric contraction. Especially in the cases with and without including viscoelastic properties of tendon (inside the Hill type model) is possible to study the difference in force acting into the bone.

SUMMARY/CONCLUSIONS

The described Hill type model of musculotendon actuator include a viscoelastic properties of tendon. The described model of tendon gives more realistic results in tendon behavior during loading. This model is good to use in musculoskeletal modeling for simulation of forward dynamics problems.

REFERENCES

Delp, S.L., Loan, J.P., (1995). *Comput. Biol. Med.,* **25**, 21-34.

Buchanan, et al.. *J Apl Biomech* **20**, 367-395, 2004.

Zajac, F.E., (1989). *Critical Reviews in Biomedical engineering,* **17**, 359-411.

Vilimek, M., (2006). *Proceedings of ASB2006 Meeting,*Abstract 46 ,2006.

ACKNOWLEDGEMENTS

This research study was supported by grant MSM 6840770012 and GACR 106/06/P304.

PATELLOFEMORAL FORCE AND STRESS BETWEEN FORWARD AND SIDE LUNGES WITH AND WITHOUT A STRIDE

Rafael F. Escamilla[1], Naiquan Zheng[2], Alan Hreljac[3], Rodney Imamura[3], Toran D. MacLeod[1], William B. Edwards[4], Glenn S. Fleisig[5], Kevin E. Wilk[6]

[1]Department of Physical Therapy, California State University, Sacramento, USA
[2]Department of Orthopaedics and Rehabilitation, University of Florida, Gainesville, FL, USA
[3]Kinesiology and Health Science Department, California State University, Sacramento, USA
[4]Department of Health and Human Performance, Iowa State University, Ames, Iowa, USA
[5]American Sports Medicine Institute and [6]Champion Sports Medicine, Birmingham, AL, USA
e-mail: rescamil@csus.edu

INTRODUCTION

It is currently unknown how patellofemoral force and stress change between forward and side lunges with a forward stride (and return back to starting position) and without a stride (stationary position). The purpose of this study was to compare patellofemoral force and stress between the forward and side lunge with and without a stride. It was hypothesized that patellofemoral force and stress would increase as knee flexion increased, would be greater with a stride compared to without a stride, and would be greater in the forward lunge compared to the side lunge.

METHODS

Eighteen subjects (9 males and 9 females) were used with an average age, mass, and height of 29±7 y, 77±9 kg, & 177±6 cm for males and 25±2 y, 60±4 kg, & 164±6 cm for females. Each subject performed the forward and side lunge with a long stride (knee over ankle at maximum knee flexion) both with and without a stride. Intensity was normalized for each exercise by having each subject their 12 repetition maximum weight, which were 49±10 kg for males and 32±7 kg for females for the forward lunge, and 55±9 kg for males and 36±9 kg for females for the side lunge. Surface electrodes were placed over the vasti muscles, rectus femoris, medial & lateral hamstrings, and gastrocnemius. Reflective markers were positioned over landmarks on the foot, ankle, knee, hip, and shoulder.

Video (60 Hz), EMG & force platform (960 Hz) data were collected during 3 repetitions of each exercise (0-90° knee flexion) and averaged. EMG data were normalized by maximum voluntary isometric contractions (MVIC).

Patellofemoral force & stress were calculated using a biomechanical knee model (Zheng et al., 1998; Salsich et al., 2003) with input variables consisting of resultant knee forces and moments, patellofemoral contact areas, and the muscle force function $F_{m(i)} = {}_{i}k_iA_i\sigma_{m(i)}[EMG_i/MVIC_i]$, where k_i was a muscle force-length variable, A_i was physiological cross sectional area (PCSA) per muscle, $\sigma_{m(i)}$ was MVIC force per unit PCSA, EMG_i and $MVIC_i$ were EMG window averages, and c_i was a weight factor adjusted in a computer optimization program. Patellofemoral force and stress as a function of lunge type and stride variation were assessed by a two-way repeated measures analysis of variance ($p < 0.01$) every 10° between 0-90°.

RESULTS AND DISCUSSION

Patellofemoral force and stress curves are shown in Figures 1 and 2. Both patellofemoral force and stress increased progressively as knee flexion increased. Between 60-0° patellofemoral force and stress were significantly greater in the forward lunge with stride compared to the side lunge with stride, but no differences were observed between the forward and side lunge without a stride. Between 50-0° patellofemoral force and stress were significantly greater in the forward lunge with stride compared to the

forward lunge without stride, but no differences were observed between the side lunge with and without a stride.

SUMMARY/CONCLUSIONS

Patellofemoral force and stress increased with knee flexion, was greater with the forward lunge with stride compared to the forward lunge without stride, and was greater in the forward lunge with stride than the side lunge with stride.

REFERENCES

Salsich et al. (2003), *Clinical Orthopaedics*, **417**, 277-284.

Zheng et al. (1998), *Journal of Biomechanics*, **31**, 963-967.

ACKNOWLEDGEMENTS

The authors would like to thank Lisa Bonacci, Toni Burnham, Juliann Busch, Kristen D'Anna, Pete Eliopoulos, & Ryan Mowbray for all their assistance during data collection and analyses.

Figure 1. Mean (SD) patellofemoral compressive force during forward and side lunges with and without a stride.

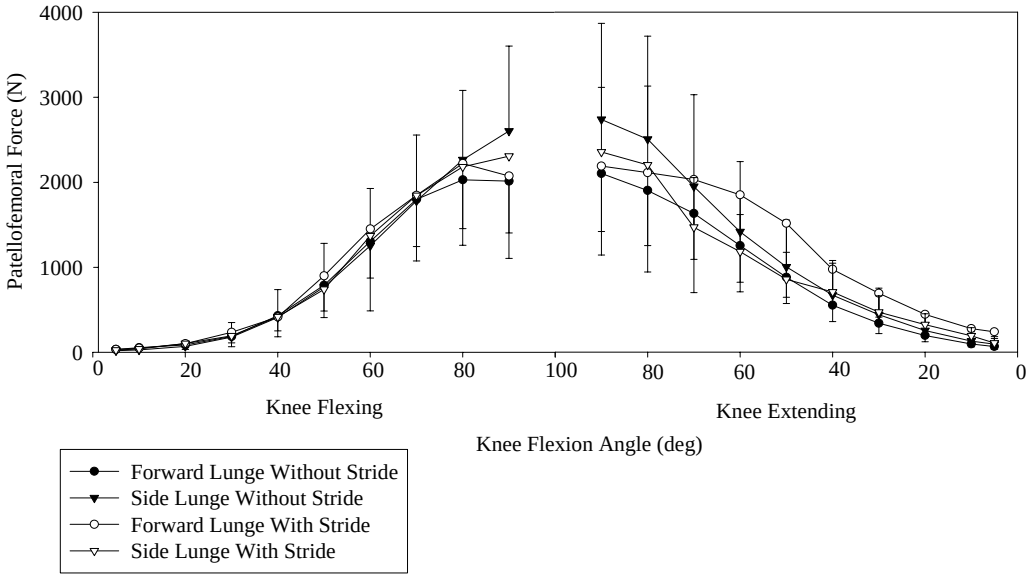

Figure 2. Mean (SD) patellofemoral stress during forward and side lunges with and without a stride.

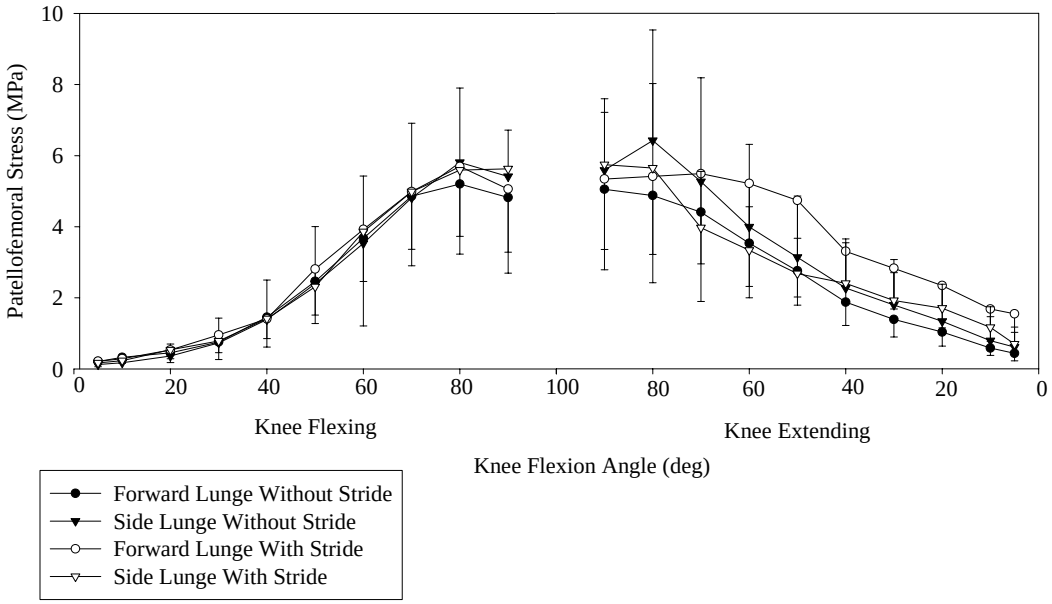

Improving models of motor unit function is best done by refining their neural mechanisms

Kevin G. Keenan and Francisco J. Valero-Cuevas
Cornell University, Ithaca, NY, USA
E-mail: fv24@cornell.edu

INTRODUCTION

Computational models of motor unit populations are implementations of the mechanisms by which neural and muscle properties are hypothesized to give rise to EMGs and force. The degree to which a model replicates experimental relations assesses how well those equations reflect the underlying mechanisms and our hypotheses of neuromuscular function. We examined the ability of the most popular motor unit model (Fuglevand et al., 1993) to replicate the scaling of EMG amplitude (Milner-Brown and Stein, 1975) and force variability (Jones et al. 2002) with mean force level.

METHODS

Our simulations are based on the forward model of recruitment of a population of motor units and production of muscle force (Fuglevand et al., 1993), with the addition of an EMG model (Farina and Merletti, 2001) that simulates the surface EMG with a planar volume conductor with muscle, fat, and skin tissues. Monte Carlo methods use repeated simulations where the specific value of each free model parameter (Table 1) is assigned by random chance from a uniform distribution (Valero-Cuevas et al., 2003). As previously described (Keenan et al., 2006) each iteration involves determining the recruitment and discharge times of a population of motor neurons (for six levels of excitatory drive), simulating the surface EMG by summing the trains of motor-unit potentials, and simulating muscle force by summing motor unit forces. Upon convergence, Monte Carlo simulations show possible model outputs as distributions of average full-wave rectified EMG amplitudes, and mean and SD of force considering the reported variability and uncertainty in motor unit parameters.

Table 1. Model parameters and the range for their uniform distributions.

Parameters	Type	Range
1) Number of motor neurons	N	150 - 500
2) Range in innervation numbers	N	1-100x
3) Recruitment range*	N	Up to 30 – 80% maximal excitation
Peak discharge rate:		
4) First recruited neuron*	N	25 – 50 pulses/s
5) Last recruited neuron*	N	25 – 50 pulses/s
6) Number of fibers	M	50,000 – 250,000
7) Fiber length	M	4 – 16 cm
8) Mean conduction velocity	M	3 – 4 m/s
9) Conduction velocity spread	M	0 – 0.5 m/s (SD)

*Model is sensitive to these parameters.
N: Neural properties; M: Muscle properties

Two fitness criteria quantified the match between simulated and experimental EMG/force and force/force-variability relations. First, we chose a slope of the log-log regression line between SD and mean force > 0.75 and < 1.25 to indicate a linear (slope = 1) scaling consistent with Signal Dependent Noise (Jones et al., 2002). Second, we chose a slope in the regression line between EMG and force of < 1.05 as a liberal estimate of a match with experimental observations (Milner-Brown and Stein, 1975).

RESULTS AND DISCUSSION

Monte Carlo simulations converged after 439 iterations, but only 3 simulations approximate the experimental relations for force/force-variability and EMG/force (Fig. 1). There was a tendency to tradeoff satisfying both fitness criteria (Fig. 1C).

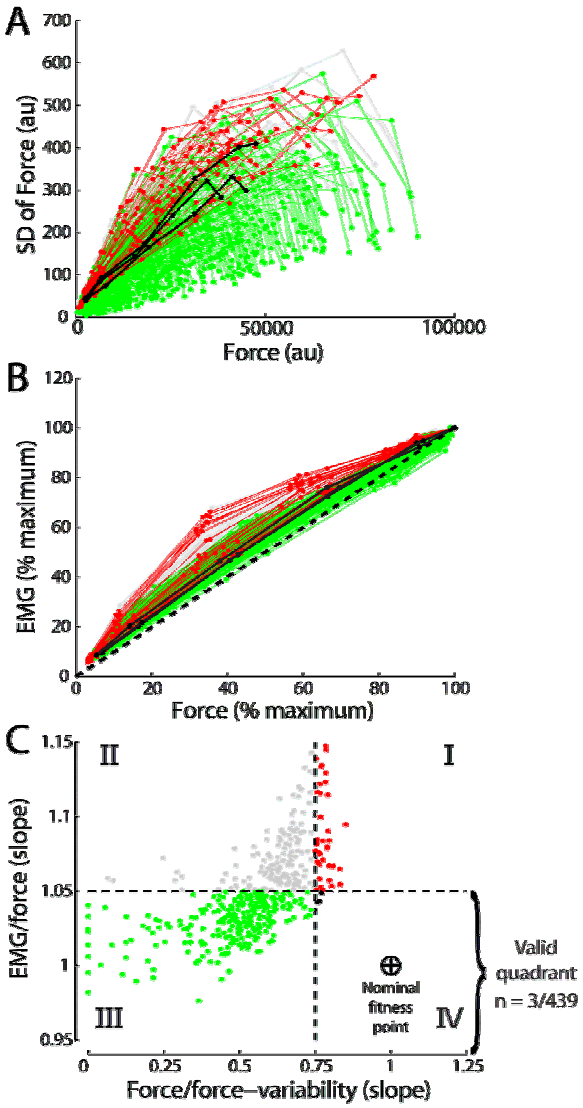

Figure 1: The model showed a predominant non-linear scaling of force variability (*A*, green) and EMG (*B*, red) with mean force across 6 excitation levels, in contrast to experimental observations. Experimental EMG/force and force/force-variability relations were replicated for only 3 of 439 Monte Carlo iterations (*A*, *B*, & *C*, black). The nominal fitness point represents the linear scaling (slopes = 1) of force variability and EMG with mean force.

A second set of 424 simulations, sampling preferentially from the neighborhood of the parameter values that produced the 3 valid simulations, converged to reveal 65 additional sets of parameter values for which the model predictions approximate the experimentally known relations. For these 68 valid simulations, the model is not sensitive to muscle properties, but very sensitive to several motor neuron properties—especially peak discharge rates and recruitment ranges (* in Table 1). Sensitivity is defined here as spanning a narrow range of values (< 50%) for valid simulations relative to full ranges in Table 1.

SUMMARY/CONCLUSIONS

Because the model is mostly sensitive to a few motor neuron properties, advancing our understanding of EMG and muscle force is best done by critically evaluating the hypothesized neural mechanisms as implemented in today's state-of-the-art models of motor unit function.

REFERENCES

Farina D, Merletti R (2001). *IEEE Trans Biomed Engin*, 48:637.

Fuglevand AJ, Winter DA, Patla AE (1993). *J Neurophysiol*, 70:2470.

Jones KE, Hamilton A, Wolpert DM (2002). *J Neurophysiol*, 88:1533.

Keenan KG, Farina D, Merletti R, Enoka RM (2006). *J Appl Physiol*, 100:1928.

Milner-Brown HS, Stein RB (1975). *J Physiol*, 246:549.

Valero-Cuevas FJ, Johanson ME, Towles JD (2003). *J Biomech*, 36:1019.

ACKNOWLEDGEMENTS

Grant Nos. AR050520 and AR052345 from the NIH, and NSF CAREER Award BES-0237258 (to F.J. Valero-Cuevas).

A BIOMECHANICAL STUDY OF VERTEBRAL ALLOMETRY IN PRIMATES

Andrew L. Schifle[1], Leah C. Anderson[1], David A. Loomis[1], Charles Kunos[3], Bruce Latimer[2], Christopher J. Hernandez [1,2]

[1] Case Western Reserve University, Cleveland, OH, USA
[2] Cleveland Museum of Natural History, Cleveland, OH, USA
[3] University Hospitals of Cleveland, Cleveland, OH, USA
E-mail: axs186@case.edu Web: mae1.cwru.edu/mmm/

INTRODUCTION

Comparative analysis of the skeleton is fundamental to the study of human evolution. Although many studies have examined the relationship between bone size/biomechanics and animal body weight in the long bones (McMahon 1975, Selker 1989), little is known regarding allometry in the spine. Our overall goal is to understand biomechanical variation in the spine among species. In this study, we determine **1)** how vertebral bone strength (as evaluated from measures of structural ridigity) varies with body weight among primates, and **2)** how mechanical efficiency (represented by the ratio of bone strength to bone mass) of vertebrae varies among primates.

METHODS

Adult thoracic (T8) vertebral specimens were selected from four species: human (*Homo sapien*), gorilla (*Gorilla gorilla*), chimpanzee (*Pan troglodyte*), and gibbon (*Hylobates lar*) (n=10 per species; 5 female, 5 male). All specimens were obtained from the Hamann-Todd osteological collection at the Cleveland Museum of Natural History. Human specimens ranged in age at death from 23-40 (31.7 ± 5.9, mean ± SD). Non-human primate specimens were skeletally mature. Body weight for human, gorilla, and chimpanzee specimens was determined from measures of femoral head volume (Ruff 1988). Body weight for gibbons was determined from femoral head diameter (McHenry 1992).

QCT scans were obtained for biomechanical analysis. Vertebrae were submerged in a 20% ethanol solution and placed under a vacuum to remove air bubbles. Axial scans were performed on a Siemens Somatom Sensation 16 QCT scanning machine (140kV, 120mA, 0.75mm slice thickness). A liquid K_2HPO_4 mineral content calibration phantom was used to determine density per voxel (ρ_{QCT}, mg/cm^3). Volumetric bone mineral density (vBMD) was computed for each vertebral body including endplates and cortex. Total bone mineral content (BMC) of the vertebral body was used as a measure of bone mass.

Structural rigidity was used as an assay of bone strength. The elastic modulus of each voxel was determined from published relationships between ρ_{QCT}, ash density, and elastic modulus (Keyak 1994, Keller 1994). The axial and anteroposterior bending rigidity of each transverse slice of the vertebra was calculated using composite beam theory (Whealan 2000, Crawford 2004). The minimum values of rigidity in each loading mode were used as indicators of bone strength, S_{axial} and $S_{bending}$. Mechanical efficiency was evaluated as the ratio of strength to bone mass (S_{axial}/BMC and $S_{bending}$/BMC, Hernandez 2006).

RESULTS AND DISCUSSION

Animal body weight spanned two orders of magnitude (6-201 kg). The axial strength increased linearly with body weight (r^2=0.82, p<0.001, Figure 1). Bending strength also increased with body weight following a power-law relationship with an exponent of 1.5 (r^2=0.95, p<0.001). Mechanical efficiency in axial compression (S_{axial}/BMC) was found to be smaller in animals with larger body weight (r^2=0.56, p<0.001, Figure 2). Conversely, mechanical efficiency in bending ($S_{bending}$/BMC) increased with body weight following a power-law relationship (r^2=0.82, p<0.001).

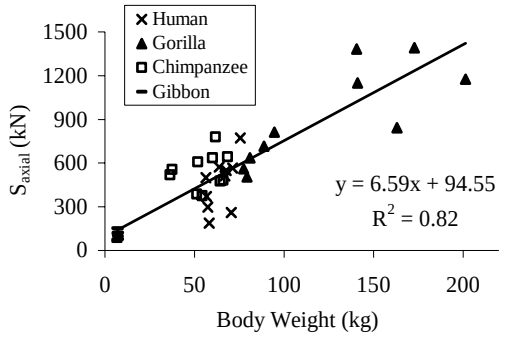

Figure 1: Strength in axial compression follows a linear relationship with body weight in human and non-human primates.

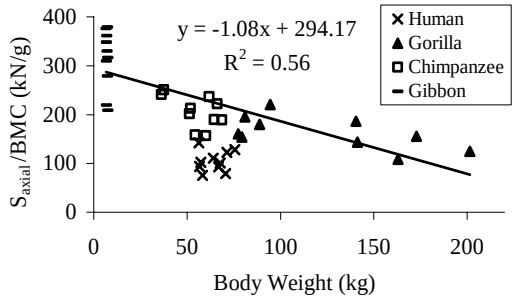

Figure 2: Mechanical efficiency in axial compression was reduced in larger animals.

In humans, mechanical efficiency in axial loading was reduced compared to non-human primates with similar body weight (p<0.001). The volumetric bone mineral density of human vertebra was significantly less than that in non-human primates (p<0.001).

SUMMARY/CONCLUSIONS

Allometric relationships are useful for accounting for differences in size while comparing species. In this study we determined the allometric relationships between vertebral bone strength and body weight in human and non-human primates. Furthermore, our analysis suggests that as primates increase in size, vertebral bone mass is utilized more efficiently in bending, but less efficiently in axial compression. The reduction in axial mechanical efficiency appears to be more pronounced in humans than in other primates of similar body weight, potentially because humans show reduced overall volumetric bone mineral density. Reduced bone density and mechanical efficiency in axial loading may help to explain why humans are susceptible to age related fractures in the spine, which are not observed in other primates.

REFERENCES

Crawford, R.P., Keaveny, T.M. (2004). *Spine*, **29**, 2248-2255.

Keller, T.S. (1994). *J. Biomech*, **9**, 1159-1168.

Keyak, J.H. et al. (1994). *J. Biomed Mater Res*, **11**, 1329-1336.

McHenry, H.M. (1992). *Am J Phys Anthropol*, **87**¸407-431.

McMahon, T.A. (1975). *Am Nat*, **109**, 547-563.

Ruff, C.B. (1988). *J. Hum Evol*, **17**, 687-714.

Selker, F., Carter, D.R. (1989). *J. Biomech*, **22**, 1175-1183.

Whealan, K.M. et al. (2000). *J Bone Joint Surg Am*, **82**, 1240-1251.

The transition between muscle coordination patterns is context dependent

Flor Alicia Medina, Madhusudhan Venkadesan, Kevin Keenan, Robert V. McNamara III, Sherry L. Backus*, Stanley Song, Carolyn Price , Francisco J Valero-Cuevas
Neuromuscular Biomechanical Laboratory, Cornell University, Ithaca, NY
*The Hospital for Special Surgery, New York, NY
E-mail: fam28@cornell.edu, fv24@cornell.edu

INTRODUCTION

The mechanical constraints for the production of finger motion and static force differ, thus joint torques and muscle coordination patterns to produce them should also differ [1]. We hypothesize that the transition between those coordination patterns should depend on the accuracy of the task. To test this hypothesis we investigated finger tapping: the abrupt transitions from motion to static force. We find that the coordination patterns for motion and force differed. Modeling the transition of the coordination patterns as a sigmoid function shows that the initiation is advanced in time when the task requires greater accuracy. This is the first study to show the tuning of complete muscle coordination patterns during a skillful everyday task.

METHODS

Eight consenting and healthy young adults rapidly transitioned from accurately moving the fingertip towards a flat target surface to producing an isometric force against it (i.e., tapping) while wearing a thimble defining a point contact [2]. Subjects tapped the horizontal surface of two pedestals: "smooth" (polished steel) and "small" (5 mm diameter) vs. "rough" (300-grit sandpaper) and "large" (11 mm diameter). The former required greater accuracy for both fingertip motion and force. Each trial consisted of 4 brief preparatory taps, followed by a tap-ramp-and-hold task where subjects ramped force magnitude and held it at maximal voluntary magnitude.

We simultaneously recorded fine wire EMG from all seven muscles of the index finger during the task [2]; and characterized the coordination pattern as the time varying 7-D unit vector of muscle forces estimated from the full-wave rectified, band-pass filtered, normalized (by MVC) EMGs weighted by physiological cross sectional areas. The temporal evolution of the coordination pattern vectors was quantified by the alignment (included angle) with respect to the reference coordination pattern defined during 80 ms of maximal static force [1]. Fig. 1 shows the evolution of the alignment from -500 to +500 ms before and after contact, respectively, for a sample trial.

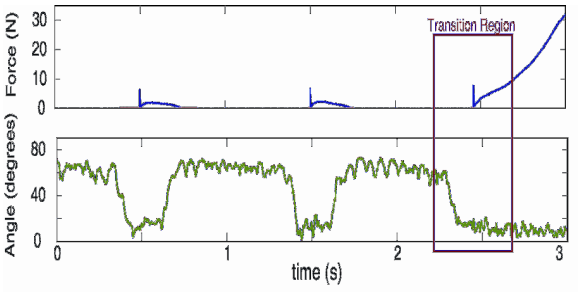

Figure 1: Coordination pattern alignment during a complete trial: preliminary taps and the tap-ramp-and-hold task.

RESULTS AND DISCUSSION

The coordination patterns for motion and force production were distinct, as shown by changes in coordination pattern (i.e., unit vector) alignment by >60 degrees (Fig. 1).

A sigmoid function characterizes and fits well the coordination pattern transition, normalized by the included angles at -500

ms and +500 ms. The average coefficient of determination ± SE was r^2 = 0.76±0.2, N=36 trials. When considering the constraints set by target texture and size, the model fits the rough-large case significantly better (average r^2 of 0.84±0.14), than the smooth-small case (r^2= 0.68±0.2), $p<0.05$. Fig. 2 shows the sigmoids fitted to each trial.

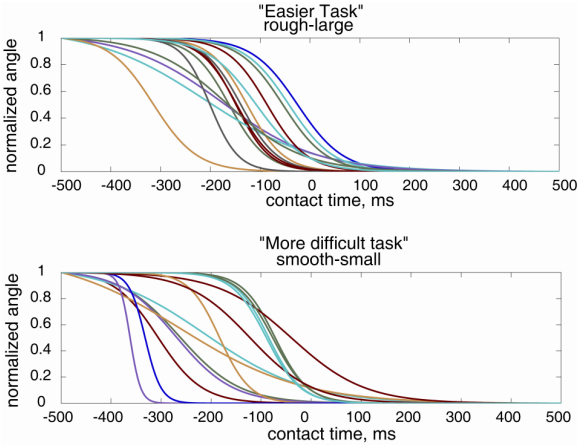

Figure 2: Fitted sigmoid for transition.

We find the transition between coordination patterns begins before contact, but the transition for the more difficult surface condition began around -300 ms, compared to -200 ms for the easier surface constraints ($p< 0.05$). Fig. 3 shows the average temporal trends of the normalized transitions, which do not overlap until ca. -230 ms.

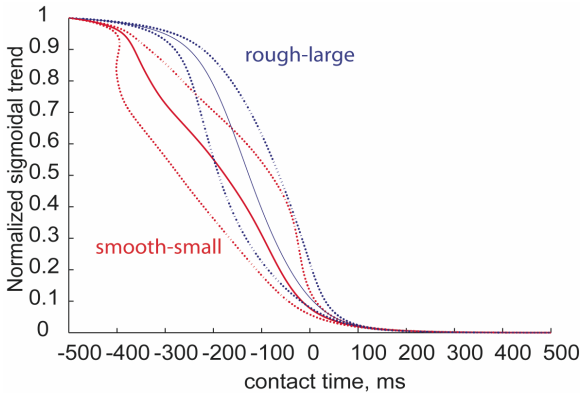

Figure 3: Normalized average sigmoidal trends (± SE) indicating an earlier transition onset for the more difficult task constraints.

SUMMARY/CONCLUSIONS

The muscle coordination patterns that produce motion and force are distinctly different, and the transition between them is well described by a sigmoid function—likely the low-pass filtering of a step change in the latent neural command by muscle activation-contraction dynamics.

The directional accuracy of force production was comparable across conditions, in spite of one having a more slippery surface. The >90% completion of the transition at contact time may signify a preference for force accuracy over motion accuracy (Fig. 3). Also, the context dependent initiation of the transition (sooner for the more difficult task) may allow time for transients in neural and muscle dynamics to die down before contact. Interestingly, however, the sigmoidal trends for the more difficult condition were less stereotypical (lower r^2 and higher residuals, $p<0.05$), suggesting a more active regulation of the coordination pattern during the transition for the task with smaller margin of error for motion and force. Mathematically speaking, the corrections for more difficult tasks likely occur in the null space of the mechanical output, and suggest that muscle redundancy may enable the nervous system to produce accurate manipulation function even when switching coordination strategies during *real world* tasks such as tapping.

REFERENCES

1.Medina, F.A., R.V. McNamara, S.L. Backus, M. Venkadesan, V.J. Santos, and F.J.Valero-Cuevas. J. Biomechanics 2006; Vol. 39 Suppl. 1, page S33. Proceedings of the WCB.

2.Valero Cuevas, F. J., J Neurophysiol 83, 1469-1479 (2000).

ACKNOWLEDGEMENTS

Grant Nos. AR050520 and AR052345 from the NIH, and NSF CAREER Award BES-0237258 (to F.J. Valero-Cuevas)

PRINCIPAL COMPONENT ANALYSIS REVEALS CONTROL STRATEGIES IN STATIC GRASP AT MULTIPLE TIME SCALES

Daniel Brown and Francisco J Valero-Cuevas
Neuromuscular Biomechanics Laboratory, Cornell University, Ithaca, NY, USA
E-mail: {db328, fv24}@cornell.edu

INTRODUCTION

The fingertip forces must satisfy force and torque equilibria to hold an object in a stable static grasp. These constraints impose specific interactions among fingertip forces the nervous system must fulfill. However, natural and unavoidable fluctuations in finger force [Slifkin 1999] perturb the system—necessitating constant corrective action. Principal component analysis (PCA) of finger forces shows a control strategy whereby the equilibrium constraints of the task and the self-perturbations of the system are controlled at different time scales.

METHODS

We asked ten consenting healthy young adults (nine right handed, one ambidextrous) to hold the test object with the thumb, middle and index fingers of the right hand in a tripod grasp. The fourth and fifth fingers were tucked away.

Subjects were asked to produce a given grasp force (6 and 12 Newtons), defined as the sum of the normal forces (i.e., norm of force vectors directed at the center of the object). This task is equivalent to holding an object of a specific weight. We instructed subjects to align a cursor representing their grasp force with the target for 95 s. We discarded the first 5 s of data to ensure we recorded steady grasp. Visual feedback was updated at 20 Hz, and force data for each finger was recorded at 400 Hz using a six DOF miniature load cell (nano-17, ATI/Industrial Automation).

We filtered force data with 8th order Butterworth high pass filters with cutoff frequencies ranging from 0.1 to 80 Hz in 30 equal log steps. For each filtered data set, PCA found the percent variance explained by the 3rd principal component (PC) as a function of frequency (Figure 1).

RESULTS

Figure 1 shows the contribution of the third PC at low frequencies to be under five percent until 1 Hz. At frequencies between roughly 1 to 10 Hz, depending on subject, the variance in the 3rd PC rises rapidly towards the theoretical maximum of 33%.

A simple differencing derivative of the traces in Figure 1 emphasizes the frequency at which the transition from a quiet to active 3rd component occurs (Figure 2). We again see peaks between 1 and 10 Hz.

DISCUSSION

We use PCA to estimate the dimensionality of finger force control during static grasp. For the three signals (normal force at each fingertip) a maximum of three dimensions (i.e., dominant PCs) is possible. When the control is primarily one- or two-dimensional, variability in additional dimensions is low, not structured and is likely noise. This can be seen in Figures 1 & 2, where at low frequency content the 3rd PC is suppressed, but at higher frequency content no such dimensionality reduction is seen.

The non-negligible variance explained by the 3rd PC likely reflects the extent to which force variability is associated with violations of the constraints and corrections by the nervous system to restore equilibrium.

We find that, when the force variability contains higher frequencies, unavoidable motor noise becomes dominant, overrides the correlations among fingers, and requires three PCs to explain the variance.

CONCLUSIONS

Below c. 1Hz, the equilibrium constraints governing stable grasp dominate the control of finger forces—as evidenced by a reduction of dimensionality in force variability. At frequencies above c. 10 Hz, the lack of dimensionality reduction suggests more independence in finger force variability due to motor noise (and possibly predictive or very short latency corrective action). Between 1 and 10 Hz, however, the increase in dimensionality is within the physiologically tenable latencies for corrections by a sensory-driven controller to enforce the constraints of the task, such as oligosynaptic reflexes or automatic grip responses [Cole 1988]. We conclude there exists a sensorimotor control system at multiple time scales to regulate the noisy neuromuscular dynamics even for static grasp.

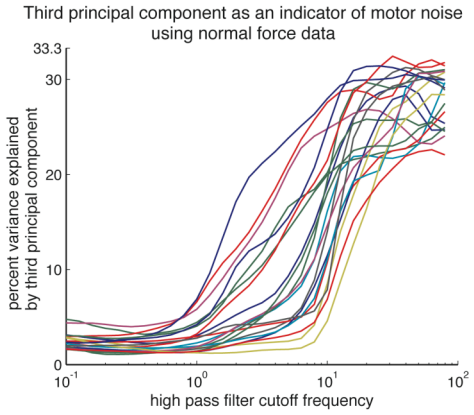

Figure 1: The percent variance explained by the 3rd principal component is minimal when low frequency content is included in the data. With higher cutoff frequencies, the 3rd PC explains a much larger portion of the variance. This suggests the presence of a physiologically tenable controller to enforce task constraints in the c. 1 and 10 Hz range.

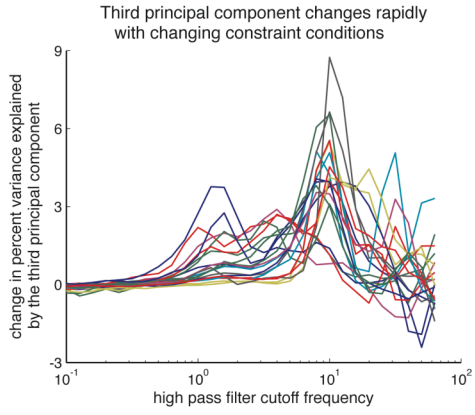

Figure 2: Calculating the derivative of the traces in Figure 1 shows a strong peak at c. 10 Hz. We propose that the dynamic control of static grasp occurs between c. 1 and 10 Hz.

REFERENCES

1. Slifkin & Newell, *J Exp Psychol* (1999) , 25: 837-851.
2. Cole & Abbs (1988) *J Neurophysiol* 60:1513-1522.

ACKNOWLEDGEMENTS

Grant Nos. AR050520 and AR052345 from the NIH, NSF CAREER Award BES-0237258 (to F.J. Valero-Cuevas), and NSF IGERT (to D. Brown).

Thanks to Drs. K. Keenan and M. Venkadesan for insightful comments.

CORTICAL NETWORKS FOR CONTROLLING INSTABILITIES IN DEXTEROUS MANIPULATION

Madhusudhan Venkadesan[1], Kristine Mosier[2], Chad Lau[3], Yang Wang[2], Francisco. J. Valero-Cuevas[1]

[1] Cornell University, Ithaca, NY, USA
[2] Indiana University School of Medicine, Indianapolis, IN, USA
[3] Purdue University, West Lafayette, IN, USA
E-mail: mv72@cornell.edu, kmosier@iupui.edu, fv24@cornell.edu

INTRODUCTION

Dexterous manipulation may be conceptualized as requiring "strength", the ability to produce fingertip forces of a specific magnitude; as well as "dexterity", the ability to dynamically regulate finger motions and, the magnitude or direction of fingertip force vectors (Valero-Cuevas, et al. 2003). Cortical activity for manipulating stable objects is being investigated (Kuhtz-Buschbeck, et al. 2001). However, cortical activity for more complex everyday tasks such as dexterous control of unstable objects remains uncharted. We employed functional magnetic resonance imaging (fMRI) to examine cortical networks engaged in controlling dynamical objects with increasing instabilities, but requiring equal strength. Fronto-parietal networks were always activated as reported previously for stable grip and pinch force, but more unstable manipulation additionally required basal ganglia activity.

METHODS

Fifteen consenting healthy right-handed adults (10M, 6F) used 3-point precision pinch to fully compress 4 springs, all requiring the same force magnitude to reach solid length. However, Spring 4 was more slender and thus the most unstable spring, whereas Spring 1 was the most stable (Fig. 1) (Valero-Cuevas, et al. 2003). Subjects used their dominant hand to perform: single compressions (compress the spring just short of solid length), cyclic compressions, or rest (holding the spring without any compression). Here, we present the pooled results from the single and cyclic compressions relative to the baseline from rest. All subjects were imaged on a Siemens 3.0 T Trio MRI scanner using standard BOLD techniques, quality assurance and motion correction techniques (Suminski, et al. 2007, Talati, et al. 2005). The raw fMRI data were processed off-line using Analysis of Functional NeuroImages (AFNI) (afni.nimh.nih.gov/afni). We performed a mixed 2-factor ANOVA to test for the effect of spring instability. We present here the: (i) mean effect maps indicating activation in response to individual springs; and (ii) conjunction maps to display overlap between the mean effects for Spring 1 and Spring 4 (most stable vs. least stable spring, respectively)

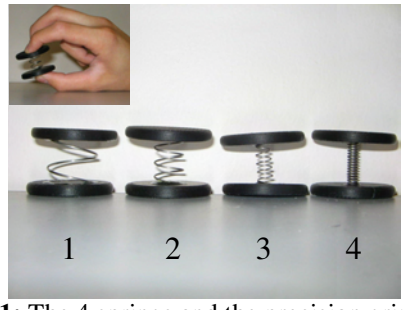

Figure 1: The 4 springs and the precision grip style used in this study are shown.

RESULTS AND DISCUSSION

We found activation consistently among the four springs in the left primary motor and

sensory cortex, the supplementary motor area (SMA; Brodmann's area 6), and bilaterally in the cerebellum. Activation was additionally observed in the bilateral prefrontal and premotor cortex (superior and inferior frontal gyrus), left putamen, and the bilateral inferior parietal lobule. ANOVA and cluster analyses were performed to identify the main effects of the springs (F-t = 4.299; p = 0.01). Two regions of interest were identified in the (contralateral) culmen of the cerebellum and the right (ipsilateral) primary sensory cortex (SI, Brodmann's Area 3) in the postcentral gyrus. Thus, the most significant difference in activation between the 4 springs occurred in the contralateral cerebellum and ipsilateral SI, suggesting that differences in dexterity are associated with SI and cerebellum.

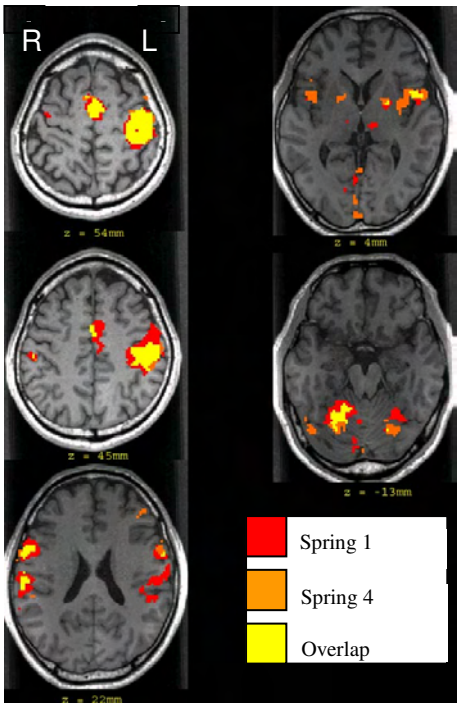

Figure 2: Conjunction maps showing regions of overlap in mean effect between Springs 1 (small dexterity value) and 4 (large dexterity value).

This effect of dexterity on cortical activity is further illustrated in the conjunction analysis which displays the spatial overlap of active clusters for Spring 1 vs. 4 (Fig. 2).

Activation overlapped in the supplementary motor cortex (SMA), predominately in the left primary motor and sensory cortex, with lesser volume in the right primary and sensory cortex, the right middle frontal gyrus, left inferior frontal gryus, and right cerebellum.

Clusters that did not overlap included activity in the bilateral thalamus, left inferior parietal cortex and left cerebellum for Spring 1, whereas Spring 4 demonstrates activity in bilateral putamen, inferior frontal gyrus and cerebellum. These data show that precision pinch compression of springs with differing dexterity requirements (but similar strength) is associated with activity in premotor, primary sensorimotor, parietal and cerebellar regions. With increasing dexterity index (increasing demand on dynamical regulation of fingertip force vectors), however, activity selectively increases in the basal ganglia and cerebellum.

CONCLUSIONS

Our results go beyond validating the well known fronto-parietal networks needed for static precision grip. We instead find alternative networks involving the basal ganglia for sensorimotor integration needed to manipulate unstable objects. These sub-networks likely form a neuro-anatomical basis for dexterous manipulation.

REFERENCES

Kuhtz-Buschbeck, J.P., et al. (2001). *Eur J Neurosci* **14**. 382.
Suminski, A.J., et al. (2007). *J Neurophysiol* **97**. 1527.
Talati, A., et al. (2005). *Percept Mot Skills* **101**. 317.
Valero-Cuevas, F.J., et al. (2003). *J Biomech* **36**. 265.

ACKNOWLEDGEMENTS

Grant Nos. AR050520 and AR052345 from the NIH, NSF CAREER Award BES-0237258, and NSF R21-HD048566 (to F.J. Valero-Cuevas).

ANKLE ANGLE AND LOCALIZED MUSCLE FATIGUE EFFECTS ON TIBIAL RESPONSE DURING HEEL IMPACTS

Adriana M. Holmes & David M. Andrews

Department of Kinesiology, University of Windsor, Windsor, Ontario, Canada
E-mail: aholmes@uwindsor.ca

INTRODUCTION

Following heel impact, the shock wave is attenuated as it travels through the musculoskeletal system as a result of active manipulation of body kinematics and joint positions (Hamill et al., 1995), as well as passive attenuation by 'wobbling masses' (e.g., muscles, soft tissues, and the heel pad) (Chu et al., 1986; Hamill et al., 1995). A decrease in the amount of shock, measured as accelerations at the knee, has been found when shank muscles were voluntarily fatigued (Flynn et al., 2004; Holmes & Andrews, 2006). However, in these studies, the relative influence of ankle angle and muscle fatigue on tibial response was not considered. Therefore, the purpose of this study was to compare the tibial response when tibialis anterior (TA) was fatigued and when not fatigued, while at the same ankle joint angle.

METHODS

Ten males and ten females participated in this study (21.8 ± 2.9 years old). An accelerometer was preloaded just medial to the tibial tuberosity; an electro-goniometer was placed across the ankle joint; and TA and lateral gastrocnemius (LG) muscle activity were recorded via EMG. Each subject's dorsiflexion angle range (min to max) was recorded, and then 4 relative positions within this full range were used for testing.

Subjects were heel-impacted into a vertically mounted force platform using a human pendulum apparatus at each of the 4 ankle angle ranges. Impacts occurred when TA was either not fatigued (NF) or fatigued (F). Dependent Measures included Peak Tibial Acceleration (PA), Time to Peak Tibial Acceleration (TPA) & Acceleration Slope (AS). AS was calculated between 30% and 70% of the time to PA (AS time) or amplitude of PA (AS amplitude).

RESULTS AND DISCUSSION

The maximum dorsiflexion angle recorded for subjects was 16.6°± 6.4°. On average, subjects were not able to maintain the same ankle angles when fatigued (Figure 1). Four ankle angle ranges of approximately 2° each were examined, where the F and NF curves overlapped (Figure 1, Table 1).

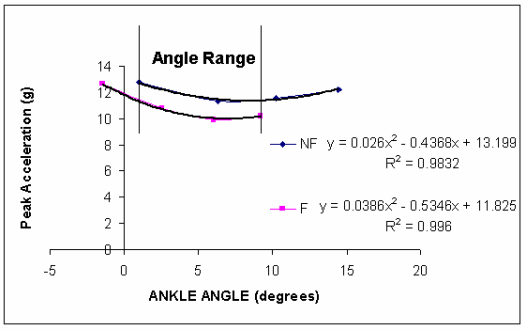

Figure 1: Peak Tibial Acceleration Across Ankle Angle Ranges for F and NF States.

Table 1: Four Ankle Angle Ranges.

1	2	3	4
1.0° -3.0°	3.0° - 5.1°	5.1° - 7.1°	7.1° - 9.2°

TA mean power frequency values decreased by over 30% following the fatigue protocol.

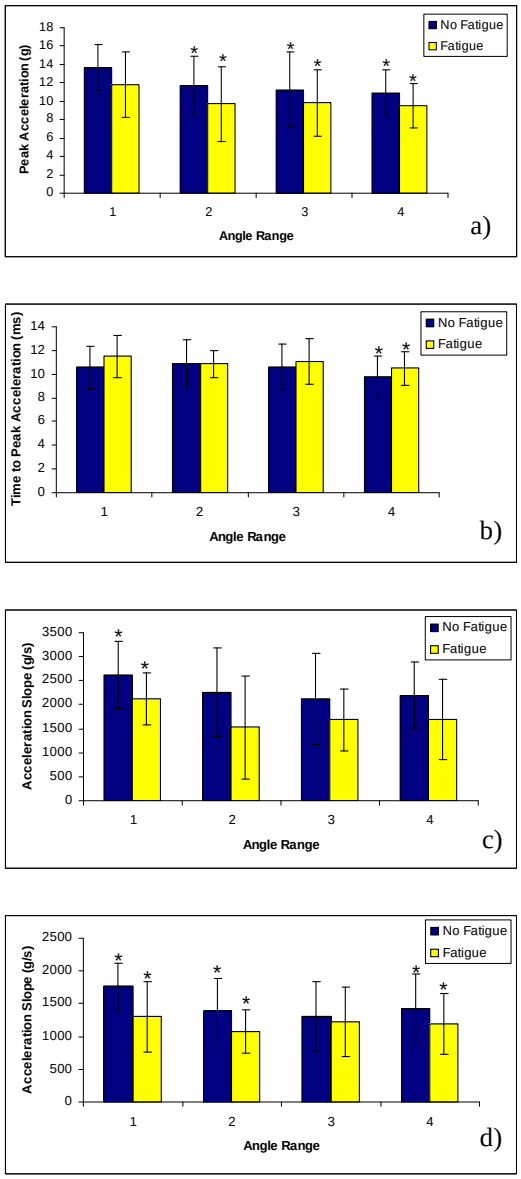

Figure 2: Fatigue effects for a) Peak Tibial Acceleration; b) Time to Peak Tibial Acceleration; c) Acceleration Slope based on Amplitude; and d) Acceleration Slope based on Time (* = $p<0.05$).

Fatigue effects were seen in PA, TPA, and AS (Figure 2a-d). An average difference of 1.1g, 1.1ms, 439g/s, and 302g/s were found between the F and NF states when the same ankle angle was recorded for PA, TPA, AS (amplitude), and AS (time), respectively. Although there was an obvious difference in magnitude between AS (amplitude) and AS (time), the same overall trends were noted. All values corresponded to those found in previous studies (Flynn et al., 2004; Holmes & Andrews, 2006).

CONCLUSIONS

The effect of ankle angle alone does not account for the differences seen in the tibial response during localized muscle fatigue. The wobbling mass reduces PA and AS, while increasing the TPA.

REFERENCES

Chu et al. (1986). *J Biomechanics*, **19**, 979 987.

Flynn et al. (2004). *Clinical Biomechanics*, **19**(7), 726-732.

Hamill et al. (1995). *Human Movement Science*, **14**, 45-60.

Holmes & Andrews (2006). *J Applied Biomechanics*, **22**, 275-284.

ACKNOWLEDGEMENTS

Thank you to NSERC for funding this project.

BLIND INFERENCE OF TENDON NETWORKS THROUGH MINIMAL TESTING

Anupam Saxena, Hod Lipson, and Francisco J. Valero-Cuevas
Cornell University, Ithaca, NY, USA
E-mail: (as574, hl274, fv24)@cornell.edu

INTRODUCTION

Hand manipulation in humans requires intricate neuromuscular interactions, which are cardinally dependent on the actuation of the *extensor mechanism*, a network of tendons acting on the phalanges. Thus, malfunction of this tendon network can critically impair manipulation. We seek to (a) decipher the functional structure of the *extensor mechanism* (i.e., topological and parameter values, often approximated by Winslow's Rhombus (Valero-Cuevas et al, in Press)) by observing the functional behavior of the digits using sparse data obtained through a set of abduction, adduction, extension and flexion tasks, (b) infer such networks via minimal testing, and (c) recognize how such networks and their functionality varies amongst healthy and diseased subjects. Here, we accomplish the first step towards this goal by using the exploration-estimation algorithm (Bongard and Lipson 2004) to simulate the inference of a hidden planar tendon network on the basis of space tests that record input-output forces.

METHODS

The exploration-estimation algorithm **(**Valero-Cuevas et al, in Press**;** Bongard and Lipson 2004**)** extracts the functional topology of a hidden system, treated as a "target" or a "black box," through a minimal number of tests (i.e., measured input-output data sets). The algorithm co-evolves populations of candidate networks and actuation tests sequentially such that more informative (as opposed to random) tests can be applied to the hidden system. This helps to evolve networks using a minimum number of tests. For problems involving large deformations, gradient-based methods—being point-to-point searches—will stall when the deformed string configurations are non-unique (i.e., simulations do not converge within specified tolerance), and function derivatives cannot be computed.

The algorithm is initialized with a random test consisting of a force input on the target and its functional response (force output). A pre-specified number of candidate networks are evolved from divided subpopulations to satisfy this input-output test. The evolved candidate networks usually vary in their simulated output force response to the same set of input forces. An input force set that causes more discrepancy in functional response (output forces) between the networks is considered more informative. We employ the variances of output forces in the candidate networks to find the most informative set of input forces to be applied to the target system next. Once identified, the new input forces are applied to the target system to procure its output force response, the experimental data is augmented by it, and then the networks are evolved to satisfy those cumulative data sets. The procedure of co-evolving networks and actuation tests continues until no further improvement in the functional behavior of the candidate networks when compared with the target is observed. Cross-validation is performed against an independent set of data extracted at the beginning of the evolution procedure.

RESULTS AND DISCUSSION

We illustrate the extraction of network topology and parameter values using the two target networks shown in Figure 1. The arrows show the directions of input forces, "squares" depict grounded nodes where reaction (output) forces are measured.

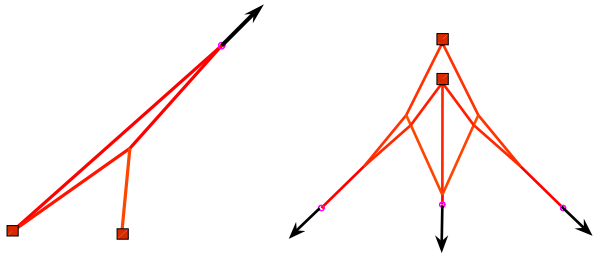

(a) (b)

Figure 1: (a) The 'A' target network, (b) The Winslow's target network.

Using the exploration-estimation algorithm described above and in detail in (Bongard & Lipson 2004), the respective networks evolved from the informative sparse data sets are shown in Figure 2. Note that the networks are functionally equivalent (Figure 3) and topologically very similar to their respective targets (cf. Figures 1 & 2).

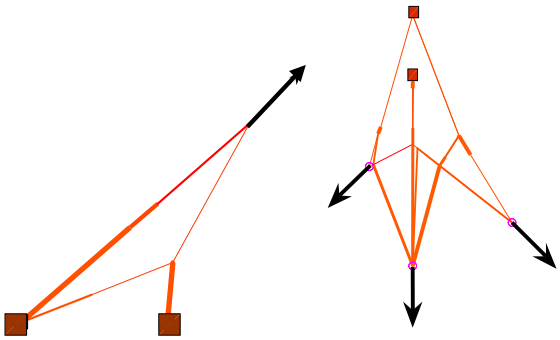

(a) (b)

Figure 2: The best evolved network obtained via minimal testing (a) of the 'A' target network; (b) of the Winslow's target network.

The cross validation errors for the two networks are shown in Figure 3, as a function of tests applied to the target system. Figure 3 compares two cases, one in which informative sets are used (solid/blue) and the other wherein random tests are employed (dashed/red). Informative tests perform statistically better than random tests on two counts (a) the cross validation errors are much smaller and (b) they converge much earlier. For the 'A' target, about 5% cross validation error is achieved using only three tests while the evolution of Winslow's rhombus takes only about 15 tests.

SUMMARY/CONCLUSIONS

We demonstrate feasibility, in simulation, in extracting tendon networks from informative sparse data, with lower cross validation errors than random tests. As a next step, we will validate our novel methods in anatomical specimens.

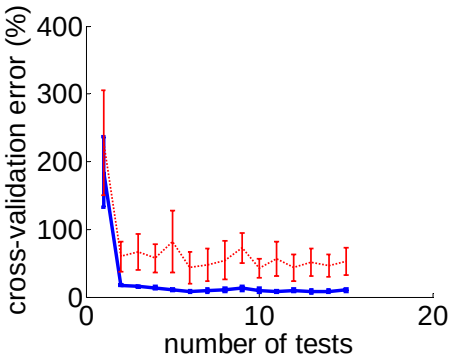

(a)

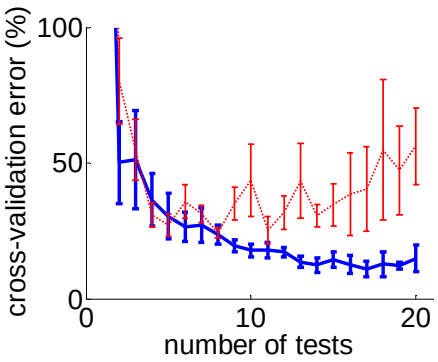

(b)

Figure 3: (a) Cross-validation error for the 'A' target network (b) the same for the Winslow's target network.

REFERENCES

1.- Valero-Cuevas FJ, Anand V, Saxena A, and Lipson H. *IEEE Trans Biomed Eng*. In Press

2.- Bongard JC and H Lipson, (2004) *Genetic and Evolutionary Computation Conference*, (GECCO '04), pp. 333-345.

ACKNOWLEDGEMENTS

The work is supported by Grant Nos. AR050520 and AR052345 from the NIH, and NSF CAREER Award BES-0237258 (to F.J. Valero-Cuevas).

WALKING WITH INCREASED PUSH-OFF DECREASES HIP FLEXION MOMENT

Cara L. Lewis [1] and Daniel P. Ferris [1]

[1] Human Neuromechanics Laboratory, University of Michigan, Ann Arbor, MI, USA
E-mail: caralew@umich.edu,
Web: http://www-personal.umich.edu/~ferrisdp/UMHNL.html

INTRODUCTION

In a simple bipedal walking model, both an impulsive push along the trailing limb (similar to ankle plantar flexion) and a torque at the hip can power level walking (Kuo 2002). Using a hip torque alone is four times more energetically costly than using only an ankle push-off impulse (Kuo 2002). This suggests a tradeoff between ankle and hip power requirements during human gait, with ankle power as the more efficient method. People with anterior hip pain may benefit from walking with increased ankle push-off if it reduces anterior hip muscle forces (Lewis and Sahrmann 2006). The purpose of this study was to test whether altering ankle push-off has an effect on the hip muscle moment during human gait. We hypothesized that changes in ankle push-off would be inversely related to the hip flexion moment.

METHODS

Five healthy female subjects (mean age: 31.8 years) walked on a custom split-belt force-measuring treadmill at 1.25 m/s. We recorded vertical, horizontal and lateral ground reaction forces (1200 Hz) as well as lower extremity kinematic data (120 Hz) from a motion capture system (Motion Analysis, Santa Rosa, CA).

Subjects walked under three conditions: Natural, Decreased Push-off and Increased Push-off. For the Natural condition, subjects walked on the treadmill without any additional instructions. For the Decreased Push-off condition, subjects were instructed to push less with their feet as they walked. Conversely, for the Increased Push-off condition, subjects were instructed to push more with their feet as they walked. Subjects practiced walking under each condition for over a minute. The Natural condition was always tested first. The order of the other two conditions was randomized.

We recorded data for 90 seconds during each condition. Data were processed in Visual3D (C-Motion, Inc, Rockville, MD) to calculate joint kinetics. Average peak moment and angular impulse (area under the moment curve) for hip flexion and ankle plantar flexion were calculated for each subject and condition. We used repeated measures ANOVAs and, when appropriate, Tukey's Honestly Significant Difference (THSD) post-hoc tests to detect differences between the three conditions.

RESULTS AND DISCUSSION

Altering push-off during walking changed the hip flexion peak moment and angular impulse. Walking with increased push-off decreased the hip flexion peak moment by ~23% and the hip flexion angular impulse by ~31% compared to walking naturally. When walking with decreased push-off, the hip flexion peak moment and angular impulse were significantly higher than in the Increased Push-off condition ($p < 0.05$).

Compared to the Natural condition, ankle plantar flexion angular impulse increased by ~14% in the Increased Push-off condition

and decreased by ~14% in the Decreased Push-off condition. There was no change in the ankle plantar flexion peak moment.

As predicted by the simple walking model, increased ankle push-off resulted in reduction of the hip flexion moment. This finding emphasizes the interchange between hip and ankle power in human gait. Increased ankle push-off during gait may help compensate for weakness or injury of the anterior hip musculature. Conversely, reduced ankle push-off power during walking may cause individuals to walk with greater hip flexion moments, increasing their risk for developing anterior hip pain. Future studies should examine subjects with anterior hip pain to determine if they have less than normal ankle push-off and if teaching them to increase ankle push-off can decrease their anterior hip pain.

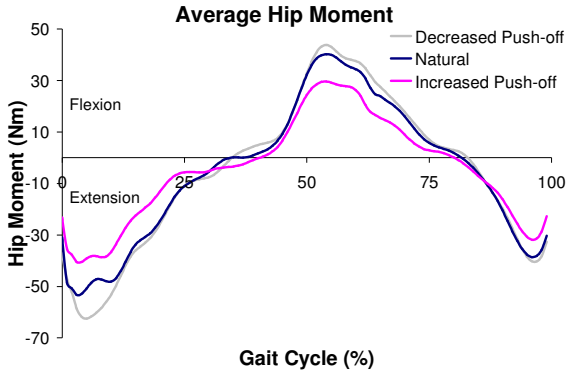

Figure 1: Average hip moment during Natural, Decreased, and Increased Push-off conditions for one representative subject.

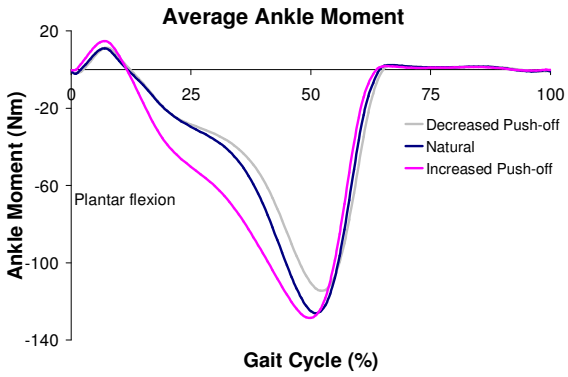

Figure 2: Average ankle moment during Natural, Decreased, and Increased Push-off condition for the same subject.

SUMMARY/CONCLUSIONS

Walking with increased push-off decreases hip flexion moment and thus, anterior hip muscle forces. People with injuries of the anterior hip musculature may benefit from gait training to increase ankle push-off.

REFERENCES

Kuo, A.D. (2002). *J Biomech Eng,* **124**, 113-120.

Lewis, C.L., Sahrmann, S.A. (2006). *Phys Ther*, **86**, 110-121.

ACKNOWLEDGEMENTS

This work was supported in part by the National Institutes of Health (HD007422 and NS45486).

Table 1: Average hip flexion and ankle plantar flexion peak moment and angular impulse for each condition (mean ± SD). * indicates difference from the Natural Condition ($p < 0.05$)

	Hip Flexion		Ankle Plantar Flexion	
Condition:	**Peak Moment (Nm)**	**Angular Impulse (Nm)**	**Peak Moment (Nm)**	**Angular Impulse (Nm)**
Decreased Push-off	37.2 ± 15.1	795.2 ± 322.4	-82.8 ± 22.7	-1844 ± 654*
Natural	36.7 ± 17.2	711.8 ± 325.1	-89.9 ± 22.6	-2123 ± 611
Increased Push-off	28.1 ± 13.3*	490.7 ± 234.5*	-85.7 ± 28.3	-2436 ± 753*

EFFECTS OF PHYSICAL ASSISTANCE ON NARROW BEAM WALKING

Antoinette Domingo and Daniel P. Ferris

Human Neuromechanics Laboratory, University of Michigan, Ann Arbor, MI, USA
E-mail: adomingo@umich.edu

INTRODUCTION

Adequate balance is needed to maintain stability and safely negotiate the environment during walking. Balance impairments are common in patients with neurologic injury and in the elderly (Shumway-Cook et al. 1988; Woollacott & Tang 1997). Designing therapeutic interventions for improving walking balance in patients could greatly improve functional mobility in millions of individuals.

Although physical assistance is often provided during motor therapy to improve balance, it is not clear how it affects motor learning of complex skills. The purpose of our study was to determine how physical assistance affects motor learning of walking balance. Physical guidance may be detrimental to learning because it changes the sensory environment and task specificity is lost. In addition, removing opportunities for errors and error correction could hinder the ability to perform the movement correctly when assistance is removed (Schmidt & Wrisberg, 2004).

In this study, two groups of subjects were evaluated before and after 30 minutes practice walking on a narrow treadmill-mounted balance beam (beam-mill) (Figure 1). The first group practiced the task without assistance, while the second group practiced with constant assistance by holding hand rails. We hypothesized that the group that practiced the task without handrails would improve their ability to walk on the beam more than the group using the handrails.

METHODS

Ten subjects walked on a treadmill mounted balance beam for 5-minute pre- and post-practice evaluations. The beam was 2.5 cm wide and 2.5 cm tall. Treadmill speed was set at 0.22 m/s. Subjects were given instructions to walk heel-to-toe and not to lean forward, twist, angle their feet away from the longitudinal direction of the beam, or use the safety harness for balance support. All subjects wore standardized shoes.

Five subjects were in each condition group: Handrails and No Handrails. The Handrails group walked on the beam-mill while holding onto bilateral handrails with light touch. The No Handrails group was not allowed to use the handrails but could move their upper extremities as they chose. The practice duration was 30 minutes with rest breaks every 10 minutes.

Figure 1: A subject walking on the treadmill mounted balance beam (beam-mill). The harness was worn for safety and did not provide support.

Subjects were evaluated over a 5-minute period during unassisted walking on the beam-mill before and after training. We

assessed beam walking performance by calculating the percentage of time the subject was on the beam (not touching the treadmill surface with either foot) and by calculating the root-mean-square (RMS) of the center of mass lateral movement. Center of mass displacement was estimated using a sacral marker (Motion Analysis Corporation, Santa Rosa, CA; 120 Hz).

RESULTS AND DISCUSSION

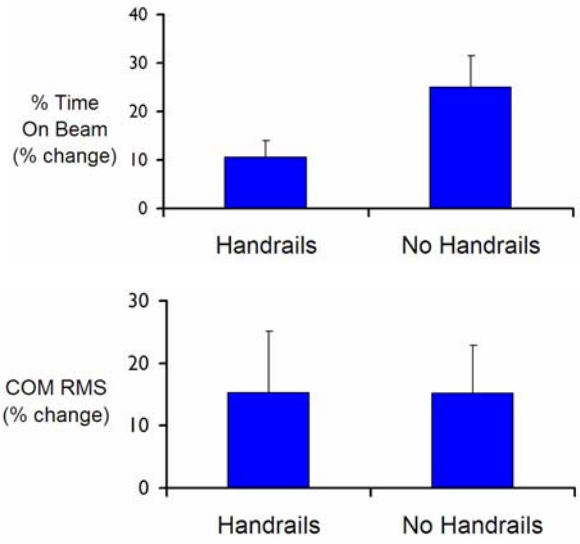

Figure 2: Percentage improvement after practice in time on the beam and medio-lateral center of mass movement for Handrails and No Handrails groups. Error bars indicate standard error of the mean.

Both groups improved in time they were able to walk on the beam (Figure 2, top), but the No Handrails group had a greater improvement (~25%) than the Handrails group (~11%). This suggests that practicing without the handrails was more beneficial for learning this difficult walking task because it allowed the subjects to explore the dynamics of the task, making and correcting movement errors (on beam 73.1% of practice time) . When subjects used the railings, error was minimized during practice (on beam 99.97% of practice time), but the opportunities to learn error correction were not present.

Both groups showed equal improvements in medio-lateral center of mass movement (Figure 2, bottom). This measurement was highly variable between subjects and may not have been sensitive enough to show differences between learning in the two groups.

SUMMARY/CONCLUSIONS

Unassisted practice appears to be more beneficial to learning walking balance than assisted practice in neurologically intact subjects. This was demonstrated by the greater improvements in time walking on the beam-mill for the No Handrails group compared to the Handrails group. The results may be limited to walking balance tasks where the subjects can already achieve a high level of performance without training. Future studies should also examine walking balance tasks where the subjects initially exhibit a low level of performance.

REFERENCES

Shumway-Cook, A., Anson D. (1988). *Arch Phys Med Rehab,* **69**, 395-400.

Woollacott, M.H., Tang, P.F. (1997). *Phys Ther,* **77**, 646-660.

Schmidt, R.A., Wrisberg, C.A. (2004). *Motor Learning and Performance.* Human Kinetics.

ACKNOWLEDGEMENTS

The authors would like to thank the members of the Human Neuromechanics Laboratory for their assistance with data collection and processing.

Walking, Skipping, and Running Produced From a Single Bipedal Model

Shawn M. O'Connor and Arthur D. Kuo

University of Michigan, Ann Arbor, MI, USA
E-mail: smoconno@umich.edu

INTRODUCTION

Human gaits such as walking and running have traditionally been treated as distinct paradigms with different dynamics. In walking, the legs are thought to act as coupled pendulums, whereas in running they compress and extend like springs. Here we show that walking, running, and even skipping can be produced entirely by the dynamic modes of a remarkably simple model which combines pendulum and spring-like behavior.

METHODS

The simple locomotion model is comprised of a single point mass at the pelvis, two axially-compliant legs with very light point mass feet, and a torsion spring acting between the legs (Figure 1). The model is a simplification of a passive bipedal running model (McGeer 1990) with the added capability of double support. We developed walking simulations that integrated equations of motion for the model and also handled discrete events such as heel-strike. We then searched for periodic gaits by varying the model parameters and initial conditions in a Newton method search.

After non-dimensionalizing the governing variables, the model has only two physical parameters: the axial and torsional leg stiffness. Gait parameters, such as the time of ground contact and step frequency, are set by tuning the two stiffness parameters and by selecting appropriate initial conditions for the simulation.

The speed and type of gait depend on physical parameters as well as the mechanical energy of the body center of mass and axial springs, which is set by the initial conditions of the model states. The model has 3 degrees of freedom during single support, and thus the model energy and movement can be divided up into three modes: inverted pendulum, pendulum, and spring-mass, which correspond to the three model states: stance angle, θ, swing angle, ϕ, and variable stance leg length, L.

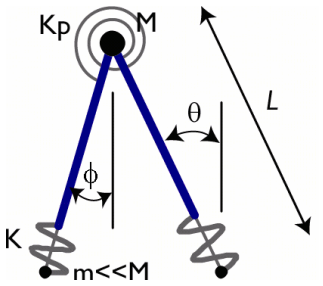

Figure 1: A two-dimensional elastic dynamic locomotion model with two stiffness parameters.

In order to compare different gaits, we developed a metric, named spring fraction, SF, that quantifies the maximum amount of energy stored in the axial stance leg spring as a fraction of the total system energy. This metric provides a basic measure of the amount of spring-mass behavior present in each gait.

$$SF = \left[0.5 \cdot K \cdot (1-L)^2\right] / E_{total}$$

RESULTS AND DISCUSSION

After adding compliant legs to our simple model, we found that the motion of both legs for an entire stride can be generated completely passively. A variety of human-like gaits may be produced with one simple

model, without enforcing ground reaction force patterns or prescribing motions. Examples of these gaits are shown in Figure 2 and directly compared with corresponding sample human data. The maximum fraction of energy stored in the stance spring for each of these gaits is then compared in Table 1.

Table 1. Comparison of the maximum elastic energy stored among bipedal gaits.

	Normal Walking	Fast Walking	Skipping	Running
Speed	1.25 m/s	1.50 m/s	1.79 m/s	2.2 m/s
SF	0.029	0.034	0.100	0.137

When walking, the model's compliant legs produce ground reaction forces and perform work on the body similar to humans. As the model walks faster and takes longer steps, more energy is stored in the stance spring and the vertical motion of the center of mass is increasingly affected by spring-mass mechanics. With increasing speed, the stance leg spring eventually stores enough energy such that the leg rebounds at mid-step and leaves the ground, producing a skipping gait. The model therefore smoothly transitions to skipping as walking speed is increased. Running can be produced with the same model parameters as for walking or skipping, but started with different initial conditions. Therefore, the distribution of system energy largely distinguishes walking and running gaits, with significantly larger amounts of energy stored in the stance spring during running, even at equivalent speeds.

Although the model parameters affect features of gait such as step frequency and contact time, the most significant difference between the demonstrated gaits lies in how the energy of the system is distributed between pendular and spring-like modes.

SUMMARY/CONCLUSIONS

We have shown that the dynamics of a variety of gaits are the result of the combination of pendulum and spring-like behavior in a simple locomotion model.

REFERENCES

McGeer, T. (1990). *Proc. R Soc. London B*, **240**, 107-134.

ACKNOWLEDGEMENTS

Supported by NIH grant R21DC6466.

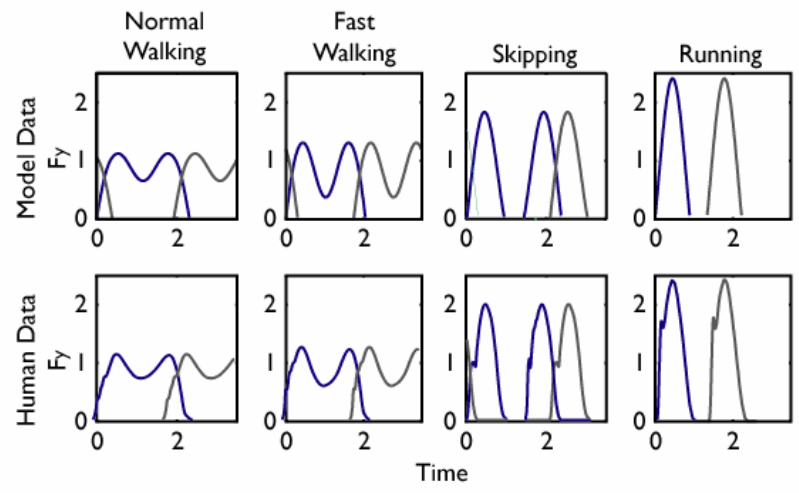

Figure 2: The simple elastic locomotion model reproduces the vertical ground reaction forces (Fy), measured in units of body weight, seen in a variety of human gaits. Time is in dimensionless units, normalized by leg length and the gravitational constant.

Visual Perturbation of Walking Balance

Shawn M. O'Connor and Arthur D. Kuo

University of Michigan, Ann Arbor, MI, USA
E-mail: smoconno@umich.edu

INTRODUCTION

Three-dimensional walking models indicate that gait may be passively stable in the anterio-posterior (A-P) direction but unstable in the medio-lateral (M-L) direction (Kuo 1999). Visual and other sensory information pertaining to side-to-side movement may therefore be more important for actively controlling balance than that for fore-aft movement. This same asymmetry is not expected during normal standing balance. Although walking and standing are controlled in different ways, center of pressure (COP) location is actively controlled in both tasks. We used a virtual reality environment to test whether oscillations added to the visual field in either the M-L or A-P directions would have a differential impact on the variability of COP during walking vs. standing.

METHODS

Six healthy subjects (aged 28 ± 3.5 yrs., mean ± s.d.) provided consent and participated in this study. Subjects received visual information while walking or standing on a split-belt instrumented force treadmill through a virtual reality display placed in front of the treadmill. The visual field consisted of a virtual dark hallway tiled with randomly placed white rectangles (Warren 1996). The display was rear-projected on a translucent 3 m x 3 m curved screen. Subjects were placed approximately 0.5 m away from the center of the screen, providing 180^o horizontal and 145^o vertical viewing angles. Head tracking was not used.

During the walking conditions, subjects walked at a constant speed of 1.25 m/s on the treadmill while viewing a speed-matched moving hallway. Subjects were exposed to sinusoidal oscillations of the visual flow in either the M-L or A-P directions at amplitudes of 0, 0.05, 0.15, 0.25, and 0.35 m and a frequency of 0.25 Hz. The effect of the oscillations was assessed by measuring root-mean-square (RMS) variability in step length and step width recorded from individual limb COP estimated at mid-step over at least 400 steps.

During the standing conditions, subjects stood on the treadmill while viewing a stationary hallway. Subjects were exposed to sinusoidal oscillations of the visual scene in either the M-L or A-P direction at amplitudes of 0 and 0.05 m and a frequency of 0.25 Hz. The effect of the oscillations was assessed by measuring RMS COP displacement in both the M-L and A-P directions over a two minute interval.

RESULTS AND DISCUSSION

Step placement variability results for the visual oscillation conditions during the walking trials are shown in Figure 1. To test whether oscillations added to the visual field in either the M-L or A-P directions would have a differential impact on the variability of foot placement we calculated the slopes of the step placement variability vs oscillation amplitude trends. Results from a one-way ANOCOVA test revealed that the slope corresponding to step width variability

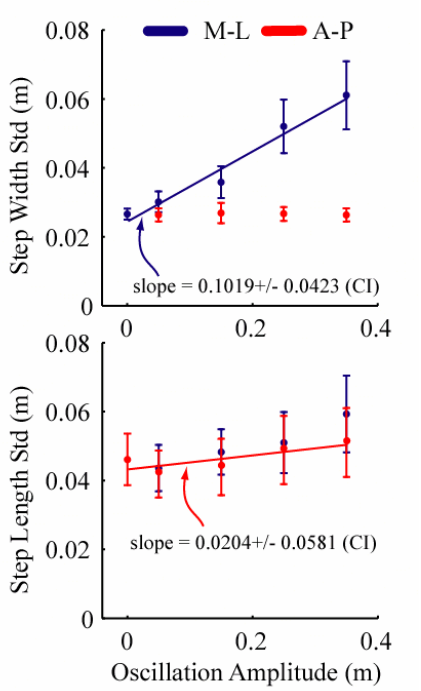

Figure 1: Comparison of M-L and A-P visual oscillations with increasing amplitude on step width and step length variability.

for M-L oscillations was significantly greater (p-value < 0.05) than the slope corresponding to step length variability for A-P oscillations. This result indicates that visual information pertaining to side-to-side movement may be more useful for controlling balance during walking than information about fore-aft movement.

To verify that this M-L sensitivity is due to walking dynamics rather than the effect of the virtual environment or the amount of visual information contained in the M-L or A-P directions, we performed a similar test for normal standing. Since only one oscillation amplitude was used, we calculated the ratio of M-L and A-P RMS COP displacement for the oscillation conditions to that of the no oscillation condition (Table 1). Results from a paired t-test revealed no significant difference between the ratio of M-L COP variability for M-L oscillations and the ratio of A-P COP variability for A-P oscillations. However, A-P oscillations also had a large effect on M-L COP, suggesting that visual information in the A-P direction may contribute greatly to standing balance in general. In any case, the sensitivity of walking to M-L visual oscillations is due to the dynamics, and not to directional sensitivity of vision.

SUMMARY/CONCLUSIONS

Visual sensory information is differentially weighted to actively control medio-lateral balance during walking, which appears to be unstable. Anterio-posterior information is de-emphasized, perhaps due to the passive stability of walking in that direction. This differential weighting is not present during standing balance. Direction-dependent weighting of sensory information may have potential applications to rehabilitation or treatment of patients with sensory loss.

REFERENCES

Kuo, A. D. (1999). *Int. J Robotics Research*, **18**, 917-930.

Warren, W.H. et al. (1996). *J Exp. Psych.*, **22**, 818-838.

ACKNOWLEDGEMENTS

Supported by NIH grant R21DC6466

Table 1: Standing RMS COP Displacement Results

Oscillation Direction / Amplitude	M-L / 0.05 m	A-P / 0.05 m
Ratio of M-L RMS COP for oscillation condition to normal	2.58±1.42	2.86±3.46
Ratio of A-P RMS COP for oscillation condition to normal	1.67±0.54	2.48±0.34

Center of Mass Velocity Redirection Predicts COM Work in Walking

[1]Peter Gabriel Adamczyk, Arthur D. Kuo
Department of Mechanical Engineering
University of Michigan, Ann Arbor, MI USA
[1]email: padamczy@umich.edu

INTRODUCTION

Humans perform simultaneous positive and negative work on the body's center of mass (COM) to redirect its velocity between single support phases, in *step-to-step transitions* (Donelan, 2002b). This work predicts a major component of the metabolic energy expended during walking (Donelan, 2002a). A simple mathematical model of dynamic walking predicts the amount of work from the COM velocity change, which in turn is predicted from step length and walking speed (Kuo, 2002). The model assumes that the step-to-step transition occurs impulsively, so it may not apply well to actual human walking, in which the transition is distributed over time, roughly coincident with double support. We tested model predictions of changes in the COM velocity's magnitude and direction, as well as the hypothesized link between velocity change and work performed on the COM, over a wide range of step lengths and speeds. We find that COM velocity change and the associated work performed on the COM by the legs are predicted well by a remarkably simple model.

METHODS

The simple dynamic walking model comprised a point mass for the COM (Fig. 1), supported by two light and rigid legs with point mass feet (Kuo, 2002). During each single support phase, the COM moves in an arc prescribed by the stance leg. Between these phases, the legs must perform work on the COM to redirect its velocity, and the change in velocity increases with both step length *s* and speed *v*. The COM velocity is predicted to undergo an angular change δ governed by the angle between the legs and therefore roughly proportional to step length, $\delta \propto s$. The amount of work performed on the COM, *W*, is predicted to be proportional to the square of velocity and the square of angular change, $W \propto \left(v^{-}\right)^2 \delta^2$.

Human walking can differ substantially from the model. Because the legs are not rigid, COM velocity need not be perpendicular to the leg as in the model, and the angular change δ need not be proportional to step length. The model's prediction for work assumes impulsive push-off and collision in sequence. In humans, these events take place and even overlap in time. The model's predictions will not hold if these assumptions are too inaccurate, and especially if humans alter how they perform the step-to-step transition at different speeds and step lengths.

We analyzed data previously collected (Donelan, 2002a) on subjects walking overground under four different types of gait variations, with a total of 24 different conditions. Ten healthy young adults walked at six different average speeds $\bar{v}$, 0.75 to 2.0 $\mathrm{m \cdot s^{-1}}$. The four variations applied these speeds to (A) normal walking at self-selected step length *s* and step frequency *f*; (B) walking with increasing *s* but at a single fixed *f* (the same as preferred at 1.25 $\mathrm{m \cdot s^{-1}}$); (C) walking with increasing *f* but at a fixed *s* (the one preferred at 1.25 $\mathrm{m \cdot s^{-1}}$),

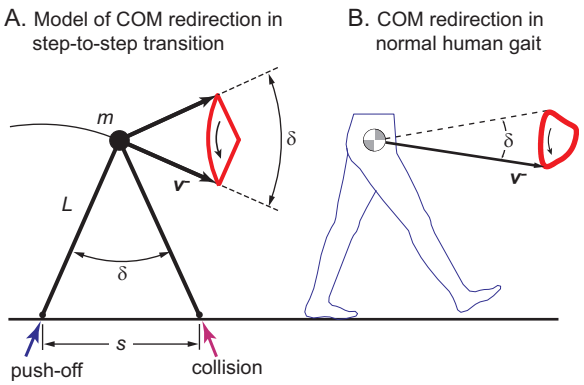

Figure 1: A) Simple model of the step-to-step transition. An impulsive push-off followed by an impulsive collision sequentially redirect the COM velocity through the angle δ. The COM velocity is perpendicular to the legs. B) These assumptions need not apply to humans, where push-off and collision occur over a longer duration and COM velocity is not always perpendicular to the legs. The work of step-to-step transitions can therefore be different between model and humans. The changes in the COM velocity are shown as a path, also known as a hodograph, running counter-clockwise. Vector $\mathbf{v}^-$ marks the velocity just before the step-to-step transition.

and finally (D) walking at a constant 1.25 $\mathrm{m \cdot s^{-1}}$, with nine different step lengths and frequencies.

We measured ground reaction forces to calculate COM velocity and the rate of COM work performed by each leg. The step-to-step transition was defined as the period between the largest differences in angle of COM velocity. We performed linear regression to test the trends predicted by the model.

RESULTS AND DISCUSSION

Angular redirection of the COM velocity was predicted by step length *s* (Fig. 2), $\delta \approx 0.30s + 0.09$, $r^2 = 0.66$. Negative step-to-step transition work was also predicted by $W^- \approx 0.80\left(v^-\right)^2 \delta^2 + 0.01$, $r^2 = 0.84$. Step length and speed therefore predict work similar to the simple model, over a very wide range of gait conditions.

These results indicate that, even though humans do not exactly follow the

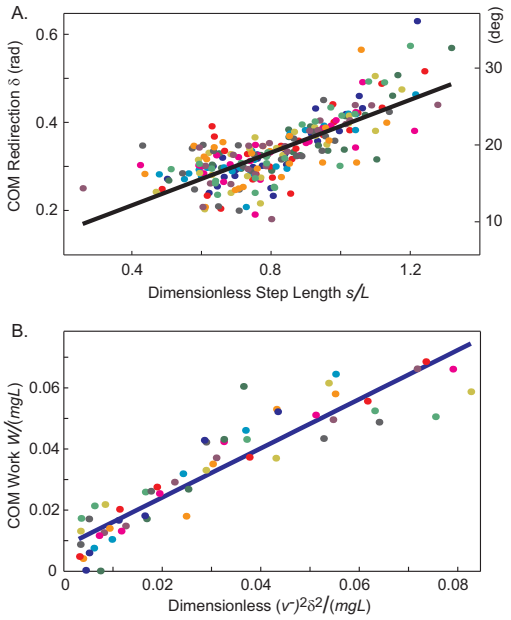

Figure 2: A) COM redirection angle δ vs. step length *s*. COM redirection increases with step length as predicted by the model, r^2 = 0.66. B) COM work performed by the leading leg *W* vs. the model prediction $\left(v^-\right)^2 \delta^2$. Step-to-step transition work is predicted well by COM velocity and angular change (r^2 = 0.84), or by walking speed and step length.

assumptions of the simple model, their COM velocity undergoes redirection similar to the model and with similar dependence on step length and speed. Humans are also fairly consistent in how they perform the step-to-step transition, so that a single model applies reasonably well to a much wider variety of speed, step length, and step frequency conditions than is observed in daily life. Step-to-step transition work, and from previous findings (Donelan et al., 2002a), the associated metabolic energy expenditure, are both predicted by speed and step length.

ACKNOWLEDGEMENTS

Supported by NIH grant R21DC6466.

REFERENCES

Donelan, J. M., R. Kram and A. D. Kuo. (2002a). *JEB* 205, 3717-27.

Donelan, J. M., R. Kram and A. D. Kuo. (2002b). *J Biomech* 35, 117-24.

Kuo, A. D. (2002). *JBME* 124, 113-20.

COMPARING METHODS OF QUANTIFYING TIBIAL ACCELERATION SLOPE

Adriana M. Holmes, Nikki L. Nolte & David M. Andrews

Department of Kinesiology, University of Windsor, Windsor, Ontario, Canada
E-mail: aholmes@uwindsor.ca

INTRODUCTION

The slope of the linear portion of shank acceleration waveforms (Figure 1) has been used to assess impact induced shock waves which are transmitted through the musculoskeletal system (Flynn et al., 2004; Holmes & Andrews, 2006). Increased loading rates have been associated with increased tibial shock travelling through the body (Hennig et al., 1993). In addition, loading rate is thought to potentially play a role in injuries to the leg during running (Nigg et al., 1995).

Previous research has used different cut-offs ranging from 10%-90% (Lafortune & Lake, 2005; Lafortune et al., 1996) to 30%-70% (Flynn et al., 2004; Holmes & Andrews, 2006) of either time to peak acceleration (PA), or PA amplitude to calculate the slope of the linear portion of the shank acceleration waveform (Figure 1). Considerable variability in acceleration slope (AS) values, and different interpretations of risk, have been reported in the literature. Therefore, the purpose of this study was to quantify differences in AS determined at various percent cut-offs between impact and PA, based on either amplitude or time.

METHODS

Ten males and ten females participated in the study (21.8 ± 2.9 years old). AS data recorded at the knee were analyzed using custom LabVIEW software (National Instruments, v. 8.2). AS was calculated based on the slope between two cut-off percentages as a function of the PA amplitude (AS amplitude) or the time to PA (AS time) (Figure 1). Nine % ranges were tested from 5-95% to 45-55% at 5% increments. A two-way ANOVA was conducted to examine any significant differences in the two methods (AS amplitude or AS time) or the nine % ranges.

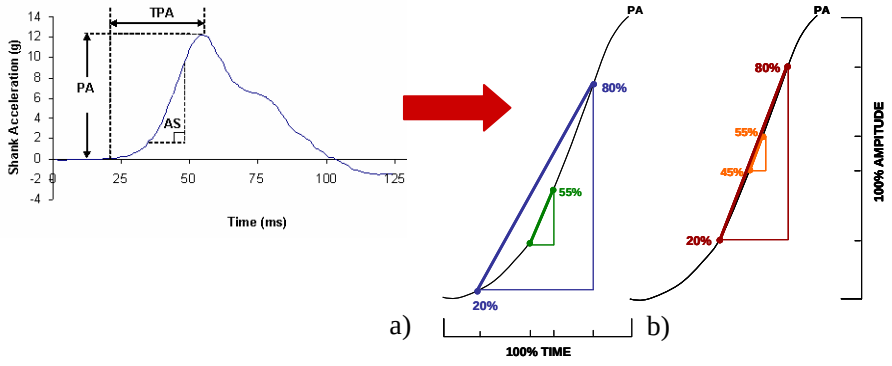

Figure 1: Sample Cut-offs for Acceleration Slope (AS) Calculations based on a) Time and b) Amplitude.

RESULTS AND DISCUSSION

AS (amplitude) values were significantly higher than AS (time) values at all levels ($p=0.00$) (Figure 2). Both AS (amplitude) and AS (time) values at the widest ranges (5-95% and 10-90%, and 5-95%, respectively), were significantly different than all other levels ($p<0.03$). AS (amplitude) values leveled off at the narrowest ranges, from 30-70% to 45-55%; while all AS (time) values above 5-95% were statistically the same. Overall, AS (amplitude) calculations are easier to track than AS (time), as amplitude measures are based on PA amplitude values which are very easy to track automatically (compared to time of impact). The AS values calculated by both methods were highly variable; yet fell within the range of those previously reported (Table 1).

CONCLUSIONS

AS (amplitude) at slope cut-offs greater than 30%, and AS (time) at cut-offs greater than 10% appear to be the most stable. Researchers need to be aware of the method used to calculate reported AS values and should consider which approach is optimal for different acceleration waveforms.

REFERENCES

Flynn, J.M. et al. (2004). *Clinical Biomechanics,* **19**, 726-732.

Holmes, A.M. & Andrews, D.M. (2006). *J. Applied Biomechanics,* **22**(4), 275-284.

Hennig et al. (1993). *J. Applied Biomechanics* **9**(4): 306-314.

Lafortune, M.A. & Lake, M.J. (1995). *J. Biomechanics,* **28**, 1111-1114.

Lafortune, M.A. et al. (1996). *J. Biomechanics,* **29**(12), 1523-1529.

Nigg et al. (1995). *J. Applied Biomechanics,* **11**, 407-432.

ACKNOWLEDGEMENTS

Thank you to NSERC for providing funding.

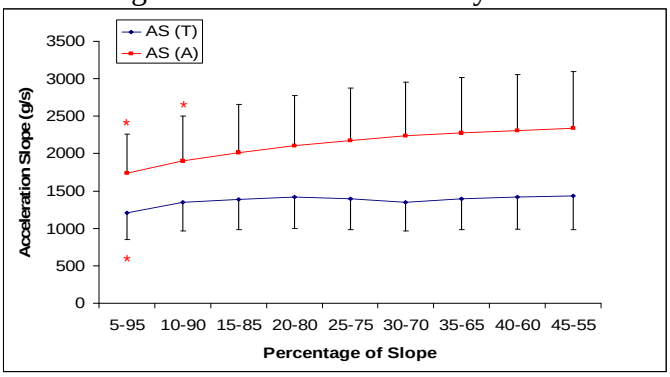

Figure 2: Acceleration Slope (AS) calculated based on Amplitude (A) or Time (T).
* = Significantly different from all percentages of slope.

Table 1: Comparison of Acceleration Slope (mean ± SD).

Reference	Acceleration Slope (g/s)
Current Study AS based on Amplitude	2121 ± 678
Current Study AS based on Time	1374 ± 406
Holmes & Andrews (2006)	1563 ± 614
Flynn et al. (2004)	2742 ± 1426
Lafortune & Lake (1995)	671 ± 220
Lafortune et al. (1996)	1150 ± 930

EFFECT OF LINEAR WHEELCHAIR VELOCITY ON A NEW MANUAL WHEELCHAIR USER JOINT INJURY INDEX

Mohammadreza Mallakzadeh, Farrokh Sassani, and Bonita J Sawatzky

The University of British Columbia, Vancouver, BC, CANADA
E-mail: mallak@mech.ubc.ca, Web: www.mech.ubc.ca

INTRODUCTION

Statistics reported by Boninger et al. (2002) indicate that manual wheelchair propulsion is associated with a high mechanical load on the upper limbs joints, which may lead to the overuse injuries and pain. Veeger et al. (1991) showed that the mechanical efficiency in wheelchair propulsion decreases by increasing the tangential velocity of the wheel. They did not however determine the effect of the velocity on the injury of the users. Dicianno et al. (1999) reported that body mass index (BMI) is another factor, which is related to the upper limb joint injury. Boninger et al. (2000) reported that frequent repetitive motion puts a person at the risk of repetitive stress injury; therefore the pushing frequency has a direct effect on the wheelchair user's joint injury.

The objectives of this study are to propose a new index for injury assessment and to verify the effect of Linear Wheelchair Velocity (LWV) on the proposed injury index.

In addition to BMI, we have used percentage of body fat to analyze its effect on the injury of the users. We have proposed a Wheelchair User Joint Injury Index (WUJII), which considers the above four parameters and reflects a value that is a representative of users' joints injury. The risk of injury may increases with higher values of WUJII. The results show that WUJII increases with respect to LWV for all subjects.

METHODS

We used 8 male as subjects for this research who have paraplegia due to a spinal cord injury with ages 19-59 years. As we had to measure a number of parameters, we used several devices to acquire the necessary data: The ©VICON Motion Analysis System, a Quickie (Sunrise Medical Inc.) wheelchair, a fabricated instrumented wheel, a heart rate monitor (HR-Polar S610™), an automatic blood pressure monitor (© 2005 A&D Medical), a fat caliper (SLIMGUIDE®), a speedometer (Filzer dB4L), a roller-rig, a special fabricated scale, and 3 personal computers.

The percentages of body fat of the subjects were determined by using the caliper for skin fold test at 4 different locations: Triceps, Biceps, Subscapula and Supraspinale. Nine semi-spherical passive markers were attached on the upper limb and trunk landmarks.

We performed experiments at three LWVs of 0.9, 1.1 and 1.3 m/s for the subjects. We measured the applied loads on the handrim by using our instrumented wheel. Each test took 3 minutes and we collected data during the last 50 seconds of each test.
Five consecutive pushing phases were analyzed for each test. The subjects

rested between the tests and their heart rates and blood pressures were measured to ensure that they have returned to the resting levels.

RESULTS AND DISCUSSION

The results show that the average WUJII ($\overline{\text{WUJII}}$) is sensitive to LWV and it increases with respect to LWV for all subjects (Figure 1).

Considering the consistent dependency of WUJII on LWV, we further modified WUJII to include LWV as one of its parameters. This allows WUJII to be a standalone measure of wheelchair user joint injury. WUJII can also be used to improve the propulsion technique for various users.

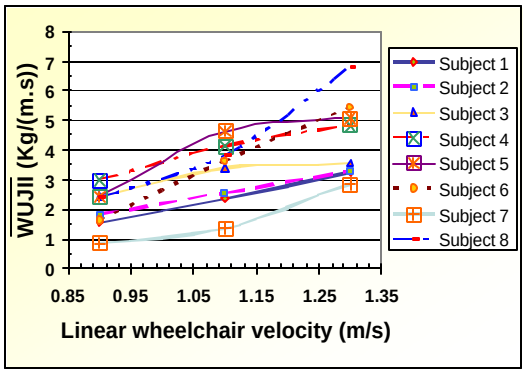

Figure 1: The values of $\overline{\text{WUJII}}$ at three linear wheelchair velocities.

Table 1 shows the mean and standard deviation (Std. Dev.) values of $\overline{\text{WUJII}}$ for the subjects at three LWVs.

CONCLUSIONS

The new Wheelchair User Joint Injury Index is reliable enough to be used in the research. Higher Linear wheelchair velocity may increase the injury and pain in the joints of the users. The new injury index can be used as a criterion to determine the optimum seat position of the wheelchair for individual users.

REFERENCES

Boninger, M.L. et al. (2000). *Arch. Phys. Med. Rehabil.*, **81**, 608-613.

Boninger, M.L. et al. (2002). *Arch. Phys. Med. Rehabil.*, **83**, 718–723.

Dicianno, B.E. (1999) *American J. Phys. Med. Rehabil.*, **78**, 177-178.

Veeger, H.E.J. et al. (1991). *Med. Sci. Sports Exerc.*, **24**, 100–107.

ACKNOWLEDGEMENTS

The authors wish to thank Dr. Thomas R. Oxland, and Dr. Antony J. Hodgson of the University of British Columbia for supporting this project and providing access to facilities.

Table 1. Mean and Std. Dev. of WUJII for the subjects at 3 linear wheelchair velocities.

Subject / Velocity (m/s)	**1**	**2**	**3**	**4**	**5**	**6**	**7**	**8**
0.9	1.55 ±0.19	1.80 ±0.39	2.45 ±0.57	2.97 ±0.22	2.41 ±0.24	1.60 ±0.25	0.86 ±0.10	2.36 ±0.17
1.1	2.34 ±0.23	2.55 ±0.33	3.39 ±0.51	4.12 ±0.42	4.63 ±0.66	3.62 ±0.61	1.35 ±0.13	3.79 ±0.42
1.3	3.27 ±0.65	3.27 ±0.15	3.54 ±0.56	4.81 ±0.80	5.08 ±0.97	5.44 ±0.59	2.87 ±0.55	6.80 ±1.04

ORIGINS OF THE LONG-RANGE CORRELATIONS IN STRIDE TIMES

Deanna H. Gates [1], Jimmy L. Su[1], and Jonathan B. Dingwell [2]

[1] Department of Biomedical Engineering, University of Texas, Austin, TX, USA
[2] Nonlinear Dynamics Laboratory, Dept. of Kinesiology, University of Texas, Austin, TX, USA
E-mail: jdingwell@mail.utexas.edu Web: http://www.edb.utexas.edu/faculty/dingwell/

INTRODUCTION

In healthy adults walking at comfortable speeds over level ground, the time series of stride times exhibits long-range correlations where each stride is correlated with thousands of prior strides (Hausdorff, 1995). When the system deteriorates due to age or disease, time series fluctuations become more uncorrelated, or random (Hausdorff, 1995). Several studies have tried to elucidate the origins on these correlations by proposing models that assume long-range correlations are regulated by *central* contol mechanisms (Ashkenazy, 2002; Hausdoff, 1995; West, 2003). While these models have been able to replicate the long-range correlations seen in stride time, they do not preclude alternative explanations. The present study set out to determine if a simple mechanical model of walking incorporating noise and minimal feedback control could generate long-range correlations similar to those observed in humans.

METHODS

We modified a simple model of bipedal walking that incorporates forward propulsion through an impulsive force applied to the trailing leg at each push-off (Kuo, 2002; Fig. 1). The push-off impulse P_i was modified to vary for each step, i, through a simple proportional feedback controller:

$$P_i = P_D + A \cdot \left[\left(P_D - P_{i-1} \right) + \xi_S U \right] + \xi_M U \quad (1)$$

where ξ_S and ξ_M represented the amplitudes of 'sensory' and 'motor output' noise terms, respectively, and U was uniformly distributed white noise on the interval [0,1].

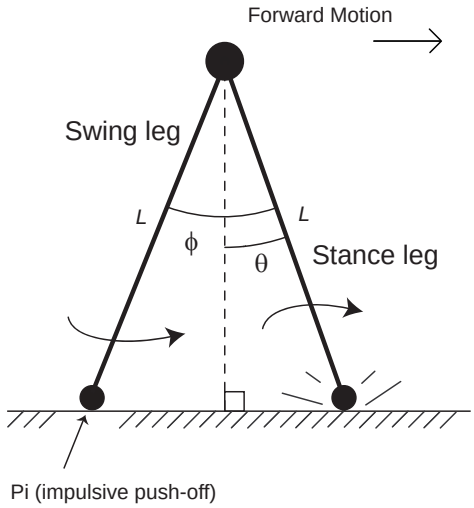

Figure 1. Diagram of the 2-D model

We generated 4000 total simulations to include 10 trials each with 400 different cobinations of sensory noise (ξ_S), motor noise (ξ_M), and feedback gain (A). In each simulation, the model took 1100 steps or 550 strides. The first 50 strides were removed prior to analysis as they may reflect some transient behavior due to initial conditions.

The stride time data from each simulation were analyzed using detrended fluctuation analysis (DFA). This method has been used extensively in the analysis of experimental time series because it reduces noise effects and removes local trends making it less likely to be affected by non-stationarities in the signal (Hausdorff, 1995). DFA pro-

duced a scaling exponent, α, which quantified how each stride interval was correlated with previous and subsequent stride intervals over different time scales. A value of α = 0.5 indicates that the time series is completely uncorrelated (i.e., white noise). Long-range correlations are present when $0.5 < \alpha \leq 1.0$ and short-range correlations exist when $\alpha < 0.5$. A single value of α was calculated for each simulation and the average of the ten trials was computed.

RESULTS AND DISCUSSION

The model ran successfully for all noise conditions with $A = 0$ and $A = 0.8$. For $A = 0.9$ and $A = 1.0$, the model became unstable at high noise levels. The model was less variable and took more time to take each stride than human walking. However, the stride times extracted from the model had the same correlation structure as that seen in healthy individuals walking at a comfortable pace. By varying the noise and feedback gain parameters, nearly any type of correlation structure could be obtained (Fig. 2). Likewise, the same type of correlation structure was obtained for multiple parameter combinations. Even in the presence of no feedback (ie. $A = 0$), the model generated long-range correlations.

SUMMARY/CONCLUSIONS

These results suggest that the long-range correlations observed in the stride interval time series of human walking could be due to the inherent biomechanical structure of the system and may not require complex central nervous system control (Gates, In Press). However, the central nervous system may still play a significant role in regulating these processes in humans. Future work must focus on determining precisely how *both* central nervous system processes *and* biomechanical factors contribute to these phenomena.

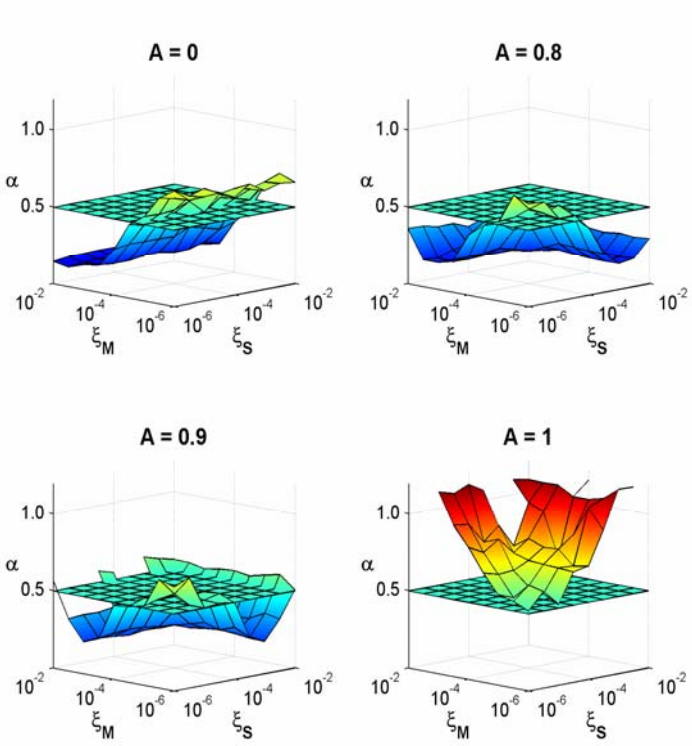

Figure 2: Changes in the correlations of stride time, α, as the model parameter values (A, ξ_M and ξ_S) were varied. The horizontal plane represents $\alpha = 0.5$ or random correlations. Above this plane, the series has long-range correlations. Below, it has short-range correlations.

REFERENCES

Ashkenazy, Y. et al., (2002) *Physica A* **316**, 662-670.

Garcia, M. et al., (1998) *J Biomech Eng* **120**, 281-288.

Gates, D. et al., (In Press) *Physica A*

Hausdorff, J.M., et al., (1995) *J Appl Physiol*, **78**, 349-358.

West, B.J., and Scafetta, N., (2003) *Phys Review E* **67**, 051917.

ACKNOWLEDGEMENTS

Supported by Whitaker Foundation grant #RG-02-0354 and NIH grant #EB003425

MOBILITY PATTERNS IN POWER WHEELCHAIR USERS AND THE IMPLICATIONS FOR MEASURING MOBILITY

Sharon Eve Sonenblum[1], Stephen Sprigle[1,2], and Chris Maurer[2]
[1]Georgia Institute of Technology, Atlanta, GA, USA; [2]Shepherd Center, Atlanta, GA, USA
E-mail: sharon.sonenblum@coa.gatech.edu

INTRODUCTION

Little literature is available concerning the mobility patterns of wheelchair users. Some generalized values of power wheelchair (PWC) use are available in terms of average distances and speeds over all subjects and days (Cooper 2002). However, the data lack the context of environment and do not identify how the movement is dispersed over time. Greater insight into PWC use and mobility patterns at home and outside will allow us to better understand the consequences of unmet mobility needs in both environments. While a study of this sort should be performed on manual wheelchair users and ambulatory persons with mobility impairments (such as those who use crutches or walkers), the burden of instrumentation makes it difficult and thus a study was first completed on PWC users.

This study aims to describe mobility patterns of PWC users in the home and outside. It also aims to describe the implications of these mobility patterns for the development of future studies and interventions for other populations with mobility impairments.

METHODS

A convenience sample of 25 adults (16 male, 9 female, mean age 46 yrs) with some affiliation to the location spinal cord injury rehabilitation center who used PWCs as their primary mobility devices were recruited for this study with IRB approval. All subjects signed informed consent forms.

Subjects' wheelchairs were instrumented with monitoring sensors for 1-2 weeks. Wheel counts were recorded on a single wheel using a reed switch and 2-4 evenly spaced Neodymium magnets. The sum of wheel counts was recorded in two second epochs on a custom data logger (Levo and Consonics, Switzerland). A Garmin GPS receiver and custom GPS logger (GeoStats, Atlanta, GA) recorded the latitude and longitude of the wheelchair every 5 seconds. GPS data was processed and used in a prompted recall interview during which we determined the subject's environment (i.e. location and indoors or outdoors) and what activities they were performing.

Post-processing of the data was done using GeoStats' software and custom Matlab code. Wheel counts were converted to distances and then bouts were computed. Bouts were defined as intentional, continuous bursts of movement beginning when a subject traveled 2 feet within four seconds and continuing until the subject traveled less than 2.5 feet over 14 seconds.

RESULTS AND DISCUSSION

Overall, most subjects wheeled very small distances (Table 1). However, the distribution of that distance was quite varied. The percent of total distance wheeled inside the home ranged from 3% to 93% (median 57%). However, the distribution of bouts was much more consistent. 16 of 21 subjects wheeled more than 60% of their bouts at home.

Table 1: Median (range) of daily wheelchair use was widely distributed over subjects.

	Distance (mi)	# Bouts
Overall	0.7 (0.1-6.6)	110 (36-281)
At Home	0.3 (0.0-0.9)	72 (5-204)
Outside	0.0 (0.0-4.4)	1 (0-31)

Wheelchair use outside was highly skewed. The median distance is representative of 15 of 21 subjects who wheeled less than 20% of their total distance outside. The remaining 6 predominantly wheeled outside.

In this study, the nature of mobility differed with environment (Table 2). Outside, subjects were more likely to travel a greater distance over a continuous bout of movement and reach a higher speed. At home, however, bouts were short and slow.

Table 2: Average bout parameters are dependent on environment.

	Distance (ft)	Duration (min)	Speed (mph)
Overall	53	0.5	1.2
At Home	23	0.4	0.6
Outside	329	1.6	2.4

The subject data presented in Figure 1 illustrates this behavior. The subject wheeled an average of 0.3 miles per day, 92% of which occurred in the home. The movement was spread out over 140 bouts and nearly 12 hours per day. The average bout went only 13 feet and only 1% of the bouts exceeded 50 feet.

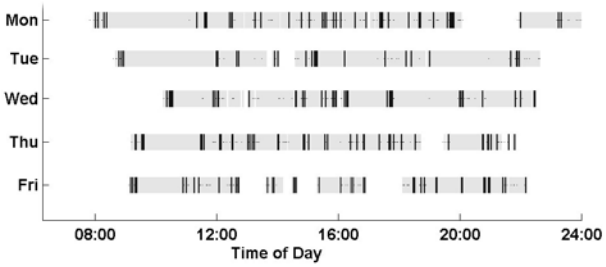

Figure 1: Wheelchair use for one subject. Gray bars indicate when subject was in wheelchair and vertical lines show mobility.

SUMMARY/CONCLUSIONS

PWC users do not have to exert additional energy to continue movement or move quickly, and yet their mobility bouts remain short and slow. Because this is likely to be true for other populations with mobility impairments, mobility should always be studied in terms of bouts as well as overall distances. When studying the biomechanics of manual wheelchair propulsion, one group found that the amount of torque needed to initiate movement is twice that needed during steady-state propulsion (Koontz, 2005). Given the prevalence of shoulder pain in people who use manual wheelchairs, this suggests that rehabilitation interventions may need to target the initial stroke of propulsion.

For persons with mobility disabilities, it appears that the predominant mobility requirement within the home is the ability to initiate movement, rather than to engage in high-speed, steady-state movement. Therefore, when studying persons with mobility impairments or developing rehabilitation interventions, one should focus on the initiation and termination of movements. Lastly, the design of mobility aids for use in the home should be optimized for safe initiation and termination of movement.

REFERENCES

Cooper, R.A., et al. (2002). *Arch Phys Med Rehabil*. **83**(2), 250-5.

Koontz, A.M. et al. (2005). *JRRD* **42**(4), 447-458.

ACKNOWLEDGEMENTS

Support was provided by NIDRR via the RERC on Wheeled Mobility and the NSF Graduate Research Fellowship Program.

A NEW TRUNK VOLUME REPRESENTATION FOR GEOMETRIC BODY SEGMENT MODELS

Jason Wicke [1] and Geneviève Dumas [2]

[1] Texas A&M – Commerce, Commerce, Texas, USA
[2] Queen's University, Kingston, Ontario, Canada
Email: jason_wicke@hotmail.com

INTRODUCTION

Geometric models (GM) are used to estimate body segment parameters (BSP), such as mass, center of mass location and moments of inertia by representing each segment as standard geometric shapes. Earlier GM used a single shape to represent an entire segment (e.g. Hanavan, 1964). Although relatively simple to use, these GM are associated with high errors for estimating BSP (Durkin & Dowling, 2003). More advanced models use a series of shapes such that the contours of the body can be followed (Jensen, 1978). These advanced GM provide the most accurate BSP estimates (Nigg, 1999).

The Jensen model uses a series of 2.0 cm thick elliptical cylinders to represent each segment, in which the width and girth dimensions are determined using photogrammetry. One of the primary limitations of this model is the use of a single shape to represent each of the segments. This is particularly an issue for the trunk segment, where a stadium shape may better represent the trunk (Sady et al., 1978). In addition, ellipses will unavoidably generate cavities in segment sections that are adjacent to other segments, such as the upper trunk and shoulder region, and the lower trunk and hips region (Figure 1). The goal of this study was to determine which shapes better represented the different regions of the trunk so that a new volume representation could be developed for GM.

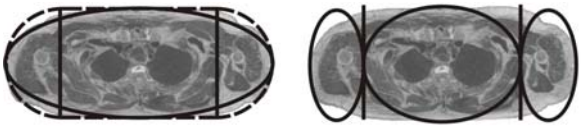

Figure 1: Upper trunk cross-section with sectioned ellipses (solid) and stadium (dashed) on right image and ellipses for the trunk and arms on left image.

METHODS

Whole body cross-sectional computed tomography (CT) scans of five male and five female Olympic athletes were used. These individuals were chosen for their muscular physique, minimizing tissue displacement while in the supine position. From the CT scans, cross-sections of four trunk regions (Table 1) were used for this study.

Table 1: Trunk regions, shapes tested and location of cross-section scans. E = Ellipse, SE = Sectioned Ellipse, SS = Sectioned Stadium.

Region	Shapes	Scan Location
Upper	E/SE/SSt	Neck of humerus
Chest	E/S	Xiphoid
Mid	E/S	Superior to iliac crest
Lower	E/SE/SSt	Max. gluteal protrusion

The four trunk cross-sections of the ten individuals were digitized in AutoCad 2000™ as were the shapes used to represent each section. The digitized area of the cross-section, each shape and the amount of over and under estimation between the cross-

section and the shape were obtained from the AutoCad properties function. A Multiple Analysis of Variance and Tukey Post Hoc was used to determine whether there were any differences in the average and error, under- and over-estimations between the shapes for each region.

RESULTS AND DISCUSSION

Across the trunk sections, the average error for the most accurate shape was within approximately ±3% error and the absolute error, which represents the maximum error of the cross sectional area estimates were all within 6.5% save the chest section (Table 1). One possible explanation for the large errors in the chest region is the lack of symmetry between the anterior and posterior contours, due to the pectoralis muscles and breasts. In the regions where the trunk was adjacent to another segment (i.e. upper and lower trunk), sectioning an ellipse that spans across the entire cross-section (e.g. trunk and arms) yielded the best results.

SUMMARY & CONCLUSIONS

Using sectioned ellipses to represent the trunk cross-section in regions where there is an adjacent segment (shoulders & thighs) eliminates the gaps generated from using separate ellipses, resulting in better volume and in turn BSP estimates.

REFERENCES

Durkin, J. L. & Dowling, J. J. (2003). Analysis of body segment parameter differences between four human populations and the estimation errors of four popular mathematical models. *Journal of Biomechanical Engineering., 125,* 515-522.

Hanavan, E. P. (1964). *A Mathematical Model of the Human Body.* (vols. AMRL-TR-64-102) Ohio: Wright-Patterson Air Force Base.

Jensen, R. K. (1978). Estimation of the biomechanical properties of three body types using a photogrammetric method. *Journal of Biomechanics, 11,* 349-358.

Nigg B.M. (1999). Inertial Properties of the Human or Animal Body. In B.M.Nigg & W. Herzog (Eds.), *Biomechanics of the Musculo-Skeletal System* (2 ed., pp. 376-399). Toronto: John Wiley & Sons.

Sady, S., Freedson, P., Katch, V. L., & Reynolds, H. M. (1978). Anthropometric model of total body volume for males of different sizes. *Human Biology, 50,* 529-540.

Table 1: Errors in using different shapes to represent the regions of the trunk. Darkened shape indicates the best representation. * and $^{+}$ = significant differences ($p < 0.05$).

		Average % Error		Over Est. % Error		Under Est. % Error		Absolute %Error	
Segment	Shape	Mean	SD	Mean	SD	Mean	SD	Mean	SD
Upper Trunk	Ellipse	-14.03	4.17	2.01	1.93	16.17	2.79	18.19	2.49
	S. Ellipse	-0.67	2.11	2.14	1.74	3.00	0.98	5.14	1.12
	S. Stadium	5.43	3.03	6.03	2.31	0.57	0.92	6.60	1.74
Chest	Ellipse	-0.50	0.72	8.28	1.70	9.05	1.75	16.34	2.34
	Stadium	7.41	3.05	11.03	1.91	3.82	1.46	14.86	1.43
Mid Trunk	Ellipse	-4.43	2.08	0.59	0.77	5.10	1.69	5.68	1.53
	Stadium	2.86	2.60	3.40	2.03	0.93	0.61	4.33	1.84
Lower Trunk	Ellipse	-18.36	1.63	0.00	0.00	12.08	0.94	18.59	1.48
	S. Ellipse	1.39	1.28	1.67	1.25	0.19	0.32	1.66	1.11
	S. Stadium	3.77	5.01	5.64	4.10	1.53	1.70	7.18	4.23

Gender Differences in Spinal Posture and User Positioning on a Prototype Seat Pan

Diana E. De Carvalho[1] Nadine M. Dunk [1], and Jack P. Callaghan[1]

[1] University of Waterloo, Waterloo, Ontario, Canada
E-mail: ddecarva@ahsmail.uwaterloo.ca

INTRODUCTION

Recent research has documented spinal posture differences between men and women when sitting in an office chair (Dunk and Callaghan 2005). Women were found to have a greater lumbar lordosis and a slightly forward leaning spine compared to men when sitting and they positioned themselves closer to the front of a seat pan. The current study was undertaken to confirm these earlier findings with subjects of a greater range of anthropometrics as well as to investigate possible differences in user positioning on a prototype pivoting seat pan both with and without a backrest (Squig model supplied by KEILHAUER, Toronto, ON, Canada). This seat pan model varies slightly from traditional pivoting seat pans by including an extra degree of freedom that allows for lateral as well as combined A/P and M/L motion of the user.

METHODS

40 subjects (20 males and 20 females), taken from a university population, were tested on the prototype without a backrest for a 15 minute trial and with a backrest for a 2 minute trial. These subjects were free of back pain for at least 12 months and were screened to bracket a wide range of anthropometrics. Mean height percentile was 56.8 (range 12.9-98.7) for males and 43.2 (range 0.2-99.1) for females. Mean weight percentile was 51.1 (range 8.2-99.7) for males and 55.1 (range 12.9-99.6) for females. Seat pressure profiles and motion analysis data were collected to give center of pressure, peak pressure, spine angles, center of mass and user position on the seat pan for the 15 minute trial. Motion analysis data alone were collected for the 2 minute trial in order to identify if interaction with the backrest altered user positioning. The subjects performed a combination of typing and mousing tasks at a computer workstation. Both desk and chair were adjusted to fit the subject prior to data collection to maintain proper ergonomics. A comfort questionnaire, including a visual analogue scale for discomfort, was administered at the beginning, at the midpoint and at the end of the 15 minute trial and once following the 2 minute trial. Statistical analysis was performed on the seat pan trials only. Information from the backrest trials was to be used in design decisions for optimal placement of the backrest.

RESULTS AND DISCUSSION

The shape and location of the thoracic and lumbar curves over the seat pan were approximately the same for all 40 subjects across all the trials. Some variability was noted in user positioning in the A/P plane, however, this was not related to either the height or mass of the individual. There was virtually no difference in seated spine height or vertical location of the lumbar curve across genders or anthropometrics.

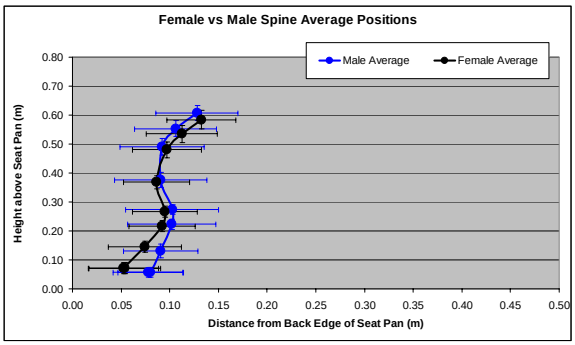

Figure 1: Average spine positions for males and females from back edge of the seat pan.

There was no relationship between percentile and A/P positioning on the seat pan. Some of the tallest subjects sat closer to the front edge of the seat pan, while some of the shorter subjects sat further back on the seat pan.

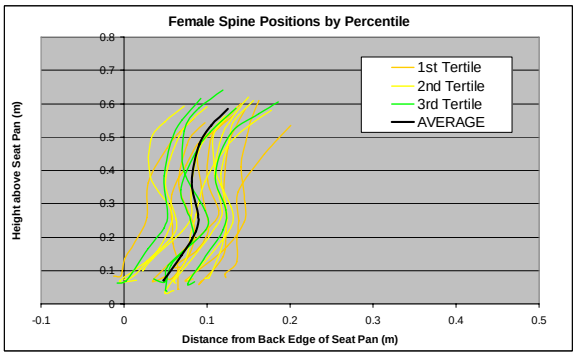

Figure 2: Female spine position on seat pan by percentile.

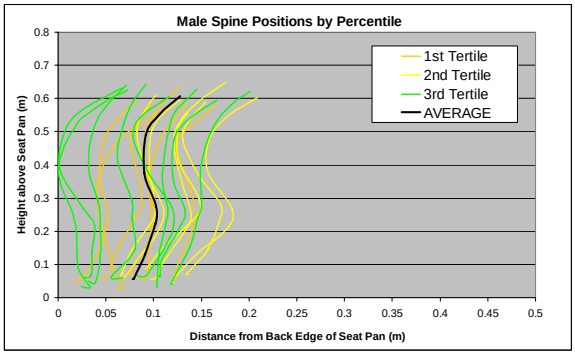

Figure 3: Male spine position on seat pan by percentile.

A major difference in female user position on the seat pan was found. Specifically, the most posterior part of the buttocks was located closer to the back edge of the chair. A slightly greater lumbar lordosis and a forward leaning posture were noted in the female subjects, agreeing with previous findings by Dunk and Callaghan (2005). A t-test was conducted on user positioning variables for the seat pan trials between men and women. The only statistically significant difference was a greater trunk angle in woman ($p<0.002479$) as measured from the vertical (more forward leaning). Both male and female subjects sat with an average 10 degree recline during the backrest trial. Seat pressure and discomfort data revealed an asymmetrical distribution of pressure favoring the left side in both male and female subjects.

SUMMARY/CONCLUSIONS

Female subjects may be more sensitive to seat pan type. This would explain the position of their center of mass posterior to the seat base to maintain balance over the pivot point of the chair. Therefore, a potential benefit of this new chair is increased utilization of the backrest. Gender differences in user positioning seen previously appear to be removed by this prototype seat pan. The pressure distribution identified could be attributed to asymmetrical demands of mousing and the additional pivoting degree of freedom in the frontal plane of the chair which warrants further investigation.

REFERENCES

Dunk,N.M. and Callaghan,J.P. (2005) Gender-based differences in postural responses to seated exposures. *Clinical Biomechanics* **20,** 1101-1110.

ACKNOWLEDGEMENTS

This study was supported by KEILHAUER.

AUTOMATED HEXAHEDRAL MESHING OF ANATOMICAL STRUCTURES USING DEFORMABLE REGISTRATION

Ritesh Bafna, Vincent A Magnotta, Nicole M. Grosland
The University of Iowa, Iowa City, IA, USA
Email: nicole-grosland@uiowa.edu, Web: www.ccad.uiowa.edu/mimx/

INTRODUCTION

The Finite Element (FE) method is a widely used numerical technique in the field of biomedical engineering for computational analysis of biological structures having irregular geometry, anisotropic material properties and complex boundary conditions. A fundamental requirement of FE analysis is an accurate 3D model. One of the challenges when using the FE method is the significant amount of time and manual intervention required to generate such models.

In this work, a new mapped meshing technique for automating the process of patient-specific FE models is presented.

METHODS

The algorithm developed here utilizes a high dimensional registration technique based upon the finite element method. This technique warps a three-dimensional hexahedral template mesh onto the desired surface definition. The algorithm uses a multi-resolution (coarse to refined mesh) approach to speed up the convergence of the algorithm.

Deformable Registration Initialization

The registration algorithm is initialized with an iterative closest point (ICP) affine registration used to bring the template mesh into rough correspondence with the subject surface; accounting for size, position, and orientation differences between the representations.

Deformable Registration The number of elements defining a desired template mesh definition may be large. Consequently, we have implemented a multi-resolution approach. A series of models increasing in refinement toward the desired template mesh are created. An extremely coarse mesh, for example, is used to establish the initial deformation field which is then applied to a more refined mesh.

To initiate the registration, the user specifies the mesh definitions (from coarse to refined), the corresponding number of iterations, and the elastic modulus to be used for each level of refinement. After the specified number of iterations at a given mesh resolution, the resulting deformation field is applied to the next level of mesh refinement. The registration process was applied iteratively until the highest resolution mesh is completed.

The forces used to drive the FE registration were derived from the distance between the surface nodes of the template mesh and the corresponding closest node on the subject surface. These forces were applied along the normal of the template mesh. The FE model deforms under the laws of non-linear continuum mechanics.

As a proof of concept, this algorithm was initially applied to warp a cubic mesh onto a spherical surface (Figure 1). Four levels of refinement were used with mesh densities ranging from 27 to 1728 elements. In addition, a template mesh of a proximal phalanx bone was created using a bounding

box projection technique (Shivanna 2006). The optimal mesh refinement was chosen for the template mesh following a convergence study. Two levels of refinement (1890 and 6765 elements) were used to warp the desired mesh to the new subject-specific proximal phalanx surface. The distance between the final mesh and the subject surface was measured along with the mesh quality.

RESULTS

The results of the warped cube onto the sphere are shown in Figure 1. The average distance between the sphere and warped mesh surface was 0.007mm. The phalanx bone is shown in Figure 2. After registration the average distance was 0.042mm. The final mesh did not contain any zero volume elements and was suitable for surface contact analysis.

CONCLUSION

This preliminary result shows that this algorithm can be applied to template mesh of one subject to generate high quality FE mesh of the same bone of different subjects. Future work would involve applying the algorithm to slightly different types of bones. Also, we would like to apply this technique to more complicated bones like the vertebrae.

REFERENCES

Shivanna K.H., *et al*. (2006). Automating patient-specific finite element model development. 9th MICCAI Conference.

ACKNOWLEDGEMENTS

The authors gratefully acknowledge the financial support provided by an NIH Award EB005973.

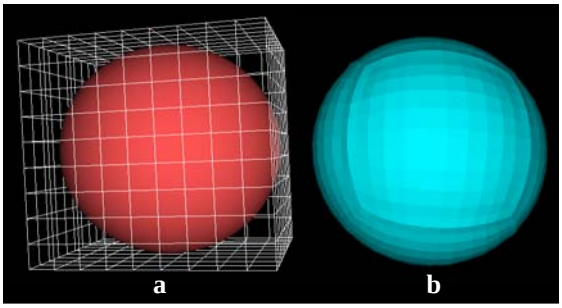

Figure 1. (a) Initial alignment of the cubic hex mesh and the surface. (b) The resulting warped solid mesh.

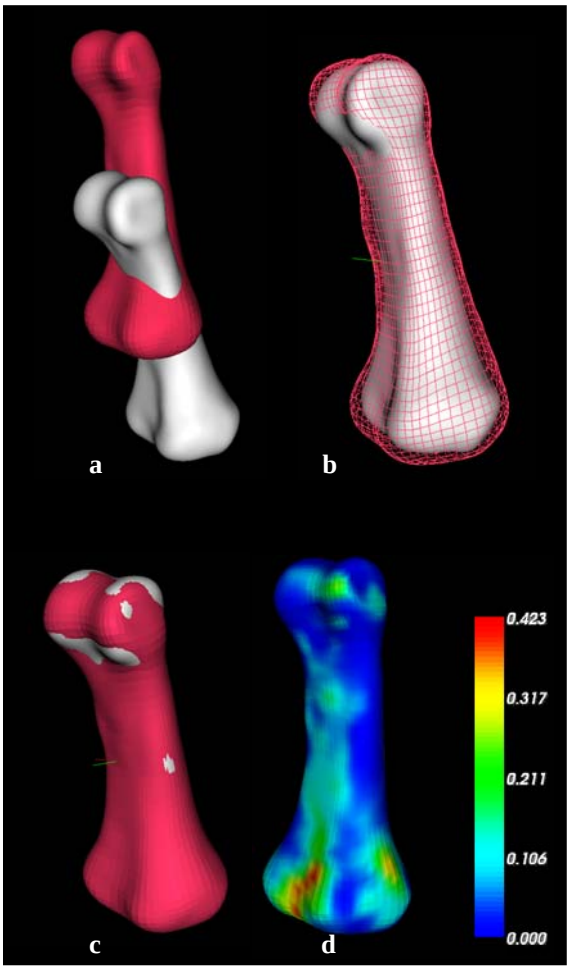

Figure 2. (a) Initial alignment of subject and template mesh. (b) Results after ICP registration. (c) The final solid mesh and subject surface. (d) Distance map between the resulting mesh and surface (units: mm).

EVALUATION OF THREE METHODS FOR DETERMINING EMG-MUSCLE FORCE PARAMETER ESTIMATES FOR THE SHOULDER MUSCLES

Christopher J. Gatti [1], Lisa Case Doro [1], Joseph E. Langenderfer [2], Amy G. Mell [1], Joseph D. Maratt [1], James E. Carpenter [1], Richard E. Hughes [1,*]

[1]Laboratory for Optimization and Computation in Orthopaedic Surgery, University of Michigan, Ann Arbor, MI
[2] Department of Engineering, University of Denver, Denver, CO
*E-mail: rehughes@umich.edu, Web: http://www-personal.umich.edu/~rehughes/index.html

INTRODUCTION

Individual muscle forces across a joint can be estimated using EMG-driven models. Multiple linear regression and principal-components regression (PCR) have been used to estimate muscle parameters. The quality of parameter estimates can also be improved by using orthogonal physical activities to generate EMG signals. The purpose of this study was to evaluate whether PCR-based estimates of shoulder muscle force-EMG relationships can be improved by incorporating orthogonal motions during the calibration trials.

METHODS

Thirteen healthy volunteers (mean age 23.4 ± 3.8 years) participated in the current study; informed consent was obtained from all study participants, and the protocol was approved by the University Institutional Review Board. Anthropometric measurements were obtained, including height, weight, and arm segment lengths. Surface and intramuscular wire electrodes were used to measure EMG activity of 12 muscles which cross the glenohumeral joint. The subject's arm was casted in 90˚ of elbow flexion with neutral forearm rotation from the midshaft of the humerus to the wrist along with a 90˚ aluminum mounting plate. Subjects were seated and restrained in a Biodex System 2 with the arm abducted 30˚ in the coronal plane with neutral humeral rotation, and the casted aluminum mounting plate was secured to a 6-DOF load cell fixture mounted on the testing apparatus. Muscle parameter calibration consisted of 3 trials each of 8 individual, sub-maximal, ramp-isometric contractions (SRICs): flexion and extension of the elbow, abduction and adduction, internal and external rotation, and flexion and extension of the shoulder. For each SRIC, subjects were instructed to steadily increase and then decrease (2-second duration each) the intensity of each action from 0 to 50% of their respective maximum voluntary isometric contraction. A custom-written LabVIEW graphical interface provided the subject with each action's 50% cutoff and a set pace at which to perform the SRIC. EMG signals were recorded at 1000 Hz and filtered using a Butterworth filter (4^{th} order, 4 Hz low-pass cutoff). Load cell data were recorded at 1000 Hz and filtered using a Butterworth filter (2^{nd} order, 8 Hz low-pass cutoff). Shoulder reaction moments were computed using subject anthropometry and the filtered moment and force data from the load cell.

One of each SRIC was grouped into a set of trials, resulting in 3 sets of trials for which muscle parameters, relating EMG to muscle force, were computed using different methods: multiple linear regression (MR), principal-components regression (PCR), and

a sequential method using principal-components regression (PCR-S). MR and PCR muscle parameters used three-axis moment data from the SRICs of the 6 actions about the shoulder. MR muscle parameters were computed following the same methods as Hughes and Chaffin (1997). For PCR, principle components were determined in conformance with Draper and Smith (1981); PCR helps to mitigate the effects of covariance, which is present in multiple regression models, by reducing the dimensionality of the data. EMG data and muscle moment arms were multiplied and used to determine the correlation matrix; the minimum number of eigenvectors required to explain 95% of the variance were retained. Muscle parameters were then computed using the retained eigenvectors and EMG and shoulder reaction moment data. PCR-S consisted of calculating muscle parameters in a sequential manner using single-axis moment data from all 8 SRICs; muscle parameters were computed from the SRIC for which they are primary agonists based on moment arms in the calibration posture. The three muscle parameter estimation methods were evaluated using three criteria: (1) the number of subjects with positive muscle parameters, (2) the coefficient of variance (COV) of the muscle parameters, and (3) the root mean square error (RMSE) between the measured and the predicted shoulder moments.

RESULTS

Performance results of each muscle parameter estimation method are presented in Table 1. PCR-S was found to yield the greatest number of subjects with at least 1 set of trials with positive muscle parameters; positive muscle parameters are desired in order to predict tensile muscle forces. PCR-S also had the smallest COV across all 3 sets of trials (averaged over all muscle parameters). MR resulted in the lowest RMSE between the measured and predicted shoulder reaction moments (averaged over all SRICs); however, MR resulted in only 4 subjects that had at least 1 set of trials with positive muscle parameters. The performance of PCR fell between that of MR and PCR-S.

CONCLUSIONS

The muscle parameter estimation methods evaluated in the current study showed a trade off with respect to the evaluation criteria. PCR-S more frequently produced physiological parameter estimates, while MR predicted shoulder reaction moments best. However, all methods yielded muscle parameters that can be used to calculate *in vivo* shoulder muscle force.

REFERENCES

Draper N.R., Smith H. (1981). *Applied Regression Analysis*. Wiley.

Hughes R.E., Chaffin D.B. (1997). *IEEE Trans Biomed Eng*, **44**, 639-642.

ACKNOWLEDGEMENTS

This study was supported by National Institutes of Health (AR048540).

Table 1: Muscle parameter estimation method performance.

Evaluation criteria	MR	PCR	PCR-S
Subjects with positive muscle parameters (#, out of 13)	4	5	11
COV (%)	177 ± 997	90 ± 373	39 ± 72
RMSE (N m)	4.10 ± 1.35	5.64 ± 1.68	9.25 ± 4.60

THE EFFECT OF MUSCLE FATIGUE ON CORRELATIONS IN TIMING ERRORS

Deanna H. Gates [1] and Jonathan B. Dingwell [2]

[1] Department of Biomedical Engineering, University of Texas, Austin, TX, USA
[2] Nonlinear Dynamics Laboratory, Dept. of Kinesiology, University of Texas, Austin, TX, USA
E-mail: jdingwell@mail.utexas.edu Web: http://www.edb.utexas.edu/faculty/dingwell/

INTRODUCTION

When a person repeatedly performs a task, their movement patterns appear to vary randomly. However, time series analyses reveal that some movement data, like synchronization errors in finger tapping (Ding, 2002), exhibit fractal long-range correlations. It has been postulated that these correlations are inherent to healthy systems and that the loss of these long-range correlations may indicate disease (Goldberger, 2002).

When a person fatigues, their coordination patterns may change (Cote, 2002; Sparto, 1997). After extreme fatigue, people will likely become more 'random' since they lose fine control over their movements due to a decrease in active motor units, slower motor unit response time and decreased proprioceptive feedback. This study determined if long-range correlations were lost due to significant muscular fatigue during a repetitive upper extremity sawing-like task.

METHODS

11 healthy right-handed subjects (26±3 yrs) sat in an adjustable chair with seat belts to ensure constant posture. They then pushed a weight back and forth along a low-friction horizontal track in time with a metronome until voluntary exhaustion. Movements of a single marker placed on the top of the handle were recorded at 60 Hz using Vicon (Oxford Metrics, Oxford, UK).

Timing errors were calculated by subtracting the time the handle marker reached a maximum or minimum from the time of the nearest metronome beep (Ding, 2002). Each timing error time series was first analyzed using detrended fluctuation analysis (DFA). This method produces a scaling exponent, α, that indicates what type of correlation exists. For $\alpha = 0.5$, the series is completely uncorrelated (i.e., white noise). Long-range correlations exist when $0.5 < \alpha \leq 1.0$ and short-range correlations exist when $\alpha < 0.5$.

Second, variability was further decomposed by postulating an explicit mapping from variability of body movements to variability at the *goal* level of the task (Cusumano, 2006). The primary *goal* of this task was to maintain time with the metronome, but many combinations of movement distance (d) and velocity (v) achieve this goal. These (d, v) combinations define the *goal equivalent manifold* (GEM), which is equal to the frequency of the metronome, f_m (Fig. 1). We then decomposed the variability in d and v into variability tangent to $(\hat{e}_T)$ and perpendicular to $(\hat{e}_P)$ the GEM:

$$\vec{\delta}_n = \delta_T \hat{e}_T + \delta_P \hat{e}_P$$

The scalar deviations $\delta_T = \vec{\delta}_n \cdot \hat{e}_T$ do *not* contribute to the timing errors, while the deviations $\delta_P = \vec{\delta}_n \cdot \hat{e}_P$ *do*. We hypothesized that correlations in δ_T and δ_P would be different reflecting different control strategies to minimize errors at the goal.

DFA was performed on timing errors and errors perpendicular to and along the GEM. Only the first and last 600 errors from each experiment were analyzed (approximately 3

minutes) to obtain 'pre' and 'post' fatigue measures. Comparisons for timing errors were made using a within subjects ANOVA. Comparisons for δ_T and δ_P were made using a 3-factor ANOVA (Subject x Direction x Pre/Post) (MINITAB 14).

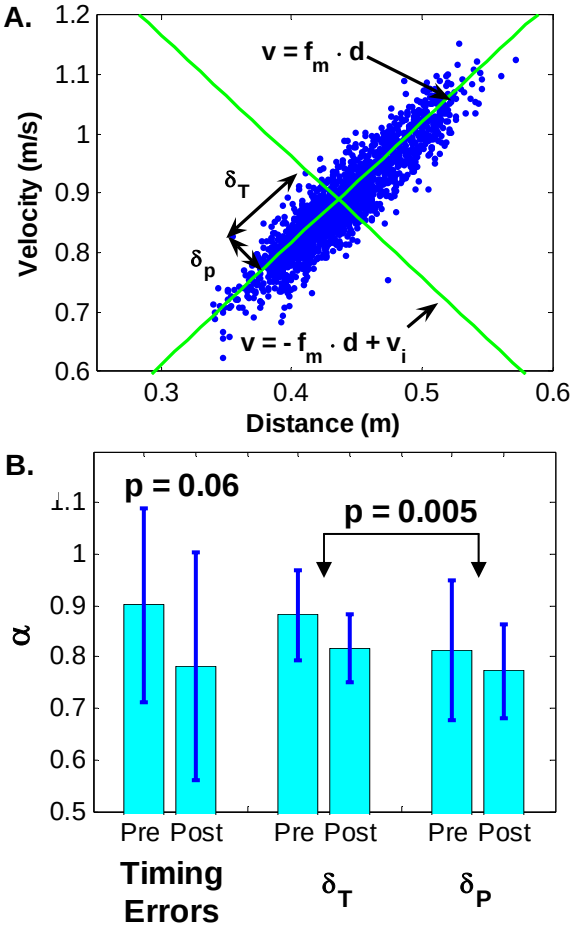

Figure 1.A. The GEM approach is illustrated. Errors are found both perpendicular to (δ_P) and along to (δ_T) the GEM.
B. Correlations tended to become more random with muscle fatigue.

RESULTS AND DISCUSSION

Subjects performed the task for 27.4 ± 8.8 minutes. DFA analysis revealed long-range correlations for timing errors (Fig. 1A). These errors tended to be somewhat more random after fatigue, but this effect was not quite significant (p = 0.06). Subjects exhibited a strong correlation between distance and velocity to stay in time with the metronome (Fig 1B). For the GEM decomposition, δ_T and δ_P errors were significantly different (p = 0.005). While pre/post fatigue differences were not significant, α tended to decrease post fatigue (p = 0.186).

SUMMARY/CONCLUSIONS

Timing errors during cyclic arm movement exhibited long-range correlations. A significant difference was found between directions of the GEM. This suggests that humans use different mechanisms to control *goal relevant* vs. *goal equivalent* movements with respect the task goal. Correlations decreased with muscle fatigue although this decrease was not significant for either analysis technique. One reason for this may be that subjects fatigued in different ways which led to large between subject variability. This study indicates that muscle fatigue may influence temporal coordination of movement. Further analysis should explore fatiguing specific muscle groups required for the task to provide consistency across subjects.

REFERENCES

Cote, J. et al. (2002) *Exp Brain Res* **147** (3): 394-398.

Cusumano, J.P. & Cesari, P. (2006) *Biol Cybern*, **94**(5): 367-379.

Ding, M., Chen, Y., Kelso, J.A.S., (2002) *Brain Cognit.* **48** (1): 98-106.

Goldberger, A. et al. (2002) *Proc Nat Acad Sci* **99** 2466-2472.

Sparto, P. et al. (1997) *Spine* **22** (22): 2647-2654.

ACKNOWLEDGEMENTS

Supported by NIH Grant #EB003425

THE EFFECT OF AGE AND PERIPHERAL ARTERIAL DISEASE ON GAIT PARAMETERS

Jessie M. Huisinga[1], Jason M. Johanning[2,3], Iraklis Pipinos[2,3], Sara A. Meyers[1], Matija Radovic[1], and Shing-Jye Chen[1]
[1] University of Nebraska at Omaha
[2] University of Nebraska Medical Center
[3] Veterans Affairs Medical Center, Omaha, NE
E-mail: jhuisinga@mail.unomaha.edu Web: biomech.unomaha.edu

INTRODUCTION

Aging produces gait changes that have been associated with impaired balance, falls, and increased risk of permanent injury (Rubenstein, 2006). These gait alterations in the healthy elderly indicate that despite absence of significant comorbidities, elderly individuals still have altered kinematic and kinetic parameters when compared to young adults (Kerrigan et al., 1998). When elderly individuals suffer from additional gait impairing diseases, the effects of aging on gait could be magnified. Peripheral Arterial Disease (PAD) is a disorder that impairs gait due to occlusion of the arteries of the lower extremities, leading to muscle ischemia and severe pain. This manifestation of atherosclerosis of the leg arteries affects approximately 10 million in USA and it is more prevalent in the elderly (Antignani, 2003). Examining the combined effects of aging and PAD on kinematic and kinetic gait parameters may help to classify how PAD magnifies gait changes that occur even in healthy elderly individuals. The purpose of this study, therefore, was to examine whether PAD exaggerates gait parameter changes normally associated with healthy aging.

METHODS

Fourteen healthy controls (age 47-85 yrs) and 20 PAD patients (age 53-87 yrs) with clinically diagnosed claudication, participated in the study. All participants were classified as either young (< 65 yrs, n=18) or elderly (> 65 yrs, n=16).

Kinematic data was collected using a 6-camera Motion Analysis system (60 Hz) while the patient walked down a 10 meter walkway at self-selected speed. At the same time, kinetic data was captured using an embedded Kistler force plate (600 Hz). Patients and controls walked pain free through a walkway at their self-selected pace for a total of 10 trials. Direct comparisons on selected kinematic and kinetic gait parameters were performed between controls and patients under 65 yrs as well as controls and patients over 65 yrs using independent t-tests.

RESULTS AND DISCUSSION

For the comparison between controls and patients under 65 yrs, all kinetic differences were found in the anteriorposterior (A/P) direction. Controls had significantly ($p<0.05$) higher peak braking force (FyB) and peak propulsion force (FyP) as compared to the patients (Figure 1). Also, Controls had significantly higher braking (IB) and propulsion (IP) impulse when normalized to stance time.

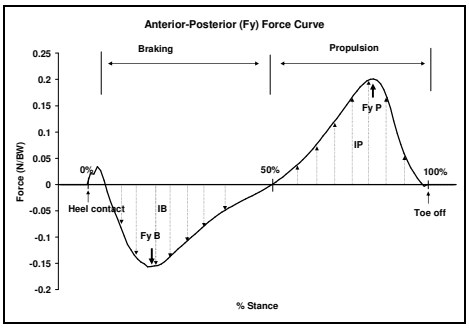

Figure 1: Reference GRF curve in A/P direction.

The increase in peak discrete point values indicates that the controls had more movement in the A/P direction. There were no significant differences in joint angles between the controls and patients under 65 yrs. Interestingly, the comparison between controls and patients over 65 yrs resulted in the same significant differences in the A/P direction with additional differences in the vertical and medial/lateral directions. The first active loading vertical peak (Fz1) was higher in the controls than the patients and the local minimum of vertical force experienced at midstance (Fzmin) was lower in the controls indicating the controls had more movement in the vertical direction as compared to the patients (Figure 2).

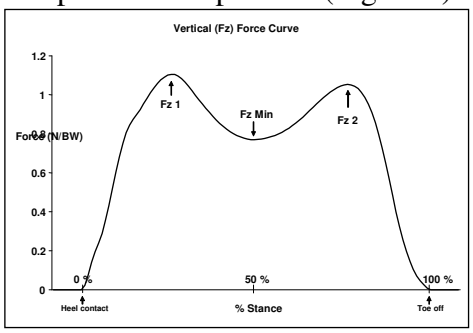

Figure 2: Reference GRF curve Vertical direction

The peak medial (FxMin) and lateral (FxMax) forces were increased in the control group (Figure 3) again indicating an increase in side-to-side movements in the controls.

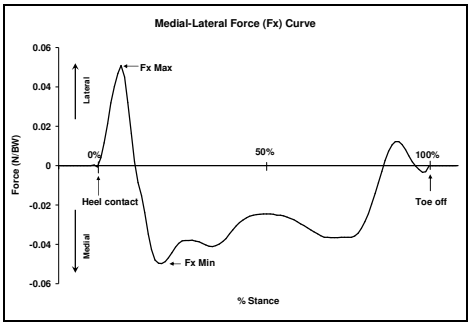

Figure 3: Reference GRF curve in M/L direction

Finally, loading rate was significantly increased in the control group, indicating a faster transfer to full weight bearing after heel strike in the control group. With respect to joint angle measures, the elderly patients had significantly increased ROM at the ankle as compared to the elderly controls. Though not significant, there was also a decrease in ROM at the knee and hip in the patients which indicates that compensations for loss of whole chain motion occur at the ankle by increasing the ROM.

SUMMARY/CONCLUSIONS

These results indicate that as PAD subjects age, differences in gait parameters increase when compared to healthy controls. The younger group differences show that compared to healthy controls, PAD subjects exhibit altered gait parameters. Differences between healthy and PAD gait have been previously shown (Scott et al., 2005), but the differences that are illuminated as the patient ages indicate that PAD exaggerates changes in both kinematic and kinetic gait parameters. The changes produced by PAD illustrate that in the presence of comorbidities, elderly gait parameters must be closely monitored in order to implement correct treatment or rehabilitation programs and provide a better quality of life.

REFERENCES

Antignani (2003) *Current Vascular Pharmacology,* **1**, 205-216.

Kerrigan, D. et al. (1998) *Arch Phys Med Rehabil,* **75**, 317-322.

Reubenstein, L. (2006) *Age & Aging*, **35**, Suppl 2:ii37-ii41.

Scott, M. et al. (2005) *Proceedings of ISB'05.* Cleveland, OH.

ACKNOWLEDGMENTS

This work supported by NIH (K25HD047194), NIDRR (H133G040118), the NRI, and the American Geriatrics Society's Dennis W. Jahnigen Award.

A Three-Dimensional Nonlinear Kinematic Finite Element Model of the Human Cervical Spine Under Dynamic Inertial Loading

Probst, B, Anderson, R[1], Hart T[2], Harris G[3], Guccione, S[4]

[1] Department of Biomedical Engineering, Tulane University, New Orleans, LA
[2] Biomedical Engineering Department, The Ohio State University, Columbus, OH
[3] National Center for Advanced Manufacturing, University of New Orleans, New Orleans, LA
[4] Department of Othropaedic Surgery, Medical College of Wisconsin, Milwaukee, WI

INTRODUCTION

State-of-the-art finite element models were developed, calibrated, validated, and exercised to realistically simulate the kinematic response of the human head and neck during any general three-dimensional acceleration. A specific case was exercised, with the exclusion of musculature, of our general hypothesis that an in vitro model can be used to test the feasibility of an in vivo finitie element model and to provide motion input data for individual motion segments for the said in vivo model. The models were developed based on motion analysis of ligamentous cervical spines, cadaveric motion analysis at the Medical College of Wisconsin (MCW), and from human research volunteer (HRV) data acquired at the National Biodynamics Laboratory (NBDL) in New Orleans.

The models exhibit biofidelic motion on the individual motion segment level, as validated by cadaveric data. Previously reported models have been validated for head motion only. Our model was validated for head motion as well as individual vertebral motion with cadaveric data for extension, flexion, and lateral inertial loads.

METHODS

Complete kinematic data sets from cadaveric studies performed at the Medical College of Wisconsin's Biomechanics Research Laboratory were obtained. Four unembalmed cadaveric human head and neck specimens, were mounted on a specially designed mini-sled pendulum. A low pulse acceleration profile with a peak of 8 g and duration of 15 milliseconds (ms) at T1, with the pendulum having an impact velocity of 5 mph and a high pulse acceleration with a peak of 14 g and duration of 15ms at T1, with a pendulum impact velocity of 7.5 mph were selected. This information was used as a standard in the calibration of the model. Data obtained included accelerations for the head and T1, angular rotational rates for the head, and displacements in three orthogonal directions for the head and C2 through C7.

Using data compiled by Williams and Belytschko (Williams and Belytschko, 1981) based on the work of Liu, et al., Francis and Lanier anatomic points representing "key points" of the vertebral bodies were used to develop the structural geometry utilizing TrueGrid® (XYZ Scientific Applications, Inc., Livermore, CA) mesh generating software.

Material properties were taken from the literature, when available, and modified based on the quasi-static mechanical testing using an in-house MTS servo-hydraulic system.

A masked prediction study was done to ensure that the model's properties were accurately described. Acceleration profiles from the NBDL, different from those of

MCW, were utilized so that numerical results would be accurate when compared to the experimental data from HRVs. The acceleration profiles utilized in the validation process were chosen specifically to match that used by Wismans (Wismans, et al., 1986) and de Jager (de Jager, et al., 1994). In addition to providing external validity, it allowed for direct comparison of this model to other previously developed models.

RESULTS AND DISCUSSION

A perfect agreement between the measured and calculated values would result in a correlation coefficient of 1.0. The correlation of the x displacement for frontal impact simulations had a minimum coefficient of 0.94. This exceeded the values of current and previous researchers of 0.7. In comparison of a low pulse 45° orientation run, the correlation of the x and y displacement for the oblique impact simulation was 0.9.

The model was also exhibited physiological phenomenon. The phenomenon of coupling was demonstrated because the model is novel in its use of accurate anatomic structures, such as the facets, and contact analysis.

In the external validation phase, the correlation value was exceeded for eighty-nine percent of the NBDL test subjects for the x-displacement at all acceleration levels in flexion runs. The correlation coefficient for the overall response for all test subjects for each acceleration profile exceeded 0.9 for the oblique runs.

SUMMARY/CONCLUSIONS

The model developed can satisfactorily represent the dynamic displacement and, therefore, dynamic acceleration behavior of the head and neck in frontal (minus x), lateral (plus y) as well as oblique (minus x plus y). This is the first finite element head neck model to be validated for frontal, lateral, and oblique impact simulations by comparisions with experimental results. Previous researchers have validated their models in a plane that corresponds to a single orthogonal axis. Oblique validation is a more severe validation test because of the three-dimensional motion involved. Multi-planar motion exists due to the direction of the load, as well as the coupling phenomenon. The agreement obtained with the oblique test is comparable to the test with single-plane motion. This agreement is an example of the robustness of the model.

This model can be further developed for the investigation of injury mechanisms. It is capable of calculating stresses within materials. It would be possible to compare calculated disc loads with experimentally known structural failure loads, and the likelihood of injury.

REFERENCES

Williams, J. and T. Belytschko (1981). A Dynamic Model of the Cervical Spine and head. AFAMRL-TR 81, **5**.

Wismans, J., H. v. Oorschot, et al. (1986). Omni-Directional Human Head-Neck Response. *Proceedings of the 30th Stapp Car Crash Conference*, SAE Paper No. 861893.

de Jager, M., A. Sauren, et al. (1994). A Three-Dimensional Head-Neck Model Validation for Frontal and Lateral Impacts. *Proceedings of the 38th Stapp Car Crash Conference*, SAE Paper No. 942211

CRITERIA FOR DYNAMIC SIMILARITY IN BOUNCING GAITS

Sharon R. Bullimore[1], Jeremy F. Burn[2] and J. Maxwell Donelan[3]

[1]Human Performance Lab, Faculty of Kinesiology, University of Calgary, Canada. [2]Departments of Anatomy and Mechanical Engineering, University of Bristol, UK. [3]Locomotion Lab, School of Kinesiology, Simon Fraser University, Canada. Email: sbullimore@kin.ucalgary.ca.

INTRODUCTION

When animals of different sizes travel at speeds corresponding to equal values of the Froude number (u^2/gL where u is speed, g is the acceleration due to gravity and L is leg length) they tend to move in a dynamically similar manner – i.e. they use close to equal values of duty factor (DF), stride length relative to leg length (RSL) and peak vertical ground reaction force relative to body weight (RPF). Consequently, the Froude number has been widely used to define equivalent speeds for comparing animals of different sizes and to predict speeds in extinct species and on other planets (Vaughan and O'Malley, 2005). However, Donelan and Kram (2000) have demonstrated, using simulated reduced gravity, that equal Froude number does not guarantee dynamic similarity, even in perfectly geometrically similar individuals. Their results have cast doubt upon the validity of using the Froude number to define equivalent speeds or to make predictions.

It has been suggested that the planar spring-mass model may be useful for defining criteria for dynamic similarity (Blickhan, 1989; Blickhan and Full, 1993; Donelan and Kram, 2000). This simple model of bouncing gaits, such as run, trot and hop, consists of a mass bouncing on a linearly elastic spring. Here we use dimensional analysis of this model to obtain criteria for dynamic similarity in bouncing gaits and to determine why dynamic similarity does not occur at equal Froude number in simulated reduced gravity.

MODEL VALIDATION

We first needed to determine whether the model accurately predicts DF, RSL and RPF in normal and reduced gravity conditions. To do this, we compared its predictions to a subset of the data of Donelan and Kram (2000). The model provided excellent predictions of DF, RSL and RPF. All predictions were within 20% of measured values and more than 90% of predictions where within 10% of measured values (Fig. 1). Prediction error either decreased, or did not change, as gravity level decreased, indicating that this is also a good model of running in simulated reduced gravity.

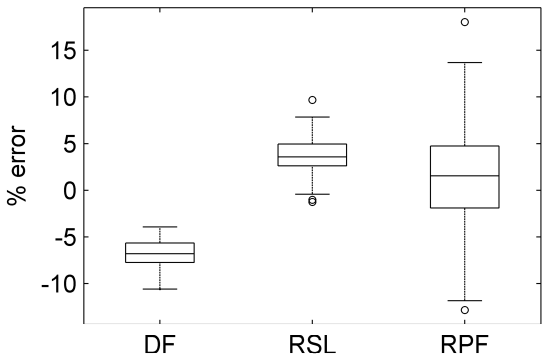

Figure 1: Percent errors in model predictions of DF, RSL and RPF.

DIMENSIONAL ANALYSIS

Buckingham's Pi-Theorem (Isaacson and Isaacson, 1975) indicated that the model parameters should be expressed as four dimensionless parameters (DPs). We

reduced this to three DPs by applying the constraint of a constant average speed of locomotion. The three DPs we used were: dimensionless leg stiffness (K), Froude number and dimensionless vertical landing velocity (V_0). All three of these DPs must be equal for bouncing gaits to be dynamically similar.

SENSITIVITY ANALYSIS

In addition to identifying criteria for dynamic similarity, it is also essential to know their relative importance. To determine this, we used sensitivity analysis. 27,000 model simulations were conducted over a physiologically relevant parameter space. At each point in the parameter space, we determined the percentage changes in DF, RSL and RPF in response to a 5% change in each DP. The relative importance of the three DPs varied with speed and gait, but was typically of the same order of magnitude, indicating that all 3 DPs are important for dynamic similarity.

REDUCED GRAVITY DATA

We reanalysed the simulated reduced gravity data of Donelan and Kram (2000) to calculate K and V_0. We found that the reason that humans do not run in a dynamically similar manner at equal Froude number in different gravity levels is that K decreases as gravity increases ($p<0.001$; Fig. 2).

CONCLUSIONS

Equal Froude number is a necessary, but not sufficient, condition for dynamic similarity in bouncing gaits. Therefore, comparing animals at equal Froude number will not necessarily eliminate size effects. Such comparisons can still be useful, however, because equal Froude number makes dynamic similarity possible and so allows fundamental differences in locomotion to be detected. Likewise, predictions of locomotion obtained by assuming dynamic similarity at equal Froude number will not always be accurate. Empirical evidence suggests that this approach can be effective in normal gravity however. More generally, dynamic similarity provides a powerful framework within which similarities and differences in locomotion can be interpreted.

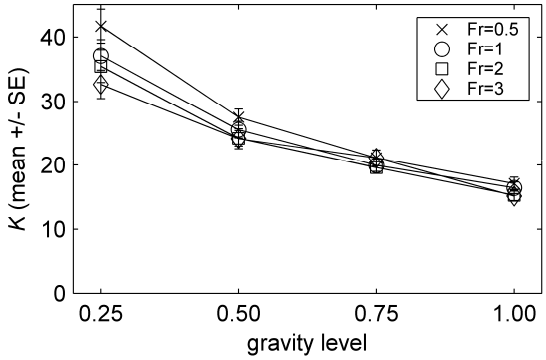

Figure 2: Decrease in K with gravity level in humans running at equal Froude (Fr) in different levels of simulated reduced gravity (multiples of Earth gravity).

REFERENCES

Blickhan, R. (1989). In *Energy transformations in cells and organisms*. Georg Thieme, 183-190.

Blickhan, R., Full, R.J. (1993). *J. Comp. Physiol. A*, **173**, 509-517.

Donelan, J.M., Kram, R. (2000). *J. Exp. Biol.*, **203**, 2405-2415.

Isaacson, E., Isaacson, M. (1975). *Dimensional Methods in Engineering and Physics*. Edward Arnold.

Vaughan, C.L., O'Malley, M.J. (2005). *Gait Posture*, **21,** 350–362.

ACKNOWLEDGEMENTS

JMD would like to thank Rodger Kram for his kind mentorship. Funding: NSERC, MSFHR, AHFMR.

Detecting the Transient Recruitment of Motor Units in the Surface Electromyogram During A Sustained Contraction

Zachary A. Riley[1], Mary E. Terry[1], Alberto Mendez-Villanueva[2], Jane C. Litsey[1], and Roger M. Enoka[1]

[1]Department of Integrative Physiology, University of Colorado, Boulder, CO, USA
[2]Faculty of Physical Activity and Sport Sciences, University of Alcala, Madrid, Spain
Email: Zachary.Riley@colorado.edu

INTRODUCTION

To sustain a submaximal force for a prolonged duration, motor units must be recruited progressively to compensate for the decline in discharge rate of the active motor units, the cessation of discharge by some motor units, and the decrease in contractile force of many muscle fibers. The recruitment of motor units is responsible for the gradual increase in the amplitude of surface electromyogram (EMG) during a fatiguing contraction. Due to the effects of amplitude cancellation, however, the surface EMG is relatively insensitive to modest changes in motor unit activity (Keenan et al. 2005). The purpose of the study was to characterize the discharge of transiently recruited single motor units during a sustained contraction, and to compare it with signals detected in the surface EMG.

METHODS

Eleven healthy adults (10 men; 27.5 ± 4.9 yrs; range, 21-35 yr) participated in the study. Twenty motor units in biceps brachii were isolated with fine wire subcutaneous electrodes and the discharge was compared with concurrently recorded surface EMG signals (Fig.1) during a sustained isometric contraction. The target force (25.4 ± 10.6% of the maximal voluntary contraction [MVC] force) was ~10% below the recruitment threshold of the motor unit (35.3 ± 11.3% MVC).

Fig. 1

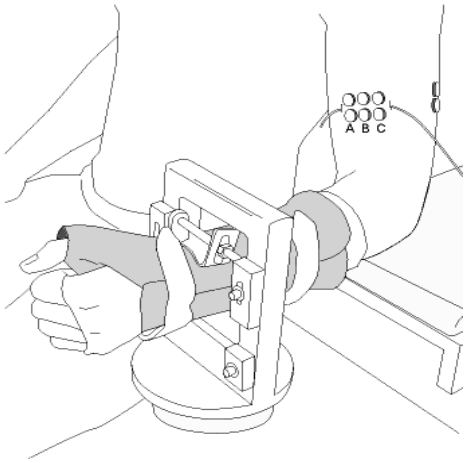

Surface EMG signals were high-pass filtered at 400 Hz (Potvin and Brown 2004; Staudenmann et al. 2007). Similarities between the surface EMG signal (rectified, smoothed 0.5 s window) and the motor unit signal (downsampled 20k to 2k, rectified, smoothed 0.5 s window) were tested with Pearson's R correlations. Processing the surface EMG also included the following steps previously used by Hunter et al. (2002): (1) rectification of the signals; (2) low-pass filtering at 2 Hz; (3) differentiation; and

(4) normalization to the average EMG of the entire signal. The threshold for the beginning and end of each burst of activity was defined as the instant when the smoothed and differentiated surface EMG signal exceeded 2.5 standard deviations above the mean that had been calculated from 25 samples at the beginning of the contraction. The minimum time between bursts was limited to 2 s and minimum burst duration was 0.5 s.

RESULTS AND DISCUSSION

Twenty motor units discharged 2-9 trains of action potentials when they were recruited. High-pass filtering the surface EMG signal with a 400-Hz cutoff significantly improved the correlation (r = 0.74, see Fig. 2) with the single motor unit signal compared with the correlation obtained with the non-filtered signal (r = 0.66, P = 0.04). The algorithm based on the high-pass filtered signal was able to detect 75% of the trains of action potentials discharged by the transiently recruited single motor units within 1.1 s of the beginning and 0.62 s of the end of each train of action potentials. The same algorithm applied to the standard band-pass filtered surface EMG only resulted in 58% of the single motor unit trains being detected.

SUMMARY/ CONCLUSIONS

These results indicate that most of the trains of action potentials discharged by motor units that were recruited transiently during a sustained contraction can be detected in the surface EMG signal with a relatively simple algorithm. In addition, high-pass filtering the surface EMG may a useful tool for isolating single motor units in a surface EMG signal.

REFERENCES

Hunter, S.K. et al. (2002). *J Appl Physiol*, **88**, 3087-3096.

Keenan, K.G. et al. (2005). *J Appl Physiol*, **98**, 120-131.

Potvin, J.R., Brown, S.H. (2004). *J Electromyogr Kinesiol*, **14**, 389-399.

Staudenmann et al. *J Biomech*, In Press.

ACKNOWLEDGEMENTS

The work was supported by a National Institute of Neurological Disorders and Stroke Grant NS043275 to RME.

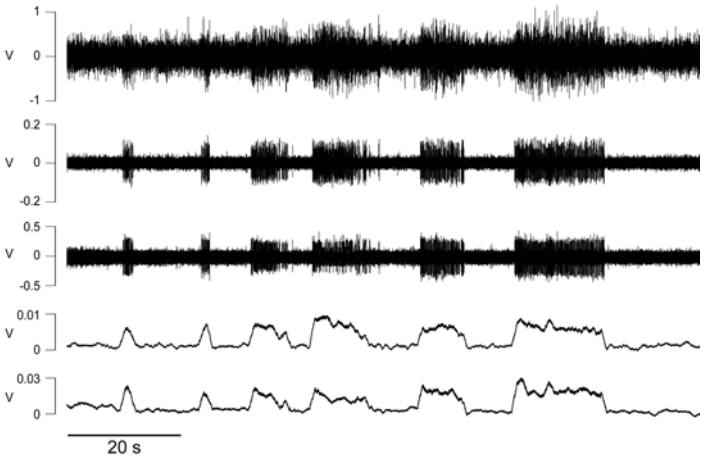

Fig 2. Representative data displaying the effect of high-pass filtering the surface EMG and the resulting method used to correlate the surface EMG signal with the single motor unit signal. The top trace represents the interference EMG detected with electrodes placed on the skin above the recording site for the single motor unit. The second trace indicates the surface EMG after high-pass filtering at 400 Hz. The third trace corresponds to the subcutaneous recording of the single motor unit activity. The fourth trace denotes the rectified and smoothed (0.5-s window) surface EMG channel after high-pass filtering. The bottom trace displays the single motor unit signal after down-sampling (20 kHz to 2 kHz), rectification, and smoothing (0.5-s window). The correlation between the bottom two traces was r = 0.89.

COMPARISON OF SPLIT DOUBLE TWISTS AND SPLIT TRIPLE TWISTS IN PAIRS FIGURE SKATING

Deborah L. King[1], Sarah L. Smith[2], Michele R. Brown[2], Jean L. McCrory[3], Barry A. Muncasy[4], Gary L. Scheirman[5]

[1]Ithaca College, Ithaca, NY, USA
[2]United States Olympic Committee, Colorado Springs, CO, USA
[3]University of Pittsburgh, Pittsburgh, PA, USA
[4]Georgia Southern University, Statesboro, GA, USA
[5]Vicon, Centennial, CO, USA
E-mail: dking@ithaca.edu, Web: www.ithaca.edu

INTRODUCTION

Pair skaters are required to perform complex throwing and lifting skills such as the split triple twist (STT) (Figure 1). The STT is said to distinguish medal winners from the rest of the competition. To the authors' knowledge, there is only one previous study on the biomechanics of STT, or any pair skill, which compared the STT of three groups of finishers at the 2002 Salt Lake Olympics (Smith, et al., 2003). With little or no data regarding the STT or similar skills in other sports, the development of the problem for this study was based on studies of figure skating jumps.

Skaters tend to perform jumps at the same height regardless of number of revolutions (King *et al.*, 1994; 2004; Albert and Miller, 1996). The prominent difference between single, double, and triple jumps is a decrease in the skater's moment of inertia about the longitudinal axis and corresponding increase in angular velocity (Aleshinsky et al., 1988; Albert and Miller, 1996). A distinguishing characteristic of higher skilled skaters as compared to lower level skaters is jump height with higher skilled skaters exhibiting higher maximum heights (King et al., 1994; 2004; Albert and Miller, 1996). The purpose of this study was to describe and compare temporal and kinematic characteristics of SDT and STT.

METHODS

Data were collected during the pair finals of the 2002 Salt Lake City Winter Olympics and 2003 International Skating Union Grand Prix Finals with four high speed (120 fps) cameras interfaced to ViconMotus pan and tilt hardware. Calibrations were performed each day using survey poles. Fourteen SDT and 15 STT were analyzed from 11 pairs. Twenty-five kinematic variables along with

Figure 1. Photo sequence of split triple twist with key events labeled.

seven temporal variables were calculated. Data from pairs with multiple SDT or STT were averaged prior to subsequent analysis. Average values and standard deviations were calculated for each variable for the SDT and STT across all teams. Paired t-tests were used to test three hypotheses at an alpha level of 0.05.

RESULTS AND DISCUSSION

Table 1 presents the average values for selected kinematic variables of the SDT and STT. There was large variability in the techniques used by the pairs to complete the SDT and STT. Average angular velocity during flight was significantly faster for the STT (3.6 ± 0.3 rev/s) as compared to the SDT (2.4 ± 0.3 rev/s) (p=0.000). This is similar to findings of double and triple jumps for which the extra revolution is completed relying almost solely on an increase in angular velocity (Aleshinsky et al., 1988; Albert and Miller, 1996). There was no significant decrease in approach speed from the SDT to the STT (p=0.570) as has been seen when comparing double to triple jumps (Albert and Miller, 1996; King et al., 1994) nor increase in maximum height (p=0.856).

Not all pairs relied entirely on increasing angular velocity for progressing from SDT to STT. Nine pairs were categorized as relying on rotation rate; three pairs relied on both rate and air time. The pairs using the combined strategy had air times over 15% longer in their STT providing at least an additional 1/4 revolution for their STT. The additional time came from increases in vertical velocity at release as well as delayed catches. Eight pairs had minor differences in air time between SDT and STT, and one pair had a decrease in time of over 15%. No pairs relied solely on increased time.

SUMMARY/CONCLUSIONS

The favored strategy for completing an extra revolution and advancing from a SDT to STT was an increase in angular velocity as is also seen in singles skating jumps. Given the reliance on increasing angular velocity, further analysis and future studies are recommended on the generation of angular momentum in the SDT and STT. Comparisons between SDT of skaters who can complete a STT to those who can not are also warranted. It is possible the SDT of the top skaters in this study is not representative of the SDT of up and coming skaters who are trying to learn the STT.

REFERENCES

Albert. W.J. and Miller, D.I. (1996). *J. App. Biomech.*, **12**, 72-87.

Aleshinsky, S.Y., et al. (1988). *Proceedings ASB'88*, 201.

King, D.L., et al., (1994). *App. Biomech.*, **10**, 51-56.

King , D.L., et al. (2004). *Sp. Biomech.*, **3**(1), 109-123.

Smith, S.L., et al (2003). *Proceedings IOC World Congress2003.*

ACKNOWLEDGEMENTS

This project was supported by the ISU, IOC/Pfiser, USFS, and USOC.

Table 1: Mean and SD for approach speed (AppSpeed), vertical velocity at release (V_{vrel}), height above ice (Height), air time (Time), and angular velocity during flight (ω_{flight}).

	AppSpeed (m/s)	**V_{vrel} (m/s)**	**Height (m)**	**Time (s)**	**ω_{flight} (rev/s)**
SDT	7.0 (± 0.5)	2.4 (± 0.6)	2.46 (± 0.15)	0.603 (± 0.059)	2.4 (± 0.3)
STT	7.1 (± 0.4)	2.7 (± 0.6)	2.45 (± 0.16)	0.639 (± 0.077)	3.6 (± 0.3)

HUMAN LOWER EXTREMITY DESIGN: ARCHITECTURE OF HUMAN HAMSTRING AND QUADRICEPS MUSCLES

Kristin M. Lieber[1,2], Jacqueline Braun[1,3], Trevor Kingsbury[1], Taylor Winters[1], Carolyn Eng[1], Samuel R. Ward[1,4], and Richard L. Lieber[1]

[1]Departments of Bioengineering, Orthopaedic Surgery, and [4]Radiology, University of California and Department of Veterans Affairs, San Diego, La Jolla, CA, USA
[2]University of Southern California, Los Angeles, CA, USA
[3]Baylor University, Waco, TX, USA
E-mail: rlieber@ucsd.edu, Web: http://muscle.ucsd.edu

INTRODUCTION

The human quadriceps and hamstring muscle groups are arguably the most thoroughly studied human muscle groups by virtue of their functional and clinical importance. This provides the motivation for us to integrate muscle, joint and tendon properties of the knee as has been accomplished for the wrist (Loren *et al.* 1996). This will enable us not only to understand the design and function of the knee, but also to recommend rationale interventional procedures that might be used to alter function or alleviate pain.

METHODS

Ten formaldehyde-fixed cadaveric lower extremities were used for this project (age: 82±10 yrs.; gender: 3 female-7 male; height 169.5±9.7 cm; weight 82.7±15.3 kg).

Muscle architectural measurements were made on the four quadriceps and four hamstrings muscles according to methods previously described (Lieber *et al.* 1990). The specific muscles studied were (n=10/muscle): Vastus lateralis (VL), vastus medialis (VM), vastus intermedius (VI), rectus femoris (RF), short head of biceps femoris (BFSH), long head of biceps femoris (BFLH), semitendinosus (ST), and semimembranosus (SM). Briefly, mass and muscle length were measured for each muscle. Fiber bundles from three to five predetermined regions of each muscle were microdissected and sarcomere length was measured in each fiber bundle using laser diffraction (Lieber *et al.* 1984) to calculate normalized fiber length and physiological cross-sectional area (PCSA) as previously illustrated (Lieber *et al.* 1990).

Statistical analysis consisted of analysis of variance (ANOVA) and *post-hoc* least-squared differences (LSD) tests were performed to make paired comparisons among muscles. All results are shown as mean ± standard error, and the significance level was α=0.05.

RESULTS AND DISCUSSION

In contrast to previous reports (Wickiewicz *et al.* 1983 and Friederich and Brand, 1990) muscle fiber lengths were not significantly different between quadriceps and hamstrings groups. However, within the quadriceps, RF fiber lengths (80.69±3.44 mm) were significantly shorter than VL (92.70±6.40 mm), VI (95.92±5.30 mm), and VM (93.12±5.41 mm) (Fig. 1, P<0.05). Similarly, within the hamstrings, SM fiber lengths (58.56±7.51 mm) were significantly shorter than the ST (124.07±12.61 mm), BFSH (105.02±8.17 mm), and BFLH (105.19±4.23 mm) (Fig. 1, P<0.05). PCSA was significantly larger in quadriceps

compared to hamstrings (P<0.05). Within quadriceps, VL PCSA (36.18±4.54 cm^2) was significantly greater than RF (14.26±1.58 cm^2), VI (22.83±3.72 cm^2), and VM (21.46±2.70 cm^2) (Fig. 1, P<0.05). Within hamstrings, the SM had a significantly larger PCSA (22.64±2.99 cm^2) than BFSH (6.07±0.48 cm^2, Fig. 1, $P < 0.05$) but was not significantly larger than any of the quadriceps muscles. Interestingly, fiber length variability was small (7%-11%) for all muscles except the ST which had the greatest coefficient of variation of all muscles (35±4%; P<0.05).

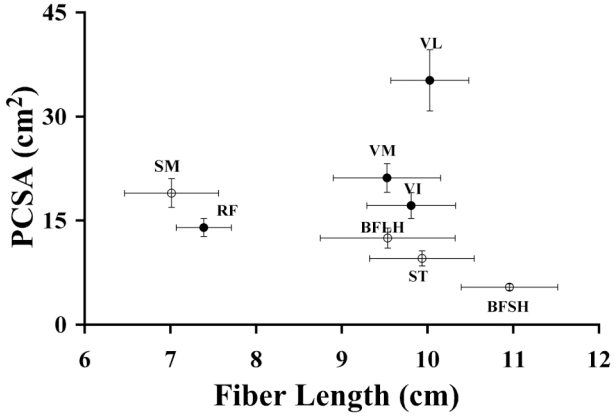

Figure 1: Scatter plot of normalized muscle fiber length *vs.* PCSA. (Hamstrings, ❍; Quadriceps, ●); Values are plotted as mean ±SEM. Abbreviations as in Methods.

These data clearly show, that considering only architectural properties, quadriceps and hamstring muscles differs primarily in their PCSA. This is not surprising, as the quadriceps (which had the largest PCSAs) are antigravity muscles at the knee. Muscle fiber lengths did not differ between muscle groups, contrary to previous reports (Wickiewicz *et al.* 1983 and Friederich and Brand, 1990). This is somewhat surprising, not only based on the "legacy" established by the two previous landmark studies, but because hamstring muscles are largely comprised of two-joint muscles. It is also interesting that the only two-joint muscle in the quadriceps (rectus femoris) had the shortest fiber length of quadriceps (Fig. 1).

Within muscle groups, hamstrings demonstrated the classic trade-off between PCSA and fiber length. Specifically, the SM had a large PCSA but short fibers while, at the other extreme, BFSH had a small PCSA but longer fibers (Fig. 1). The quadriceps did not follow this classic pattern. The VL had *both* the largest PCSA *and* the longest fibers. Functionally this would mean that the VL has both the greatest force generating capacity and the greatest excursion of the quadriceps.

SUMMARY/CONCLUSIONS

Clinically these results are important for a number of reasons. First, the data support the notion that the VL muscle is the "key" to knee function. Second, previous reports that hamstring muscles are designed for excursion is not supported by these data. In fact, as a whole, they are no different from quadriceps muscles, despite their two joint function. The specific implications of these results remain to be determined.

REFERENCES

1. Loren *et al.* (1996). *J. Biomech.* **29**, 331- 342.
2. Lieber *et al.* (1990). *J. Hand Surg.* **15A**, 244- 250.
3. Lieber *et al.* (1984). *Biophys. J.* **45**, 1007-1016.
4. Wickiewicz *et al.* (1983). *Clin. Orthop. Rel. Res*. **179**:275-283.
5. Friederich and Brand (1990). *J. Biomech*. **23**:91-95.

ACKNOWLEDGEMENTS

This work was supported by the Department of Veterans Affairs and NIH grants HD048501 and HD050837.

Can height loss across a functional spinal unit modified by static rest breaks modify cumulative compression induced injury?

Robert J. Parkinson and Jack P. Callaghan

University of Waterloo, Waterloo, ON, Canada
E-mail: rjparkin@uwaterloo.ca

INTRODUCTION

The results of multiple in vitro studies indicate that it is the central area of the endplate and vertebral body that fractures under cyclical compressive loads (Brinckmann et al. 1988; Parkinson and Callaghan 2007), indicating that this central region plays a large role in load carriage. Interestingly, it has been shown that static creep loading across the disc can force the loads experienced by the endplate towards the periphery (van Dieen et al. 2001), providing a potential mechanism to alter the load transference across the disc and change the resistance of the spinal unit to cyclic compression.

METHODS

218 porcine spinal units (C3/C4 and C5/C6) were randomly assigned to one of 15 loading groups - 3 normalized loading magnitudes (50, 70 and 90% of estimated ultimate compressive strength) and 5 normalized rest durations (0, 50, 100, 200 and 1000% of load application duration (2 seconds)). Specimens were dissected to remove excess soft tissue, mounted into custom aluminum cups via non-exothermic dental plaster and mounted into an Instron materials testing system (8872, Instron Canada, Toronto, ON, Canada). The lower aluminum cup was in contact with a metal bearing covered surface allowing unconstrained translations in the horizontal plane and rotation about the vertical axis. Once mounted, specimens were preloaded at 300N for 15 minutes. When preloading was complete specimens were cyclically loaded using a normalized physiological profile until failure occurred or a 12 hour trial time was reached. Throughout testing load and displacement were sampled at 10 Hz.

RESULTS AND DISCUSSION

Of the 218 specimens tested, 13 survived the 12 hour loading protocol (Table 1). Those specimens who received rest durations equal in length to the loading duration had the lowest occurrence of survival.

Table 1: Number of spinal units tested within each load magnitude/rest duration group. The number of surviving specimens is indicated in parentheses.

		Load Magnitude		
		50%	70%	90%
Rest Duration	0%	14(4)	16	14
	50%	14(2)	14	14
	100%	15(1)	15	14
	200%	15(3)	14	16
	1000%	14(2)	15(1)	14

As shown in our previous work (Parkinson and Callaghan 2007), load magnitude significantly altered the cumulative load tolerated prior to failure, with those loaded to a maximum of 50% tolerating significantly more load than those in the 70 or 90% groups ($p < 0.0001$). In contrast,

there was no statistically significant effect of rest duration on the cumulative load tolerated prior to failure ($p = 0.1646$), although it appears that short periods (50 or 100%) of rest may decrease the tolerance at moderate load magnitudes (figure 1).

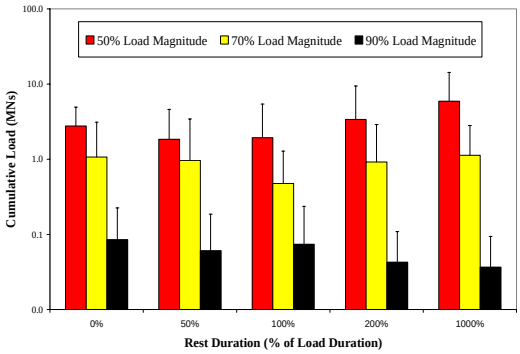

Figure 1: Average cumulative load (MNs) tolerated in each rest group (+ 1 standard deviation) separated by load magnitude.

Height loss was similarly affected by rest, with those specimens receiving short rest periods displaying the least amount of height loss prior to failure ($p = 0.0301$, figure 2). Load magnitude also significantly affected height loss, with increased load magnitudes leading to decreased height loss ($p<0.0001$), exhibiting the same pattern as cumulative load.

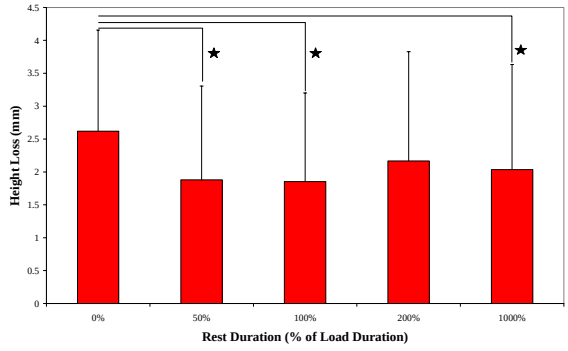

Figure 2: Average height loss (mm) at failure in each rest group (+ 1 standard deviation). Significant between group differences have been indicated with a star.

The similarities in the patterns of height loss and cumulative load tolerance may indicate a protective effect of height loss, as it has been shown that with an increase in height loss there is an increase in the amount of load carried through the annulus (Adams et al. 1996). This load redistribution may provide some relief to the central endplate region, the most common site of failure in cyclic compression. However, this relief may not translate into significantly altered load tolerance as the peripheral endplate bone may be less capable of bearing load (Lin et al. 1997).

SUMMARY/CONCLUSIONS

The results of this study have indicated that inserting periods of static rest into dynamic loading exposures is not an effective method to increase the cumulative compressive tolerance of the osteoligamentous spine, and in fact may be detrimental if the rest period is of equal duration to the loading period. This may be due to an inability to lose height within the joint, which may afford protection through load redistribution.

REFERENCES

ADAMS, M.A., et al. (1996). *Spine*, **21**, 434-438.
BRINCKMANN, P., et al. (1988). *Clin Biomech*, **3**, S1-S23.
LIN, R.M., et al. (1997). *Clin Biomech*, **12**, 331-336.
PARKINSON, R.J. and CALLAGHAN, J.P. (2007). *TIES*, **8**, 171-184.
VAN DIEEN, J.H., et al. (2001). *Clin Biomech*, **16 S1**, S135-S142.

ACKNOWLEDGEMENTS

The authors wish to thank Ms. Erin Harvey for statistical advice and Ms. Laura Malinowski for assistance in data collection.

PAD CAUSES ALTERATIONS IN THE VARIABILITY OF GAIT PATTERNS

Sara A. Myers[1], Nick Stergiou[1], Iraklis Pipinos[2,3], Jason M. Johanning[2,3], Naomi Kochi[1]
[1] University of Nebraska at Omaha
[2] University of Nebraska Medical Center
[3] Veterans Affairs Medical Center, Omaha, NE
E-mail: sfagan@mail.unomaha.edu Web: biomech.unomaha.edu

INTRODUCTION

Peripheral arterial disease (PAD) affects 8 to 12 million people in USA and is a leading cause of morbidity due to the ambulatory limitations associated with claudication. In PAD, the arteries supplying the legs are blocked by atherosclerosis, significantly reducing blood flow to the muscles. The reduced blood flow leads to inadequate levels of oxygen during physical activity and PAD patients have muscle ischemic pain and inability to walk normal distances (claudication; Nehler et al., 2003). PAD patients walk initially without pain but as the oxygen demands in the muscle increase with ongoing exercise the leg becomes progressively more ischemic and painful. Eventually, this pain causes patients to stop walking.

There are a variety of treatment options for claudicants including lifestyle modification, pharmacologic therapy and surgery. However, the degree of effectiveness of these methods is under debate. This is partially due to the inadequacy of the methods used to assess after treatment improvements in gait performance (Scherer et al., 2006). Thus, there is a need for a more sensitive quantitative tool to determine the severity of functional limitations, effectiveness of treatments, and other risks (i.e. falling) that could result from PAD. Recent literature has shown that the examination of gait variability in elderly using nonlinear analysis can describe subtle functional changes that usually go undetected using traditional approaches (Stergiou et al., 2003). Gait variability can actually be a predictor of falling in the elderly and can differentiate between pathological populations and healthy controls (Maki, 1997). Research for PAD may also benefit from a similar approach. Therefore, our purpose was to use nonlinear methods to determine gait variability in PAD patients compared to healthy controls and to determine how gait variability in PAD patients is affected by claudication.

METHODS

Fifteen PAD patients (PAD) and 15 controls (CON) walked on a treadmill while kinematics (60 Hz) were recorded using a Motion Analysis system. Walking trials of up to three minutes were captured during pain free (PF) and subsequently pain (claudication, P) conditions. Claudication was induced using a common clinical protocol where the patient walked on a treadmill, set at 10% grade and 0.67 m/s, until the onset of pain at which point the pain condition was collected. Relative lower extremity joint angles were calculated for all trials that lasted at least 30 footfalls.

The time series from the unfiltered joint angles were analyzed using the Chaos Data Analyzer Professional software (Sprott & Rowlands, 1995) to calculate the largest Lyapunov Exponent (LyE) for each trial-condition. The LyE describes variability by quantifying the exponential separation in the trajectories of the joint angles with time in state space. As nearby points separate, they diverge and produce instability. To correctly calculate the LyE, it is necessary to first reconstruct the state space by estimating the embedding dimensions and the time lag. The embedded dimension is a measure of the number of dimensions needed to unfold a given attractor, while the time lag

determines how many data points will be used in the analysis. These two parameters were calculated using custom software in MATLAB. The embedded dimension used for the study was 10 and the average time lag was 16.7. CON and PAD-PF means of LyE values were compared using independent t-tests. Paired t-tests were used to determine differences between PAD-PF and PAD-P conditions.

RESULTS AND DISCUSSION

PAD–PF patients had significantly larger LyE values as compared to CON (Table 1). Typical LyE values are around 0 for periodic data, 0.1 for chaotic data and close to 0.5 for random data (Stergiou et al., 2003). However, no differences were found between PAD-PF and PAD-P conditions. These findings collectively show that the gait pattern of PAD patients has altered variability that occurs even before the onset of pain. These changes could be one reason PAD patients have impaired balance and increased risk of falls (Gardner et al., 2001). Lack of differences between PAD-PF and PAD-P conditions may be explained by adaptation to the claudication which is now present at baseline pain free ambulation.

SUMMARY/CONCLUSIONS

PAD patients experience increased gait variability prior to the onset of claudication. The larger LyE values observed in the PAD patients indicate increased randomness in their gait patterns. These findings are similar to those found for the elderly population (Kurz and Stergiou, 2003). This increased variability observed at the ankle and the knee may result in greater uncertainty during walking and could be contributing factors to the higher prevalence of falls in PAD patients.

This study will be the basis for future work to investigate how variability in gait patterns of PAD patients is related with the increased rate of falling, evaluate more effectively different treatment methodologies, and design targeted interventions to improve walking in PAD patients.

REFERENCES

Gardner, A., Montgomery, P. (2001). *J Gerontol,* **56A,** M454-458.

Kurz, M., Stergiou, N. (2003). *Neurosci Lett,* **34,** 155-158.

Maki, B. (1997). *J Am Geriatr Soc, 45, 313-320.*

Nehler, N. et al. (2003). *Vasc Med*, **8,** 115-126.

Sprott, J., Rowlands, G. (1995). *Chaos Data Analyzer: Professional Version,* Human Kinetics Publishers.

Stergiou, N. et al. (2003) *Nonlinear Tools in Human Movement. In: Innovative Analysis of Human Movement*. Human Kinetics Publishers.

ACKNOWLEDGEMENTS

This work was supported by NIH (K25HD047194), NIDRR (H133G040118), the Nebraska Research Initiative and the American Geriatrics Society's Dennis W. Jahnigen Award

Table 1: Group means for the largest Lyapunov Exponent (mean ±SD). Significant differences ($P < .05$) between groups are marked with an asterisk (*).

LyE	Control	PAD pain	PAD pain free
Ankle	.091 ± .015	.096 ± .014	.105 ± .016*
Knee	.092 ± .014	.099 ± .019	.102 ± .011*
Hip	.101 ± .009	.100 ± .012	.100 ± .008

SAGITTAL LUMBAR INTERVERTEBRAL ANGLES IN SEATED POSTURES USING FLUOROSCOPY

Nadine M. Dunk*, Angela E. Kedgley[+], Thomas Jenkyn[+] and Jack P. Callaghan*
*Faculty of Applied Health Sciences, Department of Kinesiology, University of Waterloo
[+]Department of Mechanical and Materials Engineering, University of Western Ontario
Email: nmdunk@ahsmail.uwaterloo.ca

INTRODUCTION:

The whole body postural demands of seated tasks require an upright torso while still achieving a moderate amount of lumbo-sacral (LS) spine flexion (40% to 80% of maximum LS spine flexion (Callaghan and Dunk, 2002)). Given this evidence, the major factor in determining seated LS posture may be linked to the rotation of the pelvis. Gender-based differences in the LS spine and pelvic posture in sitting have been observed using external measurements of lumbar angle (Dunk and Callaghan, 2005). The purpose of this study was to examine x-ray images of the LS spine in order to determine the contribution of each lumbar intervertebral joint (IVJ) to the total LS curve in various standing and seated postures. Secondary purposes included examining any gender differences and a comparison of the IVJ angles with an external measurement of the LS curve.

METHODS:

Twenty-five healthy participants (12 males, 13 females) were recruited and a video fluoroscopy system was used to obtain sagittal images of the LS region ranging from the top of the sacrum to the top of the third lumbar vertebra in five standing and seated postures. External LS spine and pelvic postures were measured using accelerometers placed at L1, L3 and S2. Static images of the five postures were obtained using the digital radiography setting of the fluoroscope while accelerometer data were collected. The accelerometers provided inclinations relative to vertical. The top two corners of the sacrum and the four corners of all visible vertebral bodies (VB) were manually digitized four times for each x-ray image. Intervertebral angles were calculated as the angle between sagittal "mid-plane" lines of adjacent VBs (Frobin et al, 1996). The mid-plane line was determined as the line that intersected the mid-points between the two anterior and two posterior VB corners.

RESULTS & DISCUSSION:

The total standing ranges of motion (RoM) measured from x-rays for L3/Sac were similar for both males (40.6±2.7°) and females (39.2±2.7°) (Table 1). The total RoMs for each IVJ measured were not significantly different between genders (Table 1). These values correspond to IVJ RoM found previously in the literature (i.e. Pearcy et al., 1984).

Table 1: Total standing range of motion (RoM) for each of the three lower lumbo-sacral joints measured, including the RoM of the joints spanning L3 and the sacrum (L3/Sac – shaded column). Means (standard deviations)

	Total RoM (deg)			
	L3/4	**L4/5**	**L5/Sac**	**L3/Sac**
FEMALE	12.5° (2.0)	15.9° (2.9)	10.8° (7.2)	39.2° (9.5)
MALE	12.5° (3.1)	15.0° (4.2)	13.2° (3.7)	40.6° (9.3)

When examining the standing mid-flexion posture and both seated postures, the external L3/Sac angle showed gender differences with males exhibiting more flexion than females. There were also differences observed in the amount of L3/Sac flexion between postures (Ranges from female to male: standing mid-flexion

= 43.6 – 52.4°; upright sitting = 11.3 – 15.6°; slouched sitting = 18.6 – 28.3°). However, for both genders, each of the lower three IVJs approached their maximum flexion angles in the slouched sitting posture. In fact, in upright sitting, the L5/S1 joint for both genders was flexed more than 60% of its max RoM, supporting the idea that the LS curve is likely driven by rotation of the pelvis and lower IVJs in sitting (Figure 1). It follows that there could be increased loading of the passive tissues surrounding the lower LS IVJ, leading to pain generation and potential injury. While it appears that IVJ RoMs may not account for the biological variation between genders (Dunk and Callaghan, 2005), further study is required to form solid conclusions. The future development of a mathematical model to predict IVJ rotations from external measures during sitting may also improve estimates of the tissue loads surrounding the LS IVJs.

SUMMARY & CONCLUSIONS:
In upright sitting, there is evidence of a "bottom up" flexion pattern exhibited by the lower 3 LS IVJs. This is supported by observations that the L5/Sac joint achieved more than 60% of its max RoM in this posture and the next two adjacent IVJs (L4/L5 and L3/L4) achieved less of their maximum RoM. Although the external measurements obtained in this study corroborated the gender differences that have been previously documented in sitting, the IV joint angles as measured from x-rays do not explain these differences.

REFERENCES:
Callaghan JP, Dunk NM. *Clin Biomech*, **17,** 353-60, 2002.
Dunk NM, Callaghan JP. *Clin Biomech*, **20,** 1101-10, 2005.
Frobin W et al. *Clin Biomech*, **11,** 457-465, 1996.
Pearcy M, Portek I, Shepherd J. *Spine*, **9,** 294-297, 1984.

ACKNOWLEDGEMENTS: Mr. John Henry, X-ray technologist at London Health Sciences Centre, for his knowledge and dedication to the data collection process.

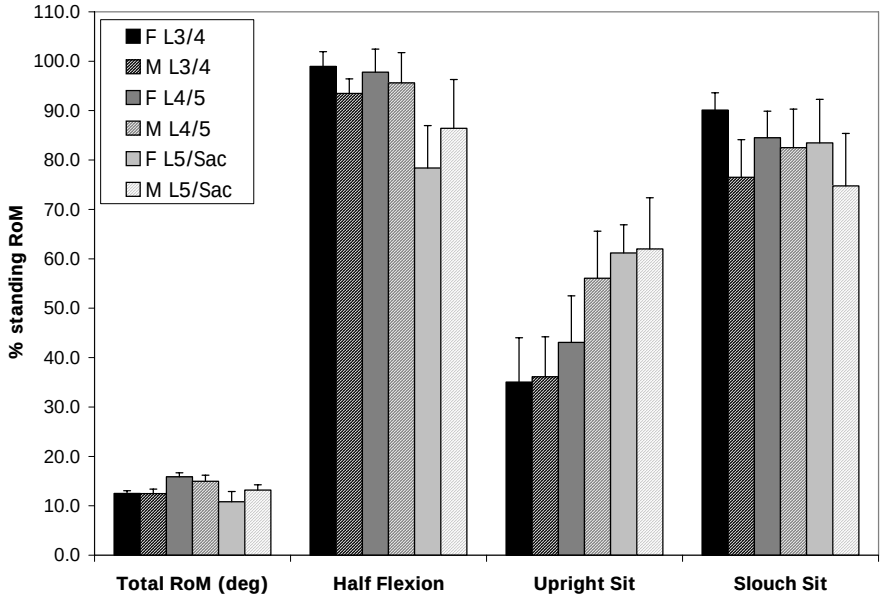

Figure 1: Intervertebral joint angles normalized to their total standing range of motion (%RoM) as measured from the full flexion posture (Total RoM (deg)).

UPPER LIMB MOMENT-GENERATING CAPACITY IN MIDDLE AGED ADULTS

Katherine Holzbaur[1,2], Garry Gold[1,2], and Wendy Murray[2,3]

[1]Stanford University, Stanford, CA, USA
[2]VA Palo Alto HCS, Palo Alto, CA, USA
[3]Northwestern University, Chicago, IL, USA
E-mail: krsholzbaur@gmail.com

INTRODUCTION

A strong relationship between muscle volume and isometric strength has been identified at the shoulder, elbow, and wrist in healthy, young adults (Holzbaur, 2007b). However, factors beyond muscle atrophy, such as increased co-contraction and decreased voluntary neural drive, contribute to the strength decreases observed in populations over the age of 65 (Klein, 2001; Hakkinen, 1996). In addition, it has been suggested that age-related muscle atrophy occurs at different rates for the elbow flexors and extensors (Klein, 2001). Few studies have investigated age-related changes in isometric strength and muscle size for middle-aged adults, and most of the data comparing isometric strength in different age groups in the upper limb are focused at the elbow. The objective of this study is to identify and characterize changes in muscle volume and isometric moment-generating capacity at the shoulder, elbow, and wrist associated with middle age.

METHODS

Ten nonimpaired subjects (5 females, 5 males, 46-60 years, average 53.2 years) were studied. All subjects provided informed consent. Isometric joint moments produced during a maximum voluntary contraction were measured for six muscle groups using a Biodex System3 (Biodex Medical Systems, Shirley, NY). Maximum shoulder abduction and adduction moments, elbow extension and flexion moments, and wrist flexion and extension moments were assessed. For each muscle group, we collected three trials of three-second duration, with 60 seconds of rest between trials. The maximum moment generated for any trial was used for analysis.

The same subjects were imaged supine in a 1.5T MRI scanner (GE Healthcare, Milwaukee, WI). Axial images were acquired from shoulder to wrist using 3D spoiled gradient echo sequences with 3 mm sections. Shoulder images were obtained with the body coil; elbow and forearm images were acquired using a flexed array long bone coil (Medical Advances, Milwaukee, WI). We reconstructed the three-dimensional geometry of the deltoid, brachioradialis, and extensor carpi ulnaris (ECU) through manual segmentation (3D-Doctor, Able Software Corp., Lexington, MA), to calculate the volumes of muscles crossing the shoulder, elbow, and wrist, respectively.

We evaluated the relationship between muscle volume and maximum isometric moment at each joint using regression analysis. We compared results for these middle-aged subjects to results from younger adults (24-37 years, average 28.6 years) previously studied using this protocol (Holzbaur, 2007b). We tested the effects of age, gender, and joint on isometric strength using a PA-GEE regression model. Finally, deltoid and brachioradialis volumes were normalized by ECU volume in each subject to allow comparisons of the distribution of

muscle volume in the upper limb (Holzbaur, 2007a).

RESULTS AND DISCUSSION

For the middle-aged adults, moment-generating capacities for shoulder abduction and adduction (Fig. 1), elbow flexion and extension, and wrist flexion were significantly correlated to the volume of a single muscle crossing that joint ($p<0.01$), with an average of 80% of variation accounted for by muscle volume. ECU volume explained 32% of wrist extension variation ($p=0.09$). For all muscle groups except wrist extension, the slope between moment and muscle volume for the middle-aged adults was within the 95% confidence interval observed for the young adults.

Age affected the isometric moments produced at the shoulder more than at the elbow or the wrist ($p<0.001$). On average, shoulder, elbow, and wrist moments produced by the middle-aged adults were 23%, 10%, and 6% smaller than those produced by the younger adults, respectively. Similarly, the ratio of muscle volumes between deltoid and ECU was significantly lower in middle-aged adults compared to younger adults (Fig. 2; $p=0.005$) while the ratio of muscle volumes between brachioradialis and ECU was comparable for the two age groups in these 20 subjects. . These results suggest a higher degree of atrophy for the shoulder muscles in the middle-aged subjects, consistent with the larger difference in isometric shoulder strength.

We conclude that, while muscle volume accounts for variability in isometric strength at a comparable level in middle-aged and younger adults, middle-aged adults exhibit relatively greater atrophy of proximal muscles compared to distal muscles. This difference in volume distribution is reflected in the isometric strength of the limb.

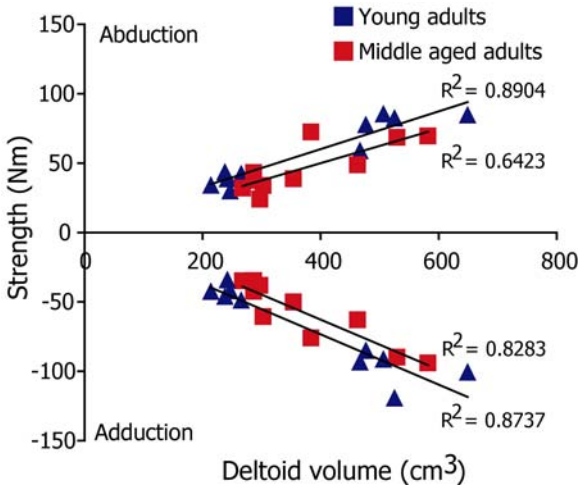

Figure 1: Moment-generating capacity of shoulder abductors and adductors compared to deltoid muscle volume.

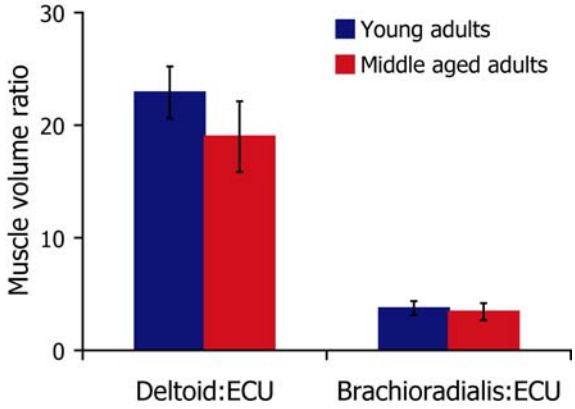

Figure 2: Ratios of muscle volume comparing deltoid, brachioradialis, and ECU.

REFERENCES

Hakkinen, K., et al. (1996). *J Gerontol A Biol Sci Med Sci*, **51A**, B21-B29.

Holzbaur, K.R.S., et al. (2007a). *J. Biomech*, **40**, 742-749.

Holzbaur, K.R.S., et al. (2007b). *J. Biomech*, in press.

Klein, C.S., et al. (2001). *J Appl Physiol*, **91**, 1341-1349.

ACKNOWLEDGEMENTS

VA RR&D Service (#A3741R). We thank Jarrett Rosenberg for statistical analysis and interpretation.

Prehension of the objects with complex friction patterns

Xun Niu, Mark L. Latash, Vladimir M. Zatsiorsky

Department of Kinesiology, The Pennsylvania State University
E-mail: xun100@psu.edu

INTRODUCTION

When people manipulate hand-held objects they adjust digit forces to the friction conditions (Johansson, Westling 1984). This study addresses the grasping of the objects at which friction beneath each digit is different from the others ('complex friction patterns'). Specifically, this study addresses three-digit prismatic grasps similar to grasping a glass with liquid. The force adjustments to the friction were classified as local and synergic.

Two hypotheses were explored: (a) The CNS does not inhibit local adjustments to friction; instead it compensates the effects of the local reactions perturbing the object equilibrium by synergic actions of other digits; (b) The CNS uses a single force distribution pattern (grasping template) for each friction set and scales the template with the load.

METHODS

Three six-component force/moment sensors were mounted on an aluminum handle; the sensors recorded forces/moments by the thumb, index and middle fingers. Caps with either rayon (friction coefficient μ=0.49) or 100-grit sand paper (μ=1.34) were affixed to the surface of the sensors. Four loads, 200 g, 400 g, 600 g or 800 g, were suspended at the bottom of the handle via a 40-cm aluminum bar to make the rotational equilibrium stable. A level was positioned at the top of the handle to visually help the subjects to keep the handle vertically oriented.

There were 32 combinations of 8 friction conditions and 4 loads, with 4 trials repeated for each combination. The friction, loads and trials were balanced in the experiment design. Eight male subjects participated in the experiment. They were instructed to hold the handle vertically in the air with natural grip force for six seconds.

Modeling and data analysis. During the performance the central controller maps the friction triplets and the load values onto the triplets of digit forces. A model, coined the *triple-product model*, was suggested to describe the mapping. The relations between the experimental conditions (friction pattern and load) and the digit forces were described via three linear relations: (1) tangential forces and load $f_i^t = k_i^{(1)} L$, (2) normal forces and tangential forces $f_i^n = k_i^{(2)} f_i^t$, and (3) normal forces and load $f_i^n = k_i^{(2)} k_i^{(1)} L$, where superscripts *n* and *t* represent normal and tangential forces, respectively, subscript *i* refers to a digit and *L* is the load. The $k_i^{(1)}$, $k_i^{(2)}$ and $k_i^{(3)}$ coefficients were computed from the relevant regression analyses. A two-way repeated measures ANOVA was performed on the coefficients with the factors LOCAL FRICTION (2 levels) and FRICTION AT OTHER DIGITS (4 levels). The degrees of freedom were corrected for sphericity with the Geisser-Greenhouse method.

RESULTS AND DISCUSSION

For $k_i^{(1)}$, the tangential forces were smaller when the thumb was at the low friction contact as compared to the high friction contact; in contrast, the VF forces were larger, see Figure 1. The repeated measures

ANOVA results are presented in Table 1. Similar relations and repeated measures ANOVA results were obtained for the index and middle fingers and for the coefficients $k_i^{(2)}$ and $k_i^{(3)}$.

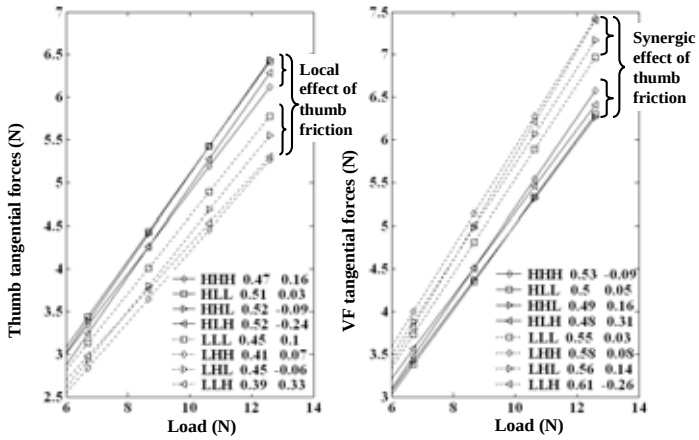

Figure 1: Local and synergic effects of the friction at the thumb contact on the tangential forces. Left panel: the thumb forces; right panel: the virtual finger (VF) forces. Group averages. The friction sets are marked as three-letter sequences where letters H or L signify the high or low friction contacts, respectively, at the thumb, middle, and ring fingers. The left panel illustrates the local effect of the thumb friction on the thumb tangential forces while the right panel illustrates the synergic effect of thumb friction on the VF forces.

Both the local and synergic effects on the digit forces were quantified. The digit forces scaled with the supported load and adjusted to both the LOCAL FRICTION and the FRICTION AT OTHER DIGITS (synergic fine-tuning). In some cases the synergic effects were manifested stronger than the adjustments to the local friction (e.g. for the middle finger tangential force). Hence, the digit force tuning to the object features arises from both (a) local adjustments to the friction at the particular digit ('independent neural networks', Burstedt et al. 1997), and (b) overall synergic reactions to the friction at other digits directed at the maintenance of the object equilibrium.

The data support the hypothesis that for each friction set the CNS specifies a certain grasping template and scales it with the load magnitude. Overall, the model approximated the results well and the correspondence between the predicted from the model and actual normal force data was within acceptable limits: the RMS was on average 1.157 ± 0.034 N.

SUMMARY/CONCLUSIONS

The study has demonstrated that: (a) digit force adjustments can be classified as local and synergic; (b) for each friction set, the central controller selects a grasping template and then scales the template with the load magnitude; (c) the digit force adjustments to the different friction patterns can be succinctly described with the suggested triple-product model.

REFERENCES

Burstedt M.K., Birznieks I., Edin B.B., Johansson R.S. (1997) *J Neurophysiol*, 78, 117–128.

Johansson R.S., Westling G. (1984). *Exp Brain Res*, 56, 550–564.

ACKNOWLEDGEMENTS

This work was supported in part by grants AR-048563, AG-018751 and NS-35032 from NIH.

Table 1. Two-way repeated measure ANOVA of $k_i^{(1)}$ coefficients, p values

	Thumb	Index	Middle
Local Friction (LF, 2 levels)	0.005	0.17	0.068
Friction at other digits (FOD, 4 levels)	0.003	0.283	0
LF×FOD	0.508	0.255	0.985

MUSCLE CONTRIBUTIONS TO BODY SEGMENT MECHANICAL POWER DURING ABLE-BODIED TOE WALKING

Kotaro Sasaki [1] Richard R. Neptune [1] Judith M. Burnfield [2] and Sara J. Mulroy [3]

[1] Department of Mechanical Engineering, The University of Texas at Austin, Austin, TX, USA
[2] Institute for Rehabilitation Science and Engineering, Madonna Rehabilitation Hospital, Lincoln, NE, USA
[3] Rancho Los Amigos National Rehabilitation Center, Downey, CA, USA
E-mail: rneptune@mail.utexas.edu, Web: http://www.me.utexas.edu/~neptune/

INTRODUCTION

Toe walking is a gait pattern associated with a variety of musculoskeletal and neurological disorders. Clinically, to distinguish primary from secondary gait deviations is critical for determining the most appropriate treatment. Previous studies have analyzed able-bodied toe walking and observed high peak ankle moments in early stance and lower values in late stance compared to heel-toe walking (Kerrigan et al., 2000, Perry et al., 2003). These differences are significant since the ankle plantar flexors are not normally active in early stance in heel-toe walking and are the primary contributors to body support and forward propulsion in late stance (e.g., Neptune et al., 2004), and therefore other muscle compensations may be necessary in order to maintain similar walking kinematics. The purpose of this study was to identify these compensatory mechanisms by quantifying differences in how muscles distribute mechanical power to the body segments between toe and heel-toe walking.

METHODS

Sagittal-plane forward dynamic simulations of toe and heel-toe walking were generated using SIMM (MusculoGraphics, Inc.) and SD/FAST (PTC). Muscle excitation patterns were fine-tuned using dynamic optimization such that the simulations reproduced experimental body-segment kinematics and ground reaction forces over a full gait cycle collected from 10 able-bodied subjects during toe and heel-toe walking at the same speed (Perry et al., 2003). A segment power analysis (Fregly and Zajac, 1996) was used to identify differences in how individual muscles generated, absorbed or transferred mechanical power among the trunk, and ipsilateral and contralateral legs during the two gait modes.

RESULTS AND DISCUSSION

The mechanical power distribution in toe walking was similar to that observed in heel-toe walking, with a few distinct exceptions. In early stance, soleus (SOL) eccentric action absorbed power from the leg and delivered it to the trunk (Fig.1: SOL, 0-20% gait cycle). The power delivered to the trunk was primarily in the vertical direction, which acted to accelerate the trunk upward to provide body support. During the same period, the gastrocnemius (GAS) absorbed power from both the trunk and leg (Fig. 1: GAS). In contrast to toe walking, the plantar flexors generated negligible power in early stance during heel-toe walking since the muscles are inactive then. The vastii (VAS) muscles functioned similarly in both toe and heel-toe walking in early stance, by absorbing power from the leg and delivering that energy to the trunk (Fig. 1: VAS, 0-20% gait cycle). However, the magnitude of the trunk vertical power was much lower in toe walking compared to heel-toe walking in order to compensate for the increased power delivered to the trunk by SOL. Similar to

VAS, the gluteus maximus contribution to trunk support in early stance also decreased.

In late stance, the magnitude of SOL power delivered to the trunk, which was directed horizontally to provide forward propulsion, decreased in toe walking (Fig. 1: SOL, ~40-60% gait cycle). This power reduction, despite an increase in excitation, was the result of the reduced capacity of SOL to generate force because of the shorter fiber lengths associated with the equinus posture (Neptune et al., 2007). As a result of this decrease in contribution to forward propulsion by SOL during toe-walking, the hamstrings (HAM) delivered more power to the trunk, primarily in the horizontal direction, in both early and late stance in toe walking (Fig. 1: HAM, 0-60% gait cycle) compared to heel-toe walking.

SUMMARY/CONCLUSIONS

Multiple compensatory mechanisms were required in toe walking, which have important implications for distinguishing primary from secondary gait deviations. These compensatory mechanisms need to be considered when determining the most appropriate treatments for equinus gait.

REFERENCES

Kerrigan, D.C. et al. (2000). *Arch Phy Med Rehab.*, **81**, 38-44.

Perry, J. et al. (2003). *Arch Phy Med Rehab.*, **84**, 7-16.

Neptune, et al. (2004). *Gait Posture*, **19**, 194-205.

Fregly, B.J, Zajac, F.E. (1996). *J. Biomech.*, **29**, 81-90.

Neptune, et al. (2007). *J. Biomech.*, **40,** 1293-1300.

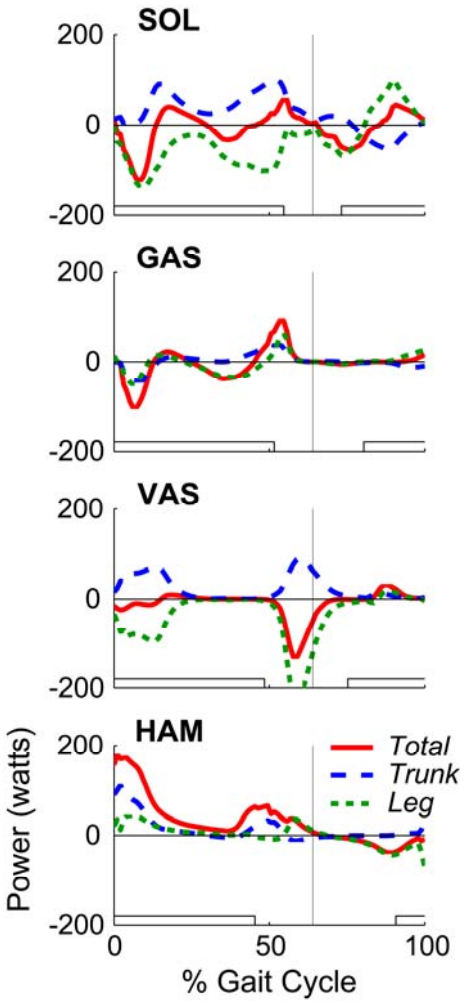

Figure 1: Musculotendon mechanical power (*Total*, solid line) and its distribution to the trunk (*Trunk*, dashed line) and ipsilateral leg (*Leg*, dotted line) during toe walking over the gait cycle. The vertical lines indicate toe-off, while the horizontal bars indicate muscle excitation timing. The power to the contralateral leg was generally small and not shown.

ACKNOWLEDGEMENTS

The authors are grateful to Dr. Phil Requejo for help with the experimental data.

THE EFFECT OF TEMPERATURE ON RESIDUAL FORCE ENHANCEMENT IN SINGLE SKELETAL MUSCLE FIBERS

Eun-Jeong Lee and Walter Herzog

University of Calgary, Calgary, AB, Canada
E-mail: ejlee@kin.ucalgary.ca, Web: www.kin.ucalgary.ca/hpl

INTRODUCTION

Residual force enhancement (or force enhancement) has been defined as an increased steady-state isometric force following stretching of an active fiber or muscle compared to the steady-state force obtained for purely isometric contractions at the corresponding length (Edman et al, 1982). Although this phenomenon has been observed consistently in skeletal muscles for more than half century, the underlying mechanism is not yet clear.

The aim of this study was to determine whether residual force enhancement is caused by specific, stretch-induced changes in cross-bridge kinetics. In a previous study, we observed a vastly increased amount of force enhancement in fibers treated with the phosphate release blocker BDM (Rassier and Herzog, 2004). This result was explained with a stretch-induced change of the ratio of weakly-to-strongly-bound cross-bridges towards the strongly bound state. Aside from using BDM, the ratio of weakly-to-strongly-bound cross-bridges can also be biased towards the weakly bound state by lowering temperature (Wang & Kawai, 2001). Therefore, we hypothesized that if force enhancement is associated with a facilitation of transition of weakly to strongly bound cross-bridges, low temperature should produce greater force enhancement than high temperature experiments.

METHODS

Single fibers (n = 11) were dissected from lumbrical muscles of the frog (*R. Pipiens*) for all experiments. Isolated fibers were suspended between a motor arm and a force transducer inside an experimental chamber filled with Ringer's solution (pH=7.2). Sarcomere lengths were measured using a laser diffraction technique. After determining the plateau of force-length relationship, an isometric reference contraction was performed at the final length. This was followed by an active stretch of 10% or 15% of optimal fiber length at a speed of 40% optimal fibre length/s. For all tests, contraction duration was 3.5s and stiffness was measured with a step stretch (20μm over 1ms) 0.2ms before deactivation. Experiments were performed at two different temperatures (7 and 20ºC). Force enhancement was measured 10ms before the length step for stiffness measurement. Force was normalized to fiber cross-sectional area and stiffness was calculated by dividing normalized force by elongation.

RESULTS AND DISCUSSION

Fiber stiffness in the force-enhanced state was similar to that observed during the isometric reference contractions. Values of force/stiffness, which are assumed to represent the average force per cross-bridge, were significantly greater in the force-enhanced state than in the isometric reference contraction (table1). This result suggests that the increased isometric force following active stretch is caused by an increase in the average force per cross-bridge rather than an increase in the number of attached cross-bridges. The average isometric reference force at 20ºC was slightly greater than that measured at 7ºC, but the difference was not statistically

significant. Stiffness was significantly increased at 7ºC compared to 20ºC (table1). Force enhancement was significantly greater at 7ºC compared to 20ºC, and correspondingly, the enhancement of ratio of force/stiffness was greater (figure1, table2).

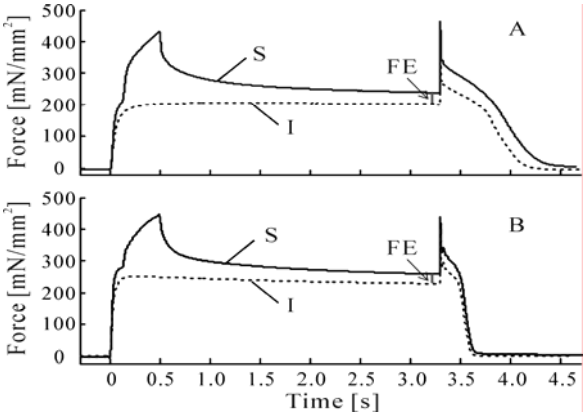

Figure 1: Raw force-time histories of active stretch (solid, S) and isometric reference contraction at the corresponding final length (dashed, I) at 7ºC (A, 18.3% FE) and 20ºC (B, 13.0% FE) temperature.

This result suggests that force enhancement at low temperatures is higher than at high temperatures, because of a bigger proportion of weakly bound cross-bridges at the low temperature and a stretch-induced facilitation of the transition of weakly to strongly bound cross-bridges. This result is consistent with previous results in which BDM was used to bias the ratio of weakly to strongly bound cross-bridges towards the weakly bound state.

SUMMARY/CONCLUSIONS

Force enhancement was greater at low compared to high temperatures, as expected, thereby supporting the hypothesis that force enhancement is associated with a stretch-induced conversion of weakly-to-strongly-bound cross-bridges.

REFERENCES

Edman, K. *et al.* (1982). *J. Gen. Physiol.*, **80**, 769-784.

Rassier, D., Herzog, W. (2004). *J. Appl. Physiol.*, **97**, 1395-1400.

Wang, G., Kawai, M. (2001). *J. Physiol.*, **531.1**, 219-234.

ACKNOWLEDGEMENTS

Canada Research Chairs Program, CIHR and NSERC of Canada

Table 1: 10% stretch. Force, Stiffness and Force/Stiffness (mean ± SE). *****Stretch significantly different from isometric reference contraction, $p<.05$. †7 ºC significantly different from 20ºC, $p<.05$.

	Force [N/mm^2]		**Stiffness [N/mm^3]**		**Force/stiffness [mm]**	
	7 ºC	20 ºC	7 ºC	20 ºC	7 ºC	20 ºC
Iso	0.172±0.017*****	0.176±0.015*	7.69±0.60†	5.81±0.57†	0.023±0.001***†**	0.031±0.002***†**
Stretch	0.189±0.017*	0.188±0.016*	7.77±0.63†	5.86±0.60†	0.025±0.001***†**	0.033±0.002***†**

Table 2: Force enhancement (FE), Stiffness enhancement (SE) and Force/Stiffness enhancement (F/stiff E) (mean ± SE). # 7 ºC significantly different from 20ºC, $p<.05$.

	10% stretch [%]			**15% stretch [%]**		
	FE #	SE	F/stiff E	FE #	SE	F/stiff E #
7 ºC	10.43 ± 1.06	1.70 ± 1.09	8.68 ± 1.25	14.36± 2.02	2.17 ± 2.08	12.06 ± 1.61
20 ºC	6.83 ± 0.61	0.65 ± 1.15	6.26 ± 1.13	9.97 ± 1.19	4.12 ± 1.41	5.73 ± 1.47

EFFECTS OF ACL INTERFERENCE SCREWS ON ARTICULAR CARTILAGE THICKNESS MEASUREMENTS WITH 1.5T AND 3T MRI

Bowers ME, Fleming BC, Tung GA, Leventhal EL, Trinh N, Crisco JJ, Kimia BB
Department of Orthopaedics, Brown Medical School/Rhode Island Hospital, Providence, RI
E-mail: Braden_Fleming@brown.edu

INTRODUCTION

ACL injury places patients at risk for early osteoarthritis (OA). Quantitative MRI (qMRI) can be used to track changes in tibiofemoral (TF) articular cartilage volume and thickness, and could provide insight into OA progression after surgical ACL reconstruction. Titanium interference screws are frequently used to fix ACL grafts. However, metallic implants can produce magnetic susceptibility artifacts with MRI, artifacts that may increase with magnetic field strength (Guermazi et al, 2003). The purpose of this study was to assess the effects of interference screws and magnetic field strength (3T vs. 1.5T) on measurements of articular cartilage thickness.

METHODS

MR Imaging: 5 fresh-frozen intact right human knees (3 female, 2 male; mean age = 56, range 51-59) were imaged on 1.5T and 3T scanners (Siemens Symphony and Trio, respectively, Erlangen, Germany) using surface knee coils. The T1-weighted WE-3D FLASH sequence (1.5mm slices) was used on the 3T scanner (Eckstein et al, 2004), and a similar sequence was adapted for use on the 1.5T magnet (2mm slices).

Test Protocol: After thawing, each knee was imaged on the two scanners with and without two 9x20mm titanium interference screws implanted (Arthrex, Inc; Naples, FL). To minimize bias, the test order was block randomized, first by screw condition (with screws vs. without), and then by magnetic field strength (1.5T vs. 3T).

Segmentation Technique: The femoral and tibial articular cartilage structures of each specimen were manually segmented in the sagittal plane and reconstructed using commercial software (Mimics 9.11; Materialise, Ann Arbor, MI). 3-D voxel models were generated and wrapped with a triangular mesh to create a virtual solid model of each cartilage structure.

Regions of Interest (ROI): We focused our thickness measurements to the regions of greatest load bearing. A cylinder was fit to the bone-cartilage interface of the femoral cartilage model of the TF joint. The notch marking the junction between the TF and patellofemoral joints on the lateral condyle was identified on sagittal MR views (Fig. 1). A line was drawn from the notch (0^o) to the center of the cylinder. Each condyle of the TF joint was then divided at 40^o, 70^o, 100^o, and 130^o from the notch point toward the posterior aspect of the condyles to create 6 patches of cartilage (3 medial, 3 lateral); the width of each patch was 20% of the overall width (M-L) of the femoral cartilage and centered about the midline of each condyle. Two patches on the tibial cartilage (1 medial, 1 lateral) were also defined by calculating the centroid of each compartment and the inertial axes of the medial compartment using MATLAB (The Mathworks, Inc., Natick, MA). The inertial axes served as a coordinate system, and the patch in each compartment was defined as the area ±20% of the overall depth (A-P) and ±15% of the overall width (M-L) from the centroid. The average thickness of each patch was calculated by the closest point algorithm using MATLAB.

Statistical Analysis: Two-way repeated measures analyses of variance were performed to compare the cartilage thickness of each ROI in response to screw condition (screws vs. no screws) and magnetic field strength (1.5T vs. 3T). Pair-wise comparisons were made with the Holm-Sidak test.

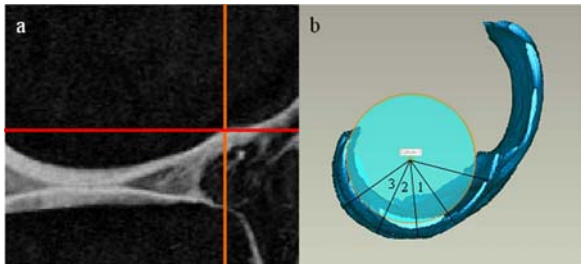

Figure 1: (a) The "notch" is marked by crosshairs on the lateral side of the TF joint, seen in the sagittal plane. (b) A cylinder was fit to the femoral condyles, with a line drawn from the notch to the cylinder axis. The location of the 3 ROIs are shown.

RESULTS

There were no significant differences in the average femoral articular cartilage thickness values due to field strength or screw condition for any ROI examined (Table 1). There were no significant differences in tibial articular cartilage thickness values at different field strengths (Table 1). There was no significant difference in the medial tibial articular cartilage thickness with different screw conditions (Table 1). However, there was a significant difference (mean 0.28mm) in the lateral tibial cartilage thickness at different field strengths (3T>1.5T, p=0.04). The difference was independent of screw condition; however, there was a trend for interaction between field strength and screw condition (p=0.06).

Table 1: Mean (standard error) thickness (mm) of each region of interest (ROI) at each field strength and screw condition. "M" denotes medial; "L" denotes lateral. "Tib" and "Fem" denote tibial and femoral, respectively. "Fem1" represents the ROI between 40-70^o, "Fem2" 70-100^o, and "Fem3" 100-130^o (see Fig. 1).

Magnet	**3T**		**1.5T**	
Screw	**Yes**	**No**	**Yes**	**No**
MTib	2.3(.07)	2.6(.07)	2.2(.07)	2.5(.07)
LTib	3.9(.05)	4.0(.05)	3.7(.05)	3.6(.05)
MFem1	1.9(.06)	2.0(.06)	1.8(.06)	1.8(.06)
MFem2	2.0(.05)	1.9(.05)	2.0(.05)	2.0(.05)
MFem3	2.0(.06)	1.9(.06)	2.0(.06)	1.9(.06)
LFem1	2.5(.05)	2.5(.05)	2.5(.05)	2.4(.05)
LFem2	2.8(.05)	2.8(.05)	2.7(.05)	2.7(.05)
LFem3	2.3(.06)	2.4(.06)	2.3(.06)	2.4(.05)

DISCUSSION

Our data demonstrate that measurements of TF articular cartilage thickness are not affected by the presence of titanium interference screws for the ACL-reconstructed patient when using the T1-WE-3D FLASH sequence at 1.5T. The lack of screw effect, however, was not independent of magnetic field strength. While the difference in thickness in the lateral compartment of the tibia between screw conditions was not statistically significant (<0.1mm; Table 1), there was a trend for interaction between these parameters at 3T. Thus, caution should be used when interpreting the mean thickness values in the lateral tibial cartilage at 3T with interference screws present. As a result, 3T and 1.5T qMRI should not be used interchangeably to assess structural changes in lateral tibial articular cartilage during longitudinal studies.

REFERENCES

Guermazi (2003). *Clin Radiol*, **58**:322 328.

Eckstein (2004). *Methods Molec Med*, **101**:191-218.

ACKNOWLEDGEMENTS

Funded by the NIH (RO1 047910S1) and the RIH Orthopaedic Foundation, Inc. We gratefully acknowledge the help of Dr. Charles B. Eaton, Dan Arcuri, Lynn Fanella, and Theodore Trafton.

COMPARISON OF TWO ALTERNATE METHODS FOR TRACKING TOE TRAJECTORY

Chris Miller [1], Brian Peters [1], Rachel Brady [1], Ajitkumar Mulavara [2], Liz Warren [2], Al Feiveson [3] and Jacob Bloomberg [3]

[1] Neurosciences Laboratory, Wyle Laboratories, Houston, TX, USA
[2] Universities Space Research Association, Houston, TX, USA
[3] NASA Lyndon B. Johnson Space Center, Houston, TX, USA
E-mail: chris.miller-1@nasa.gov

INTRODUCTION

Toe trajectory during the swing phase of locomotion has been identified as a precise motor control task (Karst, et al., 1999). The standard method for tracking toe trajectory is to place a marker on the superior aspect of the distal end of the 2nd toe (Karst, et al., 1999; Winter, 1992). However, others have based their results on a marker positioned on the lateral aspect of the 5th metatarsal head (Dingwell, et al., 1999; Osaki, et al., 2007), or on a "virtual" toe marker – computed at a distal point on the shoe based on the positions of other "real" foot markers (Begg, et al., 2007; Miller, et al., 2006). While these methods for tracking the toe may seem similar, their results may not be directly comparable. The purpose of this study was to compute toe trajectory parameters using a 5th metatarsal marker and a virtual toe marker, and compare their results with those of the standard toe marker.

METHODS

Twelve subjects gave informed consent and participated in this study, and the NASA-JSC Committee for the Protection of Human Subjects approved the protocol. Subjects wore lab-supplied shoes (Converse, North Andover, MA) with footswitches (Motion Lab Systems, Baton Rouge, LA) affixed to the soles. 3D motion of the subject's right leg and shoe was recorded using a video-based motion capture system (Motion Analysis, Santa Rosa, CA). Foot markers were placed on the top surface of the shoe over the end of the 2nd toe (rtoe), the lateral aspect of the shoe at the 5th metatarsal head (mth5), the lateral surface of the shoe at the calcaneus, and the top surface of the shoe at the site of the navicular bone. The virtual marker (vtoe) was computed during post-processing based on the positions of the navicular, calcaneal, and mth5 foot markers. The virtual-location of vtoe was at the distal end of the shoe at the second toe, at the same height on the shoe as mth5. Therefore, when the foot was flat on the walking surface, vtoe(z) = mth5(z).

Subjects walked on a treadmill for ten 60-second trials per the protocol outlined in Miller, et al. (2006). The marker positions and footswitch data were analyzed using in-house Matlab scripts (Mathworks, Inc., Natick, MA) to determine gait cycle events, kinematics of the foot, and the position of vtoe. The vertical heights of each "toe" marker were reported relative to their respective heights during a quiet stance (static) trial for reference. The analysis concentrated on three features of each toe marker: minimum vertical clearance (TCl), the first peak in early swing (Toemax1) and the second toe peak just before heel contact (Toemax2). Vertical height and %GC were calculated at the TCl, Toemax1 and Toemax2 events. A regression analysis was

performed on the vtoe and mth5 results versus rtoe (the standard) individually. If vtoe or mth5 results were analogous to rtoe, then the regression lines would have a slope equal to one and an intercept equal to zero.

RESULTS AND DISCUSSION

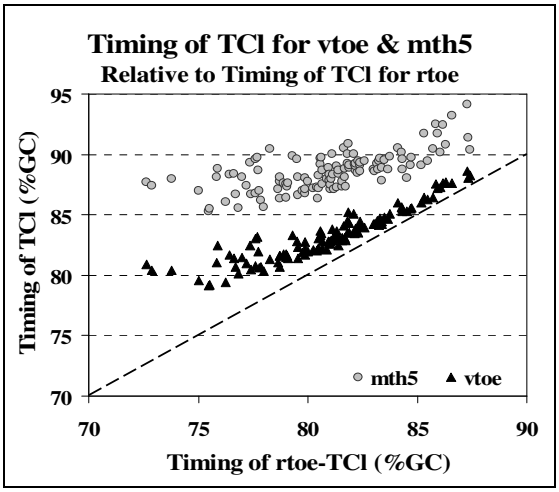

Figure 1: Per-trial averages of the timing of TCl for vtoe and mth5 relative to rtoe. The dashed line (unity) represents perfect agreement with rtoe.

Minimum mth5 marker height during swing phase occurred later in the gait cycle than minimum vtoe and rtoe height (Figure 1). Inferences based on mth5's later occurrence of TCl could result in a misinterpretation of a subject's true propensity to trip: the foot would be farther anterior of the stance leg – well past the most dangerous point during swing where floor contact would result in a fall (Winter, 1992).

The TCl results for mth5 did not compare well with rtoe (Table 1), as shown by diminished slopes, and intercepts much different than zero. The results for vtoe showed better agreement, especially for minimum height. Similar results were seen for the Toemax1 parameters. Both markers compared well with rtoe for Toemax2 parameters.

SUMMARY

The virtual toe marker (vtoe) appeared to be a better analog to rtoe than mth5 for tracking toe trajectory, especially in conditions where using the rtoe marker may be impractical.

REFERENCES

Begg R., et al. (2007). *Gait Posture,* **25(2)**, 191-8.

Dingwell J.B., et al. (1999). *Gait Posture,* **10(1)**, 21-9.

Karst G.M., et al. (1999). *J Gerontol A Biol Sci Med Sci,* **54(7)**, M343-7.

Miller C., et al. (2006). *Proceedings of ASB 2006*, #34.

Osaki Y., et al. (2007). *Exp Brain Res,* **176(3)**, 476-96.

Winter D.A. (1992). *Phys Ther,* **72(1)**, 45-53; discussion 54-6.

Table 1: Linear regression slopes and intercepts for toe clearance values and normalized gait-cycle timing using vtoe and mth5 markers when compared to rtoe (standard).

		vtoe vs. rtoe		mth5 vs. rtoe	
		Height	**Timing**	**Height**	**Timing**
TCl	**Slope (m)**	0.801	0.659	-0.004	0.391
	Intercept (b)	-6.84 mm	29.9 %GC	20.08 mm	56.9 %GC
Toemax1	**Slope (m)**	0.505	0.845	-0.111	0.771
	Intercept (b)	7.93 mm	9.7 %GC	113.5 mm	14.5 %GC
Toemax2	**Slope (m)**	1.100	0.999	0.729	1.118
	Intercept (b)	-8.06 mm	0.2 %GC	-20.0 mm	-11.8 %GC

DYNAMIC AND STATIC CHANGES IN FOOT SHAPE

Sharna Clark-Donovan, Gordon Valiant

Nike Sport Research Lab, Beaverton, OR, USA
E-mail: sharna.clark-donovan@nike.com

INTRODUCTION

Understanding the changes in foot shape that occur during static loading and active movements has implications for the design and fit of athletic footwear. It is generally accepted that the foot deforms during sporting events, however previous studies have focused on only static changes in foot shape for improved footwear fit, or the development of custom footwear (Tsung 2003, Luximon 2004, Goonetilleke 1999). Additional research on foot shape has focused on heel pad deformation and not the entire foot (DeClercq 1994, Fuller 1993).

It is important to recognize the changes in foot shape that occur during an activity, such as running, that places higher loads than standing on the foot. The purpose of this study was to quantify the changes in foot shape (length and width) that occur not only during static loading, but also during over ground running.

METHODS

Ten healthy male subjects were recruited to participate (avg. ht. 73in, avg. wt. 178 lb, shoe size USM10). All trials were performed barefoot on an elevated runway containing an embedded glass platform with mirrors below the surface to allow for filming of the plantar surface of the foot. High speed video (Vision Research Corp., Phantom v4.3.) was recorded at 1000 Hz. Three static standing trials of the right foot were completed; 1) full body weight, 2) ½ body weight, 3) non weight bearing. Additionally, ten right foot strikes on the platform while running at an 8 min/mile pace were recorded for each subject.

Circular marks were placed on the plantar surface of the foot to quantify dimensional changes. The markings were placed at the most medial and lateral points of the heel and the forefoot, and the posterior point of the heel and the anterior point of the hallux, 3rd phalange, and the second metatarsal joint space. All marks were made by the same researcher to limit variability in measurements that could result from variation in marker placement.

Heel and forefoot width changes were calculated (Image Systems, TEMA automotive) from the most medial to the most lateral points of the heel and forefoot, respectively. Length changes were measured for the distance from the posterior heel to the tip of the hallux, tip of the 3rd phalange, and the 2nd metatarsal joint space (Figs 1a & 2a).

RESULTS AND DISCUSSION

The majority of the increase in forefoot and heel width occurred with static loading. A minimal change in foot width measures from static (full body weight) loading to dynamic (running) loading was measured (Fig 1b).

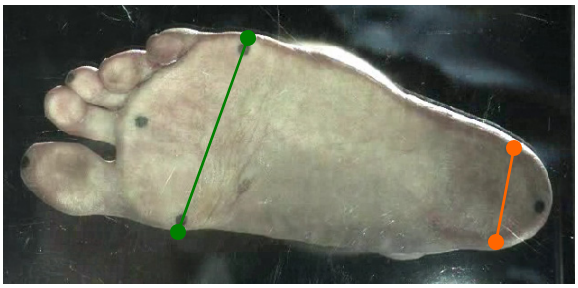

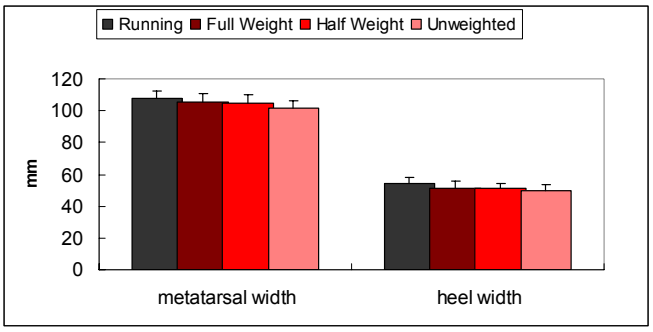

Figure 1a: Location of width measurements made, **1b:** Average foot width measures (+1SD)

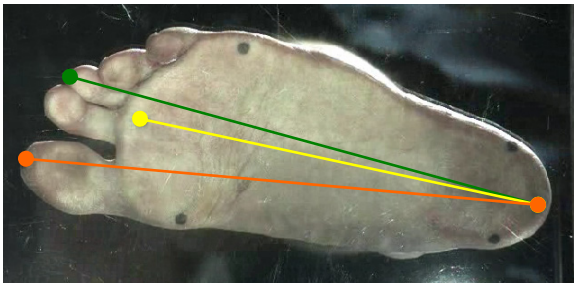

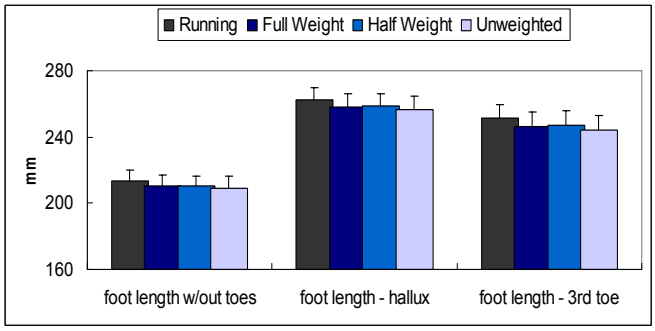

Figure 2a: Location of length measurements made, **2b:** Average foot length measures (+1SD).

As opposed to width changes, dynamic loading of the foot was responsible for most of the length changes measured. Average length changes from full body weight to running stance were 4.1mm, 4.9 mm, and 3.5mm for the heel to hallux, heel to 3rd toe, and the heel to 2nd metatarsal joint measures, respectively (Fig 2b). Much of the change in length for the hallux and third toe measures may be attributed to the large amount of dynamic movements observed in the toes.

CONCLUSION

Foot width changes from statically loaded to running were minimal (<2.5mm). A change in shoe width is 4.80mm on the Brannock device, therefore measuring shoe width while an individual is standing or walking will provide proper width fit information.

A half shoe size change on the Brannock scale is measured as a change in foot length of 4.2 mm. This research shows that there is on average a half shoe size difference in the length of the foot from the heel to the 3rd toe or the hallux during running, compared to a fully weighted position. Length changes as high as 7.1mm were observed.

Current athletic footwear construction restricts length changes to a greater degree than width changes, therefore learnings from this research can be applied to improving sizing and last design of athletic footwear.

REFERENCES

Fuller. E., Hogge. J.D. (1998). *J Am Podiatr Med Assoc*, **88**(1), 12-16.

Tsung. B.Y.S., Zhang. M. et.al. (2003) *J Rehab Res Dev*, **40**(6), 517-526

Luximon. A., Goonetilleke. R.S. (2004). *Human Factors*, **46**(2), 304-315

Goonetilleke. R.S., Luximon. A. (1999). *Human Factors*, **41**(4), 596-607

DeClercq. D, Aerts. P, Kunnen. M. (1994). *J. Biomechanics*, **27**(10), 1213-1222

Technique and Performance Level Comparisons of Male and Female Hammer Throwers

Suzanne M. Konz, PhD ATC CSCS[1] and Iain Hunter, PhD[2]

[1]Department of Health & Kinesiology, Georgia Southern University, Statesboro, GA
[2]Department of Exercise Sciences, Brigham Young University, Provo, UT

Introduction

The scientific literature has focused predominately on the characteristics of male throwers [1-9]. Literature on female throwers has been limited to anthropometric data, performance information, and case studies [10, 11]. No literature has statistically compared the differences between the throwing technique of male and female hammer throwers. Also, the literature has not explored the technique differences affecting distances thrown. The aim of this study was two-fold, to determine: 1) if there were hammer throwing technique differences between genders and 2) what technique parameters helped to determine throw distance.

Methods

The performances of the top16 male and female throwers at the 2003 WAC Finals and the top 13 male and female throwers from the 2003 USATF Nationals were examined. Video was captured using three Canon 60 Hz cameras. The best throws of each athlete were digitized and analyzed using the Peak Motus 8.5 motion analysis system.

Results

T-tests revealed that athlete mass, athlete height, velocity at release, timing components, and centripetal force were different between genders ANOVA showed that the separation between the shoulders and hips and between the shoulders and the hammer at particular positions during the throw, radius changes at certain phases of the throw, and generation of large centripetal forces helped determine throwing distance.

Discussion

Training would be aided by working on the build-up of centripetal force, the magnitude of radius changes, the separation that occurs between the shoulders and hips, and the separation between the shoulders and hammer.

Acknowledgement

This project was funded in part by USA Track & Field.

References

1. Dapena J. The pattern of hammer speed during a hammer throw and influence of gravity on its fluctuations. *Journal of Biomechanics*. 1984;17:553-9.

2. Dapena J. A kinematic study of center of mass motions in the hammer throw. *Journal of Biomechanics*. 1986;19:147-58.
3. Dapena J and ME Feltner. Influence of the direction of the cable force and of the radius of the hammer path on speed fluctuations during hammer throwing. *Journal of Biomechanics*. 1989;22:565-75.
4. Dapena J, M Gutierrez-Davila, VM Soto and FJ Rojas. Prediction of distance in hammer throwing. *Journal of Sports Sciences*. 2003;21:21-8.
5. Dapena J and C McDonald. A three-dimensional analysis of angular momentum in the hammer throw. *Medicine and Science in Sports & Exercise*. 1989;21:206-20.
6. Dapena J and MA Teves. Influence of the diameter of the hammer head on the distance of a hammer throw. *Research Quarterly in Exercise & Sport*. 1982;53:78-85.
7. Ariel GB. Biomechanical analysis of the hammer throw. *Track & Field Quarterly Review*. 1980;80:41-51.
8. Baronietz K and A Borgstom. The throwing events at the World Championships in Athletics 1995, Goteborg - technique of the worlds best throwers Part 1: shot put and hammer throw. *New Studies in Athletics*. 1995;10:43-63.
9. Gutierrez M, VW Soto and FJ Rojas. A biomechanical analysis of the individual techniques of the hammer throw finalists in the Seville Athletics World Championships 1999. *New Studies in Athletics*. 2002;17:15-26.
10. Barclay L. A breif analysis of the women's hammer throwin Seville. *Modern athlete and coach*. 2000;38:37-39.
11. Baronietz K, L Barclay and D Gathercole. Characteristics of top performances in the women's hammer throw: basics and technique of the world's best athletes. *New Studies in Athletics*. 1997;12:101-109.

PREDICTING OUTCOMES OF TREATMENT FOR STIFF-KNEE GAIT USING SUPERVISED LEARNING

Jeffrey A. Reinbolt[1], Melanie D. Fox[2], Michael H. Schwartz[3,4], and Scott L. Delp[1,2]

Departments of [1]Bioengineering and [2]Mechanical Engineering, Stanford University
Department of Orthopaedic Surgery and Biomedical Engineering, University of Minnesota[3]
Gillette Children's Specialty Healthcare, St. Paul, MN[4]
E-mail: reinbolt@stanford.edu, Web: www.stanford.edu/group/nmbl

INTRODUCTION

Stiff-knee gait is a prevalent, debilitating consequence of cerebral palsy in which swing-phase knee flexion is substantially diminished. Approximately 3 out of every 1,000 children manifest one or more of the symptoms of cerebral palsy (CDC, 2004). Stiff knee gait results in a number of related gait problems including tripping and foot-dragging due to inadequate toe clearance (Sutherland and Davids, 1993).

Outcomes following surgical treatment for stiff-knee gait are inconsistent. Some patients achieve dramatic gains in knee flexion while others show no improvement or suffer further impairment. At present, stiff-knee treatment recommendations are based on qualitative observations of the patient's gait, physical examination of muscle spasticity, inspection of gait analysis measurements, and the intuition and experience of the clinical team.

This study presents the use of supervised learning, an objective and quantitative tool, to predict treatment success for stiff-knee gait. Our goal was to determine combinations of preoperative gait measurements, or predictors, that mathematically classify the postoperative outcome, or response.

METHODS

The subjects analyzed in this study had previously undergone routine treatment-planning gait analysis at Gillette Children's Specialty Healthcare – Center for Gait and Motion Analysis, St. Paul, MN. Using inclusion and stiff-knee definitions of Goldberg *et al.* (2006) and requiring equal numbers of *good* (i.e., not-stiff) and *poor* (i.e., stiff) outcomes following treatment for stiff-knee gait, 62 subjects were identified who met these criteria.

Significant features of preoperative gait measurements separating the good and poor outcome groups were determined in two ways. First, kinematic and kinetic factors correlated with improved knee flexion (Goldberg *et al.*, 2006) were extracted from existing data. Second, kinematic, kinetic, and joint power data having the largest test statistics from a two-sample *t*-test were extracted as well.

Linear discriminant analysis (i.e., linear regression in the two-class outcome case) was used to determine the linear combination of preoperative predictors that best fits good and poor postoperative outcomes. The resulting coefficients were then used to predict postoperative outcomes for a separate set of subjects. Due to the relatively small data set, cross-validation with the 20% holdout method was used to determine performance.

RESULTS AND DISCUSSION

Several combinations of preoperative gait parameters correctly predicted postoperative outcomes at a rate higher than the inherent 50% probability of the input data (Table 1, Figure 1). The rate was highest (87.9% correct) using the combination of hip flexion and power after initial contact, knee power at peak knee extension, knee flexion velocity at toe-off, and hip internal rotation in early swing.

These preliminary results have significant clinical impact. More than 87% of treatment outcomes were predicted correctly using only five preoperative gait measurements. Nearly

70% of outcomes were predicted by a single measurement. Knee flexion velocity at toe-off was one of the most noteworthy single predictors. Good outcomes resulted in ⅔ of subjects with preoperative knee flexion velocities at toe-off above 1.2°/(% of gait cycle).

The potential to use supervised learning to predict treatment outcomes for stiff-knee gait is exciting. This study provides specific and useful preoperative predictors of postoperative outcome. Future studies are needed to determine the optimal set of predictors and if supervised learning can improve treatments.

REFERENCES

CDC (2004). *Morb Mortal Wkly Rep*, **53**, 57-59.

Goldberg, S., *et al.* (2006). *J Biomech*, **39**, 689-698.

Sutherland, D.H. and Davids, J.R. (1993). *Clin Orthop Relat Res*, **288**, 139-147.

ACKNOWLEDGEMENTS

Supported by NIH R01 HD046814 and NIH Roadmap for Medical Research U54 GM072970.

Table 1. Summary of cross-validated correct response rates for best combinations of 5 or fewer preoperative gait measurements separating the good and poor outcome groups.

Predictor (Portion of Gait Cycle)		Combination	Rate (%)
Goldberg *et al*. (2006) factors correlated with stiff-knee gait		G1-G2	**68.1**
G1. Knee flexion velocity (toe-off)		G1	67.8
G2. Average hip flexion moment (double support)		G1-G2-G5	66.4
G3. Average hip flexion moment (early swing)		G1-G2-G3-G4	63.8
G4. Average knee extension moment (double support)		G1-G2-G3-G4-G5	63.5
G5. Average knee extension moment (early swing)			
Two-sample *t*-test comparing good and poor outcome groups		T1-T2-T3-T4-T5	**82.6**
T1. Knee flexion (48.5%)	T8. Hip internal rotation (71.4%)	T6-T7-T8-T9	79.5
T2. Knee flexion (80.8%)	T9. Hip flexion (92.9%)	T2-T10-T11	78.3
T3. Hip power (43.2%)	T10. Pelvic tilt (18.7%)	T10-T11	74.1
T4. Knee abduction moment (51.6%)	T11. Hip flexion (52.0%)	T12	68.2
T5. Knee power (2.1%)	T12. Ankle power (48.3%)		
T6. Hip power (4.4%)	T13. Hip flexion (4.4%)		
T7. Knee power (40.7%)			
Combination of Goldberg *et al*. (2006) factors correlated with stiff-knee gait and two-sample *t*-test comparing good and poor outcome groups		G1-T6-T7-T8-T13	**87.9**
		G1-T8-T10-T13	87.0
		G1-T6-T10	81.9
		G1-T10	77.2

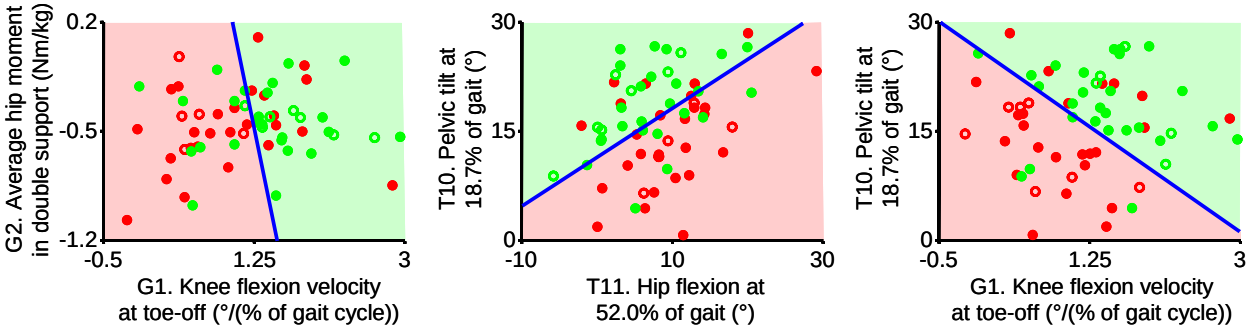

Figure 1. Scatter plots of best combinations of two preoperative gait measurements separating the good and poor outcome groups. Filled circles represent training data and open circles represent test data for one instance of cross-validation. Circle colors indicate good (green) and poor (red) postoperative outcomes. Blue lines divide the good (green shaded) and poor (red shaded) outcome prediction regions.

THE EFFECT OF COMPRESSION PANTS ON POSTURAL STEADINESS BEFORE AND AFTER TIRING EXERCISE

Gary D. Heise[1], Katharine Mack[1], and Minoru Shinohara[2]

[1]University of Northern Colorado, Greeley, CO, USA
[2]Georgia Institute of Technology, Atlanta, GA, USA
E-mail: gary.heise@unco.edu Web: www.unco.edu

INTRODUCTION

Postural steadiness is often compared between groups of healthy and unhealthy individuals and between young and old adults (Prieto et al., 1996). It has also been examined in attempts to predict falling in older adults and to determine the relative importance of vision, vestibular, and somatosensory systems in subjects of all ages (e.g., Cornilleau-Peres et al., 2005; Mackey & Robinovitch, 2005).

The popularity and prevalence of core-strengthening programs developed from dance has led to assessments of postural stability in young, healthy individuals. For example, Gerbino and colleagues recently found that college-age dancers are superior to collegiate soccer players in measures of sway index and center acquisition time (Gerbino et al., 2006).

Following this line of reasoning, balance measures may also be used to assess training aids. Manufacturers of compression pants (i.e., tights), for example, advertise that their product adds support to the musculature of the lower extremity. Overall balance may be an additional benefit of this improved support. The present study was designed to examine the effects of compression pants on postural steadiness before and after tiring exercise in a group of young, healthy women. It was expected that compression pants would improve postural steadiness.

METHODS

Eleven women, who were part of a larger study, visited the lab on three occasions, which were separated by at least two days (Mean ± SD: Age = 25.6 ± 7.3 yrs; Body Mass = 58.7 ± 5.3 kg). The three test sessions corresponded with three clothing conditions (running shorts, brand1 compression pants, brand2 compression pants), which were assigned randomly to each participant. Postural steadiness was assessed early in each session and then after tiring exercise, which included vertical jumping, an anaerobic power test, knee extensor muscle testing, and a 30-min treadmill run.

For postural steadiness measures, participants stood quietly on an AMTI force platform for 30 s, while ground reaction force (GRF) data were collected at 240 Hz. Subjects were instructed to keep their hands on their waist and direct their vision straight ahead. All tests were done with eyes open.

Center of pressure (COP) data were calculated from the final 20 s of GRF data. Dependent variables included: the root-mean-square distance from the mean COP (RDIST); the mean velocity of the COP (MVELO); and the mean frequency (MFREQ) of the COP (Prieto et al., 1996). A two factor repeated measures analysis of variance (prepost, clothing, prepost-clothing interaction) was used to detect differences in each dependent variable ($\alpha = .05$).

RESULTS AND DISCUSSION

There was a main clothing effect for MVELO as shown in Figure 1 and a main effect between pre and post testing times for MFREQ as shown in Figure 2. There were no significant differences for RDIST. Magnitudes of all measures were consistent with previously reported values from young subjects (Prieto et al., 1996).

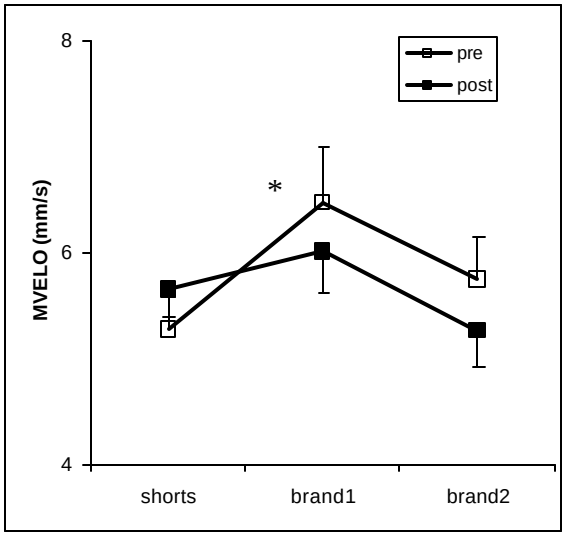

Figure 1: Mean velocity (± SE) of the COP (MVELO) for all conditions.
*brand1 > shorts, brand2 ($p < .05$)

Based on interpretations of Prieto et al. (1996), our findings show that although the level of postural steadiness was similar between all clothing conditions (i.e., no change in RDIST), the rate of regulatory activity associated with maintaining that level of postural steadiness was elevated in brand1 compression pants (MVELO). This change is likely due to a mechanical factor: brand1 compression pants effectively increased the leg stiffness, which did not reduce RDIST but only increased MVELO. This interpretation is analogous to the neural strategy of older adults stiffening the legs by increasing muscle coactivation at the ankle joint (Benjuya et al., 2004). The difference is that older adults also showed increased RDIST. The decrease in MFREQ after exercise was amplified in both compression pants conditions (see Figure 2).

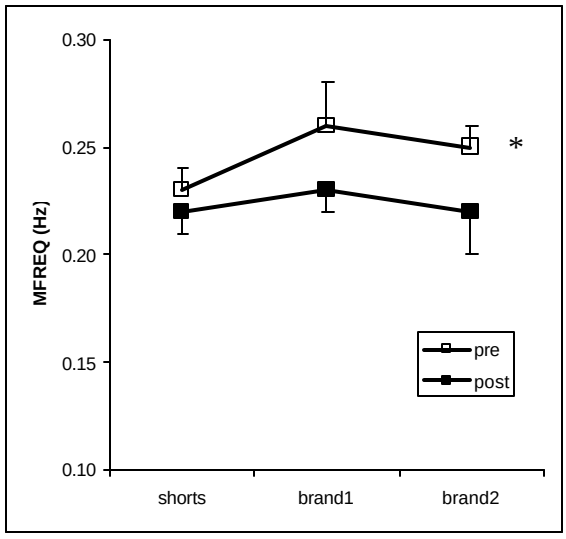

Figure 2: Mean frequency (± SE) of the COP (MFREQ) for all conditions.
*pre > post ($p < .05$).

In conclusion, after tiring exercise, there was no difference in the level of stability attained by subjects when they were wearing shorts or compression pants (variable RDIST). There was a difference in MVELO between clothing conditions and a difference in MFREQ between pre and post exercise conditions. Some compression pants may increase leg stiffness, similar to the neural strategy adapted by older adults.

REFERENCES

Benjuya, N. et al. (2004). *J Gerontology: MED*, 59A, 166-171.

Cornilleau-Peres V. et al. (2005). *Gait Posture*, **22**, 96-106.

Gerbino, P.G. et al. (2006). *Gait Posture*, doi:10.1016/j.gaitpost.2006.11.205.

Mackey, D.C. & Robinovitch, S.N. (2005). *Clin Biomech*, **20**, 776-783.

Prieto, T.E. et al. (1996). *IEEE Trans Biomed Eng*, **43**, 956-966.

Response-Surface Mapping to Generate Distributions of Forward Dynamic Simulations

Matt J. Camilleri

Sacramento City College, Sacramento, CA, USA
E-mail: camillm@scc.losrios.edu

INTRODUCTION

Muscle quantities such as force and work are estimated using forward dynamic simulations because forces cannot be measured readily. Input muscle excitations are transformed into forces that act on the body segments to produce a simulated motion. Minimizing the error between experimental and simulated data is typically implemented to compute a solution.

However, optimizing (minimizing) a single simulation to represent a distribution is problematic for several reasons. First, a single simulation provides no standard deviations with which to establish statistical confidence. Second, current simulation methods generate few quantities that can be validated against experimental data. Third, a simulation method whose explicit objective is to minimize tracking errors also tends to obscure potential manifestations of inaccuracies (tracking errors) in the neuro-musculo-skeletal model, potentially generating false confidence in the results.

Therefore the objectives of this work were to: 1) develop a method, designated the descent-ascent distributor, for generating a distribution of feasible simulation results, 2) demonstrate quantities by which to validate the distribution, and 3) demonstrate any manifestations of inaccuracies in the underlying models, revealed by the method.

METHODS

To achieve these objectives, pedaling was used as a demonstration task. Fifteen subjects pedaled at 90 rpm and 250 W. Intersegmental moments were computed by inverse dynamics. Onset angles of the leg muscles were computed from EMG data. A forward dynamic model of pedaling was used to simulate the input muscle excitations and output inter-segmental moments (Camilleri et al., in press).

The distributor had similarities to gradient-based optimization methods. A vector-valued objective function was defined by error terms (difference been simulated and experimental data), including the intersegmental moments. The distribution direction, **d**, ("descent direction" in gradient-based methods) was defined by the Jacobian, **J**, of the objective function:

$$\mathrm{d}_n = f\left(-\sum_{f=1}^{\mathrm{F}} \mathbf{J}_{nf}\right),$$

where F is the number of objective function components and n is the index of the control parameter. The Jacobian, computed from regression of the previous 20 simulations (steps), and distribution direction, were updated every 20 simulations. The use of 1) a vector-valued objective function, in which all components would unlikely be minimized simultaneously, and 2) a constant number of steps between updates of the distribution direction, ensured that new and different simulations would be generated. These simulation results were sequentially included in a distribution until it stabilized.

Statistical analyses of coordination behaviors included: 1) standard deviations of the intersegmental moments, and 2) cadence/onset-timing-angle relationships.

RESULTS AND DISCUSSION

The control parameters varied about regions of small errors (Figure 1), with associated variations in the simulated intersegmental moments (sim., Figure 2). Phasing of the pedaling frequency of the intersegmental-moment standard deviations was similar between simulations and experiments. Ninety percent of the simulated onset angles advanced and retarded with the cadence in accordance with the experimental data. A distribution of simulation results generated by the random and independent perturbation of control parameters (e.g. Monte Carlo methods) would not generate such a realistic solution.

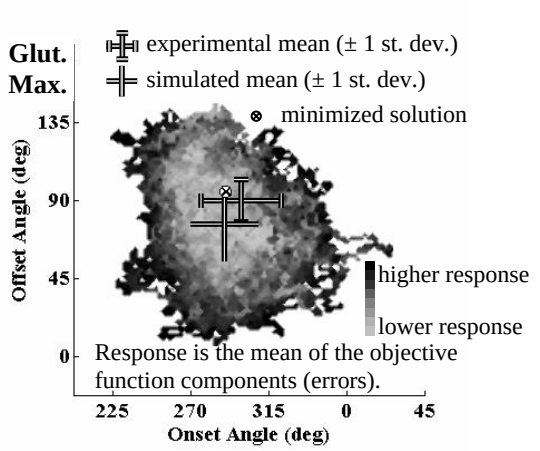

Figure 1: Minimum response surface.

Because the distributor did not explicitly minimize errors, it manifested a known inaccuracy in the model, whereas a minimized solution (tracking errors minimized; Camilleri et al., in press) obscured the inaccuracy. Pedaling is asymmetric between left and right sides (Smak et al., 1999). However, a symmetric model was implemented, as is typically done, and the distribution solution demonstrated an overestimation of the average crank power from the tracked leg, which manifests as a tracking error at the knee (Figure 2). Because of this manifestation, and the differences in simulated muscle work (Figure 3), modeling volitional pedaling as asymmetric is appropriate to generate simulations with greater confidence.

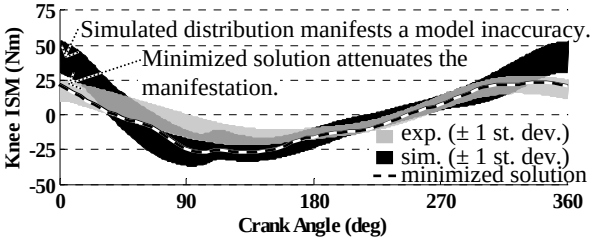

Figure 2: Knee intersegmental moment.

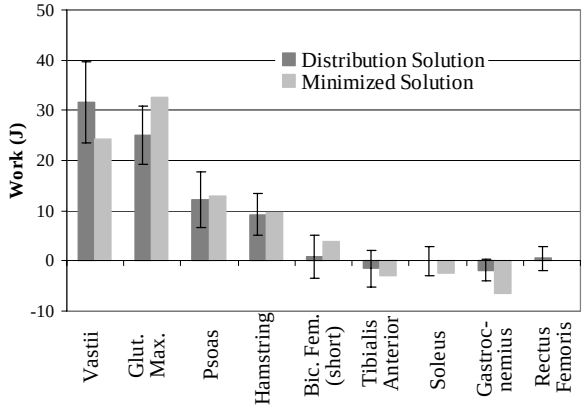

Figure 3: Muscle work per crank cycle.

SUMMARY

Implementing the descent-ascent distributor: 1) provides means and deviations for computing statistical confidence, 2) demonstrates a solution that replicates some of the coordination behaviors of pedaling, and 3) is more apt to reveal model inaccuracies. These findings support the use of the descent-ascent distributor to increase confidence in conclusions drawn from analyses of forward dynamic simulations.

REFERENCES

Camilleri, M.J. et al., *J Biomechanics*, in press.

Smak, W. et al., (1999). *J Biomechanics*, **32**, 899-906.

A Finite Element Investigation into the Effects of Minimally Invasive Treatment for Cervical Spondylotic Myelopathy

Lacey E. Bresnahan [1] Mozammil Hussain [2], Richard G. Fessler[1], Raghu N. Natarajan[2] and Gunnar B.J. Andersson [2]

[1] The University of Chicago, Chicago, IL, USA
[2] Rush University Medical Center, Chicago, IL, USA

INTRODUCTION

Cervical spondylotic myelopathy one of the most common diseases of the vertebral column frequently caused by degenerative processes (1). The degenerative changes that occur in the cervical spine result in compression of the spinal cord and nerve roots leading to radicular pain and numbness. Posterior surgical approaches for the management of cervical spondylosis are well established and among the oldest spinal procedures known. Recent advancements in minimally invasive surgical techniques have produced the same surgical result while minimizing bone and ligament resection as well as preserving the surrounding tissue (1). These surgical advancements have shown clinical improvements such as a decrease in post operative pain and improved clinical outcomes (2) however, the biomechanical impact of cervical microendoscopic decompression for stenosis (MEDS) is unknown. In this study we will quantify the change in intersegmental motion of the cervical spine in response to a decompressive laminotomy at C4-6 using the standard open procedure and the new MEDS technique.

METHODS

A three dimensional finite element model of an intact C3-T1 cervical spine motion segment was developed from the CT scan of a 38 year-old female normal subject. The model was previously validated with the *in vivo* study under diurnal compressive load of 40 – 350N (3). A compressive pre-load of 150N was simulated using the follower load technique. Two additional C3-T1 models with a C4-C6 laminectomy were developed one with traditional open posterior approach and the other a cervical MEDS approach. The open procedure was modeled by removal of the spinous process, a bilateral laminectomy and removal of the ligamentum flavum and interspinous ligaments. The cervical MEDS was modeled by unilateral removal of the right lamina and the ligamentum flavum. Moment loads were created by applying appropriate equal and opposite loads on the superior surface of C3 keeping the inferior surface of T1 fixed. A 1.5 Nm flexion, extension, axial rotation and lateral bending moments were applied to the model. The values selected represent the mean motion generated in the three principle planes computed from the *in vivo* studies. Rotation of the vertebral body was studied for the three FE models using the commercially available software ADINA.

RESULTS AND DISCUSSION

Rotation of the vertebral bodies in the sagittal, axial and coronal planes were compared between a cervical MEDS and open laminectomy at C4-6 and an intact control using finite element analysis. There was a general increase in motion at each level under all loading conditions using the open technique (Figure 1).

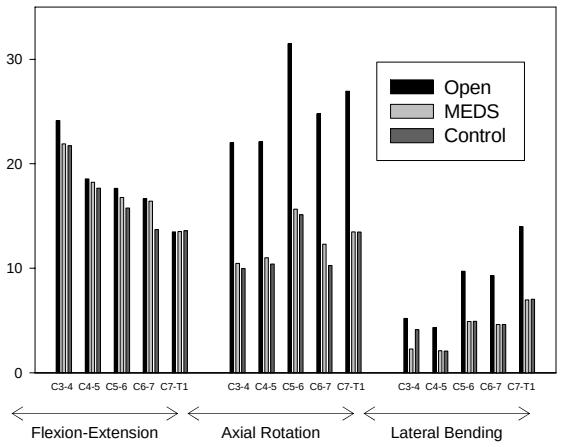

Figure 1. Change in segmental rotation for open, MEDS and control models under flexion, extension, lateral bending and axial rotation.

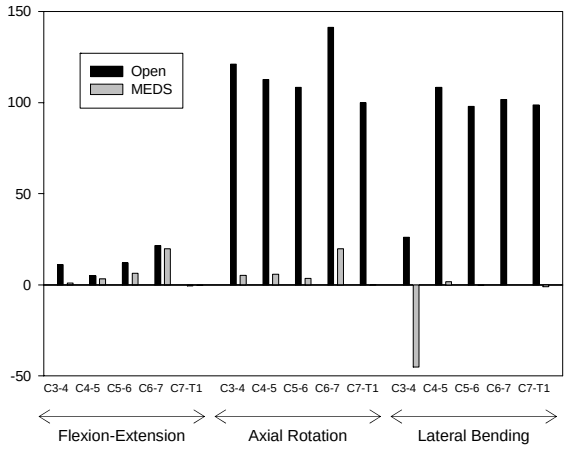

Figure 2. Change in percent segmental rotation for open and MEDS normalized to control under flexion, extension, lateral bending and axial rotation.

MEDS resulted in minimal increased motion with the most significant change at C6-7 in axial rotation and flexion-extension. Figure 2 shows the percentage change in rotation for the open and MEDS procedures standardized to an intact control model under all loading conditions. Again, there was an overall increase in motion for the open relative to the MEDS group with the largest increase in axial rotation and lateral bending. The largest increases in motion under lateral bending were seen at C4-5 for both open and MEDS resulting in a 108% and 2% change respectively relative to the control. The largest motion for axial rotation was seen at C6-7 for both groups and resulted in an increase of 141% and 20% for open and MEDS respectively. An over 100% increase in motion during axial rotation was found for each segment for the open model.

SUMMARY/CONCLUSIONS

The limitations of finite-element analysis are known. However, our application of the finite element method for comparison of segmental motion as a result of two different surgical treatments for cervical spondylotic myelopathy provide biomechanical data to verify the results seen clinically (1). Our data show that the MEDS procedure results in significant preservation of motion control compared to the open procedure for a cervical laminectomy at C4-6.

REFERENCES

1. Santiago P, Fessler RG (2007) *Neurosurgery*,**60 (Suppl 1),** S160-5.
2. Fessler RG, Khoo LT (2002) *Neurosurgery*, **51 (Suppl 5)**, S37-45.
3. Natarajan RN et al. (2000) *Spine*, **25(8)**, 955-61.

SEPARATING THE INFLUENCE OF AGE AND SPEED ON GAIT VARIABILITY

Hyun Gu Kang and Jonathan B. Dingwell

Nonlinear Biodynamics Lab, University of Texas, Austin, TX, USA
E-mail: jdingwell@mail.utexas.edu, Web: www.edb.utexas.edu/faculty/dingwell

INTRODUCTION

Gait variability has been correlated with fall risk in the elderly (Maki 1997). Older adults exhibit higher gait variability and walk slower compared to healthy young adults (Öberg 1993), but the cause of this higher variability is unclear. Slower walking is more variable in healthy young adults (Öberg 1993, Dingwell 2006). Thus, increased variability in older adults may result from simply walking slower. Alternatively, this higher variability may arise from other age-related changes, such as decreased range of motion and/or strength. This can be tested by comparing young and older adults and controlling for speeds.

Using self-selected speeds overground allows comparison between speeds, but makes it difficult to compare across subjects or groups (Öberg 1993). Interpolating variability at a fixed walking speed allows comparison between groups (Moe-Nilssen 2005), but ignores differences between individuals. Here, we quantified gait variability in both young and older adults at multiple controlled speeds, to test whether higher variability in older adults can be attributed to walking speed alone.

METHODS

Eighteen healthy older adults (age 72±6) and 17 height- and weight-matched young adults (23±3), with no orthopedic or neurological conditions, participated with informed consent. Each walked for 5 minutes on a Woodway treadmill at 80, 90, 100, 110, and 120% of preferred walking speed (PWS) (Dingwell 2006), twice at each speed. The order of presentation was randomized. VICON was used to measure motion of the trunk, pelvis, and left leg. Custom MATLAB routines were used to determine temporal-spatial gait measures, 3D joint and trunk angles, and trunk velocity. Bilateral leg strength and passive range of motion were also measured, and used to derive a composite score for strength and ROM each, using the 1st principal component from principal component analysis.

Variability of leg joint and trunk angles, and trunk velocity were quantified at each speed as MeanSD, the average of the stride-to-stride variability over the gait cycle (Dingwell 2006). The two groups and 5 speeds were compared using a repeated-measures ANOVA, with an α of $0.05 \div 18 = 0.0028$.

RESULTS AND DISCUSSION

The PWS of older adults were no different from young adults (1.29 ± 0.13 m/s, $p = 0.86$). Older adults had lower strength and ROM scores ($p < 0.001$).

Older adults exhibited higher variability at all speeds for trunk roll ($p < 0.001$). Stride time ($p < 0.02$), step length ($p < 0.005$) and trunk pitch ($p < 0.03$) trended toward the same. If 2 statistical outliers from young adults were removed, the variability of knee flexion/extension angle ($p < 0.01$), trunk velocity in anterior-posterior ($p <0.02$), and mediolateral ($p < 0.05$) directions also exhibited a similar trend. Walking speed significantly affected the variability of stride time, hip abduction/adduction angle, knee

varus/valgus angle, knee internal/external rotation, and all trunk motions ($p < 0.002$). The ankle motions were not significantly affected by age or speed.

These age-effects were no longer significant when the composite Strength and/or ROM were used as covariates in an ANCOVA model, in stride time variability ($p > 0.11$), step length variability ($p > 0.09$), MeanSD of trunk pitch ($p > 0.018$) and roll ($p > 0.01$).

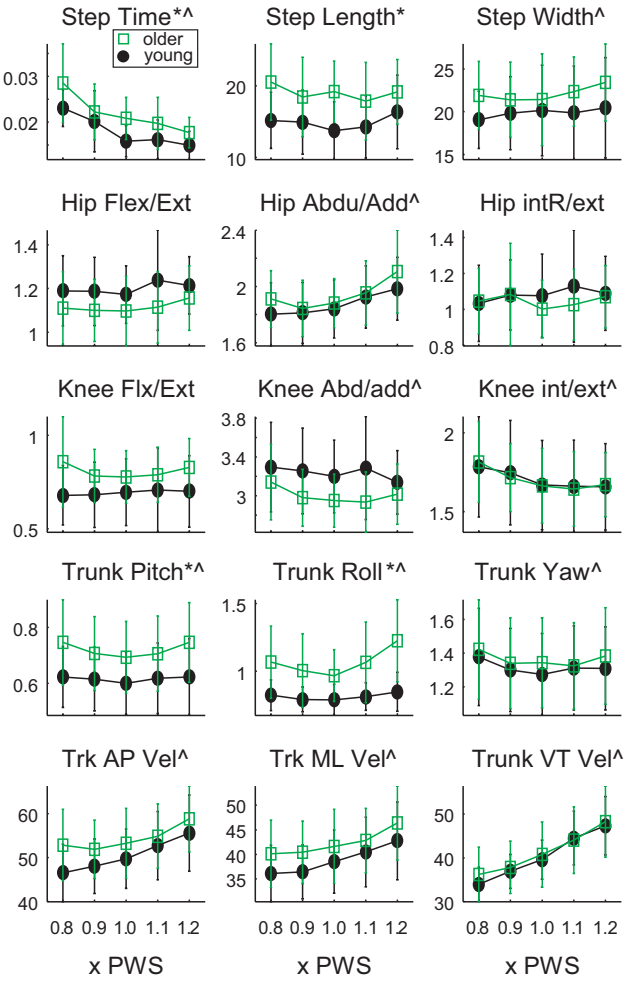

Figure 1: Variability vs. Speed. * denotes age effect; ^ denotes significant speed effect. Units: Stride Time in [s], Step length/Width in [mm], angles in degrees, and velocities in [mm/s]. AP, Anterior-posterior; ML, medio-lateral; VT, vertical.

Older adults exhibited higher variability regardless of walking speed. These differences could be attributed to their lower strength and/or flexibility. Our results agree with previous literature. Strength training and stretching interventions have reduced fall risk in some older adults (Faber 2006). Strength training also had a small, but significant reduction of gait variability (Hausdorff 2001).

Increased variability in the elderly may also come from changes in motor control. More work is needed to understand how aging affects motor functions during gait.

SUMMARY/CONCLUSIONS

This is the first comprehensive study that directly separated the issue of age-related differences in variability and the effects of walking speed. Age-related differences in variability were found regardless of walking speed. Loss of muscle strength and flexibility can explain these differences.

REFERENCES

Dingwell, J.B., Marin, L.C. (2006) *J Biomech* **39,** 444-452.

Faber, M.J., et al.(2006) *Arch Phys Med Rehabil* **87,** 885-96.

Hausdorff, J.M., et al. (2001) *J Appl Physiol* **90**, 2117-2129.

Maki, B.E. (1997) *J Am Geriatr Soc* **45,** 313-320.

Moe-Nilssen, R., Helbostad, J.L.(2005) *Gait Posture* **21,** 164-170.

Öberg, T. et al. (1993) *J Rehab Res Dev* **30,** 210-223.

ACKNOWLEDGEMENTS

Funded by Whitaker Foundation Grant # RG-02-0354 to JBD and by ASB Grant-in-Aid and A.D. Hutchinson Fellowship to HK.

DO STEP-TO-STEP TRANSITIONS INFLUENCE THE SHORT TERM LOCAL DYNAMIC STABILTIY OF GAIT?

Melissa Scott-Pandorf, Chris Arellano, and Max J. Kurz

Laboratory of Integrated Physiology, University of Houston, Houston, TX, USA
E-mail: mmscott-pandorf@uh.edu

INTRODUCTION

During walking the locomotive system must transition from one inverted pendulum arc to the next with each new step. This transition requires neural control to redirect the center of mass from a downward motion to an upward motion. Neural control of the step-to-step transitions have been suggested to play a critical role in the metabolic cost of locomotion (Kuo et al., 2005). If the step-to-step transitions require neural control for an efficient gait, it would seem plausible that control of the transitions is also involved in generating stable locomotion. Potentially, the inability to properly transition from one pendulum arc to the next may be related to the loss of stability and possibly falls. Here we use a custom built mechanical actuator to explore how the step-to-step transitions may influence the local dynamic stability of gait.

METHODS

A custom built mechanical actuator was designed to assist or resist the vertical excursion of the center of mass (COM) during the step-to-step transitions (Fig 1). The mechanical actuator consisted of a cable-spring pulley system that was attached to the subject's waist via a rock climbing harness. Different force values were obtained by stretching the rubber spring to different lengths with a hand wench. The force values were monitored with a strain gauge load cell. The horizontal force component of the spring's force was held constant (6% Body Weight) for all conditions, while the vertical force component was altered between conditions by raising or lowering the mechanical actuator (Fig 1). Raising the mechanical actuator provided a vertical assistive force during the step-to-step transition, while lowering the mechanical actuator provided a vertical resistive force during the step-to-step transition. Fifteen subjects (age: 25.2 ± 2.7 yrs; height: 1.7 ± 0.1 m; weight: 70.0 ± 10.3 kg) walked on the treadmill at a self-selected pace for four minutes while the mechanical actuator was positioned at -15, -10, 0, +10, and +15 degreesA high speed three-dimensional motion capture system (100 Hz) was used to capture the sagittal plane ankle, knee and hip joint angles.

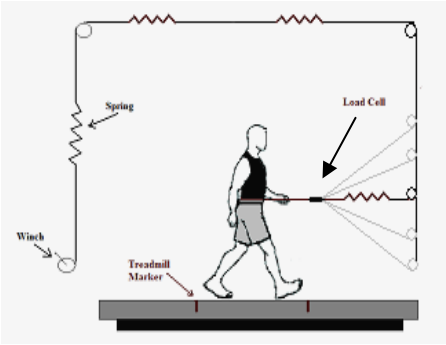

Figure 1. Mechanical actuator with experimental assist and resist angles shown.

Nonlinear time series analysis techniques were used to quantify the short term Lyapunov exponents (Dingwell & Cusumano, 2000). Lyapunov exponents quantify the local dynamic stability of the gait by determining the exponential divergence of neighboring trajectories in the reconstructed attractor. We calculated the

time lags and embedding dimensions of the respective time series to properly reconstruct the locomotive attractors (Dingwell & Cusumano, 2000). The divergence in the attractor was calculated using an algorithm by Rosenstein et al. (1993). The short term Lyapunov exponents were estimated from the slope of the divergence curve from zero to two strides (Fig 2). The larger the value of the short term Lyapunov exponent, the greater the instability in the locomotive attractor.

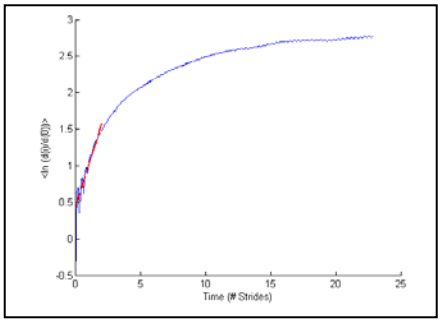

Figure 2. The slope of the divergence curve from zero to two strides.

RESULTS AND DISCUSSION

Surprisingly, no significant differences were found for the short term Lyapunov exponents of any of the lower extremity joints ($P > 0.05$). This suggests that the redirection of the COM during the step-to-step transitions may not play a large role in the local dynamic stability of gait. Possibly other neural control strategies that occur during the stance and swing phase may have a greater influence on gait stability.

Previous investigations have noted that selection of a step length influences the step-to-step transition cost of locomotion (Kuo et al., 2005). Possibly if we controlled for step length adjustment we would have seen differences in the stability.

Furthermore, it is possible that the lack of significant differences may be related to the mechanical actuator that was used in this

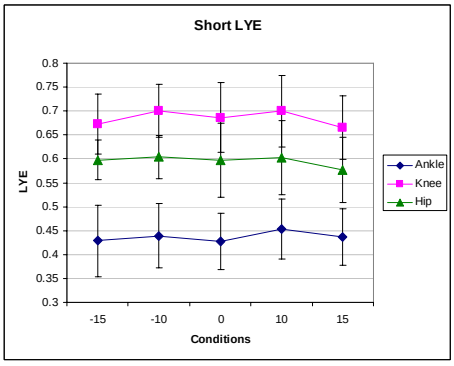

Figure 3. Short-term Lyaponuv exponents for the ankle, knee, and hip.

investigation. The vertical assistance and resistance forces during the step-to-step transition period ranged from 0% to 1.6% body weight. These force values may have been too small to impact the redirection of the COM. However, during our pilot investigation we noted that larger forces tended to alter the natural gait dynamics.

SUMMARY/CONCLUSIONS

Our investigation suggests that the step-to-step transitions may not influence the local dynamic stability of gait. However, our results should be interpreted with caution. Future studies should evaluate if changes in step length influences the local dynamic stability of gait.

ACKNOWLEDGEMENTS

Research was supported by the Texas Learning and Computational Center Grant awarded to MJK, and the Texas Space Grant Consortium Fellowship Awarded to MSP.

REFERENCES

Dingwell, J. & Cusumano, J. (2000). *Chaos* **10(4), 848-863.**

Kuo, A.D., Donelan, M. & Ruina, A. (2005). *Exer Sport Sci Rev* **33(2), 88-97.**

Rosenstein et al. (1993). *Physica D* **65**:117-134.

ROTATION OF THE LUMBAR SPINE DURING LATERAL BENDING: ADOLESCENT IDIOPATHIC SCOLIOSIS VS CONTROL SUBJECTS

Scott Campbell, MS, Kirsten Tulchin, MS, Charles Johnston, MD, and Lori Karol, MD

Texas Scottish Rite Hospital for Children, Dallas, TX, USA
Email: scott.campbell@tsrh.org

INTORDUCTION

Scoliosis is associated with a curvature of the spine in the coronal plane and a rotation of the spine about the longitudinal axis, seen clinically as a rib protuberance. During lateral bending movements, the spine flexes or extends and rotates to accomplish the maximum amount of bend. The amount of out of plane flexion/extension and rotation during lateral bending remains unknown. The current study compares flexion/extension and rotation of the lumbar spine during left and right lateral bending in two groups: females with no known spinal abnormalities and females with adolescent idiopathic scoliosis who have not undergone surgical treatment. Lateral bending was movement in the coronal plane, flexion/extension was observed in the sagittal plane, and rotation was about the longitudinal axis of the spine in the transverse plane.

METHODS

57 females underwent computerized motion analysis while performing lateral bending movements (VICON 512 Motion Analysis System, Oxford Metrics, Oxford, England). Of the 57 females, 25 were normal (control) group and 32 had adolescent idiopathic scoliosis (unfused group). The unfused group was divided into three additional subgroups based on the curve direction: 10 patients had left lumbar curves, 2 patients had right lumbar curves, and 20 had thoracic or thoracolumbar curves. Three markers were placed on the pelvis and a marker triad was placed at T12-L1. Subjects performed maximal left and right lateral bending movements. Three-dimensional Euler angles between the T12-L1 marker triad and the pelvis markers were calculated for lateral bend, flexion/extension and rotation. Flexion/extension and rotation angles were calculated at the instant of maximum lateral bend angle. The rotation of the lumbar spine was measured according to the direction it rotated. A rotation towards the bending side meant the concave side of the vertebra rotated towards the bending side.

RESULTS AND DISCUSSION

Mean lateral bending in the control group was 26.7^{o} ($\pm 5.1^{o}$) to the right and 25.5^{o} ($\pm 6.2^{o}$) to the left. Similar results were seen in the unfused group (27.2^{o} ($\pm 7.5^{o}$) right and 23.7^{o} ($\pm 6.4^{o}$) left). During lateral bending movements, 96% of the control group extended their lumbar spine, compared to 83% of the scoliosis group.

During right lateral bending, 56% of unfused subjects rotated towards the right, while 88% of the control group rotated towards the right. The inconsistent pattern of rotation towards the right side during right lateral bending in unfused subjects led to a mean spinal rotation of 1.8^{o} ($\pm 6.3^{o}$), compared to the normal group, 8.1^{o} ($\pm 7.8^{o}$) Approximately 40% of the left curve subgroup rotated towards the right during right lateral bending, as seen in Table 1. Overall, those with spinal deformity demonstrated no clear trend in the direction

of lumbar rotation during right lateral bending.

During left lateral bending, there was a greater tendency to rotate towards the same side, as 84% of unfused and 92% of controls rotated towards the left. There were no differences in the mean rotation seen during left lateral bending in the unfused and control groups, as seen in Figure 1.

Table 1: Percent of subjects with spinal rotation towards the bending side

	Left Bend (%)	Right Bend (%)
Normal (n=25)	92	88
Unfused (n=32)	84	56
Left Curves (n=10)	90	40
Right Curves (n=2)	50	100

CONCLUSIONS

The rotation of the lumbar spine during lateral bending movements normally rotates towards the direction of bend. This pattern was not found to be consistent in subjects with adolescent idiopathic scoliosis, particularly in subjects with left lumbar curves during right lateral bending. This may be due to the muscles stabilizing the lumbar spine (Alexander and Edward, 1978). The subgroup of unfused right lumbar curves only had two subjects which limit the conclusions that can be drawn for this group.

REFERENCES

Alexander and Season. (1978). *Arch Phys Med Rehabil*, 59, 314-315.

Engsberg J, et al. (2002). Spine, 27, 1346-1354.

Samuelsson L and Noren L. (1997). *Acta Orthop Scand*, 68, 273-276.

Wilk B, et al. (2006). *Spine*, 31, 309-314.

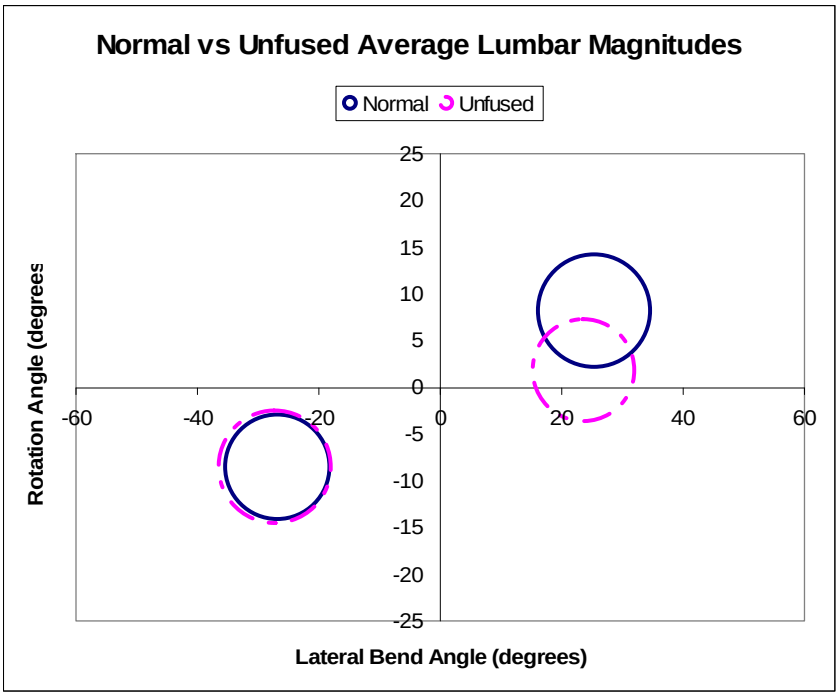

Figure 1: Spinal rotation angle during lateral bend angle. The center of the circle represents the group mean for lateral bend vs. spinal rotation. The radius of circle signifies the standard deviation of the group. Solid is controls, dashed is unfused. Negative angles represent left lateral bend and left rotation. Positive angles represent right lateral bend and right rotation.

CONTINUUM-BASED MODEL OF SKELETAL MUSCLE

G.M. Odegard [1], T.L. Haut Donahue [1], D.A. Morrow [2], and K.R. Kaufman [2]

[1] Michigan Technological University, Houghton, MI, USA
[2] Mayo Clinic/Mayo Foundation, Rochester, MN, USA
E-mail: gmodegar@mtu.edu

INTRODUCTION

Knowledge of muscle forces during given activities can provide insight into muscle physiology, musculoskeletal mechanics, neurophysiology, and motor control. However, currently available methods for clinical examination or instrumented strength testing only provide information regarding muscle groups. Musculoskeletal models are typically needed to calculate individual muscle forces.

The objective of this study is to develop a continuum-based constitutive model to describe the three-dimensional mechanical response of muscle under isochoric (volume-preserving) passive and active deformation conditions within a thermodynamic framework. The model must account for transversely-isotropic material symmetry and explicitly state the strain-energy associated with the active and passive responses of the tissue.

CONSTITUTIVE MODELING

It has been reported that skeletal muscle tissue exhibits the same mechanical behavior on both the muscle fiber- and sarcomere-associated length scales (Zajac 1989). Therefore, the mechanical behavior of skeletal muscle tissue can be modeled as a continuous and homogenous effective continuum with mathematically-defined properties and symmetry on multiple length-scale levels (Fig. 1).

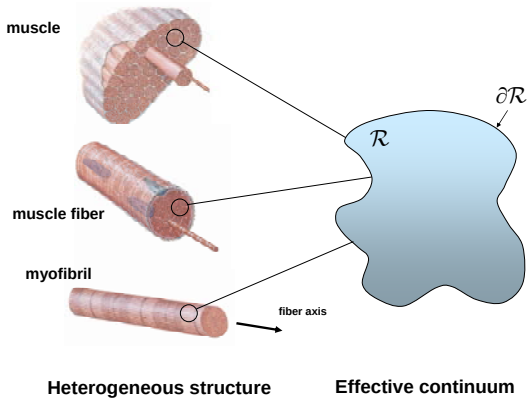

Figure 1: Effective Continuum assumption for all scale levels of skeletal muscle tissue (Netter medical illustration used with permission of Elsevier. All rights reserved.)

Following a similar approach developed for material response with internal variables (Coleman and Gurtin 1967), the strain-energy density due to the mechanical deformation, actin/myosin overlap, and muscle activation was formulated as

$$\Psi = \frac{\mu}{4}\left[\frac{1}{\alpha}\left(L_1^{\alpha}-1\right)+\frac{1}{\beta}\left(L_2^{\beta}-1\right)\right]+\frac{\gamma}{2}q\phi J_4 \qquad (1)$$

where μ, α, β, and γ are material constants; L_1, L_2, and J_4 are scalar invariants of the Green deformation tensor **C** and the structural tensors for transverse isotropy (Itskov and Aksel 2004); q is the scalar muscle activation parameter; and ϕ is the actin/myosin overlap parameter which is related to the active component of the strain-energy density. The bracketed and last term in Equation (1) represent the passive and active responses of the muscle tissue, respectively. The parameter $q = 0$ when the

muscle is unactivated and $q = 1$ when fully activated. The parameter $\phi = 1$ in the state of maximized cross-bridging. The constitutive response is given by

$$\mathbf{S} = \frac{\mu}{2}\left[\left(L_1^{\alpha-1}\right)\tilde{\mathbf{M}} - \left(L_2^{\beta-1}\right)\mathbf{C}^{-1}\tilde{\mathbf{M}}\mathbf{C}^{-1}\right] + \gamma q\phi\mathbf{M}_1 \quad (2)$$

where $\mathbf{M}_1$ and $\mathbf{M}$ are structural tensors and $\mathbf{S}$ is the 2nd Piola-Kirchhoff stress tensor.

RESULTS AND DISCUSSION

Characterization of this constitutive model using data from the literature (Jenkyn et al. 2002) results in the following values of material parameters: $\mu = 300$ kPa, $\alpha = 11.1$, $\beta = 5.3$, and $\gamma = 232$ kPa. A comparison of the total stress response for the proposed model and the Jenkyn model is shown in Figure 2 for the range of longitudinal strains (Green strain) of $-0.3 < E_{11} < 1.3$, where the x_1-axis is aligned with the fiber axis. The inset of Figure 2 is the small-strain region of the plot. The nonlinearity of the data in the small-strain region resembles the expected combined response. An inflection point exists at $E_{11} \approx 0.1$ where the active tension is decreasing and the passive tension is increasing with increasing E_{11}.

The combined passive and active stresses for the longitudinal extension show excellent agreement with the Jenkyn model. The Jenkyn model appears to be the most comprehensive model for skeletal muscle tissue currently available in the literature in that it incorporates a large range of deformation modes, albeit in two dimensions. Therefore, an accurate mathematical model of skeletal muscle tissue has been established that advances the state of muscle modeling. A set of three-dimensional experimental data is now needed to further validate the proposed model.

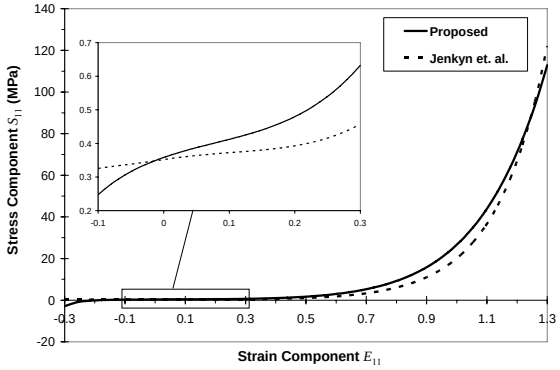

Figure 2: Total stress vs. strain diagram for fully activated skeletal muscle.

REFERENCES

Coleman, B.D., Gurtin, M.E. (1967). *J. Chem. Phys.,* **47**, 597-613.

Itskov, M., Aksel, N. (2004). *Int. J. Solids Struct.*, 41, 597-613

Jenkyn, T.R. et al. (2002). *Phys. Med. Biol.,* **47**, 4043-4061.

Zajac, F.E. (1989). *Crit. Rev. Biomed. Eng.,* **17**, 359-411.

ACKNOWLEDGEMENTS

This publication was made possible by Grant Number R01HD31476 from NIH.

A MECHANICAL CAUSE OF BODY ROTATION ABOUNT THE VERTICAL AXIS IN BASEBALL BATTING

T. Yanai
Chukyo University, Toyota, Japan
E-mail: tyanai@life.chukyo-u.ac.jp

INTRODUCTION

In baseball batting, the batter swings the bat in a circular path toward the ball to strike it. This circular path of the bat swing is generated "first by the turning of the torso and finally by action at the wrists (Adrian & Cooper, 1995)." Visual observations of batting performances suggest that the entire body, rather than the torso alone, rotates about a near-vertical axis passing through the body's center of mass. Such a rotation of the entire body could only be generated by the external forces acting eccentric to the center of mass and by the free moments acting on the body. In the present study, the moment of the ground reaction forces around the center of mass of the body and the free moment were computed separately for each leg and the contribution of each leg in generating body rotation was examined.

METHODS

After having provided written informed consent, twenty members of collegiate varsity baseball team performed the so-called "toss batting" in the Motion Analysis Laboratory. For the toss batting, the ball was tossed toward the ball-impact zone of the batter by another player kneeling on the ground at approximately 3 m away from the subject. The subject placing each leg on a force platform (9287B, Kistler Instrumentw AG, Switzerland) struck the ball toward the net located in the same field beside the tosser. After unlimited practices, each subject performed five trials of toss batting for data collection. Each trial was initiated by having the subject stand still on the force platforms in a relaxed body position. When the subject was found still and the force data became constant for more than two seconds, the subject was instructed to set ready for the toss-batting, and then he executed. For each trial, the force data was recorded with a WAD software (DKH co.Ltd., Japan). The trials were also recorded by a high speed camcorder (Fastcam-PCI, Photoron USA Inc, USA) so as to identify the instant of impact.

The mechanical cause of the body's rotation about the vertical axis passing through the CM was divided into four components; the moment of the ground reaction force acting on the front leg around the CM (Mf), the moment of the ground reaction force acting on the back leg around the CM (Mb), the free moment acting on the front leg (Ff), and the free moment acting on the front leg (Fb). The instantaneous positions of the center of mass (CM) of the performer was computed by double-integrating over time the acceleration of the CM which, in turn, was determined from the ground reaction force and the subject's body mass. The initial position of the CM for the integration was determined for the period during which the subject was standing still. The moment of the ground reaction force acting on each leg around the CM was determined by computing the cross product of the vector pointing from the CM to the center of pressure location and the ground reaction force acting on the leg. Finally contribution of each of the four components to the body's rotation was determined by time-integrating

each factor over time to determine the angular momentum generated thoroughly by that component toward the ball impact.

RESULTS AND DISCUSSION

The angular momentum of the performer's body was near zero at the instant of the front-leg touch-down (Figure 1), and it increased sharply toward the instant of impact (24 ± 4.3 kgm^2/s). The contribution of the Mf was found largest (mean=22 kgm^2/s), followed by Mb (mean=10 kgm^2/s). Ff and Fb (means = -6 kgm^2/s and -1 kgm^2/s, respectively) contributed negatively.

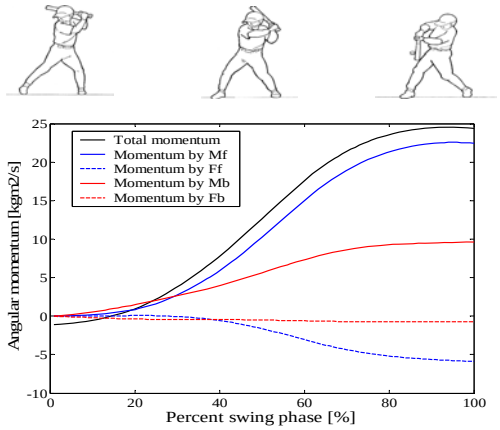

Figure 1: The mean values across the subjects for the total angular momentum of the body and their components. Swing phase initiated from the instant of front-leg touch-down and finished at the instant of ball impact.

The results clearly indicate that the rotation of the body during baseball batting is generated primarily by the moment of the ground reaction forces acting on the legs around the CM. In particular, the maximum ground reaction force generated by the front leg pushing the ground toward the homebase (mean=292 N) had a large moment arm (mean=0.52 m), having produced the largest turning effect to the body (Figure 2). The ground reaction forces acting toward or away from the pitcher had short moment arms (means=0.16 & 0.0 m for front & back leg, respectively), having produced limited moments around the CM (Figure 2). These results support the theoretical postulations described in the previous study (Messier and Owen, 1986).

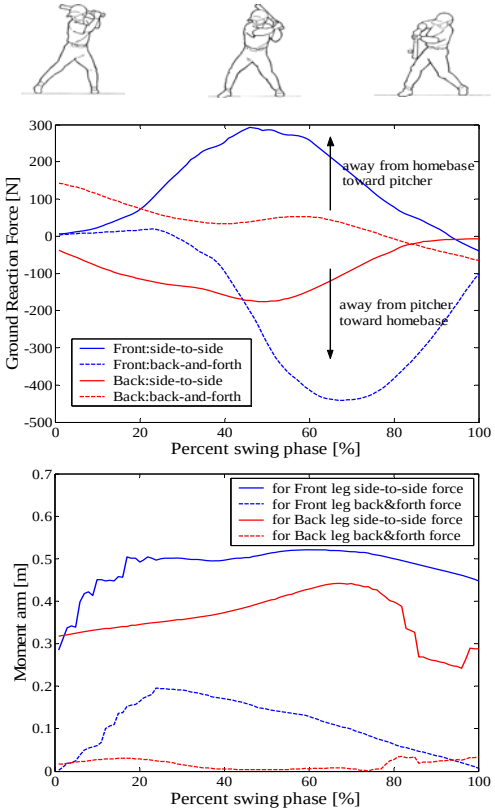

Figure 2: The mean values across the subjects for the ground reaction forces acting on the legs (above) and their moment arms (below).

The total angular momentum generated by the ground reaction forces and free moments acting on the front leg (17 ± 4.0 kgm^2/s) was found significantly greater (p=0.00) than that on the back leg (9 ± 2.2kgm^2/s). This result indicates that the front leg acts as the primary source of body rotation for bat swing.

REFERENCE

Adrian MJ and Cooper JM. *Biomechanics of Human Movement*, Brown & Benchmark, Madison, WI. 1995.

Messier SP and Owen M. (1986). *Res Quart* **57**,329-333.

PREDICTING SLOW CHANGES IN MUSCLE FATIGUE FROM KINEMATICS

Jonathan B. Dingwell[1,*] Miao Song[2], David B. Segala[2], David Chelidze[2]

[1] Nonlinear Biodynamics Lab, Department of Kinesiology, University of Texas, Austin, TX
[2] Mechanical Engineering & Applied Mechanics Dept., University of Rhode Island, Kingston, RI
* E-mail: jdingwell@mail.utexas.edu Web: http://www.edb.utexas.edu/faculty/dingwell/

INTRODUCTION

Diseases like osteoarthritis and repetitive strain injuries lead to changes in coordination that develop slowly over time. It is important, but often very difficult, to track the progression of these disease processes. By contrast, changes in movement coordination patterns can be easily measured.

When people perform repetitive tasks over extended periods of time, they develop muscle fatigue. When muscles fatigue, the body will compensate by changing the movement biomechanics to limit the use of the specific fatigued muscle(s). Continuing muscle fatigue, and/or changes in biomechanics that lead to sub-optimal movement patterns, could lead to repetitive strain injuries.

Many studies have examined changes in coordination for pre- vs. post-fatigue conditions. However, few studies have attempted to track changes in coordination over time as fatigue sets in or to correlate physiological changes (e.g., spectral shifts in EMG) with changes in coordination. Our goal was to determine if "hidden" changes in muscle fatigue could be directly inferred from easily observable changes in kinematics.

METHODS

Ten male cyclists (age 18-45 yrs; USCF Category ≥ 3) cycled to exhaustion on a Lode Excalibur Sport bicycle ergometer at 100% of their VO_2max. Subjects were given vigorous verbal encouragement throughout the trials, which lasted 4-10 min. Sagittal plane kinematic data were sampled at 120 Hz (Vicon, Oxford, UK) continuously throughout each trial. Surface EMG data were simultaneously recorded from the vastus lateralis, biceps femoris, gastrocnemius, and tibialis anterior muscles at 1080 Hz.

Muscle fatigue was assumed to evolve in a hierarchical dynamical system (Chelidze 2006, In Press; Dingwell 2007):

$$\dot{x} = f(x, \mu(\phi), t), \qquad \dot{\phi} = \varepsilon\, g(\phi, x) \qquad (1)$$

where x was a fast-time variable describing movement kinematics; ϕ was a slow-time muscle fatigue variable, which altered a parameter vector μ in the fast-time system; t was time; and ε was a small rate constant describing time scale separation. Vector spaces describing the slow-time changes in movement kinematics were extracted from

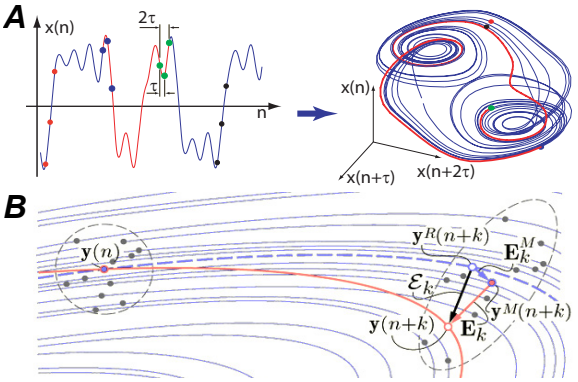

Figure 1: ***A:*** Embedding a 1-dimensional time series in a multi-dimensional vector space defining equivalent states of the system. ***B:*** Tracking function estimation: (—) is the current trajectory. (– –) is the corresponding model trajectory. $\mathbf{E}_k$ is the estimated error, $\mathbf{E}_k^M$ is the modeling error, and $\boldsymbol{\varepsilon}_k$ is the true error, or drift in the system.

the recorded fast-time time series for consecutive intermediate time intervals using *Phase Space Warping* (Fig. 1). Slow-time manifolds describing global fatigue dynamics in these feature spaces were extracted using *Smooth Orthogonal Decomposition* (SOD; Chelidze 2006, In Press). Median frequencies from the EMG data described the local fatigue dynamics in each muscle. The smooth orthogonal components from the PSW were correlated to the EMG median frequency data to determine how well these kinematic measures tracked changes in muscle fatigue. For comparison, kinematic feature vectors were also constructed using standard statistical metrics (mean, standard deviation, higher statistical moments, etc.)

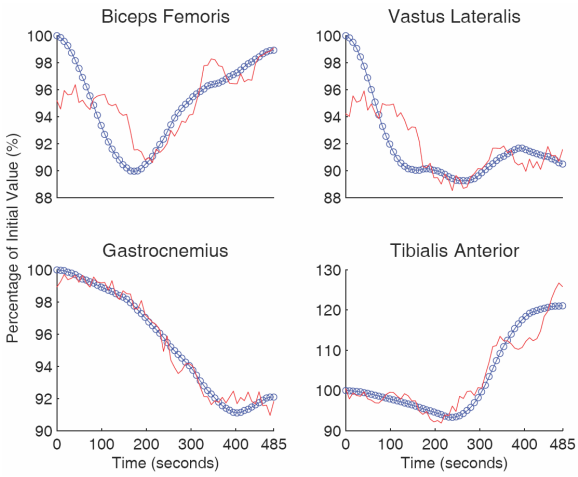

Figure 2: Projections of the first 3 PSW-based smooth orthogonal components (SOCs) for ankle angles (—) onto EMG median frequencies (−○−) for a typical subject, showing good agreement. Similar results were obtained for all subjects.

RESULTS AND DISCUSSION

There were close correlations between the EMG median frequencies and kinematics data based global fatigue features. The slow time manifolds corresponding to PSW based features fully represented the local fatigue dynamics in all the muscles as described by the EMG data (Fig. 2). By comparison, feature vectors constructed from standard statistical metrics could not recapture the slow-time scale muscle fatigue dynamics (Fig. 3).

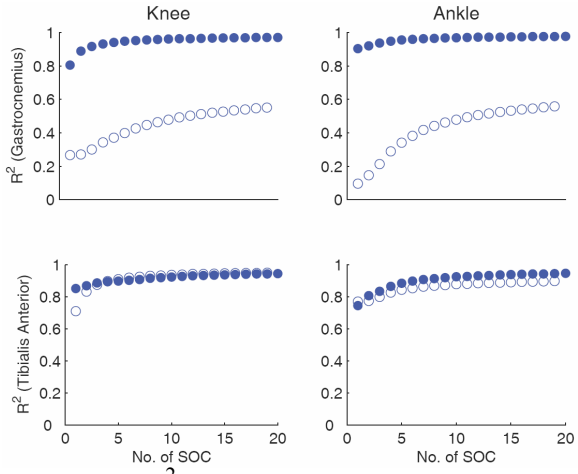

Figure 3: R^2 values for correlations between EMG median frequencies and PSW-based fits (●) for the data shown in Fig 2. Alternative fits using standard statistical metrics are shown for comparison (○).

SUMMARY/CONCLUSIONS

For this cycling task, the fatigue information present in the standard EMG analysis was fully represented in the SOD based slow time features extracted from the kinematic data. Furthermore, the SOD based analysis gave estimates of effective dimensionality of muscle fatigue dynamics. Thus, these methods may prove useful in tracking and predicting fatigue and repetitive strain injuries.

REFERENCES

Chelidze D. & Liu M. (In press). *Phil. Trans. Royal Soc. A.*

Chelidze D. & Cusumano J.P. (2006) *Phil. Trans. Royal Soc. A*, 364: 2495–2513.

Dingwell J.B. et al., (2007) *J. Biomech.*, doi:10.1016/j.jbiomech.2006.06.019.

ACKNOWLEDGEMENTS

Supported by NIH grant #EB003425 to J.B.D. and NSF grant #0237792 to D.C.

GOAL EQUIVALENT CONTROL OF VARIABILITY IN HUMAN WALKING

Jonathan B. Dingwell[1,*] Michelle A. Garel[1], Joseph P. Cusumano[2]

[1] Nonlinear Biodynamics Lab, Department of Kinesiology, University of Texas, Austin, TX
[2] Department of Engineering Science & Mechanics, Penn State University, State College, PA
* E-mail: jdingwell@mail.utexas.edu Web: http://www.edb.utexas.edu/faculty/dingwell/

INTRODUCTION

While increased gait variability has been linked to an increased risk of falls in the elderly, different gait variables exhibit different changes in variability with age and/or fall history (Brach et al. 2005; Moe-Nilssen & Helbostad, 2005). Thus, it is not clear which gait variables would be best to quantify.

For redundant tasks exhibiting equifinality, we can define an explicit mapping from variability in body movements to variability at the *goal* level of the task (Cusumano & Cesari, 2006). The *goal* of steady walking is to maintain constant speed, but many combinations of stride length (L) & stride time (T) achieve this goal. These (L, T) combinations define the "Goal Equivalent Manifold" (GEM) for walking (Fig. 1). Deviations of (L, T) *off* of the GEM negatively impact task performance (i.e., speed). Variations *along* the GEM do not. We tested the hypothesis that the temporal structure of the variability of movement deviations *along* the GEM defined for walking would differ from that for deviations *perpendicular to* the GEM.

METHODS

The goal function for steady walking is:

$$v = L_n / T_n \equiv Const \qquad (1)$$

where L_n is stride length at step n and T_n is stride time. For any constant speed v, the GEM is defined as the line $L_n = v \cdot T_n$ (Fig. 1). We then decompose the variability in L_n and T_n into variability tangent to $(\hat{e}_T)$ and perpendicular to the GEM $(\hat{e}_P)$ via:

$$\vec{\delta}_n = (\vec{\delta}_n \cdot \hat{e}_T)\hat{e}_T + (\vec{\delta}_n \cdot \hat{e}_P)\hat{e}_P \qquad (2)$$

where scalar deviations $\delta_T = \vec{\delta}_n \cdot \hat{e}_T$ are *goal equivalent*: they do *not* affect velocity, $\vec{\delta}_n$, but deviations $\delta_P = \vec{\delta}_n \cdot \hat{e}_P$ *do* directly impact speed (i.e., these are *goal-relevant* errors).

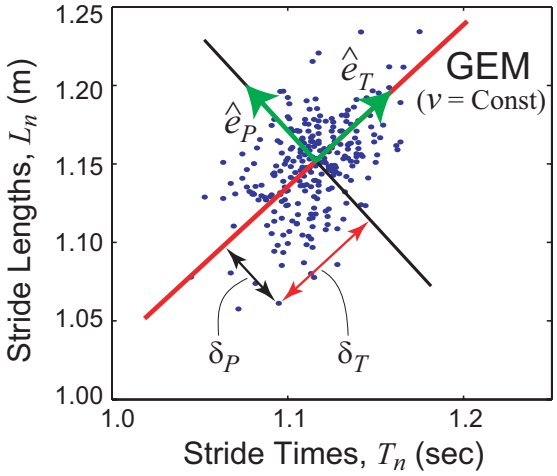

Figure 1: Stride times (T_n) and lengths (L_n) for each stride for a typical subject, showing the GEM and scalar deviations δ_T and δ_P.

Eighteen healthy elderly volunteers (age 65-85 yrs) walked on a level treadmill (Woodway USA) at their preferred self-selected constant walking speed. The 3D movements of reflective markers attached to their feet were recorded (Vicon, Oxford Metrics, Oxford, UK) continuously for 2 trials of 5 minutes and used to compute the stride length (L_n) and stride time (T_n) for each stride, n.

The GEM for each subject was constructed using their average speed across all strides, $\bar{v} = \langle L_n / T_n \rangle_n$. We then extracted time series

of deviations tangent (δ_T) and perpendicular (δ_P) to each subject's GEM (Eq. 2; Fig. 1).

Detrended fluctuation analysis (DFA; Peng et al., 1992; Hausdorff et al., 1995) was used to quantify the statistical structure of stride-to-stride variations in these δ_T and δ_P time series. DFA yields a scaling exponent, α. α = 0.5 indicates a completely random (i.e., uncorrelated) time series. $\alpha > 0.5$ implies "*persistent*" long-range correlations: i.e., deviations in one direction are more likely to be followed by more deviations in the same direction. $\alpha < 0.5$ implies "*anti-persistent*" correlations: i.e., positive and negative deviations are more likely to alternate.

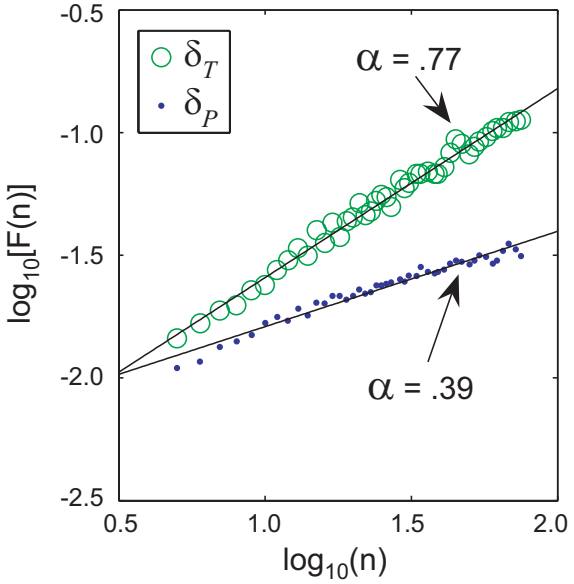

Figure 2: DFA results for deviations tangent to (δ_T) and perpendicular to (δ_P) the GEM for the data shown in Fig. 1. Similar results were obtained from all subjects.

RESULTS AND DISCUSSION

All subjects exhibited persistent long-range correlations for deviations *along* (δ_T) the GEM, but either no correlations or anti-persistence for deviations *perpendicular to* (δ_P) the GEM (Fig. 2). Across subjects, differences in correlation structure between δ_T deviations and δ_P deviations were highly statistically significant (Fig. 3).

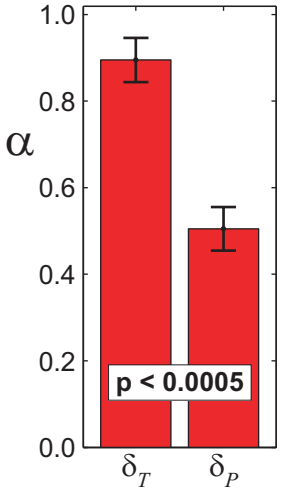

Figure 3: Means ± 95% confidence intervals for DFA slopes (α) for all 18 healthy elderly subjects for both δ_T and δ_P deviations off of the GEM. The difference between directions was highly significant ($p < 0.0005$).

SUMMARY/CONCLUSIONS

As hypothesized, the temporal structure of movement variations was significantly different *along* vs. *perpendicular to* the GEM. Deviations away from the GEM were far more likely to be redirected back towards the GEM than deviations along the GEM $[\alpha(\delta_P) << \alpha(\delta_T)]$. Thus, subjects applied greater active control to reduce these perpendicular deviations. The present approach may thus yield more appropriate variables for describing gait variability. Efforts are underway to determine how these results vary across age groups and walking speeds.

REFERENCES

Brach J.S. et al. (2005) *J. Neuroeng. & Rehabil.*, 2(1): 21-28.

Cusumano J.P. & Cesari P. (2006) *Biol. Cybern.*, 94(5): 367-79.

Hausdorff J.M. et al. (1995) *J. Appl. Physiol.*, 78(1): 349-58.

Moe-Nilssen R. & Helbostad J.L. (2005) *Gait & Posture*, 21(2): 164-170.

Peng C.K. et al. (1992) *Nature*, 356: 168-70.

ECCENTRIC BUT NOT CONCENTRIC MUSCLE WORK IS RETAINED WITH AGE IN LEVEL WALKING

Paul DeVita, Patrick Rider, Allison Gruber, Ken Steinweg, Mandana Fisher, Allison Mazzenga, Stanislaw Solnik and Tibor Hortobagyi

East Carolina University, Greenville, NC, USA
E-mail: devitap@ecu.edu, Web: http://www.ecu.edu/cs-hhp/exss/biomechlab.cfm

INTRODUCTION

It is well established that even in the absence of illness or disease aging degrades many physiological properties of skeletal muscle leading to reduced muscle strength and power (4). Loss of strength and power with age is however dependent on the type of muscle contraction with lengthening (eccentric) vs. shortening (concentric) contractions having smaller decrements (2). Loss of eccentric strength with age is further attenuated at higher angular velocities that approach those used in walking (5).

The functional consequences of the relative retention of eccentric strength with age are largely unknown. Eccentric contractions dissipate mechanical energy (i.e. do negative work) and are used by all lower extremity muscle groups in walking (1). Since eccentric but not concentric strength is well maintained with age at joint angular velocities used in walking, we hypothesize that old compared to young adults maintain eccentric (negative) work but not concentric (positive) work during level walking. The purpose of the study was to compare negative, positive, and total muscle work in the lower extremity between young and old adults during level walking at 3 speeds.

METHODS

Ground forces and 3D kinematics were obtained from 20 young (21 yr) and 20 old (77 yr) volunteers during 1.2, 1.5, and 1.8 m/s level walking after obtaining written informed consent. Inverse dynamics were used to derive 3D joint powers throughout the stride. Positive, negative, and total work were derived from these data and assumed to be due to muscle forces. 2-by-3 ANOVAs (age by speed) with $p<0.05$ were used to identify age differences and age by speed interactions followed by post hoc t-tests in the case of significant interactions.

RESULTS AND DISCUSSION

No significant interaction or age effects were seen for total negative work summed across all joints (fig 1a). A significant interaction was seen for total positive work such that the increase in positive work with increased speed was attenuated in old vs. young adults (fig 1b). Negative work was statistically identical at each joint between age groups (table 1). Significant interactions were observed for positive work at the knee and ankle joints. As in total positive work the increase in knee and ankle positive work with increased speed was attenuated in old vs. young adults. Also, positive knee work was ~30% lower in old vs. young at all speeds (t-tests, $p<0.05$).

The retention of hip concentric muscle function agrees with our previous data showing a preferential use of hip muscle work vs. work from distal knee and ankle muscles in old vs. young adults during walking (1). Previously seen reductions in knee and ankle work in walking (1) can now be more accurately interpreted as reductions in energy generating capacity of knee

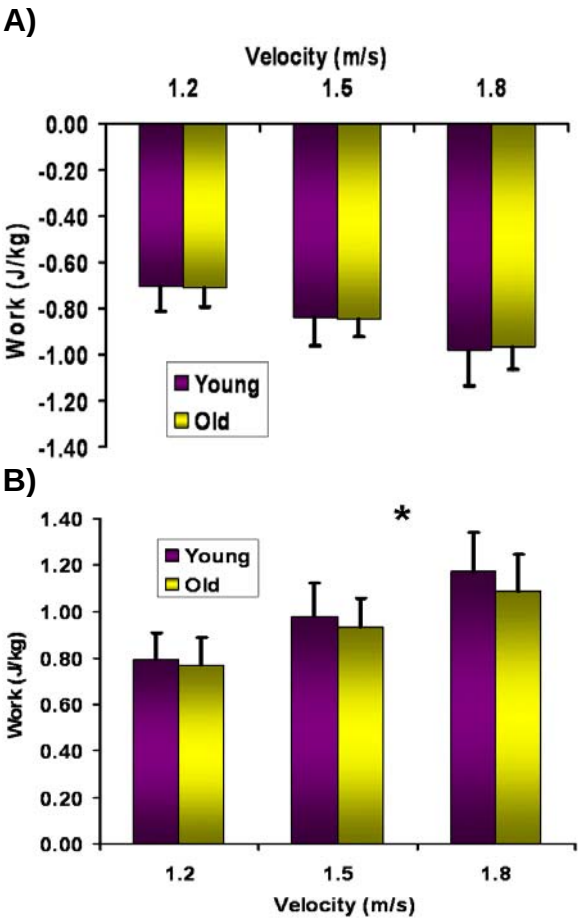

Figure 1, Total negative (A) and total positive (B) work. No significant interaction or age effect was seen in negative work. * significant age by speed interaction was seen in positive work ($p<0.05$).

extensors and ankle plantarflexors but not in their energy dissipating capacity. The retention of hip muscle function and loss of knee and ankle muscle function during walking also agrees with observations that distal vs. proximal muscles undergo larger reductions in physiological properties (3). These data show the retention of eccentric strength with age as seen isokinetically is manifested functionally during walking.

SUMMARY/CONCLUSIONS

The hypothesis was supported and showed healthy, mobile old vs. young adults retain their ability to dissipate energy during walking through lengthening contractions but have reduced capacity to generate energy through shortening contractions.

REFERENCES

1) DeVita et al., (2000), *J. Appl. Physiol.*, **88**, 1804-1811
2) Hortobagyi et al. (1995). *J. Gerontol.*, **50**, B399-406.
3) Kirkeby et al. (2000), *Histol & Histopathol* **15,** 61-71.
4) Metter et al., (1997). *J. Gerontol.*, **52**, B267-276.
5) Poulin et al., (1992). *Can J. Sport Med.*, 17, 3-7.

ACKNOWLEDGEMENTS

NIA AG16192

Table 1: Mean (sd) negative & positive work at each joint

		Negative Work			Positive Work		
		1.2 m/s	1.5 m/s	1.8 m/s	1.2 m/s	1.5 m/s	1.8 m/s
Hip	Young	-0.14*(0.05)	-0.20 (0.07)	-0.28 (0.10)	0.42 (0.09)	0.51 (0.11)	0.62 (0.12)
	Old	-0.17 (0.04)	-0.23 (0.06)	-0.29 (0.07)	0.45 (0.09)	0.56 (0.10)	0.67 (0.13)
Knee	Young	-0.31 (0.06)	-0.40 (0.07)	-0.50 (0.09)	0.14 (0.05)	0.18 (0.05)	0.23 (0.06)
*, #	Old	-0.31 (0.05)	-0.40 (0.05)	-0.50 (0.07)	0.10 (0.04)	0.13 (0.05)	0.16 (0.05)
Ankle	Young	-0.26 (0.05)	-0.24 (0.05)	-0.20 (0.05)	0.24 (0.06)	0.28 (0.09)	0.33 (0.12)
*	Old	-0.24 (0.06)	-0.22 (0.04)	-0.22 (0.04)	0.22 (0.04)	0.24 (0.05)	0.26 (0.06)

* Significant interaction effect for positive work ($p<0.05$); # Significant age effect for positive work ($p<0.05$)

INFLUENCE OF QUADRICEPS MUSCLE FORCE DISTRIBUTIONS ON CARTILAGE STRESSES AT THE PATELLOFEMORAL JOINT DURING RUNNING

Thor Besier [1] Scott Delp [1] Garry Gold [1] and Gary Beaupré [2]

[1] Stanford University, Stanford, CA, USA
[2] VA Rehabilitation Research and Development Center, Palo Alto CA, USA
E-mail: besier@stanford.edu, Web: http://nmbl.stanford.edu

INTRODUCTION

Several factors can influence the tracking of the patella, including soft tissue restraints, femoral internal rotation, and the geometry of the joint. Quadriceps muscle forces also influence the mechanics of the patellofemoral (PF) joint and are often the focus of physical therapy interventions, such as strengthening and stretching. However, the efficacy of such treatment strategies remains unclear.

Elias et al. (2006) and Dhaher & Kahn (2002) have shown the importance of the quadriceps force distribution on the medial-lateral force balance at the patella and the associated contact force and pressure. It is unknown, however, how the quadriceps force distribution influences the stresses throughout the PF joint cartilage.

The purpose of this study was to estimate the cartilage stresses within the PF cartilage during the stance phase of running (with the knee at 30° flexion) and determine the influence of altering the distribution of forces between the medial and lateral vasti to support the same net joint moment.

METHODS

Sixteen subject-specific finite element models of the PF joint were created from physically active volunteers (8 males and 8 females). The methods used to create these models are explained in detail in Besier et al. (2005). An open-MR scanner was used to obtain upright, weight-bearing images of each subject holding a squat at 30° flexion, which were used to orient the bones of the model (Figure 1).

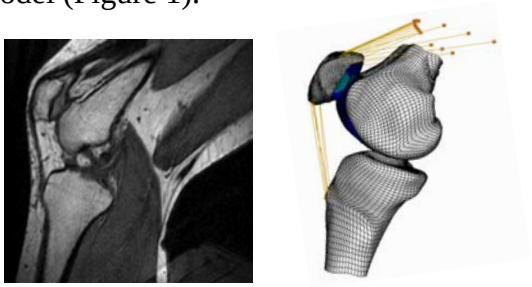

Figure 1. Weight-bearing MR image of the knee and corresponding finite element model.

The patellar tendon and quadriceps muscles were modeled as tension-only connector elements. The patellar tendon had a stiffness of 2000 N/mm. The quadriceps muscles were divided into functional groups which were activated independently. These included: vastus intermedius, rectus femoris, vastus lateralis, vastus lateralis oblique, vastus medialis, and vastus medialis oblique.

Muscle forces during running were estimated based on an EMG-driven musculoskeletal model (Lloyd & Besier, 2003) using joint kinematics and EMG data obtained from a gait analysis. Muscle forces when the knee was at 30° were used as input to the finite element model for the initial simulation. The forces in the oblique parts of vastus medialis and lateralis were determined based on their relative cross-sectional areas. Simulations were then performed in which the relative

contributions of the vastus medialis and vastus lateralis muscles where perturbed while the same net joint moment was maintained. The size of the muscle force pertubations were determined by examining the variation in muscle forces across all subjects and perturbing by one and two standard deviations from the mean muscle force. Mean and peak hydrostatic pressure and octahedral shear stresses were determined for each simulation at the layer of cartilage closest to the bone.

RESULTS AND DISCUSSION

Across all subjects the total muscle force produced by the quadriceps during stance phase when the knee was flexed 30° was 1860 ± 660 N. Vastus medialis was responsible for producing 26 ±5% of the total quadriceps force, whereas vastus lateralis produced 43 ±6% of the net quadriceps force.

These muscle forces resulted in an average PF contact area of 345 ± 72 mm^2 and a PF joint reaction force of 2059 ± 788 N. Mean hydrostatic pressures at the layer of cartilage closest to the bone were 2.1 ± 1.1 MPa in the patella and 2.5 ± 1.1 MPa in the femur. Mean octahedral shear stresses within the cartilage were 1.1 ± 0.6 MPa in the patella and 0.8 ± 0.4 MPa in the femur. Peak cartilage stresses in the patella were ~4 times greater than the average stress for both hydrostatic pressure and octahedral shear stress. Peak stresses in the femoral cartilage were 4.5 to 7 times greater than the average shear stress and hydrostatic pressure, respectively.

Increasing the contributions from the vastus medialis and vastus lateralis did not have any sizeable effect (<2%) on the *average* stresses in the PF joint cartilage.

Peak cartilage stresses, however, were more sensitive to changes in the medial-to-lateral muscle force balance. Increasing the contribution from vastus lateralis had the greatest effect on both shear stress and hydrostatic pressure (Figure 2). Shear stresses in the patella cartilage were the most sensitive to changes in muscle force distribution.

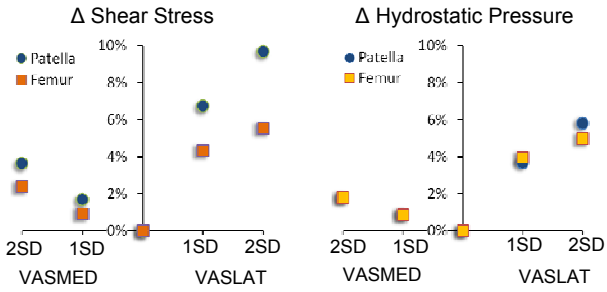

Figure 2. Percent change in cartilage stress with increasing contributions (1 or 2 standard deviations) from vastus medialis (VASMED) and vastus lateralis (VASLAT).

Cartilage stresses appear relatively insensitive to changes in the distribution of medial-to-lateral quadriceps forces, with the exception of shear stresses in the patellar cartilage. Due to its smaller physiological cross-sectional area, vastus medialis has less potential to influence cartilage stresses compared with vastus lateralis.

REFERENCES

Besier et al. (2005). *Medicine & Science in Sports & Exercise*, ***37,***1924-1930.

Dhaher & Kahn (2002). J Biomech Eng, ***124,*** 758-767.

Elias et al. (2006). *J. Biomechanics*, ***39,*** 865-872.

Lloyd. D.G. & Besier, T.F. (2003). *J. Biomechanics*, ***36***, 765-776.

ACKNOWLEDGEMENTS

Stanford Regenerative Medicine (1R-90DK071508), VA Rehab R&D (A2592R) and the NIH (EB005790-01).

GAIT ADAPTATIONS AND HIGH IMPLANT TWISTING MOMENTS DURING STAIR CLIMBING IN SUBJECTS WITH TOTAL HIP REPLACEMENTS

Kharma C. Foucher, Debra E. Hurwitz, Markus A. Wimmer

Rush University Medical Center, Chicago, IL, USA
Email: kharma_c_foucher@rush.edu, Web: www.ortho.rush.edu/Gait

INTRODUCTION

The implant twisting moment (the torque about the implant stem) has been linked to implant loosening in *in vitro* studies of total hip replacement (THR) stability. In *in vivo* testing, the implant twisting moment during stair climbing was substantially higher than during walking (Bergmann et al., 1995, 2001). To our knowledge, no one has quantified gait adaptations in subjects with THRs during stair climbing or investigated how possible gait adaptations affect the implant twisting moment during this activity. The objectives of this study were to identify gait adaptations during stair climbing and examine their effect on the implant twisting moment. Specifically the hypotheses tested were that (1) there would be significant differences in dynamic range of motion and external moments during stair climbing in subjects with THRs and normal subjects, (2) the implant twisting moment would be significantly correlated to kinetics measured during gait activities and (3) as a result of the gait adaptations, the implant twisting moment in subjects with THRs would be significantly reduced compared to normal subjects.

METHODS

15 subjects, who had undergone THR for primary hip osteoarthritis 1 year prior, and 15 normal body size matched subjects performed a stair climbing task. Institutional review board approval was received and informed consent was obtained. Dynamic hip range of motion and external moments were collected as described previously (Andriacchi et al., 1997). A parametric model was used to characterize hip contact force and implant twisting moment during stance based on subject-specific gait data (Hurwitz et al., 2003). Student's *t*-tests were used to identify differences between kinematics, kinetics, and hip forces in subjects with THRs and normal subjects. Pearson correlations were used to identify significant linear relationships between gait kinetics and hip forces.

RESULTS AND DISCUSSION

Adaptations were present during stair climbing in the THR group (Fig 1). The adduction and external rotation moments were lower in the THR group than the normal group ($p \leq 0.020$) while the peak extension moment was significantly higher in the THR group ($p = 0.012$).

The peak implant twisting moment and peak external rotation moment were significantly correlated in both subjects with THRs ($R = 0.808$, $p = 0.001$) (Fig. 2) and normal subjects ($R=0.891$, $p = 0.003$). There were no other significant correlations between peak implant twisting moment and external moments in either subject group ($p \geq 0.419$).

The peak implant twisting moment was not statistically different between the two groups (Fig. 3). The first peak contact force was significantly reduced in the THR group

(p = 0.043). The second peak contact force was similar for the two groups (p = 0.337).

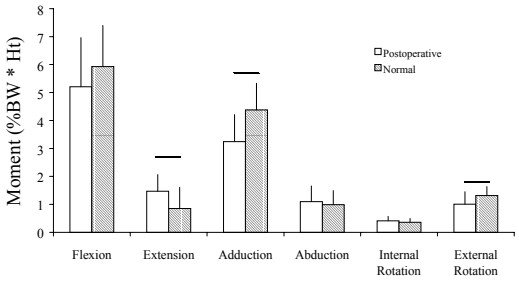

Figure 1: Gait adaptations were present during stair climbing in subjects with THRs. Bars represent significant differences between the THR and normal groups (p < 0.02).

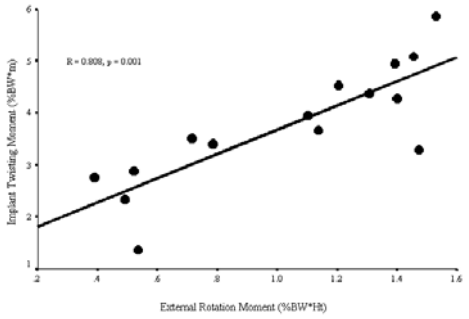

Figure 2: The peak implant twisting moment increased as the peak external rotation moment increased.

Gait adaptations during stair climbing, involved the hip abductors and mirrored those seen during level walking (Foucher et al., 2007). The positive correlation between the external rotation moment and the implant twisting moment suggests that if this moment were normal, implant twisting moments would be even higher.

Stair climbing has been implicated as a high risk activity for THR patients (Bergmann et al., 1995) because of the high implant twisting moments present relative to the overall contact force (Kotzar et al., 1995). According to Bergmann, *in vitro* studies have shown that THRs can resist a twisting moment of 1 to 5 %BW * m (1995). The implant twisting moments during stair climbing approach or exceed these values.

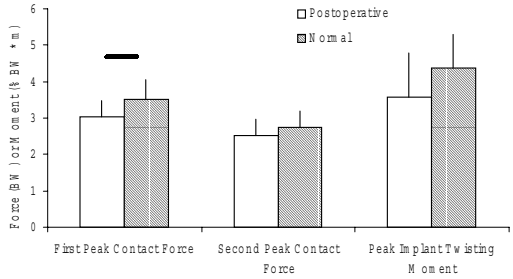

Figure 3: Hip forces in subjects with THRs and normal subjects. Bar indicates a significant difference (p = 0.043).

SUMMARY/CONCLUSIONS

Although gait adaptations were present during stair climbing, the risk for overloading the implant remains high, as adaptations did not significantly lower the implant twisting moment. The magnitude of this moment reaches values thought to be detrimental to implant longevity.

REFERENCES

Andriacchi, T.P., et al. (1997). In: Mow, V.C., Hayes, W.C. (Eds.), *Basic Orthopaedic Biomechanics 2nd edition*. New York: Raven Press, pp. 51-92.

Bergmann, G., et al. (1995). *J. Biomech,* **28**, 535-553.

Bergmann, G., et al. (2001). *J. Biomech*, **34**, 859–871.

Foucher, K.C., et al. (2007). *Trans. 53rd ORS Annual Meeting.*

Hurwitz, D.E., et al. (2003). *J. Biomech*, **36**, 113-119.

Kotzar, G.M., et al. (1995). *J. Orthop. Res.*, **13**, 945-955.

O'Connor, D.O. et al. (1996). *J. Orthop. Res.*, **14,** 769-777.

ACKNOWLEDGEMENT

Whitaker Foundation

MARROW SPACE USED FOR HIGH RESOLUTION IMAGE SEGMENTATION OF CANCELLOUS AND CORTICAL BONE

Xu, Q; Voor, MJ; Waddell, S W; Burden, R L, Jr

University of Louisville, Louisville, USA
Email: q0xu0001@gwise.louisville.edu

INTRODUCTION

Image analyses are used widely to evaluate the 3D architecture of bone in a nondestructive way. To evaluate the cancellous bone architecture and cortical structure, it is more desirable to analyze all of the cancellous bone and all of cortical bone, respectively, from a given sample region.

Because manual methods are tedious, time-consuming and subjective, efforts have been made to do segmentation automatically [1]. In the current study, we develop a novel automatic segmentation method that is useful for high throughput, high resolution image studies.

METHODS

The basic idea of our method is that a contiguous three-dimensional (3D) non-bone region that is located inside the whole bone region of interest (WBROI) can be defined as the marrow region. Any bone material that is surrounded by the marrow region is considered cancellous bone while bone that is outside of the marrow region is cortical bone. The metaphyses of proximal tibiae of rats scanned in vivo are used here to illustrate the method.

There are three steps to the segmentation:

1). Create a 3D cavity model of WBROI;
In this 3D model, using a simple threshold, all non-bone voxels of the WBROI are identified (set to 1), and all other voxels are "turned off" (set to zero).

2). Create 3D marrow model of WBROI;
The marrow region is defined based on the following observations/assumptions: For a 3D bone structure, i) Marrow voxels are connected to each other and form one and only one marrow cavity; ii) All cavities in cortex are isolated from the contiguous marrow cavity; iii) The marrow cavity is the largest cavity among all cavities found in the WBROI.

To find the marrow region, an image slice is chosen as a start point. The largest cavity (LC) in this image slice must be part of the marrow cavity. The cavity elements that are connected to LC are defined as marrow elements while considering only two slices at a time and moving in two directions through the stack. The whole marrow cavity is identified by continuing the same process from the last slice to the first slice, and then from the first slice to the last slice.

3). Create a cancellous mask and segment cancellous bone from cortical bone.
A mask is created by first dilating and then eroding the marrow region (slice by slice in 2-D) such that the mask covers only marrow and cancellous bone (Figure 1). The bone elements that are covered by this mask are cancellous bone, and the bone elements that are not covered by the mask are cortical bone.

RESULTS

Thirty-six image stacks (from OVX and sham rats scanned at different times) were processed with both a manual segmentation method and the automated method. There was excellent agreement between the two methods with the automated method requiring 5% of the time.

DISCUSSION

The present method offers a fast, automatic and objective means to segment cancellous bone from cortical bone, and also has the ability to distinguish cavities in cortex automatically and objectively.

Although the metaphyses of proximal tibiae of rats are used in this study as an example to show how the method works, the method has potential to separate cancellous bone from cortical bone of other bones with complex structure and irregular shape. The prerequisite of the method is the high resolution of the image so that marrow region and cancellous bone structure can be separately identified.

REFERENCE

[1] Helterbrand et al. (1997). *Bone*, **21**, 401-405

Figure (a) Bone tissue image with marrow in red color and bone in white color

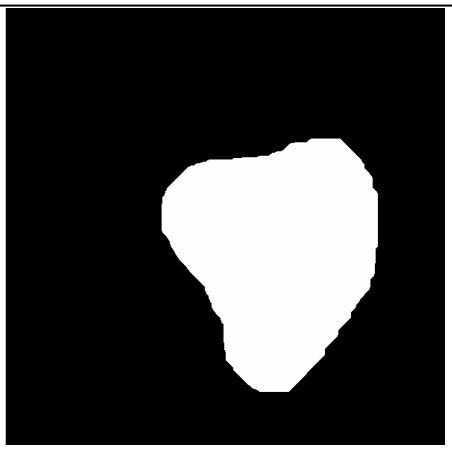

Figure (b) Dilate 2D marrow region and enlarge the image slice

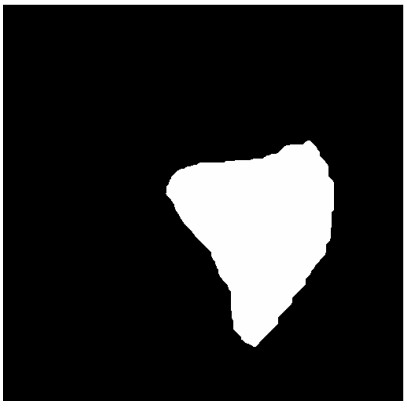

Figure (c) Fill and erode figure (b), and shrink the image slice to its original size

Figure (d) The cancellous mask is in green and blue color. Cancellous bone is in blue color. Cortical bone is in white color

Figure 1: Marrow region is dilated and eroded to find the cancellous mask

MODELING 3D KNEE TORQUE SURFACES FOR MALES & FEMALES

Andrea Laake and Laura Frey Law

Virtual Soldier Research Program, University of Iowa, Iowa City, IA, USA
E-mail: laake@engineering.uiowa.edu

INTRODUCTION

Normative static strength databases are frequently used in the biomechanics, ergonomics and clinical rehabilitation fields. However, dynamic strength has typically been limited to 2D peak torque-velocity curves that do not consider angle-specific torques. Although isolated muscle force-velocity and length-tension relationships have been studied extensively, relatively little work has included three-dimensional (3D) representations of joint torque: torque as a function of angular velocity and position. While limited 3D knee extension torque surfaces for males have been reported (Fuglevand, 1987; Marshall et al, 1990; Signorile & Applegate, 2000), little information exists for knee flexion or for females. This information could have value for modeling applications involving dynamic joint torques as a function of angle and velocity. Thus, the purpose of this study was to develop a database of maximum knee torque (flexion and extension) for men and women – combining velocity and angle-specific measures into a 3D surface. Additionally, our goal was to develop analytical representations of these data for potential implementation with biomechanical models.

METHODS

17 subjects have been recruited to date: 8 males (23 ± 2.5 yrs, 183.0 ± 6.4 cm, 84.8 ± 6.7 kg) and 9 females (23 ± 3.5 yrs; 169.5 ± 6.4 cm; 67.2 ± 12.5 kg). Written-informed consent, as approved by our Institutional Review Board, was obtained prior to all testing. The subjects warmed-up on a cycle ergometer (5 min) prior to all strength testing. Peak torques were measured using an isokinetic dynamometer (Biodex System 3, New York, USA) and the recommended Biodex standard positioning. Range of motion (ROM) limits were set from full extension (~0º) to 120º knee flexion.

Isometric torque was measured at 5 randomly-ordered positions: 15, 35, 55, 75, and 100º of knee flexion. At each position, subjects performed four, 3 sec max contractions, alternating between flexion and extension. The isokinetic protocol followed, involving randomly-ordered maximum contractions at 5 angular velocities: 60, 120, 180, 240, and 300º/s. The subjects performed several trial repetitions at each new velocity for familiarization. Subjects completed 4 to 7 maximal repetitions, increasing with velocity, for both flexion and extension.

The raw torque, position and velocity data were sampled at 1000 Hz and further analyzed using Matlab (The Math Works Inc, Natick, MA, USA). Corrections for passive tension and gravity effects were performed. Torque values were calculated for 50 velocity, angle-specific combinations. The mean (SD) male and female peak torque values were calculated and plotted as 3D surfaces (SigmaPlot, SYSTAT Software Inc, CA, USA). Analytical representations using non-uniform rational B-splines (NURBS) were determined (Mathematica, Wolfram Research Inc, USA).

RESULTS AND DISCUSSION

Peak torque values differed between males and females: 242 (± 62.4) Nm vs. 155 (± 34.3) Nm (extension) and 123 (± 19.4) Nm vs. 90 (± 52.7) Nm (flexion), respectively. To demonstrate our results, the female knee extension mean peak torque data and NURBS model are shown in Figure 1a and b, respectively.

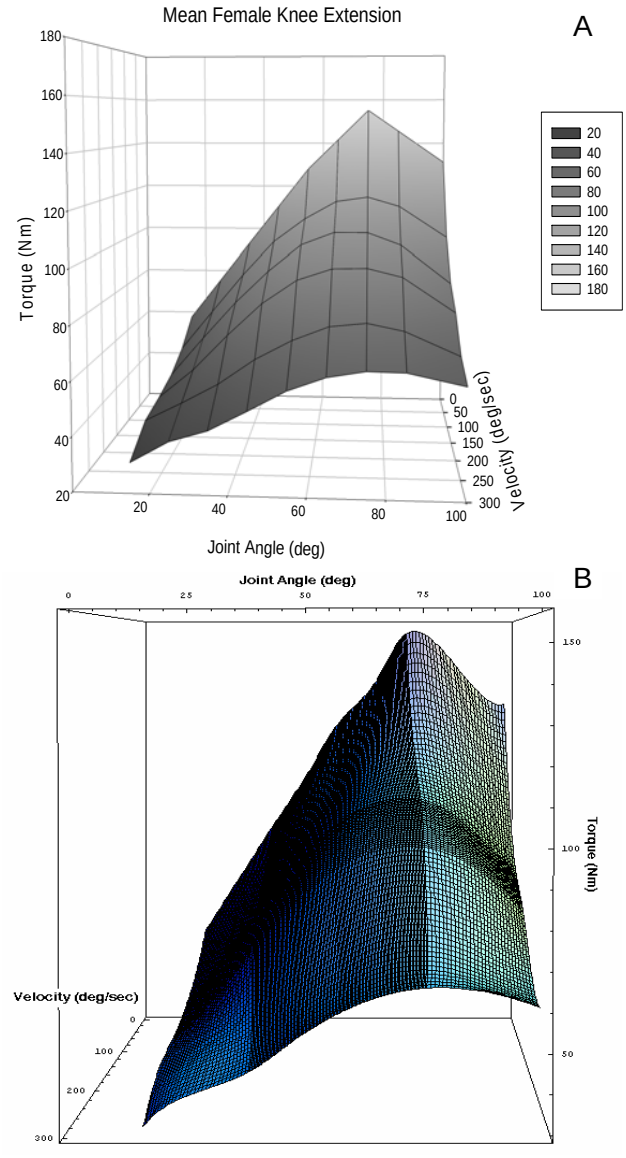

Figure 1: 3D peak torque surfaces for female knee extension: a) mean raw data, and b) NURBS model representation; (n=9).

The surfaces were consistent with Hill's (1938) force-velocity relationship, where peak torque decays with increasing velocity. The torque-angle morphology is consistent with muscle length-tension relationships (Close, 1972), despite the inclusion of muscle moment arms and multiple muscles with potentially divergent positions of optimal muscle length. The shape and position of the peak torque curves varied with velocity, demonstrating that 2D representations of strength may miss strength nonlinearities. It is interesting to note that a faint plateau effect is observed at higher velocities, similar to the results seen by Marshall et al (1990).

SUMMARY/CONCLUSIONS

With advances in human modeling, normative dynamic joint torque 3D surfaces may be increasingly valuable. Peak torque varies with both velocity and position, making 3D representations of strength ideal.

REFERENCES

Close, R.I. (1972). *Journal of Physiology*, **220**, 745-762.

Fuglevand, A.J. (1987). In: Jonsson, B. (ed) Biomechanics X-A. Human Kinetics.

Hill, A.V. (1938). *Proceedings of Royal Society*, London Ser. B **126**, 136-195.

Marshall, R.N. et al (1990). *European Journal of Applied Physiology*, **61**, 263-270.

Signorile, J.F. and Applegate, B. (2000). In: Brown, L.E. (ed) *Isokinetics in Human Performance*. Human Kinetics.

ACKNOWLEDGEMENTS

We would like to acknowledge Dr. Jingzhou Yang for his assistance with the NURBS programming.

MODELING OF THE MUSCLE/TENDON EXCURSIONS IN AN INDEX FINGER USING THE COMERCIAL SOFTWARE ANYBODY

John Z Wu [1 *], Kai-Nan An [2], Robert G. Cutlip [1], Ren G. Dong [1]

[1] National Institute for Occupational Safety and Health, Morgantown, WV, USA
[2] Mayo Clinic College of Medicine, Rochester, MN, USA
* E-mail: jwu@cdc.gov

INTRODUCTION

Biomechanical models of the hand and fingers are essential tools to explore the mechanical loading in the musculoskeletal system, which cannot be easily measured in vivo. There are multiple biomechanical models of the hand and fingers simulating different problems (e.g., Sancho-Bru et al., 2003; Brook et al., 1995). However, all these previous models are formulated analytically/numerically and are not suitable for bioengineers and scientists to deal with practical problems. The goal of our study was to develop a universal biomechanical model of the hand, which includes the factors in physiological conditions. Specifically, we develop a kinematical finger model on the platform of the commercial software Anybody (version 2.0, Anybody Technology, Aalborg, Denmark) that includes the real micro-CT-scans of the bony sections and realistic tendon/muscle attachments on the bones. The model predictions on muscle excursions in an index finger are compared with published experimental data.

METHODS

The index finger is modeled as a linkage system, based on the normative model proposed by An et al. (1979) (Fig. 1). The index finger consists of distal, middle, proximal, and metacarpal phalanges. The DIP (distal interphalangeal) and PIP (proximal interphalangeal) joints are modeled as hinges with one DOF about the z-axis; while the MCP (metacarpophalangeal) joint is modeled as a universal joint with two DOFs about the y- and z-axes. The dimensional scale of the normative finger model (An et al., 1979) is adopted into the current modeling. The attachment locations of the tendons are also defined according to the normative model. Seven muscles were included in the proposed model: Flexor profundus (FP), flexor sublimis (FS), extensor indicis (EI), extensor digitorum communis (EC), radial interosseous (RI), ulnar interosseous (UI), and lumbrical (LU). In order to better visualize the muscle/tendon attachment locations and to guide the muscle/tendon during the movements, the real bony section meshes were implemented into the proposed index finger model. These bony section meshes were obtained via micro-CT scanning of a cadaver right hand and included into the model. The predicted muscle/tendon excursions and moment arms were compared with the published experimental data (Fowler et al., 2001; An et al., 1983). Only the excursions of each individual muscle/tendon have been calculated directly in the study. The moment arm of the muscles/tendons corresponding to a particular joint is derived by differentiating the excursions with respect to that joint rotation (An et al., 1979).

RESULTS AND DISCUSSION

The variations of the muscle/tendon excursion and moment arm in response to

the flexion/extension of the DIP and PIP joints as well as the flexion/extension and adduction/abduction of the MCP joint individually are calculated and compared with the experimental data. Typical results, the moment arms of the muscles/tendons corresponding to the PIP flexion, are shown in Fig. 2. In this test, there are six relevant muscles: EI, EC, UI, LU, FS, and FP. Since the moment arms of EI and EC muscles are identical, only the result for the EI muscle is shown. The model predictions agree well with the experimental measurements that the moment arms for the FS/FP muscles are negative, while those for the other three muscles (EI/UI/LU) are positive.

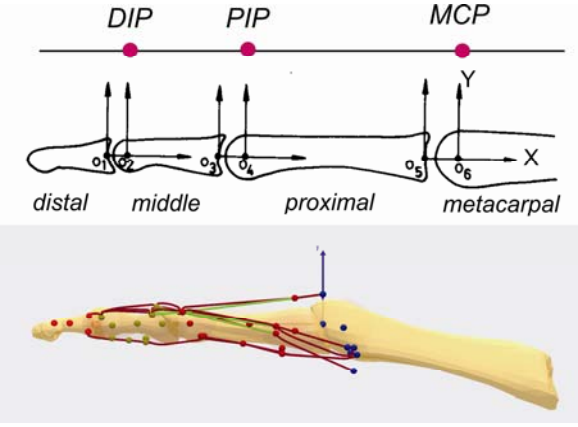

Figure 1: Schematic of the proposed finger model, which is based on the normative model (An et al., 1979). The DIP, PIP, and MCP joints are assumed to be located at O2, O4, and O6, respectively.

SUMMARY/CONCLUSIONS

In the present study, we proposed a universal model to simulate the muscle/tendon excursions and moment arms of the fingers on the platform of the commercial software AnyBody. One of the important features of the proposed model over the previous models is that the proposed approach can include the realistic bony geometries, which are associated with the muscle excursion and moment arms.

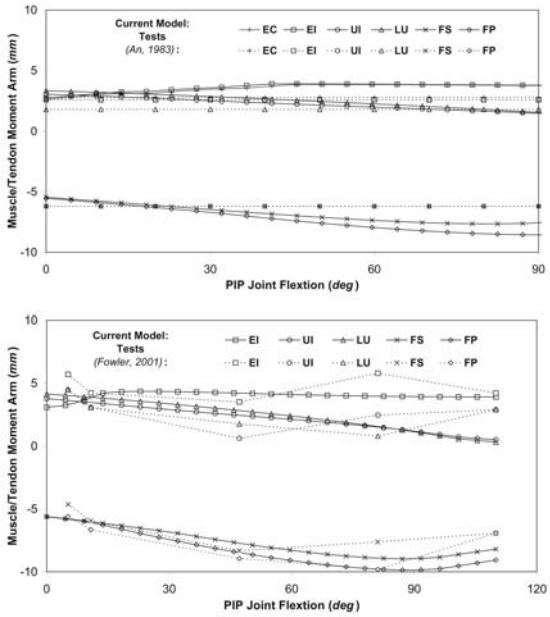

Figure 2: The predicted muscle/tendon moment arms as a function of the PIP joint flexion in comparison with the corresponding experimental data by An et al. (1983) and Fowler et al. (2001).

REFERENCES

An, K.N., Chao, E.Y., Cooney, W.P., Linscheid, R. L. (1979). *J Biomech*, 12(10):775–88.

An, K.N., Ueba, Y., Chao, E.Y., Cooney, W.P., Linscheid, R.L. (1983). *J Biomech*, 16(6):419–25.

Brook, N., Mizrahi, J., Shoham, M., Dayan, J. (1995). *Med Eng Phys* 17 (1):54–63.

Fowler, N.K., Nicol, A.C., Condon, B., Hadley, D. (2001). *J Biomech*, 34(6):791–7.

Sancho-Bru, J.L., Perez-Gonzalez, A., Vergara, M., Giurintano, D.J. (2003). *J Biomech Eng*, 125 (1):78–83.

DISCLAIMER

The findings and conclusions in this report are those of the authors and do not necessarily represent the views of the *National Institute for Occupational Safety and Health*.

MODELING OF THE DYNAMIC MUSCLE FORCE IN AN INDEX FINGER DURING TAPPING

John Z Wu [1 *], Kai-Nan An [2], Robert G. Cutlip [1], Kristine Krajnak [1], Ren G. Dong [1]
[1] National Institute for Occupational Safety and Health, Morgantown, WV, USA
[2] Mayo Clinic College of Medicine, Rochester, MN, USA
* E-mail: jwu@cdc.gov

INTRODUCTION

Since musculoskeletal disorders of the upper extremities are believed to be associated with repetitive excessive muscle force production in the hands, understanding the time-dependent muscle forces during key tapping will help to explore the mechanisms of disease initiation and development. Because the experimental evaluation of the dynamic loading in individual muscles of the hand during typing is technically difficult and expensive, researchers have studied the dynamic contact force between the fingertip and keypad, and joint angle motions, and assumed that these indices are related to the muscle/tendon excursions. The goal of the current study is to analyze the dynamic muscle forces in an index finger during typing using a universal finger model developed on a platform of the commercial software package AnyBody (AnyBody Technology Inc., Aalborg, Denmark).

METHODS

The index finger model consists of four phalanges: distal, middle, proximal, and metacarpal phalanges. These four phalanges are connected by three joints: distal interphalangeal joint (DIP), proximal interphalangeal joint (PIP), and metacarpophalangeal joint (MCP), as shown in Fig. 1. The dimensional scale of the normative finger model (An et al., 1979) is adopted into the current model. Seven muscles were included in the proposed model: flexor digitorum profundus (FP), flexor digitorum superficials (FS), extensor indicis (EI), extensor digitorum communis (EC), radial interosseous (RI), ulnar interosseous (UI), and lumbrical (LU). The responses of the index finger to tapping are simulated using an inverse dynamic technique. The time histories of impact force at the fingertip (Fig. 2a) reported by Jindrich et al. (2004) and the time-histories of DIP, PIP, and MCP joint angles during tapping reported by Kuo et al. (2006) (Fig. 2b) are applied to drive the model. The joint torques/power and muscle loading/power are predicted as a function of time.

RESULTS AND DISCUSSION

The predicted time-histories of power generated in each individual muscle as well as the total muscle power are depicted in Fig. 3(a). The predicted time-histories of the power in each joint and the total joint power are shown in Fig. 3(b). The sum of the power generated in the muscles agrees well with that in the joints, confirming that all muscle forces are transferred to the joints. Our analysis further indicates that the power generated by FP, EC, and EI muscles are predominant among all muscles, while the power transferred through MCP joint is predominant among all three joints. The predicted time-histories of muscle forces agree well with the EMG measurements made by Kuo et al. (2006) in time sequence (results not shown).

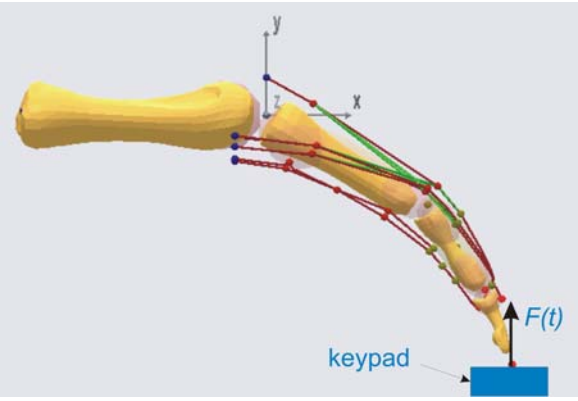

Figure 1: The finger is in contact with the keypad during tapping. The interface impact force *F(t)* is treated as external loading applied on the fingertip.

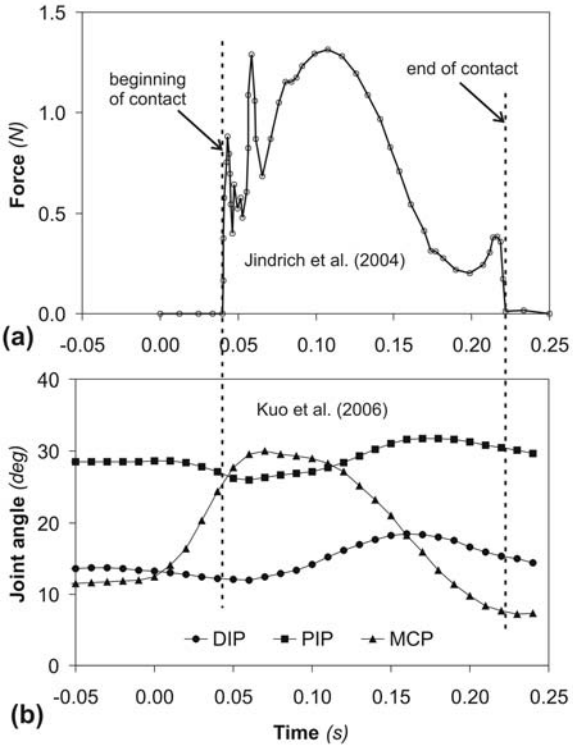

Figure 2: Time histories of representative force at fingertip (a) and joint angles (b) of an index finger during keypad strike reported by the previous researchers (Jindrich et al., 2004; Kuo et al., 2006).

SUMMARY/CONCLUSIONS

In the present study, we have theoretically analyzed the muscle forces and power generated by the muscles in an index finger during a tapping task. Our results suggested that that the powers generated by FP, EC, and EI muscles are predominant among all muscles, while the power generated in MCP joint is predominant among all three joints.

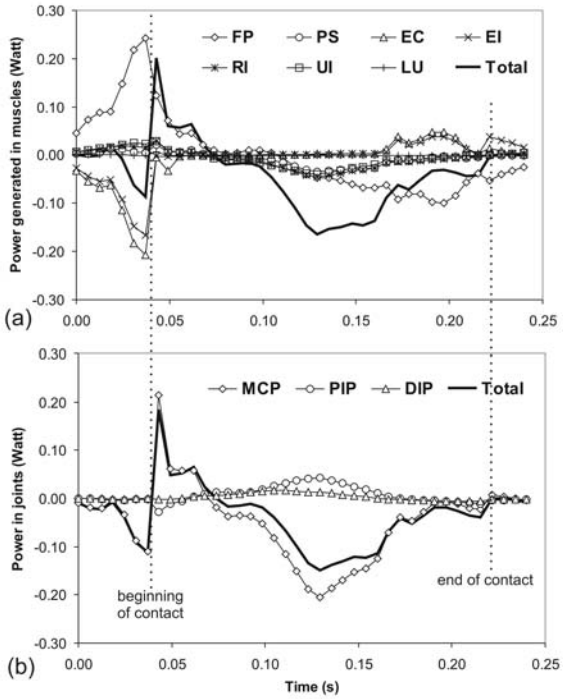

Figure 3: Predicted time-histories of power generated in each individual muscle (a) and joint (b).

REFERENCES

An, K.N., Chao, E.Y., Cooney, W.P., Linscheid, R. L. (1979). *J Biomech*, 12(10):775–88.

Kuo, P. L., Lee, D. L., Jindrich, D. L., Dennerlein, J. T. (2006). *J Biomech* 39(16): 2934-42.

Jindrich, D. L., Balakrishnan, A. D., Dennerlein, J. T. (2004). *J Biomech.* 37(10):1589-96.

DISCLAIMER

The findings and conclusions in this report are those of the authors and do not necessarily represent the views of the National Institute for Occupational Safety and Health.

GROWTH-DEPENDENT ENHANCEMENT OF MOUSE NEONATAL MUSCLE MORPHOLOGY AND CONTRACTILE FUNCTION

David S. Gokhin [1] and Richard L. Lieber [1]

[1] Departments of Orthopaedic Surgery and Bioengineering
University of California-San Diego and Veterans Affairs Medical Center, La Jolla, CA, USA
E-mail: rlieber@ucsd.edu, Web: muscle.ucsd.edu

INTRODUCTION

Postnatal skeletal muscle growth is attributable to hypertrophy of existing muscle fibers and action of myogenic stem cells, but the precise sequence of biochemical and biological events that results in muscle growth is poorly defined. A number of transcriptional regulatory molecules have been identified as mediators of skeletal muscle growth (Knapp et al., 2006). However, these studies typically consider "growth" primarily in terms of muscle mass and morphology independent of muscle quality or contractile function. As such, they do not provide insight into the nature of the development of mechanical function. Other work has focused on developmental changes in myosin heavy-chain isoform distribution (Agbulut et al., 2003), but these experiments also failed to consider contractile function.

Therefore, the objective of this study was to measure the time-course of neonatal skeletal muscle contractility and correlate these changes in muscle function with changes in tissue morphology and fiber architecture. These data are also necessary to provide a reference for studying certain muscle-specific proteins, such as nebulin (Bang et al., 2006), whose knockout is neonatal-lethal in mouse models. In such models, severe postnatal myofibrillar disorganization and muscle degeneration render invalid any comparison to mature controls. Rather, comparison to immature wild-type controls from neonatal time-points is preferred.

METHODS

Bilateral mouse hindlimbs were used at postnatal days 1, 7, 14, 21, and 28 (P1-P28; n=8/time point).

Morphology. Frozen transverse sections (thickness: 10 μm) of the tibialis anterior (TA) were generated. On one set of sections, Alexa Fluor 488-conjugated phalloidin staining was used to localize sarcomeric actin. Image analysis was performed to compute the cross-sectional area fraction of contractile material (a metric of myofibrillar concentration within muscle fibers). On another set, immunohistochemistry was used to localize pericellular laminin. Image analysis was performed to compute pixel area enclosed by laminin and thus quantify muscle fiber cross-sectional area.

Mechanics. Mouse hindlimbs were transferred to a custom muscle-testing chamber filled with Ringer solution. Hindlimbs were secured proximal to the TA with a steel pin through the femur and distal to the TA with silk suture tied around the foot and ankle, passing through the tibiotarsal joint space. Muscle length (L_m) was measured using an eyepiece crosshair reticule. Muscle fiber length (L_f) was computed as $0.6L_m$, where 0.6 is the characteristic L_f/L_m ratio for the mouse TA as determined by a pilot study. Plantarflexors were then released at the Achilles tendon and carefully resected. Dorsiflexors underwent maximal isometric stimulation using a 400-ms train of 0.3-ms

pulses delivered at 100 Hz. Isometric force was measured 3 times with 2 min between contractions. After testing, TA muscles were weighed. Maximum isometric stress was estimated by normalizing maximum isometric force to TA physiological cross-sectional area (PCSA).

Statistics. Data are presented as mean±SEM. The effect of postnatal day was assessed using one-way ANOVA with *post hoc* Fisher's PLSD analysis to locate where differences existed (α=0.05).

RESULTS AND DISCUSSION

Muscle morphology exhibited rapid postnatal maturation. The cross-sectional area fraction of contractile material increased from 0.48 at P1 to 0.92 at P28, indicating a near-total filling of the intracellular space by myofibrillar contractile material by P28 (Fig. 1A). Simultaneously, fiber cross-sectional area increased ~7-fold (Fig. 1B). Morphological maturation occurred synchronously with functional enhancement, as evidenced by a ~6-fold increase in maximum isometric stress from P1 to P28 (Fig. 1C). Certain architectural parameters followed similar growth time-courses, namely muscle mass, which increased ~4-fold (Fig. 1D), and L_f, which increased ~5-fold (Fig. 1E). Interestingly, muscle PCSA decreased by 29% from P1 to P21 but began to recover slightly by P28 (Fig. 1F). This decrease in PCSA was driven primarily by L_f increasing more rapidly than muscle mass.

SUMMARY/CONCLUSIONS

These data offer the first direct evidence for the improvement of functional quality during postnatal development of skeletal muscle. The increase in myofibrillar contractile material at least partially accounts for the functional enhancement. Future work will attempt to develop a multivariate model of isometric muscle stress production.

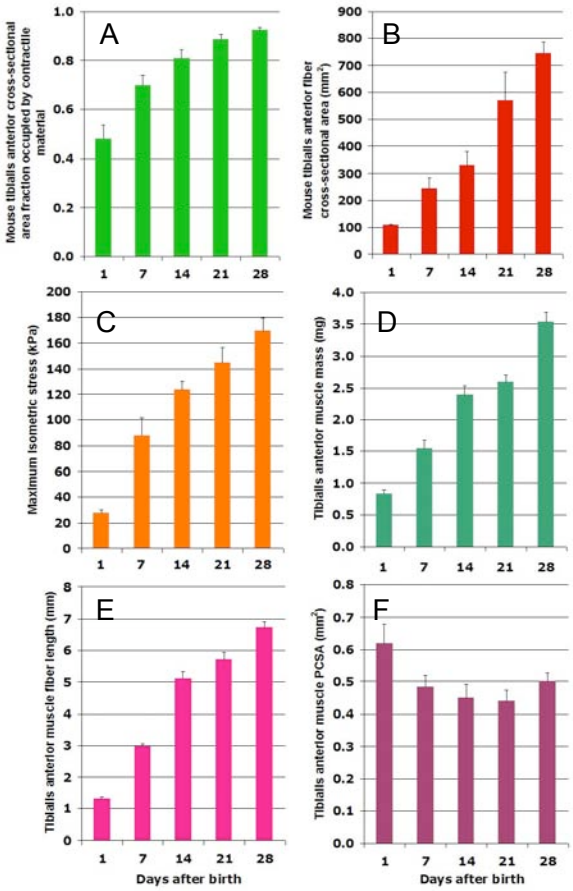

Figure 1. Muscle morphology, maximum isometric stress, mass, and muscle architecture as functions of postnatal day.

REFERENCES

Agbulut, O. et al. (2003). *Biol. Cell*, **95**, 399-406.

Bang, M.L. et al. (2006). *J. Cell Biol.*, **173**, 905-916.

Knapp, J.R. et al. (2006). *Development*, **133**, 601-610.

ACKNOWLEDGEMENTS

We acknowledge NIH grant AR40050 and the Department of Veterans Affairs.

PUSH UP BARS AND HAND POSITION AFFECT UPPER EXTREMITY MUSCLE ACTIVITY DURING THE PUSH UP EXERCISE

Steven T. McCaw[1], Amanda K. Somers[1], Siu Fong Lam[1], Mitch D. Waller[1], Aaron J. Decker[2]
[1]Illinois State University, Normal [2]Northeastern Illinois University, Chicago
email: smccaw@ilstu.edu web: www.cast.ilstu.edu/mccaw

INTRODUCTION

The push up is an upper body exercise common to many training regimens. From a prone position, the subject maintains toe-ground contact while using the upper extremity to raise and lower the extended body. The exercise utilizes the anterior chest (pectoral muscles) and posterior arm (triceps brachii) muscles, along with synergistic and stabilizing muscles in the forearm and shoulder. The use of push up bars (Figure 1) allows a user to easily alter hand position while performing the exercise to further alter muscle activity patterns. Research shows altering hand position changes muscle activation (Cogley et al. 2005; Gouvali & Boudolos 2005) and elbow joint loads (Donkers et al, 1993) during the push up. Our purpose was to determine the effect of bar use and altered hand position on muscle activity, hypothesizing that recorded muscle activity would reflect the altered loading demands of different segment orientations during the push up.


Figure 1. Push up bars

METHODS

Thirteen male university students (age: 21.8 ± 1.9 y; height: 180.8 ± 8.6 cm; mass: 85 ± 15 kg) were randomly recruited. All signed informed consent. Hand spread was controlled at 150% of the subjects biacromial width across the two hand positions (forward and laterally rotated) crossed with the use or non-use of the bars. Muscle activity was recorded (1000 Hz) using surface electrodes from the pectoralis major (PM), triceps brachii (TB), and flexor carpi ulnaris (FCU) simultaneously with opto-electronic tracking (200 Hz) of reflective markers defining the trunk, upper arm and forearm. Subjects performed five repetitions of the push ups in each of the four hand position-bar use conditions. Linear envelopes of the EMG data from each repetition were created by rectifying and digitally filtering the raw signal, and expressed as a % of an isometric reference position (% IRP). The activity of each muscle was integrated during the descent and ascent phase of each repetition, using the elbow angle to identify the phases. The five trial means of each subject were entered into a three-way (phase x hand position x bar use) repeated measures ANOVA ($\alpha = 0.05$) to identify statistically significant differences in muscle activity.

RESULTS AND DISCUSSION

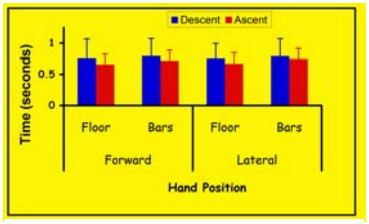

Figure 2. Phase time descriptors

Analysis of temporal aspects of the lifts indicated that it took about 100 ms longer to perform a push up using the bars (figure 2).

The grand ensemble curves of each muscle are presented in figure 3. The PM activity was not affected by hand position or bar use.

There was a significant phase by bar use interaction for the TB (figure 4); when using the bar, the TB was about 33% more active during the ascent phase. Bar use allows for greater elbow flexion during the push up, so it is likely that the TB increase reflects an increased demand for elbow extension torque in the more compromised position.

There was a significant bar use by hand position interaction for the FCU (figure 4). The muscle was more than 2x as active in the forward hand position than laterally rotated; in addition, with the hands in the forward position, there was nearly twice the activity in the FCU when using the bars, although there was no significant difference with the hands laterally rotated. When a forward hand position is used with the bars, the wrist tends to be hyperextended throughout the push up, compared to a more neutral wrist position with laterally rotated hands. With a hyperextended wrist, body weight creates a greater hyperextension torque that must be countered by an increased flexor torque. The increased FCU activity likely reflects its' recruitment to contribute to the flexor torque.

SUMMARY/CONCLUSIONS

These results indicate that both hand position and bar use affect muscle activity during the push up. Bar use affects segment orientation to increase the demands of the push up, and this effect can be maximized with hands in the forward position. Manipulating hand position and incorporating bar use provide an effective means to alter the overload and add variation to the push up exercise.

REFERENCES

1. Cogley, R., et al. (2005). *JSCR*, **19**, 628-633.
2. Donkers, M., et al. (1993). *J Biomech*, **26**, 625-632.
3. Gouvali, R. & Boudolos, K. (2005). *JSCR*, **19**, 146-151.

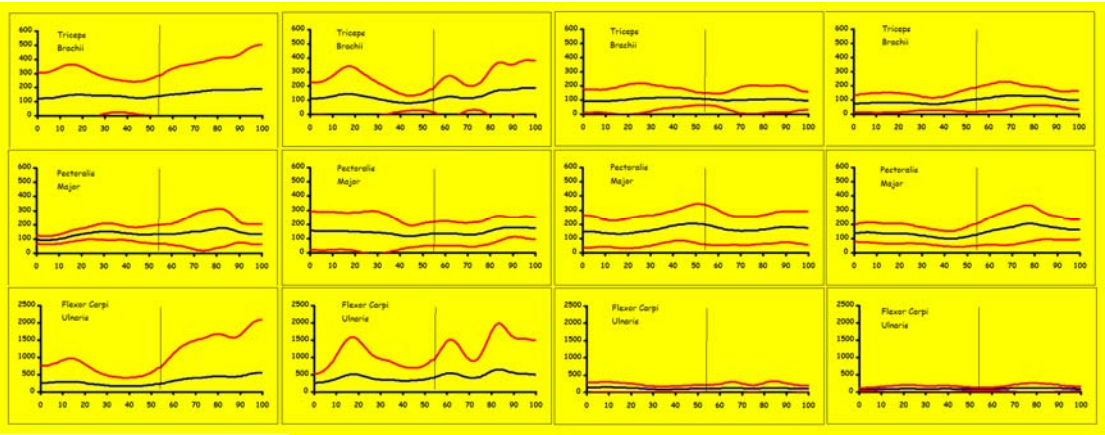

Figure 3. Grand ensemble muscle activity (blue) +/- 1 SD (red). Columns left to right: No bars, hands forward; bars, hands forward; no bars, lateral rotation; bars, lateral rotation. Haxis: % lift; Vaxis: % IRP. Vertical line mx flexion

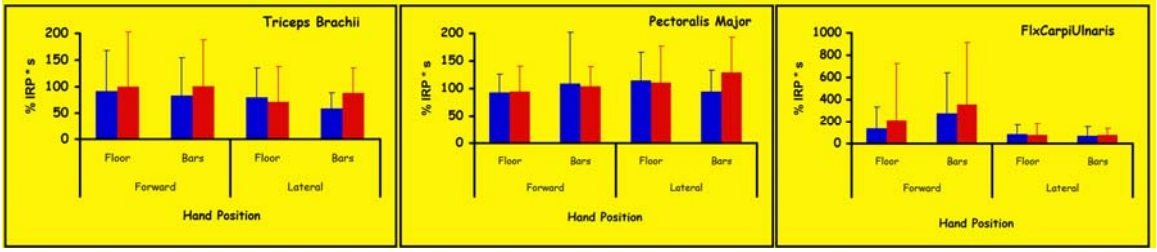

Figure 4. Descriptive statistics of integrated EMG by hand position-bar conditions.

MOVEMENT STABILITY IS AFFECTED BY MUSCLE FATIGUE

Deanna H. Gates [1] and Jonathan B. Dingwell [2]

[1] Department of Biomedical Engineering, University of Texas, Austin, TX, USA
[2] Nonlinear Dynamics Laboratory, Dept. of Kinesiology, University of Texas, Austin, TX, USA
E-mail: jdingwell@mail.utexas.edu Web: http://www.edb.utexas.edu/faculty/dingwell/

INTRODUCTION

Local dynamic stability measures how a system responds to small perturbations, such as those normally occurring during movement. Local stability has been studied during walking (Dingwell, 2006) and repetitive lifting (Granata, 2006). A common finding is that instability increases when movement speed increases (Dingwell, 2006; Granata, 2006).

Muscle fatigue may also lead to greater instability, since it decreases muscle response time (Wilder, 1996). With increased response time, the muscles might be slower to adjust in response to perturbations. One study found slight increases in local dynamic instability of the trunk with muscle fatigue during prolonged walking (Yoshino, 2004), but these effects were confounded by changes in walking speed. Therefore, this study determined how local stability was affected by muscle fatigue while subjects performed a repetitive task at a constant rate. We hypothesized that instability would increase with fatigue and that instability would increase when the height of the task was raised from sternum to shoulder level, as movements at this position are associated with shoulder injuries.

METHODS

10 healthy right-handed (28 ± 2 years) subjects sat in an adjustable chair with seat belts to help them maintain a constant posture (Fig. 1). They then pushed a weight back and forth along a low friction horizontal track in time with a metronome until volitional exhaustion. The weight was set to 15% of the subject's maximum pushing/pulling force. The height of the track was set to either sternum level (Low) or shoulder level (High). Each subject performed both tasks in random order on 2 different days. The 3-D movements of the right arm and trunk were recorded continuously at 60 Hz using VICON (Oxford Metrics, Oxford, UK). EMG were collected at 1080 Hz from 9 arm and trunk muscles. Three rotational angles of the shoulder, elbow, and wrist were calculated using Euler angles.

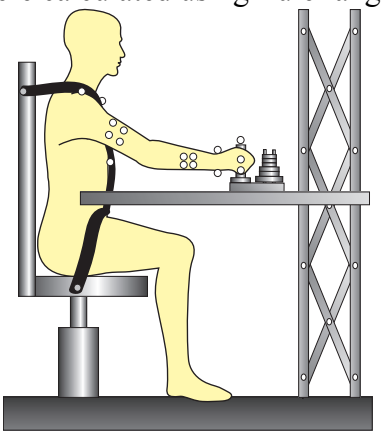

Figure 1. The experimental set-up.

Local dynamic stability is defined as the quantitative response of the system's state variables to small perturbations. Short – term local divergence exponents (λ_s*) indicate the rate of divergence of neighboring trajectories. Positive exponents indicate local instability, with larger exponents indicating greater sensitivity to local perturbations. We calculated these exponents using previously published methods (Dingwell, 2006). λ_s* was generated for each shoulder angle for the first and last minute of the trial. Data

were analyzed using a 3-factor ANOVA (Subject x Height x Pre/Post).

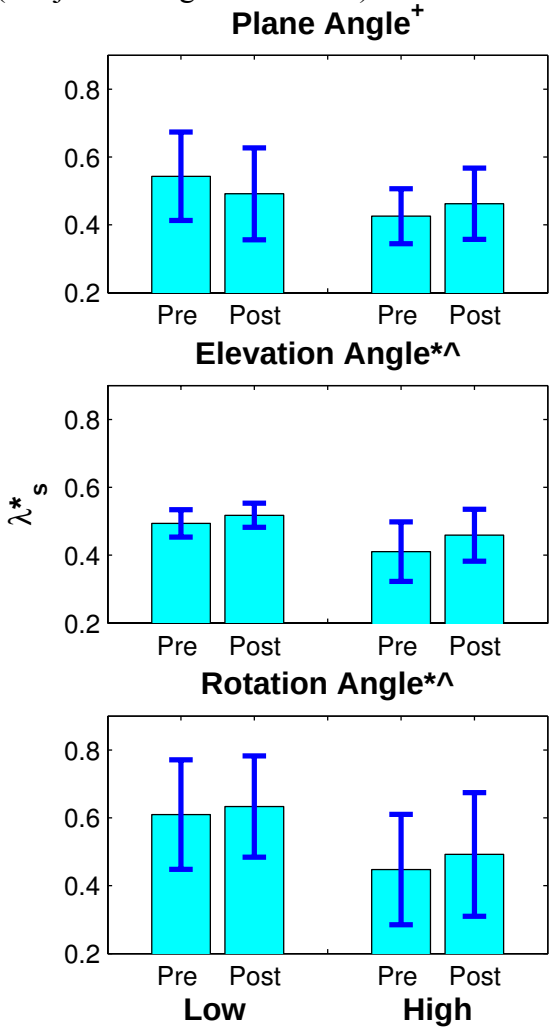

Figure 1. Local stability of all shoulder angles for pre/post and condition. Error bars represent the 95% confidence interval. * significant pre/post effect, ^ significant subject× height interaction, $^{+}$ significant pre/post× height interaction.

RESULTS AND DISCUSSION

Subjects performed the task for 24.1 ± 10.3 minutes in the Low condition and 12.1 ± 3.9 minutes in the High condition. Although there were large differences between subjects, on average, most subjects exhibited significantly greater local instability with muscle fatigue for both humeral elevation and rotation angles (Fig. 1). Subjects tended to be more unstable when the task was performed at the Low height, though this was not significant ($p = 0.329$, 0.078, and 0.081 for humeral plane, elevation, and rotation angles). There were significant subject by height interactions for elevation angle ($p = 0.001$) and rotation angle ($p < 0.001$) and a significant pre/post by height interaction for humeral plane angle ($p = 0.014$).

SUMMARY/CONCLUSIONS

Fatigue led to greater local dynamic instability for both Low and High heights. This result agrees with previous findings by Yoshino et al (Yoshino, 2004) and may indicate that individuals are at a greater risk for injury when perturbed since their capacity to respond to small perturbations is diminished. However, instability tended to *de*crease (not increase) from the low height to high height conditions. While this did not support our hypothesis, this result agrees with previous work on lumbar flexion which showed that movements in two planes were more stable than those in a single plane (Granata, 2006). As such, the trends toward decreased instability in the High task may result from the additional constraints of the task.

REFERENCES

Dingwell, J. & Marin, L., (2006) *J Biomech* **39** (3): 442-452.

Granata, K. & England, S. (2006) *Spine* **31**(10): E271-276.

Sparto, P. et al. (1997) *Spine,* **22** (22): 2647-2654.

Wilder, D. et al. (1996) Spine **21** (22): 2628-2639.

Yoshino, K., et al. (2004) *J Biomech* **37** (8): 1271-1280.

ACKNOWLEDGEMENTS

Supported by NIH Grant #EB003425

THE EFFECT OF CARDIOVASCULAR FATIGUE ON TRUNK MUSCLE ACTIVATION AND SPINE POSTURES DURING FIREFIGHTING TASKS

Diane E Gregory, Samuel J Howarth, Sonia Narula, and Jack P Callaghan

University of Waterloo, Waterloo, Ontario, Canada
E-mail: dgregory@uwaterloo.ca

INTRODUCTION

The Candidate Physical Ability Test (CPAT) is used to assess the physical fitness of firefighter candidates. The test is comprised of eight tasks which simulate real firefighting duties and demands. These tasks, whether executed during the CPAT or during a real firefighting scenario, are often performed in a cardiovascularly fatigued state. Given that cardiovascular fatigue is a large component of both the CPAT and real firefighting scenarios, it is important to understand the effect of such fatigue on firefighting tasks. Therefore the primary purpose of this study was to examine the effect of fatigue on trunk muscle activation patterns, and three-dimensional spine postures during three standard CPAT tasks. The secondary purposes of this study were to examine the effect of gender and CPAT experience (previous completion of the complete CPAT protocol) during the same standard CPAT tasks.

METHODS

Ten individuals (five male, five female) from a university population were recruited for the current study. Participants were free of any low back pain in the twelve months prior to the collection. Five of the ten participants had previous CPAT experience.

The three CPAT tasks chosen for examination were the ceiling breach and pull (ceilingBP), designed to simulate breaking or pulling down part of a ceiling; the forcible entry (forceE), designed to simulate entry through a wall or door; and the mannequin drag (mDrag), designed to simulate moving a victim. The ceilingBP involved pushing up three times on a 27.3 kg ceiling hinged door and pulling down five times on an 3.6 kg ceiling latch; with the complete cycle repeated four times. The forceE involved repetitively striking a mechanized target with a 4.5 kg sledgehammer until the target moved a given distance (generally 5-10 hits). The mDrag involved dragging a 75 kg mannequin 10.7 m followed by a 180° turn and another 10.7 m drag.

Each participant performed all three tasks (presented in random order) with as much rest in between as required by the participant while wearing a 22.7 kg CPAT regulation weight vest which is a requirement of the protocol. Each participant then completed the official CPAT fatiguing protocol which consisted of stair climbing at a rate of 60 steps/minute while wearing the 22.7 kg weight vest plus an additional 11.3 kg on the shoulders (total of 34 kg) for 3 minutes. Immediately following the fatigue protocol and the removal of the additional 11.3 kg, the participants repeated the three CPAT tasks (in the same order presented for that participant prior to fatigue) without any rest given in between.

During the tasks (both prior to and following fatigue) muscle activation and spine postures were monitored. Surface electrodes were adhered to the skin bilaterally over the

internal oblique, external oblique, lumbar erector spinae, and thoracic erector spinae. Spine posture was monitored using the Lumbar Motion Monitor (AcuPath Industrial, Biomec Inc., Cleveland, OH, USA). Variables examined included average and peak muscle activation, and average and peak spine angles, velocities, and accelerations in all three axes (flexion/ extension, lateral bend, and axial twist).

RESULTS AND DISCUSSION

Individuals showed lower average muscle activation in all four abdominal muscles during the three tasks following the fatigue protocol as compared to before (Figure 1a, $p<0.05$), while no differences in average back extensor activation were observed following the fatigue protocol. In addition, individuals showed increased average and peak spinal flexion following the fatigue protocol as compared to before (Figure 1b, $p<0.05$).

The reduced abdominal activation post fatigue may be indicative of the increased challenge of breathing. It has been shown that during a challenged breathing scenario, some individuals change their abdominal activation patterns to preferentially assist in breathing rather than to stabilize their spine (McGill et al., 1995). The cardiovascular fatigue in the current study may have induced a similar phenomenon. Since abdominal activation is cyclic in nature during a challenged breathing task, the average activation would likely be lower if compared to a static activation in the abdominals in order to maintain stability of the spine. Further, the increase in spinal flexion that was observed post fatigue may place individuals at an increased risk of spinal injury. When an individual becomes cardiovascularly fatigued, generally quality

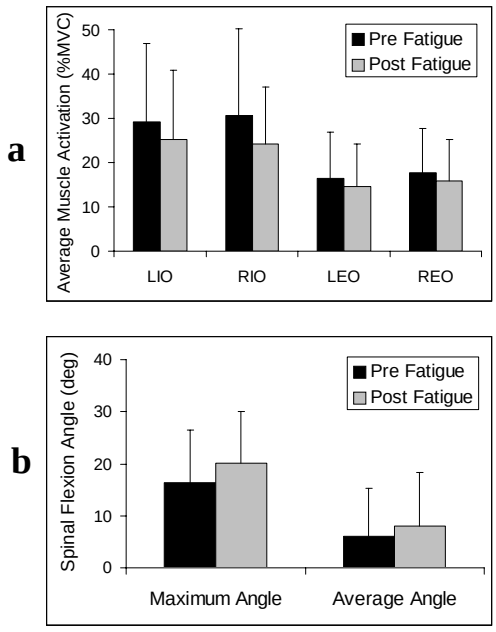

Figure 1: Significant effect of fatigue on abdominal activation (a), and spine flexion (b), $p<0.05$.

of form is lost. Poor form, combined with reduced abdominal activation and thus likely reduced spine stability, may increase the risk of injury to the individual.

SUMMARY/CONCLUSIONS

Cardiovascular fatigue is very common in firefighting scenarios. The current study demonstrated that such fatigue results in reduced abdominal activation, and increased spinal flexion, likely increasing an individual's risk of spine injury.

REFERENCES

McGill, S.M. et al (1995). *Ergonomics*, **38**, 1772-1792.

ACKNOWLEDGEMENTS

The authors wish to acknowledge UW Fitness, University of Waterloo for the use of their firefighting testing facilities.

RIGID BODY AND SPRING MODELING WITH BONE-SCREW INTERFACE TO SIMULATE PEDICLE SCREW FIXATION

Yoshimori Kiriyama [1,2] Nobutoshi Yamazaki [3] Takeo Nagura [2] Toshiyasu Nakamura [2]
Morio Matsumoto [4] Kazuhiro Chiba [2] Hideo Matsumoto [2], and Yoshiaki Toyama [2]

[1] Murayama Medical Center, Murayama, Tokyo, JAPAN
[2] Dept. of Orthopaedic Surgery, Keio University, Shinanomachi, Tokyo, JAPAN
[3] Dept. of Mechanical Engineering, Keio University, Yokohama, Kanagawa, JAPAN
[4] Dept. of Muscul. Recons. & Regen. Surg., Keio University, Shinanomachi, Kanagawa, JAPAN
E-mail: kiriyama@mmm-keio.net

INTRODUCTION

A pedicle screw fixation is one of the most effective surgical techniques for excessive spinal deformation such as scoliosis. To obtain the effective results, the screws have to be inserted into the adequate placements.

Rigid body and spring model has been used to reproduce spinal fixation surgery. The model allows us to modify various conditions and parameters under the surgery, and is a useful tool to predict the surgical outcomes and the post-operative posture.

In this study, we developed the lumbar and spinal instrument model that consisted of rigid bodies as vertebrae and springs as intervertebral stiffness. Especially, the model had the interfaces between pedicle screw and vertebra, to consider problems related to bone-screw interface such as back-out of the screw. The validation of the model was evaluated by cadaver experiment that simulated similar movement of the lumbar spine.

METHODS

Three-dimensional model of the lumbar spine and pedicle screw system were built as shown in Fig.1. Vertebrae of T12 and L1-5 were rigid bodies, and sacrum was fixed in the global coordinate system.

To reproduce the coupling motions of vertebrae, a stiffness matrix (6 by 6) linked adjacent vertebrae, because the nondiagonal coefficients in the matrix join the displacement and the load about the coupled motion. The matrix coefficients were decided from the literatures (Panjabi et al., 1994; Brickmann et al., 1991; Edwards et al., 1987).

The pedicle screws were regarded as rigid bodies. Since the vertebra was rigid body, the interfaces between screw and vertebra were modeled by pull-out springs along the pedicle screw, radial springs toward radial direction of the screw and torsion-friction torque springs around the screw. Spring constant of the pull-out spring was determined as the maximum pull-out force of 1.0 kN was generated when the screw

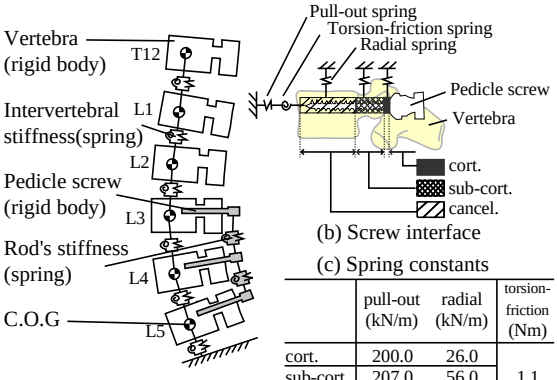

(a) Model outline

(b) Screw interface

(c) Spring constants

	pull-out (kN/m)	radial (kN/m)	torsion-friction (Nm)
cort.	200.0	26.0	1.1
sub-cort.	207.0	56.0	
cancel.	93.0	25.4	

Figure 1: The interfaces model. **note**: cort. (cortical bone), sub-cort. (sub-cortical bone), cancel. (cancelous bone)

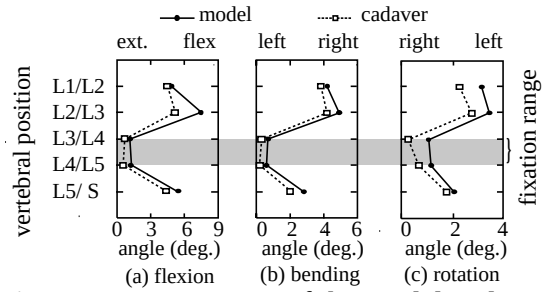

Figure 2: Comparison of the model and cadaver angles.

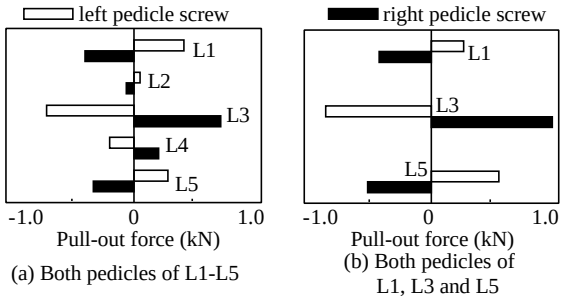

Figure 3: Pull-out forces for typical lumbar scoliosis (Cobb's angle 30 deg., right convex curve), **note**: negative (pull-out).

moved by the screw's pitch length of 2 mm (Hirano et al., 1997; Kwok et al., 1996). The radial spring constant was derived from the caudal-cepharad stiffness reported by Hirano et al. (1997). The torsion-friction spring generated a torque of 1.1 Nm independent of the rotation angle, because the average insert torque was 1.1 Nm (Kwok et al.1996; Daftari et al.1994).

The spinal rod was regarded as a column beam with a uniform cross-sectional area and material property (radious 3 mm, Young's modulous 1.1×10^2 GPa, Poisson ratio 0.3).

The postures of the model were calculated to balance the external and internal loads of a rigid body using a numerical optimization.

To validate our model, the motion of the model and that of a cadaveric lumbar spine was compared. The cadaver and the model conditions were the same as following that the pedicle screws were inserted into both pedicles of L3 to L5, and muscle forces around the lumbar spine of flexion (30 deg.), lateral bending (20 deg.) and axial rotation (10 deg.) were applied by using a custom-made spine tester (Kiriyama et al. 2006)

RESULTS AND DISCUSSION

Fig. 2 shows the vertebral angles of the computer model and cadaver specimen under the three different motions. In each motion, each vertebral angle showed a good agreement with that of cadaver experiment. The results support the validity of our rigid spring modeling. Using this model, we estimated the pull-out forces in two types of pedicle screw fixation for a typical lumbar scoliosis (Fig. 3). In both types, pull-out forces were below the maximum forces of the pedicle screws (Hirano et al., 1997).

SUMMARY/CONCLUSIONS

We built rigid body and spring model of the lumbar spine and spinal instruments that include the interface between bone and screw. The model can be used to predict various post operative conditions of the spinal fixation using pedicle screw system.

REFERENCES

Brickmann, P. and Grootenboer, H. (1991). *SPINE*, **16**, 641-646.

Daftari, T.K., et al. (1994). *J.Spin. Disord.*, **7**, 139-145.

Edwards, W.T., et al. (1987). *J. Biomech. Eng.*, **109**, 35-42.

Hirano, T. et al. (1997). *SPINE*, **22**, 2504-2510.

Kiriyama et al. (2006). *Trans. ORS*, 1309.

Kwok, A.W.L, et al. (1996). *SPINE*, **21**, 2429-2434.

Panjabi, M.M., et al (1994). *J. Bone. J. Surg.*, **76-A**, 413-424.

JOINT KINETIC CONTRIBUTIONS TO ACUTE PERFORMANCE ENHANCEMENT & DEGRADATION

Loren Z.F. Chiu and George J. Salem

University of Southern California, Los Angeles, CA, USA
E-mail: lorenchi@usc.edu Web: pt.usc.edu/labs/mbrl

INTRODUCTION

Heavy resistance exercise generates acute physiologic responses that may enhance or degrade performance. Enhancement of performance is categorized as post-activation potentiation (PAP). Alternatively, degradation of performance is the consequence of fatigue responses.

Previous reports suggest PAP enhances muscle force generated under stimulated and voluntary conditions; however, the majority of this research has been performed utilizing single-joint isometric or isokinetic exercise modalities. Recent investigations have reported immediate improvement in performance on multi-joint tasks, such as vertical jumping, following heavy resistance exercise. These investigations, however, have only reported improvements in whole-body performance (Chiu et al. 2003). Recently, we reported that weightlifting exercise enhanced vertical jump performance by acutely increasing work performed by the knee extensors and ankle plantar-flexors (Chiu et al. In Press).

The purpose of this investigation was to determine the association between changes in net joint kinetics and PAP and fatigue during weightlifting exercise.

METHODS

Men (n=6) who were actively participating in heavy resistance exercise involving weightlifting exercises (snatch, clean & jerk) were recruited for this investigation. Participants attended 3 different resistance exercise sessions, approximately one week apart. All sessions involved the clean pull exercise, but were performed at different relative intensities. The order of sessions was randomized.

#1 – 75% 1 RM/5 repetitions * 12 sets
#2 – 85% 1 RM/3 repetitions *15 sets
#3 – 95% 1 RM/1 repetition *20 sets

During exercise, subjects wore a six-degree of freedom retro-reflective marker set on their lower extremity to capture kinematics of the feet, shanks, thighs and pelvis. Video data were captured by 8 optoelectronic cameras at 120Hz. All exercise was performed standing on a force platform sampling at 1560Hz. Standard 3D inverse dynamics procedures were applied to determine peak net joint moment (NJM) and net joint power (NJP) at the ankle, knee and hip in the sagittal plane. Retro-reflective tape was also placed on the center of the barbell and average power during the second pull (BP) was calculated (Garhammer 1993).

All data were normalized to the first set of exercise and expressed as a percentage of the first set performance. Thus, a value greater than 100% indicated a potentiation response; whereas, a value less than 100% indicated a fatigue response. The maximum (>100%; i.e. potentiation) and minimum (<100%; i.e. fatigue) % values were determined. Pearson product moment correlations were utilized to determine

associations between maximum/minimum changes in performance (BP) with maximum/minimum changes in NJM and NJP.

RESULTS AND DISCUSSION

For the 75% 1 RM condition, the BP potentiation response was correlated with maximum % for NJM ($r=0.96$; $p=0.01$) and NJP ($r=0.97$; $p<0.01$) of the knee extensors. Similarly, in the 85% 1 RM condition, BP potentiation response was correlated with maximum % for NJM ($r=0.95$; $p=0.02$) and NJP ($r=0.95$; $p=0.02$) of the knee extensors. In the 95% 1 RM condition, BP potentiation response was correlated to maximum % for NJM ($r=0.93$; $p<0.01$) of the hip extensors.

These results suggest different contributions to performance enhancement dependent on the relative intensity. For lower relative intensities (75% and 85% 1 RM), performance is enhanced by increasing knee extensor NJM and NJP. However, at the higher relative intensity (95% 1 RM), performance is enhanced by increasing hip extensor NJM. This difference suggests that training at lower relative intensities will result in different acute responses, than training at heavier relative intensities.

For the 75% 1 RM condition, the BP fatigue response was correlated with minimum % value for NJM ($r=0.92$; $p<0.01$) and NJP ($r=0.89$; $p=0.02$) of the knee extensors. No significant correlations were observed for BP fatigue response and net joint kinetics in the 85% and 95% conditions.

Similar to the potentiation responses, fatigue responses also appear to be dependent on the relative intensity. For the lowest relative intensity, fatigue manifests as a decrease in the NJM generated by the knee extensors. However, at heavier relative intensities, performance decrements are not associated with decreases in NJM or NJP at the knee. It is possible that some participants fatigued their knee extensors and others fatigued their hip extensors, thus demonstrating no generalized relationship. Another explanation is that other factors, such as rate of force/torque development, time of maximum NJM/NJP, or muscle recruitment coordination are responsible for the fatigue demonstrated at higher relative intensities.

SUMMARY/CONCLUSIONS

Enhancement in performance during a high power multi-joint task is achieved by increasing peak NJM and/or NJP. The joint at which NJM/NJP is enhanced is dependent on relative intensity. Performance decrements at low relative intensities but not high relative intensities are the result of decreased NJM and NJP. The different potentiation and fatigue responses at the three relative intensities should be considered in the design of resistance training programs.

REFERENCES

Garhammer, J. (1993). A review of power output studies of Olympic and powerlifting: methodology, performance prediction, and evaluation tests. *Journal of Strength and Conditioning Research*, **7**, 76-89.

Chiu, L.Z.F. et al. (2003). Postactivation potentiation response in athletic and recreationally trained individuals. *J. Strength Cond. Res.*, **17**, 671-677.

Chiu, L.Z.F. et al. (In Press). Weightlifting exercise potentiates joint mechanical work during vertical jumping [abstract]. *Med. Sci. Sports Exerc.*

THE EVALUATION OF TRIBOLOGICAL PROPERTIES OF BIOMATERIALS USED FOR KNEE REPLACEMENTS

Radek Sedlacek, Jana Vondrova

Czech Technical University in Prague, Faculty of Mechanical Engineering, Laboratory of Biomechanics, Prague, Czech Republic, Europe Union
E-mail: radek.sedlacek@fs.cvut.cz, Web: www.biomechanics.cz

INTRODUCTION

No known surgical implant material has ever been shown to be completely free of adverse reactions in the human body. However, long-time clinical experience of use of the biomaterials has shown that an acceptable level of biological response can be expected, when the material is used in appropriate applications. This article deals with very specific wear resistance testing of biomaterials used for producing of surgical implants. This type of testing is very important for appreciation of new directions at the joint replacement design (for example in total knee replacement). The aim of this work is to evaluate the influence of different type of biomaterials and modification of UHMWPE (Ultra High Molecular Weight Polyethylene) on the wear resistance. The special experiments were carried out in collaboration with The Academy of Sciences of the Czech Republic and company MEDIN ORTHOPAEDICS Inc.

MATERIALS AND METHODS

The special wear resistance tests, called "Ring On Disc", were completely carried out with a lot of pairs of different biomaterials. The experiments were executed according to ISO 6474:1994(E). This International Standard deals with evaluation of properties of biomaterials used for production of bone replacement. The method is based on loading and rotating two pieces from biomaterials (see Figure 1).

A ring is loaded onto a flat plate from different material. The axial load that is applied on the ring is all the time constant and equal 1500±10 N. The ring is rotated through an arc of ±25° at a frequency of (1 ± 0.1) Hz for a given period of time (100 ± 1) hours. There is distilled water using as the surrounding medium.

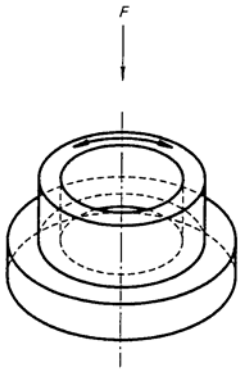

Figure 1: Schematic diagram

As a measure of wear resistance is determined and used volume of the wear track on the disc. The wear track cross-sectional area is analyzed from measured profile for each disc alone. The volume of the track is calculated from this area. After that the average volume is calculated for one group of specimens.

The profile measurements of the tested specimens were carried out using a specially adapted assembly. To determine the vertical position of points on the disc was used the digital drift sight MAHR EXTRAMESS 2001, with the sensitivity of 0.2 µm, placed in a sufficiently stiff stand. A positioning cross-table (ZEISS), containing a make-up piece (in which the disc was inserted), served for the disc shifting. The cross-table is movable in two axes by means of two

micrometric screws. Measured data were registered in a table prepared in advance.

The Experiments were carried out on the top quality testing system MTS 858 MINI BIONIX placed in "Laboratory of Biomechanics" at the Czech Technical University in Prague, Faculty of Mechanical Engineering, Department of Mechanics, Biomechanics and Mechatronics.

RESULTS AND DISCUSSION

The evaluation of the wear resistance was addict on the pertinence of different type of biomaterials and modification of UHMWPE. Totally the tests were executed in "Laboratory of Biomechanics" with 6 groups of specimens from different materials. There were 5 tested pairs in each group (means 6x5x100 hours of testing). The final parameters obtained in these tests - the wear volumes - were calculated (see Table 1). The comparison of different combinations of biomaterials used for implants producing can be implemented from this analysis.

CONCLUSIONS

We obtained the objective information about wear resistance for 6 combinations of different biomaterials and their modifications. The resulting wear volume indicates the amount of elements that are loosening during loading of the bone substitute implant in human body and describes one from the mechanical properties.

We found out the worn volume on the UHMWPE modified by crosslink is less than on the UHMWPE without modification and less then other combinations of biomaterials too. The results show the modification by crosslink is for UHMWPE material useful. Only wear resistance of combination ceramics x ceramics is better, but this combination is used only for comparison now. For next development it is purposeful to finish tests with other bone-substitute materials and increase the database with wear resistance evaluation.

REFERENCES

Sedlacek, R., Rosenkrancova, J. (2003). *Bioceramics 16*

Sedlacek, R., Rosenkrancova, J. (2004). *13th Biennial Conference of the Canadian Society for Biomechanics*, 178

Sedlacek, R., Rosenkrancova, J. (2006). *Proceedings of the 5th European Symposium on Biomedical Engineering.*

ACKNOWLEDGEMENTS

This research has been supported by the Ministry of Education of Czech Republic project No. MSM 6840770012.

Table 1: The final parameters of mechanical testing.

Material of RING	Material of DISC	Wear volume [mm^3]
Zirconia ceramics (Y-TZP)	Alumina ceramics	0,16
Vitalium alloy (Co-Cr-Mo)	Crosslink UHMWPE	4,78
Vitalium alloy (Co-Cr-Mo)	UHMWPE	5,51
Alumina ceramics (Al_2O_3)	Pressed UHMWPE	5,62
Titanium alloy (Ti_6Al_4V) with DLC	UHMWPE	6,61
Zirconia ceramics (Y-TZP)	PEEK (PolyEtherEtherKetone)	7,59

CYCLIC COMPRESSIVE LOADING FACILITATES FUNCTIONAL AND HISTOLOGICAL RECOVERY FOLLOWING STRAIN INDUCED DAMAGE IN SKELETAL MUSCLE

Timothy A Butterfield, Yi Zhao, Sudha Agarwal and Thomas M Best
The Ohio State University
E-mail: tim.butterfield@osumc.edu

INTRODUCTION

Muscle is a mechanically responsive tissue, which can perceive mechanical signals and respond via generation of corresponding intracellular signals. Muscle cells respond to biomechanical signals in a magnitude-dependent manner and lead to qualitative and quantitative changes in gene expression that initiate muscle damage or muscle repair. Trauma induced by both excessive mechanical forces and repetitive lengthening contractions can lead to the induction of proinflammatory cytokines and subsequent expression of mediators that initiate muscle damage *in vivo* (Tidball, 2002).

In fact, both the *in vitro* and *in vivo* responses of skeletal muscle to controlled loading have shown that biomechanical signals can be reparative and regenerative (Chandran et al., 2007) as well as damaging to muscle (Stekelenburg et al., 2007).

Although anecdotal clinical evidence suggests that cyclic compressive and tensile loads may improve functional recovery of skeletal muscle following eccentric exercise (EEX), this has never been implicitly tested in an *in vivo* animal model.

METHODS

Nerve cuff electrodes attached to custom made subcutaneous electrical interfaces were implanted bilaterally on the peroneal nerves of 6 adult New Zealand white rabbits. The anesthetized rabbits were placed supine in a sling with their left foot attached to a plate connected to the cam of a servo motor (Butterfield and Herzog, 2006). Supra-maximal stimulation was determined (voltage 3x α-motoneuron threshold, 150Hz). Starting with the left hindlimb, pre and post-exercise torque-angle relationships (T-Θ) were collected immediately prior to and following an EEX bout of 7 sets of 10 repetitions was performed (stimulus train duration = 350 ms) from a tibiotarsal joint angle of 95^{o}-145^{o} at 150^{o} sec^{-1} on day one.

Immediately following measurement of the post-exercise T-Θ on day 1, 30 minutes of cyclic compressive loading was applied to the left tibialis anterior (TA) via a custom built device that utilized a closed loop system that operated through both distance (position) and pressure feedback sensors. Tissue responses during compression (and shear) and tensile loading were quantified in real time with a series of piezoelectric thin film sensors applied to the muscle's surface (Fig. 1). Compressive loading was repeated for four consecutive days.

Subsequently, the right TA was subjected to the same injury protocol, but not subjected to compressive loading and served as control. On day five, final T-Θ relationships were obtained for both hindlimbs, the rabbits were euthanized and both TA were harvested for further analysis.

RESULTS AND DISCUSSION

EEX protocol resulted in similar reductions in peak isometric torque for left and right

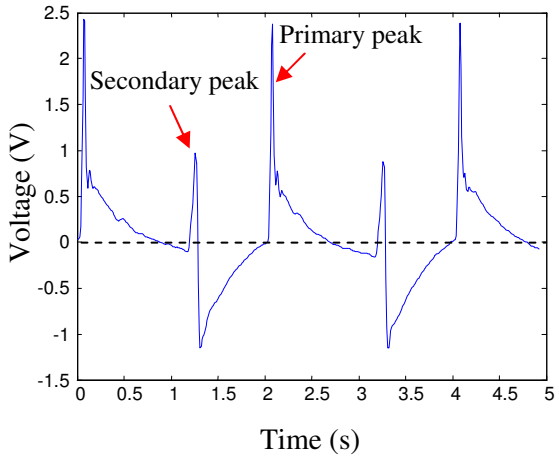

Figure 1. Force output vs. time. Data were band pass filtered in Matlab. Compression was performed at a frequency of 0.5 Hz. In this particular case, the calculated average normal stress was ~35N/cm^2.

hindlimbs (-70.5±0.02% vs -69.8.5±0.02%, p=0.624). Four days of cyclic compressive loading, facilitated recovery of peak isometric torque compared to rest only (+58.8±13.9% vs +14.2±11.3%, p=0.008), table 1.

The improvement of function following cyclic loading was corroborated via preliminary histological analysis. Multiple sections from all muscles subjected to EEX and rest exhibited a greater number of torn and necrotic fibers as well as greater cellular infiltration when compared to the EEX and cyclic loading group (Fig. 2).

In addition, four days of cyclic compressive loading resulted in a significant reduction in TA mass compared to control TA subjected to rest only (3.8 ± 0.12g vs 4.1 ± 0.14g, p-0.014), table 1.

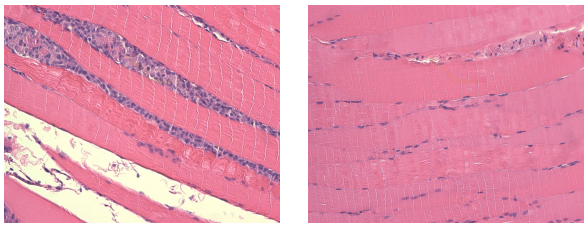

Figure 2. H&E stained sections from: **A**. TA subjected to one bout of EEX and rest for 4 days; and **B**. TA subjected to one bout of EEX, and cyclic compression for 4 days. 200x magnification.

SUMMARY/CONCLUSIONS

Compressive cyclic loading facilitates recovery of TA function following EEX induced muscle damage. This may be a result of an attenuation of the destructive cell processes, a facilitation of repair processes, or a combination of both. Future work will attempt to uncover the cellular responses to this external mechanical stimulus, and the molecular mechanisms responsible.

REFERENCES

Butterfield TA, Herzog W. (2006). *Pflügers Archiv*, **451**, 688-700.
Chandran, R et al. (2007). *Am J Physiol Cell Physiol,* In press
Stekelenburg, A et al. (2007). *J Appl Physiol,* In press
Tidball, JG (2002). *Clin Orthop*, S100-S109

ACKNOWLEDGEMENTS

Funded by the OSU Pomerene Chair in Family Medicine and NIH grant #AT00646.

Table 1: TA mass and recovery of peak isometric torque following EEX and either four days of cyclic compressive loading or rest (mean± SE).

	Cyclic Compressive Loading	Control	p-value
TA mass	3.8 ± 0.12g	4.1 ± 0.14g	p=0.014
Recovery of Isometric Torque	58.8±13.9%	14.2±11.3%	p=0.008

IS GAIT AFTER UNILATERAL TOTAL KNEE ARTHROPLASTY SIMILAR TO HEALTHY ADULTS?

Clare E. Milner
University of Tennessee, Knoxville, TN, USA. Email: milner@utk.edu

INTRODUCTION

Total knee arthroplasty (TKA) is a very successful surgery in terms of reducing pain and improving function of the affected joint. However, there are some concerns related to a predictable progression of osteoarthritis in the contralateral limb (Shakoor et al., 2002). Although walking speed is improved following TKA, it typically remains slower than that of matched controls (Walsh et al., 1998). There is some evidence that gait mechanics do not return to normal following TKA, with interlimb asymmetries in knee mechanics being reported three months after surgery (Mizner and Snyder-Mackler, 2005). There is some evidence that development and progression of osteoarthritis may be related to increased joint loading (Thambyah, 2005). This may be reflected in the magnitude of ground reaction forces after TKA, compared to healthy adults of a similar age. The attenuation of these loads via joint excursions should also be considered, particularly since abnormal knee joint mechanics have been reported in this population.

The aim of this study was to determine whether loading of the involved and the uninvolved limb following TKA was different from limb loading in healthy adults of a similar age. In particular, peak vertical ground reaction force (VGRF), instantaneous and average loading rates (ILR, ALR) and impulse (IMP) were compared among involved, uninvolved and control limbs. Furthermore, knee joint flexion at footstrike (KFLEX) and flexion excursion during weight acceptance (KEXC) were compared among the same limbs.

METHODS

These data are preliminary findings of an ongoing study of walking mechanics following TKA. Adults who were fully recovered from a previous unilateral TKA were recruited into the study. Exclusion criteria included rheumatoid arthritis, conditions likely to affect gait, and body mass index greater than 40 (extreme obesity). Healthy controls of a similar age were also recruited. All subjects provided informed consent to participate. Three-dimensional gait analysis was performed on all participants as they walked in the laboratory at their freely chosen speed (TKA 1.21 ± 0.16m/s; control 1.30 ± 0.13m/s). Five good trials were recorded using a seven camera motion capture system and two force platforms, positioned to collect consecutive steps. Ground reaction forces and knee kinematics were calculated for both lower extremities of the TKA group and the right limb of the control group. Due to the higher BMI of the TKA group, ground reaction forces were normalized to fat free mass (Deurenberg, 1991). Descriptive statistics and effect size were calculated for comparison amongst the limbs.

Data are presented for 12 subjects with TKA (age: 63 ± 6y; height: 1.72 ± 0.10m; mass: 89.1 ± 15.1kg) and 7 healthy control subjects (age: 61 ± 3y; height: 1.68 ± 0.12m; mass: 72.2 ± 19.0kg).

RESULTS AND DISCUSSION

Using effect size (ES) to indicate differences between the involved and uninvolved TKA limbs (INV, UN) and the control group (CTRL), several variables were notably decreased in the TKA limbs (Table 1). Peak

vertical ground reaction force was similar in all three limbs (ES: INV vs CTRL 0.33; UN vs CTRL -0.07). Both instantaneous and average loading rates were lower in both limbs of the TKA group (moderate to large effect) compared to the control limb (ES: ILR: INV vs CTRL 0.85,UN vs CTRL 0.70; ALR: INV vs CTRL 0.50, UN vs CTRL 0.68). However, vertical impulse was higher (large effect) in both limbs of the TKA group compared to the control limb (ES: INV vs CTRL -0.87, UN vs CTRL -0.96). The generally similar or lower loading in the TKA group compared to controls is contrary to expectations. It may be related to the reduced normal walking velocity of the TKA group. However, the higher impulse found in both limbs of the TKA group may indicate that the total load on the limbs is greater, even though the load is introduced more gradually. The significance of this for further joint degeneration is unclear.

Table 1: Ground reaction force and knee variables during walking, mean (sd)

	TKA INV	TKA UN	CTRL
VGRF	1.72 (0.26)	1.79 (0.24)	1.78 (0.12)
ILR	17.93 (5.02)	19.09 (4.56)	23.32 (7.60)
ALR	9.43 (2.76)	9.29 (1.42)	11.07 (3.80)
IMP	1.00 (0.17)	1.03 (0.20)	0.89 (0.09)
KFLEX	6.7 (6.2)	8.0 (4.8)	9.6 (2.2)
KEXC	9.8 (4.4)	12.1 (5.7)	14.7 (3.2)

There were also differences in knee joint mechanics in the TKA group compared to controls. These differences were slightly more pronounced in the involved limb, compared to the uninvolved, perhaps suggesting some interlimb asymmetry after TKA. Knee flexion excursion during loading showed the greatest differences (moderate to large effect), with excursion being smaller in both TKA limbs than the control limb (ES: INV vs CTRL -1.29; UN vs CTRL -0.57). The knee is considered to be the modulator of lower extremity stiffness, due to its flexion motion during weight acceptance. Therefore, the lower excursion may be important in terms of further deterioration of other lower extremity joints. The knee was also slightly more extended at footstrike in the TKA group compared to controls (ES: INV vs CTRL -0.70; UN vs CTRL -0.45).

These data indicate that there may be differences in knee mechanics during weight acceptance after TKA compared to controls. A more extended knee and less flexion excursion indicates a ‘stiff-knee’ gait and may reduce the shock attenuation of the lower extremity. Increased loading rates and peak during weight acceptance were expected, but not found, although the total load (impulse) was higher in the TKA group compared to controls.

SUMMARY

After unilateral TKA, both limbs exhibited less knee flexion excursion than healthy older adults. The reduction was slightly greater in the involved limb. Increased loading during weight acceptance was not found in the TKA limbs, which had peak force and loading rates similar to or lower than healthy older adults.

REFERENCES

Deurenberg, P. et al. (1991). *British J. Nutr.* **65**, 105-114.
Mizner, R.L., Snyder-Mackler, L. (2005). *J. Orthop. Res.* **23**, 1083-1090.
Shakoor N. et al. (2002). *Arth. & Rheum.* **46**, 3185-3189.
Thambyah, A. (2005). *Med. Hypotheses* **64**, 1157-1161.

MUSCLE ACTIVATION PATTERNS CHANGE THE INHERENT STIFFNESS OF THE HUMAN TRUNK

Stephen HM Brown and Stuart M McGill

Department of Kinesiology, University of Waterloo, Waterloo, ON, Canada
E-mail: shmbrown@uwaterloo.ca

INTRODUCTION

The torso musculature is quite unique in its anatomical arrangement. In particular, the abdominal wall muscles (external and internal obliques, transverse abdominis) overlay each other in a sheet-like formation and act through attachments to the abdominal and thoraco-lumbo-dorsal fascias to create a hydraulically pressurized abdomen

Most of what we know about muscle stiffness has been obtained from studies of the long strap-like muscles of the limbs. The abdominal wall muscles, however, may not be expected to stiffen in an entirely similar manner given their distinctinve architecture. In fact their ability to stiffen may be enhanced through a hydraulic mechanism, modifying intra-abdominal pressure and transferring hoop stresses around the torso (Farfan, 1973).

To date, no study has attempted to quantify the trunk stiffness inherent at varying levels of trunk muscle activation. This may elucidate the role of torso muscle activation on the hydraulic stiffening mechanisms discussed above. Therefore, the purpose of this study was to examine trunk stiffness related to torso, and in particular abdominal, muscle activation levels, in the absence of muscle reflexes.

METHODS

Nine healthy males volunteered for this study.

Each participant was secured to a jig that eliminates measurable friction and allows trunk movement about either the flexion-extension or lateral bend axis, depending upon how the participant is secured. Participants lied on their right side for the flexion-extension trials, and on their back for the lateral bend trials. Participants were then instructed to maintain one of four torso activation patterns: relaxed (minimal activation); activate EMG biofeedback (placed over the right external oblique) to 5 % MVC (light brace); activate biofeedback site to 10 % MVC (moderate brace); activate biofeedback site to 20 % MVC (heavy brace). Participants were instructed to tighten their abdominal muscles isometrically in order to achieve the desired brace levels. EMG was monitored from 14 torso muscles.

Once each participant had achieved their target activation pattern during each trial, the experimenter applied a torque such that the participant's upper body rotated (isolated at the pelvis) in the desired direction (flexion, extension, or right-side lateral bend) at a relatively constant velocity.

3-Dimensional lumbar trunk motion was recorded using an electromagnetic tracking system (Isotrak, Polhemus, Colchester, VT, USA). The moments applied to the torso were recorded by the product of the force applied perpendicular to the distal end of the upper body cradle (measured via a force transducer) and the moment arm from the location of the applied force to the level of L4/L5.

Moment-angle curves were developed and exponential curve fits of the following form were performed for each brace level/direction combination:

$$M = \lambda e^{\delta\phi} \quad (1)$$

This equation was differentiated once with respect to φ to obtain a measure of trunk angular stiffness:

$$K = \lambda\delta e^{\delta\phi} \quad (2)$$

RESULTS AND DISCUSSION

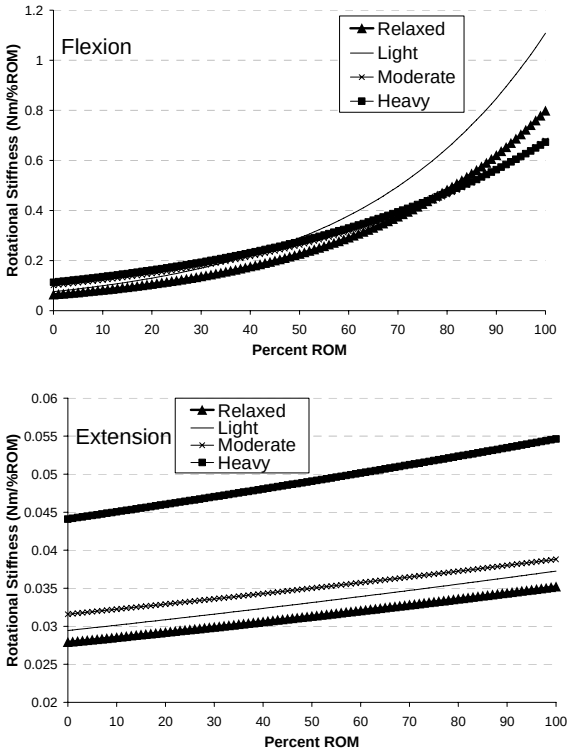

Figure 1: Stiffness (Nm/%ROM) across the ROM in each of the flexion and extension directions.

Stiffness increased exponentially at each muscle activation level in both flexion and lateral bend (Figure 1).

In flexion, from zero to approximately 40% ROM, stiffness increased with each level of abdominal brace; in lateral bend, this trend existed from zero to approximately 60% ROM. Above these ROMs higher levels of activation actually resulted in a lower stiffness level than less active states (Figure 1 flexion).

Extension stiffness, however, showed an increasing linear trend with increasing ROM for each of the muscle activation levels, and stiffness increased with each successive increase in trunk muscle activation (Figure1).

SUMMARY/CONCLUSIONS

The ability of increasing torso, and in particular abdominal, muscle activation to increase trunk stiffness is partially dependent upon trunk posture. In extension, spine stiffness increased with successive increases in muscle activation throughout the ROM. Similarly, in trunk postures most commonly adopted by individuals through daily activities (neutral to approximately 40% of maximum) spine stiffness increased in the flexion and lateral bend directions as muscle activation increased. However, towards the end ROM in both flexion and lateral bend, individuals became less stiff at the maximum abdominal muscle co-activation levels. We have previously documented similar findings whereby trunk stiffness is somewhat compromised at high levels of co-activation (Brown et al., 2006). The source or mechanism of this phenomenon is still not yet clear; future work will be directed to uncover the cause

REFERENCES

Farfan. H.F., (1973). *Mechanical Disorders of the Low Back.* Lea & Febiger, Philadelphia.

Brown, S.H.M. et al. (2006). *Spine,* **31**, E387-E393.

TRUNK MUSCLE ACTIVATION AND LOW-BACK LOADING DURING THE PERFORMANCE OF STANDARD AND SUSPENDED PUSH-UP EXERCISES

Tyson A.C. Beach, Samuel J. Howarth, and Jack P. Callaghan

Department of Kinesiology, University of Waterloo, Waterloo, ON, Canada
E-mail: callagha@healthy.uwaterloo.ca

INTRODUCTION

Push-up exercises are normally performed to challenge muscles that span upper extremity joints. However, it is also recognized that such exercises provide an effective means by which to challenge muscles of the "core", especially when the hands are in contact with a labile support surface (Freeman et al., 2006). The purpose of this study was to compare trunk muscle activation levels and resultant low-back loads when standard push-ups (STAN) and suspended push-ups (SUS) were performed (Figure 1). It was hypothesized that variables of interest would differ between the push-up exercise variants.

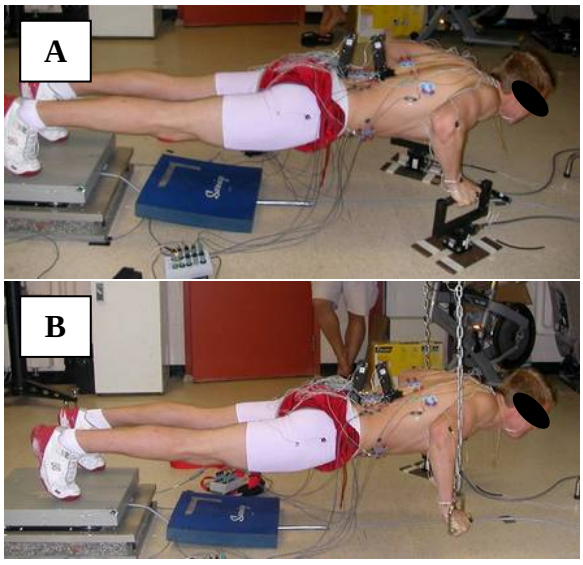

Figure 1: Bottom position of (A) standard and (B) suspended push-up exercises.

METHODS

Eleven recreationally trained male volunteers performed sets of STAN and SUS. Initial postures and the repetition rate were standardized to permit direct comparisons between exercises. The order of performance was randomized.

Surface EMG signals collected from seven bilateral trunk muscle groups (Table 1) were linear enveloped (Brereton and McGill, 1998) and normalized to peak activity levels achieved during maximal voluntary contractions (MVC).

A motion capture system (Optotrak Certus, Northern Digital Inc., Canada) provided upper body position data, and forces acting at the hand-handle interface were measured. These data were inputs for a 3D inverse dynamic linked-segment model (LSM) of the upper body to compute net L4/L5 reaction kinetics.

LSM outputs were used in conjunction with an anatomically detailed EMG-driven 3D model of the lumbar torso (Cholewicki and McGill, 1996) to estimate trunk muscle forces and subsequently L4/L5 joint contact (compression and shear) forces.

Repeated measures analyses of variance (general linear model) were used to compare dependent variables between exercises, phases (up vs. down), and where applicable, between sides of the body.

RESULTS AND DISCUSSION

When performing SUS, muscles of the abdominal wall and the latissimus dorsi were activated to levels that were significantly greater than those elicited when performing STAN (Table 1). No bilateral asymmetries in muscle activation levels were detected (Table 1). As a direct result of these increased activation levels, model-predicted muscle forces increased and consequently led to significantly greater L4/L5 compressive ($p = 0.0001$) and anterior/posterior (A/P) shear ($p = 0.0306$) forces when performing SUS. In a similar vein, muscle activation levels tended to be greater in the up-phase of both exercises (Table 1), and it followed that L4/L5 compressive ($p = 0.0391$) and A/P shear ($p = 0.0281$) forces were significantly greater in this phase of each exercise. The L4/L5 compressive loading response is encapsulated in Figure 2.

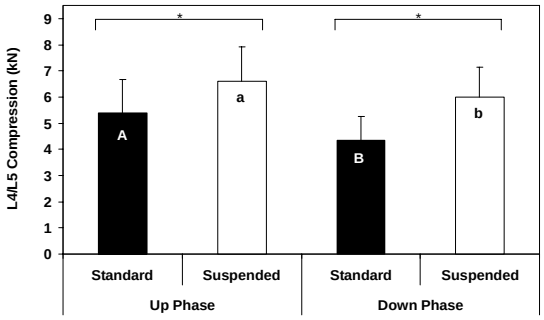

Figure 2: Comparison of L4/L5 compression forces estimated during STAN and SUS. Mean values are presented; error bars represent standard error of the mean. Bars labeled with different letters are significantly different from one another.

SUMMARY/CONCLUSIONS

In comparison to STAN, SUS appear to provide a superior abdominal muscle challenge. However, for individuals unable to tolerate high low-back compressive or shear loads, benefits gained by incorporating SUS into their training regimen may be outweighed by the potential risk of overloading low-back tissues.

REFERENCES

Brereton, L.C., McGill, S.M. (1998). *J Electromyogr Kinesiol*, **8**, 227-232.

Cholewicki, J., McGill, S.M. (1996). *Clin Biomech*, **11**, 1-15.

Freeman, S., et al. (2006). *Med Sci Sports Exerc*, **38**, 570-577.

ACKNOWLEDGEMENTS

Funding for this work was provided by the Natural Science and Engineering Research Council of Canada.

Table 1: Mean (SE) trunk muscle activation levels elicited (% MVC). RA – rectus abdominis; EO – external abdominal obliques; IO – internal abdominal obliques; LD – latissimus dorsi; T9 – upper erector spinae; L3 – lower erector spinae; L5 – multifidus surrogate.

	EXERCISE			PHASE			SIDE		
	Standard	Suspended	*p*-value	Up	Down	*p*-value	Left	Right	*p*-value
RA	13.9 (3.9)	39.5 (10.1)	0.0025	28.8 (8.8)	24.6 (8.4)	0.0342	23.9 (7.2)	29.5 (9.8)	0.5466
EO	18.2 (3.8)	26.6 (4.3)	0.0042	25.0 (4.4)	19.7 (3.9)	0.0030	23.5 (4.0)	21.3 (4.5)	0.1345
IO	15.6 (3.8)	24.1 (4.2)	0.0005	21.5 (4.6)	18.2 (3.7)	0.1687	20.1 (4.3)	19.6 (4.1)	0.9075
LD	7.1 (1.4)	11.3 (1.8)	0.0102	9.6 (1.6)	8.8 (1.8)	0.2951	9.8 (1.4)	8.6 (1.9)	0.3703
T9	11.7 (2.2)	12.5 (2.3)	0.5909	14.1 (2.5)	10.1 (1.8)	0.0163	11.0 (1.9)	13.2 (2.5)	0.3029
L3	2.2 (0.6)	4.6 (1.6)	0.0929	3.8 (1.5)	3.0 (1.0)	0.2814	3.8 (1.3)	3.0 (1.3)	0.3665
L5	1.7 (0.9)	3.2 (1.5)	0.3024	2.9 (1.5)	2.1 (0.9)	0.2117	2.7 (1.3)	2.2 (1.3)	0.6072

MUSCULAR CONTRIBUTIONS TO VERTEBRAL JOINT ROTATIONAL STIFFNESS DURING THE STANDARD PUSHUP

Samuel J. Howarth, Tyson A.C. Beach, Jack P. Callaghan

Department of Kinesiology, University of Waterloo, Waterloo, ON, Canada
E-mail: sjhowart@uwaterloo.ca

INTRODUCTION

Recent trends are promoting the use of pushups as an exercise to challenge the core trunk musculature. Evidence from Freeman et al (2006) supports this idea provided that one aims to maintain a neutral spine posture while performing the exercise.

The purpose of this study was to quantify the relative contributions of each muscle group surrounding the spine to vertebral joint rotational stiffness (VJRS) during the pushup exercise using an approach developed by Potvin and Brown (2005). It was hypothesized that the abdominal musculature would contribute more to VJRS than the posterior musculature of the lumbar spine during a standard pushup.

METHODS

Eleven males (age: 27.4 ± 2.8 years, height: 1.83 ± 0.06 m, weight: 89.4 ± 11.0 kg) volunteered to participate in the study. All participants signed an informed consent document that had been approved by the University of Waterloo's Office of Research Ethics.

All participants performed a series of 8 pushups at a cadence of one full pushup (down and up cycle) every 2 seconds.

Electromyographic (EMG) recordings were obtained bilaterally from: erector spinae at the level of the T9, L3 and L5; rectus abdominis; external abdominal obliques; internal abdominal obliques; and latissimus dorsi (Cholewicki and McGill 1996). Upper body kinematics were recorded with four position sensors (Optotrak Certus System, NDI, Waterloo, ON, Canada) and hand loads were recorded with two tri-axial force transducers (MC3A-X-500, AMTI, Watertown, MA, USA). The EMG and force transducer data were sampled at a rate of 2048 Hz while the joint kinematics were obtained at a rate of 64 Hz.

EMG signals of the aforementioned muscles collected during the pushup were full wave rectified, lowpass filtered with a 2nd order Butterworth digital filter with a cutoff frequency of 2.5 Hz, and normalized as a percentage of previously recorded maximal voluntary isometric contractions. Individual fascicle force and stiffness for a set of 118 muscle fascicles surrounding the lumbar spine were determined from a Distribution Moment model that used the normalized EMG signals as its inputs. Individual fascicle force and stiffness were multiplied by a participant-specific adjustment that accounted for differences in maximum muscle stress and muscle physiological cross sectional area. Muscular contributions to VJRS were determined using a combination of the adjusted fascicle force, stiffness and geometry (Potvin & Brown, 2005). The proportion of total VJRS for each muscle group was obtained using the methods described by Brown & Potvin (2007).

Differences between the relative contributions of individual muscle groups to VJRS were analyzed using a single factor analysis of variance and Tukey's *post hoc*

analyses. The level of statistical significance was set at $p = 0.05$ for rejecting the null hypothesis in all analyses.

RESULTS AND DISCUSSION

The VJRS contributions are dominated by the abdominal musculature. In particular, rectus abdominis contributed the most to VJRS about the flexion/extension axis at each lumbar vertebral joint while external oblique and internal oblique contributed the most to VJRS about the lateral bend and axial twist axes respectively at all lumbar vertebral joints with the exception of L5-S1 (Figure 1).

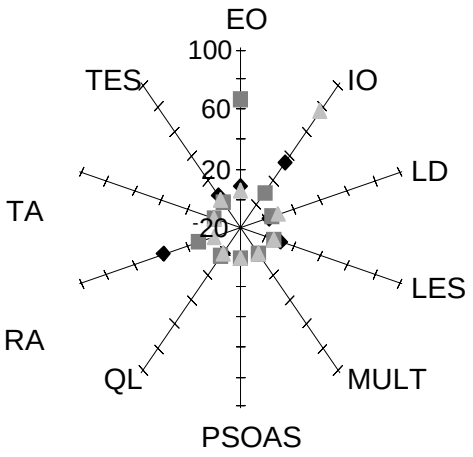

Figure 1: Proportion of VJRS for each muscle group about the flexion/extension (♦), lateral bend (■) and axial twist (▲) axes.

At L5-S1, external oblique and internal oblique contributed the most to VJRS about the axial twist and lateral bend axes respectively.

Due to the novelty of the stiffness analysis, there is no data for direct comparison of muscle contributions to VJRS during other exercises. However, the motor patterns described by Beach et al (submitted), and the neutral lumbar spine posture is similar to the motor patterns and spine posture of other abdominal training exercises (Kavcic et al, 2004), suggesting that VJRS contributions of the abdominal muscles in this study would be consistent with the VJRS outputs for other abdominal exercises. Analysis of EMG magnitudes during exercises does not include muscle morphology which is included in analyses of VJRS. Thus, VJRS can provide direct insight into the muscular stiffening mechanism during exercises.

SUMMARY/CONCLUSIONS

The pushup can be considered a challenge to the abdominal musculature. The orientation of the rectus abdominis, internal oblique, and external oblique muscles allows for these muscles to dominate the muscular contributions to VJRS about the flexion/extension, lateral bend, and axial twist axes within the lumbar spine.

REFERENCES

Beach, T.A.C. et al (submitted). Med Sci Sports Exerc.

Brown, S.H.M., Potvin, J.R. (2007). Hum Mov Sci, **26**, 113-123.

Cholewicki, J., McGill, S.M. (1996). Clin Biomech, **11**, 1-15.

Freeman, S. et al (2006). Med Sci Sports Exerc, **38**, 570-577.

Kavcic, N. et al (2004). Spine, **29**, 2319-2329.

Potvin, J.R., Brown, S.H.M. (2005). J Biomech, **38**, 973-980.

ACKNOWLEDGEMENTS

The authors would like to acknowledge the financial support of the Natural Sciences and Engineering Research Council of Canada.

UPPER EXTREMITY KINEMATICS OF CRUTCH-ASSISTED GAIT IN CHILDREN WITH MYELOMENINGOCELE

Brooke Slavens [1,2], Peter Sturm [1-3], and Gerald Harris [1-3]

[1] Orthopaedic and Rehabilitation Engineering Center, Milwaukee, WI
[2] Marquette University, Milwaukee, WI
[3] Shriners Hospitals for Children, Chicago, IL
E-mail: brooke.slavens@mu.edu

INTRODUCTION

Currently, there are limited biomechanical models for quantitative evaluation of upper extremity (UE) dynamics in children with myelomeningocele (MM). While the lower extremities have been studied extensively in MM during crutch-assisted gait (Vankoski, et al., 1997; Galli, et al., 2002; Gutierrez, et al., 2003), UE dynamics have received very limited attention (Requejo, et al., 2005). In order to study UD dynamics, a three-dimensional (3D) biomechanical model of the UEs was developed for dynamic analysis of reciprocal and swing-through Lofstrand crutch-assisted gait in children with MM.

A pediatric model that describes joint motions of the upper body during crutch-assisted gait may be a valuable tool for clinicians. The study findings may also prove useful for improving crutch prescription and in planning ambulatory rehabilitation of children with MM.

METHODS

The UE motion model includes seven rigid body segments: 1) trunk, 2) right upper arm, 3) right forearm, 4) right hand, 5) left upper arm, 6) left forearm, and 7) left hand. Three degree-of-freedom shoulder (glenohumeral) joints and two degree-of-freedom elbow and wrist joints connect the segments. The upper extremity model incorporates ISB recommendations for modeling (Wu, et al., 2005). Eighteen markers are placed on bony landmarks of the upper body in order to determine the kinematics of the trunk, shoulders, elbows and wrists during crutch-assisted gait. To calculate the kinematics of the crutches, four markers are placed strategically. Rotations are described using Euler angles (Z-X-Y order). The trunk and crutch segments are described with reference to the lab (global) coordinate system.

Nine subjects (mean ± S.D. age: 11 ± 4 years) volunteered and gave written consent to participate in the research study. All subjects had an L3 or L4 level myelodysplasia and were ambulatory using Lofstrand crutches in both reciprocal and swing-through gait patterns. Subjects who had undergone orthopaedic surgery in the past year were excluded from the study. The subjects walked at a self-selected pace using Lofstrand crutches until five successful trials were completed with each gait pattern. A 14-camera Vicon MX system captured the marker motions.

RESULTS AND DISCUSSION

The mean cadence, walking speed, stride length, and stance duration during reciprocal gait and swing-through gait were calculated. All temporal-spatial parameters were greater during swing-through gait compared to reciprocal gait, except stance duration (Table 1). Stride length and stance duration were found to be statistically different between gait patterns ($p<0.05$).

Table 1: Mean temporal-spatial parameters. *Gait patterns are significantly different ($p<0.05$)

	Cadence (steps/min)	Walking Speed (m/s)	Stride Length* (m)	Stance Duration* (s)
Reciprocal	69.55	0.46	0.77	0.62
Swing-through	77.36	0.68	1.00	0.54

The mean flexion/extension joint motion, for right and left sides, during reciprocal gait and swing-through gait were also determined (Figure 1). Although reciprocal and swing-through gait have distinguishable characteristics, the flexion/extension motions were similar throughout the gait cycles. Joint ranges of motion were greatest during swing-through gait. Significant differences were found in trunk and elbow ranges of motion between swing-through and reciprocal gait ($p<0.05$). Right and left elbow and wrist ranges of motion were significantly different during reciprocal gait.

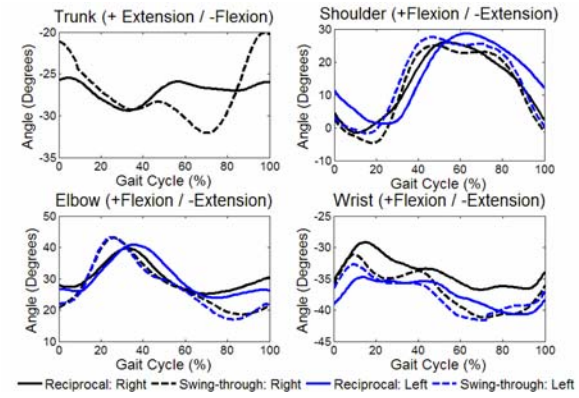

Figure 1. Joint kinematics during reciprocal and swing-through gait.

The model is effective in detecting significant differences in upper extremity joint motion. The model is considered to be suitable for further application to quantify upper extremity dynamics in pediatric subjects with MM. The information gained may be useful for developing injury prevention strategies, rehabilitation protocols, and/or improving the design of Lofstrand crutches.

SUMMARY/CONCLUSIONS

The current study aids physicians in treatment planning of children with MM, which may ultimately improve quality of life. Further subject testing is currently underway, as well as, a kinetic analysis of the UE joints. Future work includes identifying correlations among dynamics and standardized outcomes assessment tools.

REFERENCES

Vankoski, S. et al. (1997) *Dev Med Child Neurol*, **39**, 614-619.

Galli, M. et al. (2002) *Funct Neurol*, **17**, 203-210.

Gutierrez, E.M. et al. (2003) *Gait Posture*, **18**, 170-177.

Requejo, P.S. et al. (2005) *Med Eng Phys*, **27**, 19-29.

Wu, G. et al. (2005). *J. Biomechanics*, **38**, 981-992.

ACKNOWLEDGEMENTS

This project was supported by Shriners Hospitals for Children and OREC. The authors would like to thank Ms. Sahar Hassani, Ms. Kathy Reiners, Ms. Vicky Young and Mr. Adam Graf for their helpful suggestions, assistance and contributions to this project.